VYSOKÉ UČENÍ TECHNICKÉ V BRNĚ

FAKULTA CHEMICKÁ

MATERIÁLY NA BÁZI POLY(3-HYDROXYBUTYRÁTU)

HABILITAČNÍ PRÁCE

V OBORU CHEMIE, TECHNOLOGIE A VLASTNOSTI MATERIÁLŮ

MGR. RADEK PŘIKRYL, PH.D.

BRNO 2023

ABSTRAKT

Bakteriální biopolymer poly(3-hydroxybutyrát) (PHB) je pro svůj původ z obnovitelných zdrojů a svoji biodegradabilitu a biokompatibilitu zajímavým kandidátem pro některé moderní aplikace. Sám o sobě však při zpracování v tavenině vykazuje termickou nestabilitu a následnou křehkost. Tato práce se zabývá zpracováním PHB do funkčních materiálů pro 3 klíčové aplikace. V první části prezentuje vybrané výsledky v oblasti výzkumu biokompozitních materiálů pro 3D tisknutelné resorbovatelné náhrady kostní tkáně a dává do souvislosti materiálové složení, strukturu, morfologii povrchu se speciálními vlastnostmi a chováním v simulované tělesné tekutině. Ve druhé části jsou uvedeny poznatky z oblasti technologií výroby vláken metodami odstředivého zvlákňování a možnosti řízení vlastností takto vyráběné netkané textilie pro medicínské aplikace. Třetí část se zabývá technologiemi výroby povlakovaných hnojiv se zpomaleným uvolněním pro moderní agronomii a prezentuje dosažené výsledky vyvíjeného konceptu z nádobových a maloparcelních pokusů.

ABSTRACT

The bacterial biopolymer poly(3-hydroxybutyrate) (PHB) is an interesting candidate for some modern applications due to its origin from renewable sources and its biodegradability and biocompatibility. However, it exhibits thermal instability in melt processing and following brittleness. This work deals with processing PHB into functional materials for three key applications. The first part presents selected results in the field of research on biocomposite materials for 3D printable resorbable bone tissue substitutes and relates the material composition, structure, and surface morphology to special properties and behaviour in a simulated body fluid. In the second part, findings from the field of fibre production technologies using centrifugal spinning methods and the possibility of controlling the properties of the nonwoven fabric produced in this way for medical applications are presented. The third part deals with the production technologies of coated fertilizers with slow release for modern agronomy and presents the achieved results of the developed concept from the greenhouse pot and small-plot field experiments.

KLÍČOVÁ SLOVA

poly(3-hydroxybutyrát) (PHB), cirkulární ekonomika, bioplast, biokompozit, FDM 3D tisk, resorbovatelná náhrada kostní tkáně, netkaná textilie, buněčný skafold, kryty ran, hnojivo se zpomaleným a řízeným uvolňováním (CRF, SRF)

KEYWORDS

poly(3-hydroxybutyrate) (PHB), circular economy, bioplastic, biocomposite, FDM 3D printing, resorbable bone tissue replacement, nonwoven fabric, cellular scaffold, wound dressings, slow-release and controlled-release fertilizer (CRF, SRF)

PODĚKOVÁNÍ

Vědecko-výzkumná činnost je pro mne symbolem týmové práce. Dnešní doba přináší zajímavé výzvy a témata často na pomezí mnoha vědních oborů, kde je výzkum bez spolupráce nemyslitelný. I výsledků této práce bylo dosaženo intenzivní spoluprací s mnoha pro mne důležitými osobami, týmy a institucemi. Nelze zde vyjmenovat všechny, dovolím si zde alespoň zmínit osoby, které významně ovlivnily moje směřování při cestě ke zde prezentovaným výsledkům za posledních 10 let, za což jim patří moje upřímné díky.

Děkuji tímto prof. Ivaně Márové a prof. Stanislavu Obručovi za možnost nahlédnout do biotechnologie výroby PHB a vůbec za téma PHB, které umožnilo vznik Laboratoře bioplastů, jež svým aplikačním výzkumem navazuje na technologii výroby PHB. Dlouhodobá spolupráce s PhDr. Lenkou Mynářovou a celým týmem společnosti Nafigate byla klíčovým prvkem pro směřování aplikačního výzkumu i zajištění projektového i smluvního financování výzkumných prací a vnímání strategie a legislativy EU. Doc. Jiřímu Tocháčkovi vděčí náš tým za praktické základy zpracování polymerů a přístup ke zpracovatelským strojům na CEITEC. Bez osudového setkání s prof. Pavlem Alexym a jeho týmem si nedokáži představit více jak polovinu realizovaných výstupů, neboť dal šlechetně k dispozici veškeré technologie zpracování termoplastů a vždy ochotně přidal cennou odbornou radu. V oblasti výsledků s přesahem do medicíny děkuji doc. Lucy Vojtové za cenné konzultace a možnost zapojení se do jejich synergických projektů na CEITEC. Velké díky za spolupráci v oblasti povlaků hnojiv patří také doc. Petru Škarpovi z MENDELU, v oblasti biologických testů doktorce Michale Klusáček Rampichové z ÚEM AV ČR a v oblasti zpracování plastů doc. Tomáši Sedláčkovi z UTB.

Neméně důležité je pochopitelně poděkování celému mému týmu, který vždy loajálně a ochotně přijímal všechny výzvy, které nám umožnily další rozvoj a financování celé skupiny. Bez tohoto fungujícího a rozvíjejícího se týmu a ochoty si kdykoliv vzájemně pomoci by tyto výsledky ani předložená práce nevznikly.

Děkuji tímto také za podporu vedení FCH VUT a všem provozním oddělením. Jsem si vědom občas náročných a komplikovaných požadavků z mojí strany vyvolaných potřebami akutního řešení často vzniklých nestandartních situací při řešení mnoha projektů a zakázek smluvního výzkumu.

A konečně velké poděkování patří mojí rodině, která dlouhá léta musí respektovat někdy až poněkud přehnané časové pracovní vytížení a z toho plynoucí častý nedostatek energie pro aktivní rodinný život. I proto je pro mne moment odevzdání předložené práce jakýmsi pomyslným ohlédnutím za tím, co jsem se svým týmem dokázal, ale také motivací k optimalizaci životních priorit.

OBSAH

1 ÚVOD 7

2 PODNĚTY K VÝZKUMU 8

2.1 LEGISLATIVA 8

2.1.1 Legislativa na evropské úrovni 8

2.1.2 Legislativa na národní úrovni 8

2.2 BIOPLASTY 9

2.2.1 Nová generace základních typů bioplastů 10

3 POLY-3-HYDROXYBUTYRÁT 11

3.1 VLASTNOSTI PHB 11

3.2 BIOSYNTÉZA PHB 12

3.3 EXTRAKCE PHA Z MIKROBIÁLNÍ BIOMASY 12

4 TERMOPLASTY NA BÁZI PHB PRO 3D TISK 14

4.1 MOTIVACE 14

4.2 METODY A ÚSKALÍ ZPRACOVÁNÍ PHB 14

4.2.1 Krystalizace 15

4.2.2 Distribuce molekulové hmotnosti 16

4.2.3 Procesní stabilizace 16

4.2.4 Plastifikace změkčovadly 16

4.2.5 Mísení s dalšími polymery 17

4.2.6 Kompozity na bázi PHB 19

4.3 PHA MATERIÁLY PRO 3D TISK 19

4.4 BIODEGRADABILITA FINÁLNÍCH PHA BIOPLASTŮ A BIOKOMPOZITŮ 21

4.5 CÍLE 22

4.6 DOSAŽENÉ VÝSLEDKY 23

4.6.1 Zpracovatelnost a stabilizace PHB 23

4.6.2 Mísení s ostatními polymery 27

4.6.3 Aditivace změkčovadly 28

4.6.4 Nukleace 30

4.6.5 Stabilizace PHB/PLA směsí 31

4.6.6 End of life PHB/PLA směsí 32

4.6.7 FDM 3D tisk PHB kompozitů 33

4.7 PŘÍNOS 39

5 KOMPOZITY PRO FDM 3D TISK NA BÁZI PHB PRO MEDICÍNU 40

5.1 MOTIVACE 40

5.2 SOUČASNÝ STAV 40

5.3 CÍLE ... 42
5.4 DOSAŽENÉ VÝSLEDKY ... 42
5.4.1 Směsi PHB/PLA ... 42
5.4.2 Směsi PHB/PCL ... 45
5.4.3 Povrchové vlastnosti 3D tištěných skafoldů ... 46
5.4.4 Optimalizace složení směsí PHB/PLA/SN/TCP ... 48
5.4.5 Skafold pro náhradu segmentu femuru ... 51
5.5 PŘÍNOS ... 54
6 NETKANÉ MIKROVLÁKENNÉ TEXTILIE NA BÁZI PHB PRO MEDICÍNU ... 55
6.1 MOTIVACE ... 56
6.2 SOUČASNÝ STAV ... 56
6.2.1 Antimikrobiální aditiva ... 57
6.3 CÍLE ... 59
6.4 DOSAŽENÉ VÝSLEDKY ... 60
6.5 PŘÍNOS ... 66
7 AGROCHEMICKÉ APLIKACE PHB ... 67
7.1 MOTIVACE ... 67
7.2 SOUČASNÝ STAV ... 68
7.3 CÍLE ... 71
7.4 DOSAŽENÉ VÝSLEDKY ... 71
7.4.1 Testy ve vodním prostředí ... 73
7.4.2 Vegetační nádobové testy ... 74
7.4.3 Čtvrtprovozní příprava povlakovaných hnojiv ... 76
7.4.4 Polní testy ... 76
7.4.5 Optimalizace složení ... 77
7.4.6 Syntéza biomateriálů pro povlaky ... 80
7.5 PŘÍNOS ... 80
8 ZÁVĚR ... 81
9 REFERENCE ... 83
10 SEZNAM VÝSTUPŮ AUTORA NA TÉMA PRÁCE ... 104
10.1 PUBLIKACE ... 104
10.2 OSTATNÍ VÝSTUPY ... 106
10.3 VEDENÉ PRÁCE NA RELEVANTNÍ TÉMA ... 107
11 PROJEKTY ŘEŠENÉ AUTOREM ... 108

1 ÚVOD

Tato práce je kombinací komentovaného souhrnu publikovaných prací a některých původních výsledků, které nebyly týmem autora doposud publikovány. Představuje tak zaměření autora v posledních deseti letech působení na FCH VUT na pozici odborného asistenta a výzkumného pracovníka v rámci desítky získaných dotačních projektů. Společným prvkem těchto vybraných témat je biopolymer poly(3-hydroxybutyrát) (PHB) z rodiny polyhydroxyalkanoátů (PHA). Inovativní biotechnologii výroby tohoto biopolymeru a tím i celé téma přinesl na FCH VUT tým prof. Ivany Márové spolu s prof. Stanislavem Obručou. Patentem této technologie pak položili oficiálně pomyslný základní kámen výzkumnému směru PHA biopolymerů na FCH VUT, který byl motivací i pro další fakultní výzkumné skupiny. V návaznosti na výzkum technologie výroby PHA vznikly požadavky na vývoj finálních aplikací ze strany průmyslových partnerů a příležitost ke vzniku nové výzkumné skupiny v rámci Centra materiálového výzkumu FCH VUT orientované na vývoj zpracovatelských technologií PHA.

Pod autorovým vedením tak byla založena Laboratoř bioplastů s cílem hledat a vyvíjet aplikace PHB. Materiál byl testován z počátku v technologiích zpracování termoplastů a kompozitů. Následně i na základě strategie EU, která začala bioplastové aplikace spíše potlačovat, a na základě poptávky z průmyslu, bylo portfolio testovaných technologií rozšířeno. Protože je PHB spolu s ostatními kopolymery PHA vhodným kandidátem pro využití v medicíně, byla logická následná orientace týmu na materiálové technologie pro tyto aplikace. Ve spojení s 3D tiskovými technologiemi biokompozitů totiž PHB poskytuje zajímavý směr využití materiálu jako náhrady tkání ve tvaru přizpůsobeném pacientu na míru. Vlákenné membrány z těchto biomateriálů pak mohou být funkčním stavebním prvkem vrstevnaté struktury krytů ran nebo nosičem s vnitřní 3D vlákennou strukturou pro kultivaci buněk tkání. Poměrně snadná rozložitelnost PHB v podmínkách čističky odpadních vod, půdy, slané i sladké vody pak vybízela k tématům směřujícím k náhradě nebiodegradabilních materiálů v kosmetice a povlaků v agrochemických aplikacích.

Každé z výše uvedených témat má svá specifika, stanovené cíle a také jiné dosažené výsledky, které jsou snad přínosem pro poznání v oblasti zpracování biopolymeru PHA. Proto byla práce rozdělena do samostatných kapitol a ke každé jsou tyto informace uvedeny zvlášť.

Osobní motivací ke zde prezentovaným výsledkům práce byl respekt k živé i neživé přírodě a přirozeným procesům v ní, k životu jako takovému a k lidskému zdraví. S vizí bezpečného a udržitelného využívání přírodních surovin a jejich zpracování do formy funkčních materiálů a výrobků z nich, které po ukončení doby svého života nezatíží příliš životní prostředí a ideálně se stanou zdrojem pro proces dalšího využití. Ač se tato výzva zdá být neřešitelná, lze pomocí nástrojů vědy a výzkumu hledat řešení, která se alespoň tomuto ideálu budou blížit [1]. V poslední době je proto kladen čím dál větší důraz na eliminaci negativních dopadů lidské činnosti. Jedním z nosných pilířů pozitivní změny je přechod z lineární ekonomiky na cirkulární (CE). Ta se stává stále více důležitou v globálním měřítku. V posledních letech přijaly kromě Evropy i země jako Čína a Japonsko plány na podporu CE, které mají za cíl podpořit přechod na ekonomiku, která minimalizuje odpad a využívá zdroje efektivněji. A právě k tomuto záměru má přispět svým zaměřením výzkumná skupina Laboratoře bioplastů se svými výsledky, které sumarizuje předložená habilitační práce.

2 PODNĚTY K VÝZKUMU

2.1 Legislativa

2.1.1 Legislativa na evropské úrovni

Největším legislativním „balíkem“ změn v rámci EU je Zelená dohoda pro Evropu (GD) a cirkulární ekonomika (CE) je jeho základním pilířem, který se projevuje ve všech nařízeních a směrnicích. GD vytváří i rámec pro bioplasty a jejich uplatnění na trhu [2], [3].

Explicitně jsou pak cíle Zelené dohody pro EU v oblasti CE a obsaženy ve strategii Akční plán pro CE, aktuální verze vyšla v březnu 2020. Akční plán pro CE formuluje iniciativy v rámci celého životního cyklu výrobků; jeho cílem je snížit dopad spotřeby EU a do r. 2030 zdvojnásobit míru oběhového využívání materiálů v EU. Je zaměřen na způsob navrhování výrobků, podporuje procesy oběhového hospodářství, udržitelnou spotřebu a snaží se zajistit předcházení vzniku odpadu a udržení používaných zdrojů v ekonomických cyklech v EU co nejdéle [4]. Akční plán k cirkulární ekonomice směřuje k transformaci všech sektorů. Evropská komise (EK) pokračuje v plastikářské strategii z r. 2018, zaměřené, mimo jiné, na opatření, jak uchopit problém úmyslně přidávaných mikroplastů a neúmyslně uvolněných plastů, například z textilu či při opotřebovávání pneumatik [5]. Evropská komise také rozvíjí požadavky k zajištění toho, aby všechny obaly zboží na trhu EU byly do r. 2030 znovu použitelné nebo recyklovatelné ekonomicky smysluplným a prokazatelným způsobem. Do celkové strategie proto zahrnula regulatorní rámec pro bio-rozložitelné a bio-based plasty a aplikace z nich [6].

2.1.2 Legislativa na národní úrovni

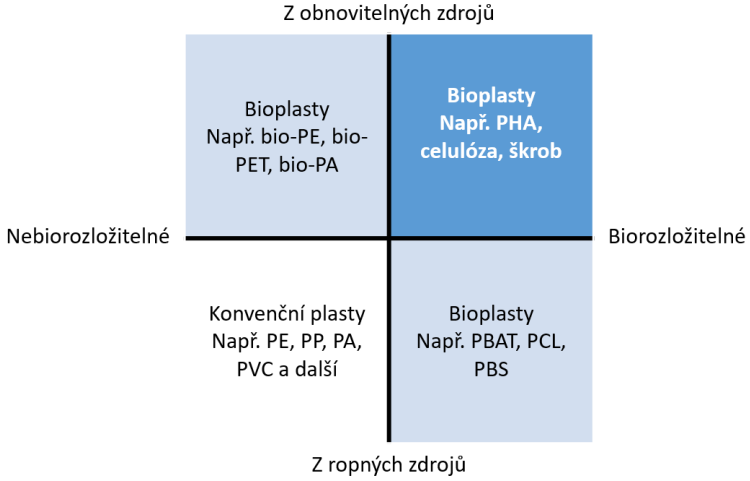
Na národní úrovni ČR byla na konci r. 2021 představena komplexní strategie pod názvem Cirkulární Česko 2040. Strategie Cirkulární Česko 2040 reflektuje nezbytnost prosazení principů oběhového hospodářství v ČR a řadí CE mezi její priority. Klade si za cíl udržet hodnotu výrobků, materiálů a zdrojů v ekonomickém cyklu tak dlouho, jak je to jen možné, a vrátit je do výrobního cyklu na konci jejich používání, přičemž se minimalizuje tvorba odpadu. Důraze je kladen na recyklaci (podporou recyklačních technologií) a na opětovné použití, zlepšením zejména v oblasti bioodpadu, textilního, stavebního a potravinového odpadu, obalů a dosloužilé elektroniky [7].

Pro průmysl, stavebnictví a energetiku je prioritou využívat druhotné suroviny. Stát ve veřejných zakázkách podpoří ty podniky, které používají výrobky s obsahem druhotných surovin a recyklátů. V oblasti produktu a designu by firmy měly zavádět v maximální možné míře nové výrobní metody využívající nejmodernější technologie k dosažení cirkulárních produktů jako např. využívání druhotných recyklovaných materiálů a předcházení vzniku odpadu při výrobě. V oblasti bioekonomiky a potravin půjde o snížení množství potravinových obalů a zefektivnění práce s bioodpadem, např. kompostováním biologicky rozložitelných odpadů nebo jejich materiálové využití. V oblasti spotřeby by měly být výrobky opětovně využívány a dostávat tak „druhý“ život. Omezit by se mělo využívání jednorázových výrobků. Největší změna je očekávaná v oblasti chování výrobců a zákazníků, tak aby byly více využívány v minulosti použité materiály či výrobky a zákazník informovaně volil, jak s nimi naloží až dosslouží.

Věda a výzkum bude finančně motivována prostřednictvím projektů zabývající se CE např. zřízením specializovaného inovačního fondu pro oběhové hospodářství, nebo zavedení inovačních voucherů pro technologie zaměřené na oběhové hospodářství. Vzdělávání v oblasti cirkulární ekonomiky poběží na všech úrovních, od těch nejnižších stupňů. [8] Využití polymerních materiálů z obnovitelných zdrojů, použití biologicky rozložitelných plastů ve smysluplných aplikacích a jejich výroba z odpadních surovin je jedním z mnoha směrů naplnění této strategie.

2.2 Bioplasty

Zájem o bioplasty v posledních letech rostl společně s uvědoměním, že nerostné suroviny nejsou nevyčerpatelné a s vizí, že je možné využít uhlík z atmosféry skrze fotosyntézy u rostlin. Nicméně předpona „bio-“ nezaručuje bezpodmínečnou udržitelnost daného materiálu. Podle stále platné definice se jedná o skupiny polymerů, které mají původ v přírodních materiálech (bio-based) NEBO jsou biodegradabilní (případně nesou obě dvě tyto vlastnosti), jak je vidět na Obr. 1. Bioplasty jsou tedy širokou skupinou materiálů a mohou být vyrobeny z různých zdrojů – kukuřice, cukrová třtina, bavlna, dřevo, houby, řasy. Některé jsou biodegradabilní jako např. polyhydroxyalkanoáty (PHA). Mezi bioplasty ale patří také bio-polypropylen a bio-PET vyrobené z rostlinných materiálů, ale shodující se chemickým složením s klasickými plasty, tedy nerozložitelné.



Obr. 1: Matice plastů podle surovinového zdroje a rozložitelnosti. Zpracováno dle [9]

Současná věda má k dispozici poznatky z téměř 200 let vývoje a využití bioplastů, jelikož první komerčně využívané plasty byly v podstatě bioplasty a začaly být využívány v průmyslovém měřítku již v polovině devatenáctého století (linoleum, ebonit, gutaperča, latex, viskóza, apod.) [10].

Kombinací fenolů a formaldehydu byl v r. 1907 vytvořen bakelit, první z řady syntetických plastů, které postupně vytlačily díky lepším materiálovým vlastnostem a nízké ceně původní bioplasty. Druhá světová válka urychlila rozvoj petrochemického průmyslu a orientaci na plasty vyrobené z ropy. Ve válečných letech byla ještě více akcentována nevýhoda bioplastů, které konkurovaly výrobě potravin.

V roce 2020 bylo celosvětově vyrobeno téměř 370 milionů tun plastů, jejich výroba vyžaduje asi 4 % fosilních zdrojů ročně. Společnost bojuje s neblahými následky znečištění životního prostředí plasty a jejich výrobou, a dle některých vědeckých týmů jsou bioplasty jednou z možností, jak tuto zátěž alespoň nějak snížit. Pozornost je soustředěna zejména na materiály vyrobitelné z odpadů a hlavním kritériem pro jejich výrobu a uplatnění na trhu je udržitelnost a environmentální stopa [11].

2.2.1 Nová generace základních typů bioplastů

Nové typy biopolymerů pro bioplasty, které se začaly vyrábět relativně nedávno v průmyslovém měřítku, jsou většinou vyrobeny z celulózy, škrobu nebo rostlinného cukru. V současnosti jsou nejvíce využívány [12]:

- Acetát celulózy (CA) - vyrábí se z bavlny, dřeva nebo jiných rostlinných materiálů a má dobré izolační vlastnosti. Používá se především pro výrobu filtrů a textilních vláken [13].
- Polylaktid (PLA) - objeven ve dvacátých letech minulého století. V r. 1989 Patrick R. Gruber zjistil, jak vyrábět PLA z kukuřice. To umožnilo firmě Novamont vývoj bioplastů pod komerční značkou MATER-BI. V r. 1997 přišla s výrobou PLA z kukuřice také firma Cargill and Dow Chemicals, a od r. 2005 tato firma funguje pod značkou NatureWorks a je jedním z hlavních výrobců PLA [14].
- Polyhydroxyalkanoáty (PHA) - tato skupina zahrnuje celou řadu polymerů, které se vyrábějí pomocí mikroorganismů, v nichž polymer vzniká jako zásobní látka. PHA biopolymery jsou biologicky odbouratelné a mají široké možnosti využití - od obalů po medicínské implantáty [15].
- Polybutylensukcinát (PBS) – může být produkován jak polymerací monomerů z petrochemických procesů tak i získaných cestou bakteriální fermentace. Vyrábí BioAmber Inc. od r. 2010 a Novamont S.p.A od r. 2016 [16].
- Termoplastický škrob (TPS) - vyrábí se z kukuřičného nebo bramborového škrobu a plastifikátoru (zejména glycerolu). Má dobré vlastnosti pro výrobu tenkostěnných obalů a tašek [17].
- Polykaprolakton (PCL) je biodegradabilní polyester (PCL) - má nízkou teplotu tání a používá se především pro výrobu medicínských implantátů, nosičů léčiv, tkáňovém inženýrství, ale také v oblasti 3D tisku výroby prototypů a jejich forem apod. [18].
- Biodegradabilní polyamid (PA) - vyrábí se z obnovitelných zdrojů, jako jsou rostlinné oleje a používá se převážně pro výrobu textilních vláken a obalů (například PA11 Rislan®) [19], [20].

Z historie bioplastů lze snadno vyvodit, že předpona bio- nezajišťuje ekologický produkt. Udržitelný bioplast by měl v rámci svého životního cyklu splňovat tyto požadavky:

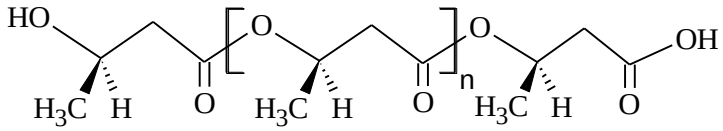
- Vstupní surovina by neměla pocházet z masivní těžby nerostných zdrojů nebo být příčinou deforestace pra/lesů. Neměla by využívat zdrojů konkurenčních s výrobou potravin a krmiv.
- Produkce bioplastů probíhá na bázi Green Chemistry, tzn. nepoužívá nebezpečných chemických látek, která jsou zdravotním rizikem pro pracovníky a zároveň rizikem kontaminace životního prostředí zejména v místě zpracování.
- Kvalita materiálu a design řešení musí přinášet řešení pro výrobky s vícenásobným použitím, protože nízká životnost produktu zvyšuje jeho environmentální stopu.
- Je nutné navrhnout a zajistit vhodný konec života výrobků (tzv. End of Life) [21]. Preferovaným a cirkulárním řešením před likvidací v kompostárně je materiálová recyklace. V případě biodegradabilních bioplastů, které je nutno likvidovat biologicky, je nutné zajistit podmínky a infrastrukturu pro ideální degradaci, a to v souladu s platnou legislativou.

Současný výzkum a vývoj se zaměřuje především na materiály z nepotravinových, obnovitelných nebo lépe odpadních zdrojů [22], jako je odpadní škrob a cukr, proteiny, odpadní celulózy, ligno-celulózy, houby a řasy [11]. Příkladem je biotechnologie výroby PHA na principu CE, která může za určitých okolností na trh přinést právě takový biomateriál s velmi širokým využitím a s důkazy o jeho environmentální stopě v podobě LCA [23].

3 POLY-3-HYDROXYBUTYRÁT

Za polyhydroxyalkanoáty (PHA) je označována široká skupina biopolymerů - bakteriálních polyesterů. Jde jak o homopolymery, tak o statistické kopolymery 3-hydroxybutanové kyseliny (3HB), 4-hydroxybutanové kyseliny (4HB), 3-hydroxyhexanové (3HHx), 3-hydroxyvalerátu (3HV), 3-hydroxyoktanoátu (3HO) a mnoha dalších monomerů [24]. V posledních letech značně vzrostl počet typů PHA biotechnologicky produkovaných jak přirozenými kmeny, tak geneticky upravenými organismy, jako např. kopolymery P(3HB-co-4HB-co3HHx) [25] , P(3HB/4HB/3HV/3HHx) [26], či acetoxyderiváty [27].

Tato práce je zaměřena primárně na poly[(R)-3-hydroxybutyrát] (PHB), lineární alifatický termoplastický polyester složený z *R* jednotek kyseliny 3-hydroxybutanové (Obr. 2). Tento polymer je známý od r. 1926, kdy jej objevil francouzský vědec Maurice Lemoigne při práci s bakteriemi rodu *Bacillus*. V buňkách existuje v amorfním stavu ve formě hydrofobních polymerních granulí (obvykle o velikosti 0,2–0,5 µm) [28]. Zde plní úlohu zásobního uhlíku a energie. Některé publikace potvrzují, že přítomnost PHA granulí v prokaryotických buňkách zvyšuje odolnost vůči stresovým faktorům, jako je vysoká nebo nízká teplota, mrazení, oxidační a osmotický tlak [29].



Obr. 2: Chemická struktura PHB

Lemoignův objev měl dlouhou cestu na trh. V r. 1983 byla založena firma Malborough Biopolymers, která nabídla PHB pod obchodním názvem Biopol [30]. V současnosti jsou největší výrobní kapacity budovány v Číně a USA, Evropa zaostává. TianAn Biologic Materials Co. Ltd. je čínský výrobce zaměřený na výrobu poly (3-hydroxybutyrát-co-3-hydroxyvalerátu) (PHBV) [31], CJ BIO zahájila výrobu P3,4HB v závodě v Pasuruanu v Indonésii [32], Danimer Scientific, se sídlem v Bainbridge (USA) vlastní patent na výrobu Nodax™ mcl-PHA [33]. Italská firma Bio-on produkující materiál MINERV-PHA™ je v současnosti v úpadku [34], avšak díky MAIP Group má novou šanci [35].

3.1 Vlastnosti PHB

Z pohledu Strategie udržitelnosti chemických látek EU má PHB tyto klíčové vlastnosti: biodegradabilita, biokompatibilita a netoxičnost. Právě ty umožňují náhradu řady látek v aplikacích, ve kterých jsou postupně zakazovány nebo omezovány – např. konvenční polymery ve formě primárních mikroplastů v kosmetice, ve formě povlaků hnojiv, jednorázových obalů ovoce a zeleniny apod.

Bakterie jsou schopné PHB produkovat s molekulovou hmotností v rozmezí od 200–3 000 kDa s polydisperzitou 2–3, v závislosti na mikroorganismu a podmínkách biotechnologického procesu [36]. Procesem extrakce se však zpravidla distribuce molekulových hmotností posunuje směrem k nižším hmotnostem. PHB je díky svojí optické čistotě vysoce krystalický, dosahuje krystalinity 55–80 %. Jeho teplota tání se pohybuje v rozmezí 170–180 °C a teplota skelného přechodu leží v intervalu 0–5 °C. Maximální rychlost krystalizace z taveniny leží v teplotním rozmezí 50–60 °C [37], [38]. Mechanické vlastnosti, jako je Youngův modul pružnosti a pevnost v tahu, se blíží vlastnostem polypropylenu (PP), deformace při porušení je však výrazně nižší než u PP. Křehkost je jednou z hlavních nevýhod PHB. Důvodem je nízká hustota nukleace a pomalá rychlost krystalizace, která

vede k tvorbě velkých sférolitů s mezitrhlinami. Další křehnutí je způsobeno sekundární krystalizací, ke které dochází během skladování při teplotě nad T_g [39]. Dalším omezením použití PHB je tepelná degradace, ke které dochází už mírně nad teplotou tání. Degradace vede ke snížení molekulové hmotnosti v důsledku štěpení řetězce podle mechanismu eliminace α-vodíku [40], [41], [42].

3.2 Biosyntéza PHB

Biosyntéza PHB v živých organismech spočívá v několika základních krocích: Prvním krokem je tvorba acetoacetyl-CoA ze dvou molekul acetyl-CoA, která je katalyzována enzymem β-ketothiolázou. Poté se acetoacetyl-CoA transformuje na (R)-3-hydroxybutyryl-CoA acetoacetyl-CoA. Třetím a posledním krokem je polymerační reakce katalyzovaná PHB syntázou vedoucí k tvorbě PHB [43].

Biotechnologická produkce PHB, respektive obecně PHA, umožňuje využívat velmi širokou základnu surovin - od levných odpadních látek, odpadních vod, řepné nebo třtinové melasy, až po rostlinné oleje a jejich mastné kyseliny, alkany a jednoduché uhlohydráty. Právě zde vznikl jeden ze strategických výzkumných záměrů Centra materiálového výzkumu FCH VUT. Myšlenka využít odpadní kuchyňský olej jako zdroj uhlíku pro biotechnologickou produkci PHB vzešla z týmu prof. Márové a prof. Obruči. Vzniklý laboratorní koncept technologie byl patentován (**V1**). Výstupní materiál byl zde charakterizován metodami termické analýzy, předmětem zájmu byla v tomto případě zejména termická stabilita stanovována nejprve na TGA, následně cyklickým měřením na DSC, kde byl vyhodnocován posun teploty tání a krystalizace. V r. 2013 již probíhaly ve výše zmíněném týmu výzkumné práce zaměřené na využití dalších typů odpadních materiálů. Protože bylo v té době záměrem využít PHA materiály i pro výrobu plastů, vznikla pod autorovým vedením Laboratoř bioplastů Centra materiálového výzkumu FCH VUT, která dále prováděla podporu materiálové charakterizace týmu biotechnologů a začala pracovat na vývoji aplikací z tohoto materiálu. Vznikla tak společná publikace **Pub 1** věnující se možnosti výroby PHA z hydrolyzovaného kávového odpadu.

3.3 Extrakce PHA z mikrobiální biomasy

K biotechnologickému kroku výroby PHA (často nazývaný up-stream) neodmyslitelně patří i následný proces extrakce (down-stream). Řízená biosyntéza v prvním procesu určuje chemickou strukturu PHA a to se všemi možnostmi, které kombinace zvoleného organismu, případně jeho genetické úpravy a chemické struktury zdroje uhlíku jako prekurzoru biochemické syntézy, nabízí. Lze také do jisté míry řídit finální distribuci molekulové hmotnosti v organismech, zejména zastavením biotechnologického procesu ve vhodný okamžik tak, aby syntetizující mikroorganismy nezačaly vzniklé PHA opět spotřebovávat. Klíčovým parametrem hodnotící úspěch tohoto kroku je však finální PHA výtěžek v procesu, tedy obsah PHA v bakteriální biomase.

Izolační proces má za úkol získat vzniklý polymer z biomasy v co nejvyšší čistotě a ideálně bez většího porušení molekulární struktury. Existují dva základní přístupy [44]:

- Rozpouštědlová extrakce za použití vhodných organických rozpouštědel
- Digesční metody narušující buněčnou membránu, ať už chemicky, enzymaticky nebo fyzikálně

Studované metody izolace PHA jsou v různém stupni TRL (Technology Readiness Level, Úroveň technologické připravenosti) [45]. Metody využívající organická rozpouštědla jsou z pohledu zachování distribuce molekulární hmotnosti a dosažené čistoty výhodnější [46]. V případě PHB je však skupina vhodných rozpouštědel poměrně malá, obsahující zejména halogenovaná rozpouštědla.

V laboratorních procesech izolace pro výzkumné účely se nejčastěji využívá referenční extrakce v chloroformu. Z pohledu legislativy je však ve velkém průmyslovém měřítku v podstatě nemožné v budoucnu takový proces extrakce využívat. Je proto zvýšený zájem o druhou skupinu izolačních metod, kde je fyzikálně chemickým způsobem rozložena buněčná stěna organismů tak, aby bylo možné nativní částice PHA od zbytků buněčných stěn následně odseparovat [47], [48]. Časté je využití NaOH [49], jeho kombinace s chlorovanými sloučeninami jako chlornan sodný [50], využití amoniaku [51], nebo surfaktantů.

Dle autorů lze využít synergii NaOH se surfaktantem Lysol (alkylbenzene sulfonate) při izolaci poly(3-hydroxybutyrátu-*co*-4-hydroxybutyrátu) (P3,4HB). Autoři dosáhli čistoty nad 93 % a výtěžku 94 % a to bez dramatického poklesu molekulové hmotnosti oproti referenční izolaci chloroformem a uvádějí, že lze tuto extrakční metodu použít pro výrobu vysoce čistého PHA pro biomedicínské aplikace [52]. Ze získaných zkušeností Laboratoře bioplastů se zpracováním PHB blendů však vyplývá, že čistota pod 97% je již velmi nevhodná pro termální zpracování. Množství zbylé biomasy způsobuje akceleraci termické degradace, což bylo viditelné na TGA i cyklických záznamech DSC. Navíc docházelo ke shlukování biomasy v polymerní tavenině a tvoření defektů způsobujících často nemožnost zpracování například do podoby rozfukované fólie nebo vláken.

Všechny izolační metody jsou optimalizovány na tři parametry – výtěžek, čistota a výsledná střední molekulová hmotnost polymeru. Je zřejmé, že zlepšením dvou libovolných parametrů je zpravidla zhoršen ten třetí a je proto třeba najít optimum pro konkrétní aplikaci. Všechny izolační metody produkují pochopitelně odpad, který je třeba v průmyslovém procesu likvidovat. Koncentrace surfaktantů, solí a organických látek včetně zbytků buněčných stěn (biomasy) je často kritickým parametrem při up-scale zkoumané technologie izolace PHA.

Protože byl tým Laboratoře bioplastů závislý na kvalitě PHB, bylo rozšířeno portfolio řešených témat i o tuto problematiku. V rámci úspěšně obhájené disertační práce Ing. Anety Pospíšilové, Ph.D. bylo jedním z cílů využít digesční metodu izolace PHB za použití mýdla. Toto mýdlo bylo připraveno zmýdelněním odpadního kuchyňského oleje, který se využívá právě jako zdroj uhlíku pro fermentační proces. V procesu výroby PHB z kuchyňského oleje byla tedy část vstupního materiálu odkloněna a využita na výrobu surfaktantu pro izolaci PHB. Po jeho využití v procesu izolace bylo mýdlo spolu s neoddělitelnými zbytky buněčných stěn vysráženo, převedeno zpět do formy mastných kyselin a využito jako zdroj uhlíku pro další fermentační proces. Tato unikátní metoda byla publikována v **Pub 2**. Optimalizací procesu izolace z pohledu koncentrace mýdla a využití proteázy bylo dosaženo při poměru hmotnosti mýdla na suchou buněčnou biomasu o hodnotě 0,125 čistoty vyšší než 95 %.

Tato metoda pak byla srovnávána s vyvíjenou a optimalizovanou alkalickou a kyselou digescí a chloroformovou extrakcí. Cílem bylo nalézt podmínky pro dosažení polymeru s dostatečnou čistotou pro kosmetické aplikace nebo dostatečnou molekulovou hmotností a čistotou pro zpracování do podoby plastu například pro 3D tisk. Vzorky PHB získané za působení alkalických činidel měly extrémně nízkou tepelnou stabilitu a teploty tání se během experimentů DSC významně snížily. GPC vzorků po izotermické degradaci potvrdilo výrazný pokles molekulové hmotnosti. Pro eliminaci hydrolýzy PHB v zásaditém prostředí byl testován přídavný krok kyselého promytí extrahovaného PHB a přídavek anhydridu kyseliny jantarové při jeho zpracování v tavenině. Molekulová hmotnost se tak snížila mnohem méně než bez této stabilizace a PHB bylo možné zpracovat v typické referenční receptuře pro výrobu struny pro 3D tisk. Výsledky byly publikovány v **Pub 3**.

4 TERMOPLASTY NA BÁZI PHB PRO 3D TISK

3D tiskem je zde v textu míněna metoda aditivní výroby třídimenzionálních předmětů. Přestože nejde formálně o tisk, termín je takto používán mezi odbornou i laickou veřejností. FDM (Fused Deposition Modeling) a FFF (Fused Filament Fabrication) pak značí tisk z polymerní taveniny, zpravidla vzniklé roztavením kalibrované tiskové struny v tiskovém extruderu.

Za datum vzniku techniky FDM je považován rok 1989 díky S. Scott Crumpovi. Pojmy 3D tisk a 3D tiskárna se však i díky dalším aditivním technologiím začaly objevovat až v druhé polovině 90. let. Roku 2004 Adrian Bowyer založil projekt RepRap (Replicating Rapid Prototyper), který zpřístupnil možnost 3D tisku běžné veřejnosti. V lednu r. 2009 byla dostupná první 3D tiskárna BfBRapMan 3D ke komerčnímu prodeji ve formě kitu. Poté v dubnu byla uvedena na trh další tiskárna společnosti MakerBot, která také stojí za online knihovnou 3D modelů Thingiverse. Firmu MakerBot koupila roku 2013 za zhruba 400 milionů dolarů společnost s názvem Stratasys [53].

Od r. 2009 dochází k prudkému rozvoji FDM 3D tisku. Ve stejném r. zahájil svoji činnost Josef Průša, který následně svými tiskárnami pro širokou veřejnost dokázal vybudovat úspěšný byznys. 3D tisk plastových výrobků v dnešní době využívají firmy nejen ve výzkumu a vývoji, při prototypování, ale také úspěšně ve výrobních procesech [54].

4.1 Motivace

S prudkým rozvojem FDM 3D tisku logicky nastal také rozvoj v oblasti materiálů pro tuto technologii. A zde vznikla příležitost hledat nová řešení pro nově vznikající segment trhu. Poptávka od spotřebitelů z průmyslové sféry i od domácích uživatelů je diametrálně jiná. Zatím co průmysl si žádal řešení s mechanickou a teplotní a chemickou odolností, domácí uživatel vyhledával často materiál s pěkným designem, snadnou tisknutelností, přírodního původu nebo materiál „se zajímavým příběhem“. V poslední době uživatele upřednostňují materiály, které při tisku neuvolňují nepříjemné emise a zajímají se o ekologické aspekty spojené s použitím tiskového materiálu. PHB vyráběné zamýšlenou a optimalizovanou technologií Hydal z odpadního kuchyňského oleje má díky využití odpadu nízkou uhlíkovou stopu a tím i svůj pozitivní příběh pro spotřebitele. Oproti ABS nezapáchá styrenem a oproti PLA nabízí díky své krystalinitě vyšší teplotní stabilitu. V neposlední řadě bylo jasné, že zvládnutí technologie 3D tisku na bázi PHA otevře dveře do velmi zajímavých a atraktivních aplikací v medicíně [55]. Společně s nadšením pro automatizaci, robotizaci, nové technologie byla vize zvládnout celý proces vývoje od surového materiálu PHB po zdařilý výtisk obrovskou výzvou.

Tomu všemu však musela zákonitě předcházet snaha zvládnout proces zpracování PHB z technologie Hydal, jeho charakterizace za účelem vstupní kontroly, aditivace z důvodu procesní stabilizace, modifikace a řízení mechanických vlastností přídavkem změkčovadel, vytváření vhodných kompozitních materiálů a sledování biodegradability a možností recyklace. Podstatné výsledky z těchto prací jsou se stručným komentářem zahrnuty do následující kapitoly.

4.2 Metody a úskalí zpracování PHB

V době vzniku záměru týmu Laboratoře bioplastů (2013) vyvinout plastový materiál na bázi PHB pocházejícího z technologie Hydal (se svými specifiky) bylo k dispozici jen několik málo publikací

s informacemi o reálném chování PHB v procesech průmyslové kompaundace. Bylo to zřejmě dáno i nedostupností dostatečného množství kvalitního PHB použitelného pro zpracování v tavenině. Většina publikací se tak z počátku opírala zejména o studium chování PHB a jeho kopolymerů připraveného do podoby fólie z roztoku chloroformu nebo lisováním materiálu ve vyhřívaných lisech.

Vlastnosti PHB a jeho kopolymerů byly zkoumány už v 70. letech 20. století. Například v publikaci z r. 1963 byla popisována molekulová hmotnost a intristická viskozita, stereoregularita i struktura krystalů PHB [56]. V r. 1971 vyšla publikace srovnávající bakteriální PHB se synteticky připraveným PHB z beta-butyrolaktonu [57] a v r. 1984 trojice publikací popisující mechanismus termální degradace PHB jak z pohledu produktů reakce [40], dopadu na molekulovou hmotnost [41] a reakčního mechanismu [42]. V publikaci [58] z r. 1994 jsou sledovány mechanické vlastnosti PHB a PHBV v závislosti na jeho tepelném zatížení (180 a 190 °C, 0–10 min) a dávané do souvislosti s měřenou molekulovou hmotností. V komunitě vědců zabývajících se tímto materiálem bylo v tu dobu zřejmé, že PHB i PHBV jsou proti konvenčním plastům velmi citlivé na parametry zpracování.

4.2.1 Krystalizace

Čisté PHB má velmi nízkou nukleační hustotu [59]. To má za následek tvorbu velkých krystalových struktur, na jejichž převážné části se tvoří mikrotrhliny, což zhoršuje mechanickou odezvu PHB [60]. Použití nukleačních činidel podporuje tvorbu menších sférolitů a konzistentnějších krystalických struktur, aby se zabránilo poruchám a jevu rekrystalizace v PHB a zajistilo se konzistentní mechanické chování PHB v čase. Z efektivně fungujících nukleantů pro PHB je znám nitrid boru [60], sacharin [59], TiO_2 [61], orotová kyselina a mastek [62]. Mastek je díky svým OH skupinám schopen v tavenině polyesteru transesterifikační reakce. Vznikne tak produkt, který působí jako nukleant [63]. Testován byl i nukleační účinek záměrně přidávaného nízkomolekulárního PHB, dle autorů vzrostla rázová houževnatost, nicméně ani v těchto materiálech se nepodařilo dosáhnout vyšší tažnosti než 8 % [64].

Jak bylo zmíněno výše, skelný přechod PHB je kolem 0 °C, proto při laboratorní teplotě mají amorfní řetězce PHB dostatečnou pohyblivost, aby pokračovaly v krystalizaci, což má neblahý vliv na mechanické vlastnosti. Bylo zjištěno, že žíhání při teplotách 120 °C nebo vyšších vede ke zlepšení jak kritického faktoru intenzity napětí, tak rychlosti uvolňování deformační energie lomové houževnatosti, která je do značné míry zachována při opětovném stárnutí [65]. Navazující práce zjistily a potvrdily, že PHB podléhá krystalizaci fyzikálním stárnutím, což způsobí zkřehnutí materiálu a omezí jeho možnosti použití, a že žíhání ovlivňuje chování PHB při lomu [66] [67] [68]. Zatím co při fyzikálním stárnutí dochází k dokonalé krystalizaci, která neposkytuje dost volného prostoru molekulám podléhat plastické deformaci, v případě vyžíhání a zchlazení vzniká nedokonalá krystalická struktura, která plastickou deformaci molekul na rozhraní umožní. Autoři také upozorňují na fakt, že teplota tání této krystalické fáze se nachází již v rozmezí od 80 do 165 °C [69] [70]. Využitím v té době poměrně nové metody modulovaného DSC bylo zjištěno, že sekundární krystalizace dále znamená také vitrifikaci části amorfních řetězců spojených s krystaly za vzniku tuhé amorfní frakce (RAF). Diskutován je také vliv RAF na krystalizaci PHB, protože jeho vitrifikace během krystalizace může bránit nebo dokonce zastavit další růst krystalů [71] [72]. Difúzní aktivační energie obou procesů krystalizace (v tavenině a ve skelném stavu) jsou srovnatelné, s tím rozdílem, že krystalizace z taveniny je difúzně řízená a probíhá 1D růstem sférolitů za konstantní nukleační rychlosti se systematičtěji orientovanou strukturou než v případě 2D krystalizací sférolitů za skelného stavu. [73]

4.2.2 Distribuce molekulové hmotnosti

Mechanické vlastnosti polymerního materiálu jsou pochopitelně závislé na jeho distribuci molekulové hmotnosti. Ne vždy autoři udávají molekulovou hmotnost (M_w) PHA před a po jeho zpracování. Jiné práce se vztahu procesních podmínek a změny M_w přímo věnují. Poznatky ze skutečného zpracování PHBV do podoby rozfukované fólie jsou diskutovány například v publikaci [74]. Výsledné fólie mají poměrně vysokou pevnost, ale nízkou tažnost (2-6 %), která je závislá na molekulové hmotnosti polymeru. Ta klesá jak s rostoucí teplotou zpracování, tak s rychlostí otáček šneku.

V publikaci [75] byly údaje o molární hmotnosti získané pomocí SEC před zpracováním použity k odhadu snížení molární hmotnosti v důsledku tepelné degradace polymeru a porovnány s experimentálními hodnotami získanými z PHB po extruzi a po extruzi s následným vstřikováním. Výsledky ukázaly, že redukce polymerního řetězce po zpracování byla vyšší, než se očekávalo, což naznačuje, že tepelná degradace nebyla hlavní příčinou poklesu M_w. V podmínkách studovaných v této práci se střih polymerního řetězce existující v procesech vytlačování a/nebo vstřikování jevil jako důležitý faktor, který je třeba vzít v úvahu při řešení velkých/průmyslových aplikací PHB.

4.2.3 Procesní stabilizace

Logickým důsledkem tohoto poznání je snaha výzkumných týmů potlačit nebo kompenzovat pokles M_w při termickém zpracování v tavenině. Vzhledem ke známému mechanismu tepelně indukovaného střihu řetězce PHB je zřejmé, že potlačení tohoto jevu lze realizovat pouze snížením procesní teploty a doby pobytu polymeru v těchto podmínkách. Z tohoto pohledu je výhodnější využít kopolymery PHA, které mají nižší teplotu tání a tím širší zpracovatelské okno. Jak bylo zmíněno výše, jednou z cest je i snížení interakcí molekul pomocí lubrikantu a tím snížení smykového namáhání v tavenině. I přes to, že nebyla prokázána role oxidačních reakcí při degradaci PHB, se v některých nových pracích stále objevuje přídavek konvenčních fenolických antioxidačních stabilizátorů [76], [77], [78] a [79].

Prokazatelný stabilizační účinek na M_w a vývoj elastického modulu pružnosti PHB po kompaundaci a vstřikování byl pozorován u přídavku výtažku z vinných pokrutin [80]. 15% přídavek zároveň snížil T_g a pevnost v tahu a zvýšil tažnost PHB, takže se aditivum zachovalo i jako plastifikátor [81]. Podobně byla testována kyselina třís lová, u které nebyl vliv na M_w prokázán [82].

Dalším způsobem změny degradačního chování polymeru je možné dosáhnout změnou chemické struktury. V publikaci [83] autoři provedli maleaci PHB v pěti stupních roubování 0,21 – 1,18 %. Teplota 5% hmotnostního úbytku se dle TGA sice posunula k vyšším hodnotám, ale maleace byla také provázena dramatickým poklesem M_w (až na desetinu pův. hodnoty u nejvyššího stupně maleace).

4.2.4 Plastifikace změkčovadly

Snaha zlepšit křehké chování PHB vedla také spoustu týmů k jeho změkčování pomocí plastifikátorů. Výběr změkčovadla zahrnuje několik důležitých kritérií. Je to například vysoký stupeň kompatibility s polymerní matricí, který je odpovědný za jeho snadnou rozpustnost a jeho schopnost fungovat jak v krystalických, tak v amorfních oblastech. Plastifikátory snižují T_g a modul pružnosti a zvyšují tažnost. Důležitá je molekulová hmotnost a chemická strukturu změkčovadla, včetně polarity, tvaru a velikosti molekuly. Zásadní je také nežádoucí migrace změkčovadla. Čím větší je molekula změkčovadla, tím nižší je jeho tlak par a tím větší je jeho stálost uvnitř polymeru. Velice rozsáhlá rešerše [84] prezentuje seznam 25 testovaných změkčovadel v PHB. Většina změkčovadel dosahuje nízkých hodnot tažnosti PHB pod 15 %. To je případ často používaného acetyltributylcitrátu (ATBC), který

dosáhl tažnosti pod 10 % a to i přesto, že je reportován posuv PHB T_g až na -30,7°C [84] [85] [86] [77]. Hranici tažnosti nad 15 % pak přesahuje dnes již velmi často používaný tributylcitrát a trietylcitrát [84]. Dle tažnosti vynikají svojí hodnotou nad 15 % také aditiva: decylester, 2-butyloctylester a hexylester kyseliny acetylsalicylové a etyl2-(3-benzoylfenyl)propanoát. Zde je nutno uvést, že materiály byly připraveny roztokově do podoby fólie a neprošly tedy zpracovatelským cyklem. Dle autorů testované deriváty s krátkým řetězcem se rychle vypařovaly a uvolňovaly ve vodném prostředí, zatímco sloučeniny s dlouhým řetězcem měly tendenci krystalizovat. V obou případech však PHB filmy během krátké doby zkřehly. Decylester kyseliny salicylové a 2-butyloktylester kyseliny salicylové byly tak autory považovány za změkčovadla vhodná pro PHB v lékařských aplikacích [87].

Publikace [88] zkoumá plastifikační účinek aditiv na bázi esterů kyseliny ferulové (esterifikováno butandiolem, pentandiolem a glycerolem). Přídavkem 30 % aditiv bylo možné dosáhnout tažnosti 250 %, ale v průběhu několika hodin docházelo ke křehnutí a snížení tažnosti na velmi malé hodnoty.

4.2.5 Mísení s dalšími polymery

Z informací výše vyplývá, že samotné PHB je klasickými postupy aditivace stabilizátory a plastifikátory jen velmi těžce zpracovatelné a výsledné mechanické vlastnosti nejsou akceptovatelné pro mnohé aplikace. Výzkumné týmy se tak velmi brzy začaly ubírat cestou vytváření směsí, a to i s výše popisovanými přísadami (např. plastifikátory, nukleačními činidly, lubrikanty, stabilizátory) na zpracovatelný termoplast s akceptovatelnými mechanickými vlastnostmi [89] [90]. PHB dodává často výslednému materiálu zajímavé vlastnosti, jako je jeho biorozložitelnost a biokompatibilita. K dispozici jsou kvalitně zpracované rozsáhlé rešerše [84], [89], [90] zahrnující přes 500 zdrojů.

Polymerní termoplastická aditiva využívaná ve směsích s PHB jsou dle původu uhlíku polymery z obnovitelných zdrojů a to buď syntetické (PLA, PBS [91], biopolymery (sem patří celá skupina PHA, termoplastický škrob), nebo polymery z fosilních zdrojů (PBAT [92], PVAc, PVA, PCL, PEG, PPG [93]. Popis aktuálního stavu z tohoto pohledu již překračuje možnosti této práce a budou zde uvedeny jen kombinace používané ve výzkumu publikovaném týmem Laboratoře bioplastů.

4.2.5.1 PHB/PVAC

Blendy s PVAc byly jedny z prvních úspěšných řešení nedostatků PHB [94]. Přestože mísením biopolymeru se syntetickým polymerem z fosilních zdrojů finální směs ztrácí jednu ze svých klíčových výhod (materiál z plně obnovitelných zdrojů), tato směs nabízela akceptovatelné mechanické vlastnosti pro řadu aplikací. PVAc je plně mísitelné s PHBV (12% HV), což dokazuje lineární závislost T_g na mísícím poměru [95]. Podobný trend byl pozorován u PHB. Analýza dle modelu Avrami ukázala, že přidání PVAc do PHB má za následek snížení celkové rychlosti krystalizace fáze PHB, ale neovlivňuje mechanismus nukleace PHB a geometrii růstu krystalů [96].

Citlivost PHB při zpracování se podařilo snížit přídavkem PVAc společně se změkčovadlem (např. ATBC), lubrikantem (glycerol monostearát) a nukleačním činidlem (sacharin). Z časové závislosti viskozity taveniny při zpracovatelské teplotě 185 °C je viditelná lepší stabilita blendu proti PHB [97].

4.2.5.2 PHB/PLA

Polylaktid (PLA) je biologicky odbouratelný termoplastický polymer patřící chemicky do skupiny polyesterů. Chirální atom uhlíku v monomerní jednotce kyseliny mléčné činí strukturu opticky aktivní. Proto existují dva stereoizomery mléčné kyseliny a výsledný polymer PLA je komerčně dostupný v mnoha typech lišících se poměrem L a D formy, který definuje jeho vlastnosti [98]: L-poly(kyselina

mléčná) (PLLA) a D-poly(kyselina mléčná) (PDLLA). PLLA je semikrystalický polymer s krystalinitou kolem 37 %, teplotou tání 170–180 °C a teplotou skelného přechodu v oblasti 60–67 °C, což přispívá ke křehkosti materiálu při teplotě okolí. PDLLA je amorfní polymer, který má teplotu skelného přechodu mezi 50–60 °C [37]. Stejně tak jsou na trhu typy lišící se distribucí M_w vhodné svým indexem toku pro vytlačování, vstřikování i vláknařské aplikace [89]. PLA má některé významné nedostatky, jako je nízká pevnost taveniny, pomalá rychlost krystalizace, špatná zpracovatelnost, vysoká křehkost, nízká houževnatost a nízká provozní teplota, které omezují jeho použití. Proto je i v jeho případě hledána možnost jeho mísení s dalšími polymery. [99]

V roztoku vysokomolekulární PLA obecně nemísitelné s vysokomolekulárním PHB, jak je vidět ze studia izotermické krystalizace, kdy při 150 a 155 °C dochází k separaci fází PHB a PLA [100]. Naproti tomu, nízkomolekulární PLA je mísitelné s vysokomolekulárním PHB a naopak [90]. V tavenině je pak za vhodných podmínek PLA s PHB mísitelné a směsi vykazují synergický efekt [101]. PLA je efektivně nukleováno PHB a přítomnost PLA stabilizuje PHB. Zejména, když je použito změkčovadlo funkční pro oba polymery, dosahují plasty na bázi těchto směsí vhodných mechanických vlastností [98].

Při smíchání v poměru 1:1 mění PLLA mechanismus krystalizace PHB a snižuje jeho teplotu krystalizace (T_c). V mísitelných směsích PHB a PLLA s nízkou M_w je při 110 °C zapotřebí 8 hodin k dokončení ko-krystalizace. V nemísitelných směsích vykazoval PLLA sníženou rychlost krystalizace způsobenou efektem zředění taveniny PHB, zatímco T_g zůstalo nezměněno [102]. Přidání PLLA k matrici PHB vede ke zvýšení T_g a T_c a poklesu T_m spolu s rozšířením píku tání, což lze vysvětlit rekrystalizací a/nebo ztluštěním lamel. Kromě toho se sníží krystalinita a počet velkých sférolitů a sníží se rychlost krystalizace PHB. V případě amorfní PDLLA sférolity PHB objemově vyplňují PDLLA inkorporovanou v intersferolitických oblastech [103].

Kompatibilita směsí PHB/PDLLA se dá zlepšit částečným zesíťováním za použití DCP. PHB tak díky zesítění vykazovalo zhoršení krystalizační schopnosti a směs vykazovala sníženou teplotu krystalizace a nižší krystalinitu, naopak došlo ke snížení teploty tání. Mechanické vlastnosti, zejména pevnost v tahu a ohybu a rázová houževnatost směsí, a také reologické vlastnosti taveniny se zlepšily [104].

4.2.5.3 PHB/PCL

PCL je biologicky odbouratelným semikrystalickým polymerem z rodiny syntetických alifatických polyesterů, který je v omezeném množství mísitelný s PHB, při vyšší koncentraci vytváří PCL domény.

V práci [105] byla vyvíjena nová biologicky odbouratelná změkčovadla na bázi kopolymeru P(3HB-co-PCL) pro zlepšení fyzikálně-chemických vlastností směsí PHB a PCL. Přidáním změkčovadel do směsí PHB/PCL se cca 4–6 zvýšila tažnost směsi PHB/PCL 50/50 ve srovnání s čistým PHB. Přídavek také snížil teplotu tání a krystalizace směsi, což umožnilo bezpečnější zpracování, přičemž nebyl pozorován žádný nepříznivý dopad na pevnost v tahu a modul pružnosti směsí.

PCL v kombinaci s PHB může zvýšit tuhost i elasticitu směsi, pokud je kompaundace provedena reaktivně za přítomnosti peroxidu [106]. Podobně je tomu u směsí PCL s PHBV, biopolymerem příbuzným PHB. Směs PHBV PCL připravená pomocí reakčního vstřikování s přídavkem dikumylperoxidu vykazuje vlastnosti lišící se od velmi pružných až po houževnaté materiály [107]. Reaktivní extruzí směsi PHBV/PCL v přítomnosti 1% síťovacího činidla 1,3,5-tri-2-propenyl-1,3,5-triazin-2,4,6(lH,3H,5H)-trion (TAIC) a peroxidu bylo dosaženo zvýšení tažnosti ze 6,7 % na 25 %. Zlepšená mezifázová kompatibilita také přispívá ke zlepšení houževnatosti směsi [108].

4.2.6 Kompozity na bázi PHB

Termoplastické kompozitní materiály představují pomyslný vrchol v konstrukci funkčních materiálů. Potkává se zde know-how z mnoha oblastí diskutovaných výše: zpracování termoplastických polymerů, řízení reologie při zpracování taveniny, problematika lubrikace, stabilizace, nukleace vhodnými aditivy a změkčování pomocí kompatibilních změkčovadel, případně reaktivní procesy modifikující celý materiálový systém. K tomu všemu však přibývá znalost vlastnosti výztuže, její kompatibilita z hlediska povrchové energie a funkčních skupin, kompatibilizace před zpracováním nebo v průběhu zpracování a zabezpečení dispergace plniva nebo výztuže ve finálním materiálu.

V případě termoplastické matrice na bázi PHA je logicky předmětem zájmu zachování biodegradability celého systému a využití přírodních obnovitelných zdrojů. Většinová část prací je tak zaměřena na obecně lignocelulózová plniva a rostlinné vlákenné výztuže. Z pochopitelných důvodů je zájem cílen hlavně na odpadní materiály, které snižují environmentální stopu vzniklého materiálu. Tuto problematiku shrnul autorský kolektiv v r. 2021 do přehledného 15 stránkového review s téměř 100 odkazy. V textu jsou uvedeny jednotlivé strategie při zpracování kompozitů [109].

Využití lignocelulózy jako plniva není v cílech ani prezentovaných výsledcích této práce, proto budou podrobněji komentovány jen zdroje zaměřující se přímo na 3D tiskové aplikace pomocí metody FDM v kapitole 4.6.7. Druhou obrovskou skupinu materiálů tvoří PHA kompozity na bázi anorganické výztuže. Díky biokompatibilitě PHA polymerů je pozornost ve výzkumu těchto kompozitů věnována jejich potenciálu využití v medicíně [110].

Širokou paletu kompozitních materiálů na bázi PLA/PHB a jejich vlastnosti shrnuje obsáhlé review [89]. Jsou zde představeny různé konstrukce materiálového složení blendů a kompozitů na bázi PLA/PHB a různých výztuží. Při bližším studiu dosažených hodnot materiálových vlastností uvedených v této publikaci se ukázalo, že jde bohužel v podstatě o neporovnatelné výsledky dosažené různými způsoby přípravy i charakterizačními technikami. A právě této oblasti částicových anorganických kompozitů pro FDM 3D tisk zamýšlených pro medicínské aplikace je věnována kapitola 5.

4.3 PHA materiály pro 3D tisk

Pro úplnost je také třeba poznamenat, že materiály na bázi PHA je možné tisknout i jinými technologiemi než FDM [111]. Tato práce však bude dále pojednávat pouze o FDM metodě tisku PHA materiálů, která byla využita ve výzkumu Laboratoře bioplastů. Materiály na bázi PHA mají díky svým vlastnostem potenciál zejména v medicíně [112] a právě tam je mířena velká část dnešních výzkumných prací [113]. Aktuální stav tohoto úzce specializovaného výzkumu je součástí kapitoly 5.2 zaměřené pouze na FDM 3D tisk PHA materiálů pro medicínu.

K dnešnímu dni existuje mnoho komerčně dostupných materiálů pro FDM 3D tisk od čistých termoplastů po kompozity, bioplasty a biokompozity z bioplastů. Do kompozitních tiskových materiálů jsou použity různé typy plniva a výztuže, typicky mikročástice, nanočástice, ale i některá krátká vlákna, aby se zlepšily vlastnosti výsledných vytištěných dílů [114].

První pokusy testovat PHB v 3D tisku metodou FDM byly nalezeny v publikaci z r. 2016 [115]. Experimenty zahrnuté v této práci ukazují, že pomocí extruderu EX2 Filabot lze polymer PHA vytlačit do konzistentního vlákna při 170 °C a rychlostí šneku 15 otáček za minutu. Vlákno bylo po průchodu vodní lázní navíjeno pomocí automatického navíjecího zařízení řízeného platformou na bázi Arduino. Jak sám autor uvádí, testy reálné tisknutelnosti však víceméně selhaly.

Lze předpokládat, že z informací o vlastnostech PHB uvedených výše bylo usouzeno, že čistý polymer PHB není vhodným materiálem pro 3D tisk. Výzkum se tak ubíral podobně jako v případě ostatních metod zpracování cestou mísení polymerů, vytváření kompozitů nebo využití kopolymerů PHA. To vše za použití vhodných změkčovadel případně reaktivních činidel. Plastický a houževnatý polymer PBS ve směsi PBS/PHB zlepšil tepelné zpracování a reologické vlastnosti [116]. Podobnou strategii zvolili v práci, kdy za účelem kompatibility špatně mísitelných PHB/PCL směsí byl použit dikumylperoxid (DCP) [117]. Výsledné materiály PHB/PCL-DCP vykazovaly mírné zvýšení prodloužení při přetržení a významné zlepšení rázové houževnatosti (7,2 $kJ \cdot m^{-2}$) ve srovnání s PHB. Dalšího snížení Youngova modulu a zlepšení rázové houževnatosti (15 $kJ \cdot m^{-2}$) bylo dosaženo začleněním nízkomolekulárního polyethylenglykolu jako změkčovadla. Tažnost však zůstala pod 10 %.

Podobný problém se špatnou mísitelností a tím i zpracovatelností do podoby tiskové struny byl řešen v případě PHBV/PLA kompatibilizací za pomocí styren-akrylátového kopolymeru s oxiranovými skupinami - známého aditiva (chain extenderu - CE) Joncryl ADR-4368. Reologická analýza prokázala zlepšení tisknutelnosti směsi PHBV:PLA:CE umožněním vyšší teploty tisku (220 °C) a dostatečné rychlosti tisku (45 $mm \cdot s^{-1}$). Práce ukázala, jak procesní parametry (teplota a rychlost tisku, tloušťka vrstvy a teplota tiskové podložky) mohou ovlivnit mechanické vlastnosti 3D výtisku. Optimalizované vzorky tisku vykazovaly vyšší modul pružnosti, pevnost i houževnatost. Tažnost nicméně opět nepřesáhla 10 %. Autoři došli k závěru, že dobrá tvorba vazby mezi jednotlivými vrstvami při tisku byla rozhodující pro zlepšení mechanických vlastností. [118].

Vliv parametrů tisku sleduje i následující publikace na materiálu PHBHx [119]. Zde je diskutována zejména problematika adheze první vrstvy k tiskové podložce a krystalizační smrštění, které má negativní efekt na warping a tím zhoršuje tisknutelnost.

Směs P3,4HB (10 mol% 4HB)/PLA byla zkoumána kolegy z FCH VUT. Reologické a mechanické vlastnosti kopolymeru byly modifikovány přidáním změkčovadel (acetyltributylcitrát) nebo smícháním s PLA. Použit je také CE Joncryl ADR4468 a fenolický antioxidant Irganox 1010. P3,4HB mírně potlačovalo tepelnou degradaci, ale nejlepší stabilizační účinek byl zjištěn v případě kopolymeru ve směsi s PLA. Dle těchto vlastností autoři konstatují, že měkčený P(3HB-co-4HB) je potenciálním kandidátem biodegradabilního polymeru pro procesy FDM [79].

V poslední době se těší zájmu přidávání přírodních plniv do biologicky odbouratelných polymerů kvůli zvýšené poptávce po biologicky odbouratelných kompozitních materiálech [120]. Výzkum se zaměřil na vývoj biokompozitního vlákna na bázi PHB/PLA, částicové výztuže 10, 20 a 30 % hydroxyapatitu (HA) a polypropylenglykolu (PPG) jako změkčovadla [121]. Přidání PPG zlepšilo zpracovatelnost během výroby filamentu a 3D tisku. Biokompozit s 10 % HA a 10 % PPG vykazoval vynikající 3D tisknutelnost. Zmíněný kompozit má vynikající mechanické vlastnosti - rázovou houževnatost 1,85 $kJ \cdot m^{-2}$, modul pružnosti v ohybu 3,2 GPa a napětí v ohybu při 2% deformaci 42,5 MPa. Autoři také uvádějí prodloužení při přetržení (6 %), které je vyšší než u komerčního PLA (4 %).

Přidání lignocelulózových vláken do polymerní matrice je jednou z cest, jak nahradit například skleněná vlákna v biokompozitech. Zajímavou prací je využití odpadního ligninu z borového dřeva jako vedlejšího produktu biorafinerie. Přídavek ligninu v PHB v množství 20 % w/w zlepšuje adhezi vrstvy během 3D tisku a zvyšuje kontaktní úhel vody. Navíc znatelně snižuje warping. Zkoušky 3D tisku byly provedeny pomocí tiskárny MakerGear™ V2 vybavené poměrně velkou tryskou 0,75 mm. Výška vrstvy byla nastavena na poměrně velkých 0,3 mm, rychlost tisku byla 1500 mm/min. Tryska

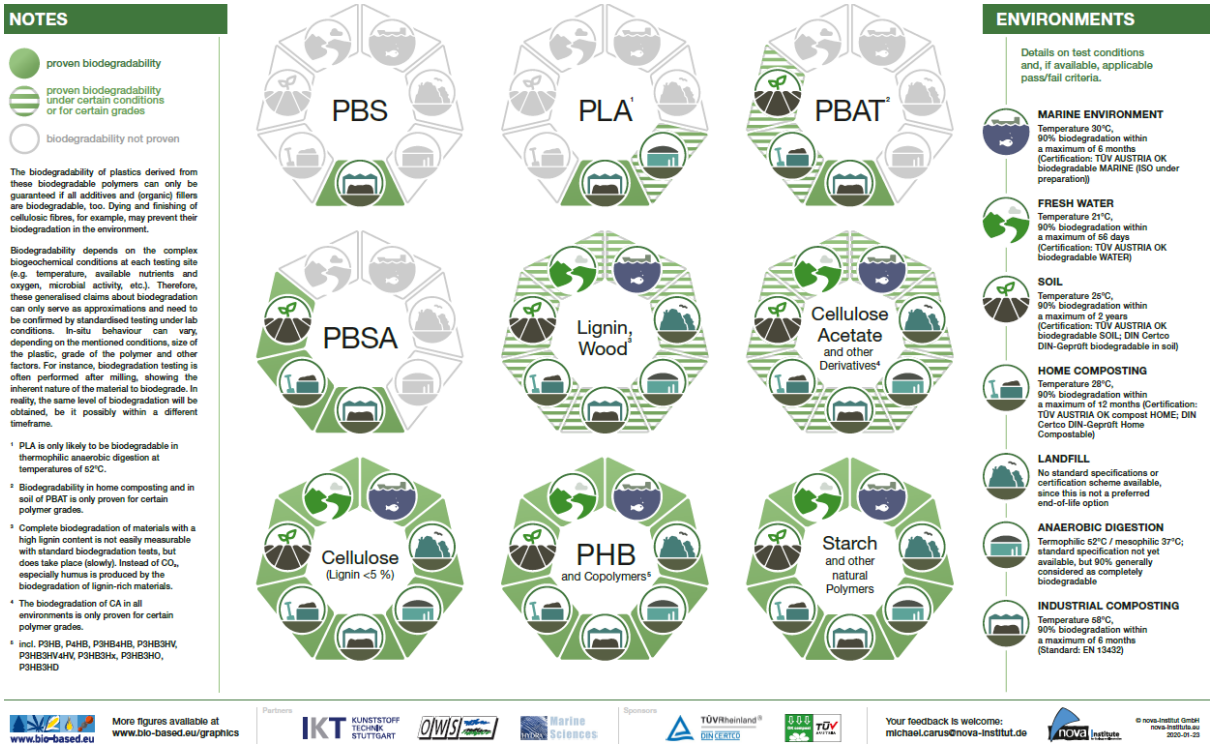
byla temperována na 190 °C a skleněná tisková podložka potažená PVA lepidlem byla vyhřívána na 40 °C [122]. Do PHA (blíže nespecifikováno, T_m 145 °C) byla také přidávána dřevní moučka (střední velikost částic 75 µm). Vzhledem k tomu, že nebyla přidávána žádná kompatibilizace ani plastifikace, výsledný materiál se choval křehce [123]. Jednou z možností je použití buničinových vláken z celulózového a papírenského průmyslu [124]. V této práci byly připraveny biokompozity z PLA, PHA a vláken sulfátové buničiny za účelem nalezení vhodného složení filamentů pro 3D tisk. Přidání 30 % sulfátových vláken k PHB/PLA nevedlo ke zlepšení mechanických vlastností. Tisknutelnost složitých geometrií byla dobrá.

PHB bylo také míseno s vícestěnnými uhlíkovými nanotrubkami (MWCNT) v množství od 0,25 do 5 % pro dosažení elektrické vodivosti biomateriálu [125]. U kompozitů byla pozorována dobrá dispergace v makro- a mikroměřítku. Přidání MWCNT mělo za následek zvýšení Youngova modulu pružnosti a snížení napětí při přetržení. Materiály úspěšně prošly test biokompatibility s buňkami MRC. Výsledky ukazují potenciál pro použití v biomedicínských elektronických zařízeních.

4.4 Biodegradabilita finálních PHA bioplastů a biokompozitů

Biodegradace je proces, při kterém se rozkládá molekulární struktura organické látky působením mikroorganismů za přítomnosti kyslíku (aerobní) na oxid uhličitý, vodu, minerální soli a novou biomasu, nebo za anaerobních podmínek za vzniku metanu. Kromě prostředí závisí biodegradace na mnoha materiálových faktorech (chemická struktura, morfologie, M_w, krystalinita, a další).

Očekávání vědců i politiků od bioplastů nyní naráží na realitu a potřebu cirkulárního přístupu. Biodegradabilita znamená ztrátu hodnoty materiálů. Proto tuto vlastnost doporučuje EK využívat pouze tam, kde je to žádoucí - např. jako bariérový povlak nebo nosič hnojiva a dalších agrochemikálií, obaly na čajové sáčky, na bioodpad, nebo materiál pro náhradu syntetických primárních mikroplastů apod. Rychlý přehled o biodegradabilitě biopolymerů poskytuje Obr. 3 [126].



Obr. 3: Biodegradabilní polymery a jejich vlastnosti v různých prostředích [126]

Aerobní degradace je pokryta zkušebními metodami ASTM D5988 [127] a D5338 [128]. Oba standardy popisují měření vývoje CO_2 s ohledem na mezofilní nebo termofilní teploty. Podle normy ASTM D5988 by biodegradace měla dosáhnout 70 % do 45 dnů a její hranice by měla být dosažena za méně než šest měsíců, aby byla považována za platnou [57]. Standard ASTM G160 [129] popisuje proces biodegradace pomocí měření úbytku hmotnosti. Anaerobní degradace je dokumentována v normách ASTM D5511 [130] a D5526 [131], které se podobají prostředí biologicky aktivních skládek. Kromě toho je cyklus následné degradace na skládce tvořený aerobní degradací následovanou anaerobní degradací diskutován v normě ASTM D7475 [132], [109].

Už v r. 1992 vyšla publikace [133] ukazující vliv teploty prostředí na rychlost biodegradace PHB a PHBV a to v prostředí půdy za laboratorních podmínek, ve vodním prostředí a kompostu. Vstřikované zkušební vzorky z PHB ve tvaru dogbone ztratily po 200 dnech při 28 °C v půdě 74–93 % původní hmotnosti. V univerzitním sladkovodním rybníku polymery degradovaly velmi pomalu; po půl roce ponoru byl zaznamenán pouze 4–7% úbytek hmotnosti. V lokální kanalizaci bylo dosaženo podobných procent úbytku hmotnosti, ale po pouhých 2 měsících. V mořské vodě docházelo k rychlé degradaci: po půl roce zůstalo 61–71 % původní hmotnosti. Rychlost degradace PHA je obtížné předpovědět, a to i při kontrole teploty, pH a obsahu vody.

Ve směsi PHB s PHBV (22% HV) s větší koncentrací PHBV klesá krystalinita a roste rychlost hydrolytického rozkladu ve fosfátovém pufru s pH 7,4 [134]. Výrazně rychlejší biodegradace PHBV než PHB byla prokázána i v kompostu [135].

Tenké filmy připravené litím z roztoku chloroformu byly podrobeny degradaci jak v pufru, tak v přítomnosti extracelulární PHB depolymerázy. Rychlost enzymatické degradace byla mnohem rychlejší než rychlost jednoduché hydrolytické degradace. K enzymatické degradaci došlo povrchovou erozí. Hmotnost a tloušťka filmu s časem klesala, zatímco M_w polyesterových filmů zůstala během enzymatické degradace téměř nezměněna. Rychlost eroze polyesteru depolymerázou klesala v řádu P3,4HB > PHB > PHBV. Rychlá eroze P3,4HB filmu PHB depolymerázou může být způsobena snadnějším atakem molekuly enzymu směrem k esterovým skupinám kopolyesterových řetězců, protože sterické bránění jednotek 4HB je menší než u jednotky 3HB nebo 3HV [136]. V případě biodegradace PHA v mořské vodě je mechanismem degradace také povrchová eroze a nejdůležitějším parametrem je teplota prostředí [137].

I vysoce krystalické PHB tedy podléhá biologickému rozkladu. Konstrukce výrobku na jeho bázi však vyžaduje často přídavek jiného polymeru, použití procesních aditiv a reakčních činidel, případně plniva a výztuže. Navíc při termické degradaci v rámci procesu zpracování PHB vznikají krotonové konce. Je tedy otázkou, jak ovlivní složení plastu a jeho zpracování finální biodegradabilitu.

4.5 Cíle

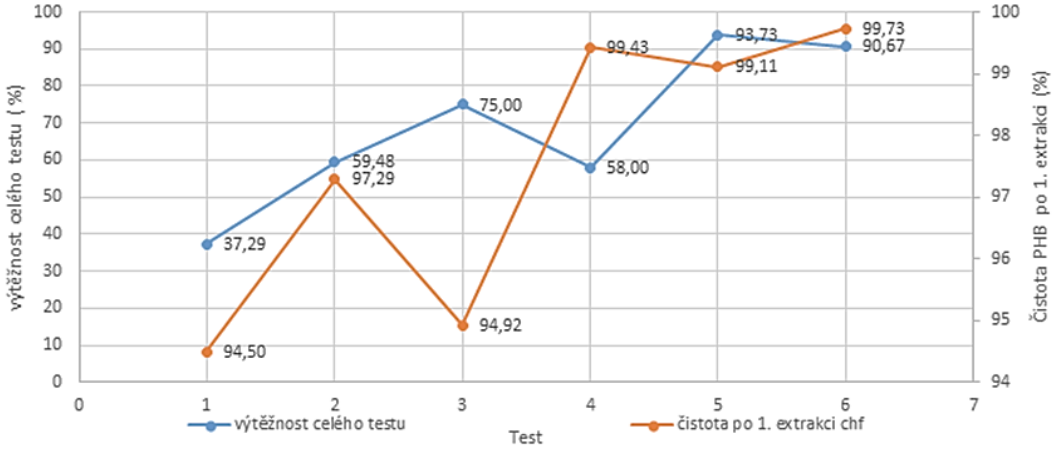
Postupně zlepšující se dostupnost a kvalita PHB HYDAL a PHB TianAn byla motivací k vytýčení v té době poměrně odvážného cíle – vyvinout a optimalizovat PHB materiál s řízenými vlastnostmi pro 3D tisk metodou FDM. Tento cíl byl také deklarován v projektové žádosti posléze úspěšně realizovaného projektu **PR 4**. Tomuto cíli však předcházel mnohem důležitější dílčí cíl - nalézt zpracovatelské postupy pro experimentální materiál PHB HYDAL a PHB TianAn do formy funkčního recyklovatelného termoplastu. A jak ukazuje výše uvedená rešerše, z pohledu dnešních publikovaných informací to byl nelehký úkol s ambiciózním cílem.

4.6 Dosažené výsledky

Tato kapitola je průvodcem vybraných výsledků publikovaných v 11 publikacích týmu Laboratoře bioplastů za posledních 10 let (Pub. 4–14) a je záměrně doplněná o některé nepublikované výsledky. K některým výsledkům jsou také uvedeny komentáře z dnešního pohledu a ve světle nově publikovaných informací z literatury.

4.6.1 Zpracovatelnost a stabilizace PHB

Práce probíhaly s experimentálním materiálem Hydal, jehož produkci zajišťovala společnost Nafigate. Vývoj procesu výroby zahrnoval jak optimalizaci upstreamu tak downstreamu, což mělo za následek proměnnou a až na výjimky zpravidla zlepšující se kvalitu produkovaného materiálu (Obr. 4). Jako zdroj uhlíku pro bakterie byl při procesu fermentace využíván použitý kuchyňský olej, který měl kolísavou kvalitu a složení. Biotechnologický proces nebyl na tyto změny citlivý, ale nevyužité látky z fermentace přecházely do druhého kroku extrakce. Obsah zbytkového oleje byl monitorován a předpokládalo se, že bude v procesu izolace odstraněn. Extrakce probíhala v chloroformovém roztoku, kdy se sedimentací oddělený polymerní roztok nástřikoval do horké vody srážecí smyčky (**V2**). Vysrážený polymer se jímal ve formě „vloček“, které se následně sušily. V případě neoptimálně provedeném izolačním procesu však přecházely estery mastných kyselin spolu s dalšími látkami do polymeru. Podobně snižovaly čistotu finálního polymeru i zbytky buněčných stěn.



Obr. 4: Vývoj kvality PHB Hydal z pohledu čistoty a dosaženého výtěžku

Tyto zbytkové látky se pak projevovaly při zpracování v tavenině jako prodegradační činidla, která urychlovala termický rozklad, drasticky snižovala střední molekulovou hmotnost, tím i viskozitu a zpracování klasickou extruzí tak v podstatě znemožňovala. I malé množství nečistoty kolem 1 % způsobuje chování viz Obr. 5. Bylo nezbytné sledovat čistotu, distribuci molekulové hmotnosti a reologické chování taveniny. Čistota matriálu byla sledována metodou GC-FID (chromatografické stanovení zastoupení esterů 3HB), ale chyba měření této metody při reálných čistotách nad 99 % byla kolem 1 %. PHB však bylo na svoji čistotu při zpracování v extruderu mnohem citlivější. Projev byl zaznamenán zejména v barevnosti (žlutosti) po přetavení v definovaných podmínkách a ve vývoji posunu barevnosti s teplotou. Vznikl proto jednoduchý vzorník zohledňující žlutost vs. čistotu, dle kterého bylo možné se jednoduše orientovat.

Distribuce molekulových hmotností byla sledována pomocí GPC. Díky častým poruchám tohoto zařízení na FCH VUT bylo z počátku měření prováděno i na dalších dvou pracovištích, výsledky však nebyly zcela souměřitelné. Hodnoty M_w se pohybovaly mezi 400–600 kDa. Důležitějším ukazatelem

kvality polymeru však byla stabilita M_w při procesu zpracování v tavenině. Protože M_w ovlivňuje reologické chování, bylo logické sledovat reologickou stabilitu při teplotě zpracování. První pokusy na rotačním reometru ARG-2 však dopadly nevalně. Metoda musí obsahovat krok, při kterém se PHB mezi deskami reometru roztaví, což je vzhledem ke konstrukci tohoto reometru a vysoké krystalinitě časové náročné a dochází k degradaci PHB už v tomto kroku. Při měření pak dochází k takovém poklesu viskozity, že tavenina odtéká z měřicích ploch a měření je zkresleno (a navíc pokaždé jinak). Ze stejného důvodu selhávalo i měření MFI. Ve spolupráci se Slovenskou technickou univerzitou v Bratislavě (STUBA) tak vznikla metodika sledování komplexní viskozity a relativní viskozity v čase při teplotách 170, 180 a 190 °C na gumárenském reometru, který disponuje zavřenou komorou. Ten navíc dokáže simulovat i vyšší smykové namáhání podobné tomu ve dvojšnekovém extruderu. Z rychlosti poklesu viskozit byla usuzována stabilita a tím i kvalita PHB. Tato metoda se používá s úspěchem do dnes.

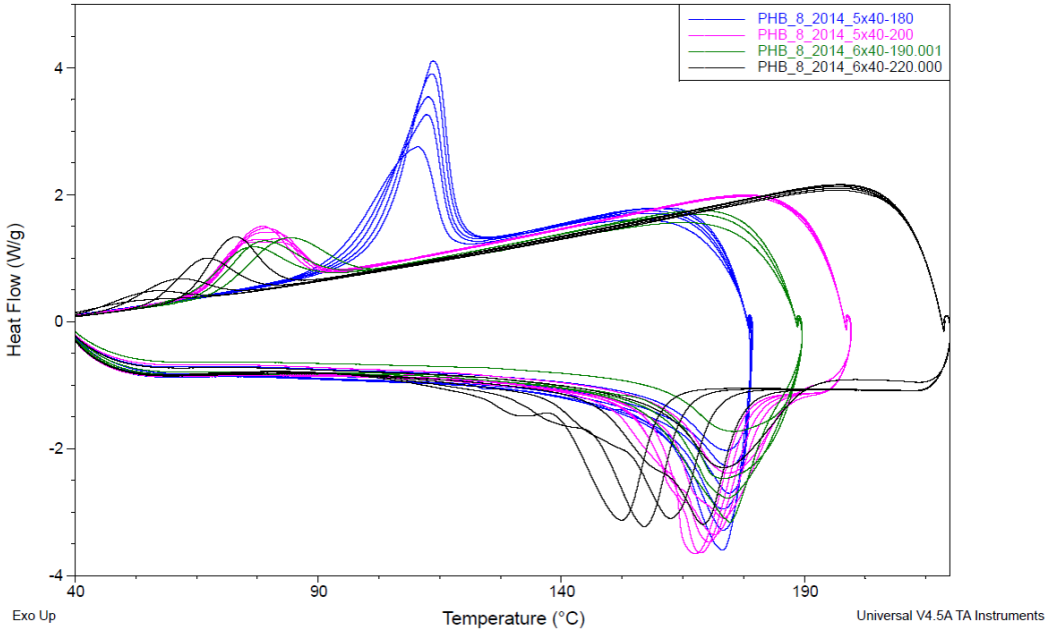


Obr. 5: Když PHB nedosahuje základních zpracovatelských parametrů…

Stabilitu materiálu bylo možné sledovat také vytvořenou metodou cyklického DSC. Vzorek je při této metodě vystaven opakujícím se cyklům ohřevu na zpracovatelskou teplotu, isotermní výdrži a následnému chlazení na 40 °C, kdy již neprobíhá krystalizace. Z rozdílů záznamu jednotlivých cyklů lze usuzovat míra stability PHB. Obr. 6 ukazuje citlivost materiálu na zpracovatelskou teplotu. Při 180 °C nedojde v DSC k úplnému roztavení materiálu. Polymer zůstává nukleován zbytky krystalické fáze a velmi rychle (při teplotách nad 110 °C) začíná při chlazení krystalizovat. Teplota tání i krystalizace se mění jen velmi málo. Už při ohřevu na 190 °C dochází k heterogenní nukleaci až při teplotách pod 90 °C. Při měření s maximem v 200 °C jsou již pozorovatelné změny v teplotě tání a při maximu v 220 °C lze již vidět prudký pokles teplot tání a krystalizace související s degradačními procesy.

Paralelně s testováním PHB Hydal a poskytování zpětné vazby k optimalizaci procesu výroby zejména v rámci projektu **PR3** probíhal výzkum v rámci **PR1** a **PR2** i na komerčních materiálech PHB. Jedním z nich bylo PHB od společnosti TianAn, který byl přepracováván v německém Biomeru pod stejnou obchodní značkou. Surový (TianAn ENMAT) i kompaundovaný polymer s 5% tributylcitrátem a nukleanty (směs BN a neznámé organické látky) byly používány pro vývoj receptur. Vycházelo se ze zkušeností se zpracováním konvenčních plastů, a proto byly nejprve testovány přídavky změkčovadel, nukleantů, lubrikantů a stabilizátorů. Testy byly prováděny na hnětiči Brabender a výsledný kompaund byl přelisován na vyhřívaném lisu do podoby zpravidla 0,5 mm tlusté fólie. Z ní byla

vyseknuta testovací tělesa ve tvaru malého dogbone 5B. Z testovaných variant materiálových složení zahrnujícího celkem 103 kombinací 40 vybraných aditiv nedosáhla žádná zásadní změny v mechanických vlastnostech. Všechny vzorky se po několika dnech za pokojové teploty chovaly křehce s tažností do 10 procent. Pozorovatelné byly změny reologie a stability materiálu při použití některých změkčovadel a stabilizátoru na bázi karbodiimidových nebo epoxidových skupin. V rámci bakalářské práce **VSKP1** byly také testovány možnosti změny struktury roubováním chlóru a flóru.



Obr. 6: Hodnocení stability PHB pomocí cyklického DSC, vliv maxima teploty při ohřevu

Z dnešního pohledu je zřejmé, že žádná zásadní změna v mechanice nastat ani nemohla. Jak vyplynulo z rešerše výše uvedené, přídavek aditiv k čistému PHB obecně neposkytuje zlepšení mechanických vlastností vlivem fyzikálního stárnutí PHB spočívajícího v dokrystalizaci amorfní fáze. Navíc, jak bylo posléze zjištěno, experimenty byly zatíženy dvěma negativními skutečnostmi. Teplota hnětiče byla řízena termostatovanou olejovou lázní. Skutečná teplota hnětiče však kolísala někdy až 20 °C pod nastavenou hodnotou (zjištěno po dvou letech po zprovoznění měřením přímo v komoře). Proto byla teplota nevhodně zvedána k 190 °C, což způsobovalo degradaci některých vzorků. Druhým problémem je samotná charakterizace vzorků z rozlisované fólie. Tato metoda byla využívána z důvodu nedostatku materiálu pro vstřikování a jak se ukázalo, i jinak funkční matriály na bázi PHA zpracované touto metodou nevykazovaly valné výsledky. Charakterizace vzorků fólií připravených z roztoku chloroformu, která se objevuje v mnohých publikacích, byla kvůli zkreslení zavržena.

Množství materiálu dostupné pro experimenty v případě PHB Hydal umožňovalo od r. 2018 navrhovat experimenty s maximální hmotností zpracovaného materiálu kolem 300 g. To umožňovalo průchod materiálu menším jednošnekovým extruderem (Haake 19 mm, L/D 25) ze ziskem cca 200 g granulátu. Záludnost zpracování PHB Hydal však navíc spočívala v jeho fyzikální formě. Díky srážení chloroformového roztoku do horké vody vznikaly 5–15 mm velké nepravidelné a velmi členité lehké útvary, které byly pracovně nazvány vločky (Obr. 7). Tyto vločky nebyl schopen dávkovat žádný z konvenčních testovaných systémů, neboť při tlaku tvořily relativně spojenou hmotu podobnou plsti. Protože byly vločky velmi měkké, nebylo je možné ani efektivně mlít na dávkovatelný prášek. Vznikla tak myšlenka pomlet tento materiál na nožovém mixeru s velmi ostrými planžetovými čepelemi. Modifikací 20L nerezového drtiče ovoce tak v laboratoři vznikl stroj, který umožnil předzpracování

tohoto problematického materiálu. Sypnost se tím zlepšila natolik, že na míru vyrobený dávkovač se spirálovým šnekem byl schopen dávkovat materiál do násypky a bylo možné jej v jednošnekovém extruderu granulovat pro následné použití v konvenčních zpracovatelských strojích.



Obr. 7: Zleva: PHB před zpracováním, drtič na ovoce, PHB po zpracování

Protože i tak bylo množství výsledného materiálu nedostatečné pro vstřikování, pro základní orientační testy mechanických vlastností byla využívána struna získaná z extruderu. Charakterizace v tahu byla prováděna s vědomím, že je ve struně materiál částečně zorientován a nelze tak vlastnosti přirovnávat ke zkušebním vstřikovaným tělesům. Nicméně se tento typ vzorku ukázal být proti těm vyseknutým z lisovaných fólií mnohem více vypovídající.

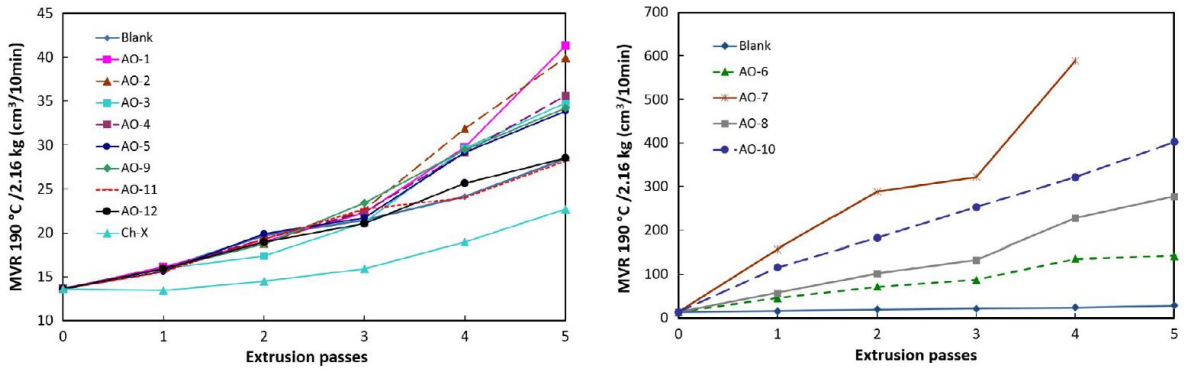
Problémem byl i proces chlazení taveniny ve formě struny, který neodpovídá teplotní historii vzorku připraveného vstřikováním, což se projeví v jeho odlišné krystalické struktuře a tím na jeho vlastnostech. Běžně používaný proces chlazení struny do záměrně dochlazované vody lze teplotním profilem přirovnat spíše k technologii výroby chill-roll fólie. Za těchto podmínek je však PHB přechlazeno ve smyslu neproběhlé krystalizace, a zůstává měkké, velmi lepivé a tedy nezpracovatelné. Při odtahu struny totiž nemá potřebnou pevnost a granulace ve střižném granulátoru zcela selhává. Z tohoto důvodu byla navržena modifikace procesu extruze a chladící lázeň byla vybavena ohřívačem nastaveným na teplotu 60 °C. PHB tak bylo ochlazováno ze zpracovatelské teploty pomaleji a docházelo k dostatečné krystalizaci tak, aby byla možná výroba struny i granulí. A teplotním profilem se vzorky struny přiblížily vzorkům vstřikovaným.

Jednou z logických otázek při zpracování PHB byla jeho procesní stabilizace. V tu dobu se autoři článků orientovali na využití antioxidantů (často právě Irganox 1010) a to bez vysvětlení důvodu použití. To vedlo k systematickému výzkumu vlivu používaných antioxidačních stabilizátorů (tabulka 1) na reologické vlastnosti PHB v průběhu vícenásobné extruze (Obr. 8). Záměrně byl přidán jeden zástupce chain extenderu, který se jevil při prvotních testech jako slibný stabilizátor reologických vlastností taveniny. Výsledky této práce byly publikovány (byť mnohem později, než reálně vznikly) v **Pub 4.**

Bylo potvrzeno, že běžné primární a sekundární antioxidanty, stejně jako multifunkční HALS, jsou v PHB neúčinné. Kromě toho, přítomnost běžných antioxidantů v matrici PHB prokázala zcela nepříznivý účinek, který zvýšil rychlost tepelného rozkladu. Prodegradační efekt struktur obsahujících atomy fosforu a dusíku s asymetrickými volnými elektronovými páry byl dokonce dramatický. Žádná z běžně používaných struktur stabilizátorů nevykazovala schopnost chránit PHB během zpracování. Smysl má pouze použití chain-extenderů, přestože nemají skutečnou schopnost polymer chránit, ale pouze kompenzovat účinky degradace.

Tabulka 1: Složení jednotlivých testovaných materiálů (Pub 4)

Blank	Base	None
AO-1	Base + 0.5 % BHT	Low-molecular phenol, 2,6-di-t-Bu substituted
AO-2	Base + 0.5% Irganox1010	High-molecular phenol, 2,6-di-t-Bu substituted
AO-3	Base + 0.5% Cyanox AO 1790	High-molecular phenol, 2-methyl-6-t-Bu substituted
AO-4	Base + 0.5% Irgafos168	Phosphite, non-hydrolyzable
AO-5	Base + 0.5% Irganox B225	Phenol-phosphite synergy blend (1:1)
AO-6	Base + 0.5% Ultranox 626	Phosphite, partially hydrolyzed
AO-7	Base + 0.5% Genox EP	Amine oxide
AO-8	Base + 0.5% Irgastab FS042	Hydroxylamine
AO-9	Base + 0.5% Irganox HP136	Lactone, benzofuranone
AO-10	Base + 0.5% Uvinul4050H	HALS, low-molecular
AO-11	Base + 0.5% Ronotec201	Vitamin E, 2,6-dimethyl substituted phenol
AO-12	Base + 0.5% natural curcuma	Low-molecular phenol, 2-methoxy substituted
Ch-X	Base + 0.5% Raschig 9000	Carbodiimide chain extender



Obr. 8: Vývoj indexu toku při vícenásobné extruzi jednotlivých vzorků se stabilizátory

4.6.2 Mísení s ostatními polymery

V rámci řešení projektů bylo cílem vyvinout materiál vhodný ke vstřikování (projekt **PR1**, výstup **V4**) a k výrobě biodegradabilních fólií pro agronomické aplikace (projekt **PR2,** výstup **V5**). Na základě negativní zkušenosti s pouhou aditivací PHB bylo hledáno řešení v podobě polymerní směsi. Na základě rešerše byly vybrány polymery PLA, PBAT, PBS, PVAc a P3,4HB jako vhodní kandidáti na další testy pro cílené aplikace. Bohužel PBS ani P3,4HB nebylo v té době dostupné v dostatečném množství a kvalitě a nebyly nakonec testovány. Dnes je již známo, že P3,4HB s vysokým podílem 4HB funguje výborně jako vysokomolekulární změkčovadlo, modifikátor houževnatosti i jako procesní stabilizátor.

PLA spolu s PVAc (v několika stupních deacylace) bylo testováno s přídavkem od 5 do 20 %. Spolu s přidávaným změkčovadlem na bázi esteru citronové kyseliny bylo možné nastavit výsledné vlastnosti z hlediska reologie a tažnosti v poměrně širokém rozsahu (5–250 %). I přes pokles tažnosti po několika dnech za laboratorní teploty vykazovaly nejtažnější vzorky 50 %. Z těchto kompaundů bylo možné připravit vzorky injekčním vstřikováním i fólie rozfukováním. Koncentrací PVAc bylo možné efektivně řídit (přesněji snižovat) rozložitelnost v laboratorním kompostu.

Vybrané receptury byly na základě požadavků agronomů obarveny modrým koncentrátem a přídavkem mletého vápence byla záměrně snížena průsvitnost fólie. Takto připravený materiál byl použit k výrobě modelových zemědělských fólií, které byly následně testovány ve dvou sezonách na záhonech s jahodami ve Výzkumném a šlechtitelském ústavu ovocnářském Holovousy s.r.o (výstup **V4**). Zde se však po dvou letech ukázalo několik zásadních problémů:

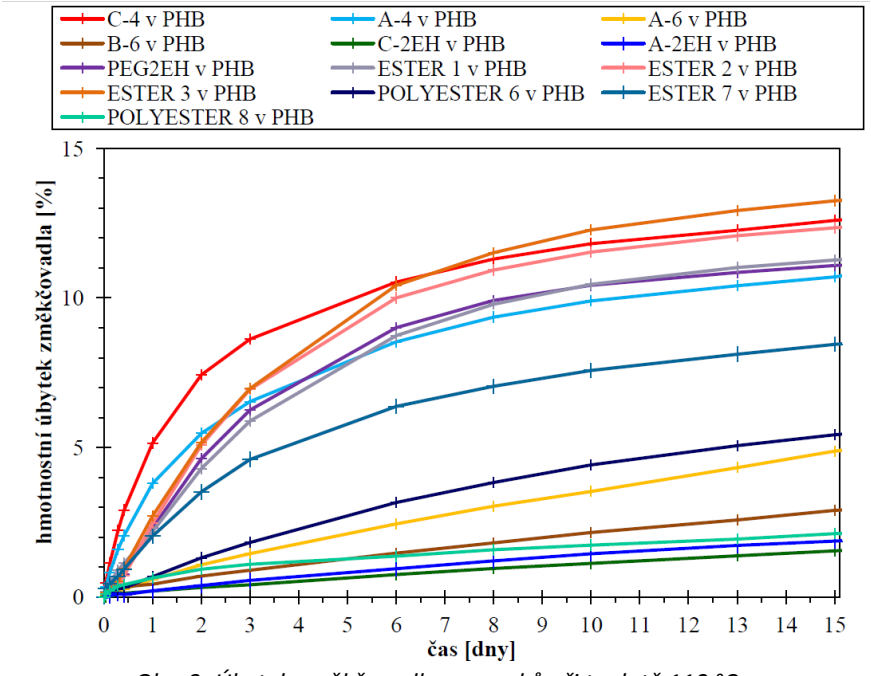
- I v kompostu nejrychleji biorozložitelné fólie nevykazovaly na reálném záhoně žádný rozklad.
- I fólie s nejvyšší tažností se v druhém roce začaly křehce drolit a generovat mikroplasty.
- Odstranění fólie ze záhonů bylo doprovázeno tvorbou mikročástic v půdě.

Synergický efekt použití stabilizátoru (Rashig 9000) byl pozorován i v těchto směsích. Směsi byly pro ověření zpracovatelnosti zkušebně kompaundovány na čtvrtprovozní lince (PIB Brno) a testovány ve vstřikovně (Plastyko Kobylí) na reálných výrobcích. Testy byly úspěšné a směs se ukázala zpracovatelná ve vstřikolisu bez jakýchkoliv problémů. Materiály bez PVAc, tedy směsi na bázi PHB/semikrystalické PLA/změkčovadlo, neposkytovaly potřebný rozsah vlastností. Vznikla hypotéza, že vyšší tažnost a houževnatost poskytuje materiálu právě přidání ryze amorfního polymeru PVAc, což doposud používané semikrystalické PLA nenabízelo. Výměnou PLLA za PDLLA bylo dosaženo potřebných vlastností i bez PVAc, čímž se zvýšila schopnost biodegradace výsledného materiálu. PVAc tak bylo vyřazeno z dalších experimentů.

4.6.3 Aditivace změkčovadly

Vlastní křehnutí bylo však nadále pozorováno na fóliích i na vstřikovaných tělesech. Aby bylo možné efektivně testovat dopad materiálových změn v receptuře a podmínek zpracování na tento proces křehnutí, byly zkoušky prováděny akcelerované – při zvýšené teplotě (110 °C). Z provedených experimentů vyplynulo, že za krátkodobé křehnutí je zodpovědné již popsané fyzikální stárnutí a za dlouhodobé pak migrace použitých nízkomolekulárních změkčovadel. Byl pozorován úbytek hmotnosti fólií i vstřikovaných dílů při vyšší teplotě, který odpovídal hmotnosti změkčovadla.

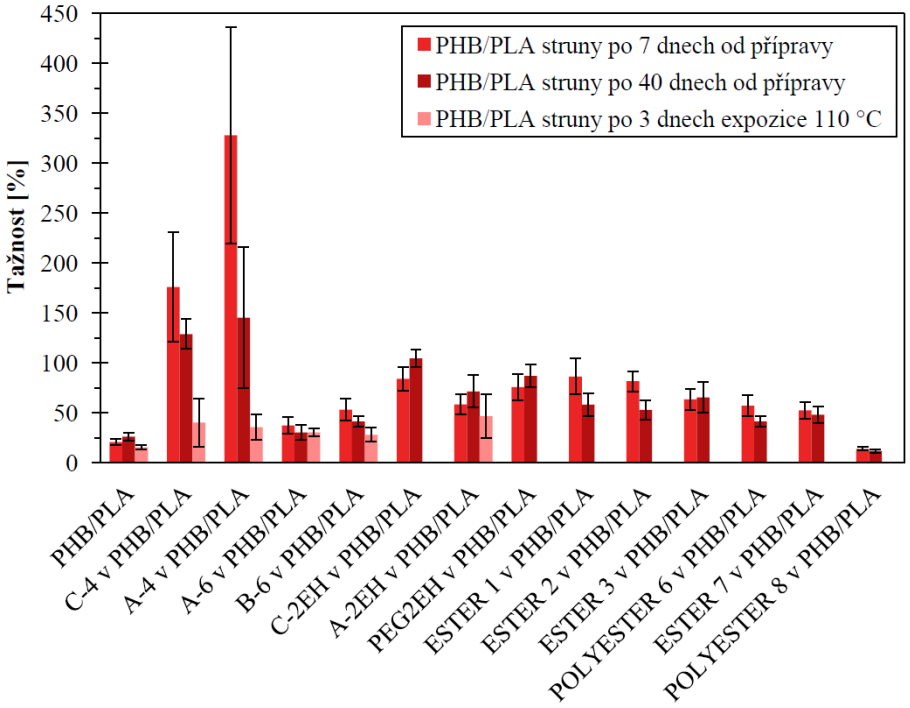
Z těchto výsledků vyplynula výzva hledat změkčovadla s větší molekulou a nižší schopností migrace na povrch, která budou mít dostatečně změkčující efekt. Byly vytipovány další komerčně dostupné estery kyseliny citronové: butyltrihexyl citrát a acetyltrihexyl citrát (Citroflex B6 a A6), PEG a jeho 2etylhexyl derivát, oligomerní adipát a další laboratorně syntetizované molekuly. Studiem efektu změkčení a rychlostí migrace změkčovadla za různých podmínek se zabývala diplomová práce **VSKP2** a v případě vláken diplomová práce **VSKP3**. Nejdůležitější výsledky ukazuje Obr. 9 a Obr. 10.



Obr. 9: Úbytek změkčovadla ze vzorků při teplotě 110 °C

Sledování hmotnosti extrudovaných strun s přídavkem 15 % změkčovadla vykazovalo obrovské rozdíly v rychlosti jeho migrace. Testem difúze změkčovadel provedeným při 110 °C v laboratorní sušárně bylo zjištěno, že komerční tributylcitrát byl nejvíce difundujícím změkčovadlem z PLA, PHB i z jejich směsi. Naopak nejméně difundujícím komerčním změkčovadlem z PLA, PHB i ze směsi PHB/PLA byl acetyltris(2-ethylhexyl)citrát. Po 15 dnech z PHB/PLA vydifundovalo jen 2,4 hm. % oproti tributylcitrátu, kterého vydifundovalo z PHB/PLA 14,3 % z dávkovaných 15 hm. %. Acetylace, butyrylace i přídavek ethylové postranní skupiny na hlavních řetězcích napomohly k zpomalení difúze změkčovadla na bázi esteru kyseliny citronové. Ze syntetizovaných změkčovadel se stalo nejméně difundujícím z PHB i PHB/PLA změkčovadlo na bázi polyesteru kyseliny mléčné s řetězci zakončenými 2-ethylhexylovými skupinami. Z PHB/PLA po 15 dnech expozice 110 °C tohoto změkčovadla vydifundovalo jen necelé 2 hm. % z předpokládaných 15 hm. %. V PLA toto změkčovadlo zkoušeno nebylo. Tam byl nejpomaleji difundujícím ze syntetizovaných změkčovadel tris(2-ethylhexyl)citrát. Naopak nejrychleji difundujícími syntetizovanými změkčovadly z PLA, PHB i PHB/PLA se stala změkčovadla na bázi esteru kyseliny 2-ethylhexanové s PEG. Některé jeho estery vydifundovaly po 15 dnech expozice při 110 °C z PHB a PHB/PLA ve stejném množství jako tributylcitrát.

Nicméně po 3 dnech expozice 110 °C směsi PHB/PLA jak s ATBC, tributylcitrátem a komerčním polyethylenglykol bis(2-ethylhexanoátem), tak se všemi testovanými syntetizovanými změkčovadly zaznamenaly rapidní zhoršení mechanických vlastností. Po 40 dnech směsi s ATBC a tributylcitrátem opět ztratily svoji houževnatost, i když ne tak výrazně jako po jejich expozici 110 °C.



Obr. 10: Tažnost strun připravených s různým změkčovadlem

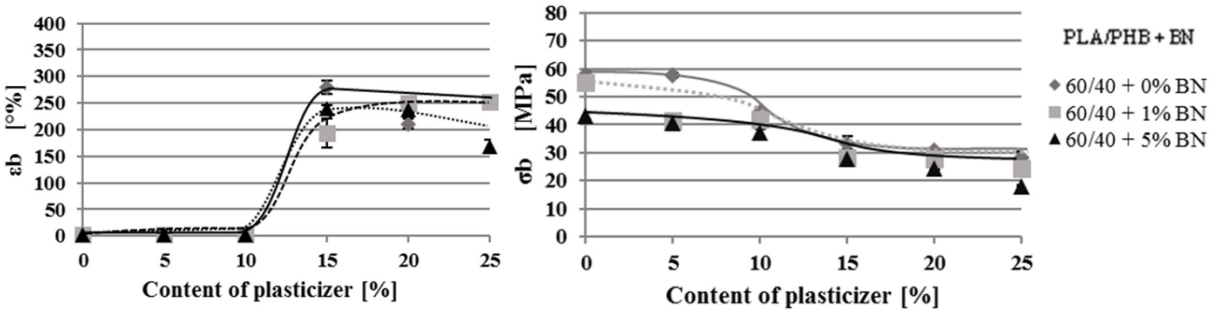
V této práci nebylo nalezeno vhodné změkčovadlo pro polymerní směs PHB/PLA, které by způsobilo vhodné mechanické vlastnosti a zároveň by jeho difúze za zvýšené teploty byla dostatečně pomalá. Některá změkčovadla se stala z hlediska mechanických vlastností účinnými změkčovadly v polymerní směsi, jako například komerční ATBC (zde A-4). Jejich difúze z plastu však byla za zvýšené teploty příliš rychlá. Na druhé straně byla nalezena změkčovadla, která z polymerní směsi za zvýšené teploty difundovala velmi pomalu, jako například syntetizované změkčovadlo na bázi polyesteru

kyseliny mléčné s řetězci zakončenými 2-ethylhexylovými skupinami, kterého po 15 dnech expozice 110 °C difundovalo z PHB/PLA směsi nejmenší množství ze všech zkoušených změkčovadel. Nicméně toto změkčovadlo způsobilo zhoršení mechanických vlastností oproti směsi neměkčené. Další práce by se proto mohly zaměřit na změkčování PHB/PLA směsi kombinací obou typů změkčovadel.

Účinnost změkčovadel lze určit také z posunu hodnoty T_g polymeru. Změkčovadla označovaná jako primární by měla T_g polymeru snížit v důsledku zvýšení pohyblivosti polymerních řetězců amorfní fáze. Stanovení je však komplikováno faktem, že PHB obsahuje jen malé množství pohyblivé amorfní fáze. Z tohoto důvodu je celková změna tepelné kapacity pomocí DSC obtížně detekovatelná.

4.6.4 Nukleace

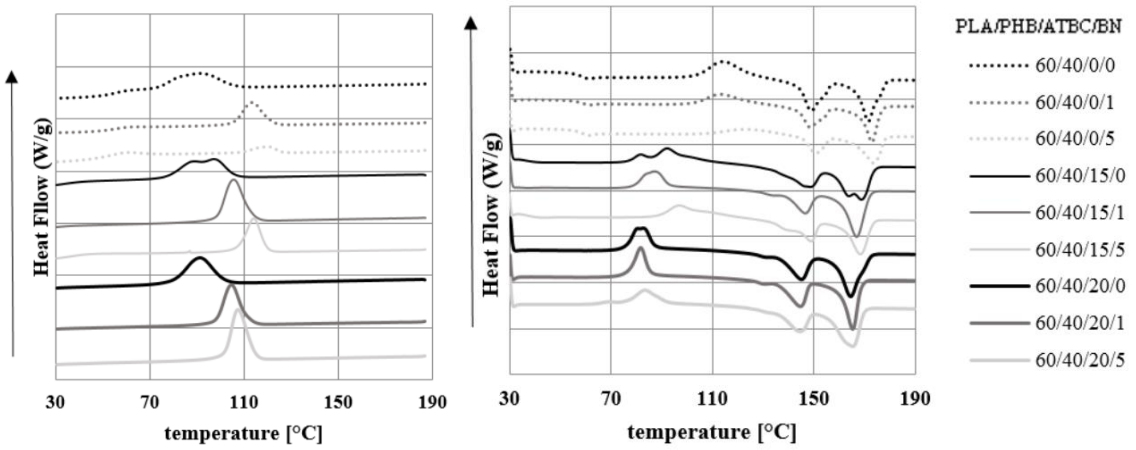
Změkčení pomocí přídavku vhodného organického změkčovadla probíhá v amorfní fázi, je však třeba řídit i strukturu krystalické fáze PHB kinetikou krystalizace. Společný záměr Laboratoře bioplastů a pracoviště prof. Alexyho na STUBA porozumět vlivu aditivace na krystalinitu a kinetiku krystalizace směsí PLA/PHB vyústil v první společnou publikaci **Pub 5 (2017)**. Vzhledem k předešlému zaměření slovenského týmu na blendy s majoritním podílem PLA aditivované krystalickým PHB, byly kompaundovány směsi semikrystalického PLA/PHB v poměru 60/40. Byl variován přídavek změkčovadla ATBC v rozmezí 0–25 % a přídavek nitridu boritého (BN) jako nukleačního činidla v dávkách 0–5 %. Sledována byla zpracovatelská stabilita směsí kompaundovaných na dvoušnekovém extruderu pomocí vyhodnocení viskozity na oscilačním reometru RPA 2000 se zavřenou komorou. Mechanické vlastnosti byly testovány na fóliích vyrobených technologií chill-roll. Pomocí DSC byla sledována krystalizace.



Obr. 11: Vliv koncentrace změkčovadla ATBC ve směsi PLA/PHB na mechanické vlastnosti a role nukleantu

Překvapivým výsledkem byla závislost tažnosti a pevnosti fólií na množství změkčovadla na Obr. 11. I z dříve provedených experimentů na směsi PHB/PVAc/PLA bylo zřejmé, že pro materiály na výrobu fólie je třeba cca 15 % změkčovadla a pro vstřikování je třeba minimálně cca 10 %. Vyšší množství změkčovadla než 15 % vedlo zpravidla k jeho velmi rychlé difúzi z tuhnoucího materiálu. V případě majority semikrystalického PLA s PHB je dle výsledků závislost koncentrace změkčovadla na pevnost a tažnost ještě ostřejší.

Jak bylo již uvedeno v rešeršní části, vysokomolekulární PLA a PHB jsou zejména v poměru blízkém 1:1 nemísitelné. Ukázaly to i výsledky v této práci, kdy jsou jasně viditelné dva píky tání (140 a 170 °C) příslušející krystalickým doménám PLA a PHB. Přídavek BN zvýšil dle předpokladu teplotu krystalizace ve všech vzorcích nezávisle na množství změkčovadla. Zvýšení koncentrace změkčovadla posunovalo s klesajícím T_g studenou krystalizaci k nižším teplotám i v případě účinné nukleace (Obr. 12).

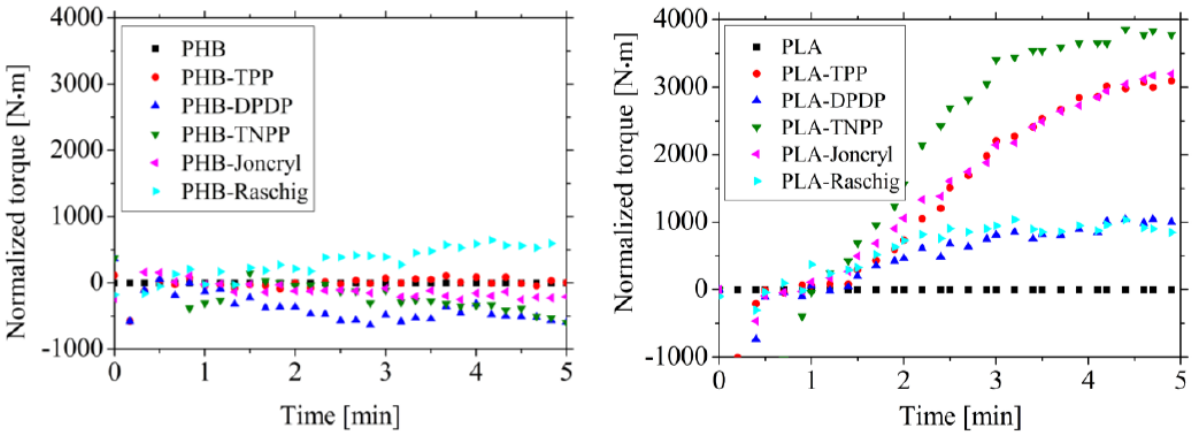


Obr. 12: Vliv přídavku ATBC na krystalizační chování PLA/PHB směsi

4.6.5 Stabilizace PHB/PLA směsí

Přestože byly omezeně mísitelné směsi PHB/PDLLA poměrně dobře zpracovatelné, bylo snahou řešit jejich stabilizaci a kompatibilizaci. Výsledky byly publikovány v **Pub 6 (2018)**. Protože se vybrané stabilizátory chovají v obou polymerech odlišně, byl navržen experiment sledující chování taveniny v přítomnosti vybraných stabilizátorů na trifenylfosfit (TPP), tris(nonylfenyl)fosfit (TNPP) a difenylisodecylfosfit (DPDP) a chain extenderů na bázi poly-(1,3,5-triisopropylfenylen-2,4-carbodiimidu) (Raschig 9000), a polymerní epoxy-styren-akrylát (Joncryl ADR-4368). Účinnost stabilizace byla sledována pomocí kroutícího momentu hnětáku PLA i PHB a jejich hodnoty kroutícího momentu po odečtení referenčního materiálu byly vyneseny v čase.

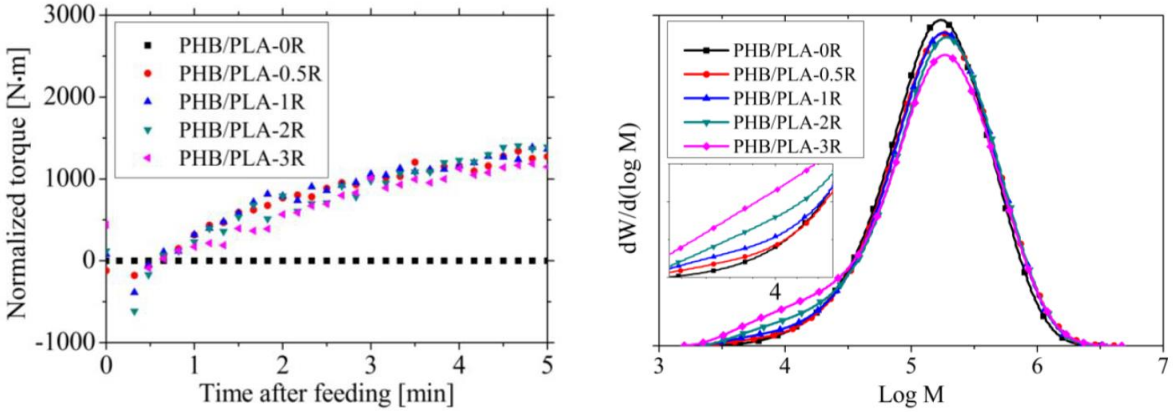
Z grafů na obrázku Obr. 13 je zřejmé, že pozitivní dopad na PHB měl pouze Rashig, což bylo v souladu s výsledkem zjištěným v předchozí práci. DPDP měl negativní dopad na viskozitu, TNPP a Joncryl také mírně negativní dopad, přídavek TPP bez měřitelného efektu. Naopak, v PLA se pozitivně projevil přídavek všech těchto aditiv. TPP a Rashig by tak mohly být vhodní kandidáti pro stabilizaci blendu. Pro optimalizaci dávky Rashig byly provedeny experimenty na blendu PHB/PLA (70/30).



Obr. 13: Vliv aditivace na reologii PHB a PLA

Jak je zřejmé z Obr. 14, už samotný 0,5% přídavek Rashigu se pozitivně projevil ve schopnosti stabilizovat reologii taveniny a jeho vyšší přídavek neměl již další vliv. Dle výsledků z GPC se při vyšší dávce než 0,5 % v tavenině hromadí nezreagovaný Rashig a ovlivňuje tak parametry vypočtené

z distribuce M_w, zejména snížení číselně střední M_w. Výsledky jsou v souladu s navazující prací jiného kolektivu [138] (2021), kde testovali přídavek polykarbodiimidu v PLA kompozitu a prokázali úspěšnou reakci prodlužování řetězce mezi karbodiimidovou skupinou a karboxylovou skupinou PLA. Optimální obsah PCDI pro nejvyšší pevnost taveniny, stabilitu filmu při vyfukování a mechanické vlastnosti byl 0,25 % aditiva. V rešeršní části review [90] (2021) je dosažený výsledek citován a zmíněn jako využitelná metoda stabilizace reologie materiálů na bázi PHB.



Obr. 14: Efekt množství přidaného aditiva Rashig na reologii a molekulovou hmotnost

4.6.6 End of life PHB/PLA směsí

4.6.6.1 Recyklace PLA/PHB směsí

Recyklace konvenčních plastů je díky legislativním změnám a tlaku uvědomělých spotřebitelů jedno z velmi diskutovaných témat. V případě bioplastů a biokompozitů je situace složitější, protože neexistuje zavedený postup separace těchto materiálů v třídících linkách. Zřejmě nejrozumnější je zpětný odběr těchto materiálů k výrobci, který zná složení a chování materiálů a je tak schopen recyklaci efektivně zabezpečit. Laboratoř bioplastů si dala za cíl vyvíjet materiály recyklovatelné z materiálového pohledu, k čemuž je nutná znalost reologického chování při násobném zpracování.

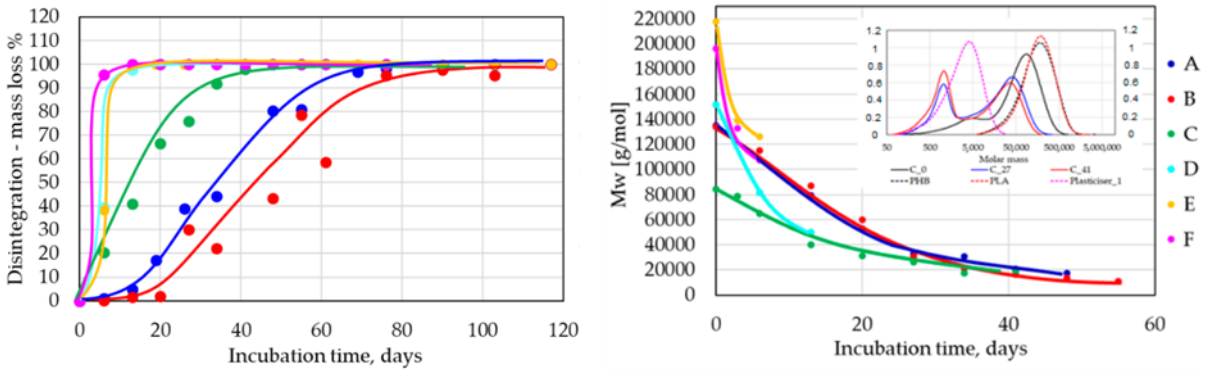
I z toho důvodu vznikla další společná práce s pracovištěm prof. Alexyho následně publikovaná v **Pub 7 (2020).** Testována byla směs PHB/PLA (55/45) s aditivy kombinovanými na míru pro injekční vstřikování. Tento blend byl od STUBA převzat partnerskou komerční společností PANARA Ltd. Nitra a dodáván pod obchodním označením NONOILEN®IM 3056-2. Materiál byl podroben vícenásobné extruzi na 19 mm jednošnekovém extruderu Brabender Plasticorder s retenčním časem cca 1 min. Pomocí reometru RPA 2000 byla sledována komplexní viskozita, tahovou zkouškou byly charakterizovány mechanické vlastnosti strun, pomocí DSC byly měřeny termické parametry a GPC bylo využito pro sledování distribuce M_w. Určována byla také odchylka barevnosti.

Celková chromatická odchylka rostla s počtem cyklů a tím s dobou setrvání v extruderu. Materiál postupně jemně tmavnul. Napětí při přetržení se pohybovalo v rozmezí 23–35 MPa a nemělo zásadní klesající tendenci. Tažnost se po prvních dvou cyklech držela na hodnotě nad 17 % a po 5 cyklech byl zaznamenán pokles na cca 5 %. Teplota tání ani skelného přechodu nevykazovaly žádnou zásadní změnu. Hmotnostně střední M_w klesala společně s klesající viskozitou, nicméně na hodnoty, které stále umožňovaly zpracování materiálu a výrobu testovacích těles vstřikováním. Lze tak tvrdit, že tyto materiály jsou z hlediska recyklovatelnosti srovnatelné s dalšími konvenčně používanými polyestery. Je nutno podotknout, že materiály neobsahovaly chain extender, zde je tedy prostor pro zlepšení.

4.6.6.2 Biodegradabilita směsí PHB/PLA

Jednou z velmi diskutovaných metod likvidace výrobků na bázi PHB po ukončení života je jeho kompostování, případně jiný způsob biodegradace. Přestože legislativa řadí biologickou likvidaci těchto materiálů v kompostárně až na poslední z možností, je snahou zachovat tuto přirozenou schopnost PHB i ve vyvíjených materiálech na jeho bázi. Toto úsilí je hnáno zkušeností se zacházením s plasty zejména v rozvojových zemích a dopadem v podobě znečištění, kterému čelí celé lidstvo.

Práce poměrně širokého týmu na toto téma započala v r. 2019 a byla v r. 2022 publikována (**Pub 8**). Pro tuto studii byly vybrány materiály zahrnující 5 odlišných receptur na bázi PLA/PHB/TPS a 3 reálných způsobů zpracování (vstřikování IM, rozfukování fólie FB, termoforming TF). Vzorky byly vystaveny účinkům biodegradace *in vitro* dle přizpůsobené metody ISO14855, dále v průmyslové kompostárně a v laboratorním komposteru při 58 °C a 28 °C simulující průmyslový a domácí kompost.



Obr. 15: Vývoj ztráty hmotnosti vzorků v čase v laboratorním komposteru a jejich molekulové hmotnosti. A – bikomponentní vstřikovaný kelímek tl. 4 mm z materiálu s TPS (vnější část) a bez TPS (vnitřní část); B a C – vstřikovaný kelímek tl. 1 mm z materiálu bez TPS a s TPS; D – fólie pro termoforming 0,35 mm bez TPS, E a F – vyfukovaná fólie tl. 0,04 mm bez a s TPS

Všechny vzorky prokázaly v laboratorním komposteru (65 °C) schopnost desintegrace na částice pod 2 mm. Všechny tři fólie se takto rozpadly do 20 dní, nejrychlejší průběh měl materiál F (s přidaným TPS). Dále následoval vstřikovaný kelímek s TPS, bikomponentní kelímek a nejpomalejší byl kelímek bez přídavku TPS (Obr. 15). Vývoj M_w klesal u fólií (D, E, F) poměrně strmě, což je zřejmě dáno i tloušťkou materiálu. U tlustostěnných vstřikovaných vzorků je směrnice poklesu menší a začíná od nižších hodnot. Vstřikování díky své zádrži v barelu zřejmě způsobilo pokles M_w už při zpracování. Vzorek C (pouze z materiálu s přidaným TPS) měl nejmenší M_w a pokles jeho rychlosti odpovídal spíše rychlosti ostatních vstřikovaných vzorků po 20 dnech. Všechny vstřikované vzorky bylo možné zachytit v pevném stavu při M_w nad 20 kDa, nižší hodnoty M_w měly už části, které nebylo možné v kompostu identifikovat.

Desintegrace je pouze orientačním měřením rozkladu materiálu v biologicky aktivním prostředí, nedává informaci o reálné přeměně plastu na CO_2 a biomasu. Z toho důvodu byla provedena měření biorozkladu v *in vitro* testu s měřením množství vygenerovaného CO_2.

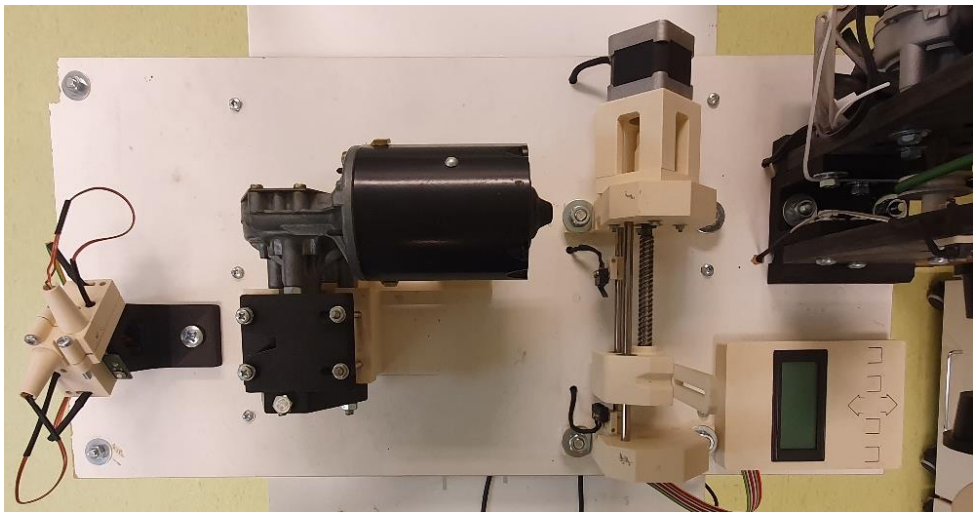
4.6.7 FDM 3D tisk PHB kompozitů

Při FDM tisku je třeba materiál dávkovat do tiskárny ve formě tiskové struny, která má předepsaný průměr a toleranci průměru i její ovality. V průmyslové praxi se dnes již běžně pro výrobu tiskové struny využívá jednošnekový extruder s kruhovou tryskou. Tok polymerní taveniny je pak dotvarován v kalibru a filament je následně chlazen ve vodní lázni nebo kaskádě temperované v případě

některých materiálů často i na teploty 50–60 °C umožňující krystalizaci materiálu. Tisková struna prochází laserovým měřidlem průměru měřicího zpravidla ve dvou na sebe kolmých osách. Na základě odchylek proti předepsanému průměru v obou těchto osách je řízena rychlost navíjení filamentu, na základě stability hodnot v čase obsluha zasahuje do teplotního profilu extruderu. Například pro nejběžnější typ struny průměru 1,75 je stanovena tolerance 1,75 ± 0,05 mm.

V laboratorním měřítku lze využít k výrobě tiskové struny i malý laboratorní jednošnekový extruder, při vhodném chování taveniny (stabilní tok) lze tiskový filament připravit i přímo na dvoušnekovém extruderu. Důležitým prvkem však zůstává systém měření průměru struny v obou rozměrech a řiditelný odtah struny ideálně s možností navíjení. S rozvojem FDM tisku odstartoval v r. 2016 v USA uvedením na trh malého extruderu s odtahem a navíjením pro výrobu 3D tiskových filamentů Filabot, byl však pro Laboratoř bioplastů cenově nedostupný. Dnes má společnost Filabot produkty pro jednoduchou výrobu tiskové struny pro domácí uživatele i firmy včetně mnohého zajímavého příslušenství [139]. Proto byl v Laboratoři bioplastů navržen, vyroben a naprogramován systém dvouosého měření průměru struny, jejího odtahu a navíjení na tiskovou cívku tak, aby společně s jednošnekovým extruderem umožnil výrobu tiskové struny s akceptovatelnou přesností, viz Obr. 16.

Tento systém je založen na optickém snímači (lineárním diodovém poli) detekujícího šířku stínu vytvářeného osvětleným filamentem. Speciálně naprogramovaný jednočipový mikropočítač zpracovává naměřená data a ta převádí pomocí matematického modelu na průměr filamentu s přesností 10 µm a hardwarově na napětí na svém analogovém výstupu [140]. Využitím dvou těchto poupravených snímačů a řídicí jednotky na platformě Arduino, která signál ze senzorů zpracovává, vznikl základ měřicí a řídicí jednotky celého systému. Pohon odtahu struny a pohon cívky byl realizován stejnosměrnými motory se šnekovými převodovkami a rastrovací vedení struny pomocí šroubovice a krokového motoru. Byla vyvinuta řídicí aplikace ovládající všechny tyto komponenty a zajišťující komunikaci s PC. To díky naprogramované aplikaci znázorňuje graficky naměřené hodnoty průměru struny. Obsluha tak může zasahovat do procesu extruze filamentu a řízením otáček extruderu a otáček odtahu nastavit proces extruze tak, aby finální filament dosahoval požadovaných parametrů. Tento systém umožnil laboratorně vyrábět relativně přesné tiskové struny, které bylo možné použít pro přesný tisk a charakterizaci tiskového materiálu.



Obr. 16: Systém pro měření průměru filamentu (vstup filamentu zleva)

Vyvíjené materiály na bázi PHB tak bylo možno testovat na zakoupených 3D tiskárnách Průša, které umožňují nastavení širokého rozsahu tiskových podmínek. Zejména v rámci přiděleného projektu **PR 4** pak bylo snahou optimalizovat vlastnosti těchto materiálů pro FDM 3D tisk. V publikaci **Pub 9** byly prezentovány první výsledky vlastností PHB kompozitních materiálů na bázi kaolinu a vápence. Zde byl řešen problém vyhodnocení negativního efektu teplotního smrštění během tisku (warping) a navržena metoda jho měření. Protože vápenec byl prodegradační zejména pro PLA obsažené v polymerní matrici, byl dále využíván pouze kaolín. Následná práce, která probíhala i v rámci řešení diplomové práce **VSKP4**, byla publikována v **Pub 10**. Optimalizace složení směsi byla založena na tříparametrovém pětiúrovňovém plánovaném experimentu (Design of Experiment - DoE), kde byly použity tyto rozsahy:

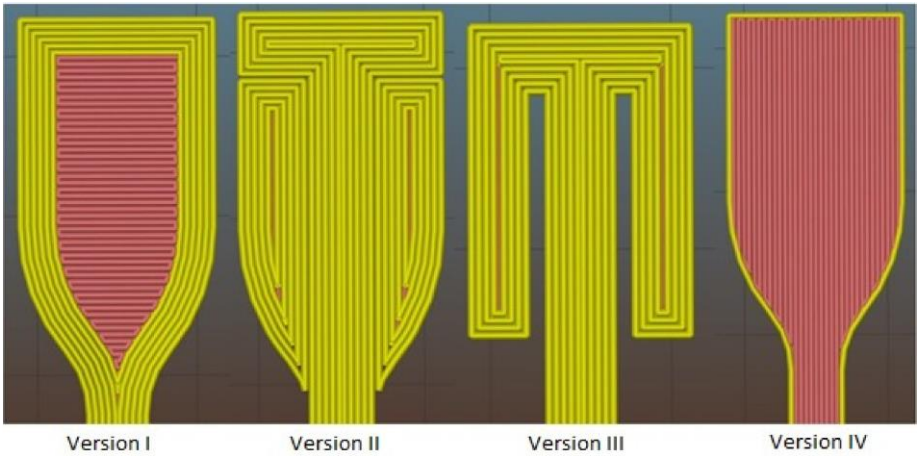
1) Obsah PHB v polymerní matrici (60 - 95 %)
2) Obsah změkčovadla 8 - 15 % (podíl hmotnosti změkčovadla ku polymerní matrici (PLA + PHB))
3) Obsah plniva kaolinu 5 - 20% (podíl hmotnosti kaolinu ku polymerní matrici (PLA + PHB))

Limity rozsahů odpovídaly kódovaným hladinám -1.682 and 1.682, střední hodnota pak kódované hladině 0. V experimentu byly sledovány základní materiálové vlastnosti jako Youngův modul pružnosti v tahu, pevnost v tahu, rázová a vrubová houževnatost, teplota měknutí při ohybovém zatížení (HDT) a koeficientu deformace při tisku (warping koeficient). Ze stanovených závislostí na výše uvedených parametrech (kódovaných hladinách) byly navrženy optimální receptury, první pro dosažení maximální hodnoty HDT a druhá pro zabezpečení minimálního koeficientu deformace při tisku. Tyto vybrané optimalizované receptury byly pro ověření reálně připraveny a charakterizovány za stejných podmínek. Výsledky ukázaly, že bylo možné touto optimalizací úspěšně dosáhnout vytýčených hodnot. Výsledek byl pak prezentován ve formě prototypu **V5**.

Využití plastifikátorů je v případě PHB směsí nepostradatelným nástrojem modifikace mechanických vlastností. Přídavek plastifikátoru ovlivňuje reologické chování taveniny, termickou stabilitu polymeru, biokompatibilitu, biodegradabilitu apod. Proto byla problematice změkčení PHB směsí pro 3D tiskové materiály věnována pozornost v experimentech, jejichž výsledky byly publikovány v úspěšném článku **Pub 11**. Jedním z cílů bylo nalézt komerční změkčovadlo vhodné pro tyto směsi. Sledován byl efekt přídavku 15 % změkčovadla na dosažené mechanické vlastnosti, ty však byly sledovány v čase a dávány do souvislostí s měřenou migrací změkčovadla z materiálu. Materiál byl testován jak ve formě tiskové struny, tak na finálním výtisku ve tvaru dogbone 5A.

Příprava testovacích těles technologií 3D tisku je pro účely charakterizace materiálu ve své podstatě nevhodná. 3D tisk vnáší do objemu materiálu defekty a i při snaze vytisknout 100% plné těleso jsou v materiálu přítomny póry. Rozhraní mezi jednotlivými liniemi není zpravidla tak pevné, jako samotný materiál. Navíc snaha o výtisk 100% plného tělesa naráží také na problém deformace tělesa při tisku, tento efekt se s požadovaným množstvím výplně zvyšuje. Na druhou stranu 3D tiskové technologie jsou uznávány jako výrobní metoda prototypů a dnes už i funkčních dílů [141]. I ty musejí splňovat specifikace výrobku z pohledu mechanických vlastností a je třeba je nějakým způsobem reprodukovatelně měřit. O co nabízí 3D tisk větší možnosti designu výrobků z pohledu tvaru, dutin, směrovosti a tvaru vnitřní výplně, nebo dokonce i výtisku ze dvou či více materiálů, o to je komplikovanější pohled na jeho chování při zatížení. To pak souvisí s parametry tiskového procesu, orientací výrobku při tisku na podložce a samozřejmě vlastností samotného tiskového materiálu.

I přes obrovský rozvoj této úspěšné technologie výroby neexistoval v r. 2017 žádný standard pro měření charakteristik 3D tištěného tělesa z termoplastů. Snahou této studie tak bylo nalézt vhodné testovací těleso pro tahovou zkoušku, které bude při tahovém namáhání co nejvíce reflektovat chování samotného materiálu. Bylo tak postupně testováno několik variant designu tělesa ve tvaru dogbone s planparalelní částí tvořenou liniemi pouze ve směru hlavní osy. Problematická se ukázala místa uchycení tělesa do čelistí a místa napojení zaoblení lopatek na planparalelní testovací část. Postupnou eliminací míst, kde vznikala nežádoucí koncentrace napětí, byl odladěn návrh spočívající ve střídání dvou vzorů (I a IV Obr. 17), který umožnil díky vzájemné orientaci linií v lopatkách dosáhnout dostatečné pevnosti k tomu, aby deformace materiálu testovacího tělesa nastávala pouze v planparalelní části. Podmínkou je dosažení dostatečné soudržnosti tiskových linií, která je nejen funkcí parametrů tisku (zejména teploty a rychlosti tisku), ale také chemické struktury materiálu. Stejně tak je třeba opticky nebo vážkově monitorovat úroveň zaplnění tělesa materiálem [141].



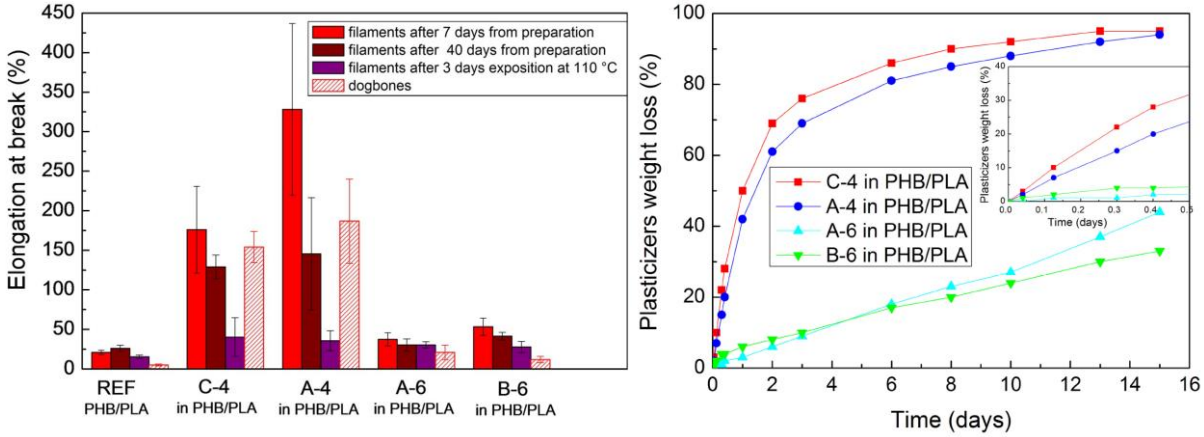
Obr. 17: Varianty návrhů lopatek testovacího tělesa ve tvaru dogbone

Dnes již existují, nebo jsou v přípravě normy, které budou snad brzy pomocníkem při sjednocení testovacích metod pro tyto složité systémy:

- ISO/ASTM 52900:2015 Additive manufacturing — General principles — Terminology
- ISO/DIS 27548 Additive manufacturing of plastics — Environment, health, and safety — Test method for determination of particle and chemical emission rates from desktop material extrusion 3D printer
- ISO/ASTM 52903:2020 Additive manufacturing — Material extrusion-based additive manufacturing of plastic materials

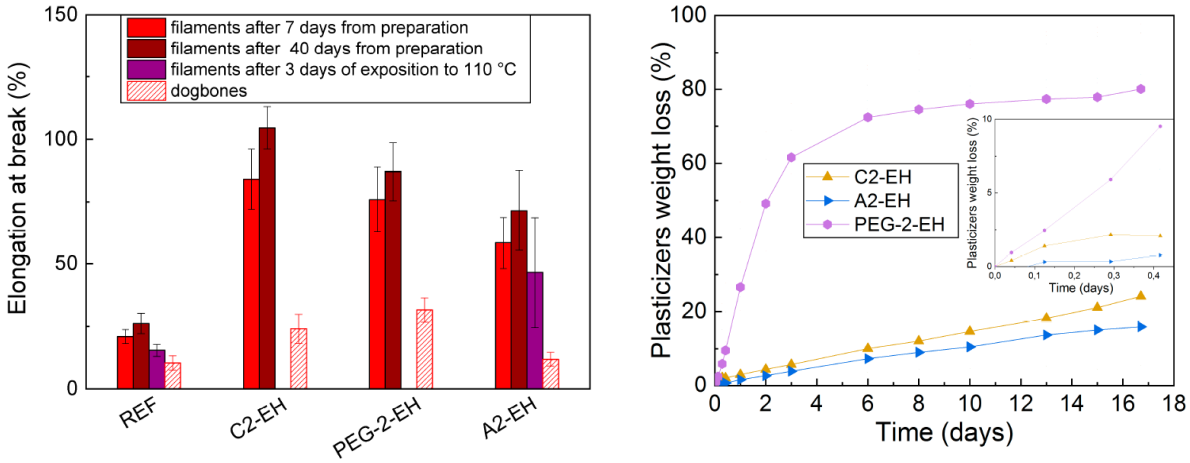
V hojně citované studii **Pub 11** byly použity čtyři komerční nízkomolekulární plastifikátory na bázi esterů kyseliny citrónové a všechny tvořili dobře mísitelnou směs PHB/PLA/změkčovadlo v poměru 60/25/15. Jejich významný změkčovací účinek a vliv na strukturu byly potvrzeny tahovými zkouškami a měřením na DSC. Zejména plastifikátory acetyltributylcitrát (A-4) a tributylcitrát (C-4) zlepšily prodloužení při přetržení o 308 % a 155 %, ve srovnání s neměkčenými směsmi. Významný plastifikační účinek potvrdily i tahové zkoušky na těchto 3D tištěných vzorcích, i když hodnoty tažnosti byly nižší než u vzorků měřených ve formě tiskového filamentu (Obr. 18a). Změkčovadla butyryltrihexylcitrát (B-6) a acetyltrihexylcitrát (A-6) zlepšila prodloužení při přetržení o 32 %, respektive o 16 %. DSC potvrdilo, že zavedení nízkomolekulárního změkčovadla do směsi PHB/PLA způsobilo větší mobilitu makromolekulárních řetězců. V důsledku toho se teploty krystalizace a tání posunuly k nižším hodnotám. Butylestery kyseliny citrónové způsobily pokles PLA T_g o 35 °C pro C-4

a o 33 °C pro A-4. Větší délka alkylových řetězců vázaných na kyselinu citrónovou naopak vykazovala horší plastifikační účinek a vedla k vyššímu PLA T_g. Z migračních testů na Obr. 18b je zřejmé, že rychlost difúze je silně závislá na velikosti molekuly změkčovadla. I z toho důvodu byly hledány další změkčovadla s vyšší molekulovou hmotností.



Obr. 18: a) Dosažené hodnoty tažnosti, b) Vývoj úniku změkčovadla z testovaného materiálu při 100 °C

V navazující práci **Pub 12** byl výběr změkčovadel postaven na etylhexyl derivátech kyseliny citronové a polyetylenglykolu s molekulovou hmotností 528–570 g·mol^{-1}. V orientačních screeningových testech totiž vycházely tyto deriváty také velmi slibně. Metodika testů byla velmi podobná jako v předešlé studii, ale byla doplněna o sledování reologické stability, měření rázové houževnatosti. Celá optimalizace tiskových parametrů byla založena na již propracované metodice hodnocení warpingu a vyhodnocení vytištěných speciálních geometrických prvků. Ty byly usazeny do obvodových stěn tělesa a následně navršeny opakovaně nad sebe. Každé patro takto vzniklé věže je pak tištěno nižší teplotou. Příliš vysoká nebo i nízká teplota se projeví nedokonalostmi v provedení detailů těchto prvků. Lze tak vizuálně vyhodnotit optimální rozsah teploty tisku a případně otestovat při tisku mezi tiskaři uznávaného standardního tělesa lodičky Benchie.

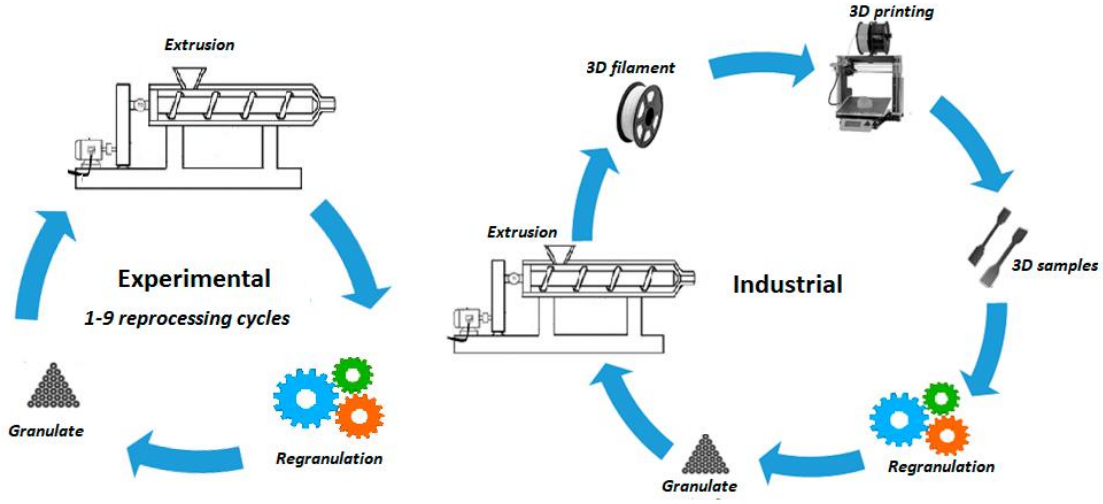


Obr. 19: a) Dosažené hodnoty tažnosti, b) Vývoj úniku změkčovadla z testovaného materiálu při 100 °C

Všechna 3 změkčovadla byla dobře mísitelná s matricí PHB-PLA, avšak tisk s PEG-2-EH vykazoval neuspokojivou kvalitu výtisků. Plastifikační účinek změkčovadel nebyl tak výrazný jako u předtím použitých citrátů (Obr. 19a) a byl potvrzen také pomocí DSC, kdy přídavek způsobil snížení T_g PLA amorfní fáze o 6 °C (C2-EH) a o 4 °C (A2-EH). Změkčovadlo PEG-2-EH překvapivě způsobilo snížení PLA T_g o 37 °C. Dále bylo provedeno měření stability viskozity pomocí oscilační reometrie a distribuce molekulové hmotnosti. Výsledky ukázaly na prodegradační chování PEG-2-EH v PHB/PLA směsích.

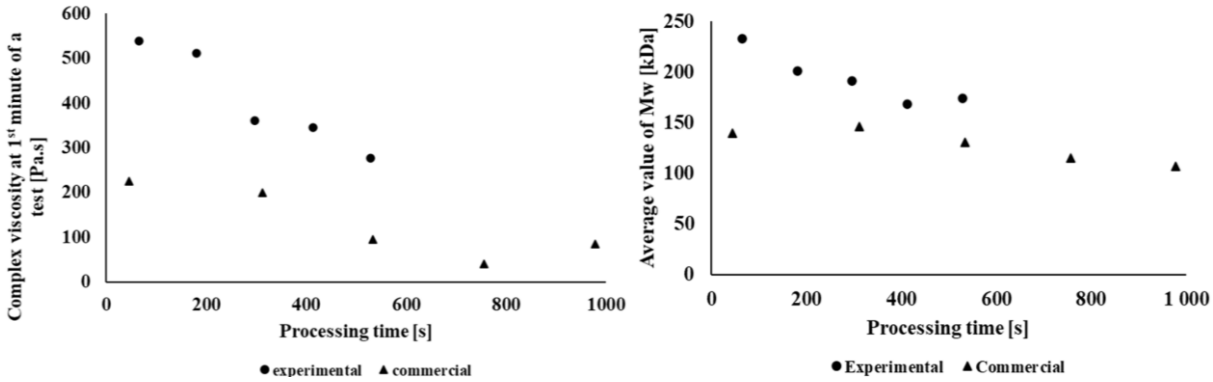
Plastifikátor PEG-2-EH také vykazoval na migračních testech poměrně velkou migraci. Tavenina s estery kyseliny citrónové (C2-EH a A2-EH) vykazovala dobrou stabilitu a změkčovadla měla nízkou tendenci migrovat ze vzorku i za poměrně nepříznivých podmínek 110 °C (Obr. 19b).

Materiály pro 3D tisk jsou často kritizovány z pohledu možností jejich recyklace. Zejména 3D tisk prototypů a často nepovedených výtisků vybízí k zamyšlení nad strategií recyklace materiálu zpět do podoby tiskové struny. Proto bylo cílem ověřit chování materiálu při klasické materiálové jednodruhové 100% recyklaci (viz **Pub 13**). Byly provedeny 2 experimenty, kde byl materiál NONOILEN® 3D 3056-2 podroben zátěži násobného procesu extruze tiskové struny (experimental) a kombinaci extruze a 3D tisku reálného vzorku (industrial/commercial) viz Obr. 20.



Obr. 20: Navržené a testované způsoby recyklace 3D tiskového materiálu na bázi PHB

Materiály byly v každém cyklu sledovány měřením následujících parametrů: komplexní viskozita taveniny pomocí reometrie, distribuce molekulových hmotností pomocí GPC, mechanické vlastnosti v tahu a ohybu na tištěných vzorcích a změna jejich barevnosti. Z výsledků lze konstatovat, že materiál dle předpokladů podléhal termické degradaci a snižovala se molekulová hmotnost a tím i viskozita taveniny (Obr. 21). I přes to, že se pohybovala i pod 100 Pa·s však bylo možné vyrobit tiskovou strunu a z ní 3D tiskem testovací vzorek.



Obr. 21: Pokles viskozity a hmotnostně střední molekulové hmotnosti během recyklačních cyklů

Se zpracovatelskou dobou také mírně rostla barevná odchylka od původní barvy referenčního vzorku a vzorek mírně tmavnul, což bylo pozorováno i u vstřikovacího typu v **Pub 7**. Napětí na mezi kluzu i napětí při porušení klesly o cca 20 % na celém rozsahu měřené doby zpracování. Tažnost

měřená na strunách už z původně nízkých hodnot cca 10 % dále nijak výrazně neklesala. U 3D tištěných těles byl po prvním cyklu zaznamenán velký pokles, nicméně materiál byl stále schopen 3D tisku. Je tedy možné tvrdit, že recyklace tohoto materiálu umožňuje jeho využití v 3D tisku v minimálně dvou cyklech, než dojde k vyššímu poklesu viskozity taveniny.

4.7 Přínos

V r. 2016 vznikl záměr vyvinout 3D tiskový materiál na bázi biodegradabilního a biokompatibilního PHB, který se opíral o do té doby získané zkušenosti se zpracováním PHB. Záměr byl od r. 2017 řešen v rámci získaného projektu PR4. V té době nebyly na VUT v Brně k dispozici laboratorní zařízení na výrobu kalibrované struny a nebyla k dispozici jednotná metodika charakterizace těles z 3D tištěných termoplastových materiálů. Ve stejném roce se také objevuje teprve první publikace na téma PHA pro FDM 3D tisk [115]. Po posledních deseti letech prudkého nárůstu publikací zabývajících se zpracováním PHA a jeho 3D tiskem mohou některé výsledky získané na začátku tohoto poměrně krátkého období působit z dnešního pohledu možná až naivně. Je však satisfakcí, že jsou klíčové publikace týmu Laboratoře bioplastů na téma 3D tisku PHB, zejm. **Pub 12** (2018 - 59 citací) a **Pub 13** (2020 - 29 citací), od r. 2019 citovány v obdobně zaměřených článcích a review (např. [142], [143], [113] a další).

Jak ukazuje i rešerše [144] vydaná r. 2018, FDM tisk materiálů na bázi PHB byl v tom roce na svém úplném počátku. Přínosem z tohoto pohledu jsou proto v tu dobu prezentované výsledky Laboratoře bioplastů s dosaženými vlastnostmi vyvíjených materiálů. Výsledky ukázaly, že je možné dosáhnout hodnot tažnosti materiálu s majoritou PHB i přes 150 %, kdy po akcelerované migraci změkčovadla dosahovaly tažnosti nad 25 %, což byla v literatuře zpravidla nedosažená hodnota (u vzorků zpracovaných v tavenině). Výtisky testovacích těles dokonce vykazovaly hodnoty tažnosti nad 100 % i po 7 dnech po vytištění.

Díky optimalizaci výroby kalibrované struny pomocí sestrojeného odtahového zařízení a vyvinuté metodice optimalizace tiskových parametrů a charakterizace 3D tištěného materiálu bylo možné dosáhnout velmi dobré kvality výtisků z těchto materiálů. Celému týmu tyto zásadní zkušenosti navíc umožnily následnou orientaci na vývoj medicínských aplikací, o kterých pojednává následující samostatná kapitola.

5 KOMPOZITY PRO FDM 3D TISK NA BÁZI PHB PRO MEDICÍNU

5.1 Motivace

Lidské zdraví je nenahraditelnou devizou člověka. Přestože má lidský organismus až neuvěřitelnou schopnost regenerace, nastávají situace, kdy je zásah do procesu hojení nezbytným krokem k záchraně zdraví anebo alespoň k minimalizaci negativních dopadů onemocnění nebo zranění. Moderní medicína se v poslední době zaměřuje na aplikace přizpůsobené přímo na míru pacienta a to nejen z pohledu vlastního farmaceutika, ale v případě, kde je to relevantní, také z pohledu tvaru aplikovaného materiálu. (protetika, dentální medicína, ortopedie, chirurgie apod.). Jednou ze slibných technologií výroby takových unikátních finálních výrobků na míru je 3D tisk. Poškození kostí je jeden z nejčastějších zdravotních problémů. I přes značnou regenerační schopnost kostní tkáně je v některých případech (například osteoporóza, tumor, infekce a další objemné defekty) nutný zásah moderní medicíny [145].

5.2 Současný stav

Jeden z nejmodernějších přístupů, které současná regenerativní medicína využívá, je tkáňové inženýrství. V tomto multidisciplinárním oboru se využívá nosiče neboli skafoldu (z anglického scaffold) jako podpůrného materiálu, který se následně osadí buňkami a/nebo případně dalšími podpůrnými látkami (růstovými faktory, léčivy atd.). Osazený skafold se použije se jako implantát k regeneraci poškozené tkáně a během hojení se zcela vstřebá. Nároky kladené na materiál skafoldu jsou vysoké, základním požadavkem je vhodná buněčná odpověď, neméně důležité jsou mechanické a povrchové vlastnosti či struktura [146]. V případě kostní tkáně musí být materiál navíc osteokonduktivní, tzn. stimulující růst kostní tkáně v místě implantátu, a osteoinduktivní neboli vyvolávající osteogenní diferenciací místních kmenových buněk [147], [148], [149].

Pro přípravu skafoldů určených pro náhrady kostní tkáně se využívá celá řada materiálů [150], [151], [152] včetně polymerů přírodního (kolagen, kyselina hyaluronová, PHA nebo celulóza) i syntetického původu (polylaktid, poly(ε-kaprolakton), poly(butylen sukcinát), a další) [153]. Velmi důležitou roli hraje i bioaktivní keramika, která se používá jak samostatně, tak pro přípravu polymerních kompozitů [154], [150], [155]. Nejčastěji využívaná jsou bioaktivní skla a vápenato-fosfátová keramika (obecně označovaná CaP), mezi kterými se využívá hlavně fosforečnan vápenatý (TCP, tricalcium phosphate) a hydroxyapatit (HA) [156]. CaP napodobují minerál přirozeně se vyskytující v kosti, jsou biokompatibilní, resorbovatelné a osteokonduktivní, jelikož vážou protein fibronektin, který poskytuje matrici pro usazení buněk [150].

Aby mohly buňky prorůst skrz celý objem skafoldu a vytvořit tak novou tkáň, musí mít skafold vhodnou 3D strukturu [157]. Existují různé techniky k vytvoření porézní struktury, jako například odlévání roztoku nebo taveniny do forem, lyofilizace, napěňování, vymývání rozpustných částic smísených se základní matricí, nebo různými technikami zvlákňování [153], [158], [159]. Ty mají značné nevýhody – nepravidelnost struktury, póry, které nejsou otevřené, nesnadná výroba pórů v oblasti 200-500 µm apod. V současné době se s úspěchem vyžívá metoda 3D tisku neboli aditivní výroby, při které se výrobek vytváří podle přesného digitálního 3D modelu a umožňuje vyrobit časově a finančně efektivně komplexní tvary včetně porézní vnitřní struktury [160], [161], [162].

Nejmasověji využívaná technika 3D tisku je FDM tisk představený v předchozí kapitole. Komerční materiály pro FDM 3D tisk zahrnují dnes celou škálu materiálů včetně: ABS, PA, PETG, PLA, PP, nebo flexibilní materiály jako TPU, či TPE. V poslední době se objevují i biodegradabilní materiály a biopolymery [144], [163], [164], [165], [166].

Pro 3D tisk skafoldů pro náhrady kostní tkáně metodou FDM tisku začal nejprve využívat poly(ε-kaprolakton (PCL). V r. 2001 publikoval Hutmacher a kol. 3D tištěná tělesa z PCL se strukturou pláství (honeycomb) a skládaných linií v různých úhlech pokládky (lay-down pattern). Pro skafold tištěný v úhlech 0/60/120° reportoval tuhost měřenou v tlaku 42 MPa. Připravené skafoldy byly osazeny lidskými fibroblasty a osteoprogenitorovými buňkami, oba typy buněk vykazovaly vhodnou adhezi a proliferaci ke skafoldu [167]. Ve stejné době, jako se začaly objevovat první výtisky z PCL, byly publikovány i výsledky tisku skafoldů pro náhradu kostí FDM 3D tiskem z polylaktidu (PLA). PLA má oproti PCL výhodu vhodnějších mechanických vlastností a lepší tisknutelnosti, je to ostatně globálně nejpoužívanější materiál pro 3D tisk. Xiong a kol. vytvořili v r. 2001 jednoduchý mřížkový skafold z PLA pelet s pevností měřenou v tlaku 8 MPa [168].

Vzhledem ke komplexním požadavkům kladeným na skafoldy je neustálá snaha jejich vlastnosti vylepšovat, a to: povrchovými úpravami; optimalizací 3D tištěné struktury; přídavkem bioaktivního plniva; nebo použitím směsí biopolymerů. Z toho důvodu lze pro každý potenciální materiál pro kostní náhrady v literatuře nalézt celou řadu dílčích studií zabývajících se buď optimalizací 3D tisku tohoto materiálu, nebo jednou z výše uvedených metod úpravy jeho výsledných vlastností (například PCL [169], [170], [171], [172], [173], kompozit PCL s TCP [174], [175], [176] nebo PCL s bioaktivním sklem [177]). Kompozitní materiál PCL/TCP byl testován dokonce *in vivo*, v r. 2010 skafold osazený lidskými mesenchymálními kmenovými buňkami (hMSC) na modelu kritického defektu stehenní kosti krys [174], 2015 na modelu prasečí dolní čelisti [175]. V současné době je PCL/TCP materiál schválený pro použití v kraniofaciální oblasti u lidí [178] a je dostupný i komerčně [179].

Vývoj 3D tisku PLA na poli kostních náhrad pomocí všech metod tisku je v review [180]. Pro skafoldy z PLA byla pozorována vhodná životaschopnost a růst osteosarkomových buněk [181] a u osteoblastů dokonce vyšší viabilita než na titanu [182]. Co se týče struktury skafoldu, v současné době se jako nejvhodnější zdá gyroidní struktura poprvé popsaná NASA r. 1970, která je optimalizovaná pro nejvyšší specifickou pevnost (vztaženou na hmotnost) [183]. V r. 2018 byly úspěšně vytisknuty gyroidní skafoldy z PLA za pomocí ve vodě rozpustitelných podpor z polyvinylalkoholu [184]. Důkladně je prostudována i mechanická odezva gyroidu [185]. Eryildiz publikoval třístupňové skafoldy se zvyšující se porozitou směrem do středu, avšak vytisklé vzorky se svou strukturou značně lišily oproti modelu ve slicovacím programu [186]. Dobré výsledky dosahuje i PLA plněná bioaktivním TCP [187], [188], [189], bioaktivním 45S5 sklem [190] a nejčastěji HA [187], [191], [192], [193], nano HA [194], [195], [196]. Pro kompozit krystalické PLLA s 50 hm. % hydroxyapatitu bylo na dvou pacientech s poraněním dolní čelisti pozorováno lepší hojení kosti než s titanem [191].

První výsledky 3D tisku polymerů ze skupiny PHA se objevují později a s použitím metody práškového spékání (Selective Laser Sintering, SLS), nejprve pro kopolymer PHBV a jeho kompozit s fosforečnanem vápenatým [197], poté v r. 2012 z PHB [198]. Pro porézní těleso za optimalizovaných podmínek byl reportován modul měřený v tlaku 23 MPa a pevnost 1,7 MPa [199]. Další studie na 3D tisk PHB metodou SLS se objevuje až v r. 2018 [200], Diermann a kol. se mezitím intenzivně věnoval

SLS 3D tisku PHBV [201], [202], [203]. V r. 2014 byly také úspěšně vytisknuty skafoldy z kompozitní pasty PHBH/biosklo ve směsi chloroformu a dimethyl sulfoxidu [204].

Termická nestabilita a komplikovaná zpracovatelnost PHA popsaná v předchozích kapitolách představuje pro 3D tisk FDM metodou velký problém. Až v r. 2016 bylo ke 3D tisku použito PHB, které prošlo maleací a bylo s přídavkem uhlíkových nanotrubek, čímž byla posunuta teplota počátku degradace [205]. Na poli materiálů pro tkáňové inženýrství se PHA z počátku objevují jako druhý polymer ve směsi s PCL [206] nebo PLA [207], [208], [209]. Například v komerčním filamentu od firmy ColorFabb obsahující 88 % PLA doplněný o PHBV [210].

Ve stejné době (2018 – 2020) naše laboratorní skupina vyvíjela směsi pro FDM 3D tisk s majoritou PHB, výsledky těchto prací jsou prezentovány v kapitole výše. Metodou FDM byly v r. 2020 vytištěny také skafoldy z PHBH, které jsou biokompatibilní s myšími 3T3 buňkami a rozložitelné v syntetické žaludeční šťávě [211] a PHBH kompozitem s acetylovanou nanocelulózou [212]. O rok později byly publikovány skafoldy z PHBV/45S5 bioskla [213]. V nedávné době se počet studií na FDM 3D tisk PHA, jejich směsí a kompozitů zvyšuje a dostává se jim více a více pozornosti [214], [215], [216], [217], [218], avšak ne všichni autoři své výsledky zakončují biologickými testy, které jsou v tomto poli nezbytné [218], [121], [119], [219].

Co se týče PHB, jako přírodní materiál nabízí v poli tkáňového inženýrství kostí přirozenou biokompatibilitu a bioresorbovatelnost. Degradační produkty PHB jsou tělu vlastní a nezpůsobují zánětlivou reakci [220]. Navíc, PHB disponuje mechanickými vlastnostmi, které jsou pro přípravu náhrad tuhých tkání vhodnější než u jiných používaných polymerů, jako kolagen, kopolymer PLA s glykolidem (PLGA), nebo PCL [221], [222], [223].

5.3 Cíle

Cílem práce je vyvinout materiál na bázi PHB vhodný pro výrobu filamentu pro FDM 3D tisk a pro použití v regenerativní medicíně, konkrétně jako skafold pro náhradu a regeneraci kostní tkáně. K dosažení cíle je nutná kombinace několika znalostí z různých oborů, a to konkrétně (i) znalosti zpracování PHB a kompaundace polymerů obecně, (ii) technologie a správné nastavení podmínek 3D tisku bioplastů, (iii) znalost odpovídajících testovacích metod pro splnění požadavků na mechanické, povrchové a biologické vlastnosti skafoldů. Podle toho se hlavní cíl výzkumu dělí na jednotlivé dílčí cíle. První dílčí cíl je navrhnout a případně optimalizovat nový biomateriál, který bude disponovat vhodnými termickými, reologickými a mechanickými vlastnostmi pro zpracování do formy 3D tiskové struny, a jeho vlastnosti charakterizovat. Druhý dílčí cíl je nalézt správné 3D tiskové podmínky pro daný materiál s pomocí know-how nově vyvinutých metod charakterizace tisknutelnosti a vlastní příprava testovacích těles pro charakterizaci. Tímto bude obohacena dosavadní materiálová základna pro FDM 3D tisk, kde se biopolymery s výjimkou PLA začínají teprve objevovat. Třetí dílčí cíl je otestovat biokompatibilitu materiálů a reakci buněk, jejich proliferaci, viabilitu, a příp. osteogenní diferenciaci, po osazení na nosiče připravené z navrhnutých materiálů.

5.4 Dosažené výsledky

5.4.1 Směsi PHB/PLA

První screeningové směsi na bázi směsi PHB/PLA vycházely z předchozích experimentů, kdy se poměr PHB/amorfní PLA 70/30 jevil jako optimální z hlediska zpracovatelnosti a výsledných mechanických

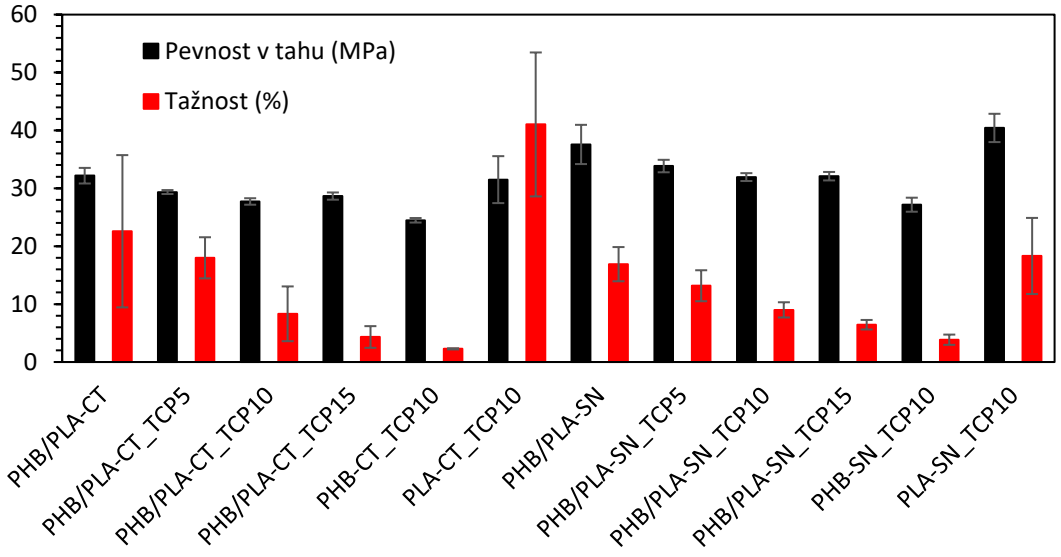
vlastností. Do směsi byl přidán plastifikátor v obsahu 12 hm%. Testovány byly dva typy změkčovadel, které se prokázaly jako netoxické, nízkomolekulární derivát kyseliny citronové Citroflex® B-6 (butyl trihexyl citrát, CT) a oligomerní adipát Syncroflex 3114 (SN). Pro zlepšení buněčné odpovědi bylo do směsi přidáváno i biokeramické plnivo, a to směs minerálů hydroxyapatitu a trikalcium fosfátu HA/TCP (D_{50} 10,8 µm, TCP směs αTCP a βTCP v poměru α/β 7/93, výrobce CN Lab Nutrition).

Celkem bylo připraveno dvanáct vzorků, šest s obsahem CT a šest s obsahem SN. U každé série byl připraven jeden neplněný vzorek obsahující oba polymery a změkčovadlo a tři plněné vzorky, viz tabulka 2. Další dva vzorky obsahovaly jen jeden z polymerů, změkčovadlo a 10 hm. % HAp/TCP.

Tabulka 2: Připravené směsi na bázi PHB/PLA

	PHB (%)	PLA (%)	Citroflex B6 (%)	TCP (%)		PHB (%)	PLA (%)	Syncroflex 3114 (%)	TCP (%)
PHB/PLA-CT	62	26	12	-	**PHB/PLA-SN**	62	26	12	-
PHB/PLA-CT_TCP5	59	25	11	5	**PHB/PLA-SN_TCP5**	59	25	11	5
PHB/PLA-CT_TCP10	56	24	11	9	**PHB/PLA-SN_TCP10**	56	24	11	9
PHB/PLA-CT_TCP15	54	23	10	13	**PHB/PLA-SN_TCP15**	54	23	10	13
PHB-CT_TCP10	80	-	11	9	**PHB-SN_TCP10**	80	-	11	9
PLA-CT_TCP10	-	80	11	9	**PLA-SN_TCP10**	-	80	11	9

Práce s těmito vzorky byla předmětem bakalářské práce Kateřiny Chaloupkové, za svobodna Svoradové, kde je možné dohledat další detaily (**VSKP5**). U připravených materiálů byly charakterizovány tepelné vlastnosti pomocí TGA a DSC, kde byl pozorován lepší změkčovací efekt aditiv Citroflex na polymerní směs oproti Syncroflex. Ze všech vzorků ve formě granulátu byly vytvořeny filamenty na 3D tisk s průměrem 1,75 mm. U vzorků byly nalezeny optimální tiskové podmínky – teplota trysky a množství extruze tzv. flow a následně mohly být vytisknuty testovací tělesa pro tahovou zkoušku, jejíž výsledky jsou na obrázku Obr. 22.



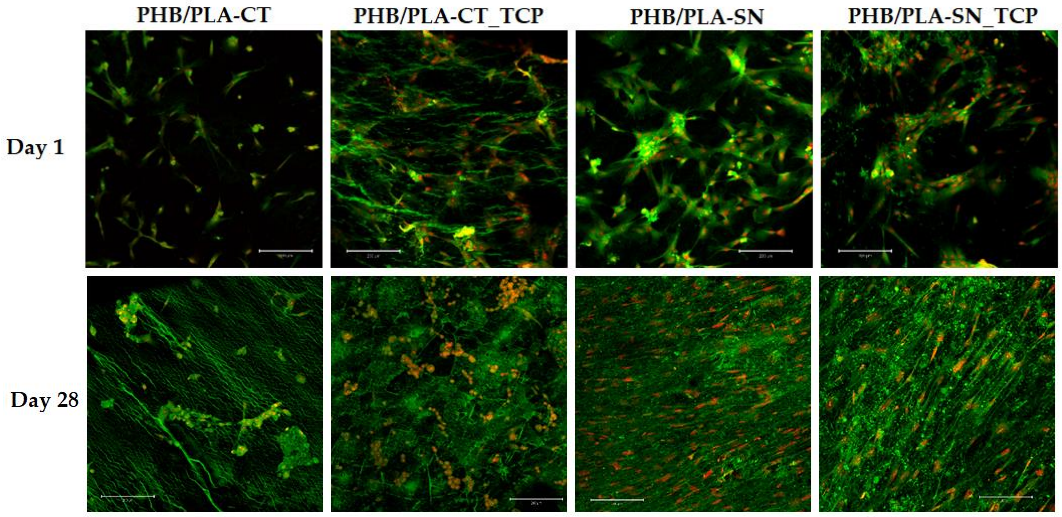
Obr. 22: Výsledné mechanické vlastnosti přepravených kompozitů

Modul pružnosti byl naměřen v rozmezí 2,2–2,6 GPa s výjimkou vzorků PLA bez přídavku PHB, kdy vzorek PLA-CT_TCP10 dosahoval až 3,3 GPa. Přídavek TCP zvýšil modul velmi málo, současně snížil pevnost i tažnost směsí. Nejvyšší pevnosti byly dosaženy u vzorků bez TCP a u vzorků PLA, a to cca 32 MPa pro vzorky změkčené Citroflexem a 38-40 MPa pro vzorky změkčené Syncroflexem.

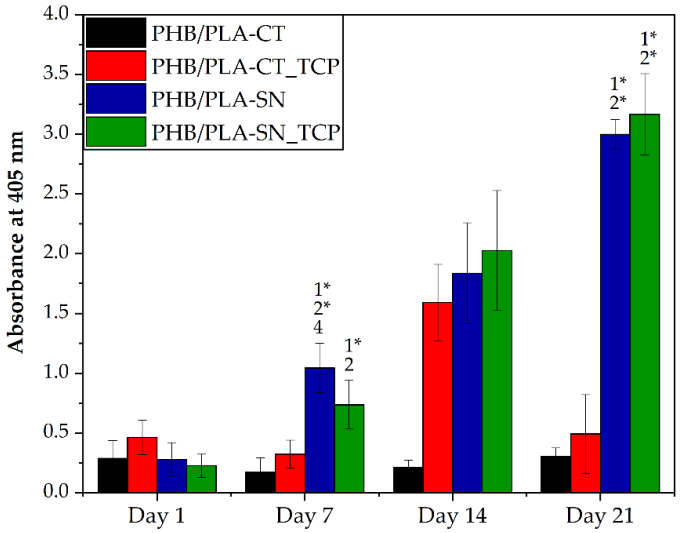
Mechanické vlastnosti kosti se v závislosti na typu kosti, věku pacienta a dalším liší. U kompaktní kosti v podélném směru je modul pružnosti v tahu kolem 18 GPa a pevnost v tahu 135 MPa, což je stále několikanásobně výš, než bylo dosaženo [224].

Výsledky testů neplněných vzorků PHB/PLA s oběma změkčovadly a odpovídající vzorky s maximálním plněním TCP, tedy PHB/PLA-CT, PHB/PLA-CT_TCP15, PHB/PLA-SN a PHB/PLA-SN_TCP15 byly publikované v **Pub 14 (2020)**. U těchto vzorků byla kromě PHB/PLA-CT_TCP15 zjištěna nižší míra warpingu při 3D tisku než u komerčního PLA Průša filamentu. Také byly zjišťovány ohybové vlastnosti důležité vzhledem k častému porušení kosti ohybovou deformací. U vzorků se SN byl z výsledků patrný žádoucí nárůst ohybového modulu i pevnosti v ohybu s rostoucím přídavkem TCP.

V neposlední řadě byla na Ústavu experimentální medicíny AVČR provedena řada biologických testů na jednoduchých skafoldech (kolečka o průměru 5 /6 mm vyražená z lisované desky o tloušťce 1 mm). Skafoldy byly sterilizovány ethylen dioxidem a osazeny lidskými mezenchymálními kmenovými buňkami (hMSC, Sciencell). Na obrázku (Obr. 23) jsou vidět fotografie z konfokální mikroskopie na začátku a konci testu, Obr. 24 prezentuje výsledky ALP testu.



Obr. 23: Vizualizace buněk na skafoldech na začátku a na konci testu



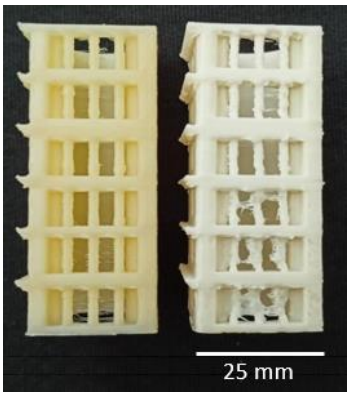
Obr. 24: Test aktivity alkalické fosfatázy

Z fotografií je vidět mnohem větší množství buněk u vzorků obsahujících adipátové změkčovadlo Syncroflex. Kromě počtu jsou také buňky rovnoměrnější rozprostřeny a mají protáhlý tvar, což

naznačuje jejich dobrou kondici. Naopak u vzorků s Citroflexem se hlavně v pozdějších stádiích testu nachází ve shlucích a neporůstají povrch skafoldu. Testy osteogenní diferenciace navíc jednoznačně potvrdily, že vzorky obsahující Syncroflex jsou pro materiál kostních náhrad vhodnější než vzorky s citrátovým změkčovadlem. U ALP testu je 21. den vidět násobně vyšší míra osteogenní diferenciace vzorků PHB/PLA-SN a PHB/PLA-SN-TCP15. Tyto dva vzorky tedy nejen že jsou vhodné pro 3D tisk metodou FDM, ale mají i potenciál pro použití jako bioaktivní materiál pro tkáňové inženýrství kostí.

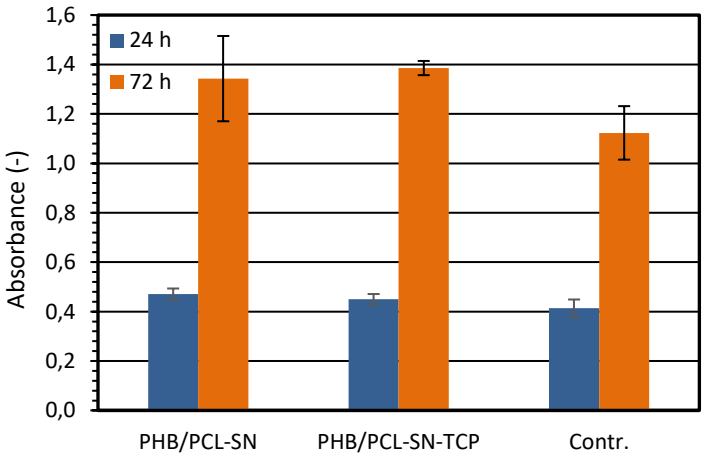
5.4.2 Směsi PHB/PCL

Na základě těchto výsledků byly studovány v rámci diplomové práce **VSKP9** i směsi obsahující místo PLA polykaprolakton, polymer tradičně využívaný pro tkáňové inženýrství kostí, jak bylo popsáno na začátku kapitoly. Byly tedy připraveny dva vzorky analogické ke dvěma nejúspěšnějším vzorkům z předchozí studie, a to PHB/PCL-SN (62 % PHB, 26 % PLA a 12 % syncroflex 3114) a PHB/PCL-SN_TCP (54 % PHB, 23 % PLA, 10 % Syncroflex 3114 a 13 % TCP). Tyto výsledky byly publikovány v **Pub 15 (2023)**. Vzhledem k rozdílné teplotě tání obou polymerů je stěžejní najít vhodnou teplotu tisku. PCL má při teplotě tání PHB nízkou viskozitu taveniny, což vede k nadbytečné extruzi materiálu a snížení geometrické přesnosti výtisku, jak je vidět na obrázku níže (Obr. 25).



Obr. 25: Teplotní věž vytištěná ze směsi PHB/PLA (vlevo) a PHB/PCL (vpravo)

Na těchto materiálech byl proveden test biokompatibility výluhů s myšími 3T3 fibroblasty, podobně jako v předchozí kapitole. Na obrázku Obr. 26 jsou uvedeny výsledky MTS testu po 24 a 72 h, kdy je vidět vynikající viabilita buněk, která je dokonce vyšší než v případě kontrolního vzorku.



Obr. 26: Výsledek cytotoxicity výluhů pro vzorky na bázi PHB/PCL

Vhodná teplota tisku je v tomto případě mnohem nižší než u směsí s PLA, a to 175 °C pro neplněný vzorek a 165 °C pro vzorek s TCP. Při těchto teplotách směsi s PCL vykazují nejnižší míru warpingu

s warping koeficientem 1,3 a 1,5 pro neplněný a kompozitní vzorek. To je nižší hodnota než pro odpovídající směsi s PLA. Hodnoty pevnosti a modulu pružnosti jsou nižší, než v případě odpovídajících analogů s PLA, což je očekávané vzhledem k mechanickým vlastnostem čistého PCL. Modul naměřený v tlaku byl 0,3 GPa pro PHB/PCL-SN a 0,4 GPa pro PHB/PCL-SN_TCP, pevnost v tlaku 15 MPa a 18 MPa ve stejném pořadí. Pevnost kompaktní kosti v tlaku je kolem 200 MPa [224].

5.4.3 Povrchové vlastnosti 3D tištěných skafoldů

Bez ohledu na materiál skafoldu, první věcí, která přichází do kontaktu s hostitelským prostředím, je jeho povrch. Během biologických testů bylo pozorováno, že povrch vylisovaných skafoldů není pro použité hMSC buňky ideální, protože z něj vrstva buněk snadno sklouzla. Proto byly dále studovány povrchové vlastnosti, které řídí adsorpci proteinů a tím pak i interakci buněk [225], [226], a to volná povrchová energie (SFE), smáčitelnost vodou – kontaktní úhel vody (WCA) a drsnost.

Největší míra adsorpce fibronektinu a albuminu je dle literatury na povrchy s WCA 40-80° [227] pro hovězí sérový albumin, fibrinogen a lidské proteiny FXII pro povrchy s WCA > 60–65° (SFE pod 36,4 $mN \cdot m^{-1}$) [228]. Co se týče povrchové energie, podle rozsáhlých studií Lima a kol. lidské fetální osteoblastické buňky (hFOB) preferují pro středně dlouhou dobu interakce hydrofilní povrchy charakterizované SFE nad 40 $mN \cdot m^{-1}$ a WCA pod 60° [229], [230].

Výsledky naměřených kontaktních úhlů a vypočtené SFE směsí PHB/PLA a PHB/PCL ve formě vylisovaných desek jsou uvedeny v tabulce 3. Voda vykazuje největší kontaktní úhel ze všech testovaných kapalin, 72–74°, kromě vzorku PHB/PLA-SN_TCP, kde je to 61°. Pro všechny materiály je WCA pod 90°, což naznačuje jejich hydrofilní povahu. Podobně pro všechny vzorky kromě PHB/PLA-SN_TCP je naměřen nejnižší kontaktní úhel s dijodmetanem - nejméně polární testovanou kapalinou.

Přidání fosfátové keramiky do směsi na bázi PHB/PLA snížilo kontaktní úhel vody o 17 % a s diethylenglykolu o 9 %, zvýšila se tedy hydrofilita materiálu. Tento jev byl popsán pro čisté PHB [231]. V případě PHB/PCL se interakce s vodou a diethylenglykolem po přídavku TCP nezměnila.

Tabulka 3: Výsledné hodnoty měřené povrchové energie

		PHB/PLA-SN	PHB/PLA-SN_TCP	PHB/PCL-SN*1	PHB/PCL-SN_TCP*1			
Kontaktní úhel ± SD (°)	Voda	74,2 ± 1,0	61,4 ± 3,4	72.7 ± 3.5	72.1 ± 4.2			
	Dijodmetan	38,1 ± 1,9	40,2 ± 2,3	22.9 ± 1.4	35.1 ± 2.2			
	Formamid	48,0 ± 1,9	36,8 ± 2,8	55.5 ± 1.8	47.7 ± 2.7			
	Diethylenglykol	42,5 ± 2,7	38,7 ± 1,5	42.2 ± 1.6	43.3 ± 0.9	PHB*2	PLA*2	PCL*3
Celková povrchová energie γ_s ($mN \cdot m^{-1}$)		40	45	40	41	40,5	33,9	30.8
Disperzní část γ_s^d ($mN \cdot m^{-1}$)		31	27	30	30	36,5	30,9	26.1
Polární část γ_s^p ($mN \cdot m^{-1}$)		9	18	10	11	4	3	4.7

*1 **Pub 15**; *2 [232]; *3 [233]

Co se týče volné povrchové energie, z připravených směsí vybočuje pouze PHB/PLA-SN_TCP, zbylé směsi dosahují přibližně 40 $mN \cdot m^{-1}$, což je podobné jako u čistého PHB, s disperzní složkou okolo 30 $mN \cdot m^{-1}$ a polární složkou okolo 10 $mN \cdot m^{-1}$. Přídavkem změkčovadla a dalších polymerů jsme tedy

schopni zvýšit polární složku SFE a zvýšit hydrofilitu materiálu. SFE a její části pro materiály na bázi PCL a PHB/PLA-SN jsou srovnatelné s polyetheruretanem [234] nebo Nylonem 6-6 [235].

S přidáním TCP keramiky do měkčené biopolymerní směsi PHB/PLA se povrchová energie zvýšila o 13 %, na 45 $mN \cdot m^{-1}$. Současně se u vzorku PHB/PLA-SN_TCP zdvojnásobila polární složka oproti vzorku bez plniva, zatímco disperzní složka se snížila o 13 %. Taková hodnota SFE polární složky je podobná jako u používaného polystyrenu nebo proteinem potažených povrchů pro tkáňové kultury [234]. Tento materiál se z tohoto pohledu jeví pro adhezi kostních buněk jako velmi vhodný.

Dalším důležitým parametrem povrchu je jeho drsnost, protože kostní buňky mají vyšší preferenci k drsnějším povrchům [236], [237], [238]. Podle studie Kunzler a kol. krysí osteoblasty na povrchu s drsností od 1 do 6 µm preferují drsnější část [239]. Drsnost 3D tištěných vzorků byla studována na materiálech PHB/PLA-SN a PHB/PLA-SN-TCP15 s použitím základního nastavení – teplota trysky 195 °C, flow 100 %, povrch složený z paralelních linií, a to tryskou 0,4 a 0,25 mm. Vyhodnocena je drsnost podél tiskové linie a napříč tiskovými liniemi pomocí konfokální mikroskopie. Výsledky jsou v tabulce 4, zatímco vizualizace povrchů je na obrázku Obr. 27.

U vzorku PHB/PLA-SF jsou dobře patrné jednotlivé řádky tiskárny. Na druhou stranu vzorek s bioaktivním fosforečnanem vápenatým má rovnoměrnější povrch, kde v případě trysky 0,4 mm není jednoznačný směr tisku a převažuje tak vliv plniva na topografii. Celkově má vzorek PHB/PLA-SN přibližně dvakrát nižší hodnoty podélné drsnosti než jeho kompozitní analog, a to z důvodu přítomnosti částic TCP. S tryskou 0,4 mm vykazoval vzorek PHB/PLA-SN drsnost jednotlivých tiskových linií 6,7 µm, což by mělo být pro růst osteoblastu dle Kunzlera vhodné.



Obr. 27: Konfokální mikroskopie povrchů 3D tištěných vzorků PHB/PLA-SN (vlevo) a PHB/PLA-SN-TCP15 (vpravo) tryskou 0,4 mm, značka měřítka symbolizuje 160 µm

Je třeba poznamenat, že tyto materiály vykazují vyšší drsnost povrchu než 3D tištěné objekty uváděné v literatuře. U čistého PLA a trysky 0,25 µm byla pomocí AFM naměřena paralelní drsnost R_q 1,2 nm (27,6 nm po ošetření plazmou), což je o 3–4 magnitudy nižší, než bylo pozorováno u našich vzorků [240]. Při použití tiskové trysky 0,4 µm bylo pomocí AFM naměřeno R_q 92 nm [241] a 367,5 nm bylo získáno z mikroskopie SEM [242].

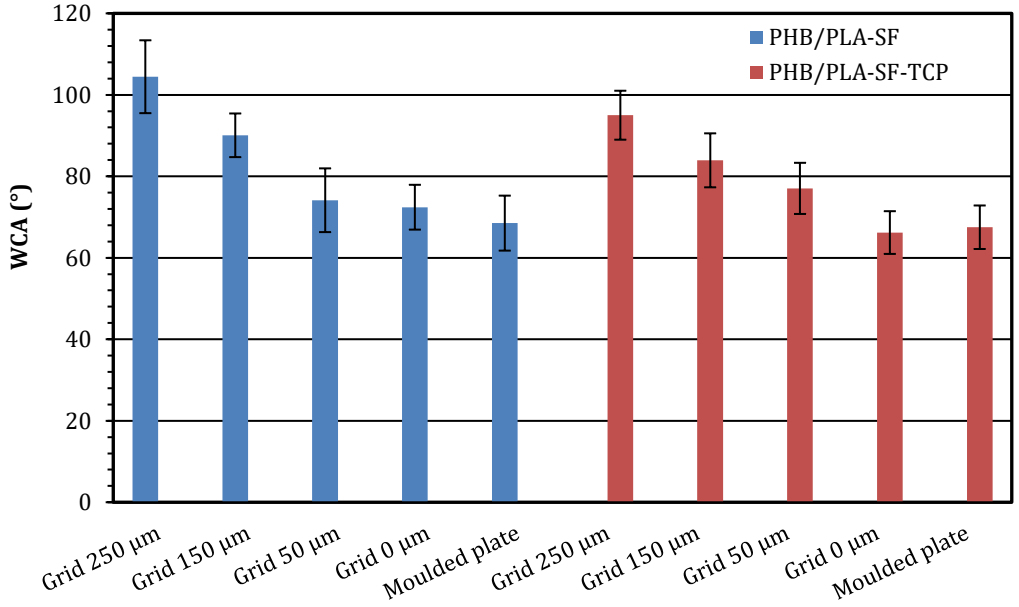
Tabulka 4: Drsnost povrchu 3D tištěných vzorků

	Podélná drsnost R_a (µm)		Příčná drsnost R_a (µm)	
Tryska (mm)	0,25	0,4	0,25	0,4
PHB/PLA-SN	2,1 ± 0,3	6,7 ± 2,5	20,7 ± 3,2	12,8 ± 1,0
PHB/PLA-SN_TCP	4,7 ± 0,6	12,4 ± 2,9	33,3 ± 3,4	12,2 ± 2,4

Příčná drsnost kolmo na směr tiskových linií je obecně vyšší než podélná (pro odpovídající materiál a průměr trysky), protože zohledňuje nejen vliv materiálového složení, ale také vliv topografie vytvořené 3D tiskem. Jedinou výjimkou je biokompozitní vzorek PHB/PLA-SN_TCP s tryskou 0,4 mm; obě hodnoty jsou srovnatelné kolem 12 µm. To potvrzuje jednotný povrch pozorovaný mikroskopem.

Při trysce 0,25 mm je příčná drsnost vyšší u vzorku PHB/PLA-SN_TCP než u směsi bez biokeramického přídavku, podobně jako v případě paralelní drsnosti. Na druhou stranu u povrchů potištěných tryskou 0,4 mm je drsnost mezi 12,2–12,8 µm pro oba materiály. V tomto případě je drsnost povrchu spíše řízena strukturou než materiálem.

U vzorků s výraznou povrchovou strukturou je ovlivněna i smáčivost vodou. Pro 3D tištěné vzorky se strukturou tvořenou paralelními liniemi a mřížkou s různou velikostí oka (50, 100, 150, a 250 µm) imitující 3D strukturu skafoldu byl změřen WCA a výsledky jsou uvedeny v grafu níže (Obr. 28). Nejnižší hodnoty WCA, kolem 70°, bylo dosaženo u lisovaných desek. 3D tištěný vzorek s plnou vrchní vrstvou (mřížka 0 µm) dosahuje WCA srovnatelného s vylisovaným vzorkem v rámci chyby měření. S výskytem mřížky na povrchu se WCA lineárně zvyšuje díky tzv. efektu lotosového květu [243]. Směrnice nárůstu je vyšší u vzorku PHB/PLA-SN, který má nižší polární složku SFE. Povrch s velikostí oka mřížky 250 µm dosáhl WCA 105° pro PHB/PLA-SN a 95° pro PHB/PLA-SN_TCP, což je 52% a 41% nárůst ve srovnání s lisovaným vzorkem. Vzhledem k výsledkům z literatury by měl být pro adhezi proteinů z testovaných povrchů nejvhodnější povrch tvořený mřížkou o velikosti oka 50–100 µm.



Obr. 28: Kontaktní úhel vody na 3D tištěných površích

5.4.4 Optimalizace složení směsí PHB/PLA/SN/TCP

V kapitole 5.4.1 byly představeny první slibné směsi pro materiály kostních náhrad. Nedosahovaly však optimálních mechanických vlastností, proto byla provedena optimalizace metodou třífaktorového pětiúrovňového plánovaného experimentu. Výsledky jsou součástí diplomové práce **VSKP7**. Byly zvoleny následujícími faktory:

1) Faktor 1 = PLA/PHB
2) Faktor 2 = bioaktivní plnivo/(PHB+PLA)
3) Faktor 3 = změkčovadlo/(PHB+PLA+plnivo)

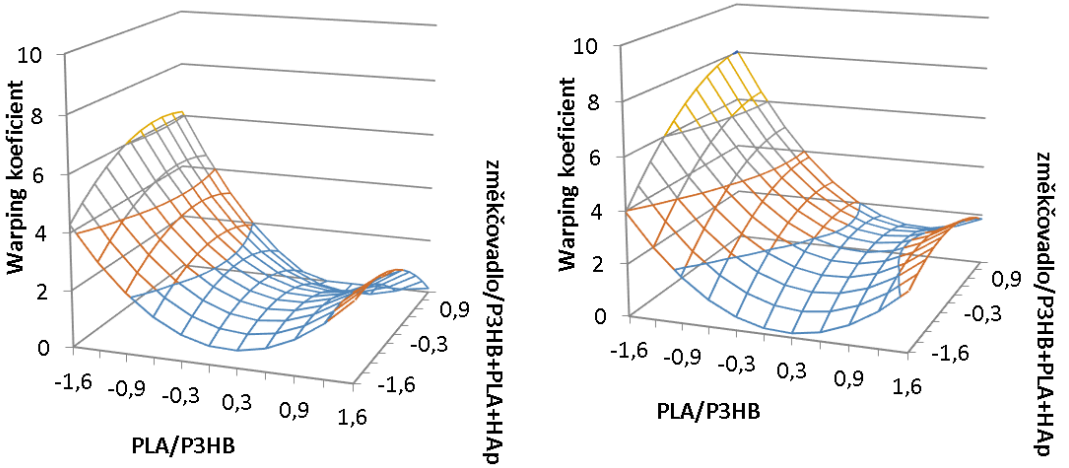
Prvním faktorem je poměr PLA/PHB v rozsahu hmotnostních poměrů 50/50–95/5 tak, aby ve směsi byla vždy majorita PHB. Ve druhém faktoru je poměr bioaktivního plniva/(PHB+PLA) v rozsahu hmotnostních poměrů 5/95–30/70, vzhledem k očekávanému limitu zpracovatelnosti při vysokém plnění. Třetí faktor byl zvolen jako změkčovadlo/(PHB+PLA+plnivo) proto, že změkčovadlo interaguje se všemi třemi složkami systému. Množství změkčovadla se z předchozích experimentů osvědčilo v rozmezí 7–11 %. Aby bylo toto rozmezí pokryto, bylo zvoleno rozmezí poměrů 5,6/94,4–12,4/87,6.

V rámci experimentu bylo připraveno celkem 20 vzorků (Tab. 5). Jako změkčovadlo byl použit osvědčený Syncroflex 3114 (SN). Bioaktivní minerál byl zakoupen od firmy Alchimika a obsahoval směs HA a TCP, označován je jako HA. Vzorky jsou uvedeny v tabulce. Jako označení vzorku bylo zvoleno zkrácené složení vzorku udávající poměr PHB/PLA, následně množství HA a poslední číslo názvu udává množství změkčovadla. Vzorky s číselným označením 9–14 mají ve svém složení vždy jeden faktor v krajní mezi experimentu. Vzorky s číselným označením 15–20 mají shodné složení a byly připraveny za účelem stanovení experimentální chyby.

Tabulka 5: Složení vzorků PHB/PLA/SN/HA pro plánovaný experiment

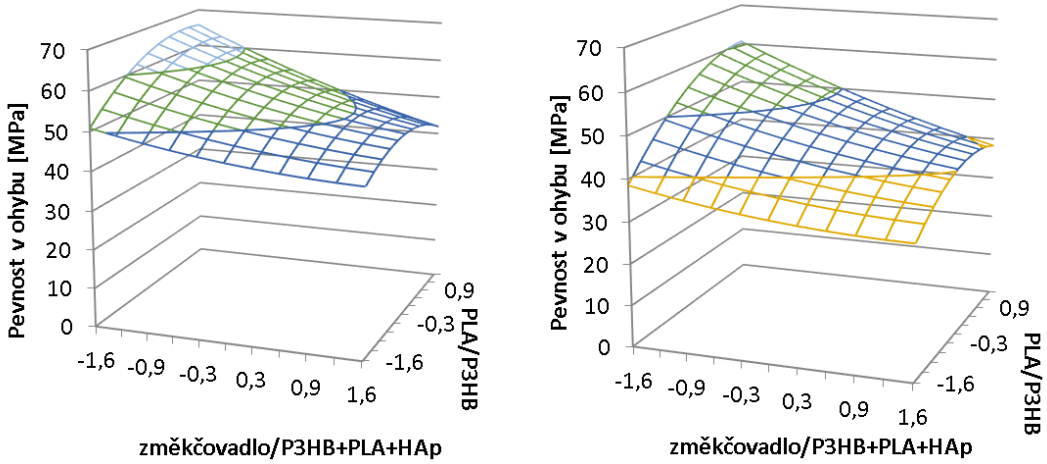
	Označení	PHB (%)	PLA (%)	SN (%)	HA (%)		Označení	PHB (%)	PLA (%)	SN (%)	HA (%)
1	80/20-11-7	66	16	7	11	**11**	66/34-5-9	57	30	9	5
2	55/45-11-7	46	37	7	11	**12**	66/34-27-9	42	22	9	27
3	80/20-24-7	55	14	7	24	**13**	66/34-18-6	50	26	6	18
4	55/45-24-7	38	31	7	24	**14**	66/34-17-12	46	24	12	17
5	80/20-10-11	63	15	11	10	**15**	66/34-18-9_1	48	25	9	18
6	55/45-10-11	44	35	11	10	**16**	66/34-18-9_2	48	25	9	18
7	80/20-23-11	53	13	11	23	**17**	66/34-18-9_3	48	25	9	18
8	55/45-23-11	36	29	11	23	**18**	66/34-18-9_4	48	25	9	18
9	95/5-18-9	70	4	9	18	**19**	66/34-18-9_5	48	25	9	18
10	50/50-18-9	37	37	9	18	**20**	66/34-18-9_6	48	25	9	18

Směsi byly kompaundovány dvoušnekového extrudéru značky LabTech (průměr šneků 16 mm, L/D 40) a 3D tiskové struny byly připraveny na jednošnekovém extrudéru HAAKE Rheomex OS (Haake Technik GmbH (průměr šneku 19 mm, L/D 30). Optimalizace 3D tiskových podmínek byla provedena metodou teplotních věží a následným měřením warping koeficientu.



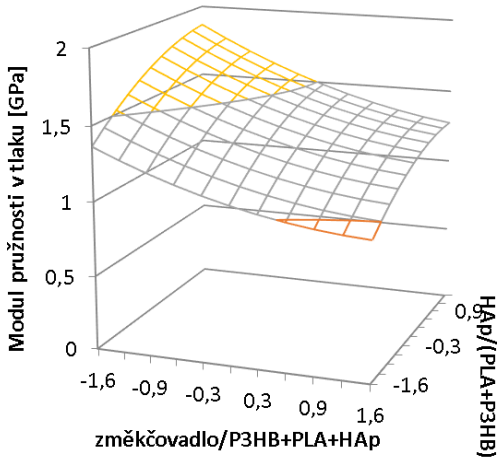
Obr. 29: Warping koeficient při nejnižším (vlevo) a nejvyšším testovaném množství HA (vpravo)

Statistickým zpracováním bylo zjištěno, že největší vliv na warping (přibližně 2–3× větší než ostatní) má faktor 1, tedy poměr polymerů PLA/ PHB. Uplatňuje se zde kombinace lineárního a kvadratického příspěvku. To je patrné na obrázku níže (Obr. 29), kde jsou znázorněny dvě plochy závislosti warping koeficientu na faktoru 1 (poměr PLA/PHA) a faktoru 3 (množství SN ve směsi) se zafixovanou hodnotou faktoru 2 (množství HA). Vlevo je plocha pro nejnižší testované množství HA, a vpravo je plocha pro nejvyšší testované množství HA. Přídavek PLA do směsi PHB/PLA snižuje warping koeficient. Zároveň vlivem kvadratického koeficientu existuje v závislosti minimum, kterého je žádoucí dosáhnout. Pro srovnání, hodnota warping koeficientu pro komerčně dostupný filament PLA (Prusa Research, Prague, Czech Republic) je 2,9 ± 0,1. Nejhůře tisknutelný je materiál s označením 95/5-18-9, který obsahuje nejvyšší obsah PHB z testovaných vzorků a je velmi křehký.



Obr. 30: Plocha pevnosti v ohybu při nejvyšším (vlevo) a nejnižším (vpravo) testovaném množství HA

U všech materiálů byly testovány mechanické vlastnosti při namáhání v ohybu a tlaku, které simulují napětí přirozeně působící na kosti. Modul pružnosti měřený v ohybu se u všech vzorků pohybuje v rozmezí 2,3–3,7 GPa. Největší vliv na něj má dle statistického vyhodnocení obsah změkčovadla, čím větší obsah, tím nižší modul. Pozitivní vliv má naopak přídavek PLA a HA, efekt je však 1–2x slabší. Závislost pevnosti v ohybu na faktoru 1, PLA/PHB, a faktoru 3 poměru změkčovadla ku zbylým složkám směsi je vidět v následujícím obrázku (Obr. 30). Stejně jako v případě modulu, faktor 1 má největší vliv a pevnost snižuje.



Obr. 31: Plocha modulu pružnosti v tlaku při středním poměru PHB/PLA

Ze zkoušky v tlaku byl vyhodnocen modul z lineární oblasti deformace (1,25-1,5 %), který se pohybuje v rozmezí 0,9–1,8 GPa, tedy o zhruba polovinu než při namáhání v ohybu Obr. 31. Vliv na

modul má pouze obsah HA, jehož přídavek modul zvyšuje, a změkčovadlo, které modul snižuje, jak je vidět v grafickém znázornění dole. Vzorky byly měřeny do 10% deformace a do této hodnoty nedocházelo k porušení a u některých vzorků ani ke kluzu, proto pevnost nebyla vyhodnocována.

Z výsledků je možné najít složení směsi, která bude mít ideální vlastnosti pro tkáňové inženýrství kostí v dosažitelném rozsahu, a to: minimální warping, maximální ohybová pevnost a maximální tlakový modul. Složení receptury, která dosahuje tyto požadavky je: 35,2 % PHB, 30,8 % PLA, 28,3 % HA a 5,6 % SN. Teoretické a dosažené vlastnosti této směsi jsou uvedeny v tabulce 6. Připravená optimalizovaná směs dosahovala o polovinu nižšího modulu v tlaku, než byla teoretická hodnota, zatímco modul naměřený v ohybu byl predikován přesně. Naměřená hodnota pevnosti v ohybu je o 18 % nižší než teoretická hodnota. Připravená směs také vykazovala mez kluzu při namáhání v tlaku kolem 9 % relativní deformace, a to s maximem 54,6 ± 1,3 MPa. Udávaná pevnost v tlaku kompaktní kosti je 205 ± 17 MPa, dosahujeme tedy přibližně čtvrtiny [224].

Tabulka 6: Teoretické a naměřené vlastnosti optimalizované směsi

	Warping koeficient (-)	Modul měřený v ohybu (GPa)	Pevnost v ohybu (MPa)	Modul měřený v tlaku (GPa)	Pevnost v tlaku (MPa)
Predikované	1,0	3,3	59,7	2,3	-
Změřené	2,54 ± 0,08	3,2 ± 0,1	48,8 ± 0,6	1,2 ± 0,1	54,6 ± 1,3

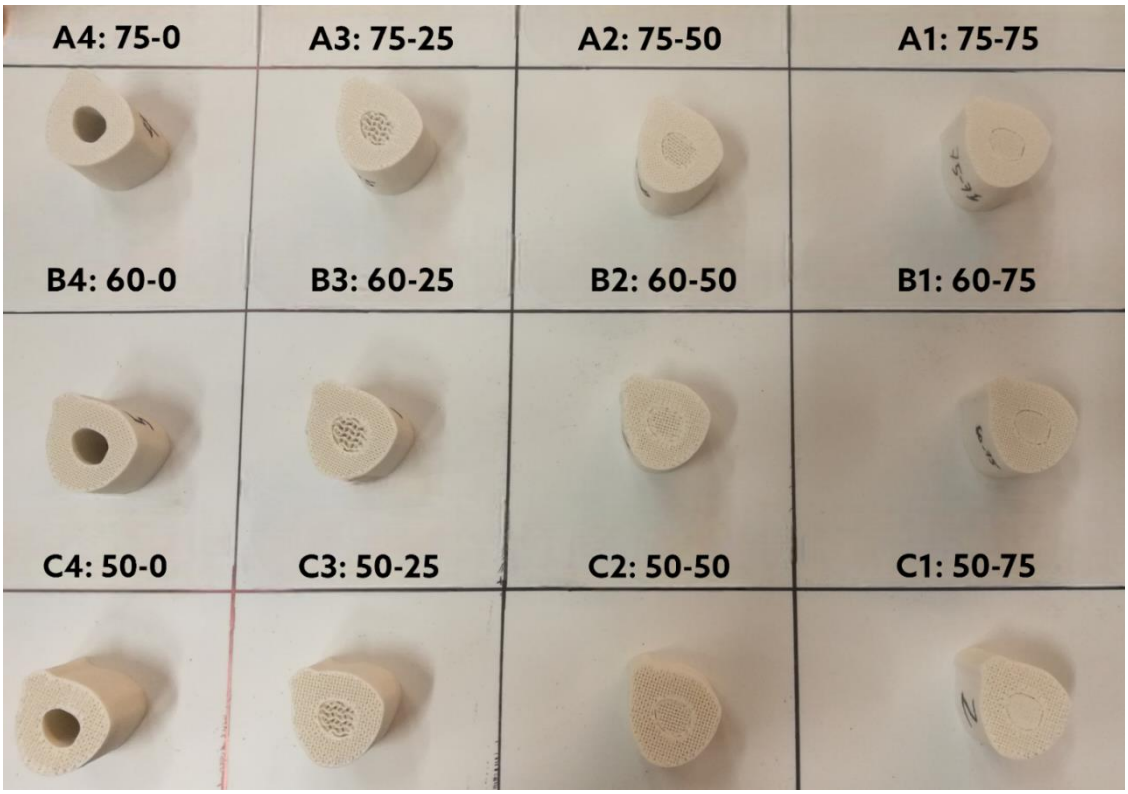
5.4.5 Skafold pro náhradu segmentu femuru

Optimalizovaná receptura PHB/PLA/TCP/HA byla využita pro návrh, výrobu a mechanickou charakterizaci anatomického modelu segmentu diafýzy femuru vytvořeného podle CT obrazů femuru skutečného pacienta v rámci diplomové práce **VSKP10**. V místě kompakty a spongiózy reálné kosti byly v 3D modelu variovány parametry výplně gyroidní struktury pomocí programu Rhinoceros 3D.

Tabulka 7: Maximální tlaková síla způsobující porušení vnitřní struktury PHB/PLA/TCP/HA anatomického modelu segmentu femuru u zvolených 12 variant vnitřní struktury (n = 10)

Varianta hustoty výplně gyroidu	A (kompakta 75 %) [kN]	B (kompakta 60 %) [kN]	C (kompakta 50 %) [kN]
1 (spongióza 75 %)	22,2 ± 0,5	15,8 ± 1,2	12,5 ± 0,8
2 (spongióza 50 %)	19,1 ± 1,1	14,5 ± 1,0	12,0 ± 0,5
3 (spongióza 25 %)	18,3 ± 0,3	13,0 ± 0,6	13,3 ± 1,0
4 (spongióza 0 %)	18,0 ± 0,5	12,8 ± 0,3	10,1 ± 0,4

Byla stanovena únosnost v tlaku dvanácti variant vytištěných 3D modelů segmentu femuru s různou procentuální hustotou jejich vnitřní gyroidní výplně (viz obrObr. 32) s výsledky uvedenými v tabulce 7. Nejvyšší síla na mezi únosnosti segmentu femuru byla dosažena se 75% výplní v místě kompakty i spongiózy (varianta A1), a to 22,20 ± 0,50 kN. Se snižující se hustotou vnitřní výplně při zachování vnější struktury únosnost klesá až na 18,00 ± 0,50 kN pro těleso varianty A4, které vnitřní část neobsahuje. Stejný trend lze pozorovat i u varianty B s vnější výplní 60 % a C s vnější výplní 50 %. Rostoucí únosnost v tlaku v závislosti na rostoucím množství materiálu je výsledek očekávaný. Přínosem jsou však reálné hodnoty únosnosti v tlaku v porovnání s porozitou materiálu, která je klíčová pro proliferaci buněk a vlastní přestavbu materiálu v kostní tkáň. Nejnižší dosažená únosnost (vzorek C4, 50% vnější výplň, bez vnitřní výplně) je 10,1 kN je v přepočtu 1030 kg, což je téměř 15 krát více než je průměrná váha člověka.



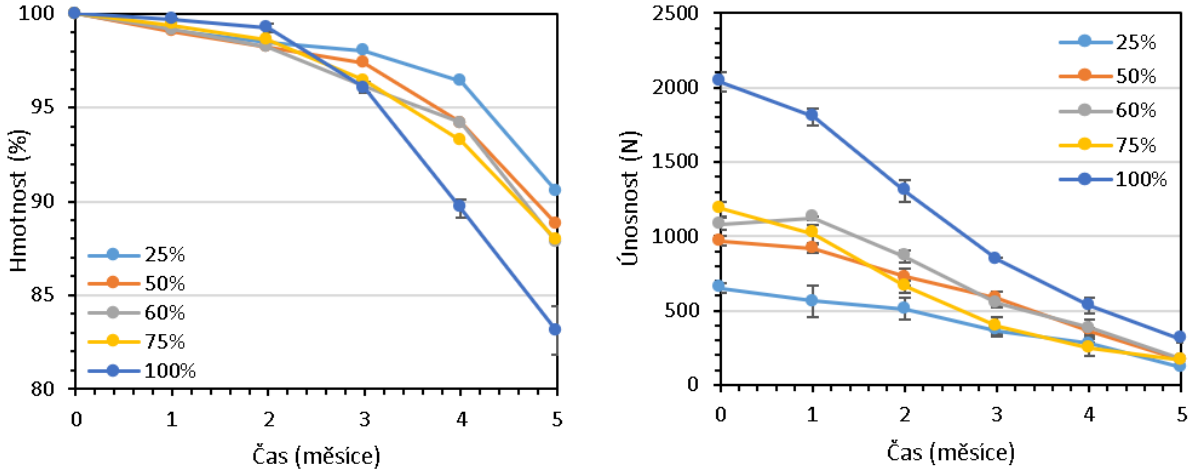
Obr. 32: Vytištěné 3D modely segmentu diafýzy femuru s různou procentuální vnitřní výplní gyroidem v místě kompaktní a spongiózní kosti

Následně byla studována možnost predikce únosnosti v tlaku nově vyvinutého anatomického modelu segmentu femuru pomocí počítačové simulace s využitím numerického modelu v programu ANSYS. Mezi naměřenými hodnotami a predikovanými byly zjištěny rozdíly v hodnotách únosnosti v tlaku. Ty byly přisouzeny odlišnostem mezi reálnou a navrženou strukturou gyroidní výplně. Tyto odlišnosti jsou způsobeny nedokonalou technikou 3D tisku v případě takto jemné struktury. Na mikroskopii byly prokázány defekty v rovinách kolmých k rovině pohybu trysky při tisku. Jde o známý problém nedokonalého spojování jednotlivých vrstev tisku, který při složitější struktuře vytváří defekty [184]. Předností gyroidní struktury je spojitost stěn, která je však díky těmto defektům narušena. Stejně tak byly pozorovány odchylky v tloušťce stěny gyroidní struktury oproti modelu.

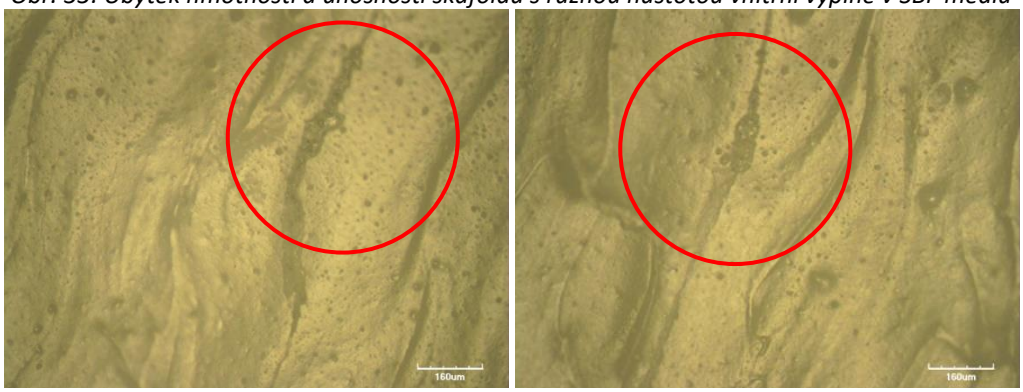
Modul pružnosti v tlaku byl zaznamenán v rozsahu 0,8–1,2 GPa se srovnatelným trendem jako v případě únosnosti v tlaku v závislosti na druhu výplně spongiózy a kompakty. Jak již bylo zmíněno, modul pružnosti kompaktní části kosti je okolo 18 ± 4 GPa, u porézní kosti v oblasti femuru je to 0,4 ± 0,3 GPa [224]. Značný rozptyl u spongiózní kosti je dán různým obsahem minerálních látek v kosti pacienta, kdy se pro krček stehenní kosti udává rozptyl modulu od 50 do 600 MPa [244]. I jiné práce publikují střední hodnotu modulu spongiózy v tlaku kolem 100–600 MPa [245], [245], [246].

V případě implementace skafoldu do těla je nutná dodatečná fixace, takže od samotného skafoldu není vyžadováno nést celou váhu pacienta. Pro úspěšnou náhradu původního materiálu kosti je i tak výhodné se co možná nejvíce přiblížit struktuře a mechanickým vlastnostem původní kosti. Zde tedy záleží na tom, zda se nahrazuje (*i*) segment kosti zasahující i do kompaktní i spongiózní části; nebo (*ii*) pouze houbovitá část, která je náchylnější k onemocnění. Pro oba případy je možné vybrat vhodnou kombinaci struktur, případně zvolit materiál s jinou mechanickou odezvou, viz předchozí kapitola.

Nakonec byla testována hydrolytická degradace 3D tištěných struktur v médiu simulujícím složení krevní plazmy (simulated body fluid, SBF) připraveného dle Kubobo a Takadama [247]. Vytištěna byla normovaná tělesa na zkoušku v tlaku s různou hustotou vnitřní výplně tvořené gyroidem, podobně jako v případě tištěných segmentů femuru (25, 50, 60, 75 a 100 %). V grafech níže je vidět úbytek hmotnosti a únosnosti v tlaku vytištěných těles v průběhu 5 měsíců (Obr. 33).



Obr. 33: Úbytek hmotnosti a únosnosti skafoldů s různou hustotou vnitřní výplně v SBF médiu



Obr. 34: Tvorba hydroxyapatitu na povrchu tištěných struktur po 2 měsících v SBF

Nejvyšší stupeň hydrolýzy viditelný jak úbytkem hmotnosti (83 % původní hmotnosti po 5 měsících) tak na změně mechanických vlastností (15 % původní únosnosti na konci testu) byl dosažen u tělesa se 100 % výplní. U těchto těles pravděpodobně probíhá autokatalýza kyselými produkty degradace, která byla popsána pro PLA [248]. Tělesa s 50, 60 a 75% výplní vykazují velmi podobný pokles hmotnosti i změnu únosnosti v tlaku. Přibližně poloviny své původní únosnosti dosahují tělesa s vnitřní výplní 25, 50 a 60 % po 3 měsících testu a tělesa s výplní 75 a 100 % již po dvou měsících. Na konci testu dosahují všechny struktury 83–91 % své původní hmotnosti a 14–18 % své původní únosnosti (v přepočtu 12–30 Kg). Při testu byl pozorován mechanismus degradace v objemu, takže se předpokládá razantní úbytek hmotnosti v dalších měsících, který je v souladu s požadavkem lékařů na plnou resorpci skafoldu během 9 měsíců. Po dvou měsících testu na testovacích skafoldech začal precipitovat hydroxyapatit z SBF media (Obr. 34). To naznačuje, že by se takové těleso v *in vivo* prostředí pokrylo bioaktivní vrstvou a bylo dobře přijato hostitelským prostředím [247].

5.5 Přínos

Navrhované řešení spočívá ve výrobě filamentu pro 3D tisk metodu FDM, který byl navržen z bioaktivního kompozitu s majoritní složkou poly(3-hydroxybutyrátu), přídavkem dalšího biopolymeru (polylaktid nebo poly(ε-kaprolakton)), netoxického změkčovadla a biokeramického plniva. Složení výsledného materiálu bylo optimalizováno s ohledem na využití v tkáňovém inženýrství pro výrobu bioresorbovatelných kostních náhrad na míru pacienta.

Kostní defekty vznikají při zlomeninách, případně následkem chorob a při operacích a jsou velmi častým případem zdravotních problémů. Tyto defekty se dnes běžně léčí implantováním kostních štěpů, ideálně přímo z těla pacienta, případně od dárce, a to stejného i jiného živočišného druhu. Tyto metody však mají několik úskalí, jako možnost přenosu nemocí, omezenou dostupnost materiálu štěpu, případně odmítnutí tělem hostitele. Výzkum v oblasti hojení kostí je proto velmi důležitým a pro lidstvo potřebným směrem, a neočekává se, že by zájem o něj v blízké době opadl. Tkáňové inženýrství a vývoj speciálních materiálů pro tyto aplikace je přístup, který překonává všechny výše zmíněné nevýhody a v současné době se značně rozvíjí ruku v ruce se speciálními technologiemi zpracování. Metoda FDM 3D tisku je jednou z nich - nabízí obrovské možnosti při navrhování tvaru výsledného kostního implantátu – skafoldu. Na rozdíl od dalších způsobů výroby je tak touto metodou možné připravit implantát pacientovi na míru přímo podle defektu kosti.

Použitý materiál PHB je dle výsledků biokompatibilní, bioresorbovatelný a má mechanické vlastnosti, které ho předurčují k použití pro náhrady tvrdých tkání, jako např. kostí. Navíc, je možné jej zpracovat jako termoplast, takže je vhodný i pro 3D tisk metodou FDM. PHB je také možné jednoduše mísit s dalšími biopolymery, případně plnivy, k další optimalizaci jeho vlastností. Tento záměr tedy nově spojuje biomateriál s obrovským aplikačním potenciálem, nejmodernější přístupy regenerativní medicíny a navíc vysoce efektivní způsob zpracování - FDM 3D tisk. Dosažené výsledky jsou velmi slibné z pohledu procesu zpracování materiálu, biokompatibility i mechanických vlastností. Dosavadní práce ukazuje, že je možné řídit materiálové vlastnosti výsledného štěpu kostní tkáně jak materiálovými vlastnostmi kompozitu (a ty jeho složením), tak volbou vnitřní struktury 3D tištěného finálního štěpu. Výsledky chování materiálu v simulované tělní tekutině ukazují postupný rozklad materiálu v rychlostech, které jsou zřejmě adekvátní pro využití tohoto materiálu v případě reálné náhrady resorbovatelné kostní tkáně. Nicméně doposud prováděné testy v SBF jsou sice důležitým, ale jen orientačním testem, který nezodpoví reálnou rychlost resorpce v těle pacienta a nemůže nahradit *in vitro* experimenty. Z toho to důvodu bude výzkumná činnost v tomto tématu pokračovat s vhodným partnerem (Ceitec, VFU Brno apod.) na charakterizaci materiálu *in vivo* v modelových organismech.

6 NETKANÉ MIKROVLÁKENNÉ TEXTILIE NA BÁZI PHB PRO MEDICÍNU

Netkané textilie jsou druhem textilií, které se vyrábějí bez tradičního procesu tkaní nebo pletení vláken. Spojování vláken do soudržné podoby se v principu realizuje pomocí chemických procesů (např. síťování gelů), tepelných procesů (např. meltblown, spunbond) nebo mechanických procesů (např. vibrační výroba plsti apod.). Zvlákňovací metody polymerních netkaných textilií využívají různé způsoby tvorby samotného polymerního vlákna. Odlišují se zejména formou, ve které polymer vstupuje do zvlákňovací hlavy, principem zvláknění, tedy v podstatě silou (typem interakce), kterou je vstupní materiál formován do podoby vlákna a způsobem záchytu vlákna do finální podoby textilie.

Polymery mohou být zvlákněny z taveniny nebo z roztoku o vhodné viskozitě, která je kromě molekulové hmotnosti vstupního polymeru, případně vhodných aditiv, následně v procesu zvláknění řízená teplotou taveniny nebo koncentrací roztoku. Hnací silou procesu formování polymeru do podoby vlákna může být odstředivá síla na rotační hlavě trysek, gravitační, nebo odtahová síla vlákna, síly vznikající při interakcí s rychle proudícím plynem, nebo elektrostatická síla. Vytvořené vlákno je pak zachytáváno buď na tzv. kolektory nebo mřížky anebo na nosnou vrstvu často v podobě kovového nebo polymerního pásu, jiné netkané textilie, papíru apod. Síly, které přitlačí vlákno do vznikající struktury netkané textilie mohou být odstředivé, elektrostatické, magnetické nebo může být vlákno unášeno proudem vzduchu vedeným skrze prodyšnou nosnou vrstvu [249]. Mnohé metody využívají kombinaci více těchto jednotlivých principů [250]. Při některých metodách se využívá finální fixace vláken do vzniklé struktury netkané textilie kalandrováním.

Netkané textilie mají mnoho výhod a nacházejí široké uplatnění v medicíně v oblasti tkáňového inženýrství. Zde se v kontaktu s tkání používají nejčastěji buď jako prodyšné krycí membrány, nebo jako nosiče buněčných kultur, na kterých mohou buňky adherovat a růst. V druhém případě netkané textilie poskytují strukturální podporu novým buňkám tkání a umožňují difuzi živin a odpadních látek mezi buňkami a okolím. Tento proces je důležitý například při vytváření tkání a orgánů *in vitro*, které se pak mohou použít k léčbě nebo nahrazení poškozených tkání a orgánů v lidském těle.

Netkané textilie lze připravit s vlastnostmi na míru aplikaci. Jejich tloušťku, porozitu, velikost vlákna a hustotu sítě lze řídit procesem výroby. Biokompatibility textilie a nízké toxicity lze dosáhnout vhodným výběrem materiálu. Kombinací parametrů výrobního procesu, výběrem materiálu a případně aditiv lze pak nastavit mechanické vlastnosti. Umožňuje to dosáhnout flexibilních textilií, které mohou být tvarovány do různých forem, což umožňuje jejich použití pro různé typy tkání a orgánů. V případě, že je použit materiál schopný resorpce v organismu, může se tato netkaná textilie postupně rozkládat v těle a přetvářet na novou tkáň bez negativní reakce imunitního systému. Netkané textilie lze také modifikovat za účelem schopnosti uvolňovat účinné/léčivé látky inkorporované do materiálu resorbujících vláken. Do materiálu vláken lze také zabudovat vhodná aditiva, která ovlivňují diferenciaci buněk [251].

Polyhydroxyalkanoáty, na které je tato práce zaměřena, trpí nestabilitou svojí chemické struktury při procesech zpracování v tavenině. Viskozita taveniny, která je nutná pro zavedené průmyslové procesy výroby netkaných textilií Meltblown a Spunbond, musí být poměrně nízká z důvodu toku taveniny úzkými tryskami a nutného dloužení rozfukem vzduchu. Požadované hodnoty MFI se pohybují v rozmezí 30–1500 g·10 minut^{-1} [252].

Tato spodní hranice je však v technologické praxi požadována často mnohem vyšší. Viskozita PHB je poměrně strmě závislá na teplotě taveniny, ale teplota potřebná k dosažení takových hodnot viskozity přesahuje použitelný teplotní rozsah zpracování PHB [39]. Dochází tak k tepelné degradaci, tedy štěpení řetězců, snižování celé distribuce molekulové hmotnosti za tvorby krotonových a karboxylových konců. V případě nedokonale čištěného PHB, a tedy přítomnosti zbytkových proteinů a buněčných stěn, dochází navíc k napalování degradačních produktů těchto látek na stěny trysky a jejich zalepování, což působí v procesu zvláknění komplikace. Tyto zkušenosti získané při vývoji blendů pro zvlákňování PHB v tavenině byly jedním z impulsů k rozšíření portfolia zkoumaných technologií o roztokové metody.

6.1 Motivace

Biokompatibilita PHB, jeho prokázaná resorbovatelnost v lidském těle rozkladem na produkty tělu vlastní (hydroxymáselná kyselina), s jeho přírodním původem, a tím i biodegradovatelností v přírodních podmínkách, jsou důvodem velkého zájmu o tento materiál i v medicínských aplikacích [253]. Zejména ve vlákenné formě, která eliminuje křehkost, jako jednu ze slabých stránek PHB, lze dosáhnout materiálů flexibilních a poddajných, a to bez chemické modifikace PHB. Klasické zvlákňovací techniky termoplastických materiálů z taveniny mohou sice produkovat kvalitní vlákno na bázi PHB, jde však z výše zmíněných procesních důvodů zpravidla o blend s dalšími polymery, aditivy a stabilizátory, což je v případě využití pro tkáňové inženýrství zdrojem komplikací z pohledu biokompatibility a toxicity. Navíc, při zpracování termoplastů na bázi PHB v tavenině není možné se vyhnout termické degradaci polymerního řetězce a vzniku nežádoucích produktů těchto degradačních reakcí. Naopak v případě využití zvlákňovacích technik z roztoku je možné zachovat strukturní vlastnosti PHB (jeho molekulovou hmotnost, optickou i chemickou čistotu) a za předpokladu kompletního odstranění rozpouštědla z finálního produktu je výsledným materiálem čisté, termicky nedegradované PHB. Pochopitelným předpokladem pro tento výsledek je vhodně izolovaný a dostatečně čistý materiál již na vstupu. Vhodnou volbou parametrů technologie zvláknění z roztoku lze dosáhnout netkaných textilií s širokým rozmezím distribuce průměrů vláken, jejich orientace [254], [255] a stejně tak i široké škály velikosti prostoru mezi vlákny (porozity), což umožňuje nastavit jejich prodyšnost a případně i filtrační schopnosti. Proto tyto netkané textilie nabízejí poměrně velký potenciál ve využití jako kryty ran. Technologicky navíc dávala smysl návaznost na procesy extrakce PH3B, které v té době probíhaly v chloroformu, a byl tak přímo k dispozici vhodný roztok jako vstupní produkt do technologie odstředivého zvlákňování. Extrakce v chloroformu byla posléze z důvodu negativního environmentálního dopadu odsunuta do pozadí a nahrazena procesy využívající detergenty. Záměrem mnohých technologů i výzkumníků zabývajících se extrakcí PHA a jejich zvlákňováním z roztoku je nahradit chloroform za rozpouštědlo šetrnější k strojům, lidskému zdraví i životnímu prostředí [256].

6.2 Současný stav

Odstředivé zvlákňování polymerů do podoby mikro a nanovlákna je proces známý už od devadesátých let 20. století, kdy se objevují první patenty [257]. Je zde prezentováno technické řešení základních typů rotačních zvlákňovacích hlav s tryskami. Práce [258] shrnuje předpokládané vztahy mezi procesními parametry (viskozita zvlákňovaného média, povrchové napětí, rotační rychlost hlavy, vzdálenost trysky od osy rotace, průměr trysky a vzdálenost sběrných kolektorů od

trysky) a finální tloušťkou vlákna. Stejně tak autoři v publikaci [259] ukazují možnost využít Berryho číslo (*Be*) jako procesní faktor, který lze podobně jako při elektrospinningu použít k popisu vlivu interakcí polymerních řetězců na vlákna o výsledném průměru. Obecně platí, že pro výrobu nanovláken pomocí odstředivého zvlákňování by *Be* mělo překročit kritickou hodnotu Be^*, při které jsou koncentrace a viskozita adekvátně vysoké a polymerní řetězce jsou dostatečně propletené. Naopak, je-li *Be* nižší než Be^*, neadekvátní interakce řetězců bude mít za následek špatnou tvorbu vláken [259].

Podobně je teorie procesních parametrů CFS diskutována v publikaci [260]. Dle autorů je při procesu výroby nanovláken třeba vzít v úvahu tři významné materiálové parametry, kterými jsou povrchové napětí, viskozita a rychlost odpařování rozpouštědla. Kromě toho pak do výsledku vstupují další procesní parametry, jako je rotační rychlost zvlákňovací trysky, její průměr a vzdálenost od kolektorů. Ostatní parametry nemají tak významný vliv [261]. I v mnoha dalších publikacích je snahou autorů popsat vlivy procesních parametrů na výslednou strukturu vláken i za pomoci složitějších modelů [261], [262], [263], [264], [265], [266], [267].

Vlastnosti CFS vláken i vliv reologických vlastností roztoku použitých polymerů na tyto výsledné vlastnosti vlákna jsou velmi často porovnávány s ES technologií [268], [269]. Dle publikace se ze stejného roztoku etylcelulózy s polyvinylpyrrolidonem (PVP) ve směsi etanol s vodou metodou CFS vytváří při určitých poměrech porézní strukturu vlákna, zatím co vlákna z ES nevykazovala žádnou porozitu [270]. Podobně vlákna z PCL vyrobená pomocí CFS (zde jako *Rotary Jet Spinning* RJS) vykazovala vyšší drsnost oproti vláknům z ES [271]. Přesto, že jsou distribuce průměru vláken, morfologie jejich povrchu i porozita netkané textile často poměrně odlišné i za použití stejného polymeru, tvorba vlákna je vždy řízena zejména interakcí molekul v rozpouštědle. Publikace [272] porovnává tyto procesy na polyvinylalkoholových a PVP vláknech. Zatímco ES poskytlo rovinné 2D vrstvy vláken, CFS poskytlo objemné 3D struktury, podobné vatě. Společným znakem procesů bylo, že střední průměr vlákna se zvyšoval se zvyšující se koncentrací polymeru v roztoku (což přímo souvisí se zvyšující se viskozitou roztoků) a vlákna z odstředivého zvlákňování měla větší střední průměr. Bylo však zjištěno, že korelace mezi průměry vláken a viskozitami roztoku byly významně silnější pro vlákna z CFS ve srovnání s vlákny z ES technologie. Nicméně elektrostatické zvlákňování dokázalo vyrobit vlákna z relativně zředěných roztoků (10 hm. % polymerů), zatímco odstředivé zvlákňování bylo schopno získat vlákna z velmi viskózních roztoků, kde elektrostatické zvlákňování již nevytvářelo žádná vlákna.

6.2.1 Antimikrobiální aditiva

Možnost mísit polymerní roztok s funkčními aditivy s antimikrobiálním účinkem a z něj následně vyrábět vlákenné netkané textilie podněcuje výzkum mířící k medicínským aplikacím, k antimikrobiálním obalům potravin, k vývoji filtračních materiálů a bioelektronických senzorů pro "smart textiles" [273]. Využívají se jak anorganické látky (např. jod v PVP/vinyl-acetátových vláknech [274], tak nanočástice z dusičnanu stříbrného v teplotně zesíťovaném gelu [275] nebo v polyvinylalkohol-co-vinylacetátu [276], nanočástice stříbra v PLA vláknech pro obaly potravin [277], v celulosových vláknech [278], nanočástice mědi v matricích z PVP a polyethylenoxidu (PEO) z roztoků PVP/ethanol a PEO/voda [279], oxid zinečnatý a hydroxyapatit v PLA [280]. Objevují se i aplikace aditiv organických látek často na přírodní bázi jako karboxymetylchitosan v polyetylenoxidových vláknech [281], virgin kokosový olej [282], kyselina třís lová s pullulanem v chitosanových vláknech

[283] a ve vláknech z chitosan/polyvinylalkoholu [284], česnekový extrakt v polyvinylpyrrolidonových vláknech [285], tymiánový esenciální olej v polyakrylonitrilových vláknech [286], cinamaldehyd v chitosanových vláknech [287] a nebo syntetické antibiotikum ciprofloxacin v PLA/želatina [288].

I přes to, že materiály PHA i metoda odstředivého zvlákňování jsou známé poměrně dlouho, publikací na téma odstředivě zvlákněného PHA nebylo do dnešní doby nijak mnoho publikováno. Nejstarší dohledanou publikací na toto téma je dvojice navázaných prací týmu autora L. J. R. Fostera z r. 2001 [289] a 2003 [290]. Práce se zaměřuje na charakterizaci připravených PHB vláken z pohledu morfologie, termických vlastností a interakce s vybranými kmeny buněk. Diskutovaná je problematika nedostatečné adheze buněk na vlákna PHB a možnosti úpravy povrchu vláken hydrolýzou povrchu v alkalickém a kyselém prostředí. Prezentovány jsou výsledky *in vitro* degradace vláken v kyselém i alkalickém prostředí a pomocí SEM, DSC a FTIR je vysvětlován mechanismus rozpadu vláken. Obě práce také ukazují souvislosti a vliv použitého rozpouštědla (chloroform vs. dichlormetan), čistotu PHB (technická čistota v.s. dodatečně přečištěné) a použitá aditiva (pektin a alginát sodný) na dosaženou strukturou netkané textilie a morfologii vlákna. Publikované výsledky ukazují potenciál PHB pro aplikace v oblasti hojení ran a vyzdvihují možnost použití technologie odstředivého zvláknění PHB pro výrobu netkaných textilií se zabudovanými, s roztokem PHB nemísitelnými, účinnými látkami do vlákna.

Zajímavou možnost s antimikrobiálními vlastnostmi nabízí hypericin izolovaný například z Hypericum perforatum (třezalky tečkované). Přestože je v klasické farmacii používaný zejména pro léčbu depresí a úzkostných stavů, v novodobých publikacích je prezentován i jako zajímavý přírodní fotosenzibilizátor. Má široké spektrum absorbance s maximy při 545 a 595 nm a širokým rozsahem emisních vlnových délek s maximem při 594 a 640 nm a je tedy vhodný pro fotokatalýzu iniciovanou viditelným světlem [291]. Tuto účinnou látku zabudoval do PHB odstředivě zvlákněných netkaných textilií tým pana M. Berana [292]. V této práci byla využita modifikovaná metoda odstředivého zvlákňovaní s rotačními kolektory. Do 2% roztoku PHB v chloroformu byl přidán 14,8% extrakt z třezalky v rozpouštědle methanol:aceton (2:1, w:w) tak, aby byla finální koncentrace 0,3 % ve výsledném zvlákněném roztoku. Článek nebyl zaměřen na charakterizaci fyzikálních vlastností vláken, úsilí bylo věnováno měření kvantifikace singletového kyslíku a antibakteriálních vlastností vláken v případě Escherichia coli při expozici viditelným světlem. Ten byl úspěšně prokázán, což otevírá možnosti využít materiál v mnoha oblastech tkáňového inženýrství tam, kde je třeba posílit boj proti gramnegativním bakteriím.

Na záměr netkané textilie s antimikrobiálním povrchem navazuje práce publikovaná v r. 2018, která se zabývá využitím šťávy z kyselých pomerančů (sour orange juice – SOJ) jako přírodního aditiva na povrchu PHB vláken vyrobených odstředivým zvlákňováním [293]. Účinky tohoto komplexního přírodního aditiva byly popsány v několika dalších publikacích [294], [295]. Byla hodnocena antibakteriální aktivita proti běžným grampozitivním a gramnegativním bakteriím (Staphylococcus aureus, resp. Escherichia coli) a také buněčná adheze a životaschopnost 3T3 myších fibroblastů. Scaffoldy PHB/SOJ vytvořené ponořením PHB netkané textilie vyrobené odstředivým zvlákněním do pomerančové šťávy vykazovaly antibakteriální aktivitu. Testy na buňkách ukázaly vhodné prostředí pro buněčný růst a uchycení buněk. Výsledky této studie otevírají nové možnosti pro výrobu vláknitých materiálů pro biomedicínské aplikace s multifunkčními vlastnostmi za použití přírodních látek.

Jedním z dalších přístupů vytvoření antimikrobiálního materiálu na bázi PHA je modifikace povrchu vláken v plazmatu, vakuovým naprašováním atomů kovu nebo roztokovým pokovením povrchu částicemi stříbra [296]. Tyto úpravy jsou funkční, jejich toxikologická ne/závadnost je dnes často diskutována. Úpravy povrchu mají také zásadní vliv na výslednou povrchovou energii a tím na smáčivost. Zatím co samotná úprava plazmatickým výbojem dle předpokladu zvýšila povrchovou energii a to zejména její polární složku a tím snížila kontaktní úhel vody, depozice kovových vrstev na povrch PHB kontaktní úhel vody zvýšila a to v závislosti na tloušťce kovové vrstvy.

Na mikrovlákna z PHB vyrobená metodou CFS imobilizoval tým z Prahy Endoinulinázu z Aspergillus niger Inulinase® Novozym 960 [297]. Vyvinuli tak biokatalyzátor pro výrobu probiotického oligosacharidu a inulooligosacharidu. Vlákna ve formě vaty o tloušťkách v rozsahu 1–3 µm byla vyrobena z 5% roztoku PHB v chloroformu na zařízení s rotační polyamidovou nádobou zvonovitého tvaru. Vlákna byla nabotnána v bezvodém etanolu, následně byl přebytek ethanolu odstraněn a vlákna byla důkladně promyta demineralizovanou vodou. Promytá vlákna byla inkubována v 50 ml kapaliny Inulinase® Novozym 960. Nakonec byla vlákna důkladně promyta demineralizovanou vodou, vysušena při pokojové teplotě a zvážena hydrofobními interakcemi.

Nejnovější publikací na téma CFS PHA materiálů je studie belgického kolektivu autorů [298]. Zabývá se zvlákněním kopolymeru P3HBcoHHx s molární koncentrací 10,55 % hydroxyhexanoátu v roztocích chloroformu s proměnnou koncentrací polymeru. Viskozita roztoku řízená koncentrací polymeru byla považována za nezávislou proměnnou ve vztahu k měřeným veličinám popisující vytvořená vlákna. Charakterizována byla tloušťka vláken a jejich morfologie, termické vlastnosti (krystalinita a teplota tání) a mechanické vlastnosti v tahu. Autoři uvádí kritickou koncentraci, kdy dochází k úspěšnému zvláknění do formy netkané textilie bez vysokého zastoupení kapek. Tu stanovují na základě měřené závislosti Zero-shear viskozity na koncentraci polymeru v roztoku a korelují se získanými vlákny. Zvláknění probíhalo na laboratorně vytvořeném systému rotační dvouramennou hlavou osazenou tryskami 0,6 mm [261]. Autoři upozorňují na složitost porovnání mechanických vlastností vlákenné struktury netkané textilie. Mechanická odezva těchto materiálů v tahu je silně závislá na distribuci tloušťky vláken a jejich orientaci v textilii. Tyto vlastnosti jsou dány procesními parametry technologie, které se mezi autory velmi výrazně liší.

6.3 Cíle

Všechny tyto výše popsané podněty a fakta vedly zejména v rámci projektu **PR 9** a **PR 12** v týmu Laboratoře bioplastů k vědecko-výzkumné činnosti zaměřující se na procesy zpracování PHB do formy funkčních netkaných textilií pro medicínské aplikace metodou odstředivého zvlákňování. Cílem bylo a stále je připravit netkanou textilii na bázi PHA s řiditelnými vlastnostmi (mechanické vlastnosti, morfologie, interakce s kapalinami a buňkami). Předpokladem je možnost ovlivnit tyto parametry aditivy na základě analogie se zpracováním v tavenině. Využití mísení kopolymerů PHA s různými vlastnostmi, přídavek jiného biopolymeru nebo přídavek změkčovadla byly materiálové a procesní možnosti, které v případě odstředivého zvláknění PHA nebyly zatím publikovány.

Z pohledu budoucí možné aplikace je dlouhodobým cílem tyto netkané textilie otestovat ve třech případech využití:

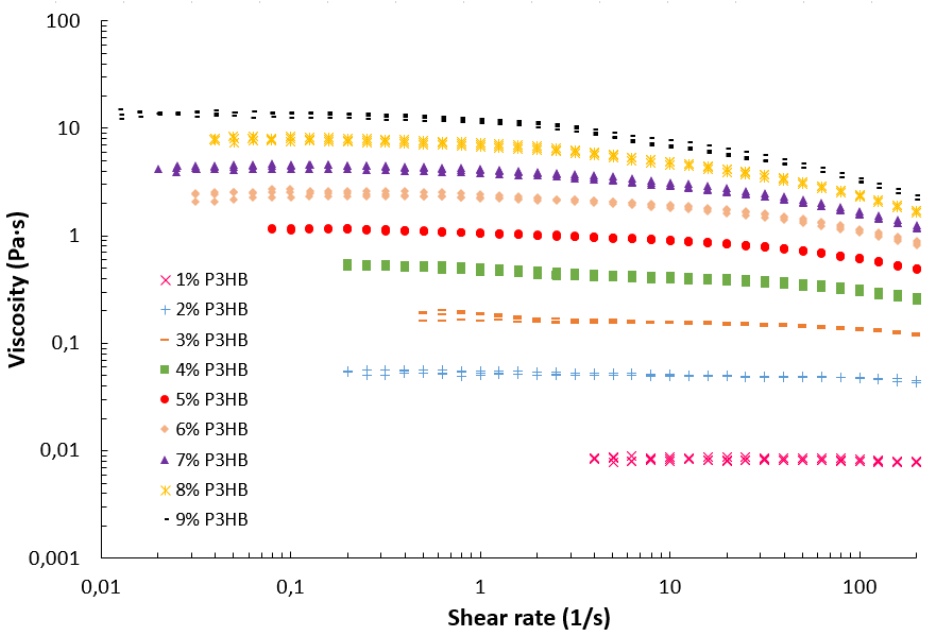
- kryty ran, v budoucnu s antimikrobiálními vlastnostmi s možnostmi pomalého nebo lépe řízeného uvolňování účinné látky (**PR 9**),

- funkčního substrátu pro kultivaci buněk s prostorovou strukturou imitující přirozené prostředí buňky (**PR 9**),
- filtračního materiálu pro osobní ochranu dýchacích cest před viry a bakteriemi. Zde se nabízelo využití přírodních aditiv na bázi fenolických pryskyřic s antibakteriálním a antivirotickým účinkem. Tento záměr vznikl a byl rozvíjen v rámci projektu **PR 11** řešeného na CEITEC VUT pod vedením doc. Lucy Vojtové.

Ve všech případech je záměrem otestovat výrobu navržených řešení v průmyslovém měřítku technologie odstředivého zvlákňování u průmyslového partnera.

6.4 Dosažené výsledky

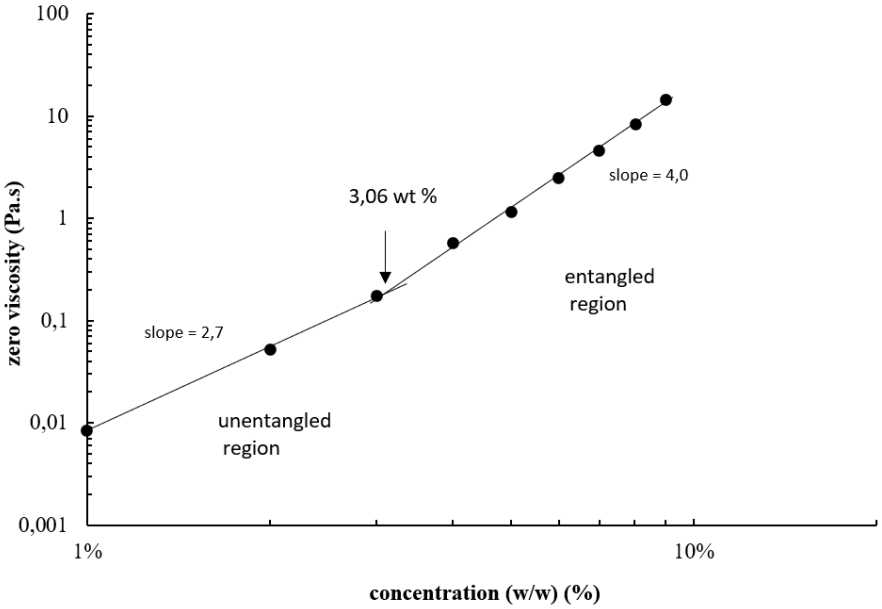
Klíčovými vlastnostmi pro úspěšné zvláknění čistého polymeru odstředivým zvlákněním z roztoku je bezesporu viskozita polymerního roztoku řízená interakcí rozpouštědla a polymeru, jeho koncentrací a distribucí jeho molekulové hmotnosti. Jak popisují publikace [299], [300], [301], existují intervaly koncentrace roztoku, kdy je závislost logaritmu intristické viskozity na logaritmu jeho koncentrace lineární, avšak s jinou konstantou. V těchto intervalech dochází v roztoku k odlišné interakci řetězců polymeru s rozpouštědlem, což se projeví jiným chováním při elektrospiningu (ES) i odstředivém zvlákňování (CS). Podobnost chování roztoku v procesech CS a ES je běžně využívána. U PHB jsou pozorovány dva intervaly oddělené kritickou viskozitou. Pod touto viskozitou dochází k tvorbě kapiček, nad kritickou viskozitou k tvorbě vláken. U některých polymerů byly pozorovány 3 rozhraní, které ukazují na schopnost tvořit kapky, tvořit kapky s vlákny a v posledním intervalu tvořit pouze vlákna. Zřejmě díky širší distribuci molekulových hmotností PHB jsou pozorovatelné jen tyto dva ne zcela ostré intervaly. Obrázek níže (Obr. 35) ukazuje tokové křivky PHB v závislosti na smykové rychlosti při různých koncentracích PHB v chloroformu.



Obr. 35: Reologické chování roztoku PHB v chloroformu v závislosti na jeho koncentraci

Z těchto křivek byly určeny zero-shear viskozity a ty vyneseny v závislosti na koncentraci roztoku. Průsečíkem přímek lineárních závislostí v grafu na Obr. 36 níže byla vyhodnocena kritická viskozita 3 %. Ta by měla vyústit v tvorbu vláken a omezit vznik kapek. Stanovená hodnota je v souladu s experimentálně pozorovaným chováním při přípravě vláken v rámci diplomové práce **VSKP6**.

3% roztok tvořil při 4000 ot/min spolu s vlákny i kapky, na vláknech z 5% roztoku již kapky pozorovány nebyly. V případě 8000 ot/min byly kapky pozorovány i z 5% roztoku, ze 7% roztoku se pak vytvářela vlákna bez kapek. Výsledek je také ve shodě s publikací [301], kde byla stanovena kritická viskozita na hodnotě cca 3,5 %.



Obr. 36: Závislost zero shear viskozity na koncentraci PHB v roztoku chloroform

Podobně byly získány hodnoty kritické viskozity pro směsi PHB s kopolymerem 15 % P3,4HB a směsí PHB s 10 % změkčovadla Syncroflex. Hodnota kritické viskozity u směsi s P3,4HB byla stanovena na hodnotu 2,5 %, použití aditiva Syncroflex naopak umožnilo zvlákňovat roztoky vyšších koncentrací, což zvýšilo i produkční rychlost.

Během práce s roztoky PHA v chloroformu stabilizovaného etanolem byl pozorován již publikovaný jev snížení viskozity v čase skladování roztoku. Pokles je způsoben poklesem molekulových hmotností polymeru hydrolýzou v kyselém prostředí HCL vzniklé oxidací chloroformu [300]. Zajímavým zjištěním byla také zrychlená degradace polymerních řetězců v prostředí chloroformu stabilizovaného amylenem na denním světle. Proto nebylo možné tento chloroform jako rozpouštědlo využívat, neboť zvláknění z těchto roztoků o rychle klesající viskozitě nebylo možné.

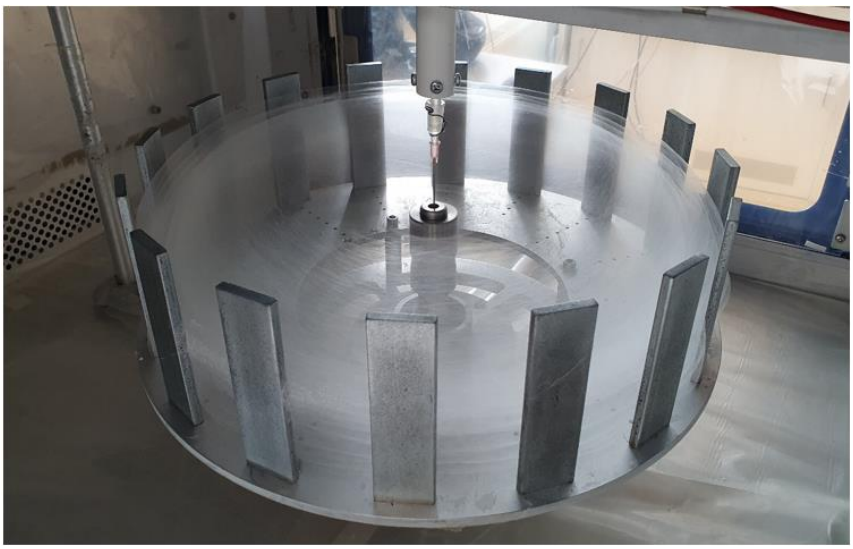
Během dvou let vývoje těchto PHB vlákenných textilií byly v rámci dvou diplomových prací (**VSKP6** a **VSKP8**) testovány příměsi 3 změkčovadel - acetyltributylcitrát (Citroflex A4), polyadipát (Syncroflex 3114-LQ) a komerční plně biobased polyester EMERY MC2192 (dnes pod značkou EDENOL2192). Podobně byly roztoky PHB modifikovány přídavkem pomocných polymerů (amorfní PDLLA, PCL a PEG 1000 a P3,4HB). Všechny binární směsi kromě PEG, který byl s PHB nedostatečně mísitelný, se podařilo úspěšně zvláknit a modifikovat tak výsledné vlastnosti vláken.

Zvlákňování probíhalo technologií odstředivého zvlákňování na přístroji FibeRio CycloneL1000. Přístroj je nastaven k produkci vláken z 2 ml zásobníku v rotační hlavě. Aby byla produkce vláken kontinuální a bylo lépe řízeno dávkování, byla provedena úprava a použita injekční stříkačka naplněná roztokem polymeru napojená na injekční pumpu (LAMBDA VIT-FIT (HP)). Roztok polymeru byl dávkován touto pumpou hadičkou až do zvlákňovací hlavy skrze dávkovací jehlu 18G o vnějším průměru 1,2 mm. Na Obr. 37 je zobrazena zvlákňovací hlava s upraveným kontinuálním dávkováním.



Obr. 37: Přístroj FibeRio CycloneL1000 s upraveným kontinuálním dávkováním

Na rotační hlavě jsou upevněny dvě výměnné zvlákňovací jehly se standardním bajonetovým uchycením. Nejlepších výsledků bylo dosaženo použitím zvlákňovacích jehel 30 G. Jsou to jehly s vnějším průměrem 0,3 mm a zkosením 11°. Dávkování roztoků bylo po optimalizaci zvoleno konstantní o rychlosti cca 2,5 ml/min. K získání kokonů vláken o přibližně stejné hmotnosti bylo trvání jednoho zvlákňovacího cyklu 2 min pro 7% roztoky a 2,5 min pro 5% roztoky polymerů. Vzdálenost kolektorů byla také neměnná a to 130 mm od zvlákňovací hlavy. Rozložení 16 kolektorů o rozměrech 115 × 32 × 7 mm bylo rovnoměrné po celém obvodu. Nejčastěji měnícím se procesním parametrem byla rychlost otáčení zvlákňovací hlavy. Ta byla nastavena tak, aby probíhala stabilní tvorba mikrovláken do formy tzv. kokonu viz Obr. 38. Pro většinu vzorků byla ideální rychlost zvlákňování 10 tis. ot/min.

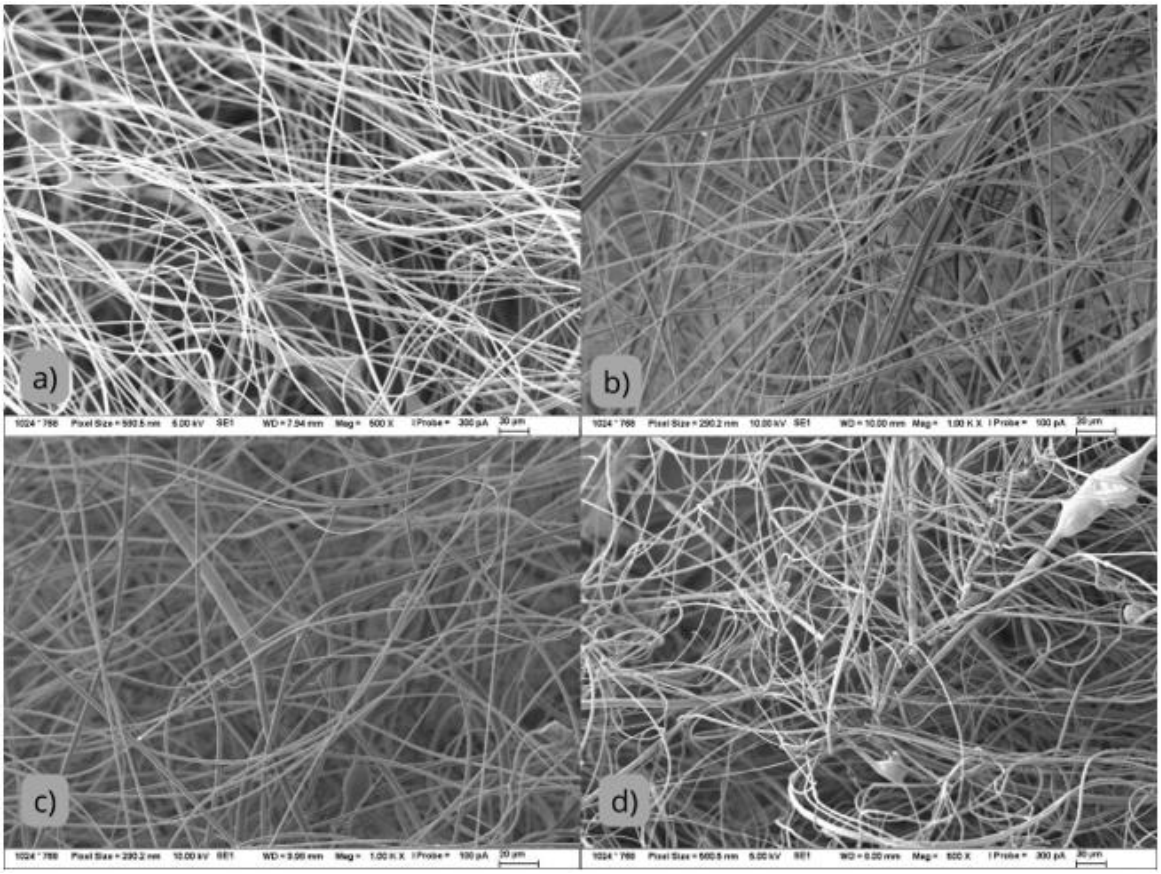


Obr. 38: Ukázka úspěšně zvlákněného polymerního roztoku do objemného „kokonu“

Paralelně byly vybrané úspěšné roztoky testovány na průmyslovém zvlákňovacím zařízení ve společnosti NanoSpace Techology. Tato technologie přizpůsobená výrobě planárních vzorků v metráži neposkytuje již objemné vlákenné struktury ve formě vaty, ale plošnou formu náhodně orientovaných vláken s gramáží 2-20 g/m^2 na pomocné nosné textilii. Vzhledem k odlišné konstrukci zvlákňovací hlavy a využití odlišných směsných rozpouštědel není výsledek srovnatelný. Proto byly vybrané materiály testované v obou formách – planárních membránách z průmyslu a vaty

z laboratorního zvláknění. Tyto testy poskytly důležitou informaci o použitelnosti navržených materiálů v průmyslové praxi.

Jeden vybraný příklad možnosti, kde se přídavkem pomocného polymeru podařilo zlepšit stabilitu procesu zvláknění i kvalitu samotných vláken je na Obr. 39. Jak bylo patrné již při samotném procesu zvlákňování, přídavek 15 % P3,4HB do PHB umožnil velmi stabilním procesem vytvořit nadýchaný kokon vláken, který na rozdíl od čistého PHB neobsahoval tolik slepených vláken. Vyšší přídavek P3,4HB než 15 % pak vedl k již nehomogenní struktuře vláken. Podobného efektu bylo dosaženo přídavkem 10 % změkčovadla Syncroflex, výroba na laboratorním stroji byla stabilnější a výkon výrobní průmyslové linky byl také prokazatelně vyšší a zlepšila se i kvalita vláken v membráně.

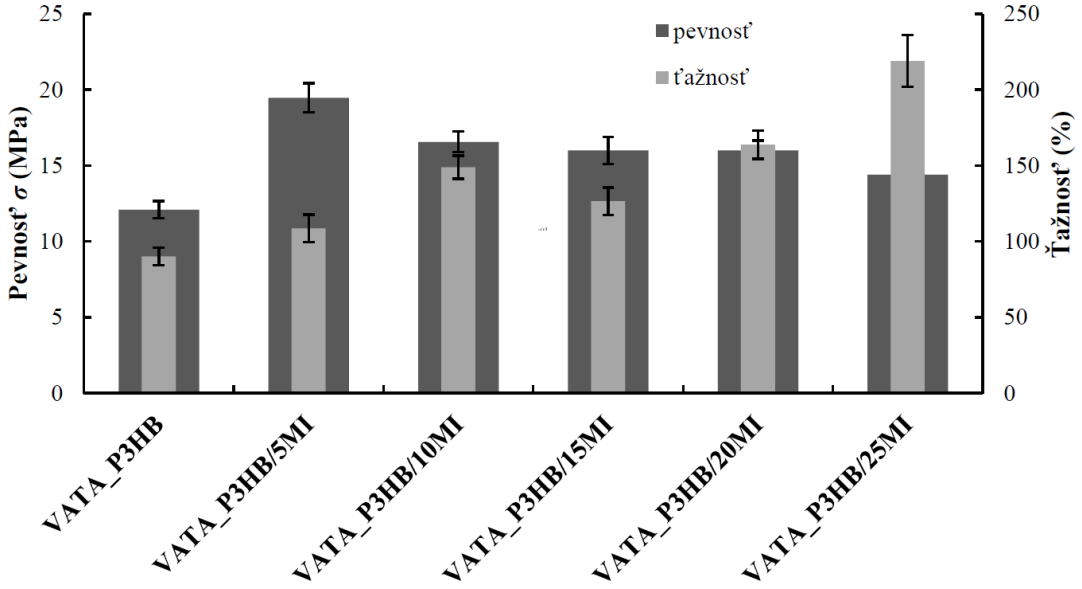


Obr. 39: SEM snímky laboratorně připravených vláken z a) PHB, b) PHB+15%P3,4HB, c) PHB+20 % P3,4HB (zvětšení 1000×) a d) PHB+25 % P3,4HB (zvětšení 500×)

Předmětem výzkumu byl dopad přídavku aditiv na mechanické vlastnosti a tedy možnost jejich řízení. Pro jednoduchou charakterizaci odpovídající procesu manipulace s planárními membránami i vlákny ve formě vaty byla zvolena tahová zkouška. Z planárních membrán byly vyseknuty vzorky tvaru dogbone. Z laboratorně připravených vláken ve formě vaty byly z kokonu, vždy ve stejném směru s ohledem na orientaci kokonu při výrobě, vystřiženy svazky, které byly uchyceny do čelistí. Vzorky byly podrobeny základní tahové zkoušce při deformační rychlosti 10 mm/min. Stanoveny byly hodnoty maximální síly a napětí a maximální deformace při porušení (poklesu síly pod 20 % z naměřeného maxima). Napětí bylo vypočteno jako poměr síly a efektivní plochy, která byla odvozena ze známé hmotnosti vzorku a hustoty polymeru. Sledován byl zejména vliv přídavku aditiv na mechanickou odezvu v tahu (Obr. 40). Přestože je měření takto subtilních vzorků zatíženo významnou chybou, vliv přídavku změkčovadla ve všech variantách byl prokazatelný a zvyšoval maximální deformaci. U formy vata byla tažnost PHB s přídavkem 10 % změkčovadla Syncroflex

135 % oproti referenčnímu PHB (90 %), u planárních membrán byla tažnost celkově nižší, účinek (cca 150 % původní hodnoty) změkčení však stejný (z 10 na 15 %).

Přídavek kopolymeru P3,4HB také způsobil zvýšení tažnosti netkaných textilií a to až na 220 % při 25% zastoupení P3,4HB v polymerní směsi. Nutno podotknout, že tato vlákna nebyla z hlediska morfologie příliš homogenní. Jako optimální se při výrobě i z hlediska morfologie jevil přídavek 15 % P3,4HB. V tomto případě z cca 90% tažnosti bylo dosaženo 125 %, v případě pevnosti z 12 MPa zvýšení na 16 MPa. Tyto změny jsou dány nejen rozdílným složením polymerní směsi, ale také zřejmě jinou strukturou sítě vláken a jejich vazbou způsobenou jinou viskozitou roztoku a afinitou vznikajících vláken dopadajících na ta ostatní. Testy zvláknění čistého P3,4HB vedly sice po optimalizaci také k tvorbě vláken na kolektorech, ale nebylo možné je z nich sejmout. Vlákna byla příliš měkká a lepkavá a při dotyku se shlukla do jednoho celku. I malé množství P3,4HB ve směsi tak zřejmě působí pozitivně na pevnost sítě, protože zpevňuje spojení vláken v místě jejich dotyku. Jeho vyšší koncentrace vede ke změkčení samotného vlákna. Tuto teorii by bylo vhodné ověřit přípravou samotného vlákna a měřením jeho vlastností.



Obr. 40: Vliv přídavku P3,4HB (MI) na mechanické vlastnosti netkaných textilií připravených ve formě vaty.

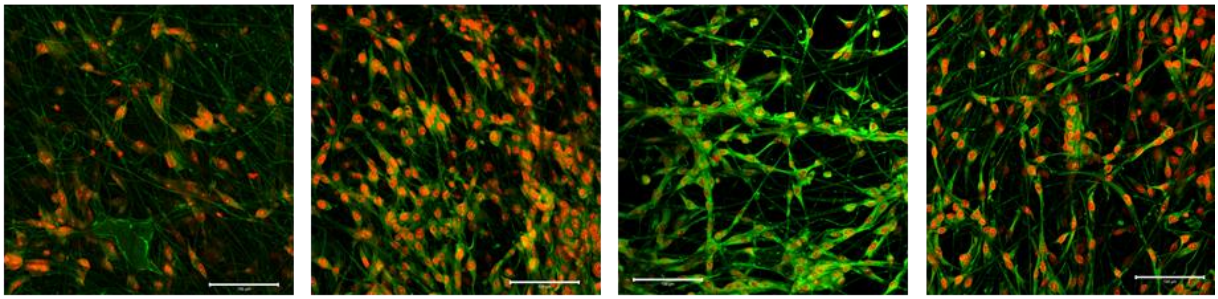
Z důvodu uvažované aplikace do tkáňového inženýrství byla otestována mechanická odezva v tahu za sucha i v prostředí vody. PHB s přídavkem P3,4HB i změkčovadla se chovají v obou prostředích v podstatě srovnatelně.

Pro obě aplikace kryty ran i 3D substráty pro buňky je důležitá interakce povrchu s vodou. Kryty ran mohou využít hydrofilní i hydrofobní povahu materiálu. Vhodným vrstvením těchto rozdílných textilií lze řídit difuzi exsudátu, propustnost pro plyny a vodní páru, sorpci a sorpční kapacitu exsudátu apod. Při aplikaci textilie do živného roztoku v testovacích jamkách (wellplate) je třeba spíše hydrofilního charakteru povrchu. Byla proto u připravených materiálů testována i volná povrchová energie a interakce s vodou. Kontaktní úhel vody na těchto materiálech se pohyboval kolem 110° což je obecně považováno za nesmáčivý materiál. Díky této povaze nebyl materiál ani nijak savý.

Dosáhnout lepší smáčivosti těchto materiálů lze obecně několika způsoby. Chemická či plazmochemická modifikace povrchu oxidací i chemická modifikace roubováním vhodných molekul/skupin na povrch tenkých vláken je pro biomateriály bez funkčních skupin zpravidla spojena s procesem degradace. Proto byl hledán méně drastický způsob. Jednou z cest je enzymatická úprava

povrchu, kdy působením enzymu dojde k modifikaci povrchu vlákna enzymatickým štěpením molekul na povrchu nebo navázáním enzymu na upravovaný povrch. Proto byla otestována interakce lipázy s referenčními PHB vlákny a to ve dvou koncentracích lipázy ve vodném roztoku, který na PHB vlákna působil 24 hod. Výsledný kontaktní úhel po vyprání v destilované vodě a vysušení dosahoval cca 25°, což bylo provázeno také naměřenou změnou nasákavosti upravených textilií. XPS analýza povrchu ukázala přítomnost cca 3,5 at. % uhlíku, který zřejmě pocházel z lipázy navázané na povrch textilie.

Z planárních vzorků zamýšlených pro kryty ran i z textilií ve formě vaty pro využití jako 3D nosiče buněk byly výsekem připraveny kruhové vzorky průměru 6 mm do 96 jamkových wellplate. Výška objemovaného vzorku tvořící tvar čočky byla cca 2 mm. Série takto připravených vzorků byla podrobena testům hodnocení cytotoxicity na myších 3T3 fibroblastech. Hodnocena byla metabolická aktivita, proliferace buněk a penetrace buněk do 3D substrátů.



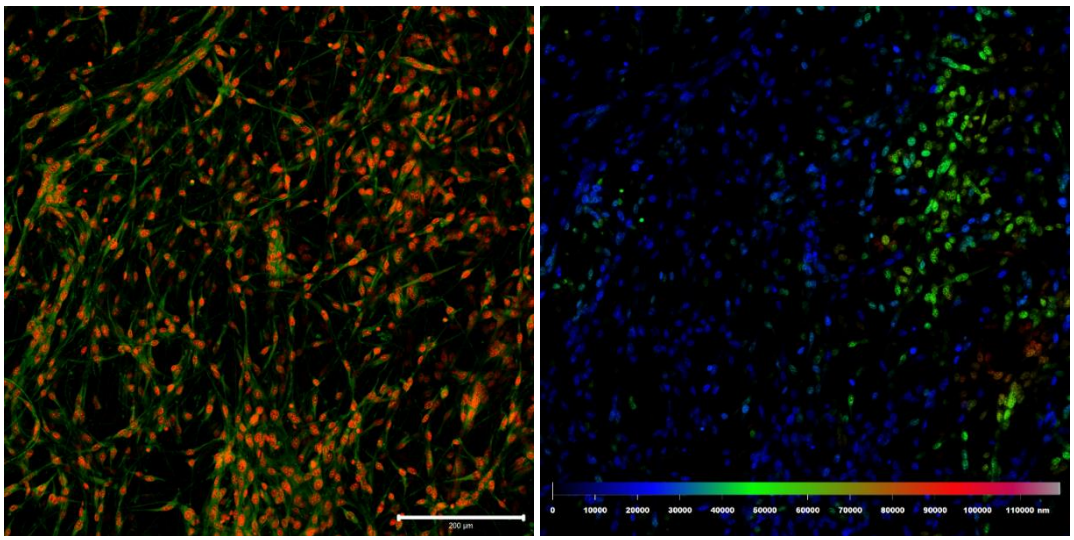
Obr. 41: Příklad buněčné distribuce ve vlákenných laboratorně připravených nosičích z PHB + 15 % P3,4HB v 1., 7., 14. a 12. den. Buněčná jádra byla obarvena propidium jodidem (červeně), intracelulární membrány pomocí DiOC6(3) (zeleně), měřítko 100 µm.

Výsledky tří setů vzorků různého složení prokázaly, že všechny PHB vlákenné nosiče i s výše uvedenými zvolenými aditivy nevykazovaly toxicitu vůči 3T3 buňkám a ochotně adherovaly na vlákna (Obr. 41). Dle metabolické aktivity měřené pomocí MTS testu dosáhly buňky na laboratorně připravených nosičích s přídavkem P3,4HB po fázi rychlého růstu po 14 dnech konfluence. Vysokých hodnot metabolické aktivity pak dosahovaly planární vzorky z průmyslové linky a vlákna upravená lipázou.

Buněčná proliferace na vlákenných nosičích byla měřena pomocí kvantifikace buněčné DNA. Rychlost nárůstu počtu buněk se zvětšovala s přídavkem P3,4HB, což také korelovalo s rostoucím množstvím kapiček a defektů vláken. Jak bylo pozorováno z mikroskopických snímků, buňkám se daří právě na těchto místech adherovat. Stejný výsledek (množství defektů a na nich buňky) byl pozorován u vláken z čistého PHB.

Proliferace buněk a jejich penetrace do hloubky porézní vlákenné struktury byly pozorovány pomocí konfokálního mikroskopu ve čtyřech časových intervalech. Z obrázků z kanálu propidium jodidu (buněčná jádra), byly následně připraveny hloubkové projekce (příklad na Obr. 42). Pro tento účel je softwarově určité hloubce z nosiče přiřazena barva na barevné škále. Je tak zobrazeno, do jaké hloubky nosiče buňky penetrovaly. Je však nutné brát v úvahu, zda jde o skutečnou penetraci buněk, kdy v jedné oblasti je možné vidět buňky z různých vrstev, nebo zda jde o lokální nerovnost vzorku. Metoda má tedy svá omezení a je jen orientační. Z výsledků lze vyčíst, že v poréznějších laboratorně připravených strukturách byly nalezeny buňky i v hloubce 130 µm, zatím co v planárních vlákenných nosičích z průmyslové linky pouze v cca 50 µm. Vzhledem k tomu, že byly v těchto hloubkách nalezeny buňky již v prvním intervalu odběru, je pravděpodobné, že tyto buňky „propadly“ do této hloubky již při osazení a dále se v těchto vrstvách rozmnožovaly. Nejde tedy o penetraci buněk

z vrstvy do vrstvy. Fibroblasty mají tendenci růst po vlákně, které je však v těchto substrátech preferenčně orientováno v planární rovině s minimem vláken v rovině kolmé. Z tohoto důvodu byl zahájen test konceptu přípravy kruhových nosičů s preferenční orientací vláken v kolmém směru, který bude poskytovat zcela odlišnou možnost proliferace buněk skrze nosič.



Obr. 42: Zobrazení buněk na nosiči s 15 % P3,4HB 21. den (měřítko 200 um) a jejich hloubková barevná projekce (barevná škála odpovídá 0–110 µm)

V rámci projektu Techbikom (**PR 12**) pod vedením doc. Ing. Lucy Vojtové, Ph.D. byly vyvíjeny textilie s přídavkem extraktů s antimikrobiálním účinkem. Extrakty byly připraveny zahraničním partnerem projektu z kůry odpadního smrkového dřeva a následně přidávány do zvlákňovacího roztoku. Po optimalizaci viskozity a procesních podmínek byla úspěšně připravena netkaná textilie, která byla podrobena charakterizaci antimikrobiálního účinku, který se úspěšně prokázal jak proti gramnegativním tak grampozitivním mikroorganismům. Tyto vzorky byly také podrobeny měření cytotoxicity a biokompatibility na 3T3 fibroblastech a byly zhodnocené jako biokompatibilní. To otevírá další možnosti pro budoucí témata výzkumu směrem k medicínským aplikacím.

6.5 Přínos

Práce v této oblasti ukázaly, že PHB lze zpracovat bez tepelného namáhání roztokově do formy vlákenné netkané textilie a její vlastnosti lze řídit přídavkem aditiv podobně jako v případě zpracování v tavenině. Přídavek změkčovadla adipátového typu i kopolymeru P3,4HB umožnil změnit odezvu textilie na mechanické namáhání v tahu. Podařila se zvýšit deformovatelnost textilie bez jejího porušení, což usnadnilo manipulovatelnost s touto subtilní membránou například v případě využití v oblasti krytů ran. V obou testovaných případech byly výsledné materiály biokompatibilní s použitými 3T3 fibroblasty. Využitá technologie odstředivého zvláknění je přenositelná do průmyslového měřítka. Testovaná roll-to-roll technologie produkuje z hlediska porozity odlišnou textilii vhodnou například k výrobě plně biodegradabilních membrán s filtrační účinností vhodnou i pro ochranné osobní prostředky. Byl také laboratorně úspěšně ověřen koncept výroby biokompatibilní membrány s antimikrobiálním účinkem indukovaným přídavkem extraktu fenolických látek získaných z odpadní kůry dřevozpracovatelského průmyslu. Tyto výsledky z doby posledních 2,5 let jsou nyní se zúčastněnými týmy dalších organizací zpracovávány do dvou publikací. Získané poznatky budou nyní uplatněny při konstrukci kompozitních materiálů hydrogel-vlákno pro kryty ran.

7 AGROCHEMICKÉ APLIKACE PHB

PHB je se svými vlastnostmi danými plně přírodním původem velmi zajímavý kandidát na využití v agrochemických aplikacích, a to jako bariérová biologicky rozložitelná vrstva s definovanou propustností pro dusíkaté nutrienty, fungicidy, herbicidy apod.

7.1 Motivace

Zemědělství jako jeden z nejdůležitějších segmentů naší společnosti musí díky populačnímu růstu vyprodukovat více potravin, krmiva pro zvířata, surovin pro rostoucí trh biopaliv a dalších látek z biologických zdrojů, a to v rámci udržitelného hospodářství i v době klimatické krize. Bez použití hnojiv by bylo potřeba čtyřikrát více půdy pro zajištění celosvětové sklizně a obdělávaná plocha by musela zabírat téměř polovinu všech bezledových kontinentů, na rozdíl od 15 % z celkového počtu plochy půdy, potřebné již v r. 2000 [302].

Význam hnojiv pro lidskou populaci je neoddiskutovatelný. Bez Haber-Boschovy syntézy amoniaku (komercializované v r. 1913) a následných syntetických sloučenin dusíku a jejich aplikací bychom nebyli schopni vyprodukovat více než polovinu dnešních světových potravin [302]. V příštích 80 letech je předpokládán prudký nárůst populace o 2-3 miliardy lidí. Bude tudíž kladen ještě větší důraz na produkci plodin, čímž se rapidně zvýší i potřeba hnojiv [303], [304]. Hnojiva poskytují rostlinám základní makroživiny (dusík/fosfor/draslík), kde je hlavně dusík nezbytný a rozhodující pro růst rostlin [305]. Avšak špatná absorpce živin z hnojiv a související ztráty dusíku v půdě, vodě a vzduchu způsobují kaskádu ekologických problémů [306]. Navzdory skutečnosti, že používání dusíkatých hnojiv hraje zásadní roli při uspokojování poptávky po rostlinné produkci, je účinnost využití dusíku, vzhledem k jejich nadměrnému používání, relativně nízká (obecně mezi 25–50 %) a často vede ke ztrátám nadbytečného dusíku z agroekosystému [307]. Mezi environmentální problémy s tím souvisejícími patří migrace dusičnanů do řek, jezer, rybníků a podzemních vod, v důsledku čehož dochází k eutrofizaci a rozšiřování mrtvých zón i ve vodách pobřežních oceánů. Atmosférická depozice čpavku a dusičnanů také ovlivňuje přírodní ekosystémy; dochází k vyšším emisím oxidu dusného (N_2O), který je nyní třetím nejvýznamnějším skleníkovým plynem po CO_2 a CH_4 [302]. Nadměrné používání hnojiv může způsobit okyselení půdy, vyčerpání půdních kationtů a snížení příjmu uhlíku a kontaminaci půdy těžkými kovy. To vše negativně ovlivňuje zdraví zvířat a lidí, životní prostředí, biodiverzitu a klima [308], [309]. Ještě výraznější ztráty dusíku v životním prostředí, ke kterým bude docházet s rostoucí populací, by bylo možné snížit střídmější konzumací masa, nízko-bílkovinným krmením zvířat, lepším agronomickým hospodařením, portfóliem zahrnujícím dělené aplikace a vyvážené používání hnojiv, cílené zemědělství, optimalizované střídání plodin a použití hnojivových sloučenin s pomalým uvolňováním [302].

Hnojiva s řízeným a s pomalým uvolňováním (controlled-release fertilizers - CRF a slow-release fertilizers - SRF) poskytují účinnější, ekonomičtější a bezpečnější způsob dodávání živin rostlinám. Jsou schopny udržet živiny v půdě po delší dobu, a ty jsou tak rostlinám k dispozici v požadované koncentraci. Efektivita využití živin (Nitrogen Use Efficiency - NUE) se tedy zlepšuje díky méně častému dávkování a sníženému odstraňování živin z půdy deštěm nebo zavlažováním, což také snižuje rizika pro životní prostředí [305], [310], [311], [312]. Hnojiva s pomalým nebo řízeným

uvolňováním jsou dobrou alternativou ke konvenčním minerálním hnojivům a jejich použití umožňuje snížit dávku hnojiva dokonce až o 20 % nebo 30 % doporučené hodnoty pro dosažení stejného výnosu [313].

Dle Nařízení evropského parlamentu a rady (EU) 2019/1009 [314], odstavce KSM 9, může Hnojivový výrobek EU obsahovat polymery jiné než polymery s živinami pouze v případech, kdy je účelem polymeru:

a) regulovat pronikání vody do částic živin, a tedy uvolňování živin (v tom případě se polymer obvykle označuje jako „povrchově aktivní látka“),
b) zvýšit schopnost hnojivového výrobku EU zadržet vodu nebo jeho smáčitelnost, nebo
c) spojovat materiál ve hnojivovém výrobku EU náležejícím do KFV 4.

Ode dne 16. července 2026 musí tyto polymery uvedené v bodě a) a b) splňovat kritéria biologické rozložitelnosti stanovená akty v přenesené pravomoci uvedenými v čl. 42 odst. 5. Nejsou-li taková kritéria stanovena, nesmějí být v žádném hnojivovém produktu EU uvedeném na trh po daném datu takové polymery obsaženy.

Pokud jde o polymery uvedené v bodě 1 písm. a) a b), za rozumně předvídatelných podmínek použití hnojivového výrobku EU nesmí ani polymer, ani vedlejší produkty vznikající při jeho rozkladu vykazovat žádný celkově nepříznivý účinek na zdraví zvířat či rostlin nebo na životní prostředí. Polymer musí obstát ve zkoušce akutní toxicity pro růst rostlin, zkoušce akutní toxicity pro žížaly a ve zkoušce inhibice nitrifikace půdními mikroorganismy.

Kritériem pro SRF hnojivo je dle normy EN 13266/2009 zpomalené uvolnění živin tak, aby se za 24 hodin ve vodě uvolnilo max. 15 % živin a za 28 dní max 75 %, přičemž nejméně 75 % hmotnostního podílu živin musí být uvolněno v určeném čase uvolnění [315]. Norma popisuje i způsob měření kinetiky uvolnění živin ve vodním prostředí.

V souladu s Evropskou zelenou dohodou (European Green Deal) – část Farm to Fork, nařízení EU o hnojivech (Fertilizing Products Regulation FPR) a akčním plánem oběhového hospodářství (Circular Economy Action Plan) tak čelí výrobci významným výzvám. Budou muset přizpůsobit své současné postupy novým požadavkům FPR, včetně kritérií biologické rozložitelnosti materiálů pro polymerní povlaky hnojiv s řízeným uvolňováním [305], [316]. Farm to Fork pak definuje jako jeden z cílů snížení spotřeby agrochemikálií až o 50 % do r. 2030. Další regulací v této oblasti přináší EU Sustainable Chemistry Strategy. Je proto nezbytný vývoj hnojiv s řízeným uvolňováním založených na ekologicky šetrných a bezpečných netoxických materiálech s biologicky odbouratelnými povlaky. Jedním z mála dostupných alternativ ke stávajícím řešením je využití vlastností polyhydroxyalkanoátů (PHA) – konkrétně PHB.

7.2 Současný stav

Hnojiva s pomalým uvolňováním jsou obvykle popisována jako „sloučeniny s nízkou rozpustností s komplexní/vysokomolekulární chemickou strukturou, které uvolňují živiny prostřednictvím mikrobiálního nebo chemického rozkladu této sloučeniny“ [305], [317]. Hnojiva s řízeným uvolňováním (CRF) lze popsat jako „produkty obsahující zdroje ve vodě rozpustných živin, jejichž uvolňování do půdy je řízeno povlakem naneseným na hnojivo“ [305], [313]. SRF se obvykle dělí na „kondenzační produkty močovinových aldehydů, hnojiva s fyzikální bariérou (potažená nebo zabudovaná do matrice) a super granule. CRF je podmnožinou SRF, která spadá do kategorie hnojiv

s fyzickou bariérou“ [305]. Současné komerční CRF s polymerním povlakem jsou často vyrobeny z termoplastického materiálu, jako jsou polyolefiny, polyvinylidenchloridy a kopolymerů, které se nemohou snadno rozkládat v půdě a v průběhu času se v půdě hromadí. Obecně platí, že CRF obsahující syntetické, biologicky neodbouratelné polymery se po uvolnění živin akumulují v půdě (až 50 kg/ha za rok), kde zbytkové polymery zůstávají a způsobují tzv. bílé znečištění [305], [318].

Celý proces uvolňování CRF probíhá ve třech hlavních fázích: pronikání vody (nebo vodní páry) do systému CRF, rozpouštění živin a uvolňování živin systémem CRF. Rychlost a účinnost každého stupně závisí na mnoha faktorech, které ovlivňují celkový profil uvolňování CRF. Tyto faktory lze klasifikovat následovně: faktory závislé na povlaku, faktory závislé na tvaru a velikosti hnojiv a faktory dané půdou a její mikrobiální aktivitou [319].

PHA nalezly uplatnění v nejrůznějších oblastech díky jejich biokompatibilitě, biodegradabilitě a (u některých semikrystalických typů) nízké propustnosti pro malé molekuly plynů jako H_2O, CO_2 a O_2, což je velmi podstatná vlastnost pro použití v hnojivech s pomalým uvolňováním. Pro dosažení ještě lepších bariérových vlastností je třeba prostup malých molekul skrze amorfní část povlaku zpomalit prodloužením jejich difúzních cest. To lze podpořit využitím částicových plniv nebo nanoplniv, aditiv, jako jsou nukleační činidla, změkčovadla nebo také mísením s jinými biodegradovatelnými polymery [320].

Metody přípravy systémů SRF na bázi PHA lze dle aktuálně dostupných literárních zdrojů rozdělit na 3 skupiny, které využívají NPK, KNO_3, NH_4NO_3 nebo močovinu:

- granule nebo fólie z termoplastických kompozitních materiálů na bázi PHA připravených v tavenině, kde je zpravidla přítomno další pomocné organické nebo anorganické plnivo, které pomáhá zpomalit uvolnění živin
- emulzně připravené mikročástice obsahující anorganický nosič s navázanou dusíkatou látkou
- peleta, tableta nebo granule dusíkaté sloučeniny s případným obsahem organického nebo anorganického plniva povlakované tenkou vrstvou PHA

SRF hnojiva na bázi kompozitu připraveného kompaundací PHB a modifikovaného bentonitu a NPK byly testovány v rámci publikace [321]. Účinnost hnojiva byla testována na rostlinách salátu setém v nádobových pokusech, v testu však nebyla zahrnuta pozitivní reference nepovlakovaného hnojiva o stejné dávce. Kinetika uvolňování živin splňovala normou daná kritéria pro SRF, kompozice však obsahovala jen 5 % NPK. To bylo zlepšeno na hodnotu 20 % v návazné práci stejných autorů [322]. Výsledkem bylo hnojivo, ze kterého se však dle autorů uvolní jen 37 % živin. Podobně byly vyvíjeny kompozity na bázi PHB, škrobu, glycerolu a montmorillonitu s obsahem 10 % NPK nebo KNO_3 [323] a v návazné práci stejného týmu s až 50% živin [324]. První práce zahrnuje popis dle Fickova zákona, k charakterizaci využívá konduktometrické měření koncentrace iontů nutrientů. Dle uvedených výsledků je po 60 hodinách uvolněno 100 % KNO_3 a 60 % NPK. Není však jasné, zda je v případě NPK měřen jen dusík nebo i ostatní nutrienty. V případě druhé publikace je měřeno uvolnění jen po dobu 25 hodin, kdy obě varianty s 50 % hnojiva přesáhly hranici dovoleného maxima 15 % vyloužených živin na 40 %.

V tavenině PHB byly společně s nutrienty zapracovány také plniva na bázi celulózy. 50 % KNO_3 v PHB a vlákny z bagasy byly míseny v hnětiči a následně podrobeny testu uvolnění živin. Bagasa zde zpomalovala uvolňování KNO_3. K charakterizaci byly nasazeny modely Korsmeyer–Peppas, Peppas–Sahlin, Higuchi. Nicméně dle grafů je jasné, že po 200 hod. byly vyplaveny všechny nutrienty [325].

V případě publikace popisující charakterizaci extrudovaných profilů z PHBV, celulózových vláken z olejových palem a KNO_3 je uvedena jen biodegradabilita jako úbytek celkové hmotnosti pelety (dle obrázku průměru 25 mm). Dle autorů se peleta rozloží do 16 týdnů. Kinetika uvolnění dusíku není prezentována [326]. Kompozice PHB, TPS a celulózy s 50 % KNO_3 byla připravena kombinací roztokové a extruzní techniky [327]. Po 24 hodinách testu ve vodě však bylo všechno KNO_3 uvolněno.

18 gramové pelety z PHBHx s vlákny z palmy (v poměru 70/30) a 15 % NPK byly testovány při růstu mladých palem olejných. Kinetika uvolňování byla sledována konduktometricky, ale nebyla přepočtena na procentuální hodnotu výluhu z celkové dávky hnojiva. Výsledky ukázaly, že PHA-CRF podporoval růst rostlin i půdní mikroflóru. Začlenění rostlinných vláken (surových nebo mletých) do PHA-CRF usnadnilo počáteční uvolňování některých hnojiv z PHA-CRF pravděpodobně kvůli absorpci vody. Další uvolňování hnojiv z PHA-CRF bylo podpořeno degradací PHA půdními mikroorganismy, což následně vedlo ke zvýšení prospěšných mikrobů v rhizosféře a ke zvýšení růstu rostlin [328].

V publikacích [329] a [330] je prezentována formulace močoviny postupně uvolňovaného z matrice PHB vyplněné přírodním nanočásticovým montmorilonitem. Mikrokapsule byly připraveny roztokovou metodou z chloroformového roztoku PHB a pomocných látek (PVAc, škrob). Je uvedeno, že dle normy měřená biodegradace připravených mikrokapsulí probíhá téměř lineárně po dobu 120 dní, nicméně zde chybí informace o uvolnění močoviny. Příprava probíhala pouze na laboratorní úrovni, navíc s malým obsahem močoviny (max. 20 %) v poměru k celkové formulaci.

Skupina prof. Volové na Sibiřské federální univerzitě v Krasnojarsku vyvinula a v laboratorních podmínkách testovala formulace pesticidů a hnojiv s prodlouženým účinkem založené na PHB. Testovanými formami byly filmy, granule nebo pelety PHB a pelety pak doplněné o výplň z přírodních materiálů (rašelina, dřevo, jíl), nesoucí agrochemikálie. Výzkumné práce shrnují informace o interakci PHB a použitých chemikálií, závislosti účinnosti na tvaru nosiče, strukturní, fyzikální a mechanické vlastnosti vyvinutých formulací, data o kinetice uvolňování chemikálií z matrice do půdy v laboratorních podmínkách a zhodnocení efektivity systému s postupným uvolňováním oproti komerčním formulacím. Dále se skupina věnovala hodnocení biodegradability a vlivu na složení půdních mikroorganismů. Na základě vstupních parametrů byly pro experimenty vybrány herbicid metribuzin, fungicid tebuconazol a hnojiva močovina a dusičnan amonný. Použití výplňového materiálu (rašelina, dřevo, jíl) umožnilo zpravidla urychlení biodegradace nosné matrice a zlevnění formulace, zatímco obalení (coating) pelet vrstvou polymeru degradaci jádra pelety zpomaluje. Použitím různých poměrů vstupních surovin, velikostí a tvaru pelet lze nastavit kinetiku uvolňování hnojiva. Vliv má samozřejmě také rozpustnost a další fyzikální vlastnosti použitého pesticidu nebo hnojiva. Jednotlivé formulace byly testované v laboratoři v půdních mikroekosystémech a jsou připravené jako prototypy pro další testování v reálných podmínkách [331], [332], [333]. Využití PHB pro uvolňování herbicidů a fungicidů je vedle CRF jedním z velmi zajímavých směrů s velkým potenciálem a je v plánu tento směr rozvíjet, nicméně zde nyní nebude dále komentován.

Povlakovaná hnojiva na bázi směsi PHBHx, PCL a dusičnanu amonného a technologie jejich laboratorní přípravy prezentoval tým z Japonska [334]. Kuličky ledku obalené ručně pásky z fólie připravené z roztoku chloroformu byly následně v lisu zahřáty tak, aby došlo k zatavení fólie do celistvého obalu. Připravené SRF bylo testováno ve vodním prostředí a v půdě. Výsledky ukazují, že povlak z čistého PHBHx má velmi malou propustnost pro vodu a tím i pro dusíkaté ionty. Přídavek PCL urychluje uvolňování nutrientů, poměr PHBHx/PCL 80/20 vyhovuje požadavkům na SRF. Po

14 týdnech ve vodě se uvolnilo cca 40 % NO_3^-. Autoři jsou si vědomi poněkud komplikovaného upscale této technologie. Přesto, že použili chloroform při laboratorní přípravě fólií, odkazují na možnost výroby fólií z PHB vyfukováním nebo technologií chill-roll. Uvádějí, že organická rozpouštědla jsou drahá a jejich uvolňování během kroku sušení může mít negativní dopady na životní prostředí. Potahování ve vodě rozpustnými polymery mělo potenciál zmírnit problémy s náklady a znečištěním, ale uvolňování živin je zpravidla příliš rychlé, aby splnilo kritéria SRF.

7.3 Cíle

Cílem výzkumu v této oblasti bylo využít vlastnosti přírodního biodegradabilního polymeru PHB ke konstrukci hnojiv s pomalým uvolňováním. V době sestavování projektu byla známá a předpokládaná následující fakta:

- PHB bude v technologii Hydal dostupné za cenu cca 4 €/kg
- PHB bude v technologii Hydal extrahováno chloroformem, ve výrobní technologii tak bude k dispozici 5% roztok PHB v chloroformu, který lze na výrobu hnojiva případně využít.
- Močovina je výborným dusíkatým hnojivem, její použití bez inhibitoru ureázy nebude možné, pokud nebude pozvolna uvolňována SRF hnojivem.
- Ledek amonný je výborným zdrojem dusíku pro rostliny, jeho zpracování je však problematické z pohledu bezpečnostních rizik
- Z procesu výroby po extrakci PHB vystupuje odpadní biomasa ve formě prášku a obsahuje fosfor a dusík
- Fosfor z biomasy lze vysrážet do formy struvitu, který je možné použít taktéž k hnojení.

7.4 Dosažené výsledky

Na základě výše uvedených faktů a informací z literární rešerše byly stanoveny koncepty možného řešení. Strategií bylo vytvořit jádro z rozpustného hnojiva a to opatřit povlakem na bázi PHB s řízenou tloušťkou, která bude definovat rychlost difuze. Povlak by měl navíc díky mikrobiální aktivitě degradovat a skrze póry jeho narušené struktury by se mělo postupně uvolňovat hnojivo. Základem proto byly nejdříve lisované pelety dusíkatého hnojiva opatřené přídavkem PHB prášku a případně dalších přísad jako je struvit a biomasa. Tyto pelety byly následně roztokovou metodou opatřeny povlakem na bázi PHB.

V průběhu řešení projektu došlo k několika zásadním změnám. Technologie Hydal začala využívat bezchloroformovou izolaci, chloroform spolu s mnoha VOC (volatile organic compounds) byly považovány z hlediska ekologie za nepřípustné v procesu izolace a podobně i v procesu výroby hnojiv. To vedlo výzkumný tým k přehodnocení způsobu roztokové přípravy povlaků, podařila se najít alternativa vhodného rozpouštědla k tomuto účelu alespoň ve smyslu snížení zdravotních rizik. Chloroform byl nahrazen „zeleným rozpouštědlem“ dioxolanem, který je netoxický, nekarcinogenní a šetrnější k životnímu prostředí [335].

Přestože je PHB považováno obecně za biodegradabilní a legislativa jej uvádí jako jeden z referenčních biodegradabilních polymerů, je třeba monitorovat reálné chování těchto materiálů v půdě za běžných podmínek a popsat jeho vliv na chování půdních mikroorganismů. K tomu jsou třeba citlivé analytické metody, které by měly umět poskytnout hodnoty koncentrace měřeného polymeru v půdě s dostatečnou přesností a citlivostí. Vzhledem k termické nestabilitě PHB a jeho

degradačním reakcím na kyselinu krotonovou není možné spoléhat se pouze na detekci 3HB kyseliny nebo jejich esterů. Situaci také komplikuje fakt, že PHB je nativně obsaženo v půdních bakteriích. Problematika je pospána v review o těchto metodách v **Pub 17**.

Pelety vyvíjeného hnojivového systému byly z velké části připravovány precizně na laboratorním ručním lisu a manuálně povlakovány (tzv. dip coating). Pro ověření možnosti zavedení do výroby byl koncept pelet o vybraném složení otestován v technologii průmyslové peletizace. Následně na těchto průmyslově připravených peletách bylo provedeno povlakování v průmyslu dostupnou technologií dražování v dražovacím bubnu.

Složení směsí pro přípravu pelet bylo navrženo na základě zkušeností popsaných v literatuře. Navíc, jak bylo při vývoji zjištěno, PHB v peletách neplní roli jen jako zpomalovač rychlosti uvolňování, ale z hlediska technologie povlakování jako modifikátor povrchu pelety a adhezní můstek k povlaku. Močovina i ledek jsou materiály velmi polární a z důvodu jejich rozdílné povrchové energie oproti PHB v chloroformovém roztoku nebylo možné čisté hnojivové pelety (100 % hnojiva v peletách) roztokem PHB v chloroformu v dražovacím bubnu povlakovat. Takto vytvořený povlak totiž ulpíval přednostně na stěnách dražovacího bubnu a díky nedostatečné adhezi byl velmi defektní. V případě mísení PHB do matrice hnojiva bylo tímto možno dosáhnout dostatečné adheze povlaku k peletě.

Preciznější optimalizace procesu s použitím roztoku na bázi dioxolanu, který měl i vhodnější viskozitu k povlakování než v případě chloroformu (v rámci projektu **PR 5**) a pozdější optimalizace rychlosti dávkování roztoku do dražovacího bubnu v rámci bakalářské práce **VSKP11** ukázala, že je možné realizovat povlak i na pelety čisté močoviny bez adhezního můstku. Variace obsahu PHB v peletě však prokázala, že malé množství PHB v peletě zlepšuje kvalitu povlaku z pohledu kinetiky uvolňování hnojiva ve vodném i půdním prostředí. Práce také ukázala důležitou roli čistoty rozpouštědla dioxolanu. V případě využití levnějšího dioxolanu o 90% čistotě oproti 99% standartně používané, docházelo k formování velmi nedokonalého a defektního povlaku.

Tab 8: Složení laboratorně připravených pelet na hydraulickém lisu

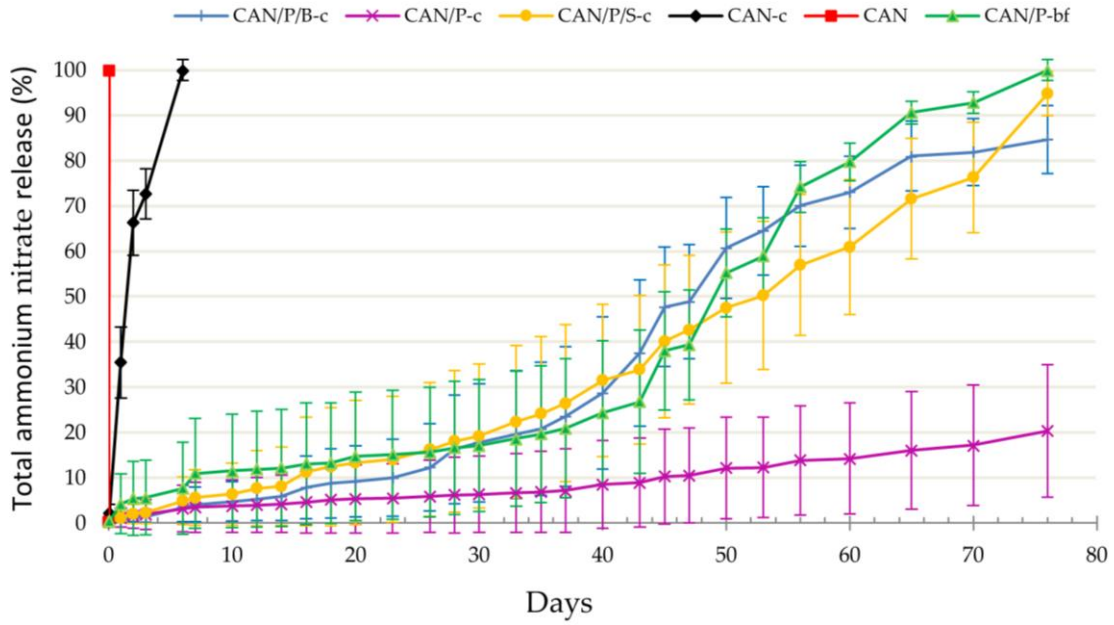
Composition of 6-Fold Manually Coated Fertilizer Pellets	
CAN/P/B-$_C$	50% CAN + 50% biomass + coating P3HB in dioxolane
CAN/P-$_C$	50% CAN + 50% P3HB + coating P3HB in dioxolane
CAN/P/S-$_C$	50% CAN + 25% P3HB + 25% struvite + coating P3HB in dioxolane
CAN-c	100% CAN + coating P3HB in dioxolane
CAN	100% CAN (positive reference)
CAN/P-$_{bf}$	50% CAN + 50% P3HB + biodegradable polymeric film (encapsulation)

Vlastnosti vybraných povlakovaných pelet byly charakterizovány ve vodném prostředí destilované vody a v rámci spolupráce s MENDELU byla účinnost hnojiv sledována ve vegetačních nádobových experimentech a následně i v rámci testu na polních parcelách. Výsledky z první části experimentu a řešení projektu **PR 5** byly publikovány v **Pub 18**. Zde byl využit dusičnan amonný (AN) v komerční kompozici (Calcium Amonium Nitrate – CAN), který obsahuje 27 % dusíku a 21 % dolomitu. Pomleté práškové hnojivo bylo homogenizováno s práškovým PHB, či struvitem nebo sušenou biomasou z výroby PHB (Nafigate). Sušená biomasa obsahovala cca. 60 % PHB. Práškové materiály hnojiva a aditiv byly poté manuálně stlačeny pomocí hydraulického lisu do formy tablety o hmotnosti 0,5 g, výšce 4 mm a průměru 10 mm. Tabulka 8 ukazuje sérii připravených pelet.

Testy povlakování dip-coatingem byly provedeny v roztoku PHB v chloroformu (7%) a v dioxolanu (6%). Vrstvy z roztoku v dioxolanu byly uniformní a roztok byl dostatečně filmotvorný.

7.4.1 Testy ve vodním prostředí

Vyrobené pelety byly podrobeny testu uvolňování dusíkatých iontů ve vodném prostředí. Toto poskytuje obraz o kvalitě povlaku a jeho stabilitě ve vodě. Rychlost prostupu dusíkatého hnojiva ideální nedefektní membránou na bázi PHB je velmi malá a řízená difúzí touto membránou. Přestup hnojiva do vodního prostředí skrze tento povlak je proto zpravidla řízen zejména přítomností defektů nebo rychlostí jejich vzniku. Příkladem typického vzniku nových defektů je difuze vody do pelety, její bobtnání a díky mechanickému napětí v povlaku pak vznik pórů a trhlin. V tomto testu při použití destilované vody se neuvažuje biologická degradace povlaku. Pro stanovení úbytku ledku z pelety byla využita vážková a konduktometrická metoda.



Obr. 43: Úbytek dusičnanu amonného z připravených pelet ve vodném prostředí.

Jak lze vidět z Obr. 43, v případě potahovaných pelet obsahujících 100% CAN bylo naměřeno velmi rychlé uvolňování. Polovina AN se z těchto pelet uvolnilo přibližně po 1,5 dnech a vše během 6 dnů. Přilnavost povlaku pravděpodobně nebyla dostatečná a vrstva byla defektní. Uvolňování dusičnanu amonného z potahovaných pelet obsahujících struvit, biomasu a pelety potažené fólií na bázi PHB vykazovalo podobný sigmoidní průběh uvolňování hnojiva. Polovina dusičnanu amonného byla uvolněna z pelet obsahujících struvit 53. den, u pelet obsahujících biomasu přibližně 48. den a u pelet s fólií přibližně 49. den. Na konci měření (76. den) se z fólií potažených pelet uvolnil všechen dusičnan amonný, z pelet obsahujících struvit 95 % AN a z pelet obsahující biomasu 85 % AN. Významně nejméně AN se uvolnilo z potahovaných pelet obsahujících 50 % CAN a 50 % PHB - pouze 20 %, což byl skvělý výsledek. Křivka uvolňování dusíku z amonného hnojiva má v tomto intervalu téměř lineární průběh, což svědčí o velmi kvalitně provedeném povlaku srovnatelným s povlaky ze syntetických polymerů [305]. Tento zřejmě bezdefektní povlak mohl vzniknout díky zlepšené adhezi povlaku PHB (rozpuštěného v dioxolanu) k peletám tohoto složení, obsahující PHB i v peletě. Výsledky těchto testů tak ukazují, že tyto pelety mají potenciál pro postupné uvolňování dusíku i v půdním prostředí.

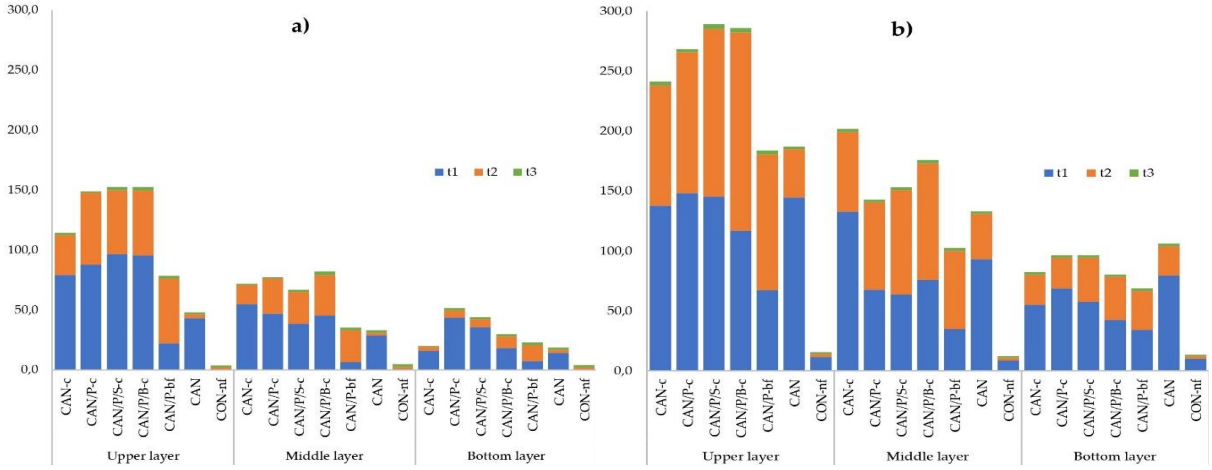
Boyandin a kol. [333] zkoumali uvolňování dusičnanu amonného ve vodném prostředí v peletách s šestinásobným povlakem PHB v chloroformu. Jejich pelety obsahovaly pouze 25 % dusičnanu amonného a zbytek tvořil PHB nebo jiné přísady (dřevěná moučka). Testování ve vodě v této studii trvalo pouze sedm dní. Z obalovaných pelet obsahujících dusičnan amonný a PHB se po sedmi dnech uvolnilo (18,3 ± 7,9) % hnojiva a z obalovaných pelet obsahujících rovněž dřevnou moučku se uvolnilo (13,4 ± 7,9) % hnojiva. Naše obalované pelety obsahující hnojivo s 50 % PHB nebo struvitu nebo biomasy měly po sedmi dnech pouze 3,5-5,7 % uvolněného dusičnanu amonného. Pelety ve fóliích uvolnily 11,5 % dusičnanu amonného.

7.4.2 Vegetační nádobové testy

Reálné chování hnojiva se zpomaleným uvolňováním lze nasimulovat v laboratorních podmínkách bez přirozené půdy jen velmi těžko. Do procesu uvolňování hnojiva z testovaných pelet nezasahují v reálných podmínkách jen fyzikální parametry (teplota, vlhkost a jejich průběh v čase, pH), ale zejména biologické procesy v půdním okolí pelety, které jsou navíc samy na těchto fyzikálních veličinách závislé. Pro úplnost je třeba zmínit i dopad mechanické manipulace s peletami při procesu výroby, skladu, aplikace apod. Vegetační nádobové a zejména polní testy jsou tedy klíčové pro pozorování reálného efektu navržených hnojiv. I ty polní však budou ovlivněny skutečnými sezónními podmínkami v dané lokalitě (parametry půdy a aktuálního počasí). Proto byly na Mendelově univerzitě v Brně provedeny nádobové testy ve vegetační hale s kontrolovanou teplotou a zálivkou. Cílem nádobového vegetačního pokusu bylo ověření účinku aplikace coatovaných hnojiv na vývoj a růst kukuřice SY Orpheus (Oseva, a.s., Bzenec, ČR) a na dynamiku uvolnění dusíku v půdě. Pokus probíhal v Mitscherlichových vegetačních nádobách (na 6,5 kg půdy). Během vegetace byly prováděny tyto půdní analýzy a analýzy rostlin ve třech termínech:

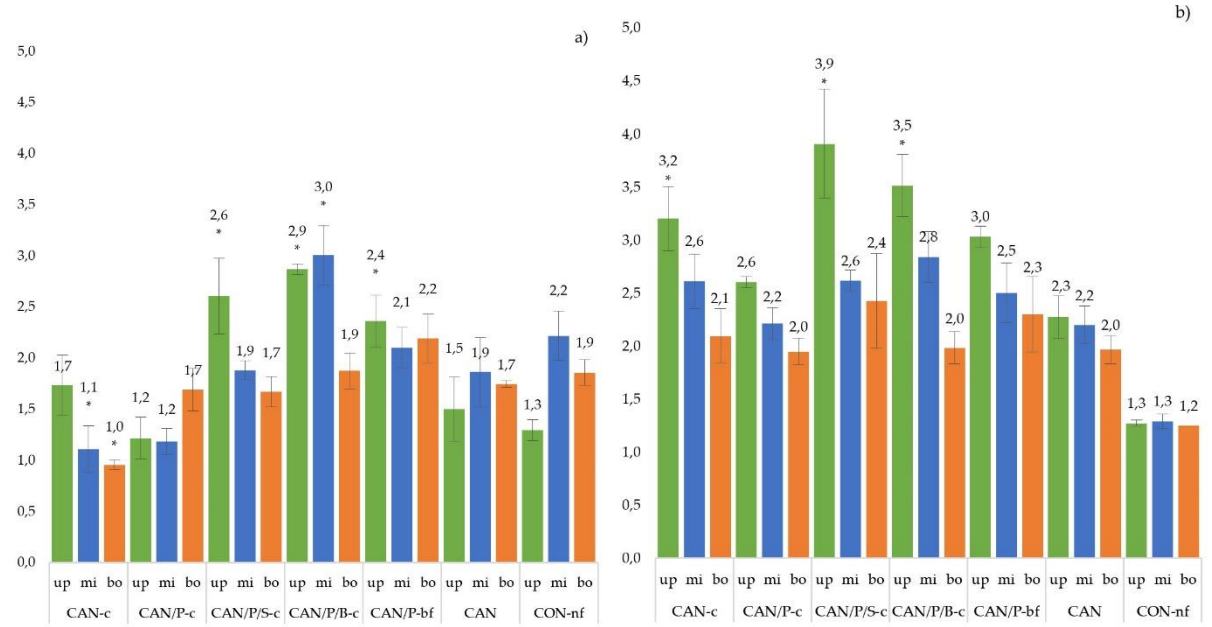
- odběr půdy ze 3 hloubek půdního profilu (v každém termínu vždy ze 4 nádob). Stanovení obsahu N_{min} (amonného (NH_4^+) a nitrátového dusíku (NO_3^-) v půdě – ve všech termínech
- hmotnost sušiny nadzemní části rostlin – ve všech termínech
- obsah N v nadzemní hmotě rostlin – ve všech termínech
- další analýzy jako stanovení chlorofylu v listu, vegetačního indexu, kořenové kapacity – na konci experimentu

Rozbory půdy a rostlin byly zhodnoceny statistickými metodami (program STATISTICA 12) metodou analýzy variance s následným testováním dle Tukeye, při 95 % hladině významnosti ($P \leq 0,05$). Statisticky průkazné rozdíly u sledovaných veličin (v grafech označeny *) jsou vztaženy vždy k necoatovaným produktům stejného typu hnojiva. Výsledky pokusů v nádobách prokázaly, že testovaná potahovaná hnojiva CAN je možno použít ke zlepšení účinnosti využití živin (nutrient use efficiency), snížení ztrát dusíku a minimalizaci znečištění životního prostředí díky postupnému dodávání dusíku rostlinám během vegetace. Uvolňování dusíku z obalovaných CAN hnojiv ovlivnilo dynamické změny obsahu minerálního dusíku v půdě během vegetace kukuřice. Obsahy N_{min} a jeho iontových forem (NO_3^-, NH_4^+) byly v půdě stanoveny ve třech termínech (t1–t3). Dynamika uvolňování sledovaných forem minerálního dusíku z hnojiv je uvedena na Obr. 44. Je zřejmé, že coatovaná hnojiva mají tendenci zadržovat dusík v půdě (v půdním profilu), přispívají k eliminaci jeho ztrát vyplavováním a tím zvyšují účinnost hnojení.



Obr. 44: Dynamika uvolňování a) amonné a b) dusičnanové formy dusíku (mg/kg půdy) testovaných variant s negativní referencí bez hnojiva CON-nf

V půdních rozborech provedených v 9. týdnu po zasetí je evidentní, že rostliny vyčerpaly minerální dusík z půdy. Svědčí o tom velmi nízké obsahy amonných a dusičnanových forem dusíku ve všech půdních vrstvách (Obr. 45). Avšak i v tomto termínu u obou forem dusíku existují zjevné rozdíly mezi použitými variantami hnojiv. Významně nejvyšší zásoby NH_4^+ a NO_3^- byly zjištěny u variant hnojených coatovanými hnojivy (zejména CAN/P/S-c, CAN/P/B-c) a zapouzdřeným hnojivem CAN/P-bf.



Obr. 45: Obsah a) amonné a b) dusičnanové formy dusíku na konci testu v jednotlivých hloubkových profilech půdy.

Ačkoli dostatek dostupného dusíku může být nezbytný pro přímou spotřebu rostlin, nadměrný obsah může zvýšit jeho ztráty v půdě. Jedním z důležitých aspektů obalovaných hnojiv je proto uvolňování živin optimální rychlostí vhodnou pro příjem rostlinami. Aplikace těchto potahovaných hnojiv CAN prokázala pozitivní vliv na průběh uvolňování N_{min} (NO_3^-, NH_4^+) a pozitivní dopad na další měřené parametry podrobně prezentované v **Pub 18 se svými grafickými přílohami**.

7.4.3 Čtvrtprovozní příprava povlakovaných hnojiv

V rámci projektu **PR 5** byla také testována technologie strojní výroby povlakovaných pelet. Pomocí peletizačního stroje bylo na Výskumnom ústave chemickej technológie (VÚCHT) připraveno přibližně 22 kg válcovitých peletek obsahujících dusíkaté hnojivo a PHB. Z bezpečnostních důvodů byla pro tento typ pelet vybrána na prášek mletá močovina, neboť ledek amonný není možné bezpečně zpracovávat v přítomnosti dalšího organického uhlíku (plánovaného přídavku PHB). Močovina je nejkoncentrovanějším tuhým dusíkatým hnojivem (46 % dusíku N). Po aplikaci probíhá v půdě rozklad močoviny na amonný a nitrátový dusík. Rozsah použití močoviny jako půdního hnojiva je velmi široký a zahrnuje prakticky všechny plodiny. Může být použita jak před zasetím, tak i v průběhu vegetace. Účinnost použití močoviny jako zdroje dusíku na velmi kyselých, silně alkalických půdách nebo těsně po vápnění může být výrazně nižší než u srovnatelných oblastí s pH neutrálními půdami. Močovina je vhodná pro hnojení polních plodin náročných na dusík (kukuřice, okopaniny, řepka).

Pelety byly v prvních verzích vyrobeny peletizací zhomogenizované práškové směsi močoviny a PHB v poměru 1:1. 7% roztok PHB v dioxolanu pro coating byl připravován pod zpětným chladičem a později pak v autoklávu (95 °C, tlak cca 1,25 bar). Tímto způsobem byl, za stálého míchání 600 ot./min, roztok PHB připraven již za 20−25 minut. Povlakování probíhalo dávkováním roztoku do dražovacího bubnu, kde se promíchávaly připravené pelety. Byly tak úspěšně naneseny souvislé vrstvy povlaku na peletkách bez viditelných defektů. Byla hledána optimální tloušťka povlaku změnou objemu aplikovaného roztoku. Po optimalizaci bylo na jednu várku hnojivových peletek (900 g) v dražovacím bubnu aplikováno cca. 2000 ml 7,4–7,9% roztoku PHB v 1,3-dioxolanu. Tyto pelety byly dále testovány ve vodním a půdním prostředí formou polních testů na parcelách.

7.4.4 Polní testy

Polní testy probíhaly na Školním zemědělském podniku Mendelovy univerzity u obce Žabčice, 25 km jižně od Brna. Tato oblast se nachází v nadmořské výšce 179 m, v jihomoravské suché oblasti s typickým vnitrozemským klimatem a jedná se o jednu z nejteplejších oblastí v České republice. Před aplikací hnojiv a zasetím kukuřice byla provedena klimatická a půdní charakteristika, ze které se vycházelo při vyhodnocování experimentu. Půda v předchozích nádobových testech byla stejná jako z této parcely. Pokus byl založen pro čtyři varianty: kontrola − negativní reference (bez hnojiva), pozitivní reference (močovina bez povlaku) a pelety připravené na peletizéru 50:50 (močovina:PHB) povlakované roztokem připravovaným pod zpětným chladičem a v autoklávu. Každá varianta byla založena ve čtyřech opakováních/parcelách o ploše 15 m^2.

K experimentu byla opět použita zrna kukuřice odrůdy SY Orpheus. Setba kukuřice a aplikace hnojiv byly provedeny 16. 4. 2021 a 27. 5. 2021 byl aplikován herbicid MAISTER POWER od společnosti Bayer S.A.S. (Lyon, Francie), v množství 1,5 l/ha. Dne 21. 10. 2021 proběhla sklizeň. Poté byl zjištěn výnos zrna kukuřice a hmotnost tisíce semen (HTS). Tato data byla vyhodnocena metodou jednofaktorové analýzy variance v programu STATISTICA 12 (s následným testováním dle Fischera, při 95% hladině významnosti). Z hodnot výnosu zrna a hmotnost tisíce semen (HTS) nejsou patrné statisticky významné rozdíly mezi výnosy při aplikaci 100% nepovlakované močoviny a povlakovaných variant hnojiv. Výsledky studia kvality kukuřice, konkrétně obsah N a škrobu a produkce bílkovin a škrobu jsou teprve zpracovávány.

7.4.5 Optimalizace složení

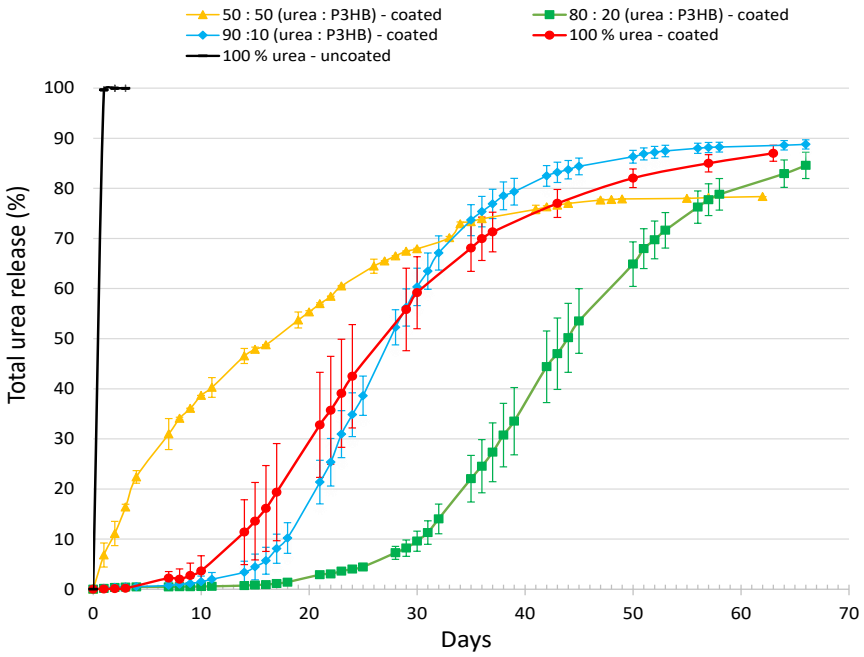
Z těchto prvních polních testů je patrné, že přítomnost poměrně vysokého množství PHB nemá negativní vliv na růst rostlin při tomto způsobu hnojení. Na základě těchto výsledků testů byla provedena optimalizace složení hnojivových formulací se záměrem snížit obsah PHB ve finálním produktu. Po optimalizaci procesních podmínek byla provedena peletizace směsí močoviny:PHB v poměrech 50:50 (kontrolní série pro porovnání s prvními výsledky), 80:20, 90:10 a 100:0. Pelety byly následně povlakovány dle postupu výše v dražovacím bubnu roztokem 7% PHB v dioxolanu připraveného v autoklávu. Plánovaná hmotnost PHB povlaku byla navržena na 20 % hmotnosti povlakované pelety. Stanovení hmotnosti pelet před a po povlakování včetně dvoudenní doby sušení však ukázalo na významnou odchylku od zamýšlené hodnoty. Zejména pelety o poměru močovina:PHB 80:20 a 90:10 vykazovaly 35–40% nárůst hmotnosti, což bylo způsobeno neoptimalizovanou rychlostí a způsobem dávkování roztoku do pelet v rotačním bubnu. Při rychlejším průtoku se nestačil dostatečně dioxolan odpařovat a zůstával částečně absorbovaný do pelety a částečně v povlaku. Sušení při vyšších teplotách nebylo možné, protože způsobovalo popraskání povlaku. Defektní byly povlaky pelet v poměru 50:50, které sice vykazovaly téměř správnou hodnotu přírůstku hmotnosti PHB, ale zřejmě vlivem přítomnosti většího množství dioxolanu nabotnaly, popraskaly a díky tomu se také následně lépe odpařil dioxolan. V podstatě správnou hodnotu přírůstku hmotnosti (18 %) vykazovaly jen pelety z čisté močoviny, které neměly možnost absorbovat dioxolan do pelety. Snížená hmotnost je dána ztrátami ulpíváním PHB na povrchu rotačního bubnu při povlakování.

Tyto pelety byly poté testovány ve vodném prostředí a vegetačních nádobových testech. Výsledky uvolňování močoviny ve vodním prostředí jsou patrny z Obr. 46. Až na sérii 50:50, která, jak bylo zmíněno, měla defektní povlak, nebylo z coatovaných pelet během prvních deseti dní uvolněno téměř žádné hnojivo a křivky vykazují správný esovitý průběh v souladu s teorií popsanou výše.

Délka lagfáze se zvyšuje s množstvím PHB v peletě. I zde se tedy potvrdil předpoklad, že obsah PHB v peletě umožňuje připravit odolnější povlak. Pelety se 100 % močoviny mají až na kratší lagfázi velmi podobný průběh uvolňování, k uvolnění 50 % hnojiva došlo po třech týdnech a 80 % po šesti týdnech. Tyto výsledky jsou velmi pozitivní, jelikož bylo možné připravit funkční povlak i bez PHB v peletě. Bylo to zřejmě způsobeno pomalejší rychlostí dávkování coatovacího roztoku oproti prvním experimentům. V půdním prostředí je však očekáván příspěvek mikrobiální aktivity k tvorbě defektů a tím zrychlení uvolnění živin z pelety. U pelet 80:20 byl průběh uvolňování močoviny první čtyři týdny velmi mírný, bylo uvolněno pouze 7 % hnojiva. Poté začala močovina difundovat do vody rychleji. Po více než šesti týdnech byla uvolněna pouze polovina dávky dusíkatého hnojiva. K uvolnění 80 % došlo až po více než 60 dnech. Tato varianta se díky vysokému zastoupení hnojiva v matrici a zároveň jeho značně zpomalenému uvolňování jeví jako nejoptimálnější.

Pro srovnání účinnosti tohoto povlaku je možné uvést příklady prezentované v některých publikacích. Např. u pelet 100% močoviny povlakovaných roztokem polystyrenu (PS) došlo k uvolnění 80 % hnojiva po cca 28 dnech, přičemž zastoupení povlaku PS na peletách tvořilo zhruba 10 % [336]. Zde vyvíjená hnojiva s PHB jakožto zcela biodegradabilním přírodním povlakem tedy dosahují ve vodním prostředí dokonce i lepších výsledků, než syntetický nerozložitelný PS. Z ostatních biopolymerů je díky své nízké ceně často studován také škrob, avšak samotný jej nelze použít.

U škrobu, v podobě akrylamidového hydrogelu vyztuženého nanočásticemi přírodního uhlí, bylo dosaženo uvolnění 70 % živin během 21 dní [337].

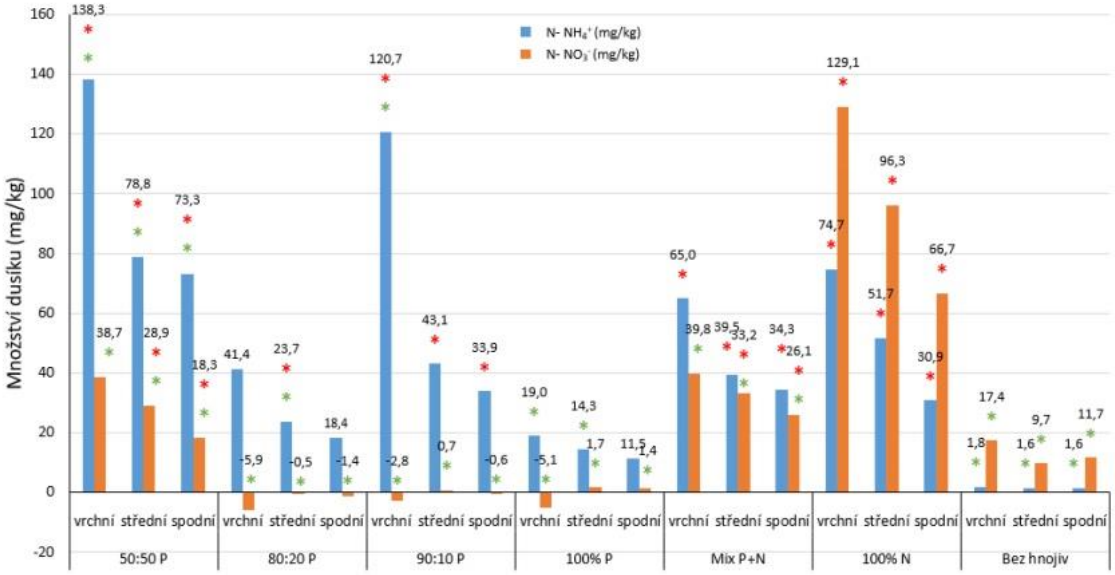


Obr. 46: Průběh uvolňování močoviny ve vodě ze strojně připravených pelet

Při nádobových testech vedených byly pelety sledovány i z pohledu jejich soudržnosti. Po dvou týdnech v půdním prostředí držely povlakované pelety všech variant svůj tvar, ale u části pelet došlo k částečnému porušení povlaku a absorpci vody. Po čtyřech týdnech se defektní pelety 50:50 již rozpadaly, byly nasáklé vodou a drolily se, u některých se již objevila plíseň. Pelety 80:20 a 90:10 držely svůj tvar lépe, nicméně u některých pelet byl povlak také porušen. K narušení povlaku docházelo zejména na koncích pelet. Povlakované pelety se 100 % močoviny byly už zcela vyprázdněné. Po šesti týdnech v půdě se pelety všech variant při vyjímání z půdy rozpadaly.

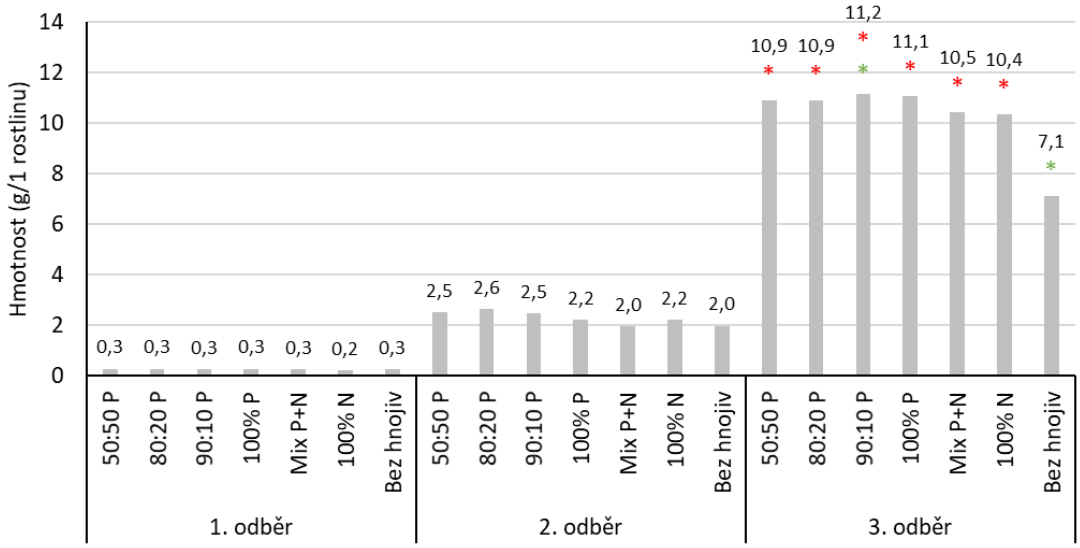
Z výsledků v době sepisování práce byly k dispozici pouze výsledky stanovení NH_4^+ a NO_3^- v půdě z prvního odběru. Hodnoty koncentrací byly vztaženy k negativní referenci (variantě bez hnojiva), jelikož určité množství minerálního dusíku se v půdě nachází i přirozeně. Významná je koncentrace především ve vrchní vrstvě, u které vysoké množství NH_4^+ indikuje riziko volatilizace, a ve spodní vrstvě, ze které je při vysokém obsahu NO_3^- usuzováno, že nedochází ke zpomalenému uvolňování kvůli rychlé nitrifikaci.

Po prvních dvou týdnech se hnojivo dle očekávání nejrychleji uvolnilo u pozitivní reference (100% nepovlakovaná močovina), u které je nejvyšší hodnota obsahu NO_3^- ve všech vrstvách, jelikož došlo k velmi rychlému uvolnění hnojiva a nitrifikaci NH_4^+ (Obr. 47). Je patrný rozdíl oproti ostatním povlakovaným peletám, u kterých byl prokázán zpomalující účinek díky povlaku a zabránění vyplavování NO_3^- iontů do spodních vrstev již v prvním termínu. K rychlému uvolnění močoviny došlo také u povlakovaných pelet 50:50, které mají vysoké hodnoty obsahu NH_4^+. Díky povlakové vrstvě však nedošlo k tak rychlé nitrifikaci. Uvolnění močoviny ale proběhlo rychleji, než u ostatních povlakovaných variant. I v půdním prostředí tedy bylo potvrzeno, že povlaková vrstva je u této varianty defektní. U varianty (mix 1/3 100% nepovlakovaná močovina + 2/3 80:20 povlakovaná) došlo k rozpuštění nepovlakované močoviny a jsou zde tedy také vyšší hodnoty obsahu NH_4^+ i NO_3^-.



Obr. 47: Obsah amonné a dusičnanové formy dusíku při prvním odběru (statisticky významný rozdíl od negativní reference; * statisticky významný rozdíl od pozitivní reference; P - povlakované; N - nepovlakované)*

U povlakovaných pelet 80:20 bylo uvolňování močoviny pomalejší, což dokazují nižší hodnoty NH_4^+. Hodnoty NO_3^- vyšly záporně, jedná se však pouze o odchylky při odečtu přirozeného dusíku v půdě. Půda hnojená povlakovanými peletami 90:10 vykázala vysoký obsah NH_4^+ ve vrchní vrstvě, u kterých tedy hrozí volatilizace. Obsah NO_3^- ale zaznamenán nebyl. Nízké hodnoty byly naměřeny také u povlakované 100% močoviny, nicméně je předpoklad, že vzhledem k absenci PHB v matrici, a tedy horší adhezi povlaku k peletám, došlo v dalším odběru ke skokovému nárůstu uvolněného množství.



Obr. 48: Vývoj hmotnosti sušiny nadzemní části rostlin pro jednotlivé varianty čtvrtprovozních pelet s různým obsahem močoviny : PHB (statisticky významný rozdíl od negativní reference; * statisticky významný rozdíl od pozitivní reference; P - povlakované; N - nepovlakované)*

V rámci tohoto nádobového testu pak byly týmem na MENDELU opět měřeny další parametry půdy a rostlin, které jsou již k dispozici pro všechny tři termíny odběrů. U vývoje hmotnosti sušiny nadzemní části rostlin (znázorněn na Obr. 48) nebyly po prvním ani po druhém odběru zaznamenány

mezi hmotnostmi statisticky významné rozdíly. Po třetím odběru, tedy po šesti týdnech, již byly patrné rozdíly mezi variantami s povlakovanými a nepovlakovanými hnojivy a u všech hnojených variant byly naměřeny výrazně vyšší hodnoty než u negativní reference (variantě bez hnojiva). U varianty 90:10 byly dokonce naměřeny statisticky významné hodnoty oproti pozitivní referenci (100% nepovlakovaná urea). Podobně byla naměřena statisticky významná odchylka u obsahu chlorofylu u varianty 80:20. Byl tedy pozorován pozitivní vliv povlakovaných hnojiv na růst nadzemních částí rostlin. Výsledky jsou nyní zpracovávány do formy článku.

7.4.6 Syntéza biomateriálů pro povlaky

Jedním ze směrů využití PHB je příprava reaktivních polyesterů. Vhodnou depolymerací například odpadního nebo nekvalitního PHA lze připravit oligomerní PHA. Ty lze pak využít pro biosource vytvrditelné povlaky. I v souvislosti s výzkumem materiálů pro povlakování hnojiv byla tomuto tématu věnována pozornost. Například při alkoholýze katalyzované paratoluensulfonovou kyselinou byly laboratorně připraveny metyl- a etylestery 3HB. Tato reakce byla vedena v mikrovlnném poli, což ji oproti klasické reakci za zvýšené teploty značně urychlilo a umožnilo její průběh za teploty, kdy je konkurenční degradační reakce na krotonový konec ještě násobně pomalejší. Získané alkylestery 3HB byly pak funkcionalizovány akrylovou kyselinou při reakci s anhydridem akrylové kyseliny za katalýzy 2-ethylhexanoátem draselným. Kinetika reakcí a jejich výtěžky byly popsány v **Pub 19.**

7.5 Přínos

Jak dokazují dosavadní vědecké práce, PHB je bezesporu slibným kandidátem pro výrobu hnojiv se zpomaleným uvolňováním z pohledu jeho bariérových vlastností a biodegradability. Z rešerše však vyplývá, že je obtížné dodržet limit maximální rychlosti uvolňování a to zejména, pokud má formulace vyšší obsah hnojiva než 50 %. Formulace založené na v tavenině zpracovaných "kompozitech" autorům publikací uvedených výše v tomto směru selhávaly. Pro tým Laboratoře bioplastů byl motivací úspěch týmu prof. Volové s peletami povlakovanými roztokem PHB v chloroformu, ale jimi dosažená maximální hranice 50% obsahu živin v peletě byla námi stanovena jako akceptovatelné minimum s cílem přiblížit se k 80 %. Legislativní změny také přispěly k náhradě chloroformu a volbě dioxolanu jako rozpouštědla pro povlakovací roztok. Výhodou jsou nižší zdravotní rizika při práci s dioxolanem. Nevýhodou je jeho hořlavost a vysoká cena na evropském trhu. Momentálně je ale možné zakoupit dioxolan na čínském trhu, který je 9krát levnější a cena je téměř na úrovni běžných rozpouštědel, jako např. aceton (cca 3,5 USD/1 kg dioxolanu).

V rámci projektu **PR 5** se podařilo naplnit výše uvedené cíle a prokázat, že lze tyto formulace vyrábět i strojně, byť z pohledu objemu stále v laboratorním měřítku. Vyvinuté formulace byly testovány nejen v nádobových experimentech, ale také v jedné sezóně v maloparcelních testech na kukuřici. Tento (z pohledu statistiky v agronomii stále nevýznamný) test ukázal, že je možné PHB technologicky zpracovat ve formě bariérového obalu do funkčního systému dusíkatého hnojiva, který splňuje základní parametry hnojiva se zpomaleným uvolňováním. Výsledky zaujaly Lovochemii a.s., která projevila zájem o spolupráci v rámci připravovaného a dnes již realizovaného projektu Národního centra kompetence materiálů pro 21. století - dílčího projektu Biopolymery pro agrochemické aplikace. Na základě výsledků publikovaných v článku **Pub 18** byl tým laboratoře Bioplastů osloven při přípravě evropského projektu HORIZON-JU-CBE-2023-IA-02 Production of safe, sustainable, and efficient bio-based fertilisers to improve soil health and quality.

8 ZÁVĚR

Tato práce prezentuje záměry a výsledky autora a jeho týmu v oblasti zpracování biopolymeru PHB do podoby vybraných aplikací. Jak je v textu postupně ukázáno, PHB z nynějšího pohledu a zkušeností bude mít vždy spoustu limitů zejména v případě klasických termoplastových aplikací. Jeho křehnutí spojené s jeho vysokou krystalinitou a fyzikálním stárnutím nad jeho teplotou skelného přechodu 0 °C lze jen velmi těžko potlačit bez zásahu do chemické struktury tohoto polymeru. To umožňuje například proces reaktivní kompaundace s vhodnými síťovacími činidly, chainextendery a dalšími polymery. Při vhodně zvolené stabilizaci a kompatibilizaci těchto často omezeně mísitelných komponent může vzniknout materiál s akceptovatelnými vlastnostmi pro vybrané aplikace. V případě aplikace v medicíně je však tato metoda problematická z pohledu zajištění biokompatibility a cytotoxicity. V ostatních aplikacích vyvstává otázka ceny za takový materiál, jehož mechanické vlastnosti nepřevyšují i levné konvenční plasty, zejména v době, kdy biodegradabilita není (až na několik málo jmenovaných aplikací) ani legislativou pro většinu plastových aplikací uznávána za výhodu a kdy recyklaci těchto materiálů komplikuje pochopitelná nepřipravenost třídících systémů na tyto materiály.

V mnoha zde citovaných publikacích se objevuje šlechetný záměr nahradit alespoň část plastových výrobků materiály z obnovitelných zdrojů za účelem snížení uhlíkové stopy. To je ve světle faktu, že jen 4 % fosilních zdrojů jsou použity k výrobě plastů, cíl s poměrně malým dopadem. Chybí také zpravidla LCA analýza dokládající, že je tento záměr vůbec teoreticky uskutečnitelný.

Laboratoř bioplastů si začala tato fakta před 5 lety uvědomovat. Po pochopení problémů a limitů spojených se zpracováním a vlastnostmi PHB a seznámení se se záměrem legislativy EU se proto orientovala jen na aplikace PHB, u kterých má smysl využít jeho vlastnosti biodegradability a biokompatibility jako přidané hodnoty. Získané dovednosti, znalosti i zkušenosti z výše popsané experimentální práce a vývoje s průmyslovými partnery tak byly dále využity pro vývoj materiálu na bázi PHB pro medicínu a její 3D tištěné aplikace, kosmetiku, agronomii a termoplastové speciality, které vytyčila stávající legislativa jako vhodné pro výrobu z bioplastů.

Jedním ze zásadních výsledků bylo nalezení funkční a poměrně atypické kombinace PHB a amorfního PLDLA. Spolu s vhodným změkčovadlem vybraným na základě poměrně širokého screeningu a hodnocení kinetiky jeho migrace z polymerní směsi byly vyvinuty funkční a zpracovatelné termoplastické směsi s majoritou PHB. Ty byly mimo jiné optimalizovány i pro 3D tisk z taveniny metodou FDM. Technologie výroby kompaundu i struny a vlastnosti při tisku byly ověřeny v průmyslovém výrobním procesu společnosti Fillamentum. I dle aktualizované rešerše to byl první reálně vyrobitelný a tisknutelný materiál s majoritou P3HB. Tyto úspěšné směsi byly také základem pro následný vývoj termoplastů a jejich kompozitů pro resorbovatelné náhrady kostní tkáně. Tištěné struktury z těchto materiálů byly sledovány z pohledu mechanických vlastností, kinetiky poklesu hmotnosti a molekulové hmotnosti v prostředí simulované tělní tekutiny, z pohledu biokompatibility a diferenciace mezenchymálních buněk a z pohledu role morfologie povrchu při jejich proliferaci. Výsledky byly využity pro modelový návrh náhrady segmentu femuru stehenní kosti, který byl v několika variantách vyroben 3D tiskem a testován s vizí budoucích *in vivo* experimentů.

PHB bylo testováno i v procesech roztokového zpracování do formy vláken a funkčních bariérových povlaků. Z chloroformového roztoku PHB s vybranými aditivy byly metodou odstředivého zvláknění z roztoku připravovány vlákenné struktury netkaných textilií s řízenými mechanickými vlastnostmi. Bylo zjištěno, že přídavek P3,4HB nebo adipátového změkčovadla efektivně modifikuje nejen mechanickou odezvu výsledné textilie, ale taktéž stabilizuje vlastnosti a kvalitu vláken a zvyšuje výkon laboratorní i poloprovozní linky, která využívá odlišný netoxický rozpouštědlový systém. Všechny varianty netkaných textilií byly biokompatibilní a netoxické pro 3T3 fibroblasty. U vysoce porézní struktury laboratorně připravených vzorků byla konfokálním mikroskopem prokázána požadovaná proliferace buněk do vlákenné struktury. Optimalizace porozity a monitoring buněk v řezu scaffoldu bude předmětem navazující práce.

Vynikajících výsledků bylo také dosaženo aplikací povlaku PHB připraveného z roztoku dioxolanu na dusíkaté hnojivo. Takto vytvořené hnojivo splňovalo kritéria aktuální legislativy na hnojiva se zpomaleným uvolňováním a biodegradabilitu jeho povlaku. Ve srovnání s aktuálně publikovanými výsledky bylo dosaženo velmi pomalého uvolňování s možností jeho řízení na míru pěstované vegetaci v poměrně širokém rozsahu. Koncept byl ověřen na technologiích existujících v průmyslu. Výsledný produkt byl úspěšně testován ve vegetačních nádobových experimentech i na maloparcelních testech.

Výsledky tak dokazují, že PHB má i přes jeho některé negativní vlastnosti obrovský potenciál v aplikacích, které mohou přispět ke snížení zátěže způsobené lidskou činností. Vzhledem ke stále se rozvíjejícím způsobům výroby různých PHA biopolymerů, a s tím spojenou problematikou kvality produktu a jejich stability, bude stále třeba hledat způsoby efektivního zpracování těchto zajímavých materiálů. Nutností pak bude začlenění těchto materiálu do procesů a principů cirkulární ekonomiky tak, aby benefity jeho využití převládaly nad nevýhodami, které jako i každý jiný materiál s sebou také přináší.

Ve všech zde prezentovaných řešených záměrech a projektech byla moje hlavní role zejména vedoucího výzkumné skupiny, školitele 4 doktorských studentů a vedoucího několika závěrečných prací. V pozici manažera projektů, které zajišťovaly financování celé skupiny o cca 9 osobách. Osobním přínosem pro řešenou problematiku a vznik výsledků byly i tyto konkrétní činnosti:

- Optimalizace dávkování PHB Hydal do technologií zpracování
- Provedení širokého screeningu aditiv pro PHB a jejich testování
- Zavedení výzkumu a vývoje biomateriálů na bázi PHB pro FDM 3D tiskové procesy
- Vývoj a výroba biodegradabilních fólií pro agronomii
- Návrh a realizace technologie laboratorní výroby 3D tiskové struny
- Návrh laboratorního systému dloužení polymerních pásků a vláken
- Optimalizace procesů odstředivého zvláknění roztoků PHB s aditivy
- Návrh laboratorní technologie výroby biodegradovatelných abrazivních částic pro kosmetiku
- Návrh záměru bezodpadové extrakce PHB využitím surfaktantů ze vstupní suroviny pro fermentaci

9 REFERENCE

[1] *Science to Protect Public Health and the Environment: EPA Research Program Overview 2016–2019*. s. 1-35. Dostupné z: https://www.epa.gov/sites/default/files/2015-10/documents/strap_2016_overview_508.pdf

[2] Zelená dohoda pro Evropu. *Evropská rada*. Dostupné z: https://www.consilium.europa.eu/cs/policies/green-deal/

[3] *SDĚLENÍ KOMISE EVROPSKÉMU PARLAMENTU, RADĚ, EVROPSKÉMU HOSPODÁŘSKÉMU A SOCIÁLNÍMU VÝBORU A VÝBORU REGIONŮ: Nový akční plán pro oběhové hospodářství, Čistší a konkurenceschopnější Evropa*. Brusel, 2020, ročník 2020. Dostupné z: https://eur-lex.europa.eu/legal-content/CS/TXT/HTML/?uri=CELEX:52020DC0098

[4] Circular economy action plan: The EU's new circular action plan paves the way for a cleaner and more competitive Europe. *An official website of the European Union*. Dostupné z: https://environment.ec.europa.eu/strategy/circular-economy-action-plan_en

[5] *Microplastics: The EU aims to address the growing volume of microplastics in the environment.*. Dostupné z: https://environment.ec.europa.eu/topics/plastics/microplastics_en

[6] *Plastics strategy: The EU's plastics strategy aims to transform the way plastic products are designed, produced, used and recycled in the EU.*. Dostupné z: https://environment.ec.europa.eu/strategy/plastics-strategy_en

[7] Cirkulárnímu Česku jsme o krok blíž. Vláda schválila první Akční plán pro cirkulární ekonomiku do roku 2027. Ministerstvo *životního prostředí.* Dostupné z: https://www.mzp.cz/cz/news_20230621_Cirkularnimu-Cesku-jsme-o-krok-bliz-Vlada-schvalila-prvni-Akcni-plan-pro-cirkularni-ekonomiku-do-roku-2027

[8] *Akční plán Cirkulární Česko 2040 pro období 2022-2027*. s. 1-112. Dostupné z: https://www.mzp.cz/C1257458002F0DC7/cz/news_20230621_Cirkularnimu-Cesku-jsme-o-krok-bliz-Vlada-schvalila-prvni-Akcni-plan-pro-cirkularni-ekonomiku-do-roku-2027/$FILE/AP_C%C4%8C_2040.pdf

[9] GOEL, Vishal, Priyanka LUTHRA, Gurpreet KAPUR a S. RAMAKUMAR. Biodegradable**/**Bio-plastics: Myths and Realities. Journal of Polymers and the Environment. 2021, 29(10), 3079-3104. ISSN 1566-2543. DOI: 10.1007/s10924-021-02099-1

[10] ALTMAN, Rebecca. The myth of historical bio-based plastics. Science. 2021, 373(6550), 47-49. ISSN 0036-8075. DOI: 10*.1126/science.abj1003*

[11] CHOUDHARY, Priyvart, Amritanshu PATHAK, Pankaj KUMAR, Chetana S a Nishesh SHARMA. Commercial *production of* bioplastic from organic waste–derived biopolymers viz-a-viz waste treatment: A minireview. Biomass Conversion and Biorefinery. ISSN 2190-6815. DOI: 10.1007/s13399-022-03145-1

[12] ROSENBOOM, Jan-Georg, Robert LANGER a Giovanni TRAVERSO. Bioplastics for a circular economy. Nature Reviews Materials. 2022, 7(2), 117-137. ISSN 2058-8437. DOI: *10.1038/*s41578-021-00407-8

[13] ROHMAWATI, Baiti, Fatin ATIKAH NATA SYA'IDAH, Rhismayanti RHISMAYANTI, Dante ALIGHIRI a Willy TIRZA EDEN. Synthesis of Bioplastic-based Renewable Cellulose *Acetate from* Teak Wood (Tectona grandis) Biowaste Using Glycerol-Chitosan Plasticizer. Oriental Journal of Chemistry. 2018, 34(4), 1810-1816. ISSN 0970020X. DOI: 10.13005/ojc/3404014

[14] MADHAVAN NAMPOOTHIRI, K., Nimisha NAIR a Rojan JOHN. An overview of the recent developments in polylactide (PLA) research. Bioresource Technology. 2010, 101(22), 8493-8501. ISSN 09608524. DOI: 10.1016/j.biortech.2010.05.092

[15] KESSLER, B., R. WEUSTHUIS, B. WITHOLT a G. EGGINK. Production of Microbial Polyesters: Fermentation and Downstream Processes. BABEL, Wolfgang a Alexander STEINBÜCHEL, ed., Wolfgang BABEL, Alexander STEINBÜCHEL. *Biopolyesters*. Berlin, Heidelberg: Springer Berlin Heidelberg, 2001, s. 159-182. Advances in Biochemical Engineering/Biotechnology. ISBN 978-3-540-41141-3. DOI: 10.1007/3-540-40021-4_5

[16] ALIOTTA, Laura, Maurizia SEGGIANI, Andrea LAZZERI, Vito GIGANTE a Patrizia CINELLI. A *Brief Review of* Poly (Butylene Succinate) (PBS) and Its Main Copolymers: Synthesis, Blends, Composites, Biodegradability, and Applications. Polymers. 2022, **14**(4). ISSN 2073-4360. DOI: 10.3390/polym14040844

[17] SIROHI, Ranjna, Shikhangi SINGH, Ayon TARAFDAR et al. Thermoplastic starch. *Biomass*, Biofuels, Biochemicals. Elsevier, 2021, s. 31-49. ISBN 9780128218884. DOI: 10.1016/B978-0-12-821888-4.00011-3

[18] LABET, Marianne a Wim THIELEMANS. Synthesis of polycaprolactone: a review. Chemical Society Reviews. *2009, 38(12)*. ISSN 0306-0012. DOI: 10.1039/b820162p

[19] SACCHI, Maria, João MARCICANO a Fernando VASCONCELOS. Biodegradable Polyamide 6.6 for Textile Application. Journal of *Management and Sustainability*. 2021, 11(2). ISSN 1925-4733. DOI: 10.5539/jms.v11n2p100

[20] YAMANO, Naoko, Norioki KAWASAKI, Sayuri IDA a Atsuyoshi NAKAYAMA. Biodegradation of *polyamide 4 in seawater. Polymer* Degradation and Stability. 2019, 166, 230-236. ISSN 01413910. DOI: 10.1016/j.polymdegradstab.2019.05.032

[21] FREDI, Giulia a Andrea DORIGATO. Recycling of bioplastic waste: A review. Advanced Industrial and Engineering Polymer Research. 2021, 4(*3), 159-177.* ISSN 25425048. DOI: 10.1016/j.aiepr.2021.06.006

[22] FAHIM, I.S., H. CHBIB a Hamada MAHMOUD. The synthesis, production & *economic feasibility of manufacturing* PLA from agricultural waste. Sustainable Chemistry and Pharmacy. 2019, 12. ISSN 23525541. DOI: 10.1016/j.scp.2019.100142

[23] NARODOSLAWSKY, M. LCA of PHA Production – Identifying the Ecological Potential of Bio-plastic. Chemical and Biochemical Engineering Quarterly. 2015, *29(2), 299-305.* ISSN 03529568. DOI: 10.15255/CABEQ.2014.2262

[24] REHAKOVA, Veronika, Iva PERNICOVA, Xenie KOURILOVA et al. Biosynthesis of versatile PHA copolymers by thermophilic members of the genus *Aneurinibacillus. International Journal of Biological* Macromolecules. 2023, 225, 1588-1598. ISSN 01418130. DOI: 10.1016/j.ijbiomac.2022.11.215

[25] LIU, Qian a Guo-Qiang CHEN. *In vitro* biocompatibility and degradation of terpolyester 3HB-co-4HB-co-3HHx, consisting of 3-hydroxybutyrate, 4-hydroxybutyrate and 3-hydroxyhexanoate. Journal of Biomaterials Science, Polymer Edition. 2012, 19(11*)*, 1521-1533. ISSN 0920-5063. DOI: 10.1163/156856208786140391

[26] VOLOVA, Tatiana, Olga VINOGRADOVA, Natalia ZHILA, Ivan PETERSON, Evgeniy KISELEV, Alexander VASILIEV, Aleksey SUKOVATIY a Ekaterina SHISHATSKAYA. Properties of a novel quaterpolymer P(3HB/4HB/3HV/3HHx). Polymer. 2016, 101, 67-74. ISSN 00323861. DOI: 10.1016/j.polymer.2016.08.048

[27] JUNG, Kuno, Roland HANY, Daniel RENTSCH, Tazio STORNI, Thomas EGLI a Bernard WITHOLT. Characterization of New Bacterial Copolyesters Containing *3-Hydroxyoxoalkanoates* and Acetoxy-3-hydroxyalkanoates**.** Macromolecules. 2000, 33(23), 8571-8575. ISSN 0024-9297. DOI: 10.1021/ma000829y

[28] LAUZIER, C., R.H. MARCHESSAULT, P. SMITH a H. CHANZY. Structural study of isolated poly(β-hydroxybutyrate) granules. Polymer. 1992, 33(*4), 823-827.* ISSN 00323861. DOI: 10.1016/0032-3861(92)90343-U

[29] OBRUCA, Stanislav, Petr SEDLACEK, Eva SLANINOVA, Ines FRITZ, Christina DAFFERT, Katharina MEIXNER, Zuzana SEDRLOVA a Martin *KOLLER. Novel* unexpected functions of PHA granules. Applied Microbiology and Biotechnology. 2020, 104(11), 4795-4810. ISSN 0175-7598. DOI: 10.1007/s00253-020-10568-1

[30] *PALMEIRO-SÁNCHEZ, Tania, Vincent O'FLAHERTY a* Piet LENS. Polyhydroxyalkanoate bio-production and its rise as biomaterial of the future. Journal of Biotechnology. 2022, **348,** 10-25. ISSN 01681656. DOI: 10.1016/j.jbiotec.2022.03.001

[31] *TianAn Biologic Materials Co., Ltd...* Dostupné z: http://www.tianan-enmat.com/

[32] *CJ BIO inaugurates 5,000 tonne PHA facility. Dostupné z: https://www.bioplasticsmagazine*.com/en/news/meldungen/20220502-PHA.php

[33] *Nodax® is 100% renewable* and is produced from readily available feedstocks: Danimer Scientific Uses Proprietary Processing to Produce Environmentally Responsible PHA.. Dostupné z: https://danimerscientific.com/pha-beginning-of-life/

[34] NOTA STAMPA BIO-ON: Bio-on news.. Dostupné z: http://www.bio-on.it/news.php

[35] Bio-On is back, saved by the Maip group. Bioplastic *Magazine.* Dostupné z: https://www.bioplasticsmagazine.com/en/news/meldungen/20230313_bio-on_maip.php

[36] KHANNA, Shilpi a Ashok SRIVASTAVA. Recent *advances* in microbial polyhydroxyalkanoates. Process Biochemistry. 2005, **40**(2), 607-619. ISSN 13595113. DOI: 10.1016/j.procbio.2004.01.053

[37] STEINBÜCHEL, A. a M. HOFRICHTER. Biopolymers. Chichester: Wiley-VCH, 2003. ISBN 35-273-0230-1.

[38] DOS SANTOS, Antonio, *Luiz OLIVEIRA DALLA VALENTINA, Andrey HIDALGO SCHULZ a Márcia TOMAZ* DUARTE. From Obtaining to Degradation of PHB: Material Properties. Part I. Ingeniería y Ciencia. 2017, 13(26), 269-298. ISSN 17949165. DOI: 10.17230/ingciencia.13.26.10

[39] HÄNGGI, Urs J. Virgin PHB has thermoplastic properties, but is not a thermoplast. s. 1-9. Dostupné z: https://*www.biomer.de/K*%C3%96LN2018**.**pdf

[40] GRASSIE, N., E.J. MURRAY a P.A. HOLMES. The thermal degradation of poly(-(d)-β-hydroxybutyric acid): Part 1—Identification and quantitative analysis of *products. Polymer Degradation* and Stability**.** 1984, 6(1), 47-61. ISSN 01413910. DOI: 10.1016/0141-3910(84)90016-8

[41] GRASSIE, N., E.J. MURRAY a P.A. HOLMES. The thermal degradation of poly(-(d)-β-hydroxybutyric acid): Part 2—Changes in molecular weight*. Polymer Degradation and* Stability. 1984, 6(2), 95-103. ISSN 01413910. DOI: 10.1016/0141-3910(84)90075-2

[42] GRASSIE, N., E.J. MURRAY a P.A. HOLMES. The thermal degradation of poly(-(d)-β-hydroxybutyric acid*):* Part 3—The reaction mechanism. Polymer Degradation and Stability. 1984, 6(3), 127-134. ISSN 01413910. DOI: 10.1016/0141-3910(84)90032-6

[43] ALVES, Mariane, Karine MACAGNAN, Amanda RODRIGUES et al. Poly(3-hydroxybutyrate*)-P(*3HB)**:** Review of Production Process Technology. Industrial Biotechnology. 2017, 13(4), 192-208. ISSN 1550-9087. DOI: 10.1089/ind.2017.0013

[44] ZAPLETAL, M a J TREJBAL. Izolace polyhydroxyalkanoátů z mikrobiální biomasy. Chemické Listy. 110(12), 860–867. Dostupné z: http*://www.*chemicke-listy.cz/ojs3/index.php/chemicke-listy/article/view/120

[45] SAAVEDRA DEL OSO, M., M. MAURICIO-IGLESIAS a A. HOSPIDO. Evaluation and optimization of the environmental performance of PHA downstream processing. *Chemical Engineering* Journal. 2021, 412. ISSN 13858947. DOI: 10.1016/j.cej.2020.127687

[46] KOLLER, Martin, Lukáš MARŠÁLEK, Miguel DE SOUSA DIAS a Gerhart BRAUNEGG. Producing microbial polyhydroxyalkanoate (PHA) biopolyesters in *a sustainable* manner. New Biotechnology. 2017, 37, 24-38. ISSN 18716784. DOI: 10.1016/j.nbt.2016.05.001

[47] KOLLER, Martin. Established and advanced approaches for recovery of microbial polyhydroxyalkanoate (PHA) biopolyesters from surrounding microbial *biomass*. The EuroBiotech Journal. 2020, 4(3), 113-126. ISSN 2564-615X. DOI: 10.2478/ebtj-2020-0013

[48] MADKOUR, Mohamed, Daniel HEINRICH, Mansour ALGHAMDI, Ibraheem SHABBAJ a Alexander STEINBÜCHEL. PHA Recovery from Biomass. Biomacromolecules. 2013, 14(9), 2963-2972*. ISSN* 1525-7797. DOI: 10.1021/bm4010244

[49] MOHAMMADI, Mitra, Mohd HASSAN, Yoshihito SHIRAI et al. Separation and Purification of Polyhydroxyalkanoates from Newly Isolated Comamonas sp. EB172 by Simple Digestion with Sodium Hydroxide. Separation Science and Technology. 2012, 47(3), 534-541. ISSN 0149-6395. DOI: 10.1080/01496395.2011.615788

[50] RODRIGUES, Ana, Rita FRANCA, Madalena DIONÍSIO, Chantal SEVRIN, Christian GRANDFILS, Maria REIS a Nídia LOURENçO. Polyhydroxyalkanoates from a Mixed Microbial Culture: *Extraction Optimization and Polymer Characterization.* Polymers. 2022, 14(11). ISSN 2073-4360. DOI: 10.3390/polym14112155

[51] BURNIOL-FIGOLS, Anna, Ioannis SKIADAS, Anders DAUGAARD a Hariklia GAVALA. Polyhydroxyalkanoate (PHA) purification through dilute aqueous ammonia digestion at elevated temperatures. Journal of Chemical Technology & Biotechnology. 2020, 95(5), *1519-1532*. ISSN 0268-2575. DOI: 10.1002/jctb.6345

[52] IRDAHAYU, Nik, Kannusamy SHANTINI, Kai-Hee HUONG*, Sevakumaran* VIGNESWARI, Nursolehah AZIZ, Mohd. AZIZAN a Al-Ashraf AMIRUL. En route to economical eco-friendly solvent system in enhancing sustainable recovery of poly(3-hydroxybutyrate- co -4-hydroxybutyrate) copolymer. *Engineering in Life Sciences*. 2017, **17**(9), 1050-1059. ISSN 16180240. DOI: 10.1002/elsc.201600217

[53] První zmínky o 3D *tisku.* 3d-tiskni.cz. Zlín, 2020. Dostupné z: https://3d-tiskni.cz/prvni-zminky-o-3d-tisku/

[54] Náš příběh. Prusa Research. Praha: Prusa Research, 2022. Dostupné z: https://www.prusa3d.com/cs/stranka/nas-pribeh_875/

[55] BUJ-CORRAL, Irene, Aitor TEJO-OTERO a Felip FENOLLOSA-ARTÉS. Use of FDM Technology in Healthcare Applications: Recent Advances. DAVE, Harshit K. a J. Paulo DAVIM**,** ed., Harshit DAVE, J. DAVIM. Fused Deposition Modeling Based 3D Printing. Cham: Springer International Publishing, 2021, s. 277-297.

Materials Forming, Machining and Tribology. ISBN 978-3-030-68023-7. DOI: 10.1007/978-3-030-68024-4_15

[56] ALPER, R., D. LUNDGREN, R. MARCHESSAULT a W. COTE. Properties of poly-3-hydroxybutyrate. *I. General considerations concerning the naturally occurring* polymer. Biopolymers**.** 1963, 1(6), 545-556. ISSN 0006-3525. DOI: 10.1002/bip.360010605

[57] SHELTON, J., Jerome LANDO a Dennis AGOSTINI. Synthesis and characterization of poly(β-hydroxybutyrate). Journal of Polymer Science Part B: Polymer Letters. 1971, 9(3), 173-178. ISSN 04492986. DOI: 10.1002/pol.1971.110090303

[58] HOFFMANN, A., S. KREUZBERGER a G. HINRICHSEN. Influence of thermal *degradation on* tensile strength and Young's modulus of poly(hydroxybutyrate). Polymer Bulletin. 1994, 33(3), 355-359. ISSN 0170-0839. DOI: 10.1007/BF00314274

[59] EL-HADI, A, R SCHNABEL, E STRAUBE, G MÜLLER a S HENNING. Correlation between degree of *crystallinity, morphology,* glass temperature, mechanical properties and biodegradation of poly (3-hydroxyalkanoate) PHAs and their blends. Polymer Testing. 2002, 21(6), 665-674. ISSN 01429418. DOI: 10.1016/S0142-9418(01)00142-8

[60] PUENTE, Jorge, Antonella ESPOSITO, Frédéric CHIVRAC a Eric DARGENT. Effect of boron nitride as a nucleating agent on *the crystallization of* bacterial poly(3-hydroxybutyrate). Journal of Applied Polymer Science. 2013, 128(5), 2586-2594. ISSN 00218995. DOI: 10.1002/app.38182

[61] JAQUES, Nichollas, Ingridy SILVA, Manoel BARBOSA NETO, Andreas RIES, Eduardo CANEDO a Renate WELLEN. Effect of heat cycling on melting *and crystallization of PHB*/TiO2 compounds**.** Polímeros. 2018, 28(2), 161-168. ISSN 1678-5169. DOI: 10.1590/0104-1428.12416

[62] JACQUEL, Nicolas, Koichirou TAJIMA, Nobuo NAKAMURA, Hideo KAWACHI, Pengju PAN a Yoshio INOUE. Nucleation mechanism of polyhydroxybutyrate and poly(hydroxybutyrate- co -hydroxyhexanoate) crystallized by orotic acid as a nucleating agent. Journal of Applied Polymer Science. *2010, 115(2),* 709-715. ISSN 00218995. DOI: 10.1002/app.30873

[63] KAI, Weihua, Yong HE a Yoshio INOUE. Fast crystallization of poly(3-hydroxybutyrate) and poly(3-hydroxybutyrate-co-3-hydroxyvalerate) with talc and boron nitride as nucleating *agents*. Polymer International. 2005, 54(5), 780-789. ISSN 0959-8103. DOI: 10.1002/pi.1758

[64] CAL, Andrew, Brian GRUBBS, Lennard TORRES, Timothy RIIFF, Rena KIBBLEWHITE, William ORTS a Charles LEE. Nucleation and plasticization with recycled low-molecular-weight poly-3-hydroxybutyrate toughens virgin poly-3-hydroxybutyrate. Journal of Applied Polymer Science. 2019, **136**(17). ISSN 0021-8995. DOI: 10.1002/app.47432

[65] HOBBS, J. K. The fracture of poly(hydroxybutyrate)Part I Fracture mechanics study during ageing. *Journal of* Materials Science**.** 1998, 33(10), 2509-2514. ISSN 0022-2461. DOI: 10.1023/A:1004384631218

[66] HOBBS, J. a P. BARHAM. The fracture of poly(hydroxybutyrate)Part II Fracture mechanics study after annealing. Journal of Materials Science. 1998, 33(10), 2515-2518. *ISSN* 0022-2461. DOI: 10.1023/A:1004336715288

[67] HOBBS, J. a P. BARHAM. The fracture of poly(hydroxybutyrate) Part III Fracture morphology in thin films and bulk systems. Journal of *Materials Science. 1999, 34(19),* 4831-4844. ISSN 00222461. DOI: 10.1023/A:1004659726586

[68] DE KONING, G. J. M. Embrittlement and Rejuvenation of Bacterial Poly[(R)-3-hydroxybutyrate]. FISHMAN, Marshall L., Robert B. FRIEDMAN a Samuel J. HUANG, ed., Marshall FISHMAN*, Robert* FRIEDMAN, Samuel HUANG. Polymers from Agricultural Coproducts. Washington, DC: American Chemical Society, 1994, s. 188-201. ACS Symposium Series. ISBN 9780841230415. DOI: 10.1021/bk-1994-0575.ch013

[69] DE KONING, G.J.M. a P.J. LEMSTRA. Crystallization phenomena in bacterial poly[(R)-3-hydroxybutyrate]: 2. Embrittlement and rejuvenation. Polymer. *1993, 34(19),* 4089-4094. ISSN 00323861. DOI: 10.1016/0032-3861(93)90671-V

[70] DE KONING, G.J.M., A.H.C. SCHEEREN, P.J. LEMSTRA, M. PEETERS a H. REYNAERS. Crystallization phenomena in bacterial poly[(R)-3-hydroxybutyrate]: 3. Toughening via *texture changes. Polymer.* 1994, **35**(21), 4598-4605. ISSN 00323861. DOI: 10.1016/0032-3861(94)90809-5

[71] CESàRO, Attilio, Luciano NAVARINI a Renzo PEPI. A modulated DSC analysis of microbial biocompatible polyesters. Thermoch. Acta. 1993, 227, 157-166. ISSN 00406031. DOI: 10.1016/0040-6031(93)80259-D

[72] DI LORENZO, Maria a René ANDROSCH. Crystallization of Poly[(R)-3-hydroxybutyrate]. DI LORENZO, Maria Laura a René ANDROSCH, ed., Maria DI LORENZO, René ANDROSCH. Thermal Properties of Bio-based *Polymers. Cham:* Springer International Publishing, 2019, s. 119-142. Advances in Polymer Science. ISBN 978-3-030-39961-0. DOI: 10.1007/12_2019_50

[73] YUXIAN, An, Li LIXIA, Dong LISONG, Mo ZHISHEN a Feng ZHILIU. Nonisothermal Crystallization and Melting Behavior ofPoly(b-hydroxybutyrate)–Poly(vinyl-acetate) Blends. Journal of Polymer Science Part B: Polymer Physics. 1999, 37(5), 443-450. ISSN 0887-6266. DOI: 10.1002/(SICI)1099-0488(19990301)37:5<443::AID-POLB4>3.0.CO;2-Bopen_in_newISSN

[74] RENSTAD, Rasmus, Sigbritt KARLSSON a Ann-Christine ALBERTSSON. Influence of processing parameters on the molecular weight and mechanical properties of poly(3-hydroxybutyrate-co-3-hydroxyvalerate). *Polymer Degradation and Stability*. 1997, 57(3), 331-338. ISSN 01413910. DOI: 10.1016/S0141-3910(97)00028-1

[75] PACHEKOSKI, Wagner, Carla DALMOLIN a José AGNELLI. The influence of the industrial processing on the degradation of poly(hidroxybutyrate) - PHB. *Materials Research*. 2013, 16(2), 237-332. ISSN 1980-5373. DOI: 10.1590/S1516-14392012005000180

[76] QUISPE, Mayte, Olivia LÓPEZ a Marcelo VILLAR. Antioxidant Efficiency of Irganox® 1010 on Processing and Properties of Plasticized Poly(3-Hydroxybutyrate) Films. *Journal of Composites and Biodegradable Polymers*. 2021, 9, 7-16. ISSN 2311-8717. DOI: 10.12974/2311-8717.2021.09.02

[77] WANG, Liang, Wenfu ZHU, Xiaojuan WANG, Xianyu CHEN, Guo-Qiang CHEN a Kaitian XU. Processability modifications of poly(3-hydroxybutyrate) by plasticizing, blending, and stabilizing. *Journal of Applied Polymer Science*. 2008, 107(1), 166-173. ISSN 00218995. DOI: 10.1002/app.27004

[78] BOTANA, Adrian, Mariana MOLLO, Patricia EISENBERG a Rosa TORRES SANCHEZ. Effect of modified montmorillonite on biodegradable PHB nanocomposites. *Applied Clay Science*. 2010, 47(3-4), 263-270. ISSN 01691317. DOI: 10.1016/j.clay.2009.11.001

[79] KOVALCIK, Adriana, Jiri SMILEK, Michal MACHOVSKY et al. Properties and structure of poly(3-hydroxybutyrate-co-4-hydroxybutyrate) filaments for fused deposition modelling. *International Journal of Biological Macromolecules*. 2021, 183, 880-889. ISSN 01418130. DOI: *10*.1016/j.ijbiomac.2021.04.183

[80] ANGELINI, Stefania, Pierfrancesco CERRUTI, Barbara IMMIRZI, Merima POSKOVIC, Gabriella SANTAGATA, Gennaro SCARINZI a Mario MALINCONICO. From Microbial Biopolymers to Bioplastics: Sustainable Additives for PHB Processing and Stabilization. KALIA, Vipin Chandra, ed., Vipin KALIA. *Microbial Factories*. New Delhi: Springer India, 2015, s. 139-160. ISBN 978-81-322-2594-2. DOI: 10.1007/978-81-322-2595-9_10

[81] PERSICO, Paola, Veronica AMBROGI, Antonio BARONI, Gabriella SANTAGATA, Cosimo CARFAGNA, Mario MALINCONICO a Pierfrancesco CERRUTI. Enhancement of poly(3-hydroxybutyrate) thermal and processing stability using a bio-waste derived additive. *International Journal of Biological Macromolecules*. 2012, 51(5), 1151-1158. ISSN 01418130. DOI: 10.1016/j.ijbiomac.2012.08.036

[82] AURIEMMA, Maria, Amodio PISCITELLI, Rossana PASQUINO, Pierfrancesco CERRUTI, Mario MALINCONICO a Nino GRIZZUTI. Blending poly(3-hydroxybutyrate) with tannic acid: Influence of a polyphenolic natural additive on the rheological and thermal behavior. *European Polymer Journal*. 2015, 63, 123-131. ISSN 00143057. DOI: 10.1016/j.eurpolymj.2014.12.021

[83] CHEN, Cheng, Bin FEI, Shuwen PENG, Yugang ZHUANG, Lisong DONG a Zhiliu FENG. The kinetics of the thermal decomposition of poly(3-hydroxybutyrate) and maleated poly(3-hydroxybutyrate). *Journal of Applied Polymer Science*. 2002, 84(9), 1789-1796. ISSN 0021-8995. DOI: 10.1002/app.10463

[84] TURCO, Rosa, Gabriella SANTAGATA, Iolanda CORRADO, Cinzia PEZZELLA a Martino DI SERIO. *In vivo* and Post-synthesis Strategies to Enhance the Properties of PHB-Based Materials: A Review. *Frontiers in Bioengineering and Biotechnology*. 2021, 8. ISSN 2296-4185. DOI: 10.3389/fbioe.2020.619266

[85] PANAITESCU, Denis, Cristian NICOLAE, Adriana FRONE, Ioana CHIULAN, Paul STANESCU, Constantin DRAGHICI, Michaela IORGA a Mona MIHAILESCU. Plasticized poly(3-hydroxybutyrate) *with improved melt processing and balanced properties*. Journal **of** Applied Polymer Science. 2017, 134(19). ISSN 00218995. DOI: 10.1002/app.44810

[86] ERCEG, Matko, Tonka KOVAČIĆ a Ivka KLARIĆ. Thermal degradation of poly(3-hydroxybutyrate) plasticized with acetyl tributyl citrate. Polymer Degradation and Stability. 2005, 90(2), 313-318. *ISSN 01413910*. DOI: 10.1016/j.polymdegradstab.2005.04.048

[87] KUNZE, Carmen, Thomas FREIER, Sven KRAMER a Klaus-Peter SCHMITZ. Anti-inflammatory prodrugs as plasticizers for biodegradable implant materials based *on poly(3-hydroxybutyrate)*. Journal **of** Materials Science: Materials in Medicine. 2002, 13(11), 1051-1055. ISSN 09574530. DOI: 10.1023/A:1020392606225

[88] LONGÉ, Lionel, Laurent MICHELY, Antoine GALLOS et al. Improved Processability and Antioxidant Behavior of Poly(3-hydroxybutyrate) in Presence of Ferulic Acid-Based Additives. *Bioengineering*. 2022, 9(3). ISSN 2306-5354. DOI: 10.3390/bioengineering9030100

[89] NASER, Ahmed, Ibrahim DEIAB, Fantahun DEFERSHA a Sheng YANG. Expanding Poly(lactic acid) (PLA) and Polyhydroxyalkanoates (PHAs) Applications: A Review on Modifications and Effects. *Polymers*. 2021, 13(23). ISSN 2073-4360. DOI: 10.3390/polym13234271

[90] BRIASSOULIS, Demetres, Philippos TSEROTAS a Ioanna-Georgia ATHANASOULIA. Alternative optimization routes for improving the performance of poly(3-hydroxybutyrate) (PHB) based plastics. *Journal of Cleaner Production*. 2021, 318. ISSN 09596526. DOI: 10.1016/j.jclepro.2021.128555

[91] PHUA, Y., A. PEGORETTI, T. ARAUJO a Z. ISHAK. Mechanical and thermal properties of poly(butylene succinate)/poly(3-hydroxybutyrate- co -3-hydroxyvalerate) biodegradable blends. *Journal of Applied Polymer Science*. 2015, 132(47), -. ISSN 00218995. DOI: 10.1002/app.42815

[92] DE MATOS COSTA, Anna, Raquel SANTOS, Edson ITO, Laura DE CARVALHO a Eduardo CANEDO. Melt and cold crystallization in a poly(3-hydroxybutyrate) poly(butylene adipate-co-terephthalate) blend. *Journal of Thermal Analysis and Calorimetry*. 2019, 137(4), 1341-1346. ISSN 1388-6150. DOI: 10.1007/s10973-019-08027-9

[93] CYRAS, V., A. VÁZQUES, Ch. ROZSA, N. GALEGO FERNÁNDEZ, L. TORRE a J. KENNY. Thermal stability of P(HB-co-HV) and its blends with polyalcohols. *Journal of Applied Polymer Science*. 2000, 77(13), 2889-2900. DOI: 10.1002/1097-4628(20000923)77:13<2889::AID-APP11>3.0.CO;2-O

[94] GRECO, Pietro a Ezio MARTUSCELLI. Crystallization and thermal behaviour of poly(d(—)-3-hydroxybutyrate)-based blends. *Polymer*. 1989, 30(8), 1475-1483. ISSN 00323861. DOI: 10.1016/0032-3861(89)90219-X

[95] CHANG, Ling, Yin-Hsuan CHOU a Eamor WOO. Effects of amorphous poly(vinyl acetate) on crystalline morphology of poly(3-hydroxybutyric acid-co-3-hydroxyvaleric acid). *Colloid and Polymer Science*. 2011, 289(2), 199-211. ISSN 0303-402X. DOI: 10.1007/s00396-010-2330-7

[96] AN, Yuxian, Lisong DONG, Lixia LI, Zhishen MO a Zhiliu FENG. Isothermal crystallization kinetics and melting behavior of poly(β-hydroxybutyrate)/poly(vinyl acetate) blends. *European Polymer Journal*. 1999, 35(3), 365-369. ISSN 00143057. DOI: 10.1016/S0014-3057(98)00145-1

[97] AHMED EL-HADI, RAINER SCHNABEL, EKKEHARD STRAUBE, GERT MÜLLER, M. RIEMSCHNEIDER. Effect of Melt Processing on Crystallization Behavior and Rheology of Poly(3-hydroxybutyrate) (PHB) and its Blends. *Macromolecular Materials and Engineering*. 2002, 287(5), 363-372. ISSN 1438-7492. DOI: 10.1002/1439-2054(20020501)287:5<363::AID-MAME363>3.0.CO;2-D

[98] ABDELWAHAB, Mohamed, Allison FLYNN, Bor-Sen CHIOU, Syed IMAM, William ORTS a Emo CHIELLINI. Thermal, mechanical and morphological characterization of plasticized PLA–PHB blends. *Polymer Degradation and Stability*. 2012, 97(9), 1822-1828. ISSN 01413910. DOI: 10.1016/j.polymdegradstab.2012.05.036

[99] NOFAR, Mohammadreza, Dilara SACLIGIL, Pierre CARREAU, Musa KAMAL a Marie-Claude HEUZEY. Poly (lactic acid) blends: Processing, properties and applications. *International Journal of Biological Macromolecules*. 2019, 125, 307-360. ISSN 01418130. DOI: 10.1016/j.ijbiomac.2018.12.002

[100] LU, Huiqiang, Sergei KAZARIAN a Harumi SATO. Simultaneous Visualization of Phase Separation and Crystallization in PHB/PLLA Blends with In Situ ATR-FTIR Spectroscopic Imaging. *Macromolecules*. 2020, 53(20), 9074-9085. ISSN 0024-9297. DOI: 10.1021/acs.macromol.0c00713

[101] OLEJNIK, Olga, Anna MASEK a Jakub ZAWADZIłłO. Processability and Mechanical Properties of Thermoplastic Polylactide/Polyhydroxybutyrate (PLA/PHB) Bioblends. *Materials*. 2021, 14(4). ISSN 1996-1944. *DOI: 10.3390*/ma14040898

[102] ZHANG, Jianming, Harumi SATO, Tsuyoshi FURUKAWA, Hideto TSUJI, Isao NODA a Yukihiro OZAKI. Crystallization Behaviors of Poly(3-hydroxybutyrate) and Poly(l -lactic acid) in Their Immiscible and Miscible Blends. *The Journal of Physical Chemistry B*. 2006, 110(48), 24463-24471. ISSN 1520-6106. DOI: 10.1021/jp065233c

[103] GUNARATNE, L.M. a R.A. SHANKS. Miscibility, melting, and crystallization behavior of poly(hydroxybutyrate) and poly(D,L-lactic acid) blends. *Polymer Engineering & Science*. 2008, 48(9), 1683-1692. ISSN 00323888. DOI: 10.1002/pen.21051

[104] DONG, Weifu, Piming MA, Shifeng WANG, Mingqing CHEN, Xiaoxia CAI a Yong ZHANG. Effect of partial crosslinking on morphology and properties of the poly(β-hydroxybutyrate)/poly(d,l-lactic acid) blends. *Polymer Degradation and Stability*. 2013, 98(9), 1549-1555. ISSN 01413910. DOI: 10.1016/j.polymdegradstab.2013.06.033

[105] CHEN, Haiying, Farshad OVEISSI, Sean DALY, Zahra SHAHRBABAKI, Sina NAFICY a Fariba DEHGHANI. A green and biodegradable plasticizer from copolymers of poly(β-hydroxybutyrate- co -ε-caprolactone). Journal of *Applied Polymer* Science. 2022, 139(22). ISSN 0021-8995. DOI: 10.1002/app.52240

[106] GARCIA-GARCIA, D., E. RAYÓN, A. CARBONELL-VERDU, J. LOPEZ-MARTINEZ a R. BALART. Improvement of the compatibility between poly(3-hydroxybutyrate) and poly(ε-caprolactone) by reactive extrusion with dicumyl *peroxide. European Polymer Journal.* 2017, 86, 41-57. ISSN 00143057. DOI: 10.1016/j.eurpolymj.2016.11.018

[107] GRIMALDI, M., B. IMMIRZI, M. MALINCONICO, E. MARTUSCELLI, G. ORSELLO, A. RIZZO a M. VOLPE. Reactive processing — property relationships in *biodegradable* blends useful **for** prosthesis application. Journal of Materials Science. 1996, 31(23), 6155-6162. ISSN 0022-2461. DOI: 10.1007/BF00354432

[108] ZYTNER, Peter, Feng WU, Manjusri MISRA a Amar MOHANTY. Toughening of Biodegradable Poly(3-hydroxybutyrate- co -3-hydroxyvalerate)/Poly(ε-caprolactone) Blends by In Situ Reactive Compatibilization. ACS Omega. 2020, 5(25*), 14900-14910.* ISSN 2470-1343. DOI: 10.1021/acsomega.9b04379

[109] ROBLEDO-ORTÍZ, Jorge, Martín GONZÁLEZ-LÓPEZ, Alan MARTÍN DEL CAMPO a Aida PÉREZ-FONSECA. Lignocellulosic Materials as Reinforcement of Polyhydroxybutyrate and its Copolymer with Hydroxyvalerate: A Review. *Journal of Polymers* and the Environment. 2021, 29(5), 1350-1364. ISSN 1566-2543. DOI: 10.1007/s10924-020-01979-2

[110] MISRA, Superb, Sabeel VALAPPIL, Ipsita ROY a Aldo BOCCACCINI. Polyhydroxyalkanoate (PHA)/Inorganic Phase Composites for Tissue Engineering Applications. Biomacromolecules. 2006, 7(*8), 2249-2258.* ISSN 1525-7797. DOI: 10.1021/bm060317c

[111] CHIULAN, Ioana, Adriana FRONE, Călin BRANDABUR a Denis PANAITESCU. Recent Advances in 3D Printing of Aliphatic Polyesters. Bioengineering. 2018, **5**(1). ISSN 2306-5354. DOI: 10.3390/bioengineering5010002

[112] FAIDALLAH, Rawabe, Muammel HANON, Zoltán SZAKÁL a István OLDAL. Biodegradable Materials Used in FDM 3D Printing Technology: *A* Critical Review**.** Journal of Modern Mechanical Engineering and Technology. 2022, 9, 90-105. ISSN 2409-9848. DOI: 10.31875/2409-9848.2022.09.11

[113] MEHRPOUYA, Mehrshad, Henri VAHABI, Massimiliano BARLETTA, Pascal LAHEURTE a Valérie LANGLOIS. Additive manufacturing of polyhydroxyalkanoates (PHAs) biopolymers: Materials, printing *techniques, and applications. Materials Science* and Engineering: C. 2021, 127. ISSN 09284931. DOI: 10.1016/j.msec.2021.112216

[114] DEY, Arup, Isnala ROAN EAGLE a Nita YODO. A Review on Filament Materials for Fused Filament Fabrication. Journal of Manufacturing and *Materials Processing*. 2021, **5**(3). ISSN 2504-4494. DOI: 10.3390/jmmp5030069

[115] WOUTER DECONINCK. Extrusion of Polyhydroxyalkanoate Filament For Use in 3D Printers. Virgínia, 2016. Bakalárska práce. College of *William & Mary.*

[116] SABALINA, Alisa, *Sergejs GAIDUKOVS, Maksims JURINOVS, Liga GRASE a* Oskars PLATNIEKS. Fabrication of poly(lactic acid), poly(butylene succinate), and poly(hydroxybutyrate) bio-based and biodegradable blends for application in *fused* filament fabrication-based 3D printing. Journal of Applied Polymer Science. 2023, 140(28). ISSN 0021-8995. DOI: 10.1002/app.54031

[117] LAOUTID, Fouad, Hadrien LENOIR, Adriana MOLINS SANTAEULARIA, Antoniya TONCHEVA, Tim SCHOUW a Philippe DUBOIS. Impact-Resistant Poly(3-Hydroxybutyrate)/Poly(ε-Caprolactone)-Based Materials, through Reactive Melt Processing, for Compression-Molding and 3D-Printing Applications. Materials. 2022, 15(22). ISSN 1996-1944. DOI: 10.3390/ma15228233

[118] VIGIL FUENTES, Miguel, Suman THAKUR, Feng WU, Manjusri MISRA, Stefano GREGORI a Amar MOHANTY. Study on the 3D printability of poly(3-hydroxybutyrate-co-3-hydroxyvalerate)/poly(lactic acid) blends

with chain extender using fused *filament* fabrication. Scientific Reports. 2020, 10(1). ISSN 2045-2322. DOI: 10.1038/s41598-020-68331-5

[119] IVORRA-MARTINEZ, Juan, Miguel PEYDRO, Jaume GOMEZ-CATURLA, Lourdes SANCHEZ-NACHER, Teodomiro BORONAT a Rafael BALART. The effects of processing parameters on mechanical properties of 3D-printed polyhydroxyalkanoates parts. Virtual and Physical Prototyping. 2023, 18(1*)*. ISSN 1745-2759. DOI: 10.1080/17452759.2022.2164734

[120] RAJAN, Kumaresan, Mahendran SAMYKANO, Kumaran KADIRGAMA, Wan HARUN a Md. RAHMAN. Fused deposition modeling: process, materials, parameters, properties, and applications. The International Journal *of Advanced Manufacturing* Technology. 2022, 120(3-4), 1531-1570. ISSN 0268-3768. DOI: 10.1007/s00170-022-08860-7

[121] KANABENJA, Warrayut, Kunanon PASSARAPARK, Thanaporn SUBCHOKPOOL, Nithiwach NAWAAUKKARATHARNANT, Allen ROMÁN, Tim OSSWALD, Chuanchom AUMNATE a Pranut POTIYARAJ. 3D printing filaments from plasticized *Polyhydroxybutyrate/Polylactic acid blends reinforced with hydroxyapatite*. Additive Manufacturing. 2022, 59. ISSN 22148604. DOI: 10.1016/j.addma.2022.103130

[122] VAIDYA, Alankar, Christophe COLLET, Marc GAUGLER a Gareth LLOYD-JONES. Integrating softwood biorefinery lignin into polyhydroxybutyrate composites and application in 3D printing. Materials Today Communications. 2019, 19, 286-296. ISSN 23524928. DOI: 10.1016/j.mtcomm.2019.02.008

[123] TIAN, Jing, Run ZHANG, Yihui WU a Ping XUE. Additive manufacturing of wood flour/polyhydroxyalkanoates (PHA) fully bio-based composites based on *micro-screw extrusion* system. Materials & Design. 2021, 199. ISSN 02641275. DOI: 10.1016/j.matdes.2020.109418

[124] RODRÍGUEZ-FABIà, Sandra a Gary CHINGA-CARRASCO. Effects of a poly(hydroxyalkanoate) elastomer and kraft pulp fibres on biocomposite properties and three-dimensional (3D) printability of filaments for *fused deposition modelling*. Journal of Bioresources and Bioproducts. 2022, 7(3), 161-172. ISSN 23699698. DOI: 10.1016/j.jobab.2022.03.002

[125] DAN, Li, Qiuli CHENG, Ravin NARAIN, Beate KRAUSE, Petra PÖTSCHKE a Anastasia ELIAS. Three-Dimensional Printed and Biocompatible Conductive Composites Comprised of Polyhydroxybutyrate and Multiwalled Carbon Nanotubes. Industrial & *Engineering Chemistry Research.* 2021, 60(2), 885-897. ISSN 0888-5885. DOI: 10.1021/acs.iecr.0c04753

[126] Biodegradable Polymers in Various Environments According to Established Standards and Certification Schemes: New updated version of the poster. Renewable Carbon Publications. Dostupné z: https://renewable-carbon.eu/publications/product/biodegradable-polymers-in-various-environments-according-to-established-standards-and-certification-schemes-graphic-pdf/

[127] ASTM D5988-18: Standard Test Method for Determining Aerobic Biodegradation of Plastic Materials in Soil. West Conshohocken, US: ASTM International*, 2018, 6* s. ASTM D5988-18.

[128] *ASTM D5338-15(2021): Standard Test Method for Determining Aerobic Biodegradation of Plastic Materials* Under Controlled Composting Conditions, Incorporating Thermophilic Temperatures. West Conshohocken, US: ASTM International, 2021.

[129] *ASTM G160 − 12: Standard Practice for Evaluating Microbial Susceptibility of Nonmetallic Materials By Laboratory Soil Burial. West Conshohocken, US*: ASTM International, 2019.

[130] *ASTM D5511 − 18: Standard Test Method for Determining Anaerobic Biodegradation of Plastic Materials Under High-Solids Anaerobic-Digestion* Conditions. West Conshohocken, US: ASTM International, 2018.

[131] *ASTM D5526 − 18: Standard Test Method for Determining Anaerobic Biodegradation of Plastic Materials Under Accelerated Landfill Conditions*. West Conshohocken, US: ASTM International, 2018.

[132] *ASTM D 7475 − 20: Standard Test Method for Determining the Aerobic Degradation and Anaerobic Biodegradation of Plastic* Materials under Accelerated Bioreactor Landfill Conditions. West Conshohocken, US: ASTM International, 2020.

[133] *MERGAERT, J., C. ANDERSON, A. WOUTERS, J. SWINGS a K. KERSTERS. Biodegradation of polyhydroxyalkanoates. FEMS Microbiology Letters.* 1992, 103(2-4), 317-321. ISSN 03781097. DOI: 10.1111/j.1574-6968.1992.tb05853.x

[134] SATOH, Hidenori, Naoko YOSHIE a Yoshio INOUE. Hydrolytic degradation of blends of poly(3-hydroxybutyrate) with poly(3-hydroxybutyrate-co-3-hydroxyvalerate). *Polymer.* 1994, 35(2), 286-290. ISSN 00323861. DOI: 10.1016/0032-3861(94)90692-0

[135] YUE, C.L., R.A. GROSS a S.P. MCCARTHY. Composting studies of poly (β-hydroxybutyrate-co-/gb-hydroxyvalerate). *Polymer Degradation and Stability*. 1996, 51(2), 205-210. ISSN 01413910. DOI: 10.1016/0141-3910(95)00201-4

[136] DOI, Yoshiharu, Youko KANESAWA, Masao KUNIOKA a Terumi SAITO. Biodegradation of microbial copolyesters: poly(3-hydroxybutyrate-co-3-hydroxyvalerate) and poly*(3-hydroxybutyrate-co-4-hydroxybutyrate). Macromolecules.* 1990, 23(1), 26-31. ISSN 0024-9297. DOI: 10.1021/ma00203a006

[137] DOI, Yoshiharu, Youko KANESAWA, Naoki TANAHASHI a Yoshiharu KUMAGAI. Biodegradation of microbial polyesters in the marine environment. Polymer Degradation and Stability. 1992, 36(2), 173-177. ISSN *01413910. DOI:* 10.1016**/**0141-3910(92)90154-W

[138] AKARADECHAKUL, Kornchanok, Peerapong CHANTHOT, Noppadon KERDDONFAG a Cattaleeya PATTAMAPROM. The effect of polycarbodiimide chain extender on thermal stability and mechanical properties of biobased poly(lactic acid)/natural rubber blown films. *Journal of Plastic Film & Sheeting*. 2022, **38**(3), 396-415. ISSN 8756-0879. DOI: 10.1177/87560879211058679

[139] Filabot. USA: Filabot. Dostupné z: https://www.filabot.com/

[140] *Filament* Width Sensor Prototype Version 3. Ultimaker Thingiverse. MakerBot Industries, 2023. Dostupné z: https://www.thingiverse.com/thing:454584

[141] DIZON, John, Alejandro ESPERA, Qiyi CHEN a *Rigoberto* ADVINCULA. Mechanical characterization of 3D-printed polymers. Additive Manufacturing. 2018, 20, 44-67. ISSN 22148604. DOI: 10.1016/j.addma.2017.12.002

[142] PUPPI, Dario, Gianni PECORINI a Federica CHIELLINI. Biomedical Processing of Polyhydroxyalkanoates. Bioengineering. *2019, 6*(4). ISSN 2306-5354. DOI: 10.3390/bioengineering6040108

[143] HAN, Syaza, Mastura TAHA, Muhd MANSOR a Muhamad RAHMAN. Investigation of *tensile* and flexural properties of kenaf fiber-reinforced acrylonitrile butadiene styrene composites fabricated by fused deposition modeling. Journal of Engineering and Applied Science. 2022, 69(1). ISSN 1110-1903. DOI: 10.1186/s44147-022-00109-0

[144] CHIULAN, Ioana, Adriana FRONE, Călin BRANDABUR a Denis PANAITESCU. Recent Advances in 3D Printing of Aliphatic Polyesters. Bioengineering. 2018, 5(1). *ISSN 2306-5354. DOI:* 10**.**3390/bioengineering5010002

[145] DIMITRIOU, Rozalia, Elena JONES, Dennis MCGONAGLE a Peter GIANNOUDIS. Bone regeneration: current concepts and future directions. BMC Medicine. 2011, 9(1). ISSN 1741-7015. DOI: 10.1186/1741-7015-9-66

[146] BROWN, Justin, Sangamesh KUMBAR a Cato LAURENCIN. Bone Tissue Engineering. Biomaterials Science. Elsevier, *2013,* s. 1194-1214**.** ISBN 9780123746269. DOI: 10.1016/B978-0-08-087780-8.00113-3

[147] TOKTAM GHASSEMI AT ALL. Current Concepts in Scaffolding for Bone Tissue Engineering. The *Archives* of Bone and Joint Surgery. 2018, 6(2), 90-99. DOI: 10.22038/abjs.2018.26340.1713

[148] ZENG, Jian-Hua, Shi-Wei LIU, Long XIONG et al. Scaffolds for the *repair of bone defects in clinical studies*: a systematic review. Journal of Orthopaedic Surgery and Research. 2018, 13(1). ISSN 1749-799X. DOI: 10.1186/s13018-018-0724-2

[149] FATTAHIAN, Hamidreza, Kimia MANSOURI a Nikta MANSOURI. Biomaterials, substitutes, and tissue engineering in bone repair: current and future concepts. Comparative Clinical *Pathology. 2019, 28*(4), 879-891. ISSN 1618-5641. DOI: 10.1007/s00580-017-2507-2

[150] GARCÍA-GARETA, Elena, Melanie COATHUP a Gordon BLUNN. Osteoinduction of bone grafting materials for bone repair and regeneration. Bone. *2015, 81, 112-121*. ISSN 87563282. DOI: 10.1016/j.bone.2015.07.007

[151] SHEIKH, Zeeshan, Shariq NAJEEB, Zohaib KHURSHID, Vivek VERMA, Haroon RASHID a Michael GLOGAUER. Biodegradable Materials for *Bone* Repair and Tissue Engineering Applications. Materials. 2015, 8(9), 5744-5794. ISSN 1996-1944. DOI: 10.3390/ma8095273

[152] QU, Huawei, Hongya FU, Zhenyu HAN a Yang SUN. Biomaterials for bone tissue engineering scaffolds: a review. RSC Advances. 2019, *9*(45), 26252-26262. ISSN 2046-2069. DOI: 10.1039/C9RA05214C

[153] PUPPI, D., F. CHIELLINI, A.M. PIRAS a E. CHIELLINI. Polymeric materials for bone and cartilage *repair.* Progress in Polymer Science. 2010, 35(4), 403-440. ISSN 00796700. DOI: 10.1016/j.progpolymsci.2010.01.006

[154] LU, Haiping, Yinghong ZHOU, Yaping MA, Lan XIAO, Wenjun JI, Yi ZHANG a Xin WANG. Current Application of *Beta-Tricalcium Phosphate in Bone* Repair and Its Mechanism to Regulate Osteogenesis. Frontiers in Materials. 2021, 8. ISSN 2296-8016. DOI: 10.3389/fmats.2021.698915

[155] FILIP, Diana, Vasile-Adrian SURDU, Andrei PADURARU a Ecaterina ANDRONESCU. Current Development in Biomaterials—Hydroxyapatite and Bioglass for Applications in Biomedical Field: A Review. Journal of Functional Biomaterials. 2022, *13(4)*. ISSN 2079-4983. DOI: 10.3390/jfb13040248

[156] SAMAVEDI, Satyavrata, Abby WHITTINGTON a Aaron GOLDSTEIN. Calcium phosphate ceramics in bone tissue engineering: A review of properties and their influence on cell behavior. *Acta Biomaterialia.* 2013, 9(9), 8037-8045. ISSN 17427061. DOI: 10.1016/j.actbio.2013.06.014

[157] ABBASI, Naghmeh, Stephen HAMLET, Robert LOVE a Nam-Trung NGUYEN. Porous scaffolds for bone regeneration. Journal of Science: Advanced Materials and Devices. *2020, 5*(1), 1-9. ISSN 24682179. DOI: 10.1016/j.jsamd.2020.01.007

[158] RAEISDASTEH HOKMABAD, Vahideh, Soodabeh DAVARAN, Ali RAMAZANI a Roya SALEHI. Design and fabrication of porous *biodegradable scaffolds: a strategy for tissue* engineering. Journal of Biomaterials Science, Polymer Edition. 2017, **28**(16), 1797-1825. ISSN 0920-5063. DOI: 10.1080/09205063.2017.1354674

[159] CHOCHOLATA, Petra, Vlastimil KULDA a Vaclav BABUSKA. Fabrication of Scaffolds for Bone-Tissue Regeneration. Materials. 2019, 12(4). *ISSN 1996-1944. DOI:* 10.3390/ma12040568

[160] NGO, Tuan, Alireza KASHANI, Gabriele IMBALZANO, Kate NGUYEN a David HUI. Additive manufacturing (3D printing**)**: A review of materials, methods, applications and challenges. *Composites Part B: Engineering*. 2018, **143,** 172-196. ISSN 13598368. DOI: 10.1016/j.compositesb.2018.02.012

[161] ZHANG, Qiliang, Jian ZHOU, Peixuan ZHI, Leixin LIU, Chaozong LIU, Ao FANG a Qidong ZHANG. 3D printing method for bone tissue engineering scaffold. Medicine in *Novel Technology and Devices*. 2023, 17. ISSN 25900935. DOI: 10.1016/j.medntd.2022.100205

[162] BOSE, Susmita, Sahar VAHABZADEH a Amit BANDYOPADHYAY. Bone tissue engineering using 3D printing. Materials Today. 2013, 16(12), 496-504. *ISSN 13697021. DOI:* 10.1016/j.mattod.2013.11.017

[163] SHUNMUGASUNDARAM, M., Ahmed MAUGHAL a M. AJAY KUMAR. A review of bio-degradable materials *for* fused deposition modeling machine. Materials Today: Proceedings. 2020, 27, 1596-1600. ISSN 22147853. DOI: 10.1016/j.matpr.2020.03.267

[164] MANOJ, Aluri a Ramesh PANDA. Biodegradable Filament for 3D Printing Process: A Review. Engineered Science. 2022, 18, *11-19*. ISSN 2576988X. DOI: 10.30919/es8d616

[165] RIGOTTI, Daniele a Alessandro PEGORETTI. Additive manufacturing with biodegradable polymers. Biodegradable Polymers, *Blends* and Composites. Amsterdam: Elsevier, 2022, s. 611-679. ISBN 9780128237915. DOI: 10.1016/B978-0-12-823791-5.00026-0

[166] KOVALCIK, Adriana. Recent Advances in 3D Printing of Polyhydroxyalkanoates: A Review. *The EuroBiotech Journal.* 2021, 5(1), 48-55. ISSN 2564-615X. DOI: 10.2478/ebtj-2021-0008

[167] DIETMAR W. HUTMACHER A KOL. Mechanical properties and cell cultural response of *polycaprolactone scaffolds designed* and fabricated via fused deposition modeling. Journal of Biomedical Materials Research. 2001, 55**(**2), 203-216. DOI: 10.1002/1097-4636(200105)55:2<203::AID-JBM1007>3.0.CO;2-7

[168] XIONG, Zhuo, Yongnian YAN, Renji ZHANG a Lei SUN. Fabrication of porous poly(l-lactic acid) scaffolds for bone tissue engineering *via precise extrusion. Scripta* Materialia. 2001, 45(7), 773-779. ISSN 13596462. DOI: 10.1016/S1359-6462(01)01094-6

[169] ZEIN, Iwan, Dietmar HUTMACHER, Kim TAN a Swee TEOH. Fused deposition modeling of novel scaffold architectures for tissue engineering applications. Biomaterials. *2002, 23*(4), 1169-1185. ISSN 01429612. DOI: 10.1016/S0142-9612(01)00232-0

[170] RAI, B. The effect of rhBMP-2 on canine osteoblasts seeded onto 3D bioactive polycaprolactone scaffolds. Biomaterials. 2004, 25(24), 5499-5506. ISSN 01429612. DOI: 10.*1016/j*.biomaterials.2004**.**01.007

[171] TEO, Erin, Shin-Yeu ONG, Mark KHOON CHONG, Zhiyong ZHANG, Jia LU, Shabbir MOOCHHALA, Bow HO a Swee-Hin TEOH. Polycaprolactone-based fused deposition modeled mesh for delivery of antibacterial agents to infected wounds. Biomaterials. *2011, 32(1*), 279-287. ISSN 01429612. DOI: 10.1016/j.biomaterials.2010.08.089

[172] DOMINGOS, M., F. CHIELLINI, A. GLORIA, L. AMBROSIO, P. BARTOLO a E. CHIELLINI. Effect of process

parameters on the morphological and mechanical properties of 3D Bioextruded poly(ε-caprolactone) scaffolds**.** Rapid Prototyping Journal. 2012, 18(1), 56-67. ISSN 1355-2546. DOI: 10.1108/13552541211193502

[173] PARK, SuA, GeunHyung KIM, Yong JEON, YoungHo KOH a WanDoo KIM. 3D polycaprolactone scaffolds with controlled pore structure using a *rapid* prototyping system**.** Journal of Materials Science: Materials in Medicine. 2009, 20(1*)*, 229-234. ISSN 0957-4530. DOI: 10.1007/s10856-008-3573-4

[174] RAI, Bina, Jane LIN, Zophia LIM, Robert GULDBERG, Dietmar HUTMACHER a Simon COOL. Differences between *in vitro* viability and differentiation and *in vivo* bone-forming efficacy of *human mesenchymal* stem cells cultured on PCL–TCP scaffolds. Biomaterials. 2010, 31(*31), 7960-7970*. ISSN 01429612. DOI: 10.1016/j.biomaterials.2010.07.001

[175] KONOPNICKI, Sandra, Basel SHARAF, Cory RESNICK, Adam PATENAUDE, Tracy POGAL-SUSSMAN, Kyung-Gyun HWANG, Harutsugi ABUKAWA a Maria TROULIS. Tissue-Engineered Bone With 3-Dimensionally Printed *β-Tricalcium Phosphate and Polycaprolactone Scaffolds and* Early Implantation: An *In Vivo* Pilot Study in a Porcine Mandible Model. Journal of Oral and Maxillofacial Surgery. 2015, 73(5), 10161-101611. ISSN 02782391. DOI: 10.1016/j.joms.2015.01.021

[176] DÁVILA, J., M. FREITAS, P. INFORçATTI NETO, Z. *SILVEIRA,* J. SILVA a M. D'ÁVILA. Fabrication of PCL/β-TCP scaffolds by 3D mini-screw *extrusion printing. Journal of Applied Polymer Science*. 2016, 133(15**)**, -. ISSN 00218995. DOI: 10.1002/app.43031

[177] KORPELA, Jyrki, Anne KOKKARI, Harri KORHONEN, Minna MALIN, Timo NÄRHI a Jukka SEPPÄLÄ. Biodegradable and bioactive porous scaffold structures prepared using fused deposition modeling. Journal of Biomedical Materials Research *Part B: Applied* Biomaterials. 2013, 101(4), 610-619. ISSN 15524973. DOI: 10.1002/jbm.b.32863

[178] SPARKS, David, Jay WIPER, Thomas LLOYD et al. Protocol for the BONE-RECON trial: *a single-arm* feasibility trial for critical sized lower limb BONE defect RECONstruction using the mPCL-TCP scaffold system with autologous vascularised corticoperiosteal tissue transfer. *BMJ Open*. 2023, **13**(5). ISSN 2044-6055. DOI: 10.1136/bmjopen-2021-056440

[179] Biomendex. Tampere: Biomendex, 2023. Dostupné z: https://biomendex.com/

[180] CHEN, Xibao, Gang CHEN, Gang WANG, Peizhi ZHU a Chunxia GAO. Recent Progress on 3D-Printed Polylactic Acid and Its Applications in Bone Repair. Advanced Engineering Materials. 2020, *22(4)*. ISSN 1438-1656. DOI: 10.1002/adem.201901065

[181] GREGOR, Aleš, Eva FILOVÁ, Martin NOVÁK et al. Designing of PLA scaffolds for bone tissue replacement fabricated by ordinary commercial 3D printer. Journal of Biological Engineering. 2017, 11(1). ISSN 1754-1611. DOI: 10.1186/s13036-017-0074-3

[182] WURM, Matthias, Tobias MÖST, Bastian BERGAUER, Dominik RIETZEL, Friedrich NEUKAM, Sandra CIFUENTES a Cornelius WILMOWSKY. In-vitro evaluation of Polylactic acid (PLA) manufactured by fused deposition modeling. *Journal of Biological Engineering*. 2017, **11**(1). ISSN 1754-1611. DOI: 10.1186/s13036-017-0073-4

[183] SCHOEN, Alan. INFINITE PERIODIC MINIMAL SURFACES WITHOUT SELF-INTERSECTIONS. Washington, D. C, 1970. NATIONAL AERONAUTICS AND SPACE ADMINISTRATION.

[184] GERMAIN, Loïc, Carlos FUENTES, Aart VAN VUURE, Anne DES RIEUX a Christine DUPONT-GILLAIN. 3D-printed biodegradable gyroid scaffolds for tissue engineering applications. Materials & Design. 2018, 151, 113-122. ISSN *02641275. DOI:* 10.1016/j.matdes.2018.04.037

[185] ALIZADEH-OSGOUEI, Mona, Yuncang LI, Alireza VAHID, Arash ATAEE a Cuie WEN. High strength porous PLA gyroid scaffolds manufactured via fused deposition modeling for tissue-engineering *applications. Smart Materials in Medicine.* 2021, 2, 15-25. ISSN 25901834. DOI: 10.1016/j.smaim.2020.10.003

[186] ERYILDIZ, Meltem. Fabrication of Drug-Loaded 3D-Printed Bone Scaffolds with Radial Gradient Porosity. Journal of Materials Engineering and Performance. 2023, 32(9), 4249-4257. ISSN 1059-9495. DOI: 10.1007/s11665-022-07490-0

[187] XIONG, Z. Fabrication of porous scaffolds for bone tissue engineering via low-temperature deposition. Scripta Materialia. 2002, 46(11), 771-776. ISSN 13596462. DOI: 10.1016/S1359-6462(02)00071-4

[188] DRUMMER, Dietmar, Sandra CIFUENTES-CUÉLLAR a Dominik RIETZEL. Suitability of PLA/TCP for fused deposition modeling. Rapid Prototyping Journal. 2012, 18(6), 500-507*. ISSN 1355-2546.* DOI: 10.1108/13552541211272045

[189] ELHATTAB, Karim, Sarit BHADURI a Prabaha SIKDER. Influence of Fused Deposition Modelling Nozzle Temperature on the Rheology and Mechanical Properties of 3D Printed β-Tricalcium Phosphate (TCP*)/Polylactic Acid (PLA) Composite. Polymers.* 2022, **14**(6). ISSN 2073-4360. DOI: 10.3390/polym14061222

[190] DISTLER, Thomas, Niklas FOURNIER, Alina GRÜNEWALD, Christian POLLEY, Hermann SEITZ, Rainer DETSCH a Aldo BOCCACCINI. Polymer-Bioactive Glass Composite Filaments for 3D Scaffold Manufacturing by Fused Deposition Modeling: Fabrication and Characterization. Frontiers in Bioengineering and Biotechnology. 2020, 8. ISSN 2296-4185. DOI: 10.3389/fbioe.2020.00552

[191] *MATSUO*, Akira, Hiroshige CHIBA, Hidetoshi TAKAHASHI, Jun TOYODA a Harutsugi ABUKAWA. Clinical application of a custom-made bioresorbable raw particulate hydroxyapatite/poly-l-lactide mesh tray for mandibular reconstruction. Odontology. *2010, 98(1), 85-88*. ISSN 1618-1247. DOI: 10.1007/s10266-009-0111-x

[192] ESPOSITO CORCIONE, Carola, Francesca GERVASO, Francesca SCALERA, Francesco MONTAGNA, Alessandro SANNINO a Alfonso MAFFEZZOLI. The feasibility of printing polylactic acid-nanohydroxyapatite composites using a low-cost *fused deposition modeling* 3D printer**.** Journal of Applied Polymer Science. 2017, 134(13). ISSN 00218995. DOI: 10.1002/app.44656

[193] SENATOV, F.S., K.V. NIAZA, A.A. STEPASHKIN a S.D. KALOSHKIN. Low-cycle fatigue behavior of 3d-printed PLA-based porous scaffolds*. Composites Part B*: Engineering. 2016, 97, 193-200. ISSN *13598368. DOI:* 10.1016/j.compositesb.2016.04.067

[194] ESMAEILI, Saeid, Hossein AKBARI AGHDAM, Mehdi MOTIFIFARD, Saeed SABER-SAMANDARI, Amir MONTAZERAN, Mohammad BIGONAH, Erfan SHEIKHBAHAEI a Amirsalar KHANDAN. A porous polymeric–hydroxyapatite scaffold used for femur fractures *treatment: fabrication, analysis*, and simulation. European Journal of Orthopaedic Surgery & Traumatology. 2020, 30(1), 123-131. ISSN 1633-8065. DOI: 10.1007/s00590-019-02530-3

[195] DUBINENKO, Gleb, *Aleksey ZINOVIEV, Evgeny BOLBASOV, Anna* KOZELSKAYA, Evgeniy SHESTERIKOV, Victor NOVIKOV a Sergei TVERDOKHLEBOV. Highly filled poly(l -lactic acid)/hydroxyapatite composite for 3D printing of personalized bone *tissue engineering scaffolds. Journal of* Applied Polymer Science. 2021, 138(2). ISSN 0021-8995. DOI: 10.1002/app.49662

[196] ESPOSITO CORCIONE, Carola, Francesca SCALERA, Francesca GERVASO, Francesco MONTAGNA, Alessandro SANNINO a Alfonso MAFFEZZOLI. One-step solvent-free process for the fabrication of *high loaded PLA*/HA composite filament for 3D printing. Journal of Thermal Analysis and Calorimetry. 2018, 134(1), 575-582. ISSN 1388-6150. DOI: 10.1007/s10973-018-7155-5

[197] DUAN, Bin, Wai CHEUNG a Min WANG. Optimized fabrication of Ca–P/PHBV nanocomposite scaffolds via selective laser sintering for bone tissue engineering. Biofabrication. *2011, 3(1)*. ISSN 1758-5082. DOI: 10.1088/1758-5082/3/1/015001

[198] PEREIRA, Tatiana, Marcelo OLIVEIRA, Izaque MAIA, Jorge SILVA, Marysilvia COSTA a *Rossana THIRÉ. 3D Printing of* Poly(3-hydroxybutyrate) Porous Structures Using Selective Laser Sintering. Macromolecular Symposia. 2012, 319(1), 64-73. ISSN 10221360. DOI: 10.1002/masy.201100237

[199] PEREIRA, T.F., M.A.C. SILVA, M.F. OLIVEIRA, I*.A.* MAIA, J.V.L. SILVA, M.F. COSTA a R.M.S.M. *THIRÉ. Effect* of process parameters on the properties of selective laser sintered Poly(3-hydroxybutyrate) scaffolds for bone tissue engineering. Virtual and Physical Prototyping. 2012, **7**(4), 275-285. ISSN 1745-2759. DOI: 10.1080/17452759.2012.738551

[200] SASKA, Sybele, Luana PIRES, Mariana COMINOTTE et al. Three-dimensional printing and *in vitro* evaluation of poly(*3-hydroxybutyrate) scaffolds* functionalized with osteogenic growth peptide for tissue engineering. Materials Science and Engineering: C*. 2018, 89, 265-273*. ISSN 09284931. DOI: 10.1016/j.msec.2018.04.016

[201] DIERMANN, Sven, Mingyuan LU, Yitian ZHAO, Luigi-Jules VANDI, Matthew DARGUSCH a Han HUANG. Synthesis, microstructure, and mechanical behaviour of a unique porous PHBV scaffold manufactured using selective laser sintering. Journal of the Mechanical Behavior of Biomedical Materials. 2018, 84, 151-160. ISSN 17516161. DOI: 10.1016/j.jmbbm.2018.05.007

[202] DIERMANN, Sven, Mingyuan LU, Grant EDWARDS, Matthew DARGUSCH a Han HUANG. *In vitro* degradation of a unique porous PHBV scaffold manufactured using selective laser sintering. Journal of Biomedical Materials Research Part A*. 2019, 107*(1), 154-162. ISSN 15493296. DOI: 10.1002/jbm.a.36543

[203] DIERMANN, Sven, Mingyuan LU, Matthew DARGUSCH, Lisbeth GRøNDAHL a Han HUANG. Akermanite reinforced PHBV scaffolds manufactured using selective laser sintering. Journal of Biomedical Materials Research Part *B*: Applied Biomaterials. 2019, 107(8), 2596-2610. ISSN 1552-4973. DOI: 10.1002/jbm.b.34349

[204] ZHAO, Shichang, Min ZHU, Jianhua ZHANG, Yadong ZHANG, Zhongtang LIU, Yufang ZHU a Changqing ZHANG. Three dimensionally printed mesoporous bioactive glass and poly(3-hydroxybutyrate-co-3-hydroxyhexanoate) composite scaffolds for bone regeneration. *Journal of Materials Chemistry* B. 2014, 2(36). ISSN 2050-750X. DOI: 10.1039/C4TB00838C

[205] WU, C. a H. LIAO. Interface design of environmentally friendly carbon nanotube-filled polyester composites: Fabrication, characterisation, functionality and application. Express Polymer Letters. *2017,* 11(3)**,** 187-198. ISSN 1788618X. DOI: 10.3144*/expresspolymlett.2017.20*

[206] KOSORN, Wasana, Morakot SAKULSUMBAT, Paweena UPPANAN, Pakkanun KAEWKONG, Surapol CHANTAWEROAD, Jaturong JITSAARD, Kriskrai SITTHISERIPRATIP a Wanida JANVIKUL. PCL/PHBV blended three dimensional scaffolds fabricated by fused deposition modeling and responses of chondrocytes to the scaffolds*. Journal of Biomedical Materials Research* Part B: Applied Biomaterials. 2017, 105(5), 1141-1150. ISSN 15524973. DOI: 10.1002/jbm.b.33658

[207] FINDRIK BALOGOVÁ, Alena, Radovan HUDÁK, Teodor TÓTH, Marek SCHNITZER, Jozef FERANC, Dušan BAKOŠ a Jozef ŽIVČÁK. Determination of geometrical and viscoelastic properties of PLA/PHB samples made by additive manufacturing for urethral substitution. *Journal of Biotechnology.* 2018, 284, 123-130. ISSN 01681656. DOI: 10.1016/j.jbiotec.2018.08.019

[208] ECKER, Josef, Ivana BURZIC, Andreas HAIDER, Sabine HILD a Harald RENNHOFER. "Improving the impact strength of PLA and its blends with PHA in fused layer modelling ". Polymer Testing. *2019, 78*. ISSN 01429418. DOI: 10.1016/j.polymertesting.2019.105929

[209] RYDZ, Joanna, Jakub WŁODARCZYK, Jennifer GONZALEZ AUSEJO et al. Three-Dimensional Printed PLA and PLA/PHA Dumbbell-Shaped Specimens: Material Defects and Their Impact on Degradation Behavior. Materials. 2020, 13(8). ISSN 1996-1944. DOI: 10.3390/ma13082005

[210] GONZALEZ AUSEJO, Jennifer, Joanna RYDZ, Marta MUSIOł et al. A comparative study of three-dimensional printing directions: The degradation and toxicological profile of a PLA/PHA blend*. Polymer* Degradation and Stability. 2018, 152, 191-207. ISSN 01413910. DOI: 10.1016/j.polymdegradstab.2018.04.024

[211] KOVALCIK, Adriana, Leire SANGRONIZ, Michal KALINA, Katerina SKOPALOVA, Petr HUMPOLÍČEK, Maria OMASTOVA, Norbert MUNDIGLER a Alejandro MÜLLER. Properties of scaffolds prepared by fused deposition modeling of poly(hydroxyalkanoates). International Journal of Biological Macromolecules. 2020, 161, 364-376. ISSN 01418130. DOI: *10.1016/*j.ijbiomac.2020.06.022

[212] GIUBILINI, Alberto, Gilberto SIQUEIRA, Frank CLEMENS, Corrado SCIANCALEPORE, Massimo MESSORI, Gustav NYSTRÖM a Federica BONDIOLI. 3D-Printing Nanocellulose-Poly(3-hydroxybutyrate- co -3-hydroxyhexanoate) Biodegradable Composites by Fused Deposition *Modeling. ACS Sustainable Chemistry &* Engineering. 2020, 8(27), 10292-10302. ISSN 2168-0485. DOI: 10.1021/acssuschemeng.0c03385

[213] ARÁOZ, Beatriz, Emine KARAKAYA, Ana GONZÁLEZ WUSENER, Rainer DETSCH, Juan BIZZOTTO, Geraldine GUERON, Aldo BOCCACCINI a Élida HERMIDA. 3D printed poly(hydroxybutyrate-co-hydroxyvalerate)—45S5 bioactive glass composite resorbable scaffolds suitable *for bone regeneration. Journal of Materials Research.* 2021, 36(19), 4000-4012. ISSN 0884-2914. DOI: 10.1557/s43578-021-00272-9

[214] FINDRIK BALOGOVÁ, Alena, Marianna TREBUŇOVÁ, Gabriela IŽARÍKOVÁ et al. *In Vitro* Degradation of Specimens Produced from PLA/PHB by Additive Manufacturing in Simulated Conditions. Polymers. *2021, 13(10)***.** ISSN 2073-4360. DOI: 10.3390/polym13101542

[215] VOLPINI, Valentina, Alberto GIUBILINI, Lorenzo CORSI, Andrea NOBILI a Federica BONDIOLI. Characterization of biocompatible scaffolds manufactured by fused filament fabrication of *poly(3-hydroxybutyrate- co -3-hydroxyhexanoate). Royal Society Open Science*. 2022, 9(4). ISSN 2054-5703. DOI: 10.1098/rsos.211485

[216] KOHAN, Miroslav, Samuel LANCOŠ, Marek SCHNITZER, Jozef ŽIVČÁK a Radovan HUDÁK. Analysis of PLA/PHB Biopolymer Material with Admixture of Hydroxyapatite and Tricalcium Phosphate for Clinical Use. Polymers. *2022, 14(24)***.** ISSN 2073-4360. DOI: 10.3390/polym14245357

[217] YE, Xiangling, Yongqiang ZHANG, Tao LIU et al. Beta-tricalcium phosphate enhanced mechanical and

biological properties of 3D-printed polyhydroxyalkanoates scaffold for bone *tissue engineering.* International Journal of Biological Macromolecules. 2022, 209, 1553-1561. ISSN 01418130. DOI: 10.1016/j.ijbiomac.2022.04.056

[218] DONG, Xue, Ishani PREMARATNE, Kemal SARIIBRAHIMOGLU et al. 3D-printed poly-4-hydroxybutyrate bioabsorbable scaffolds for nipple reconstruction. Acta Biomaterialia. 2022, 143, 333-343. ISSN 17427061. DOI: 10.1016/j.actbio.2022.*02.040*

[219] GIELISCH, Matthias, Diana HEIMES, Daniel G. E. THIEM, C. BOESING, M. KRUMPHOLTZ, B. AL-NAWAS a Peer W. KÄMMERER. Steam-sterilized and degradable fused filament fabrication-printed polylactide/polyhydroxyalkanoate surgical guides for dental implants*: Are they* accurate enough for static navigation?. *International Journal of Bioprinting*. 2022, **9**(2). ISSN 2424-8002. DOI: 10.18063/ijb.v9i2.655

[220] CHEN, Guo-Qiang a Qiong WU. The application of polyhydroxyalkanoates as tissue engineering materials. Biomaterials. 2005, 26(33), 6565-6578. ISSN 01429612. DOI: 10.1016/j.biomaterials.2005.04.036

[221] LIM, Janice, Mingliang YOU, Jian LI a Zibiao LI. Emerging bone tissue engineering via Polyhydroxyalkanoate (PHA)-based scaffolds. Materials Science and Engineering: C. 2017, 79, 917-929. ISSN 09284931. DOI: 10.1016/j.msec.2017.05.132

[222] BUTT, Fatima, Nawshad MUHAMMAD, Almas HAMID, Muhammad MONIRUZZAMAN a Faiza SHARIF. Recent progress in the utilization of biosynthesized polyhydroxyalkanoates for biomedical applications – Review. International Journal *of Biological Macromolecules.* 2018, **120**, 1294-1305. ISSN 01418130. DOI: 10.1016/j.ijbiomac.2018.09.002

[223] GREGORY, David, Caroline TAYLOR, Annabelle FRICKER, Emmanuel ASARE, Santosh TETALI, John HAYCOCK a Ipsita ROY. Polyhydroxyalkanoates and their advances for biomedical applications. Trends in Molecular Medicine. 2022, *28(4), 331-342*. ISSN 14714914. DOI: 10.1016/j.molmed.2022.01.007

[224] WANG, Xiaojian, Shanqing XU, Shiwei ZHOU et al. Topological design and additive manufacturing of porous metals for bone scaffolds and orthopaedic implants: A review. Biomaterials. *2016, 83, 127-141*. ISSN 01429612. DOI: 10.1016/j.biomaterials.2016.01.012

[225] NEDĚLA, Oldřich, Petr SLEPIČKA a Václav ŠVORČÍK. Surface Modification of Polymer Substrates for Biomedical Applications. Materials. 2017, 10(10). ISSN 1996-1944. DOI: 10.3390/ma10101115

[226] CAI, Shuxiang, Chuanxiang WU, Wenguang YANG, Wenfeng LIANG, Haibo YU a Lianqing LIU. Recent advance in surface modification for regulating cell adhesion and behaviors. Nanotechnology Reviews**.** 2020, 9(1), 971-989. ISSN 2191-9097. DOI: 10.1515/ntrev-2020-0076

[227] WEI, Jianhua, Toshio IGARASHI, Naoto OKUMORI, Takayasu IGARASHI, Takashi MAETANI, Baolin LIU a Masao YOSHINARI. Influence of surface wettability on competitive protein adsorption and initial *attachment of osteoblasts.* Biomedical Materials. 2009, 4(4). ISSN 1748-6041. DOI: 10.1088/1748-6041/4/4/045002

[228] XU, Li-Chong a Christopher SIEDLECKI. Effects of surface wettability and contact time on protein adhesion to biomaterial surfaces. Biomaterials. 2007, 28(22), 3273-3283. ISSN 01429612. DOI: 10.1016/j.biomaterials.2007.03.032

[229] LIM, Jung, Xiaomei LIU, Erwin VOGLER a Henry DONAHUE. Systematic variation in osteoblast adhesion and phenotype with substratum surface characteristics. Journal of Biomedical *Materials Research.* 2004, 68(**3**), 504-512. ISSN 0021-9304. DOI: 10.1002/jbm.a.20087

[230] LIM, Jung, Michael SHAUGHNESSY, Zhiyi ZHOU, Hyeran NOH, Erwin VOGLER a Henry DONAHUE. Surface energy *effects* on osteoblast spatial growth and mineralization. Biomaterials. 2008, 29(12), 1776-1784. ISSN 01429612. DOI: 10.1016/j.biomaterials.2007.12.026

[231] SHISHATSKAYA, E., I. KHLUSOV a T. VOLOVA. A hybrid PHB–hydroxyapatite composite for biomedical application: production, *in vitro* and *in vivo* investigation. Journal of Biomaterials Science, Polymer Edition. 2012, 17(5), 481-498. ISSN 0920-5063. DOI: 10.1163/156856206776986242

[232] SMITH, R. a R. PITROLA. Influence of casting substrate on the surface free energy of various polyesters. Journal of Applied Polymer Science. 2002, 83(5), 997-1008. ISSN 0021-8995. DOI: 10.1002/app.2280

[233] LINS, Luanda, Valeria BUGATTI, Sébastien LIVI a Giuliana GORRASI. Ionic Liquid as Surfactant Agent of Hydrotalcite: Influence on the *Final Properties of Polycaprolactone Matrix*. Polymers. 2018, 10(1). ISSN 2073-4360. DOI: 10.3390/polym10010044

[234] VAN DER VALK, P., A. VAN PELT, H. BUSSCHER, H. DE JONG, Ch. WILDEVUUR a J. ARENDS. Interaction of

fibroblasts and *polymer surfaces: relationship between* surface free energy and fibroblast spreading. Journal of Biomedical Materials Research. 1983, **17**(5), 807-817. ISSN 0021-9304. DOI: 10.1002/jbm.820170508

[235] OWENS, D. a R. WENDT. Estimation of the surface free energy of polymers. Journal of Applied Polymer Science. 1969, 13(8)*, 1741-1747*. ISSN 00218995. DOI: 10.1002/app.1969.070130815

[236] MARCHISIO, Marco, Maristella DI CARMINE, Rita PAGONE, Adriano PIATTELLI a Sebastiano MISCIA. Implant surface roughness influences osteoclast proliferation and differentiation. Journal of Biomedical Materials *Research* Part B**:** Applied Biomaterials. 2005, 75(2), 251-256*. ISSN* 1552-4973. DOI: 10.1002/jbm.b.30287

[237] MUSTAFA, Kamal, Joanna WROBLEWSKI, Blanca LOPEZ, Ann WENNERBERG, Kjell HULTENBY a Kristina ARVIDSON. Determining *optimal* surface roughness of TiO 2 blasted titanium implant material for attachment, *proliferation* and differentiation of cells derived from human mandibular alveolar bone. Clinical Oral Implants Research. 2001, 12(5), 515-525. ISSN 09057161. DOI: 10.1034/j.1600-0501.2001.120513.x

[238] DELIGIANNI, Despina, Nikoleta KATSALA, Petros KOUTSOUKOS a Yiannis MISSIRLIS. Effect of surface roughness of hydroxyapatite on human bone marrow cell adhesion, proliferation, differentiation and detachment *strength.* Biomaterials. 2000, 22(1), 87-96. ISSN 01429612. DOI: 10.1016/S0142-9612(00)00174-5

[239] KUNZLER, Tobias, Tanja DROBEK, Martin SCHULER a Nicholas SPENCER. Systematic study of osteoblast and fibroblast response to roughness by means of surface-morphology gradients. Biomaterials. 2007, 28(13)*, 2175-2182*. ISSN 01429612. DOI: 10.1016/j.biomaterials.2007.01.019

[240] WANG, Mian, Pelagie FAVI, Xiaoqian CHENG, Negar GOLSHAN, Katherine ZIEMER, Michael KEIDAR a Thomas WEBSTER. Cold *atmospheric* plasma (CAP) surface nanomodified 3D printed polylactic acid (PLA) scaffolds for bone regeneration. Acta Biomaterialia. 2016, 46, 256-265. ISSN 17427061. DOI: 10.1016/j.actbio.2016.09.030

[241] JAIDEV, L.R. a Kaushik CHATTERJEE. Surface functionalization of 3D printed polymer scaffolds to augment stem cell response. Materials & Design. *2019, 161,* 44-54. ISSN 02641275. DOI: 10.1016/j.matdes.2018.11.018

[242] FENG, Kuan-Che, Adriana PINKAS-SARAFOVA, Vincent RICOTTA et al. The influence of roughness on stem cell differentiation using 3D printed polylactic acid scaffolds. Soft *Matter*. 2018, 14(48), 9838-9846. ISSN 1744-683X. DOI: 10.1039/C8SM01797B

[243] GENTLEMAN, Molly a Eileen GENTLEMAN. The role of surface free energy in osteoblast–biomaterial interactions. International Materials Reviews. 2014, 59(8), 417-429*. ISSN 0950-6608*. DOI: 10.1179/1743280414Y.0000000038

[244] HABA, Yvonne, Ralf SKRIPITZ, Tobias LINDNER, Martin KÖCKERLING, Andreas FRITSCHE, Wolfram MITTELMEIER a Rainer BADER. Bone *Mineral Densities and Mechanical Properties* of Retrieved Femoral Bone Samples in relation to Bone Mineral Densities Measured in the Respective Patients. The Scientific World Journal. 2012, **2012,** 1-7. ISSN 1537-744X. DOI: 10.1100/2012/242403

[245] ROHLMANN, Antonius, Hans ZILCH, Georg BERGMANN a Reinhard KOLBEL. Material properties of femoral cancellous bone in axial loading. Archives of Orthopaedic and Traumatic Surgery. 1980, 97(2), 95-102. ISSN 0344-8444. DOI: 10.1007/BF00450930

[246] UCHIYAMA, T., T. TANIZAWA, H. MURAMATSU, N. ENDO, H.E. TAKAHASHI a T. HARA. Three-dimensional microstructural analysis of human trabecular bone in relation to its mechanical properties. Bone. 1999, *25(4), 487-491*. ISSN 87563282. DOI: 10.1016/S8756-3282(99)00188-X

[247] KOKUBO, Tadashi a Hiroaki TAKADAMA. How useful is SBF in predicting *in vivo* bone bioactivity*?. Biomaterials.* 2006, 27**(**15), 2907-2915. ISSN 01429612. DOI: 10.1016/j.biomaterials.2006.01.017

[248] ELSAWY, Moataz, Ki-Hyun KIM, Jae-Woo PARK a Akash DEEP. Hydrolytic degradation of polylactic acid (PLA) and its composites. Renewable and *Sustainable Energy Reviews. 2017, 79, 1346-1352*. ISSN 13640321. DOI: 10.1016/j.rser.2017.05.143

[249] SKRIVANEK, Josef, Pavel HOLEC, Ondrej BATKA, Martin BILEK a Pavel POKORNY. Optimization of the Spinneret Rotation Speed and Airflow Parameters for the Nozzleless Forcespinning of a Polymer Solution. Polymers. 2022, 14(5). *ISSN 2073-4360.* DOI: 10.3390/polym14051042

[250] CHANG, Wei-Min, Cheng-Chien WANG a Chuh-Yung CHEN. The combination of electrospinning and

forcespinning: Effects on a viscoelastic jet and a single nanofiber. Chemical Engineering Journal. 2014, 244, 540-551. ISSN 13858947. DOI: 10.1016/j.cej.2014.02.001

[251] DOS SANTOS, Danilo, Daniel CORREA, Eliton MEDEIROS, Juliano OLIVEIRA a Luiz MATTOSO. Advances in Functional Polymer Nanofibers: From Spinning Fabrication Techniques to Recent Biomedical Applications. ACS Applied Materials & Interfaces. 2020, 12(41), 45673-45701. ISSN 1944-8244. DOI: 10.1021/acsami.0c12410

[252] DRABEK, Jiri a Martin ZATLOUKAL. Meltblown technology for production of polymeric microfibers/nanofibers: A review. Physics of Fluids. 2019, 31(**9**). ISSN 1070-6631. DOI: 10.1063/1.5116336

[253] PULINGAM, Thiruchelvi, Jimmy APPATURI, Thaigarajan PARUMASIVAM, Azura AHMAD a Kumar SUDESH. Biomedical Applications of Polyhydroxyalkanoate in Tissue Engineering. Polymers. *2022, 14*(11). ISSN 2073-4360. DOI: 10.3390/polym14112141

[254] LOORDHUSWAMY, Amalorpava, Venkat KRISHNASWAMY, Purna KORRAPATI, Senthilram THINAKARAN a Giri RENGASWAMI. Fabrication of highly *aligned fibrous scaffolds* for tissue regeneration by centrifugal spinning technology. Materials Science and Engineering: C. 2014, 42, 799-807. ISSN 09284931. DOI: 10.1016/j.msec.2014.06.011

[255] BADROSSAMAY, Mohammad, Kartik BALACHANDRAN, Andrew CAPULLI et al. Engineering hybrid polymer-protein super-aligned nanofibers via rotary jet spinning. *Biomaterials*. 2014, **35**(10), 3188-3197. ISSN 01429612. DOI: 10.1016/j.biomaterials.2013.12.072

[256] PHA biosynthesis, recovery, and application. Delft, 2022. Disertační práce. Delft University of Technology.

[257] VOELKER, H., H. ZETTLER, W. FATH a K. BERBNER. PRODUCTION OF FIBERS BY CENTRIFUGAL SPINNING. US. 5,494,616.

[258] STOJANOVSKA, Elena, Emine CANBAY, Esra PAMPAL et al. A review on non-electro nanofibre spinning techniques. RSC Advances. 2016, 6(87), 83783-83801. ISSN 2046-2069. DOI: 10.1039/C6RA16986D

[259] ZHANG, Xiangwu a Yao LU. Centrifugal Spinning: An Alternative Approach to Fabricate Nanofibers at High Speed and Low Cost. Polymer *Reviews. 2014,* 54(4**)**, 677-701. ISSN 1558-3724. DOI: 10.1080/15583724.2014.935858

[260] ZHANG, Zhiming, Jun SUN, H.L. YUAN, R.K. AGARWAL, P. TANDON a E.X. WANG. Research on the development of the centrifugal spinning. MATEC Web of Conferences. 2017, 95. ISSN 2261-236X. DOI: 10.1051/matecconf/20179507003

[261] MERCHIERS, Jorgo, Carina MARTÍNEZ NARVÁEZ, Cheryl SLYKAS, Naveen REDDY a Vivek SHARMA. Evaporation and Rheology Chart the Processability Map for Centrifugal Force *Spinning. Macromolecules.* 2021, 54(23), 11061-11073. ISSN 0024-9297. DOI: 10.1021/acs.macromol.1c01799

[262] LU, Yao, Ying LI, Shu ZHANG, Guanjie XU, Kun FU, Hun LEE a Xiangwu ZHANG. Parameter study and characterization for polyacrylonitrile nanofibers fabricated via centrifugal *spinning process. European Polymer* Journal. 2013, 49(12), 3834-3845. ISSN 00143057. DOI: 10.1016/j.eurpolymj.2013.09.017

[263] DIVVELA, Mounica, An-Cheng RUO, Yevgen ZHMAYEV a Yong JOO. Discretized modeling for centrifugal spinning of *viscoelastic liquids.* Journal of Non-Newtonian Fluid Mechanics. 2017, 247, 62-77. ISSN 03770257. DOI: 10.1016/j.jnnfm.2017.06.005

[264] ZHMAYEV, Yevgen, Mounica DIVVELA, An-Cheng RUO, Tao HUANG a Yong JOO. The jetting behavior of viscoelastic Boger fluids during centrifugal spinning. Physics of Fluids. 2015, 27(12). ISSN 1070-6631. DOI: 10.1063/1.4936391

[265] NOROOZI, S., W. ARNE, R.G. LARSON a S.M. TAGHAVI. Centrifugal spinning of viscoelastic nanofibres. Journal of Fluid Mechanics. *2022, 934.* ISSN 0022-1120. DOI: 10.1017/jfm.2021.1135

[266] NOROOZI, S., H. HASSANZADEH, W. ARNE, R.G. LARSON a S.M. TAGHAVI. Centrifugal spinning of polymeric solutions: Experiments and modelling. Journal of Non-Newtonian Fluid Mechanics. 2023, 313. ISSN 03770257. DOI: 10.1016/j.jnnfm.2022.104971

[267] *RIAHI, Daniel N. On Strain* Hardening of Nonlinear Polymeric Jets During Forcespinning. International Journal of Applied and Computational Mathematics. 2018, 4(1). ISSN *2349-5103. DOI:* 10.1007/s40819-017-0448-8

[268] XU, Huaizhong, Shinichi YAGI, Sherry ASHOUR, Lei DU, Md HOQUE a *Lin TAN. A Review on* Current

Nanofiber Technologies: *Electrospinning, Centrifugal Spinning, and Electro-Centrifugal Spinning. Macromolecular Materials and* Engineering. 2023, 308(3). ISSN 1438-7492. DOI: 10.1002/mame.202200502

[269] HLAVATÁ, J., T. SUCHÝ, M. ŠUPOVÁ, M. POKORNÝ a E. KOŠTÁKOVÁ. A comparison *of* the centrifugal **force** spinning and electrospinning of collagen under different conditions: international conference, NANOCON. Brno: Tanger, 2018. ISBN 9788087294710.

[270] HOU, Teng, Xianglong LI, Yishen LU a Bin YANG. Highly porous fibers prepared by centrifugal spinning. Materials & Design. 2017, 114, 303-311. ISSN 02641275. DOI: 10.1016/**j**.matdes.2016.11.019

[271] MACHADO-PAULA, M.M., M.A.F. CORAT, M. LANCELLOTTI et al. A comparison between electrospinning and rotary-jet spinning to produce PCL fibers with low bacteria colonization. *Materials Science and* Engineering: C**.** 2020, 111. ISSN 09284931. DOI: 10.1016/j.msec.2020.110706

[272] RIHOVA, Martina, Ahmet INCE, Veronika CICMANCOVA, Ludek HROMADKO, Klara CASTKOVA, David PAVLINAK, Lucy VOJTOVA a Jan MACAK. Water-born 3D nanofiber mats *using* cost-effective centrifugal spinning: comparison with electrospinning process. Journal of Applied Polymer Science. 2021, 138(5). ISSN 0021-8995. DOI: 10.1002/app.49975

[273] SHAH, Mudasir, Bilal PIRZADA, Gareth PRICE, Abel SHIBIRU a Ahsanulhaq QURASHI. Applications of nanotechnology in smart textile industry: A critical review. Journal of Advanced Research. *2022, 38, 55-75*. ISSN 20901232. DOI: 10.1016/j.jare.2022.01.008

[274] SEBE, István, Barnabás SZABÓ, Zsombor NAGY, Dóra SZABÓ, László ZSIDAI, Béla KOCSIS a Romána ZELKÓ. Polymer *structure and antimicrobial activity of* polyvinylpyrrolidone-based iodine nanofibers prepared with high-speed rotary spinning technique. International Journal of Pharmaceutics. 2013, 458(1), 99-103. ISSN 03785173. DOI: 10.1016/j.ijpharm.2013.10.011

[275] GUNGOR, Melike, Merve SAGIRLI, Mehmet CALISIR, Sule SELCUK a Ali KILIC. Developing centrifugal spun thermally cross-linked gelatin based fibrous biomats for *antibacterial wound* dressing applications. Polymer Engineering & Science. 2021, 61(9), 2311-2322. *ISSN 0032-3888. DOI:* 10.1002/pen**.**25759

[276] RZAYEV, Zakir, Demet ERDÖNMEZ, Kübra ERKAN, Murat ŞIMşEK a Ulviye BUNYATOVA. Functional Copolymer/Organo-MMT Nanoarchitectures. XXII. Fabrication *and Characterization of Antifungal* and Antibacterial Poly (Vinyl Alcohol-co-Vinyl Acetate/ODA-MMT/AgNPs Nanofibers and Nanocoatings by e-Spinning and c-Spinning Methods. International Journal *of Polymeric Materials and Polymeric Biomaterials*. 2014, **64**(5), 267-278. ISSN 0091-4037. DOI: 10.1080/00914037.2014.936599

[277] MARTÍN-ALONSO, María, Valentina SALARIS, Adrián LEONÉS et al. Centrifugal Force-Spinning to Obtain Multifunctional Fibers of PLA Reinforced with Functionalized Silver Nanoparticles. Polymers. *2023, 15(5).* ISSN 2073-4360. DOI: 10.3390/polym15051240

[278] XU, Fenghua, Baicheng WENG, Luis MATERON, Anxiu KUANG, Jorge TRUJILLO a *Karen LOZANO. Fabrication of cellulose fine* fiber based membranes embedded with silver nanoparticles via Forcespinning. Journal of Polymer *Engineering.* 2016, 36(3), **269-278**. ISSN 2191-0340. DOI: 10.1515/polyeng-2015-0092

[279] HASAN, Md, Ramiro GONZALEZ, Ari MUNOZ, Luis MATERON, Jason PARSONS a Mataz ALCOUTLABI. Forcespun polyvinylpyrrolidone/copper and polyethylene oxide/copper composite fibers and their use as antibacterial agents. *Journal of Applied* Polymer Science. 2022, 139(11). ISSN 0021-8995. DOI: 10.1002/app.51773

[280] PADILLA-GAINZA, Victoria, Heriberto RODRÍGUEZ-TOBÍAS, Graciela MORALES et al. Development of zinc oxide/hydroxyapatite/poly(*D,L-lactic acid) fibrous scaffold for tissue engineering applications. Biomaterials Advances. 2022, 133.* ISSN 27729508. DOI: 10.1016/j.msec.2021.112594

[281] LI, Chen, Yu HUANG, Renhao LI et al. Fabrication and properties of carboxymethyl chitosan/polyethylene oxide composite *nonwoven mats* by centrifugal spinning. Carbohydrate Polymers. 2021, 251. ISSN 01448617. DOI: 10.1016/j.carbpol.2020.117037

[282] PRIYANTO, Aan, Dian HAPIDIN a Khairurrijal KHAIRURRIJAL. Potential Loading of Virgin Coconut Oil into Centrifugally-Spun Nanofibers for Biomedical Applications. ChemBioEng Reviews. 2022, 9(4), *393-408.* ISSN 2196-9744**.** DOI: 10.1002/cben.202100043

[283] XU, Fenghua, Baicheng WENG, Robert GILKERSON, Luis MATERON a Karen LOZANO. Development of tannic acid/chitosan/pullulan composite nanofibers from aqueous solution for potential applications as wound dressing. Carbohydrate Polymers. 2015, *115, 16-24.* ISSN 01448617. DOI:

10.1016/j.carbpol.2014.08.081

[284] XU, Fenghua, Baicheng WENG, Luis MATERON, Robert GILKERSON a Karen LOZANO. Large-scale production of a ternary composite nanofiber membrane for wound dressing *applications. Journal of* Bioactive and Compatible Polymers. 2014, 29(6), 646-660. ISSN 0883-9115. DOI: 10.1177/0883911514556959

[285] ZAHRA, Fathiyah, Ahmad FAUZI, Muhammad MIFTAHUL MUNIR a Khairurrijal KHAIRURRIJAL. Synthesis and Characterization of Rotary Forcespun Polyvinylpyrrolidone Fibers Loaded by Garlic (Allium sativum) Extract. IOP Conference Series: Materials Science *and Engineering.* 2019, **515**. ISSN 1757-899X. DOI: 10.1088/1757-899X/515/1/012005

[286] SALUSSOGLIA, Ana, Clovis DE SOUZA, Eduardo TANABE a Mônica LOPES AGUIAR. Evaluation of filter media covered with spun fibres and containing thyme essential oil with antimicrobial properties. *Environmental Technology.* 2022, 43(2), 301-310. ISSN 0959-3330. DOI: 10.1080/09593330.2020.1786167

[287] CREMAR, L., J. GUTIERREZ, J. MARTINEZ, L. MATERON, R. GILKERSON, F. XU a K. LOZANO. Development of antimicrobial chitosan based nanofiber dressings for wound healing applications. Nanomedicine Journal. 2018, 5(1), *6-14. DOI:* 10.22038/nmj.2018.05.002

[288] XIA, Lei, Linlin LU, Yuxia LIANG a Bowen CHENG. Fabrication of centrifugally spun prepared poly(lactic acid)/gelatin/ciprofloxacin nanofibers for *antimicrobial* wound dressing**.** RSC Advances. 2019, 9(61), 35328-35335. ISSN 2046-2069. DOI: 10.1039/C9RA07826F

[289] FOSTER, L., S. DAVIES a B. TIGHE. Centrifugally-spun polyhydroxybutyrate fibres: Effect of process solvent on structure, morphology and cell response. Journal of Biomaterials Science, Polymer *Edition.* 2012, 12**(**3), 317-336. ISSN 0920-5063. DOI: 10.1163/156856201750180843

[290] FOSTER, L.J.R. a B.J. TIGHE. Centrifugally spun polyhydroxybutyrate fibres: accelerated hydrolytic degradation studies. Polymer Degradation and Stability. 2005, 87(1), 1-10. *ISSN 01413910*. DOI: 10.1016/j.polymdegradstab.2003.11.012

[291] SAW, Constance, Paul HENG a Malini OLIVO. Potentiation of the Photodynamic Action of Hypericin. Journal of Environmental Pathology, Toxicology and Oncology. *2008, 27*(1), 23-33. ISSN 0731-8898. DOI: 10.1615/JEnvironPatholToxicolOncol.v27.i1.30

[292] BERAN, Milos, Ales HORNA, Viktor VORISEK, Eliska BERKOVA, Radka KORINKOVA, Vojtech TROUSIL a Marketa HRUBANOVA. Antimicrobial polyhydroxybutyrate submicron fiber mat loaded *with extract* of Hypericum perforatum. Journal of Plant Biotechnology. 2022, 49(3), 257-270. ISSN 1229-2818. DOI: 10.5010/JPB.2022.49.3.257

[293] AKIA, Mandana, Nataly SALINAS, Cristobal RODRIGUEZ, Robert GILKERSON, Luis MATERON a Karen LOZANO. Texas Sour Orange Juice Used in *Scaffolds for* Tissue Engineering**.** Membranes. 2018, 8(3). ISSN 2077-0375. DOI: *10.3390/membranes8030038*

[294] HERATH, H., M. CHAMIKARA, D. DISSANAYAKE, M. DISSANAYAKE, M. ISHAN, S. RAJAPAKSE a S. SOORIYAPATHIRANA. A Comparative Assessment of the Antibacterial Activity in Fruit *Juice of* Sri Lankan Sweet Orange Cultivars vis a vis Sour Orange. Journal of Agricultural Sciences – Sri Lanka. 2016, **11**(1), 13-23. ISSN 2386-1363. DOI: 10.4038/jas.v11i1.8076

[295] AKIA, Mandana, Cristobal RODRIGUEZ, Luis MATERON, Robert GILKERSON a Karen LOZANO. Antibacterial activity of polymeric nanofiber membranes impregnated with Texas sour orange juice. *European Polymer Journal.* 2019, 115, **1-5**. ISSN 00143057. DOI: 10.1016/j.eurpolymj.2019.03.019

[296] SLEPIČKA, P., Z. MALÁ, S. RIMPELOVÁ a V. ŠVORČÍK. Antibacterial properties of modified biodegradable PHB non-woven fabric. Materials Science and Engineering: C. *2016, 65, 364-368.* ISSN 09284931. DOI: 10.1016/j.msec.2016.04.052

[297] BERAN, Milos, Jitka PINKROVÁ, Marian URBAN a Josef DRAHORÁD. Immobilisation of endoinulinase on polyhydroxybutyrate microfibers. Czech Journal of Food Sciences. 2016, 34(6), 541-546*.* ISSN 12121800. DOI: 10.17221/72/2016-CJFS

[298] VANHEUSDEN, Chris, Jan VANMINSEL, Naveen REDDY, Pieter SAMYN, Jan D'HAEN, Roos PEETERS, Anitha ETHIRAJAN a Mieke BUNTINX. Fabrication of poly(3-hydroxybutyrate-co-3-hydroxyhexanoate) Fibers Using Centrifugal Fiber Spinning: Structure, Properties and Application Potential. *Polymers*. 2023, **15**(5). ISSN 2073-4360. DOI: 10.3390/polym15051181

[299] WANG, Chi, Chia-Hung HSU a I.-Hwe HWANG. Scaling laws and internal structure for characterizing electrospun poly[(R)-3-hydroxybutyrate] fibers. *Polymer*. 2008, **49**(19), 4188-4195. ISSN 00323861. DOI:

10.1016/j.polymer.2008.07.033

[300] OL'KHOV, A. A., O. V. STAROVEROVA, M. A. GOL'DSHTRAKH, A. V. KHVATOV, K. Z. GUMARGALIEVA a A. L. IORDANSKII. Electrospinning of biodegradable poly-3-hydroxybutyrate. Effect of the characteristics of the polymer solution. *Russian Journal of Physical Chemistry B*. 2016, **10**(5), 830-838. ISSN 1990-7931. DOI: 10.1134/S1990793116050213

[301] BYCHUK, M. A., N. R. KIL'DEEVA, M. A. KURINOVA, N. V. BOGDANOV, M*. V. KALININ,* A. **V**. NOVIKOV a G. A. VIKHOREVA. Electrospinning of Biodegradable Polymer Scaffolds. *Fibre Chemistry*. 2015, **46**(6), 345-348. ISSN 0015-0541. DOI: 10.1007/s10692-015-9618-9

[302] SMIL, V. Nitrogen Cycle and World Food Production. World Agriculture. 2011, 2, *9-13.*

[303] World Population Prospects 2019: Highlights (ST/ESA/SER.A/423). 1. New York: United Nations, 2019. ISBN 978-92-1-148316-1.

[304] ADAM, David. How far will global population rise? Researchers can't agree. Nature. 2021, 597(7877), 462-465. ISSN *0028-0836*. DOI: 10.1038/d41586-021-02522-6

[305] LAWRENCIA, Dora, See WONG, Darren LOW et al. Controlled Release Fertilizers: A Review on Coating Materials and Mechanism of Release. Plants. 2021, 10(2). ISSN 2223-7747. DOI: *10.3390/plants10020238*

[306] GALLOWAY, James, Alan TOWNSEND, Jan ERISMAN et al. Transformation of the Nitrogen Cycle: Recent Trends, Questions, and Potential Solutions. Science. *2008, 320(*5878), **889-892**. ISSN 0036-8075. DOI: 10.1126/science.1136674

[307] ZHANG, Xin, Eric DAVIDSON, Denise MAUZERALL, Timothy SEARCHINGER, Patrice DUMAS a Ye SHEN. Managing nitrogen for sustainable development. *Nature. 2015, 528*(7580), 51-59. ISSN 0028-0836. DOI: 10.1038/nature15743

[308] BISHT, Nikita a Puneet SINGH CHAUHAN. Excessive and Disproportionate Use of Chemicals Cause Soil Contamination and Nutritional *Stress. L.* LARRAMENDY, Marcelo a Sonia SOLONESKI, ed., Marcelo L. LARRAMENDY, Sonia SOLONESKI. Soil Contamination - Threats and Sustainable Solutions. IntechOpen, 2021. ISBN 978-1-83880-753-5. DOI: 10.5772/intechopen.94593

[309] FAN, Liang-tseng a Satish SINGH. Controlled Release. Berlin, Heidelberg: Springer Berlin Heidelberg, 1989. ISBN 978-3-642-74509-6. DOI: 10.1007/*978-3-642-74507-2*

[310] GIL-ORTIZ, Ricardo, Miguel NARANJO, Antonio RUIZ-NAVARRO, Sergio ATARES*, Carlos* GARCÍA, Lincoln ZOTARELLI, Alberto SAN BAUTISTA a Oscar VICENTE. Enhanced Agronomic Efficiency Using a New Controlled-Released, Polymeric-Coated Nitrogen Fertilizer in Rice. *Plants*. 2020, **9**(9). ISSN 2223-7747. DOI: 10.3390/plants9091183

[311] *COLE, Janet, Michael SMITH, Chad PENN, Becky CHEARY a* Kelley CONAGHAN. Nitrogen, phosphorus, calcium, and magnesium applied individually or as a slow release or controlled release fertilizer increase growth and yield and affect macronutrient and micronutrient concentration and content of field-grown tomato plants. *Scientia Horticulturae*. 2016, **211**, 420-430. ISSN 03044238. DOI: 10.1016/j.scienta.2016.09.028

[312] CONG, Zhao, Shen YAZHEN, Du CHANGWEN, Zhou JIANMIN, Wang HUOYAN a Chen XIAOQIN. Evaluation of Waterborne Coating for Controlled-Release Fertilizer Using Wurster Fluidized Bed. *Industrial & Engineering Chemistry Research*. 2010, **49**(20), 9644-9647. ISSN 0888-5885. DOI: 10.1021/ie101239m

[313] M.E. TRENKEL. Slow- and Controlled-Release and Stabilized Fertilizers: An Option for Enhancing Nutrient Use Efficiency in Agriculture. 2. Paris, France: IFA, 2010. ISBN 978-2-9523139-7-1.

[314] NAŘÍZENÍ EVROPSKÉHO PARLAMENTU A RADY (EU) 2019/1009 ze dne 5. června 2019. 2019, ročník 2019, číslo 1009. Dostupné z: https://eur-lex.europa.eu/legal-content/CS/TXT/HTML/?uri=CELEX:32019R1009&qid=1692348367505

[315] ČSN EN 13266. Pozvolně působící hnojiva - Stanovení uvolňování živin - Metoda pro povrchově upravená hnojiva. 2009.

[316] JACOB HANSEN AT ALL. Fertilizers Europe 2019/20 OVERVIEW. 1-32. Dostupné z: https://www.fertilizerseurope.com/wp-content/uploads/2020/07/AR-2019_20_32-pager-screen.pdf

[317] SHAVIV, Avi. Controlled Release Fertilizers. *Frankfurt,* Germany: In Proceedings of the IFA International Workshop on Enhanced-Efficiency Fertilizers, 2005.

[318] LUBKOWSKI, Krzysztof, Aleksandra SMOROWSKA, Barbara GRZMIL a Agnieszka KOZŁOWSKA. Controlled-Release Fertilizer Prepared Using a Biodegradable Aliphatic Copolyester of Poly(butylene succinate) and

Dimerized Fatty Acid. Journal of Agricultural and Food Chemistry. 2015, **63**(10), 2597-2605. ISSN 0021-8561. DOI: 10.1021/acs.jafc.5b00518

[319] GANETRI, Ikram, Youness ESSAMLALI, Othmane AMADINE, Karim DANOUN, Soumia ABOULHROUZ a Mohamed ZAHOUILY. Controlling factors of slow or controlled-release fertilizers. Controlled Release Fertilizers for Sustainable Agriculture. Elsevier, 2021, s. 111-129. ISBN 9780128195550. DOI: 10.1016/B978-0-12-819555-0.00007-8

[320] SIRACUSA, Valentina a Nadia LOTTI. Biobased Plastics for Food Packaging. Reference Module in Food Science. Elsevier, 2018. ISBN *9780081005965. DOI:* 10.1016/B978-0-08-100596-5.22413-X

[321] DAITX, Tales, Vanessa *LIMA, Marcelo GRYCZAK, Cesar PETZHOLD, Larissa CARLI a Raquel MAULER. Poly(hydroxybutyrate)-based* systems behavior on the controlled release of NPK fertilizers. Polymers *for Advanced* Technologies. 2020, **31**(11), 2579-2587. ISSN 1042-7147. DOI: 10.1002/pat.4985

[322] *DAITX, Tales, Marcelo GIOVANELA, Larissa CARLI a Raquel MAULER. Biodegradable polymer/clay* systems for highly controlled release of NPK fertilizer. Polymers for Advanced Technologies. 2019, 30(3), 631-639. *ISSN* 10427147. DOI: 10.1002/pat.4499

[323] SOUZA, Josiane, Camila *CHIAREGATO a Roselena FAEZ. Green Composite Based on PHB and Montmorillonite for* KNO3 and NPK Delivery System*. Journal of Polymers* and the Environment. 2018, 26(2), 670-679. ISSN 1566-2543. DOI: 10.1007/s10924-017-0979-4

[324] SOUZA, Josiane, Adriana DE *CAMPOS, Débora FRANçA a* Roselena FAEZ. PHB and Montmorillonite Clay Composites as KNO3 and NPK Support for a Controlled Release. Journal of Polymers and the Environment. 2019, 27(*9), 2089-2097.* ISSN 1566-2543. DOI: 10.1007/s10924-019-01498-9

[325] CHIAREGATO, Camila, *Claudinei SOUZA a* Roselena FAEZ. The fertilizer release into water and soil as the biodegradation process in the sustainable material enhancing the fertilizer efficiency. Environmental Technology & Innovation. 2021, 22. ISSN *23521864. DOI: 10.1016/*j.eti.2021.101417

[326] HARMAEN, A., A. KHALINA, H. ALI a I. AZOWA. Thermal, Morphological, and Biodegradability Properties of Bioplastic Fertilizer Composites Made of Oil Palm Biomass, *Fertilizer, and Poly(hydroxybutyrate-co-valerate).* International Journal of Polymer Science. 2016, 2016, *1-8.* ISSN 1687-9422. DOI: 10.1155/2016/3230109

[327] FRANçA, Débora, Luciana ANGELO, Claudinei SOUZA a Roselena FAEZ. Biobased Poly(3-hydroxybutyrate)/Starch/Cellulose Nanofibrils for Nutrients Coatings. ACS Applied Polymer Materials. *2021, 3(6)*, 3227-3237. ISSN 2637-6105. DOI: 10.1021/acsapm.1c00418

[328] MURUGAN, Paramasivam, Su ONG, Rokiah HASHIM, Akihiko KOSUGI, Takamitsu ARAI a *Kumar SUDESH. Development and* evaluation of controlled release fertilizer using P(3HB-co-3HHx) on oil palm plants (nursery stage) and soil microbes. *Biocatalysis and Agricultural Biotechnology*. 2020, **28**. ISSN 18788181. DOI: 10.1016/j.bcab.2020.101710

[329] ARJONA, J., F. VALENZUELA-DIAZ, H. WIEBECK, S. WANG a M. SILVA-VALENZUELA. Evaluation of Urea Encapsulation by Microcapsules of PHB/MMT and PHB/OMMT Nanocomposites. *LI,* Bowen, Jian LI, Shadia IKHMAYIES et al. Characterization of Minerals, *Metals, and Materials 2018*. Cham: Springer International Publishing, 2018, s. 365-372. The Minerals, Metals & Materials Series. ISBN 978-3-319-72483-6. DOI: 10.1007/978-3-319-72484-3_39

[330] DE CARVALHO ARJONA, Jessica, Maria DAS GRAçAS SILVA-VALENZUELA, Shu-Hui WANG a Francisco VALENZUELA-DIAZ. Biodegradable Nanocomposite Microcapsules for Controlled Release of Urea. *Polymers.* 2021, 13(5). ISSN 2073-4360. DOI: 10.3390/polym13050722

[331] VOLOVA, T., Ekaterina SHISHATSKAYA, Natalia ZHILA, Svetlana PRUDNIKOVA a Anatoly BOYANDIN. New generation formulations of agrochemicals: current trends and *future priorities. Palm Bay,* Florida: Apple Academic Press, 2019. ISBN 9781771887496.

[332] VOLOVA, Tatiana, Svetlana PRUDNIKOVA a Anatoly BOYANDIN. Biodegradable poly-3-hydroxybutyrate as a fertiliser carrier. Journal of the Science of Food and Agriculture. 2016, *96(12), 4183-4193.* ISSN 00225142. DOI: 10.1002/jsfa.7621

[333] BOYANDIN, Anatoly, Eugenia KAZANTSEVA, Daria VARYGINA a Tatiana VOLOVA. Constructing Slow-Release Formulations of Ammonium Nitrate Fertilizer Based on Degradable Poly(3-hydroxybutyrate). Journal of Agricultural and *Food Chemistry.* 2017, **65**(32), 6745-6752. ISSN 0021-8561. DOI: 10.1021/acs.jafc.7b01217

[334] EZEMA, Chinonso, Toshihiko OOI a Ken'ichiro MATSUMOTO. Heat-Press Technique for Coating

Ammonium Nitrate Granules with Biodegradable Hydrophobic Polymer Blend of Poly(3-hydroxybutyrate-co -3-hydroxyhexanoate) and Poly(*ε-caprolactone). ACS Agricultural* Science & Technology. 2022, 2(6), 1179-1186. ISSN 2692-1952. DOI: 10.1021/acsagscitech.2c00061

[335] YABUENG, Nuttipon a Suchada NAPATHORN. Toward non-toxic and simple recovery process of poly(3-hydroxybutyrate) using the green solvent 1,3-dioxolane. *Process Biochemistry*. 2018, **69**, 197-207. ISSN 13595113. DOI: 10.1016/j.procbio.2018.02.025

[336] YANG, Yue-chao, Min ZHANG, Yuncong LI, Xiao-hui FAN a Yu-qing GENG. Improving the Quality of Polymer-Coated Urea with Recycled Plastic, Proper Additives, and Large Tablets. *Journal of Agricultural and Food Chemistry*. 2012, **60**(45), 11229-11237. ISSN 0021-8561. DOI: 10.1021/jf302813g

[337] SALIMI, Mehri, Elaheh MOTAMEDI, Babak MOTESHAREZEDEH, Hossein HOSSEINI a Hossein ALIKHANI. Starch-*g*-poly(acrylic acid-co-acrylamide) composites reinforced with natural char nanoparticles toward environmentally benign slow-release urea fertilizers. *Journal of Environmental Chemical Engineering*. 2020, **8**(3). ISSN 22133437. DOI: 10.1016/j.jece.2020.103765

10 SEZNAM VÝSTUPŮ AUTORA NA TÉMA PRÁCE

10.1 Publikace

Biopolymer PHB

Pub 1. OBRUCA, Stanislav, Pavla BENESOVA, Sinisa PETRIK, Jana OBORNA, **Radek PRIKRYL** and Ivana MAROVA, 2014. Production of polyhydroxyalkanoates using hydrolysate of spent coffee grounds. September 2014. B.m.: Elsevier BV. Available at: DOI: 10.1016/j.procbio.2014.05.013

Pub 2. POSPISILOVA, Aneta, Ivana NOVACKOVA and **Radek PRIKRYL**, 2021. Isolation of poly(3-hydroxybutyrate) from bacterial biomass using soap made of waste cooking oil. April 2021. B.m.: Elsevier BV. Available at: DOI: 10.1016/j.biortech.2021.124683

Pub 3. POSPISILOVA, Aneta, Veronika MELCOVA, Silvestr FIGALLA, Premysl MENCIK and **Radek PRIKRYL**, 2021. Techniques for increasing the thermal stability of poly[(R)-3-hydroxybutyrate] recovered by digestion methods. November 2021. B.m.: Elsevier BV. Available at: DOI: 10.1016/j.polymdegradstab.2021.109727

Bioplasty na bázi PHB

Pub 4. TOCHÁČEK, Jiří, **Radek PŘIKRYL**, Přemysl MENČÍK, Veronika MELČOVÁ and Silvestr FIGALLA, 2021. The chances of thermooxidation stabilization of poly(3-hydroxybutyrate) during processing–A critical evaluation. 26. February 2021. B.m.: Wiley. Available at: DOI: 10.1002/app.50647

Pub 5. PERD'OCHOVÁ, D, K TOMANOVÁ, P ALEXY, J BOČKAJ, J FERANC, R PLAVEC, L OMANÍKOVÁ, P JURKOVIČ and **R PŘIKRYL**, 2017. The influence of additives on crystallization of blends based on polylactid acid. November 2017. B.m.: IOP Publishing. Available at: DOI: 10.1088/1757-899x/266/1/012014

Pub 6. MELCOVA, Veronika, **Radek PRIKRYL**, Premysl MENCIK and Jiří TOCHACEK, 2019. Processing Stabilization of Poly(3-Hydroxybutyrate)/Poly(Lactic Acid) Blends with Oligomeric Carbodiimide. May 2019. B.m.: Trans Tech Publications, Ltd. Available at: DOI: 10.4028/www.scientific.net/msf.955.7

Pub 7. PLAVEC, Roderik, Slávka HLAVÁČIKOVÁ, Leona OMANÍKOVÁ, Jozef FERANC, Zuzana VANOVČANOVÁ, Katarína TOMANOVÁ, Ján BOČKAJ, Ján KRUŽELÁK, Elena MEDLENOVÁ, Ivana GÁLISOVÁ, Lucia DANIŠOVÁ, **Radek PŘIKRYL**, Silvestr FIGALLA, Veronika MELČOVÁ and Pavol ALEXY, 2020. Recycling possibilities of bioplastics based on PLA/PHB blends. December 2020. B.m.: Elsevier BV. Available at: DOI: 10.1016/j.polymertesting.2020.106880

Pub 8. FOGAŠOVÁ, Mária, Silvestr FIGALLA, Lucia DANIŠOVÁ, Elena MEDLENOVÁ, Slávka HLAVÁČIKOVÁ, Zuzana VANOVČANOVÁ, Leona OMANÍKOVÁ, Andrej BACO, Vojtech HORVÁTH, Mária MIKOLAJOVÁ, Jozef FERANC, Ján BOČKAJ, Roderik PLAVEC, Pavol ALEXY, Martina REPISKÁ, **Radek PŘIKRYL**, Soňa KONTÁROVÁ, Anna BÁREKOVÁ, Martina SLÁVIKOVÁ, Marek KOUTNÝ, Ahmad FAYYAZBAKHSH and Markéta KADLEČKOVÁ, 2022. PLA/PHB-Based Materials Fully Biodegradable under Both Industrial and Home-Composting Conditions. 30. September 2022. B.m.: MDPI AG. Available at: DOI: 10.3390/polym14194113

Biokompozity pro FDM 3D tisk na bázi PHB

Pub 9. MENCIK, Premysl, Veronika MELCOVA, Sona KONTAROVA, **Radek PRIKRYL**, Dagmara PERDOCHOVA and Martina REPISKA, 2019. Biodegradable Composite Materials Based on Poly(3-Hydroxybutyrate)

for 3D Printing Applications. May 2019. B.m.: Trans Tech Publications, Ltd. Available at: DOI: 10.4028/www.scientific.net/msf.955.56

Pub 10. MENČÍK, Přemysl, **Radek PŘIKRYL**, Štěpán KROBOT, Veronika MELČOVÁ, Soňa KONTÁROVÁ, Roderik PLAVEC, Jan BOČKAJ, Vojtech HORVÁTH and Pavol ALEXY, 2022. Evaluation of the Properties of PHB Composite Filled with Kaolin Particles for 3D Printing Applications Using the Design of Experiment. 19. November 2022. B.m.: MDPI AG. Available at: DOI: 10.3390/ijms232214409

Pub 11. MENČÍK, Přemysl, **Radek PŘIKRYL**, Ivana STEHNOVÁ, Veronika MELČOVÁ, Soňa KONTÁROVÁ, Silvestr FIGALLA, Pavol ALEXY and Ján BOČKAJ, 2018. Effect of Selected Commercial Plasticizers on Mechanical, Thermal, and Morphological Properties of Poly(3-hydroxybutyrate)/Poly(lactic acid)/Plasticizer Biodegradable Blends for Three-Dimensional (3D) Print. 3. October 2018. B.m.: MDPI AG. Available at: DOI: 10.3390/ma11101893

Pub 12. KONTÁROVÁ, Soňa, **Radek PŘIKRYL**, Veronika MELČOVÁ, Přemysl MENČÍK, Matyáš HORÁLEK, Silvestr FIGALLA, Roderik PLAVEC, Jozef FERANC, Jiří SADÍLEK and Aneta POSPÍŠILOVÁ, 2020. Printability, Mechanical and Thermal Properties of Poly(3-Hydroxybutyrate)-Poly(Lactic Acid)-Plasticizer Blends for Three-Dimensional (3D) Printing. 23. October 2020. B.m.: MDPI AG. Available at: DOI: 10.3390/ma13214736

Pub 13. PLAVEC, Roderik, Vojtech HORVÁTH, Slávka HLAVÁČIKOVÁ, Leona OMANÍKOVÁ, Martina REPISKÁ, Elena MEDLENOVÁ, Jozef FERANC, Ján KRUŽELÁK, **Radek PŘIKRYL**, Silvestr FIGALLA, Soňa KONTÁROVÁ, Andrej BACO, Lucia DANIŠOVÁ, Zuzana VANOVČANOVÁ and Pavol ALEXY, 2022. Influence of Multiple Thermomechanical Processing of 3D Filaments Based on Polylactic Acid and Polyhydroxybutyrate on Their Rheological and Utility Properties. 11. May 2022. B.m.: MDPI AG. Available at: DOI: 10.3390/polym14101947

3D tisknutelné kompozity na bázi PHB pro medicínu

Pub 14. MELČOVÁ, Veronika, Kateřina SVORADOVÁ, Přemysl MENČÍK, Soňa KONTÁROVÁ, Michala RAMPICHOVÁ, Věra HEDVIČÁKOVÁ, Věra SOVKOVÁ, **Radek PŘIKRYL** and Lucy VOJTOVÁ, 2020. FDM 3D Printed Composites for Bone Tissue Engineering Based on Plasticized Poly(3-hydroxybutyrate)/poly(d,l-lactide) Blends. 27. November 2020. B.m.: MDPI AG. Available at: DOI: 10.3390/polym12122806

Pub 15. KROBOT, Štěpán, Veronika MELČOVÁ, Přemysl MENČÍK, Soňa KONTÁROVÁ, Michala RAMPICHOVÁ, Věra HEDVIČÁKOVÁ, Ema MOJŽIŠOVÁ, Andrej BACO and **Radek PŘIKRYL**, 2023. Poly(3-hydroxybutyrate) (PHB) and Polycaprolactone (PCL) Based Blends for Tissue Engineering and Bone Medical Applications Processed by FDM 3D Printing. 22. May 2023. B.m.: MDPI AG. Available at: DOI: 10.3390/polym15102404

Netkané mikrovlákenné textilie na bázi PHB pro medicínu

Pub 16. ABDEL-MOHSEN, A.M., R.M. ABDEL-RAHMAN, I. KUBENA, L. KOBERA, Z. SPOTZ, M. ZBONCAK, **R. PRIKRYL**, J. BRUS and J. JANCAR, 2020. Chitosan-glucan complex hollow fibers reinforced collagen wound dressing embedded with aloe vera. Part I: Preparation and characterization. February 2020. B.m.: Elsevier BV. Available at: DOI: 10.1016/j.carbpol.2019.115708

Agrochemické aplikace PHB

Pub 17. FOJT, Jakub, Jan DAVID, **Radek PŘIKRYL**, Veronika ŘEZÁČOVÁ and Jiří KUČERÍK, 2020. A critical review of the overlooked challenge of determining micro-bioplastics in soil. November 2020. B.m.: Elsevier BV. Available at: DOI: 10.1016/j.scitotenv.2020.140975

Pub 18. KONTÁROVÁ, Soňa, **Radek PŘIKRYL**, Petr ŠKARPA, Tomáš KRIŠKA, Jiří ANTOŠOVSKÝ, Zuzana GREGUŠKOVÁ, Silvestr FIGALLA, Vojtěch JAŠEK, Marek SEDLMAJER, Přemysl MENČÍK and Mária MIKOLAJOVÁ, 2022. Slow-Release Nitrogen Fertilizers with Biodegradable Poly(3-hydroxybutyrate) Coating: Their Effect on the Growth of Maize and the Dynamics of N Release in Soil. 14. October 2022. B.m.: MDPI AG. Available at: DOI: 10.3390/polym14204323

Pub 19. JAŠEK, Vojtěch, Jan FUČÍK, Lucia IVANOVÁ, Dominik VESELÝ, Silvestr FIGALLA, Ludmila MRAVCOVA, Petr SEDLACEK, Jozef KRAJČOVIČ and **Radek PŘIKRYL**, 2022. High-Pressure Depolymerization of Poly(lactic acid) (PLA) and Poly(3-hydroxybutyrate) (PHB) Using Bio-Based Solvents: A Way to Produce Alkyl Esters Which Can Be Modified to Polymerizable Monomers. 1. December 2022. B.m.: MDPI AG. Available at: DOI: 10.3390/polym14235236

10.2 Ostatní výstupy

10.2.1 Patent

V1 MÁROVÁ, I.; OBRUČA, S.; PŘIKRYL, R.; VUT v Brně: Způsob produkce polyhydroxyalkanoátů (PHA) na olejovém substrátu. 304183, patent. (2013) (8%)

10.2.2 Poloprovoz

V2 PŘIKRYL, R.; MELČOVÁ, V.; MENČÍK, P.; POHLUDKA, D.; PACÁKOVÁ, Z.; BOLYÓ, J.: DELTA-01; Funkční zařízení na srážení. Nafigate Corporation a.s., Prosek, Praha. (16 %)

10.2.3 Ověřená technologie

V3 PŘIKRYL, R.; MENČÍK, P.; MELČOVÁ, V.; KONTÁROVÁ, S.; FIGALLA, S.; POSPÍŠILOVÁ, A.: 3D tisková struna KOMP 5-5; Technologie výroby polymerní směsi s majoritním obsahem poly-3-hydroxybutyrátu (PHB) pro výrobu 3D tiskových strun. FCH VUT v Brně. (ověřená technologie)

10.2.4 Prototyp

V4 PŘIKRYL, R.; MENČÍK, P.; TOCHÁČEK, J.; POHLUDKA, D.: HYDAL-F; Biodegradabilní fólie na bázi polyhydroxybutyrátu. Výzkumný ústav ovocnářský, Holovousy - fólie v reálných podmínkách FCH VUT - vzorky fólie. (20 %)

V5 PŘIKRYL, R.; MELČOVÁ, V.; KONTÁROVÁ, S.; FIGALLA, S.; POSPÍŠILOVÁ, A.; MENČÍK, P.: Fialment KOMP 5-5; Prototyp tiskové struny na bázi PHB. FCH VUT v Brně. (16 %)

10.2.5 Funkční vzorek

V6 PŘIKRYL, R.; PALOUŠEK, D.; MENČÍK, P.; VESPALEC, A.; KRČMA, M.; ŠKAROUPKA, D.: Design obličeojvé polomasky pro výrobu termoformingem 01; Obličejová polomaska realizovaná pomocí termoformingu. FCH VUT v Brně, Purkyňova 464/118, Brno 612 00. URL: http://intranet.ustavkonstruovani.cz/project-documentations/edit/399. (30 %)

V7 PŘIKRYL, R.; BÁLKOVÁ, R.; TOCHÁČEK, J.; MENČÍK, P.; KUČERA, F.; PETRŮJ, J.: Hydal I; Plast pro injekční vstřikování na bázi poly-3-hydroxybutyrátu HYDAL-Powder. FCH VUT v Brně, Nafigate corporation. (30 %)

10.3 Vedené práce na relevantní téma

VSKP1 Melčová Veronika, PhD.: Modifikace polyhydroxybutyrátu roubováním funkcních skupin, 2015

VSKP2 Stehnová Ivana, Ing.: Vliv chemické struktury změkčovadla na vlastnosti bioplastu na bázi polyhydroxybutyrátu, diplomová práce, 2018

VSKP3 Štulrajterová Lujza, Ing.: Vlastnosti vláken na bázi polyhydroxybutyrátu, diplomová práce, 2018

VSKP4 Horálek Matyáš, Ing.: Biokompozity na bázi polyhydroxybutyrátu pro 3D tisk, diplomová práce, 2019

VSKP5 Chaloupková Kateřina, Ing.: Biokompozitní materiál pro 3D tisk v regenerativní medicíně, bakalářská práce, 2020

VSKP6 Gregušková Zuzana, Ing.: Mikrovlákna na bázi polyhydroxybutyrátu pro medicínské aplikace, diplomová práce, 2021

VSKP7 Chaloupková Kateřina, Ing.: Optimalizace biokompozitu na bázi poly(3-hydroxybutyrátu) s ohledem na tisknutelnost a mechanické vlastnosti, diplomová práce, 2022

VSKP8 Kecíková Alžběta, Ing.: Příprava mikrovlákenných struktur na bázi kopolymeru PHB, diplomová práce, 2022

VSKP9 Krobot Štěpán, Ing.: Materiály na bázi PHB pro 3D tisk medicínských aplikací, diplomová práce, 2022

VSKP10 Nečas Aleš, Ing.: Vliv vnitřní struktury na mechanické vlastnosti 3D tištěného segmentu femuru z nového optimalizovaného biokompozitu, diplomová práce, 2023

VSKP11 Bobková Magdalena, Bc.: Povlakovaná hnojiva se zpomaleným uvolňováním na bázi PHB, bakalářská práce, 2022, vedoucí Ing. Soňa Kontárová, Ph.D.

11 PROJEKTY ŘEŠENÉ AUTOREM

PR 1. **TAČR GAMA**, TG01010054-1, **Průmyslová receptura na vstřikování z biopolymeru PHA**, zahájení: 01.10.2014, ukončení: 30.09.2016, řešitel dílčího projektu

PR 2. **TAČR EPSILON**, TH01011353, **Vývoj nového výrobního postupu pro biotechnologii Hydal**, zahájení: 01.02.2015, ukončení: 31.05.2016, řešitel za organizaci

PR 3. **TAČR DELTA**, TF02000062, **Transfer biotechnologie Hydal do Číny**, zahájení: 01.02.2016, ukončení: 31.12.2018, vedoucí výzkumné skupiny

PR 4. **MPO TRIO**, FV20480, **Vytvoření nové materiálové základny pro 3D printing z Hydal PHA**, zahájení: 01.06.2017, ukončení: 31.12.2019 řešitel za organizaci

PR 5. **MPO TRIO**, FV40095, **Smart Fertilizers**, zahájení: 01.04.2019, ukončení: 31.12.2021, řešitel za organizaci

PR 6. **MPO TRIO**, FV40094, **Vývoj nové materiálové základny na základě Hydal PHA pro náhradu mikroplastů**, zahájení: 01.04.2019, ukončení: 31.12.2021, vedoucí výzkumné skupiny

PR 7. ***Eurostars*****,** 7D19010, **RIMPLAN**, zahájení: 2019, ukončení: 2022, (v rámci Nafigate)

PR 8. **TAČR TREND**, FW01010513**, Vývoj produkčního systému velkoformátové aditivní výroby vysoce plněných odpadních termoplastů**, zahájení: 01.02.2020, ukončení: 31.12.2023, vědecký pracovník

PR 9. **OP PIK Aplikace 8**, EG20_321/0024676, **Nové cirkulární biotechnologie a biomedicínské aplikace**, zahájení: 1.12.2020, ukončení: 31.5.2023, řešitel za organizaci

PR 10. **H2020-BBI-JTI-2020**, BioSupPack - **Demonstrative process for the production and chemical recycling of environmentally safe, superior bio-based packaging by plasma integration in the value chain**, zahájení: 01.05.2021, ukončení: 31.10.2024, vedoucí výzkumné skupiny

PR 11. **TAČR Kappa**, TO01000309, ProfiBone - **Low-temperature 3D Printing of Bio-Functionalized Ceramic Bone Implants with Adjustable Mechanical Properties**, zahájení 1.1.2021, ukončení 31.12.2023, vědecký pracovník (Ceitec)

PR 12. **Interreg,** ATCZ287, **Technologie na zpracování odpadní biomasy lesního průmyslu pro pokročilé polymerní kompozity, zahájení** 01.01.2022 , ukončení 31.12.2022, výzkumný pracovník (Ceitec)

PR 13. **TAČR NCK**, TN02000051/009, **Technologie zpracování odpadních kalů z recyklace plastů**, zahájení 1.3.2023, ukončení 31.12.2024, řešitel dílčího projektu za organizaci

PR 14. **TAČR NCK**, TN02000051/012, **Bioplasty pro agrochemické aplikace**, zahájení 1.6.2023, ukončení 31.5.2026, řešitel dílčího projektu za organizaci



VYSOKÉ UČENÍ TECHNICKÉ V BRNĚ

FAKULTA CHEMICKÁ

PŘÍLOHA K HABILITAČNÍ PRÁCI

V OBORU CHEMIE, TECHNOLOGIE A VLASTNOSTI MATERIÁLŮ

MGR. RADEK PŘIKRYL, PH.D.

BRNO, 2023

Process Biochemistry 49 (2014) 1409–1414

Contents lists available at ScienceDirect

Process Biochemistry

journal homepage: www.elsevier.com/locate/procbio

Short communication

Production of polyhydroxyalkanoates using hydrolysate of spent coffee grounds

Stanislav Obruca [a,*], Pavla Benesova [a], Sinisa Petrik [a], Jana Oborna [b], Radek Prikryl [c], Ivana Marova [a]

[a] Materials Research Centre, Faculty of Chemistry, Brno University of Technology, Purkynova 118, 612 00 Brno, Czech Republic
[b] Institute of Chemistry and Technology of Environmental Protection, Faculty of Chemistry, Brno University of Technology, Purkynova 118, 612 00 Brno, Czech Republic
[c] Institute of Material Chemistry, Faculty of Chemistry, Brno University of Technology, Purkynova 118, 612 00 Brno, Czech Republic

ARTICLE INFO

Article history:
Received 24 February 2014
Received in revised form 20 May 2014
Accepted 21 May 2014
Available online 29 May 2014

Keywords:
Spent coffee grounds
Polyhydroxyalkanoates
PHA
Burkholderia cepacia
Detoxification

ABSTRACT

Spent coffee grounds (SCG) are solid fraction wastes deriving from coffee industries, the disposal of which represents a serious environmental issue. This work aims at the conversion of hydrolysate of SCG (SCGH) into polyhydroxyalkanoates (PHA) by *Burkholderia cepacia*. The bacteria was capable of SCGH utilization and production of copolymer of 3-hydroxybutyrate and 3-hydroxyvalerate [P(HB-co-HV]. Levulinic acid present in SCGH probably served as the precursor of 3HV for the copolymer biosynthesis. To improve the PHA yields, various detoxification methods were tested. The extraction of polyphenols from SCG by ethanol prior to the hydrolysis seems to be the most promising, since, apart from the fact that it enhanced the PHA yields by about 25%, polyphenols extracted from SCG may represent important side products, because they might be used for the production of functional foods and other high value products.
© 2014 Elsevier Ltd. All rights reserved.

1. Introduction

Polyhydroxyalkanoates (PHA) are polyesters synthesized and stored in bacterial cells in the form of intracellular granules. Bacteria use PHA as carbon, energy and reducing power storage materials. PHA have attracted much attention as biodegradable alternative to traditional petrochemical plastics, their properties and potential applications were extensively reviewed by Philip et al. [1].

Among PHA, the homopolymer of 3-hydroxybutyrate, poly(3-hydroxybutyrate) (PHB), is the most abundant and the best characterized polymer to date. However, PHB possesses several properties, such as high crystallinity, melting point temperature and low flexibility, which complicate its processing and also limit the range of its application. The mechanical properties of this polymer can be significantly improved by the incorporation of 3-hydroxyvalerate (3HV) units into the PHA structure resulting in the formation of poly(3-hydroxybutyrate-*co*-3-hydroxyvalerate) [P(HB-co-HV)] with better mechanical properties and processability [2].

Since about 45% of the total costs of PHA production are ascribed to carbon sources, such as refined glucose or sucrose [3], cheap wastes or side products of agriculture and food industry are used as inexpensive carbon substrates improving thus the economic feasibility of the PHA production [4]. Moreover, cellulosic and hemicellulosic biomass are considered being very promising renewable sources for the biotechnological production of fuels and chemicals, including PHA [5]. Therefore, the PHA production from *Burkholderia cepacia*, *Burkholderia sacchari* [6] and *Ralstonia eutropha* [7] has been reported by utilizing sugarcane bagase hydrolysate. More recently, Pan and his colleagues studied the PHA production from detoxified sugar maple hemicellulosic hydrolysate by *B. cepacia* [8,9], Zhang et al. utilized oil palm empty fruit bunch for the PHB production using *Bacillus megatrerium* [10] and *B. sacchari* was employed for the PHA production from wheat straw hydrolysate [11].

Coffee is one of the world' most popular beverages and has grown steadily in commercial importance during the last 150 years. Nowadays, coffee is, after petroleum, the second largest traded commodity in the world. In 2010 the worldwide annual production of coffee beans exceeded 8 million tons [12]. During the preparation of coffee beverage or the manufacturing of instant coffee, raw coffee powder is mixed with hot water or steam under the conditions of favoring the release of aroma compounds and other coffee-bean constituents into the liquid, which generates solid residues known

* Corresponding author. Tel.: +420 541 149 486; fax: +420 541 211 697.
E-mail address: Stana.O@seznam.cz (S. Obruca).

http://dx.doi.org/10.1016/j.procbio.2014.05.013
1359-5113/© 2014 Elsevier Ltd. All rights reserved.

as spent coffee grounds (SCG). On an average, the manufacturing of one ton of green coffee generates about 650 kg of SCG [12]. Despite the fact that this waste stream of coffee industry has been considered as a raw substrate for the production of various compounds such as polyphenols [13,14], bioethanol [15,16], biodiesel [16,17] or mannooligosaccharides [18], the most of this residue remains unutilized, being discharged to the environment or burned for elimination, which can be considered neither as environmentally friendly nor economically feasible techniques [12].

We have recently investigated the utilization of oil extracted from SCG for the PHA production [19]. Hence, we aimed at the valorization of residual SCG after the oil extraction. To our best knowledge, there is no report on the utilization of cellulosic biomass of SCG for the biosynthesis of polyhydroxyalkanoates. Therefore, in the present work, the ability of *B. cepacia* to produce PHA from SCG was tested. Moreover, various detoxification methods were used to improve the fermentability of SCG based media and thus, the PHA yields obtained on this substrate.

2. Materials and methods

2.1. Raw material preparation

Spent coffee grounds (SCG) were obtained from a coffee automat machine at the Faculty of Chemistry, Brno University of Technology, Czech Republic. The waste material was firstly dried to the constant weight (80 °C for 24 h). The coffee oil extraction was performed with n-hexane as described by Al-Hamamre et al. [17]. To hydrolyze the hemicelluloses of raw material, 15% (w/v) SCG were firstly treated by 1 vol.% H_2SO_4 for 90 min at 121 °C [16]. In the next step, the enzymatic digestion was used to break up cellulose releasing fermentable saccharides. Therefore, pH of the suspension after the acidic hydrolysis was set to 4.5 (10 M NaOH) and cellulose was treated by 0.5% (vol/vol) of Celluclast 1.5 L (Novozymes A/S, Bagsværd, Denmark) at 50 °C under permanent shaking (150 rpm) for 24 h [16]. At the end of the process the solids obtained after enzyme treatments (representing approx. 30% of SCG after oil extraction) were removed by filtration and the permeate, called spent coffee grounds hydrolyzate (SCGH), was used for the cultivation media preparation and the PHA production.

2.2. Analysis of SCGH composition

The concentration of dry matter was estimated by drying 10 ml of SCGH to constant weight at 105 °C. Ash content was determined as the weight of solids obtained after the incubation of 2 ml of SCG-media at 800 °C for 2 h. Subsequently, the phosphorus content of ash was measured by Ion Chromatography (850 Professional IC, Metrohm, Switzerland) using Metrosep A Supp 7-250/4.0 column. Particular sugars contents (cellobiose, glucose, mannose, galactose and arabinose) were estimated by liquid chromatography (pump LCP 4020, thermostat LCO 101, degasser DG-1210, refractometric detector RIDK 102; Ecom, Czech Republic) with REZEX-ROA column (150 mm × 4.6 mm, 5 μm; Phenomex, USA). The determination of total sugars by Somogyi-Nelson method was employed for routine analysis of sugars. The concentrations of levulinic acid, 5-hydroxymethyfurfural and furfural were determined by gas chromatography equipped with flame ionization detector (GC-FID, Trace GC Ultra, Thermo Scientific) according to Omari et al. [20]. The concentration of nitrogen compounds was determined by Kjehdal method and the overall protein content was calculated using the conversion factor of 6.25. The total phenolics content was estimated using the Folin–Ciocalteu reagent method [21]. All analyses were performed at least in triplicate and the results were evaluated as mean values with SD values.

2.3. Microorganisms and cultivations

B. cepacia CCM 2656 (ATCC 17759) was purchased from the Czech Collection of Microorganisms. The bacterial culture was cultivated in mineral salt medium described by Bertrand et al. [22]. SCGH, salt solutions and microelement solutions were autoclaved separately (115 °C, 20 min) and then aseptically reconstituted at room temperature prior to the inoculation to reach desired portion of SCGH in the medium and final concentration of salts. The cultivations were performed in Erlenmeyer flasks (volume 250 ml) containing 50 ml of the cultivation media. The temperature was set to 30 °C and the agitation to 180 rpm. After 72 h of cultivation, the cells were harvested (centrifugation, 8000 × g, 5 min) and the biomass as well as the PHB yields were determined as described below. All cultivations were performed in triplicate.

Table 1
Composition of SCGH used in this study (150 g SCG per liter).

Parameter	Concentration/value
Dry solid matter ($g\,l^{-1}$)	98.4 ± 0.1
Ash ($g\,l^{-1}$)	27.6 ± 0.8
Conductivity ($mS\,cm^{-1}$)	23.2
PO_4^{3-} ($g\,l^{-1}$)	0.32 ± 0.03
Total nitrogen (wt.%)	0.162 ± 0.1
Proteins (N × 6.25) ($g\,l^{-1}$)	10.2 ± 0.6
Polyphenols ($g\,l^{-1}$)	3.6 ± 0.1
Levulinic acid ($g\,l^{-1}$)	1.72 ± 0.19
5-Hydroxymethyl furfural ($g\,l^{-1}$)	0.15 ± 0.03
Furfural ($g\,l^{-1}$)	*n.d.*
Total sugars ($g\,l^{-1}$)	50.1 ± 2.2
Cellobiose ($g\,l^{-1}$)	2.7 ± 0.3
Galactose ($g\,l^{-1}$)	17.3 ± 0.3
Mannose ($g\,l^{-1}$)	23.6 ± 0.6
Arabinose ($g\,l^{-1}$)	2.8 ± 0.2
Glucose ($g\,l^{-1}$)	3.9 ± 0.2

Results are in form average ± standard deviation.
n.d. – not detected.

2.4. PHA analysis

The biomass concentration was analyzed gravimetrically, the samples were centrifuged and the cells were washed with 5% (vol/vol) Triton X (10 ml) and distilled water, respectively, and afterwards they were dried (105 °C) to the constant weight. The PHB content of dried cells was analyzed by gas chromatography (Trace GC Ultra, Thermo Scientific, USA) as reported by Brandl et al. [23]. Commercially available P(HB-co-HV) (Sigma–Aldrich, Germany, HV content 12 mol.%) was used as a standard; benzoic acid was used as an internal standard. The molecular weight of PHB was determined by gel permeation chromatography (Agilent 1100 Series; column PLgel Mixed B (300 9 7.5 mm; 10 lm)).

The Differential Scanning Calorimetry (DSC) (204 F1, Netzsch) was used for determination of thermal properties of produced material as described elsewhere [2]. Thermogravimetric apparatus (TGA) (Q500; TA Instruments) was used for evaluation of thermal stability of the PHB.

2.5. Detoxification of SCGH

Several methods which should reduce the amount of toxic substances in SCGH were tested in this study. Polyphenols were extracted from SCG prior to its hydrolysis using various mixtures of distilled water and ethanol (0, 30, 45 and 60 vol.% of ethanol). The polyphenol extraction from 20 g of SCG was performed using 40 ml of particular solvent for 2 h at 50 °C under constant shaking (150 rpm). After the extraction, SCG was filtered, dried and hydrolyzed as described above. The control was prepared identically; however, SCG was not subjected to the extraction.

Further, the overliming was performed with SCGH (after hydrolysis) as described by [8], also the activated charcoal (AC) detoxification was employed; AC was mixed with SCGH in the ratio of 1:20 (w/v) and stirred for 1 h at 60 °C [8].

3. Results and discussion

3.1. Composition of SCGH

To hydrolyze SCG, the combination of diluted acid hydrolysis (1% H_2SO_4) of hemicelluloses and enzymatic execution of cellulose was applied. This approach yielded liquid hydrolysate of SCG (SCGH) the composition of which is shown in Table 1. The total concentration of sugars was determined to be 50.1 $g\,l^{-1}$ (by the hydrolysis of 150 $g\,l^{-1}$ of SCG), the major sugars identified in SCGH are mannose (23.6 $g\,l^{-1}$) and galactose (17.3 $g\,l^{-1}$) followed by glucose (3.9 $g\,l^{-1}$), arabinose (2.8 $g\,l^{-1}$) and cellobiose (2.7 $g\,l^{-1}$). Unlike in other hemicellulose hydrolysates such as wheat straw [13] or maple hemicellulosic hydrolysate [10] containing significant portion of pentoses, SCGH contains only low portion of arabinose. The fact that hexoses are substantially dominating sugars of SCGH may be an important factor positively influencing the PHA production. The metabolic pathways of hexoses utilization generates larger amount of energy, which might, in consequence, enhance the PHB yields. Lopes et al. reported the theoretical ATP/3HB monomer ratio being 3 mol/mol in case of xylose compared to the value of 7 mol ATP/mol 3HB in glucose [24].

The analysis also focused on chemical compounds which might complicate the fermentability of SCGH. SCGH contains significant portion of ash (27.6 g l^{-1}) which may be attributed to the application of H_2SO_4 during acidic hydrolysis and NaOH for subsequent neutralization of SCGH. High concentration of salts may cause the inhibition of bacterial growth due to the induction of osmotic stress. On the contrary, it was observed that mild osmotic stress may support PHA biosynthesis [25]. Moreover, SCGH contains also high amounts of potentially toxic substances such as polyphenols, 5-hydromethylfurfural (5HMF) and levulinic acid (LA). 5HMF and LA are the products of hexoses degradation under high temperature and acidic conditions [20].

3.2. PHB production from SCGH employing B. cepacia

B. cepacia ATCC 17759 is a gram-negative bacterium which is generally considered as one of the most promising candidates for the PHA production from hemicellose and cellulose hydrolysates because, apart from the fact that it is able to utilize various hexoses and pentoses, it also tolerates antimicrobial substance [6,8,9]. Therefore, *B. cepacia* was employed for the PHA production from SCGH.

At first, *B. cepacia* was cultivated in media with various portions of SCGH for 72 h. The results are provided in Table 2. The highest biomass and also PHA yields (4.91 and 2.69 g l^{-1}) were achieved when the medium contained 30 vol.% of SCGH. Lower portion of SCGH probably did not provide sufficient amount of the substrates, on the contrary, higher amount of SCGH in the cultivation media revealed rather inhibition effect on the biomass as well as PHB yields. LA and 5HMF are not present in SCGH in the amounts which could result in strong inhibition of the cell growth because it was reported that the growth of *B. cepacia* was not affected by LA up to 5 g l^{-1} and by 5HMF up to 1.0 g l^{-1} [8], which is far above their concentration in SCGH. Oppositely, polyphenolics are in SCGH in the concentration (3.6 g l^{-1}) that can cause toxic effect, because Pan et al. [8] reported than the growth of *B. cepacia* was strongly inhibited by the presence of 2.0 g l^{-1} of polyphenol vanillin. Moreover, in their further publication Pan et al. observed that synergistic inhibitory effects occurred in the presence of multiple inhibitors when *B. cepacia* was grown on wood hydrolysate [9]. This may be an explanation for the *B. cepacia* growth inhibition in the presence of higher amount of SCGH and why simple dilution may solve the problems accompanying the presence of inhibitors in SCGH. Since all the production parameters including yield coefficient $Y_{P/S}$ were the highest when the SCGH portion in media was set at 30 vol.%, this dilution of SCGH was used as optimal in further experiments.

Furthermore, *B. cepacia* was capable of accumulation of copolymer P(HB-*co*-HV). It is likely that LA present in SCGH, which was already reported to be transformed into 3HV by *B. cepacia* [26], served as the primary precursor of 3HV. The portion of 3HV in copolymer increased with the amount of SCGH in the cultivation media, which may be attributed to rising concentration of the 3HV precursors.

3.3. Time course of PHA production by B. cepacia on SCGH

In order to get deeper insight into the process of PHA production from SCGH by *B. cepacia*, the biomass, PHB yields, individual sugar concentrations and other parameters were recorded during the cultivation, the results of the experiments are shown in Fig. 1. During the time course of cultivation, the biomass concentration was steadily growing accompanied by the increase of PHA content in the biomass. The cultivation was finished after 77 h, at this cultivation time the biomass concentration, the PHA content in the biomass and the PHA yields reached 4.90 g l^{-1}, 57.26 wt.% and 2.81 g l^{-1}, respectively.

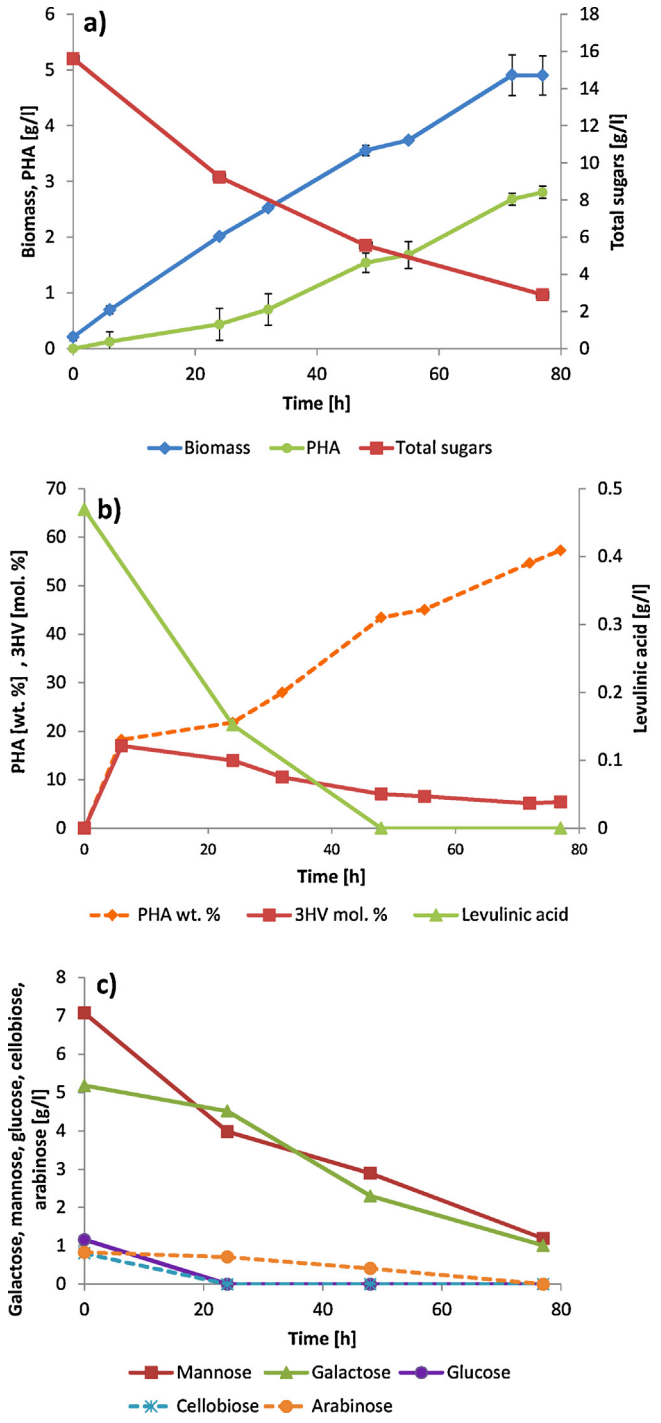


Fig. 1. Time course of biomass, PHA and particular sugars concentrations during cultivation of *B. cepacia* on SCGH.

LA was completely exhausted during initial 48 h of cultivation, which corresponded with the development of ratio of 3HB to 3HV in copolymer, because the portion of 3HV in copolymer decreased during the course of cultivation. Therefore, it is likely that at the beginning of the cultivation the copolymer with high portion of 3HV was synthetized, the amount of 3HV decreased with the reduction of levulinic acid level and, once the LA was completely utilized, the bacterial culture synthetized PHB homopolymer. This explanation is in accordance with the results of DSC study, which suggested, that at the 77th h of cultivation the polymer was a blend of PHB homopolymer and P(HB-co-HV) copolymer (see below).

Table 2
Production of PHB from SCGH employing *B. cepacia*.

SCGH portion in media (vol.%)	CDW ($g l^{-1}$)	PHA (wt.%)	PHA ($g l^{-1}$)	3HV (mol.%)	Sugars consumed ($g l^{-1}$)	$Y_{P/S}$
15	3.24 ± 0.34	25.36 ± 1.61	0.82 ± 0.10	4.5 ± 0.1	7.52	0.11
30	4.91 ± 0.10	54.79 ± 1.23	2.69 ± 0.07	5.0 ± 0.2	11.93	0.23
50	2.78 ± 0.27	34.04 ± 0.10	0.94 ± 0.08	8.7 ± 0.1	16.85	0.06
65	2.71 ± 0.11	29.74 ± 3.21	0.81 ± 0.09	9.4 ± 0.4	18.37	0.04

Results are in form average ± standard deviation.
CDW stands for cell dry weight.
3HV represents content of 3-hydroxyvalerate in P(HB-co-HV) copolymer.

The carbon catabolite repression (CCR) represents a serious problem when dealing with lignocellulosic hydrolysates as fermentation substrates. CCR is caused by preferential consumption of one of the sugars, which may in turn result in the accumulation of other sugars (usually pentoses) to potentially inhibiting concentrations when the fed-batch cultivation strategy is applied [11]. The growth of *B. cepacia* on SCGH was accompanied by the utilization of sugars present in SCGH. All the sugar of SCGH were consumed gradually during the whole course of cultivation, however, glucose and cellobiose were exhausted as the first (Fig. 1C). Since SCGH contains only low portion of pentose, in particular arabinose, and; moreover, this sugar is consumed along with mannose and galactose, CCR should not occur during the PHA production from SCGH employing *B. cepacia*.

When the cultivation was finished, polymer was extracted from the cells to study its properties thoroughly. The molecular weight (M_w) and the polydispersity index of the polymer were determined to be 2.62×10^5 and 3.33, respectively. The DSC study revealed two peaks corresponding to melting temperatures of the polymer: 170.2 and 162.3 °C (see Supplementary materials). This indicates that the polymer might be a blend of P(HB-co-HV) (lower melting temperature) and homopolymer PHB (higher melting temperature) [2]. The TGA analysis shown that polymer started to degrade and lose weight at a temperature of about 230 °C, the maximum weight-loss rate was determined as 285.3 °C.

3.4. Detoxification of SCGH

Several detoxification methods were applied to improve the fermentability of SCGH. At first, phenolic compounds can be extracted from SCG prior to their hydrolysis which should reduce their amount in SCGH. Zuoro and Lavecchia reported that coffee phenolics could be extracted by the mixture of water and ethanol [13]; therefore several concentrations of ethanol were tested. Furthermore, apart from the extraction of polyphenols prior to hydrolysis, also the methods of SCGH detoxification after the hydrolysis were tested. The overliming (OL) can be effective due to the precipitation or chemical destabilization of inhibitors and activated charcoal (AC) can improve the fermentability of SCGH by the absorbtion of phenolic compounds [8]. The influence of tested detoxification methods on total sugars and inhibitors concentrations in SCGH is shown in Table 3.

The application of post-hydrolysis detoxification methods resulted in significant removal of polyphenols where the introduction of activated charcoal seems to be more efficient than the overliming. However, both approaches also caused significant loss of fermentable sugars (from 19.3% to 34.6%), which is undesirable side effect of the detoxification procedure. On the other hand, when polyphenols were extracted from SCG prior to the hydrolysis, no significant elimination of sugars was observed. The efficiency of removal of phenolic compounds increased with rising concentration of ethanol in the extraction mixture from 18.3% to 36.9%. All the detoxification methods tested in this work reduced also the amount of LA (from 5.2% to 64.8%) and 5HMF (from 10.2% to 84.3%).

In order to further investigate the effect of detoxification methods on the PHA production from SCGH, the set of shake-flask experiments was performed using non-detoxified SCGH as a control, the results are provided in Table 4. Among the detoxification methods tested, the extraction of polyphenols from SCG by 30% ethanol prior to their hydrolysis seems to be the most efficient, because this approach improved the PHA yields more than about 25% in comparison with the control culture. Aside from the positive effect of phenolic compounds extraction on the PHA production from SCG prior its hydrolysis, this detoxification strategy offers also additional advantage, because extracted phenolic compounds can represent important side-product of the intended technology. SCG contain large amounts of chlorogenic acid and its derivatives collectively referred to as chlorogenic acids which provide many health benefits to humans [27]. For instance the pharmacokinetic studies demonstrated that about one-third of ingested chlorogenic acids are absorbed in the stomach and proximal duodenum, while the remaining are cleaved by gut microflora into caffeic and quinic acids [28]. Interestingly, the latter compounds have recently been shown to possess the neurotrophic and neuroprotective properties [29,30]. Hence, phenolics extracted from SCG prior to its hydrolysis can be used for the production of high value products such as functional foods or dietary supplements.

The product yield coefficient $Y_{P/S}$ obtained in this study for PHA production on SCGH employing *B. cepacia* reached 0.27, which is

Table 3
Effect of different SCGH detoxification methods on concentration of total sugars and microbial inhibitors.

	Total sugars		Polyphenols		Levulinic acid		5HMF	
	c ($g l^{-1}$)	E^* (%)	c ($g l^{-1}$)	E^* (%)	c ($g l^{-1}$)	E^* (%)	c ($g l^{-1}$)	E^* (%)
Control	49.4 ± 4.9		3.68 ± 0.03		1.58 ± 0.13		0.147 ± 0.060	
EtOH 0%	53.0 ± 1.3	−7.4	3.01 ± 0.04	18.3	0.56 ± 0.03	64.8	0.109 ± 0.002	25.9
EtOH 30%	52.6 ± 0.6	−6.6	2.84 ± 0.11	22.7	0.79 ± 0.05	49.9	0.114 ± 0.019	22.5
EtOH 45%	47.3 ± 8.7	4.4	2.41 ± 0.01	34.5	0.57 ± 0.02	64.0	0.090 ± 0.066	38.9
EtOH 60%	46.0 ± 0.2	6.9	2.32 ± 0.06	36.9	0.59 ± 0.07	62.8	0.132 ± 0.001	10.2
AC	39.9 ± 2.1	19.3	1.66 ± 0.02	55.0	0.63 ± 0.20	60.3	0.070 ± 0.004	52.6
OL	34.6 ± 1.1	30.0	2.96 ± 0.06	19.7	1.49 ± 0.36	5.2	0.023 ± 0.000	84.3

Results are in form average ± standard deviation.
E^* stands for elimination of particular substance in comparison with control in %.

Table 4
PHA production by *B. cepacia* on detoxified SCGH.

	CDW ($g l^{-1}$)	PHA (wt.%)	PHA ($g l^{-1}$)	3HV (mol.%)	Sugars consumed ($g l^{-1}$)	$Y_{P/S}$
Control	5.42 ± 0.48	49.08 ± 0.70	2.66 ± 0.24	8.1 ± 0.8	9.77	0.27
EtOH 0%	4.86 ± 0.23	52.37 ± 2.47	2.54 ± 0.17	5.6 ± 0.4	12.83	0.20
EtOH 30%	5.49 ± 0.40	56.01 ± 1.79	3.08 ± 0.24	4.2 ± 0.2	12.97	0.24
EtOH 45%	5.20 ± 0.32	49.99 ± 3.20	2.60 ± 0.23	6.0 ± 0.7	10.83	0.24
EtOH 60%	5.02 ± 0.32	51.33 ± 4.80	2.58 ± 0.29	5.1 ± 0.6	10.45	0.25
AC	4.78 ± 0.34	56.79 ± 0.00	2.72 ± 0.19	6.1 ± 0.5	10.45	0.26
OL	7.40 ± 0.47	23.47 ± 6.56	1.74 ± 0.50	11.6 ± 0.5	6.77	0.26

Results are in form average ± standard deviation.
CDW stands for cell dry weight.
3HV represents content of 3-hydroxyvalerate in P(HB-co-HV) copolymer.
SCGH portion in cultivation media was set to be 30 vol.%.

more than comparable to data reported for PHA production on other lignocellulose hydrolysates such as bagasse hydrolysate using *B. cepacia* (0.23) [6] or *R. eutropha* (0.08) [7]. Similar results were also obtained on oil palm empty fruit bunch by *Bacillus megaterium* (0.27) [10] and on wood hydrolysate by *B. cepacia* (0.19) [8].

Thus, this study suggested a novel promising waste substrate for the PHA production – spent coffee grounds. World-wide coffee production has been steadily growing and it is accompanied by the production of waste-products, especially SCG. Therefore SCG are available in millions of tons, because, on an average, the processing of one ton of green coffee generates about 650 kg of SCG [13]. Hence, there is high amount of potential substrate for the PHA production from SCG, especially in coffee producing countries. On the other hand, also Europe belongs among regions with strong coffee industry and high per capita consumption [31]. Furthermore, SCG are highly pollutant due to the presence of organic material that requires a great quantity of oxygen in order to degrade. Being discharged to the environment, they can cause contamination and environmental pollution problems and, furthermore, simply piled up, they can ferment and produce spontaneous combustion [15]. Therefore, the conversion of SCG into PHA by *B. cepacia* can represent theoretically economically feasible process (due to low cost of entering substrate); and, moreover, also ecologically friendly approach to the elimination of potentially problematic wastes.

Acknowledgement

This work was supported by project "Centre for Materials Research at FCH BUT" No. CZ.1.05/2.1.00/01.0012 from European Regional Development Fund (ERFD) and by the project "Excellent young researcher at BUT" No. CZ.1.07./2.3.00/30.0039. Authors kindly thank to Dr. Tomas Opravil (Brno University of Technology, Czech Republic) for collection of spent coffee grounds.

Appendix A. Supplementary data

Supplementary data associated with this article can be found, in the online version, at doi:10.1016/j.procbio.2014.05.013.

References

[1] Philip S, Keshavarz T, Roy I. Polyhydroxyalkanoates: biodegradable polymers with a range of applications. J Chem Technol Biotechnol 2007;82:233–47.
[2] Lee WH, Loo CY, Nomura CT, Sudesh K. Biosynthesis of polyhydroxyalkanoate copolymers from mixtures of plant oils and 3-hydroxyvalerate precursors. Bioresour Technol 2008;99:6844–51.
[3] Choi J, Lee SY. Factors affecting the economics of polyhydroxyalkanoate production by bacterial fermentation. Appl Microbiol Biotechnol 1999;51:12–21.
[4] Koller M, Bona R, Braunegg G, Hermann C, Horvat P, Kroutil M, et al. Production of polyhydroxyalkanoates from agricultural waste and surplus materials. Biomacromolecules 2006;6:561–5.
[5] Wyman CE, Decker SR, Himmel ME, Brady JW, Skopec CE, Viikari L. Hydrolysis of cellulose and hemicellulose. In: Dumitriu S, editor. Polysaccharides: structural diversity and functional versatility. second ed. New York: CRC Press; 2004. p. 995–1034.
[6] Silva LF, Taciro MK, Ramos MEM, Carter JM, Pradella JCG, Gomez JGC. Poly-3-hyroxybutyrate (P3HB) production by bacteria from xylose, glucose and sugarcane bagasse hydrolysate. J Ind Microbiol Biotechnol 2004;31:245–54.
[7] Yu J, Stahl H. Microbial utilization and biopolyester synthesis of bagasse hydrolysates. Bioresour Technol 2008;99:8042–8.
[8] Pan W, Perrotta JA, Stipanovic AJ, Nomura CT, Nakas JP. Production of polyhydroxyalkanoates by *Burholderia cepacia* ATCC 17759 using detoxified sugar maple hemicellulosic hydrolysate. J Ind Microbiol Biotechnol 2012;39:459–69.
[9] Pan W, Nomura CT, Nakas JP. Estimation of inhibitory effects of hemicellulosic wood hydrolysate inhibitors on PHA production by *Burkholderia cepacia* ATCC 17759 using response surface methodology. Bioresour Technol 2012;125:275–82.
[10] Zhang Y, Sun W, Wang H, Geng A. Polyhydroxybutyrate production from oil palm empty fruit bunch using *Bacillus megaterium* R11. Bioresour Technol 2013;147:307–14.
[11] Cesario MT, Raposo RS, de Almeida MCMD, van Keulen F, Ferreira BS, de Fonseca MMR. Enhanced bioproduction of poly-3-hydroxybutyrate from wheat straw lignocellulosic hydrolysates. New Biotechnol 2014;31:104–13.
[12] Murthy PS, Naidu MM. Sustainable management of coffee industry by-products and value addition – a review. Resour Conserv Recycl 2012;66:45–58.
[13] Zuorro A, Lavecchia R. Spent coffee grounds as a valuable source of phenolic compounds and bioenergy. J Clean Prod 2012;34:49–56.
[14] Machado EMS, Rodriguez-Jasso RM, Teixeira JA, Mussatto SI. Growth of fungal strains on coffee industry residues with removal of polyphenolic compounds. Biochem Eng J 2012;60:87–90.
[15] Mussatto SI, Machado EMS, Carneiro LM, Teixeira JA. Sugars metabolism and ethanol production by different yeast strains from coffee industry wastes hydrolysates. Appl Energy 2012;92:763–8.
[16] Kwon EE, Yi H, Jeon YJ. Sequential co-production of biodiesel and bioethanol with spent coffee grounds. Bioresour Technol 2013;136:475–80.
[17] Al-Hamamre Z, Foerster S, Hartmann F, Kroger M, Kaltschmitt M. Oil extracted from spent coffee ground as a renewable source for fatty acid methyl ester manufacturing. Fuel 2012;96:70–6.
[18] Asano I, Umemura M, Fujii S, Hoshino H, Iino H. Effects of mannooligosaccharides from coffee mannan on fecal microflora and defecation in healthy volunteers. Food Sci Technol Res 2004;10:93–7.
[19] Obruca S, Petrik S, Benesova P, Svoboda Z, Eremka L, Marova I. Utilization of oil extracted from spent coffee grounds for sustainable production of polyhydroxyalkanoates. Appl Microbiol Biotechnol 2014, http://dx.doi.org/10.1007/s00253-014-5653-3 (in press).
[20] Omari KW, Besaw JE, Kerton FM. Hydrolysis of chitosan to yield levulinic acid and 5-hydroxymethylfurfural in water under microwave irradiation. Green Chem 2012;14:1480–7.
[21] Marova I, Parilova K, Friedl Z, Obruca S, Duronova K. Analysis of phenolic compounds in lager beers of different origin: a contribution to potential determination of the authenticity of Czech beer. Chromatographia 2011;73:S83–95.
[22] Bertrand JL, Ramsay BA, Ramsay JA, Chavarie C. Biosynthesis of poly-p-hydroxyalkanoates from pentoses by *Pseudomonas pseudoflava*. Appl Environ Microb 1990;56:3133–8.
[23] Brandl H, Gross RA, Lenz RW, Fuller RC. *Pseudomonas oleovorans* as a source of poly(beta-hydroxyalkanoates) for potential application as a biodegradable polyester. Appl Environ Microb 1988;54:1977–82.
[24] Lopes M, Rocha R, Zanotto S, Gomez J, Silva L. Screening of bacteria to produce polyhydroxyalkanoates from xylose. World J Microbiol Biotechnol 2009;25:1751–6.
[25] Obruca S, Marova I, Svoboda Z, Mikulikova R. Use of controlled exogenous stress for improvement of poly(3-hydroxybutyrate) production in *Cupriavidus necator*. Folia Microbiol 2010;55:17–22.
[26] Keenan TM, Tanenbaum SW, Stipanovic AJ, Nakas JP. Production and characterization of poly-beta-hydroxyalkanoate copolymers from *Burkholderia cepacia* utilizing xylose and levulinic acid. Biotechnol Prog 2004;20:1697–704.
[27] Brezova V, Slebodova A, Stasko A. Coffee as a source of antioxidants: an EPR study. Food Chem 2009;114:859–68.

[28] Stalmach A, Steiling H, Williamson G, Crozier A. Bioavailability of chlorogenic acids following acute ingestion of coffee by humans with an ileostomy. Arch Biochem Biophys 2010;501:98–105.
[29] Sul DG, Kim HS, Lee DH, Joo SS, Hwang KW, Park SY. Protective effect of caffeic acid against beta-amyloid-induced neurotoxicity by the inhibition of calcium influx and tau phosphorylation. Life Sci 2009;84:257–62.
[30] Jeong CH, Jeong HR, Choi GN, Kim DO, Lee U, Heo HJ. Neuroprotective and anti-oxidant effects of caffeic acid isolated from *Erigeron annuus* leaf. Chin Med 2011;24:6–25.
[31] European Coffee Report. European Coffee Federation; 2012/2013. Available online at http://www.ecf-coffee.org/publications

Bioresource Technology 326 (2021) 124683

Contents lists available at ScienceDirect

Bioresource Technology

journal homepage: www.elsevier.com/locate/biortech

Short Communication

Isolation of poly(3-hydroxybutyrate) from bacterial biomass using soap made of waste cooking oil

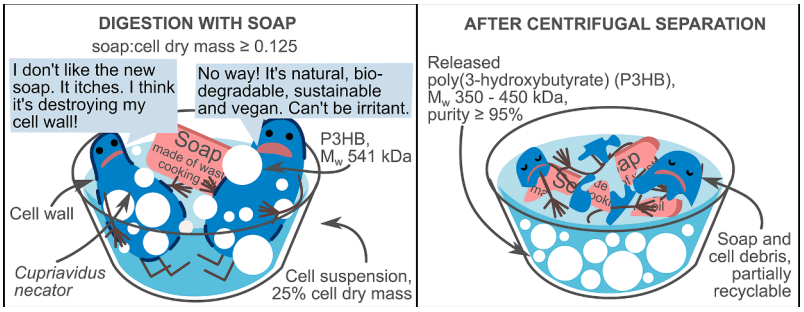
Aneta Pospisilova *, Ivana Novackova, Radek Prikryl

Faculty of Chemistry, Brno University of Technology, Purkynova 118, Brno, Czech Republic

HIGHLIGHTS

- Fatty acid salts (soap) made from waste cooking oil serve as an alternative surfactant for the isolation of PHB from bacterial biomass.
- This surfactant can be easily precipitated from the wastewater by acidification, which facilitates wastewater treatment.
- The precipitate is utilized in the process as a substrate for biomass production.
- High purity and recovery of the product was achieved without a significant decrease in molecular weight.

GRAPHICAL ABSTRACT



ARTICLE INFO

Keywords:
PHA
P3HB
Recovery
Downstream process
Isolation

ABSTRACT

The aim of this work was to develop a soap-based method for the isolation of poly(3-hydroxybutyrate) from bacterial biomass. The method consisted of adding soap derived from waste cooking oil to a concentrated (25%) biomass suspension, heating and centrifugal separation. Purity above 95% could be achieved with soap:cell dry mass ratios at least 0.125 g/g, making the method comparable to other surfactant-based protocols. Molecular weights M_w of products from all experiments were between 350 and 450 kDa, being high enough for future material applications. Addition of hydrochloric acid to the wastewater led to the precipitation of soap and part of non-P3HB cell mass. The resulting precipitate was utilized as a carbon source in biomass production and increased substrate-to-P3HB conversion.

1. Introduction

Poly(3-hydroxybutyrate) (P3HB) is the best known natural polyhydroxyalkanoate (PHA). It is produced by many organisms (Koller et al., 2017), out of which the bacterium *Cupriavidus necator* is the most significant in industrial practice. It can be grown on primary feedstock (cane sugar, vegetable oil…) or, preferably, secondary feedstock (molasses, whey…) (Choi and Lee, 1997; Koller et al., 2017). P3HB is considered a possible alternative to commonly used plastics, especially for material applications where the biodegradability is required (Sirohi et al., 2020). For a viable industrial production of P3HB, the cost-effective and environmentally friendly isolation method is a key step. Furthermore, the isolation method should lead to high purity of the material and minimal decrease of molecular weight (Koller, 2020).

Currently, two main strategies are used for the P3HB isolation – extraction and digestion. Extraction of P3HB usually employs

* Corresponding author.
E-mail addresses: pospisilova-a@seznam.cz (A. Pospisilova), xcnovackova@fch.vutbr.cz (I. Novackova), prikryl@fch.vutbr.cz (R. Prikryl).

https://doi.org/10.1016/j.biortech.2021.124683
Received 12 November 2020; Received in revised form 2 January 2021; Accepted 4 January 2021
Available online 16 January 2021
0960-8524/© 2021 Elsevier Ltd. All rights reserved.

halogenated solvents, mainly chloroform and dichloromethane. Resulting polymer is reportedly very pure and has high molecular weight, but the environmental and occupational hazards associated with these solvents are high (Koller, 2020; López-Abelairas et al., 2015). Several non-halogenated solvents can also be used (Jacquel et al., 2008). Their main disadvantages are high cost and complicated recycling.

The digestion methods may employ different agents (or their mixtures) able to disrupt the cell membranes and to dissolve or solubilize non-P3HB cell mass (NPCM). Main advantages of the digestion methods are relative simplicity and less hazardous operation. Quality of the product and economy of operation depends on the reagent used – methods with acids, bases, and oxidants are reportedly economical and have low carbon footprint, but considerably decrease the molecular weight of the polymer (López-Abelairas et al., 2015; Jiang et al., 2015; Kim et al., 2003). In contrast, highly selective methods with surfactants, enzymes, or other organisms cause negligible degradation of the polymer, but are still rather uneconomical (Jacquel et al., 2008; Gonzalez et al., 2020). In all digestion methods, liquid waste containing NPCM is formed, leading to difficult wastewater treatment (Jacquel et al., 2008). Methods for upcycling this waste stream are under development (Yadav et al., 2020).

In this study, the feasibility of P3HB recovery from *C. necator* by non-traditional surfactant was explored. The surfactant, fatty acid sodium salts ("soap") was prepared from waste cooking oil which is a cheap and sustainable starting material. Dependence of P3HB purity on soap:cell dry mass (CDM) ratio was determined and the effectiveness of additional digestion agent protease was tested. Molecular weight was monitored to ensure that the product would be suitable for material applications in the future. Another goal was to efficiently utilize wastewater resulting from digestion. The advantage of soap over conventional surfactants is that it precipitates by acidification to form free fatty acids (Samorì et al., 2015; Kaoru, 2019), which were reported to be a suitable substrates for *C. necator* (Sharma et al., 2016). Experiments with acidification of wastewater and the use of a precipitate were performed.

2. Materials and methods

2.1. Soap preparation

Waste cooking oil was obtained from Nafigate Corporation (Czech Republic). According to the supplier, it was a mixture of used oils, collected for the sake of recycling, having saponification value 186 mg KOH/g, acid value 5 mg KOH/g and containing mainly oleic, linoleic, palmitic and stearic acid triacylglyceroles, diacylglyceroles, free fatty acids and oxidised forms of the above. Iodine value and peroxide value were analyzed iodometrically according to AOAC methods (AOAC, 2021a; AOAC, 2021b).

NaOH (26.5 g, 0.663 mol) was dissolved in water (76 g) and mixed with 200 g of waste cooking oil (0.663 mol of saponifiable groups; calculated from saponification value). The mixture was vigorously stirred at 80 °C. The conversion of NaOH was monitored acidimetrically (1 M HCl, phenolphthalein) in 0.5 h intervals and the reaction was considered completed when the conversion was $>$ 98%. Then the mixture was left to cool at room temperature.

2.2. Digestion of biomass using soap

Biomass was produced by Nafigate Corporation via the fermentation of waste cooking oil by *C. necator* H16. Specific procedure for biomass production is described in patent application (Marova et al., 2014). The biomass was shipped and stored frozen at −20 °C. It contained 50% CDM, out of which 75% was P3HB. The P3HB in biomass had M_w = 541 000 g/mol.

Two series of experiments with different doses of soap were carried out. The first series used a protease (Sigma–Aldrich; from *Bacillus licheniformis* ⩾2.4 U/g) as an additional digestion agent, the second did not. The ratio (w/w) of soap to CDM ranged from 0 to 1.

For each experiment, the biomass was diluted with water to contain 25% CDM. The mixture was heated to 95 °C for 0.5 h and cooled to 80 °C. Soap was dissolved in the mixture and pH was measured. If pH was <9, it was increased to 9–9.5 by the addition of 20% NaOH. The mixture was stirred for 1 h at 80 °C and then cooled to 55 °C. For experiments involving protease, the enzyme (0.01 ml/g CDM) was added in this stage. Then the mixture was stirred at 55 °C for 1 h and pH was measured. If pH was <9, it was increased to 9–9.5 with 20% NaOH solution. The mixture was heated to 95 °C and centrifuged (10 000 g/10 min/60 °C). The supernatant was separated, same volume of boiling water was added to the pellet, and resulting mixture was centrifuged (10 000 g/10 min/60 °C). Washing with hot water was repeated twice more. The supernatants were stored for further workup (see Section 2.3). The pellet was dried at 105 °C to constant weight.

2.3. Precipitation of supernatant

Supernatants from PHB digestion were acidified to pH 3 using 2.5 M HCl. The mixture was centrifuged and the precipitate (stable, semisolid oily emulsion) was separated from the transparent yellow liquid. Dry weight of the precipitate was measured thermogravimetrically. The precipitate was stored at 4 °C prior to use (see Section 2.4).

2.4. Use of the precipitate for biomass production

Cultivations of inoculum of bacterial strain *C. necator* H16 (CCM 3726) were performed in 100 ml Erlenmeyer flasks with 50 ml of the Nutrient Broth medium (peptone 10.0 g/l, beef extract 10.0 g/l, NaCl 5.0 g/l) during 24 h at 30 °C with constant shaking at 180 rpm, when culture was inoculated from cryoculture.

Subsequent cultivations focused on comparison of growth potential and PHB producing capability using different substrates were performed in mineral salts medium consisting of 1 g/l $(NH4)_2SO_4$, 1.02 g/l KH_2PO_4, 11.1 g/l $Na_2HPO_4 \cdot 12\ H_2O$, 0.2 g/l $MgSO_4 \cdot 7\ H_2O$ and 1 mL/l mineral elements solution MES (9.7 g/l $FeCl_3$, 7.8 g/l $CaCl_2 \cdot 2H_2O$, 0.156 g/l $CuSO_4 \cdot 5\ H_2O$, 0.119 g/l $CoCl_2 \cdot 6H_2O$, 0.118 g/l $NiCl_2$ in 0.1 M HCl). As carbon sources, waste cooking oil, precipitate, and their mixture were used. Final concentrations of substrates in the cultivation media were 20 g/l for the sole ones and 10 + 10 g/l for mixture. All cultivations were performed in two parallel 250 ml Erlenmeyer flasks with 100 ml media (inoculation ratio 10 %) under permanent shaking at 180 rpm at 30 °C for 72 h, when the cultivations were stopped, cells were harvested and analysed. All substrates (sole ones or the mixture) were prepared twice to obtain statistically more valuable results. To determine the content of biomass gravimetrically, 10 ml of cultures in duplicates from each flask were centrifuged (6 000 rpm; 5 min), washed with distilled water and centrifuged once more. Then the pellets were dried to constant weight and the concentration of biomass was expressed in g/l as CDM. The data for every type of substrate were obtained from two parallel cultivations as mentioned previously, when two values for each Erlenmeyer flask were determined, i.e. averages were taken from four individual values.

2.5. Analysis

Purity of P3HB was analysed as methyl esters of 3-hydroxybutyric acid by gas chromatography as reported previously (Obruca et al., 2014). Molecular weight was measured by GPC using 185 Agilent HPLC series 1100 chromatograph with PLgel mixed-c 5 μm, 7.5x300 mm column, with chloroform as the mobile phase. 12 polystyrene standards (0.2–2000 kDa) were used for calibration.

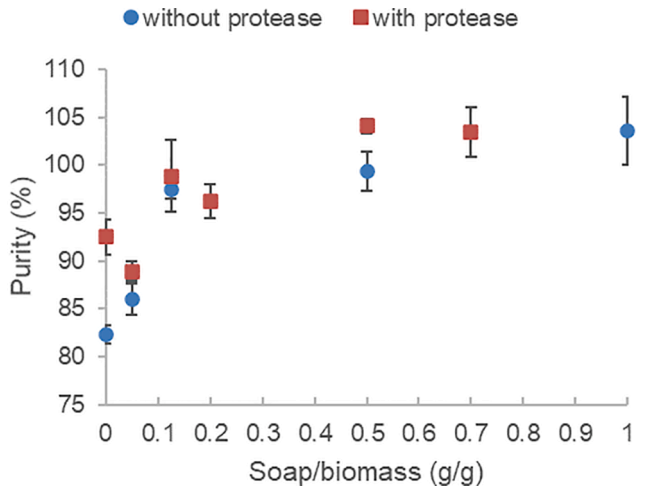


Fig. 1. Purity of P3HB from soap-based method. Error bars represent 95% confidence intervals.

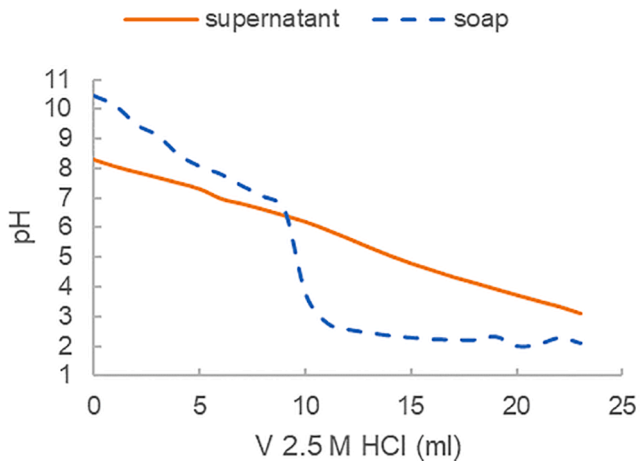


Fig. 2. Titration curves: 1. supernatant (0.2 g/g CDM of soap used for digestion; supernatant contains 10 g of soap in 550 ml), 2. soap (10 g in 550 ml of water).

3. Results and discussion

3.1. Soap preparation

The main feedstock for the preparation of soap was waste cooking oil. High degree of deterioration was evident mainly sensorially (dark color, odor) and by a higher acid value (5 mg KOH/g). The oil was rich in unsaturated fatty acids (iodine value 96 g/100 g), and partially oxidized, as indicated by the peroxide value 20 meq/kg.

The soap was prepared by ordinary saponification of the oil with one equivalent of NaOH at 80 °C. Time needed for the reaction was 2.5 h, after which the soap was obtained as a pale yellow waxy solid. Neither the purification of the oil nor the purification of generated soap was necessary. Despite being contaminated with frying and saponification byproducts, the soap performed comparably to pure commercially available surfactant (see Section 3.2).

3.2. Digestion of biomass using soap

To quantify the influence of soap concentration and protease addition on the purity of P3HB, experiments with different doses of soap were performed. The experiments were carried out at higher temperatures than usual for surfactant-based methods. At low temperatures, the mixtures tended to be very viscous, which disabled efficient stirring and centrifugal separation. pH was maintained alkaline because soap is fully efficient only at higher pH. However, the susceptibility of P3HB to alkaline hydrolysis had to be considered (Burniol-Figols et al., 2020). pH between 9 and 9.5 led to optimal performance and minimal molecular weight loss.

As expected, the purity of P3HB increased with increasing amount of soap and with protease as can be seen in Fig. 1. Plotted values follow a similar trend as in SDS-based method, published previously by Kim et al. (2003) who achieved > 95% purity if the SDS:CDM ratio was at least 0.3. Soap was seemingly more effective, leading to > 95% with soap:CDM at least 0.125. The result was surprising because soap is generally considered inferior in terms of solubilization and denaturation power (Holmberg, 2019). Probable explanation is that alkaline pH and high temperature in the soap-based method enhanced the digestion.

In addition to purity, other important parameters were monitored – molecular weight, recovery, and color of the product. Molecular weight M_w of all products was between 350 000–450 000 Da (65–83% of the original value in biomass) and the recovery was 80–100 %. No relationship between the dose of soap or protease addition was found. The small differences in M_w could be explained by little differences in pH and by the experimental error of the GPC method. Differences in recovery were probably caused by the experimental error – with a viscous supernatant and a rather soft pellet, decantation occasionally led to product loss. Dose of soap and especially the presence of the enzyme affected color – with increasing amount of soap and with the protease, the product became significantly paler.

Based on the experiments, soap:CDM ratio between 0.125 and 0.5, preferably 0.2, combined with the protease was evaluated as the most promising experimental setup. The product obtained at these conditions had high enough purity and beige color, making it together with high molecular weight suitable for material applications.

3.3. Precipitation of supernatant

Supernatants were acidified to convert soap to free fatty acids. Principally similar reaction was previously described by Samorì et al. (2015) whose digestion method was based on high doses of a "switchable anionic surfactant" ammonium laurate (surfactant:CDM up to 2). In Samori's method, acidification of the supernatant produced lauric acid in 98% yield that could be used for the preparation of the surfactant again. Supernatants from soap-based digestion reacted differently. The titration curve had a practically flat shape (Fig. 2), indicating the acid-base reaction of more compounds with different pK_A values. Dry weights of the precipitates were significantly higher than the theoretical yields of fatty acids, indicating that a considerable portion of NPCM precipitated together with the fatty acids. Relative content of NPCM in precipitate was dependent on soap:CDM ratio – the more soap used for digestion, the lower content of NPCM in the precipitate. This may explain the sufficient purity of Samori's fatty acid – with higher amount of the surfactant, the amount of NPCM in the precipitate could be negligible. Precipitates from soap-based digestion with lower doses of

Table 1
Results of laboratory-scale cultivation. WCO stands for waste cooking oil, CDM stands for cell dry mass, S.D. stands for standard deviation.

Substrate	Substrate dry weight (g/l)	CDM ± S.D. (g/l)	P3HB ± S.D. (%)	P3HB ± S.D. (g/l)	**Substrate conversion (%)**
20 g/l WCO (control)	20	10.6 ± 0.3	80.9 ± 2.7	8.6 ± 0.2	**43**
10 g/l WCO + 10 g/l precipitate	14.5	12.5 ± 0.2	70.6 ± 2.3	8.8 ± 0.2	**61**
20 g/l precipitate	9	7.5 ± 0.2	42.8 ± 1.6	3.2 ± 0.1	**36**

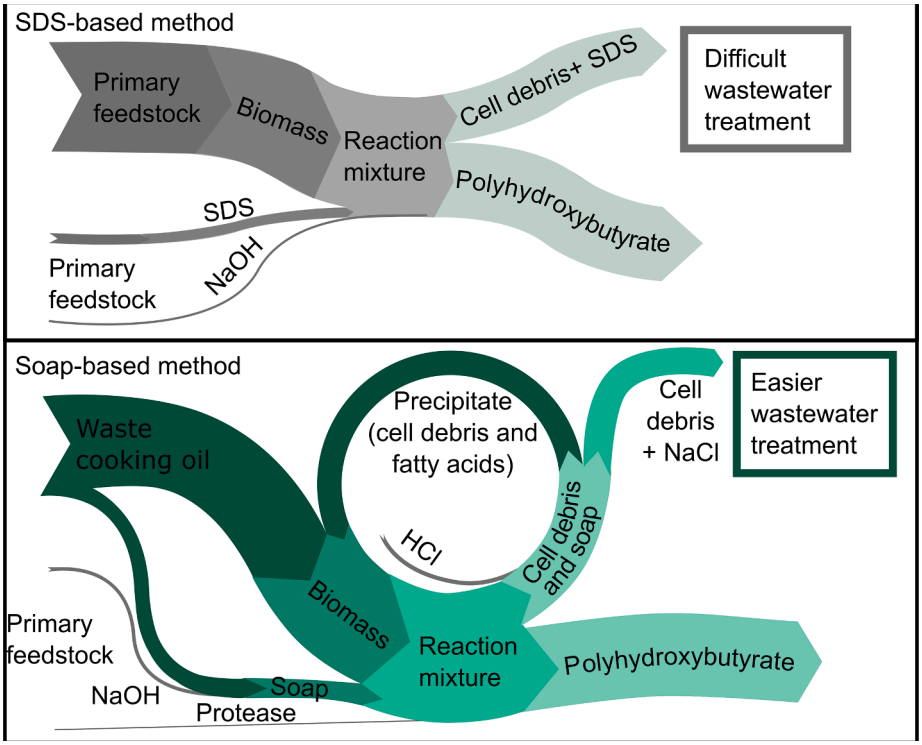


Fig. 3. Comparison of SDS-based biomass digestion described previously (Chen, 2009) and soap-based biomass digestion (this work). Line widths are proportional to weights.

soap (soap:CDM 0.125–0.5) contained 48–26% of NPCM as impurity. Due to the complex and diverse character of NPCM, attempts to remove it were not performed. Instead, the precipitate was used as a substrate for fermentation (Section 3.4).

3.4. Use of precipitate for biomass production

Laboratory-scale fermentation tests showed that the precipitate or its mixture with a standard substrate (waste cooking oil) could be readily used as a substrate for bacteria to produce bacterial biomass. For reference, the standard substrate was fermented in the same manner. Results are in Table 1.

As the table shows, there was a synergy between precipitate and waste cooking oil – more substrate was converted to P3HB if a mixture of the above was used as a carbon source. The reason could be the emulsifying properties of the precipitate which made the oil more bioavailable. Pure precipitate did not perform so well as the mixture or oil alone. High amount of hydrolyzed protein in the precipitate could be the reason. *C. necator* accumulates P3HB faster in N-deficient environment (Ahn et al., 2015) and thus nitrogen-rich precipitate may slow down the process.

Based on these results, the process shown in Fig. 3 was designed, the material flows were calculated (counting with soap:CDM ratio 0.2) and compared with the SDS-based method published previously (Chen, 2009).

4. Conclusions

Soap-based isolation method produced a high-molecular-weight P3HB, potentially suitable for material applications. Soap:CDM ratio at least 0.125 was needed to reach > 95% purity of the product and the relationship between the soap dose and purity showed a similar trend as in the method with the standard surfactant (SDS). Effect of protease on analytical purity was less pronounced but positively affected the product's color. After digestion, the soap was precipitated from the wastewater and the precipitate was advantageously utilized in biomass production. Future research will focus on upscale, optimization of the separation step and material research of the P3HB thus obtained.

CRediT authorship contribution statement

Aneta Pospisilova: Conceptualization, Methodology, Investigation, Writing - original draft, Validation. **Ivana Novackova:** Methodology, Investigation, Writing - original draft. **Redek Prikryl:** Supervision, Project administration.

Declaration of Competing Interest

The authors declare that they have no known competing financial interests or personal relationships that could have appeared to influence the work reported in this paper.

Acknowledgement

Authors acknowledge the support of Brno University of Technology through the project FCH-S-20–6340. Ivana Novackova is Brno Ph.D. Talent Scholarship Holder – Funded by the Brno City Municipality.

References

Ahn, J., Jho, E.H., Nam, K., 2015. Effect of C/N ratio on polyhydroxyalkanoates (PHA) accumulation by Cupriavidus necator and its implication on the use of rice straw hydrolysates. Environ. Eng. Res. 20, 246–253. https://doi.org/10.4491/eer.2015.055.

AOAC, a. Iodine Value of Fats and Oils, Wijs method 993.20.

AOAC, b. Peroxide Value of Oils and Fats 965.33.

Burniol-Figols, A., Skiadas, I.V., Daugaard, A.E., Gavala, H.N., 2020. Polyhydroxyalkanoate (PHA) purification through dilute aqueous ammonia digestion at elevated temperatures. J. Chem. Technol. Biotechnol. 95, 1519–1532. https://doi.org/10.1002/jctb.6345.

Chen, X., 2009. Method for separating, extracting and purifying poly-β) hydroxyalkanoates (PHAs) directly from bacterial fermentation broth. US Patent 7,582,456.

Choi, J.i., Lee, S.Y., 1997. Process analysis and economic evaluation for poly(3-hydroxybutyrate) production by fermentation. Bioprocess Eng. 17, 335–342.https://doi.org/10.1007/s004490050394.

Gonzalez, K., Navia, R., Liu, S., Cea, M., 2020. Biological approaches in polyhydroxyalkanoates recovery. Curr. Microbiol. 1–10.

Holmberg, K., 2019. Ullmann's Encyclopedia of Industrial Chemistry. Wiley-VCH, Weinheim. chapter Surfactants. pp. 1–56.https://doi.org/10.1002/14356007.a25_747.pub2.

Jacquel, N., Lo, C.W., Wei, Y.H., Wu, H.S., Wang, S.S., 2008. Isolation and purification of bacterial poly(3-hydroxyalkanoates). Biochem. Eng. J. 39, 15–27. https://doi.org/10.1016/j.bej.2007.11.029.

Jiang, Y., Mikova, G., Kleerebezem, R., van der Wielen, L.A., Cuellar, M.C., 2015. Feasibility study of an alkaline-based chemical treatment for the purification of polyhydroxybutyrate produced by a mixed enriched culture. Amb Express 5, 5. https://doi.org/10.1186/s13568-015-0096-5.

Kaoru, N., 2019. Production process for polyhydroxyalkanoate. JP2019041606A.

Kim, M., Cho, K.S., Ryu, H.W., Lee, E.G., Chang, Y.K., 2003. Recovery of poly(3-hydroxybutyrate) from high cell density culture of Ralstonia eutropha by direct addition of sodium dodecyl sulfate. Biotechnol. Lett. 25, 55–59. https://doi.org/10.1023/a:1021734216612.

Koller, M., 2020. Established and advanced approaches for recovery of microbial polyhydroxyalkanoate (PHA) biopolyesters from surrounding microbial biomass. EuroBiotech J. 4, 113–126. https://doi.org/10.2478/ebtj-2020-0013.

Koller, M., Maršálek, L., de Sousa Dias, M.M., Braunegg, G., 2017. Producing microbial polyhydroxyalkanoate (PHA) biopolyesters in a sustainable manner. New Biotechnol. 37, 24–38. https://doi.org/10.1016/j.nbt.2016.05.001.

López-Abelairas, M., García-Torreiro, M., Lú-Chau, T., Lema, J., Steinbüchel, A., 2015. Comparison of several methods for the separation of poly(3-hydroxybutyrate) from Cupriavidus necator H16 cultures. Biochem. Eng. J. 93, 250–259. https://doi.org/10.1016/j.bej.2014.10.018.

Marova, I., Obruca, S., Prikryl, R., 2014. Method of producing polyhydroxyalkanoates (PHA) from oil substrate. WO2014032633A1.

Obruca, S., Benesova, P., Oborna, J., Marova, I., 2014. Application of protease-hydrolyzed whey as a complex nitrogen source to increase poly(3-hydroxybutyrate) production from oils by Cupriavidus necator. Biotechnol. Lett. 36, 775–781.

Samorì, C., Basaglia, M., Casella, S., Favaro, L., Galletti, P., Giorgini, L., Marchi, D., Mazzocchetti, L., Torri, C., Tagliavini, E., 2015. Dimethyl carbonate and switchable anionic surfactants: two effective tools for the extraction of polyhydroxyalkanoates from microbial biomass. Green Chem. 17, 1047–1056. https://doi.org/10.1039/C4GC01821D.

Sharma, P.K., Fu, J., Spicer, V., Krokhin, O.V., Cicek, N., Sparling, R., Levin, D.B., 2016. Global changes in the proteome of Cupriavidus necator H16 during poly-(3-hydroxybutyrate) synthesis from various biodiesel by-product substrates. AMB Express 6, 36. https://doi.org/10.1186/s13568-016-0206-z.

Sirohi, R., Prakash Pandey, J., Kumar Gaur, V., Gnansounou, E., Sindhu, R., 2020. Critical overview of biomass feedstocks as sustainable substrates for the production of polyhydroxybutyrate (PHB). Bioresour. Technol. 311, 123536 https://doi.org/10.1016/j.biortech.2020.123536.

Yadav, B., Pandey, A., Kumar, L.R., Tyagi, R., 2020. Bioconversion of waste (water)/residues to bioplastics – a circular bioeconomy approach. Bioresour. Technol. 298, 122584 https://doi.org/10.1016/j.biortech.2019.122584.

Polymer Degradation and Stability 193 (2021) 109727

Contents lists available at ScienceDirect

Polymer Degradation and Stability

journal homepage: www.elsevier.com/locate/polymdegradstab

Techniques for increasing the thermal stability of poly[(R)-3-hydroxybutyrate] recovered by digestion methods

Aneta Pospisilova*, Veronika Melcova, Silvestr Figalla, Premysl Mencik, Radek Prikryl

Faculty of Chemistry, Brno University of Technology, Purkynova 118 Brno, Czech Republic

ARTICLE INFO

Article history:
Received 26 August 2021
Revised 20 September 2021
Accepted 21 September 2021
Available online 22 September 2021

Keywords:
Polyhydroxyalkanoate
Polyhydroxybutyrate
Poly[(R)-3-hydroxybutyrate]
PHB
P3HB
Recovery
Isolation
Degradation
Stability

ABSTRACT

This work deals with the thermal stability of poly[(R)-3-hydroxybutyrate] (PHB) obtained by different isolation methods. PHB was recovered from bacteria by digestion with three different reagents (acid, base, surfactant) and by chloroform extraction as a reference. Thermal stability of the samples was investigated by differential scanning calorimetry, isothermal degradation with hot press, and gel permeation chromatography and was compared with the stability of commercially available PHB. PHBs recovered by digestion with alkaline reagents were found to be thermally unstable, compared to the extracted polymer and the commercially available one. Two different techniques for stabilization of PHB obtained by digestion methods were tested wash with acid solution or addition of carboxylic acid or anhydride before heating. Both methods proved to significantly increase the thermal stability.

© 2021 Elsevier Ltd. All rights reserved.

1. Introduction

poly[(R)-3-hydroxybutyrate] (PHB) is a natural polyester synthesized mainly by bacteria as an energy storage compound. As a biosourced and biodegradable polymer, it is considered a possible substitute for certain petrol-based plastics. It is usually recovered from microbial biomass by solvent extraction or digestion. During extraction, the biomass is mixed with an organic solvent which dissolves PHB. In digestion, the biomass is mixed with a solution of a reagent that dissolves or solubilizes cell debris, while leaving solid PHB particles undissolved [1,2].

One of the factors that limit the wider use of PHB in the plastic industry is its high price. The high price is partly due to high recovery costs PHB is usually recovered from bacteria by extraction with large volumes of expensive and hazardous halogenated solvents. However, it was reported that the cost and environmental burden could be reduced by using digestion methods instead of solvent extraction. Especially digestion with alkalis and acids seems beneficial in terms of price and carbon footprint. On the other hand, these methods lead to a polymer with lower molecular weight [3,4]. Digestion with surfactants or combination of surfactant with alkali is another simple and economical approach and usually leads to PHB with higher molecular weight [5–7].

Another obstacle is the poor melt processability of PHB, that is caused mainly by its low thermal stability. Above its melting temperature (around 170 °C) the molecular weight of the polymer significantly decreases within minutes, which makes melt processing very challenging [8]. Molecular weight affects many processing and mechanical parameters, such as melting point, melt viscosity, or tensile strength. With lower molecular weight, the mechanical properties deteriorate significantly [9]. Therefore, high molecular weight and good thermal stability are the key factors for production of useful PHB-based plastic products.

Unfortunately, PHBs obtained by cost-effective digestion methods are usually much less stable than PHBs from solvent extraction. The lower stability is reportedly caused by trace impurities such as cell debris and residues of digestion agents [3,6,10–12]. Influence of the impurities on thermal stability of PHB is not yet fully understood. It has been established [8] and is generally accepted that very pure PHB (obtained by repeated precipitation from halogenated solvent) thermally decomposes mainly via a random chain scission mechanism (Fig. 1) It is less clear, however, what happens if other compounds (impurities or additives) are heated together with the polymer. Some authors assume that random chain scission is still the main mechanism of polymer decomposition and

* Corresponding author.
E-mail addresses: pospisilova-a@seznam.cz (A. Pospisilova), xcmelcova@fch.vut.cz (V. Melcova), xcfigallas@vut.cz (S. Figalla), mencik@fch.vut.cz (P. Mencik), prikryl@fch.vutbr.cz (R. Prikryl).

https://doi.org/10.1016/j.polymdegradstab.2021.109727
0141-3910/© 2021 Elsevier Ltd. All rights reserved.

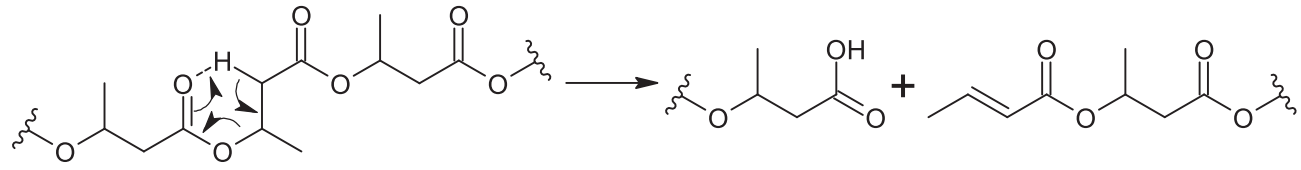


Fig. 1. Random chain scission.

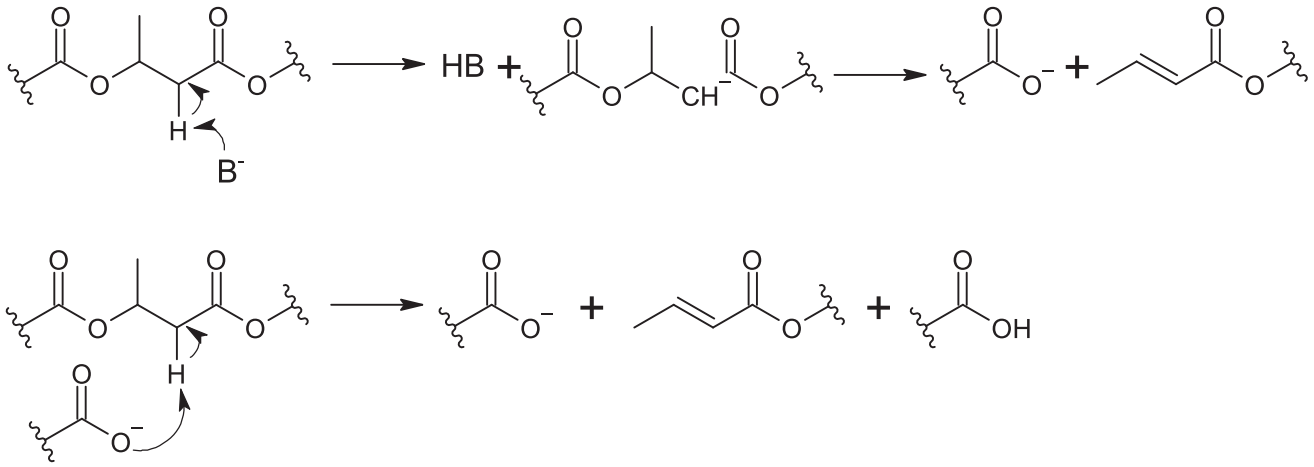


Fig. 2. E1cB mechanism of PHB degradation. First, the base reacts with PHB, leading to cleavage of the polymer chain. Negatively charged carboxylate is formed on one chain end and can cleave another polymer molecule, which propagates the reaction.

that various compounds accelerate (or decelerate) this reaction. For example, metal cations, which are hard Lewis acids, are thought to facilitate the scission by bonding to a carboxyl group, which thereby facilitates the formation of a double bond [13,14]. However, only some hard Lewis acids (Ca^{2+}, Mg^{2+}) truly enhance the reaction, while others (Al^{3+}) do not [13]. Some authors argue that cis-elimination is a concerted, non-catalyzed, synchronous intramolecular reaction, and therefore should not be affected by matrix influences [11,15].

For thermal degradation of PHB in the presence of bases, such as carboxylate chain end, carboxylic acid salts, or inorganic carbonates, E1cB mechanism was proposed [16,17] (Fig. 2). This mechanism may explain the low thermal stability of PHBs obtained by digestion at alkaline conditions, described by several authors [3,6,10], and the negative effect of alkaline additives on thermal stability, a phenomenon described by many others [13,17–21].

Clearly, one of the ways to cheaper and more sustainable production of PHB for plastic industry is to improve the digestion methods to give a more thermally stable polymer. Assuming the main reason for low thermal stability are basic residues, such as reagent molecules, carboxylate chain ends, or impurities, it can be expected that simple neutralization should improve the thermal stability. It has been previously reported that acid wash increased the thermal stability of synthetic [14,17] and commercially available (i.e., obtained by a method unknown to the public) PHB [14,22,23] but its effectiveness on PHB obtained by digestion methods has not yet been reported. In this work, the acid wash was tested on PHB obtained by three digestion reagents - acid, alkali, and surfactant. Effect of acidic additives, such as nonvolatile organic acids and anhydrides was also investigated. These additives have previously been used in blends containing PHB and thermoplastic starch. It is believed that their protective effect was due to the reaction with OH groups in the thermoplastic starch [24]. It can be assumed that under melt processing conditions they will also react with basic functional groups to form neutral or less basic by-products and thus stabilize the PHB.

2. Experimental procedures

2.1. Materials

Commercial PHB sample was provided by Biomer (Germany). Chloroform, EtOH, and MeOH were obtained from Lach-ner LLC (Czech Republic). H_2SO_4 and NaOH were supplied by Penta Chemicals Unlimited (Czech Republic). Protease from *Bacillus licheniformis* (2.4 U/g), citric acid, succinic acid, stearic acid, maleic anhydride, and succinic anhydride were obtained from Sigma-Aldrich (Germany). NaClO solution (4.7%, technical) was provided by Bochemie a.s. (Czech Republic). The PHB standard for GC was obtained from Nafigate Corporation (Czech Republic) and was repeatedly purified by dissolution in chloroform and precipitation with n-propanol prior to use. Tributyl citrate was provided by Vertellus Holdings LLC (USA). Waste cooking oil (saponification value 186 mg KOH/g, acid value 5 mg KOH/g, iodine value 96 g/100 g, peroxide value 20 meq/kg) and *Cupriavidus necator* H16 biomass (cell dry weight=49%, PHB in cell dry weight=73%) were obtained from Nafigate Corporation Ltd. Soap was prepared from the waste cooking oil according to a previously described procedure [7].

2.2. Methods

2.2.1. Alkaline digestion

The previously published procedure [4] was adapted. Briefly, 12 g of dried biomass was mixed with NaOH solution, prepared from 9.36 g NaOH in 459 ml of water. The mixture was stirred at 37 °C for 4 h and centrifuged. White pellet was washed twice with water and then with ethanol. Finally, the product was dried at 60 °C for 5 h.

2.2.2. Soap-based digestion

The previously published procedure [7] was adapted. Briefly, 40 g of frozen biomass was diluted with water (40g) and heated to 95 °C for 0.5 h. Then it was cooled to 80 °C and mixed with soap (4 g). pH was increased from 8.7 to 9.3 with 0.25 ml of 20% NaOH. Then the mixture was stirred at 80 °C for 1 h and cooled to 55 °C. Protease (0.2 g) was added, and the mixture was stirred at 55 °C for 1 h. pH was maintained above 9 by adding 20% NaOH (0.9 ml in total). The mixture was heated to 95 °C and centrifuged (10 min, 10 000 g, 60 °C). The pellet containing PHB was diluted to 80 ml with hot water and centrifuged again. The washing with hot water was repeated twice more. Finally, the product was dried at 105 °C to a constant weight, which took 2 h.

2.2.3. Acid digestion

The previously published procedure [4] was adapted. Briefly, 24 g of frozen biomass was diluted with water (240 ml) and mixed with 96% H_2SO_4 (8.75 g). The mixture was stirred at 80 °C for 6 h and then alkalized to pH = 10 with 20% NaOH (32 ml). After centrifugation (5 000 g, 15 min), the white pellet was diluted with water (240 ml) and centrifuged again. Then the pellet was bleached with 3% NaClO (200 g) for 1 h at 25 °C. The mixture was centrifuged and washed with 2 × 240 ml of water. Finally, the product was dried at 105 °C to a constant weight, which took 2 h.

2.2.4. Chloroform extraction

5 g of dried biomass was extracted with 95 g of boiling chloroform and filtered. The polymer solution was precipitated by slow addition to 400 ml of cold methanol. Then the product was dried at 70 °C for 0.5 h.

2.2.5. Acid wash

Preparation of acid-washed samples followed the digestion methods described above (Sections 2.2.1, 2.2.2, 2.2.3), but the last wash with water was modified - the aqueous suspension was acidified to pH = 3 - 3.5 with 3% H_2SO_4 before centrifugation.

2.2.6. Incorporation of additives

1 g of dry PHB was homogenized with mortar and pestle with a given additive (1 - 10% wt.), until a fine homogeneous powder was formed.

2.2.7. Thermal degradation under isothermal conditions

Each sample (ca 1 g) was heated 5 min at 190 °C in a laboratory hot press Qnubu Rosin Press. The degree of thermal degradation was then evaluated by GPC.

2.2.8. Analysis

For GPC, samples (5 mg) were dissolved in chloroform (1 ml) at 70 °C and filtered through 0.45 μm PTFE syringe filters. GPC was performed on a 185 Agilent HPLC series 1100 chromatograph with PLgel mixed-c 5 μm, 7.5 × 300 mm column, with chloroform as the mobile phase. 12 polystyrene standards (0.2 - 2000 kDa, Agilent Technologies Inc., USA) were used for calibration. Purity of PHB was analyzed as a methyl ester of 3-hydroxybutyric acid by gas chromatography as reported previously [25]. FTIR measurements were conducted on Bruker Tensor 27 machine in ATR mode on diamond in spectral area 4000 - 600 cm^{-1}, with resolution 4 cm^{-1} and number of frames 32. For DSC, around 10 mg of sample was hermetically sealed into aluminum pans. Four heating cycles were measured using DSC 2500 from TA Instruments. In each cycle, samples were heated to 190 °C (10 °C/min) annealed for 5 min at 190 °C and cooled to 0 °C (10 °C/min).

3. Results and discussion

3.1. PHB samples and their properties

Samples were prepared by three different digestion methods and one extraction method - H_2SO_4 treatment followed by NaClO bleaching (acid digestion), NaOH digestion (alkaline digestion) and digestion with fatty acid sodium salt and proteolytic enzyme (soap-based digestion) according to published procedures [4,7] Chloroform extraction was inspired by the published procedure [26] but the volumes of solvents were decreased for a more convenient operation. The low yield of chloroform extraction could be explained by low volume of solvent and suboptimal filtration settings that led to the material loss. In the other methods, the yields were comparable with those previously published. As expected, PHB obtained by harsh, nonselective digestion methods (alkaline, acidic) had significantly lower molecular weight than the polymer prepared from the same biomass by milder soap-based digestion or by chloroform extraction (Table 1).

All three digestion methods had one thing in common - the polymer was recovered from an alkaline mixture. Even the so-called acid method requires alkaline workup, otherwise the purity of the polymer would not be sufficient [27]. Despite repeated washing with water, the pH of aqueous suspensions in the last washing steps were roughly the same as before washing (Table 1). This may be due to the low solubility or strong adsorption of the basic impurities on PHB. Other insoluble basic species, possibly responsible for the high pH, could be negatively charged carboxylate groups at the ends of PHB chains.

All samples had a purity around 95% or more, making them suitable for common industrial applications. For certain purposes, such as solution spinning and film making, the solubility is another important parameter. It was found out that PHB obtained by alkaline and soap-based digestion did not fully dissolve in the most common solvent (chloroform). The samples contained a substantial amount of insoluble impurity that could be filtered off, washed, dried, and quantified gravimetrically. By FTIR, the impurity was identified as mainly protein. Commercial PHB formed a lightly opalescent solution, but the amount of insoluble matter was negligible. Other two samples formed clear solutions, without any detectable insoluble impurity.

3.2. Thermal stability

The samples were isothermally treated to assess their processability. Heating at 190 °C for 5 min was chosen because it corresponds to realistic conditions for melt processing of the polymer [28]. As expected, all samples degraded significantly. Even reference samples (chloroform-extracted and commercial PHBs) dropped to about half of their original molecular weight (Fig. 3). This degradation rate is in good agreement with previously published results for high-purity PHB [8] and therefore it is likely caused mainly by the random chain scission.

In samples recovered by digestion, the thermal degradation was much more severe. Especially samples from alkaline and soap-based digestion were found to be extremely unstable, with the molecular weight after melting being only 5% or 10% of that before melting. Significant level of degradation was even visible - their melts after 5 min of heating had very low viscosity, solidified at low temperature and spontaneously cracked upon cooling. The fast degradation was also observed by cyclic DSC, where the clearest sign of degradation was the decrease of melting point, as shown in Fig. 4. After four cycles, the melting temperature of PHB from soap and alkaline digestion dropped under 130 °C, while the other samples remained at values typical for PHB, that are around 170 °C.

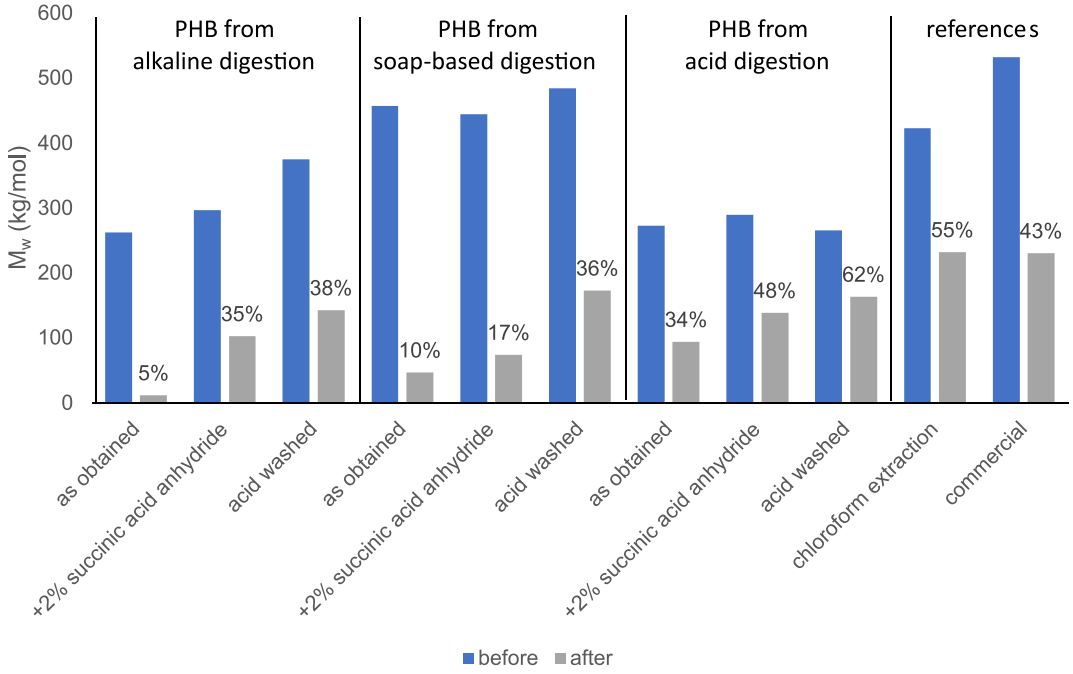


Fig. 3. Weight-average molecular weight of PHB before and after isothermal degradation for 5 min at 190 °C. Numbers above the columns represent the fractions of the original molecular weight M_w(5 min)/M_w(0).

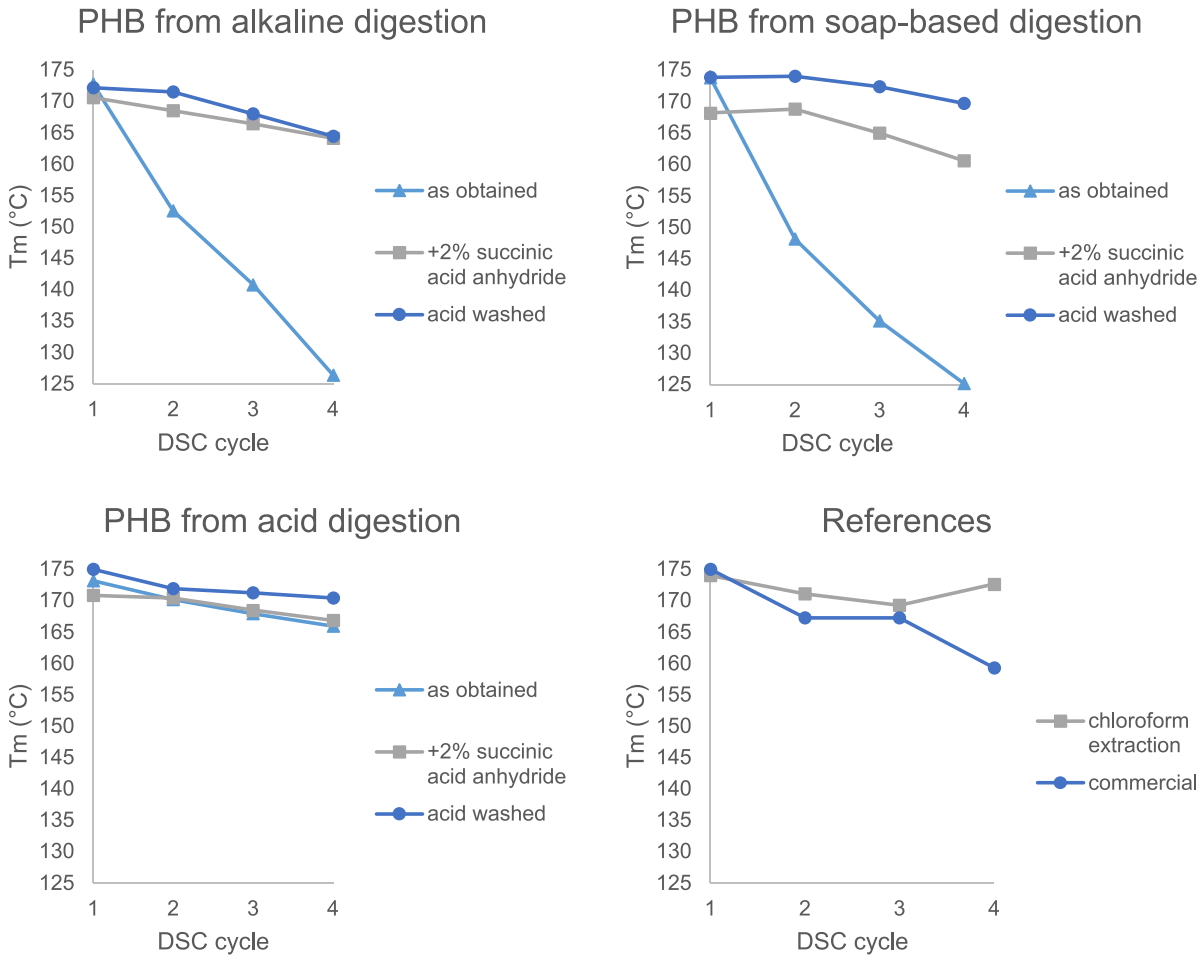


Fig. 4. Melting points of PHBs after 1 4 DSC cycles. Each DSC cycle included heating to 190 °C, annealing at 190 °C for 5 min, and cooling.

Table 1
Preparation and properties of the PHB samples. s.d. stands for standard deviation. CII stands for chloroform-insoluble impurity.

preparation method	pH at the last aqueous wash	yield (%)	purity ± s.d. (%)	CII (%)	M_w (kg/mol)
alkaline digestion	11.7	76	98 ± 3	4.2	263
soap-based digestion	9.9	94	95 ± 3	1.3	457
acid digestion	9.0	94	95 ± 1	0	273
chloroform extraction	n.a.	60	95 ± 2	0	423
commercial	n.a.	n.a.	99 ± 1	0	532

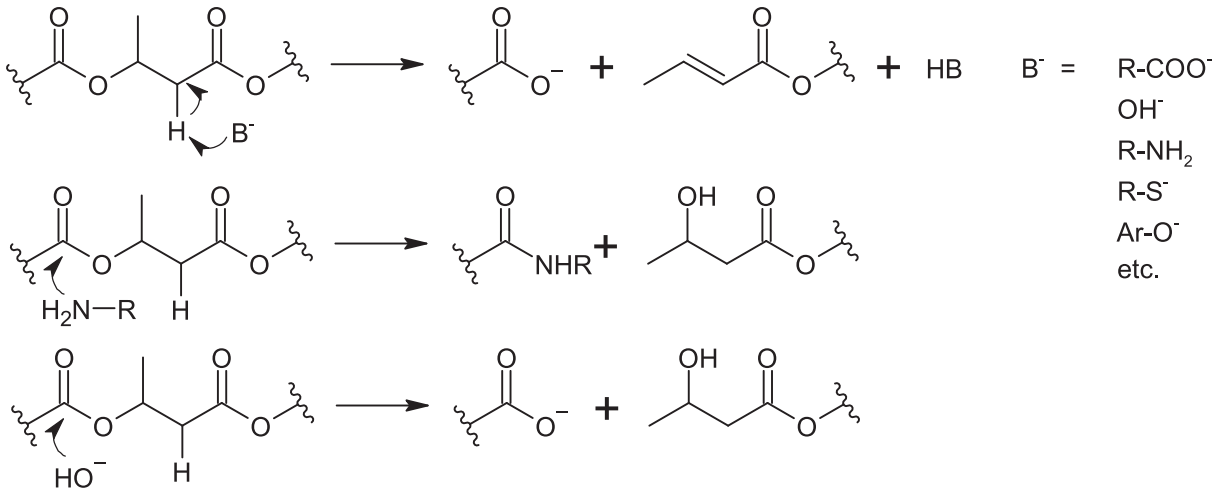


Fig. 5. Hypothetical mechanisms of impurity-induced thermal degradation of PHB.

We can hypothesize that PHBs carboxylate chain ends or residues of hydroxide and fatty acid salts were the major cause of the degradation. Other impurities, such as protein, may also play a role - protein side chains in their basic form are highly reactive and could decompose PHB via substitution or elimination. (Fig. 5) This could explain the slightly higher thermal stability of the PHB obtained by acid digestion, that did not contain the protein-rich impurity.

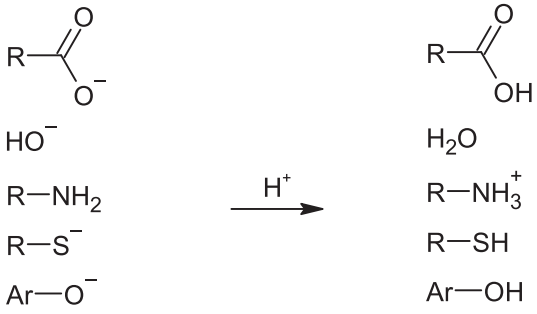


Fig. 6. Neutralization of basic residues by acid wash.

3.3. Methods for increasing the thermal stability of PHB

3.3.1. Wash with acid

Acid wash did not require any major change in the recovery procedures. Last aqueous wash was only slightly modified - after mixing the pellet with water, the pH was decreased with several drops of diluted acid. The rest of the isolation procedure was identical. This little change dramatically affected the thermal stability of the samples cyclic DSC shows that the melting point remained close to 170 °C even after the fourth cycle (Fig. 4). Furthermore, the molecular weight after isothermal degradation dropped much less than in untreated samples (Fig. 3). For the sake of simplicity, only the results of sulfuric acid treatment were shown. However, the effect seemed to be general - treatment with citric acid or hydrochloric acid solution stabilized the polymer, too. This corresponds to the hypothesis that any strong enough acid should have a significant stabilizing effect. All functional groups mentioned above (Fig. 5) have pK_a higher than 3.5. Therefore, decreasing the pH below 3.5 should restrict their ability to act as base or nucleophile and thus mitigate the thermal instability of the PHB. (Fig. 6)

3.3.2. Acidic additives

Another strategy for increasing the thermal stability of PHB is the addition of an acidic stabilizer directly before melt processing. This strategy might be beneficial for those who do not have control over the recovery process and want to simply improve the thermal stability. Suitable stabilizers should be nonvolatile, readily available, nontoxic, and environmentally friendly. Therefore, organic acids (citric, succinic, stearic) and anhydrides (succinic, maleic) were investigated. For initial screening, the additives (1 - 10%) were homogenized with PHB from soap-based digestion. The mixtures underwent isothermal degradation (as described in Section 2.2.6) and were rated visually (color, brittleness). Citric and succinic acid were found to be effective in stabilization of the polymer against thermal degradation but led to significant coloration of the melt. Contrary, stearic acid did not stabilize the polymer significantly and did not cause any coloration either. Optimal additives proved to be anhydrides (succinic, maleic) that were effective stabilizers and did not significantly impair color.

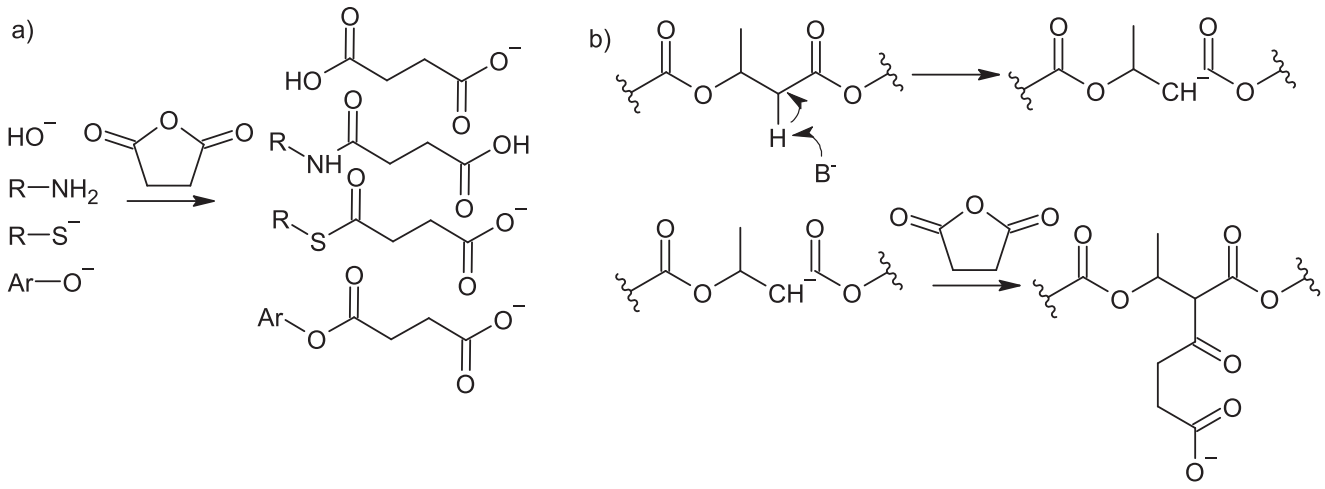


Fig. 7. Hypothetical mechanisms of stabilization with succinic anhydride. It may react with highly basic groups to less basic species (a) or it may prevent the elimination by grafting to the anionic degradation intermediate (b).

Thermal degradation of PHBs from different digestion methods with 2% of succinic acid anhydride was studied in more detail. Anhydride-stabilized PHB was in all cases more stable than untreated, as can be seen from the cDSC results (Fig. 4). However, isothermal degradation experiments showed that it was slightly less stable than the corresponding acid-washed PHB (Fig. 3). This may be caused by lower homogeneity of the mixture or by different reactivity (Fig. 7). Nevertheless, the anhydride proved to have positive effect and may be useful whenever acid wash is impractical.

4. Conclusion

This work describes two successful techniques for stabilizing PHB obtained by digestion methods - addition of an acidic stabilizer and acid wash. Cyclic DSC experiments showed that PHB samples recovered using alkaline reagents had extremely low thermal stability and the melting points significantly decreased during the DSC experiments. GPC of the samples after isothermal degradation confirmed a severe decrease of molecular weight. Both the addition of anhydride and acid wash mitigated this effect after the treatments, the polymers had a melting point around 170 °C until the last scan. Molecular weight decreased much less, too. Acid wash had a stronger stabilizing effect than the addition of an acidic stabilizer (succinic anhydride). Mechanisms of the stabilizing effects were proposed, too, and will be experimentally studied in the future.

Declaration of Competing Interest

The authors declare no known competing financial interests that could have appeared to influence the work reported in this paper.

Acknowledgments

Authors acknowledge the support of Ministry of Industry and Trade through the project CZ.01.1.02/0.0/0.0/20_321/0024676 New circular biotechnologies and biomedical applications and of Brno University of Technology through the project FCH-S-21-7553 of the Specific University Research Grant.

References

[1] C. Pérez-Rivero, J.P. López-Gómez, I. Roy, A sustainable approach for the downstream processing of bacterial polyhydroxyalkanoates: state-of-the-art and latest developments, Biochem. Eng. J. 150 (2019) 107283, doi:10.1016/j.bej.2019.107283.
[2] M. Koller, Established and advanced approaches for recovery of microbial polyhydroxyalkanoate (PHA) biopolyesters from surrounding microbial biomass, EuroBiotech J. 4 (3) (2020) 113–126, doi:10.2478/ebtj-2020-0013.
[3] Y. Jiang, G. Mikova, R. Kleerebezem, L.A. van der Wielen, M.C. Cuellar, Feasibility study of an alkaline-based chemical treatment for the purification of polyhydroxybutyrate produced by a mixed enriched culture, AMB Express 5 (1) (2015) 5, doi:10.1186/s13568-015-0096-5.
[4] M. Lpez-Abelairas, M. Garca-Torreiro, T. L-Chau, J. Lema, A. Steinbchel, Comparison of several methods for the separation of poly(3-hydroxybutyrate) from *cupriavidus necator* H16 cultures, Biochem. Eng. J. 93 (2015) 250–259, doi:10.1016/j.bej.2014.10.018.
[5] N. Jacquel, C.-W. Lo, Y.-H. Wei, H.-S. Wu, S.S. Wang, Isolation and purification of bacterial poly(3-hydroxyalkanoates), Biochem. Eng. J. 39 (1) (2008) 15–27, doi:10.1016/j.bej.2007.11.029.
[6] C. Samorì, M. Basaglia, S. Casella, L. Favaro, P. Galletti, L. Giorgini, D. Marchi, L. Mazzocchetti, C. Torri, E. Tagliavini, Dimethyl carbonate and switchable anionic surfactants: two effective tools for the extraction of polyhydroxyalkanoates from microbial biomass, Green Chem. 17 (2) (2015) 1047–1056, doi:10.1039/C4GC01821D.
[7] A. Pospisilova, I. Novackova, R. Prikryl, Isolation of poly(3-hydroxybutyrate) from bacterial biomass using soap made of waste cooking oil, Bioresour. Technol. 326 (2021) 124683.
[8] N. Grassie, E. Murray, P. Holmes, The thermal degradation of poly(-(d)-beta-hydroxybutyric acid): Part 2 changes in molecular weight, Polym. Degrad. Stab. 6 (2) (1984) 95–103.
[9] A. Hoffmann, S. Kreuzberger, G. Hinrichsen, Influence of thermal degradation on tensile strength and Young's modulus of poly(hydroxybutyrate), Polym. Bull. 33 (3) (1994) 355–359.
[10] A. Burniol-Figols, I.V. Skiadas, A.E. Daugaard, H.N. Gavala, Polyhydroxyalkanoate (PHA) purification through dilute aqueous ammonia digestion at elevated temperatures, J. Chem. Technol. Biotechnol. 95 (5) (2020) 1519–1532, doi:10.1002/jctb.6345.
[11] F.-D. Kopinke, M. Remmler, K. Mackenzie, Thermal decomposition of biodegradable polyesters–I: poly(β-hydroxybutyric acid), Polym. Degrad. Stab. 52 (1) (1996) 25–38.
[12] B. Kunasundari, C.R. Arza, F.H. Maurer, V. Murugaiyah, G. Kaur, K. Sudesh, Biological recovery and properties of poly(3-hydroxybutyrate) from *Cupriavidus necator* H16, Sep. Purif. Technol. 172 (2017) 1–6.
[13] K.J. Kim, Y. Doi, H. Abe, Effect of metal compounds on thermal degradation behavior of aliphatic poly(hydroxyalkanoic acid)s, Polym. Degrad. Stab. 93 (4) (2008) 776–785.
[14] K.J. Kim, Y. Doi, H. Abe, Effects of residual metal compounds and chain-end structure on thermal degradation of poly(3-hydroxybutyric acid), Polym. Degrad. Stab. 91 (4) (2006) 769–777.
[15] F.-D. Kopinke, K. Mackenzie, Mechanistic aspects of the thermal degradation of poly(lactic acid) and poly(β-hydroxybutyric acid), J. Anal. Appl. Pyrolysis 40 (1997) 43–53.
[16] M. Kawalec, G. Adamus, P. Kurcok, M. Kowalczuk, I. Foltran, M.L. Focarete, M. Scandola, Carboxylate-induced degradation of poly(3-hydroxybutyrate)s, Biomacromolecules 8 (4) (2007) 1053–1058.
[17] M. Kawalec, M. Sobota, M. Scandola, M. Kowalczuk, P. Kurcok, A convenient route to PHB macromonomers via anionically controlled moderate-temperature degradation of PHB, J. Polym. Sci., Part A 48 (23) (2010) 5490–5497.
[18] E. Hablot, P. Bordes, E. Pollet, L. Avérous, Thermal and thermo-mechanical degradation of poly(3-hydroxybutyrate)-based multiphase systems, Polym. Degrad. Stab. 93 (2) (2008) 413–421.

[19] K. Csomorova, J. Rychlỳ, D. Bakoš, I. Janigova, The effect of inorganic additives on the decomposition of poly(beta-hydroxybutyrate) into volatile products, Polym. Degrad. Stab. 43 (3) (1994) 441–446.
[20] Y. Ke, Z. Qu, G. Wu, Y. Wang, Thermal and in vitro degradation properties of the NH_2-containing PHBV films, Polym. Degrad. Stab. 105 (2014) 59–67.
[21] H. Ariffin, H. Nishida, Y. Shirai, M.A. Hassan, Highly selective transformation of poly [(R)-3-hydroxybutyric acid] into trans-crotonic acid by catalytic thermal degradation, Polym. Degrad. Stab. 95 (8) (2010) 1375–1381.
[22] M. Larsson, O. Markbo, P. Jannasch, Melt processability and thermomechanical properties of blends based on polyhydroxyalkanoates and poly(butylene adipate-*co*-terephthalate), RSC Adv. 6 (50) (2016) 44354–44363.
[23] C.R. Arza, P. Jannasch, F.H. Maurer, Network formation of graphene oxide in poly(3-hydroxybutyrate) nanocomposites, Eur. Polym. J. 59 (2014) 262–269.
[24] P. Alexy, K. Tomanova, Z. Vanovcanova, R. Plavec, J. Feranc, J. Bockaj, L. Omanikova, D. Bakos, I. Hudec, M. Galambos, et al., Biodegradable Polymeric Mixture and Method for its Preparation, US Patent App. 16/646,482, 2020.
[25] S. Obruca, P. Benesova, J. Oborna, I. Marova, Application of protease-hydrolyzed whey as a complex nitrogen source to increase poly(3-hydroxybutyrate) production from oils by *cupriavidus necator*, Biotechnol. Lett. 36 (4) (2014) 775–781.
[26] A. Burniol-Figols, C. Varrone, A.E. Daugaard, S.B. Le, I.V. Skiadas, H.N. Gavala, Polyhydroxyalkanoates (PHA) production from fermented crude glycerol: study on the conversion of 1,3-propanediol to PHA in mixed microbial consortia, Water Res. 128 (2018) 255–266.
[27] J. Yu, L.X. Chen, Cost-effective recovery and purification of polyhydroxyalkanoates by selective dissolution of cell mass, Biotechnol. Prog. 22 (2) (2006) 547–553.
[28] J. Tocháček, R. Přikryl, P. Menčík, V. Melčová, S. Figalla, The chances of thermooxidation stabilization of poly(3-hydroxybutyrate) during processing–a critical evaluation, J. Appl. Polym. Sci. 138 (27) (2021) 50647.

Check for updates

Received: 1 October 2020 | Revised: 1 February 2021 | Accepted: 7 February 2021

DOI: 10.1002/app.50647

ARTICLE

Applied Polymer SCIENCE WILEY

The chances of thermooxidation stabilization of poly (3-hydroxybutyrate) during processing–A critical evaluation

Jiří Tocháček[1] | Radek Přikryl[2] | Přemysl Menčík[2] | Veronika Melčová[2] | Silvestr Figalla[2]

[1]CEITEC – Central European Institute of Technology, Brno University of Technology, Brno, Czech Republic

[2]Faculty of Chemistry, Brno University of Technology, Brno, Czech Republic

Correspondence
Jiří Tocháček, CEITEC Central European Institute of Technology, Brno University of Technology, Purkyňova 656/123, 612 00 Brno, Czech Republic.
Email: jiri.tochacek@ceitec.vutbr.cz

Funding information
Ministry of Education, Youths and Sports of the Czech Republic, Grant/Award Number: CEITEC 2020 (LQ1601) and the Specific University Research Grant through the project FCH-S-20-6340 Advanced materials and material technologies

Abstract

The performance of a series of thermooxidation stabilizers was investigated in poly(3-hydroxybutyrate) (PHB) during processing by multiple extrusion at 190°C. The issue was to find out if PHB may be processing stabilized or not. Phenols of different steric hindrance, phosphites, amine oxide, hydroxylamine, lactone, hindered amine and carbodiimide were tested as potential stabilizers and their efficiencies compared with non-stabilized polymer as a reference. Multiple extrusion data was evaluated using the processing degradation index (PDI) formerly designed for polypropylene. Changes in molecular weight were monitored as well. The results have shown that none of the stabilizing structures, currently successfully used in other polymers, have the ability to protect PHB. This indirectly implies that no radical chain scission takes place during PHB processing, i.e. no thermooxidation takes place. Moreover, nearly all of the tested structures act as prodegradants in PHB, some of them very strong. The strongest ones contain P or N atoms with asymmetrical free electron pairs in their molecules that evidently accelerate the main degradation mechanism of PHB—thermally induced cis-elimination.

KEYWORDS

biopolymers and renewable polymers, degradation, extrusion, polyesters, stabilization

1 | INTRODUCTION

Poly(3-hydroxybutyrate) (PHB) first described in the twenties of the past century has been known as a biosourced polymer with a great future, proposed as a potential substitute of some petrochemical based polymers, Figure 1. In numerous papers its properties were compared to those of polypropylene, but PHB high tendency to crystallization resulting in consequent brittleness still made its comparison problematic and its practical use limited. A lot of attention was paid to improving its properties, especially to elimination of high crystallinity resulting in very low strain at break making its application problematic.[1–3]

Investigating mechanical properties, many scientific papers reported PHB processed under laboratory conditions. In these papers tensile test specimens were cut from the films prepared by solution casting from chloroform.[4–6] This approach did not provide full information on polymer behavior, since it skipped the step of extrusion which is inevitable in processing on industrial scale. Thus, the papers reporting processing using single- or twin-screw extrusions or kneading techniques were found to be much closer to reality.[7–9]

During extrusion, polymers commonly undergo degradation due to high temperatures and thermomechanical stress, both under the limited access to oxygen. In the case of PHB the processing temperature

 © 2021 Wiley Periodicals LLC.

window is limited by its melting point 175–180°C and the upper threshold 200–220 °C above which the volatiles start to be released. In the course of processing, hydrolysis leading to the formation of acidic and alcoholic functionalities and random scission by cis-elimination leading to the crotonic acid derivatives may take place, Figure 2. Both occur statistically within the polymer chain and decrease its molecular weight.[10–12]

While hydrolysis at high temperatures, typical for esters, may be prevented by drying, decomposition by cis-elimination is purely temperature dependent and needs no other reactant. Beside the main ester functionalities, PHB polymer backbone is composed of hydrocarbon parts that may be affected by heat and mechanical stress during processing and subsequently oxidized. The problem of PHB stability concerns especially its extrusion. Relatively narrow processing window 180–190°C and sensitivity to processing by extrusion induce a question if there is a way how to protect PHB during processing and make it more resistant to higher temperatures, higher screw rotation speed and longer residence time in the barrel. At this point published literature data is inconsistent, some papers report the use of thermooxidation stabilization by phenols, some by phenol-phosphite blends, some use only phosphite and many other do not use thermooxidation protection at all.[6,12–16] Some information on stabilization appeared already in the 80s; however, it was not supported by accessible experimental results.[12] Also our laboratory results were not unambiguous so that we decided to generate enough experimental data in order to elucidate this problem. A series of polymer stabilizers (antioxidants) was investigated with respect to their possible use in PHB during processing in order to answer the question if PHB can be efficiently stabilized or not. Presently, protective agents such as chain extenders are used as well. Their effect on PHB matrix is more provable and they are sometimes presented as "stabilizers" but their mechanism of action is different.[17,18] They do not retard thermooxidation itself, but they heal the consequences of thermal or hydrolytic decomposition. They react with free carboxylic and hydroxyl functionalities, forming new cross-links in polymer and increasing the viscosity of polymer melt. The action of chain extenders was not the area of our interest but one of them tested in this work was used as a reference.

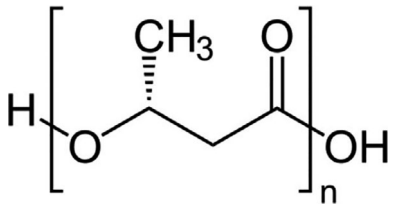


FIGURE 1 Poly(3-hydroxybutyrate) structure (PHB)

2 | MATERIALS

Poly(3-hydroxybutyrate) Biomer PHB—a custom compound with 0.5% boronitride (BN) and 5% tributyl citrate (TBC) provided by Biomer (dr. Haenggi). The following compounds were used as stabilizers: Butylated hydroxytoluene (BHT, Sigma–Aldrich); 1,3,5-Tris(4-t-butyl-3-hydroxy-2,6-dimethylbenzyl)isocyanurate (Cyanox 1790, Cytec); Pentaerythrityl tetrakis[3-(3,5-di-tert-Bu-4-hydroxyphenyl)propionate] (Irganox1010; BASF); Tris (2,4-di-t-Bu-phenyl)phosphite (Irgafos 168, BASF); Irganox B225 blend (BASF); Bis(2,4-di-t-butylphenyl)pentaerythrityl diphosphite (Ultranox 626, Addivant); Bis(hydrogenated rape-oil alkyl)methyl amine, N-oxides (Genox EP, Chemtura); distearyl hydroxylamine (Irgastab FS042, BASF); 5,7-di-t-butyl-3-(3,4-di-methylphenyl)-3H-benzofuran-2-one (HP136, Ciba); N,N′-bis (2,2,6,6-tetramethyl-4-piperidyl)-N,N′-diformyl hexamethylenediamine (Uvinul 4050H, BASF); D,L-α-tocoferol (Ronotec 201, Roche); Natural curcuma (food grade); Polymeric carbodiimide (Stabilizer 9000, Raschig).

Native PHB granulate received from the supplier was surface treated with 0.2% TBC, then blended with 0.5% stabilizer and compounded.

3 | METHODS AND MEASUREMENT

Extrusion experiments involving both compounding and multiple extrusion were carried out using a laboratory

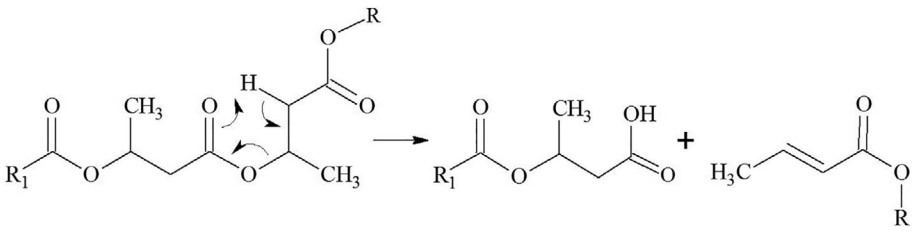


FIGURE 2 Poly(3-hydroxybutyrate) (PHB) thermal decomposition by cis-elimination[11]

HAAKE single-screw extruder, D = 19 mm, L/D = 30 at temperatures 190, 190, 185 and 180°C (hopper to die)/ 60 rpm; nozzle diameter 3 mm. Polymer melt was water quenched at 60°C and pelletized. Before each extrusion polymeric material was dried at 60°C for 2 h. Multiple extrusion was realized by 5-fold extruder pass, after each one polymer melt-volume rate (MVR) was measured on Dynisco LMI5000 melt-indexer at 190°C/2.16 kg (EN ISO 1133). Compounding step was denoted as zero extrusion, multiple extrusions 1 to 5. Thermogravimetric analysis (TGA) was carried out on TGA Q500 at 50–400°C temperature range, using samples 10–13 mg under the atmosphere of nitrogen (60 ml/min). Average molecular weights were determined by means of SEC method using Agilent Technologies 1100 Series. Instrument is equipped with isocratic pump, fraction collector, refractive index detector and autosampler. PLgel 10 μm mixed B column thermostated to 30°C with chloroform as the eluent at a flow rate 1 ml/min. Calibration using 12 standards 1.6–1100 kDa.

4 | RESULTS AND DISCUSSION

The tested series of stabilizing structures was designed in order to cover the most important stabilization mechanisms widely utilized in industry as well as the mechanisms marginal but existing and capable of potential interference with radical thermooxidation scission of hydrocarbons.

The class of sterically hindered phenols is represented by the fully hindered low molecular BHT (AO-1), fully hindered high-molecular Irganox 1010 (AO-2), partly hindered high-molecular Cyanox AO 1790 (AO-3) and low-hindered, low-molecular weight vitamin E and curcuma (AO-11 and 12). All these structures act as "chain breaking antioxidants" and interfere with radical oxidative scission of hydrocarbons by eliminating alkylperoxyl radicals. Consequently they form relatively stable fenoxyl radicals, the stability of which is dependent on the degree of 2,6- sterical hindrance of active phenolic moiety.[19–21]

Organic phosphites applied as secondary stabilizers are represented by non-hydrolysable Irgafos 168 (AO-4), its synergistic 1:1 blend with phenol Irganox B225 (AO-5) and partially hydrolyzed Ultranox 626 (AO-6). Phosphites are often described as hydroperoxide decomposers, but their reaction mechanism is more complex and beside hydroperoxides they also react with alkoxyl and alkylperoxyl radicals.[19,20,22] Phenol-phosphite synergistic blends such as AO-5 are widely used in industry. The efficiency of phosphites also depends on their hydrolyzability, which in some cases positively contributes to the overall stabilization performance. In this respect partially hydrolyzed AO-6 is a typical example.[23]

The structures such as aminoxide, hydroxylamine and lactone (AO-7 to 9) belong to those known but marginally used. They possess the ability to react with C-centered radicals formed during processing and prevent their oxidation.[19] Their overall efficiencies and price/performance ratios, however, are not much advantageous, as well as their administrative (patent) and hygienic limitations. This all makes their practical use limited. Nevertheless, the reactions of their structures are highly specific so that they had to be involved in this series as well.

AO-10 is a representative of hindered amine light stabilizers (HALS) class. Despite not being processing stabilizer, it was also enrolled in the series due to its complex mechanism. HALS are known by the ability to react with C-centered, alkoxyl and alkylperoxyl radicals, as well as the ability to non-radically decompose hydroperoxides and neutralize acidic species in polymer.[19,20,24] Beside protection from the effects of light, HALS are very efficient thermooxidation stabilizers. This is the main reason of involving AO-10 in this screening series.

The last one—carbodiimide Stabilizer 9000 (Ch-X) has nothing to do with polymer thermooxidative protection. Despite it is often presented as "stabilizer," it reacts with hydrolytic scission intermediates, forms crosslinks, and partially improves the properties of polymer matrix. Its use in the series was only illustrative and it served as another reference for the stabilizers tested.[17]

Investigation of stabilization efficiencies was carried out by multiple extrusion. This approach has been frequently used for polyolefins, where the basic cylinder temperatures 240°C for HDPE and 260°C for PP are usually used in order to cause the maximum thermomechanical deterioration of the material tested. In the case of PHB, this method had not been applied yet, so that the optimum processing conditions providing applicable data had to be set at first. Definition of optimum processing temperature was carried out with the basic PHB matrix additivated with 0.5% BN and 5% TBC, no other additives were used.

As shown in Figure 3 processing temperature 180°C appeared to be low, the changes in MVR were minimum and occurred relatively late. On the other hand, processing at 200°C increased MVR so far that it was unmeasurable after 5th extrusion. These extremes delimited 190°C as the optimum temperature providing reasonable degree of deterioration and well measurable MVR.

In order to provide an evidence that degradation changes due to extrusion are not caused by the thermal

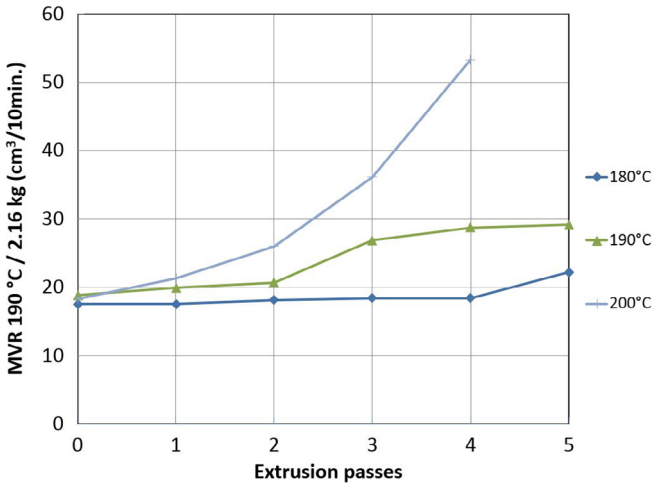


FIGURE 3 Poly(3-hydroxybutyrate) (PHB) - multiple extrusion at 60 rpm carried out at 180, 190 and 200°C [Color figure can be viewed at wileyonlinelibrary.com]

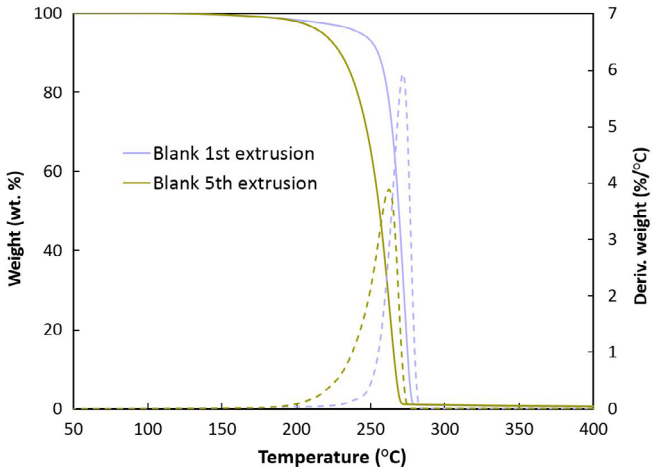


FIGURE 4 Thermogravimetric analysis (TGA) of blank under N_2 atmosphere determined after first and fifth extrusion at 180–190°C [Color figure can be viewed at wileyonlinelibrary.com]

decomposition of PHB itself, TGA analysis of Blank after 1st and 5th extrusion was carried out, Figure 4, Table 1. It can be seen that the purely thermal stability of Blank is sufficient and at 180–190°C temperature range used for extrusions remains practically unchanged even after five extrusions. Deterioration due to fifth extrusion decreases the onset of thermal decomposition down to 200°C that is still at least 10°C above the maximum processing temperature applied in extruder. Moreover, even the minimum mass loss (1 to 1.4%) observed at processing temperatures may be more accounted for the partial loss of TBC added as plasticizer, originally present in PHB at 5% concentration.

Polymer behavior during processing was evaluated by means of multiple extrusion at 190°C/60 rpm with PHB formulated such as shown in Table 2.

TABLE 1 TGA - temperatures indicating 1% and 5% mass loss

	Temperature (°C)	
	1% loss	5% loss
Blank–first extrusion	180.8	243.3
Blank–fifth extrusion	180.1	217.8

Abbreviation: TGA, thermogravimetric analysis.

TABLE 2 PHB sample coding and formulations (base: 0.5% boronitride, 5.2% tributylcitrate)

Sample	Formulation	Stabilizer type
Blank	Base	None
AO-1	Base +0.5% BHT	Low-molecular phenol, 2,6-di-tBu substituted
AO-2	Base +0.5% Irganox 1010	High-molecular phenol, 2,6-di-t-Bu substituted
AO-3	Base +0.5% Cyanox AO 1790	High-molecular phenol, 2-methyl-6-t-Bu substituted
AO-4	Base +0.5% Irgafos 168	Phosphite, non-hydrolyzable
AO-5	Base +0.5% Irganox B225	Phenol-phosphite synergy blend (1:1)
AO-6	Base +0.5% Ultranox 626	Phosphite, partially hydrolysed *(30–34% free DTBP)*
AO-7	Base +0.5% Genox EP	Amine oxide
AO-8	Base +0.5% Irgastab FS042	Hydroxylamine
AO-9	Base +0.5% Irganox HP136	Lactone, benzofuranone
AO-10	Base +0.5% Uvinul 4050H	HALS, low the -molecular
AO-11	Base +0.5% Ronotec 201	Vitamin E, 2,6-dimethyl substituted phenol
AO-12	Base +0.5% natural curcuma	Low-molecular phenol, 2-methoxy substituted
Ch-X	Base +0.5% Stabilizer 9000	Carbodiimide chain extender

Abbreviation: PHB, poly(3-hydroxybutyrate).

The results attained were rather surprising and stabilizers could be divided into two groups according to the performance. In the first group depicted in Figure 5 it is evident that performance of stabilizers practically does not differ up to 3rd extrusion and exhibits processing stability comparable with that of unstabilized polymer. During 4th and 5th extrusions, the phenols, phosphites and their combinations, despite being very efficient in other

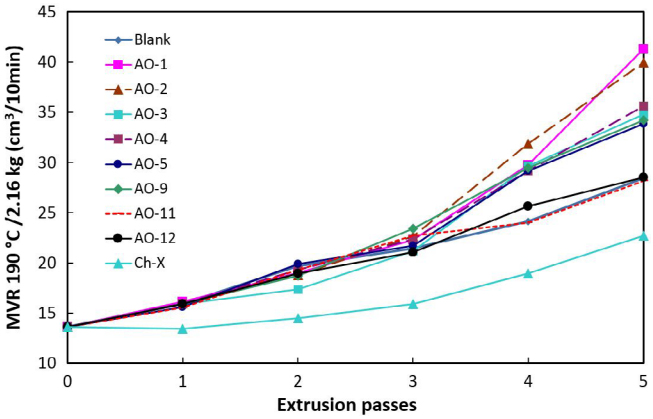


FIGURE 5 Poly(3-hydroxybutyrate) (PHB) + base + 0.5% stabilizer - multiple extrusion at 190°C/60 rpm [Color figure can be viewed at wileyonlinelibrary.com]

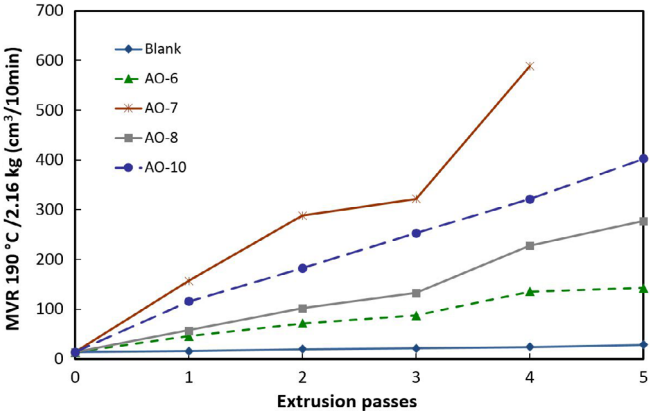


FIGURE 6 Poly(3-hydroxybutyrate) (PHB) + base + 0.5% stabilizer - multiple extrusion at 190°C/60 rpm [Color figure can be viewed at wileyonlinelibrary.com]

polymers, act prodegradatively and visibly decrease the processing stability of polymer. Natural antioxidants such as curcuma and vitamin E (AO-11, AO-12) behave completely neutrally and do not affect processing stability of polymer during the whole test.

A visibly different (and relatively the best) performance is exhibited by carbodiimide chain extender (Ch-X). Much less increased MVR compared to the non-stabilized reference polymer is a result of Ch-X reaction mechanism, forming bonds among polymer chains, changing morphology and consequently increasing the viscosity of polymer melt. Being not the issue of this work, however, the use of Ch-X only illustrates how different its effect in PHB can be.

The performance of the second group of stabilizers was found completely different, Figure 6. Compared to the reference Blank, they all exhibit extremely intensive increase in MVR starting even within the 1st extrusion, with AO-7 the fifth extrusion was not possible at all. Except AO-10 which is not a processing stabilizer, all the remaining ones performing more or less efficiently in other polymers act as very strong prodegradants in PHB. In order to quantify the extent of deterioration due to multiple extrusion, processing degradation index (PDI) was calculated according to Equation (1). PDI is a useful tool describing the processing deterioration of polymer by one single parameter.[25] The higher it is, the higher degree of degradation polymer exhibits.

$$\mathrm{PDI} = \frac{(\mathrm{MFI}_0 + \mathrm{MFI}_1 + \ldots + \mathrm{MFI}_n) - (n+1)\mathrm{MFI}_0}{(n+1)\mathrm{MFI}_0} 100 = \frac{(\mathrm{MFI}_1 + \ldots + \mathrm{MFI}_n) - n\mathrm{MFI}_0}{(n+1)\mathrm{MFI}_0} 100 \quad (1)$$

where MFI is the melt flow index (rate) and 0 to n is the number of extrusion.

The use of PDI was originally designed for polypropylene (PP), the processing degradation of which goes exclusively through the chain scission mechanism. In such a case, changes due to processing are reliably reflected by MFI, which is increased with increasing chain scission. All under the condition that no other interfering reactions such as cross-linking take place. Despite polypropylene and PHB differ in chemistry of their degradation, the chain scission as a prevailing mechanism is their common feature. In PHB the possible re-esterification reactions leading to the certain portion of chain extension take place only at the beginning of heating where terminal hydroxyl groups initially present in polymer are consumed. With consequent chain scission due to cis-elimination no new terminal hydroxyl groups are released. Possible release of hydroxyl groups due to hydrolysis is prevented by the patient drying of pellets before each extrusion. These facts show that the portion of possible cross-links related to the main polymer chain scission is negligible in PHB and the calculation of PDI originally proposed for PP may be applied directly without any changes. Not having exact data on PHB melt density, MVR were used instead of MFI, Figure 7.

PDI allowing the direct comparison of processing stability indicates that the common phenols, phosphites and their blends in the first group decrease processing stability 1.2 to 1.5 times, while in the second group 10 up to 37 times. No effect can be seen with AO-11 and 12, the relatively positive effect of Ch-X cannot be used for consideration due to its different mechanism of action.

During multiple extrusion most of the MVR values were found between 13 and 320 dg/min. Within the measured series some typical MVRs roughly covering this interval were selected and molecular weights of these samples were determined. Their plot against MVR is

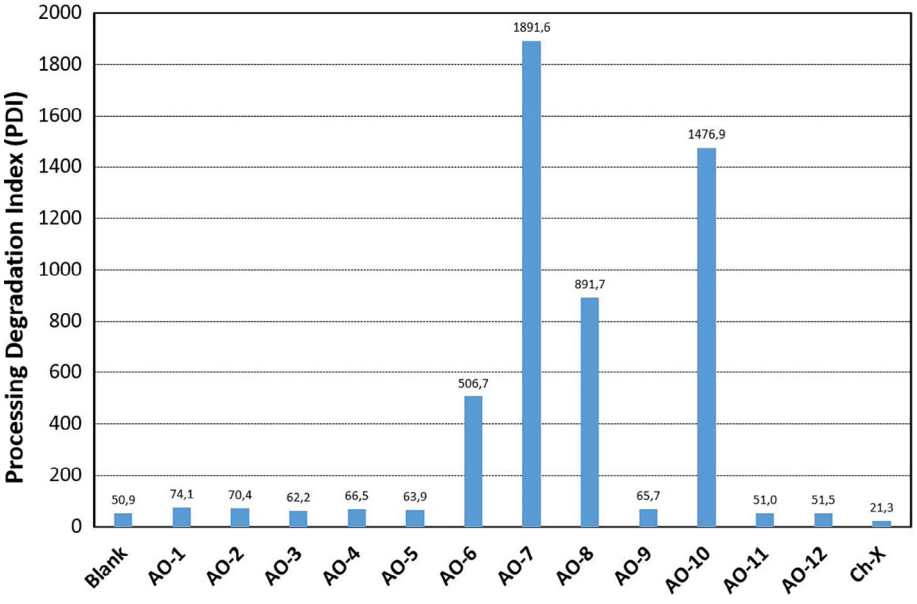


FIGURE 7 Processing degradation index (PDI) calculated for particular stabilizers based on multiple extrusion data [Color figure can be viewed at wileyonlinelibrary.com]

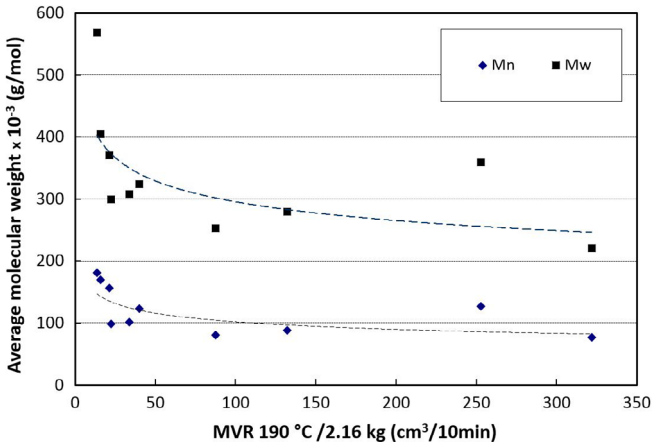


FIGURE 8 Molecular weights versus melt volume rate (MVR) [Color figure can be viewed at wileyonlinelibrary.com]

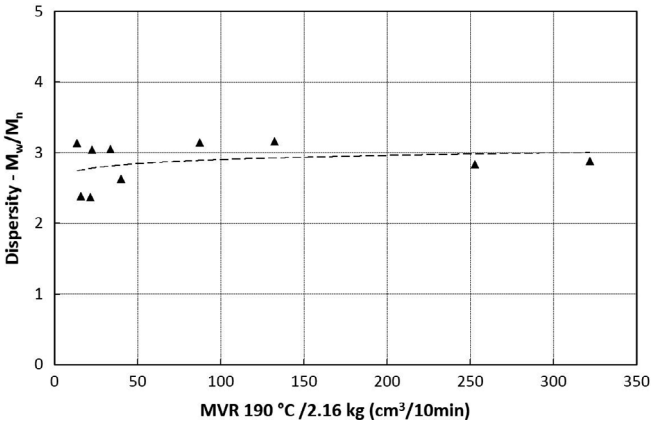


FIGURE 9 Dispersity M_w/M_n versus melt volume rate (MVR)

shown in Figure 8, dispersities given by M_w/M_n ratio in Figure 9.

The highest molecular weights are reflected in the lowest MVR values. The most intensive drop in molecular weights is connected with the primary increase of MVR at the initial extrusion steps, while with a higher extent of degradation indicated by higher MVR values, molecular weights decrease only moderately. Concerning the dispersities, some slight increase may again be connected with the beginning of processing but further on their dependence on MVR is very flat and exhibiting only minimum changes. Broken lines in Figures 8 and 9 only depict the trends. This indicates that the effect of mechanical stress preferably attacking the longest chains in PP and usually leading to the narrowing of M_w/M_n ratio [26,27] is much less important at processing of PHB. The main degradation mechanism – cis-elimination is mostly temperature dependent, takes place statistically along all polymer chains regardless of their lengths and prevails. This results in keeping the M_w/M_n ratio more or less constant.

Color development due to extrusions is shown in Figure 10. One can observe that the color of PHB itself is brownish and the addition of stabilizers does not change it so far. The exceptions are AO-6 and AO-12. In case of AO-6 the formation of discolored species can be accounted for the reaction between phosphitic species of hydrolyzed stabilizer and PHB, while the yellow color of AO-11 is the inherent property of its active component - curcuma. Considering the effect of multiple extrusion, the discoloration is not any dramatic as well. The changes are mostly very moderate and even the pronounced prodegradation effect exhibited by stabilizers AO-7,8,10 does not result in adequate worsening of color.



FIGURE 10 Color development due to multiple extrusion at 190°C/60 rpm (* = fourth extrusion) [Color figure can be viewed at wileyonlinelibrary.com]

The results of this work show that none of the thermooxidation stabilizer systems improved the stability of PHB during processing. The absence of their stabilization efficiency indirectly indicates that throughout extrusion at 180–190°C no hydrocarbon part of PHB is oxidized and no radical scission takes place. In such a case the typical protective actions of antioxidants such as chain breaking mechanism or hydroperoxide decomposition are of no use. The revealed completely adverse effect making them to act as prodegradants stem from their chemical structures. The highest prodegradation effect was observed with structures containing P and N atoms with asymmetrical free electron pairs that may act as nucleophilic catalysts of cis-elimination. A similar effect on PHB thermal decomposition at processing temperatures between 180 and 220°C has already been reported for glycerol, while its triacetyl derivative exhibited no effect.[28] Relatively low prodegradation effect of AO-4, AO-5 also containing phosphite functionality may be caused by the presence of bulky aromatic substituents limiting the steric accessibility of P free electron pair.

5 | CONCLUSIONS

This work answered the question if PHB could be stabilized by the currently known antioxidants or not. A specially selected series of stabilizers involving the structures most used as well as those used marginally was tested as protective agents for PHB processing. It was confirmed that common primary and secondary antioxidants, as well as multifunctional HALS, are ineffective in PHB and the potential of their mechanism of action cannot be utilized. This also indirectly confirmed the fact that no radical scission takes place in PHB during extrusion at temperatures 180–190°C. Beside this, the presence of common antioxidants in PHB matrix has shown a completely adverse effect that increased the rate of thermal decomposition where practically no oxygen was involved. The prodegradation effect of the structures containing phosphorus and nitrogen atoms with asymmetric free electron pairs was even dramatic. Finally, it can be concluded that none of the commonly used stabilizer structures exhibits the ability to protect PHB during processing and its presence in the matrix is not only useless but in some cases may be even harmful. In such a case only the use of chain extenders makes sense, despite they do not have a real ability to protect polymer but only ”rectify the damage” caused by preceding degradation.

ACKNOWLEDGMENTS

The results of this research have been acquired within CEITEC 2020 (LQ1601) project and Advanced materials

and material technologies project No. FCH-S-20-6340 of the Specific University Research Grant, both with the financial contribution of the Ministry of Education, Youth and Sports of the Czech Republic.

ORCID

Jiří Tocháček https://orcid.org/0000-0001-9983-2461

REFERENCES

[1] G.-Q. Chen, R.-C. Luo, in *Polyhydroxyalkanoate blends and composites. Biodegradable polymer blends and composites from renewable resources* (Ed: L. Yu), John Wiley & Sons. Inc., Hoboken, New Jersey **2009**, p. 191.
[2] A. J. dos Santos, L. V. Oliveira Dalla Valentina, A. A. Hidalgo Schulz, M. A. Tomaz Duarte, *Ingeniería y Ciencia* **2017**, *13*, 269.
[3] C. F. Jasso-Gastinel, *Modification of polymer properties*, Elsevier, Amsterdam **2017**.
[4] I. Bibers, V. Tupureina, A. Dzene, M. Kalnins, *Mech. Compos. Mater.* **1999**, *35*, 357.
[5] S. Xu, R. Luo, L. Wu, K. Xu, G.-Q. Chen, *J. Appl. Polym. Sci.* **2006**, *102*, 3782.
[6] L. Wang, W. Zhu, X. Wang, X. Chen, G.-Q. Chen, K. Xu, *J. Appl. Polym. Sci.* **2008**, *107*, 166.
[7] W. M. Pachekoski, J. A. M. Agnelli, L. P. Belem, *Mater. Res.* **2009**, *12*, 159.
[8] P. Alexy, P. Bugaj, J. Feranc, M. Pavlačková, K. Tomanová, F. Benovič, R. Plavec, M. Mihalovič, M. Botošová, *Chem. Listy* **2011**, *105*, s241.
[9] A. El-Hadi, R. Schnabel, E. Straube, G. Mueller, M. Riemschneider, *Macromol. Mater. Eng.* **2002**, *287*, 363.
[10] N. Grassie, E. J. Murray, P. A. Holmes, *Polym. Degrad. Stab.* **1984**, *6*, 47.
[11] N. Grassie, E. J. Murray, P. A. Holmes, *Polym. Degrad. Stab.* **1984**, *6*, 95.
[12] N. Grassie, E. J. Murray, P. A. Holmes, *Polym. Degrad. Stab.* **1984**, *6*, 127.
[13] L.P. Costa, L.H. Carvalho, T.G. Almeida, E.L. Canedo. Stabilization during processing of PHB/organoclay. 2nd Brazilian conference on composite materials-BCCM2, Sao José dos Campos-SP, September 15–18, **2014**
[14] V. Melčová, Polyhydroxybutyrate modification by grafting of functional groups. Bachelor's thesis Brno University of Technology, Czech Republic, **2015**
[15] L. Palkovský. Processing stability of poly(3-hydroxybutyrate) (PHB). Bachelor's thesis, Brno University of Technology, Czech Republic, **2017**
[16] R. M. R. Wellen, E. L. Canedo, M. S. Rabello, G. J. M. Fechine, *Mat. Res* **2016**, *19*, 759.
[17] JONCRYL ADR-4368C, BASF technical literature, p.1–8, 25-Jan-08 (BASF)
[18] V. Melčová, R. Přikryl, P. Menčík, J. Tocháček, *Mater. Sci. Forum* **2019**, *955*, 7.
[19] H. Zweifel, *Stabilization of Polymeic Materials*, Springer-Verlag, Berlin, Heidelberg **1998**.
[20] R. Gächter, H. Müller, *Plastics Additives*, 3rd ed., Hanser Publishers, Munich, Vienna, N.Y **1990**.
[21] R. Wolf, B. L. Kaul, *Plastics, Additives. Ullman's Encyclopedia of Industrial chemistry*, Vol. A20, VCH Publishers, Inc., Weinheim, Germany **1992**.
[22] K. Schwetlick, W. D. Habicher, *Die Angew. Makromol. Chem.* **1995**, *232*, 239.
[23] J. Tocháček, J. Sedlář, *Polym. Degrad. Stab.* **1995**, *50*, 345.
[24] J. Pospíšil, P. P. Klemchuk, *Oxidation Inhibition in Organic Materials, Vol. II*, CRC Press, Boca Raton, Florida **1990**.
[25] J. Tocháček, J. Jančář, *Polym. Test.* **2012**, *31*, 1115.
[26] J. Tocháček, S. Hermannová, J. Jančář, J. Kalfus, *Chem. Listy* **2008**, *102*, 1228.
[27] J. Tocháček, J. Jančář, J. Kalfus, P. Zbořilová, Z. Buráň, *Polym. Degrad. Stab.* **2008**, *93*, 770.
[28] I. Janigová, I. Lacík, I. Chodák, *Polym. Degrad. Stab.* **2002**, *77*, 35.

SUPPORTING INFORMATION

Additional supporting information may be found online in the Supporting Information section at the end of this article.

How to cite this article: Tocháček J, Přikryl R, Menčík P, Melčová V, Figalla S. The chances of thermooxidation stabilization of poly(3-hydroxybutyrate) during processing–A critical evaluation. *J Appl Polym Sci*. 2021;e50647. https://doi.org/10.1002/app.50647

PAPER • **OPEN ACCESS**

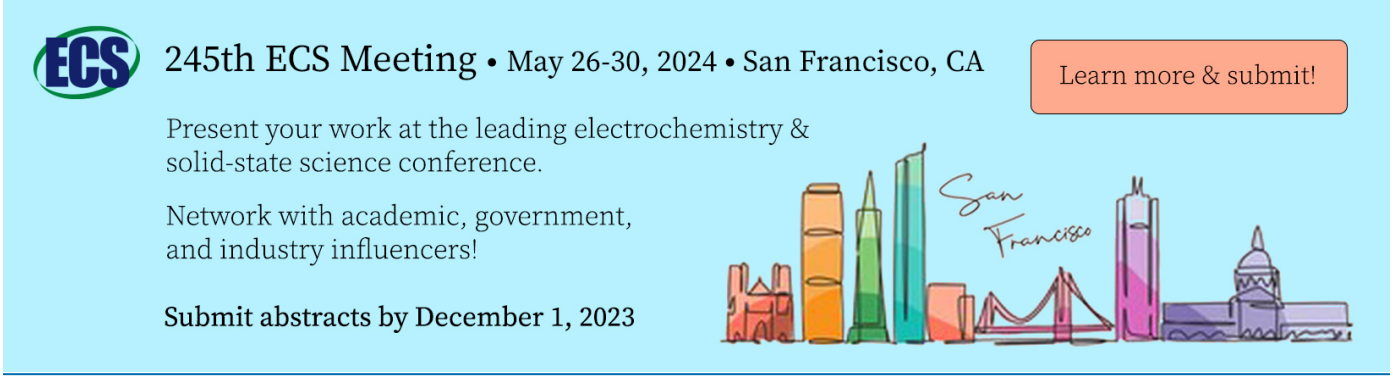
The influence of additives on crystallization of blends based on polylactid acid

To cite this article: D Perd'ochová *et al* 2017 *IOP Conf. Ser.: Mater. Sci. Eng.* **266** 012014

View the article online for updates and enhancements.

You may also like

- Cytotoxicity and biocompatibility of biomaterials based in polyhydroxybutyrate reinforced with cellulose nanowhiskers determined in human peripheral leukocytes
Horacio Vieyra, Esmeralda Juárez, Ulises Figueroa López et al.
- Characterization of bioplastics produced by haloarchaeon Haloarcula sp strain NRS20 using cost-effective carbon sources
Nashwa Hagagy, Amna A N Saddiq, Hend M Tag et al.
- Poly (3-hydroxybutyrate-*co*-15 mol% 3hydroxyhexanoate)/ZnO nanocomposites by solvent casting method: a study of optical, surface, and thermal properties
J Vishnu Chandar, S Shanmugan, D Mutharasu et al.



This content was downloaded from IP address 147.229.117.37 on 09/10/2023 at 08:09

IOP Conf. Series: Materials Science and Engineering **266** (2017) 012014 doi:10.1088/1757-899X/266/1/012014

The influence of additives on crystallization of blends based on polylactid acid

D Perďochová[1], K Tomanová[1], P Alexy[1], J Bočkaj[1], J Feranc[1], R Plavec[1], L Omaníková[1], P Jurkovič[1] and R Přikryl[2]

[1]Slovak University of Technology, Faculty of Chemical and Food Technology, Institute of Natural and Synthetic Polymers, Department of Plastics, Rubber and Fibers, Radlinského 9, 812 37 Bratislava, Slovakia,
[2]Brno University of Technology, Institute of Material Chemistry, Faculty of Chemistry, Purkyňova 118, 612 00 Brno, Czech Republic

dagmaraperdochova@gmail.com

Abstract. The sustainable development consists of the effort of replacing commonly used polymer materials for the biodegradable ones. They do not have sufficient physical and mechanical properties, therefore they have to be modified by producing various ratio mixtures or with the additives. Improving their processability and properties is an important challenge to be afforded before using these materials on the market. One way to improve the properties of these materials is to prepare their blends [1]. The most common way of the preparation of packaging materials is the injection moulding, where the crystallization of material is very important. That is the reason the crystallization has become one of the most studied characteristics of biodegradable blends based on PLA / PHB. The work is a contribution to works that deal with the description of the structure of PLA / PHB blends, which have been modified by the addition of various types of additives, mainly nucleating agents and plasticizers [2]. The films of these blends keep approximately unchanged mechanical properties after two weeks of storage. The presence of plasticizer (ATBC) and nucleating agent (BN) has no significant impact on the processing stability of PLA/PHB blends. The results show that the combination of the plasticizer and nucleating agent greatly affects the process of crystallization of PLA/PHB blends as well as the ratio of polymers and the heat treatment process.

1. Introduction

Nowadays, the most commonly used materials are polymers, both synthetic and natural. Their expansion is based on their good physical properties, mechanical properties, and also because of low production costs. The increasing consumption of conventional synthetic polymeric materials is the cause of the growing problem of their disposal. At the same time, we are faced with an ecological problem. For this reason, efforts are being made to replace conventional plastics (PE, PP, PS and others) with biodegradable plastics and therefore more environmentally friendly. One possibility how to solve this problem can be by the production of biodegradable plastics. Biodegradable polymers, especially those from renewable resources and their blends, are playing an important role in the field of research of new materials. Of all of the potential products made from annually renewable resources, polylactic acid (PLA) is currently the most interesting. This biopolymer is 100% renewable, it can be

Content from this work may be used under the terms of the Creative Commons Attribution 3.0 licence. Any further distribution of this work must maintain attribution to the author(s) and the title of the work, journal citation and DOI.
Published under licence by IOP Publishing Ltd

easily composted and has comparable properties to commercially-known plastics [3,4]. The second group of studied polymers are polyhydroxyalkanoates, biopolymers synthesized by the action of microorganisms. As in the case of polylactic acid, these are polymers with similar properties to conventional plastics, they are completely biodegradable and have potential as a biodegradable substitute. The simplest and most commonly used poly-β-hydroxyalkanoate is poly-β-hydroxybutyrate (PHB) [5]. Polymers that are produced from natural resources and are capable of being decomposed in nature have worse physical and mechanical properties than conventional polymer materials and therefore, use of them in demanding applications and to replace conventional plastics, they have to be modified in some ways. One way to modify the properties of these materials is to prepare their blends. This method of the preparation can achieve a synergistic improvement in properties in the comparison with the pure components [6]. The properties of polymeric materials are generally improved during processing in accordance with the requirements of the final product application. One important factor for setting the processing conditions is the understanding and description of the polymer structure, which affects the final properties of the product. Based on the supramolecular structure, we can predict and control the resulting behaviour of polymeric materials [7]. Polymer blends are prepared as a result of improved processing and utility properties together with various additives and modifiers. The plasticizers are one of the most commonly applied additives to improve the processability and flexibility of the final product. Since the most common method of preparing polymeric materials is injection moulding where crystallization of the material is a very important factor, crystallization has become one of the most studied characteristics of PLA / PHB blends [8]. At the same time the crystallization is followed by the effect of other additives, nucleating agents on the crystallization process itself and their effect on the resulting mechanical properties. The present work is a contribution to the number of works dealing with the description of the crystalline structure of PLA / PHB blends which have been modified by the addition of various types of additives, mainly nucleating agents and plasticizers.

2. Materials

Polylactid acid $(C_3H_4O_2)_n$ – Ingeo 4043D, Mw = 202 kDa, PDI = 2,18 ; D-isomer content 4,2 %. Nature Works, USA
Polyhydroxybutyrate $(C_4H_6O_2)_n$, Mw = 608 kDa, PDI = 4,23; homopolymer P3HB - Biomer, Nemecko
Ester-type plasticizer – acetyltributylcitrate (ATBC), Jungbunzlauer, Nemecko (0, 5, 10, 15, 20, 25%wt.)
Nucleating agent – Boron Nitride (BN), Momentive, USA (BN – 0, 1, 5 % wt.)

3. Experimental

3.1 Blends preparation

Biodegradable blends based on PLA/PHB (60/40 w/w) with the specific content of additives were prepared using twin screw extruder (L/D = 40, D = 16 mm) at temperature 160 – 170 – 180 – 180 – 185 – 185 – 185 – 180 – 175 – 170 °C (direction hopper – head). Extruded materials were chilled in water and granulated into small pellets. Pellets were dried at 70°C for 2 hours in hot air oven and consequently used for rheological and DSC measurements.

3.2 Processing stability

The oscillation rheometer RPA 2000 was used for processing stability testing of prepared blends. Timed test was done at three temperatures: 170, 180, 190°C, the angle of strain was 30° and oscillation frequency was 60 cpm. For correct evaluation of temperature influence on the rate of polymer degradation based on the decrease of complex viscosity, the elimination of differences in initial viscosity was done by recalculation of complex viscosity using the formula (1):

$$\eta^*_{rel}(t) = \eta^*(t) / \eta^* \quad (1)$$

where $\eta^*_{rel}(t)$ is relative complex viscosity at time t, $\eta^*(t)$ is complex viscosity at time t and η^* is complex viscosity at the start of the test.

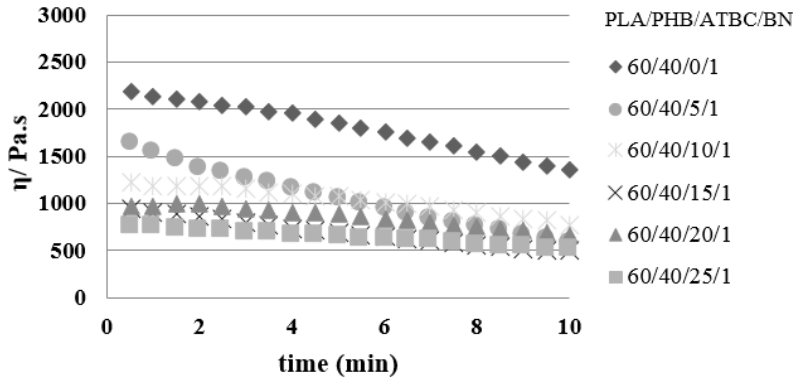
3.3 Films preparation
For films preparation was used single-screw Brabender extruder (screw diameter 19 mm, L/D=25) as well as chill-roll technology was used. Prepared films were used for measuring the mechanical properties. The selected temperature profile of the single screw extruder in the head → hopper direction was as follows: 170-180-180-170 ° C.

3.4 Mechanical properties measurement
Tensile strength at break (*σb*) and the elongation at break (*εb*) were determined according to ISO 527 standard using Zwick machine at cross-head speed 50 mm/min. Strips 15mm width were used as testing pieces.

3.5 DSC measurement
DSC (Mettler Toledo) was used for studying the crystallization properties of prepared blends under specific conditions. The flow of purge gas of nitrogen was 50ml/min. Standard aluminium crucibles were used. Measuring program:
1. Heating 10 K/min, 30-190 °C
2. Isothermal process 190 °C, 3 min
3. Cooling 10 K/min, 190-30 °C
4. Isothermal process 30 °C, 3 min
5. Heating 10 K/min, 30-190 °C

4. Results and discussion
The work deals with the study of influence of plasticizer and nucleating agent on crystallization process and the resulting thermal and physical properties of PLA/PHB blends.

4.1 Processing stability
The indication of the first stages of degradation process of polymers can be easily detected using the oscillation rheometer. Changes in relative complex viscosity of the prepared blends were taken as the indicator of processing stability. According to article [9], it was shown that changes in relative complex viscosity reflect changes in molecular weight of degraded polymer very well. The example of dependency of complex viscosity and relative complex viscosity on test time for PLA/PHB blends including 1% wt. of nucleating agent and different concentration of plasticizer is shown in Figure 1.



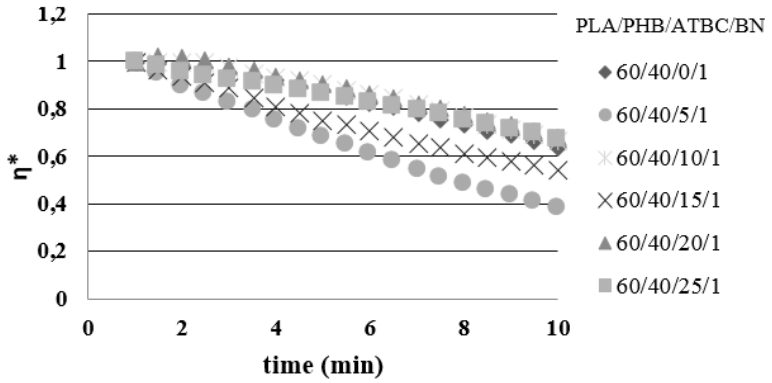


Figure 1. The dependency of complex viscosity and relative complex viscosity on test time for PLA/PHB blends including 1% wt. of nucleating agent and different concentration of plasticizer

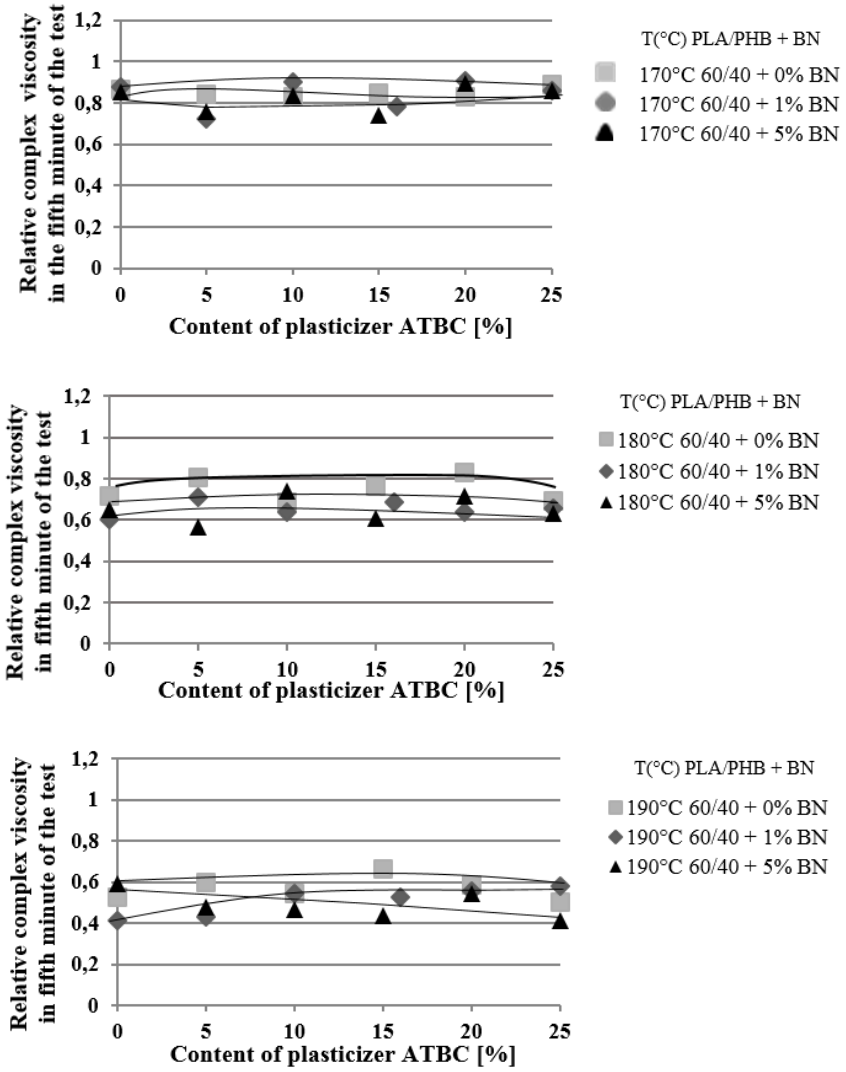


Figure 2. The dependency of relative complex viscosity in the fifth minute of the test on content of plasticizer and nucleating agent BN at different temperatures (170 °C, 180 °C, 190 °C).

According to results shown in Figure 2 it can be seen that the viscosity of the blends in the fifth minute of the test, because of the thermo-mechanical stress caused by oscillatory rheometer, gradually decreases with temperature and it indicates that the increasing temperature causes the expected increase of degradation of the polymer blends. Differences in relative complex viscosity are significant but slightly. The effect of the presence of the nucleating agent, as well as the influence of the concentration of plasticizer is minimal and the observed differences can be considered to be within the experimental variability. Consequently, neither the plasticizer nor the nucleating agent has a negative effect on the processing stability or rheological characteristics of the studied blends.

4.2 Mechanical properties

The PLA / PHB blends were prepared according to method mentioned in chapter 3.1. Subsequently, the physical-mechanical properties of PLA / PHB blends were measured according to method mentioned in chapter 3.4 after sample preparation at time intervals 24 hours, a week and 2 weeks after the extrusion. The conditions for storage of samples were 50% relative humidity and 25°C. Nucleating agent BN is also used as a filler in high performance in polymer blends, which greatly improves thermal conductivity. In film production, this property of BN appears to have been evident. The addition of a larger amount of BN (5 wt.%) has a positive effect on the processing properties either during the production of the pellets or the film, probably due to the better thermal conductivity of the prepared blends. Whether cooling in a water bath or cooling on chill rolls, it is likely that a faster heat transfer occurs, resulting in the stiffness of string and a reduced stickiness of the films on the chill rolls. For all samples (PLA/PHB : 60/40 w/w ratio), physical-mechanical properties were maintained after 2 weeks of storage. For this reason, in the following, we only summarize the PLA / PHB blends, depending on the different plasticizer and nucleating agent content after 2 weeks of storage. The elongation at break for 60/40 w/w PLA / PHB blends (Figure 3) with 0, 1 and 5 wt.% of nucleating agent is noted after the addition of 15 %wt. of the plasticizer, and above this plasticizer concentration no change are observed in the elongation with the increase amount of the plasticizer. The addition of the nucleating agent does not affect the elongation at break and value of ε_b can to be considered as similar except the highest concentration of both additives when the elongation at break is slightly lower.

The tensile strength at break (Figure 4) decreases with the addition of 0-15% of plasticizer, the most significant decreasing can be observed in the range of 10-15%, from 15% of plasticizer we do not notice a significant change in tensile strength at break. The differences in tensile strength at break caused by presence of nucleating agent are more significant in case of low concentration of plasticizer to compare with differences at higher concentration of plasticizer, which are very small.

Based on described mechanical properties of prepared blends the marginal effect of presence of nucleating agent was observed in case of both tensile parameters. More significant effect was noticed in the case of presence of plasticizer as additive in different concentrations.

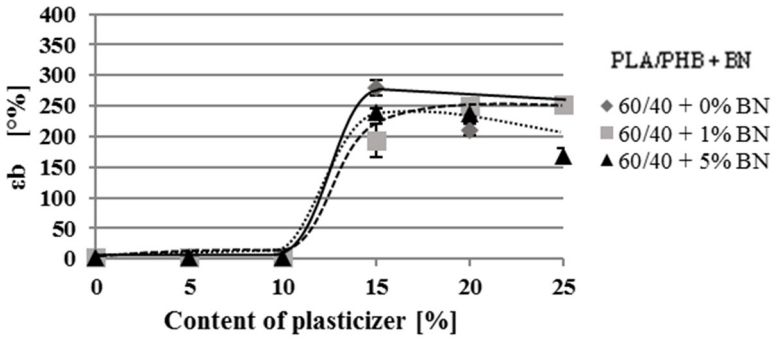


Figure 3. The dependency of elongation at break on content of plasticizer after two weeks of storage.

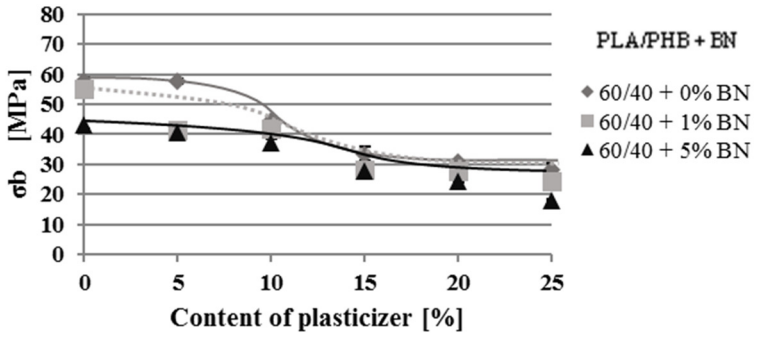


Figure 4. The dependency of tensile strength at break on content of plasticizer after two weeks of storage.

4.3 Thermal properties

The thermal properties of prepared blends were studied by DSC, especially the crystallization process. It is well known that the first heating curve is significantly influenced by the sample´s thermal history. The thermal history of prepared samples was erased by first heating run which is not reported because it reflects more thermal history of the sample preparation than real material characteristics. Only cooling and the second heating curves are presented in Figure 5 and Figure 7. The curves of cooling are shown in Figure 5, dependency of crystallization temperature Tc (peak) on nucleation agent as well as plasticizer concentration is shown in Figure 6. It can be seen that the addition of nucleating agent significantly influences the crystallization of PLA/PHB blends. The crystallization peak is shifted to a higher temperature in comparison to blank PLA/PHB blend. The changes of Tc depend also on plasticizer concentration. With increasing content of plasticizer, crystallization peak of nucleated blends is shifted to lower temperature. It means, that during the cooling of the melt, the crystallization process starts earlier as an effect of nucleation agent and it starts later as an effect of plasticizer, probably because plasticizer allows better mobility of the polymer chains. It can be predicted that the presence of other types of plasticizers can exhibit more or less strong effect on crystallization process of PLA/PHB blends in presence of nucleating agent in dependency of interaction between plasticizers and polymers. It means that by suitable selection of nucleation agent and plasticizer as additive in combination, the temperature of crystallization can be modified.

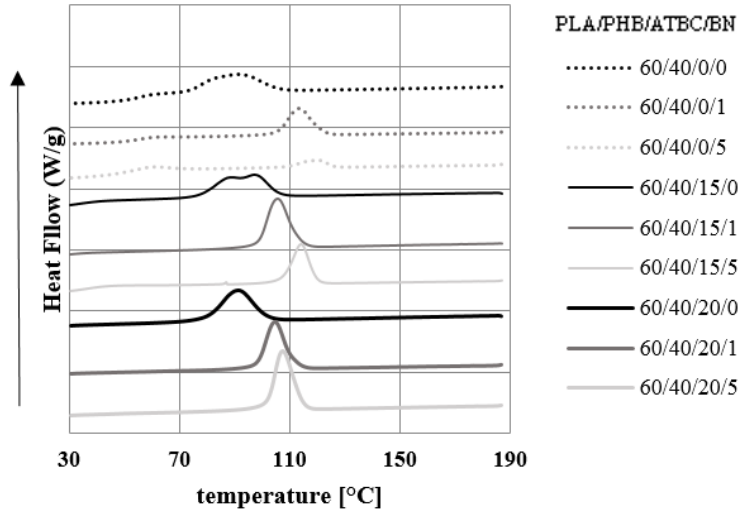


Figure 5 The curves of cooling of prepared blends. Ratio: PLA/PHB/plasticizer/nucleating agent.

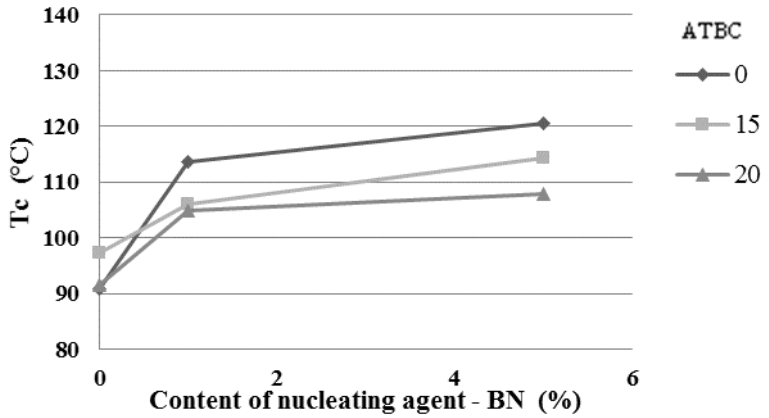


Figure 6 The dependency of Tc on nucleation agent content for various concentration level of plasticizer.

The curves of the second heating are shown in Figure 7, where three processes can be observed - the cold crystallisation, the melting of PLA and the melting of PHB. The effect of cold crystallization is present due to low rate of crystallization of PLA during cooling of samples. The dependency of Tcc as the peak value on both additives concentration is shown in Figure 8. The difference in nucleating activity is observed according to presence of nucleating agent as well as plasticizer. The Tcc of cold crystallization is shifted to higher temperature with increasing content of nucleating agent, mainly if blend contains no plasticizer. On the other hand, the increasing content of plasticizer shifts Tcc to lower temperature. This effect allows to modify crystallization process via the processing condition during the processing (temperature of the mould, in injection moulding process for example). Figure 9 shows the dependencies of Tm for PLA as well as for PHB on both additives concentration. Both melting temperatures (for PLA and PHB polymers in the blend) are strongly shifted to lower values by plasticizer concentration. The activity of nucleating agent is influenced by plasticizer as well. It can be seen, based on DSC results, that the crystallization of the blends and the type of crystals formed can be significantly influenced by the influence of the additives.

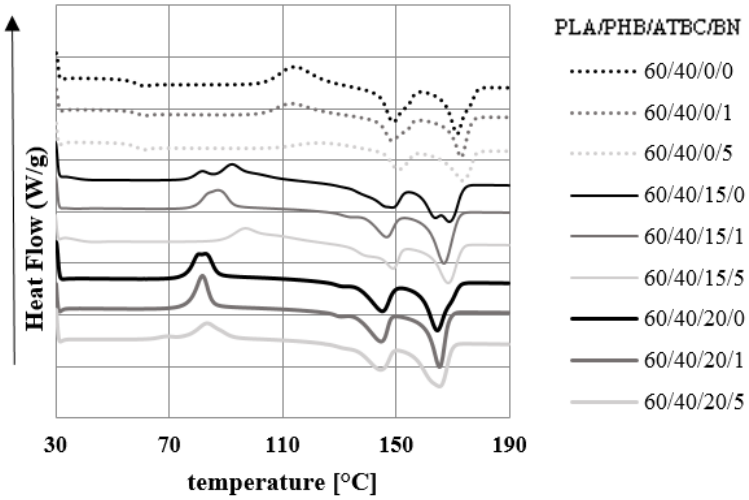


Figure 7. The curves of the second heating of prepared blends. Ratio: PLA/PHB/plasticizer/nucleating agent.

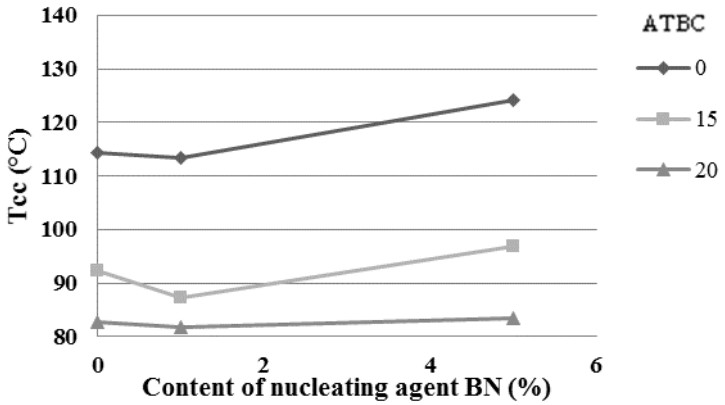


Figure 8. The dependency of Tcc on nucleating agent concentration for various levels of plasticizer content.

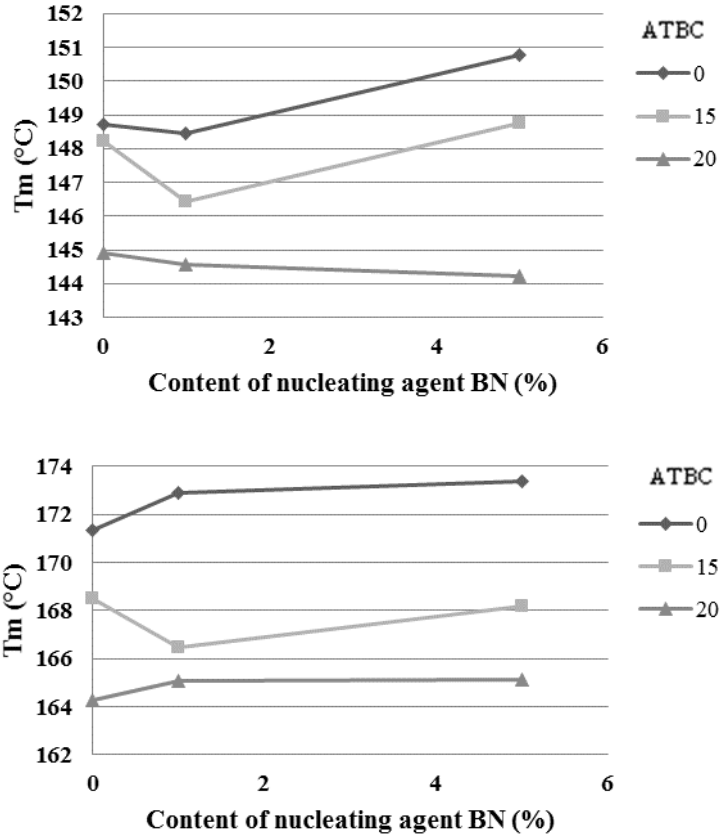


Figure 9. The dependency of Tm on nucleating agent concentration for various levels of plasticizer content.

Polymorphism, but also the process of cold crystallization and melting, is significantly affected. Generally, the nucleating agent (BN) increases the rate of crystallization process of PLA / PHB blends and the plasticizer improves the mobility of the segments to shift the temperature of melting and cold crystallization to lower temperature during the heating of the blend.

5. Conclusion

Neither the plasticizer nor the presence of a nucleating agent has significant impact on the processing stability of PLA / PHB blends. The addition of the nucleating agent has negative impact on the physical-mechanical properties of prepared blends as compared to blends without nucleating agent, especially in the case of tensile strength at break (σb) which decreases compared to samples without nucleating agent. The elongation at break significantly improves over 10% of plasticizer content. Additives, in our case nucleating agent and plasticizer, affect the crystallization process. In general, the nucleating agent (BN) improves nucleating activity of PLA/PHB blends and plasticizer allows better mobility of the chains that results in lower crystallization temperature. The next study will be based on optimizing the composition and processing conditions of PLA/PHB blends.

Acknowledgements

This work was supported by the Slovak Research and Development Agency (Project No. APVV-14-0301 and No. APVV-14-0175)

References

[1] Armentano I, Fortunati E and Burgos N, 2015 Processing and characterization of plasticized PLA/PHB blends for biodegradable multiphase systems *Polymer Letters* **9** 583–596
[2] Lim J S, Park K I and Chung G S 2013 Effect of composition ratio on the thermal and physical properties of semicrystalline PLA/PHB-HHx composites *Materials Science and Engineering* 2131–2137
[3] Gautam R, Bassi A S and Yanful EK 2007 A Review of Biodegradation of Synthetic Plastic and Foams *Appl Biochem Biotechnol* **141** 85-108
[4] Steinbuchel A and Merchessault R H 2005 Biopolymers for medical and pharmaceutical applications. *Polylactides* ISBN 978-3-527-311 186-219
[5] Ansari S and Fatma T. 2014 Polyhydroxybutyrate - a Biodegradable Plastic and its Various Formulations *International Journal of Innovative Research in Science, Engineering and Technology* **3** 9494–9499
[6] Abdelwahab M A and Flynn A 2012 Thermal, mechanical and morphological characterization of plasticized PLA–PHB blends. *Polymer Degradation and Stability* **97** 1822-1828
[7] Gerard T 2014 Polylactide/poly(hydroxybutyrate-co-hydroxyvalerate) blends: Morphology and mechanical properties. *Express Polymer Letters* **8** 609-617
[8] Kaufman S H and Falcetta J J 1977 Introduction to Polymer Science and Technology *Wiley* NY 13-23
[9] Mikušová M, Mihalík M, Alexy P, Tomanová K, Plavec R, Bočkaj J and Vanovčanová Z 2014 Method for testing of processing stability of biodegradable polyesters based on oscillation rheometry. *KGK-Kautschuk Gummi Kunststoffe* ISSN 0848-3276 51-54

Processing stabilization of poly(3-hydroxybutyrate)/poly(lactic acid) blends with oligomeric carbodiimide

MELCOVA Veronika[1, a *], PRIKRYL Radek[1, b], MENCIK Premysl[1, c] and TOCHACEK Jiri[2, d]

[1]Faculty of Chemistry, Brno University of Technology, Purkynova 464/118, CZ-612 00 Brno
[2]CEITEC, Purkynova 123, CZ-612 00 Brno

[a]xcmelcova@fch.vut.cz, [b]prikryl@fch.vut.cz, [c]mencik@fch.vut.cz, [d]jiri.tochacek@ceitec.vutbr.cz

Keywords: Poly(3-hydroxybutyrate), poly(lactic acid), carbodiimide, stabilization, reactive extrusion.

Abstract. Reactivity of five reactive agents with two biopolyesters, poly(3-hydroxybutyrate) (PHB) and poly(lactic acid) (PLA), was studied *in situ* during processing in laboratory kneader with simultaneous recording of a melt torque. Among them only Raschig, an oligomeric carbodiimide based additive, was proven to enhance melt viscosity of both. In order to find out the most efficient level of this additive for stabilizing of both polymers and PHB/PLA (70/30 w/w) blend, different concentrations were studied by means of melt torque monitoring, rheology time tests and gel permeation chromatography. Results showed the same trend for neat polymers and their blend. Addition of more than 0.5 % wt. did not have any further positive effect on molecular weight or complex viscosity of the melt. Higher amount is not consumed during the reaction and is left in the sample. Therefore, this amount was used for processing stability studies on PHB/PLA blends by subsequent extrusion cycles. Melt volume-flow rate of extruded samples was obtained and results showed lower values for all stabilized blends comparing to the first extrusion sample of non-stabilized blend. At the same, stability of the blends is secured up to the third extrusion cycle.

Introduction

Poly(3-hydroxybutyrate) (PHB) is a biodegradable and biobased polymer from the group of microbial polyesters polyhydroxyalkanoates [1]. Poly(lactic acid) (PLA) is a biobased polyester hydrolysable at composting conditions [2]. Both polymers are subjects of up-to-date research mainly due to global plastics pollution. However, both possess several drawbacks which are frequently overcome by blending these two polymers together although they are not miscible in the whole concentration range. PHB/PLA blend compatibility, mechanical and rheological properties can be improved by partial cross-linking with dicumyl peroxide [3]. However, radical reactions lead to unwanted drop in molecular weight (MW) and to the formation of hardly identifiable structures.

When processing these two polymers, final morphology (and therefore properties) of the system is driven mainly by their viscosity difference. Viscosity of pristine PHB is lower than that of PLA and is further decreased due to the β-scission degradation reaction [4]. Therefore, finding a suitable non-radical stabilizing reagent is beneficial for blend compatibilization as well.

As for PLA, various articles have been published describing reactive modification of PLA by means of non-radical reaction. Most used reagent appears to be a multi-functional epoxide styrene-acrylic oligomeric chain extender (commercial names Joncryl or CESA) [5]–[10]. Its addition leads to long chain branched structure with increased MW and MW distribution as an epoxy group from this reagent attacks a carboxyl group of PLA. Moreover, the addition of polymeric carbodiimide as a chain extender [5] and stabilizing agent [11] has been published. Carbodiimide is able to react with carboxyl and hydroxyl end groups of PLA, newly formed moisture and lactic acid and therefore compensates the effects of degradation. At 210 °C PLA is stabilized for up to 30 minutes [11]. Further, phosphite compounds such as tris(nonylphenyl) phosphite (TNPP) [5],[12], triphenyl

phosphite (TPP) [12] and tris-(2,4-di-tert-butylphenyl) phosphite [12] are proven to react with PLA in the melt. MW of PLA doubled with the incorporation of 2%wt. of TPP [12]. Star-like or tree-like molecules of PLA can be achieved through a two-step reaction with pyromellitic dianhydride with triglycidyl isocyanurate [13].

Arza et al studied the effect of bis(3,4-epoxycyclohexylmethyl) adipate, 2,2'-bis(2-oxazoline), trimethylolpropane tris(2-methyl-1-aziridinepropionate), TPP, TNPP, polycarbodiimide, and poly(methyl metharylate-co-glycidyl methacrylate) (GMM.MMA) addition to PHB. Samples were cocasted from chloroform solution and tested via rheology. The authors claimed only minor improvement on PHB melt stability with polycarbodiimide and GMM.MMA. [14] *Martelli et al* reported only slight stabilizing effect of polycarbodiimide on PHB [15].

This article is focused firstly on the performance of selected reactive additives with PHB and PLA during processing *in situ*. Secondly, the most effective additive was used for stabilizing PHB/PLA blend with PHB majority. Similar study on the blend was not reported up to date.

Experimental

Materials PHB with a production name Hydal, kindly provided by Nafigate, was used to prepare kneaded samples. Biomer® P309 (with nucleating agent and 5%wt. of plasticizer) granules were used for multiple extrusions. PLA Ingeo™ 4060D (amorphous PDLLA, referred to as PLA) was provided by NatureWorks LLC in the form of pellets and used as received. Raschig 9000 (referred to as Raschig), poly-(1,3,5-triisopropylphenylene-2,4-carbodiimide) of MW $2–3 \cdot 10^4$ g/mol was kindly provided from RASCHIG GmbH. TPP, TNPP and diphenyl isodecyl phosphite (DPDP) were purchased from Kingyorker. Joncryl ADR-4368 (referred to as Joncryl), of MW 6800 g/mol was purchased from BASF SE. All reagents were used as received.

Reactive kneading Melt compounding of all the samples was performed using a 25 ml internal chamber Brabender laboratory kneader operating at 175 °C and 45 RPM. Total sample weight was kept 30 g. Polymer granules were fed into the chamber within 2 minutes and homogenized continuously for 1 min. Subsequently, reagent was added to the mixture and the reaction was carried out for 5 minutes after feeding. The time evolution of torque (N·m) was recorded during the whole processing experiment (8 min) (analogous to [3]). Polymer granules were dried in an oven at 60 °C for 2 h before processing. First series contained samples of neat polymers with 2 wt% of reactive agent – TPP, TNPP, DPDP, Joncryl or Raschig. In the second series, the samples of PHB/PLA blend (70/30 w/w) with different amounts of Raschig were prepared. Samples are marked PHB/PLA-XR, where X is the amount of Raschig in weight percent (0; 0.5; 1; 2; 3).

Multiple Extrusions Multiple extrusion cycles were performed in HAAKE™ Rheomex OS 19 mm, L/D = 30, single screw extruder. Setting of temperature zones from hopper to die was as follows: 180 °C - 180 °C - 170 °C - 160 °C, rotational speed 60 RPM. Extruded profiles were put into water bath with temperature 60 °C in order to finish the crystallization process, air dried and fed into the pelletizing machine. Before processing and before each cycle, raw materials/blends were dried in a polymer dryer at 60 °C. Total amount of 1 kg of a mixture was submitted to six extrusion cycles. After each cycle, 60 g of the sample was collected to further analysis. This way 6 samples of non-stabilized and 6 samples of PHB/PLA (70/30 w/w) stabilized with 0.5 % of Raschig blend were prepared. Samples are marked PHB/PLA-X and PHB/PLA-R-X, respectively, where X stands for the number of extrusion cycle (1–6).

Gel permeation chromatography (GPC) MW averages and polydispersity indexes for both neat and modified polymers and blends were measured using GPC. Measurements were performed on Agilent Technologies 1100 Series instrument equipped with isocratic pump, fraction collector and autosampler. PLgel 10 μm mixed B column thermostated to 30 °C with chloroform as the eluent at a flow rate 0.1 ml/min. Linear polystyrene standards with narrow distribution were used to gain the calibration curve (10 points in calibration). Instrument is equipped with refractive index detector. For the measurement, 5 mg of sample was used.

Rheology Viscosity during 10 minute time test was studied by means of rheology measurements. Rotational Stress Control (CMT) TA Rheometer AR-G2 with environmental Test Chamber (ETC) system was used and parallel plate geometry with diameter 25 mm was chosen for all the measurements. Gap was adjusted to appropriate value according to the sample being approximately 800 μm. The time sweep (TS) procedure contained firstly pre-heating and then small amplitude oscillation in order to settle down the sample before measurement. The measurement itself was performed for 10 min at 190 °C, frequency of 0.833 Hz (50 oscillations per minute) was used. Amplitude of deformation was chosen 10 % in order to simulate conditions during processing. Samples for rheology measurements were prepared by pressing approximately 5 g of kneaded samples between two metal plates using hydraulic laboratory press machine to prepare films. Films were then shaped pressed into rounded specimens with a diameter 25 mm.

Melt volume-flow rate In order to characterize processing properties of extruded blends, their melt volume rate was determined. Measurements were performed on LMI 5000 melt indexer from Dynisco in automatic mode. Inner diameter of die was 2 mm; total weight applied to the sample 2.16 kg. All measurements were carried out at 190 °C after 5 min of pre-heating at this temperature. The amount of 5 g of material in the form of granules was transferred into the barrel and packed properly. Melt volume flow through the die was automatically recorded in ml/10 min.

Results and discussion

Reactive additive selection In this work, firstly the reactivity of different reactive agents in amount of 2 % towards neat PHB and PLA was investigated. Five additives were studied – TPP, DPDP, TNPP, Joncryl and Raschig. Melt reactions were carried out in a laboratory kneader with simultaneous recording of the melt torque. Melt torque showed expected decrease in time as a result of thermal degradation. In order to better evaluate additives´ contribution, parts of the melt torque-time curves after feeding were normalized by subtracting the values of neat polymer. Resulting graphs for both polymers are shown in Fig. 1.

As can be seen from the figure, among all tested compounds, only Raschig was proven to enhance melt torque of both PHB and PLA and therefore was chosen for further experiments. Enhancement of torque indicates an increase in viscosity of the melt, due to a chain extension/crosslinking reaction. Although the rest of the additives were effective in increasing the melt torque of PLA during compounding, their effect on PHB was contrary or none. This may be explained by pro-degrading or lubricating effect of the reagents.

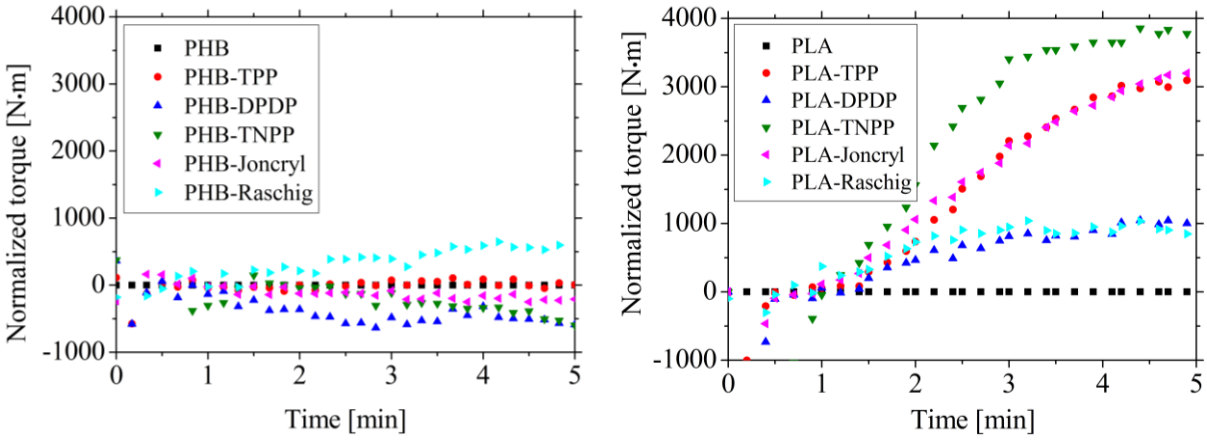


Fig. 1 Normalized torque curves of reactive processing of PHB and PLA

Kneading of Raschig concentration line In order to out find the most efficient amount of Raschig for stabilizing PHB/PLA (70/30 w/w) blend, kneading experiments with different amounts of Raschig were performed. In Figure 2, there is *in situ* measured melt torque plotted against time after feeding for the blend samples with different amounts of Raschig. Normalized torque was

calculated as described in the previous part. As can be seen from the figure, melt torque curves of all samples are comparable and independent on the Raschig amount. According to these results, 0.5 % appears to be an optimum amount of Raschig to gain a maximum possible increase in melt torque.

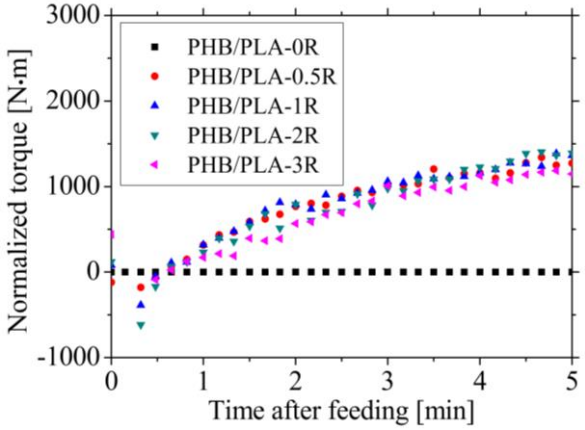


Fig. 2 Normalized torque curves of PHB/PLA blends with different amounts of Raschig

Rheology time sweep with complementary MW determination The influence of the amount of Raschig addition in kneaded samples was further studied by means of rheology and GPC. Time dependence of complex viscosity during 10 minutes time test can be seen in Fig. 3. All samples with Raschig showed approximately two times higher complex viscosity after kneading compared to the non-reactive blend. Complex viscosity of reactive samples was higher during the whole time test. Moreover, the slope of its decrease is lower than in the case of neat PHB/PLA sample. There are two possible explanations for this behaviour. This may indicate, that the reaction between polymers and Raschig continues during the test. Or that a reacted matrix of polymers and Raschig with different rheological properties was formed. However, there is no significant difference between individual reactive samples.

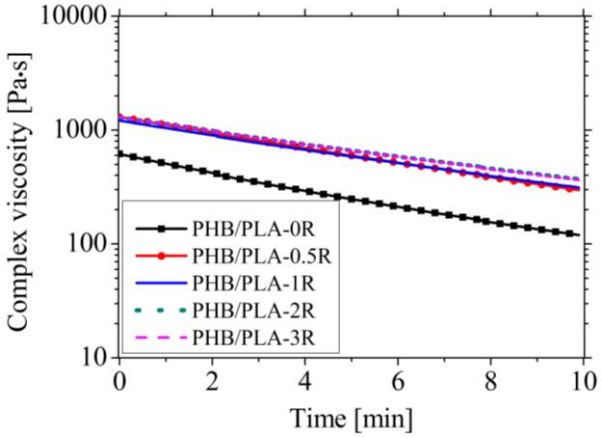


Fig. 3 Complex viscosity determined by time sweep of kneaded PHB/PLA samples

The results of GPC analysis are listed in Table 1 and visually presented in Fig. 4. Starting with 89 kg/mol, number average MW is linearly decreased with the addition of Raschig. Weight average MW is higher than neat PHB/PLA blend for all reactive samples and polydispersity index (PDI) is linearly increased with Raschig addition. The reason of this behaviour can be found in Fig. 4. In GPC curves of reactive samples, there is a fraction of MW of approximately 10^4 g/mol. As reported in Raschig data sheet, its M_w is $2–3 \cdot 10^4$ g/mol and therefore this GPC signal is attributed to the presence of non-reacted Raschig. This idea is supported by the fact that the area corresponding to the described low-molecular fraction is wider with increasing amount of Raschig (see cut-out of Fig. 4). Accordingly, number average molecular weight decreased as it is sensitive to the presence of low-molecular weight fraction and MW distribution became broader.

Table 1 GPC results of PHB/PLA samples with Raschig addition

Sample	PHB/PLA-0R	PHB/PLA-0.5R	PHB/PLA-1R	PHB/PLA-2R	PHB/PLA-3R
M_n (kg/mol)	89	86	78	69	53
M_w (kg/mol)	231	253	248	250	242
PDI	2.6	3.0	3.2	3.6	4.5

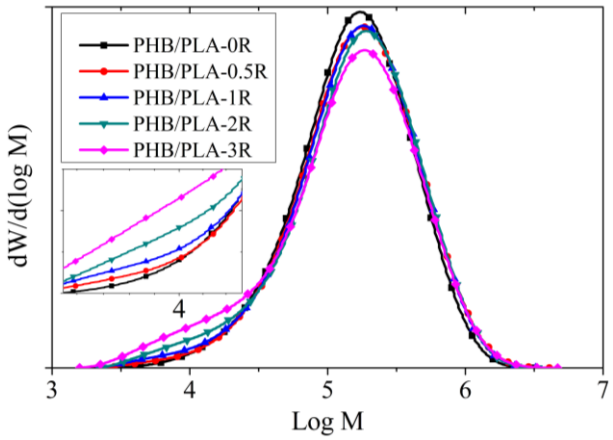


Fig. 4 GPC curves of kneaded PHB/PLA-Raschig samples

Both results showed the same trend as indicated during kneading. The addition of more than 0.5 % wt. did not have any further positive effect on blend molecular weight or complex viscosity of the melt. Greater amount of Raschig is not consumed during the reaction and is left in the mixture as demonstrated by GPC measurement.

Melt volume-flow index The thermo-mechanical degradation of PHB/PLA blends during processing was monitored by measurements of MVI. A clear difference between flow behaviour of non-stabilized and stabilized (0.5 % of Raschig) blends can be seen from the results in Table 2. Raschig samples from all extrusion cycles show lower MVI (higher viscosity) than corresponding non-stabilized samples. The influence of Raschig addition is especially significant in the case of sixth extrusion sample as its MVI is still lower than that of the first extrusion sample of PHB/PLA. Melt volume-flow index remains stable up to 3 extrusion cycles.

Table 2 The results of MVI measurement

	MVI [ml/10 min]					
Extrusion cycle	1.	2.	3.	4.	5.	6.
PHB/PLA	6.78	6.70	6.77	7.12	7.39	7.72
PHB/PLA-R	5.49	5.45	5.42	5.58	5.76	5.99

Summary

Instrumented kneading test of selected additives proved Raschig, an oligomeric carbodiimide, to be the only one reactive stabilizer towards both poly(3-hydroxy butyrate) and poly(lactic acid) as it led to the increase of melt torque during processing. Therefore, in the following experiments Raschig was used for stabilizing of PHB/PLA 70/30 w/w blend. With the addition of 0.5%wt. of Raschig, a maximum increase of melt torque during kneading compared to the non-stabilized PHB/PLA blend was attained. Furthermore, complex viscosity of stabilized blend was increased and rheology properties were not further improved with greater amount of Raschig. The effect of Raschig addition on molecular weight of the blends was more complex. Above 0.5%wt., unreacted residue of Raschig caused the number average molecular weight to drop significantly and polydispersity to rise. Weight average molecular showed the highest value for blend with 0.5 %wt. of Raschig. Processing stability of PHB/PLA blend during six multiple extrusion cycles was determined via melt volume-flow measurements. After six extrusion cycles, Raschig blend MVI is lower than that

of the non-stabilized after the first extrusion cycle. This confirms a suitability of using Raschig for stabilizing PHB/PLA blend during processing.

Acknowledgements

This work was supported by the FCH BUT-Sustainability and Development project No. LO1211 at Materials Research Centre and by the project Light functional materials based on natural polymers No. FCH-S-18-5448 of the Specific University Research Grant. Both provided by the Ministry of Education, Youth and Sports of the Czech Republic.

References

[1] A. Steinbüchel, M. Hofrichter, Biopolymers: Polyesters I, Wiley-VCH, Weinheim, 2002.

[2] E. Castro-Aguirre, F. Iñiguez-Franco, H. Samsudin, X. Fang, and R. Auras, Poly(lactic acid)—Mass production, processing, industrial applications, and end of life, Adv. Drug Deliv. Rev. 107 (2016) 333-366.

[3] W. Dong, P. Ma, S. Wang, Effect of partial crosslinking on morphology and properties of the poly(β-hydroxybutyrate)/poly(D,L-lactic acid) blends, Polym. Degrad. Stab. 98 (2013) 1549-1555.

[4] F.D. Kopinke, K. Mackenzie, Mechanistic aspects of the thermal degradation of poly(lactic acid) and poly(β-hydroxybutyric acid), J. Anal. Appl. Pyrolysis 40-41 (1997) 43-53.

[5] N. Najafi, M.C. Heuzey, P.J. Carreau, Crystallization behavior and morphology of polylactide and PLA/clay nanocomposites in the presence of chain extenders, Polym. Eng. Sci. 53 (2013) 1053-1064.

[6] M. Nerkar, J.A. Ramsay, B.A. Ramsay, M. Kontopoulou, Dramatic improvements in strain hardening and crystallization kinetics of PLA by simple reactive modification in the melt state, Macromol. Mater. Eng. 299 (2014) 1419-1424.

[7] A. Jaszkiewicz, A.K. Bledzki, R. van der Meer et. al, How does a chain-extended polylactide behave?, Polym. Bull. 71 (2014) 1675-1690.

[8] N. Najafi, M.C. Heuzey, P.J. Carreau, P.M. Wood-Adams. Control of thermal degradation of polylactide (PLA)-clay nanocomposites using chain extenders, Polym. Degrad. Stab. 97 (2012) 554-565.

[9] Y. Wang, Ch. Fu, Y. Luo, Ch. Ruan, Y. Zhang, Y. Fu. Melt synthesis and characterization of poly(L-lactic acid) chain linked by multifunctional epoxy compound, J. Wuhan. Univ. Technol. 25 (2010) 774-779.

[10] S. Pilla, S.G. Kim, G.K. Auer, S. Gong, Ch.B. Park, Microcellular extrusion-foaming of polylactide with chain-extender, Polym. Eng. Sci. 49 (2009) 1653-1660.

[11] L. Yang, X. Chen, X. Jing. Stabilization of poly(lactic acid) by polycarbodiimide, Polym. Degrad. Stab. 93 (2008) 1923-1929.

[12] J. Xie, R. Yang, Preparation and characterization of high-molecular-weight poly(L-lactic acid) by chain-extending reaction with phosphites, J. Appl. Polym. Sci. 124 (2012) 3963-3970.

[13] J. Liu, L. Lou, W. Yu, Long chain branching polylactide, Polymer 51 (2010) 5186-5197.

[14] C.R. Arza, P. Jannasch, P. Johansson et al, Effect of additives on the melt rheology and thermal degradation of poly[(R)-3-hydroxybutyric acid], J. Appl. Polym. Sci. 132 (2015).

[15] S.M. Martelli, M. Pietrini, E.G. Fernandes, E. Chiellini, Poly[(R)-3-hydroxy butyrate] melt processing, J. Polym. Environ. 21 (2013): 39-45.

Polymer Testing 92 (2020) 106880

Contents lists available at ScienceDirect

Polymer Testing

journal homepage: http://www.elsevier.com/locate/polytest

Recycling possibilities of bioplastics based on PLA/PHB blends

Roderik Plavec [a,*], Slávka Hlaváčiková [a], Leona Omaníková [a], Jozef Feranc [a], Zuzana Vanovčanová [a], Katarína Tomanová [a], Ján Bočkaj [a], Ján Kruželák [a], Elena Medlenová [a], Ivana Gálisová [a], Lucia Danišová [a], Radek Přikryl [b], Silvestr Figalla [b], Veronika Melčová [b], Pavel Alexy [a]

[a] Institute of Natural and Synthetic Polymers, Faculty of Chemical and Food Technology, Slovak University of Technology, Radlinského 9, 812 37, Bratislava, Slovak Republic

[b] Institute of Materials Science, Faculty of Chemistry, Brno University of Technology, Purkyňova 464/118, 612 00, Brno, Czech Republic

A B S T R A C T

The study is focused on modelling the evaluation of recyclability of the biodegradable blend using multiple extrusion of selected composition of PLA/PHB blend which had been more deeply studied before. It was shown that the multiple extrusion reduces viscosity of the tested blend due to multiple thermomechanical stresses and the material was partially degraded. Partial degradation was demonstrated by measuring of molecular characteristics. The degree of degradation of the tested material was determined with relatively high accuracy after creating a colour space/viscosity. Multiple processing and subsequent degradation of the tested material did not negatively affect thermal properties, as well as strength characteristics of the blend. It was concluded that the biodegradable polymer blend of the PLA/PHB type is suitable for multiple processing and material recycling can be applied for this type of bioplastics.

1. Introduction

In the last decades, modern living conditions have led to a dramatic increase of the consumption of polymers (especially plastics). This continued increase in the use of plastics has brought along an increase of amount of plastics in the waste stream motivating greater interest in recycling and reuse of plastics [1]. Nearly 448 million tons of plastics which are produced every year consume about 8% of the world's fossil resources. If the current strong increase in plastic consumption continues as expected, the plastic sector will use 20% of total crude oil consumption by 2050 [2]. Ecological aspects together, as well as rising raw material prices cause a higher utilization of renewable raw materials for a plastics production [3].

Logically, biodegradable materials from renewable sources are a very important option in achieving the goals of sustainable development and reducing negative environmental impact. The advantage of biodegradable materials from renewable sources is especially their biodegradation in biologically active environment and their contribution in lowering carbon footprint. Biodegradable plastics have a wide range of applications, mostly in packaging and agriculture, as well as, due to their biocompatibility, in the field of biocompatible biomaterials. The most common biodegradable plastics are polymer blends which contain thermoplastic starch (TPS) and aliphatic/aromatic polyesters such as polylactic acid (PLA), polycaprolactone (PCL), polybutylene adipate terephthalate (PBAT) and polyhydroxybutyrate (PHB) [4,5].

PLA, which benefits from origin from renewable sources and is biodegradable in the industrial compost environment, has attracted attention in the previous decades. It has become an economically viable commodity of plastics industry used for the production of common use products and packaging materials as trays, bottles or films [6,7].

The second biodegradable polymer in the studied polymer blend was polyhydroxybutyrate (PHB). Because PHB is relatively brittle, expensive and sensitive to thermal degradation, it is usually advantageous to use it in polymer blends to promote overall properties instead of producing it in pure form [8]. PHB can be plasticized with dioctyl phthalate, 1,4-cyclohexanedimethanol dibenzoate, tert-butylphenyl phosphate, PEG, triacetyl glycerol, tributyrin, dodecanol, lauric acid, trilaurin and low molecular weight poly (adipate) [9–11].

Both polymers PLA and PHB are biodegradable polyesters and are used in consumer products by several industries due to their biocompatibility and biodegradability. They have comparable thermal and mechanical properties as the properties of some common polymers, which has aroused considerable interest in investigating their physical and processing properties for potential applications [12–14]. PLA and PHB are known to have poor processing properties and are brittle at the room temperature [15]. PLA has better mechanical performance than

* Corresponding author. .
E-mail address: roderik.plavec@stuba.sk (R. Plavec).

https://doi.org/10.1016/j.polymertesting.2020.106880
Received 12 April 2020; Received in revised form 10 September 2020; Accepted 25 September 2020
Available online 29 September 2020
0142-9418/© 2020 Elsevier Ltd. This is an open access article under the CC BY-NC-ND license (http://creativecommons.org/licenses/by-nc-nd/4.0/).

PHB while PHB displays better barrier properties [16–18]. Several authors have proposed blending PLA and PHB as a strategy to modify unfavorable characteristics and improve properties of each virgin polymer [19–23].

Previous studies of PLA/PHB blends have shown that the miscibility between the two polymers depends on the molecular weight of the second component [12,24–26]. PHB is miscible with low molecular weight PLA in the melt throughout the composition range, while mixtures of PHB with high molecular weight PLA shows biphasic separation [24,25]. Similarly, the PLA component is miscible with low molecular weight PHB (Mw = 9400) in a melt with a PHB content of up to 50% by weight and is immiscible with high molecular weight PHB and commercial grade bacterial PHB [15,26]. The properties of PLA/PHB mixtures also depend on the composition, chemical or physical crosslinking and processing conditions. Zhang et al. [16] investigated the morphology, structure, crystallization, thermal properties, mechanical properties and biodegradation of PLA/PHB mixtures, which were prepared by melt mixing. The PLA/PHB blend in ratio of components 75/25 showed improved mechanical properties, thermal decomposition temperature and the presence of some interactions. In general, PLA/PHB mixtures exhibit better barrier properties than PLA [17,27], but still relatively low strain at break values (improvements lower than 1%) [19,22]. To overcome this drawback, the incorporation of plasticizers have been proposed, resulting in a decrease in glass transition temperature (Tg), a better material processability and an improvement in its flexibility [17,19,28,29]. For example, elongation at break values (εb) reported for PLA/PHB (75:25 w/w) blended with different plasticizers are in the range of 6%–15% for poly (ethylene glycol) (PEG) [17], D-limonene [22] and Lapol 108 [19], and 90% for acetyl tributyl citrate (ATBC) [28]. In addition, acetyl tributyl citrate (ATBC) have also proved to be effective in accelerating the disintegration process under composting conditions [28]. The patent EP2710076B1 [30] shows that blending PLA and PHB in a suitable ratio with adding a suitable type of plasticizer improve mechanical properties and even increase flexibility of PLA/PHB blends. The presence of a plasticizer suppresses the degradation induced by thermomechanical stress during processing of studied polymer blend. Yang et al. [31] focused on the use of degraded PHB as a plasticizer for the production of PLA-based polymers by extrusion. The results obtained were very promising because the inoculated PLA with 20% (w/w) of PHB oligomers showed a high ductility and toughness. In addition, the new polymeric composition had an elongation at break 66 times higher than pure PLA. Another way to improve the compatibility of the PLA/PHB blends is to use a compatibilizer. These compatibilizers include glycidyl methacrylate (GMA) [29,32] or poly (vinyl acetate) (PVAc) [33–36]. PLA/PHB blend has various applications; however, some materials should be added to the blends to endow the desired properties.

PLA/PHB blends are biodegradable materials commonly investigated for food packaging applications [22]. One of the potential application fields of these materials is as a film. It has been reported that 25 wt% of PHB produced a reinforcement effect on PLA matrix [16]. Arrieta et al. in different studies [22,37–39] investigated the behavior of PLA/PHB blends with various plasticizers for food packaging applications. They showed that natural terpene D-limonene (LIM) as plasticizer raised the crystallinity of PLA and resulted in flexible films. They also showed that PHB played a reinforcing role in the PLA matrix and hence improved the oxygen barrier properties and surface water resistance. Similar results were reported on the effect of ATBC on the mechanical and disintegration behavior of electrospun fibers of PLA/PHB blends. Electrospun nanofibers of PLA/PHB blends were successfully developed by Nicosia et al. [40] for air filtration and antibacterial applications. The PHB/PLA composite due to its high mechanical strength had been recommended also for medical implantation [41]. PLA blends with a copolymer of PHB named poly (3-hydroxybutyrateco-4-hydroxybutyrate) (P (3HB-*co*-4HB)) were studied in Refs. [42–44] for packaging applications. The blends were found to be immiscible, but of high compatibility. The crystallization rate of PLA, the strain at break and biodegradability were improved in the presence of P (3HB-co-4HB). PLA/PHA blends could be helpful compostable materials for long-term agricultural applications, including row covers and landscape fabrics [45]. The blends PLA/PHB for their improved utility properties and improved biodegradability were also investigated for using in additive manufacturing - 3D printing [46,47].

Broniarz et al. [48] proposed that a blend composed of 70 wt%. PLA with 30 wt% PHB could be used as an effective candidate for the gel polymer electrolyte used in Li-ion battery applications since the membrane fabricated from PLA/PHB blend exhibited attractive merits, such as high porosity, high conductivity, and high electrochemical stability.

Since PLA/PHB have gain considerably interesting during the last decade, it is interesting to recycle these widely applied formulations.

However, biodegradable plastics from renewable resources also exhibit number of disadvantages such as brittleness, degradation during processing but also their impossibility of material recycling with commonly used synthetic plastics. For this reason, there is currently very little scientific work on material recycling of biodegradable polymer materials. However, in view of circular economy in terms of environmental protection, it is desirable to explore a possibility of re-using such materials through material recycling.

Various plastic waste management strategies have been studied, ranging from reuse and recycling (Mechanical, Chemical, Feedstock) to thermolysis/recovery processes [49–51]. From the point of view of energy and the environment, the research works [52–55] emphasized that a mechanical recycling strategy is the most appropriate plastic waste management option for relatively clean and homogeneous plastic and bioplastic waste in comparison with landfill or incineration alternatives.

Mechanical recycling allows directly recovery of plastic solid waste for reuse in the production of new plastic products [49,51,53,56], and can use traditional technologies and commonly used processing machines such as conventional extruders and injection moulding machines.

Due to the fact that the process results in different degrees of degradation of the polymer, mechanical recycling is limited by the number of repeated processing cycles [57]. Material recycling has been commonly used for many years in the management of plastic waste resulting from the industrial processing of polymeric materials [58,59]. Also according to European strategy for plastics in circular economy [60] by 2030 all plastic packaging placed on the EU market should be either reusable or able to be recycled in a cost-effective manner and more than half of all plastics waste generated in Europe should be recycled. According to this strategy [60] also innovative materials and alternative feedstock for plastics production should be developed and used where evidence clearly shows that they are more sustainable compared to the non-renewable alternatives. The degradation of the polymer in the extruder is one of the main factors that can adversely affect the material quality of plastics during material recycling. The term deterioration of material quality means processing deterioration, deterioration of mechanical or thermal properties of the material, as well as electrical and optical properties or appearance and aesthetic properties of the material [61,62]. Polymer degradation during processing also reduces the productivity of re-used material due to viscosity differences mixing recycled and virgin polymer to receive applicable products. Degradation is affected by many factors such as shear stress, temperature, humidity, pH, presence of oxygen, UV radiation and presence of other processing additives (for example stabilizers) [63,64]. The growing amount of generated plastic waste, legislative requirements and increased interest of people in environmental protection are the reason to use plastics in the highest number of “living” cycles. Therefore, it is very important to recognize the effect of multiple extrusion of different polymer materials on the final properties of these materials. Several publications have been published on multiple uses of conventional synthetic plastics, such as PP, PE or PVC [65–72], where changes in the final properties of materials based on multiple material extrusion are described. However, until now only few scientific works have been

devoted to describing changes in properties of biodegradable materials from renewable sources during multiple processing of these materials in experimental way [73,74].

PLA is one of the most studied bioplastics related to recyclability. PLA can biodegrade under certain conditions, such as in the presence of oxygen and moisture [75]. Although PLA is biodegradable, which significantly reduces the negative impact of PLA waste on the environment, it is important to recycle the material and investigate changes in the properties of PLA during its multiple processing. Multiple extrusion of PLA up to 10 times was investigated by Żenkiewicz et al. [76] using a twin-screw extruder followed by laboratory injection moulding machine, for preparation of the test samples. The tensile strength values of PLA did not significantly depend on the number of extrusion cycles. Another study [77] on PLA reprocessing (containing 92% L-lactide and 8% D-lactide) showed that only the tensile modulus remains constant with thermomechanical cycles of up to seven injection mouldings. Conversely, stress and tensile stress, modulus, hardness and rheological factors generally show reduced values. The viscosity of PLA decreases significantly (from 3960 to 713 Pa s) after only one injection cycle. The mechanical properties of recycled PLA have become too poor for the industrial use of the polymer.

In Badia work [78], the influence of multiple thermomechanical processing on the structure and properties of the amorphous type of PLA was studied. Due to the multiple processing of amorphous PLA the molecular weight in this case as well and the studied properties of the polymer deteriorate decreased, especially after the 2nd processing transition in the case of injection moulding.

In Agüeo's work [79], it was found that the effect of multiple extrusion of PLA leads mainly to a decrease in the elongation at break and also the impact strength. PLA is sensitive to the hydrolysis of ester bonds, but during extrusion in the first three processing cycles no significant degradation of the material occurs and PLA can be recycled in the three cycles of extrusion. The Rivas article [80] studied the properties of PHB after multiple extrusion (3 cycles of recycling). During reprocessing, the mechanical properties deteriorated significantly, when the tensile strength of the material after triple extrusion reached less than 50% of the original value of the tensile strength.

The mixture of copolymer polyhydroxybutyrate/polyhydroxyvalerate (PHBV) and PLA has been investigated for recycling by extrusion and injection moulding [81]. Compared to the PHBV, the mixture of PHBV and PLA was more stable in thermomechanical degradation where mechanical properties (tensile strength, elongation at break and impact strength) remained more or less stable even after six cycles of reprocessing. Preservation of mechanical properties has revealed the stabilizing effect of PLA in PHBV/PLA blends, which opens up a promising opportunity to expand polyhydroxyalkanoates recycling and applications.

This study describes the effect of multiple extrusion on final mechanical, thermal and optical properties, as well as processing stability of commercial available biodegradable polymer blends under trademark NONOILEN® based on PLA and PHB. NONOILEN® represents modern plastic material fulfilling all ecological requirements based on main circular economy principles. It is polymeric blend which combines various benefits of basic components and eliminate their weaknesses. NONOILEN® consists of PLA, PHB, plasticizers and eventually nucleating agent, antiblocking agent or other additives according to specifics of given applications. Mainly esters of citric acid are applied in role of plasticizers or some oligomeric esters of di- or more carboxylic acids, preferably esters of adipic or citric acid. All these plasticizers can be produced based on renewable materials and they are ecologically safe without any negative effect on human or animal health.

Table 1
Basic properties of NONOILEN® IM 3056–2.

Parameter	Unit	Value
MFI	g/10 min at 2,16 kg, 180 °C	5.8
Density	g/cm^3	1.2
Tensile strength at break	MPa	49.1
Elongation at break	%	2.8

Note: The results assigned to the zero processing cycle and the results at the extrusion time 0 correspond to the results of the virgin polymer mixture NONOILEN® IM 3056–2 (with PLA/PHB ratio = 45/55).

2. Experimental

2.1. Materials

NONOILEN® IM 3056–2 is an injection moulding grade of PLA/PHB based blend produced by Panara Ltd. Slovakia. PLA/PHB ratio in the blend was 45/55 by weight. NONOILEN® IM 3056–2 was used as delivered.

The basic properties of polymer blend NONOILEN® IM 3056–2 are described in Table 1.

2.2. Methods of samples preparation and experiments

2.2.1. Multiple extrusion

Tested biodegradable polymer blend was processed by single-screw extruder Plasticorder Brabender equipped with a screw of 19 mm in diameter, L/D = 25, compression ratio 1:3. Head of extruder was equipped with the circular cross section die nozzle, diameter 2 mm. Temperature profile of the extruder was: 170-190-185-180 °C in direction from hopper to head and speed of screw was 55 min$^{-1.}$ Material retention time in extruder of each cycle was 58 s. The strand cooled by air on belt was taken for evaluating of measured properties from each extrusion cycle. Diameter of strand was 1.8 mm. The final number of testing cycles (extrusions) was 11, and thermomechanical stability, mechanical and thermophysical properties and colorimetric changes were tested after each processing cycle.

2.2.2. Processing (thermomechanical) stability

Thermomechanical stability was measured using the oscillation rheometer RPA 2000 from Alpha Technologies. The timed test was used to determine processing stability of polymer blend according to the method described in the paper [82]. The angle of strain was 60° and frequency was 50 cpm. The time period of all tests in each cycle was 10 min at the testing temperature 180 °C. For the correct evaluation of temperature effect on the rate of polymer degradation based on the decreasing of complex viscosity, the elimination of differences of initial viscosity was done by recalculation of complex viscosity to the values of relative complex viscosity using the following formula:

$$\eta^*_{rel}(t) = \eta^*(t)/\eta^*_0 \quad (1)$$

where $\eta^*_{rel}(t)$ is the relative complex viscosity at the time t, $\eta^*(t)$ is the complex viscosity at the time t and η^*_0 is initial complex viscosity at the start of test.

2.2.3. Mechanical properties measurement

Mechanical properties were measured by using the prepared strands from each extrusion cycle. The strands had a circular cross-section with a diameter of 2,0 mm. Tensile strength at break (σ_b) and the elongation at break (ε_b) were determined according to ISO 527 standard by the Zwick machine at cross-head speed 1 mm/min in the deformation range of 0–3%. When deformation reaches value 3% of elongation, the cross-head speed increased up to 50 mm/min.

Table 2
Conditions for DSC measurements.

		Ramp	Set temperature (°C)	Time (min)
1.	Conditioning	isothermal	0	1
2.	Heating	10 °C/min.	200	20
3.	Conditioning	isothermal	200	1

2.2.4. Thermophysical properties measurement

The differential scanning calorimetry (DSC) was used for the determination of basic thermophysical properties such as glass transition temperature, crystallization temperature and melting temperature of samples after 0; 2; 4; 6; 8; 10 and 11 cycles were measured. The conditions for DSC measurements are summarized in Table 2.

2.2.5. Measurements of colour changes

Colour of tested samples was measured on prepared strands according to the CIE Lab colour scale relative to the standard illuminant D65 over a white background by the reflection spectrophotometer (Techkon SpectroDens). The aperture diameter of the measuring port was 3 mm. Illuminating and viewing selected configuration of this instrument was CIE diffuse/10° geometry and the CIE 1964 supplementary standard colorimetric observer. Colour difference was calculated using formula [2]:

$$\Delta E^*_{a,b} = \sqrt{(\Delta L^*)^2 + (\Delta a^*)^2 + (\Delta b^*)^2} \quad (2)$$

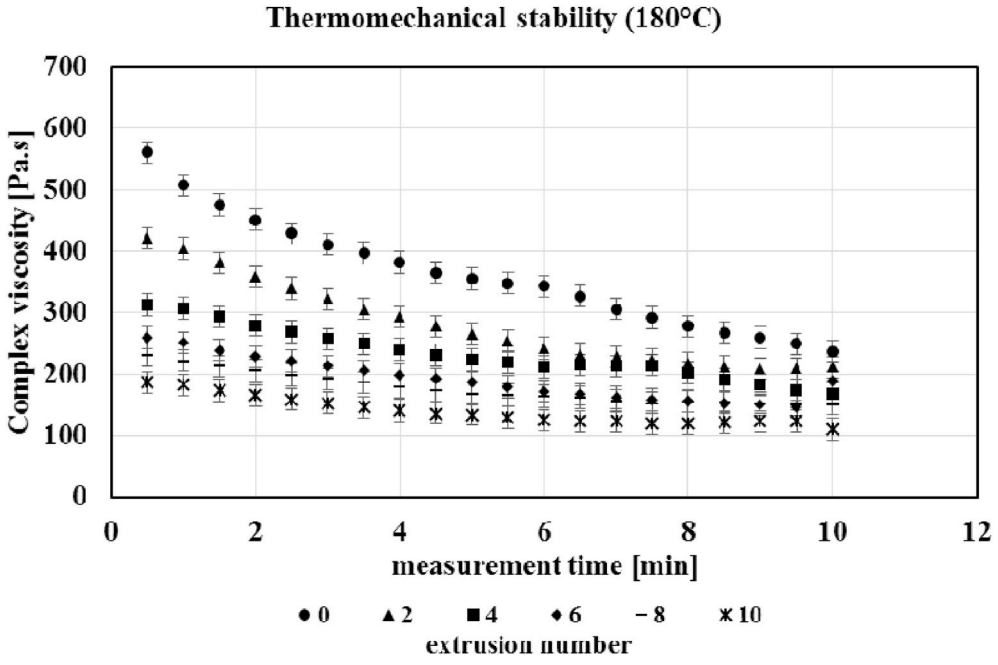


Fig. 1. Dependency of complex viscosity on measurement time for each processing cycle.

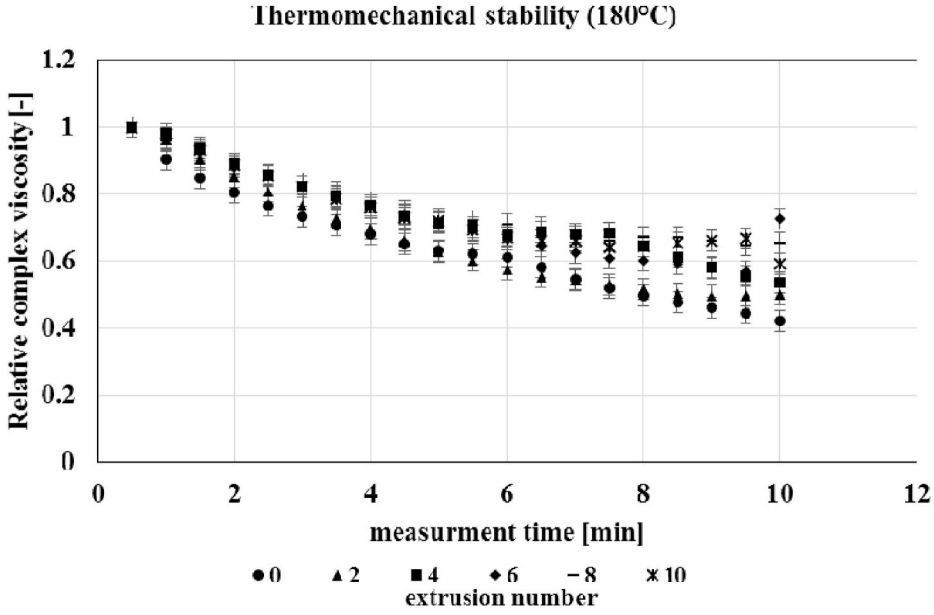


Fig. 2. Dependency of relative complex viscosity on measurement time for each processing cycle.

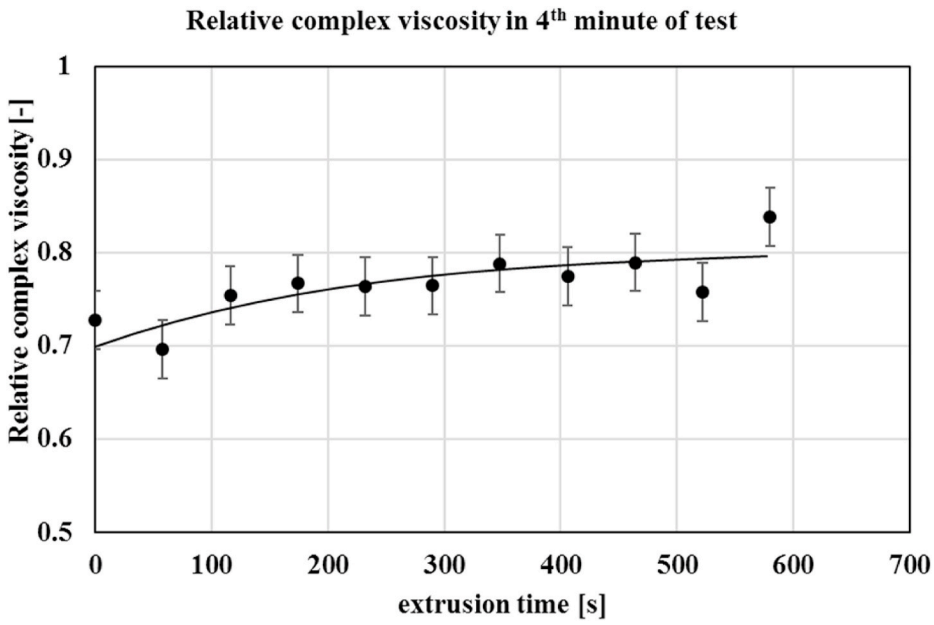


Fig. 3. Dependency of relative complex viscosity on extrusion time of blend at the 4th minute of the test.

2.3. Molecular characteristics

Molar mass of the tested material was determined by gel permeation chromatography. Measurements were performed by the Agilent Technologies 1100 Series instrument equipped with isocratic pump, and an autosampler. PL gel 5 μm mixed C column was tempered to 30 °C with chloroform as the eluent at the flow rate 1 ml/min. Linear polystyrene standards with narrow distribution were used to gain the calibration curve (10 points in calibration). Instrument was equipped with refractive index detector. 5 mg of sample was used for the measurement.

3. Results and discussion

3.1. Processing stability

It is well known that biopolyesters, such as PLA and especially PHB, are very sensitive to degradation during thermomechanical loading, which negatively affects processing properties by rapid viscosity decreasing. This viscosity decrease causes deterioration of the mechanical properties and many other properties of polymeric materials containing these polymers. The effect of multiple extrusion on degradation of polymers is usually described via evaluating of melt flow index (MFI) changes. However, by this method it is not possible to obtain accurate viscosity values of the material at a given time. Also, the MFI measurement of various processing processes does not include material degradation that occurs directly during measurement, alternatively at the filling of the MFI device or at melting of polymeric material before MFI measuring.

For this reason, the oscillation rheometry measurement was chosen for evaluation of processing stability according to the conditions which are described in Ref. [82]. It can be seen from Fig. 1 that due to the multiple treatment of the tested material by extrusion, the absolute values of complex viscosity decrease. There is also a contribution to the decrease in viscosity due to the test time during which the sample is subjected to thermomechanical stress in the oscillating field of the rheometer. Since all factors affecting viscosity are constant during the test, it can be assumed that the decrease in complex viscosity is due to the decrease in molar mass, indicating material degradation. To compare the rate of degradation of the material based on a different number of processing cycles in the extruder, the parameter of relative complex viscosity was introduced according to equation [1]. This eliminates viscosity differences at the beginning of the test. Fig. 2 shows the dependence of relative complex viscosity on the retention time of the sample in the rheometer under oscillation stress as a function of the number of processing cycles. As can be seen from Figs. 1 and 2, the absolute values of viscosity logically decrease with number of processing cycles. Relative scale of complex viscosity shows that the rate of degradation slowly decreases with the number of processing cycles. It shows that the main degradation process is significant mainly in the first cycles. On the other hand, the latest extrusion cycle shows a small increase in relative viscosity during the oscillation test similarly to the absolute values of viscosity in Fig. 1 (0, 2 and 4 cycles). It can be explained by possible reaction between blend components. This phenomenon was also observed in the article [81].

The change in degradation rate after multiple processing of Nonoilen in a single screw extruder is better visible if the relative complex viscosity is correlated to the retention time in the extruder. In Fig. 3 the relative complex viscosity in the 4th minute of the timed test is shown as a dependency on total processing time in the extruder. It can be seen that the rate of degradation of the material exhibits only marginal changes which are covered by experimental error. It means that the rate of degradation practically does not depend on the time of thermomechanical loading during extrusion in a single screw. All samples after 4 min in the oscillating rheometer reach approximately from 70% to 80% of their initial viscosity.

It can be stated that the formation of a polymer blend of the PLA/PHB type had in our case a very positive effect on the processing stability of biodegradable polymer blends in comparison with the PLA or PHB polymers themselves, where already at the 3rd (PHB) resp. 5th (PLA) during the processing transition there is such a large decrease in viscosity due to degradation that the material cannot be subsequently processed [78–80]. The positive effect of blending PLA/PHAs on processing stability was also demonstrated in the article [81], where during 6 processing passes the decrease in viscosity compared to the non-recycled blend was minimal.

3.2. Molecular characteristics

Molecular weight as well as distribution of molecular weight were evaluated based on GPC measurements. The distribution curves for 0, 3,

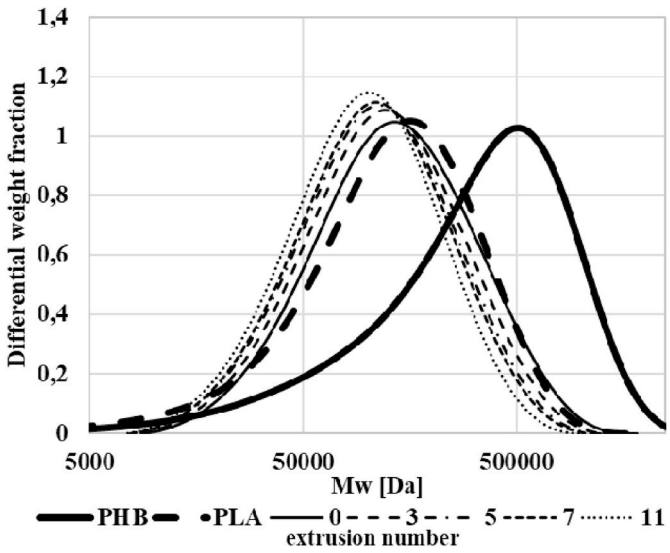


Fig. 4. Distribution of molar mass in dependency on various processing passes.

5, 7 and 11 passing through the extruder are shown in Fig. 4. It is interesting that Nonoilen with ratio of PLA/PHB 45/55 exhibits smooth distribution curve and does not exhibit multiple maxima corresponding to original polymers. GPC measurements of PLA and PHB were realised with the same polymers which were used for Nonoilen blend production. Both PLA and PHB were kindly delivered by Panara company. With the increasing of the pass number the maximum of distribution curves is shifted to lower molecular weights due to a partial degradation of components. Figs. 5 and 6 show very good correlation between extrusion time, molecular weight and complex viscosity. It means, that oscillation rheometry method which was used for processing degradation study reflects changes in molecular weight very well.

3.3. Colour changes

Degradation process during processing of polymers usually also causes changes in colour. The colour changes as results of multiple processing of Nonoilen were evaluated. The dependence of ΔE parameter on cumulative processing time which represents the total chromatic declination from the white standard is shown in Fig. 7 and the dependency of L coordinate on the cumulative extrusion time is shown in Fig. 8. It is clearly seen that the degradation of the tested grade of Nonoilen directly affects the colour difference (ΔE) when ΔE increases with the extrusion time. The decreasing of the L coordinate confirms that the samples after longer extrusion time become darker. Fig. 9 shows the colour change of the material. It is seen that the material darkens with a higher extrusion number. The results of identifying the colour changes during the processing of Nonoilen PLA/PHB biodegradable and bio-based blend simultaneously with the previous results show that also colour changes very well reflect degradation process and they are in very good correlation with viscosity and molecular mass of the tested polymeric material.

Colour changes were also investigated during multiple processing of amorphous type of PLA [79], where also due to multiple processing there is a decrease in lightness and an increase in colour difference of the tested samples.

3.4. Thermophysical properties

Thermal properties were measured and evaluated using DSC measurements – Fig. 10. Based on evaluation of dependency of the thermal properties on extrusion time it can be stated that the extrusion time has a

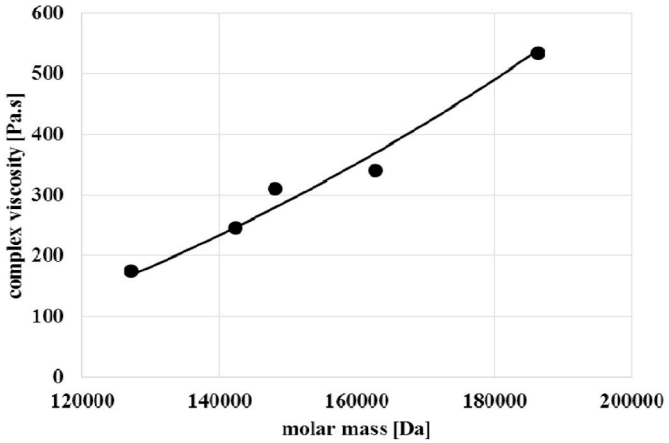


Fig. 6. Dependency of complex viscosity on the 4th minute of oscillation test on initial molecular weight of the tested sample.

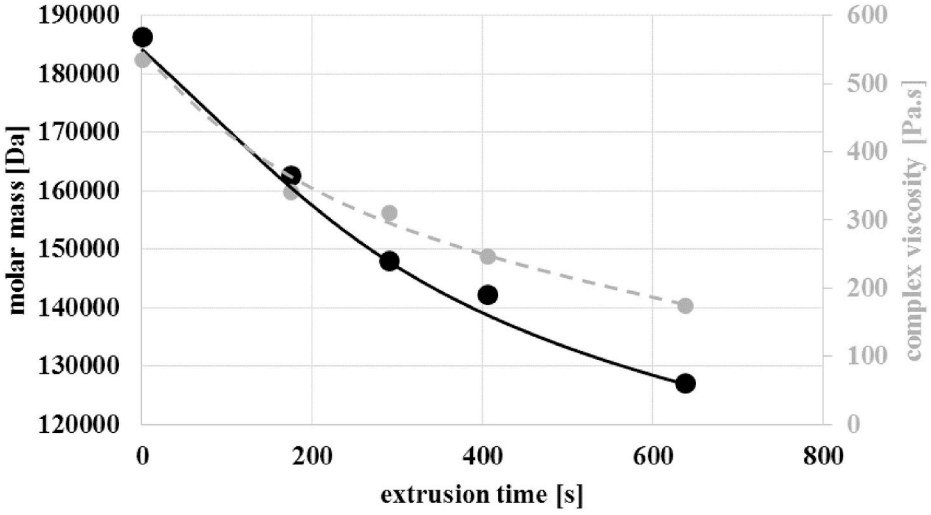


Fig. 5. Dependency of molar mass and complex viscosity on extrusion time of material.

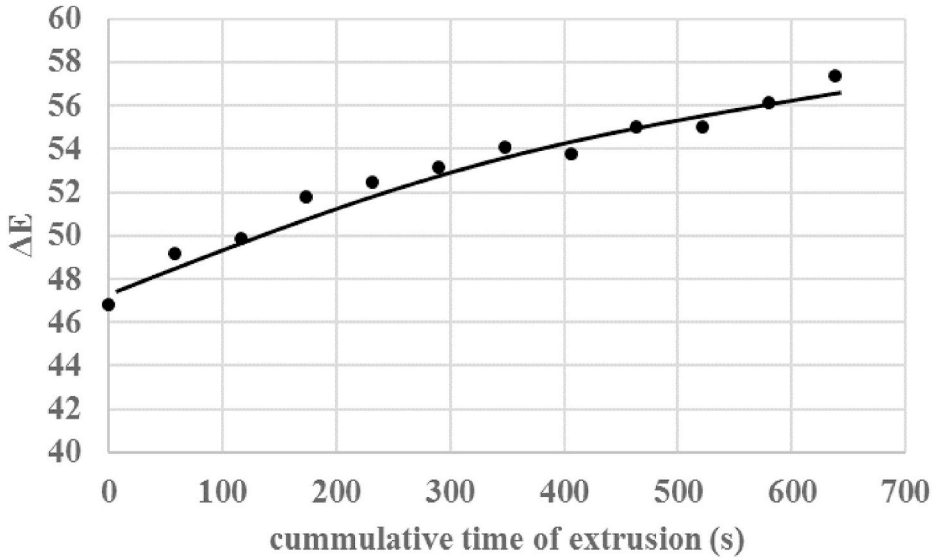


Fig. 7. Dependency of colour change on complex viscosity of the studied blend.

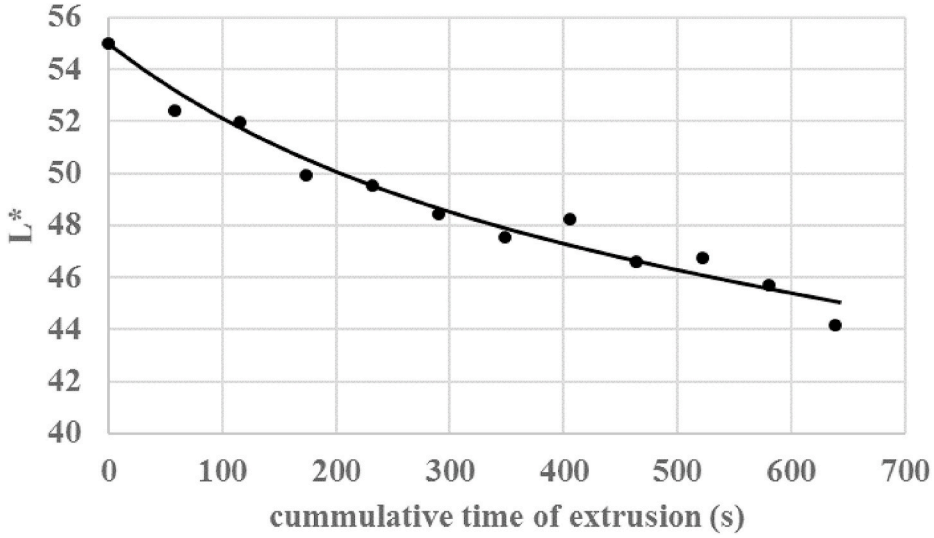


Fig. 8. Dependency of lightness on time of extrusion of the studied blend.

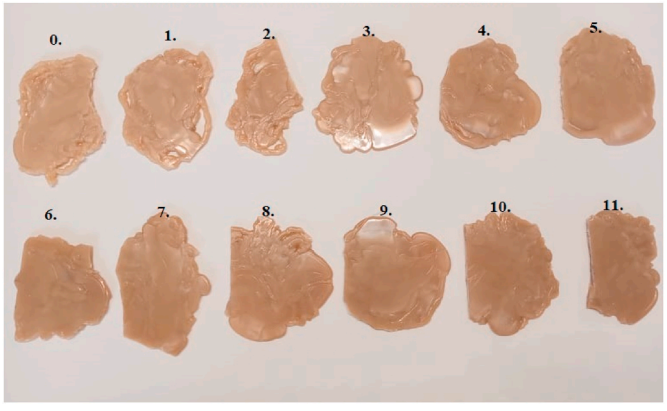


Fig. 9. Colour changes of material after different processing cycles (0.-11.).

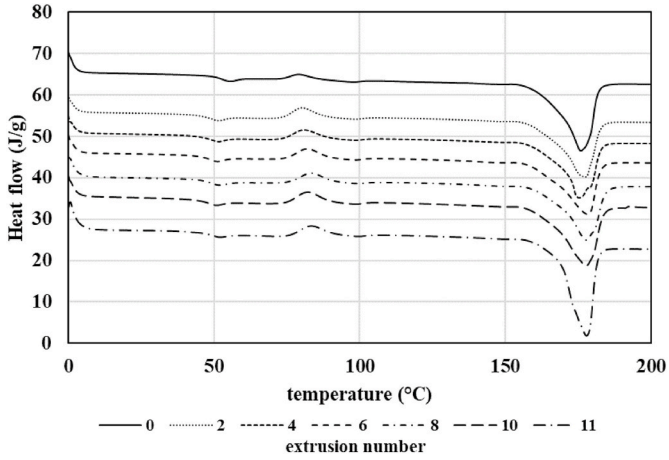


Fig. 10. DSC thermograms of each processing cycle.

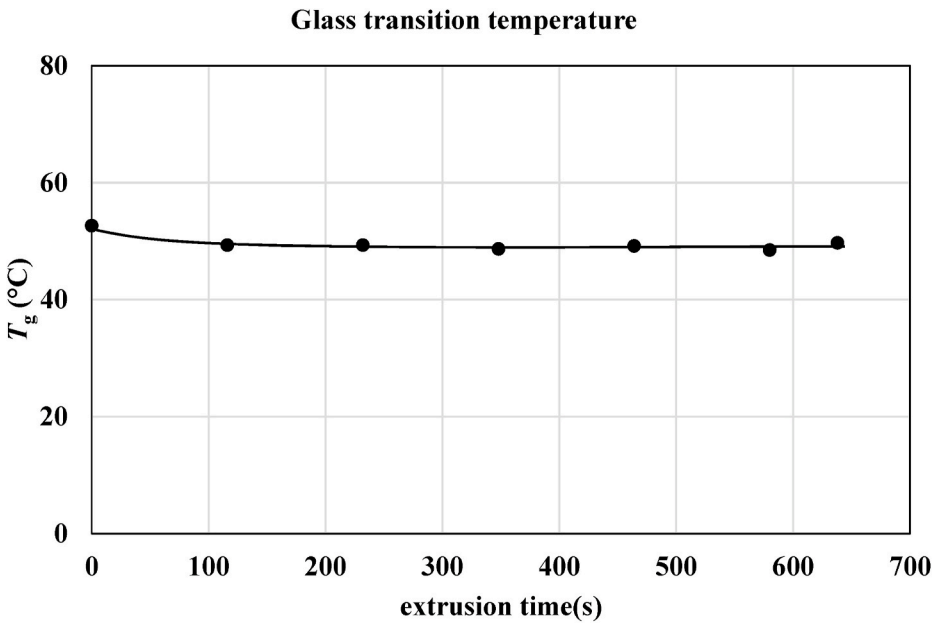


Fig. 11. Dependency of glass transition temperature on extrusion time.

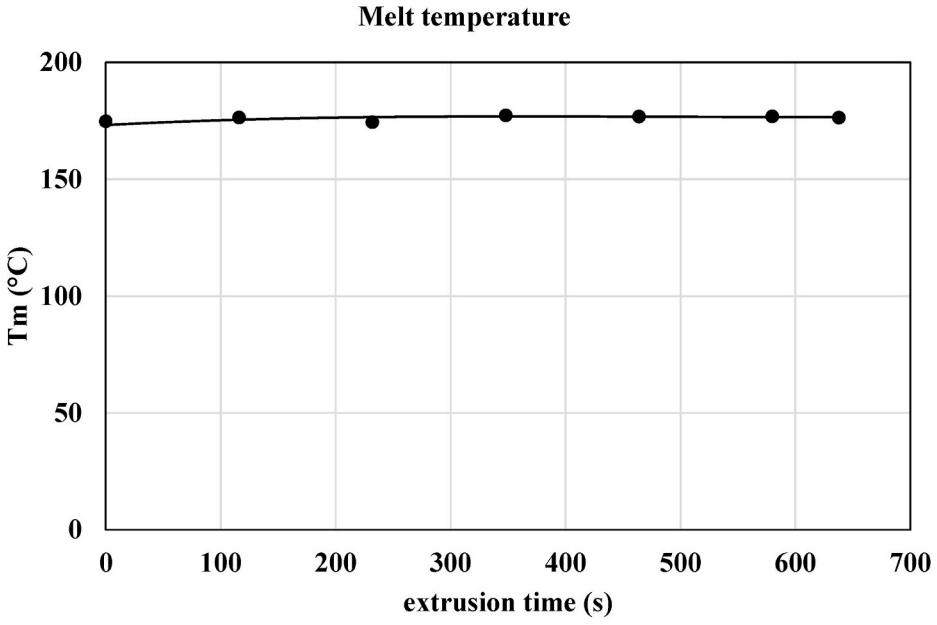


Fig. 12. Dependency of melt temperature on extrusion time.

minimal influence on thermal properties of the material as the difference between glass transition temperature of the individual materials after multiple processing does not exceed 3 °C. The dependency of glass transition temperature on extrusion time is visible in Fig. 11, where the material without any processing cycle has the highest value of T_g (52.5 °C). After processing the glass transition, the temperature of the material decreases to the value about 49.5 °C. This result also corresponds to scientific works [78,79,81], where with multiple processing of the PLA itself resp. Of the PLA/PHBV polymer blend, there is only a minimal effect on the Tg of the tested material. Also, the melting point of the crystallites and the melting enthalpy of the crystallites are practically without changes in dependency on the extrusion time (Figs. 12 and 13). In this case, it should be noted that in other scientific works that have dealt with multiple thermomechanical processing of PLA and PLA/PHAs [77–79,81], the enthalpy of crystallization and enthalpy of melting of crystallites increase due to multiple processing and thus the crystallinity of the polymer or polymer blend is increasing. We suppose that this phenomenon is caused by a significant decrease in viscosity, which the authors report, and thus by better mobility of polymer macromolecules compared to the polymer blends studied by us. Interestingly, the studied biodegradable polymer blend shows only one crystallite melting peak. From DSC results, it can be predicted that, despite partial degradation of the material during multiple processing, there is no significant change in thermal properties and no significant change in crystallinity of the material. This may indicate that due to the multiple processing, the barrier properties and strength characteristics

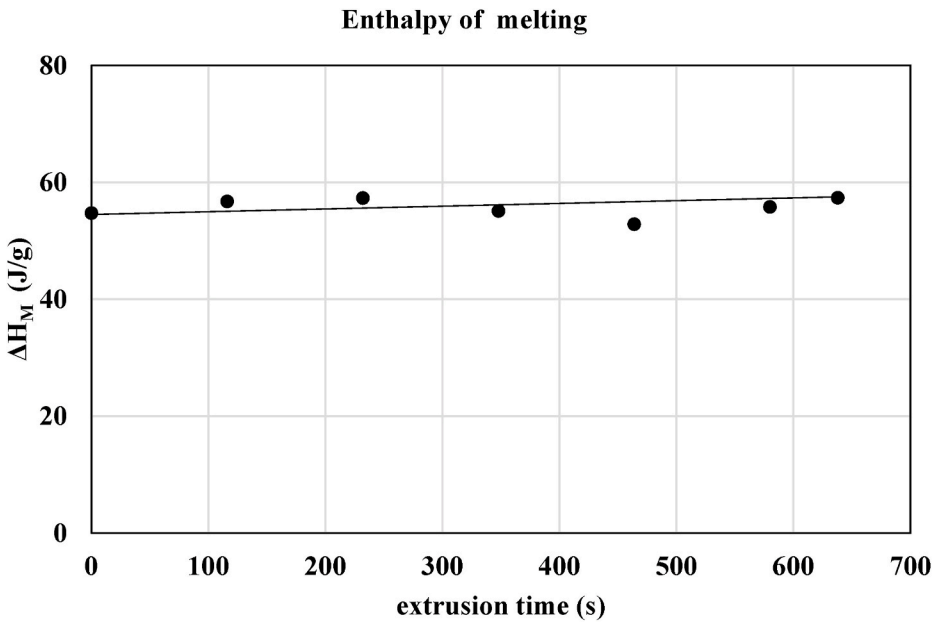


Fig. 13. Dependency of melting enthalpy on extrusion time.

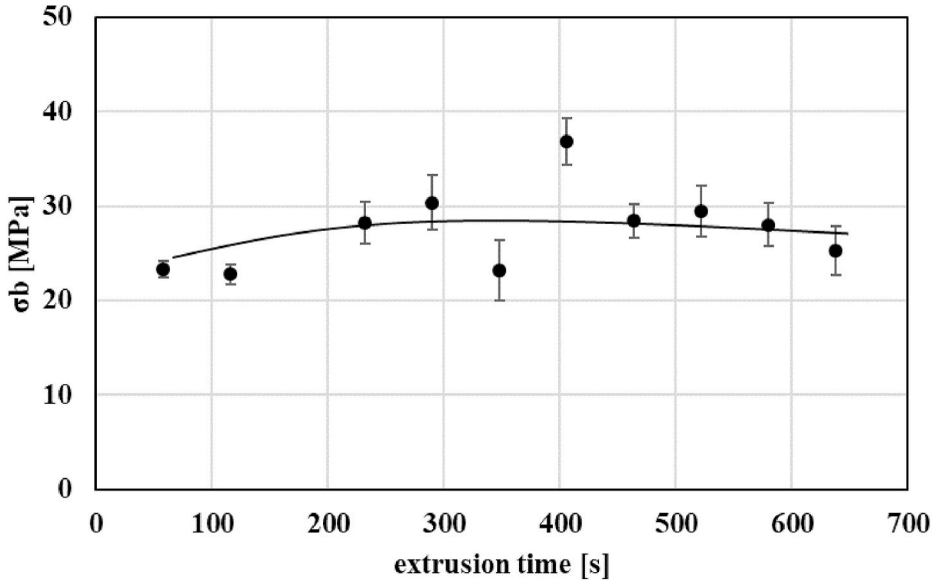


Fig. 14. The dependency of strength at break on extrusion time of the tested blend.

of the test material will not deteriorate.

3.5. Mechanical properties

Evaluation of tensile strength and elongation at break in dependency on cumulative extrusion time shows, that tensile strength varied between 23 and 35 MPA approx. (Fig. 14). Elongation at break falls down only in the first stages of extrusion time and after 200 s no changes can be observed on graph presented in Fig. 15. During multiple extrusion process, the tested blend exhibited relatively stable values of tensile strength of break in the range from 23 to 35 MPa. Decreasing of the relative elongation at break values can be connected also with material degradation and with reduction of polymer chains length.

Even in this case, it can be stated that the PLA/PHB mixture is more suitable for multiple processing compared to the PLA or PHB polymers themselves, because in the case of PHB [80] the tensile strength decreases by more than 50% after only three processing cycles compared to the initial value and in the case of PLA after the 7th processing transition, the values of tensile strength decrease from the initial value of 65 MPa to the value of 25 MPa [77]. However, it should be emphasized that in this case it was a multiple injection of material, where higher shear rate affects on the material. With multiple extrusion of PLA, the values of strain at break decrease by about 10% from the initial strain at break values (from 55 MPa to 50 MPa) after the 6th processing cycle [79]. In our case, the decrease in strength did not occur even after the 11th processing cycle.

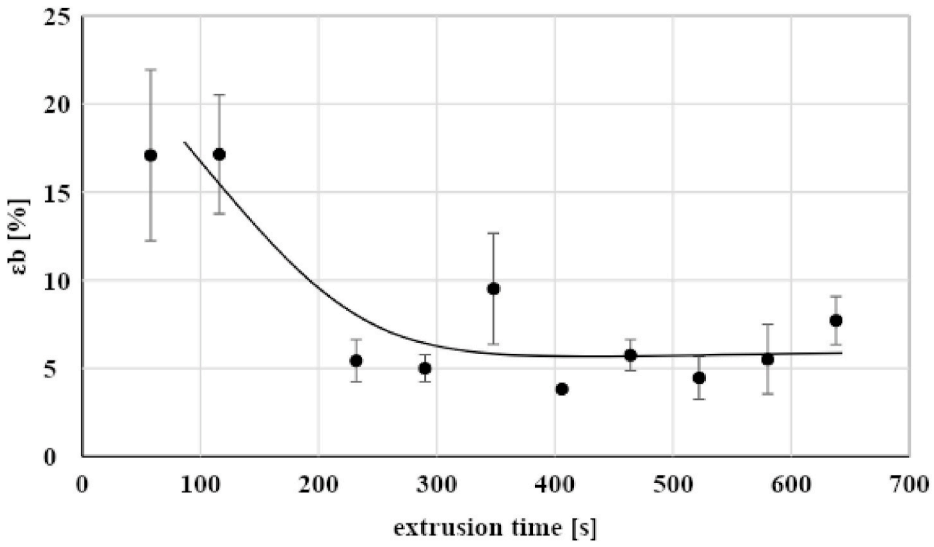


Fig. 15. Dependency of elongation at break on extrusion time of the tested blend.

4. Conclusion

Influence of multiple extrusion as a model for material recycling of biodegradable PLA/PHB blend on basic blend properties was studied. Increased extrusion (processing) time causes reducing of viscosity of the tested blend. On the other hand, rate of degradation did not increase due to longer extrusion time. Decreasing of molecular weight was confirmed using GPC. The average molecular weight as well as polydispersity index decrease as an effect of multiple reprocessing of the blend. Degradation of the material was also reflected in the change of material colour, which was determined by the CIE Lab colour space coordinates (ΔE, L *). The degree of degradation of the tested material can be determined with relatively high accuracy after creating a colour space/complex viscosity curve using this method. We consider a positive result that the multiple processing and subsequent degradation of the tested material did not negatively affect thermal properties of the blend. Increased diffusion of the plasticizer from the polymer matrix did not appear and there was not observed increasing glass transition temperature or crystallite melting point. Interestingly, the mixture exhibited the character of a miscible mixture at a molecular level, assuming from the presence of only one melting peak of the crystallites. Also, multiple processing did not affect negatively the strength characteristics of the blend, even though there was a slight increase in tear strength. Conversely, the flexibility of the material decreased by multiple processing, but in general, this parameter in absolute values was close to the initial values of the original blend. To the decrease of elongation at break occurs just after 2nd processing cycle. It follows that until the 2nd processing cycle, the material retains its original user properties, while until this time no changes were observed in the processing of the polymeric material, which would be caused by a decrease in viscosity due to degradation. Despite the decrease in elongation at break, it can be stated that the studied mixtures retained similar values of mechanical properties as the non-recycled PLA/PHA polymer blends studied in the articles [16,18,83,84]. Recycled Nonoilen blends could be used in the applications that do not require high material flexibility.

From the results shown in this work, it can be stated that compared to PLA and PHB polymers themselves, the PLA/PHB blend has better resistance against degradation at multiple thermomechanical stress, which has a positive effect on the processing process and mechanical properties of the tested material. It should be emphasized that in the case of the tested polymer blend PLA/PHB we were able to perform 11 processing passes without significant changes of studied properties, especially of rheological and mechanical properties of the material, unlike PHB itself, where the authors were able to perform 3 processing passes [80] and in the case of PLA, where the authors prepared a maximum of 10 processing passes [77].

It can be concluded that the biodegradable polymer blend of the PLA/PHB type is suitable for material recycling.

CRediT authorship contribution statement

Roderik Plavec: Conceptualization, Writing - original draft, Methodology. **Slávka Hlaváčiková:** Investigation, Writing - review & editing. **Leona Omaníková:** Methodology, Investigation. **Jozef Feranc:** Resources. **Zuzana Vanovčanová:** Visualization. **Katarína Tomanová:** Investigation. **Ján Bočkaj:** Resources. **Ján Kruželák:** Formal analysis. **Elena Medlenová:** Resources. **Ivana Gálisová:** Project administration. **Lucia Danišová:** Investigation. **Radek Přikryl:** Supervision. **Silvestr Figalla:** Validation. **Veronika Melčová:** Investigation. **Pavel Alexy:** Supervision.

Declaration of competing interest

The authors declare that they have no known competing financial interests or personal relationships that could have appeared to influence the work reported in this paper.

Acknowledgement

This work was supported by the grants of Research and Development Agency APVV 17–304 and APVV-17-0078 and by the Bioplastics for circular economy project No. FCH–S-19-6100 of the Specific University Research Grant provided by the Ministry of Education, Youth and Sports of the Czech Republic.

References

[1] F. Deri, K. Hamad, M. Kaseem, Recycling of Waste from Polymer Materials: an Overview of the Recent Works, 2013, pp. 2801–2812.
[2] The World Economic Forum, The New Plastics Economy – Rethinking the Future of Plastics, 2016.
[3] Plastic the mag. Did you say "Bio-Based"? Plastic the Mag (2012). http://plastics-themag.com/Wanted—renewable-plastic-resources.
[4] C. Bastioli, *Handbook of Biodegradable Polymers.* s.L, Rapra Technology Limited, 2005.
[5] K. Van De Velde, P. Kiekens, Biopolymers: Overview of Several Properties and Consequences on Their Applications, 2002, pp. 433–442.
[6] M. Shibata, K. Ozawa, N. Teramoto, R. Yosomiya, H. Takeishi, Biocomposites Made from Short Abaca Fiber and Biodegradable Polyesters, 288, 2003, pp. 35–43.

[7] K. Meinander, M. Niemi, J. Hakola, J.-F. Selin, Polylactides – degradable polymers for fibres and films, Macromol. Symp. 123 (1997) 147–153.
[8] A. Soroudi, I. Jakubowicz, Recycling of bioplatics, their blends and biocomposies: A review, Eur. Polym. J. (2013) 2839–2858.
[9] R.C. Baltieri, L.H. Innocentini Mei, J. Bartoli, Study of the influence of plasticizerson the thermal and mechanical properties of poly(3-hydroxybutyrate) compounds, Macromol. Symp. 197 (2003) 33–44, 2003.
[10] N. Yoshie, K. Nakasato, M. Fujiwara, K. Kasuya, H. Abe, Y. Doi, Effect of low molecular weight additives on enzymatic degradation of poly(3-hydroxybutyrate), Polymer 41 (2000), 3227e34. 2000, Vol. 41.
[11] M. Pizzoli, M. Scandola, G. Ceccorulli, Crystallization and melting of isotactic poly (3-hydroxy butyrate) in the presence of a low molecular weight diluent, Macromolecules 35 (2002) 3937–3941, 2002.
[12] L. Cartier, T. Okihara, Y. Ikada, H. Tsuji, J. Puiggali, B. Lotz, Epitaxial crystallization and crystalline polymorphism of polylactides, Polymer 41 (25) (2000) 8909–8919.
[13] T. Iwata, Y. Aoyagi, M. Fujita, H. Yamane, Y. Doi, Y. Suzuki, et al., Processing of a strong biodegradable poly[(R)-3-hydroxybutyrate] fiber and a new fiber structure revealed by micro-beam X-ray diffraction with synchrotron radiation, Macromol. Rapid Commun. 25 (11) (2004) 1100–1104.
[14] J. Zhang, Y. Duan, H. Sato, H. Tsuji, I. Noda, S. Yan, et al., Crystal modifications and thermal behaviour of poly(l-lactic acid) revealed by infrared spectroscopy, Macromolecules 38 (19) (2005) 8012–8021.
[15] J.W. Park, Y. Doi, T. Iwata, Uniaxial drawing and mechanical properties of poly [(R)-3-hydroxybutyrate]/poly(l-lactic acid) blends, Biomacromolecules 5 (4) (2004) 1557–1566.
[16] M. Zhang, N.L. Thomas, Blending polylactic acid with polyhydroxybutyrate: the effect on thermal, mechanical, and biodegradation properties, Adv. Polym. Technol. 30 (2) (2011) 67–79.
[17] M.P. Arrieta, M.D. Samper, J. Lopez, A. Jimenez, Combined effect of poly (hydroxybutyrate) and plasticizers on polylactic acid properties for film intended for food packaging, J. Polym. Environ. 22 (2014) 460–470.
[18] M.L. Iglesias Montes, D.A. D'Amico, L.B. Manfredi, V.P. Cyras, Effect of natural glyceryl tributyrate as plasticizer and compatibilizer on the performance of bio-based polylactic acid/poly(3-hydroxybutyrate) blends, J. Polym. Environ. 27 (2019) 1429–1438.
[19] M.A. Abdelwahab, A. Flynn, B.-S. Chiou, S. Imam, W. Orts, E. Chiellini, Thermal, mechanical and morphological characterization of plasticized PLA–PHB blends, Polym. Degrad. Stabil. 97 (2012) 1822–1828.
[20] I. Armentano, E. Fortunati, N. Burgos, F. Dominici, F. Luzi, S. Fiori, A. Jimenez, K. Yoon, J. Ahn, S. Kang, J.M. Kenny, Bio-based PLA_PHB plasticized blend films: processing and structural characterization, LWT - Food Sci. Technol. (Lebensmittel-Wissenschaft -Technol.) 64 (2015) 980–988.
[21] V. Jost, R. Kopitzky, Blending of polyhydroxybutyrate-co-valerate with polylactic acid for packaging applications – reflections on miscibility and effects on the mechanical and barrier properties, Chem. Biochem. Eng. Q. 29 (2015) 221–246.
[22] M.P. Arrieta, J. Lopez, A. Hernandez, E. Rayon, Ternary PLA-PHB-Limonene blends intended for biodegradable food packaging applications, Eur. Polym. J. 50 (2014).
[23] Y. Ma, Y. Wang, Development of PLA - PHB - Based Biodegradable Active Packaging and its Application to Salmon, 2018, pp. 1–8, 2018.
[24] N. Koyama, Y. Doi, Miscibility of binary blends of poly[(R)-3-hydroxybutyric acid] and poly[(S)-lactic acid], Polymer 38 (7) (1997) 1589–1593.
[25] E. Blumm, A.J. Owen, Miscibility, crystallization and melting of poly(3-hydroxybutyrate)/poly(L-lactide) blends, Polymer 36 (21) (1995) 4077–4081.
[26] I. Ohkoshi, H. Abe, Y. Doi, Miscibility and solid-state structures for blends of poly [(S)-lactide] with atactic poly[(R, S)-3-hydroxybutyrate], Polymer 41 (15) (2000) 5985–5992.
[27] I. Armentano, E. Fortunati, N. Burgos, F. Dominici, F. Luzi, S. Fiori, A. Jimenez, Processing and Characterization of Plasticized PLA/PHB Blends for Biodegradable Multiphase Systems, 9, 2015, pp. 583–596.
[28] M.P. Arrieta, E. Fortunati, F. Dominici, J. Lopez, J.M. Kenny, Bionanocomposite films based on plasticized PLA-PHB/cellulose nanocrystal blends, Carbohydr. Polym. 121 (2015) 265–275.
[29] S. Wang, P. Ma, R. Wang, Y. Zhang, Mechanical, thermal and degradation properties of poly(D, L-lactide)/poly(hydroxybutyrate-co-hydroxyvalerate)/poly (ethylene glycol) blend, Polym. Degrad. Stabil. 93 (7) (2008) 1364–1369.
[30] P. Alexy, I. Chodák, D. Bakoš, P. Bugaj, M. Pavlacková, K. Tomanová, F. Benovic, R. Plavec, M. Mihalik, *BIOLOGICALLY DEGRADABLE POLYMERIC COMPOSITION WITH HIGH DEFORMABILITY. 20140039096* Bratislava, 11 Apr 2012 (Application).
[31] X. Yang, J. Clénet, H. Xu, K. Odelius, M. Hakkarainen, Two step extrusion process: from thermal recycling of PHB to plasticized PLA by reactive extrusion grafting of PHB degradation products onto PLA chains, Macromolecules (2015) 2509–2518.
[32] M. Kumar, S. Mohanty, S.K. Nayak, M. Rahail Parvaiz, Effect of glycidyl methacrylate (GMA) on the thermal, mechanical and morphological property of biodegradable PLA/PBAT blend and its nanocomposites, Bioresour. Technol. 101 (21) (2010) 8406–8415.
[33] A.M. El-Hadi, Effect of processing conditions on the development of morphological features of banded or nonbanded spherulites of poly(3-hydroxybutyrate) (PHB) and polylactic acid (PLLA) blends, Polym. Eng. Sci. 51 (11) (2011) 2191–2202.
[34] O. Martin, L. Avérous, Poly(lactic acid): plasticization and properties of biodegradable multiphase systems, Polymer 42 (14) (2001) 6209–6219.
[35] L.V. Labrecque, R.A. Kumar, V. Davé, R.A. Gross, S.P. McCarthy, Citrate esters as plasticizers for poly(lactic acid), J. Appl. Polym. Sci. 66 (8) (1997) 1507–1513.
[36] S. Jacobsen, H.G. Fritz, Plasticizing polylactide-the effect of different plasticizers on the mechanical properties, Polym. Eng. Sci. 39 (7) (1999) 1303–1310.
[37] M.P. Arrieta, J. López, E. Rayón, A. Jimenez, Disintegrability under composting conditions of plasticized PLA/PHB blends, Polym. Degrad. Stabil. 108 (2014) 307–318.
[38] M.P. Arrieta, M.M. Castro-Lopez, E. Rayón, L.F. Barral-Losada, J.M. LopezVilariño, J. López, M.V. GonzaÍez-Rodríguez, Plasticized poly(lactic acid) −poly (hydroxybutyrate) (PLA−PHB) blends incorporated with catechin intended for active food-packaging applications, J. Agric. Food Chem. 62 (2014) 10170–10250.
[39] M.P. Arrieta, J. López, J.M. Kenny, L. Peponi, Development of flexible materials based on plasticized electrospun PLA–PHB blends: Structural, thermal, mechanical and disintegration properties, Eur. Polym. J. 73 (2015) 433–446.
[40] A. Nicosia, W. Gieparda, J. Foksowicz-Flaczyk, J. Walentowska, D. Wesołek, B. Vazquez, F. Prodi, F. Belosi, Air filtration and antimicrobial capabilities of electrospun PLA/PHB containing ionic liquid, Separ. Purif. Technol. 154 (2015) 154–160.
[41] A.K. Bledzki, A. Jaszkiewicz, Mechanical performance of biocomposites based on PLA and PHBV reinforced with natural fibres - A comparative study to PP, Compos. Sci. Technol. 70 (2010) 1687–1696.
[42] L. Han, C. Han, H. Zhang, S. Chen, L. Dong, Morphology and properties of biodegrad able and biosourced polylactide blends with poly(3-hydroxybutyrate-co-4-hydroxybutyrate), Polym. Compos. 33 (2012) 850–859.
[43] Y. Weng, L. Wang, M. Zhang, X. Wang, Y. Wang, Biodegradation behavior of P (3HB,4HB)/PLA blends in real soil environments, Polym. Test. 32 (2013) 60–70.
[44] H. Li, X. Lu, H. Yang, J. Hu, Non-isothermal crystallization of P(3HB-co-4HB)/PLA blends crystallization kinetic, melting behavior and crystal morphology, J. Therm. Anal. Calorim. 122 (2015) 817–829.
[45] M. Gao, Z. Ren, S. Yan, J. Sun, X. Chen, An optical microscopy study on the phase structure of poly(L-lactide acid)/poly(propylene carbonate) blends, J. Phys. Chem. B 116 (2012) 9832–9837.
[46] J. Gonzalez Ausejo, J. Rydz, M. Musioł, Wanda Sikorska, et al., Three-dimensional printing of PLA and PLA/PHA dumbbell-shaped specimens of crisscross and transverse patterns as promising materials in emerging application areas: Prediction study, Polym. Degrad. Stabil. 156 (2018) 100–110.
[47] J.G. Ausejo, J. Rydz, M. Musioł, W. Sikorska, M. Sobota, J. Włodarczyk, G. Adamus, H. Janeczek, I. Kwiecień, A. Hercog, B. Johnston, H.R. Khan, V. Kannappan, K. R. Jones, M.R. Morris, A comparative study of three-dimensional printing directions: the degradation and toxicological profile of a PLA/PHA blend, Polym. Degrad. Stabil. 152 (2018) 191–207.
[48] M. Osinska-Broniarz, W. Gieparda, D. Wesolek, A. Martyla, R. Przekop, A. Sierczynska, Preparation and characterization of gel polymer electrolytes based on electrospun PLA/PHB membranes for lithium-ion batteries, ECS Transactions 70 (2015).
[49] J. Hopewell, R. Dvroak, E. Kosior, Plastics Recycling: Challenges and Opportunities, 2009, pp. 2115–2126.
[50] R. Clift, Overview Clean Technology - the Idea and the Practice, 1997, pp. 347–350.
[51] S.M. Al-Salem, P. Lettieri, J. Baeyens, Recycling and recovery rotes of plastic solid waste: A review, Waste Manag. (2009) 2625–2643.
[52] U. Arena, M.L. Mastellone, F. Perugini, Life cycle assessment of a plastic packaging recycling system, Int. J. Life Cycle Assess. (2003) 92–98.
[53] F. Perugini, M.L. Mastellone, U. Arena, A life cycle assessment of mechanical and feedstock recycling options for management of plastic packaging wastes, Environ. Prog. (2005) 246–259.
[54] D. Lazarevic, et al., Plastic waste management in the context of a European recycling society: comparing results and uncertainties in a life cycle perspective, Resour. Conserv. Recycl. (2010) 246–259.
[55] V. Piemonte, Bioplastic waste: The best final disposition for energy saving, J. Polym. Environ. (2011) 988–994.
[56] M.M. Fisher, Plastics Recycling, *Plastics and the Environment*, 2004, pp. 563–627 [book auth.] J. Wiley.
[57] R. Hatti-Kaul, L.J. Nilsson, B. Zhang, S. Lundmark, Designing biobased recyclable polymers for plastics: a review, Trends Biotechnol. (2020) 50–67.
[58] F. LaMantia, Handbook of Plastics Recycling, 2002.
[59] M. Żenkiewicz, M. Kurcok, Effects of compatibilizers and electron radiation on thermomechanical properties of composites consisting of five recycled polymers, Polym. Test. 27 (2008).
[60] European commision, A European Strategy for Plastics in a Circular Economy, 16.1, 2018. Brussels : s.n.
[61] H. Hisken, S. Moss, R. J-Pauquet, H. Zweifel, Degradation of polyolefins during melt processing, Polym. Degrad. Stabil. 34 (1991) 279–293.
[62] H. Kometani, T. Matsumura, T. Suga, T. Kanai, Quantitative analysis for polymer degradation in the extrusion process, Int. Polym. Process. (2006) 24–31.
[63] H. Hu, R. Zhang, Z. Kong, K. Wang, J. Zhu, Bio-based poly(butylene furandicarboxylate)-b-poly(ethylene glycol) copolymers: the effect of poly (ethylene glycol) molecular weight on thermal properties and hydrolysis degradation behavior, Advanced Industrial and Engineering Polymer Research 2 (2019) 167–177.
[64] T. Sawaguchi, D. Sasaki, A. Takamura, On the entanglement-based mechanism in thermal degradation of vinyl polymers, Polym. Degrad. Stabil. 169 (2019).
[65] E. Pock, C. Kiss, Á. Janecska, E. Epacher, B. Pukánszky, Effect of chain structure on the processing stability of high-density polyethylene, Polym. Degrad. Stabil. 85 (2004).
[66] S. Al-Malaika, X. Peng, Metallocene ethylene-1-octene copolymers: effect of extrusion conditions on thermal oxidation of polymers with different comonomer content, Polym. Degrad. Stabil. 92 (2007) 2136–2149.
[67] Stabilization of metallocene ethylene-1-octene copolymers during multiple extrusions, Polym. Degrad. Stabil. 93 (2008) 1619–1631.

[68] H.M. da Costa, V.D.V. Ramos, M.C.G. Rocha, Rheological properties of polypropylene during multiple extrusion, Polym. Test. 24 (2005) 86–93.
[69] H.M. da Costa, V.D.V. Ramos, M.G. Márcia de Oliveira, Degradation of polypropylene (PP) during multiple extrusion: thermal analysis, mechanical properties and analysis of variance, Polym. Test. 26 (2007) 676–684.
[70] S.V. Canevarolo, Chain scission distribution function for polypropylene degradation during multiple extrusion, Polym. Degrad. Stabil. 70 (2000) 71–76.
[71] E. Ramirez-Vargas, D. Navarro-Rodriquez, A.I. Blanqueto-Menchaca, B.M. Huerta-Martinez, M. Palacios-Mezta, Degradation effects on the rheological and mechanical properties of multi-extruded blends of impact-modified polypropylene and poly(ethylene-co-vinyl acetate), Polym. Degrad. Stabil. 86 (2004) 301–307.
[72] J. Tocháček, J. Jančář, J. Kalfus, P. Zbořilová, Z. Buráň, Degradation of polypropylene impact-copolymer during processing, Polym. Degrad. Stabil. 93 (2008) 770–775.
[73] F.R. Beltran, V. Lorenzo, J. Acosta, M.U. de la Orden, J. Martínez Urreaga, Effect of simulated mechanical recycling processes on the structure, J. Environ. Manag. 216 (2018) 25–31.
[74] F.R. Beltrán, Celia Infante, M. Ulagaresde la Orden, Joaquín Martínez Urreaga, Mechanical recycling of poly(lactic acid): Evaluation of a chain extender and a peroxide as additives for upgrading the recycled plastic, J. Clean. Prod. 219 (2019) 46–56.
[75] D. Helfenbein, Development of Recycling of PLA Sheet into PLA Pellets without Undergoing Process, 2011.
[76] M. Żenkiewicz, J. Richert, P. Rytlewski, K. Moraczewski, M. Stepczynska, T. Karasiewicz, Characterisation of multi-extruded poly(lactic acid), Polym. Test. (2009) 412–418.
[77] I. Pillin, N. Montrelay, A. Bourmaud, Y. Grohens, Effect of hermo-mechanical cycles on the physico-chemical properies of poly(lactic acid), Polym. Degrad. Stabil. (2008) 321–328.
[78] J.D. Badia, E. Strömberg, S. Karlsson, A. Ribes-Greus, Material valorisation of amorphous polylactide. Influence of thermo-mechanical degradation on the morphology, segmental dynamics, thermal and mechanical performance, Polym. Degrad. Stabil. 97 (4) (2012) 670–678.
[79] A. Agüero, M. del Carmen Morcillo, et al., Study of the influence of the reprocessing cycles on the final properties of polylactide Pieces obtained by injection molding, Polymers 11 (2019).
[80] L.F. Rivas, S.A. Casarin, et al., Reprocessability of PHB in extrusion: ATR-FTIR, tensile tests and thermal studies, Polímeros 27 (2017) 122–128.
[81] I. Zembouai, S. Bruzaud, M. Kaci, A. Benhamida, Y.-M. Corre, Y. Grohens, Mechanical recycling of poly(3-hydroxybutyrate-co-3-hydrxyvalerate)/polylactide based blends, J. Polym. Environ. (2014) 449–459.
[82] M. Mikušová, M. Mihalík, P. Alexy, K. Tomanová, R. Plavec, J. Bočkaj, Z. Vanovčanová, Method for testing of processing stability of biodegradable polyesters based on oscillation rheometry, KGK - Kautsch. Gummi Kunstst. 3 (2014) 51–54.
[83] I. Armentano, E. Fortunati, N. Burgos, F. Dominici, F. Luzi, K. Yoon, Processing and characterization of plasticized PLA/PHB blends for biodegradable multiphase systems, Express Polym. Lett. 9 (2015) 583–596.
[84] T. Gerard, T. Budtova, A. Podshivalov, S. Bronnikov, Polylactide/poly (hydroxybutyrate-co-hydroxyvalerate) blends: Morphology and mechanical properties, Express Polym. Lett. 8 (2014) 609–617.

polymers

MDPI

Article

PLA/PHB-Based Materials Fully Biodegradable under Both Industrial and Home-Composting Conditions

Mária Fogašová [1], Silvestr Figalla [2,*], Lucia Danišová [1], Elena Medlenová [1], Slávka Hlaváčiková [1], Zuzana Vanovčanová [1], Leona Omaníková [1], Andrej Baco [1], Vojtech Horváth [1], Mária Mikolajová [1], Jozef Feranc [1], Ján Bočkaj [1], Roderik Plavec [1], Pavol Alexy [1], Martina Repiská [1], Radek Přikryl [2], Soňa Kontárová [2], Anna Báreková [3], Martina Sláviková [3], Marek Koutný [4], Ahmad Fayyazbakhsh [4] and Markéta Kadlečková [4]

1 Institute of Natural and Synthetic Polymers, Faculty of Chemical and Food Technology, Slovak University of Technology, Radlinského 9, 812 37 Bratislava, Slovak Republic
2 Institute of Materials Science, Faculty of Chemistry, Brno University of Technology, Purkyňova 464/118, 612 00 Brno, Czech Republic
3 Department of Landscape Engineering, Hortyculture and Landscape Engineering Faculty, Slovak University of Agriculture, Hospodárska 7, 949 76 Nitra, Slovak Republic
4 Department of Environmental Protection Engineering, Faculty of Technology, Tomas Bata University in Zlín, Nad Ovčírnou III 3685, 760 01 Zlín, Czech Republic
* Correspondence: xcfigallas@vutbr.cz

Abstract: In order to make bioplastics accessible for a wider spectrum of applications, ready-to-use plastic material formulations should be available with tailored properties. Ideally, these kinds of materials should also be "home-compostable" to simplify their organic recycling. Therefore, materials based on PLA (polylactid acid) and PHB (polyhydroxybutyrate) blends are presented which contain suitable additives, and some of them contain also thermoplastic starch as a filler, which decreases the price of the final compound. They are intended for various applications, as documented by products made out of them. The produced materials are fully biodegradable under industrial composting conditions. Surprisingly, some of the materials, even those which contain more PLA than PHB, are also fully biodegradable under home-composting conditions within a period of about six months. Experiments made under laboratory conditions were supported with data obtained from a kitchen waste pilot composter and from municipal composting plant experiments. Material properties, environmental conditions, and microbiology data were recorded during some of these experiments to document the biodegradation process and changes on the surface and inside the materials on a molecular level.

Keywords: polylactic acid (PLA); polyhydroxybutyrate (PHB); blend polymeric material; biodegradation; industrial compost; home-compost

check for updates

Citation: Fogašová, M.; Figalla, S.; Danišová, L.; Medlenová, E.; Hlaváčiková, S.; Vanovčanová, Z.; Omaníková, L.; Baco, A.; Horváth, V.; Mikolajová, M.; et al. PLA/PHB-Based Materials Fully Biodegradable under Both Industrial and Home-Composting Conditions. *Polymers* **2022**, *14*, 4113. https://doi.org/10.3390/polym14194113

Academic Editors: Piotr Bulak and Beom Soo Kim

Received: 5 September 2022
Accepted: 23 September 2022
Published: 30 September 2022

Publisher's Note: MDPI stays neutral with regard to jurisdictional claims in published maps and institutional affiliations.

Copyright: © 2022 by the authors. Licensee MDPI, Basel, Switzerland. This article is an open access article distributed under the terms and conditions of the Creative Commons Attribution (CC BY) license (https://creativecommons.org/licenses/by/4.0/).

1. Introduction

Biodegradable polymers are one of the possible alternatives to conventional polymeric materials that can, for specific applications, provide the benefit of biological decomposition without leaving unwanted litter or potentially dangerous microplastics [1,2]. However, biodegradable polymers and materials based on them are significantly different in the conditions needed for their biodegradation and in the time frame of their biodegradation [3–5]. Ideally, for a given application, we need a material that fulfils the necessary application properties and most important mechanical properties and at the same time can biodegrade under the conditions related to the particular application. It is often difficult to find or develop a material that fulfils all of those requirements.

Mainly with the aim to achieve suitable processing and mechanical and barrier properties for a given application, real polymer materials are often blends of several polymers

and contain various additives and fillers [6–8]. The whole material has to be biodegradable, which means that correct selection of individual components is very important and can significantly affect its biodegradability. The plasticizer triacetin, used in a study by Sedničková et al. [9], was tested with PLA and PLA/PHB blends, and the materials were exposed to biodegradation in compost at 58 °C. The results of the study prove higher sensitivity of PHB (polyhydroxybutyrate) towards biodegradation in comparison with that of PLA under the same conditions. Additionally, the plasticizer triacetin degraded faster in comparison with PLA. The study also showed that changes in material composition (e.g., amount of plasticizer) might change the biodegradation rate. Another bio-based plasticizer, acetyl-tri-n-butyl citrate (ATBC), in combination with polyethylene glycol (PEG) was also tested as a component of PLA/PHB blends [10]. The material exhibits disintegration under composting conditions in less than one month. The ability of PHB to act as a nucleating agent in PLA/PHB blends slowed down the disintegration, while plasticizer content accelerated it.

It is expected in many cases that waste containing biodegradable plastics is collected along with other primarily plant-based organic waste and it is further treated in municipal or agricultural composting plants. In general, materials suitable for such an end-of-life should comply with EN 13432 standard describing procedures for testing under so-called industrial composting conditions [11]. According to this standard, industrial composting requires an elevated temperature (55–60 °C) in combination with relatively high water activity expressed as water content (approximately 60% w/w) and the presence of oxygen. Under such conditions, several criteria must be met: (i) The disintegration of the material from at least 90% must take place within 12 weeks, (ii) 90% mineralization of the composted material must be achieved in less than six months, which is usually measured from evolved CO_2, and (iii) the material should not have a negative effect on compost quality (no or minimal heavy metal content, no ecotoxicity) [12].

The description above, however, does not correspond to the conditions on a typical simple composting plant where temperatures over 50 °C can be achieved for about two to three weeks maximally [13]. Then, the process continues in a milder mesophilic temperature range. To address this issue, a group of standards was formulated describing so-called "home-composting" (Vicotte OK compost HOME, AS 5810 Austrian standard) [14]. Here, besides other requirements, the temperature should be kept between 20 and 30 °C during the biodegradation test. Despite the fact that some commercially used materials declared as compostable polymers are often used in applications where composting is meant to be the final stage of life of these materials, they do not meet these requirements and therefore are not compostable. Chemical and biological processes, in general, are, to some extent, accelerated with temperature [15,16]. For example, PLA needs temperatures well over 50 °C to initiate the biodegradation process, which is possibly related to the glass transition temperature of PLA occurring in approximately the same temperature range [17]. This fact was demonstrated, e.g., by Sedničková et al. [9] in a study, where the biodegradation of PLA was measured in compost incubations at 25, 37, and 58 °C for 119 days. The mineralization achieved at 58 °C was 92.3%, but only 19.5% at 37 °C and 14.9% at 25 °C. Other studies showed no or limited PLA biodegradation under mesophilic conditions [18,19].

Moreover, in reality, the almost complete mineralization must be achieved within six months, most of the time at relatively mild temperatures, to make the material compatible with the typical composting plant operation settings [12]. As a consequence, today, typical relatively simple composting plants with no fundamental process control possibilities often tend to reject biodegradable polymer materials, even those labelled as compostable, because, according to their experiences, these items do not decompose fast enough, complicate operations at the plant, and contaminate the resulting compost [20,21].

Another prospective material, PHB, also produced from renewable resources [22,23], can, in contrast to PLA, reach 100% mineralization in five weeks under mild conditions, e.g., in the soil [24]. This polymer itself does not have sufficient processing and mechanical properties for many applications.

The main aim of this study is to demonstrate the biodegradation of the original bio-based biodegradable materials and some model products made of these materials under conditions corresponding to industrial composting (58 °C) and some of them even under conditions corresponding to home-composting (28 °C) in a reasonable time frame. The samples were also evaluated in a real municipal composting plant. Other supporting methods were performed to follow the biodegradation process. This study is meant to show that the presented materials with very good mechanical and processing properties are also biodegradable and fully compatible with common composting technology in a simple municipal composting plant or even in the proper home-compost.

2. Materials and Methods

2.1. Materials

Samples made of PLA/PHB or PLA/PHB/TPS (thermoplastic starch) blends for this study were developed for various processing technologies and applications. Thermoplastic starch TPS was prepared by blending corn starch + glycerol 70/30 in a twin screw extruder at 160 °C. The used plasticizers are based on esters of citric acid. Blends according to composition in Table 1 were prepared by blending in a co-rotating twin screw extruder with the following parameters: L/D = 44, D = 26 mm, temperature profile from hopper to head: 50-160-170-170-170-170-170-170-160-160 °C, screw speed 150 rpm. The blends were cooled in a water bath and pelletized. All blends were sent to production companies that made the test products. The basic characteristics of all the used blends are listed (Table 1).

Table 1. Basic characteristics of the tested materials.

Blend No.	Blend Technology	PLA Ingeo 4043D %wt.	PHB Enmat Y1000 %wt.	ATBC Citrofol B2 %wt.	TPS %wt.	MFI	P	TS	ε	T_g
IM 2	Injection moulding	40	50	10	0	5.8	1.2	31	8	N/A
IM 1	Injection moulding	30	40	5	25	35	1.3	34	5	53
TF -1	Thermoforming	65	30	5	0	6.2	1.2	28	36	N/A
FB 2	Film blowing	70	15	15	0	18	1.2	18	330	28
FB 1	Film blowing	50	10	15	25	33	1.3	11	288	24

MFI, melt flow index, 180 °C, 2.16 kg, g/10 min; P, density g/cm^3; TS, tensile strength at break, MPa; ε, elongation at break, %; T_g, glass transition temperature, °C.

The test specimens based on PLA/PHB or PLA/PHB/TPS are listed in Table 2. Cups were produced by the company KS-PT s.r.o. (Slovakia), the thermoforming sheet was produced in Panara a.s. (Slovakia), and blown films were produced in Topstav s.r.o. (Slovakia) in their pilot (Panara a.s.) plant or production plant (KMS-PT s.r.o. and Topstav s.r.o.). The smaller picture of the sample represents the specific used test specimen for biodegradation testing in home-compost, industrial compost, and an electric composter.

Table 2. Products that were tested for biodegradation and compostability.

Sample	Grade No	Thickness	Description
A, bicomponent cup  	IM 2 (Inner layer) IM 1 (Outer layer)	1–6 mm, average 4 mm	Bicomponent cup

Table 2. *Cont.*

Sample	Grade No	Thickness	Description
B, 500 mL cup  	IM 2	1 mm	Cup for beverages and beer, mainly for festivals
C, 200 mL cup  	IM 1	1 mm	Cup for drinks suitable mainly for dining restaurants and canteens
D, sheet for thermoforming  	TF 1	0.35 mm	Semiproduct (sheet) for subsequent thermoforming technology, for various packaging applications
E, blown film  	FB 2	0.04 mm	Blown film, e.g., for bags, suitable for various packaging applications
F, blown film  	FB 1	0.04 mm	Blown film e.g., for bags, mainly for waste bags for biowaste collection

2.2. Biodegradation Testing by CO_2 Production Quantification

Composting biodegradation tests were performed according to the adapted and miniaturized ISO 14855 method in 500 mL biometric flasks with septum-equipped stoppers. Mature compost from a nearby municipal composting facility (TSZ Ltd., Zlín, Czech Republic) was used in this part of the study. This test was done at 58 °C for industrial composting and at 28 °C to simulate home-composting conditions. Into each flask, 2.5 g of dry-weight compost, 5 g of perlite, and 1 mL of mineral salt medium were weighed, and the water content of the substrate mixture was eventually adjusted to 60% by the addition of sterile drinking water. One hundred milligrams of the samples were cut into 5 × 5 mm fragments that were placed in each sample flask. For each sample, three flasks plus 4 blank flasks were used. The internal production of CO_2 in blank incubations was always subtracted to calculate the net sample mineralization. Headspace gas was sampled

at appropriate intervals through the septum with a gas-tight needle and conducted through a capillary into a gas analyzer (UAG, Stanford Instruments, Sunnyvale, CA, USA) to determine the amount of CO_2. Biodegradation percentage (D_t) was calculated as

$$D_t = \frac{(CO_2)_t - (CO_2)_b}{ThCO_2} \times 10 \quad (1)$$

where $(CO_2)_t$ is the released CO_2 by each sample, $(CO_2)_b$ is the CO_2 produced by the blank flasks, and ($ThCO_2$) is the theoretical CO_2 from the sample. A flash elemental analyzer 1112 (Thermo Fisher Scientific, Waltham, MA, USA) was used to measure the carbon content of the samples.

2.3. Compostability Testing in an Electric Composter

A small electric composter GG 02 from the JRK company (Slovakia) was used for biodegradation testing while the samples were incubated together with kitchen waste. The effective volume of the composter was 40–50 liters. The temperature was 65 °C during the whole operation time, except for one hour per day when the temperature increased to 75 °C to ensure the hygienization of the content. The internal stirrer was activated for 20 min during each hour, providing altered mixing sequences in forward and reverse directions. The biodegradation process was initiated according to the user manual using the original ACIDULO® bacteria culture. Samples of PLA/PHB or PLA/PHB/TPS blends were inserted into the composter two weeks after the stabilization of the process in the composter. Each day, 0.5–1.0 kg of kitchen food waste was added to the composter. The samples were weighed before being inserting into the composter. Only one sample was measured for every composition because of technical reasons of the experiments. The content of the composter was removed each week and sieved through a sieve with a mesh size of 2 × 2 mm. Pieces larger than 2 mm (which did not pass through the sieve) were collected from the fraction above the sieve. The collected samples were washed in water, subsequently dried in an air oven for 1 h at 90 °C, and weighed with precision of 0.0001 g. Then, the samples were returned to the composter immediately after weighing. Biodegradation was evaluated as the percentage of disintegration. Microbiology inside the composter was monitored with DNA isolation and sequencing following an already established methodology [25].

2.4. Disintegration Testing in a Municipal Composting Plant

The disintegration of samples was tested also in the municipal composting facility of the city of Nitra (Nitra District, Southwest Slovakia) under real conditions of industrial composting. The compost pile consisted of approximately 11 m^3 of biodegradable municipal waste (a family house garden and public greenery plant-based waste). Disintegration testing was realized in two independent 12-week-long composting cycles. The first cycle was realized from 6 July 2019 to 27 September 2019, and the second cycle—from 16 July 2020 to 12 October 2020 on a dedicated roofed site. Both cycles followed a certified methodology [26]. The samples were weighed and enclosed in a plastic net with a 2 × 2 mm mesh diameter. The cut samples were inserted to approximately 2/3 of the height of the compost pile (Figure 1).

Right below the samples, probes were placed to measure the temperature and humidity inside the compost pile. The data were continuously monitored and recorded. The samples were inspected every 2–3 weeks; sample packages were carefully removed from the pile, visually inspected, and photographed. Afterwards, they were again inserted to 2/3 of the height of the compost pile. The residues of the samples were dried and weighed at the end of the cycle. Biodegradation was evaluated as the percentage of disintegration. The outside air temperature (in both cycles) was about 22 °C on average.



Figure 1. The compost pile and the plastic net with the cut samples.

During the first cycle, only one specimen was tested from each sample. The average value of humidity during the entire monitored period was 39.3% (vol). The average value of inner temperature during the first cycle was 62.6 °C. During the second cycle, two specimens were tested for each sample. The average humidity during the entire monitored period was 35% vol. The average inner temperature during the second cycle was 61.1 °C.

2.5. Material Characterization Methods

SEM microscopy. Surface changes on the tested films were observed using SEM. The samples were coated by a gold/platinum alloy using Balzers SCD 050 sputtering equipment. TESLA BS 300 was used for the observation of samples composted in an electric composter, and JEOL F 7500 SEM (JEOL, Tokio, Japan) was used for the samples from an industrial city composting plant. Phenom Pro Desktop SEM (Thermo Fisher Scientific, Waltham, MA, USA) was used for laboratory experiments under industrial and home-composting conditions.

Thermophysical properties' measurement. Differential scanning calorimetry (DSC) was used for the determination of basic thermophysical properties such as glass transition temperature, crystallization temperature, and melting temperature of samples after 0, 6, and 13 days of composting. The conditions for DSC measurements are in Table 3.

Table 3. Conditions for DSC measurements.

Phase	Ramp	Temperature, °C	Time, min
1. Conditioning	isothermal	0	1
2. Heating	10 °C/min	200	20
3. Conditioning	isothermal	200	1

Gel permeation chromatography (GPC) measurements. Samples (5 mg) were dissolved in chloroform (1 mL) at 70 °C and filtered through 0.45 µm polytetrafluoroethylene (PTFE) syringe filters. GPC was performed in a 185 Agilent HPLC series 1100 chromatograph (Santa Clara, CA 95051, United States) with a PLgel mixed-c 5 µm, 7.5 × 300 mm column, with chloroform as the mobile phase. Twelve polystyrene standards (0.2–2000 kDa) were used for calibration.

3. Results and Discussion

3.1. Characterization of the Studied Materials

PLA/PHB- and PLA/PHB/TPS-based materials and final products (films, sheets, and cups) are described in Tables 1 and 2. The materials were developed to be compostable in industrial compost or even under home-composting conditions while still having favorable

processing and service properties and containing an important proportion of PLA, which is probably the most available bio-based polymer but still considered to be non-biodegradable under home-composting conditions. All specimens listed in Table 2 were tested in the electric composter, municipal composting plant, and laboratory tests under industrial composting conditions. Samples in the film form (D, E, F) were also tested for biodegradability in a laboratory test under home-composting conditions. The selection of these samples for home-composting was based on their relatively low thickness and on the assumption that home-composting conditions are less aggressive than those in industrial composting, especially for the PLA component of the materials [27,28].

3.2. Biodegradability in the Laboratory Test under Industrial and Home-Composting Conditions

All samples were exposed to the laboratory test under industrial composting conditions (58 °C). It was expected that based on the composition of the samples; they all should be completely mineralized under these conditions. For the thick-wall samples without TPS (A and B), more time to reach 100% mineralization was assumed.

Three samples for each composition were measured, including the reference sample (cellulose). The average standard deviation for all tested compositions was ±8.6 for the industrial composting conditions. Mineralization of 100% was obtained for all tested samples after about 90 days of incubation (Figure 2). No sample except E exhibited a lag phase. Sample E contained the highest amount of PLA (70%), so this typical feature of PLA compost biodegradation was demonstrated in this sample [28,29]. All other samples, which degraded without a lag phase, contained at least 30% of easily biodegradable PHB and/or TPS, which were able to smooth out the lag phase in the biodegradation curve under industrial compost conditions. In the case of E, the PHB phase was probably closed inside the dominant PLA phase. After the lag phase, mineralization went on exponentially, and the sample reached complete mineralization as the first one. The mineralization was also fast for other film samples D and F, with F being faster at the beginning, which probably reflected its higher content of easily biodegradable TPS and plasticizers (40%) in comparison to that in D (5%). Surprisingly, the mineralization was also fast for a relatively thick (1 mm) sample C with high PHB and TPS contents (65%). The slowest degradation was observed in the case of both thick samples A (4 mm) and B (1 mm). TPS-containing cups exhibited slightly faster biodegradation in very good correlation with the cup's construction (thickness). Interestingly, the thickness of the sample, at least to some extent, did not play a very significant role. The thin film F composed of a PLA/PHB/TPS blend exhibited a course of biodegradation similar to that of the thick sample C. Both were made of a comparable formulation, but if TPS was not present in the composition, thickness played a more important role (samples B, D, and E were TPS-free formulations). Possibly, the TPS phase could initiate early disintegration of the sample and thus circumvent the importance of thickness.

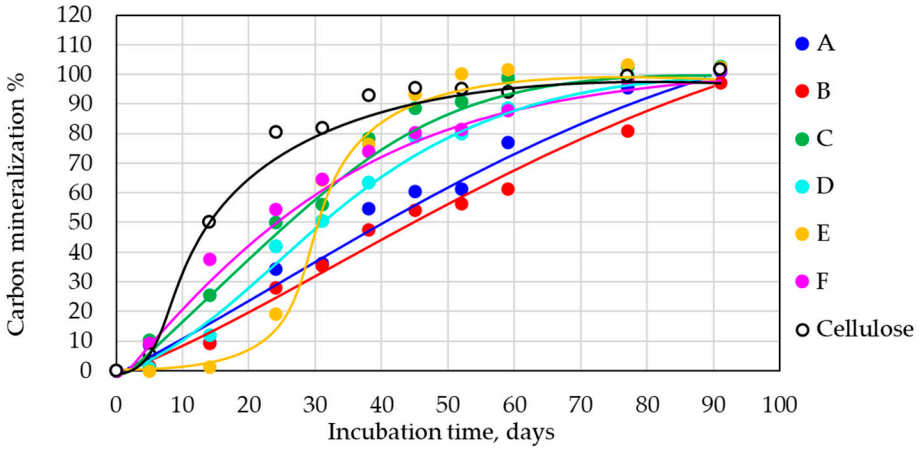


Figure 2. Mineralization of samples under industrial composting conditions, 58 °C.

The selected samples were removed from the compost after incubation, and they were observed in SEM to evaluate microbial colonization and deterioration of the material's surface (Figure 3). After only 10 days in the compost, all materials were densely colonized, and the density of the biofilm was clearly increased with the time of exposure. It was not possible to identify the microorganisms present, but the morphological appearance suggested filamentous thermophilic actinobacteria with distinguishable round endospores. The erosion of the surface was also clearly apparent.

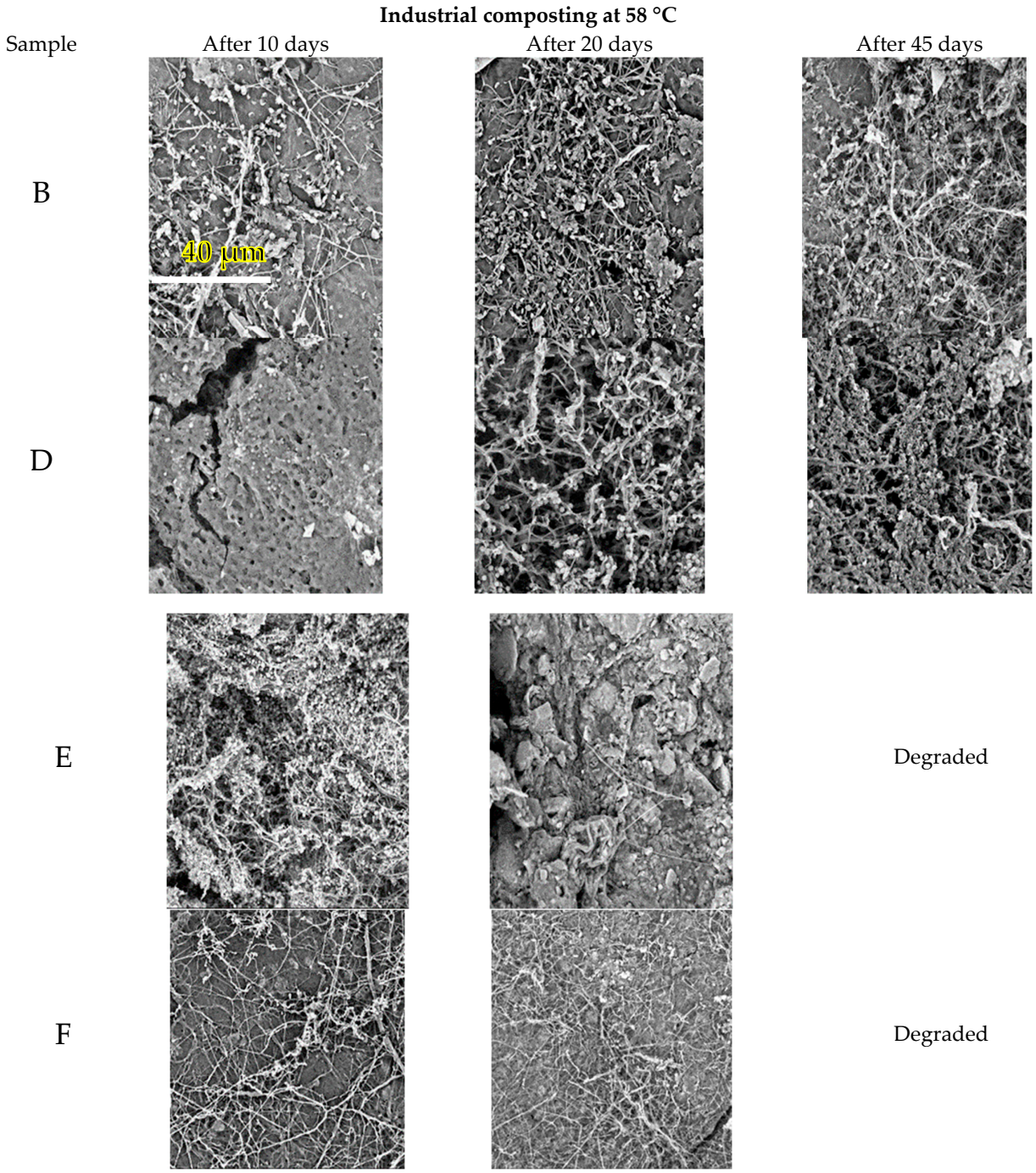


Figure 3. Scanning electron microscopy survey of the sample surface during the biodegradation test at 58 °C (industrial composting condition). Magnification of 5000×. Specifications according to Table 2 (B—500 mL cup, D—sheet for thermoforming, E—blown film and F—blown film with TPS).

Film samples D, E, and F were selected for biodegradation under home-composting conditions (28 °C, Figure 4). From our previous experiences [28,29] and the majority of the scientific literature on the topic [30], it should be expected that the PLA fraction of the materials should not be mineralized under such conditions.

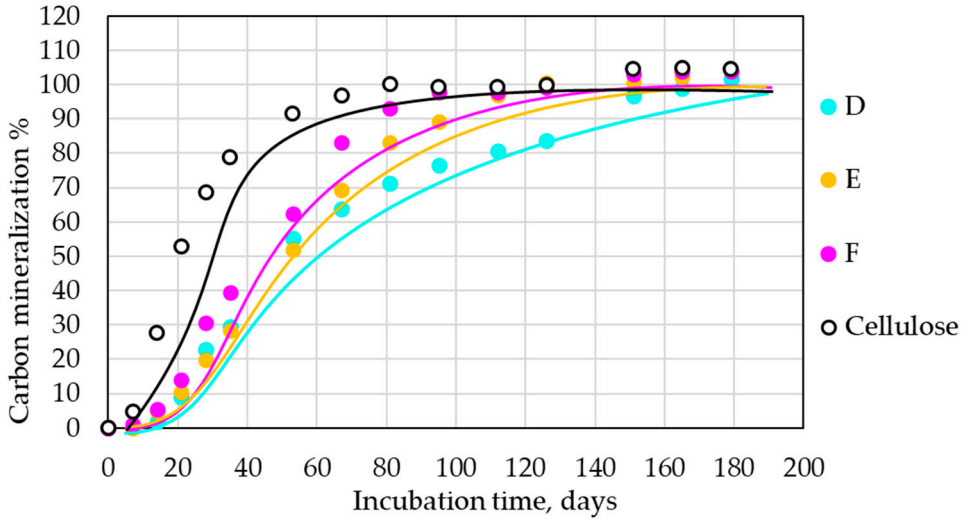


Figure 4. Mineralization of samples under home-composting conditions, 28 °C.

Three samples for each composition were measured, including the reference sample (cellulose). All samples exhibited total mineralization in a period of about 180 days. The average standard deviation for all tested compositions was ±3.9 for the home-composting conditions. An about 15-day-long lag phase occurred for all tested samples. Additionally, the curves for the tested samples were not so far from that of the cellulose reference and had the expected order. The thin film of the PLA/PHB/TPS blend (F) exhibited the fastest biodegradability, followed with a minimal gap by the thin film sample without TPS (E). In this case, apparently, thickness and plasticizer played a significant role; the thick film made of PLA/PHB without TPS and at lower plasticizer content (D) degraded significantly slower than did the thin film with higher plasticizer content (E).

When observed in SEM (Figure 5), the samples from the home-compost experiments, in general, showed a much lower degree of surface colonization if compared with that in the industrial compost experiment, which can be explained by the fact that at this temperature, a completely different microbial community was present. Again, filamentous (actinomyces most probably) but also rod-shaped bacteria were discernible (e.g., Figure 5F, 30 days). (1) (2) (3) Cavities and cracks were gradually formed. At this temperature, fungi were very active, with their extracellular enzymes probably degrading the material even if they were not seen attached to the surface.

A very important result from the environmental as well as practical points of view is the fact that PLA/PHB-blend samples degraded fully at home-compost conditions. It means that 100% mineralization was reached despite the general opinion that PLA is not able to biodegrade at temperatures below its T_g, (about 55 °C) under home-compost conditions and therefore only the mineralization of the non-PLA part of the blends could be expected. The blending of PLA and PHB in the hot melt state probably causes re-esterification reactions, leading to the formation of PLA/PHB co-polyesters. The easily biodegradable PHB segments in such a co-polyester can promote a release of low MW fragments that are prone to further biodegradation [27]. It is very difficult to investigate the occurrence and extent of re-esterification by standard analytical methods, but the results from the home-composting biodegradation can be considered as proof. This is indeed a significant discovery not only for the eventual compositing "at home" but also for industrial composting plants. In these usually municipal facilities, the composting process is quite simple and not always fully controlled, so the thermophilic phase of

the composting process could be too brief or not sufficiently hot to initiate total PLA mineralization. Problems have been reported with various items from PLA-based material labelled as "compostable", and often, such items are no longer accepted in these plants. Additionally, this will prevent microplastic formation, one of the most-closely watched environmental risks studied recently.

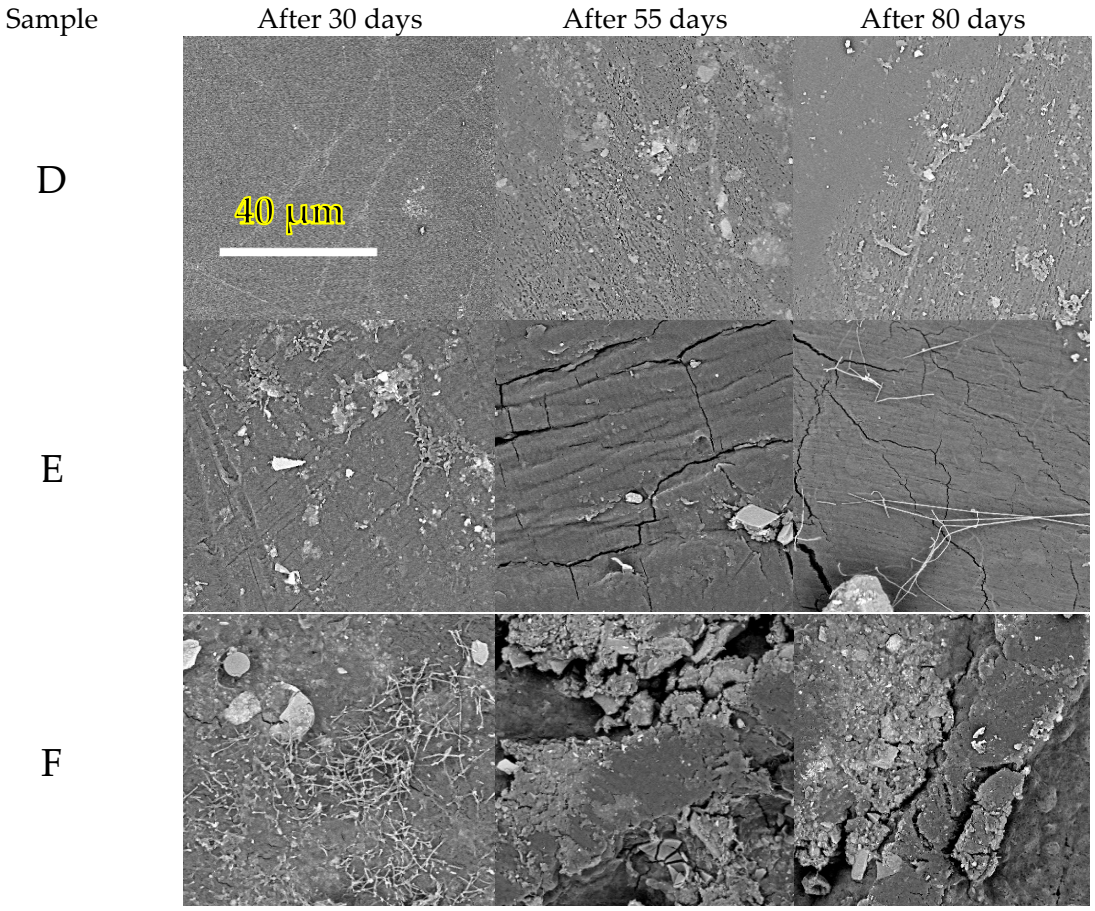


Figure 5. Scanning electron microscopy survey of the sample surface during the biodegradation test at 28 °C (home-composting conditions). Magnification of 5000×. Specifications according to Table 2 (D—sheet for thermoforming, E—blown film and F—blown film with TPS).

3.3. Composting in the Electric Composter

All samples in Table 2 were also tested in a small electric composter. Test specimens of 10 × 7 cm with the original thickness were inserted into the composter. Biodegradation was evaluated as weight losses in percentages; it can also be stated that the degree of disintegration was evaluated. The results presented in Figure 6 show differences between the disintegration of individual samples. The disintegration of all film samples was very fast, and all films were disintegrated into pieces smaller than 2 mm after 20 days. The cup containing TPS (C) exhibited fast disintegration into particles smaller than 2 mm after 40 days. The other two cups (B, PLA/PHB-based; A, TPS-containing cup) were disintegrated after a very similar time period, while the combined cup A was slightly faster. The comparison of biodegradation curves based on CO_2 measurements (in industrial compost conditions and home-compost conditions (Figure 6) and disintegration curves (Figure 6) can provide an important insight into the problem of the eventual formation of microplastics.

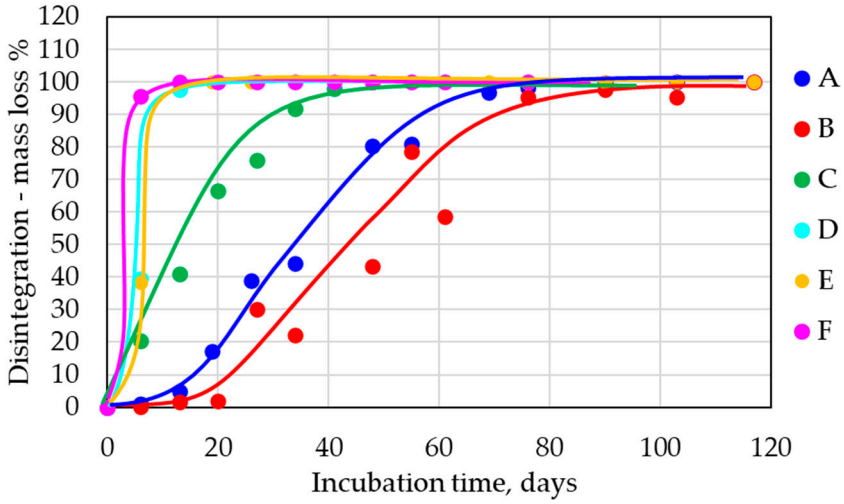


Figure 6. The disintegration of tested samples in a small electric composter, expressed as weight loss.

In Figure 7, sample C is shown as a typical example of all three cups. It means that the composting process in this case ensured direct microbial conversion of the materials to CO_2 with a relatively short disintegration step. On the contrary, the films rapidly disintegrated into smaller particles, and the mineralization followed immediately. This observation in the case of films was given by the low mechanical strength of the samples and the mechanical strain during the mixing inside the composter. A thick cup was more resistant to mechanical breakdown than thin films were before the samples became too brittle due to the biodegradation process. A similar effect was also observed when home-composting and electric composter biodegradation were compared in the case of sample E (Figure 7), where, logically, a more significant delay of mineralization after disintegration was detected. These results show that the studied materials really also underwent mineralization in home-composting conditions, and eventual fragments/microplastics after their disintegration were readily mineralized.

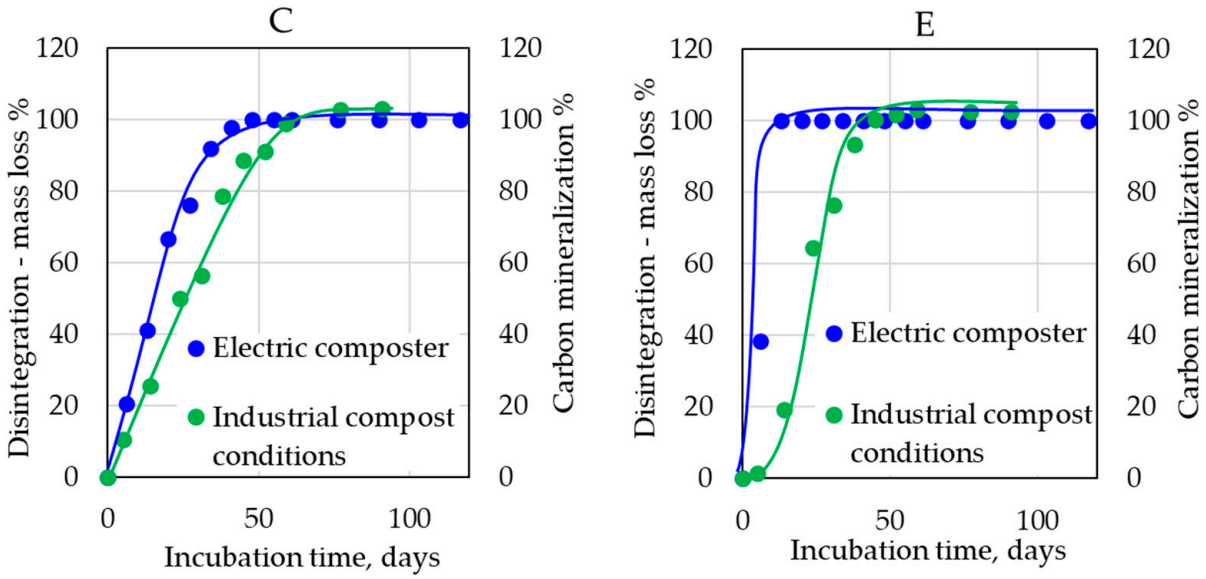


Figure 7. Comparison of biodegradation curves measured as CO_2 in industrial compost conditions (58 °C) for samples C and E and in home-compost conditions (28 °C) for sample E with disintegration curves obtained using an electric composter for samples C and E.

All tested samples exhibited well-visible changes in the surface morphology after only 6 days of incubation, as can be seen in the SEM figures. Thick samples B without TPS and

C with TPS that were not disintegrated instantly are shown as examples (Figure 8). The microscopic observation is in perfect correlation with the results of biodegradation and disintegration testing discussed previously. Cavities of various dimensions and depths were created in relation to the sample´s composition, which resulted in the enlargement of the surface area and acceleration of the biodegradation process.

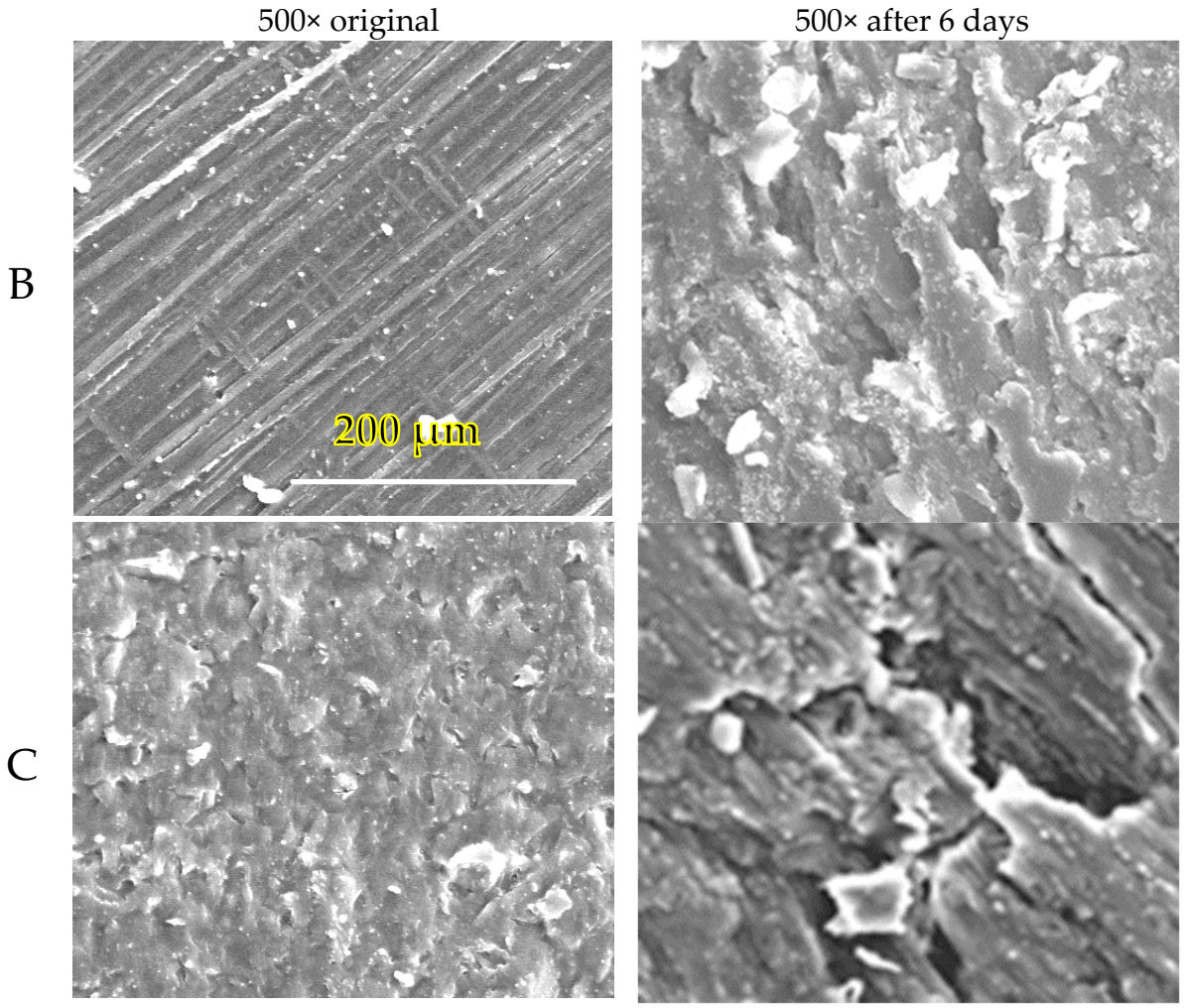


Figure 8. SEM images of the tested samples before composting and after 6 days of incubation in an electric composter. Specifications according to Table 2. (B—500 mL cup and C—200 mL cup with TPS).

The composition of the bacterial community was described by next-generation 16S r DNA metagenome sequencing in different stages of the process. The design of the composter and its operation exhibited a severe limitation for the bacterial community. Very high operation temperature (65 °C) and a daily hygienization period (75 °C) put even thermophilic bacteria on the limit of their survival. These parameters should be adjusted to provide a better environment for the compost microflora; however, it is not the topic of this study. Evidently (Figure 9), the community was dominated by thermophilic spore-forming taxa (Bacilli, Actinobacteria). The presence of other taxa like Bacteroidia, Negativicutes, and even Clostridia witness probably the presence of anaerobic pockets inside the compost. The introduced inoculum strongly influenced the initial stage, then, the gradual increase of the other taxa with time could be seen.

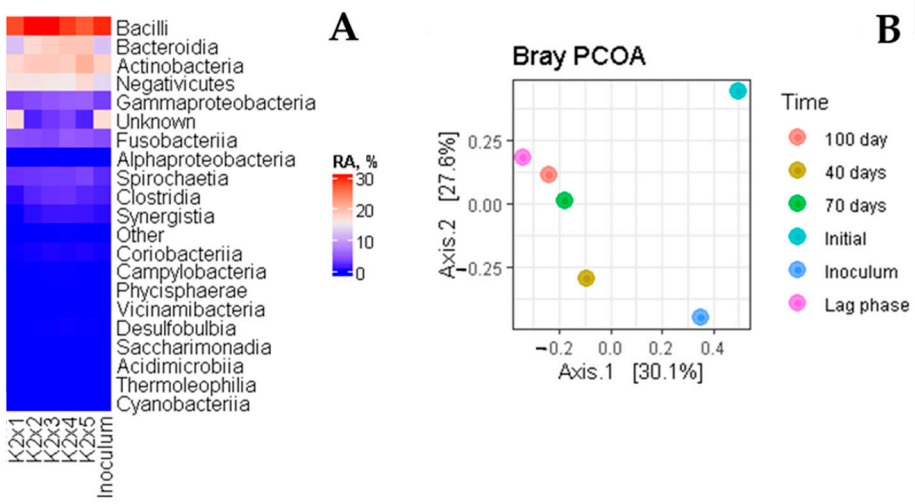


Figure 9. The bacterial community inside an electric composter. (**A**): heatmap at class taxonomic level, RA, relative abundance. (**B**): PCoA scatter plot.

3.4. Composting at the Municipal Composting Plant

The study of compostability under real conditions and verification of the results from the laboratory and the electric composter were realized in two composting cycles at Nitra municipal composting plant (Slovakia). Samples B, C, and F were tested during the first cycle. All investigated (Table 2) samples were tested in the second cycle. The first and second cycles were realized separately, the first one during the summer of 2019 and the second one during the summer of 2020. The main difference between the first and second cycles was in the humidity curve of the compost substrate (Figure 10). During the first cycle, the composting process started with a high level of moisture which then decreased over time. The moisture profile in the second cycle was exactly the opposite. In both cases, pure pulp paper (pure cellulose) was used as a reference. Biodegradation was evaluated from the weight losses after 12 weeks of incubation.

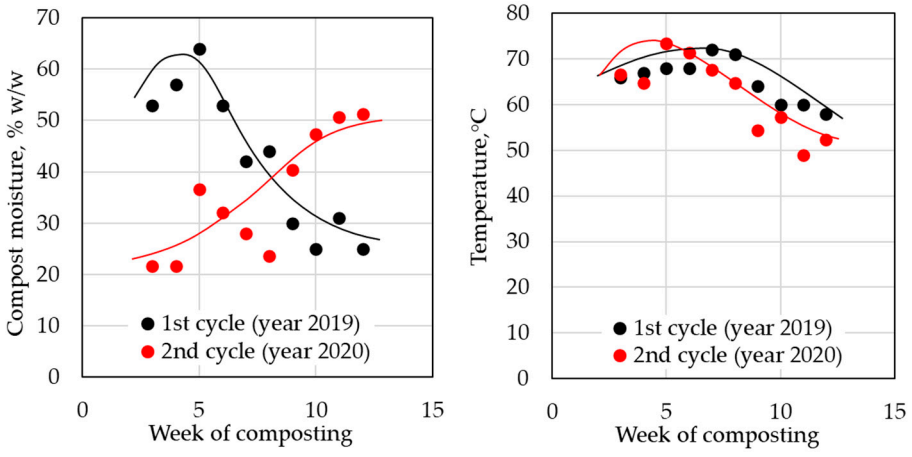


Figure 10. Moisture and temperature profiles during composting in a municipal composting plant.

Significant differences in the first cycle (year 2019) were observed in the degradation of the pulp paper reference in both cycles (Figures 11 and 12). While temperature profiles were very similar in both cycles, the trends of the compost substrate humidity differed significantly. The first stages of composting in the second cycle proceeded apparently at insufficient humidity, which could explain why in the second cycle, the compost was not sufficiently active for the biodegradation of the reference material. Suitable moisture content is an essential parameter for the composting process, especially during the initial

hot phases of the composting. The pulp paper reference was not found in the first cycle of composting after 12 weeks, while in the second cycle, with low humidity in the first stages of composting, lower than 50% weight loss was observed (Figure 12), and the paper still preserved its original shape (Figure 11).

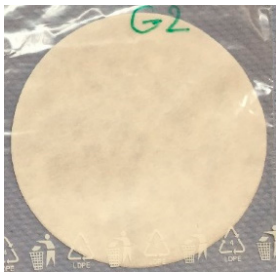
Original pulp paper before composting	Pulp paper after 12 weeks in the first composting cycle (year 2019)	Pulp paper after 12 weeks in the second composting cycle (year 2020)
	Pulp paper was not found	

Figure 11. Pulp paper reference material before industrial composting and after 12 weeks of composting.

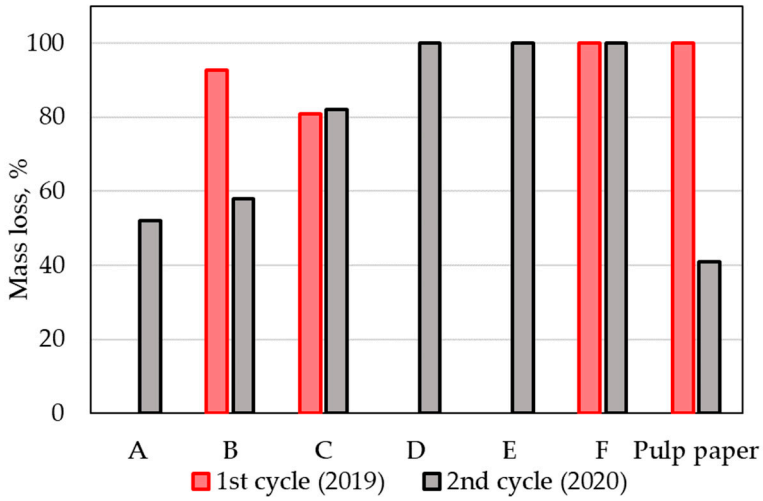


Figure 12. Weight losses of the tested samples after 12 weeks of incubation in the first and second composting cycles at a municipal composting plant.

The investigated samples provided very interesting results regarding the above-discussed differences between both composting cycles. Despite the humidity profile, film samples degraded completely in both composting cycles (sample F in the first composting cycle, as well as samples D, E, F in the second composting cycle). A thick cup sample containing TPS (sample C) degraded equally in both cycles, and the humidity profile had a small effect on their biodegradation. The thick sample without TPS (cup sample B) and the combined cup (sample A) were probably more sensitive to the moisture content but still biodegraded substantially. In general, the samples in the study biodegraded comparably or even better than the cellulose reference did in the described real-condition experiment.

The surface morphology of the samples was also studied in the second cycle of the industrial composting experiment. Film samples could not be analyzed because they were decomposed completely; all other samples exhibited significant changes in surface morphology (Figure 13). Similarly, as with the samples from the electric composter, strong surface erosion was observed.

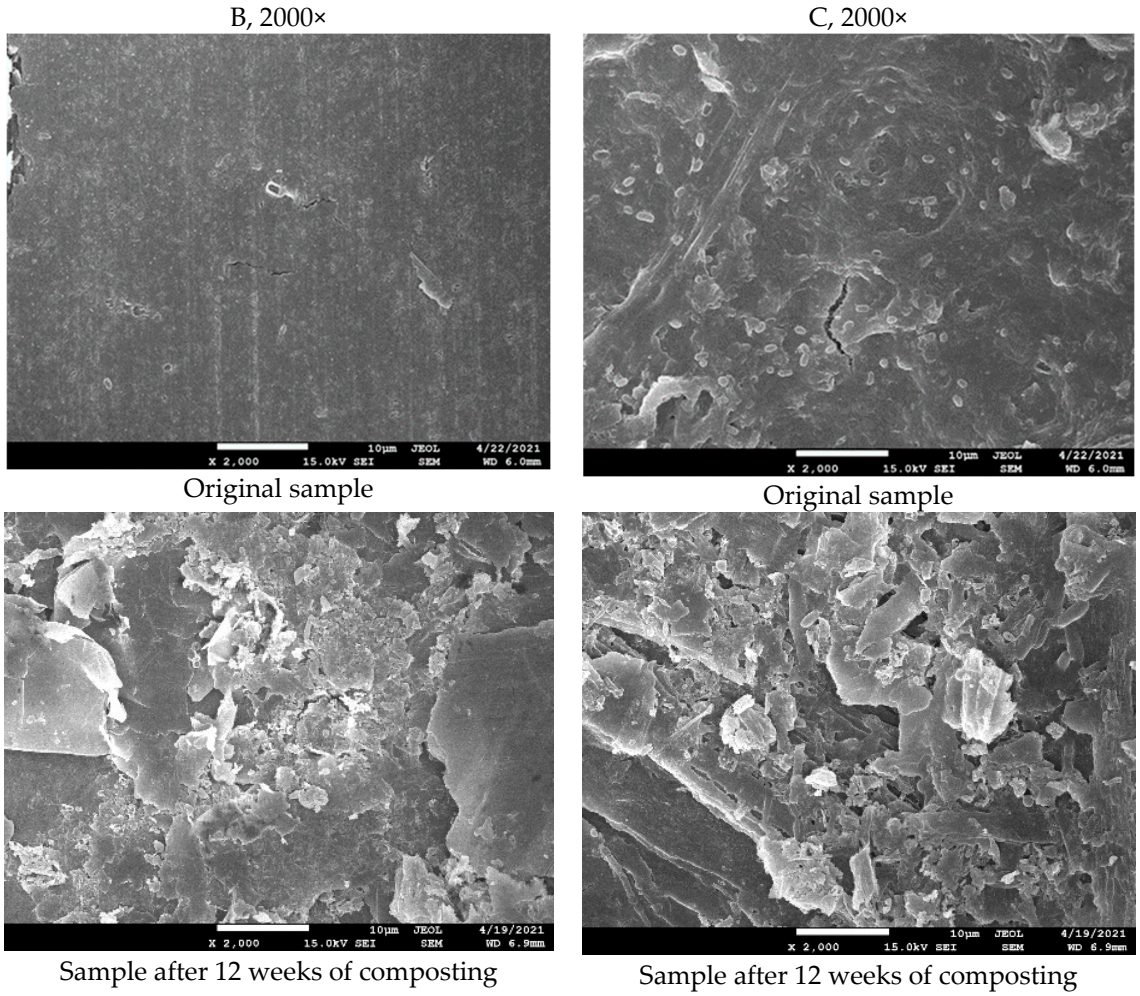


Figure 13. SEM images after 12 weeks of incubation at a municipal composting plant (second cycle).

3.5. Changes in the Material Properties during the Composting Experiments

In the case of the electric composter, after each period, molecular weight distributions were measured by GPC. It must be noted that GPC measurements were realized with solid, nondegraded residuals of composted materials. GPC curves of unprocessed PLA and PHB used in the blends were also analyzed, and the records are shown (Figure 13, insert). Partial degradation due to blending and then processing of the blend during sample preparation was noticeable for each sample. The degradation caused by processing only in the melt state was not very extensive; only in the case of sample C was its extent more significant. This can relate to the presence of glycerol in TPS and possible alcoholysis of PHB by glycerol [31,32]. The intense shift of the main peaks to lower molecular weights after composting was visible mainly in the case of thick cup samples. In addition, the appearance of low-molecular-weight fractions was clearly seen in GPC records. The last indicated fraction produced by the biodegradation process exhibited an average molecular weight (MW) of about 1000 g/mol. Lower MW fractions (below 500 g/mol) were probably easily mineralized. The fast gradual decrease of MW was observed for all samples (Figure 14).

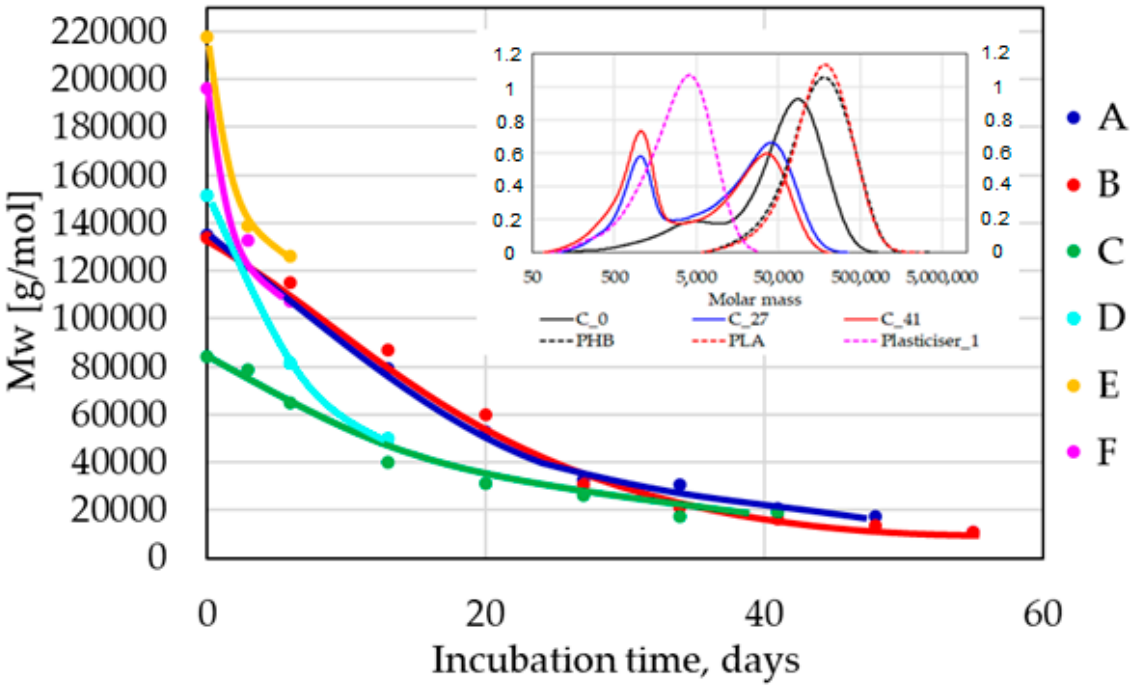


Figure 14. MW evolution during incubation in an electric composter. The GPC records of sample C after 0, 27, and 41 days of composting are shown as an example (insert).

Regardless of the original MW, all samples that did not biodegrade exhibited similar MW values after 30 days of composting. It means that the degradation process ran not only on the surface of the samples but also in the bulk of the materials. Only short time periods were evaluated in the case of film samples because already after 14 days of composting, no film sample could be retrieved.

The process at the municipal composting plant also caused a dramatic decline in MW below 1000 g/mol, as shown for selected samples (Figure 15). Such low-molecular-weight substances are considered to be easily and rapidly biodegradable during the following composting period.

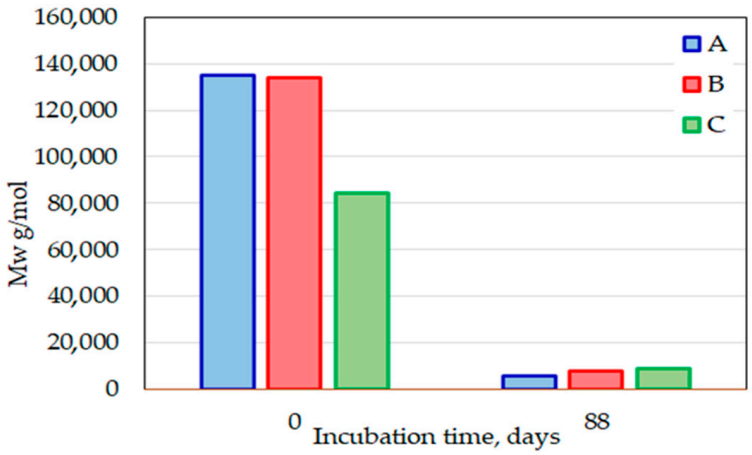


Figure 15. Comparison of MW for cup samples before composting and after 12 weeks in the second composting cycle (2020).

The mentioned changes in polymer structure were also confirmed by DSC measurements realized on solid residuals after each evaluated period of composting process in the electric composter (Figure 16).

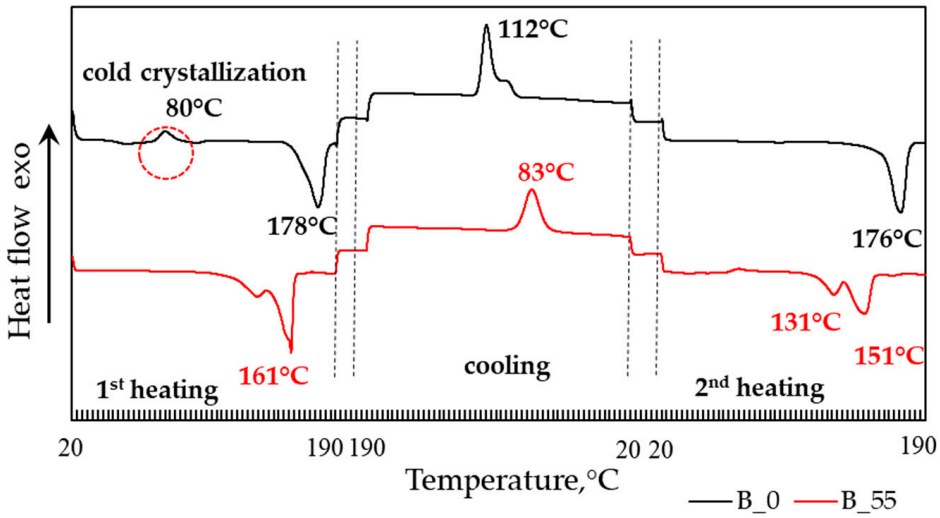


Figure 16. DSC curves of sample B before composting (B_0) and after 55 days of composting (B_55) in an electric composter.

Significant changes were visible in the first heating as well as in the cooling and the second heating cycle. The temperatures of melting were significantly shifted to lower values after 55 days of composting; after the same period, the crystallization temperature was significantly decreased. The composting caused the disappearance of the cold crystallization peak visible in the original sample, and the melting peak was split in two. Quantitative analysis of DSC measurements (Figure 17) also showed that the changes in thermograms in the first run were not connected only to the consumption of the amorphous phase, but significant changes in the molecular structure occurred. This was confirmed by the decrease of crystallization enthalpy as well as of the melting enthalpy in the second heating cycle when the record of the sample was no longer affected by its previous thermal and other history.

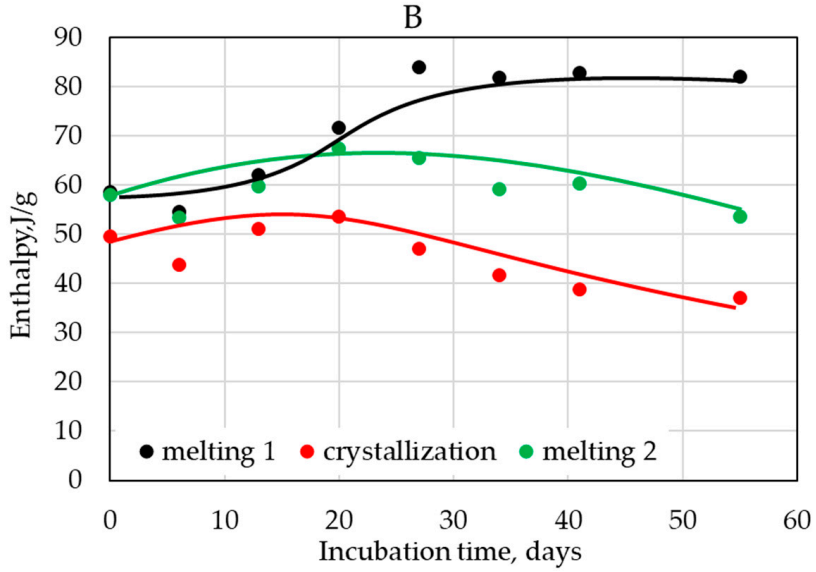


Figure 17. Evolution of enthalpies of melting and crystallization during the incubation in an electric composter for sample B.

4. Conclusions

This detailed study presents results from composting experiments in several experimental settings, all aimed at the group of PLA/PHB blend materials with various compositions and, depending on the particular material, also containing citric-acid-ester-based

plasticizers and thermoplastic starch (TPS). All tested samples were in their real final product forms and shapes.

It was found that the studied PLA/PHB-based blends were fully biodegradable under industrial composting conditions as well as in an electric composter, which was designed for the composting of kitchen waste. A very important result from this study is the observation that some of the studied materials, despite their high PLA contents, could fully biodegrade under home conditions. The result is explained by the assumption that PLA could react with PHB during the blending in the melt form, and this reactive extrusion process could induce re-esterification of both polymer components. This extrusion process was intentionally designed with such a purpose. The easily biodegradable PHB segments can promote the polymer chains' scission and ultimately complete biodegradation of the materials under home-composting conditions.

Evaluation of GPC, DSC, and SEM data showed that during the composting of studied PLA/PHB blends, the changes in the molecular structure and morphology proceeded not only on the surface but also in the bulk of the materials. SEM images showed that already in the first stages of biodegradation, not only macroscopic disintegration but also biological decomposition of the materials took place on the surface, causing an enlargement of the specific surface area and thus the acceleration of the biodegradation process.

A very important result was the verification that disintegration and mineralization as the two main processes during biodegradation of materials could run in the case of the studied PLA/PHB blends not only in sequence but also in parallel. This was observed mainly in the case of thicker specimens like cups, but also in the case of thin products like films where the disintegration was extremely rapid but the mineralization phase was delayed only shortly. Based on these results, it can be concluded that these PLA/PHB materials do not leave microplastics in the environment after industrial as well as after home-composting processes. The composting experiment in a municipal composting plant confirmed and verified the laboratory results. During two independent testing cycles, it was found that the studied PLA/PHB materials degraded comparably or even faster than the pure cellulose reference did.

Author Contributions: Conceptualization, R.P. (Roderik Plavecand); methodology, M.F. and M.K. (Marek Koutný); validation, R.P. (Radek Přikryl); formal analysis, E.M., S.H., J.B. and M.R.; investigation, M.F., S.F., L.O., V.H., A.F. and M.S.; data curation, A.B. (Andrej Bacoand) and S.K.; writing—original draft preparation, L.D. and S.F.; visualization, M.M. and A.B. (Anna Báreková); supervision, P.A. and M.K. (Markéta Kadlečková); project ad-ministration, E.M., Z.V. and J.F. All authors have read and agreed to the published version of the manuscript.

Funding: This research was funded by Internal Grant Agency with grant number IGA/FT/2022/006, Slovak Research and Development Agency with grant number APVV-20-0256 and APVV-20-0193, Operational Program Integrated Infra-structure within the project "Demand-driven research for the sustainable and innovative food", Drive4SIFood 313011V336, co-financed by the European Regional Development Fund and project FCH-S-21-7553 of the Specific University Research Grant.

Institutional Review Board Statement: Not applicable.

Data Availability Statement: The study did not report any data.

Acknowledgments: This work was supported by an internal grant IGA/FT/2022/006, APVV-20-0256, APVV-20-0193, Operational Program Integrated Infrastructure within the project "Demand-driven research for the sustainable and innovative food", Drive4SIFood 313011V336, co-financed by the European Regional Development Fund and project FCH-S-21-7553 of the Specific University Research Grant.

Conflicts of Interest: The authors declare no conflict of interest.

References

1. Duraj-Thatte, A.M.; Manjula-Basavanna, A.; Courchesne, N.-M.D.; Cannici, G.I.; Sánchez-Ferrer, A.; Frank, B.P.; Hag, L.V.; Cotts, S.K.; Fairbrother, D.H.; Mezzenga, R.; et al. Water-processable, biodegradable and coatable aquaplastic from engineered biofilms. *Nat. Chem. Biol.* **2021**, *17*, 732–738. [CrossRef]
2. Xia, Q.; Chen, C.; Yao, Y.; Li, J.; He, S.; Zhou, Y.; Li, T.; Pan, X.; Yao, Y.; Hu, L. A strong, biodegradable and recyclable lignocellulosic bioplastic. *Nat. Sustain.* **2021**, *4*, 627–635. [CrossRef]
3. Ghosh, K.; Jones, B.H. Roadmap to Biodegradable Plastics—Current State and Research Needs. *ACS Sustain. Chem. Eng.* **2021**, *9*, 6170–6187. [CrossRef]
4. Liao, J.; Chen, Q. Biodegradable plastics in the air and soil environment: Low degradation rate and high microplastics formation. *J. Hazard. Mater.* **2021**, *418*, 126329. [CrossRef]
5. Šašinková, D.; Serbruyns, L.; Julinová, M.; FayyazBakhsh, A.; De Wilde, B.; Koutný, M. Evaluation of the biodegradation of polymeric materials in the freshwater environment—An attempt to prolong and accelerate the biodegradation experiment. *Polym. Degrad. Stab.* **2022**, *203*, 110085. [CrossRef]
6. Arockiam, A.J.; Subramanian, K.; Padmanabhan, R.; Selvaraj, R.; Bagal, D.K.; Rajesh, S. A review on PLA with different fillers used as a filament in 3D printing. *Mater. Today Proc.* **2021**, *50*, 2057–2064. [CrossRef]
7. Ko, E.; Kim, T.; Ahn, J.; Park, S.; Pak, S.; Kim, M.; Kim, H. Synergic Effect of HNT/oMMT Bi-filler System for the Mechanical Enhancement of PLA/PBAT Film. *Fibers Polym.* **2021**, *22*, 2163–2169. [CrossRef]
8. Shanmugam, V.; Rajendran, D.J.J.; Babu, K.; Rajendran, S.; Veerasimman, A.; Marimuthu, U.; Singh, S.; Das, O.; Neisiany, R.E.; Hedenqvist, M.S.; et al. The mechanical testing and performance analysis of polymer-fibre composites prepared through the additive manufacturing. *Polym. Test.* **2020**, *93*, 106925. [CrossRef]
9. Sedničková, M.; Pekařová, S.; Kucharczyk, P.; Bočkaj, J.; Janigová, I.; Kleinová, A.; Jochec-Mošková, D.; Omaníková, L.; Perd'ochová, D.; Koutný, M.; et al. Changes of physical properties of PLA-based blends during early stage of biodegradation in compost. *Int. J. Biol. Macromol.* **2018**, *113*, 434–442. [CrossRef]
10. Arrieta, M.P.; López, J.; Rayón, E.; Jiménez, A. Disintegrability under composting conditions of plasticized PLA&PHB blends. *Polym. Degrad. Stab.* **2014**, *108*, 307–318. [CrossRef]
11. Rahman, H.; Bhoi, P.R. An overview of non-biodegradable bioplastics. *J. Clean. Prod.* **2021**, *294*, 126218. [CrossRef]
12. Lee, P.-K.; Choi, B.-Y.; Kang, M.-J. Assessment of mobility and bio-availability of heavy metals in dry depositions of Asian dust and implications for environmental risk. *Chemosphere* **2015**, *119*, 1411–1421. [CrossRef]
13. Yu, Z.; Tang, J.; Liao, H.; Liu, X.; Zhou, P.; Chen, Z.; Rensing, C.; Zhou, S. The distinctive microbial community improves composting efficiency in a full-scale hyperthermophilic composting plant. *Bioresour. Technol.* **2018**, *265*, 146–154. [CrossRef]
14. Altieri, R.; Seggiani, M.; Esposito, A.; Cinelli, P.; Stanzione, V. Thermoplastic Blends Based on Poly(Butylene Succinate-co-Adipate) and Different Collagen Hydrolysates from Tanning Industry—II: Aerobic Biodegradation in Composting Medium. *J. Polym. Environ.* **2021**, *29*, 3375–3388. [CrossRef]
15. Mengqi, Z.; Shi, A.; Ajmal, M.; Ye, L.; Awais, M. Comprehensive review on agricultural waste utilization and high-temperature fermentation and composting. *Biomass Convers. Biorefinery* **2021**, *24*, 1–24. [CrossRef]
16. Schulte, P.M. The effects of temperature on aerobic metabolism: Towards a mechanistic understanding of the responses of ectotherms to a changing environment. *J. Exp. Biol.* **2015**, *218*, 1856–1866. [CrossRef]
17. Iovino, R.; Zullo, R.; Rao, M.A.; Cassar, L.; Gianfreda, L. Biodegradation of poly(lactic acid)/starch/coir biocomposites under controlled composting conditions. *Polym. Degrad. Stab.* **2008**, *93*, 147–157. [CrossRef]
18. Apinya, T.; Sombatsompop, N.; Prapagdee, B. Selection of a Pseudonocardia sp. RM423 that accelerates the biodegradation of poly(lactic) acid in submerged cultures and in soil microcosms. *Int. Biodeterior. Biodegrad.* **2015**, *99*, 23–30. [CrossRef]
19. Narancic, T.; Verstichel, S.; Chaganti, S.R.; Morales-Gamez, L.; Kenny, S.T.; De Wilde, B.; Padamati, R.B.; O'Connor, K.E. Biodegradable Plastic Blends Create New Possibilities for End-of-Life Management of Plastics but They Are Not a Panacea for Plastic Pollution. *Environ. Sci. Technol.* **2018**, *52*, 10441–10452. [CrossRef]
20. Accinelli, C.; Abbas, H.K.; Bruno, V.; Nissen, L.; Vicari, A.; Bellaloui, N.; Little, N.S.; Shier, W.T. Persistence in soil of microplastic films from ultra-thin compostable plastic bags and implications on soil Aspergillus flavus population. *Waste Manag.* **2020**, *113*, 312–318. [CrossRef]
21. Bandini, F.; Frache, A.; Ferrarini, A.; Taskin, E.; Cocconcelli, P.S.; Puglisi, E. Fate of Biodegradable Polymers Under Industrial Conditions for Anaerobic Digestion and Aerobic Composting of Food Waste. *J. Polym. Environ.* **2020**, *28*, 2539–2550. [CrossRef]
22. Koskimäki, J.J.; Kajula, M.; Hokkanen, J.; Ihantola, E.-L.; Kim, J.H.; Hautajärvi, H.; Hankala, E.; Suokas, M.; Pohjanen, J.; Podolich, O.; et al. Methyl-esterified 3-hydroxybutyrate oligomers protect bacteria from hydroxyl radicals. *Nat. Chem. Biol.* **2016**, *12*, 332–338. [CrossRef] [PubMed]
23. Opgenorth, P.H.; Korman, T.P.; Bowie, J.U. A synthetic biochemistry module for production of bio-based chemicals from glucose. *Nat. Chem. Biol.* **2016**, *12*, 393–395. [CrossRef] [PubMed]
24. Siracusa, V.; Rocculi, P.; Romani, S.; Rosa, M.D. Biodegradable polymers for food packaging: A review. *Trends Food Sci. Technol.* **2008**, *19*, 634–643. [CrossRef]
25. Šerá, J.; Serbruyns, L.; De Wilde, B.; Koutný, M. Accelerated biodegradation testing of slowly degradable polyesters in soil. *Polym. Degrad. Stab.* **2020**, *171*, 109031. [CrossRef]

26. Vaverková, M.; Adamcová, D.; Kotovicová, J.; Toman, F. Evaluation of biodegradability of plastics bags in composting conditions. *Ecol. Chem. Eng. S* **2014**, *21*, 45–57. [CrossRef]
27. Husárová, L.; Pekařová, S.; Stloukal, P.; Kucharzcyk, P.; Verney, V.; Commereuc, S.; Ramone, A.; Koutny, M. Identification of important abiotic and biotic factors in the biodegradation of poly(l-lactic acid). *Int. J. Biol. Macromol.* **2014**, *71*, 155–162. [CrossRef]
28. Stloukal, P.; Kalendova, A.; Mattausch, H.; Laske, S.; Holzer, C.; Koutny, M. The influence of a hydrolysis-inhibiting additive on the degradation and biodegradation of PLA and its nanocomposites. *Polym. Test.* **2015**, *41*, 124–132. [CrossRef]
29. Stloukal, P.; Pekařová, S.; Kalendova, A.; Mattausch, H.; Laske, S.; Holzer, C.; Chitu, L.; Bodner, S.; Maier, G.; Slouf, M.; et al. Kinetics and mechanism of the biodegradation of PLA/clay nanocomposites during thermophilic phase of composting process. *Waste Manag.* **2015**, *42*, 31–40. [CrossRef]
30. Jašo, V.; Glenn, G.; Klamczynski, A.; Petrović, Z.S. Biodegradability study of polylactic acid/ thermoplastic polyurethane blends. *Polym. Test.* **2015**, *47*, 1–3. [CrossRef]
31. Janigová, I.; Lacík, I.; Chodák, I. Thermal degradation of plasticized poly(3-hydroxybutyrate) investigated by DSC. *Polym. Degrad. Stab.* **2002**, *77*, 35–41. [CrossRef]
32. Špitalský, Z.; Lacík, I.; Lathová, E.; Janigová, I.; Chodák, I. Controlled degradation of polyhydroxybutyrate via alcoholysis with ethylene glycol or glycerol. *Polym. Degrad. Stab.* **2006**, *91*, 856–861. [CrossRef]

Biodegradable composite materials based on poly(3-hydroxybutyrate) for 3D printing applications

MENCIK, Premysl[1*], MELCOVA, Veronika[1], KONTAROVA, Sona[1], PRIKRYL, Radek[1], PERDOCHOVA, Dagmara[2], REPISKA, Martina[2]

[1] Brno University of Technology, Faculty of Chemistry, Purkynova 464/118, 612 00 Brno, Czech Republic

[2] Slovak University of Technology in Bratislava, Faculty of Chemical and Food Technology, Radlinskeho 9, 812 37 Bratislava, Slovak Republic

*mencik@fch.vutbr.cz

Keywords: Poly(3-hydroxybutyrate), Kaolin, Limestone, Bio-composite, 3D print.

Abstract. Presented work deals with the development of bio-source and biodegradable composite material for 3D printing. Polymer blend based on poly(3-hydroxybutyrate) (60 wt%) and poly(lactic acid) (25 wt%) plasticized with tributyl citrate (15 wt%) was used as a matrix. This base blend was filled with 10 vol% of kaolin or limestone. Zinc stearate was used for the surface treatment of the limestone samples. The mechanical and thermal properties of the composites, as well as their behavior during 3D printing process, were compared with unfilled blend and commercial poly(lactic acid) based 3D printing filament. Warping behavior, one of the main problems of 3D printing materials, was studied by means of warp coefficient. Cross-sections of specimens 3D printed under the same processing conditions were observed by the optical microscope. In the case of composite samples, individual filaments were separated. Despite the separation, composites filled with kaolin and with surface treated limestone exhibited satisfying mechanical properties. Scanning electron microscopy analysis confirmed good particle distribution of the samples with kaolin and surface treated limestone. No significant particle agglomerates were formed in the composites with limestone proving good dispersion ability of zinc stearate. Thermogravimetric analysis and Differential scanning calorimetry analysis showed no degradation effect of the used fillers on base polymer matrix. Observed results indicate that kaolin and surface treated limestone are suitable fillers for the bio-source composites used for 3D printing.

Introduction

3D printing as one of the method of additive manufacturing is currently on the rise and thanks to its financial availability it starts to spread outside specialized manufacturing and rapid prototyping centers. Thanks to the printing speed and availability of the 3D printers it is the most common method in population mainly for private usage. Manufacturers of 3D printing materials produce a large variety of materials, but most commonly on petrochemical base. This makes space for development of new bioplastic materials which could be used for 3D printing. The scientific world pays lots of attention to 3D printing from metals, or resins cured by UV or blue light. The Fused filament fabrication (FFF) 3D printing method can be found in publications focusing on pharmacy [1, 2] or special usage of commercial materials [3].

Warping is one of the biggest problems in 3D printing using this method. It is the process during which the printed object starts to twist and the edges rise up from the printing bed. From the point of view of material structure it is the inner tension in the printed object caused by gradual shrinkage of individual layers. The reason of this malfunction is a combination of the temperature shrinkage of the plastic and its crystallization. Nucleated and highly crystalline polymers exhibit higher level of warping during 3D printing in comparison with amorphous materials. It is possible to partially eliminate these negative effects by choosing the suitable printing condition and/or by addition of

filler to the polymer matrix. No comprehensive or even standardized testing method of printing properties has been constituted at present time.

Printing properties might be positively affected by usage of reinforced materials. Mechanical properties such as tensile strength or fracture toughness might be also improved by this. We must also mention the potential complication during 3D printing of composites, mainly agglomeration of the filler and congestion of the printer's die [4].

Biopolymers and bioplastics are continuously building stronger position on the market and their usage in 3D printing brings a large challenge. One of the most promising candidates is poly(3-hydroxy butyrate) (P3HB) [5]. This biopolymer got an attention of many research centers thanks to possibility of its producing from the food waste resources [6, 7]. Besides economic advantages, such as a low price of the raw materials, there is an important fact of full P3HB compostability, its degradability in soils and both fresh and sea water [8, 9]. Therefore P3HB and composites based on it are the main focus of this article.

Experimental

Used Materials Poly(3-hydroxy butyrate) (PHB) (Biomer - T22), poly(lactic acid) (PLA) (Natureworks - Ingeo 4060D), tri-n-butyl citrate (Vertellus - Citroflex® 4), kaolin (Sedlecky kaolin a. s. - Sedlec Ia), limestone (Piotrovice - WW-2), zinc stearate (Sigma Aldrich).

Samples Preparation The examined samples were prepared by the twin screw extrusion on the LabTech machine using the downward temperature profile from 180°C on the feeding zone to 150°C on the die and the 100 RPM of screw.

Unfilled matrix was prepared as follows: 60 wt% PHB, 25 wt% PLA and 15 wt% plasticizer tributyl citrate. 10 vol% of filler was added to the matrix for the preparation of composite samples. Presence of zinc stearate acted as interfacial compatibilizer. The detailed conception of the samples in weight parts is displayed in Table 1.

Table 1 Weight parts of prepared composite samples

Sample	PHB	PLA	Plasticizer	Kaolin	Limestone	Zinc Stearate
Unfilled matrix	60	25	15			
Komp.1	60	25	15	23		
Komp.2	60	25	15		24	
Komp.3	60	25	15		24	5

The raw material for 3D print - 3D print filament - had been prepared on single screw extruder HAAKE™ Rheomex OS. Extruded filament was cooled in water bath at 60°C and continuously winded. A biaxial optical control of the filament diameter, calibrated to value of 1.75 mm, was installed before the winding device.

The macroscopic structure of printed composite samples and samples with unfilled matrix was observed by optical microscopy. The microstructure and level of particle dispersion (in case of composites) was observed by the Scanning electron microscopy (SEM). The mechanical properties were examined by tensile tests.

Testing samples for both tensile and warp analyses had been prepared by FFF 3D printing method using Prusa i3MK2 and Prusa i3MK3 printers. The 3D printing was performed at the temperature range from 195°C to 190°C without heating of the printing bed. While printing the test samples, the polymer melt is deposited collinearly directly one next to the other in perimeters, which should compose a compact object. During the warping sample printing (shown in Fig. 1), the height of the sample printed before its separation from the bed was observed. The theoretical height of the sample was then divided by the measured value to get the value of warp coefficient as shown in the Eq. 1. The intended theoretical height of the sample was 10 mm.

$$\text{Warp coefficient} = \frac{\text{theoretical warp specimen height}}{\text{maximum printed height}}. \quad (1)$$



Fig. 1 The V-shaped test warping specimen

The thermal behavior of all samples and crystallization behavior of composites was observed by differential scanning calorimetry (DSC) and thermogravimetric analysis (TGA) method. The outputs of the mechanical tests and printing behavior of samples were compared with commercial material for 3D printing – Prusa PLA Natural, which is considered to be a low warping material.

Results and Discussion

The microstructure distribution of the composites filler was observed using SEM. For the composite sample Komp.1 (not presented here) SEM micrograph shows well dispersed lamellar kaolin particles. These particles are dispersed uniformly and without significant agglomerates.

Fig. 2a shows the sample Komp.2, where sharp edges of limestone particle agglomerates of size from 1 to 3 micrometers can be observed. The particles separated from the matrix proved low interphase compatibility. Matrix in the far field from the particles shows fragile behavior. It is demonstrated by the sharp fracture patterns.

Fig. 2b shows fracture area of the sample Komp.3. The particle agglomerates aren't significantly smaller than those of the Komp.2 sample but exhibit better compatibility with the matrix. The particles are apparently well blended with the matrix. The matrix surrounding the particles does not show sharp fracture patterns compared to Fig. 2a, which can be a proof of certain level of the matrix softening by stearate.

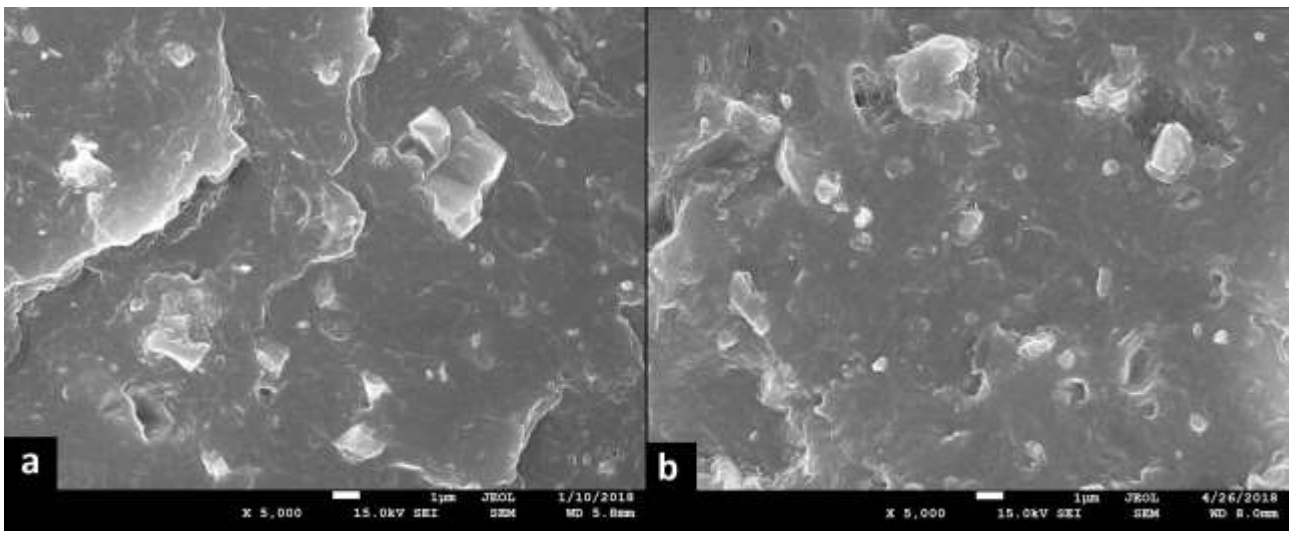


Fig. 2 SEM micrographs of limestone particles distribution in Komp.2 and Komp.3 samples

Warp coefficient value of examined biomaterials was compared with that of commercial 3D printing materials based on PLA (see Fig.3). Even the unfilled matrix reached less than half of the warp coefficient value compared to the commercial material. Among examined composite samples, the lowest warp coefficient was observed with sample Komp.1. On the other hand, filling with the limestone impaired the printing properties which were indicated by increased warp coefficient of the sample Komp.2. The sample Komp.3 shows lower warping in comparison with the sample

Komp.2, even compared to the unfilled matrix. The zinc stearate improves printing behavior of the composite filled by limestone.

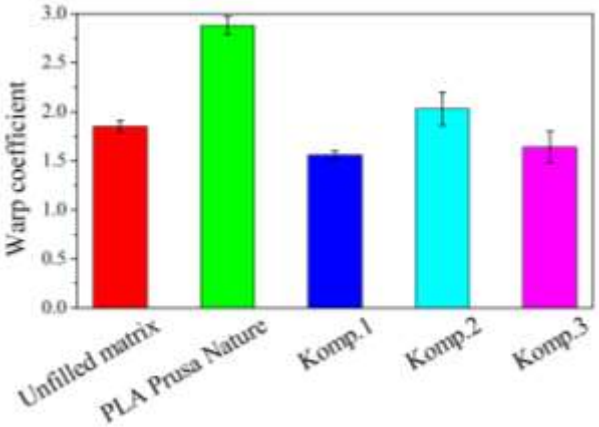


Fig. 3 Warp coefficient of unfilled polymers and composite samples filled with kaolin and limestone

Fig. 4 shows cross-section fragile fracture areas of examined samples, which were printed in order to compare the macroscopic structure. Fig. 4a shows the fracture area of commercial material PLA Prusa Natural. There are no visible significant voids in between individual perimeters and sample seems to be compact. Fig. 4b shows the fracture area of the unfilled matrix. Only a small amount of tight vacancies can be seen on the right side. The rest of the sample volume is very well joined together and creates a monolithic mass. Fig. 4c shows voids enlarging in Komp.1 on the right side of the photography. The rest of the sample exhibits very good homogeneity of material. Filling of the composite with kaolin caused slightly worse joining of the perimeters during 3D printing. Fig. 4d shows the fracture area of the composite Komp.2. Large vacancies can be seen among individual perimeters. It means that under these printing conditions the melt viscosity is insufficient for creation of the compact object. The same result was observed with sample Komp.3.

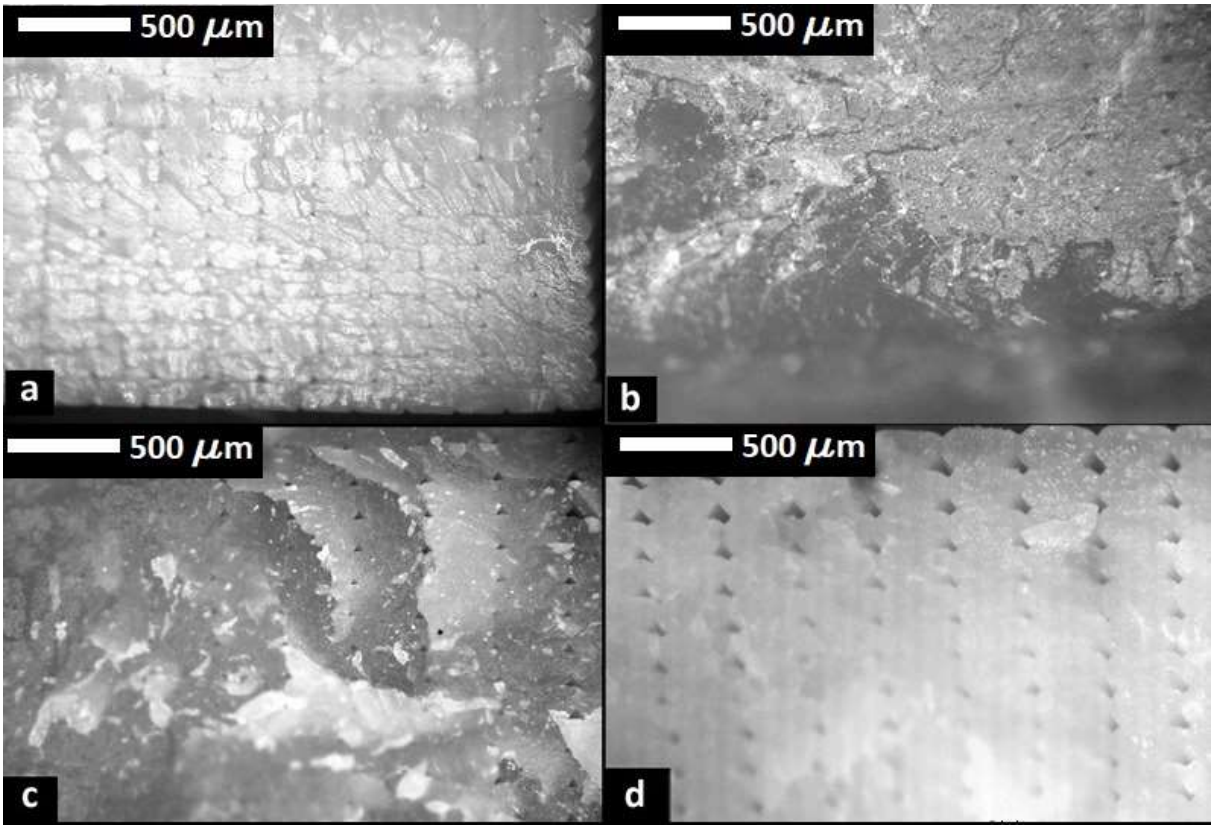


Fig. 4 Macrostructure of 3D printed samples a) PLA Prusa Natural, b) Unfilled matrix, c) Komp.1, d) Komp.2

Tensile tests had been performed to analyze mechanical properties of the samples. None of the composite samples had shown a significant increase of Young's modulus, comparing with the unfilled matrix. Moreover all of the composite samples show lower tensile strength then the unfilled matrix. It is caused by insufficient interface adhesion of the filler to the matrix from the microscopic point of view. From the macroscopic point of view, the decrease of tensile strength is partly caused by heterogenity of the samples, as described above. All composites samples exhibited decrease of elongation at break compared to the unfilled matrix. Only sample Komp.3 had higher elongation probably thanks to plasticization function of zinc stearate.

The crystallization properties were observed by DSC. The section of second cooling cycle curve is shown in Fig. 5 on the right. The addition of the filler in composite samples slightly increased the crystallization temperature (3 to 5°C) compared to the unfilled matrix. It shows poor nucleation ability of kaolin and limestone. This slight temperature increase is not significant for our polymer matrix. Both unfilled matrix and composite samples then crystallize relatively slowly, which correspond with good warping test results. All this range of crystallization temperatures is acceptable for 3D print application.

Table 2 Comparison of the tensile test results

Sample	Modulus [GPa]	Strength [GPa]	Elongation at break [%]
PLA Prusa Natural	3,3 ± 0,1	62,5 ± 2,6	7 ± 1
Unfilled matrix	0,7 ± 0,1	18,7 ± 1,1	111 ± 45
Komp.1	0,8 ± 0,2	15,4 ± 0,9	11 ± 3
Komp.2	0,8 ± 0,2	15,8 ± 0,4	37 ± 13
Komp.3	0,8 ± 0,1	16,8 ± 1,0	63 ± 10

The thermogravimetric analysis was performed to examine the thermal stability of the composites and unfilled matrix. The output thermogram of the weight loss (%) and thermal decomposition rate derivation (%/°C) can be seen in Fig. 5 on the left. Slow weight loss, caused by plasticizer migration out from the sample, can be observed from ca. 150°C. The first peek of thermal degradation belongs to PHB, the second one (the lower one) shows the thermal degradation of PLA. The thermal stability of composites is not significantly influenced by the presence of the filler.

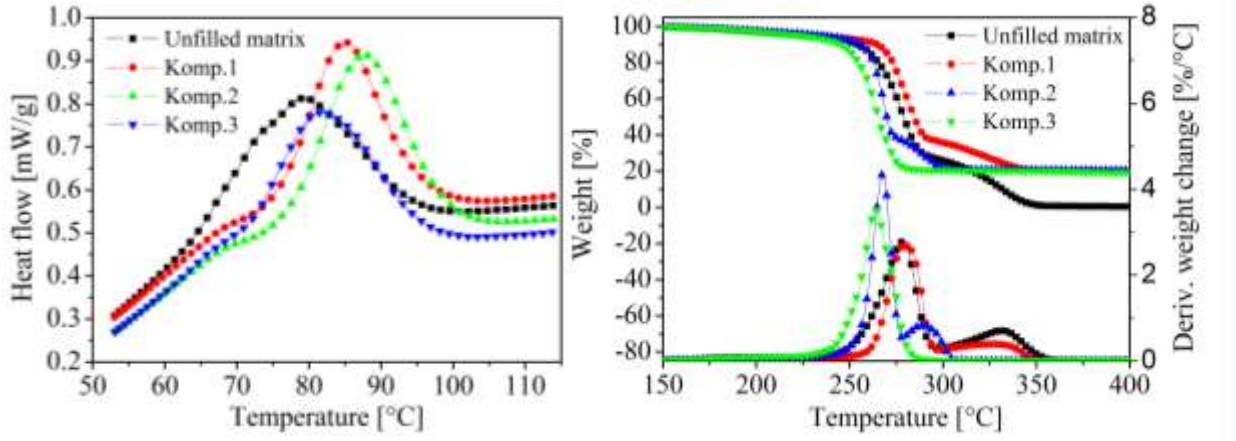


Fig. 5 Thermogravimetric (left) and DSC (right) curves of prepared composites

Conclusion

Plasticized biopolyester matrix based composites with major content of PHB were prepared. PHB/PLA/plasticizer matrix was filled with inorganic filler (kaolin, limestone). Composite sample Komp.1 (filled with kaolin) exhibits very good interface adhesion and particles dispersion on SEM. Good interfacial adhesion, in case of samples filled with limestone, was observed only after adding of the zinc stearate (compatibilizer). The sample Komp.1 also exhibits good macroscopic homogeneity of the 3D printed objects. On the other hand, in case of composite sample Komp.2

(filled with limestone) large vacancies between 3D printed perimeters were observed. This inhomogeneity had not been decreased even with adding of zinc stearate. Composite samples Komp.1 together with Komp.3 (limestone with zinc stearate) showed the lowest warp coefficient. The results of composite samples tensile tests didn't show a significant increase of Young's modulus comparing the unfilled matrix. Thus the filler in composite samples obviously does not fulfill the reinforcing role. None of the fillers caused significant nucleation of the matrix and didn't act as the thermal degradation catalyzer, from the point of view of thermal behavior.

All of the samples, composites and unfilled matrix, could be processed by 3D printing. Composites have lower warp coefficient and higher tensile strain in compare to commercial PLA based 3D printing material. It means that examined materials provide better processability during 3D printing with better mechanical properties of final printed object. PHB based biomaterials are then a promising alternative in the range of the 3D printing materials.

Acknowledgement

This work was supported by the Materials Research Centre, which is supported by the Ministry of Education, Czech Republic (project No. LO1211).

References

[1] G. Kollamaram, et al., Low temperature fused deposition modeling (FDM) 3D printing of thermolabile drugs, Int. J. Pharm. 545 (2018) 144–152.

[2] D. Smith, Y. Kapoor, G. Klinzing and A. Procopio, Pharmaceutical 3D printing: Design and qualification of a single step print and fill capsule, Int. J. Pharm. 544 (2018) 21–30.

[3] S. Chen, J. Lu and J. Feng, 3D-Printable ABS Blends with Improved Scratch Resistance and Balanced Mechanical Performance, Ind. Eng. Chem. Res. 57 (2018) 3923–3931.

[4] E. Çantı and M. Aydın, Effects of micro particle reinforcement on mechanical properties of 3D printed parts, Rapid Prototyping J. 24 (2018) 171–176.

[5] I. Vroman and L. Tighzert, Biodegradable Polymers, Materials. 2 (2009) 307–344.

[6] I. Marova, S. Obruca, R. Prikryl, Patent CZ 304183 B6 (2013).

[7] P. Suriyamongkol, R. Weselake, S. Narine, M. Moloney and S. Shah, Biotechnological approaches for the production of polyhydroxyalkanoates in microorganisms and plants — A review, Biotechnol. Adv. 25 (2017) 148–175.

[8] K. Gonda, D. Jendrossek and H. Molitoris, Fungal degradation of the thermoplastic polymer poly-β-hydroxybutyric acid (PHB) under simulated deep sea pressure, Hydrobiologia. 426 (2000) 173–183.

[9] N. Altaee, G. El-Hiti, A. Fahdil, K. Sudesh and E. Yousif, Biodegradation of different formulations of polyhydroxybutyrate films in soil, SpringerPlus, 5:762. doi: 10.1186/s40064-016-2480-2.

International Journal of
Molecular Sciences

MDPI

Article

Evaluation of the Properties of PHB Composite Filled with Kaolin Particles for 3D Printing Applications Using the Design of Experiment

Přemysl Menčík [1,*], Radek Přikryl [1], Štěpán Krobot [1], Veronika Melčová [1], Soňa Kontárová [1], Roderik Plavec [2], Jan Bočkaj [2], Vojtech Horváth [2] and Pavol Alexy [2]

[1] Institute of Material Chemistry, Faculty of Chemistry, Brno University of Technology, Purkyňova 464/118, 612 00 Brno, Czech Republic
[2] Institute of Natural and Synthetic Polymers, Faculty of Chemical and Food Technology, Slovak University of Technology in Bratislava, Radlinského 9, 812 37 Bratislava, Slovakia
* Correspondence: mencik@fch.vut.cz; Tel.: +42-07-2043-5473

Abstract: In the presented work, poly(3-hydroxybutyrate)-PHB-based composites for 3D printing as bio-sourced and biodegradable alternatives to synthetic plastics are characterized. The PHB matrix was modified by polylactide (PLA) and plasticized by tributyl citrate. Kaolin particles were used as a filler. The mathematical method "Design of Experiment" (DoE) was used to create a matrix of samples for further evaluation. Firstly, the optimal printing temperature of the first and upper layers was determined. Secondly, the 3D printed samples were tested with regards to the warping during the 3D printing. Testing specimens were prepared using the determined optimal printing conditions to measure the tensile properties, impact strength, and heat deflection temperature (HDT) of the samples. The results describe the effect of adding individual components (PHB, PLA, plasticizer, and filler) in the prepared composite sample on the resulting material properties. Two composite samples were prepared based on the theoretical results of DoE (one with the maximum printability and one with the maximum HDT) to compare them with the real data measured. The tests of these two composite samples showed 25% lower warping and 8.9% higher HDT than was expected by the theory.

Keywords: 3D printing; FDM; PHB; composite; Design of Experiment; kaolin

check for updates

Citation: Menčík, P.; Přikryl, R.; Krobot, Š.; Melčová, V.; Kontárová, S.; Plavec, R.; Bočkaj, J.; Horváth, V.; Alexy, P. Evaluation of the Properties of PHB Composite Filled with Kaolin Particles for 3D Printing Applications Using the Design of Experiment. *Int. J. Mol. Sci.* **2022**, *23*, 14409. https://doi.org/10.3390/ijms232214409

Academic Editors: Ivo Kuřitka, Miroslav Mrlík and Tomáš Sedláček

Received: 31 October 2022
Accepted: 16 November 2022
Published: 19 November 2022

Publisher's Note: MDPI stays neutral with regard to jurisdictional claims in published maps and institutional affiliations.

Copyright: © 2022 by the authors. Licensee MDPI, Basel, Switzerland. This article is an open access article distributed under the terms and conditions of the Creative Commons Attribution (CC BY) license (https://creativecommons.org/licenses/by/4.0/).

1. Introduction

Poly(3-hydroxybutyrate) is one of the most examined members of the polyhydroxyalkanoate polymer family. It is a highly crystalline, naturally sourced biopolymer synthesized by bacteria and biodegradable in an environment at ambient conditions [1]. PHB is a thermoplastic material with some of its properties, such as melting temperature, glass transition temperature, crystallinity, and tensile strength being very similar to polypropylene. However, PHB is significantly more brittle than PP [2]. It is also not well thermally stable [3]. Due to its high crystallinity and processing temperature, PHB has a high tendency to shrink or warp during 3D printing. Generally, warping could be reduced by the improvement of the adhesion of printed material to the printing bed or by setting the printing parameters precisely [4]. In recent years PHB has also had attention for its biocompatibility. With various 3D printing techniques on the rise, PHB is very much in use in the tissue engineering field. Concerning the FDM 3D printing of neat PHB, this usually turns out to have very poor results due to the significant brittleness of PHB. Several studies have investigated PHB and its copolymers as potential scaffold materials in a diverse range of tissue engineering applications [5,6]. A very effective approach to reduce warping and improve printability is the blending of PHB with another biopolymer or the addition of

filler. PHB is miscible with polyethylene oxide, polyvinyl acetate, polymethyl methacrylate, polycaprolactone, or polylactic acid at different ratios and temperatures [7].

Polylactide (PLA) is well known for its biocompatibility and compostability [8], and it is also well-compatible with PHB, enhancing the 3D printing properties of the mixture [9]. It is characterized by high tensile strength, tensile modulus, and low elongation, which makes it more than suitable for load-bearing applications [10]. Neat PHB, PHB-PLA, or other PLA blends are used in medicine for the 3D printing of scaffolds and hard tissue substitutes [11–13]. Up to now, PLA is also the most widely used material for 3D printing by FDM in terms of biodegradable and nonbiodegradable materials.

Palm fibres, lignin, or cellulose nanofibrils may be used as an organic filler, which decreases the warping of the PHB and, at the same time, does not influence biodegradability [14–17]. Many kinds of inorganic fillers, such as iron and copper particles, have been used to reduce thermal expansion and increase thermal conductivity for other technical plastic matrices [18,19]. Short glass or carbon fibres are suitable for enhancing mechanical properties [20,21]. Montmorillonite nanoclay has also been used to increase mechanical properties [22]. Many other materials like alumina, Zn, and Ti oxides can also be utilized [23]. Several previous works focusing on the evaluation of the influence of other inorganic fillers have also demonstrated kaolin as a usable filler for the bio-source PHB/PLA matrix composites used for 3D printing. The mechanical properties and printability of the kaolin-filled composite do not deteriorate, while differential scanning calorimetry proves there is no degradable effect of the kaolin on the matrix [24]. In another study, kaolin was used to enhance the flow properties of the plastic and showed the potential to be used as a rheological modifier [25].

In some studies, the influence of filler concentration on the mechanical properties of PHB composites has been determined [26], but not with respect to its printability. In others, the effect of printing parameters on tensile properties has been studied [27]. For an unambiguous choice of the appropriate composition of materials for 3D printing, knowledge of the effects of the individual components in a polymer mixture is essential. Design of Experiment (DoE) is one of the methods used to describe the influence of individual material components on the properties under study [28,29] or to predict the final mechanical properties [30]. In this work, the influence of kaolin filler, plasticizer, and PLA content on the mechanical, thermal, and 3D printing properties of PHB-based composites was established using the DoE method.

Ultimately, the Design of Experiment proved to be suitable for outlining the properties of composite material. Six optimal compositions (Comp_O_1 to Comp_O_6) were determined and it was confirmed that the calculated values are achievable after 3D printing and measuring of these compositions.

2. Results and Discussion

2.1. Optimization of 3D Printing Temperature

It was essential to find the optimal 3D printing temperature for all studied materials as they were used for 3D printing of the samples for all the following tests. The visually estimated temperatures from the temperature tower are summarized in Table 1. Optimal printing temperatures were mainly in the range of 175 to 185 °C.

The optimal printing temperatures for five reference samples (Comp_15 to Comp_20) were determined to be 180 ± 5 °C. The deviation of 5 °C was caused by the temperature regulation of the 3D printer.

Since the evaluation of the precision of geometric elements is only visual, the results are relatively highly burdened by the observer's individuality. In the steps to follow, the value of optimal temperature will be more specified.

Table 1. The range of optimal printing temperatures of composites observed from the temperature tower.

Sample	Optimal Printing Temperature (°C)	Sample	Optimal Printing Temperature (°C)
Comp_1	185–175	Comp_11	180–175
Comp_2	180–175	Comp_12	180–175
Comp_3	175 and 200	Comp_13	200
Comp_4	200–195	Comp_14	180–175
Comp_5	200–195 and 180–175	Comp_15	180–175
Comp_6	200 and 180–175	Comp_16	180–175
Comp_7	200–195 and 175	Comp_17	185–175
Comp_8	200–195 and 180–175	Comp_18	180–175
Comp_9	200–175	Comp_19	175
Comp_10	175	Comp_20	175
		Comp_21	200–175

2.2. Determination of Warping Coefficient

Before the warping coefficient of all examined samples could be determined, it was necessary to find the printing temperature of the first layer. The printing temperature of the first layer is one of the most crucial parameters of FDM 3D printing. The first layer is the only one in direct contact with the printing bed and may have a different temperature (T_1) from the rest of the printed layers (T_2). The T_1 temperature must be high enough to ensure that the first layer adheres perfectly to the printing bed. On the other hand, it must not be too high to prevent excessive melting and degradation of the printed material. The T_2 temperature is usually lower for PLA-like materials to maintain a satisfactory shape of the printed part and avoid shrinkage. In addition, due to the low thermal stability of PHB, degradation is prevented.

A warping test with variable temperature T_1 and fixed temperature T_2 = 185 °C was conducted on the sample Comp_21, where T_2 was obtained from the temperature tower. Figure 1 shows the dependence of the warping coefficient on the printing temperature of the first layer (T_1). The results showed that the optimal printing temperature T_1 in this case equalled 195 °C when the warping coefficient reached the lowest values, and thus, the influence of warping was at a minimum. Below this temperature, the polymer melt had a low viscosity and did not adhere sufficiently to the printing bed. On the other hand, above the optimum temperature, there was already a large difference between T_1 and T_2. The printer´s extruder did not have time to cool down and, therefore, printed several layers on top of each other at a higher temperature than T_2. This caused deformation of the bottom of the printed specimen and intensified warping. Temperature T_1 was used further for all tested samples.

Test of warping during 3D printing was performed for all samples and all temperatures in the range of their optimal printing temperatures. The resulting temperatures with the lowest warping coefficient for each sample are presented in Table 2. From the warping test, the optimal printing temperature was further specified and the warping coefficient was calculated. Table 2 also shows that regarding the warping coefficient values, the optimal printing temperature for sample Comp_21 was 190 °C. This was a slightly higher temperature than the one used in the previous test, but this deviation was to determine whether the optimal printing temperature T_1 was negligible.

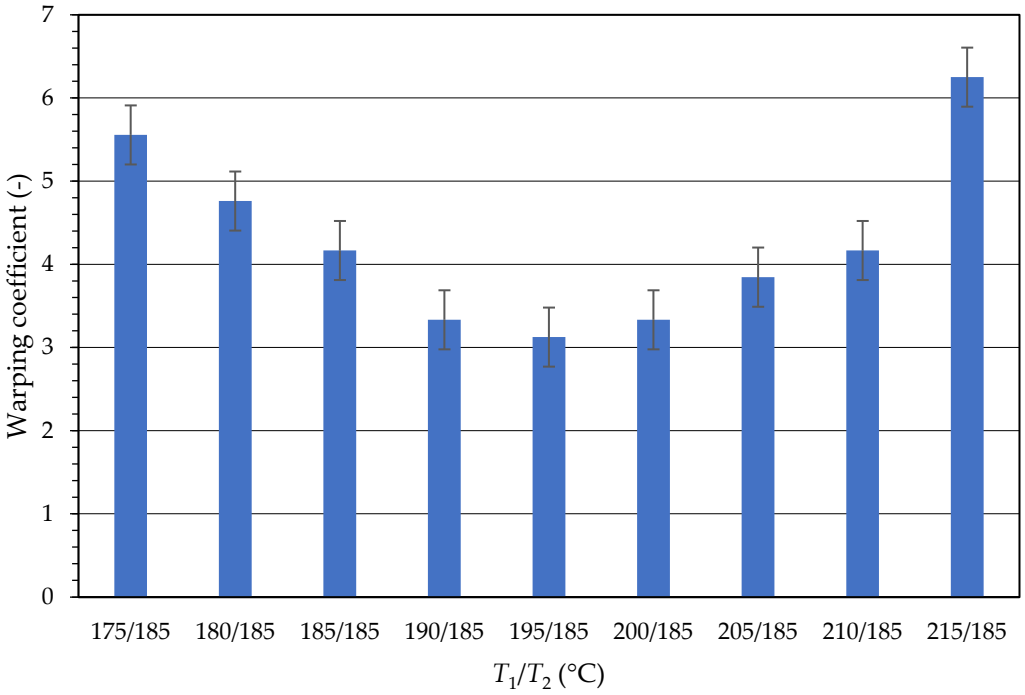


Figure 1. The dependence of the first-layer temperature (T_1) on the warping coefficient of the material.

Table 2. The optimal composite printing temperatures based on the warping test and warping coefficient.

Sample	Printing Temperature T_2 (°C)	Warping Coefficient	Sample	Printing Temperature T_2 (°C)	Warping Coefficient
Comp_1	185	3.2 ± 0.1	Comp_11	185	4.5 ± 0.0
Comp_2	185	4.0 ± 0.2	Comp_12	185	5.0 ± 0.0
Comp_3	195	3.5 ± 0.2	Comp_13	190	3.7 ± 0.2
Comp_4	185	7.1 ± 0.0	Comp_14	185	4.8 ± 0.3
Comp_5	185	4.0 ± 0.2	Comp_15	185	4.2 ± 0.0
Comp_6	185	6.7 ± 0.6	Comp_16	195	4.6 ± 0.6
Comp_7	185	4.4 ± 0.3	Comp_17	185	4.0 ± 0.2
Comp_8	185	6.7 ± 0.6	Comp_18	185	4.4 ± 0.3
Comp_9	185	1.3 ± 0.0	Comp_19	185	4.0 ± 0.2
Comp_10	185	4.0 ± 0.2	Comp_20	185	4.2 ± 0.0
			Comp_21	190	1.5 ± 0.0

Temperatures obtained from the warping test were used for 3D printing of the testing samples for all following tests. The optimal printing temperatures were relatively close together, which indicates that they were not significantly dependent on the ratio between the individual components in the composite samples.

2.3. Tensile Test

Young's modulus of elasticity E and tensile strength σ values were obtained from the tensile test of the samples. The results of elongation at break were burdened with a significant standard deviation and therefore were not published.

The results of Young's modulus report showed that all three DoE factors were statistically relevant. The lowest level of significance was for parameter b_1. Therefore, factor x_1 was fixed on coded level 0, which means the middle of its range. Figure 2a shows the plot of dependence of Young's modulus of elasticity on the sample's composition represented by factors x_2 and x_3. With increasing plasticiser content, e.g., with increasing

factor x_2, Young's modulus linearly decreased. With increasing kaolin content in the material, e.g., with increasing factor x_3, modulus E also increased until it reached a maximum. Further increase of kaolin content did not affect the modulus E increase, and the value of E was relatively constant beyond this maximum point. Filling with kaolin resulted in a toughening effect, and the E value increased up to this kaolin concentration. Also, the viscosity of the melted polymer during 3D printing was too high, and the connection of the printed layers was weaker beyond this point. Moreover, the high viscosity of polymer melt during 3D printing created larger voids, which decreased thermal stability (HDT). This trend was also confirmed in a full range of factor x_1, e.g., in ranges of PLA content.

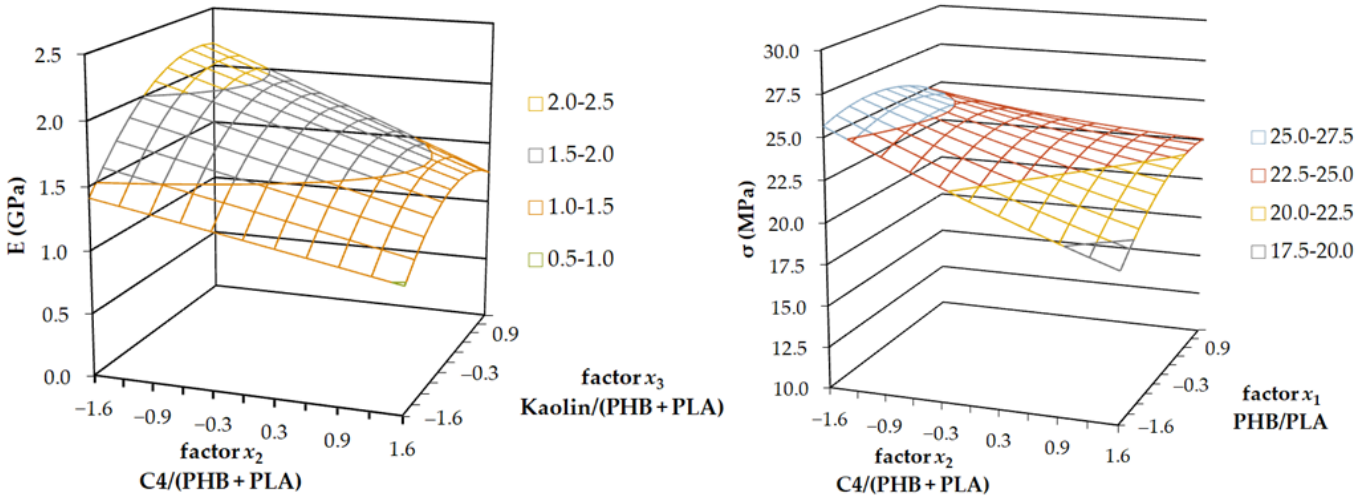


Figure 2. The 3-axis plots of the tensile test results; Young's modulus of elasticity (**left**) and tensile strength (**right**).

The results of the tensile strength report showed that only parameter b_2 was statistically relevant (content of plasticizer C4), whereas the other two parameters were not. The lowest level of significance was shown by parameter b_3, and therefore factor x_3 was fixed on coded level 0. The plot of dependence of tensile strength σ on the DoE factors x_2 and x_1 is presented in Figure 2b. Although, since factor x_1 was not statistically relevant, we cannot evaluate and comment on its influence on tensile strength. The tensile strength decreased linearly with the increasing content of C4 in the mixture. This result indicated the functioning plasticization ability of C4, which caused plastic deformation to occur at even lower loads. The shape of the stress-strain curve showed normative shape A, which means that the first local maximum corresponded with the tensile strength of the sample.

2.4. Unnotched and Notched Charpy Impact Test

The unnotched Charpy impact test results implied that the factors x_1 and x_2 were statistically relevant. Interestingly, although factor x_3 corresponded with kaolin content, it was not statistically relevant and thus fixed on coded level 0. The graph in Figure 3a shows the dependence of unnotched impact strength (a_{cU}) on the content of plasticiser, e.g., factor x_2, which increased linearly. This result again confirmed the proper functioning of plasticizer C4 in the samples. The highest value of impact strength was measured for the lowest content of PHB in the mixture. The dependence of impact strength on PHB content was non-linear. The lowest measured value was located on coordinate $x_1 = 0.6$, and from this point on, it increased slightly again. The further increase of a_{cU} values could have been caused by the weaker connections of the 3D printed layers at higher filler contents.

The plot for the notched Charpy impact test, which is illustrated in Figure 3b, is somewhat different than for the unnotched. In this case, the statistically relevant factors were x_2 and x_3. Factor x_1 was not relevant and fixed on coded level 0. The value of notched impact strength (a_{cN}) increased non-linearly with the increasing content of the

plasticiser. It also increased with the increasing content of kaolin particles. This effect was, however, more relevant for the higher content of plasticiser because of better dispersion of the particles in the plasticized matrix, which corresponded with slower crack propagation.

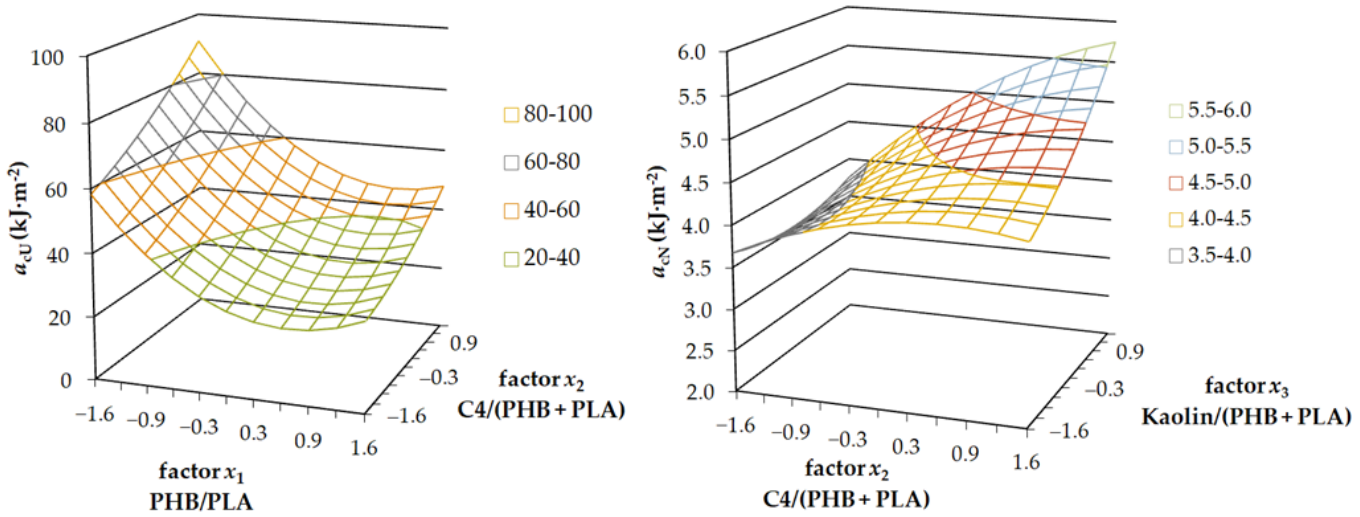


Figure 3. The 3-axis plots of the unnotched (**left**) and the notched (**right**) Charpy impact test results.

2.5. Heat Deflection Temperature Test

The Heat Deflection Temperature (HDT) Test reported all the factors as statistically irrelevant, with x_3 being the least significant of all. Increasing the filling concentration with kaolin showed a smooth linear improving effect on the HDT, but the overall effect was negligible. Factor x_3 was fixed on coded level 0, and the plot was created using factors x_1 and x_2. The decreasing trend of the HDT with increasing content of plasticizer C4 (factor x_2) is evident from the results presented in Figure 4. The dependence of the HDT on factor x_1 was non-linear, with the maximum point in coded level 0.4. The HDT decreased beyond this point, probably because of weaker connections of the 3D printed layers. This non-linear trend was less significant at higher kaolin contents.

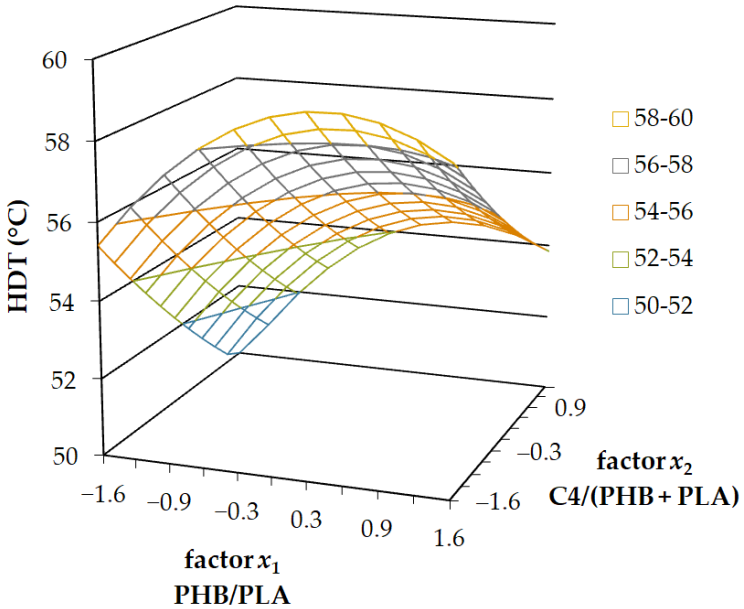


Figure 4. The 3-axis plot of the Heat Deflection Temperature Test results at 1.82 MPa load.

2.6. Optimal Composition of Samples

Regarding the DoE results, the optimal composition of the composite samples, which should, by theory, achieve the maximum value of measured property in each of the tests performed, was determined using the MS Excel Solver function. The optimal material compositions of the samples (Comp_O_1 to Comp_O_6) and the theoretical maximum values of the measured properties are presented in coded levels in Table 3. The material property aimed to maximize and is marked in bold for each composition.

Table 3. The optimal compositions of samples according to the DoE results.

Factor/Property	Comp_O_1	Comp_O_2	Comp_O_3	Comp_O_4	Comp_O_5	Comp_O_6
x_1	0.369	−0.049	−1.682	−1.682	−1.682	0.436
x_2	−1.682	−1.682	1.682	1.682	−0.141	−1.682
x_3	1.200	1.682	−1.682	1.682	−0.739	1.682
E (GPa)	**2.3**	2.2	0.4	0.8	1.2	2.2
σ (MPa)	26.2	**26.4**	18.6	19.5	22.4	26.3
a_{cU} (kJ/m^2)	21.8	22.9	**109.0**	83.3	79.2	21.7
a_{cN} (kJ/m^2)	3.6	3.7	4.2	**5.9**	4.3	3.7
Warping coefficient	14.3	25.0	2.1	2.2	**1.6**	50.0
HDT (°C)	60.9	61.3	48.4	50.1	51.4	**61.5**

Two samples were prepared to confirm that the optimal compositions calculated by theory to achieve the maximum values of measured properties corresponded with the real ones. Sample Comp_O_5 had optimal composition to achieve the lowest warping coefficient, and Comp_O_6 had the highest HDT. The material composition of Comp_O_5 and Comp_O_6 is given in Table 4.

Table 4. The actual weight percentage composition of the prepared samples.

wt%	Comp_O_5	Comp_O_6
PHB	48.6	67.3
PLA	32.3	7.7
C4	10.4	9.3
Kaolin	8.7	15.7

Samples Comp_O_5 and Comp_O_6 were subjected to the Temperature Tower Test to obtain the range of usable printing temperatures. According to the results, the temperature 195 °C was chosen as the ideal printing temperature for both samples. All further testing specimens were printed at 195 °C for the first layer (T_1) and also for all other layers (T_2).

The analysis of the warping coefficient was performed on the mixture Comp_O_5 optimized for low warping. Five testing specimens were used for the test, and the mean value was compared with the theoretical value obtained from the DoE. The mixture Comp_O_6 was optimized for high-temperature stability and subjected to the HDT Test. Eight testing specimens were used for the test, and the mean value was compared with the theoretical value obtained from the DoE. Another six HDT testing specimens were annealed in a laboratory oven for 2 h at 80 °C to achieve another increasement in thermal stability. These samples were named An_Comp_O_6. All the results obtained are given in Table 5.

Table 5. The results of the warping test and the HDT Test of optimised mixtures.

Sample	Warping Coefficient	Warping Coefficient by DoE	HDT (°C)	HDT by DoE (°C)
Comp_O_5	1.3 ± 0.1	1.6	-	-
Comp_O_6	-	-	64.3 ± 2.7	61.5
An_Comp_O_6	-	-	76.0 ± 6.1	-

The obtained value of the warping coefficient was up to 25% lower than anticipated from the results of the DoE. This makes a difference of another two successfully printed layers within the printed sample. In terms of the HDT, the experimentally acquired values were up to 8.9% higher than the theoretical ones obtained from the DoE. It was even possible to increase the value of the HDT by up to 33.5% by annealing the sample. This occurred due to the secondary crystallization of PHB in the samples.

3. Materials and Methods

3.1. Materials

Poly(3-hydroxyburyrate) Biomer® T22 (PHB), polylactid NatureWorks Ingeo™ 4060D (PLA), and plasticizer Vertellus Citroflex® 4 (C4) were used to prepare the polymer matrix. Kaolin Sedlec Ia was used as a filler. Both polymers were dried at 60 °C for 2 h before processing.

3.2. Sample Preparation

Composite blends were prepared by twin screw extruder, LabTech, Sorisole, Italy, with an L/D ratio of 40 and a screw diameter of 16 mm. The temperature profile of extrusion was 80/170/180/180/180/180/180/170/160/150 °C from feeder to die, and the speed of the screw was set to 100 RPM. The filament from the extruder was cooled in a water bath and cut by a strand pelletizer. All material granulates were dried before the next processing.

Filaments for 3D printing were prepared by a single screw extruder, Thermo Fischer Scientific, Waltham, MA, USA, with an L/D ratio of 25. The temperature profile of extrusion was 185/180/175/170 °C from feeder to die, and the speed of the screw was set to 25 RPM. The extruded filament was cooled down in the water bath and winded on spools by a custom-made filament winder.

All testing samples were 3D printed by FDM printer Prusa i3MK3 controlled by V3.9.0 firmware version (Prusa Research a.s., Prague, Czech Republic), and using 0.4 mm E3D V6 nozzle.. All G-codes were prepared in PrusaSlicer, software version 1.41.2. PrusaSlicer is based on an open-source platform Slic3r, which is licensed under the GNU Affero General Public License, version 3. The layer height was 0.2 mm. The printing speed was set to 40 mm/s for perimeters, and 60 mm/s for rectilinear infill. The printing speed of the first layer was 70% of the printing speed of the other layers. The infill density was set to 100% to create the entirely filled samples. The print profile used was taken from the profile for PLA. Therefore, the printed sample was cooled by a fan at 100% from the second layer.

3.3. Optimization of 3D Printing Temperature

The Temperature Tower Test (TTT) samples were printed from each prepared composite blend [31]. They consisted of 6 floors, where each floor was made up of 8 different geometric elements. The 3D printing began at 220 or 195 °C, and each consecutive floor above the previous one was printed at a temperature 5 °C lower. The geometric elements from each floor were evaluated visually to determine the optimal printing temperature.

3.4. Determination of Warping Coefficient

Warping is a negative effect manifested by a warping coefficient. The warp testing samples [31] were printed for warping analysis. The height of the printed sample was observed during printing to the point when the specimen began to warp and detach from the printing bed. The theoretical total height of the sample (10 mm) was divided by the maximum height reached by the sample. The resulting value is the warping coefficient. This relation is shown in Equation (1).

$$Warping\ coefficient = \frac{Total\ theoretical\ height\ of\ the\ sample\ (10\ mm)}{Maximum\ height\ reached\ by\ the\ sample} \quad (1)$$

3.5. Tensile Test

Standardised double-paddle testing specimens (dogbones 5A with cross Section 4 × 2 mm) were 3D printed according to the ČSN EN ISO 527-2. The tensile test was performed using the universal testing machine ZWICK Z010 with a 10 kN load cell. The test speed of the measurement was set to 5 mm/min in the deformation range of 0.05–0.25% to determine Young's modulus and to 50 mm/min for the rest of the tests performed. The dogbone 5A test samples were 3D printed with a longitudinally oriented printing trajectory [31]. The number of tested specimens was at least 5 for each tested series.

3.6. Unnotched and Notched Charpy Impact Test

Both tests of impact strength were performed using CEAST Resil Impactor Junior with pendulum hammer 2.7 J. The rectangular testing samples were 3D printed according to ISO 179. The 2 mm deep V-notch with a tip radius of 0.25 mm radius machined on one face was made using a CEAST Power-Driven Notchvis cutting machine. Samples were tested in the edgewise position.

3.7. Heat Deflection Temperature Test

The Heat Deflection Temperature (HDT) Test was performed according to the ČSN EN ISO 294-4 standard using a custom-made laboratory testing machine. Samples for the test were 3D printed and measured in a flatwise position. The samples after 3D printing could not be measured at the lower load allowed by the standard (0.455 MPa) because of the internal tension and therefore were measured using a 1.82 MPa load only.

3.8. Design of Experiment—Composition of Samples

To cover the broadest possible range of resulting material properties the 3-factor, 5-level Design of Experiment (DoE) was compiled. The following limits were chosen:

- The content of PHB ranged from 60 to 95 wt%
- The content of plasticizer C4 ranged from 8 to 15 wt%
- The content of kaolin filler ranged from 5 to 20 wt%

The first factor of the experiment (x_1) was the PHB to PLA ratio, the second factor (x_2) was the plasticizer to total polymer content ratio (C4/(PHB + PLA)), and the third factor (x_3) was the filler to total polymer content ratio (Kaolin/(PHB + PLA)). The limit values, mean values, and steps of the experiment in coded and real values are listed in Table 6. The limit values in coded levels −1.682 and 1.682 correspond with the limit composition of the samples. The mean value is located on the coded coordinate 0. The confidence interval was 95%.

Table 6. Limit values of DoE and steps in coded and real levels.

	Limit Values of the Experiment					
Factors	**−1.682**	**−1**	**0**	**1**	**1.682**	**Step**
x_1-PHB/PLA	1.5000	5.0476	10.2490	15.4510	18.9990	5.202
x_2-C4/(PHB/PLA)	0.0870	0.1051	0.1317	0.1583	0.1765	0.027
x_3-Kaolin/(PHB/PLA)	0.0526	0.0925	0.1509	0.2094	0.2492	0.058

Subsequently, the mathematical matrix of samples was built from the limit values in (from limits in Table 6). The values of factors in coded and real levels are summarized in Table 7. The samples starting with Comp_15 up to Comp_20 have the same material composition and provide information about the repeatability and accuracy of the tests. They were tested in random order with all other samples, and the statistical relevance of measurement was established from the results.

Table 7. The composition of the samples in coded and real levels of DoE.

	Factors in Coded Levels			Factors in Real Levels		
Sample	**PHB/PLA**	**C4 (PHB+PLA)**	**Kaolin (PHB+PLA)**	**PHB/PLA**	**C4 (PHB+PLA)**	**Kaolin (PHB+PLA)**
Comp_1	−1	−1	−1	5.0476	0.1051	0.0925
Comp_2	1	−1	−1	15.4510	0.1051	0.0925
Comp_3	−1	1	−1	5.0476	0.1583	0.0925
Comp_4	1	1	−1	15.4510	0.1583	0.0925
Comp_5	−1	−1	1	5.0476	0.1051	0.2094
Comp_6	1	−1	1	15.4510	0.1051	0.2094
Comp_7	−1	1	1	5.0476	0.1583	0.2094
Comp_8	1	1	1	15.4510	0.1583	0.2094
Comp_9	−1.682	0	0	1.5000	0.1317	0.1509
Comp_10	1.682	0	0	18.9990	0.1317	0.1509
Comp_11	0	−1.681	0	10.2490	0.0870	0.1509
Comp_12	0	1.681	0	10.2490	0.1765	0.1509
Comp_13	0	0	−1.681	10.2490	0.1317	0.0526
Comp_14	0	0	1.681	10.2490	0.1317	0.2492
Comp_15-20	0	0	0	10.2490	0.1317	0.1509

Regarding the given limit values and DoE factors, it was possible to determine the final composition of all testing samples. The actual sample composition is listed in Table 8. The sample Comp_21, not containing the filler, was added to the list for the first estimation of 3D printing conditions.

Table 8. The actual composition of testing samples.

Sample	**PHB (wt%)**	**PLA (wt%)**	**C4 (wt%)**	**Kaolin (wt%)**
Comp_1	69.7	13.8	8.8	7.7
Comp_2	78.4	5.1	8.8	7.7
Comp_3	66.7	13.2	12.7	7.4
Comp_4	75.1	4.9	12.7	7.4
Comp_5	63.5	12.6	8.0	15.9
Comp_6	71.5	4.6	8.0	15.9
Comp_7	61.0	12.1	11.6	15.3
Comp_8	68.7	4.4	11.6	15.3
Comp_9	46.8	31.2	10.3	11.8
Comp_10	74.1	3.9	10.3	11.8
Comp_11	73.6	7.2	7.0	12.2
Comp_12	68.6	6.7	13.3	11.4
Comp_13	76.9	7.5	11.1	4.4
Comp_14	66.0	6.4	9.5	18.0
Comp_15-20	71.0	6.9	10.3	11.8
Comp_21	60.9	26.1	13.0	0

Experimental data were plotted in 3D wave graphs. The graphs show the dependence of the measured value on two statistically relevant DoE factors. The third, less relevant or even irrelevant factor was fixed at a constant level coded as 0. Equation (2) was used to plot the graphs. Parameters x_1, x_2, and x_3, represent DoE factors, PHB/PLA, C4/(PHB + PLA), and Kaolin/(PHB + PLA) respectively.

$$y = b_0 + b_1x_1 + b_2x_2 + b_3x_3 + b_{11}{x_1}^2 + b_{22}{x_2}^2 + b_{33}{x_3}^2 + b_{12}x_1x_2 + b_{13}x_1x_3 + b_{23}x_2x_3 \quad (2)$$

Statistically relevant parameters b_i and thus relevant factors x_i were calculated for each test from the mathematical analysis of standard deviations of the measurements and critical values.

4. Conclusions

Poly(3-hydroxybutyrate) (PHB)-based composites for 3D printing were successfully prepared in the presented work. A mathematical matrix of samples with different material compositions was designed based on the Design of Experiment (DoE) method. The basic range of the usable printing temperatures was determined by the Temperature Tower Test. The optimal printing temperature of the first layer (T_1) was found to be 195 °C. It was determined by a warping test performed during 3D printing and chosen as the optimal printing temperature for all samples.

The testing specimens were 3D printed under the found optimal conditions. The mechanical properties of the composites improved with increasing filler content (kaolin particles) until they reached the maximum point. The polymer melt showed too high a viscosity to achieve the optimal connection of the printed layers beyond this point during 3D printing. With further increasements of the filler content, the mechanical properties remained either constant or even deteriorated. Tensile strength and the heat deflection temperature (HDT) deteriorated with increasing kaolin content, but on the other hand, the printability of materials, represented by a low warping coefficient, improved.

In the end, six optimal compositions (Comp_O_1 to Comp_O_6) were established to provide the highest Young´s modulus, tensile strength, unnotched, and notched impact strength, warping coefficient, and HDT, based on the results of the DoE.

Two material compositions calculated by theory with minimum warping coefficient and maximum HDT (Comp_O_5 and Comp_O_6) were prepared based on the DoE results and 3D printed to confirm that the theoretically determined highest values of the examined properties of these compositions were achievable after their measurement. These samples performed up to 25% lower warping coefficient and up to 8.9% higher HDT after they were measured than was anticipated from the theoretical results calculated by the DoE. Another increasement of HDT, by up to 33.5%, was achieved by annealing the samples (An_Comp_O_6).

In conclusion, the Design of Experiment proved to be suitable for outlining the properties of composite material as it consisted of many components, which could vary in their content. Six optimal compositions were determined and it was confirmed that the calculated values were achievable after 3D printing the compositions and measuring them. The DoE method saves much time and raw materials, as several samples with the most optimal properties can be prepared, and there is no need to prepare and test all of the possibilities.

Author Contributions: Conceptualization, P.M. and R.P. (Radek Přikryl); methodology, P.M. and R.P. (Radek Přikryl); validation, P.M., R.P. (Radek Přikryl) and P.A.; formal analysis, V.M., Š.K. and V.H.; investigation, P.M., Š.K., V.M., S.K., V.H., J.B. and R.P. (Roderik Plavec); resources, R.P. (Radek Přikryl) and P.A.; data curation, P.M., Š.K., V.M. and S.K.; writing—original draft preparation, P.M.; writing—review and editing, Š.K., V.M., S.K. and R.P. (Roderik Plavec); supervision, R.P. (Radek Přikryl) and P.A.; project administration, R.P. (Radek Přikryl) and P.A.; funding acquisition, R.P. (Radek Přikryl) and P.A. All authors have read and agreed to the published version of the manuscript.

Funding: Authors acknowledge the funding by Brno University of Technology through the project FCH-S-20–6340, Slovak Research and Development Agency with grant number APVV-20-0193 and Operational Program Integrated Infrastructure for the project "Center for Medical Bioadditive Research and Production (CEMBAM), code ITMS2014 +: 313011V358, co-financed by the European Regional Development Fund".

Data Availability Statement: Not aplicable.

Conflicts of Interest: The authors declare no conflict of interest.

References

1. Savenkova, L.; Gercberga, Z.; Nikolaeva, V.; Dzene, A.; Bibers, I.; Kalnin, M. Mechanical properties and biodegradation characteristics of PHB-based films. *Process Biochem.* **2000**, *35*, 573–579. [CrossRef]
2. Lenz, R.W.; Marchessault, R.H. Bacterial polyesters: Biosynthesis, biodegradable plastics and biotechnology. *Biomacromolecules* **2005**, *6*, 1–8. [CrossRef]

3. Sato, H.; Dybal, J.; Murakami, R.; Noda, I.; Ozaki, Y. Infrared and raman spectroscopy and quantum chemistry calculation studies of C–H· · · O hydrogen bondings and thermal behavior of biodegradable polyhydroxyalkanoate. *J. Mol. Struct.* **2005**, *744–747*, 35–46. [CrossRef]
4. Rahim, T.N.A.T.; Abdullah, A.M.; Md Akil, H. Recent developments in fused deposition modeling-based 3D printing of polymers and their composites. *Polym. Rev.* **2019**, *59*, 589–624. [CrossRef]
5. Kramschuster, A.; Turng, L.-S. 17—Fabrication of tissue engineering scaffolds. In *Handbook of Biopolymers and Biodegradable Plastics*; Ebnesajjad, S., Ed.; (Plastics Design Library); William Andrew Publishing: Boston, MA, USA, 2013; pp. 427–446. ISBN 978-1-4557-2834-3. [CrossRef]
6. Zeng, J.-H.; Liu, S.-W.; Xiong, L.; Qiu, P.; Ding, L.-H.; Xiong, S.-L.; Li, J.-T.; Liao, X.-G.; Tang, Z.-M. Scaffolds for the repair of bone defects in clinical studies: A systematic review. *J. Orthop. Surg. Res.* **2018**, *13*, 33. [CrossRef]
7. Sin, L.T.; Rahmat, A.R.; Rahman, W.A.; Ebnesajjad, S. *Handbook of Biopolymers and Biodegradable Plastics*, 1st ed.; Ebnesajjad, S., Ed.; (Plastics Design Library); William Andrew Publishing: Boston, MA, USA, 2013. Available online: https://www.elsevier.com/books/handbook-of-biopolymers-and-biodegradable-plastics/ebnesajjad/978-1-4557-2834-3 (accessed on 21 July 2022).
8. Vitetta, L.; Coulson, S.; Thomsen, M.; Nguyen, T.; Hall, S. Probiotics, D-lactic acidosis, oxidative stress and strain specificity. *Gut Microbes* **2017**, *8*, 311–322. [CrossRef] [PubMed]
9. Gonzalez Ausejo, J.; Rydz, J.; Musioł, M.; Sikorska, W.; Sobota, M.; Włodarczyk, J.; Adamus, G.; Janeczek, H.; Kwiecień, I.; Hercog, A.; et al. A comparative study of three-dimensional printing directions: The degradation and toxicological profile of a PLA/PHA blend. *Polym. Degrad. Stab.* **2018**, *152*, 191–207. [CrossRef]
10. Madhavan Nampoothiri, K.; Nair, N.R.; John, R.P. An overview of the recent developments in polylactide (PLA) research. *Bioresour. Technol.* **2010**, *101*, 8493–8501. [CrossRef] [PubMed]
11. Kovalcik, A.; Sangroniz, L.; Kalina, M.; Skopalova, K.; Humpolíček, P.; Omastova, M.; Mundigler, N.; Müller, A.J. Properties of scaffolds prepared by fused deposition modeling of poly(hydroxyalkanoates). *Int. J. Biol. Macromol.* **2020**, *161*, 364–376. [CrossRef]
12. Saska, S.; Pires, L.C.; Cominotte, M.A.; Mendes, L.S.; de Oliveira, M.F.; Maia, I.A.; da Silva, J.V.L.; Ribeiro, S.J.L.; Cirelli, J.A. Three-dimensional printing and in vitro evaluation of poly(3-hydroxybutyrate) scaffolds functionalized with osteogenic growth peptide for tissue engineering. *Mater. Sci. Eng. C Mater. Biol. Appl.* **2018**, *89*, 265–273. [CrossRef] [PubMed]
13. Findrik Balogová, A.; Hudák, R.; Tóth, T.; Schnitzer, M.; Feranc, J.; Bakoš, D.; Živčák, J. Determination of geometrical and viscoelastic properties of PLA/PHB samples made by additive manufacturing for urethral substitution. *J. Biotechnol.* **2018**, *284*, 123–130. [CrossRef]
14. Wu, C.-S.; Liao, H.-T.; Cai, Y.-X. Characterisation, biodegradability and application of palm fibre-reinforced polyhydroxyalkanoate composites. *Polym. Degrad. Stab.* **2017**, *140*, 55–63. [CrossRef]
15. Vaidya, A.A.; Collet, C.; Gaugler, M.; Lloyd-Jones, G. Integrating softwood biorefinery lignin into polyhydroxybutyrate composites and application in 3D printing. *Mater. Today Commun.* **2019**, *19*, 286–296. [CrossRef]
16. Mousavioun, P.; George, G.; Doherty, W. Environmental degradation of lignin/poly(hydroxybutyrate) blends. *Polym. Degrad. Stab.* **2012**, *97*, 1114–1122. [CrossRef]
17. Uzun, G.; Aydemir, D. Biocomposites from polyhydroxybutyrate and bio-fillers by solvent casting method. *Bull. Mater. Sci.* **2017**, *40*, 383–393. [CrossRef]
18. Hwang, S.; Reyes, E.I.; Moon, K.; Rumpf, R.C.; Kim, N.S. Thermo-mechanical characterization of metal/polymer composite filaments and printing parameter study for fused deposition modeling in the 3D printing process. *J. Electron. Mater.* **2015**, *44*, 771–777. [CrossRef]
19. Nikzad, M.; Masood, S.H.; Sbarski, I. Thermo-mechanical properties of a highly filled polymeric composites for fused deposition modeling. *Mater. Des.* **2011**, *32*, 3448–3456. [CrossRef]
20. Zhong, W.; Li, F.; Zhang, Z.; Song, L.; Li, Z. Short fiber reinforced composites for fused deposition modeling. *Mater. Sci. Eng. A* **2001**, *301*, 125–130. [CrossRef]
21. Tekinalp, H.L.; Kunc, V.; Velez-Garcia, G.M.; Duty, C.E.; Love, L.J.; Naskar, A.K.; Blue, C.A.; Ozcan, S. Highly oriented carbon fiber–polymer composites via additive manufacturing. *Compos. Sci. Technol.* **2014**, *105*, 144–150. [CrossRef]
22. Weng, Z.; Wang, J.; Senthil, T.; Wu, L. Mechanical and thermal properties of ABS/montmorillonite nanocomposites for fused deposition modeling 3D printing. *Mater. Des.* **2016**, *102*, 276–283. [CrossRef]
23. Torrado, A.R.; Shemelya, C.M.; English, J.D.; Lin, Y.; Wicker, R.B.; Roberson, D.A. Characterizing the effect of additives to ABS on the mechanical property anisotropy of specimens fabricated by material extrusion 3D printing. *Addit. Manuf.* **2015**, *6*, 16–29. [CrossRef]
24. Mencik, P.; Melcova, V.; Kontarova, S.; Prikryl, R.; Perdochova, D.; Repiska, M. Biodegradable composite materials based on poly(3-hydroxybutyrate) for 3D printing applications. *Mater. Sci. Forum* **2019**, *955*, 56–61. [CrossRef]
25. Tawfik, M.; Ahmed, N.; Ward, A. *Characterization of Kaolin-Filled Polymer Composites*; Society of Plastic Engineers: Houston, TX, USA, 2018. Available online: https://www.researchgate.net/profile/A-Ward/publication/326405402_Characterization_of_kaolin-filled_polymer_composites/links/5b4b1462a6fdccadaecbf1f1/Characterization-of-kaolin-filled-polymer-composites.pdf (accessed on 30 October 2022).
26. Senatov, F.; Anisimova, N.; Kiselevskiy, M.; Kopylov, A.; Tcherdyntsev, V.; Maksimkin, A. Polyhydroxybutyrate/hydroxyapatite highly porous scaffold for small bone defects replacement in the nonload-bearing parts. *J. Bionic Eng.* **2017**, *14*, 648–658. [CrossRef]

27. Auffray, L.; Gouge, P.-A.; Hattali, L. Design of experiment analysis on tensile properties of PLA samples produced by fused filament fabrication. *Int. J. Adv. Manuf. Technol.* **2022**, *118*, 4123–4137. [CrossRef]
28. Munawar, M.A.; Schubert, D.W.; Khan, S.M.; Rehman, M.A.U.; Gull, N.; Islam, A.; Sabir, A.; Shafiq, M.; Haider, B.; Azam, M.; et al. Investigation of functional, physical, mechanical and thermal properties of TiO2 embedded polyester hybrid composites: A design of experiment (DoE) study. *Prog. Nat. Sci. Mater. Int.* **2018**, *28*, 266–274. [CrossRef]
29. Salahshoori, I.; Seyfaee, A.; Babapoor, A.; Neville, F.; Moreno-Atanasio, R. Evaluation of the effect of silica nanoparticles, temperature and pressure on the performance of PSF/PEG/SiO2 mixed matrix membranes: A molecular dynamics simulation (MD) and design of experiments (DOE) study. *J. Mol. Liq.* **2021**, *333*, 115957. [CrossRef]
30. Kumar, S.; Priyadarshan; Ghosh, S.K. Statistical and computational analysis of an environment-friendly MWCNT/NiSO4 composite materials. *J. Manuf. Process.* **2021**, *66*, 11–26. [CrossRef]
31. Menčík, P.; Přikryl, R.; Stehnová, I.; Melčová, V.; Kontárová, S.; Figalla, S.; Alexy, P.; Bočkaj, J. Effect of selected commercial plasticizers on mechanical, thermal, and morphological properties of poly(3-hydroxybutyrate)/poly(lactic acid)/plasticizer biodegradable blends for three-dimensional (3D) print. *Materials* **2018**, *11*, E1893. [CrossRef]

materials

MDPI

Article

Effect of Selected Commercial Plasticizers on Mechanical, Thermal, and Morphological Properties of Poly(3-hydroxybutyrate)/Poly(lactic acid)/ Plasticizer Biodegradable Blends for Three-Dimensional (3D) Print

Přemysl Menčík [1], Radek Přikryl [1], Ivana Stehnová [1], Veronika Melčová [1], Soňa Kontárová [1,*], Silvestr Figalla [1], Pavol Alexy [2] and Ján Bočkaj [2]

[1] Institute of Material Chemistry, Faculty of Chemistry, Brno University of Technology, Purkyňova 464/118, 612 00 Brno, Czech Republic; mencik@fch.vut.cz (P.M.); prikryl@fch.vut.cz (R.P.); xcstehnova@fch.vut.cz (I.S.); xcmelcova@fch.vut.cz (V.M.); xcfigallas@fch.vut.cz (S.F.)

[2] Institute of Natural and Synthetic Polymers, Faculty of Chemical and Food Technology, Slovak University of Technology in Bratislava, Radlinského 9, 812 37 Bratislava, Slovakia; pavol.alexy@stuba.sk (P.A.); jano.bockaj@gmail.com (J.B.)

* Correspondence: kontarova@fch.vut.cz; Tel.: +420-604-455-762

Received: 21 August 2018; Accepted: 28 September 2018; Published: 3 October 2018



Abstract: This paper explores the influence of selected commercial plasticizers structure, which are based on esters of citric acid, on mechanical and thermal properties of Poly(3-hydroxybutyrate)/Poly(lactic acid)/Plasticizer biodegradable blends. These plasticizers were first tested with respect to their miscibility with Poly(3-hydroxybutyrate)/Poly(lactic acid) (PHB/PLA) blends using a kneading machine. PHB/PLA/plasticizer blends in the weight ratio (wt %) of 60/25/15 were then prepared by single screw and corotating meshing twin screw extruders in the form of filament for further three-dimensional (3D) printing. Mechanical, thermal properties, and shape stability (warping effect) of 3D printed products can be improved just by the addition of appropriate plasticizer to polymeric blend. The goal was to create new types of eco-friendly PHB/PLA/plasticizers blends and to highly improve the poor mechanical properties of neat PHB/PLA blends (with majority of PHB) by adding appropriate plasticizer. Mechanical properties of plasticized blends were then determined by the tensile test of 3D printed test samples (dogbones), as well as filaments. Measured elongation at break rapidly enhanced from 21% for neat non-plasticized PHB/PLA blends (reference) to 328% for best plasticized blends in the form of filament, and from 5% (reference) to 187% for plasticized blends in the form of printed dogbones. The plasticizing effect on blends was confirmed by Modulated Differential Scanning Calorimetry. The study of morphology was performed by the Scanning Electron Microscopy. Significant problem of plasticized blends used to be also plasticizer migration, therefore the diffusion of plasticizers from the blends after 15 days of exposition to 110 °C in the drying oven was investigated as their measured weight loss. Almost all of the used plasticizers showed meaningful positive softening effects, but the diffusion of plasticizers at 110 °C exposition was quite extensive. The determination of the degree of disintegration of selected plasticized blend when exposed to a laboratory-scale composting environment was executed to roughly check the "biodegradability".

Keywords: plasticizers; poly(hydroxybutyrate)/poly(lactic); mechanical properties; thermal properties; biodegradable polymeric blends; 3D printing

1. Introduction

Bioplastics have gained significant attention from the researches, manufacturers, customers, and investors worldwide over the past 25 years as the bio-alternatives for various fossil-resource based products. The pollution of the environment that is caused by plastics, the disappearance of landfill space, diminishes of petroleum resources, and the interest in controlling the toxic gases emissions are ranked among the reasons for this attention. The term "biopolymer" refers to polymers that are bio-based, biodegradable, or both; so, among the benefits of bioplastics from biopolymers that are based on renewable resources (or even on waste materials) is reduced carbon dioxide production during the bioplastics synthesis and their biodegradability [1–4].

Biobased material has some or all of its carbon produced from renewable resources like corn or sugar cane, or is produced in yeast, bacteria, or algae. The conditions for the determination of biobased content of polymeric materials are described in the European standard CEN/TS 16295:2012 [4].

Under appropriate conditions of moisture, temperature, and oxygen availability, the biodegradation leads to the fragmentation or disintegration of plastics with no toxic or environmentally harmful residue [5]. According to CEN/TR 15932:2010, biodegradable polymers are able to completely degrade to low molecular products (carbon dioxide, methane, water) and the biomass (mineralization and bioassimilation) through the chain scission in the backbone [6]. Specific test conditions, environments, and time-scales for laboratory tests are defined in European standards (EN ISO 14851:2004, EN ISO 14852:2004, EN ISO 17556:2004, EN ISO 14855-1:2007/AC:2009, EN ISO 14855-2:2009) [7–11]. Complete biodegradation is a combination of physical and enzymatic processes (where the chain scission is caused by human, animal, or fungi cell activity). The biodegradation progress is monitored by the measurement of oxygen uptake and carbon dioxide production. A special case of biodegradability is the compostability, where the degradation of a sample takes place in a soil being strongly influenced by composting conditions, such as the substrate properties, the microbial activity, the water content, and pH (EN ISO 13432:200/AC:2005, EN ISO 14995:2006) [4,12,13].

Although high costs of biodegradable polymers and the lack of regulation and composting facilities still prevent the massive distribution of bioplastics, the hypothetical global bioplastics production capacity is expected to increase from around 2.05 million tons in 2017 to approximately 2.44 million tons in 2022 [1,14]. Generally, bioplastics are used in a growing number of markets, from packaging, catering products, consumer electronics, automotive, agriculture/horticulture, toys and textiles to medical applications, and a number of other segments. Well-investigated biopolymers, such as PLA and PHAs, are the main drivers of production capacity growth [14].

PHA includes a group of microbial polyester polymers and copolymers (150 different PHA monomers have been reported yet). These bio-based biodegradable linear polyesters feature a wide array of physical and mechanical properties depending on their chemical composition. The occurrence of short-chain-length PHA (scl-PHA) with 3–5 carbon atoms per unit is the most common [15,16]. The PHAs production is estimated to triplicate the capacities in next five years [14]. PHAs are stored as intracellular carbon and energy reserve granules in diverse Gram-negative and Gram-positive bacteria from a range of substrates, including sugars and fatty acids [15].

Poly(lactic acid) (PLA), $-[CH(CH_3)COO]_n-$ is very versatile aliphatic polyester that features excellent barrier properties and is available in the form of high-performance PLA grades that are a good replacement for PS (polystyrene), PP (polypropylene), and ABS (acrylonitrile butadiene styrene) in more demanding applications [14,17]. PLA is synthesized from renewable resources through lactic acid fermentation and it is highly transparent, colorless, glossy, and rigid thermoplastic material [18,19]. The properties of PLA are dependent on the ratio between D and L enantiomers. The disadvantages of this polymer are its low heat distortion temperature (softening above 60 °C) and also its inability to quickly biodegrade at ambient temperature [18]. The tensile properties of PLA can vary widely depending on whether it is annealed or oriented, or on its degree of crystallinity [19,20].

The combination of these non-toxic, biodegradable, and biocompatible materials (PHAs, PLA) with three-dimensional (3D) printing technologies is useful, especially for the biomedical field

(scaffolds, implants), art objects, precise replicas of archeological objects, and for prototyping and the manufacture of spare parts for automotive, airplanes, etc. [17]. PLA, as biodegradable polymer, is already used in 3D printing industry. Biodegradable PLA/PHA polymeric blends are also applicable for 3D printing, even in industry at the time [21]. Their printability is good.

Fused Deposition Modeling (FDM) is the most productive technology used in low-cost 3D printers. A plastic filament used in this method is pushed through heated extrusion nozzle, melted and deposited on the bed in a tailored shape. The software that processes a STL (stereolithography) or CAD (computer-aided design) file, mathematically slicing and orienting the model for the building process, is embodied in this method [22]. The FDM method is applied in this work for the preparation of 3D printed dogbones (double-paddle shaped testing elements), which are further used for tensile tests. Usually, it is necessary to deal with the warping problem, which occurs especially during the printing of large parts, where the internal temperature of printed object tends to vary. Our materials are printed at high temperature (190 °C, the temperature of the extrusion nozzle) onto the printing bed (which has ambient temperature) and cooled with an integrated fan for quick solidification. This usually causes the shrinkage and it can lead to the deformation through the warping, which can lead to the detachment from printing bed and to the product destruction [23]. The warping wasn´t relevant in the case of our 3D printed dogbones.

Although PLA and Poly(3-hydroxybutyrate (PHB) can be potentially used as biodegradable and biocompatible alternatives to conventional polymers by many industrial sectors, both PLA and PHB have a few disadvantages. PHB is tough, fragile, and brittle in nature and it has poor processing properties. Blending with amorphous polymer, such as poly(D,L-lactic acid), is proposed to reduce the crystallinity of PHB, so that the applications of PHB can be expanded [3,24]. In spite of blending, these neat PHB/PLA blends are still stiff and brittle materials with poor mechanical properties and thermal degradation close to its melting point, limiting its processability [25]. Poor ductile properties can be well improved by the addition of plasticizer.

Plasticizers are an important class of low molecular weight non-volatile compounds that were homogeneously incorporated in a material (usually plastics or elastomer) that are widely used in polymer industries as additives. The primary role of such substances is lowering the glass transition temperature (T_g), the melting temperature (T_m), and improving the flexibility, the distensibility, and the processability of biopolymers [26,27]. Plasticizers reduce the tension of deformation, hardness, density, viscosity, and electrostatic charge of a polymer, and at the same time, they increase the polymer chain flexibility, resistance to fracture, and dielectric constant [26,28]. The additions of plasticizer thus influence the mechanical properties—reduce the toughness, the tensile strength, and increase the elongation at break. Other properties are also affected, such as the degree of crystallinity, optical clarity, electric conductivity, fire behavior, and the resistance to biological degradation, amongst other physical properties [28]. Among the most significant plasticizers are various monomeric esters of phthalic, phosphoric, adipic, sebacic, citric, and ricinoleic acids, furthermore chlorinated paraffins and low-molecular weight polyesters [26,27].

Plasticizers can be divided into two principal groups: primary and secondary. Primary plasticizers lower the glass transition temperature T_g and increase the elongation and softness of the polymer. Secondary plasticizers, when added to the polymer alone, do not bring about such changes and may also have limited compatibility with the polymer. However, when added to the polymer in the presence of a primary plasticizer, secondary plasticizers enhance the plasticizing performance of the primary plasticizer [29]. In this current study, the primary plasticizers that externally plasticized the polymeric blends were used.

The principle disadvantage of external plasticizing is the migration of the plasticizer from the plasticized material to other contacting media. This process includes the diffusion of the plasticizer from bulk material towards the surface, the interface phenomena, and the sorption or evaporation into the surrounding medium [28]. One of the consequences of the plasticizer decrement is the loss of the material elasticity and ductility. In addition, the plasticizer leakage from the material can

be the cause of surrounded media contamination (medical application issues). Among the main factors that affect the plasticizer migration are the type and the concentration of the plasticizer, its molecular weight, branching, and polarity. Low-molecular weight plasticizers tend to leak away from the polymeric material easier. The more linear the plasticizer's structure, the more extraction rate and migration occurred when compared to more branched plasticizers. The plasticizer migration is also affected by the type of polymer, its molecular weight, and its compatibility with the plasticizer; and, by the plasticization process and homogeneity of the product. The migration is also influenced by the conditions of the migration test (type of contact, time, temperature, polymer probe, specimen thickness). Higher temperatures simplify the plasticizer migration, while lower temperatures decelerate the migration [27,29–35].

In this current study, four commercial monomeric plasticizers that are based on esters of citric acid were used. The plasticizers miscibility with PHB/PLA blends in the weight ratio (wt %) of 85 (polymer)/15 (plasticizer) was confirmed using a kneading machine. The PHB/PLA/plasticizer blends in the weight ratio of 60/25/15 were then prepared by single screw and corotating meshing twin screw extruders in the form of filaments (for further 3D printing). The mechanical properties of plasticized blends were determined by tensile test of filaments as well as 3D printed dogbones. The diffusion of plasticizers from blends that were exposed at 110 °C in the drying oven was also investigated. The determination of the degree of disintegration of selected plasticized blend when exposed to a laboratory-scale composting environment was executed to roughly check their biodegradability. The Modulated Differential Scanning Calorimetry (MDSC) was performed to check the thermal properties of the plasticized blends and Scanning Electron Microscopy (SEM) was used to check their morphology. The goal was to create new types of eco-friendly PHB/PLA/plasticizers blends and to highly improve poor mechanical properties of neat PHB/PLA blends (with majority of PHB), by adding appropriate plasticizer.

These environmentally friendly PHB/PLA/plasticizer blends with the majority of PHB are biocompatible and suitable for 3D printing technology, and thus for biomedical applications and prototyping. Additionally, such type of eco-friendly blends, containing the PHB majority, can be well compostable. PHB can be prepared, even from waste cooking oil, so, unlike other types of biodegradable bioplastics, it does not require the agricultural feedstock, such as corn, potato, sugar cane, or sugar beet [36,37]. Quite many plasticizers were tested with PHB or PLA apart to improve their thermal and mechanical properties for various applications. Only some studies have focused on improving the thermal and mechanical properties of PHB/PLA/plasticizer blends, but always with the PLA majority.

Armentato et al. [38] investigated binary and ternary films made of PLA, 15% PHB and OLA (oligomeric lactic acid), which were prepared under optimized extrusion conditions, followed by a filmature procedure. The mechanical, thermal, morphological, and functional properties were investigated as the function of OLA composition ratio (15, 20, and 30 wt % of OLA by weight).

Arrieta et al. [25] blended PLA with PHB (75:25 wt % ratio) to increase the crystallinity. The plasticizers acetyl(tributyl citrate) (ATBC) and poly(ethylene glycol) (PEG) were added in the amount of 15 wt % when PLA/PHB blends achieved the melt state, to increase the processability and ductility. Each blend was then processed into biodegradable flexible film with improved properties for food packaging.

Abdelwahab et al. [3] investigated a blend of PLA (75% by weight) and PHB (25%) with a polyester plasticizer (Lapol 108) at two different concentrations (5 and 7% by weight per 100 parts of the blends).

This paper describes the influence of four plasticizers on thermal, mechanical, and morphological properties of plasticized PHB/PLA blends, but with the PHB majority. This kind of work has not been likely published yet, and thus it is unique in this context.

2. Materials and Methods

2.1. Materials

Poly-3-hydroxybutyrate (P3HB Biomer®, ρ = 1.23 g·cm^{-3}, M_w = 410,000 g·mol^{-1}) was provided by Biomer Company (Krailling, Germany) [39]. The polymer was in the form of white powder.

The PLA used in this study is poly(D,L-lactic acid), which is amorphous at T_g around 60 °C. This amorphous PLA was chosen for its ability to reduce the overall crystallinity content in our PHB/PLA/plasticizers blends, which are further used for 3D printing. Amorphous polylactic acid (aPLA) granules (Ingeo™ 4060D, M_w = 180 000 g·mol^{-1}, T_g = 55–60 °C, ρ = 1.24 g·cm^{-3}) were supplied by NatureWorks LLC (Minnetonka, MIN, USA) Company [40].

Four monomeric commercial plasticizers that are selected for this study are based on esters of citric acid, as provided by Vertellus Holdings LLC Company (Indianapolis, IN, USA), with trademark Citroflex® [41]. Their commercial and chemical names, molecular weights, and labels can be seen in Table 1. Their structure can be seen in Figure 1.

Table 1. Commercial and chemical names of used plasticizers, their molecular weights, and labels.

Commercial	Chemical Name	Molecular Weight (g·mol^{-1})	Plasticizer's Label
Citroflex® 4	Tributyl Citrate	360.4	C-4
Citroflex® A-4	Acetyl tributyl Citrate	402.5	A-4
Citroflex® A-6	Acetyl trihexyl Citrate	486	A-6
Citroflex® B-6	n-Butyryl tri-n-hexyl Citrate	514	B-6

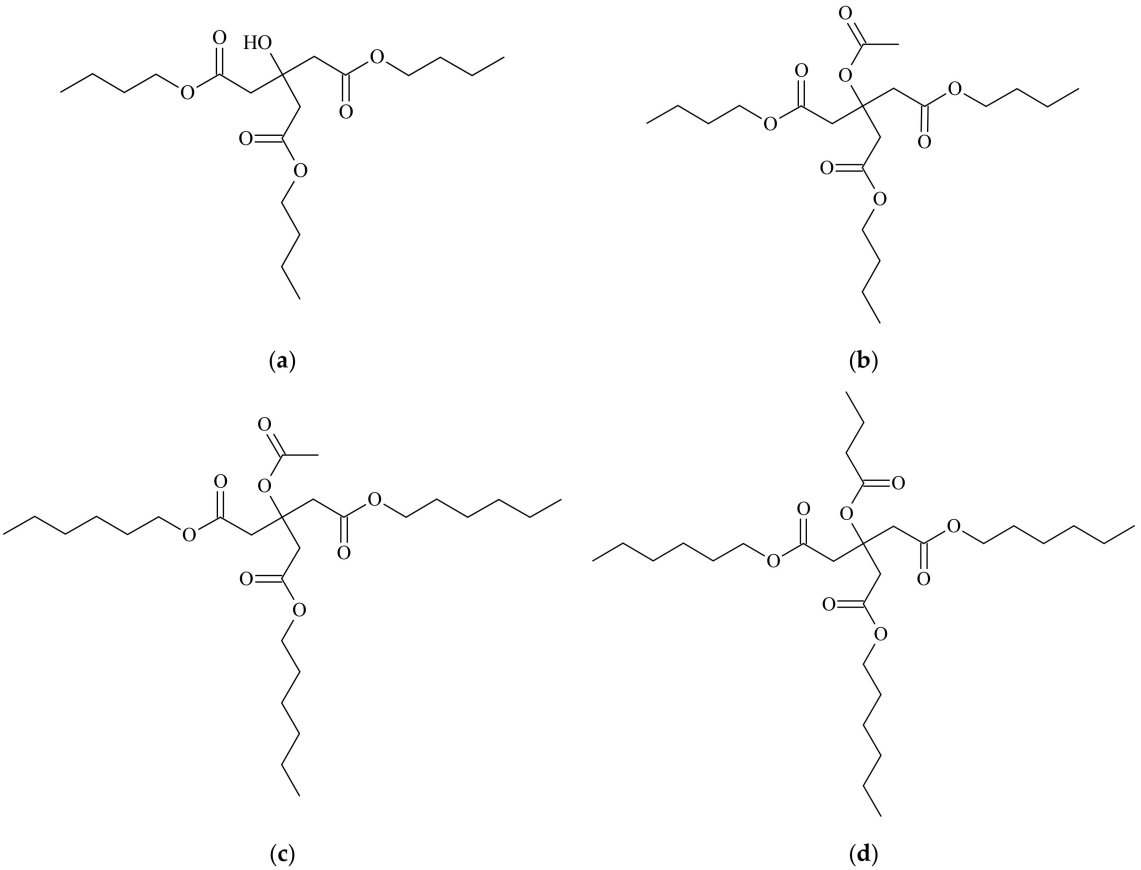


Figure 1. (**a**) Plasticizer C-4 structure; (**b**) Plasticizer A-4 structure; (**c**) Plasticizer A-6 structure; and (**d**) Plasticizer B-6 structure.

2.2. Plasticizers Miscibility with PLA/PHB Polymers

The miscibility of plasticizers with PHB/PLA polymer mixture was tested using the kneading machine PLASTI-CORDER Brabender. Citroflex® plasticizers were kneaded with PHB/PLA mixture in the weight ratio (wt %) of 60 PHB:25 PLA:15 plasticizer. Non-plasticized PHB/PLA was kneaded as a reference for the comparison (70 PHB:30 PLA). The total weight of each sample before the kneading process was 30 g. The process of kneading plasticizers with the PHB/PLA mixtures was performed at 178–180 °C (chamber temperature) at 45 rev./min, and the kneading process of reference was performed at 180 °C. The PHB/PLA mixture was dosed into the PLASTI-CORDER Brabender machine (Brabender GmbH & Co. KG, Duisburg, Germany) first and then kneaded for 1.5 min. Then, the plasticizer was added and the kneading process continued for following 3.5 min in the case of C-4, A-4 and B-6 plasticizers and for 4.5 min in the case of A-6 plasticizer. The total kneading time of PHB/PLA with plasticizers (sample dosing with kneading) was 6–7 min. The total kneading time of reference was 9 min. The gearbox torque dependence on the total plasticization time was measured and the miscibility was evaluated.

2.3. Preparation of Plasticized PHB/PLA Blends

PHB and PLA polymers were firstly pre-treated by drying at 80 °C in the drying oven (Memmert, Schwabach, Germany) for 2 h to eliminate possible absorbed water. As the first step, the corotating meshing twin screw extruder with the screw auger parameters D = 16 mm and L/D = 40, from Labtech Engineering Company (Samutprakarn, Thailand), was used for the preparation of plasticized PHB/PLA blends. The total weight of each sample for extrusion was 350 g. The chamber temperature profile from hopper to nozzle was set to 160–175–175–75–175–175–175–170–165–160 °C and the rotational speed of screw was set to 130 rev./min. The PHB/PLA blends in the weight ratio of 70/30 (wt %) (reference) as well as the PHB/PLA/plasticizer blends in the weight ratio of 60/25/15 (wt %) were extruded in the form of filaments. Four Citroflex® plasticizers were used one by one. Unfortunately, the filament, which was pulled from the nozzle, had diverse non-defined thickness and diameter and so it was unsuitable for 3D printing. Therefore, the filaments were pulled through the water tank (water with ambient temperature) and then the filaments were pulled into the granulator to get pellets, which are later used for the second extrusion.

The PHB/PLA (reference) pellets and the PHB/PLA/plasticizer pellets that were prepared by twin screw extruder, were at first pre-treated by drying at 80 °C for 2 h in the drying oven. Then single screw extruder HAAKE™ Rheomex OS (Haake Technik GmbH, Vreden, Germany) was used for the second extrusion in order to achieve the filaments with a defined diameter of 1.75 mm. The chamber temperature profile from hopper to nozzle was set to 185–175–170–150 °C and the rotational speed of screw was set to 25 rev./min. The filament that extruded from the nozzle was pulled out into the draw-off device through the calibration mechanism located in the water tank. Water was tempered by the thermostat at 60 °C in order to finish the polymer crystallization. Prepared PHB/PLA/plasticizer filaments with defined diameter were then used for further characterizations and for 3D printing.

2.4. Modulated Differential Scanning Calorimetry—Thermal Characterization

The thermal properties of prepared samples were determined using the combination of modulated and conventional differential scanning calorimetry (MDSC and DSC, respectively). The measurements were performed on TA Instruments model DSC 2500 (TA Instruments, New Castle, DE, USA) under nitrogen atmosphere. The samples (approx. 13 mg) were sealed in hermetic aluminium pans. Firstly, they were cooled down to −50 °C and then kept in isothermal mode for 5 min. Afterwards, MDSC scan from −50 to 80 °C was carried out at average heating rate of 3 °C/min with the period of 60 s and modulation amplitude of 1.25 °C. This ensured that measured properties corresponded to as prepared samples without further thermal stress. Subsequently, two DSC scans (heating rate 10 °C/min), the first from 80 to 190 °C and the second from −30 to 190 °C, were performed. The glass transition temperature

T_g was determined from the MDSC curve of reversing heat capacity. The melting temperature T_m and the crystallization temperature T_c were determined from the conventional DSC scans. The crystallinity X_c was calculated from the measured data using the following equation:

$$X_c = \frac{\Delta H_m}{\Delta H_m^0} \cdot 100\%, \quad (1)$$

where ΔH_m, and ΔH_m^0 (J/g) are the enthalpy of second melting peak and the enthalpy of fusion of 100% crystalline polymer (146 J/g for PHB), respectively.

2.5. Migration Tests—Plasticizers Diffusion from PHB/PLA Blends

First experiments with the plasticizers diffusion from our blends were performed by the Thermogravimetric Analysis (TA Q500, TA Instruments, New Castle, Delaware USA). However, it was not possible to determine the diffusion speed exactly, as some of the plasticizers showed too long evaporation from the surface. Therefore another test was conducted. 5 g of extruded PHB/PLA/plasticizer pellets and 5 g of extruded PHB/PLA pellets (reference) were compression moulded on a laboratory hotpress to obtain planar samples of 0.70–0.72 mm thickness. The heating temperature of press desk was set to 190 °C. The laboratory press with the sample was closed during 0.5 min and the presswork itself lasted for 1 min. The samples of 3 × 3 cm square shape proportions were then cut from these moulded pressed planar samples, wiped by the napkin paper moistened in ethanol, laid down on the PET foil, and put into the drying oven heated to 110 °C with 50% air circulation. The samples were taken out from the drying oven after 1, 3, 7, 10 h, and 1, 2, 3, 6, 8, 10, 13, 15 days, and then they were wiped by the napkin paper moistened in ethanol and measured while using analytical balance. The dependencies of plasticizer's weight loss from PHB/PLA planar samples on the time of exposition to 110 °C were evaluated.

2.6. Tensile Tests—Mechanical Characterization

The elongation at break, the Young´s modulus, and the tensile strength were determined under ambient conditions, using the universal measurement device Zwick Z 010 (ZwickRoell GmbH & Co., Ulm, Germany). The tensile tests of non-plasticized extruded PHB/PLA samples (references), as well as plasticized PHB/PLA samples, were carried out using the load indicator with the maximal tensile force of 500 N and with pneumatic grips. The deformation rate was initially set to 5 mm/min to determine the elastic modulus, and then enhanced to 50 mm/min. The measurements were carried out without using the extensometer. The filaments with defined diameter were tested after three days of exposition to 110 °C in the drying oven and after 7 and 40 days after their preparation by extrusion. Double-paddle testing samples (dogbones, ~(5 × 2 × 75) mm, tensile test measurements approach CSN EN ISO 527-1) were 3D printed from mentioned extruded filaments (PHB/PLA reference sample and all PHB/PLA/plasticizer samples), and they were measured using Zwick Z 010 after seven days following the 3D printing [42]. The reported values were the average of at least seven measurements. The data points were the mean value of each measurement, with the error bars in each graph representing the standard deviation.

2.7. 3D Printing

The dogbone samples for tensile tests were printed on PRUSA i3 MK2 3D printer (Prusa Research s.r.o., Praha, Czech Republic) by the FDM technology from PHB/PLA/plasticizer filaments with defined diameter, as mentioned above. AutoCAD (ver. 2018, Autodesk Inc., San Rafael, CA, USA) and Slic3r (software version 1.3.0, free software, developed by Alessandro Ranellucci) program were used for 3D virtual modeling and mathematical slicing. The dogbones were printed at 190 °C (195 °C during the first layers printing for better adhesion to the printing bed), at ambient conditions, without

additional air cooling and bed heating. 3D printing was executed approximately six months after the filaments preparation.

The evolution of 3D printed dogbone models that were prepared for further tensile tests can be seen in Figure 2.

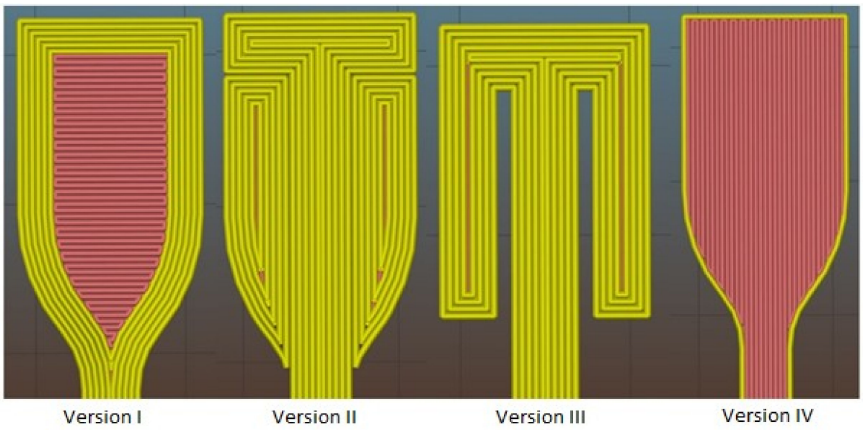


Figure 2. Evolution of three-dimensional (3D) printed dogbones prepared for tensile tests.

The Version I was created by simple import of fabricated model to Slic3r program and uploading to the printer. But, during the tensile test with dogbones of Version I, the delamination of perimeters occurred (illustrated by yellow color), and so the measured samples did not provide relevant results. To solve this problem, Version II was designed, where the perimeters of dogbone neck were elongated up to the upper part. The paddleboards were created from two parts. Unfortunately, during the tensile test, the defect at the point of paddleboard and neck connection occurred, because the printer created an inclusion in the paddleboard corner by releasing a large amount of melting. The inclusion acted as a disruption initiator and cracked untimely. The aim of Version III was to eliminate this problem, but the pressure of grips was not strong enough to hold the sample. The deformation then occurred in upper cross-sectional part and disagreed with real dogbone strength. The final Version (that could not be illustrated in Figure 2) was created by the combination of 10 laminas of Version I and IV, which alternate regularly (five from each Version). The delamination of the neck in its extending part was eliminated by the insertion of vertical infill (illustrated by red color) and the vertical fracture of samples was eliminated by the combination with horizontal infill.

2.8. Scanning Electron Microscopy—Morphology Characterization

The Scanning Electron Microscopy (SEM) micrographs of dogbone areas that were fractured after tensile tests were obtained with the EVO® LS 10 (Zeiss Company, Oberkochen, Germany), operated at 10 kV. The samples were coated with a gold-palladium layer in vacuum conditions to increase their electrical conductivity. The micrographs were registered at 100× magnification. This method was used for the following samples (in wt %): 70PHB/30PLA (reference) and 60PHB/25PLA/15plasticizer samples (where all four Citroflex® plasticizers A-4, C-4, A-6, B-6 were used).

2.9. Determination of the Degree of Disintegration

The determination of the disintegration of plastic materials under simulated composting conditions in a laboratory-scale test was executed according to IS/ISO 20200 [43]. Unfortunately, the method is not applicable to the determination of real biodegradability of plastic materials under garden or industrial composting conditions. The solid matrix used consists of synthetic solid waste inoculated with matured compost that was taken from a commercial garden composting plant. The pieces of plastic test material are composted with this prepared solid matrix. The degree of disintegration is determined after a composting cycle, by sieving the final matrix through a 2 mm

sieve in order to recover the non-disintegrated residues. The reduction in mass of the test sample is considered as disintegrated material and is used to calculate the degree of disintegration [43]. The composition of synthetic waste used in this method was: sawdust, rabbit-feed, ripe compost, corn-starch, saccharose, cornseed oil, and urea. The box with a lid made of polypropylene, having the dimensions of (30 × 20 × 10) cm, was used as a composting reactor. Two defined holes were made in the middle of two 20 cm sides to provide the gas exchange between inner atmosphere and outer environment. As samples, PHB/PLA/A-4 (60/25/15 in wt %) were used in the form of thin films with the dimensions approximately (6.5 × 10 × 0.08) cm. Two identical films were located in each box. The solid matrix was prepared manually by mixing different components that are mentioned above. Each box was filled by solid matrix up to the middle. Beforehand weighed and measured samples were laid on this matrix and covered with further matrix. Prepared content was then equally washed down by distilled water to overall 55% of humidity. Each reactor was closed, weighed, and placed in the air-circulation oven maintained at constant temperature of 58 °C for a minimum period of 45 days and maximum of 90 days, so that the samples were disintegrated under thermophilic conditions. The reactors were then weighed, water was added to restore the initial mass, or to restore the mass to 80% or 70% of the initial mass, the waste was stirred, and all of these actions were executed in particular days according to IS/ISO 20200. Also, other parameters, like visual appearance, odor, and color, were observed and the photos were taken.

3. Results and Discussion

3.1. Plasticizers Miscibility with PHB/PLA

Citroflex® plasticizers were kneaded with PHB/PLA mixture in the weight ratio (wt %) of 60 PHB:25 PLA:15 plasticizer, using the kneading machine PLASTI-CORDER Brabender (Brabender GmbH & Co. KG, Duisburg, Germany) equipped with two counter rotating sigma blades.

In Figure 3, you can see the gearbox torque dependence (kN·m) on the time when plasticizer was added to PHB/PLA mixture (PHB/PLA mixture was already dosed during 1 min and kneaded for 1.5 min). These dependencies are compared with the reference sample (neat 70 PHB:30 PLA in wt %). As can be seen from Figure 3, the gearbox torque first declined to 0 kN·m after the plasticizer addition due to the lubrication of Sigma Blades by plasticizer. The blades could move freely, and the torque resistance approached zero. Afterward, the plasticizer started to mix with PHB/PLA, so the gearbox torque increased and achieved the maximum, which corresponds to the whole mixture viscosity increase. Achieved maximum should mean the moment of plasticizer blending with PHB/PLA. Citroflex® plasticizers in 15% concentration were miscible with PHB/PLA during maximum 7 min of total kneading time. It corresponds to maximum 4.5 min from plasticizer addition. All the plasticizers were successfully kneaded with PHB/PLA mixture. The plasticizers B-6, C-4 and A-4 were kneaded into PHB/PLA mixture faster than the plasticizer A-6. The influence of plasticizer structure on measured dependencies can be seen especially when the plasticizers A-4 and A-6 are compared. The plasticizer A-6 with longer polymeric chains (acetyl trihexyl citrate) needed a longer time to be kneaded into PHB/PLA mixture than the plasticizer A-4 with shorter polymeric chain (acetyl tributyl citrate). On the other hand, the most branched plasticizer B-6 (butyryl trihexyl citrate), which should theoretically be kneaded for the longest time with PHB/PLA mixture, actually needed the shortest time. Branched plasticizer B-6 seems to have weak cohesive forces and it thus tends to disperse well between PHB and PLA molecules at higher kneading temperature.

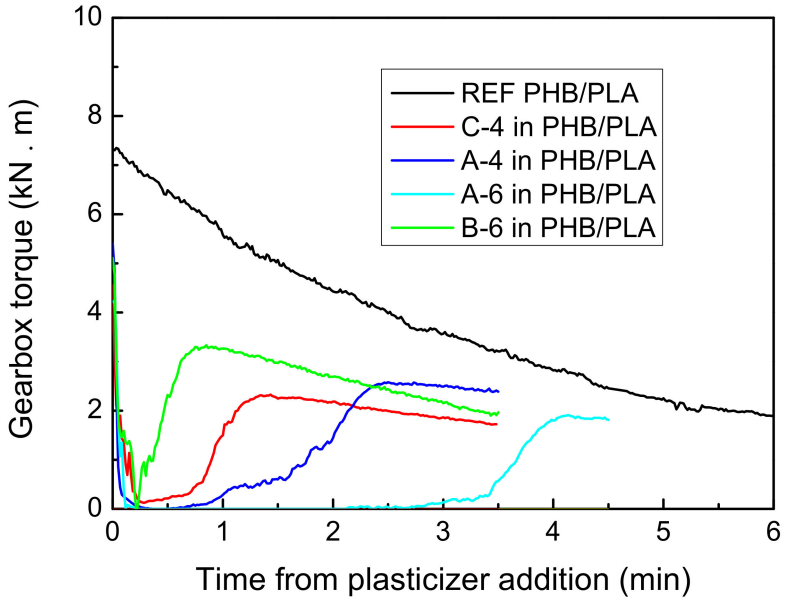


Figure 3. Gearbox torque dependence on the time elapsed from the addition of plasticizers to Poly(3-hydroxybutyrate/Poly(lactic acid) (PHB/PLA) mixture.

3.2. Differential Scanning Calorimetry—Thermal Behavior

The thermal behavior of PHB/PLA/plasticizer samples and non-plasticized reference sample was observed while using the combination of modulated and conventional differential scanning calorimetry (MDSC and DSC, respectively). Due to high amount of rigid fraction in PHB, its glass transition temperature could not be detected. The effect of the plasticizer on PHB thermal properties was observed by means of melting and crystallization temperatures shifts (Figures 4 and 5, respectively), as well as by the crystallinity change. In the case of PLA fraction in blends, the change in T_g was monitored and it is presented in Figure 6. All the evaluated data are listed in Table 2.

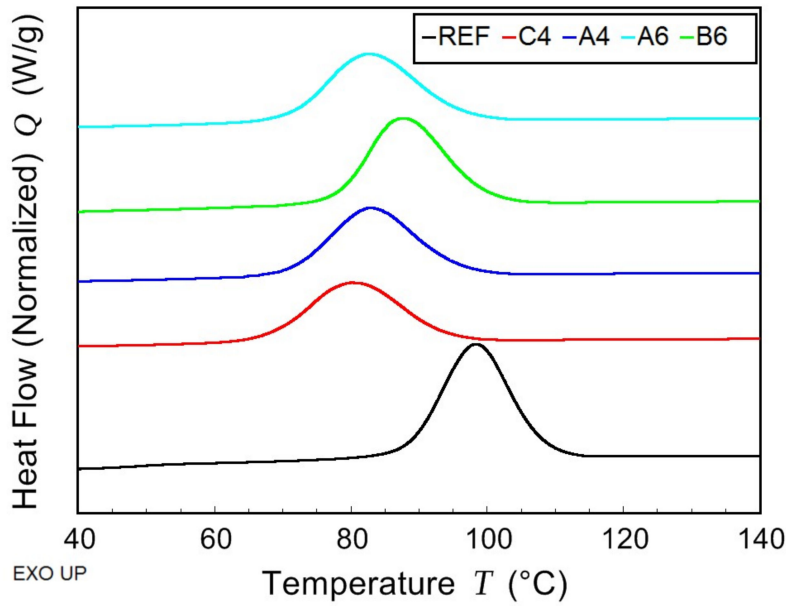


Figure 4. Differential scanning calorimetry (DSC)—first cooling scan of non-plasticized reference sample (REF) and PHB/PLA/Plasticizer (where the plasticizers are: C-4, A-4, B-6, and A-6).

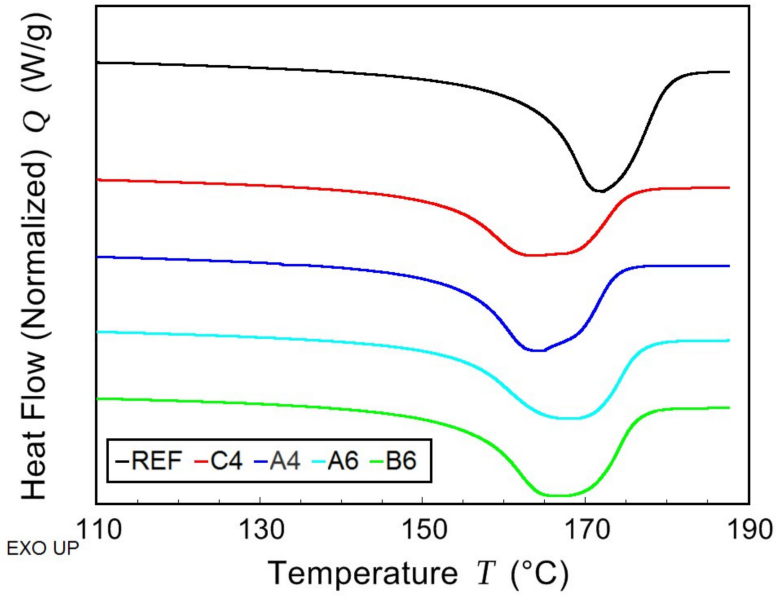


Figure 5. DSC—second heating scan of non-plasticized reference sample (REF) and PHB/PLA/Plasticizer (where the plasticizers are: C-4, A-4, B-6, and A-6).

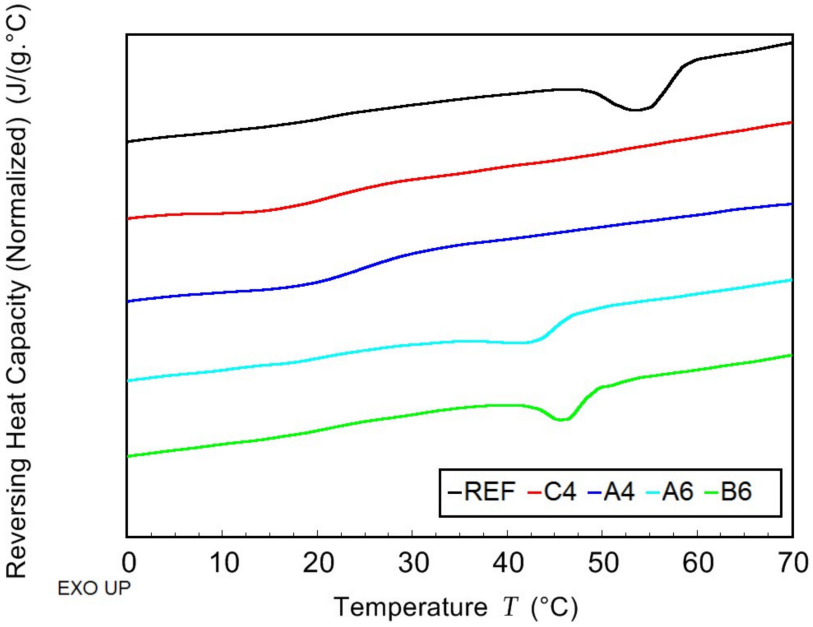


Figure 6. Reversing heat capacity gained from Modulated Differential Scanning Calorimetry (MDSC) scan of non-plasticized reference sample (REF) and PHB/PLA/Plasticizer (where the plasticizers are: C-4, A-4, B-6, and A-6).

Table 2. MDSC and DSC parameters of PHB/PLA/Plasticizer samples and non-plasticized reference.

Sample	MDSC Scan	First Cooling DSC Scan		Second Heating DSC Scan		
	$T_{g,\,PLA}$ (°C)	T_c (°C)	H_c (J/g)	T_m (°C)	H_m (J/g)	X_c (%)
REF	58.4	98	54.6	172	64.0	63
C-4	23.3	80	37.1	163	48.3	55
A-4	25.5	83	39.9	164	51.8	59
B-6	49.8	88	46.0	167	57.4	66
A-6	45.9	82	41.4	168	52.7	60

The introduction of low molecular plasticizer into PHB/PLA blend caused greater mobility of macromolecular chains. As a consequence, the crystallization and the melting temperatures were shifted to lower temperatures. The most significant drop was observed in the case of C-4 (tributyl citrate), where, as compared to the reference, T_c was lower by 18 °C and T_m was lower by 9 °C. The crystallinity was reduced in all samples except for that with B-6 (butyryl trihexyl citrate). In a semicrystalline polymer, low molecular additives are retained in amorphous phase in between crystallites. In a blend of semicrystalline (PHB) and amorphous (PLA) polymer, such additives are expected to be ejected into amorphous polymer during the crystallization. Therefore, the plasticizing effect is more apparent when observing the change of PLA T_g. Butyl esters of citric acid caused a decrease of PLA T_g by 35 °C for C-4 and by 33 °C for A-4 (acetyl tributyl citrate). Increased length of alkyl chains that are linked to citric acid conversely showed a worse plasticizing effect and led to T_g higher than 40 °C. At the same time, there is the effect of alkyl chain that is attached to –OH end of citrate molecule as butyryl trihexyl citrate exhibits the highest PLA T_g of all the samples. Both of the blends with B-6 and A-6 (acetyl trihexyl citrate) are expected to behave glassy at laboratory temperature.

3.3. Migration Tests—Plasticizers Diffusion from PHB/PLA Blends

The plasticizers diffusion from PHB/PLA/plasticizer (60/25/15 in wt %) samples was evaluated as their weight loss (%) after up to 15 days of exposition to 110 °C in the drying oven.

The weight loss (%) of C-4, A-4, A-6, and B-6 plasticizers after 1, 3, 7, 10 h, and 1, 2, 3, 6, 8, 10, 13, and 15 days of exposition to 110 °C can be seen in Figure 7. The plasticizers began to migrate rapidly after 10 h of exposition, especially in the case of C-4 (tributyl citrate) and A-4 (acetyl tributyl citrate). On the other hand, 15 days of exposition to 110 °C must be considered as a hard thermal condition for bioplastics. They are not expected to be exposed to so severe conditions during their ordinary use. The plasticizers most resistant to diffusion are B-6 (butyryl trihexyl citrate) and A-6 (acetyl trihexyl citrate), while C-4 and A-4 plasticizers had up to 95% weight loss after 15 days of exposition. Stable plasticizers B-6 and A-6 showed only 33 and 44% weight loss after 15 days of exposition and their weight loss proceeded gradually. The influence of plasticizer structure on the diffusion is well noticeable. C-4 plasticizer with –OH group, the smallest carbon amount and the least branched chain showed the fastest diffusion from the PHB/PLA/plasticizer sample. A-4, A-6, and B-6 plasticizers vary by the length of alkyl chains linked to citrate molecule and the most branched plasticizer B-6 with the largest molecular weight showed the best stability and tendency not to diffuse from the sample. This influence of structure on the diffusion agrees with [28–32].

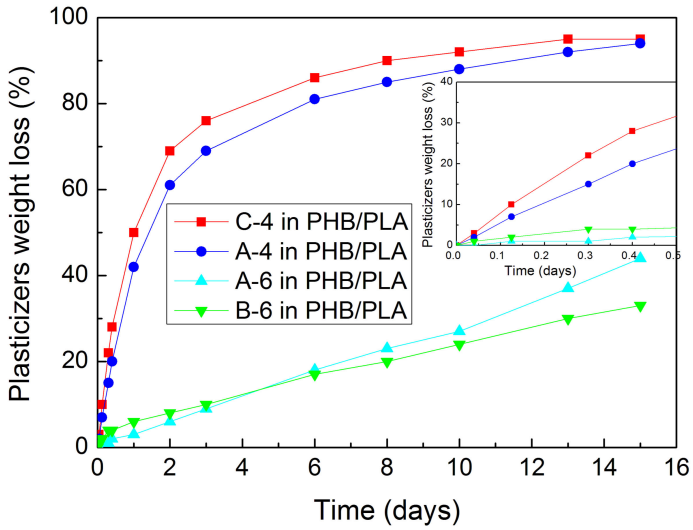


Figure 7. Plasticizers weight loss (%) from PHB/PLA/plasticizer blends after up to 15 days of exposition to 110 °C in the drying oven.

3.4. Tensile Tests—Mechanical Behavior

The tensile tests were measured on samples containing PHB/PLA/plasticizer (60/25/15 in wt %). Measured samples were in the form of extruded filaments and dogbones 3D printed from these filaments. The appearance of 3D printed dogbone can be seen in Figure 8.



Figure 8. 3D printed dogbone for tensile tests (PHB/PLA/A-4).

The tensile tests were carried out on filaments after seven and 40 days from extrusion, on filaments after three days of exposition to 110 °C in the drying oven and on 3D printed dogbones after seven days from printing. The results were compared with neat PHB/PLA (70/30 in wt %) as reference. With respect to plasticizers efficiency, the elongation at break is the most important value for us. In Figure 9, we can see the plasticizers influence on measured elongation at break (%) when compared with non-plasticized reference. All four Citroflex® plasticizers have positive softening effect in PHB/PLA polymers.

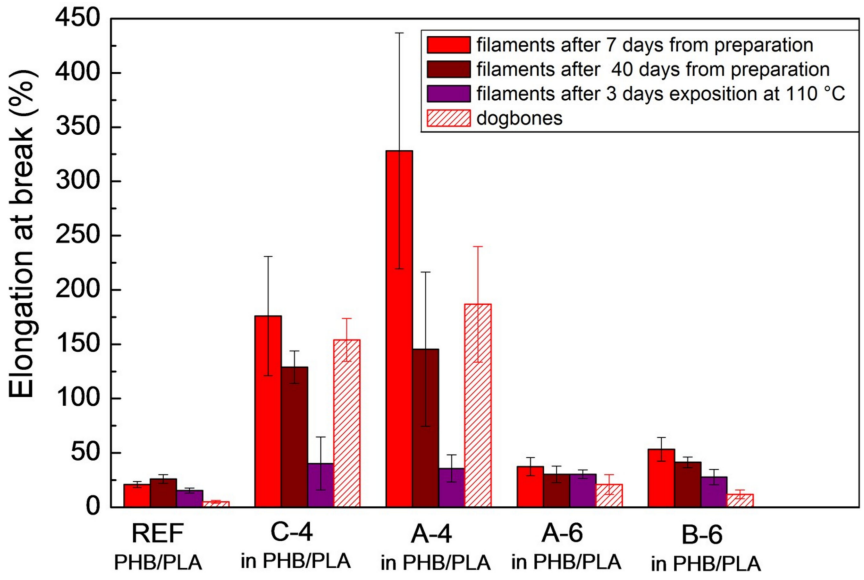


Figure 9. Elongation at break (%) of neat PHB/PLA (reference), PHB/PLA/plasticizers filaments, and 3D printed dogbones.

The plasticizers A-6 (acetyl trihexyl citrate) and B-6 (butyryl trihexyl citrate) improved the elongation at break (measured after seven days from filament preparation) only slightly: from 21% for non-plasticized PHB/PLA filament samples to 37% and 53% for plasticized ones, respectively. Their plasticizing effect is insignificant, on the other hand these plasticizers are more resistant to diffusion (as was discussed in the Migration tests chapter). The results from the migration tests were also confirmed by the tensile tests measurements, since the elongation at break of blends with A-6 and B-6 plasticizers only slightly decreased after three days of exposition to 110 °C. The blends with A-6 and B-6 plasticizers are relatively resistant to the aging, as was confirmed by the tensile tests measurement after 40 days from the preparation. Weaker softening effect of these two plasticizers, but their stronger resistivity against aging and exposition to higher temperature is caused by their structure: increased length of alkyl chains linked to the citrate molecule and more branched structure. It corresponds well with the MDSC results, where A-6 and B-6 plasticizers showed minor T_g reduction,

and hence worse plasticizing effect. The elongation at break of dogbones with A-6 and B-6 plasticizers confirmed a weaker plasticizing effect, which is probably due to 6-month old filament from which the dogbones were made.

On the contrary, significant plasticizing effect was achieved by using two plasticizers with the shortest length of alkyl chains: C-4 (tributyl citrate) and A-4 (acetyl tributyl citrate). The elongation at break measured after 7 days from preparation (filament extrusion) increased from 21% for non-plasticized reference to 176% for PHB/PLA/C-4 sample, and even to 328% for PHB/PLA/A-4 sample. The aging effect was most apparent for A-4 plasticizer, but still, A-4 seems to have the most significant plasticizing effect. It was confirmed by the tensile test measurements with dogbones samples. The A-4 plasticizer structure differs from C-4 only by the acetyl group that was attached to the citrate molecule. Significant plasticizing effect of C-4 and A-4 plasticizers was confirmed also by the MDSC measurements, where T_g of PLA fraction was strongly decreased in the case of samples with these plasticizers.

Meaningful plasticizing effect was depreciated by three days of exposition to 110 °C. Such thermal conditions caused massive plasticizer diffusion from the sample, especially in the case of low-molecular plasticizers with shortest alkyl chains. After the exposition, the elongations at break of samples with C-4 and A-4 plasticizers were comparable to samples containing A-6 and B-6 plasticizers. It agrees with the results from the migration test, where the samples with A-4 and C-4 plasticizers evinced an extensive diffusion. Still, the plasticizing effect was slightly preserved, even after hard thermal conditions.

The Young's modulus (GPa) and the tensile strength (MPa) of measured PHB/PLA/plasticizer samples and non-plasticized reference can be seen in Tables 3 and 4. Stronger softening effect of A-4 and C-4 plasticizers and their intense diffusion from samples after three days of exposition to higher temperature can be observed also from these results, for example from lower Young's modulus values for the samples with C-4, A-4 plasticizers and the increase of these values after three days of exposition to 110 °C. The tensile strength values of plasticized samples were comparable for all the plasticizers; the change of values can be seen especially after three days of exposition to 110 °C in the case of A-4 and mainly C-4 plasticizers.

Table 3. Young's modulus (GPa) of measured PHB/PLA/plasticizer samples and PHB/PLA reference.

Sample	Young's Modulus (GPa)			
	Filaments—7 Days after Preparation	Filaments—40 Days after Preparation	Filaments—after 3 Days at 110 °C	Dogbones—7 Days after Printing
REF	0.57 ± 0.07	0.45 ± 0.12	0.59 ± 0.06	2.41 ± 0.13
C-4	0.16 ± 0.01	0.17 ± 0.00	0.41 ± 0.08	0.66 ± 0.05
A-4	0.15 ± 0.01	0.17 ± 0.01	0.34 ± 0.03	0.69 ± 0.02
A-6	0.32 ± 0.03	0.32 ± 0.03	0.30 ± 0.02	1.16 ± 0.06
B-6	0.33 ± 0.02	0.30 ± 0.02	0.27 ± 0.05	1.46 ± 0.13

Table 4. Tensile strength (MPa) of measured PHB/PLA/plasticizer samples and PHB/PLA reference.

Sample	Tensile Strength (MPa)			
	Filaments—7 Days after Preparation	Filaments—40 Days after Preparation	Filaments—after 3 Days at 110 °C	Dogbones—7 Days after Printing
REF	43.3 ± 1.0	42.9 ± 1.9	44.8 ± 0.5	39.1 ± 1.6
C-4	18.9 ± 0.5	20.4 ± 0.6	30.8 ± 2.6	19.8 ± 0.3
A-4	19.5 ± 0.5	20.2 ± 0.8	26.4 ± 1.6	20.3 ± 0.8
A-6	20.1 ± 0.9	22.5 ± 0.4	22.9 ± 0.4	22.1 ± 1.0
B-6	19.8 ± 0.5	20.7 ± 0.5	20.1 ± 0.6	23.5 ± 1.0

Armentato et al. [38] found that the addition of OLA produced a significant reduction of the T_g values of PLA/PHB blends and it confirmed the plasticizing effect of OLA resulting in the increase of molecular mobility of the polymer structure. Single T_g value was observed in all the studied formulations and no apparent phase separation was detected, confirming high compatibility between

OLA and the PLA/PHB matrix. The introduction of OLA in 15 and 20 wt % did not result in a significant change in the PLA/PHB thermal stability. But, the thermal stability was decreased with 30 wt % of OLA. Considerable improvement of ductile properties of PLA/PHB/OLA blends was demonstrated. The introduction of OLA caused significant decrease of the tensile strength. When the OLA concentration increased, the elongation at break increased. The elongation at break was improved from 140% for non-plasticized PLA/15PHB blends to 370% for PLA/15PHB/30OLA blend. Also the oxygen and water vapor barrier properties were improved in the consequence of higher crystallinity of plasticized PLA/PHB blends. The PLA/PHB blend with 30 wt % OLA was selected as the optimum formulation, since it offered the best compromise between ductile and oxygen and water vapor barrier properties with no migration problems for the application as food packaging material [38].

According Arrieta et al. [25], their obtained PLA/PHB blends showed improved oxygen barrier properties and lowered water incorporation. PHB improved the interface interaction between PLA and plasticizers. Only one T_g value was observed for all formulations with plasticizers, suggesting the good miscibility between different components in the amorphous region. The addition of ATBC or PEG to the polymer matrices caused the T_g depression in all plasticized films. This reduction in T_g was higher in films plasticized with PEG. Decreased modulus, tensile strength, and increased elongation at break were caused by both plasticizers. Blends that were plasticized with ATBC showed higher flexibility and thermal stability than those with PEG (elongation at break improved from 2.0% for the PLA/PHB blend to 182% for the PLA/PHB/ATBC blends). PLA/PHB/ATBC blends showed higher oxygen barrier properties and hydrophobicity than those with PEG and appeared to be more effective [25].

Abdelwahab et al. [3] investigated the thermal and mechanical properties of their blends. The DSC curves of PLA/PHB blends exhibited two T_g values, which indicated that these blends were immiscible. However, the addition of Lapol to the system decreased the T_g values of PHB and PLA in the system and slightly increased the crystallinity and the temperature corresponding to the onset of decomposition for a polymer. It was attributed to higher thermal stability of Lapol. The Young´s modulus and the tensile strength were decreased by the addition of Lapol in PLA/PHB system, while the elongation at break only slightly increased (from 7% to 15%) [3].

3.5. Scanning Electron Microscopy—Morphology Characterization

The SEM micrographs of 3D printed dogbones areas that were fractured after the tensile tests can be seen in Figure 10. The micrographs were registered only at 100× magnification, but almost complete views on fractured areas were obtained. The PHB/PLA reference blend (70/30 in wt %, Figure 10a) seems to have homogeneous surface, with no apparent phase separation, suggesting the good interaction between both polymers, despite larger PHB content. However, the reference fracture surface is not very smooth; the laminas extracted during the tensile test are evident. There are also apparent holes, caused by 3D printing. The holes are larger especially near the top of the sample, where the filament laminas did not fit tightly. The laminas located near the bed and printed earlier are better fused, linked and pressed by upper laminas. This effect is apparent even from the micrographs of plasticized blends, see Figure 10b–e (60PHB/25PLA/15plasticizer in wt %). Although mechanical properties of non-plasticized (reference) and plasticized samples are different, their fracture areas on micrographs seem to be quite similar. Assumed ductile fracture patterns are not so apparent on the micrographs with plasticized samples. Micrographs seem to be similar compared to assumed rigid fracture of non-plasticized reference. The plasticizers with strong softening effect, like C-4 (tributyl citrate) and A-4 (acetyl tributyl citrate), seem to be well miscible with the polymer matrix, the surface is more compact and smooth, especially in case of C-4 plasticizer (Figure 10b,c). It corresponds well with MDSC and tensile tests results. A-6 (acetyl trihexyl citrate) and B-6 (butyryl trihexyl citrate) plasticizers with a weaker softening effect in PHB/PLA matrix have apparently less compact structure with huge holes on the micrographs, especially in the case of A-6 (Figure 10d,e). Larger A-6 and B-6 plasticizers molecules probably are not uniformly miscible with the polymer matrix, therefore

they have higher viscosity and such material is predisposed not to fuse well in 3D printed laminas at the same printing conditions. But generally, all of these plasticizers are low-molecular and hence applicable in 3D printing. 3D printing process might be improved in order to avoid the presence of voids. Temperature enhancement during printing should decrease viscosity of melting and cause better fluidity. Furthermore diameter measurements of filament incoming to printer jet and continual flow calibration according to these measurements could help with this problem; and, probably also gradient modification of the height of the layers, where the height of the bottom layers (near to the printing bed) are higher than of those at the top of printed sample.

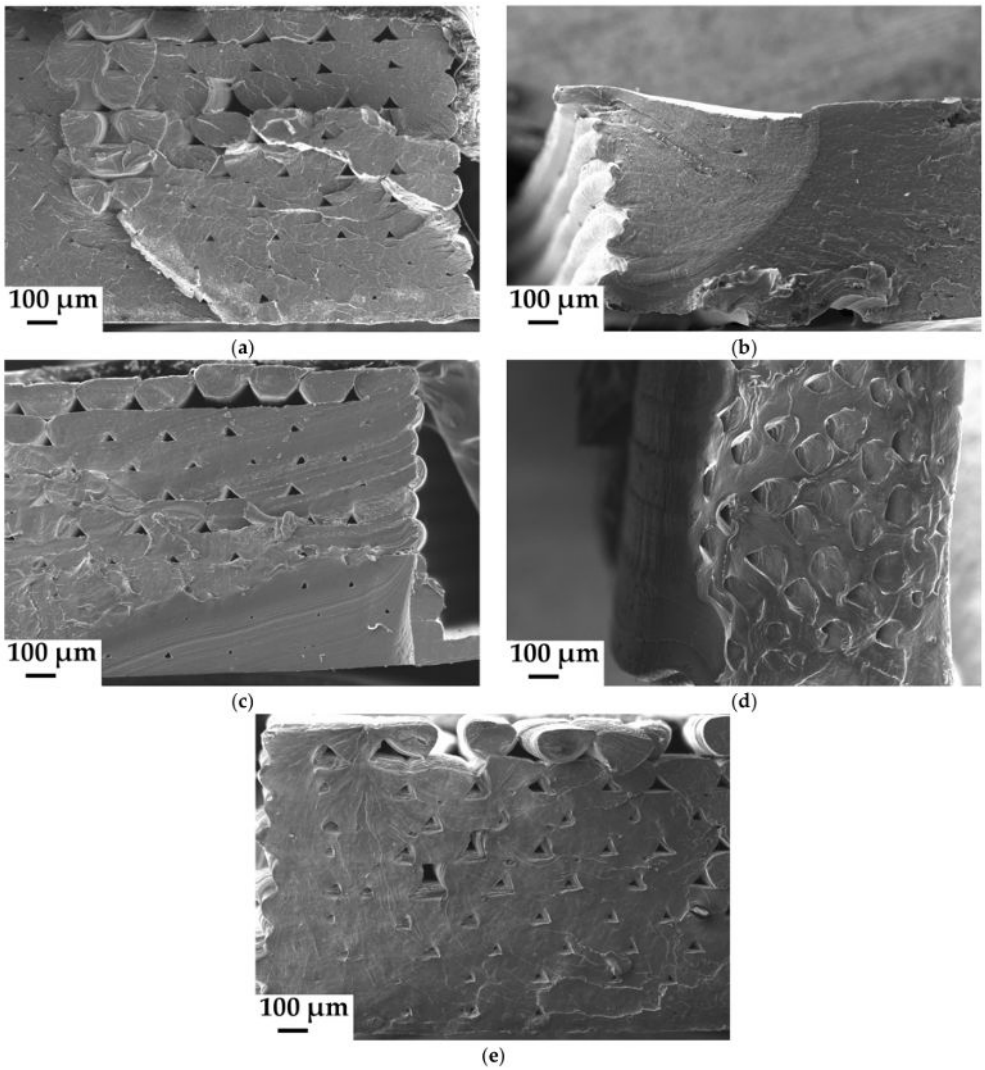


Figure 10. Scanning Electron Microscopy (SEM) micrographs of 3D printed dogbones fractured during tensile tests and made of: (**a**) PHB/PLA (reference); (**b**) PHB/PLA/C-4; (**c**) PHB/PLA/A-4; (**d**) PHB/PLA/A-6; and, (**e**) PHB/PLA/B-6.

Arrieta et al. [25] inspected fractured SEM micrographs of PLA/PHB/ATBC (A4) films that showed ductile fracture patterns where the plastic deformations were present.

3.6. Determination of the Degree of Disintegration

This laboratory-scale test was executed according to IS/ISO 20200 under simulated composting thermophilic conditions (at 58 °C). The parameters, like visual appearance, odor, and color were observed and some photos were taken, as can be seen in Figure 11. PHB/PLA/plasticizer sample (60/25/15 in wt %) in the form of film was chosen for this test, with acetyl tributyl citrate as a plasticizer

(A-4). The weight of PHB/PLA/A-4 film at the beginning of test was 3.0287 g. Particular sticking of the composting medium on the sample film surface was observed in the 4th day of the experiment. More distinct composting medium sticking on the film surface happened then gradually and was very distinct already in the 12th day of experiment. Concurrently, the medium turned brown. First, small sample degradation signs were observed till the 32nd day of experiment. In the 46th day of experiment, the sample film was smaller only by 5%, but it was very brittle. Subsequently, distinct degradation happened and in the 55th day of the experiment only 25% remained from the original film. Only 5% of the sample remained in the 60th day and the disintegration was completely finished in the 65th day from the test initiation. The subjective rating of the degree of disintegration—preserved sample amount (in %, estimated only by visual observation) can be seen in Table 5.

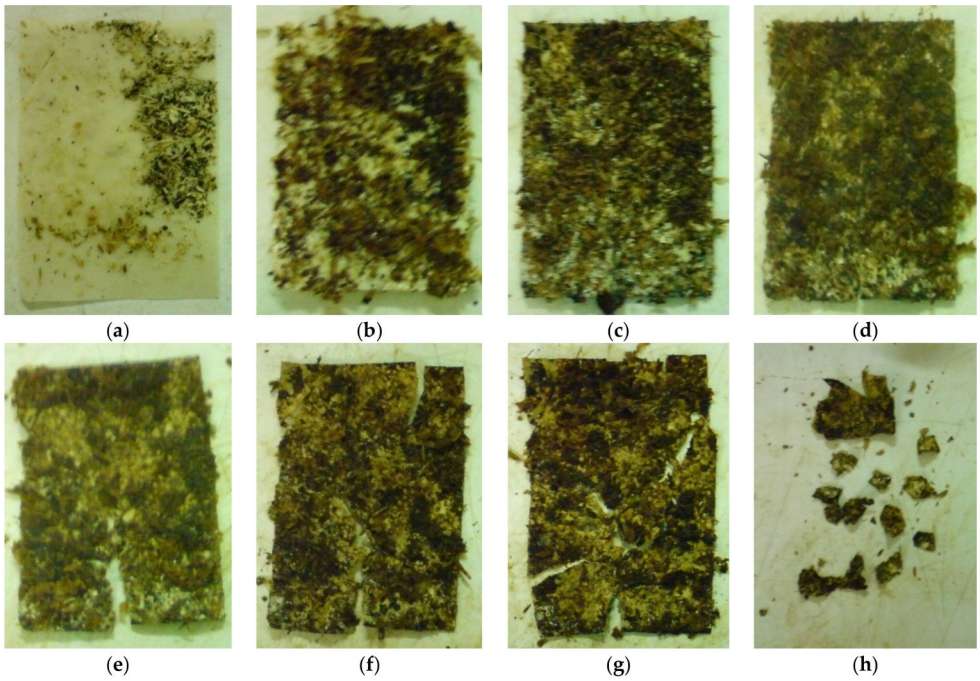


Figure 11. Determination of the degree of disintegration—photos of sample during the test: (**a**) 4th day; (**b**) 12th day; (**c**) 25th day; (**d**) 29th day; (**e**) 32nd day; (**f**) 35th day; (**g**) 42nd day; and, (**h**) 55th day.

Table 5. Subjective rating of the degree of disintegration during test—preserved sample amount (in %).

Day	**1**	**4**	**6**	**12**	**14**	**15**	**18**	**20**	**25**	**29**	**32**	**35**	**39**	**42**	**46**	**55**	**60**	**65**
(%)	100	100	100	100	100	100	100	100	100	100	99	98	97	97	95	25	5	0

The samples were disintegrated under thermophilic condition during 65 days. According to IS/ISO 20200, the samples have to be disintegrated until 90 days. Despite positive results, this method is not applicable to the determination of biodegradability of plastic materials under real composting conditions. Still, the determination of the degree of disintegration test brought important information about possible biodegradability under composting conditions.

Other, accurate biodegradable tests of our plasticized matrix with various plasticizers that were performed at water (fresh and salt) and at soil are running at these days. Namely, that is "Determination of the ultimate aerobic biodegradability of plastic materials in an aqueous medium-method by measuring the oxygen demand in a closed respirometer" (ISO 14851:1999), "Water quality—Guidance for determination of biodegradability in the marine environment" (ISO 16221:2001) and "Plastics-Determination of the ultimate aerobic biodegradability in soil by measuring the oxygen demand in a respirometer or the amount of carbon dioxide evolved" (ISO 17556:2003) [9,44,45]. Extensive results from these tests will be part of another publication.

4. Conclusions

PHB/PLA/plasticizer melt blends in the weight ratio (wt %) of 60/25/15 were successfully prepared by the corotating twin screw extruder and then by single screw extruder to achieve blended filaments with defined diameters for further 3D printing. Four commercial low molecular plasticizers based on esters of citric acid were used, and all of them were well miscible with PHB/PLA matrix (with PHB majority). Their significant softening effect and structure influence were confirmed by tensile tests and MDSC measurements. Especially, acetyl tributyl citrate (A-4) and tributyl citrate (C-4) plasticizers improved the elongation at break by 308% and 155%, respectively, when compared to non-plasticized PHB/PLA blends. The dogbone samples for tensile tests were designed and successfully printed by 3D printer (FDM technology). Significant plasticizing effect was confirmed also by tensile tests with 3D printed dogbones, although the values of measured elongation at break of dogbones were lower than those for the samples measured in the filament form. Butyryl trihexyl citrate (B-6) and acetyl trihexyl citrate (A-6) plasticizers also had positive softening effect, but considerably smaller as compared to A-4 and C-4 plasticizers. B-6 and A-6 plasticizers improved the elongation at break by 32% and 16%, respectively. MDSC confirmed that the introduction of low molecular plasticizer into PHB/PLA blend caused greater mobility of macromolecular chains. As a consequence, the crystallization and melting temperatures were shifted to lower values. Butyl esters of citric acid caused a decrease of PLA T_g by 35 °C for C-4 and by 33 °C for A-4. Increased length of alkyl chains linked to citric acid conversely showed worse plasticizing effect and it led to higher PLA T_g. The migration tests—the diffusion of all four plasticizers from PHB/PLA matrix were performed. The plasticizers that softened the best, showed also large diffusion after 15 days of exposition to 110 °C in the drying oven. The influence of plasticizer structure on the diffusion was well noticeable. SEM micrographs of 3D printed dogbones fractured by tensile tests showed more compact areas without large holes in the case of samples with A-4 and C-4 plasticizers. PHB/PLA/A-4 sample in the form of film was disintegrated under thermophilic conditions (according to IS/ISO 20200) during 65 days, still, other biodegradability tests have to be done. The goal was to create a new type of eco-friendly PHB/PLA/plasticizer blends and highly improve the poor mechanical properties of neat PHB/PLA blends (with majority of PHB) by the addition of appropriate plasticizer. All four examined plasticizers are applicable and are suitable also for 3D printing technology, but mainly tributyl citrate and acetyl tributyl citrate are the best for the improvement of ductile properties.

Author Contributions: R.P., P.A. and P.M. conceived and designed the experiments; J.B., I.S, P.M., V.M. and S.K. performed the experiments; I.S., V.M. and S.K. analyzed the data; R.P. and S.F. contributed materials/analysis tools; P.M., S.K., V.M. wrote and edited the paper; P.A., R.P., S.F., I.S. and J.B. participated in the analysis, discussion and reviewed the manuscript.

Funding: This research was funded by the Ministry of Education, Youth and Sports of the Czech Republic Project No. LO1211 - Material Research Centre at Faculty of Chemistry, Brno University of Technology, project Light functional materials based on natural polymers No. FCH-S-18-5448 of the Specific University Research Grant. Farther by Ministry of Industry and Trade Czech Republic project No. FV20480, and by Slovak research and Development Agency project No. APVV-14-301 and APVV-17-304.

Acknowledgments: We would like to thank all subjects who volunteered in the study.

Conflicts of Interest: The authors declare no conflict of interest.

References

1. Byun, Y.; Kim, Y.T. Bioplastics for Food Packaging: Chemistry and Physics. In *Innovations in Food Packaging*, 2nd ed.; Han, Y.H., Ed.; Academic Press: Cambridge, MA, USA, 2014; pp. 353–368. ISBN 9780123946010.
2. Koller, M. Advances in Polyhydroxyalkanoate (PHA) Production. *Bioengineering* **2017**, *4*, 88. [CrossRef] [PubMed]
3. Abdelwahab, M.H.; Flynn, A.; Chiou, B.-S.; Imam, S.; Orts, W.; Chiellini, E. Thermal, mechanical and morphological characterization of plasticized PLA-PHB blends. *Polym. Degrad. Stab.* **2012**, *97*, 1822–1828. [CrossRef]

4. Imre, B.; Pukánszky, B. Compatibilization in bio-based and biodegradable polymer blends. *Eur. Polym. J.* **2013**, *49*, 1215–1233. [CrossRef]
5. Rhim, J.-W.; Park, H.-M.; Ha, Ch.-S. Bio-nanocomposites for food packaging applications. *Prog. Polym. Sci.* **2013**, *38*, 1629–1652. [CrossRef]
6. *Plastics. Recommendation for Terminology and Characterisation of Biopolymers and Bioplastics*, 1st ed.; BSI: Brussels, Belgium, 2010.
7. *Determination of the Ultimate Aerobic Biodegradability of Plastic Materials in an Aqueous Medium. Method by Measuring the Oxygen Demand in a Closed Respirometer*, 1st ed.; BSI: Brussels, Belgium, 2004.
8. *Determination of the Ultimate Aerobic Biodegradability of Plastic Materials in an Aqueous Medium: Method by analysis of Evolved Carbon Dioxide*, 1st ed.; BSI: Brussels, Belgium, 2004.
9. *Plastics. Determination of the Ultimate Aerobic Biodegradability in Soil by Measuring the Oxygen Demand in a Respirometer or the Amount of Carbon Dioxide Evolved*, 1st ed.; BSI: Brussels, Belgium, 2003.
10. *Determination of the Ultimate Aerobic Biodegradability of Plastic Materials Under Controlled Composting Conditions—Method by analysis of Evolved Carbon Dioxide: Part 1: General Method*, 1st ed.; BSI: Brussels, Belgium, 2003.
11. *Determination of the Ultimate Aerobic Biodegradability of Plastic Materials Under Controlled Composting Conditions—Method by Analysis of Evolved Carbon Dioxide—Part 2: Gravimetric Measurement of Carbon Dioxide Evolved in a Laboratory-Scale Test*, 1st ed.; BSI: Brussels, Belgium, 2009.
12. Pagga, U. Biodegradability and Compostability of Polymeric Materials in the Context of the European Packaging Regulation. *Polym. Degrad. Stab.* **1998**, *59*, 371–376. [CrossRef]
13. Kale, G.; Kijchavengkul, T.; Auras, R.; Rubino, M.; Selke, S.E.; Singh, S.P. Compostability of Bioplastic Packaging Materials: An Overview. *Macromol. Biosci.* **2007**, *7*, 255–277. [CrossRef] [PubMed]
14. European Bioplastics. Available online: http://docs.european-bioplastics.org/publications/EUBP_Facts_and_figures.pdf (accessed on 19 June 2018).
15. Urtuvia, V.; Villegas, P.; González, M.; Seeger, M. Bacterial production of the biodegradable plastics polyhydroxyalkanoates. *Int. J. Biol. Macromol.* **2014**, *70*, 208–213. [CrossRef] [PubMed]
16. Khanna, S.; Srivastava, A.K. Recent Advances in Microbial Polyhydroxyalkanoates. *Process. Biochem.* **2005**, *40*, 607–619. [CrossRef]
17. Chiulan, I.; Frone, A.N.; Brandabur, C.; Panaitescu, D.M. Recent Advances in 3D Printing of Aliphatic Polyesters. *Bioengineering* **2018**, *5*, 2. [CrossRef] [PubMed]
18. Zhang, M.; Thomas, N.L. Blending Polylactic Acid with Polyhydroxybutyrate: The Effect on Thermal, Mechanical, and Biodegradation Properties. *Adv. Polym. Tech.* **2011**, *30*, 67–79. [CrossRef]
19. Xiao, L.; Wang, B.; Yang, G.; Gauthier, M. Poly(Lactic Acid)-Based Biomaterials: Synthesis, Modification and Applications. In *Biomedical Science, Engineering and Technology*; InTech: London, UK, 2012; pp. 247–282. ISBN 978-953-307-471-9.
20. Garlotta, D. A Literature Review of Poly(Lactic Acid). *J. Polym. Environ.* **2001**, *9*, 63–84. [CrossRef]
21. ColorFabb. Available online: https://colorfabb.com/ (accessed on 21 September 2018).
22. Sanatgar, R.H.; Campagne, Ch.; Nierstrasz, V. Investigation of the adhesion properties of direct 3D printing of polymers and nanocomposites on textiles: Effect of FDM printing process parameters. *Appl. Surf. Sci.* **2017**, *403*, 551–563. [CrossRef]
23. Salentijn, G.I.J.; Oomen, P.E.; Grajewski, M.; Verpoorte, E. Fused Deposition Modeling 3D Printing for (Bio)analytical Device Fabrication: Procedures, Materials, and Applications. *Anal. Chem.* **2017**, *89*, 7053–7061. [CrossRef] [PubMed]
24. Wasantha, L.M.; Gunaratne, K.; Shanks, R.A. Miscibility, Melting, and Crystallization Behavior of Poly(hydroxybutyrate) and Poly(D,L-lactic acid) Blends. *Polym. Eng. Sci.* **2008**, *48*, 1683–1692. [CrossRef]
25. Arrieta, M.P.; Samper, M.D.; López, J.; Jiménez, A. Combined Effect of Poly(hydroxybutyrate) and Plasticizers on Polylactic acid Properties for Film Intended for Food Packaging. *J. Polym. Environ.* **2014**, *22*, 460–470. [CrossRef]
26. Da Silva, M.A.; Vieira, M.G.A.; Maçumoto, A.C.G.; Beppu, M.M. Polyvinylchloride (PVC) and natural rubber films plasticized with a natural polymeric plasticizer obtained through polyesterification of rice fatty acid. *Polym. Test.* **2011**, *30*, 478–484. [CrossRef]

27. Wypych, G. *Handbook of Plasticizers*, 3rd ed.; ChemTec Publishing: Toronto, ON, Canada, 2017; ISBN 978-1-5231-0906-7. Available online: https://app.knovel.com/hotlink/toc/id:kpHPE00024/handbook-plasticizers/handbook-plasticizers (accessed on 26 June 2018).
28. Białecka-Florjańczyk, E.; Florjańczyk, Z. Solubility of Plasticizers, Polymers and Environmental Pollution. In *Thermodynamics, Solubility and Environmental Issues*, 1st ed.; Letcher, T.M., Ed.; Elsevier: Amsterdam, The Netherlands, 2007; pp. 397–408. ISBN 978-0-444-52707-3.
29. Cadogan, D.F.; Howick, C.J. Plasticizers. In *Ullmann's Polymers and Plastic: Products and Processes*; Wiley VCH: Weinheim, Germany, 2016; Volume 1, pp. 581–600. ISBN 978-3-527-33823-8.
30. Marcilla, A.; García, S.; García-Quesada, J.C. Study of the migration of PVC plasticizers. *J. Anal. Appl. Pyrolysis* **2004**, *71*, 457–463. [CrossRef]
31. Marcilla, A.; García, S.; García-Quesada, J.C. Migrability of PVC plasticizers. *Polym. Test.* **2008**, *27*, 221–233. [CrossRef]
32. Ambrogi, V.; Brostow, W.; Carfagna, C.; Pannico, M.; Persico, P. Plasticizer migration from cross-linked flexible PVC: Effects on tribology and hardness. *Polym. Eng. Sci.* **2001**, *52*, 211–217. [CrossRef]
33. Sun, X.S. Plastics Derived from Starch and Poly(Lactic Acids). In *Bio-Based Polymers and Composites*, 1st ed.; Wool, R.P., Ed.; Elsevier: Burlington, MA, USA, 2005; pp. 369–410. ISBN 978-0-12-763952-9.
34. Godwin, A.D. Plasticizers. In *Applied Plastics Engineering Handbook*, 1st ed.; Kutz, M., Ed.; Elsevier: Waltham, MA, USA, 2011; pp. 487–501. ISBN 978-1-4377-3514-7.
35. Vieira, M.G.A.; Da Silva, M.A.; Dos Santos, L.O.; Beppu, M.M. Natural-based plasticizers and biopolymer films: A review. *Eur. Polym. J.* **2011**, *47*, 254–263. [CrossRef]
36. Ivana, M.; Obruca, S.; Prikryl, R. Process for Preparing Polyhydroxyalkanoates (PHA) on Oil Substrate. U.S. Patent Application No. PCT/CZ2013/000100, 23 August 2018.
37. Hydal. Available online: https://www.hydalbiotech.com/our-technologies (accessed on 26 June 2018).
38. Armentato, I.; Fortunati, E.; Burgos, N.; Dominici, F.; Luzi, F.; Fiori, S.; Jimenéz, A.; Yoon, K.; Ahn, J.; Kang, S.; et al. Processing and characterization of plasticized PLA/PHB blends for biodegradable multiphase systems. *Express Polym. Lett.* **2015**, *9*, 583–596. [CrossRef]
39. Biomer: Biodegradable Polymers. Available online: http://www.biomer.de/IndexE.html (accessed on 26 June 2018).
40. NatureWorks. Available online: https://www.natureworksllc.com/ (accessed on 26 June 2018).
41. Vertellus Citroflex® Platicizers. Available online: http://www.vertellus.com/products/plastics-polymers/citroflex-plasticizers/ (accessed on 26 June 2018).
42. *Determination of Tensile Properties - Part 1: General Principles*, 2nd ed.; CEN: Brussels, Belgium, 2012.
43. *Plastics—Determination of the Degree of Disintegration of Plastic Materials under Simulated Composting Conditions in A Laboratory-Scale Test*, 2nd ed.; ISO: Geneva, Switzerland, 2015.
44. *Determination of the Ultimate Aerobic Biodegradability of Plastic Materials in an Aqueous Medium—Method by Measuring the Oxygen Demand in A Closed Respirometer*, 1st ed.; BIS: New Delhi, India, 1999.
45. *Water Quality—Guidance for Determination of Biodegradability in the Marine Environment*, 1st ed.; ISO: Geneva, Switzerland, 2001.



© 2018 by the authors. Licensee MDPI, Basel, Switzerland. This article is an open access article distributed under the terms and conditions of the Creative Commons Attribution (CC BY) license (http://creativecommons.org/licenses/by/4.0/).

materials

MDPI

Article

Printability, Mechanical and Thermal Properties of Poly(3-Hydroxybutyrate)-Poly(Lactic Acid)-Plasticizer Blends for Three-Dimensional (3D) Printing

Soňa Kontárová [1,*], Radek Přikryl [1], Veronika Melčová [1], Přemysl Menčík [1], Matyáš Horálek [1], Silvestr Figalla [1], Roderik Plavec [2], Jozef Feranc [2], Jiří Sadílek [3] and Aneta Pospíšilová [1]

1 Institute of Materials Chemistry, Faculty of Chemistry, Brno University of Technology, Purkyňova 464/118, 612 00 Brno, Czech Republic; prikryl@fch.vut.cz (R.P.); xcmelcova@fch.vut.cz (V.M.); mencik@fch.vut.cz (P.M.); xchoralek@fch.vut.cz (M.H.); xcfigallas@fch.vut.cz (S.F.); xcpospisilovaan@fch.vut.cz (A.P.)

2 Institute of Natural and Synthetic Polymers, Faculty of Chemical and Food Technology, Slovak University of Technology in Bratislava, Radlinského 9, 812 37 Bratislava, Slovakia; roderik.plavec@stuba.sk (R.P.); jozef.feranc@stuba.sk (J.F.)

3 Polymer Institute Brno, Tkalcovská 36/2, 602 00 Brno, Czech Republic; jiri.sadilek@polymer.cz

* Correspondence: kontarova@fch.vut.cz; Tel.: +42-06-0445-5762

Received: 24 September 2020; Accepted: 21 October 2020; Published: 23 October 2020



Abstract: This paper investigates the effect of plasticizer structure on especially the printability and mechanical and thermal properties of poly(3-hydroxybutyrate)-poly(lactic acid)-plasticizer biodegradable blends. Three plasticizers, acetyl tris(2-ethylhexyl) citrate, tris(2-ethylhexyl) citrate, and poly(ethylene glycol)bis(2-ethylhexanoate), were first checked whether they were miscible with poly(3-hydroxybutyrate)-poly(lactic acid) (PHB-PLA) blends using a kneading machine. PHB-PLA-plasticizer blends of 60-25-15 (wt.%) were then prepared using a corotating meshing twin-screw extruder, and a single screw extruder was used for filament preparation for further three-dimensional (3D) fused deposition modeling (FDM) printing. These innovative eco-friendly PHB-PLA-plasticizer blends were created with a majority of PHB, and therefore, poor mechanical properties and thermal properties of neat PHB-PLA blends were improved by adding appropriate plasticizer. The plasticizer also influences the printability of blends, which was investigated, based on our new specific printability tests developed for the optimization of printing conditions (especially printing temperature). Three-dimensional printed test samples were used for heat deflection temperature measurements and Charpy and tensile-impact tests. Plasticizer migration was also investigated. The macrostructure of 3D printed samples was observed using an optical microscope to check the printing quality and printing conditions. Tensile tests of 3D printed samples (dogbones), as well as extruded filaments, showed that measured elongation at break raised, from 21% for non-plasticized PHB-PLA reference blends to 84% for some plasticized blends in the form of filaments and from 10% (reference) to 32% for plasticized blends in the form of printed dogbones. Measurements of thermal properties (using modulated differential scanning calorimetry and oscillation rheometry) also confirmed the plasticizing effect on blends. The thermal and mechanical properties of PHB-PLA blends were improved by the addition of appropriate plasticizer. In contrast, the printability of the PHB-PLA reference seems to be slightly better than the printability of the plasticized blends.

Keywords: plasticizers; poly(hydroxybutyrate)-poly(lactic); 3D printing; printability; citrates; poly(ethylene glycol) PEG; biodegradable polymeric blends

1. Introduction

Environmental issues caused by plastics have induced rising concern towards "biopolymers", polymers that are biodegradable or bio-based or can be both. Bioplastics made from biopolymers already serve as alternatives for many petroleum-based commodities and have a predicted global production capacity of around 2.62 million tons for 2023. Researchers are trying to seek bioplastics which have comparable or even better properties to those of petroleum-based plastics. Bioplastics are already used in an increasing number of branches, e.g., packaging, catering products, agriculture, coatings and adhesives, toys, textiles, electronics, automotive, building and construction, medical applications, and many other sectors. Biopolymers PLA (poly(lactic acid)) and PHAs (polyhydroxyalkanoates) are generally well-researched and are the prime leaders of biopolymers production capacity growth [1–7].

PHAs are bio-based and biodegradable linear polyesters and copolymers with a broad range of mechanical and physical properties, which depend on PHA chemical composition. The production capacity of PHAs is expected to triple from 2018 to 2023 [7]. PHAs are embedded as intracellular carbon and energy reserve granules in different Gram-positive and Gram-negative bacteria from a number of substrates, including sugars and fatty acids [8]. The most common presence of short-chain-length PHAs (scl-PHA) are those with 3–5 carbon atoms per unit [8,9]. The subject of our study is poly(3-hydroxybutyrate) (PHB), the most researched and widely used representative of the PHAs group. The advantage of PHB is the possibility of its preparation also from waste cooking oil so it does not require agronomical feedstock [10,11].

Poly(lactic acid) (PLA), -$[CH(CH_3)COO]_n$-, is a highly transparent, glossy, colorless, and rigid thermoplastic material with great barrier properties. This aliphatic polyester is synthesized from lactic acid, which is produced by the fermentation of renewable resources and is available in the form of high-performance PLA grades that are a good replacement for PP (polypropylene), PS (polystyrene), and ABS (acrylonitrile butadiene styrene) in many demanding applications [7,12–16]. The ratio between D and L enantiomers influences the properties of PLA. Among the disadvantages of PLA are their low heat distortion temperatures (HDTs): softening above 60 °C. A disadvantage is also its incapability of fast biodegrading at ambient temperature [13]. The tensile properties of PLA can be various and are influenced by its degree of crystallinity and whether it is annealed or oriented [14,17].

Due to nontoxicity, biodegradability, and biocompatibility, these PHB (poly(3-hydroxybutyrate)) and PLA blends can be useful together with three-dimensional (3D) printing technologies, especially for biomedicine (implants, scaffolds), art, archeology (replicas), and for prototyping and manufacture of reserve parts for the automotive industry, airplanes, etc. [12,18–20]. While PLA has great printability and is commonly used in 3D printing, printability of pure PHB (synthesized by bacterial fermentation) is more complicated due to its high crystallinity. It is related mostly to warping (overall shrinkage is caused not only by thermal shrinkage but in addition also crystallization shrinkage occurring during melt cooling). The principal disadvantage for the printing of PHB is that its melting temperature (around 170–180 °C) is too close to the degradation temperature. Thus, its printability is limited by this relatively small processing window. Filaments of PLA-PHA polymeric blends are already used for 3D printing also in industry, and its printability is good due to the majority of PLA [21,22].

In this study, fused deposition modeling (FDM) technology is used. This technology is very productive also while using low-cost 3D printers. A plastic filament (in our study PHB-PLA-plasticizer filament) used in the FDM method is pushed through an extrusion nozzle heated to a particular temperature and is melted and deposited on the printing bed in the desired conformation. A part of the FDM method is the software that compiles an STL (stereolithography) or CAD (computer-aided design) file, mathematically slicing and orienting the model for the building process [23]. This method is used in our work for the preparation of 3D printed dogbones (double-paddle shaped testing samples) from PHB-PLA-plasticizer material, which are further used for tensile tests, HDT measurements, Charpy, and tensile-impact tests. Before the printing of a test specimen, the printability had to be tested to setup the best printing conditions (especially printing temperature). The warping problem can occur especially during the printing of large parts because the internal temperature of a printed object during printing tends to vary. PHB-PLA-plasticizer materials are printed at high extrusion nozzle

temperatures (180-195 °C) onto the printing bed, which is at room temperature. An integrated fan is used for cooling and for quick solidification of the material. The shrinkage which is usually caused by this situation can lead to deformation through warping. As a result, detachment from the printing bed and the destruction of products usually occur [24]. In general, FDM "printability" is not well defined and there are not standard specifications describing printability, probably due to the many types of printers, methods, and printing parameters that can influence the printability of the final product. The printability of our PHB-PLA-plasticizer blends and warping were tested according to practical tests designed by our research group. These tests are focused on determining the appropriate temperature of the extrusion nozzle, especially the temperature at which geometrical shapes are printed with the best quality (designed temperature tower test, see Materials and Methods) and with minimal warping (designed warping test specimen). These newly designed tests are applicable for all materials and FDM printers and can be useful tools to set up the best temperature of the extrusion nozzle for the printing of the desired products.

To take advantage of PLA and PHB as biocompatible and biodegradable alternatives to customary polymers in industry, some disadvantages must be overcome. Toughness, fragility, brittleness, and poor processing properties of neat PHB can be exceeded by blending with poly(D,L-lactic acid). This amorphous polymer can reduce the crystallinity of PHB and so expand the range of applications of PHB [3,25]. Still, neat PHB-PLA blends are brittle and stiff materials, have poor mechanical properties, and due to thermal degradation near to its melting point also have limited processability [26]. The addition of plasticizer can improve poor mechanical properties, especially poor ductility. These non-volatile low molecular weight compounds, used as additives in the polymer industry, are able to lower the melting temperature (T_m), the glass transition temperature (T_g), and improve the flexibility and the processability of biopolymers [27,28]. The addition of plasticizers can influence a lot of properties: they can decrease the tension of deformation, density, hardness, viscosity, they can increase resistance to fracture, dielectric constant, the polymer chain flexibility, and they can influence optical clarity, the degree of crystallinity, electric conductivity, the resistance to biological degradation, and fire conductivity [27,29]. A lot of plasticizers have already been investigated, such as various monomeric esters of adipic, phosphoric, phthalic, citric, ricinoleic and sebacic acids, chlorinated paraffin, and low-molecular-weight polyesters [27,28].

Two commercial and synthesized eco-friendly primary plasticizers that are based on esters of citric acid (acetyl tris(2-ethylhexyl) citrate, tris(2-ethylhexyl) citrate), and poly(ethylene glycol) bis(2-ethylhexanoate) were used in this current study. The goal was to improve the poor mechanical properties of neat PHB-PLA blends (with the majority of PHB) by adding an appropriate plasticizer and to make new types of eco-friendly PHB-PLA-plasticizer blends which are suitable for later application as scaffolds in biomedicine. Our previous research [30] was concerned with PHB-PLA-plasticizer, where different plasticizers, including tributyl citrate and acetyl tributyl citrate, were used. In this current study, also printability, which is necessary to be well explored for the printing of scaffold and other products, is investigated. At the beginning, the miscibility of new plasticizers with PHB-PLA blends in the weight ratio (wt.%) of 85polymer-15plasticizer was checked using a kneading machine. The 60PHB-25PLA-15 plasticizer blends (in wt.%) were then prepared by corotating meshing twin-screw extruder, and next, a single screw extruder was used for filaments preparation (for further 3D printing). The printability of 3D samples printed from these blends was judged according to our newly designed tests. The printability test "Temperature tower" could reveal the best nozzle printing temperature for each PHB-PLA-plasticizer blend and also compared the influence of particular plasticizers on the printability of geometrical shapes. The printability test "Warping specimen" revealed the influence of particular plasticizers on warping. In addition, the best nozzle printing temperatures, at which the warping during printing was minimal, were found. Thus, the optimization of printing conditions via printing tests allowed us to print PHB-PLA-plasticizer test specimens (for further mechanical, thermal, and optical tests) with the best obtainable printing quality. The printing quality was finally checked using the 3DBenchy test. The mechanical properties of these plasticized blends were further estimated

using tensile tests of filaments as well as 3D printed dogbones, which were printed at optimized conditions after printability tests. 3D printed dogbones were used also for Charpy and tensile-impact tests. The migration of plasticizers from blends, which is the principal disadvantage of external plasticizing (especially in the case of linear plasticizer's structure compared to branched [31–37]) was also investigated by exposing blends to 110 °C in the drying oven. Modulated differential scanning calorimetry (MDSC) was used to investigate the thermal properties of our blends, as well as the HDT (with 3D printed test specimens), and oscillation rheometry (RPA 2000) measurements. The macrostructure of 3D printed samples, printed at the conditions adjusted according to printability tests, and their printing quality was checked using an optical microscope.

Papers engaged in the improvement of the thermal and mechanical properties of PLA-PHB blends using plasticizers have already been published but always with a PLA majority. Among the investigated plasticizers are, e.g., oligomeric lactic acid [38], acetyl tributyl citrate and poly(ethylene glycol) [26,39], polyester plasticizer (Lapol 108) [3]. Papers dealing with the printability of PLA or PHB or different biobased polymer are even rarer. Diederichs et al. [40] investigated how to improve the printability of biobased poly(trimethylene terephthalate) (PTT) with additives such as chain extenders (CEs) and impact modifiers. They were able to prepare 3D printed complete and warpage-free samples because of the modifications made in processing and printing parameters, and with the assistance of additives. The 3D printing quality of seven PLA grades analyzed based on MFI (melt flow index), density, SEM (scanning electron microscopy), and DSC (differential scanning calorimetry) was investigated by Wang et al. [41]. They also found that commercial PLA3D850 is a promising material for 3D printing in the case that PHB is used as a blending partner (80-20 PLA-PHB by weight) and that this blending leads to a fully biodegradable material with good processability and no need for annealing.

Our research describes the influence of three plasticizers on printability and the mechanical and thermal properties of plasticized PHB-PLA blends, with a majority of PHB. Research of our blends with acetyl tris(2-ethylhexyl) citrate, tris(2-ethylhexyl) citrate, and poly(ethylene glycol) plasticizers and the section describing the "printability" of PHB-PLA-plasticizer blends has not been published yet, and thus, it is unique in this context. Our printability tests developed for the optimization of printing conditions could be useful also for the case of other materials and types of printers. Our PHB-PLA-plasticizer blends are suitable for 3D printing, biomedical applications and prototyping. The advantage of blends with a majority of PHB is their ability to be well compostable and biodegradable.

2. Materials and Methods

2.1. Materials

Poly-3-hydroxybutyrate (PHB Biomer®, ρ = 1.23 g·cm^{-3}, M_w = 410,000 g·mol^{-1}) was provided by Biomer Company (Krailling, Germany) in the form of white powder [42]. In our study amorphous poly(D,L-lactic acid) (PLA) with T_g around 60 °C is used. Amorphous PLA was chosen for its ability to reduce the overall crystallinity content in our PHB-PLA-plasticizers blends, which are further used for 3D printing. Amorphous PLA granules (Ingeo™ 4060D, M_w = 180 000 g·mol^{-1}, T_g = 55–60 °C, *rho* = 1.24 g·cm^{-3}) were supplied by NatureWorks LLC (Minnetonka, MN, USA) Company [43].

Monomeric commercial plasticizer used in this research is based on the ester of citric acid (acetyl tris(2-ethylhexyl) citrate) and is provided by Jungbunzlauer Suisse AG (Basel, Switzerland), with the Citrofol® trademark [44]. An additional monomeric plasticizer based on the ester of citric acid (tris(2-ethylhexyl) citrate) was synthesized for this study. Another commercial plasticizer, poly(ethylene glycol) bis(2-ethylhexanoate), was provided by Merck KGaA (Darmstadt, Germany) [45]. The plasticizers described by commercial and chemical names, molecular weights, and labels can be seen in Table 1. Their structure can be seen in Figure 1.

Table 1. Commercial and chemical names of used plasticizers and their molecular weights and labels.

Commercial	Chemical Name	Molecular Weight (g·mol^{-1})	Plasticizer's Label
Citrofol® AHII	acetyl tris(2-ethylhexyl) citrate	570	A2-EH
poly(ethylene glycol) bis (2-ethylhexanoate)		650	PEG-2-EH
Synthetized	**Chemical Name**	**Molecular Weight (g·mol^{-1})**	**Plasticizer's Label**
-	tris(2-ethylhexyl) citrate	528	C2-EH

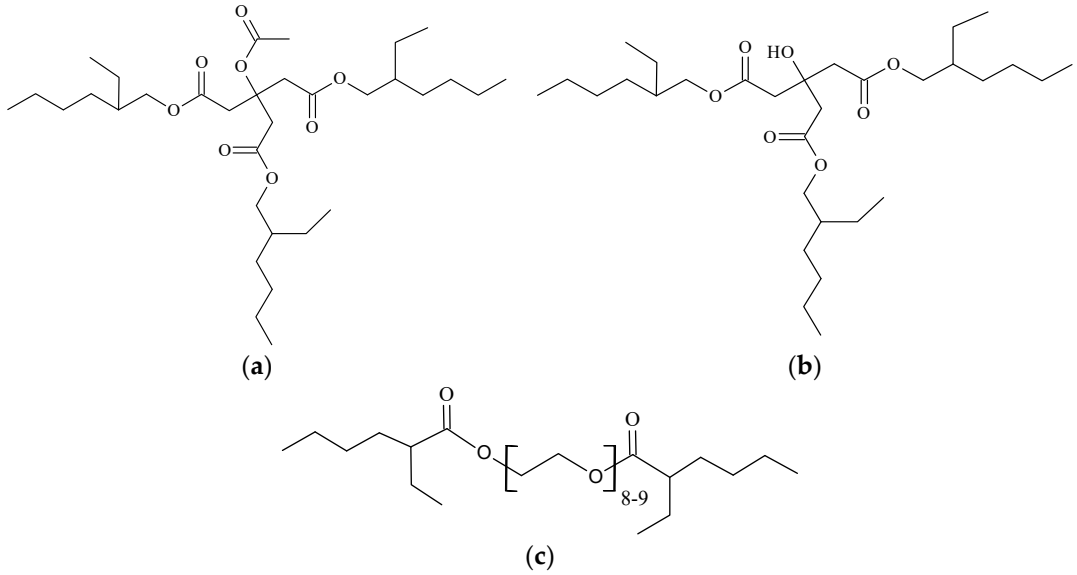


Figure 1. (**a**) Plasticizer A2-EH structure; (**b**) plasticizer C2-EH expected structure; and (**c**) plasticizer PEG-2-EH structure.

2.2. Plasticizers Miscibility with PLA-PHB Polymers

60PHB-25PLA-15 plasticizer samples (in wt.%) and a non-plasticized 70PHB-30 PLA reference sample were kneaded using a kneading machine and according to conditions described in our previous work [30]. There were only small changes in the process: the weights of samples were 50 g (before the kneading). Sample dosing (PHB-PLA mixture) into the Brabender machine (Brabender GmbH & Co. KG, Duisburg, Germany) took 1 min, and then, the mixture was kneaded for another 2 min before plasticizer was added. The kneading process continued for the following 6 min. The total kneading time of PHB-PLA-plasticizer samples as well as PHB-PLA reference was 9 min.

2.3. Preparation of Plasticized PHB-PLA Blends

The 70PHB-30PLA blends (in wt.%) (reference), as well as the 60PHB-25PLA-15 plasticizer blends (in wt.%), were extruded using two extruders according to conditions described in our previous work [30]. Citrofol® (A2-EH), C2-EH, and PEG-2-EH were used as plasticizers stepwise. Conditions and process details were the same as in our previous work, except the total weights of each sample for extrusion, which were 1000 g for plasticized samples and 850 g for reference. Filaments with well-defined thicknesses and diameters were prepared for further 3D printing.

2.4. 3D Printing

The dogbone samples prepared for further tensile tests and sample bars (80 × 10 × 4) mm prepared for further HDT measurements, Charpy and tensile-impact strength tests and for the observations using optical microscopy were first designed using AutoCAD (ver. 2018, Autodesk Inc., San Rafael, CA, USA) and Slic3r (software version 1.3.0, free software, developed by Alessandro Ranellucci).

These programs were used for 3D virtual modeling and mathematical slicing. The 3D model for the printing of dogbone specimens was designed by our group and is described in detail in our previous work [30]. Sample bars were also designed using Slic3r and uploaded to the printer. Their 3D model was generated simply by only perimeters (100%) using no infill.

All test specimens were printed on a PRUSA i3 MK3 3D printer (Prusa Research s.r.o., Praha, Czech Republic) using FDM technology from PHB-PLA-plasticizer filaments with a defined diameter, as mentioned above. The dogbones and sample bars were printed at 180–195 °C (195 °C during the printing of first layers for better adhesion to the printing bed), without additional air cooling and bed heating. Specific printing temperatures for each PHB-PLA-plasticizer sample were selected according to our printability test results (described below), where the temperature tower, the warping, and 3DBenchy tests were examined. Other basic printing parameters for testing samples can be seen in Table 2. Three-dimensional printing was executed approximately three months after preparation of the filaments.

Table 2. Basic printing parameters.

Basic Printing Parameters	Dogbone	Temperature Tower, Warping, 3DBenchy, Other Testing Samples
Filament diameter (mm)	1.75 ± 0.05	1.75 ± 0.05
Nozzle diameter (mm)	0.4	0.4
Layer height (mm)	0.2	0.2
Perimeters printing speed ($mm \cdot s^{-1}$)	40	45
Infill printing speed ($mm \cdot s^{-1}$)	60	200
Bed heating (°C)	20	20
Fan (%)	100	100

2.5. Printability Tests

The printability tests were designed for the optimization of printing conditions, in order to improve the structural homogeneity and thus mechanical properties of our samples. The printing temperature was optimized via temperature tower tests and warping tests designed by our team. Final verification of adjusted printing conditions proceeded via the Benchy test.

2.5.1. Temperature Tower

One of the most important 3D printing parameters is the temperature of the printing nozzle. The'printability temperature interval for each PHB-PLA-plasticizer blend was examined via a test specimen temperature tower, designed by our team [46], with the help of Autodesk Fusion 360 software (ver. 2018, Autodesk Inc., San Rafael, CA, USA). The temperature tower (see Figure 2) was designed regarding the printability speed, amount of used material, and number of various geometric elements. The temperature tower consists of six identical floors and each of them contains eight different geometric elements. The dimensions of the temperature tower are approximately (60 × 25 × 25) mm. It is possible to set up individual printing temperatures for each floor. Three temperature towers were 3D printed in the case of each PHB-PLA-plasticizer blend, first in the temperature interval 220–195 °C (220 °C the first floor, each following floor 5 °C less than the previous floor, 195 °C the last floor), second in the temperature interval 195–170 °C, and third in the temperature interval 180–155 °C. Ideal temperatures for each PHB-PLA-plasticizer blend were then visually evaluated by the comparison of floors one to another and by the measurement of dimensional variations of printed geometric elements compared to the software model. Among the observed geometric elements, there were colonnade and bridges between floors (Figure 2A), horizontal circle holes and overhangs between floors (Figure 2B), diagonal crossbar and rectangle holes (Figure 2C), roundness of the wall (Figure 2D,E), and vertical circle hole and eventual stringing in it (Figure 2E). In addition, the color of each floor was checked and compared. The darker coloration of some floors, especially during the printing with

higher nozzle temperatures, suggested material degradation and inapplicable nozzle temperature. The temperature tower provides information about the range of applicable printability temperatures and ideal temperature for a particular material, together with warping test results.

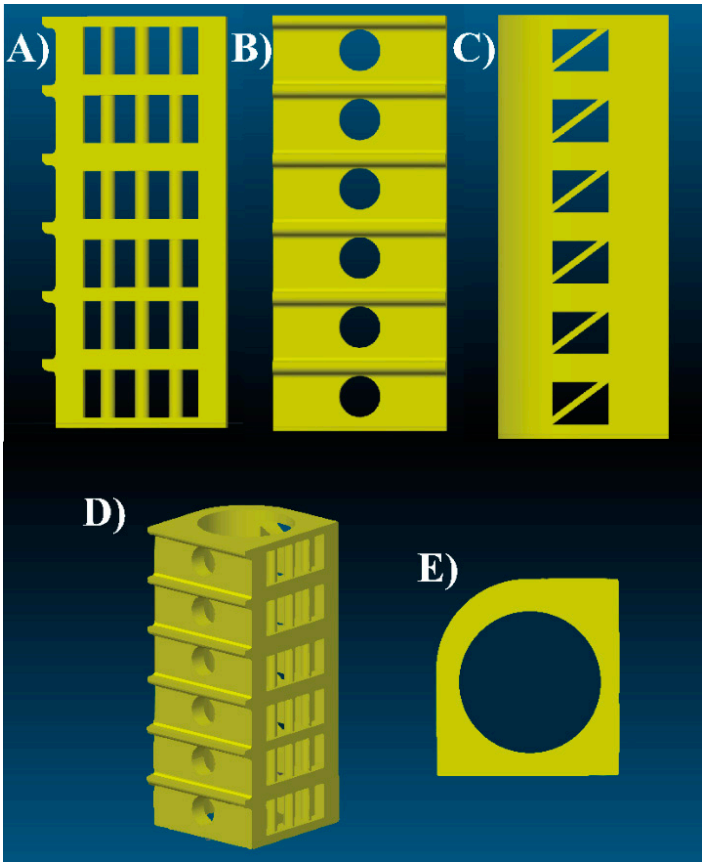


Figure 2. Temperature tower model: (**A**–**C**) lateral views, (**D**) axonometric view, (**E**) top view [46].

2.5.2. Warping

A standardized method, enabling easy, quick, and repetitive measurements of warping of 3D printed materials is not currently available. Hence, our team designed the test specimen, which fulfills the demands for repeatable warping measurements. The warping specimen consists of a square platform (20 × 20) mm and a stuck beam (60 × 10 × 10) mm, which adhere to the bed only via one peripheral wall [46] (Figure 3).

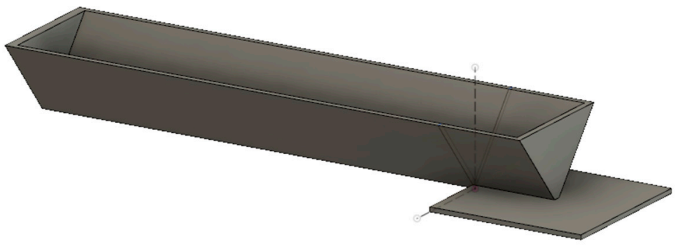


Figure 3. Three-dimensional model of designed warping test specimen [46].

The warping during the printing of the test specimen causes the lifting of a stuck beam at the opposite end from the square platform. The first detachment of a stuck beam from the bed occurred during the printing of the warping specimen, and the height of the layer (value of *z*-axis during printing subtracted from the printer) was observed and recorded. The designed total height of the warping test

specimen (10 mm) was then divided by the recorded value, and in this way, the warping coefficient was calculated (Equation (1)). The later the negative effect of warping starts to manifest, the lower the warping coefficient and therefore the material is more printable.

$$\text{warping coefficient} = \frac{\text{designed height of warping test specimen}}{\text{height of warping test specimen achieved during printing}} \quad (1)$$

Several applicable temperatures, based on the temperature tower results, were selected for 3D printing of warping specimens printed from each PHB-PLA-plasticizer filament. The temperatures, for which the warping coefficient was the lowest, were then applied for 3D printing of test specimens from each PHB-PLA-plasticizer filament. These test specimens were subjected to tensile tests, HDT, Charpy and tensile-impact strength tests, and observations using optical microscopy. The first layer temperature during the 3D printing was always set to 195 °C for better adhesion to the printing bed. This value was experimentally established as the best for PHB-PLA-plasticizer filaments [46].

2.5.3. 3D Benchy

The 3D Benchies were printed for each PHB-PLA-plasticizer filament at printing temperatures optimized via the temperature tower and warping tests. Resultant printing temperatures varied in the range of 180–195 °C (the first layers were printed at 195 °C). Printed 3D Benchies were then visually evaluated [47], and thus, the adjusted printing conditions were revised.

2.6. Modulated Differential Scanning Calorimetry—Thermal Characterization

The combination of modulated and conventional differential scanning calorimetry (MDSC and DSC, respectively) was used for the thermal properties measurements of prepared PHB-PLA-plasticizer and PHB-PLA reference samples. The measurements were performed according to ASTM D 3417-99 standard specification [48]. Process details and measurements conditions were the same as in our previous work; for further details please see [30].

2.7. Oscillation Rheometry—Thermal Characterization

The oscillation rheometer RPA 2000 (Alpha Technologies GmbH, Germany, Schwabach) with parallel biconical chambers geometry was used for the rheology measurements according to the methodology tailored for bioplastics [49]. All PHB-PLA-plasticizer samples and PHB-PLA reference were subjected to a 10 min timed test at 180 °C. The used frequency was 0.833 Hz (50 oscillations per minute). The amplitude of deformation was chosen to be 30% in order to simulate the conditions during processing. The samples for rheology measurements were in the form of granules prepared from PHB-PLA-plasticizer filaments. The tests were carried out for 7 and 40 days after the preparation of the pellets.

For the evaluation of the degradation rate under thermal and shear loading, the relative complex viscosity was calculated for each sample according to the formula:

$$\eta^*_{rel}(t) = \frac{\eta^*(t)}{\eta^*(0)} \quad (2)$$

where $\eta^*_{rel}(t)$ is relative complex viscosity in time t, $\eta^*(t)$ is complex viscosity in time t, and $\eta^*(0)$ is complex viscosity at the start of the timed test.

2.8. GPC–Gel Permeation Chromatography

MW (Molecular Weights) averages and polydispersity indexes for both neat and modified polymers and blends were measured using gel permeation chromatography (GPC). The measurements were performed using an Agilent Technologies 1100 Series instrument equipped with an isocratic pump, fraction collector, and autosampler. PLgel 10 μm MIXED-B column was thermostated to 30 °C

with chloroform as the eluent at the flow rate of 0.1 mL/min. Linear polystyrene standards with narrow distribution were used to gain the calibration curve (10 points in calibration). The instrument is equipped with a refractive index detector. For the measurement, 5 mg of sample was used.

2.9. HDT—Heat Deflection Temperature

A custom-made apparatus for the HDT measurements of plastics under flexural load in flatwise position was used for the testing of 3D printed PHB-PLA-plasticizer samples, according to CSN EN ISO 75 standard specifications [50]. Three-dimensional printed sample bars, (their 3D model was formed from perimeters only) with (80 × 10 × 4) mm dimensions, were immersed under load in a heat-transfer medium (silicon oil) provided with the means of raising the temperature by (2 ± 0.2) °C/min. The load applied to the specimen center to give the maximum fiber stresses was 1.82 MPa and 0.455 MPa (Standard Method A and B), respectively. When the test bar deflected by 341 µm, the temperature of the medium was recorded. Two sample bars of all PHB-PLA-plasticizer and PHB-PLA reference samples were subjected to measurements simultaneously for a given load.

2.10. Migration Tests—Plasticizers Migration from PHB-PLA Blends

Migration tests of PHB-PLA-plasticizer samples were performed in a drying oven heated to 110 °C. The time of exposition to the higher temperature varied from 1 h up to 16.7 days. Details of measurement conditions and preparation of samples for testing are described in our previous work. Please see [30].

2.11. Tensile Tests—Mechanical Characterization

The mechanical properties of PHB-PLA-plasticizer samples (as well as reference), especially Young's modulus, the elongation at break, and the tensile strength, were determined using the device and according to measurement conditions described in our previous work. Please see [30]. The samples in the form of filaments and 3D printed double-paddle testing samples (dogbones, ~(4 × 2 × 75) mm were measured. The test approached the CSN EN ISO 527-1 standard [51]. For each sample, at least twelve tensile test measurements were carried out.

2.12. Charpy and Tensile-Impact Strength Tests—Mechanical Characterization

Charpy V-notched as well as Charpy un-notched tests were performed using Charpy pendulum Zwick 5113.100 (ZwickRoell GmbH & Co., Ulm, Germany) according to CSN EN ISO 179-1/eA and ISO 179-1/eU standard specifications at ambient conditions [52]. The sample bars (80 × 10 × 4) mm were 3D printed from all PHB-PLA-plasticizer filaments (3D model was generated simply by only perimeters) and half of them were notched (notch Type A). 2.7 J and 10.8 J hammers were used for the measurements of impact energy. Ten V-notched and 10 un-notched 3D printed PHB-PLA-plasticizer specimens were always measured in the edgewise position. The measurements were carried out 7 days after 3D printing. The Charpy un-notched and notched impact strengths, a_{cU}, and a_{cN} (kJ/m^2), were calculated from measured and corrected impact energies E_c (J). Because the breakage did not occur in the case of some flexible PHB-PLA-plasticizer specimens, we decided to also add the determination of tensile-impact strength.

The tensile-impact strength tests were performed using a Charpy pendulum impact hammer (type BPI-25COMC.10, ZwickRoell GmbH & Co., Ulm, Germany), according to CSN EN ISO 8256 standard specifications at ambient conditions [53]. The sample bars (80 × 10 × 4) mm were 3D printed from all PHB-PLA-plasticizer filaments (3D model was generated simply by only perimeters) and were notched according to the standard (type 1 notches, type 1 test specimens). A 7.5 J pendulum hammer was used with the deflection angle of 147°, and the tests were performed according to method A. The measurements were carried out 7 days after 3D printing. The notched tensile-impact strengths, a_{tN} (kJ/m^2), of all PHB-PLA-plasticizer specimens were calculated from measured and corrected tensile-impact energies, E_c (J).

2.13. Optical microscopy—Structural Characterization

The sample bars (80 × 10 × 4) mm were 3D printed from all PHB-PLA-plasticizer filaments (3D model was generated simply by only perimeters). Three-dimensional printed samples were kept in the refrigerator for 30 min and then disrupted via grip and hammerlock to achieve a brittle fracture. The brittle fractures of all PHB-PLA-plasticizer samples were observed using an Olympus SZ51 optical microscope (Olympus Europa Holding GmbH, Hamburg, Germany), with the ocular WHSZ10x-H/22, 4x zoom magnification, 40 total magnifications, and transmitted LED illumination.

3. Results

3.1. Plasticizers Miscibility with PHB-PLA

Acetyltris(2-ethylhexyl)citrate (A2-EH), poly(ethylene glycol)bis(2-ethylhexanoate) (PEG-2-EH), and tris(2-ethylhexyl)citrate (C2-EH) plasticizers were kneaded with PHB-PLA mixture in the weight ratio (wt.%) 60PHB-25PLA-15 plasticizer.

The gearbox torque dependence (kN·m) on the time after the plasticizer was added to the PHB-PLA mixture can be seen in Figure 4. The PHB-PLA mixture had already been dosed for 1 min and kneaded for 2 min. These dependencies (of plasticized samples) are compared with the reference sample (70-30 PHB-PLA in wt.%). In the case of PEG-2-EH (see Figure 5), the gearbox torque first declined to 0 kN·m after the plasticizer addition due to the lubrication of the blades by the plasticizer. These results are in agreement with our previous work, in the case of C-4 and A-4 plasticizers [30]. The torque resistance approached zero because the blades could move freely. After, the gearbox torque increased, because the plasticizer started to mix with PHB-PLA. Finally, the gearbox torque achieved the maximum, which corresponds to the moment of the plasticizer blending with the PHB-PLA. All plasticizers (in the concentration of 15%) were miscible with PHB-PLA within maximally 6 min of total kneading time, which corresponds to a maximum of 3 min from when the plasticizers were added. The addition of C2-EH and A2-EH plasticizers did not cause the gearbox torque declination to 0 kN·m, which may mean a smaller lubrication effect of these plasticizers. The plasticizer C2-EH were kneaded into the PHB-PLA mixture faster than the plasticizers A2-EH and PEG-2-EH. The plasticizer with the acetyl group in the structure (A2-EH) needs more kneading time. This result is in good agreement with our previous work [30], where the plasticizer with the acetyl group A-4 (acetyl tributyl citrate) needed more kneading time compared to the plasticizer C-4 (tributyl citrate). The plasticizer structure also became evident for PEG-2-EH, where the kneading time was the longest due to a longer polymeric chain. As can be seen, all selected plasticizers were successfully kneaded with the PHB-PLA mixture.

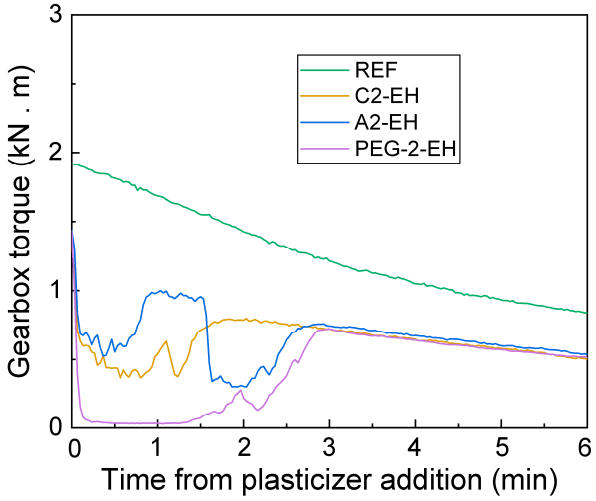


Figure 4. Dependence of gearbox torque on the time elapsed from the addition of plasticizers to the poly(3-hydroxybutyrate) and poly(lactic acid) (PHB-PLA) mixture.

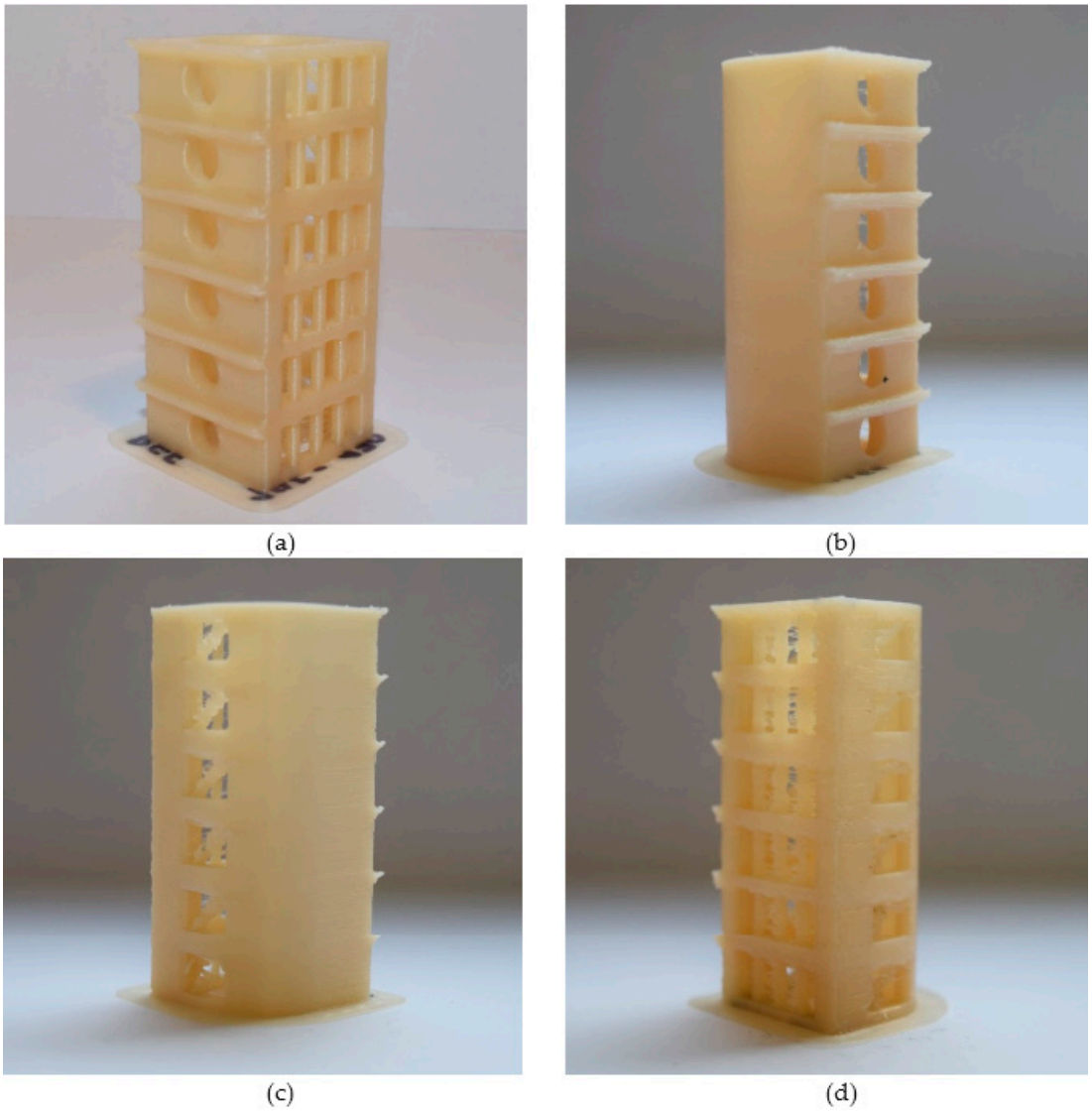


Figure 5. Examples of temperature towers 3D printed at 195–170 °C (minus 5 °C for each floor) from PHB-PLA-plasticizer filaments: (**a**) reference without plasticizer, (**b**) with C2-EH plasticizer, (**c**) with A2-EH, (**d**) with PEG-2-EH.

3.2. 3D Printing and Printability Tests

Printability tests, specifically the temperature tower, warping test, and Benchy test, were carried out for the optimization of printing conditions, especially of printing temperature.

3.2.1. Temperature Tower

The range of applicable printing temperatures was gathered via the temperature tower test described in Materials and Methods (Section 2.5.1.).

The temperature of the last floor of each temperature tower, which was successfully and completely printed (before the next floor printing failed due to too low temperature), can be seen in Table 3. In the case of higher temperatures (temperature towers in the range 220–195 °C), all floors were successfully printed. Contrariwise, the material degradation due to higher temperature can be seen as darker floor coloration, and thus, higher temperatures were not selected into the range of applicable printing temperatures. Equally, the printing with low temperatures is not well reproducible (due to the fluctuation of the nozzle temperature and other printing conditions), although geometric elements are very well printed at lower

temperatures. Moreover, the layers do not hold together so well, and sometimes, delamination can occur during printing at lower temperatures. The evaluated range of applicable printing temperatures are given in Table 3. As can be seen, the range of applicable temperatures for all PHB-PLA-plasticizer filaments was 160–195 °C. In contrast, the filament with a non-plasticized reference has the largest range of applicable temperatures (160–200 °C). Subjective evaluation (marks from 1–5, where 1 is the best) of stringing, some geometric elements (especially colonnade and diagonal crossbar in a rectangle), and undesirable holes in the 3D printed structure can be seen in Table 4. This table contains only a few elements as an example of possible evaluation, although all geometric elements of the temperature tower might be evaluated (as was described in Section 2.5.1). The average marking from this subjective evaluation for all temperature towers can also be seen in Table 4. The printability of geometric elements of the reference sample (without plasticizer) is the best and for the largest range of temperatures. In contrast, the PHB-PLA-PEG-2-EH filament had the worst printability of geometric elements. The filaments with C2-EH and A2-EH had sufficient printability of geometric elements (comparable to reference sample) but only at the lowest temperatures. It seems that it is caused by lower viscosity of their melting during printing at higher temperatures and so shapes of geometric elements collapsed more than during printing at lower temperatures.

Table 3. Evaluation of 3D printed temperature towers.

PHB-PLA-Plasticizer Filament	Temp. Range (°C)	Last Printed Floor (°C)	Range of Applicable Temperatures (°C)
REF (PHB-PLA)	220–195	220	200–195
	195–170	170	195–170
	180–155	160	180–160
C2-EH	220–195	220	-
	195–170	170	190–180
	180–155	160	180–160
A2-EH	220–195	220	-
	195–170	170	180–175
	180–155	155	180–165
PEG-2-EH	220–195	220	-
	195–170	170	195, 180
	180–155	155	165

Table 4. Visual evaluation of the geometric elements of some of the 3D printed temperature towers via marks 1–5 (1 is the best).

PHB-PLA-Plasticizer Filament	Temp. Range (°C)	Stringing	Colonnade	Diagonal	Holes in Structure	Average Mark
REF (PHB-PLA)	220–195	4	3	3	2	3
	195–170	2	1	1	3	1.75
	180–155	1	2	1	3	1.75
C2-EH	220–195	5	5	5	1	4
	195–170	4	4	5	3	4
	180–155	2	2	3	3	2.5
A2-EH	220–195	5	4	5	1	3.75
	195–170	4	4	5	1	3.5
	180–155	2	1	2	3	2
PEG-2-EH	220–195	5	5	5	4	4.75
	195–170	5	5	5	3	4.5
	180–155	4	3	4	2	3.25

This evaluation via the comparison of printed elements is rather subjective and requires some practice. Hence, the temperature tower gave us information only about the range of applicable temperatures. These ranges of applicable temperatures were then optimized via the warping tests to obtain one "ideal" temperature for the printing of specimens for mechanical and thermo-mechanical characterizations. These specimens must be printed reproductively and, due to their size, also with the lowest warping. Thus, despite the fact that the printability of geometric elements is best at a particular temperature, this temperature is not suitable for printing the specimens for testing.

Extreme temperatures (too high or low) must be taken into consideration, and it is not suitable to include them in the applicable temperatures. This method is possible to apply more exactly using image analysis of geometric elements. However, visual evaluation was fully sufficient for the selection of the range of applicable temperatures in our case. Image analysis of geometric elements could be useful, e.g., in the case of scaffold printing and other products with a demand for high-level accuracy. The advantages of the temperature tower are the possibility to examine a wide range of materials printed within a wide range of temperatures and to debug the printing conditions on different types of printers. The examples of 3D printed temperature towers from PHB-PLA-plasticizer filaments can be seen in Figure 5.

3.2.2. Warping

For each PHB-PLA-plasticizer sample, warping specimens were printed for each chosen applicable temperature. The temperature of the first layer for each specimen was set to 195 °C (according to the experience with our material [46]). The warping coefficient is a dimensionless quantity and was calculated as described in Materials and Methods (see Equation (1)). The later the negative effect of warping started to manifest, the lower the warping coefficient is and the better is the printability of a material. In Table 5 we can see the results of warping coefficient measurements. The best warping coefficient (the lowest) and appropriate printing temperature is highlighted for each PHB-PLA-plasticizer filament. As can be seen, the warping coefficient is usually lower with decreasing temperature. In the case of the non-plasticized reference, the lowest warping (1.1 ± 0.1) was achieved at 180 °C, filaments with PEG-2-EH plasticizer had the lowest warping (2.0 ± 0.2) at 180 °C. Filament with A2-EH plasticizers had comparable warping (1.8 ± 0.0)-(2.0 ± 0.1) at all temperatures, so we decided that 185 °C would be the best temperature for the printing. The exception was in the case of filament with C2-EH plasticizer, where the warping coefficient was higher with decreasing temperature. In contrast, the lowest warping for C2-EH filament (2.3 ± 0.1) was achieved at a higher temperature of 195 °C. The reason for this effect is not clarified now.

Table 5. Warping coefficient calculated from warping specimen measurements carried out at some applicable temperatures (which were selected from the temperature tower results).

PHB-PLA-Plasticizer	Printing Temperature (°C)	Warping Coefficient	Selected Temperature for Specimen Printing (°C)
REF (PHB-PLA)	205	2.1 ± 0.1	180
	200	1.4 ± 0.0	
	195	1.6 ± 0.0	
	190	1.6 ± 0.0	
	185	1.3 ± 0.0	
	180	1.1 ± 0.1	
C2-EH	195	2.3 ± 0.1	195
	190	2.5 ± 0.2	
	185	2.6 ± 0.2	
	180	3.6 ± 0.3	
A2-EH	190	1.8 ± 0.0	185
	185	1.8 ± 0.0	
	180	2.0 ± 0.1	
PEG-2-EH	190	2.7 ± 0.1	180
	185	3.0 ± 0.1	
	180	2.0 ± 0.2	

Although the printability of geometric elements in the case of C2-EH and A2-EH plasticizer is best when printing at lower temperatures (180–155 °C), the warping seems to be better at higher temperatures.

This quick method is established on unaided vision, is subjective, and the measurements should be carried out by one person to minimalize the error rate. This method is suitable for a basic overview and comparison of printing properties between samples. In the case of more complicated and accurate samples (e.g., scaffolds), more precise measurements would be employed.

3.2.3. Test Specimen Printing and Verification of Printing Conditions Using 3D Benchy

Final verification of adjusted printing conditions, especially printing temperatures, proceeded via the Benchy test. Benchies were printed at the same printing conditions as the test specimen samples (described in Tables 2 and 5) from all PHB-PLA-plasticizer filaments. Printed 3D Benchies were then visually evaluated [47], and the printing conditions were revised. Although there are many possible signs for the Benchy evaluation, we subjectively marked only some of them 1–5 (where 1 is the best) and this way visually examined the quality of printed Benchies. We were interested in signs which were related to the material properties rather than to the adjustment of our printer. In Tables 6 and 7, we can see some chosen Benchy signs (shape features [47] and other signs related to the material) and their subjective marking. In Table 8, the average mark of all PHB/-PLA-plasticizer Benchies calculated from this evaluation can be seen. The Benchy from the reference filament (without plasticizer) has the best printability. The Benchies printed from filaments with A2-EH and C2-EH plasticizers also had comparable printability. The printability of Benchy printed from filament with PEG-2-EH plasticizer seemed to be the worst. The examples of 3D Benchies printed from PHB-PLA-plasticizer filaments can be seen in Figure 6.

Table 6. Subjective visual evaluation of 3D Benchies: some of their chosen signs related to the material properties. Subjective marking (1–5, where 1 is the best).

PHB-PLA-Plasticizer	Hull	Stringing	Elephant Foot	Text Details	Cylindrical Shapes
REF (PHB/PLA)	3	2	1	1	3
C2-EH	4	3	3	2	4
A2-EH	4	2	3	3	3
PEG-2-EH	4	5	3	4	5

Table 7. Subjective visual evaluation of 3D Benchies: other chosen signs related to the material properties. Subjective marking (1–5, where 1 is the best).

PHB-PLA-Plasticizer	Square Shapes	Overhang Surfaces	Horizontal Holes	Layers Visibility	Warping
REF (PHB-PLA)	2	4	3	3	3
C2-EH	2	3	3	5	3
A2-EH	2	2	3	4	3
PEG-2-EH	2	5	4	4	4

Table 8. Average marking (1–5, where 1 is the best) of subjective evaluation of 3D Benchies.

PHB-PLA-Plasticizer	Average Mark
REF (PHB-PLA)	2.5
C2-EH	3.2
A2-EH	2.9
PEG-2-EH	4

The Benchies were printed at nozzle temperatures selected via the warping test. The evaluation of benchies confirmed these temperatures (see Table 5) as the most suitable for the printing of testing specimens.

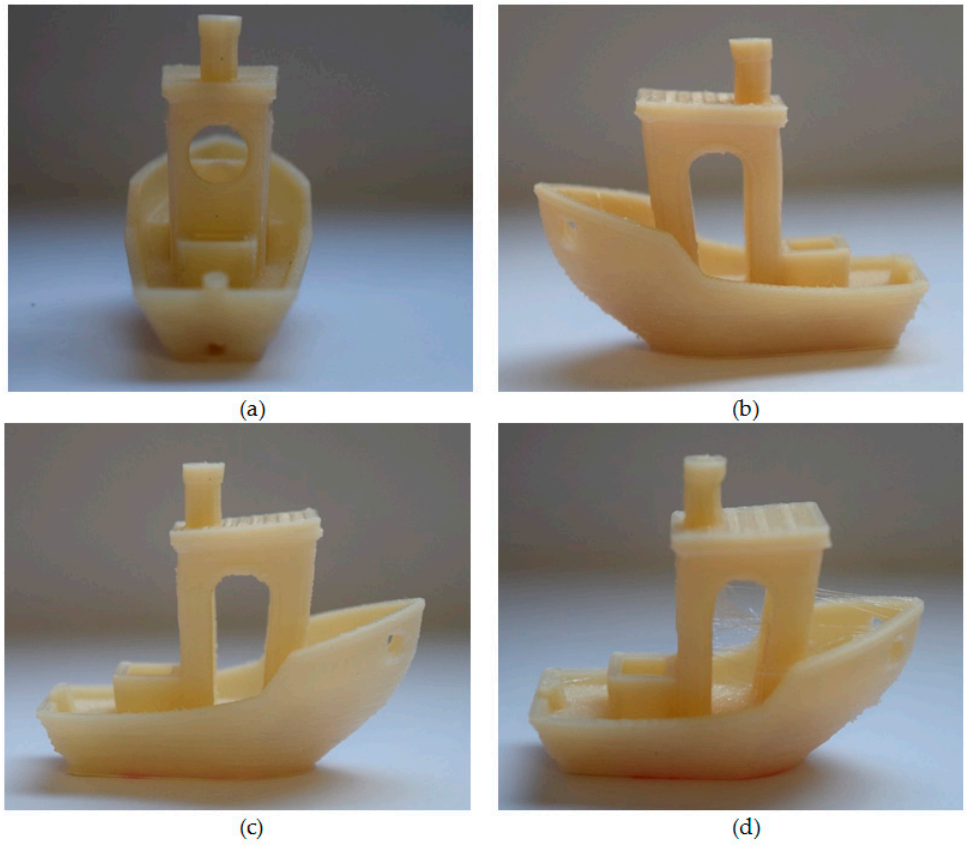


Figure 6. Three-dimensional Benchies printed under the conditions optimized via the temperature tower and warping tests, from all PHB-PLA-plasticizer filaments: (**a**) reference without plasticizer, (**b**) with C2-EH plasticizer, (**c**) with A2-EH, (**d**) with PEG-2-EH.

3.3. Modulated Differential Scanning Calorimetry—Thermal Characterization

The combination of modulated and conventional differential scanning calorimetry (MDSC and DSC, respectively) was used for observation of the thermal behavior of PHB-PLA-plasticizer samples and a non-plasticized sample (reference). The glass transition temperature of PHB could not be detected due to the high amount of rigid fraction in PHB. With the help of the melting and crystallization temperatures shifts and using the crystallinity change, the effect of the plasticizers on the thermal properties of PHB could be observed (Figures 7 and 8, respectively). In Figure 9 we can see the change in T_g in the case of PLA fraction in blends. Measured and evaluated data are presented in Table 9.

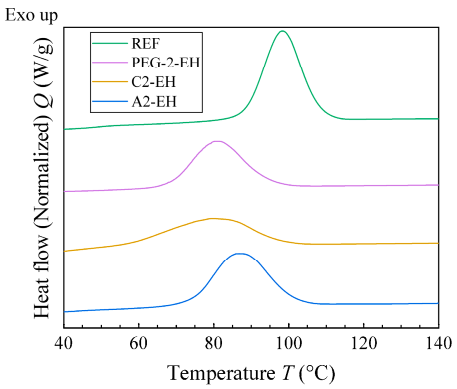


Figure 7. First cooling scan (differential scanning calorimetry (DSC)) of the non-plasticized reference sample (REF) and PHB-PLA-plasticizer blends (the plasticizers are PEG-2-EH, C2-EH, and A2-EH).

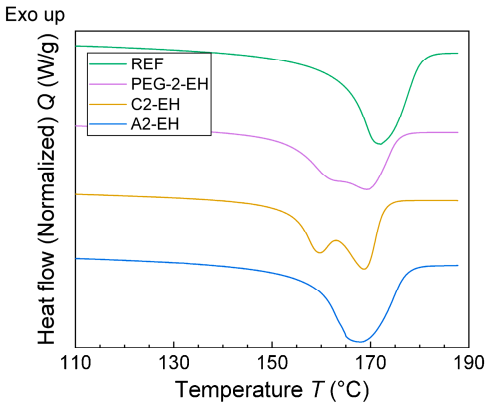


Figure 8. Second heating scan (DSC) of the non-plasticized reference sample (REF) and PHB-PLA-plasticizer blends (the plasticizers are PEG-2-EH, C2-EH, and A2-EH).

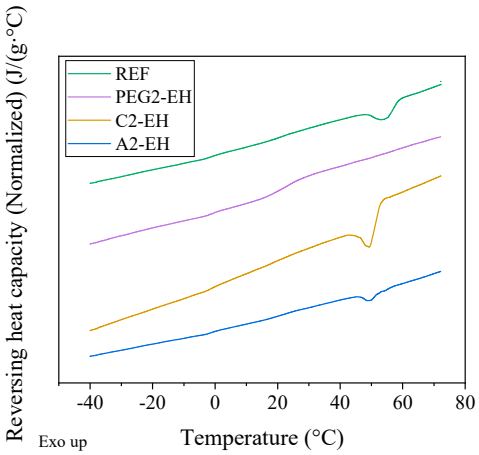


Figure 9. Reversing heat capacity (from modulated differential scanning calorimetry (MDSC) scan) of the non-plasticized reference sample (REF) and PHB-PLA-plasticizer blends (the plasticizers are PEG-2-EH, C2-EH, and A2-EH).

Table 9. MDSC and DSC parameters of PHB-PLA-plasticizer samples and non-plasticized reference.

Sample	MDSC Scan	First Cooling DSC Scan		Second Heating DSC Scan		
	$T_{g,\,PLA}$ (°C)	T_c (°C)	H_c (J/g)	T_m (°C)	H_m (J/g)	X_c (%)
REF	58.4	98	54.6	172	64.0	62.6
C2-EH	52.2	79	43.0	169	48.0	54.8
A2-EH	54.3	86	45.7	168	57.6	65.8
PEG-2-EH	21.7	81	32.0	169	47.9	54.7

Low molecular plasticizer introduced into the PHB-PLA blend should cause greater mobility of macromolecular chains. Consequently, the melting and the crystallization temperatures should be shifted to lower temperatures. The melting temperature, T_m, of PHB-PLA-plasticizer blends was not significantly shifted as compared to the non-plasticized reference. C2-EH, PEG-2-EH, and A2-EH plasticizers shifted especially for the crystallization temperature, where T_c was lower by 19 °C in the case of C2-EH (as compared to the reference), by 17 °C in the case of PEG-2-EH, and by 12 °C in the case of A2-EH. Low molecular plasticizers are retained in the amorphous phase in between crystallites in the case of a semicrystalline polymer. In the case of our blend of PHB semicrystalline and PLA amorphous polymer, we assumed that additives (plasticizers) are ejected into the amorphous polymer during crystallization. Thus, the plasticizing effect is more evident when we are monitoring the change of PLA T_g. PLA T_g in the case of esters of citric acid decreased only slightly by 6.2 °C for C2-EH

and only by 4.1 °C for A2-EH. Thus, in the case of C2-EH and A2-EH plasticizers, increased length of alkyl chains (compared to tributyl citrate and acetyl tributyl citrate from our previous work [30]) caused a worse plasticizing effect and led to T_g being higher than 52 °C. A2-EH plasticizer exhibits the highest PLA T_g and T_c temperatures of all plasticized samples and seems to have the worst plasticizing ability. Both blends, with A2-EH and C2-EH, are expected to be glassy at laboratory temperature. PEG-2-EH plasticizer with its long but not-branched structure, which seems to have a great plasticizing effect, caused the decrease of PLA T_g by almost 37 °C and the decrease of T_c by 17 °C, as compared to the reference. On the contrary, the melting temperature, T_m, of blends with PEG-2-EH plasticizer decreased by only 3 °C.

The crystallinity of PHB (X_c in%) in the reference and plasticized blends was calculated from the melting enthalpy (H_m (J/g)) measured during the second heating DSC scan (Table 9). The non-plasticized reference had the crystallinity of PHB 63%. Samples plasticized using PEG-2-EH and C2-EH had lower crystallinity of PHB (about 55%). The plasticizer A2-EH had even higher crystallinity (66%) than the reference. This could explain the worst plasticizing effect of A2-EH.

3.4. Oscillation Rheometry—Thermal Characterization

The oscillation rheometry (RPA measurements) was carried out 7 and 40 days after the blend preparation. Complex viscosity (Pa·s) of all PHB-PLA-plasticizer samples measured after 7 days from the preparation of pellets can be seen in Figure 10. For better comparison, the relative complex viscosity for all samples was evaluated as well. All plasticized samples had apparently lower complex viscosity during the test compared to the reference. The blends with PEG-2-EH plasticizer had the lowest complex viscosity at the beginning of the measurement and the largest decrease of complex viscosity, similarly to the blend with C2-EH plasticizer. The blend with PEG-2-EH plasticizer showed the most significant degradation of the polymeric matrix among all plasticized blends. It correlates well with subjective printability results, where the plasticizers C2-EH and PEG-2-EH had the worst printability.

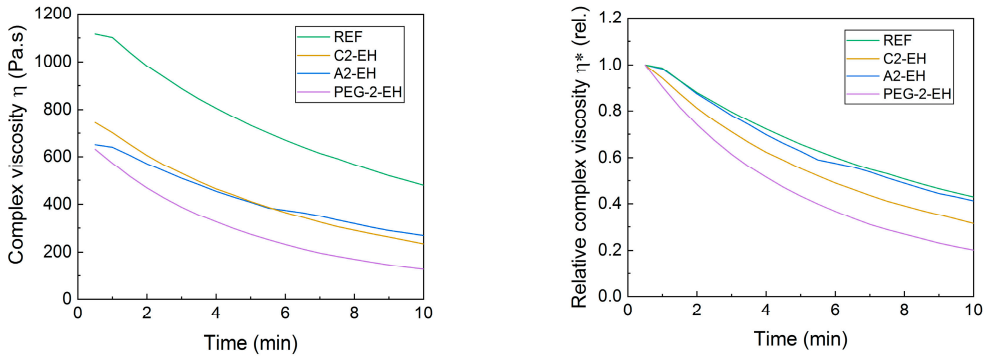


Figure 10. Complex viscosity (**a**) and relative complex viscosity (**b**) evaluated from oscillation rheometry (RPA) measurements of the non-plasticized reference sample (REF) and PHB-PLA-plasticizer blends (where the plasticizers are PEG-2-EH, C2-EH, and A2-EH). Measured 7 days after the preparation of blends.

The complex viscosity (Pa·s) of all PHB-PLA-plasticizer samples measured after 40 days from the preparation of pellets can be seen in Figure 11. While the blends with A2-EH plasticizer seem to have a little higher complex viscosity at the beginning of the measurement (after 40 days of aging), in contrast, the blends with PEG-2-EH plasticizer had a little lower complex viscosity at the beginning of the measurement, compared to the measurements carried out after 7 days. Complex viscosities of the reference and the sample with C2-EH measured after 40 days correspond to the measurements after 7 days from the preparation of pellets. At the end of the measurement after 40 days, the blends with PEG-2-EH plasticizer had lower complex viscosity. The relative complex viscosity can be also seen

in Figure 11. The shapes of relative complex viscosity curves of blends with A2-EH plasticizer seem to be shifted from the reference down towards C2-EH, compared to the measurements after 7 days. The blends with PEG-2-EH plasticizer had the lowest relative complex viscosity.

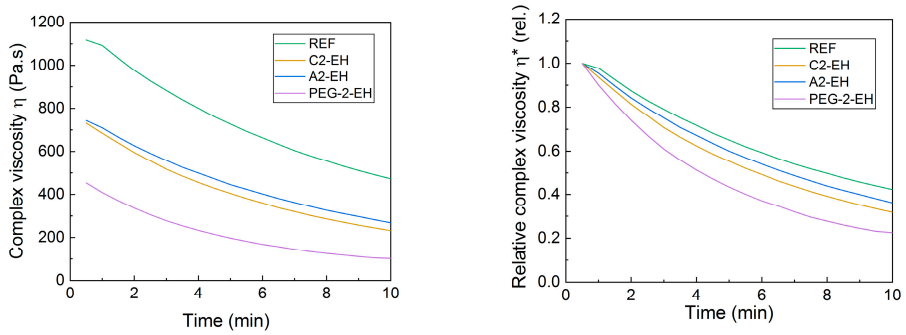


Figure 11. Complex viscosity (**a**) and relative complex viscosity (**b**) evaluated from RPA measurements of the non-plasticized reference sample (REF) and PHB-PLA-plasticizer blends (where the plasticizers are PEG-2-EH, C2-EH, and A2-EH). Measured 40 days after the preparation of blends.

In order to detect what happened to the blend with PEG-2-EH plasticizer and to confirm its degradation, GPC (gel permeation chromatography) measurements were additionally performed.

The differential distribution of molecular weights for all PHB-PLA-plasticizer samples and the reference can be seen in Figure 12. The curves correspond to the PHB-PLA distribution of molecular weights, and as can be seen, the reference and other plasticized samples except for the sample with PEG-2-EH plasticizer had a similar distribution of molecular weights. Plasticized samples (except for PEG-2-EH) even caused the shift to larger molecular weights, compared to the reference. The distribution of molecular weights of the PHB-PLA-PEG-2-EH sample is significantly shifted to lower molecular weights, so PHB-PLA from this sample is evidently degraded during the processing, which confirms the RPA results. Figure 12 displays only the principal peak of polymer elution. Plasticizers are not displayed in this graph, but they created an individual peak (under 1000 g/mol). Regarding high measurement error in this area (on the periphery of the range of our GPC column), these peaks are not displayed. The influence of contained plasticizer on the properties of solvent (or GPC analysis result) is theoretically possible, but we do not think this influence is radical in practice. Sample concentration for GPC analysis was 0.5% and during elution was further diluted below 0.005%. The measurements were carried out identically and with a similar error, so we think it justifies this kind of comparison.

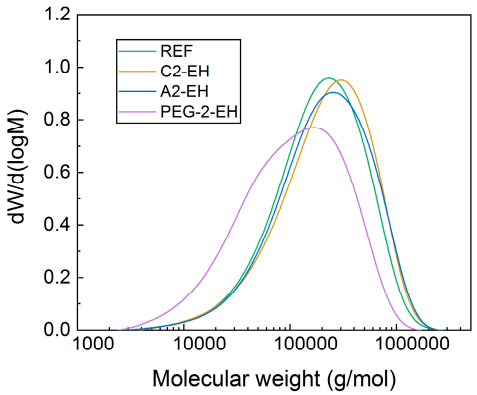


Figure 12. Gel permeation chromatography (GPC) measurements of the non-plasticized reference sample (REF) and PHB-PLA-plasticizer blends (where the plasticizers are PEG-2-EH, C2-EH, and A2-EH).

3.5. HDT—Heat Deflection Temperature—Thermal Characterization

In Figure 13, you can see the HDT for all the PHB-PLA-plasticizer samples and for the reference. As you can see, the plasticizing effect manifests itself by decreasing the HDT under both loads, compared to the reference. The HDTs of the plasticized samples measured under a higher load of 1.8 MPa were decreased only slightly, compared to the reference, specifically, in decreasing order from the reference (HDT = 57.7 °C): A2-EH, PEG-2-EH, C2-EH (HDT = 48.1 °C). The differences in the HDT are slightly more apparent for the measurements under a lower load of 0.455 MPa. The HDT decreased: from reference (96.8 °C), through the blends with plasticizers C2-EH (70.8 °C), A2-EH to PEG-2-EH (67.9 °C). The differences between the measured HDTs of the plasticized samples are relatively small.

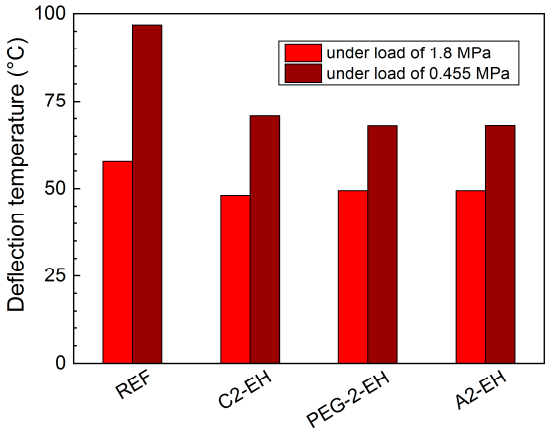


Figure 13. Heat distortion temperature (HDT) measurements of the non-plasticized reference sample (REF) and PHB-PLA-plasticizer blends (where the plasticizers are PEG-2-EH, C2-EH, and A2-EH).

3.6. Migration Tests—Plasticizers Migration from PHB-PLA Blends

The tests of plasticizer migration from samples were performed at 110 °C in a drying oven (as was described in Materials and Methods). We observed plasticizer weight loss (%) after, up to 16.7 days.

The weight loss (%) of C2-EH, A2-EH, and PEG-2-EH plasticizers from samples after 1, 3, 7, 10 h, and 1, 2, 3, 6, 8, 10, 13, 15, and 16.7 days of exposition can be seen in Figure 14.

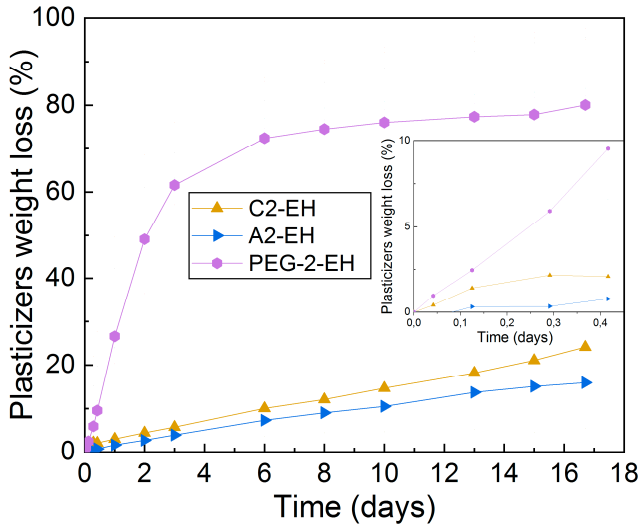


Figure 14. Weight loss of plasticizers (%) from PHB-PLA-plasticizer blends after up to 16.7 days of exposition to 110 °C in the drying oven.

The plasticizer PEG-2-EH started to migrate very fast after 10 h of exposition. The PEG-2-EH plasticizer showed up to 80.0% weight loss at the end of the test. In contrast, the plasticizers which showed the best resistivity to diffusion were C2-EH and A2-EH. Their weight loss proceeded gradually and showed only 24% and 16% weight loss at the end of the test, respectively.

Our previous study [30] showed the rapid migration of tributyl citrate and acetyl tributyl citrate plasticizers. These plasticizers had smaller molecular weight and shorter lengths of alkyl chains linked to citrate molecules. On the other hand, C2-EH and A2-EH plasticizers have longer side alkyl chains, are more branched, and have a greater molecular weight. Thus, C2-EH and A2-EH plasticizers demonstrated the best migration stability and did not diffuse from the sample so much.

PEG-2-EH plasticizer has a greater molecular weight but has a linear non-branched structure and migrates also very fast. The GPC (gel permeation chromatography) confirmed its degradation effect on PHB-PLA. This influence of structure on diffusion is in good agreement with [29–34].

The weight loss (%) measurements were also carried out on the reference sample. An insignificant decrease in the reference weight loss was measured, which we attribute to water evaporation (0.3% after 1 h, 0.4% after 2–16.7 days). These continuous values were subtracted from other samples with plasticizers.

3.7. Tensile Tests—Mechanical Characterization

The tensile tests were performed on PHB-PLA-plasticizer filaments after 7 and 40 days from the extrusion and after three days of exposition to 110 °C in the drying oven and on 3D printed dogbones after 7 days from printing.

The elongation at break is for us the most interesting quality considering plasticizer efficiency. In Figure 15, we can see the measured elongation at break (%) of all PHB-PLA-plasticizer samples compared with the non-plasticized reference. The plasticizers' influence can be clearly seen, and all three plasticizers have a positive softening effect in PHB-PLA polymers.

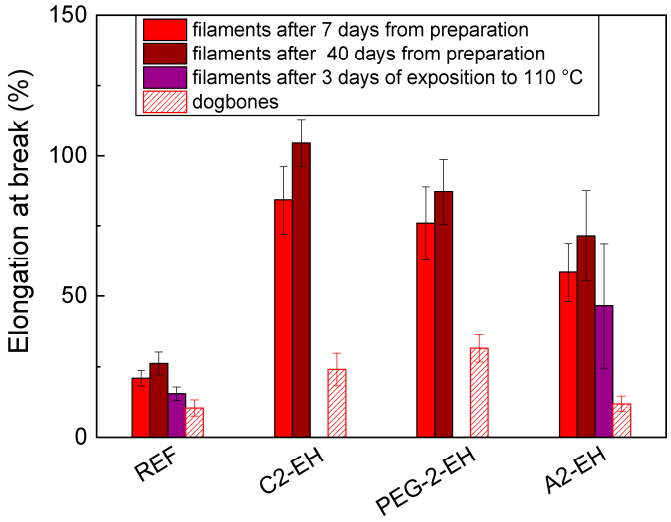


Figure 15. Elongation at break (%) of neat PHB-PLA (reference), PHB-PLA-plasticizers filaments, and 3D printed dogbones.

The plasticizers A2-EH, C2-EH, and PEG-2-EH improved the elongation at break (measured after seven days from the filament preparation) rather slightly: from 21% for non-plasticized PHB-PLA filament samples to 58% (A2-EH), 84% (C2-EH), and 76% (PEG-2-EH) for plasticized filaments. The plasticizing effect of these plasticizers is not so significant; on the other hand, they showed better resistivity to diffusion (except PEG-2-EH, as was proved in the migration tests Section 3.6). Their elongation at break measured after 40 days is even slightly higher than that after 7 days, as well as the elongation at break of the non-plasticized reference measured after 40 days. We assumed that

this is within the frame of measurement error. Nevertheless, the blends with A2-EH and C2-EH plasticizers are relatively resistant to aging. The plasticizer structure apparently influenced the results. Their weaker softening effect was influenced by their more branched structure and increased length of alkyl chains linked to the citrate molecule. On the other hand, they have stronger resistivity to aging and higher temperatures. The MDSC measurements correspond with tensile test results, where A2-EH and C2-EH plasticizers showed smaller T_g reduction and thus worse plasticizing effect. The PEG-2-EH plasticized sample seems to be an exception; according to the migration tests, this plasticizer is not resistant to diffusion at higher temperatures. However, it seems to be resistant to aging. The elongation at break of the blends with A2-EH plasticizer decreased only slightly after three days of exposition to 110 °C. On the contrary, the filaments with C2-EH and PEG-2-EH plasticizers after three days of exposition to 110 °C were so fragile that the elongation at break could not have been measured. This is the consequence of PEG-2-EH sensitivity to higher temperatures, confirmed by the RPA measurements. The elongation at break of dogbones with A2-EH, C2-EH, and PEG-2-EH plasticizers confirmed the weaker plasticizing effect.

Tensile test measurements of filaments with A-4 and C-4 plasticizers have already been published in our previous work [30], and these results can serve as a comparison with other plasticizers, to see how plasticizer structure influences elongation at break.

In Tables 10 and 11 we can see Young's modulus (GPa) and the tensile strength (MPa) of the PHB-PLA-plasticizer samples and non-plasticized reference. The weaker softening effect of plasticizers can be seen also from these results. The tensile strength values of the plasticized samples were comparable for all the plasticizers except for PEG-2-EH, which showed lower tensile strength measured 7 days after preparation. The samples with A2-EH plasticizer had comparable values of tensile strength not only 7 and 40 days after preparation, but also after 3 days at 110 °C.

Table 10. Young's modulus (GPa) of PHB-PLA-plasticizer samples and of PHB-PLA reference.

Sample	Young's Modulus (GPa)			
	Filaments—7 Days after Preparation	Filaments—40 Days after Preparation	Filaments—after 3 Days at 110 °C	Dogbones—7 Days after Printing
REF	0.57 ± 0.07	0.45 ± 0.12	0.59 ± 0.06	0.64 ± 0.21
C2-EH	0.34 ± 0.01	0.34 ± 0.03	Fragile-not measured	0.71 ± 0.11
A2-EH	0.33 ± 0.02	0.30 ± 0.01	0.31 ± 0.05	0.72 ± 0.08
PEG-2-EH	0.15 ± 0.01	0.18 ± 0.01	Fragile-not measured	0.56 ± 0.06

Table 11. Tensile strength (MPa) of PHB-PLA-plasticizer samples and of PHB-PLA reference.

Sample	Tensile Strength (MPa)			
	Filaments—7 Days after Preparation	Filaments—40 Days after Preparation	Filaments—after 3 Days at 110 °C	Dogbones—7 Days after Printing
REF	43.26 ± 1.00	42.86 ± 1.92	44.84 ± 0.49	40.90 ± 1.46
C2-EH	19.20 ± 0.76	18.92 ± 0.71	Fragile-not measured	26.11 ± 1.25
A2-EH	21.09 ± 0.70	18.72 ± 0.75	19.68 ± 1.38	26.74 ± 1.77
PEG-2-EH	15.11 ± 0.38	18.01 ± 0.58	Fragile-not measured	17.70 ± 0.73

Armentato et al. [38] investigated PLA-PHB-lactic acid oligomers (OLA) blends and achieved significant improvement of ductile properties by the introduction of OLA. OLA caused a meaningful decrease of the tensile strength, and the elongation at break increased with the increasing of OLA concentration. They achieved an improvement of elongation at break from 140% for non-plasticized 85PLA-15PHB blends to 370% for a 55PLA-15PHB-30OLA blend.

Arrieta et al. [26] observed decreased tensile strength and modulus and increased elongation at break with A4 and PEG plasticizers. Blends plasticized with A4 had higher thermal stability and

flexibility than blends plasticized with PEG. They achieved an improvement of elongation at break from 2.0% for the PLA-PHB blend to 182% for the PLA-PHB-A4 blends. Ductile properties of PLA-PHB blends were not clearly improved by the addition of PEG plasticizer.

Abdelwahab et al. [3] investigated the PLA-PHB-Lapol system. The addition of Lapol into the PLA-PHB system caused a decrease of Young's modulus and the tensile strength and a slight increase of elongation at break from 7% to 15%.

3.8. Charpy and Tensile-Impact Strength Tests—Mechanical Characterization

Twenty sample bars (80 × 10 × 4) mm were 3D printed from all PHB-PLA-plasticizer filaments (3D model was generated simply by only perimeters), half of them were notched (V-notch Type A) and half of them were left un-notched. The measurements were carried out 7 days after 3D printing. The Charpy un-notched and notched impact strengths, a_{cU}, and a_{cN} (kJ/m^2), were calculated from measured and corrected impact energies, E_c (J). Because un-notched breakage did not occur in the case of too flexible PHB-PLA-PEG-2-EH specimens (even with a 10.8 J hammer), we decided to supplement the tests also using the determination of tensile-impact strength. V-notched breakage occurred in the case of all PHB-PLA-plasticizer specimens with a 2.7 J hammer, except for the specimen with PEG-2-EH plasticizer, where the 10.8 J hammer was necessary to break the specimen.

The tensile-impact strength measurements were carried out 7 days after 3D printing. The notched tensile-impact strengths, a_{tN} (kJ/m^2), of all PHB-PLA-plasticizer specimens were calculated from measured and corrected tensile-impact energies, E_c (J).

As can be seen in Figure 16, PHB-PLA samples with C2-EH and A2-EH plasticizers almost did not influence evaluated Charpy and tensile-impact strength, A_n (kJ/m^2), as compared to the non-plasticized reference. In the case of a sample with A2-EH plasticizer, un-notched Charpy and notched tensile-impact strength are even slightly lower. Their evaluated impact strength is within the error frame, especially the tensile-impact measurements had quite a large error frame. The evaluated impact strength was not influenced only by the material properties, but also by the structure of the 3D printed specimens. The breakage in the case of tensile-impact tests proceeded along 3D printed perimeters. The enhancement of impact strength measured from V-notched Charpy and notched tensile-impact is apparent for the samples with PEG-2-EH plasticizers. Notched tensile-impact strength of PHB-PLA-PEG-2-EH samples only slightly increased to 11 kJ/m^2, as compared to 5 kJ/m^2 of the non-plasticized reference.

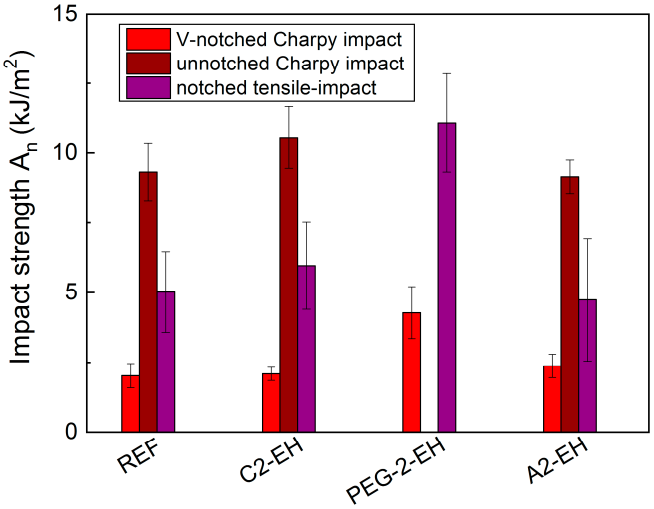


Figure 16. Charpy and tensile-impact measurement-evaluated impact strength of neat PHB-PLA (reference) and PHB-PLA-plasticizer filaments.

3.9. Optical Microscopy—Structural Characterization

The brittle failures of all PHB-PLA-plasticizer samples were optically analyzed using Olympus SZ51 an optical microscope (see Materials and Methods). The samples were 3D printed under the conditions optimized via the temperature tower and warping tests, equal to conditions which were applied also to the printing of testing specimens for mechanical and thermal characterizations. This elemental verification of 3D printed structure via optical microscopy is a cheap and easy way to check the printing settings and conditions. In Figure 17, we can see that the structures of all PHB-PLA-plasticizer samples are quite compact and free of large holes and missing filaments, which means this is quite a good setting of printing conditions. The biggest holes and the potential for upgrading the printing conditions (especially printing temperature) can be seen on the reference and A2-EH samples. Generally, the printing conditions seem to be adjusted well.

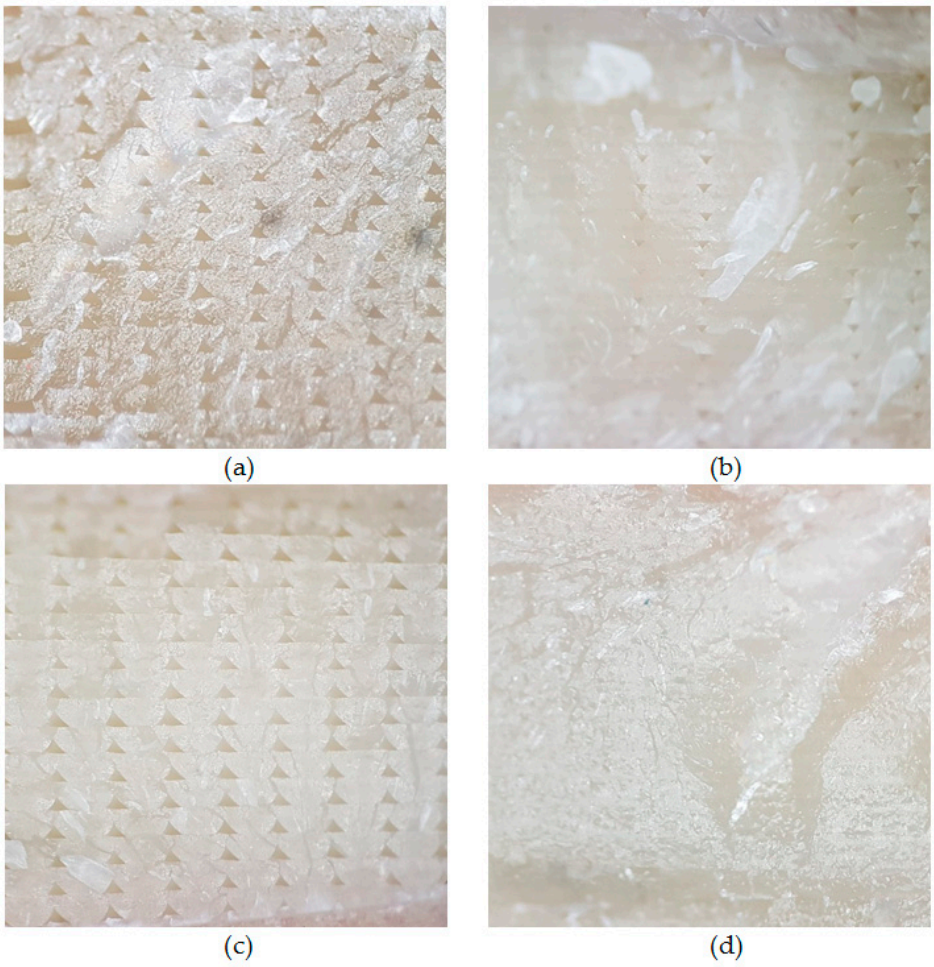


Figure 17. The surface of 3D printed samples using optical microscopy: (**a**) reference without plasticizer, (**b**) with C2-EH plasticizer, (**c**) with A2-EH, (**d**) with PEG-2-EH.

4. Conclusions

Poly(3-hydroxybutyrate)-poly(L,D-lactic acid)-plasticizer blends in the weight ratio (wt.%) of 60-25-15 were successfully prepared using a corotating twin-screw extruder and then using a single screw extruder to achieve filaments with defined diameters for further 3D printing via the fused deposition modeling method. Three low molecular plasticizers were used. Two of them were based on esters of citric acid (acetyl tris(2-ethylhexyl) citrate (A2-EH) and tris(2-ethylhexyl)citrate (C2-EH)), and the last one is poly(ethylene glycol) bis(2-ethylhexanoate) (PEG-2-EH). All plasticizers were well miscible with the PHB-PLA matrix (with PHB majority). The printability of 3D samples printed

from these blends was judged according to newly designed tests—the "Temperature tower" and the "Warping specimen". The influence of particular plasticizers on the printability of geometrical shapes and on warping was investigated. Due to these tests, we revealed the best nozzle printing temperature for each PHB-PLA-plasticizer blend, which varied in the range of 180-195 °C. After this optimization, we were able to print the testing samples with the best printing quality and with minimal warping for further mechanical, thermal, and optical measurements. The printing quality of the test specimens was then checked using an optical microscope and the 3DBenchy test. The 3DBenchies from all PHB-PLA-plasticizer filaments were successfully printed and visually marked. The used plasticizers seemed to have a quite similar influence on the "printability", except for PEG-2-EH, with which the worst Benchy was printed.

The softening effect of plasticizers was not so significant. They improved the elongation at break rather slightly: from 21% for non-plasticized PHB-PLA filament samples to 58% in the case of A2-EH, 84% in the case of C2-EH, and 76% in the case of PEG-2-EH. In spite of the fact that the values of measured elongation at break of 3D printed dogbones were lower than those of the samples measured in the filament form, dogbone tensile tests measurements also confirmed a less meaningful but sufficient plasticizing effect.

The minor softening effect of plasticizers was confirmed using MDSC. Still, the introduction of low molecular plasticizer into the PHB-PLA blend caused greater mobility of macromolecular chains. Consequently, the melting temperatures and the crystallization were slightly shifted to lower values. The plasticizing effect is more evident when observing the change of PLA T_g because low molecular additives are retained in the amorphous phase in between crystallites in the case of a semicrystalline polymer. C2-EH and A2-EH plasticizers showed a slight plasticizing effect, where the PLA T_g was decreased only by 6 °C (C2-EH) and by 4 °C (A2-EH). Surprisingly, the plasticizer PEG-2-EH caused a decrease of PLA T_g by 37 °C. Heat distortion temperature and the viscosity measurements using oscillation rheometry were executed as well. Gel permeation chromatography measurements were additionally performed to detect what happened to the PHB-PLA blend with PEG-2-EH plasticizer and confirmed the degradation of the polymer matrix due to the presence of PEG-2-EH.

Migration tests were performed in order to investigate the migration of all three plasticizers from the PHB-PLA matrix. The plasticizer PEG-2-EH showed quite large migration after 16.7 days of exposition to 110 °C in the drying oven. The influence of plasticizer structure on the migration process was well noticeable; esters of citric acid with larger molecular weight (C2-EH and A2-EH) showed the best stability and tendency not to migrate from the sample.

Charpy and tensile-impact tests were also carried out. The PHB-PLA samples with C2-EH and A2-EH plasticizers had negligible influence on evaluated Charpy and tensile-impact strength, A_n (kJ/m^2), as compared to the non-plasticized reference. The improvement of impact strength measured from V-notched Charpy and notched tensile-impact is slightly apparent for the samples with PEG-2-EH plasticizer. The notched tensile-impact strength of the PHB-PLA-PEG-2-EH sample increased to 11 kJ/m^2, as compared to 5 kJ/m^2 of the non-plasticized reference. The evaluated impact strength was not influenced only by the material properties, but also by the structure of the 3D printed specimens. The breakage in the case of tensile-impact tests proceeded along 3D printed perimeters.

The goal was to create a new type of PHB-PLA-plasticizer blends, to sufficiently improve poor mechanical properties of neat PHB-PLA blends (with a majority of PHB) via the addition of appropriate plasticizer and mainly to investigate the printability of these blends. All three examined plasticizers are applicable and also suitable for 3D printing technology and will be later investigated especially in biomedicine as scaffolds.

Author Contributions: Conceptualization, S.K., R.P. (Radek Přikryl), V.M., P.M. and M.H.; Data curation, S.K., R.P. (Roderik Plavec), J.F. and J.S.; Formal analysis, S.K., R.P. (Radek Přikryl), V.M., P.M., M.H., S.F., R.P. (Roderik Plavec), J.F., J.S. and A.P.; Investigation, S.K., V.M., P.M., M.H., S.F., R.P. (Roderik Plavec), J.F., J.S. and A.P.; Methodology, S.K., R.P. (Radek Přikryl) and M.H.; Project administration, R.P. (Radek Přikryl); Resources, R.P. (Radek Přikryl), P.M., S.F., R.P. (Roderik Plavec), J.F., J.S. and S.P.; Writing—original draft, S.K. and V.M.;

Writing—review & editing, S.K., R.P. (Radek Přikryl), V.M., P.M. and A.P. All authors have read and agreed to the published version of the manuscript.

Funding: This research was funded by the Ministry of Industry and Trade Czech Republic Project No. FV20480, by the Ministry of Education, Youth and Sports of the Czech Republic Project No. LO1211 and No. FCH-S-19-6100 of the Specific University Research Grant, and by the Slovak Research and Development Agency project APVV-17-304.

Acknowledgments: We would like to thank Ivana Stehnová-Bajzová for the performing of some older experiments and also all subjects who volunteered in the study.

Conflicts of Interest: The authors declare no conflict of interest.

References

1. Byun, Y.; Kim, Y.T. Bioplastics for Food Packaging: Chemistry and Physics. In *Innovations in Food Packaging*, 2nd ed.; Han, Y.H., Ed.; Academic Press: Cambridge, MA, USA, 2014; pp. 353–368. ISBN 9780123946010. [CrossRef]
2. Koller, M. Advances in Polyhydroxyalkanoate (PHA) Production. *Bioengineering* **2017**, *4*, 88. [CrossRef] [PubMed]
3. Abdelwahab, M.H.; Flynn, A.; Chiou, B.-S.; Imam, S.; Orts, W.; Chiellini, E. Thermal, mechanical and morphological characterization of plasticized PLA-PHB blends. *Polym. Degrad. Stab.* **2012**, *97*, 1822–1828. [CrossRef]
4. D'Anna, A.; Arrigo, R.; Frache, A. PLA/PHB Blends: Biocompatibilizer Effects. *Polymers* **2019**, *11*, 1416. [CrossRef]
5. Frone, A.N.; Batalu, D.; Chiulan, I.; Oprea, M.; Gabor, A.R.; Nicolae, C.-A.; Raditoiu, V.; Trusca, R.; Panaitescu, D.M. Morpho-Structural, Thermal and Mechanical Properties of PLA/PHA/Cellulose Biodegradable Nanocomposites Obtained by Compression Molding, Extrusion, and 3D Printing. *Nanomaterials* **2020**, *10*, 51. [CrossRef]
6. García-Campo, M.J.; Boronat, T.; Quiles-Carrillo, L.; Balart, R.; Montanes, N. Manufacturing and Characterization of Toughened Poly(lactic acid) (PLA) Formulations by Ternary Blends with Biopolyesters. *Polymers* **2018**, *10*, 3. [CrossRef]
7. European Bioplastics. Available online: http://docs.european-bioplastics.org/publications/EUBP_Facts_and_figures.pdf (accessed on 20 March 2020).
8. Urtuvia, V.; Villegas, P.; González, M.; Seeger, M. Bacterial production of the biodegradable plastics polyhydroxyalkanoates. *Int. J. Biol. Macromol.* **2014**, *70*, 208–213. [CrossRef] [PubMed]
9. Khanna, S.; Srivastava, A.K. Recent Advances in Microbial Polyhydroxyalkanoates. *Process. Biochem.* **2005**, *40*, 607–619. [CrossRef]
10. Marova, I.; Obruca, S.; Prikryl, R. Process for Preparing Polyhydroxyalkanoates (PHA) on Oil Substrate. International Patent Application No. PCT/CZ2013/000100, 23 August 2013.
11. Nafigate Corporation. Available online: https://www.nafigate.com/biotechnology (accessed on 22 October 2020).
12. Chiulan, I.; Frone, A.N.; Brandabur, C.; Panaitescu, D.M. Recent Advances in 3D Printing of Aliphatic Polyesters. *Bioengineering* **2018**, *5*, 2. [CrossRef]
13. Zhang, M.; Thomas, N.L. Blending Polylactic Acid with Polyhydroxybutyrate: The Effect on Thermal, Mechanical, and Biodegradation Properties. *Adv. Polym. Tech.* **2011**, *30*, 67–79. [CrossRef]
14. Xiao, L.; Wang, B.; Yang, G.; Gauthier, M. Poly(Lactic Acid)-Based Biomaterials: Synthesis, Modification and Applications. In *Biomedical Science, Engineering and Technology*; InTech: London, UK, 2012; pp. 247–282. ISBN 978-953-307-471-9. [CrossRef]
15. Nguyen, V.K.; Nguyen, T.T.; Pham Thi, T.H.; Pham, T.T. Effects of Pulp Fiber and Epoxidized Tung Oil Content on the Properties of Biocomposites Based on Polylactic Acid. *J. Compos. Sci.* **2020**, *4*, 56. [CrossRef]
16. Correa-Pacheco, Z.N.; Black-Solís, J.D.; Ortega-Gudiño, P.; Sabino-Gutiérrez, M.A.; Benítez-Jiménez, J.J.; Barajas-Cervantes, A.; Bautista-Baños, S.; Hurtado-Colmenares, L.B. Preparation and Characterization of Bio-Based PLA/PBAT and Cinnamon Essential Oil Polymer Fibers and Life-Cycle Assessment from Hydrolytic Degradation. *Polymers* **2020**, *12*, 38. [CrossRef] [PubMed]
17. Garlotta, D. A Literature Review of Poly(Lactic Acid). *J. Polym. Environ.* **2001**, *9*, 63–84. [CrossRef]
18. Ma, C.; Jiang, L.; Wang, Y.; Gang, F.; Xu, N.; Li, T.; Liu, Z.; Chi, Y.; Wang, X.; Zhao, L.; et al. 3D Printing of Conductive Tissue Engineering Scaffolds Containing Polypyrrole Nanoparticles with Different Morphologies and Concentrations. *Materials* **2019**, *12*, 2491. [CrossRef] [PubMed]

19. Wasti, S.; Adhikari, S. Use of Biomaterials for 3D Printing by Fused Deposition Modeling Technique: A Review. *Front. Chem.* **2020**, *8*, 315. [CrossRef] [PubMed]
20. Puppi, D.; Pecorini, G.; Chiellini, F. Biomedical Processing of Polyhydroxyalkanoates. *Bioengineering* **2019**, *6*, 108. [CrossRef] [PubMed]
21. ColorFabb. Available online: https://colorfabb.com/ (accessed on 30 March 2020).
22. Kong, D. Development of Polylactic Acid-Polyhydroxybutyrate Blends for Packaging Applications. Master's Thesis, RMIT University, Melbourne, Australia, 2017.
23. Sanatgar, R.H.; Campagne, C.; Nierstrasz, V. Investigation of the adhesion properties of direct 3D printing of polymers and nanocomposites on textiles: Effect of FDM printing process parameters. *Appl. Surf. Sci.* **2017**, *403*, 551–563. [CrossRef]
24. Salentijn, G.I.J.; Oomen, P.E.; Grajewski, M.; Verpoorte, E. Fused Deposition Modeling 3D Printing for (Bio)analytical Device Fabrication: Procedures, Materials, and Applications. *Anal. Chem.* **2017**, *89*, 7053–7061. [CrossRef]
25. Wasantha, L.M.; Gunaratne, K.; Shanks, R.A. Miscibility, Melting, and Crystallization Behavior of Poly(hydroxybutyrate) and Poly(D,L-lactic acid) Blends. *Polym. Eng. Sci.* **2008**, *48*, 1683–1692. [CrossRef]
26. Arrieta, M.P.; Samper, M.D.; López, J.; Jiménez, A. Combined Effect of Poly(hydroxybutyrate) and Plasticizers on Polylactic acid Properties for Film Intended for Food Packaging. *J. Polym. Environ.* **2014**, *22*, 460–470. [CrossRef]
27. Da Silva, M.A.; Vieira, M.G.A.; Maçumoto, A.C.G.; Beppu, M.M. Polyvinylchloride (PVC) and natural rubber films plasticized with a natural polymeric plasticizer obtained through polyesterification of rice fatty acid. *Polym. Test.* **2011**, *30*, 478–484. [CrossRef]
28. Wypych, G. *Handbook of Plasticizers*, 3rd ed.; ChemTec Publishing: Toronto, ON, Canada, 2017; ISBN 978-1-5231-0906-7.
29. Białecka-Florjańczyk, E.; Florjańczyk, Z. Solubility of Plasticizers, Polymers and Environmental Pollution. In *Thermodynamics, Solubility and Environmental Issues*, 1st ed.; Letcher, T.M., Ed.; Elsevier: Amsterdam, The Netherlands, 2007; pp. 397–408. ISBN 978-0-444-52707-3.
30. Menčík, P.; Přikryl, R.; Stehnová, I.; Melčová, V.; Kontárová, S.; Figalla, S.; Alexy, P.; Bočkaj, J. Effect of Selected Commercial Plasticizers on Mechanical, Thermal, and Morphological Properties of Poly(3-hydroxybutyrate)/Poly(lactic acid)/Plasticizer Biodegradable Blends for Three-Dimensional (3D) Print. *Materials* **2018**, *11*, 1893. [CrossRef]
31. Cadogan, D.F.; Howick, C.J. Plasticizers. In *Ullmann's Polymers and Plastic: Products and Processes*; Wiley VCH: Weinheim, Germany, 2016; Volume 1, pp. 581–600. ISBN 978-3-527-33823-8.
32. Marcilla, A.; García, S.; García-Quesada, J.C. Study of the migration of PVC plasticizers. *J. Anal. Appl. Pyrolysis* **2004**, *71*, 457–463. [CrossRef]
33. Marcilla, A.; García, S.; García-Quesada, J.C. Migrability of PVC plasticizers. *Polym. Test.* **2008**, *27*, 221–233. [CrossRef]
34. Ambrogi, V.; Brostow, W.; Carfagna, C.; Pannico, M.; Persico, P. Plasticizer migration from cross-linked flexible PVC: Effects on tribology and hardness. *Polym. Eng. Sci.* **2001**, *52*, 211–217. [CrossRef]
35. Sun, X.S. Plastics Derived from Starch and Poly(Lactic Acids). In *Bio-Based Polymers and Composites*, 1st ed.; Wool, R.P., Ed.; Elsevier: Burlington, MA, USA, 2005; pp. 369–410. ISBN 978-0-12-763952-9.
36. Godwin, A.D. Plasticizers. In *Applied Plastics Engineering Handbook*, 1st ed.; Kutz, M., Ed.; Elsevier: Waltham, MA, USA, 2011; pp. 487–501. ISBN 978-1-4377-3514-7.
37. Vieira, M.G.A.; Da Silva, M.A.; Dos Santos, L.O.; Beppu, M.M. Natural-based plasticizers and biopolymer films: A review. *Eur. Polym. J.* **2011**, *47*, 254–263. [CrossRef]
38. Armentato, I.; Fortunati, E.; Burgos, N.; Dominici, F.; Luzi, F.; Fiori, S.; Jimenéz, A.; Yoon, K.; Ahn, J.; Kang, S.; et al. Processing and characterization of plasticized PLA/PHB blends for biodegradable multiphase systems. *Express Polym. Lett.* **2015**, *9*, 583–596. [CrossRef]
39. Rogovina, S.; Zhorina, L.; Gatin, A.; Prut, E.; Kuznetsova, O.; Yakhina, A.; Olkhov, A.; Samoylov, N.; Grishin, M.; Iordanskii, A.; et al. Biodegradable Polylactide–Poly(3-Hydroxybutyrate) Compositions Obtained via Blending under Shear Deformations and Electrospinning: Characterization and Environmental Application. *Polymers* **2020**, *12*, 1088. [CrossRef]

40. Diederichs, E.V.; Picard, M.C.; Chang, B.P.; Misra, M.; Mielewski, D.F.; Mohanty, A.K. Strategy To Improve Printability of Renewable Resource-Based Engineering Plastic Tailored for FDM Applications. *ACS Omega* **2019**, *4*, 20297–20307. [CrossRef]
41. Wang, S.; Capoen, L.; D'hooge, D.R.; Cardon, L. Can the melt flow index be used to predict the success of fused deposition modelling of commercial poly(lactic acid) filaments into 3D printed materials? *Plast. Rubber Compos.* **2018**, *47*, 9–16. [CrossRef]
42. Biomer: Biodegradable Polymers. Available online: http://www.biomer.de/IndexE.html (accessed on 30 March 2020).
43. NatureWorks. Available online: https://www.natureworksllc.com/ (accessed on 30 March 2020).
44. Jungbunzlauer Specialties. Available online: https://www.jungbunzlauer.com/en/products/specialties.html (accessed on 30 March 2020).
45. Merck. Available online: https://www.merckmillipore.com/CZ/cs/product/Polyethylene-glycol-600,MDA_CHEM-807486 (accessed on 30 March 2020).
46. Horalek, M. Biocomposites based on Polyhydroxybutyrate for 3D Printing. Master's Thesis, Brno University of Technology, Brno, Czech Republic, 2019.
47. #3D Benchy: Measure and Calibrate. Available online: http://www.3dbenchy.com/dimensions/ (accessed on 21 January 2020).
48. *Standard Test Method for Enthalpies of Fusion and Crystallization of Polymers by Differential Scanning Calorimetry (DSC)*; ASTM D 3147-99; ASTM: New York, NY, USA, 1999.
49. Mikusova, M.; Mihalik, M.; Alexy, P.; Tomanova, K.; Plavec, R.; Bockaj, J.; Vanovcanova, Z. Method for testing of Processing Stability of biodegradable Polyesters based on Oscillation Rheometry. *Kautsch. Gummi Kunstst.* **2014**, *67*, 51–54.
50. *Plastics—Determination of Temperature of Deflection under Load—Part 2: Plastics and Ebonite*; ISO 75-2:2013; CEN: Brussels, Belgium, 2013.
51. *Determination of Tensile Properties—Part 1: General Principles*, 2nd ed.; ISO 527-1:2012; CEN: Brussels, Belgium, 2012.
52. *Plastics—Determination of Charpy Impact Properties—Part 1: Non-Instrumented Impact Test*; ISO 179-1:2000; CEN: Brussels, Belgium, 2000.
53. *Plastics—Determination of Tensile-Impact Strength*; ISO 8256:2004; CEN: Brussels, Belgium, 2004.

Publisher's Note: MDPI stays neutral with regard to jurisdictional claims in published maps and institutional affiliations.



© 2020 by the authors. Licensee MDPI, Basel, Switzerland. This article is an open access article distributed under the terms and conditions of the Creative Commons Attribution (CC BY) license (http://creativecommons.org/licenses/by/4.0/).

polymers

MDPI

Article

Influence of Multiple Thermomechanical Processing of 3D Filaments Based on Polylactic Acid and Polyhydroxybutyrate on Their Rheological and Utility Properties

Roderik Plavec [1,*], Vojtech Horváth [1], Slávka Hlaváčiková [1], Leona Omaníková [1], Martina Repiská [1], Elena Medlenová [1], Jozef Feranc [1], Ján Kruželák [1], Radek Přikryl [2], Silvestr Figalla [2], Soňa Kontárová [2], Andrej Baco [1], Lucia Danišová [1], Zuzana Vanovčanová [1] and Pavol Alexy [1]

[1] Institute of Natural and Synthetic Polymers, Faculty of Chemical and Food Technology, Slovak University of Technology, Radlinského 9, 812 37 Bratislava, Slovakia; vojtech.horvath@stuba.sk (V.H.); slavka.hlavacikova@stuba.sk (S.H.); leona.omanikova@stuba.sk (L.O.); martina.repiska@stuba.sk (M.R.); elena.medlenova@stuba.sk (E.M.); jozef.feranc@stuba.sk (J.F.); jan.kruzelak@stuba.sk (J.K.); andrej.baco@stuba.sk (A.B.); lucia.danisova@stuba.sk (L.D.); zuzana.vanovcanova@stuba.sk (Z.V.); pavol.alexy@stuba.sk (P.A.)

[2] Institute of Materials Chemistry, Faculty of Chemistry, Brno University of Technology, Purkyňova 464/118, 612 00 Brno, Czech Republic; prikryl@fch.vut.cz (R.P.); xfigalla@fc.vut.cz (S.F.); kontarova@fch.vut.cz (S.K.)

* Correspondence: roderik.plavec@stuba.sk

Abstract: This study focused on material recycling of a biodegradable blend based on PLA and PHB for multiple applications of biodegradable polymeric material under real conditions. In this study, we investigated the effect of multiple processing of a biodegradable polymer blend under the trade name NONOILEN®, which was processed under laboratory as well as industrial conditions. In this article, we report on testing the effect of blending and multiple processing on thermomechanical stability, molecular characteristics, as well as thermophysical and mechanical properties of experimental- and industrial-type tested material suitable for FDM 3D technology. The results showed that the studied material degraded during blending and subsequently during multiple processing. Even after partial degradation, which was demonstrated by a decrease in average molecular weight and a decrease in complex viscosity in the process of multiple reprocessing, there was no significant change in the material's thermophysical properties, either in laboratory or industrial conditions. There was also no negative impact on the strength characteristics of multiple processed samples. The results of this work show that a biodegradable polymer blend based on PLA and PHB is a suitable candidate for material recycling even in industrial processing conditions. In addition, the results suggest that the biodegradable polymeric material NONOILEN® 3D 3056-2 is suitable for multiple uses in FDM technology.

Keywords: material recycling; polyhydroxybutyrate; polylactic acid; 3D printing

check for updates

Citation: Plavec, R.; Horváth, V.; Hlaváčiková, S.; Omaníková, L.; Repiská, M.; Medlenová, E.; Feranc, J.; Kruželák, J.; Přikryl, R.; Figalla, S.; et al. Influence of Multiple Thermomechanical Processing of 3D Filaments Based on Polylactic Acid and Polyhydroxybutyrate on Their Rheological and Utility Properties. *Polymers* **2022**, *14*, 1947. https://doi.org/10.3390/polym14101947

Academic Editors: Eleonora Ferraris and Lorenzo Moroni

Received: 11 April 2022
Accepted: 9 May 2022
Published: 11 May 2022

Publisher's Note: MDPI stays neutral with regard to jurisdictional claims in published maps and institutional affiliations.

Copyright: © 2022 by the authors. Licensee MDPI, Basel, Switzerland. This article is an open access article distributed under the terms and conditions of the Creative Commons Attribution (CC BY) license (https://creativecommons.org/licenses/by/4.0/).

1. Introduction

In recent years, consumer lifestyles have led to a dramatic increase in the consumption of polymers (especially plastics). In 2019, 368 million tons of plastic material were produced worldwide, of which, 57.9 million tons of plastic material were produced in the EU [1].

The use of plastics is continuing to increase which is significantly increasing plastic waste production, and therefore there is greater interest in recycling and reusing plastics. In 2018, 9.4 million tons of plastic waste were recycled in the EU [2,3]. According to the EU directive 2018/852, at least 65% by weight of all packaging waste must be recycled in EU countries by 2025 and up to 70% by weight of all packaging waste by 2030 [4].

In this article, we present the possibility of material recycling of biodegradable and biobased polymeric materials in the form of 3D filaments based on polylactic acid and polyhydroxybutyrate suitable for additive manufacturing (AM).

Additive manufacturing, also known as three-dimensional (3D) printing, is an additive automated manufacturing process that uses digital 3D designs to prepare specific three-dimensional objects. In fact, it is a set of methods based on layered or spatial storage technologies that use computer-aided design (CAD) software to create physical 3D objects. These production methods allow the direct production of shape-complex products with precisely defined shapes [5].

Three-dimensional (3D) printing is a relatively new technique which dates back to 1980, but it is evolving dynamically. It includes the production of 3D spatial objects based on digital models. Currently, synthetic and biodegradable materials are both used for 3D printing. The range of polymers used in additive manufacturing includes thermoplastics [6], thermosets [7], elastomers [8], hydrogels [9], functional polymers, polymer blends [10], composites [11], and biological systems [12], which have already enabled the creation of value-added materials. Metals or ceramics are also used in 3D printing, and a combination of different types of fillers is currently being researched [13–15]. The gradually growing interest by industries as well as the general public in additive production is reflected in increasing investments in this area [16]. Additive manufacturing can increasingly compete with traditional production processes, such as injection molding in the case of plastics or CNC processing in the case of metals.

The most well-known 3D printing technology is fused deposition modeling (FDM), which is widely used in research and many industrial sectors. FDM is used to create models, prototypes, as well as end products. It is an inexpensive and simple way of producing prototypes or products, and it is often used to produce complex products. Fused deposition modeling (FDM) is a widely used 3D printing technology for polymer and composite filaments due to its flexible and fast printing process, low cost, variety of materials, and high strength as well as toughness of materials [17]. Several successful applications of FDM technology have been published in the literature associated with various industries, such as aerospace engineering [18], the automotive industry [19], and bioengineering [20–23]. Three-dimensional printing is considered to be an environmentally friendly processing technology because its use reduces the generation of plastic waste and also, theoretically, it can use recycled polymers. These benefits have the potential to increase resource efficiency in production by reducing waste production, which contributes to the development of a circular economy (CE) system [24,25]. Among the polymers used in FDM, the most commonly reported polymers are polylactic acid (PLA) and acrylonitrile-butadiene styrene (ABS) copolymer [26].

There are several reasons why the development and use of bioplastics have recently gained significant attention in FDM technology. These reasons include environmental pollution caused by conventional synthetic plastic materials, a reduction in crude oil resources, and interest in controlling toxic gas emissions. The term “bioplastic”, in general, refers to polymer materials that are either biobased or biodegradable, or both [27–30].

Biodegradable materials from renewable sources contribute to sustainable development as well as reduce the negative impacts of polymeric materials on the environment. The main advantage of biodegradable materials from renewable sources is their biodegradability in a biologically active environment, and therefore their contribution to reducing the carbon footprint [2,31,32]. This means that additive production using biomaterials can contribute to many areas of a circular economy, such as saving input materials as well as their recycling and reuse [33,34]. FDM technology is also widely used in medicine and tissue engineering, for example, for the development of customized scaffolds for a wide range of biomaterials [22,35,36]. In addition, FDM technology can generate biomimetic scaffolds due to its ability to produce multi-material structures and push soft biomaterials such as hydrogels [37–39]. Despite the clear advantages of biopolymers obtained from renewable raw materials, some properties of these materials are inferior to those of commonly used plastics, in particular, thermal and mechanical properties, as well as processing stability. Therefore, scientists are trying to find bioplastics that have comparable or even better properties than synthetic (petroleum-based) plastics. Biodegradable materials from

renewable sources (biopolymers) used in FDM technology include polylactic acid (PLA), mainly due to its excellent biocompatibility, good biodegradability, and high mechanical strength [40,41]. Polylactic acid is a transparent, colorless, and solid thermoplastic material. It is synthesized from lactic acid (its dilactide), which is produced by fermentation of renewable raw materials. PLA is a chiral compound, which gives it various rheological, mechanical, and thermal properties. Polylactic acid may be a suitable replacement for PP (polypropylene), PS (polystyrene), or ABS (acrylonitrile butadiene styrene) in industrial applications [42–45]. PLA has been evaluated as the most suitable material for 3D printing by the FDM method because it requires a relatively low print temperature (low die and pad temperature) and also has excellent adhesion to the 3D printer pad [46]. However, this material also has certain drawbacks, in particular, very high brittleness and poor shape stability at temperatures above 60–70 °C. In addition, PLA is sensitive to thermomechanical and hydrolytic degradation during thermomechanical processing [47], with cleavage of the polymer chain, which causes a decrease in molecular weight and inner viscosity. During its use, the polymer may be sensitive to thermal, photochemical, and hydrolytic degradation, which also contributes to reducing its molecular weight [48,49]. Its shortcomings also include the fact that it is not biodegradable in home compost. For these reasons, the possibility of modifying polylactic acid in order to minimize its undesirable properties has been investigated [45].

One possible modification to improve the insufficient properties of PLA is to prepare polymer blends with another biopolymer. An alternative is the use of polyhydroxyalkanoates, which are obtained from renewable raw materials and are fully biodegradable and compostable. Polyhydroxyalkanoates (PHA) are a class of biopolyesters that can be produced naturally by bacteria. The most commonly used type of PHA is poly (3-hydroxybutyrate). Due to its biocompatibility and biodegradability, PHB has attracted attention especially for its possible applications in biomedical areas, for example, as scaffolds for tissue engineering. PHB is a thermoplastic polyester classified as a biopolymer that is produced by microorganisms such as *Ralstonia eutropha* under non-equilibrium growth conditions [50,51]. It is a semi-crystalline polyester with a high level of crystallinity. Although PHB is a fully biodegradable biopolymer, when used alone, it is relatively brittle, expensive, and sensitive to thermomechanical degradation during processing [2]. It is usually used in polymer blends to modify the resulting properties instead of applying it in pure form [2,52,53]. Several authors have suggested blending PLA and PHB as a strategy to address deficient material characteristics and improve the properties of the original polymer [29,53–56]. Previous studies of PLA/PHB blends have shown that the miscibility between the two polymers depended on the molecular weight of the second component [57–59]. The properties of PLA/PHB blends have also been shown to depend on the composition, chemical or physical crosslinking, and processing conditions. PLA/PHB blends alone show relatively low values of flexibility [29,60]. To overcome this disadvantage, it has been proposed to incorporate plasticizers into a PLA/PHB blend, which leads to a reduction in the glass transition temperature (T_g), better processability of the material, and improved flexibility [61–63]. The EP2710076B1 patent [64] shows that blending PLA and PHB and a suitable type of plasticizer improves the mechanical properties and even increases the flexibility of the PLA/PHB blend. The most significant prerequisite for using these materials is the production of cast and blown films, but it has been found that they are also suitable for use in FDM 3D printing technology [65,66]. Studies by [45,65] examined the printability of PLA/PHB blends using various laboratory-prepared and commercial-type plasticizers, with improved dimensional stability and warping reduction by using 15 wt% plasticizer, as well as a positive effect on printability itself and improved physical and mechanical properties (especially impact strength and elongation at break) as compared with PLA/PHB blends without plasticizers and also as compared with PLA itself. Another study examined the effect of temperature and printing conditions of extruded PLA/PHB filament [67]. The contact time as well as the surface contact area were found to affect the crystalline phase of the blends and their subsequent biodegradability.

Since PLA/PHB blends have recently been widely researched in the field of additive production and also in other branches of the plastics industry due to their positive properties, it is interesting to examine the possibility of their material recycling, especially in terms of a circular economy and environmental protection. Researchers [68–71] have emphasized that a mechanical recycling strategy is the most appropriate plastic waste management option for the recovery of relatively clean and homogeneous plastic waste as compared with landfill or incineration alternatives. Mechanical recycling allows direct recovery of solid plastic waste for re-use in the production of new plastic products [72–74] and can use traditional technologies and commonly used processing machines such as conventional extruders and injection molding machines. Due to the fact that the recycling process results in a polymer with varying degrees of degradation, mechanical recycling is limited by the number of repeated processing cycles [75]. Material recycling has commonly been used for many years in the management of plastic waste from the industrial processing of polymeric materials [76,77]. According to the European Strategy for Plastics in the Circulating Economy [78], by 2030, all plastic packaging placed on the EU market should be either reusable or recyclable in a cost-effective way and more than half of all plastic waste generated in Europe should be recycled. According to this strategy [78], innovative materials and alternative starting materials for plastics production should also be developed and used if the evidence clearly shows that they are more sustainable as compared with non-renewable alternatives.

Polymer degradation in an extruder is one of the main factors that can adversely affect the quality of plastic material during its recycling. The term deterioration of a material means deterioration of processability, the mechanical or thermal material properties, as well as the electrical and optical properties, or the appearance and aesthetic properties of the material [79,80]. Due to these effects, recycled plastics are usually used for the production of low technical value products (down cycling). Polymer degradation during processing also reduces the productivity of the reused material due to differences in the viscosities of the recycled and virgin polymers when they are blended to obtain the respective products. Degradation is affected by many factors, such as shear stress, temperature, humidity, pH, the presence of oxygen, UV radiation, and the presence of other technological additives (such as stabilizers) [81,82]. The growing amount of plastic waste produced, legislative requirements, and the increased interest of people in protecting the environment are reasons for the use of plastics in the largest possible number of "life" cycles. Therefore, it is very important to recognize the effect of multiple extrusions of different polymeric materials on the final properties of these materials. However, so far, only a small number of scientific articles have been devoted to experimentally describing changes in the properties of biodegradable types of renewable materials after multiple treatments of these materials [83,84], most of which have dealt with the reprocessing of PLA itself.

Multiple extrusions of PLA (10 processing cycles) were investigated in [85]. Samples were prepared using a twin-screw extruder. In this case, the tensile strength values of PLA did not depend significantly on the number of extrusion cycles. Another study [86] on PLA reprocessing showed that with multiple thermomechanical processing only the tensile modulus remained constant for up to seven injection cycles. Other tested mechanical properties as well as rheological properties decreased by multiple processing by injection. The viscosity of the PLA obtained using a shear rate gradient from 0.01 s^{-1} to 100 s^{-1} decreased significantly (from 3960 to 713 Pa) after the first processing cycle. The mechanical properties of recycled PLA after multiple treatments have been reported to become insufficient for subsequent industrial use. In [87], the influence of multiple thermomechanical processing on the structure and properties of an amorphous PLA type was studied. As a result of multiple processing of amorphous PLA, there was a decrease in molecular weight and, subsequently, a decrease in other tested properties of PLA after the second processing cycle. In [88], it was found that the effect of multiple extrusion of PLA led mainly to a reduction in elongation at break and also to a reduction in impact strength. The authors of [89] studied the effect of multiple processing on the properties of PHB itself and were able

to regranulate PHB in three cycles. During the material recycling of PHB, its mechanical properties deteriorated significantly when the tensile strength of the material after triple extrusion reached less than 50% of the original tensile strength value.

Material recycling of PLA/PHB blends with the addition of a suitable plasticizer was tested in [2]. It was found that the molecular weight as well as the viscosity of the tested materials decreased due to multiple treatments. Nevertheless, after repeated processing, there was no decrease in the strength characteristics or a change in the thermal properties of the blends. It was proven in this work that it was possible to implement up to 11 processing cycles from PLA/PHB polymer blends with the addition of a suitable plasticizer. Despite the fact that PLA/PHB polymer blends are completely biodegradable in a suitable biological environment, in order to save raw material resources, it is important to know their material recycling potential and the associated reuse before such materials are composted. Such a procedure would significantly increase the ecological and economic value of using polymeric materials based on PLA/PHB, which directly corresponds to the principles of the circular economy.

In this article, we focus on the effect of multiple processing on the final mechanical and thermal properties, as well as the processing stability of a PLA/PHB blend intended for 3D printing under the designation NONOILEN® 3D 3056-2, which was processed in both laboratory and industrial conditions at an industrial partner.

2. Experimental Methods

2.1. Materials and Methods of Samples' Preparation

This work deals with the study of the recyclability of a biodegradable polymer blend intended for 3D printing technology under the trade name NONOILEN® 3D 3056-2, which is a biodegradable polymeric material prepared from polylactic acid, polyhydroxybutyrate, and oligomer plasticizer. The concentration of PLA in the tested polymer blend is above 10%, the concentration of PHB is above 30%, and the concentration of suitable plasticizer is less than 15%. The exact composition of the blend was provided by Panara a.s., producer of NONOILEN® 3D 3056-2. This type of blend is suitable for FDM processing by 3D printing technology, and was used as a basis for examining the possibility of multiple processing of the material with the possibility of its subsequent material recycling.

The process of material recycling (multiple extrusion) of the studied biodegradable polymer blend was carried out in two different processing streams.

For the study of experimental material recycling (under laboratory conditions), first, the material recycling of the tested blend was carried out under laboratory conditions at the Institute of Natural and Synthetic Polymers, Slovak University of Technology, in Bratislava, where the material was blended on a laboratory twin-screw extruder from the Labtech company and the resulting material was cyclically processed on a single-screw extruder (Plasticorder, Brabender, Duisburg, Germany).

2.1.1. Polymer Blend Preparation for the Study of Experimental Recycling

The polymer blend NONOILEN® 3D 3056-2 for experimental recycling was prepared according to the recipe provided by Panara a.s. using a laboratory twin-screw extruder LTE16 from the Labtech company. The diameters of the screws were 16 mm and the L/D ratio was 40. The geometric arrangement of the screws was co-rotating with intermeshing. The screw speed was set at 150 min^{-1}. The operating temperature profile of the device in the direction of the hopper to the head which consisted of 10 heating zones was as follows: 60–140–5 × 190–160–150–150 °C.

2.1.2. Multiple Extrusion of the NONOILEN® 3D 3056-2 Experimental Samples

The tested polymer blend based on PLA/PHB was processed several times on a Plasticorder Brabender single-screw extruder with a nozzle with a circular cross-section and a diameter of 2 mm. The screw speed was set at 55 min^{-1}. The total retention time of the material in the device was 58 s. The temperature profile of the device in the direction of

the hopper to the head was as follows: 170–185–190–180 °C. The granulate was fed into the device via a hopper. The melt was forced through a die into a water bath where the filaments were cooled, and then granulated. In total, the material was processed 9 times.

2.1.3. Study of Industrial Material Recycling (in Real Conditions)

In the second processing stream, the blend with the same composition was prepared and further recycled under industrial conditions at the Fillamentum Manufacturing Czech company, Hulín, Czech Republic using a twin-screw extruder LTE 26 from the Labtech company, Praksa, Thailand. The screw diameter was 26 mm and the L/D ratio was 40. The geometric arrangement of the screws was co-rotating with intermeshing. The screw speed was set at 400 min^{-1} and the material was repeatedly processed, firstly by extrusion into filaments, and then by FDM technology (3D printing) into test specimens. Then, the prepared 3D specimens were mechanically ground into granules, from which the filaments were prepared in the next step.

2.1.4. Polymer Blend Preparation for the Study of Material Recycling in Industrial Conditions

The polymer blend NONOILEN® 3D 3056-2 for recycling in real conditions was provided by the Fillamentum Manufacturing Czech Co. as a commercially available material in the form of filaments suitable for 3D printing using FDM technology. Then, the provided filaments were processed using a 3D printer and the printed samples were mechanically granulated and reprocessed by extrusion again to the filament form on a Plasticorder Brabender single-screw extruder. In the case of studying the possibility of material recycling of the tested blend in real conditions, this blend was repeatedly thermomechanically stressed by a combination of processing using a single-screw extruder (filament production) and processing using a 3D printer (preparation of 3D samples).

2.2. Multiple Extrusion of the NONOILEN® 3D 3056-2 Industrial Samples

The samples were prepared using a Plasticorder Brabender single-screw extruder with a die with a circular cross-section. The temperature profile used in the direction from the hopper to the head was as follows: 170–185–190–180 °C. The granules were fed into the device via a hopper. The melt was extruded through a nozzle into a water bath, where the prepared filaments were cooled and wound on a spool. The diameters of the prepared filaments were 1.5 mm $\pm$ 0.05 mm.

2.3. Preparation of the Samples by 3D Printing from Industrial Samples of NONOILEN® 3D 3056-2

Samples were prepared by 3D printing. Tensile bars were printed on a PRUSA i3MK3 3D printer, Praque, Czech Republic. The prepared filaments were introduce into a 3D printer, where they were melted, and then printed in a form of tensile bars. The diameter of the nozzle of the 3D printer was 0.4 mm and its temperature was 190 °C. The temperature of the printer pad was 20 °C. The height of the printed layer was 0.2 mm and number of the layers was 10. The printing speed was 40 mm/s.

The process of mechanical recycling in experimental and industrial conditions is shown in Figure 1 and the designation of each studied sample is stated in Table 1.

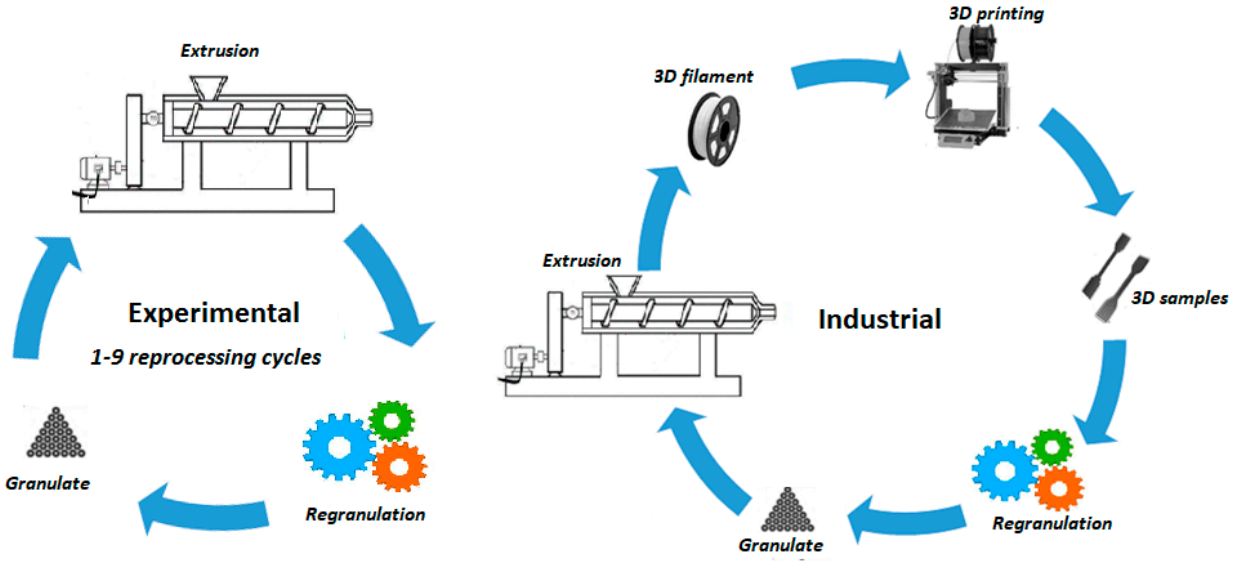


Figure 1. The process of mechanical recycling in experimental and industrial conditions.

Table 1. Processing passes of the PLA/PHB blend suitable for 3D printing.

Experimental Recycling			
Extrusion Number/Sample Name	**Processing Equipment**	**Processing Time (Seconds)**	
1 (E)	Twin-screw extruder (blending)	65	
2 (E)	Single-screw extruder	123	
3 (E)	Single-screw extruder	181	
4 (E)	Single-screw extruder	239	
5 (E)	Single-screw extruder	297	
6 (E)	Single-screw extruder	355	
7 (E)	Single-screw extruder	413	
8 (E)	Single-screw extruder	471	
9 (E)	Single-screw extruder	529	
Industrial Recycling			
Extrusion Number/Sample Name	**Processing Equipment**	**Processing Time (Seconds)**	**Product**
1 (I)	Twin-screw extruder (blending) *	45	Polymer blend
2 (I)	Single-screw extruder *	295	1st Filament
3 (I)	3D printer	312	1st 3D sample
4 (I)	Single-screw extruder	517	2nd Filament
5 (I)	3D printer	534	2nd 3D sample
6 (I)	Single-screw extruder	739	3rd Filament
7 (I)	3D printer	756	3rd 3D sample
8 (I)	Single-screw extruder	961	4th Filament
9 (I)	3D printer	978	4th 3D sample

* 1st and 2nd processing passes of the polymer blend were prepared in cooperation with the Fillamentum Manufacuring Czech company at their industrial processing facilities. Note: The symbol after the processing cycle number indicates how the material was recycled (I—in industrial conditions; E—in laboratory conditions).

3. Experiments

The experiments were performed to describe the effects of multiple processing of the tested biodegadable polymer blend on its rheological and utility properties, in laboratory (experimental) as well as real (industrial) conditions. The aim was to investigate the

possibility of material recycling of the tested biodegradable polymer blend based on PLA and PHB.

3.1. Processing (Thermomechanical) Stability

Testing of the processing stability of the biodegradable polymer blend samples was performed on an RPA 2000 oscillating rheometer, Wilmington, DE, USA. The tested samples were measured at a temperature of 190 °C. The preheating time was 1 min and the total duration of the test was 10 min. The oscillation frequency was 50 CPM and the oscillation angle was 60°. The samples were tested at a shear rate of 22 s^{-1}. The dependences of the complex viscosity on the test time were determined. For a better comparison of the results, since the samples did not have the same viscosity at the beginning of the test, the dependence of the relative complex viscosity on time was evaluated as the indicator of degradation. The mathematical formula for calculating the relative complex viscosity is $\eta^*_{rel.}(t) = \frac{\eta^*(t)}{\eta^*(0)}$, where $\eta^*_{rel.}(t)$ is the relative complex viscosity in time t, $\eta^*(t)$ is the complex viscosity in time t, and $\eta^*(0)$ is the complex viscosity at the beginning of the test [90].

It should be noted that testing of the effect of multiple processing on processing stability, thermal properties, and physical-mechanical properties was performed under the same conditions for samples of both recycling processing streams.

3.2. Molecular Characteristics

Molar mass of the tested material was determined by gel permeation chromatography. The measurements were performed using an Agilent Technologies 1100 Series, Santa Clara, CA, USA instrument equipped with an isocratic pump, and an autosampler. A PLgel 5 µm mixed C column was tempered to 30 °C with chloroform as the eluent at a flow rate of 1 mL/min. Linear polystyrene standards with narrow distribution were used to gain the calibration curve (10 points in calibration). The instrument was equipped with a refractive index detector.

3.3. Color Changes Measurement

Color changes was measured on prepared 3D printed samples according to the CIE Lab color scale relative to the standard illuminant D65 over a white background using a reflection spectrophotometer (Techkon SpectroDens, Königstein, Germany). The aperture diameter of the measuring port was 3 mm. The selected illuminating and viewing configuration of this instrument was CIE diffuse/10° geometry and the CIE 1964 supplementary standard colorimetric observer. Total chromatic change was calculated using Equation (1):

$$\Delta E^*_{a,b} = \sqrt{(\Delta L^*)^2 + (\Delta a^*)^2 + (\Delta b^*)^2} \quad (1)$$

3.4. Measurement of Thermal Properties

The thermal properties of the studied blend were measured using a differential scanning calorimetry on a Mettler-Toledo Inc., Worthington, OH, USA instrument. The basic thermal characteristics such as the glass transition temperature, the crystallization temperature, and the melting point of the crystallites were evaluated from the measurements. The conditions for measuring of thermal properties are summarized in Table 2.

Table 2. Conditions for measuring thermal properties.

	Ramp	Set Temperature (°C)	Time (min)
Conditioning	isothermal	0	1
1st Heating	10 °C/min	200	20
Conditioning	isothermal	200	3
Cooling	10 °C/min	0	20
Conditioning	isothermal	0	3
2nd Heating	10 °C/min	200	20

The heat difference required for heating by 1 K between the sample and the standard was measured. The standard in this case was an empty cup. Nitrogen was used as the inert gas and the evaluation software was SW STARe 16.30.

3.5. Measurement of Mechanical Properties

The measurement of mechanical properties was performed using a Zwick/Roell, Ulm, Germany testing device at a cross-head speed of 50 mm/min. The distance between the heads of the testing device was 50 mm and the working distance of the extensiometer was 20 mm. From the obtained tensile curves, the following mechanical parameters were determined: relative elongation at break (ε_b), tensile strength at break (σ_b), yield strength (σ_y), and Young's modulus (E). Mechanical properties were measured from prepared filaments and also from dogbone-shaped samples.

3.6. Flexural Test

The three-point bending test was performed on a UMZ-3K tester from the MICRO-EPSILON, Ortenburg, Germany company. The tested samples were prepared in the form of a filament with a circular cross-section as part of the material recycling testing under industrial conditions. The distance of the extreme support points was set to 24 mm in this test. The load was applied using a load pin in the middle of the span length with a cross head speed of 2 mm/min. During the test, the stress-strain dependency of the test specimen was recorded.

Flexural strength was evaluated by Equation (2):

$$\sigma_{max} = \frac{8 \cdot F_{max} \cdot g}{\pi \cdot d^3} \quad (2)$$

where F_{max} is the maximal developed force during the flexural test, d is the filaments diameter, and g is the distance between supports

Young's modulus was evaluated as the slope of the first linear function area of dependency of flexural strength on sample deformation.

Deformation at flexural strength was evaluated like a cross point of the tangents line of the first and second linear function area of dependency of flexural strength on sample deformation.

4. Results

4.1. Processing Stability

Figure 2 shows the dependence of complex viscosity on the material time in the oscillation field of the rheometer of individual processing cycles of the PLA/PHB blend NONOILEN® 3D 3056-2 from Panara, a.s., Nitra, Slovak Republic company recycled in laboratory conditions. It can be seen from the graph that due to the longer retention of the material in the oscillating rheometer, the complex viscosity decreases, which is a demonstration of material degradation under thermomechanical loading. A decrease in complex viscosity also occurs due to multiple processing of the polymeric material. From this, it can be deduced that the investigated material degrades under thermomechanical loading in laboratory conditions. Degradation of recycled material under industrial conditions also occurs as a result of multiple treatments, as is clearly seen in Figure 3. Degradation of the material preferably occurs during filament processing. The largest decrease in complex viscosity during the test of thermomechanical stability is exhibited by Sample 2(I), but the largest decrease in the values of complex viscosity between two identical products processed with higher processing number occurs between the preparation of the first and the second filament (extrusion number 2(I) vs. 4(I)). On the contrary, the processing of the material using FDM 3D printing technology does not have a negative impact on the processing stability of the tested material. Since the experimental (laboratory) and industrial processing equipment differ from each other, both in terms of construction and also in different retention time of the material during processing, to compare the results between commercial and laboratroy tested material, we chose extrusion times as the comparison

parameter. The total processing time of the material for each processing pass of the tested polymeric blend is given in Table 1. Figure 4 shows a comparison of the complex viscosity of an experimental sample and a sample processed under real (industrial) processing conditions. During the blending under industrial conditions, the material is thermomechanically loaded by different processing conditions as compared with blending of the experimental polymer blend (different shear stress of the material during blending, different time of retention), which causes a higher rate of material degradation during blending as compared with material blending under laboratory conditions.

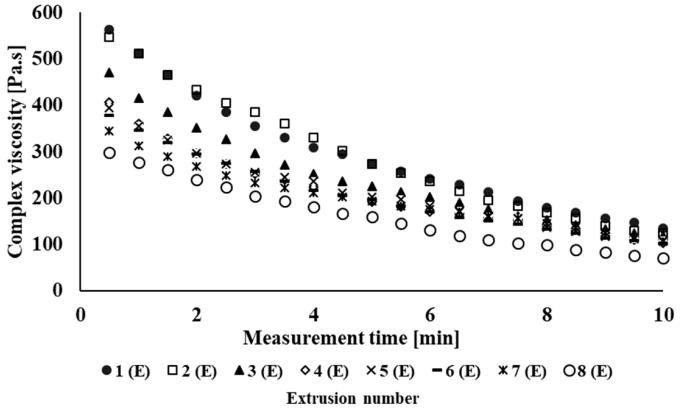


Figure 2. Dependence of complex viscosity on measurement time for NONOILEN® 3D 3056-2 experimental samples prepared in laboratory conditions.

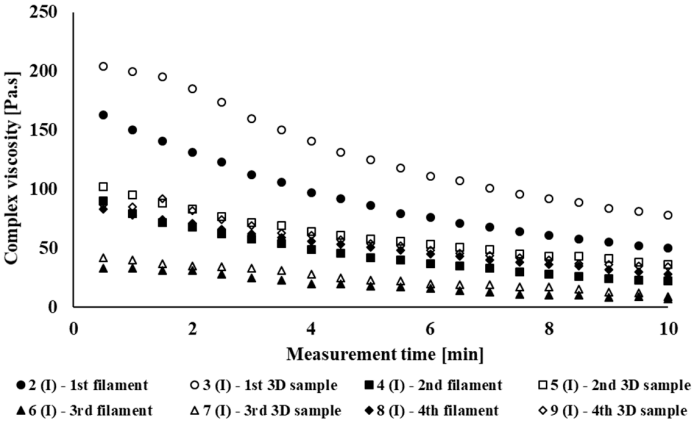


Figure 3. Dependence of complex viscosity on measurement time for commercially processed NONOILEN® 3D 3056-2 samples.

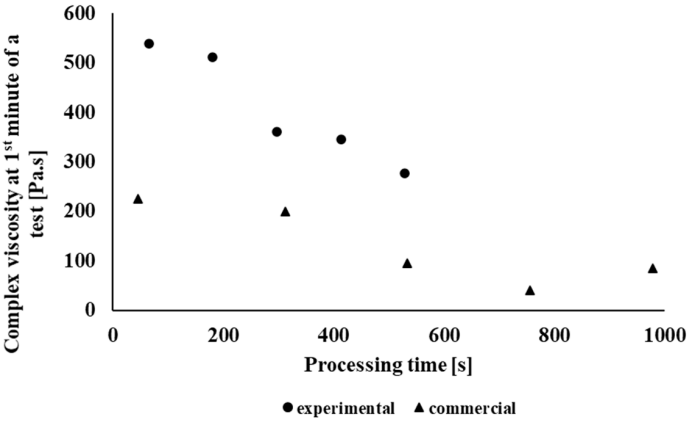


Figure 4. Dependence of the complex viscosity in the 1st minute of the test in an oscillating rheometer on the processing time of the NONOILEN® 3D 3056-2 material.

4.2. Molecular Characteristics

To better understand the problem of degradation of the studied biodegradable polymer blend based on PLA and PHB, we performed measurements of molecular characteristics of individual processing cycles of the polymer blend, which were processed in experimental, and subsequently, in real production conditions. Figure 5 shows the molar mass distributions for the individual processing cycles of the material tested in both processing conditions. In both cases, due to multiple treatments, the molar masses shift to lower values, which is due to the degradation of the material during the multiple thermomechanical loading. The biggest difference between the molar mass distributions in laboratory (experimental) processing of the tested material and processing in a commercial processing machine is the absence of macromolecules with the highest molar mass ($\overline{M_w}$ above 10^6 Da) in the case of industrial processing. This result is consistent with the results described in the processing stability test, where the commercially processed material showed lower complex viscosity values than the material processed under laboratory conditions.

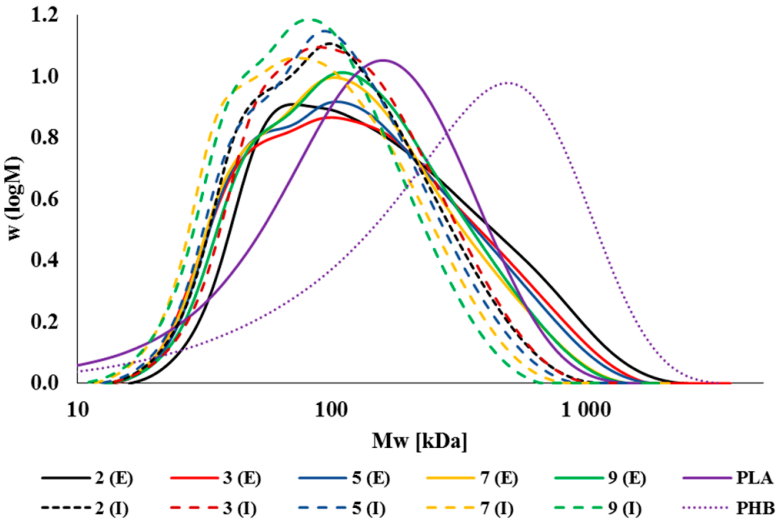


Figure 5. Molar mass distribution of individual processing cycles of experimental and industrial types of the NONOILEN® 3D 3056-2 material.

The different influences of processing on the material's molecular characteristics are clearly shown in Figure 6; the dependence of the molar mass on the retention time of the material in the processing equipment is shown, where a more significant decrease in the molar mass occurs during the experimental processing of the studied material. In both processing alternatives, however, the longer total processing time causes a decrease in the average molar mass. There is a very good correlation of results between the processing stability of the tested materials and their average molar mass (Figure 7), both in the case of laboratory and industrial samples of individual processing passes.

In the case of the polydispersity index (Figure 8), the situation is different. Due to the absence of large macromolecules ($\overline{M_w}$ above 10^6 Da) in the case of blend samples processed under industrial conditions, these samples show a narrower distribution curve than in the case of blend samples processed under laboratory conditions. In the case of laboratory-processed samples, a decrease in polydispersity is visible due to multiple processing of the material, and thus, longer retention of the material in the processing equipment. During industrial processing of the material, the polydispersity index changes only minimally due to multiple processing, because the main molar mass reduction of the highest molar mass fractions was run during the blend preparation. The lower polydispersity index values for samples processed during industrial recycling was caused by the fact that, in the case of blending the polymer blend under industrial conditions, a twin-screw extruder with a higher processing time and a higher shear stress was used as compared with the

laboratory blending equipment. Macromolecules with lower $\overline{M_w}$ are more stable against thermomechanical degradation during processing because of lower viscosity and lower shear stresses in the melt.

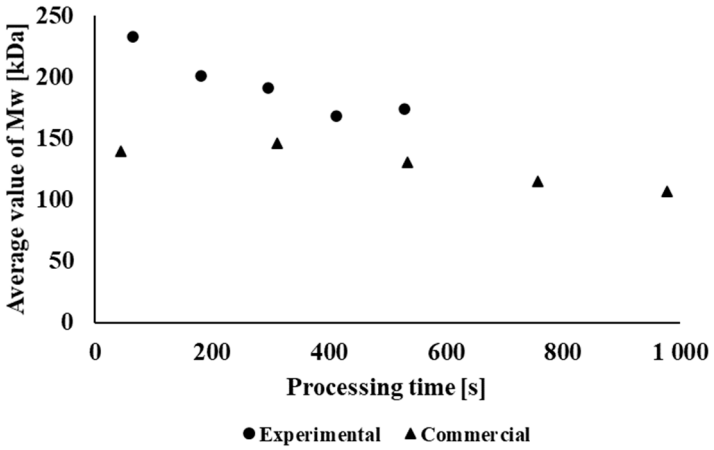


Figure 6. Dependence of the average molar mass as a function of the total retention time of the material in the processing equipment.

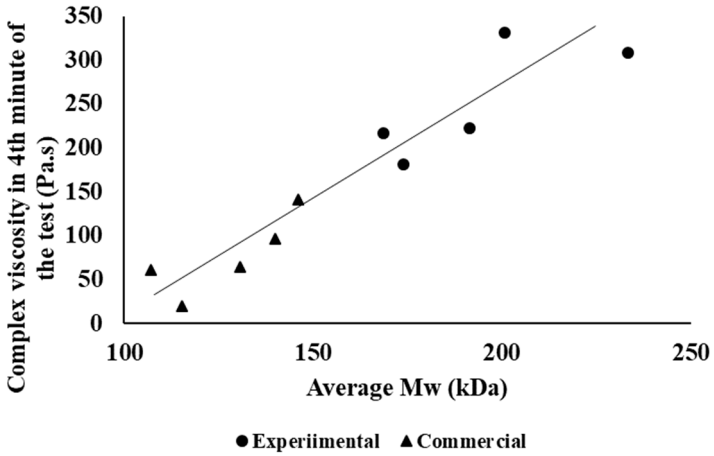


Figure 7. Dependence of complex viscosity in the 4th minute of the processing stability test on the average molar mass of the material.

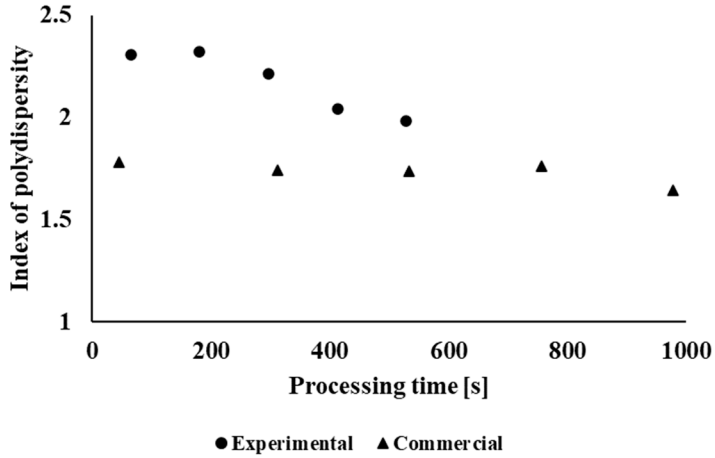


Figure 8. Dependence of the polydispersity index on the total retention time of the material in the processing equipment.

From the study of material degradation during multiple processing in machines, we found that, due to multiple thermomechanical processing, the tested material partially degrades, which was associated with a decrease in its molar mass and a subsequent decrease in material viscosity. It should be noted that the starting blends themselves differed in viscosity. Greater degradation of the material occurs during its processing under industrial conditions, which is due to the different construction of industrial equipment, different shear stress of the material, as well as different retention time of the material in the processing equipment. However, the positive fact is that both in the laboratory, and subsequently in the research phase directly at the industrial partner, we were able to realize nine processing passes, which would ultimately mean that the tested blend would be usable at least four times under industrial conditions before its ecological recovery in the form of biodegradation would be necessary.

4.3. Color Changes

As multiple material processing in the processing machines results in material degradation, which often results in darkening of the material, we examined the color changes accompanying material recycling. Figure 9 shows the measured tensile specimens after 3D printing of industrially processed material, where the first dogbone represents the third processing cycle, the second dogbone represents the fifth processing cycle, the third dogbone represents the seventh processing cycle, and the fourth dogbone represents the last, i.e., ninth processing cycle of the NONOILEN® 3D 3056-2 material.

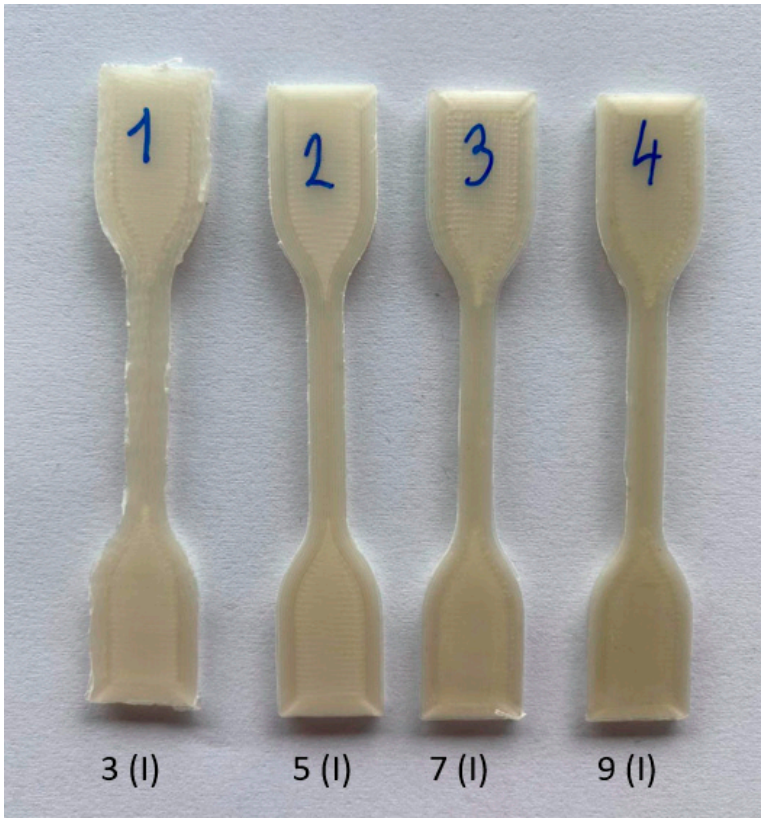


Figure 9. 3D printed samples after multiple processing (3rd, 5th, 7th, and 9th processing transition) of the industrial type sample, NONOILEN® Fillamentum for NATURE.

Figure 10 shows the dependence of the brightness of the material on the retention time of the material in the device for extruded 3D objects of industrially processed sample types and for filaments of the experimentally processed tested polymer blend. It can be seen that during recycling under laboratory conditions, due to the extrusion process, the brightness

values decrease, and thus, the material darkens. In the case of samples prepared by 3D printing, the brightness values change minimally. It can also be seen from the dependence of the color difference of the material (Figure 11) on the time in the device that the color difference is larger as compared with the initial sample in the case of material processing under laboratory conditions; in industrial processing the color difference changes minimally.

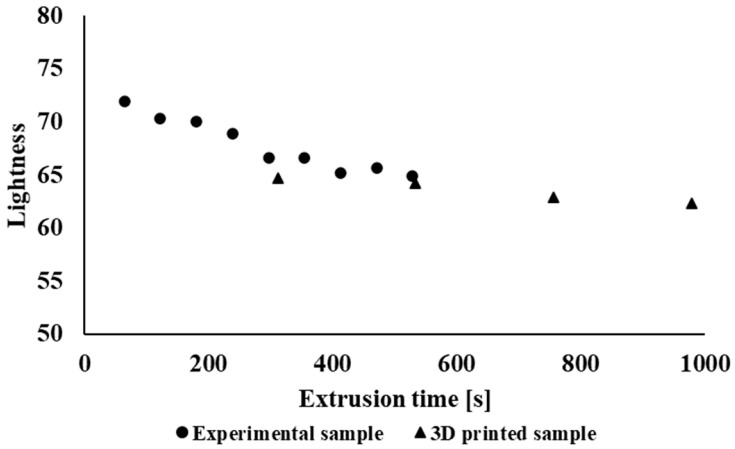


Figure 10. Dependence of material lightness on material retention time in equipment for experimental samples as well as 3D printed objects of industrially processed samples of NONOILEN® 3D 3056-2.

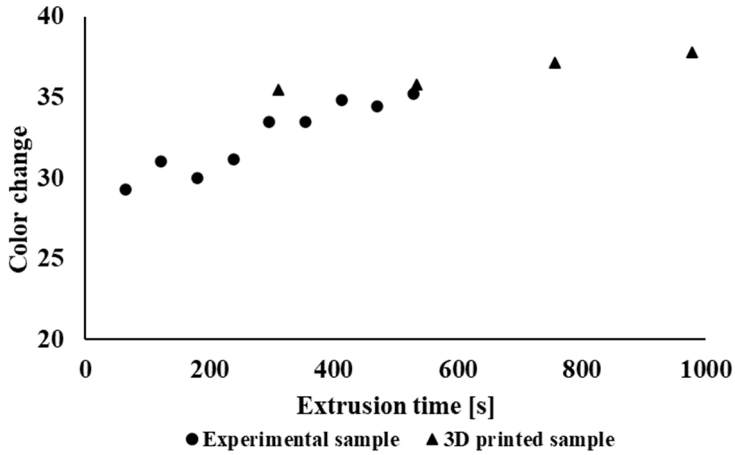


Figure 11. Dependence of the color difference of the material on the retention time of the material in the processing equipment.

Significant color change in samples processed under laboratory conditions occurs due to differential degradation of the primary non-recycled polymer blend during its blending when the blend prepared under industrial conditions already shows lower lightness values due to degradation during blending of the polymer blend. For this reason, in the process of multiple processing under industrial conditions, such a significant color change can no longer occur as in the case of processing samples prepared under laboratory conditions.

In the case of experimental and industrial processing of samples, different effects of processing equipment on processing stability, molecular characteristics, and color changes of the biodegradable polymer blend type NONOILEN® 3D 3056-2 were found. In the following section, the effects of multiple processing on the thermal and physical-mechanical properties were tested to clarify the possibility of material recycling of the tested biodegradable polymeric material. The material was also processed first in laboratory conditions, and then in industrial (commercial) processing directly at the industrial partner.

4.4. Thermophysical Properties

The thermophysical properties were measured using the DSC method, with first heating of the samples, cooling, and then second heating (Figures 12–14). For illustration, in these figures, thermograms are plotted for the first and ninth processing passes in the case of the experimental part of the study. In the case of mechanical recycling in industrial conditions, in the graph, thermograms are plotted for the first and the fourth filaments and for the first and last (fourth) printed 3D samples. The process of thermophysical measurements measured by DSC of other tested samples was comparable with the given thermograms. The thermophysical characteristics of the processing passes for the experimental and industrial samples are summarized in Table 3. Based on the evaluation of thermal properties of individual processing cycles prepared in laboratory and industrial conditions, we found that multiple processing of the tested blend had only a minimal effect on its thermophysical characteristics, regardless of the processing equipment on which the polymeric material was processed. By comparing the different technological equipment on which the materials were processed, only slight deviations were recorded at the values of the glass transition temperature (T_g) depending on the used technology, while the samples prepared under laboratory conditions showed a glass transition temperature from 2 to 3.5 °C higher than in the case of samples prepared on industrial equipment (filaments and 3D samples). Due to multiple processing of the material, the values of the cold crystallization temperature and the melting point of the crystallites do not significantly change. In the case of cooling, all processing transitions of the tested material show a crystallization peak, where there is also no shift in the crystallization temperature values due to multiple processing. In addition, due to multiple treatments, the enthalpy of melting crystallites, crystallization, and cold crystallization does not change, despite the fact that multiple treatments cause degradation of the material accompanied by a decrease in molar mass. The results indicate that in both cases of multiple processing (in laboratory and industrial conditions) the ratio of crystalline and amorphous phase is without significant changes with multiple processing during recycling. However, the thermophysical properties are slightly influenced by the processing equipment as well as the blending process of the original (non-recycled) polymer blend, especially in the case of influencing the glass transition temperature and temperature of cold crystallization.

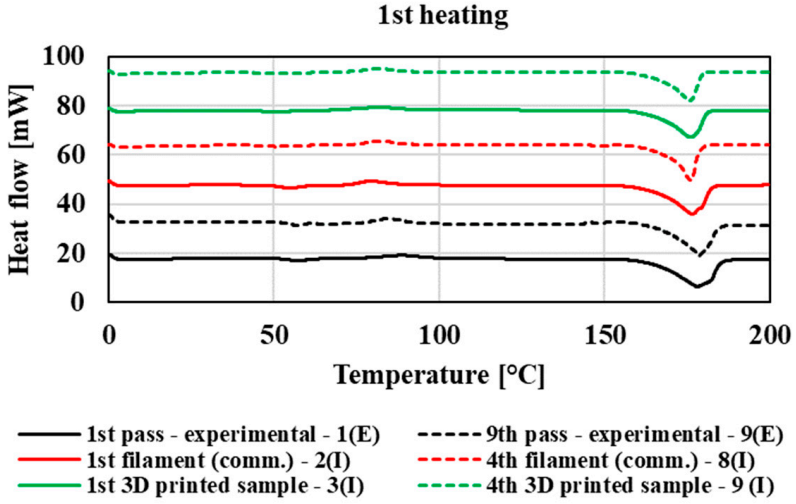


Figure 12. DSC thermogram of 1st heating for experimental and commercial type polymeric material.

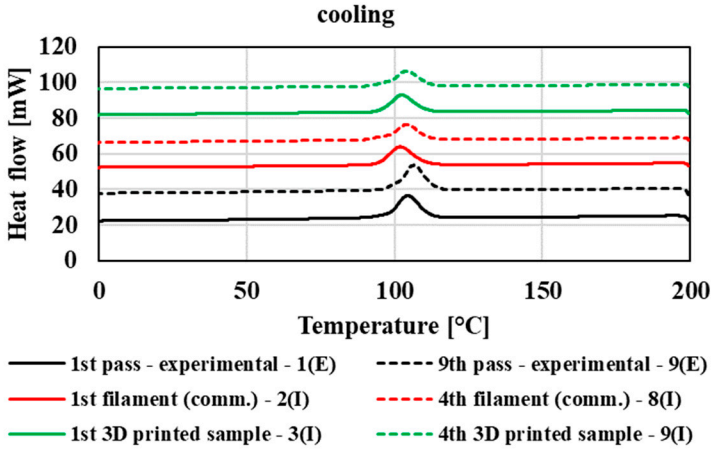


Figure 13. DSC thermogram of cooling heating for experimental and commercial type polymeric material.

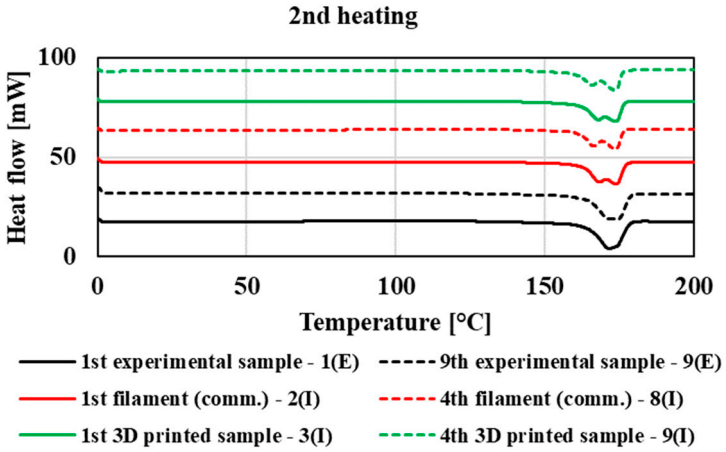


Figure 14. DSC thermogram of 2nd heating for experimental and commercial type polymeric material.

Table 3. Thermophysical characteristics of studied samples (processing passes).

Sample	Experimental Samples					Industrial Samples				
	1 (E)	**3 (E)**	**5 (E)**	**7 (E)**	**9 (E)**	**1 (I)**	**3 (I)**	**5 (I)**	**7 (I)**	**9 (I)**
T_g [°C]	53.76	54.75	54.67	54.73	54.74	48.58	46.75	47.76	49.11	48.28
T_{cc} [°C]	88.80	84.80	84.00	84.33	84.99	79.31	82.47	83.15	83.67	82.00
ΔH_{cc} [J/g]	6.46	9.56	9.38	8.16	8.70	5.90	4.95	7.03	6.20	6.65
T_m [°C]	177.36	177.09	178.26	177.60	179.78	175.84	176.08	177.38	175.09	175.06
ΔH_m [J/g]	56.75	53.93	53.57	53.30	50.28	57.70	55.46	55.17	53.99	53.92
T_{cc} [°C]	105.12	106.26	107.19	107.50	107.36	102.52	102.65	104.01	105.32	104.36
ΔH_c [J/g]	46.06	45.45	47.23	45.52	46.69	46.57	43.33	44.53	41.31	42.83

4.5. Mechanical Properties

Multiple processing during material recycling and the associated degradation of the material can also have an adverse effect on the mechanical properties of the studied polymeric material, while degradation often leads to a decrease in strength characteristics as well as a decrease in flexibility of polymeric material. Therefore, when measuring mechanical properties, basic physical-mechanical parameters such as yield strength, tensile strength, and relative elongation at break were evaluated. The mechanical properties of the tested processing cycles were evaluated separately for experimental samples and separately for commercial types of samples (filament, 3D object), while the values of mechanical properties were related to the total extrusion time. Figure 15 shows the dependence of

the yield strength on the total retention time of the material in the processing machine. In the case of specimens prepared by 3D printing (3D samples), it was not possible to determine the yield strength of the material. By comparing the experimental samples and the commercial filament, which has been repeatedly treated, it showed that multiple treatments did not have a significantly negative effect on the yield strength. This effect could be predicted based on the unchanged amorphous phase/crystallinity ratio, as mentioned in comments about the DSC measurements. It can also be stated that multiple processing does not negatively affect the tensile strength (Figure 16) of the studied experimental and industrially processed types of samples. In the case of strength characteristics, no significant effect of the used processing equipment was recorded. In the case of relative elongation at break (Figure 17), it can also be seen that multiple processing under laboratory conditions has minimal effect on its values. On the contrary, processing in industrial conditions has a greater impact on the flexibility of the material. In this case, there was a decrease in the elongation at break after the preparation of the second filament. The decrease in elongation at break was due to the lower molar mass of these samples and the absence of long macromolecular chains during material blending on industrial equipment. Based on the fact that this type of blend is not intended for high flexible products (initial elongation at break is not so high), the changes in this parameter do not significantly devaluate the application properties of the final product.

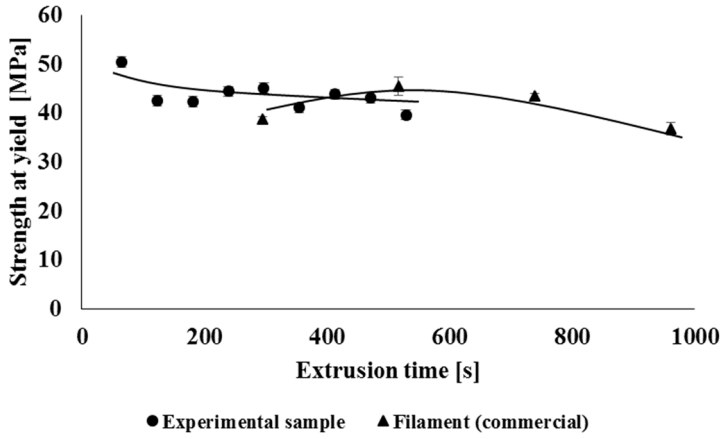


Figure 15. Dependence of strength at yield on the total processing time of the polymeric material.

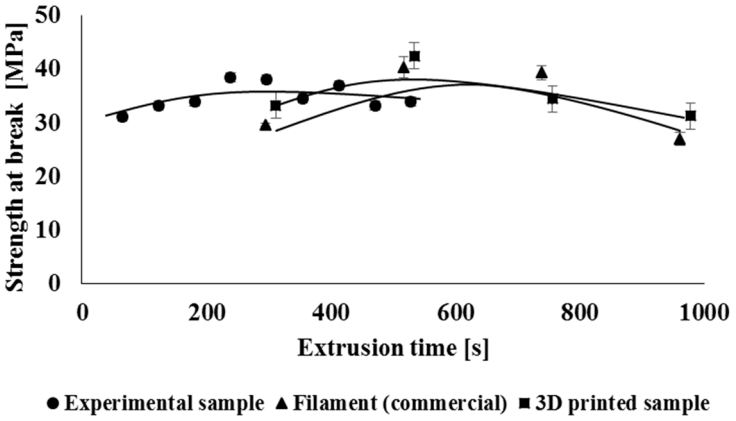


Figure 16. Dependence of tensile strength at break on the total processing time of the polymeric material.

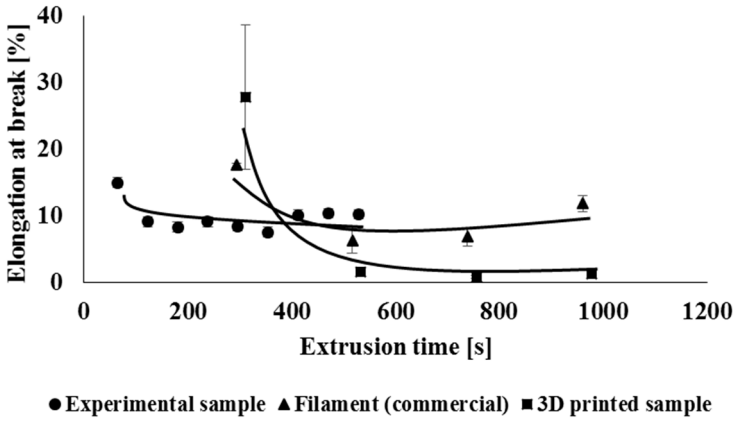


Figure 17. Dependence of the elongation at break on the total processing time of the polymeric material.

Scientific articles [91,92] state that, in addition to the decrease in molecular weight due to degradation, the deterioration in mechanical strength may also be caused due to the moisture content of polyesters, including PLA and PHB. In this case, due to multiple treatments, the strength characteristics were affected only minimally. That means that the possible different moisture contents of the samples after their multiple processing did not have a significant effect on the strength characteristics of the studied samples.

4.6. Flexural Test

Flexural strength provides information about the material's ability to withstand deformation under stress. The flexural test was investigated on the filaments prepared in the process of industrial recycling. Figure 18 shows a slight decrease in the maximum flexural strength values of the individual samples due to multiple processing (recycling) of the tested polymeric material. The decrease in flexural strength values of the tested samples is caused by partial degradation during processing, when the molar mass of the polymer blend decreases, but the decrease in maximum flexural strength even after nine processing cycles of the polymer blend shows only 7% of the value as compared with the original non-recycled sample. In addition, only minimal changes during multiple processing occurred in the case of deformation at the flexural strength (Figure 19) and also in the evaluation of Young's modulus (Figure 20), when the values of the investigated parameters were in the range of statistical measurement errors even after multiple processing as compared with non-recycled material.

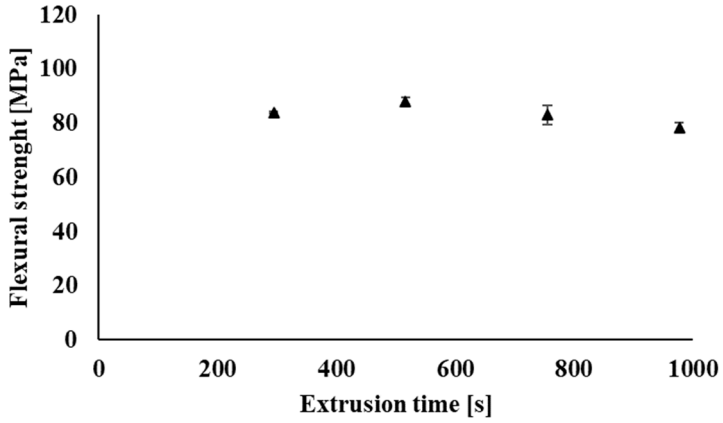


Figure 18. Dependence of maximum flexural strength on the total processing time of the material in the form of filaments processed under industrial conditions.

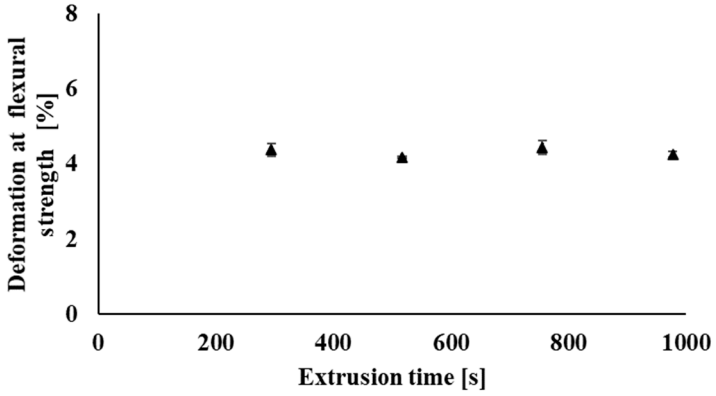


Figure 19. Dependence of flexural strength deformation on the total processing time of the material in the form of filaments processed under industrial.

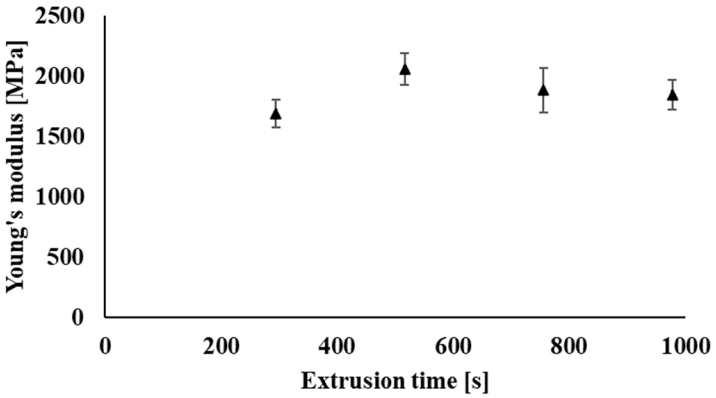


Figure 20. Dependence of Young's modulus on the total processing time of the material in the form of filaments processed under industrial conditions.

During the 3D printing test, it was noted that multiple processing of material had no negative impact on the 3D printing. The tested material can be printed under the same conditions as fresh (unrecycled) material even after multiple processing (the same printing temperature, pad temperature, and printing speed). There were no increases in side effects such as warping, delamination of layers, or deformation of the 3D-printed model observed during the 3D printing of objects (samples) made of multiple processed material.

5. Conclusions

In this study, we investigated the possibility of material recycling of a biodegradable polymer blend based on PLA and PHB under the trade name NONOILEN prepared under laboratory and industrial conditions. Biodegradable polymers were tested in two different processing streams, namely in laboratory and industrial conditions, to compare the impact of multiple processing on processing stability, molecular characteristics, thermophysical properties, mechanical properties, and color changes of the tested materials.

During the testing of processing stability of the studied material, it was found that the extended extrusion time in multiple processing caused degradation of the material due to cyclic thermomechanical loading, which was reflected in a decrease in the complex viscosity values of the tested material after multiple processing. A more significant decrease in complex viscosity due to multiple processing occurred in the polymeric material tested under laboratory conditions, especially at the third thermomechanical loading of the material (Sample 3(E)). In the case of testing the processing stability of the material processed under industrial conditions, the complex viscosity of the non-recycled material was lower as compared with the complex viscosity of material tested under laboratory (experimental) conditions, due to different types of multiple processing of material in

laboratory and in industrial conditions. The highest decrease in viscosity, in the case of the industrial type of tested blend, was observed during the blending process of the polymer blend. Subsequently, a significant decrease in processing stability during the process of multiple processing (material recycling) under industrial conditions occurred during the fourth processing cycle (Sample 4(I)).

Degradation of the material was also proven by a GPC analysis, which showed that, in the case of industrial processing of this polymer blend, the degradation of long macromolecular segments occurred preferentially in the blending process of the biodegradable polymer blend. During multiple processing, a more pronounced decrease in the average molecular weight occurred, in the case of experimentally prepared samples, which had, however, a higher initial average molecular weight. The value of the average molecular weight stabilized in the range from 120 to 160 kDA, even after multiple processing, both in the case of experimentally processed samples and in the case of industrially processed samples. Nevertheless, it was possible to process the tested biodegradable material in both laboratory and industrial conditions in up to nine processing cycles, which, from an industrial point of view, means that after preparing the polymer blend it is possible to prepare the filaments and to use them to print an object in four consecutive recurring cycles.

It is positive that, even after partial degradation of the material due to multiple processing, there is no significant change in its thermophysical properties, either in laboratory or industrial conditions. The difference between thermophysical properties (mainly T_g) of experimental and industrial samples was given by the different degradations of the tested material in the process of blending.

There is also no negative impact on the strength characteristics of multiple processed samples. These results correspond with results described in [2], where material recycling of PLA/PHB blends suitable for injection molding were tested.

The results obtained in this work indicate that a biodegradable and biobased polymer blend based on PLA and PHB is a suitable candidate for material recycling even in industrial processing conditions. The largest differences in tested rheological and utility properties between the samples processed under experimental as well as industrial conditions were recorded during the actual blending of the biodegradable polymer blend on the different blending devices. The results of this scientific work suggest that the biodegradable polymeric material NONOILEN® 3D 3056-2 is suitable for multiple uses in FDM technology, which could lead to significant savings in input materials in 3D printing, for example, in the event of defective prints.

Author Contributions: Conceptualization, R.P. (Roderik Plavec); methodology, S.K.; validation, L.D.; formal analysis, L.O., R.P. (Radek Přikryl) and S.F.; investigation, R.P. (Roderik Plavec), V.H., E.M. and A.B.; resources, J.K.; data curation, M.R.; writing—original draft preparation, R.P. (Roderik Plavec) and S.H.; writing—review and editing, S.H. and R.P. (Radek Přikryl); visualization, Z.V.; supervision, P.A.; project administration, R.P. (Roderik Plavec); funding acquisition, J.F. All authors have read and agreed to the published version of the manuscript.

Funding: This work was supported by scientific grants from the Agency for Science and Research of the Slovak Republic APVV 20-0193 and APVV 20-0256 and FCH-S-21-7553 of the Specific University Research Grant, Brno University of Technology. The scientific work was created with the support of the Fillamentum Manufacturing Czech company.

Conflicts of Interest: The authors declare no conflict of interest.

References

1. Plastics Europe. Plastics-the Facts. 2020. Available online: https://www.plasticseurope.org/en/resources/publications/4312-plastics-facts-2020 (accessed on 7 March 2022).
2. Plavec, R.; Hlaváčiková, S.; Omaníková, L.; Feranc, J.; Vanovčanová, Z.; Tomanová, K.; Bočkaj, J.; Kruželák, J.; Medlenová, E.; Gálisová, I.; et al. Recycling possibilities of bioplastics based on PLA/PHB blends. *Polym. Test.* **2020**, *92*, 106880. [CrossRef]
3. Hamad, K.; Kaseem, M.; Deri, F. Recycling of waste from polymer materials: An overview of the recent works. *Polym. Degrad. Stab.* **2013**, *98*, 2801–2812. [CrossRef]

4. Parliament, Directive 2018/852 of the European. Packaging and Packaging Waste. Available online: https://eur-lex.europa.eu/legal-content/EN/TXT/HTML/?uri=CELEX:32018L0852&from=EN (accessed on 7 March 2022).
5. Li, J.; Wu, C.; Chu, P.K.; Gelinsky, M. 3D printing of hydrogels: Rational design strategies and emerging biomedical applications. *Mater. Sci. Eng. R Rep.* **2020**, *140*, 100543. [CrossRef]
6. Cicala, G.; Latteri, A.; Del Curto, B.; Russo, A.L.; Recca, G.; Farè, S. Engineering Thermoplastics for Additive Manufacturing: A Critical Perspective with Experimental Evidence to Support Functional Applications. *J. Appl. Biomater. Funct. Mater.* **2017**, *15*, 10–18. [CrossRef] [PubMed]
7. Kleinfehn, A.P.; Lindemann, J.A.L.; Razvi, A.; Philip, P.; Richardson, K.; Nettleton, K.; Becker, M.L.; Dean, D. Modulating Bioglass Concentration in 3D Printed Poly(propylene fumarate) Scaffolds for Post-Printing Functionalization with Bioactive Functional Groups. *Biomacromolecules* **2019**, *20*, 4345–4352. [CrossRef] [PubMed]
8. Yu, K.; Xin, A.; Du, H.; Li, Y.; Wang, Q. Additive manufacturing of self-healing elastomers. *NPG Asia Mater.* **2019**, *11*, 7. [CrossRef]
9. Ramiah, P.; Du Toit, L.C.; Choonara, Y.E.; Kondiah, P.P.D.; Pillay, V. Hydrogel-Based Bioinks for 3D Bioprinting in Tissue Regeneration. *Front. Mater.* **2020**, *7*, 76. [CrossRef]
10. Chen, S.; Zhang, Q.; Feng, J. 3D printing of tunable shape memory polymer blends. *J. Mater. Chem. C* **2017**, *5*, 8361–8365. [CrossRef]
11. Shin, D.-Y.; Lee, J.S.; Koo, B.-R.; Ahn, H.-J. Hierarchical hybrid nanostructure of 1T-tungsten disulfide quantum dots/multihollow capillary bundle-type mesoporous carbon for ultrafast and ultrastable lithium storage. *Chem. Eng. J.* **2021**, *412*, 15. [CrossRef]
12. Munaz, A.; Vadivelu, R.K.; John, J.S.; Barton, M.; Kamble, H.; Nguyen, N.-T. Three-dimensional printing of biological matters. *J. Sci. Adv. Mater. Devices* **2016**, *1*, 1–17. [CrossRef]
13. Gibson, I.; Rosen, D.W.; Stucker, B. The Use of Multiple Materials in Additive Manufacturing. *Addit. Manuf. Technol.* **2010**, 436–449. [CrossRef]
14. Ligon, S.C.; Liska, R.; Stampfl, J.; Gurr, M.; Mülhaupt, R. Polymers for 3D Printing and Customized Additive Manufacturing. *Chem. Rev.* **2017**, *117*, 10212–10290. [CrossRef]
15. Sanatgar, R.H.; Campagne, C.H.; Nierstrasz, V. Investigation of the adhesion properties of direct 3D printing of polymers and nanocomposites on textiles: Effect of FDM printing process parameters. *Appl. Surf. Sci.* **2017**, *403*, 551–563. [CrossRef]
16. Gupta, N.; Weber, C.; Newsome, S. *Additive Manufacturing: Status and Opportunities*; Science and Technology Policy Institute: Washington, DC, USA, 2012; pp. 1–35.
17. Yao, T.; Ye, J.; Deng, Z.; Zhang, K.; Ma, Y.; Ouyang, H. Tensile failure strength and separation angle of FDM 3D printing PLA material: Experimental and theoretical analyses. *Compos. Part B Eng.* **2020**, *188*, 107894. [CrossRef]
18. Chua, C.K.; Leong, K.F.; Lim, C.S. *Rapid Prototyping: Principles and Applications*, 3rd ed.; World Scientific Publishing Company: Singapore, 2010.
19. Pham, D.; Dimov, S.S. *Rapid Manufacturing: The Technologies and Applications of Rapid Prototyping and Rapid Tooling*; Springer Science & Business Media: Berlin/Heidelberg, Germany, 2012.
20. Wurm, M.C.; Möst, T.; Bergauer, B.; Rietzel, D.; Neukam, F.W.; Cifuentes, S.C.; Von Wilmowsky, C. In-vitro evaluation of Polylactic acid (PLA) manufactured by fused deposition modeling. *J. Biol. Eng.* **2017**, *11*, 29. [CrossRef] [PubMed]
21. Bose, S.; Vahabzadeh, S.; Bandyopadhyay, A. Bone Tissue Engineering Using 3D Printing. *Mater. Today* **2013**, *16*, 496–504. [CrossRef]
22. Chia, H.N.; Wu, B.M. Recent advances in 3D printing of biomaterials. *J. Biol. Eng.* **2015**, *9*, 4. [CrossRef]
23. Abouzaid, K.; Guessasma, S.; Belhabib, S.; Bassir, D.; Chouaf, A. Printability of co-polyester using fused deposition modelling and related mechanical performance. *Eur. Polym. J.* **2018**, *108*, 262–273. [CrossRef]
24. Gebler, M.; Schoot Uiterkamp, A.J.M.; Visser, C. A global sustainability perspective on 3D printing technologies. *Energy Policy* **2014**, *74*, 158–167. [CrossRef]
25. Yadav, D.; Garg, R.K.; Ahlawat, A.; Chhabra, D. 3D printable biomaterials for orthopedic implants: Solution for sustainable and circular economy. *Resour. Policy* **2020**, *68*, 101767. [CrossRef]
26. Pinho, A.C.; Amaro, A.M.; Piedade, A.P. 3D printing goes greener: Study of the properties of post-consumer recycled polymers for the manufacturing of engineering components. *Waste Manag.* **2020**, *118*, 426–434. [CrossRef] [PubMed]
27. Youngjae, B.; Young, T.K. Chapter 14—Bioplastics for Food Packaging: Chemistry and Physics. In *Innovations in Food Packaging*, 2nd ed.; Han, J.H., Ed.; Academic Press: Cambridge, MA, USA, 2014; pp. 353–368.
28. Koller, M. Advances in Polyhydroxyalkanoate (PHA) Production. *Bioengineering* **2017**, *4*, 88. [CrossRef] [PubMed]
29. Abdelwahab, M.A.; Flynn, A.; Chiou, B.S.; Imam, S.; Orts, W.; Chiellini, E. Thermal, mechanical and morphological characterization of plasticized PLA–PHB blends. *Polym. Degrad. Stab.* **2012**, *97*, 1822–1828. [CrossRef]
30. Imre, B.; Pukánszky, B. Compatibilization in bio-based and biodegradable polymer blends. *Eur. Polym. J.* **2013**, *49*, 1215–1233. [CrossRef]
31. Bastioli, C. *Handbook of Biodegradable Polymers*; Walter de Gruyter GmbH & Co. KG: Berlin, Germany, 2020.
32. Van de Velde, K.; Kiekens, P. Biopolymers: Overview of several properties and consequences on their applications. *Polym. Test.* **2002**, *21*, 433–442. [CrossRef]
33. van Wijk, A.J.M.; van Wijk, I. *3D Printing with Biomaterials: Towards a Sustainable and Circular Economy*; IOS Press: Amsterdam, The Netherlands, 2015.

34. Cisneros-López, E.O.; Pal, A.K.; Rodriguez, A.U.; Wu, F.; Misra, M.; Mielewski, D.K.; Kiziltas, A.; Mohanty, A.K. Recycled poly(lactic acid)–based 3D printed sustainable biocomposites: A comparative study with injection molding. *Mater. Today Sustain.* **2020**, *7*, 100027. [CrossRef]
35. Haro, F.B.; Burgo, J.M.D.A.D.; D'Amato, R.; Islán, M.; Heras, E.S.; Alonso, J.M.G.; Mendez, J.A.J. Monitoring an Analysis of Perturbations in Fusion Deposition Modelling (FDM) Processes for the Use of Biomaterials. *J. Med. Syst.* **2019**, *43*, 109. [CrossRef]
36. Corcione, C.E.; Gervaso, F.; Scalera, F.; Padmanabhan, S.K.; Madaghiele, M.; Montagna, F.; Sannino, A.; Licciulli, A.; Maffezzoli, A. Highly loaded hydroxyapatite microsphere/PLA porous scaffolds obtained by fused deposition modelling. *Ceram. Int.* **2018**, *45*, 2803–2810. [CrossRef]
37. Tellis, B.; Szivek, J.; Bliss, C.; Margolis, D.; Vaidyanathan, R.; Calvert, P. Trabecular scaffolds created using micro CT guided fused deposition modeling. *Mater. Sci. Eng. C* **2008**, *28*, 171–178. [CrossRef]
38. Rimington, R.P.; Capel, A.J.; Christie, S.D.; Lewi, M.P. Biocompatible 3D printed polymers via fused deposition modelling direct C 2 C 12 cellular phenotype in vitro. *Lab Chip* **2017**, *17*, 2982–2993. [CrossRef]
39. Singh, B.N.; Panda, N.N.; Mund, R.; Pramanik, K. Carboxymethyl cellulose enables silk fibroin nanofibrous scaffold with enhanced biomimetic potential for bone tissue engineering application. *Carbohydr. Polym.* **2016**, *151*, 335–347. [CrossRef] [PubMed]
40. Jammalamadaka, U.; Tappa, K. Recent Advances in Biomaterials for 3D Printing and and tissue engineering. *J. Funct. Biomater.* **2018**, *9*, 22. [CrossRef] [PubMed]
41. Rojas-Martínez, L.; Flores-Hernandez, C.; López-Marín, L.; Martinez-Hernandez, A.; Thorat, S.; Vasquez, C.R.; Del Rio-Castillo, A.; Velasco-Santos, C. 3D printing of PLA composites scaffolds reinforced with keratin and chitosan: Effect of geometry and structure. *Eur. Polym. J.* **2020**, *141*, 110088. [CrossRef]
42. Zhang, M.; Thomas, N.L. Blending polylactic acid with polyhydroxybutyrate: The effect on thermal, mechanical, and biodegradation properties. *Adv. Polym. Technol.* **2011**, *30*, 67–79. [CrossRef]
43. Chiulan, I.; Frone, A.N.; Brandabur, C.; Panaitescu, D.M. Recent Advances in 3D Printing of Aliphatic Polyesters. *Bioengineering* **2017**, *5*, 2. [CrossRef]
44. Xiao, L.; Wang, B.; Yang, G.; Gauthier, M. Poly (lactic acid)-based biomaterials: Synthesis, modification and applications. *Biomed. Sci. Eng. Technol.* **2012**, *11*, 247–282.
45. Kontárová, S.; Přikryl, R.; Melčová, V.; Menčík, P.; Horálek, M.; Figalla, S.; Plavec, R.; Feranc, J.; Sadílek, J.; Pospíšilová, A. Printability, Mechanical and Thermal Properties of Poly(3-Hydroxybutyrate)-Poly(Lactic Acid)-Plasticizer Blends for Three-Dimensional (3D) Printing. *Materials* **2020**, *13*, 4736. [CrossRef]
46. Upadhyay, R.K.; Mishra, A.K.; Kumar, A. Mechanical Degradation of 3D Printed PLA in Simulated Marine Environment. *Surf. Interfaces* **2020**, *21*, 100778. [CrossRef]
47. Scaffaro, R.; Botta, L.; Passaglia, E.; Oberhauser, W.; Frediani, M.; Di Landro, L. Comparison of different processing methods to prepare poly(lactid acid)-hydrotalcite composites. *Polym. Eng. Sci.* **2013**, *54*, 1804–1810. [CrossRef]
48. Le Marec, P.E.; Ferry, L.; Quantin, J.-C.; Bénézet, J.-C.; Bonfils, F.; Guilbert, S.; Bergeret, A. Influence of melt processing conditions on poly(lactic acid) degradation: Molar mass distribution and crystallization. *Polym. Degrad. Stab.* **2014**, *110*, 353–363. [CrossRef]
49. Tuna, B.; Ozkoc, G. Effects of Diisocyanate and Polymeric Epoxidized Chain Extenders on the Properties of Recycled Poly(Lactic Acid). *J. Polym. Environ.* **2016**, *25*, 983–993. [CrossRef]
50. Lim, J.; You, M.; Li, J.; Li, Z. Emerging bone tissue engineering via Polyhydroxyalkanoate (PHA)-based scaffolds. *Mater. Sci. Eng. C* **2017**, *79*, 917–929. [CrossRef] [PubMed]
51. Chen, G.-Q.; Wu, Q. The application of polyhydroxyalkanoates as tissue engineering materials. *Biomaterials* **2005**, *26*, 6565–6578. [CrossRef] [PubMed]
52. Wang, S.; Capoen, L.; D'hooge, D.R.; Cardon, L. Can the melt flow index be used to predict the success of fused deposition modelling of commercial poly(lactic acid) filaments into 3D printed materials? *Plast. Rubber Compos.* **2018**, *47*, 9–16. [CrossRef]
53. Soroudi, A.; Jakubowicz, I. Recycling of bioplastics, their blends and biocomposites: A review. *Eur. Polym. J.* **2013**, *49*, 2839–2858. [CrossRef]
54. Armentano, I.; Fortunati, E.; Burgos, N.; Dominici, F.; Luzi, F.; Fiori, S.; Jiménez, A.; Yoon, K.; Ahn, J.; Kang, S.; et al. Bio-based PLA_PHB plasticized blend films: Processing and structural characterization. *LWT* **2015**, *64*, 980–988. [CrossRef]
55. Jost, V.; Kopitzky, R. Blending of polyhydroxybutyrate-co-valerate with polylactic acid for packaging applications-reflections on miscibility and effects on the mechanical and barrier properties. *Chem. Biochem. Eng. Q.* **2015**, *29*, 221–246. [CrossRef]
56. Ma, Y.; Li, L.; Wang, Y. Development of PLA-PHB-based biodegradable active packaging and its application to salmon. *Packag. Technol. Sci.* **2018**, *31*, 739–746. [CrossRef]
57. Blumm, E.; Owen, A.J. Miscibility, crystallization and melting of poly(3-hydroxybutyrate)/poly(L-lactide) blends. *Polymer* **1995**, *36*, 4077–4081. [CrossRef]
58. Koyama, N.; Doi, Y. Miscibility of binary blends of poly[(R)-3-hydroxybutyric acid] and poly[(S)-lactic acid]. *Polymer* **1997**, *38*, 1589–1593. [CrossRef]
59. Ohkoshi, I.; Abe, H.; Doi, Y. Miscibility and solid-state structures for blends of poly[(S)-lactide] with atactic poly[(R,S)-3-hydroxybutyrate]. *Polymer* **2000**, *41*, 5985–5992. [CrossRef]
60. Arrieta, M.P.; Lopez, J.; Hernandez, A.; Rayon, E. Ternary PLA-PHB-Limonene blends intended for biodegradable food packaging applications. *Eur. Polym. J.* **2014**, *50*, 255–270. [CrossRef]

61. Arrieta, M.P.; Samper, M.D.; Lopez, J.; Jiménez, A. Combined Effect of Poly(hydroxybutyrate) and Plasticizers on Polylactic acid Properties for Film Intended for Food Packaging. *J. Polym. Environ.* **2014**, *22*, 460–470. [CrossRef]
62. Arrieta, M.; Fortunati, E.; Dominici, F.; López, J.; Kenny, J. Bionanocomposite films based on plasticized PLA–PHB/cellulose nanocrystal blends. *Carbohydr. Polym.* **2015**, *121*, 265–275. [CrossRef] [PubMed]
63. Wang, S.; Ma, P.; Wang, R.; Zhang, Y. Mechanical, thermal and degradation properties of poly(D, L-lactide)/poly(hydroxybutyrate-co-hydroxyvalerate)/poly(ethylene glycol) blend. *Polym. Degrad. Stab.* **2008**, *93*, 1364–1369. [CrossRef]
64. Alexy, P.; Chodák, I.; Bakoš, D.; Bugaj, P.; Pavlacková, M.; Tomanová, K.; Benovic, F.; Plavec, R.; Mihalik, M. Biologically Degradable Polymeric Composition with High Deformability. WO2012141660A1, 11 April 2012. Available online: https://patents.google.com/patent/WO2012141660A1/ (accessed on 7 March 2022).
65. Menčík, P.; Přikryl, R.; Stehnová, I.; Melčová, V.; Kontárová, S.; Figalla, S.; Alexy, P.; Bočkaj, J. Effect of Selected Commercial Plasticizers on Mechanical, Thermal, and Morphological Properties of Poly(3-hydroxybutyrate)/Poly(lactic acid)/Plasticizer Biodegradable Blends for Three-Dimensional (3D) Print. *Materials* **2018**, *11*, 1893. [CrossRef]
66. Fuentes, M.A.V.; Thakur, S.; Wu, F.; Misra, M.; Gregori, S.; Mohanty, A.K. Study on the 3D printability of poly(3-hydroxybutyrate-co-3-hydroxyvalerate)/poly(lactic acid) blends with chain extender using fused filament fabrication. *Sci. Rep.* **2020**, *1*, 10.
67. Ausejo, J.G.; Rydz, J.; Musioł, M.; Sikorska, W.; Janeczek, H.; Sobota, M.; Wlodarczyk, J.; Szeluga, U.; Hercog, A.; Kowalczuk, M. Three-dimensional printing of PLA and PLA/PHA dumbbell-shaped specimens of crisscross and transverse patterns as promising materials in emerging application areas: Prediction study. *Polym. Degrad. Stab.* **2018**, *156*, 100–110. [CrossRef]
68. Lazarevic, D.; Aoustin, E.; Buclet, N.; Brandt, N. Plastic waste management in the context of a European recycling society: Comparing results and uncertainties in a life cycle perspective. *Resour. Conserv. Recycl.* **2010**, *2*, 246–259. [CrossRef]
69. Perugini, F.; Mastellone, M.L.; Arena, U. A life cycle assessment of mechanical and feedstock recycling options for management of plastic packaging wastes. *Environ. Prog.* **2005**, *2*, 246–259. [CrossRef]
70. Piemonte, V. Bioplastic Wastes: The Best Final Disposition for Energy Saving. *J. Polym. Environ.* **2011**, *19*, 988–994. [CrossRef]
71. Arena, U.; Mastellone, M.L.; Perugini, F. Life Cycle assessment of a plastic packaging recycling system. *Int. J. Life Cycle Assess.* **2003**, *8*, 92–98. [CrossRef]
72. Fisher, M. Plastics recycling. In *Plastics and the Environment*; John Wiley & Sons, Inc.: Hoboken, NJ, USA, 2003.
73. Al-Salem, S.M.; Lettieri, P.; Baeyens, J. Recycling and recovery rotes of plastic solid waste: A review. *Waste Manag.* **2009**, *10*, 2625–2643. [CrossRef]
74. Hopewell, J.; Dvorak, R.; Kosior, E. Plastics recycling: Challenges and opportunities. *Philos. Trans. R. Soc. B Biol. Sci.* **2009**, *364*, 2115–2126. [CrossRef] [PubMed]
75. Hatti-Kaul, R.; Nilsson, L.J.; Zhang, B.; Lundmark, S. Designing Biobased Recyclable Polymers for Plastics: A Review. *Trends Biotechnol.* **2020**, *1*, 50–67. [CrossRef] [PubMed]
76. Mantia, F.L.A. *Handbook of Plastics Recycling*; iSmithers Rapra Publishing, Rapra Technology Limited: Shropshire, UK, 2002.
77. Żenkiewicz, M.; Kurcok, M. Effects of compatibilizers and electron radiation on thermomechanical properties of composites consisting of five recycled polymers. *Polym. Test.* **2008**, *27*, 420–427. [CrossRef]
78. European Commission. *Communication from the Commission to the European Parliament, the Council, the European Economic and Social Committee and the Committee of the Regions A European Strategy for Plastics in a Circular Economy*; COM/2018/028; European Commission: Brussels, Belgium, 2019.
79. Hinsken, H.; Moss, S.; Pauquet, J.-R.; Zweifel, H. Degradation of polyolefins during melt processing. *Polym. Degrad. Stab.* **1991**, *34*, 279–293. [CrossRef]
80. Kometani, H.; Matsumura, T.; Suga, T.; Kanai, T. Quantitative Analysis for Polymer Degradation in the Extrusion Process. *Int. Polym. Process.* **2006**, *21*, 24–31. [CrossRef]
81. Hu, H.; Zhang, R.; Kong, Z.; Wang, K.; Ying, W.B.; Wang, J.; Zhu, J. Bio-based poly(butylene furandicarboxylate)-b-poly(ethylene glycol) copolymers: The effect of poly(ethylene glycol) molecular weight on thermal properties and hydrolysis degradation behavior. *Adv. Ind. Eng. Polym. Res.* **2019**, *2*, 167–177. [CrossRef]
82. Sawaguchi, T.; Sasaki, D.; Takamura, A. On the entanglement-based mechanism in thermal degradation of vinyl polymers. *Polym. Degrad. Stab.* **2019**, *169*, 108990. [CrossRef]
83. FBeltrán, R.; Lorenzo, V.; Acosta, J.; de la Orden, M.U.; Urreaga, J.M. Effect of simulated mechanical recycling processes on the structure and properties of poly(lactic acid). *J. Environ. Manag.* **2018**, *216*, 25–31. [CrossRef]
84. Beltrán, F.R.; Infante, C.; de la Orden, M.U.; Urreaga, J.M. Mechanical recycling of poly(lactic acid): Evaluation of a chain extender and a peroxide as additives for upgrading the recycled plastic. *J. Clean. Prod.* **2019**, *219*, 46–56. [CrossRef]
85. Żenkiewicz, M.; Richert, J.; Rytlewski, P.; Moraczewski, K.; Stepczyńska, M.; Karasiewicz, T. Characterisation of multi-extruded poly(lactic acid). *Polym. Test.* **2009**, *28*, 412–418. [CrossRef]
86. Pillin, I.; Montrelay, N.; Bourmaud, A.; Grohens, Y. Effect of thermo-mechanical cycles on the physico-chemical properties of poly(lactic acid). *Polym. Degrad. Stab.* **2008**, *93*, 321–328. [CrossRef]
87. Badia, J.D.; Strömberg, E.; Karlsson, S.; Ribes-Greus, A. Material valorisation of amorphous polylactide. Influence of thermo-mechanical degradation on the morphology, segmental dynamics, thermal and mechanical performance. *Polym. Degrad. Stab.* **2012**, *97*, 670–678. [CrossRef]

88. Agüero, A.; Morcillo, M.d.C.; Quiles-Carrillo, L.; Balart, R.; Boronat, T.; Lascano, D.; Torres-Giner, S.; Fenollar, O. Study of the Influence of the Reprocessing Cycles on the Final Properties of Polylactide Pieces Obtained by Injection Molding. *Polymers* **2019**, *11*, 1908. [CrossRef] [PubMed]
89. Rivas, L.F.; Casarin, S.A.; Cavalcante, N.; Alencar, M.I.; Agnelli, J.A.M.; de Medeiros, E.S.; de Oliveira Wanderley Neto, A.; de Oliveira, M.P.; de Medeiros, A.M.; Ferreira e Santos, A.S. Reprocessability of PHB in extrusion: ATR-FTIR, tensile tests and thermal studies. *Polímeros* **2017**, *27*, 122–128. [CrossRef]
90. Mikušová, M.; Mihalík, M.; Alexy, P.; Tomanová, K.; Plavec, R.; Bočkaj, J.; Vanovčanová, Z. *Method for Testing of Processing Stability of Biodegradable Polyesters Based on Oscillation Rheometry*; Kautschuk Gummi Kunstoffe: Heidelberg, Germany, 2014; Volume 67, pp. 51–54.
91. Ma, Y.; Zhang, W.; Wang, Z.; Wang, Z.; Xie, Q.; Niu, H.; Guo, H.; Yuan, Y.; Liu, C. PEGylated poly(glycerol sebacate)-modified calcium phosphate scaffolds with desirable mechanical behavior and enhanced osteogenic capacity. *Acta Biomater.* **2016**, *44*, 110–124. [CrossRef]
92. Wang, Z.; Ma, A.; Wang, Y.X.; Liu, Y.; Chen, K.; Wu, K.; Yu, S.; Yuan, Y.; Liu, C. Urethane-based low-temperature curing, highly-customized and multifunctional poly (glycerol sebacate)-co-poly (ethylene glycol) copolymers. *Acta Biomater.* **2018**, *71*, 279–292. [CrossRef]

polymers

MDPI

Article

FDM 3D Printed Composites for Bone Tissue Engineering Based on Plasticized Poly(3-hydroxybutyrate)/poly(D,L-lactide) Blends

Veronika Melčová [1,*], Kateřina Svoradová [1], Přemysl Menčík [1], Soňa Kontárová [1], Michala Rampichová [2], Věra Hedvičáková [2], Věra Sovková [2], Radek Přikryl [1] and Lucy Vojtová [3,*]

1 Institute of Material Chemistry, Faculty of Chemistry, Brno University of Technology, Purkyňova 464/118, 612 00 Brno, Czech Republic; xcsvoradova@vutbr.cz (K.S.); mencik@fch.vut.cz (P.M.); kontarova@fch.vut.cz (S.K.); prikryl@fch.vut.cz (R.P.)

2 Institute of Experimental Medicine, Czech Academy of Sciences, Vídeňská 1083, 142 20 Prague 4, Czech Republic; Michala.rampichova@iem.cas.cz (M.R.); vera.lukasova@iem.cas.cz (V.H.); vera.sovkova@iem.cas.cz (V.S.)

3 CEITEC—Central European Institute of Technology, Brno University of Technology, Advanced Biomaterials, Purkyňova 656/123, 612 00 Brno, Czech Republic

* Correspondence: xcmelcova@fch.vutbr.cz (V.M.); lucy.vojtova@ceitec.vutbr.cz (L.V.); Tel.: +420-774-564-737 (V.M.); +420-541-149-832 (L.V.)

Received: 31 October 2020; Accepted: 23 November 2020; Published: 27 November 2020



Abstract: Tissue engineering is a current trend in the regenerative medicine putting pressure on scientists to develop highly functional materials and methods for scaffolds' preparation. In this paper, the calibrated filaments for Fused Deposition Modeling (FDM) based on plasticized poly(3-hydroxybutyrate)/poly(D,L-lactide) 70/30 blend modified with tricalcium phosphate bioceramics were prepared. Two different plasticizers, Citroflex (*n*-Butyryl tri-*n*-hexyl citrate) and Syncroflex (oligomeric adipate ester), both used in the amount of 12 wt%, were compared. The printing parameters for these materials were optimized and the printability was evaluated by recently published warping test. The samples were studied with respect to their thermal and mechanical properties, followed by biological in vitro tests including proliferation, viability, and osteogenic differentiation of human mesenchymal stem cells. According to the results from differential scanning calorimetry and tensile measurements, the Citroflex-based plasticizer showed very good softening effect at the expense of worse printability and unsatisfactory performance during biological testing. On the other hand, the samples with Syncroflex demonstrated lower warping tendency compared to commercial polylactide filament with the warping coefficient one third lower. Moreover, the Syncroflex-based samples exhibited the non-cytotoxicity and promising biocompatibility.

Keywords: additive manufacturing; fused deposition modeling; poly(3-hydroxybutyrate); polylactide; tricalcium phosphate; regenerative medicine; tissue engineering; bone scaffolds

1. Introduction

Skeletal damage is among the most common health issues, mostly originating from osteoporosis and traumatic fractures [1,2]. A huge effort of scientists and commercial sector is applied to an investigation of new efficient and patient friendly treatment methods, such as tissue engineering.

Tissue engineering (TE) is one of the modern concepts in regenerative medicine. This multi-disciplinary approach connects the knowledge from the fields of medicine and biology with material sciences. In TE, the scaffold as a supportive material, which may be seeded with cells and/or other supplementary

factors, is prepared in vitro and used as an implant for affected tissue regeneration. In orthopedics, TE finds application when the extent of the bone injury excludes the self-healing by natural processes of ossification. At the same time, it should offer superior performance to other methods of regenerative medicine exploited in such cases, as the bone autographs or allografts [3–6].

A suitable 3D structure needs to be ensured so that the entire interior of a scaffold is accessible for cells' migration regardless of whether the material is cultivated with cells in vitro or the cells originate from the patient's body [7]. Polymeric scaffolds for tissue engineering with such 3D structures can be technologically prepared in several ways, such as by casting a solution or a melt into molds, by lyophilization, foaming, eluting porogenic particles, or by various spinning techniques [7–10]. Currently, a relatively new fabrication method of 3D printing (known as additive manufacturing) is also being successfully used. 3D printed product is created layer by layer according to an accurate digital 3D model. Hence the biggest advantage of this method is the ability to produce time and cost effectively complex shapes, including porous internal structures [11].

There are several 3D printing techniques which use different types of input materials and are reviewed elsewhere [12]. For the preparation of scaffolds for bone tissue replacement, the use of Selective Laser Sintering (SLS) method, where a powder is fusioned by laser beam, was published [13–15]. 3D printing technique used in this article is based on the Fused Deposition Modeling (FDM) in which a plastic filament of exact diameter is led to a heated nozzle, where it is melted and extruded onto a substrate, where it forms the first layer of formed object. This method becomes increasingly popular mainly due to its low cost, high speed, and simplicity [16–18]. Common materials for FDM printers are mainly polylactide (PLA) and acrylonitrile butadiene styrene (ABS), but other conventional polymers, composites and biopolymers are also getting more attention at present [19–22].

Disk shaped scaffolds were successfully prepared by FDM from semi-crystalline PLA and seeded with human fetal osteoblasts. According to the authors, FDM has not affected the biocompatibility of PLA in any way, although the cell growth was more pronounced in the control sample (polystyrene) than in PLA. This may be related to the resulting surface of the scaffold, which was not optimized in this work [23]. The first studies focusing on FDM 3D printing of biodegradable polyhydroxyalkanoates (PHA) have also appeared. PHA are a group of microbial polyesters which are biocompatible and biodegradable and therefore promising candidates for a scaffold material [24,25]. Recently, FDM printed scaffolds from poly(3-hydroxybutyrate-*co*-3-hydroxyhexanoate) (PHBH) were evaluated regarding their thermal, rheological, and mechanical properties. In addition, their cytocompatibility with mouse embryonic fibroblast cells and the biodegradation in synthetic gastric juice were tested, showing overall better results than PLA scaffolds [26]. Moreover, poly(3-hydroxybutyrate-3-hydroxyvalerate) (PHBV) another widely studied representative of PHA group, was blended with PLA and used for 3D printing of dumbbell specimens for mechanical tests. The material was shown to be non-toxic toward human embryonic kidney cells and normal human lung fibroblasts [27].

With a great success, composite materials combining the advantage of easy polymer processability and ceramic filler bioactivity are often investigated for TE scaffolds. Hydroxyapatite (HA), natural inorganic component of bone, and tricalcium phosphate (TCP) are two most abundant examples. These illers were reported to be applicable for FDM 3D printing in PLA [28] or polycaprolactone (PCL) matrix [29–31]. Although HA has the closest chemical structure to that of a bone mineral, it is the least soluble of calcium phosphate ceramics used. Moreover, stochiometric HA is osteoconductive, but not osteoinductive unlike TCP, which possesses both these properties. At the same time, TCP is more soluble and therefore its biosorption is faster [32]. Konopnicky et al. studied 3D printed constructs made from TCP filled PCL (50 wt.% of the filler) seeded with porcine bone marrow progenitor cells to treat man-made mandible defects in minipigs. Eight weeks after the surgery, the seeded scaffolds showed better bone penetration depth than the controls [30].

With this article we wish to contribute to the common goal of improvement of current treatment methods by exploiting functional, biodegradable polymers and additives and state-of-the-art preparation method. The goal is to develop a material with suitable thermal and mechanical

properties to be processed by FDM 3D printing method. At the same time, this material has to meet all the conditions for being used in vivo in tissue engineering of bones namely to be osteoconductive, osteoinductive, osteogenic, resorbable or degradable [3,6]. To achieve this, we used the following materials: (i) poly(3-hydroxybutyrate) (PHB), the most published and commercially successful PHA polymer, which has all the above-mentioned features of PHA family; (ii) amorphous PLA, which contributes to the processability and mechanical properties of the resulting material; (iii) plasticizers varying in molecular weight and chemical structure to further improve overall properties and printability; and (iv) TCP to promote a good response of the materials in vivo. Our research group drawn from its unique experience with FDM 3D printing of PHB/PLA blends [33,34].

2. Materials and Methods

2.1. Preparation of Composites

Four composite samples based on plasticized blend of poly(3-hydroxybutyrate) Y1000P from TianAn Biologic Materials (Ningbo City, China, abbreviated PHB) and amorphous poly(D,L-lactide) Ingeo 4060D from NatureWorks (Minnetonka, MN, USA, abbreviated PLA) were used for all studies. Citroflex®B-6 (*n*-Butyryl tri-*n*-hexyl citrate, abbreviated as CT) from Vertellus Holdings LLC Company (Indianapolis, IN, USA) and Syncroflex TM 3114 (oligomeric adipate ester, referred as abbr. SN) from Croda (Rawcliff, UK) were used as plasticizers. Tricalcium phosphate blend (αTCP = 7%, βTCP = 93%, abbr. TCP) (CN Lab Nutrition, Shaanxi, China) was added to the matrix as a bioactive filler. The mean particle size of TCP is 10.8 μm as measured by laser diffraction using HELOS analyzer by Sympatec GmbH (Remlingen, Germany).

The composition of prepared biocomposites is given by Table 1. All samples were compounded using the corotating meshing twin screw extruder, from Labtech Engineering Company (Samutprakarn, Thailand, D = 16 mm, and L/D = 40). The temperature setting of individual zones of the extruder was 160–175–175–175–175–175–175–170–165–160 °C from a hopper to a nozzle and the rotational speed of screw was set to 130 rev.·min^{-1}. The total weight of each sample for extrusion was 500 g.

Table 1. The composition of prepared samples: the basic mixture is composed of 12% of plasticizer and the remaining 88% is PHB/PLA in the ratio of 70/30. For filled samples, 15 wt.% of TCP is added to the mixture.

	Amount (wt.%)				
Sample	**PHB**	**PLA**	**Citroflex**	**Syncroflex**	**TCP**
PHB/PLA-CT	62	26	12	0	0
PHB/PLA-CT_TCP	54	23	10	0	13
PHB/PLA-SN	62	26	0	12	0
PHB/PLA-SN_TCP	54	23	0	10	13

2.2. Thermal Characterization

2.2.1. Differential Scanning Calorimetry

Differential scanning calorimetry (DSC) measurements were performed on DSC 2500 (TA Instruments, New Castle, DE, USA). The samples were subjected to two heating runs from 10 to 195 °C with the heating rate of 10 °C·min^{-1}. All measurements were carried out under the nitrogen atmosphere. The polymer sample masses were approximately 10 mg. Aluminum pans with samples were hermetically sealed before the measurement. The crystallinity was calculated from DSC measurement according the equation:

$$X_c = \frac{\Delta H_m}{\Delta H_m^0} \cdot 100\%, \quad (1)$$

where ΔH_m, and $\Delta H^0{}_m$ (J/g) are the enthalpy of fusion from the second heating cycle and the enthalpy of fusion of 100% crystalline polymer (146 J/g for PHB), respectively.

2.2.2. Thermogravimetric Analysis

The curves from thermogravimetric analysis (TGA) were obtained using Q500 TG analyzer (TA Instruments, New Castle, DE, USA). After the equilibration at 40 °C, the samples were heated to 550 °C at the heating rate of 10 °C·min^{-1} under nitrogen atmosphere. Subsequently, the temperature ramp continued to 600 °C at the same heating rate under air atmosphere.

2.3. Preparation of 3D Printing Filaments

Granules prepared in the first step were processed using the HAAKE™ Rheomex OS single screw extruder (Haake Technik GmbH, Vreden, Germany) into the form of 3D printing filaments. The chamber temperature profile from a hopper to a nozzle was set to 185–175–170–150 °C and the rotational speed of screw was kept 25 rev.·min^{-1}. The filament was firstly pulled into the water tank tempered to 60 °C. Secondly, the filament was directed to the draw-off device with the calibration unit in order to ensure a constant diameter of the filament of 1.75 mm.

2.4. 3D Printing and Printability Tests

Original Prusa i3 MK3 3D printer (Prusa Research, Prague, Czech Republic) was used for all studies. Maximum printing space of this printer is 250 × 210 × 200 mm ($x \times y \times z$), the resolution of x and y axes is 10 µm and the resolution of z axis is 5 µm. The basic printing parameters of used printer are given in Table 2.

Table 2. Basic printing parameters of used 3D printer.

Filament diameter	1.75 mm
Nozzle diameter	0.4 mm
Layer height	0.2 mm
Width of printed layer	0.45 mm
Perimeter printing speed	45 mm·s^{-1}
Fill print speed	200 mm·s^{-1}
Bed temperature	20 °C
Cooling fan power	100%

Prepared biocomposites underwent the tests especially designated by our research group for the purpose of evaluating the printability. Firstly, the temperature of the nozzle was optimized by the Temperature Tower Test (TTT). In this test, two towers composed of several identical floors containing different geometrical elements are used. Each floor is printed with different temperature, which allows us to visually evaluate the quality of the print and the optimal printing temperature. Further details can be found in our previous publication [33].

Afterwards, the filling study aiming at proper setting of the parameter flow—volume passed through the extruder, was conducted to ensure optimal density and compactness of 3D printed specimens and therefore meaningful mechanical properties. A crucial factor to which an attention must be paid is the filament diameter. If the diameter is higher than desired 1.75 mm, the printer feeds excessive material which leads to the deterioration of mechanical properties and specimen surface or even to nozzle clogging. Opposite to this, thinner filament will cause the specimen to be underfilled with voids between individual perimeters. Such a sample will not be sintered properly which will manifest during the mechanical tests. Therefore, three samples (bars with dimensions of 30 × 10 × 4 mm) with different setting of flow value were printed. Typically, 95, 100 and 105% of flow was used for all samples and a broader range was studied when necessary. Samples were frozen (−18 °C) and observed using SZ51 optical microscope from Olympus (Tokyo, Japan).

Last but not least, warping—a negative phenomenon occurring during 3D printing was quantified using the printing conditions optimized by previous tests (two temperatures and one value of flow). In the warping test, the specimen consists of square platform on which a V-shaped beam adhering to bed only by its edge is connected. During printing, warping causes the front part beam to lift and detach from the bed. The maximum printed height before this happens is recorded and used for the calculation of the warping coefficient:

$$warping\ coefficient = \frac{theoretical\ height\ of\ warping\ test\ specimen\ (10\ \text{mm})}{height\ of\ warping\ test\ specimen\ achieved\ during\ printing} \quad (2)$$

The test is thoroughly described in our previous publication [33]. The results are shown as mean ± standard deviation (SD) from five testing specimens.

2.5. Mechanical Testing

2.5.1. Tensile Test

Standardized double-paddle testing specimens (dogbones 5A with cross section 4 × 2 mm, according to the CSN EN ISO 527) were 3D printed from prepared filaments. The G-code for printing the dogbones was made by regular alternating of two layers (i) the first layer is formed by simple import of fabricated model to original PrusaSlicer software (Prusa Research, Prague, Czech Republic) with adjusting the perimeters to form the entire neck of the dogbone and (ii) the second layer is formed manually by inserting infill parallel to the longest dimension of the dogbone. The development of this G-code is described in our previous work [34]. The Zwick-Roel Z010 (ZwickRoell GmbH & Co., Ulm, Germany) device with load indicator of maximum tensile force 1 kN and pneumatic grips with 2.5 kN maximum gripping force were used for the measurements. The deformation rates for the determination of Young's elastic modulus and for the rest of the test were set to 5 mm·min^{-1} and 50 mm·min^{-1}, respectively. However, the Young's modulus was determined without the extensometer. All measurements were carried out 10 days after the sample preparation to ensure that the material aging process after the preparation is finished. The elongation at break, the Young´s modulus, and the tensile strength were determined as the average of at least six measurements, and the results are shown as mean ± SD.

2.5.2. Flexure Test

The three-point bending test of studied materials was performed according to the CSN EN ISO 178 standard method A. Rectangular testing specimens with dimensions of 80 × 10 × 4 mm were 3D printed from prepared filaments. The G-code for 3D printing was created in original PrusaSlicer software (Prusa Research, Prague, Czech Republic) so that the entire volume of the specimen was composed from perimeters. The Zwick-Roel Z010 (ZwickRoell GmbH & Co., Ulm, Germany) device with load indicator of maximum force 1 kN was used for the measurements. The radius of loading nose and supports was 5 mm, the support span was 64 mm. The flexural modulus was determined from the deformation range of 0.05–0.25%. The test speed was set to 2 mm·min^{-1}. A limit deformation of 5% was also set. The results in the graph are mean average from six samples with error bars from SD.

2.6. In Vitro Tests on Scaffolds

The granules of prepared composites were compression molded in a laboratory hot press to obtain plates with the thickness of approximately 1 mm. Round specimens with the diameter of 6 mm were cut off from these plates for 96 well plates (MTS assay, DNA quantification, ALP activity measurement) and with the diameter of 10 mm for 48 well plates (confocal microscopy and PCR analysis). Prepared scaffolds were sterilized (Military University Hospital Prague) with ethylene dioxide and seeded with human mesenchymal stem cells (hMSC, Sciencell, Carlsbad, CA, USA). To enhance an osteogenic differentiation of cells, used culture medium contained Eagle's minimal essential medium (α-MEM)

with 10% of fetal bovine serum (FBS), 1% of penicillin/streptomycin, 100 nM of dexamethasone, 10 mM of β-glycerol phosphate and 50 μg·mL^{-1} of ascorbic acid-2-phosphate. Cells were seeded in the density of 100 × 10^3 hMCS in 125 μL of culture medium on 48 well plate and 15 × 10^3 hMSC in 41 μL of culture medium on 96 well plates. After two hours of adhesion, the medium was filled to the volume of 750 μL in the case of 48 well plate and 250 μL in the case of 96 well plate. hMSCs were seeded also on the bottom of the 96 well plates for some assays (tissue culture polystyrene abbreviated PS). Half of the medium was changed every week. MTS test, DNA quantification, osteogenic differentiation quantification and visualization of cells were conducted after 1, 7, 14, 21, and 28 days of the experiment.

2.6.1. Metabolic Activity Assay

The scaffolds were transferred to the clean plates and 100 μL of growth medium (without osteogenic supplements) and 20 μL of MTS substrate((3-(4,5-dimethylthiazol-2-yl)-5-(3-carboxy-methoxyphenyl)-2 -(4-sulfo-phenyl)-2H-tetrazolium) (Sigma Aldrich, St. Louis, MO, USA) was added. After two hours of incubation at 37 °C, the amount of formazan formed by metabolizing the MTS substrate was determined spectrophotometrically from 100 μL transferred to a new well plate. The absorbance of the solutions was measured at 490 nm with 690 nm as a reference wavelength using the microplate reader Infinite®M200 PRO from Tecan (Männedorf, Switzerland). The absorbance of the MTS solution incubated with scaffolds without seeded cells was subtracted from the values.

2.6.2. DNA Quantification

The proliferation of the cells on scaffolds was determined using DNA quantification. After MTS measurement, the scaffolds were transferred into 200 μL of lysis buffer composed of 10 mM tris(hydroxymethyl) aminomethane (Tris), 1mM ethylenediamine-tetraacetic acid (EDTA), 0.2% Triton-X-100 and distilled water. Subsequently, the samples were subjected to three freeze/thaw cycles, between which the samples were roughly vortexed. 200 μL of Quant-iT™ dsDNA Assay Kit reagent and 10 μL of cell lysate were added to 96 well plate. The fluorescence of the reagent after the reaction with DNA from the lysate was measured using the multiplate fluorescence reader Infinite®M200 PRO from Tecan (Männedorf, Switzerland) at λ_{ex} = 485 nm and λ_{em} = 528 nm. The DNA content was determined according to the calibration curve using the standards in the kit.

2.6.3. Cell Visualization

The fluorescent staining and confocal microscopy were used for the cell visualization. The samples were fixed with frozen methyl alcohol (−20 °C) for 10 min and rinsed with phosphate buffered saline (PBS, pH 7,4). Afterwards, the samples were incubated with DiOC6(3) (3,3'-diethyl-hexacarbocyanine iodide, Invitrogen, Molecular Probes, 1 μg·mL^{-1} in PBS) at room temperature for 45 min. For the nuclei visualization, the incubation of samples with propidium iodide (Sigma Aldrich, St. Louis, MO, USA, 5 μg·mL^{-1} in PBS) followed. Subsequently, the samples were rinsed with PBS three times and observed using the LSM 5 DUO confocal microscope Zeiss (Oberkochen, Germany). Used wavelengths were λ_{ex} = 488 nm and λ_{em} = 520 nm in the case of DiOC6(3) and λ_{ex} = 560 nm and λ_{em} = 580 nm in the case of propidium iodide.

2.6.4. Alkaline Phosphatase Activity

Alkaline phosphatase (ALP), being an early marker of osteogenic differentiation, was determined on days 1, 7, 14, and 21 of the experiment. The scaffolds were rinsed in PBS and incubated at room temperature for 30 min with 100 μL of ALP substrate (p-nitrophenyl phosphate liquid substrate system; Sigma Aldrich, St. Louis, MO, USA). After 30 min, the reaction was stopped by adding 50 μL of 2M NaOH and the amount of produced p-nitrophenol was determined by measuring the absorbance at 405 nm with the microplate reader Infinite®M200 PRO from Tecan (Männedorf, Switzerland). The absorbance of ALP substrate incubated with scaffolds without seeded cells was subtracted from the values.

2.6.5. Osteogenic Differentiation Analysis

The samples were transferred to a 1.5 mL test tube with lysis buffer (RLT buffer) and crushed with a tweezer. RNA of the samples was isolated using the Qiagen RNeasy Mini Kit (Hilden, Germany) according to the manufacturer's protocol. The RNA concentration was determined spectrophotometrically as the absorbance at 260/280 nm with the microplate reader Infinite®M200 PRO from Tecan (Männedorf, Switzerland). Subsequently, cDNA was synthetized using the RevertAid H Minus First Strand cDNA Synthesis Kit from Thermo Scientific (Waltham, MA, USA). The real-time polymer chain reaction (RT-PCR) was performed to multiply the amount of cDNA. The gene sequences for osteogenic markers RunX2 (86 bp, RUNX2, Hs01047973_m1, Thermo Scientific), type I collagen (66 bp, COL1A1 Hs00164004_m1,Thermo Scientific), osteocalcin (138 bp, BGLAP Hs01587814_g1, Thermo Scientific) and the reference gene (eukaryotic elongation factor, EEF-1, Hs00265885_g1, Thermo Scientific) as well were quantified using the TaqMan Mater Mix and TaqMan probes. The fluorescence intensity was measured with the Light Cycler 480 from Roche (Basel, Switzerland). The thermo cycling parameters were 95 °C for 10 min; 95 °C for 10 s, 60 °C for 10 s (45 cycles); and 40 °C for 1 min. All samples were scaled relative to the median of the EEF1 expression level. The gene expression data were analyzed using the $2^{(-\Delta Ct)}$ method (relative quantification). Also, hMSCs prior to seeding on the scaffolds (day 0) and hMSCs cultured in differentiation medium seeded on the bottom of the wells (PS) were evaluated.

2.6.6. Immunohistochemical Staining

Based on the previous results, PHB/PLA-SN and PHB/PLA-SN_TCP samples were selected for immunohistochemical staining. Osteocalcin and type I collagen were visualized using indirect immunofluorescence staining on days 14, 21, and 28 and on days 14 and 21, respectively. The samples were firstly rinsed in PBS and fixed with frozen methyl alcohol (−20 °C) for 10 min. Secondly, they were rinsed in PBS and incubated in the solution containing 0.1% of Triton-X-100 (Sigma Aldrich, St. Louis, MO, USA) and 1% of bovine serum albumin (BSA) in PBS. Afterwards, the samples were incubated over night at 4 °C with primary rabbit antibody in the case of osteocalcin (rabbit anti-osteocalcin IgG, Peninsula Laboratories, dilution 1:20, San Carlos, CA, USA) or mouse antibody in the case of type I collagen (mouse anti-collage type I IgG, DSHB, dilution 1:20, Iowa city, IA, USA) determination. Incubated samples were rinsed with PBS with 0.05% of Tween-20 (Sigma Aldrich, St. Louis, MO, USA) for 5, 10 and 15 min. Subsequently, the samples were rinsed in PBS and supplemented with respective secondary antibodies containing Alexa Fluor 488 fluorophore (goat anti-mouse, Biotech; goat anti-rabbit, LifeTechnologies, OR, USA). The incubation in the dark at laboratory temperature took 45 min. Rinsing with PBS with 0.05% of Tween-20 for 5, 10 and 15 min followed. Afterwards, the samples were rinsed with PBS, incubated for 5 min with propidium iodide (5 $\mu g \cdot mL^{-1}$) and rinsed with PBS three times. The Zeiss LSM 5 DUO was used for imagining with the wavelengths set to λ_{ex} = 488 nm and λ_{em} = 520 nm for Alexa fluor 488 and λ_{ex} = 560 nm and λ_{em} = 580 nm for propidium iodide.

2.6.7. Statistical Analysis

Data obtained from DNA test and MTS quantification were tested in the SigmaStat 3.5 software (Systat Software, Inc., San Jose, CA, USA). The one-way analysis of variance (ANOVA) and the Tukey/Student-Newman-Keuls methods were used. The level of significance was set at lower than 0.05 or lower than 0.001 (indicated by * in the graphs).

3. Results

3.1. Thermal Properties of Prepared Materials

The study of thermal properties of prepared materials was performed by DSC measurements. DSC scans of first cooling cycle and second heating cycle are depicted in Figure 1 and measured values are listed in Table 3.

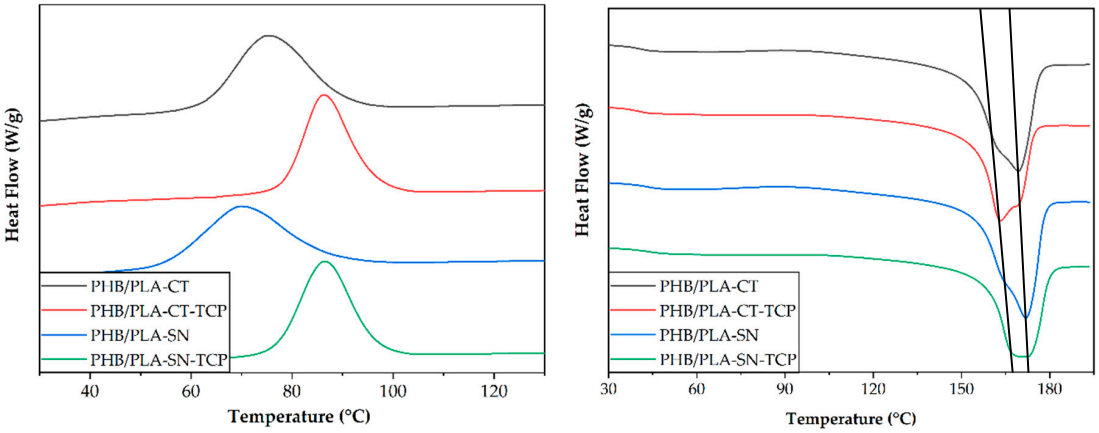


Figure 1. First cooling and second heating DSC scans of prepared materials.

Table 3. Thermal properties of tested materials.

	Glass Transition Temperature PLA T_g (°C)	Crystallization Temperature PHB T_{c1} (°C)	Melting Temperature PHB T_{m2} (°C)	Crystallinity PHB X_{c1}
PHB/PLA-CT	42.8	75.6	169.3	59.9
PHB/PLA-CT_TCP	41.1	86.3	163.3	56.7
PHB/PLA-SN	40.8	69.8	171.9	61.1
PHB/PLA-SN_TCP	42.3	86.6	169.9	59.1

As can be seen from the cooling scan, the crystallization temperature (PHB T_{c1}) of both composite samples (PHB/PLA-CT_TCP and PHB/PLA-SN_TCP) is higher than in the case of non-filled plasticized PHB/PLA blend. The increase in crystallization temperature due to nucleation effect of TCP is from 76 to 86 °C for Citroflex and from 70 to 87 °C for Syncroflex. The melting curves of all samples exhibited a double peak typical for PHB. The Citroflex-based samples had lower melting temperature (PHB T_{m2}) than the Syncroflex-based samples and the temperature decreased further with TCP addition to 163 °C for PHB/PLA-CT_TCP. The crystallinity calculated according to the equation (1) lying in the range of 56–61%, is the lowest for the sample PHB/PLA-CT_TCP.

In the blend of highly crystalline PHB and amorphous PLA, the plasticizer is expected to be located in the amorphous, PLA enriched phase. Therefore, the plasticizer is supposed to affect the glass transition of PLA (PLA T_g). In all samples, the PLA T_g was in the range of 41–43 °C, not affected by the presence of TCP.

3.2. Thermal Stability of Prepared Composites

The resulting TGA curves are shown in Figure 2 and the degradation temperatures in Table 4. As you can see from the figure, all samples had two-step decomposition, the first step corresponding to PHB and the second one to PLA decomposition. No visible step corresponding to the plasticizer is visible as both plasticizers decompose together with the polymers. However, at approximately 250 °C the samples with Citroflex show a greater weight loss than the samples with Syncroflex indicating that this plasticizer is more volatile.

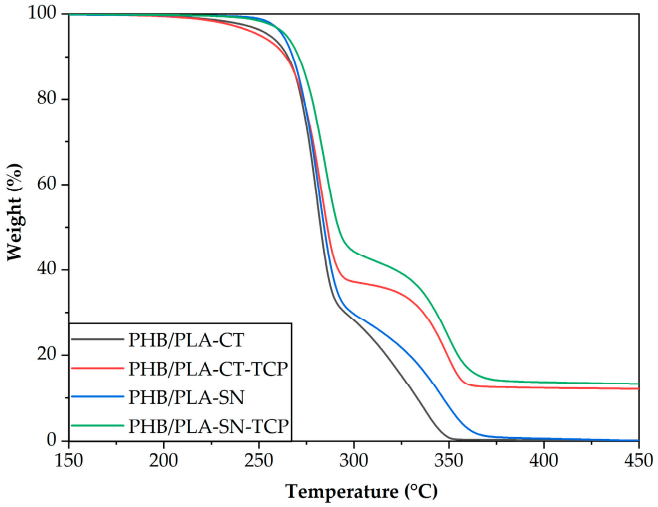


Figure 2. TGA curves of prepared samples.

Table 4. The results of TGA.

	Maximum Rate of Degradation		Residue Amount *w*% at 600 °C
	PHB T_d (°C)	PLA T_d (°C)	
PHB/PLA-CT	281	337	-
PHB/PLA-CT_TCP	283	348	11.9
PHB/PLA-SN	281	346	-
PHB/PLA-SN_TCP	284	348	12.9

The degradation temperature of neat PHB (PHB T_d) is 286 °C, while in studied blends it varies from 281 to 284 °C. The degradation temperature of neat PLA (PLA T_d) is 343 °C. In the case of PHB/PLA-CT sample, the temperature was lowered to 337 °C. The rest of the samples showed increased degradation temperature, up to 348 °C for both filled samples. It can be concluded that TCP does not act as a pro-degradant in PHB/PLA/plasticizer blends.

The amount of TCP determined by TGA was 11,9 wt.% for PHB/PLA-CT_TCP and 12.9 wt.% for PHB/PLA-SN_TCP. In the former, the deviation is attributed to the material inhomogeneity.

3.3. Optimal Printing Conditions and Printability

We managed to FDM 3D print the testing specimens from all prepared biocomposite filaments. Firstly, the TTT was executed. The geometric elements (colonnade, bridges, circle hole, overhangs) located on each floor of temperature tower printed with the nozzle temperatures ranging from 180 to 220 °C were visually evaluated (as described in [33]). This test provided us with the information about optimal nozzle temperature which was used for further printing tests. The optimization of flow parameter was executed as well, providing us with indirect information about the thickness of prepared filaments. The final optimized conditions can be seen in Table 5 together with the results of warping test. As can be seen from the table, the optimal temperature lies between 190–195 °C for all samples except for PHB/PLA-CT in which it is 5 °C lower. The optimal flow setting is 100% for all samples except for PHB/PLA-CT_TCP, which exhibited 90% probably due to the filament diameter slightly higher than 1.75 mm.

The warping coefficient was measured according to [33] for both temperatures identified by TTT. By definition, lower warping coefficient means lower warping during the printing. To give a basic idea about the meaning of specific values of warping coefficient, the commercial Beige PLA filament (Prusa Research, Prague, Czech Republic) has the warping coefficient of 2.9 ± 0.1 and therefore the goal is to reach comparable or lower values. Based on the results presented in Table 5, measured samples exhibited even lower warping coefficient in the range from 1.9 to 2.6 except for the

sample PHB/PLA-B6_TCP. Both plasticized samples, PHB/PLA-CT and PHB/PLA-SN have comparable warping coefficient (2.0–2.2) favoring higher of the two tested temperatures. The addition of TCP led to the increase of unwanted warping phenomenon in the case of both plasticizers especially for higher printing temperature. However, this effect is much stronger for Citroflex samples as the PHB/PLA-CT_TCP as the only sample shows higher warping than commercial material. The warping coefficient of this sample was one third higher than for unfilled reference for the printing temperature of 190 °C. On the other hand, the warping level of PHB/PLA-SN_TCP sample for the printing temperature of 190 °C was comparable to the plasticizer unfilled samples. When using higher temperature, the printability worsened.

Table 5. Optimized printing conditions and the results of warping test.

	Optimal Nozzle Temperature (°C)	Optimal Flow (%)	Warping Coefficient (-)		
			185 °C	190 °C	195 °C
PHB/PLA-CT	185–190	100	2.2 ± 0.1	2.0 ± 0.1	
PHB/PLA-CT_TCP	190–195	90		3.0 ± 0.2	3.2 ± 0.3
PHB/PLA-SN	190–195	100		2.1 ± 0.1	2.0 ± 0.1
PHB/PLA-SN_TCP	190–195	100		2.2 ± 0.2	2.5 ± 0.1

3.4. Tensile Properties of Prepared Biocomposites

The results of the tensile test of 3D printed standardized tensile testing specimens, 5A dogbones, can be seen in Table 6. The Young modulus (E modulus, E_T) of PHB/PLA blend plasticized with Citroflex and Syncroflex is comparable within the measurement error of around 2.3–2.4 GPa. However, the tensile strength (σ_{max}) of unfilled sample with Citroflex is lower than that of Syncroflex unfilled sample (32.2 ± 1.3 MP vs. 37.6 ± 3.4 MPa, respectively). Simultaneously, the elongation at break (ε_{max}) for the sample PHB/PLA-CT is higher than in the case of PHB/PLA-SN but with greater deviation at the same time (22.6 ± 13.1% for Citroflex and 16.9 ± 3.0% for Syncroflex). When TCP as a bioactive filler is added to these blends, the modulus is slightly increased (the highest 2.6 ± 0.1 GPa value is achieved for PHB/PLA-CT_TCP) due to the addition of high-modulus fraction to the matrix. At the same time, the tensile strength drops, the decrease of approximately 12% and 15% from the original value for Citroflex and Syncroflex samples, respectively, is observed. This is attributed to the samples' inhomogeneity caused by the presence of TCP crystals.

Table 6. The results of tensile test.

	Young's Modulus E_T (GPa)	Tensile Strength σ_{max} (MPa)	Elongation at Break ε_{max} (%)
PHB/PLA-CT	2.3 ± 0.1	32.2 ± 1.3	22.6 ± 13.1
PHB/PLA-CT_TCP	2.6 ± 0.1	28.3 ± 0.8	3.4 ± 2.0
PHB/PLA-SN	2.4 ± 0.2	37.6 ± 3.4	16.9 ± 3.0
PHB/PLA-SN_TCP	2.5 ± 0.0	32.1 ± 0.7	6.4 ± 0.8

As well, the elongation at break significantly decreased with the TCP addition in comparison to the unfilled samples. PHB/PLA-CT_TCP reaches only 15% of the value of elongation at break of unfilled PHB/PLA-CT sample. As for Syncroflex, this decrease is to 38% of original value. However, the sample PHB/PLA-SN_TCP reached the elongation at break of 6.4 ± 0.8%, which is almost twice the value of corresponding sample with citrate-based plasticizer causing probably unwanted reactions with TCP, which is acid-sensitive.

3.5. Flexural Properties of Prepared Materials

To observe the materials deformation behavior during bending, the flexural test was conducted on 3D printed rectangular testing specimen with results presented in Figure 3.

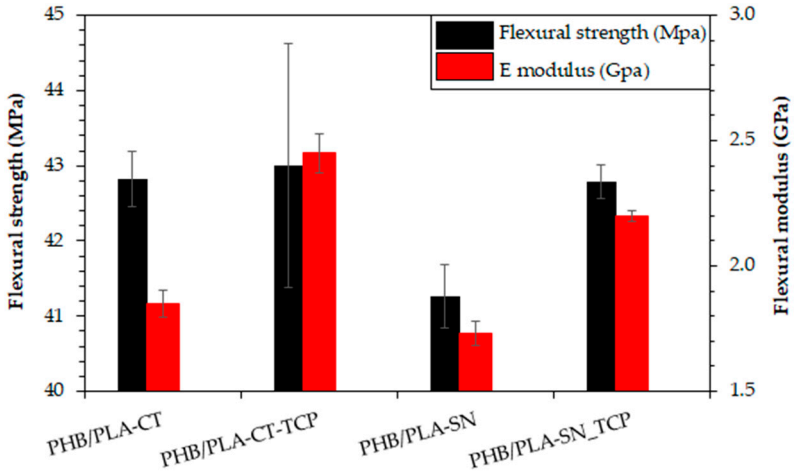


Figure 3. The results of flexural test of 3D printed specimen.

The flexural modulus is overall lower than the tensile modulus, being between 1.7–1.9 GPa for the samples without TCP. The reason for that is probably the fact that this modulus reflects the properties of only small specific locations on the surface of the sample. Significant increase is observed with the addition of TCP, up to 2.5 ± 0.1 GPa and 2.2 ± 0.0 GPa for the samples plasticized with Citroflex and Syncroflex, respectively. The flexural strength is comparable among all samples, ranging from 41.3 (PHB/PLA-SN) to 43.0 MPa (PHB/PLA-CT_TCP). As for Syncroflex samples, slight increase is observed with the addition of filler.

3.6. In Vitro Testing on Scaffolds

3.6.1. Cell Proliferation and Metabolic Activity

To evaluate the cell proliferation on prepared scaffolds, the DNA quantification was performed. This test determined the overall number of cells proliferated on samples. The metabolic activity of cells was measured via the MTS assay.

The results of DNA quantification are depicted in Figure 4. On day 1, the cell adhesion was statistically higher in the samples containing Syncroflex compared to the samples with Citroflex plasticizer. The sample PHB/PLA-CT had very low amount of DNA until day 28 of the experiment and seems to be worse in terms of its biocompatibility. The sample containing Citroflex plasticizer and TCP, PHB/PLA-CT_TCP, had low DNA values on days 1 and 7, followed by an increase on day 14. In the following days however, the number of cells decreased again. On the samples containing Syncroflex, cell proliferation occurred mainly during the first seven days, after which the values were rather stable. The highest amount of DNA was observed in the late phase of the experiment, especially for the sample PHB/PLA-SN.

The results of metabolic activity measurement are shown in Figure 5. On the first day of the experiment, the samples PHB/PLA-CT and PHB/PLA-SN_TCP showed the highest metabolic activity but still much lower than the control PS plastic showed. For the rest of the experiment however, the sample PHB/PLA-CT had the lowest metabolic activity of all samples, which might be due to the citrate-based plasticizer and some of its releasing residues. The values were generally lower for the samples containing Citroflex plasticizer, than for those with Syncroflex. However, the TCP addition to citrate-based samples improving the cell metabolic activity especially in the later stages might be probably due to the neutralizing effect of the basic released TCP interacting with possible acid-residues from Citroflex. Regarding the samples with Syncroflex, the values of metabolic activity were higher or comparable for the sample containing TCP than for the sample without bioactive filler proving no unwanted side reactions between the plasticizer and TCP. Moreover, from day 7 the values of absorbance are not statistically different from a control plastic.

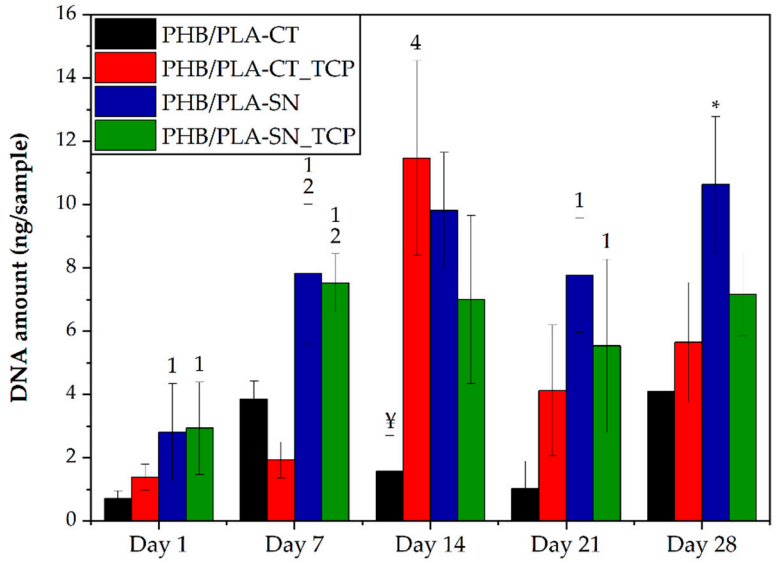


Figure 4. Cell proliferation. The number above the column indicates statistically significantly higher values compared to the column of that number, $p < 0.05$. * means the statistically highest value of all groups for a given day, ¥ means the statistically lowest value of all groups for a given day.

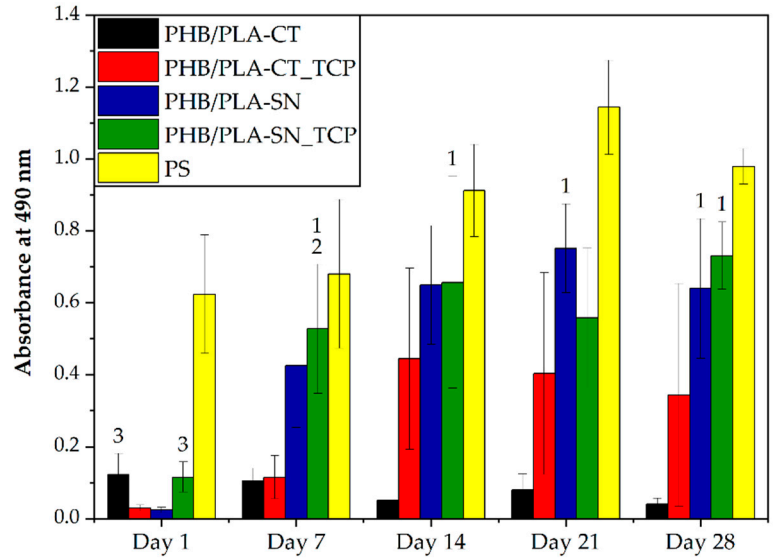


Figure 5. Metabolic activity of cells on the scaffolds. The numbers above the column indicate statistically significantly higher values compared to the column of that number, $p < 0.05$.

To sum up, the result of the MTS assay was similar to the result of DNA quantification showing higher cell proliferation and viability on the samples with Syncroflex compared to those with CT.

To gain comprehensive information, also the number and the shape of the cells on scaffolds were observed using confocal microscopy. The results can be seen in Figure 6. The difference between Citroflex and Syncroflex samples is prominent, confirming the results of MTS test and DNA quantification.

On day 1 of the test, the highest number of cells forming a thick network over most of the area of the scaffold was observed on the sample PHB/PLA-CT. Nevertheless, from day 7 until the end of the experiment only a few cells were observed in the case of this sample. The cells formed clusters and they all had round shape indicating their poor condition not suitable for their proliferation. The sample with Citroflex plasticizer and TCP, PHB/PLA-CT_TCP, showed high number of cells during the first and seventh days of the experiment, but after that the situation was similar to the case of its filler-free reference.

In contrast, a profound increase of the number of cells was visible on the seventh day of the experiment for both samples with Syncroflex. From then on, the cells formed a confluent layer. For some samples, this layer peeled off due to the smooth surface of the scaffold.

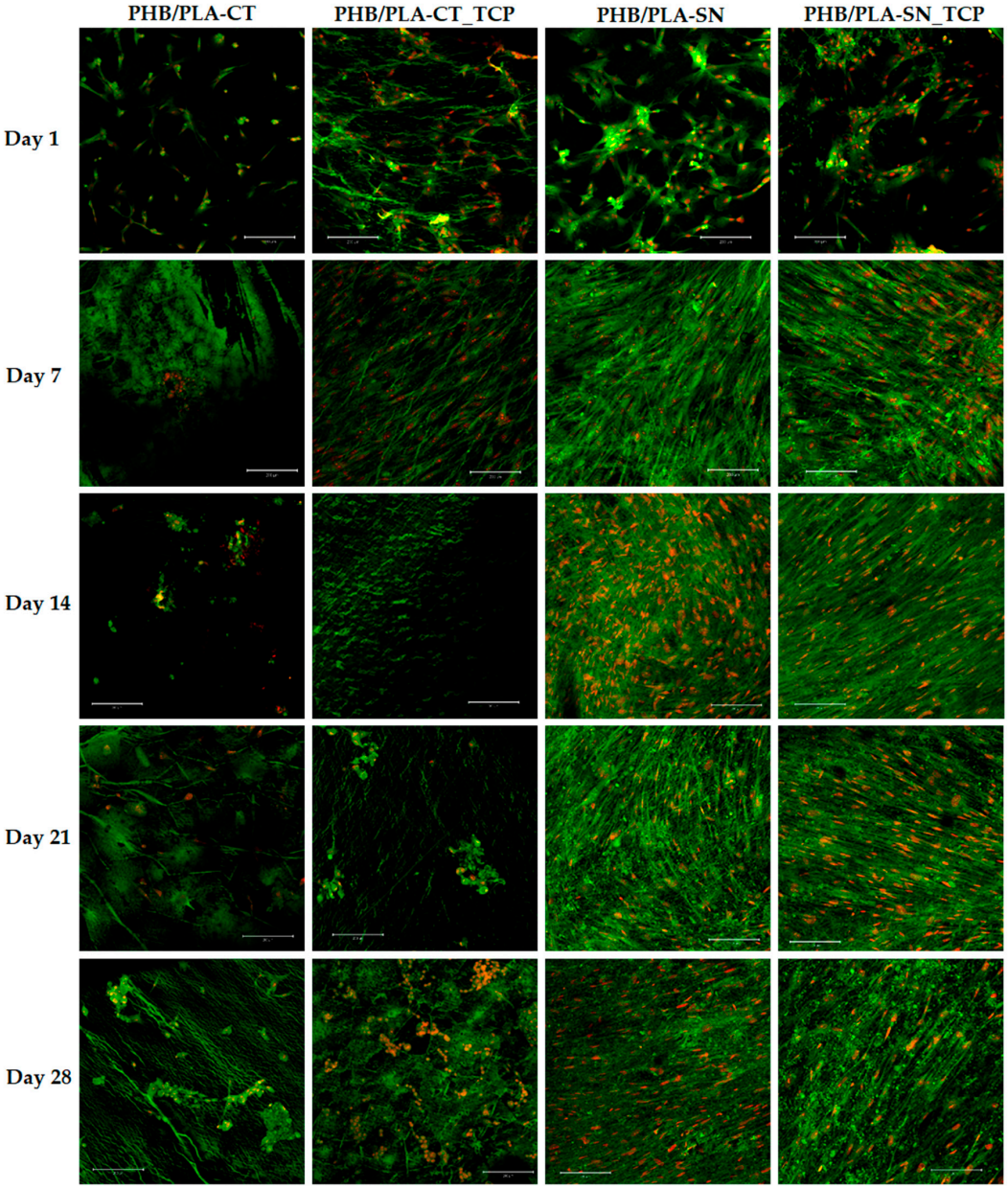


Figure 6. hMSCs on scaffolds from tested materials, magnification 100×, the bar is 200 µm.

3.6.2. Osteogenic Differentiation of Cells

The osteogenic differentiation of hMSCs on scaffolds was monitored by ALP activity and real-time PCR analysis in all samples, and by immunohistochemical staining only in the samples containing Syncroflex as the samples containing Citroflex had insufficient number of cells on the scaffolds.

Figure 7 depicts the results of ALP assay of tested materials. On day 1, the values were low and comparable among all samples. The following days, the sample PLA/PHB-CT containing citrate-based plasticizer remained on its original value. After the TCP addition the amount of ALP reached the maximum on day 14 and then dropped again to the initial value on day 21. The samples with Syncroflex exhibited statistically higher values of produced ALP than the samples with CT, especially on day 21 of the experiment, where the difference is profound.

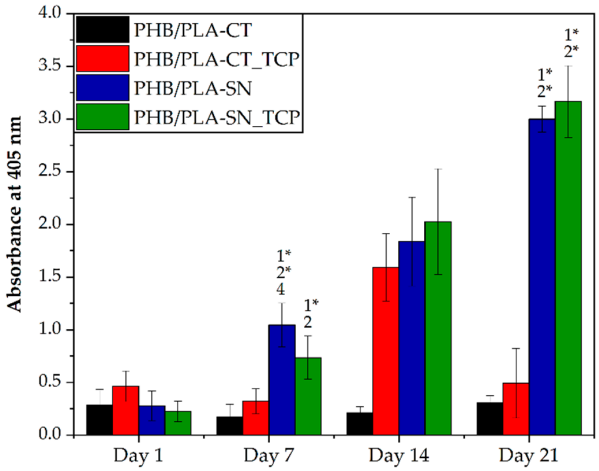


Figure 7. The results of ALP assay. The numbers above the column indicate statistically significantly higher values compared to the column of that number for $p < 0.05$ and $p < 0.001$ with *.

The expression of typical osteogenic markers was monitored via real-time PCR analysis and is shown in Figure 8.

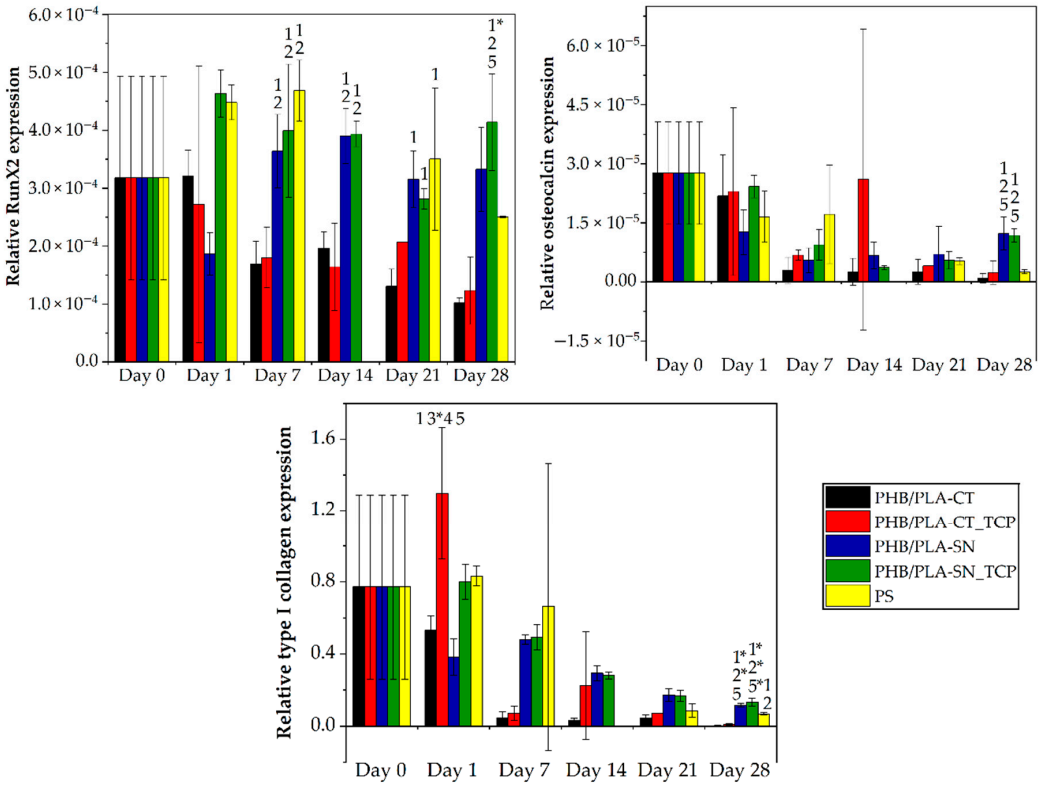


Figure 8. Gene expression of osteogenic markers RunX2, collagen I and osteocalcin. The numbers above the column indicate statistically significantly higher values compared to the column of that number for $p < 0.05$ and $p < 0.001$ with *.

RunX2, the marker of early osteogenic differentiation, was expressed in comparable quantity during the experiment for individual samples. The highest expression level was observed for the samples with Syncroflex, PHB/PLA-SN and PHB/PLA-SN_TCP. The expression of both type I collagen and osteocalcin, the marker of late osteogenic differentiation, dropped during the experiment for all samples. In the late stage of the analysis (days 21 and 28), the highest amount of expressed type I collagen was detected again in the samples containing Syncroflex. Regarding osteocalcin, no

statistically significant difference was observed until the 28th day of the test, when Syncroflex samples showed the highest values.

Although rather low levels of expression of osteocalcin and type I collagen were measured by RT-PCR analysis, both markers could be visualized by confocal microscopy after immunohistochemical staining (see Figure 9 for osteocalcin and Figure 10 for type I collagen). Both proteins were detected for both studied samples, PHB/PLA-SN and PHB/PLA-SN_TCP, on all monitored days.

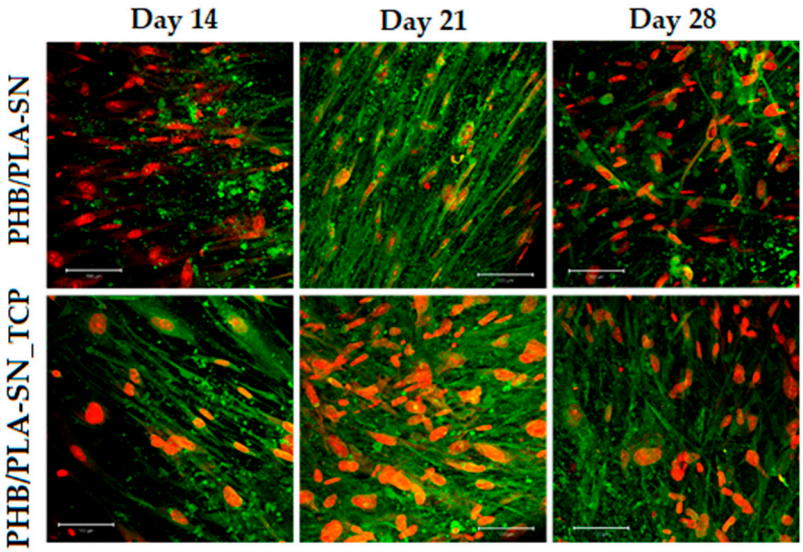


Figure 9. Osteocalcin staining, cell nuclei are red and osteocalcin green, magnification 200×, the bar is 100 μm.

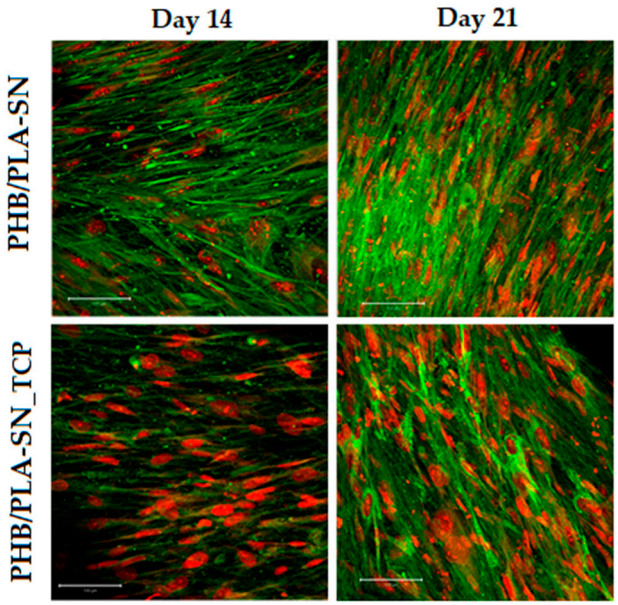


Figure 10. Collagen I staining, cell nuclei are red and collagen is green, magnification 200×, the bar is 100 μm.

4. Discussion

Two series of samples based on poly(3-hydroxybutyrate) (PHB) and poly(D,L-lactide) (PLA) blend were compounded, one with *n*-Butyryl tri-*n*-hexyl citrate (Citroflex, CT) and one with oligomeric adipate ester (Syncroflex, SN) as a plasticizer. For each plasticizer, unfilled reference sample and composite sample with 13 wt.% of tricalcium phosphate (TCP) were prepared. Therefore, both the

difference between the performance of these two plasticizers and the effect of bioactive filler addition were studied.

The difference of used plasticizers from the viewpoint of thermal properties of resulting materials observed by Differential Scanning Calorimetry (DSC) is negligible. The Citroflex samples exhibit lower melting temperature of PHB, the glass transition temperature of PLA being around 42 °C is comparable for all samples. TCP acts as a nucleating agent increasing the temperature of crystallization of about 10–15 °C. Moreover, the addition of TCP does not decrease the thermal stability of the blend, contrariwise the temperature of maximum degradation rate of both polymers is higher for both composite samples than for their unfilled reference as measured by Thermogravimetric analysis.

All samples were successfully extruded to the form of 3D printing filaments with the precise diameter of 1.7–1.8 mm followed by Fused Deposition Modeling 3D printing of testing specimen for subsequent test. To ensure the highest quality of printed objects, two crucial 3D printing parameters, the nozzle temperature and the flow were optimized by the temperature tower test (TTT) and the filling study, respectively. The printability of these blends was also evaluated applying new, recently published Warping Test (see [33]). The optimum printing temperature range obtained from TTT was in the range of 190–195 °C for all samples except for PHB/PLA-CT, for which it was slightly lower, 185–190 °C, corresponding to the results from DSC measurement. Lower melting and processability temperatures of this sample indicate more profound plasticizing effect of Citroflex than Syncroflex.

The warping test further specified the optimum printing temperature, generally being the higher one of the two selected by TTT for unfilled samples and the lower temperature of the two for the samples filled with TCP. The composite sample with Citroflex plasticizer showed the highest level of warping of all tested samples. On top of that, this sample showed even higher warping levels than commercial PLA Prusa filament. On the contrary, the composite sample with Syncroflex reached the same printability as unfilled reference at the printing temperature of 190 °C. All Syncroflex samples achieved better warping properties than commercial Prusa PLA filament subjected to identical testing conditions.

The mechanical testing confirmed Citroflex to have better plasticizing effect on studied PHB/PLA blend. The samples with Citroflex had lower tensile Young modulus, tensile strength and at the same time higher elongation at break than corresponding samples with Syncroflex. The TCP addition influenced the tensile modulus very slightly (E modulus increased from 2.3–2.4 to 2.5–2.6 GPa). At the same time, the tensile strength was reduced by about 12–15% to values close to 30 MPa. In the case of our samples, the tensile strength also corresponds with the yield strength and therefore its change cannot be explained by higher probability of cracking with the addition of filler. We attribute this effect to an imperfect adhesion between the polymer matrix and the filler, which manifests itself more profoundly in the tensile test, where the bulk properties are measured. In addition, the elongation at break drops with the addition of TCP to 3.4% for Citroflex and to 6.4% for Syncroflex sample. The flexural modulus of unfilled samples is lower than the tensile modulus, reaching the values of 1.7–1.9 GPa and is profoundly increased with the addition of the filler. Opposite to this, the flexural strength is comparable for all tested samples. To put these values into context, although the mechanical properties of bones are highly age and body part dependent, the modulus of compact bone in longitudinal direction (corresponds to measured values from tensile test) is reported to be 17.9 ± 3.9 GPa and the strength of 135 ± 15.6 MPa [6]. This 7-fold difference in the tensile modulus and 4.5-fold in the tensile strength represents a huge space for future development. The increase in these parameters can be achieved for example by varying the composition of the blends—lower amount of plasticizer with simultaneous higher amount of the filler; or by tuning the structure of 3D printed object.

Moreover, the set of in vitro tests of proliferation and viability and also the osteogenic differentiation of human mesenchymal stem cells (hMSC) on scaffolds prepared from studied materials was executed. The scaffolds were disks of 6 or 10 mm diameter and 1 mm thickness shape cut from compression molded plates.

Overall, the samples with Syncroflex showed superior performance compared to the samples with CT. The sample PHB/PLA-CT had consistently the worst results of all performed in vitro tests

albeit showing promising properties for 3D printing and good mechanical properties. The cell growth on this sample was almost non-existent and observed cells had round shape and existed in clusters indicating their bad condition. The alkaline phosphatase (ALP) activity was minimal during all days of the test. RunX2, a marker of osteogenic differentiation, was detected, but in the lowest amount of all samples and osteocalcin and collagen were measured only the first day of the experiment. Mildly better results were observed in the case of PHB/PLA-CT_TCP, its corresponding filled sample. The number of metabolically active cells was higher than that for PHB/PLA-CT, but also with the higher measurement error. As observed by microscope, although the number of cells was higher, their shape and overall condition were poor. The ALP activity showed an increase up to the 14th day of the experiment and then a drop followed. On day 21 of the experiment, the values of both Citroflex samples were very close to each other. The expression of osteogenic markers for PHB/PLA-CT_TCP was extremely low and again comparable to the sample PHB/PLA-CT. To conclude, the Citroflex plasticizer has the potential to be used for producing blends suitable for 3D printing. Nevertheless, these tests proved low biocompatibility of such material hence being inappropriate for the medical applications in human body.

The Syncroflex-based samples on the other hand demonstrated excellent cell proliferation during the entire course of the test, with PHB/PLA-SN with the most cellular DNA detected. The same trend was observed for metabolically active cells. The visualization using confocal microscope revealed that the cells formed a confluent layer and had a natural elongated shape proving their good condition. No major difference between the two Syncroflex samples was detected by these tests. The same applies when it comes to the measurement of ALP activity, both samples, PHB/PLA-SN and PHB/PLA-SN_TCP, exhibited a continuous increase throughout the test reaching comparable values on the last day. The expression of RunX2 for the sample PHB/PLA-SN_TCP reached higher value than the control on the 28th day of the test. The levels of expression of osteocalcin and type I collagen were rather low, but these proteins were visualized by immunohistochemical staining and were present during all tested days. Syncroflex proved to be a suitable plasticizer for PHB/PLA blend. Both samples, unfilled reference and prepared composite were not only suitable for the 3D printing applications but also demonstrated excellent results of in vitro tests which shows their potential for use as the material for stem cell-seeded scaffolds for regenerative medicine of bones.

5. Conclusions

To conclude, *n*-Butyryl tri-*n*-hexyl citrate (CT) plasticizer is a suitable plasticizer for poly(3-hydroxybutyrate) (PHB)/poly(D,L-lactide) (PLA) blends leading to improved processability and mechanical properties. However, the samples with Citroflex showed poor biocompatibility properties in in vitro test excluding them from the future research in the field of tissue engineering.

Both studied materials containing PHB/PLA and Syncroflex plasticizer, with and without the tricalcium phosphate (TCP) addition, are suitable for the 3D printing by FDM method and at the same time exhibit promising properties to be used as materials for bone tissue scaffolds. However, the in vitro testing revealed that the scaffold design needs to be adjusted mainly by means of surface topography. Therefore, further research will take place in the direction of tuning the surface and mechanical properties of developed blends.

Author Contributions: Conceptualization, L.V. and R.P.; Data curation, S.K. and M.R.; Formal analysis, V.M., K.S., P.M., S.K., M.R., V.H., V.S., L.V. and R.P.; Funding acquisition, M.R., L.V. and R.P.; Investigation, V.M., K.S., P.M., S.K., V.H. and V.S.; Methodology, P.M., M.R., L.V. and R.P.; Project administration, R.P.; Resources, V.M., P.M., M.R., L.V. and R.P.; Supervision, M.R., L.V. and R.P.; Visualization, V.M. and M.R.; Writing—original draft, V.M.; Writing—review & editing, M.R., L.V. and R.P. All authors have read and agreed to the published version of the manuscript.

Funding: This study has been supported by the Czech Science Foundation grant no. 18-09306S, by the Ministry of Industry and Trade of the Czech Republic Project No. FV20480, by the Specific University Research Grant through the project FCH-S-20-6340 and by the project CEITEC 2020 (LQ1601) with financial support from the Ministry of Education, Youth and Sports of the Czech Republic under the National Sustainability Programme II.

Conflicts of Interest: The authors declare no conflict of interest.

References

1. Amin, S.; Achenbach, S.J.; Atkinson, E.J.; Khosla, S.; Melton, L.J. Trends in Fracture Incidence: A Population-Based Study Over 20 Years. *J. Bone Miner. Res.* **2014**, *29*, 581–589. [CrossRef] [PubMed]
2. Johnell, O.; Kanis, J.A. An estimate of the worldwide prevalence and disability associated with osteoporotic fractures. *Osteoporos. Int.* **2006**, *17*, 1726–1733. [CrossRef] [PubMed]
3. Brown, J.L.; Kumbar, S.G.; Laurencin, C.T. Bone tissue engineering. In *Biomaterials Science: An Introduction to Materials in Medicine*, 3rd ed.; Elsevier: Amsterdam, The Netherlands, 2013; pp. 1194–1214.
4. Laurencin, C.T.; Ambrosio, A.M.A.; Borden, M.D.; Cooper, J.A. Tissue Engineering: Orthopedic Applications. *Annu. Rev. Biomed. Eng.* **1999**, *1*, 19–46. [CrossRef] [PubMed]
5. Fattahian, H.; Mansouri, K.; Mansouri, N. Biomaterials, Substitutes, And Tissue Engineering in Bone Repair. *Comp. Clin. Path.* **2019**, *28*, 879–891. [CrossRef]
6. Qu, H.; Fu, H.; Han, Z.; Sun, Y. Biomaterials for bone tissue engineering scaffolds: A review. *RSC Adv.* **2019**, *9*, 26252–26262. [CrossRef]
7. Hollister, S.J. Scaffold Design and Manufacturing: From Concept to Clinic. *Adv. Mater.* **2009**, *21*, 3330–3342. [CrossRef]
8. Chocholata, P.; Kulda, V.; Babuska, V. Fabrication of Scaffolds for Bone-Tissue Regeneration. *Materials* **2019**, *12*, 568. [CrossRef]
9. Sloviková, A.; Vojtová, L.; Jančář, J. Preparation and modification of collagen-based scaffold for tissue engineering. *Chem. Pap.* **2008**, *62*, 417–422. [CrossRef]
10. Švachová, V.; Vojtová, L.; Pavliňák, D.; Vojtek, L.; Sedláková, V.; Hyršl, P.; Alberti, M.; Jaroš, J.; Hampl, A.; Jančář, J. Novel electrospun gelatin/oxycellulose nanofibers as a suitable platform for lung disease modeling. *Mater. Sci. Eng. C* **2016**, *67*, 493–501. [CrossRef]
11. Balletti, C.; Ballarin, M.; Guerra, F. 3D printing: State of the art and future perspectives. *J. Cult. Herit.* **2017**, *26*, 172–182. [CrossRef]
12. Ngo, T.D.; Kashani, A.; Imbalzano, G.; Nguyen, K.T.; Hui, D. Additive manufacturing (3D printing): A review of materials, methods, applications and challenges. *Compos. Part B Eng.* **2018**, *143*, 172–196. [CrossRef]
13. Pereira, T.F.; Oliveira, M.; Maia, I.A.; Da Silva, J.V.L.; Costa, M.; Thiré, R.M.D.S.M. 3D Printing of Poly(3-Hydroxybutyrate) Porous Structures Using Selective Laser Sintering. *Macromol. Symp.* **2012**, *319*, 64–73. [CrossRef]
14. Lee, S.; Zhou, W.Y.; Wang, M.; Cheung, W.L.; Ip, W.Y. Selective Laser Sintering of Poly(L-Lactide) Porous Scaffolds for Bone Tissue Engineering. *J. Biomim. Biomater. Tissue Eng.* **2008**, *1*, 81–89. [CrossRef]
15. Saska, S.; Pires, L.C.; Cominotte, M.A.; Mendes, L.S.; de Oliveira, M.F.; Maia, I.A.; da Silva JV, L.; Ribeiro SJ, L.; Cirelli, J.A. Three-Dimensional Printing and in Vitro Evaluation of Poly(3-Hydroxybutyrate) Scaffolds Functionalized with Osteogenic Growth Peptide for Tissue Engineering. *Mater. Sci. Eng. C* **2018**, *89*, 265–273. [CrossRef] [PubMed]
16. Boparai, K.S.; Singh, R.; Singh, H. Development of rapid tooling using fused deposition modeling: A review. *Rapid Prototyp. J.* **2016**, *22*, 281–299. [CrossRef]
17. Carrell, J.; Gruss, G.; Gomez, E. Four-dimensional printing using fused-deposition modeling: A review. *Rapid Prototyp. J.* **2020**, *26*, 855–869. [CrossRef]
18. Dhinakaran, V.; Kumar, K.M.; Ram, P.B.; Ravichandran, M.; Vinayagamoorthy, M. A review on recent advancements in fused deposition modeling. *Mater. Today Proc.* **2020**, *27*, 752–756. [CrossRef]
19. Ligon, S.C.; Liska, R.; Stampfl, J.; Gurr, M.; Mülhaupt, R. Polymers for 3D Printing and Customized Additive Manufacturing. *Chem. Rev.* **2017**, *117*, 10212–10290. [CrossRef]
20. Mohan, N.; Senthil, P.; Vinodh, S.; Jayanth, N. A review on composite materials and process parameters optimisation for the fused deposition modelling process. *Virtual Phys. Prototyp.* **2017**, *12*, 47–59. [CrossRef]
21. Chiulan, I.; Frone, A.N.; Brandabur, C.; Panaitescu, D.M. Recent Advances in 3D Printing of Aliphatic Polyesters. *Bioengineering* **2018**, *5*, 2. [CrossRef]
22. Shunmugasundaram, M.; Maughal, A.A.B.; Ajay Kumar, M. A review of bio-degradable materials for fused deposition modeling machine. *Mater. Today Proc.* **2020**, *27*, 1596–1600. [CrossRef]

23. Wurm, M.C.; Möst, T.; Bergauer, B.; Rietzel, D.; Neukam, F.W.; Cifuentes, S.C.; Von Wilmowsky, C. In-vitro evaluation of Polylactic acid (PLA) manufactured by fused deposition modeling. *J. Biol. Eng.* **2017**, *11*, 1–9. [CrossRef] [PubMed]
24. Lim, J.; You, M.; Li, J.; Li, Z. Emerging bone tissue engineering via Polyhydroxyalkanoate (PHA)-based scaffolds. *Mater. Sci. Eng. C* **2017**, *79*, 917–929. [CrossRef] [PubMed]
25. Butt, F.I.; Muhammad, N.; Hamid, A.; Moniruzzaman, M.; Sharif, F. Recent progress in the utilization of biosynthesized polyhydroxyalkanoates for biomedical applications—Review. *Int. J. Biol. Macromol.* **2018**, *120*, 1294–1305. [CrossRef] [PubMed]
26. Kovalcik, A.; Sangroniz, L.; Kalina, M.; Skopalova, K.; Humpolíček, P.; Omastova, M.; Mundigler, N.; Müller, A.J. Properties of scaffolds prepared by fused deposition modeling of poly(hydroxyalkanoates). *Int. J. Biol. Macromol.* **2020**, *161*, 364–376. [CrossRef] [PubMed]
27. Gonzalez Ausejo, J.; Rydz, J.; Musioł, M.; Sikorska, W.; Sobota, M.; Włodarczyk, J.; Adamus, G.; Janeczek, H.; Kwiecień, I.; Hercog, A.; et al. A comparative study of three-dimensional printing directions: The degradation and toxicological profile of a PLA/PHA blend. *Polym. Degrad. Stab.* **2018**, *152*, 191–207. [CrossRef]
28. Esposito Corcione, C.; Scalera, F.; Gervaso, F.; Montagna, F.; Sannino, A.; Maffezzoli, A. One-step solvent-free process for the fabrication of high loaded PLA/HA composite filament for 3D printing. *J. Therm. Anal. Calorim.* **2018**, *134*, 575–582. [CrossRef]
29. Xuan, Y.; Tang, H.; Wu, B.; Ding, X.; Lu, Z.; Li, W.; Xu, Z. A specific groove design for individualized healing in a canine partial sternal defect model by a polycaprolactone/hydroxyapatite scaffold coated with bone marrow stromal cells. *J. Biomed. Mater. Res. Part A* **2014**, *102*, 3401–3408. [CrossRef]
30. Konopnicki, S.; Sharaf, B.; Resnick, C.; Patenaude, A.; Pogal-Sussman, T.; Hwang, K.-G.; Abukawa, H.; Troulis, M.J. Tissue-Engineered Bone With 3-Dimensionally Printed β-Tricalcium Phosphate and Polycaprolactone Scaffolds and Early Implantation: An In Vivo Pilot Study in a Porcine Mandible Model. *J. Oral Maxillofac. Surg.* **2015**, *73*, 1016.e1–1016.e11. [CrossRef]
31. Dávila, J.L.; Freitas, M.S.; Inforçatti Neto, P.; Silveira, Z.C.; Silva JV, L.; d'Ávila, M.A. Fabrication of PCL/B-TCP Scaffolds By 3D Mini-Screw Extrusion Printing. *J. Appl. Polym. Sci.* **2016**, *133*, 133. [CrossRef]
32. Samavedi, S.; Whittington, A.R.; Goldstein, A.S. Calcium phosphate ceramics in bone tissue engineering: A review of properties and their influence on cell behavior. *Acta Biomater.* **2013**, *9*, 8037–8045. [CrossRef]
33. Kontárová, S.; Přikryl, R.; Melčová, V.; Menčík, P.; Horálek, M.; Figalla, S.; Plavec, R.; Feranc, J.; Sadílek, J.; Pospíšilová, A. Printability, Mechanical and Thermal Properties of Poly(3-Hydroxybutyrate)-Poly(Lactic Acid)-Plasticizer Blends for Three-Dimensional (3D) Printing. *Materials* **2020**, *13*, 4736. [CrossRef]
34. Menčík, P.; Přikryl, R.; Stehnová, I.; Melčová, V.; Kontárová, S.; Figalla, S.; Alexy, P.; Bočkaj, J. Effect of Selected Commercial Plasticizers on Mechanical, Thermal, and Morphological Properties of Poly(3-hydroxybutyrate)/Poly(lactic acid)/Plasticizer Biodegradable Blends for Three-Dimensional (3D) Print. *Materials* **2018**, *11*, 1893. [CrossRef]

Publisher's Note: MDPI stays neutral with regard to jurisdictional claims in published maps and institutional affiliations.

© 2020 by the authors. Licensee MDPI, Basel, Switzerland. This article is an open access article distributed under the terms and conditions of the Creative Commons Attribution (CC BY) license (http://creativecommons.org/licenses/by/4.0/).

polymers

MDPI

Article

Poly(3-hydroxybutyrate) (PHB) and Polycaprolactone (PCL) Based Blends for Tissue Engineering and Bone Medical Applications Processed by FDM 3D Printing

Štěpán Krobot [1,*], Veronika Melčová [1], Přemysl Menčík [1], Soňa Kontárová [1], Michala Rampichová [2], Věra Hedvičáková [2], Ema Mojžišová [3], Andrej Baco [4] and Radek Přikryl [1,*]

[1] Institute of Material Chemistry, Faculty of Chemistry, Brno University of Technology, Purkyňova 464/118, 612 00 Brno, Czech Republic
[2] Institute of Experimental Medicine, CAS, Vídeňská 1083, 142 20 Praha, Czech Republic
[3] Institute of Natural and Synthetic Polymers, Faculty of Chemical and Food Technology, Slovak University of Technology in Bratislava, Radlinského 9, 812 37 Bratislava, Slovakia
[4] PANARA, a.s., Krškanská 21, 949 05 Nitra, Slovakia
* Correspondence: stepan.krobot@vutbr.cz (Š.K.); prikryl@fch.vut.cz (R.P.); Tel.: +420-608-877-566 (Š.K.); +420-606-454-546 (R.P.)

Abstract: In the presented work, poly(3-hydroxybutyrate)–PHB-based composite blends for bone medical applications and tissue engineering are prepared and characterized. PHB used for the work was in two cases commercial and, in one case, was extracted by the chloroform-free route. PHB was then blended with poly(lactic acid) (PLA) or polycaprolactone (PCL) and plasticized by oligomeric adipate ester (Syncroflex, SN). Tricalcium phosphate (TCP) particles were used as a bioactive filler. Prepared polymer blends were processed into the form of 3D printing filaments. The samples for all the tests performed were prepared by FDM 3D printing or compression molding. Differential scanning calorimetry was conducted to evaluate the thermal properties, followed by optimization of printing temperature by temperature tower test and determination of warping coefficient. Tensile test, three-point flexural test, and compression test were performed to study the mechanical properties of materials. Optical contact angle measurement was conducted to determine the surface properties of these blends and their influence on cell adhesion. Cytotoxicity measurement of prepared blends was conducted to find out whether the prepared materials were non-cytotoxic. The best temperatures for 3D printing were 195/190, 195/175, and 195/165 °C for PHB-soap/PLA-SN, PHB/PCL-SN, and PHB/PCL-SN-TCP, respectively. Their mechanical properties (strengths ~40 MPa, moduli ~2.5 GPa) were comparable with human trabecular bone. The calculated surface energies of all blends were ~40 mN/m. Unfortunately, only two out of three materials were proven to be non-cytotoxic (both PHB/PCL blends).

Keywords: 3D printing; FDM; poly(3-hydroxybutyrate); bone tissue engineering; scaffold; biocompatibility; polycaprolactone; polylactic acid

check for updates

Citation: Krobot, Š.; Melčová, V.; Menčík, P.; Kontárová, S.; Rampichová, M.; Hedvičáková, V.; Mojžišová, E.; Baco, A.; Přikryl, R. Poly(3-hydroxybutyrate) (PHB) and Polycaprolactone (PCL) Based Blends for Tissue Engineering and Bone Medical Applications Processed by FDM 3D Printing. *Polymers* **2023**, *15*, 2404. https://doi.org/10.3390/polym15102404

Academic Editor: Swee Leong Sing

Received: 30 March 2023
Revised: 10 May 2023
Accepted: 19 May 2023
Published: 22 May 2023

Copyright: © 2023 by the authors. Licensee MDPI, Basel, Switzerland. This article is an open access article distributed under the terms and conditions of the Creative Commons Attribution (CC BY) license (https://creativecommons.org/licenses/by/4.0/).

1. Introduction

Bioplastics and biodegradable polymers are attracting attention not only for their eco-friendliness but also for their biocompatibility. This quality allows them to be implanted into the human body without causing harm and later absorbed and fully disintegrated. As a result, these polymers are being used in medicine and medical applications to improve regeneration, restore damaged tissues, and shorten healing time. Among the polymers utilized in medical applications are poly(3-hydroxybutyrate), polylactic acid, poly(glycolic) acid, and polycaprolactone, as well as their blends and copolymers [1,2].

Tissue engineering is a highly advanced method utilized in modern regenerative medicine. The primary component of tissue engineering is a scaffold, which is a porous

structure that provides support for various cells and becomes integrated into the human body. Among the most prevalent health problems, bone damage remains a significant concern. Osteoporosis and traumatic fractures, particularly in older individuals, are common causes of bone damage [3,4]. The scaffold material used in bone tissue engineering must possess certain properties that are essential for successful bone growth at the implant site. Firstly, the material must be osteoconductive, which means it should facilitate bone growth. Additionally, it must be osteoinductive, meaning it should induce the differentiation of local stem cells that are present in the bone marrow into osteogenic cells. For the cells to form new tissue, the scaffold material should have appropriate porosity and a 3D structure that allows cells to grow through the entire volume of the scaffold [5–7]. High demands are placed on scaffold properties, making 3D printing the ideal method to meet these requirements. The use of 3D-printed scaffolds has shown great potential in improving treatment for certain medical conditions, shortening healing time, and reducing waste production. Tissue engineering has recently incorporated 3D printing to produce scaffolds from biocompatible polymer blends, allowing for enhanced properties. Among the most commonly used polymers for 3D printed scaffolds are biodegradable ones, including polylactic acid, poly(3-hydroxybutyrate), and polycaprolactone [8,9].

Poly(3-hydroxybutyrate) (PHB) is a biopolymer that is synthesized by bacteria and is highly crystalline. It is also biodegradable under natural conditions [10]. PHB has properties that are comparable to those of polypropylene (PP), including similar melting temperature, glass transition temperature, crystallinity, and tensile strength. However, PHB is considerably more brittle than PP [11,12].

PHB is the most published and commercially successful polyhydroxyalkanoate polymer, which was found to be miscible with other biodegradable polymers such as polycaprolactone (PCL) or polylactic acid (PLA) at different ratios and with inorganic particle fillers such as montmorillonite nanoclay, kaolin, or tricalcium phosphate (TCP) [13–17]. Blending PHB with another biopolymer or the addition of filler is a very effective approach to improve the printability of prepared materials. TCP, as well as hydroxyapatite (HAp), have high bioactivity and have been used as bone substitute materials. Furthermore, mesenchymal stem cells (MSCs) can be induced to differentiate into osteogenic lineages in vivo using tricalcium phosphate (TCP) [18–21].

Polycaprolactone (PCL) is widely used in tissue engineering to manufacture different types of stents due to its good biocompatibility and shape retention properties. PCL has a low melting point, making it ideal for 3D printing, and it has been extensively studied as a scaffold material for tissue engineering due to its ability to support cell attachment, proliferation, and differentiation [22–24]. PCL scaffolds have been used for a variety of tissue engineering applications, including bone regeneration [25–28]. PCL scaffolds have been shown to have several advantages over other scaffold materials [29]. PCL degrades slowly over time, which allows for the gradual release of growth factors and other signaling molecules that can promote tissue regeneration. Additionally, PCL has been shown to have good mechanical properties, which can help maintain the structural integrity of the scaffold over time [30,31].

Tissue engineering and regenerative medicine face several challenges, particularly in bone tissue engineering, which hinder their progression to clinical practice. The main challenges are the need for a synergistic combination of biomaterials, cells, and factor therapy to induce new functional bone regeneration, the development of widely investigated biomaterial scaffolds with appropriate micro- and nano-structural properties, and the incorporation of biomimetic properties and growth factors. Other challenges include improving the biofunctionality, antimicrobial behavior, biocompatibility, and stem cell differentiation efficiencies of implants. Bone biofabrication using additive manufacturing techniques is suggested as a possible solution to these challenges. Additionally, animal and human trials are essential, and there is a need for close collaboration between medical doctors and biomaterials scientists to address critical problems and advance the field [32–35].

This work focuses on research on the 3D printing of scaffolds based on PHB biodegradable polymeric blends for tissue engineering and bone medical applications. The objective is to create a material that possesses appropriate thermal and mechanical properties, making it capable of being processed through FDM 3D printing. Additionally, it is essential for the material to be non-cytotoxic while also having the potential to be osteoconductive, osteoinductive, or osteogenic. The influence of material composition on cell proliferation was also established [36].

2. Materials and Methods

2.1. Materials

A total of three composite polymer blends were used in the research. Two blends were based on a plasticized blend of poly(3-hydroxybutyrate) (PHB) EDW 2394 from TianAn (Ningbo City, China) and polycaprolactone (PCL) Capa® 6500 from Perstorp (Malmö, Sweden) with the same composition as the PHB/PLA blends studied in our previous work [37]. The third material was based on poly(3-hydroxybutyrate) produced by the chloroform-free soap route (abbreviated as PHB-soap) [38] and amorphous poly(D,L-lactide) (PLA) Ingeo 4060D from NatureWorks (Minnetonka, MN, USA). All three materials were plasticized using Syncroflex TM 3114 (oligomeric adipate ester, abbreviated as SN) from Croda (Rawcliff, UK), and a tricalcium phosphate blend (αTCP = 7%, βTCP = 93%, abbreviated as TCP) from CN Lab Nutrition (Shaanxi, China) was added to the matrix as a bioactive filler. The mean particle size of TCP was 10.8 µm measured by laser diffraction using a HELOS analyzer by Sympatec GmbH (Remlingen, Germany). The composition of prepared biocomposites is given in Table 1.

Table 1. The composition of prepared and used materials: the basic mixture was composed of 12% of plasticizer, and the remaining 88% is PHB-soap/PLA or PHB/PCL in a ratio of 70/30. For filled samples, 15 wt% of TCP was added to the mixture.

	Amount (wt%)				
Material	**PHB or PHB-Soap**	**PLA**	**PCL**	**SN**	**TCP**
PHB-soap/PLA-SN	62	26	0	12	0
PHB/PCL-SN	62	0	26	12	0
PHB/PCL-SN-TCP	54	0	23	10	13

The extrusion process was performed using a corotating meshing twin screw extruder from Labtech Engineering Company (Samutprakarn, Thailand) (D = 16 mm, and L/D = 40), with the temperature setting of individual zones 80–180–180–180–180–175–170–160–160–160 °C from a hopper to a nozzle and a rotational speed of the screw set to 150 rev.·min^{-1}. The total weight of each sample for extrusion was 500 g.

2.2. 3D Printing Filaments

The HAAKE™ Rheomex OS single screw extruder (Haake Technik GmbH, Vreden, Germany) was used to process granules of prepared materials into 3D printing filaments. The chamber temperature profile from a hopper to a nozzle was set at 185–175–170–160 °C, while the screw's rotational speed was maintained at 20 rev.·min^{-1}. To ensure a constant diameter of the filament of 1.75 mm, the filament was directed to the calibration unit after being pulled through the water tank tempered to 60 °C, and the draw-off device passed through the air dryer before being wound onto a coil.

2.3. Differential Scanning Calorimetry (DSC)

Three newly prepared polymer blends, namely PHB-soap/PLA-SN, PHB/PCL-SN, and PHB/PCL-SN-TCP, were subjected to differential scanning calorimetry (DSC) to evalu-

ate their thermal properties. The samples were measured in two forms, granulate (marked as "_G") and prepared 3D printing filament (marked as "_F").

DSC measurements were conducted on DSC 2500 (TA Instruments, New Castle, DE, USA) under a nitrogen atmosphere. The samples were first cooled to −30 °C and then subjected to two heating cycles to 200 °C with a heating rate of 10 °C·min^{-1}. Aluminum pans with samples were hermetically sealed before the measurement, and the polymer sample masses were approximately 10 mg.

The crystallinity of the samples was calculated using Equation (1), where ΔH_m and ΔH^0_m (J/g) are the enthalpy of fusion from the second heating cycle and the enthalpy of fusion of 100% crystalline polymer (146 J/g for PHB and 139 J/g for PCL), respectively:

$$X_c = \frac{\Delta H_m}{\Delta H^0_m} \cdot 100\ (\%) \quad (1)$$

2.4. Parameters of 3D Printers

The specimens were printed using Original Prusa i3 MK3S and MK3 FDM 3D printers controlled by V3.9.0 firmware version, manufactured by Prusa Research a.s. in Prague, Czech Republic. The MK3S printer, equipped with a 0.25 mm diameter nozzle, was utilized for printing specimens intended for optical contact angle measurement (OCA), surface roughness analysis, and in vitro tests on scaffolds. On the other hand, the MK3 printer, which features a 0.4 mm diameter nozzle, was used for printing specimens intended for the temperature tower test, warping test, tensile test, three-point flexural test, and compression test.

All G-codes were prepared in PrusaSlicer, software version 1.41.2. PrusaSlicer is based on an open-source platform called Slic3r, licensed under the GNU Affero General Public License, version 3. The print profile used was taken from the profile for PLA. Therefore, the printed sample was cooled by a fan at 100% from the second layer. The flow value of 100% was used for all samples, except when the prepared 3D printing filaments tended to be a little bit thicker than the desired 1.75 mm, in which case the flow was changed to 95%.

The maximum printing space of both printers is 250 × 210 × 200 mm (x × y × z), with the resolution of the x and y-axes being 10 µm and the resolution of the z-axis being 5 µm. The basic printing parameters of the MK3S and MK3 printers are provided in Table 2.

Table 2. Basic printing parameters of Prusa i3 MK3S and MK3 FDM 3D printers used for printing all specimens.

Parameter	MK3S	MK3
Filament diameter	1.75 mm	1.75 mm
Nozzle diameter	0.25 mm	0.4 mm
Layer height	0.15 mm	0.2 mm
Width of a printed layer	0.3 mm	0.45 mm
Perimeter printing speed	45 mm·s^{-1}	45 mm·s^{-1}
Fill print speed	200 mm·s^{-1}	200 mm·s^{-1}
Bed temperature	20 °C	20 °C
Cooling fan power	100%	100%

2.5. Optimization of 3D Printing Temperature

The 3D printing filaments underwent tests to assess their printability and determine the ideal processing conditions. The temperature tower test (TTT) was used to optimize the temperature of the nozzle. The test involved three towers, with the first tower having a temperature range of 220–195 °C, the second tower having a range of 195–170 °C, and the third tower having a range of 175–150 °C. The temperature range started with the highest temperature at the bottom and gradually decreased by 5 °C to the lowest temperature at the top. A separate article provides further details [39].

2.6. Determination of Warping Coefficient

There were two aspects to optimizing warping during 3D printing. First, the optimal printing temperature (or temperatures) was determined based on the TTT, along with one or two additional temperatures 5 °C above and below. To test for warping, a smaller value of the warping coefficient was preferred. Further information about this test is provided in our previous publication [39].

Once the optimal printing temperature for a particular material was determined, it was used for all subsequent printings of that material. The first temperature of the pair was used to print the brim and the first layer of the specimen, while the second temperature was used for printing all remaining layers.

For PHB-soap/PLA-SN, the flow was set to 100%, the fan was disabled, and the printing speed was set to 80%. This ensured that each printed layer had enough time to cool down before the next layer was printed.

2.7. Compression Moulding and 3D Printing of Testing Specimens

The process of compression molding was employed to produce granules of composite materials using a hydraulic laboratory press Qnubu Rosin Press (Qnubu, Parets del Vallès, Spain). To begin the process, 5 g of granulate was evenly distributed on the press plate. A spacer grid with a thickness of 1 mm was used to determine the final thickness of the plate. The press plates were inserted between the top and bottom platforms that were heated to a temperature of 190 °C. The molding process took 100 s under a pressure of 20 MPa. Once the process was complete, the press plates were removed, and the molded plate was allowed to cool at laboratory temperature for one minute. Finally, the press plates were rapidly cooled under running water until the molded plate could be removed.

2.8. 3D Printing of Testing Specimens

The original PrusaSlicer software (Prusa Research a.s., Prague, Czech Republic) was used to create the G-codes for 3D printing all specimens. Standardized double-paddle testing specimens (dogbones 5A) with a cross-section of 4 × 2 mm, according to the CSN EN ISO 527-2, were printed for tensile testing. The G-code for 3D printing the dogbones involved regular alternating of two layers. The first layer was created by importing the fabricated model to the PrusaSlicer software and adjusting the perimeters to form the entire neck of the dogbone. The second layer was formed manually by inserting infill parallel to the longest dimension of the dogbone. A separate article described the development of this G-code [40].

For the three-point flexural test, rectangular testing specimens with dimensions of 80 × 10 × 4 mm were printed. The G-code was created so that the entire volume of the specimen consisted exclusively of perimeters. In cases where specimens contained PCL, the bed was heated to 60 °C to facilitate removal.

Rectangular testing specimens with dimensions of 10 × 4 × 10 mm were printed for the compression test. Testing specimens for all the mechanical tests were printed using all five polymer blends prepared. In cases where specimens contained PCL, the bed was heated to 60 °C to facilitate removal after the end of printing.

2.9. Mechanical Testing

To evaluate the properties of the prepared materials, three mechanical tests were conducted, including tensile, three-point flexural, and compression tests. The measurements were carried out 7 days after the sample preparation to ensure the completion of the material crystallization process. The average of at least six measurements was taken for each test, and the results were presented as mean ± SD.

For the mechanical tests, the ZwickRoell Z010 device from ZwickRoell GmbH & Co. (Ulm, Germany). was used. The tensile, flexural, and compression tests were conducted according to the CSN EN ISO 527, CSN EN ISO 178, and CSN EN ISO 604 standard methods,

respectively. The details of the testing conditions for tensile and flexural tests can be found in our previous article [37].

In the compression test, a load indicator with a maximum force of 10 kN was utilized, and the preload was set to 1 N. The compression modulus was determined from the deformation range of 1.25–1.50%. The test speed was set to 1 mm·min^{-1}, and the limit deformation for the end of the measurement was set to 10%.

2.10. Optical Contact Angle Measurement (OCA) and Surface Energy Evaluation

The surface energy of all five materials was determined by measuring molded plates made from their melt. Contact angles and their standard deviations were used to calculate surface energy, including dispersive and polar components, using an OCA 10 (Dataphysics, Filderstadt, Germany) with SCA-2000 software (Xi'an, China). Four liquids were used in the measurement, including water, diiodomethane, formamide, and diethylene glycol, with water and diethylene glycol acting as polar liquids and diiodomethane and formamide as nonpolar liquids. The average of at least ten drops was taken to determine the results, which are presented as mean ± SD. The contact angle with a certain liquid indicates the degree of effort required by the liquid to minimize its contact with the surface.

The OWRK method (Owens, Wendt, Rabel, and Kaelble) was employed, and results for each liquid were added according to the corresponding research methodology, including Rabel for water, Owens et al. for diiodomethane, Rabel for formamide, and Erbyl for diethylene glycol.

2.11. Cytotoxicity Measurement

To determine whether the newly prepared materials (PHB-soap/PLA-SN, PHB/PCL-SN, and PHB/PCL-SN-TCP) were suitable for use in tissue engineering, cytotoxicity tests were conducted on these materials. The materials were sterilized with ethylene oxide, and the culture of their extracts was used with osteoblastic cell line MC3T3-E1 fibroblasts to evaluate their biocompatibility. The cells were subjected to metabolic activity assay and visualization using optical microscopy. The biocompatibility of the samples is essential for their use in tissue engineering applications. The test was performed in accordance with EN ISO 10993.

The extracts were prepared by incubating the samples (6 mm in diameter, sterilized using ethylene oxide) in growth medium DMEM (Sigma Aldrich) supplemented with 10% fetal bovine serum and 1% antibiotics (Penicillin/Streptomycin) at 37 °C for 48 h, 250 µL/sample. 3T3 mice fibroblasts were seeded in a growth medium in a 96-well plate with a density of 2×10^3 cells per well and cultured with the extracts for 24 and 72 h at 37 °C and 10% CO_2. After 24 h, 200 µL of the extract was added to each well.

Cell morphology and proliferation were observed using optical microscopy 24 and 72 h after seeding (microscope Olympus IX51, camera Olympus DP80), and the MTS assay (CellTiter 96® AQueous One Solution Cell Proliferation Assay; Promega) was performed to assess cell viability. Cells were incubated in MTS solution (20 µL) and 100 µL of the fresh culture medium at 37 °C for 2 h. The MTS substrate was metabolized by mitochondrial enzymes to violet formazan, which absorbs light at 490 nm. The absorbance of the solution (100 µL) was measured using a microplate reader (Infinite M200 PRO, Tecan, Switzerland) at 490 nm and reference wavelength 690 nm. The absorbance of the pure medium with MTS substrate was subtracted from the values.

The MTS test uses a new type of tetrazolium dye, which ultimately results in an aqueous, soluble formazan product. The tetrazolium dye used in the MTS assay is 3-(4,5-dimethylthiazol-2-yl)-5-(3-carboxymethoxyphenyl)-2-(4-sulfophenyl)-2H-tetrazolium. The formation of the soluble formazan dye occurs in the presence of phenazine methosulfate (PMS), which serves as an intermediate electron acceptor, transferring electrons from NADH to reduce the tetrazolium dye, forming the soluble formazan product. The main difference between MTT and MTS assay is that MTT assay has an additional step associated with the solubilization of formazan crystals, whereas MTS assay is not associated with

the solubilization of formazan crystals. Therefore, the MTS test is more effective and less time-consuming.

The MTS assay was performed on six independently prepared samples, and the data were statistically evaluated using SigmaStat 12.0 (Systat, Palo Alto, CA, USA). Quantitative data are presented as mean values ± standard deviation (SD). The statistical significance between a pair of groups was determined by the ANOVA test and Student–Newman–Keuls test for post hoc analysis if the data passed the normality test and the test of equality of variances. If the data were without normal distribution, statistical significance between a pair of groups was determined using Kruskal–Wallis One Way Analysis of Variance on Ranks and Dunn's multiple comparisons test for post hoc analysis. A p-value less than 0.05 was considered statistically significant. Margin values were not included due to the variability of the measured results, but at least four samples were used for the statistical evaluation.

3. Results

3.1. Thermal Properties of Prepared Materials and Filaments for 3D Printing

Differential Scanning Calorimetry (DSC)

Table 3 displays the crystallization temperatures (T_c) and crystallinities (X_c) of PHB and PCL. The measured melting temperature (T_m) of PHB-soap was between 168.2–169.7 °C, while PCL was between 52.0–54.2 °C. Therefore, the melting temperatures were not included in the table. The crystallinity of PHB-soap remained relatively stable in both granulate and filament forms, with only a 0.9% change. Moreover, the thermal properties of PHB-soap, such as the melting and crystallization temperatures, were not affected by the process of preparing 3D printing filament from granulate by extrusion.

Table 3. The results of DSC measurement; N/A used where not applicable.

Material	T_c, PHB (°C)	X_c, PHB (%)	T_c, PCL (°C)	X_c, PCL (%)
PHB-soap/PLA-SN_G	78.3	58.9	N/A	N/A
PHB-soap/PLA-SN_F	78.8	58.0	N/A	N/A
PHB/PCL-SN_G	78.4	69.9	2.2	45.7
PHB/PCL-SN_F	87.6	61.5	28.4	59.2
PHB/PCL-SN-TCP_G	88.8	83.5	−2.5	13.5
PHB/PCL-SN-TCP_F	86.5	64.2	25.0	51.3

When comparing the thermal properties of PHB-soap and commercial PHB, it was found that only the T_c of the PHB/PCL-SN_G blend was comparable to that of PHB-soap/PLA-SN in granulate and filament form. In all other blends, the T_c was approximately 10 °C greater than that of PHB-soap. Additionally, the crystallinity (X_c) of commercial PHB blends was always higher than that of PHB-soap.

It was observed that TCP and the process of filament extrusion have a nucleating effect on commercial poly(3-hydroxybutyrate), leading to an increase in T_c. In contrast, TCP does not nucleate PCL, but the process of filament extrusion does, resulting in an increase in T_c and crystallinity.

3.2. Optimisation of Processing Conditions and Printability Testing of Prepared 3D Printing Filaments

3.2.1. Temperature Tower Test (TTT)

Table 4 presents all the results obtained from the temperature tower test (TTT). Figure 1 illustrates an example of 3D-printed temperature towers. Each tower provided a range of applicable temperatures, and the quality of the printed geometric elements on each tower was considered to determine the best temperature or range of temperatures for 3D printing. After conducting the TTT, the optimal temperature or temperatures for 3D printing were determined to be 190–185 °C for PHB-soap/PLA-SN, 170 °C for PHB/PCL-SN, and 170–165 °C for PHB/PCL-SN-TCP. These temperatures were then utilized for the warping test.

Table 4. The results of the temperature tower test (TTT); floor/floors with the best printed geometric element within a single tower; N/A used when no temperature or interval could be selected as the best.

Material	Temperature Range (°C)	Stringing	Colonnade	Diagonal	Holes in Structure	Last Printed Floor (°C)	Best Temperature (°C)
PHB-soap/PLA-SN	220–195	N/A	N/A	N/A	N/A	195	N/A
	195–170	190–170	190–170	185	185–170	170	190–170
	175–150	175–165	175–170	170	175–165	160	175–170
PHB/PCL-SN	220–195	N/A	N/A	N/A	N/A	195	N/A
	195–170	N/A	N/A	N/A	N/A	170	N/A
	175–150	170	170	170	170	165	170
PHB/PCL-SN-TCP	220–195	N/A	N/A	N/A	N/A	195	N/A
	195–170	N/A	N/A	N/A	195–170	170	170
	175–150	N/A	N/A	165	175–165	165	165

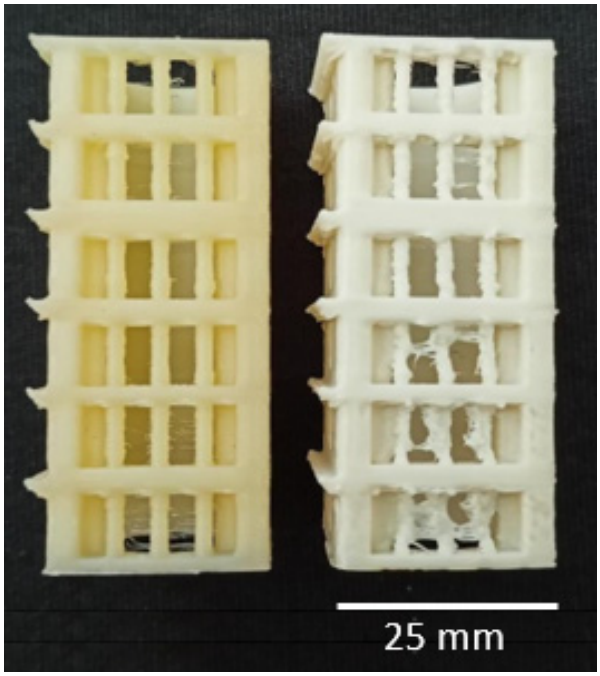


Figure 1. An image of 3D printed temperature towers of PHB-soap/PLA-SN (temperature range 195–170 °C) with optimal quality of printed elements (**left**) and PHB/PCL-SN-TCP (temperature range 220–195 °C) with non-optimal quality of printed elements (**right**).

3.2.2. Warping Test

Table 5 presents the results of the warping test. A linear trend can be observed in the warping coefficient for PHB/PCL-SN, where the coefficient decreases with increasing temperature. However, in the case of the PCL blend with TCP, the warping coefficient increases. It should be noted that the dependency plot was based on only three points, and additional data would be required to further support this observation. Taking into account all the results from the TTT and warping test, the final processing temperatures for the 3D printing of the three prepared composite materials were determined. The processing temperatures selected were 195/190 °C for PHB-soap/PLA-SN, 195/175 °C for PHB/PCL-SN, and 195/165 °C for PHB/PCL-SN-TCP.

Table 5. The results of the warping test (the lowest warping coefficients are highlighted in green).

Material	Temperature (°C)	Average Warping Coefficient ± SD (-)
PHB-soap/PLA-SN	190	2.59 ± 0.08
	185	3.06 ± 0.11
PHB/PCL-SN	175	1.26 ± 0.02
	170	1.30 ± 0.02
	165	1.55 ± 0.03
PHB/PCL-SN-TCP	175	1.81 ± 0.04
	170	1.65 ± 0.03
	165	1.53 ± 0.03

3.3. Mechanical Properties

3.3.1. Tensile Test

The results of the tensile test are presented in Figure 2, which illustrates that the addition of TCP to the PHB/PCL blend results in a reduction of the blend's tensile strength by 10.5%. Additionally, the ductility of the blend decreases as the TCP performs the function of a stress concentrator. On the other hand, the addition of TCP increases Young's modulus by 28.6%, which is typical for fillers.

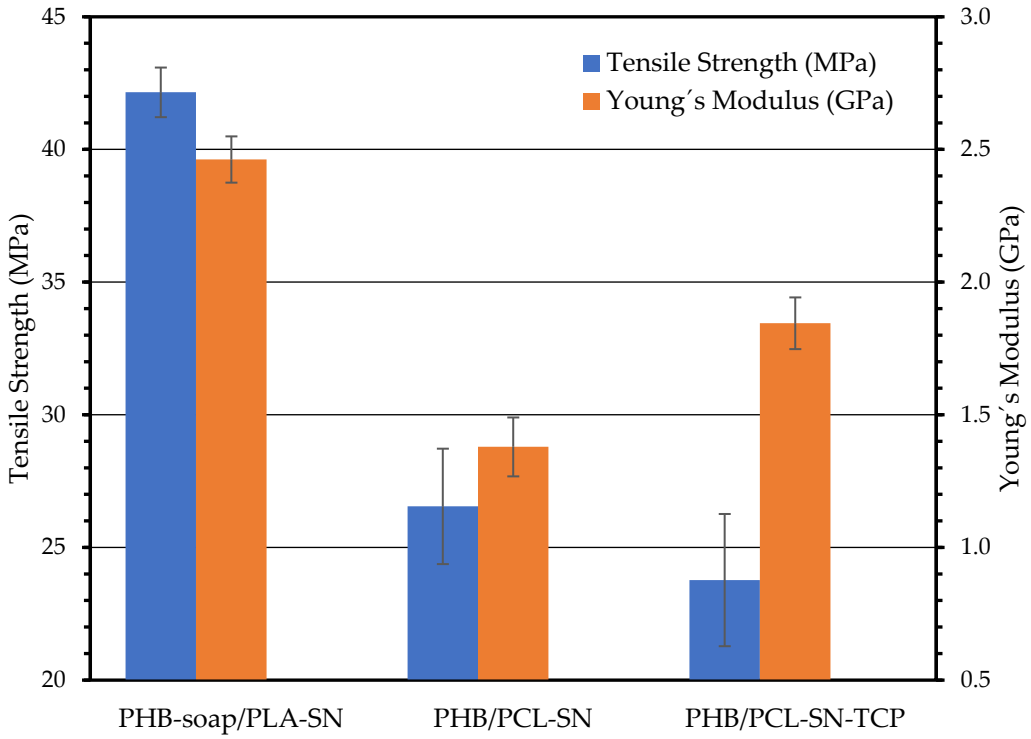


Figure 2. The results of tensile test of 3D printed dogbones.

In comparison to their PHB/PLA counterpart, PHB/PCL blends exhibit lower values of measured characteristics because PCL is more ductile at room temperature than PLA due to its lower glass transition temperature (T_g) of −60 °C compared to PLAs 60 °C, which results in more ductile specimens.

3.3.2. Three-Point Flexural Test

The graph in Figure 3 presents all the results obtained from the flexural test. As in the case of the tensile test, PHB/PCL blends do not reach such mechanical properties in comparison to PHB-soap/PLA. The addition of TCP to the PHB/PCL blend enhanced

flexural strength by 11.1% and flexural modulus by 36.4%, providing reinforcement against bending stress. These results confirm the assumption that PCL blends exhibit lower mechanical properties than PLA blends due to the lower glass transition temperature of PCL and that the addition of a bioactive filler (TCP) helps to at least partially improve these mechanical properties.

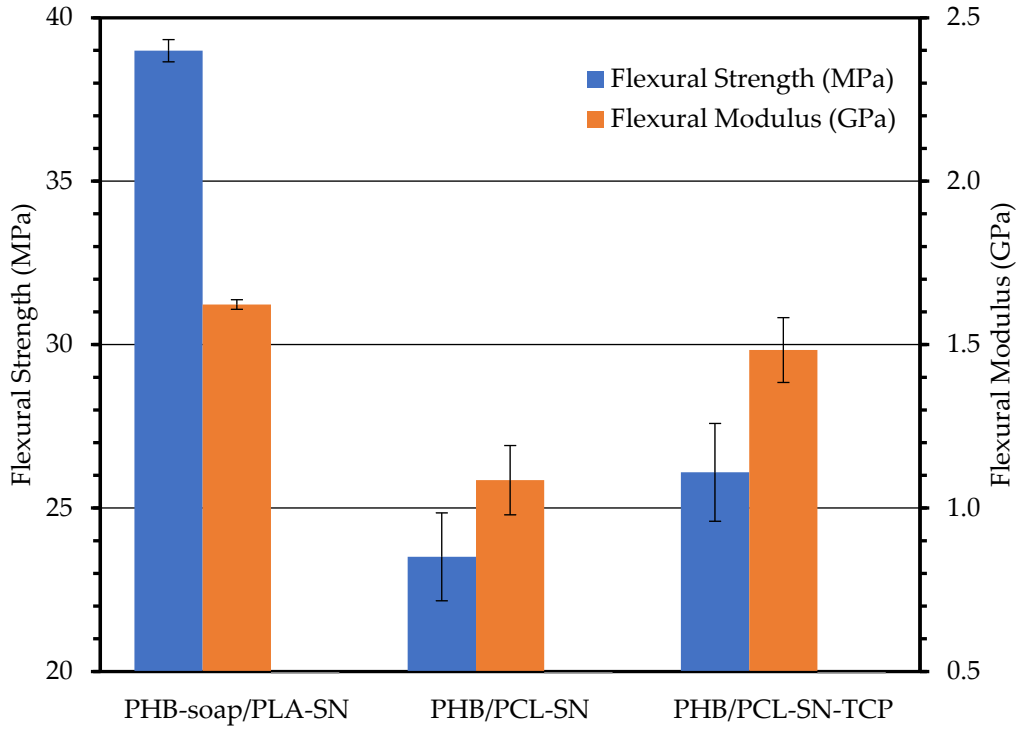


Figure 3. The results of a three-point flexural test of 3D printed specimens.

3.3.3. Compression Test

The compression test results are illustrated in Figure 4, showing that the addition of TCP to the PHB/PCL blend significantly increases compressive strength and compression modulus. The reinforcement of the specimens against pressure accounts for the improvement in mechanical properties. Compared to PHB/PCL blends, PHB/PLA blend exhibits higher mechanical properties, as confirmed by the three tests.

In terms of mechanical properties, the PHB/PLA blend displays the highest strength during compression testing, although the strengths during tensile and flexural tests are also comparable to those during compression tests. During the tensile test, the specimens show the highest modulus, while the flexural and compression moduli are relatively lower.

When comparing the mechanical test results with human trabecular bone, which is a porous and relatively poorly calcified material, the moduli can range between 0.01–3 GPa, and the strengths between 0.1–30 MPa, depending on the bone type, its location in the body, and the orientation of applied stress [41].

The addition of TCP into the blends has a positive impact on Young's modulus, flexural strength, flexural modulus, compressive strength, and compression modulus. However, it decreases the tensile strength and ductility of the 3D-printed specimens of the PHB/PCL blend. The positive influence on mechanical properties is more significant and critical for scaffolds intended for bone tissue engineering, even though the ductility decreases.

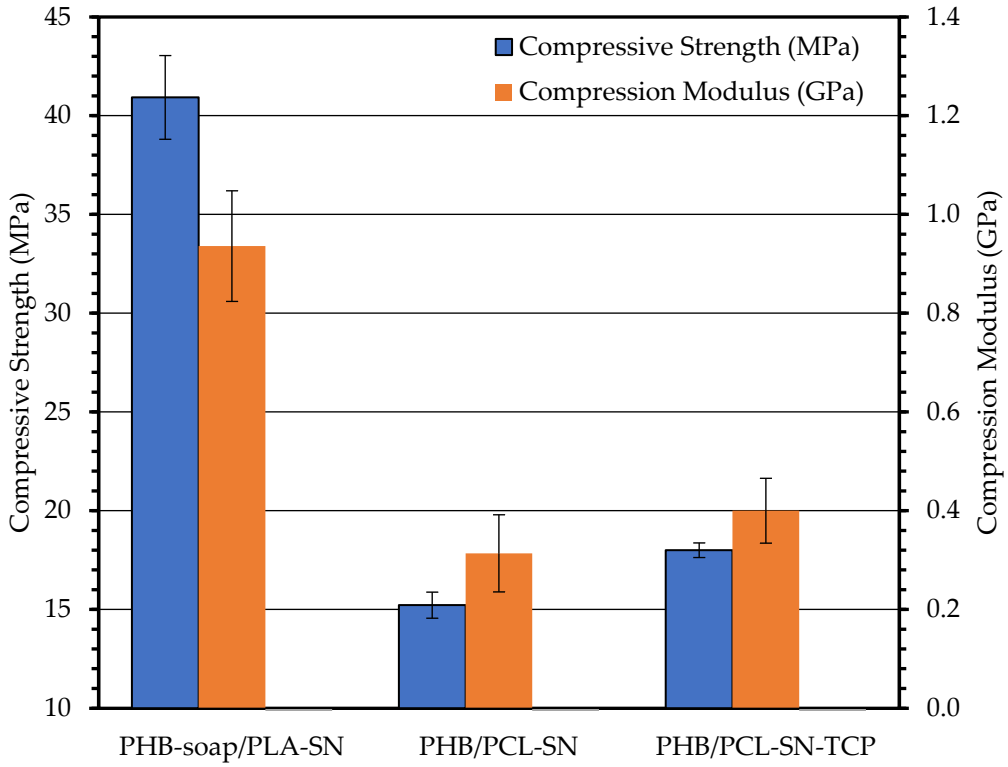


Figure 4. The results of compression test of 3D printed specimens.

3.4. Surface Properties and Their Influence on Cell Adhesion

Optical Contact Angle Measurement (OCA) and Surface Energy Calculation of Prepared Materials

Table 6 presents the results of optical contact angle measurement (OCA) conducted on molded plates of all three composite materials. The contact angle of water was the greatest among all liquids used, with a value of 84.6° for the PHB-soap blend. This indicates that all prepared materials exhibit nonpolar hydrophobic character, repelling polar liquids. Diethylene glycol, the second polar liquid used, showed the second-greatest contact angle only in the case of the PHB-soap/PLA blend. However, the contact angles of all other remaining liquids were very similar to that of diethylene glycol, with a difference of only approximately 2°, probably due to its comparatively lower polarity than water. In three of five cases, the lowest contact angle was observed for diiodomethane, with PHB/PCL-SN exhibiting the lowest contact angle of just 22.9°. This further confirms the hydrophobic nature of all five materials, as diiodomethane is the least polar of all four liquids used. Figure 5 illustrates the difference between good and poor wetting.

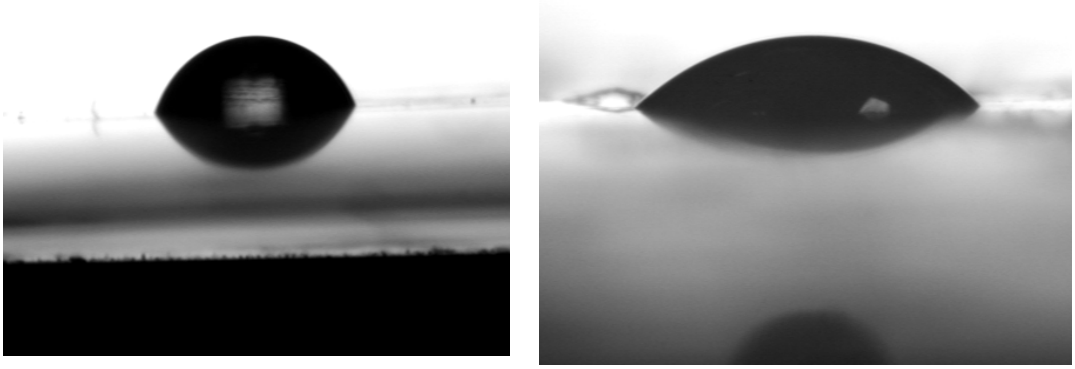


Figure 5. An image of PHB-soap/PLA-SN surface with a water drop (**left**) and PHB/PCL-SN-TCP surface with diethylene glycol (**right**).

Table 6. Optical contact angle measurement (OCA) and surface energy of molded specimens.

Material	Liquid	Contact Angle (°) ± SD	Surface Energy (mN/m)	Dispersive Component	Polar Component
PHB-soap/PLA-SN	Water Diiodomethane Formamide Diethylene glycol	84.6 ± 2.6 39.2 ± 1.7 38.7 ± 2.5 42.3 ± 2.0	40	35	5
PHB/PCL-SN	Water Diiodomethane Formamide Diethylene glycol	72.7 ± 3.5 22.9 ± 1.4 55.5 ± 1.8 42.2 ± 1.6	40	30	10
PHB/PCL-SN-TCP	Water Diiodomethane Formamide Diethylene glycol	72.1 ± 4.2 35.1 ± 2.2 47.7 ± 2.7 43.3 ± 0.9	41	30	11

All materials had a very similar surface energy of around 40 mN/m, with a dispersive component of approximately 30 mN/m and a polar component of 10 mN/m, similar to PMMA or PEO [42]. PHB-soap/PLA-SN showed a dispersive component 5 mN/m greater and a lower polar component by the same amount compared to all other materials, indicating even less polarity and more hydrophobicity. The calculated surface energies of all materials (40 mN/m) were found to be suitable for cell growth and proliferation according to previously published studies [43,44].

The surface energy of PHB homopolymer is 47 mN/m with a dispersive component of 38 mN/m and a polar component of 9 mN/m [45]. On the other hand, the surface energy of PLA is 36 mN/m with a dispersive component of 27 mN/m and a polar component of 9 mN/m [46], while PCL has a surface energy of 31 mN/m with a dispersive component of 26 mN/m and a polar component of 5 mN/m [47].

3.5. Cytotoxicity Measurement

The impact of the extracts of the materials on 3T3 fibroblasts was used to determine their cytotoxicity. After the addition of the extracts, the metabolic activity of the cells was evaluated by performing the MTS test at 24 and 72 h, as presented in Figure 6. PHB-soap/PLA-SN exhibited the lowest absorbance value after 24 h, while the blends of PHB/PCL had nearly equivalent absorbance values. The PHB/PCL-SN-TCP absorbance value was comparable to that of the control group. Meanwhile, the value of PHB/PCL-SN was statistically higher. The blends of PHB/PCL showed increased metabolic activity, with absorbance levels higher than those of the control group. However, PHB-soap/PLA-SN exhibited very low metabolic activity and displayed cytotoxicity.

The cells in the control group that were cultured in a normal medium appeared healthy, and their population increased up to day 3, as presented in Table 7. The cells that were cultured in extracts of PHB/PCL-SN and PHB/PCL-SN-TCP displayed good morphology and formed a confluent layer after 72 h. The group with PHB-soap/PLA-SN extracts exhibited fewer cells compared to the other groups, and even though some of the cells in this group proliferated, the rest underwent apoptosis.

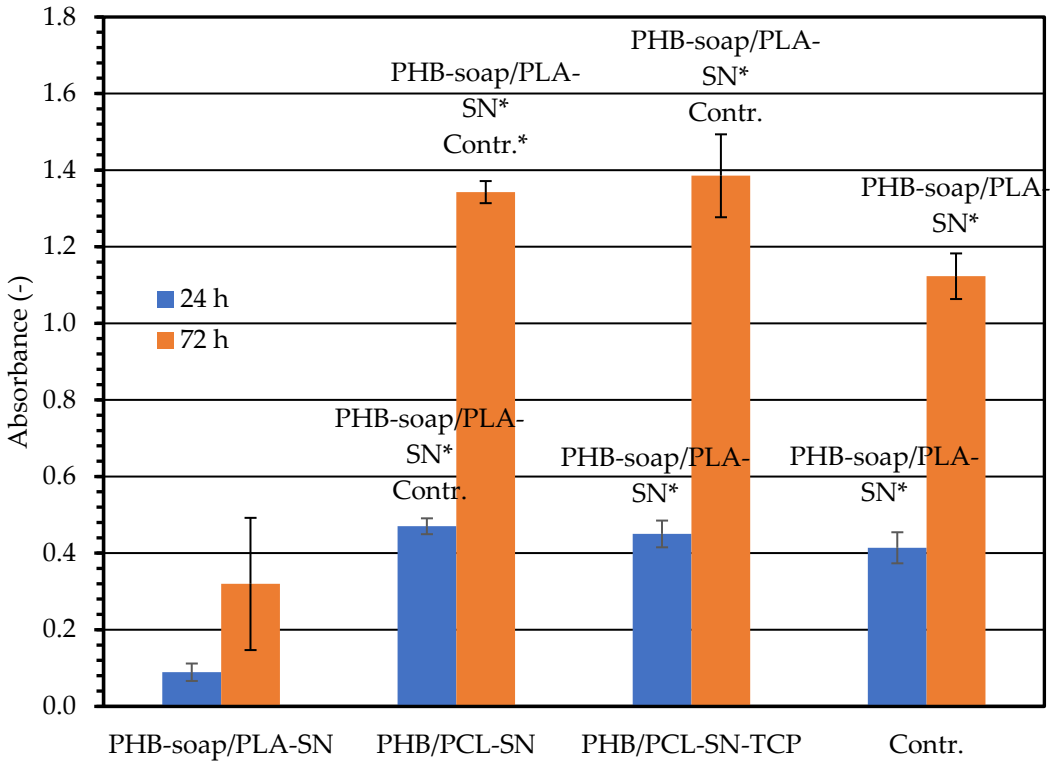
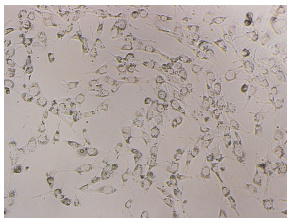
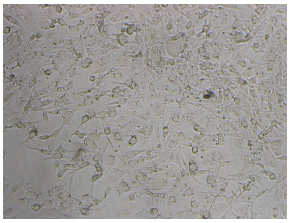
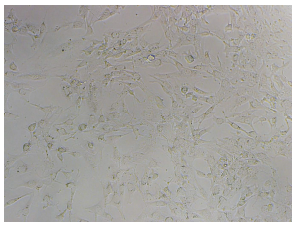
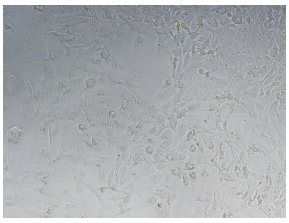
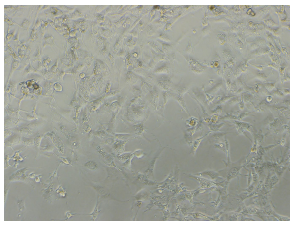
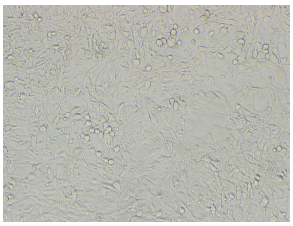
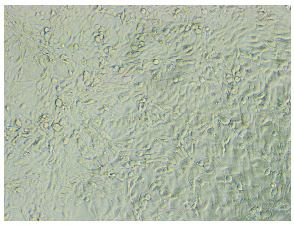
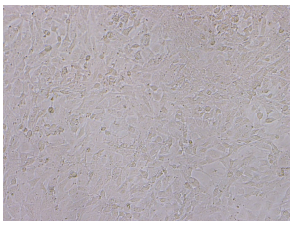


Figure 6. Metabolic activity of 3T3 fibroblasts cultured in extracts measured using MTS test 24 and 72 h after seeding. 3T3 fibroblasts cultured in growth medium were used as a control (Contr.). The labels above the columns sign statistical significance ($p < 0.05$, * $p < 0.001$).

Table 7. The cells cultured in extracts were visualized using optical microscopy 24 and 72 h after seeding; magnification 100×.

Time	PHB-Soap/PLA-SN	PHB/PCL-SN	PHB/PCL-SN-TCP	Contr.
24 h				
72 h				

4. Discussion

Optimal printing temperatures of 195/190 °C for PHB-soap/PLA-SN, 195/175 °C for PHB/PCL-SN, and 195/165 °C for PHB/PCL-SN-TCP were identified. The measured melting temperature (T_m) of PHB-soap was found to be between 168.2–169.7 °C, while that of PCL was between 52.0–54.2 °C. It was observed that TCP and the process of filament extrusion had a nucleating effect on commercial poly(3-hydroxybutyrate), leading to an increase in T_c. Despite the fact that the mechanical properties of PHB/PCL blends were lower than those of PHB-soap/PLA in all mechanical tests, they still compared favorably

with human trabecular bone. These blends exhibited strengths of approximately 40 MPa and moduli of around 2.5 GPa. Furthermore, the materials prepared were found to be hydrophobic, with surface energies of approximately 40 mN/m. Unfortunately, PHB-soap/PLA-SN was found to be cytotoxic, while PHB/PCL-SN and PHB/PCL-SN-TCP were non-cytotoxic and biocompatible. Therefore, these two PHB/PCL blends hold great potential for future research in tissue engineering.

Ecker et al. developed blends of polylactic acid (PLA) with an amorphous copolymer of polyhydroxyalkanoates (PHA), where the specific composition of the PHA copolymer was not disclosed. The temperature used for 3D printing was 205 °C for the entire sample, and the printing bed was heated to 80 °C. The resulting mechanical properties of the PLA/PHA blend, with tensile strengths of approximately 40 MPa and Young's moduli of 2.5 GPa, were comparable to those observed for the novel material PHB-soap/PLA, which was prepared by a chloroform-free extraction process. Furthermore, the crystallinity of the PLA/PHA blend was found to be approximately 55%, which is consistent with the observed thermal properties of the PHB-soap/PLA blend. These findings suggest that PHB-soap extracted by the chloroform-free process exhibits similar properties to commercially available PHB extracted using traditional solvents. Moreover, the printing temperature of PHB-soap/PLA was only 10 °C lower than the PLA/PHA blend, and bed heating was not required, indicating that PHB-soap/PLA may be a promising candidate for 3D printing applications [7].

Abdelwahab et al. investigated the preparation of a blend consisting of 75 wt% polylactic acid (PLA) and 25 wt% poly(3-hydroxybutyrate) (PHB), which were plasticized with 5 and 7 wt% of a polyester plasticizer, Lapol 108. The resulting blends exhibited crystallinity values ranging from 36 to 40%. However, despite the attempts to improve the mechanical properties of the blends, the tensile strength and Young's modulus remained poor, measuring only 15 MPa and 1.2 GPa, respectively [48].

In this study, Wang et al. investigated the potential to enhance the mechanical properties of PLA filaments by blending them with PHB in an 80/20 weight ratio. The optimal 3D printing temperature for the PLA/PHB blend was found to be 190 °C, which was lower than that of neat PLA (210 °C). The presence of PHB domains resulted in a decrease in Young's modulus and tensile strength from 3.6 GPa to 3.4 GPa and from 66 MPa to 55 MPa, respectively. However, annealing the samples resulted in a significant improvement in their mechanical properties, with Young's modulus even exceeding that of neat PLA [49].

Laoutid et al. prepared PHB/PCL blends by reactive extrusion. In this study, the mechanical properties of PHB/PCL blends were significantly improved by the addition of DCP as a compatibilizing promotor and grafting agent, as well as low molecular weight PEG as a plasticizer. The resulting materials showed that the thermal stability of the blend was slightly improved, with a bimodal PHB melting endotherm indicating the occurrence of grafting and crosslinking reactions. With the ratio of PHB/PCL shifted from 80/20 to 60/40, Young's modulus decreased from 1.4 GPa to 700 MPa and tensile strength from 34.5 MPa to 19.1 MPa. PCL is above its T_g at ambient conditions, which results in the deterioration of mechanical properties with higher PCL content [50].

Regrettably, none of the studies presented in this research delved into the biocompatibility of the prepared blends. Their main focus was on enhancing processing techniques and mechanical properties. Nonetheless, the novel materials showcased in this study possess a significant advantage in terms of their properties being similar to, or even better than, those examined in previous publications.

These findings propose that PHB/PCL blends hold great potential for future research in bone regeneration applications, as they can substitute or aid damaged bone tissues. Additionally, leveraging 3D printing technology to develop patient-specific implants and scaffolds using these materials could boost the success rates of bone regeneration surgeries and reduce the need for invasive surgeries and implant rejection. Furthermore, the study's results emphasize the importance of conducting thorough cytotoxicity testing for new biomaterials to guarantee their biocompatibility and safety for use in medical applications.

Taken together, the findings of this study represent a promising step toward the development of novel biomaterials for tissue engineering and medical bone applications, with the potential for future clinical translation.

5. Conclusions

The objective of this study was to explore the potential of 3D printable polymer blends for bone medical applications and tissue engineering. The objective was to develop a material that possesses appropriate thermal and mechanical properties, making it capable of being processed through FDM 3D printing. Additionally, it is essential for the material to be non-cytotoxic while also having the potential to be osteoconductive, osteoinductive, or osteogenic.

In conclusion, this work presents the preparation and characterization of PHB-based composite blends for bone medical applications and tissue engineering. The PHB used was obtained by both commercial and chloroform-free routes and blended with PLA or PCL, plasticized by oligomeric adipate ester, and supplemented with TCP particles. The blends were processed into 3D printing filaments and tested for their thermal, mechanical, surface, and cytotoxic properties. The best temperatures for 3D printing were determined for each blend, and their mechanical properties were found to be comparable to human trabecular bone. However, only two out of the three blends were non-cytotoxic, indicating further development is required for some of the materials tested. Overall, the results show the potential of these PHB-based composite blends for use in bone medical applications and tissue engineering.

Author Contributions: Conceptualization, R.P., V.M., P.M., Š.K.; methodology, R.P., P.M., M.R.; validation, Š.K., V.M., S.K.; formal analysis, Š.K., V.M., M.R.; investigation, Š.K. (Štěpán Krobot), V.M., M.R., V.H., E.M., A.B.; resources, R.P., E.M.; data curation, Š.K., V.M.; writing—original draft preparation, Š.K.; writing—review and editing, Š.K., V.M., S.K.; supervision, R.P., V.M., P.M.; project administration, R.P.; funding acquisition, R.P., V.H., S.K. All authors have read and agreed to the published version of the manuscript.

Funding: Authors acknowledge the funding by Brno University of Technology by the Specific University Research Grant through the project FCH-S-23-8208, and Operational Program Integrated Infrastructure for the project "Center for Medical Bioadditive Research and Production (CEMBAM), code ITMS2014 +: 313011V358, co-financed by the European Regional Development Fund".

Institutional Review Board Statement: Not applicable.

Informed Consent Statement: Not applicable.

Data Availability Statement: The data are available upon reasonable request from the corresponding author.

Conflicts of Interest: Author Andrej Baco was employed by the company PANARA. The remaining authors declare that the research was conducted in the absence of any commercial or financial relationships that could be construed as a potential conflict of interest.

References

1. Kramschuster, A.; Turng, L.-S. 17—Fabrication of Tissue Engineering Scaffolds. In *Handbook of Biopolymers and Biodegradable Plastics*; Ebnesajjad, S., Ed.; Plastics Design Library; William Andrew Publishing: Boston, MA, USA, 2013; pp. 427–446. [CrossRef]
2. Surisaeng, J.; Kanabenja, W.; Passornraprasit, N.; Aumnate, C.; Potiyaraj', P. Polyhydroxybutyrate/Polylactic Acid Blends: An Alternative Feedstock for 3D Printed Bone Scaffold Model. *J. Phys. Conf. Ser.* **2022**, *2175*, 12021. [CrossRef]
3. Amin, S.; Achenbach, S.J.; Atkinson, E.J.; Khosla, S.; Melton, L.J. Trends in Fracture Incidence: A Population-Based Study over 20 Years. *J. Bone Miner. Res.* **2014**, *29*, 581–589. [CrossRef] [PubMed]
4. Johnell, O.; Kanis, J.A. An Estimate of the Worldwide Prevalence and Disability Associated with Osteoporotic Fractures. *Osteoporos. Int.* **2006**, *17*, 1726–1733. [CrossRef] [PubMed]
5. Gregor, A.; Filová, E.; Novák, M.; Kronek, J.; Chlup, H.; Buzgo, M.; Blahnova, V.; Lukášová, V.; Bartoš, M.; Nečas, A.; et al. Designing of PLA Scaffolds for Bone Tissue Replacement Fabricated by Ordinary Commercial 3D Printer. *J. Biol. Eng.* **2017**, *11*, 31. [CrossRef] [PubMed]

6. Esposito Corcione, C.; Gervaso, F.; Scalera, F.; Montagna, F.; Sannino, A.; Maffezzoli, A. The Feasibility of Printing Polylactic Acid–Nanohydroxyapatite Composites Using a Low-Cost Fused Deposition Modeling 3D Printer. *J. Appl. Polym. Sci.* **2017**, *134*, 44656. [CrossRef]
7. Ecker, J.V.; Burzic, I.; Haider, A.; Hild, S.; Rennhofer, H. Improving the Impact Strength of PLA and Its Blends with PHA in Fused Layer Modelling. *Polym. Test.* **2019**, *78*, 105929. [CrossRef]
8. Shunmugasundaram, M.; Baig Maughal, A.A.; Kumar, M.A. A Review of Bio-Degradable Materials for Fused Deposition Modeling Machine. *Mater. Today Proc.* **2020**, *27*, 1596–1600. [CrossRef]
9. Kovalcik, A.; Sangroniz, L.; Kalina, M.; Skopalova, K.; Humpolíček, P.; Omastova, M.; Mundigler, N.; Müller, A.J. Properties of Scaffolds Prepared by Fused Deposition Modeling of Poly(Hydroxyalkanoates). *Int. J. Biol. Macromol.* **2020**, *161*, 364–376. [CrossRef]
10. Savenkova, L.; Gercberga, Z.; Nikolaeva, V.; Dzene, A.; Bibers, I.; Kalnin, M. Mechanical Properties and Biodegradation Characteristics of PHB-Based Films. *Process Biochem.* **2000**, *35*, 573–579. [CrossRef]
11. Lenz, R.W.; Marchessault, R.H. Bacterial Polyesters: Biosynthesis, Biodegradable Plastics and Biotechnology. *Biomacromolecules* **2005**, *6*, 1–8. [CrossRef]
12. Kaygusuz, B.; Özerinç, S. Improving the Ductility of Polylactic Acid Parts Produced by Fused Deposition Modeling through Polyhydroxyalkanoate Additions. *J. Appl. Polym. Sci.* **2019**, *136*, 48154. [CrossRef]
13. Ebnesajjad, E. (Ed.) *Handbook of Biopolymers and Biodegradable Plastics*, 1st ed.; Elsevier: Amsterdam, The Netherlands, 2012. Available online: https://www.elsevier.com/books/handbook-of-biopolymers-and-biodegradable-plastics/ebnesajjad/978-1-4557-2834-3 (accessed on 7 February 2022).
14. Dubinenko, G.; Zinoviev, A.; Bolbasov, E.; Kozelskaya, A.; Shesterikov, E.; Novikov, V.; Tverdokhlebov, S. Highly Filled Poly(L-Lactic Acid)/Hydroxyapatite Composite for 3D Printing of Personalized Bone Tissue Engineering Scaffolds. *J. Appl. Polym. Sci.* **2021**, *138*, 49662. [CrossRef]
15. Wurm, M.C.; Möst, T.; Bergauer, B.; Rietzel, D.; Neukam, F.W.; Cifuentes, S.C.; von Wilmowsky, C. In-Vitro Evaluation of Polylactic Acid (PLA) Manufactured by Fused Deposition Modeling. *J. Biol. Eng.* **2017**, *11*, 29. [CrossRef]
16. Moghaddaszadeh, A.; Seddiqi, H.; Najmoddin, N.; Ravasjani, S.A.; Klein-Nulend, J. Biomimetic 3D-Printed PCL Scaffold Containing a High Concentration Carbonated-Nanohydroxyapatite with Immobilized-Collagen for Bone Tissue Engineering: Enhanced Bioactivity and Physicomechanical Characteristics. *Biomed. Mater.* **2021**, *16*, 65029. [CrossRef]
17. Konopnicki, S.; Sharaf, B.; Resnick, C.; Patenaude, A.; Pogal-Sussman, T.; Hwang, K.-G.; Abukawa, H.; Troulis, M.J. Tissue-Engineered Bone With 3-Dimensionally Printed β-Tricalcium Phosphate and Polycaprolactone Scaffolds and Early Implantation: An In Vivo Pilot Study in a Porcine Mandible Model. *J. Oral Maxillofac. Surg.* **2015**, *73*, 1016.e1–1016.e11. [CrossRef]
18. Zeng, J.-H.; Liu, S.-W.; Xiong, L.; Qiu, P.; Ding, L.-H.; Xiong, S.-L.; Li, J.-T.; Liao, X.-G.; Tang, Z.-M. Scaffolds for the Repair of Bone Defects in Clinical Studies: A Systematic Review. *J. Orthop. Surg.* **2018**, *13*, 33. [CrossRef]
19. Qu, H.; Fu, H.; Han, Z.; Sun, Y. Biomaterials for Bone Tissue Engineering Scaffolds: A Review. *RSC Adv.* **2019**, *9*, 26252–26262. [CrossRef]
20. Ghassemi, T.; Shahroodi, A.; Ebrahimzadeh, M.H.; Mousavian, A.; Movaffagh, J.; Moradi, A. Current Concepts in Scaffolding for Bone Tissue Engineering. *Arch. Bone Jt. Surg.* **2018**, *6*, 90–99.
21. Findrik Balogová, A.; Trebuňová, M.; Ižaríková, G.; Kaščák, Ľ.; Mitrík, L.; Klímová, J.; Feranc, J.; Modrák, M.; Hudák, R.; Živčák, J. In Vitro Degradation of Specimens Produced from PLA/PHB by Additive Manufacturing in Simulated Conditions. *Polymers* **2021**, *13*, 1542. [CrossRef]
22. Wang, F.; Tankus, E.B.; Santarella, F.; Rohr, N.; Sharma, N.; Märtin, S.; Michalscheck, M.; Maintz, M.; Cao, S.; Thieringer, F.M. Fabrication and Characterization of PCL/HA Filament as a 3D Printing Material Using Thermal Extrusion Technology for Bone Tissue Engineering. *Polymers* **2022**, *14*, 669. [CrossRef]
23. Jiao, Z.; Luo, B.; Xiang, S.; Ma, H.; Yu, Y.; Yang, W. 3D Printing of HA / PCL Composite Tissue Engineering Scaffolds. *Adv. Ind. Eng. Polym. Res.* **2019**, *2*, 196–202. [CrossRef]
24. Siddiqui, N.; Asawa, S.; Birru, B.; Baadhe, R.; Rao, S. PCL-Based Composite Scaffold Matrices for Tissue Engineering Applications. *Mol. Biotechnol.* **2018**, *60*, 506–532. [CrossRef] [PubMed]
25. Arif, Z.U.; Khalid, M.Y.; Noroozi, R.; Sadeghianmaryan, A.; Jalalvand, M.; Hossain, M. Recent Advances in 3D-Printed Polylactide and Polycaprolactone-Based Biomaterials for Tissue Engineering Applications. *Int. J. Biol. Macromol.* **2022**, *218*, 930–968. [CrossRef]
26. Dwivedi, R.; Kumar, S.; Pandey, R.; Mahajan, A.; Nandana, D.; Katti, D.S.; Mehrotra, D. Polycaprolactone as Biomaterial for Bone Scaffolds: Review of Literature. *J. Oral Biol. Craniofacial Res.* **2020**, *10*, 381–388. [CrossRef] [PubMed]
27. Hou, Y.; Wang, W.; Bartolo, P. Investigation of Polycaprolactone for Bone Tissue Engineering Scaffolds: In Vitro Degradation and Biological Studies. *Mater. Des.* **2022**, *216*, 110582. [CrossRef]
28. Yang, X.; Wang, Y.; Zhou, Y.; Chen, J.; Wan, Q. The Application of Polycaprolactone in Three-Dimensional Printing Scaffolds for Bone Tissue Engineering. *Polymers* **2021**, *13*, 2754. [CrossRef] [PubMed]
29. Seyedsalehi, A.; Daneshmandi, L.; Barajaa, M.; Riordan, J.; Laurencin, C.T. Fabrication and Characterization of Mechanically Competent 3D Printed Polycaprolactone-Reduced Graphene Oxide Scaffolds. *Sci. Rep.* **2020**, *10*, 22210. [CrossRef]

30. Hutmacher, D.W.; Schantz, T.; Zein, I.; Ng, K.W.; Teoh, S.H.; Tan, K.C. Mechanical Properties and Cell Cultural Response of Polycaprolactone Scaffolds Designed and Fabricated via Fused Deposition Modeling. *J. Biomed. Mater. Res.* **2001**, *55*, 203–216. [CrossRef]
31. Zimmerling, A.; Yazdanpanah, Z.; Cooper, D.M.L.; Johnston, J.D.; Chen, X. 3D Printing PCL/NHA Bone Scaffolds: Exploring the Influence of Material Synthesis Techniques. *Biomater. Res.* **2021**, *25*, 3. [CrossRef]
32. Amini, A.R.; Laurencin, C.T.; Nukavarapu, S.P. Bone Tissue Engineering: Recent Advances and Challenges. *Crit. Rev. Biomed. Eng.* **2012**, *40*, 363–408. [CrossRef]
33. Riester, O.; Borgolte, M.; Csuk, R.; Deigner, H.-P. Challenges in Bone Tissue Regeneration: Stem Cell Therapy, Biofunctionality and Antimicrobial Properties of Novel Materials and Its Evolution. *Int. J. Mol. Sci.* **2021**, *22*, 192. [CrossRef]
34. Ikada, Y. Challenges in Tissue Engineering. *J. R. Soc. Interface* **2006**, *3*, 589–601. [CrossRef]
35. Orciani, M.; Fini, M.; Di Primio, R.; Mattioli-Belmonte, M. Biofabrication and Bone Tissue Regeneration: Cell Source, Approaches, and Challenges. *Front. Bioeng. Biotechnol.* **2017**, *5*, 17. [CrossRef]
36. Krobot, Š. Materiály Na Bázi P3HB pro 3D Tisk Medicínských Aplikací. In *Poly(3-Hydroxybutyrate) Based Materials for 3D Printing in Medical Applications*; Vysoké Učení Technické v Brně, Fakulta Chemická, Ústav Chemie Materiálů: Brno, Czech Republic, 2023.
37. Melčová, V.; Svoradová, K.; Menčík, P.; Kontárová, S.; Rampichová, M.; Hedvičáková, V.; Sovková, V.; Přikryl, R.; Vojtová, L. FDM 3D Printed Composites for Bone Tissue Engineering Based on Plasticized Poly(3-Hydroxybutyrate)/Poly(D,L-Lactide) Blends. *Polymers* **2020**, *12*, 2806. [CrossRef]
38. Pospisilova, A.; Novackova, I.; Prikryl, R. Isolation of Poly(3-Hydroxybutyrate) from Bacterial Biomass Using Soap Made of Waste Cooking Oil. *Bioresour. Technol.* **2021**, *326*, 124683. [CrossRef]
39. Kontárová, S.; Přikryl, R.; Melčová, V.; Menčík, P.; Horálek, M.; Figalla, S.; Plavec, R.; Feranc, J.; Sadílek, J.; Pospíšilová, A. Printability, Mechanical and Thermal Properties of Poly(3-Hydroxybutyrate)-Poly(Lactic Acid)-Plasticizer Blends for Three-Dimensional (3D) Printing. *Materials* **2020**, *13*, 4736. [CrossRef]
40. Menčík, P.; Přikryl, R.; Stehnová, I.; Melčová, V.; Kontárová, S.; Figalla, S.; Alexy, P.; Bočkaj, J. Effect of Selected Commercial Plasticizers on Mechanical, Thermal, and Morphological Properties of Poly(3-Hydroxybutyrate)/Poly(Lactic Acid)/Plasticizer Biodegradable Blends for Three-Dimensional (3D) Print. *Materials* **2018**, *11*, 1893. [CrossRef]
41. Morgan, E.F.; Unnikrisnan, G.U.; Hussein, A.I. Bone Mechanical Properties in Healthy and Diseased States. *Annu. Rev. Biomed. Eng.* **2018**, *20*, 119–143. [CrossRef]
42. Żenkiewicz, M. Methods for the Calculation of Surface Free Energy of Solids. *J. Achiev. Mater. Manuf. Eng.* **2007**, *24*, 137–145.
43. Schakenraad, J.M.; Busscher, H.J.; Wildevuur, C.R.H.; Arends, J. The Influence of Substratum Surface Free Energy on Growth and Spreading of Human Fibroblasts in the Presence and Absence of Serum Proteins. *J. Biomed. Mater. Res.* **1986**, *20*, 773–784. [CrossRef]
44. van der Valk, P.; van Pelt, A.W.J.; Busscher, H.J.; de Jong, H.P.; Wildevuur, C.R.H.; Arends, J. Interaction of Fibroblasts and Polymer Surfaces: Relationship between Surface Free Energy and Fibroblast Spreading. *J. Biomed. Mater. Res.* **1983**, *17*, 807–817. [CrossRef] [PubMed]
45. Zubairi, S.I.; Bismarck, A.; Mantalaris, A. The Effect of Surface Heterogeneity on Wettability of Porous Three Dimensional (3-D) Scaffolds of Poly(3-Hydroxybutyric Acid) (PHB) and Poly(3-Hydroxybutyric-Co-3-Hydroxyvaleric Acid) (PHBV). *J. Teknol.* **2015**, *75*, 305–312. [CrossRef]
46. Mehrabi Mazidi, M.; Edalat, A.; Berahman, R.; Hosseini, F. Highly-Toughened Polylactide- (PLA-) Based Ternary Blends with Significantly Enhanced Glass Transition and Melt Strength: Tailoring the Interfacial Interactions, Phase Morphology, and Performance. *Macromolecules* **2018**, *51*, 4298–4314. [CrossRef]
47. Lins, L.; Bugatti, V.; Livi, S.; Gorrasi, G. Ionic Liquid as Surfactant Agent of Hydrotalcite: Influence on the Final Properties of Polycaprolactone Matrix. *Polymers* **2018**, *10*, 44. [CrossRef] [PubMed]
48. Abdelwahab, M.A.; Flynn, A.; Chiou, B.-S.; Imam, S.; Orts, W.; Chiellini, E. Thermal, mechanical and morphological characterization of plasticized PLA–PHB blends. *Polym. Degrad. Stab.* **2012**, *97*, 1822–1828. Available online: https://www.sciencedirect.com/science/article/pii/S0141391012002108 (accessed on 8 May 2023). [CrossRef]
49. Wang, S.; Daelemans, L.; Fiorio, R.; Gou, M.; D'hooge, D.R.; De Clerck, K.; Cardon, L. Improving Mechanical Properties for Extrusion-Based Additive Manufacturing of Poly(Lactic Acid) by Annealing and Blending with Poly(3-Hydroxybutyrate). *Polymers* **2019**, *11*, 1529. [CrossRef]
50. Laoutid, F.; Lenoir, H.; Molins Santaeularia, A.; Toncheva, A.; Schouw, T.; Dubois, P. Impact-Resistant Poly(3-Hydroxybutyrate)/Poly(ε-Caprolactone)-Based Materials, through Reactive Melt Processing, for Compression-Molding and 3D-Printing Applications. *Materials* **2022**, *15*, 8233. [CrossRef]

Disclaimer/Publisher's Note: The statements, opinions and data contained in all publications are solely those of the individual author(s) and contributor(s) and not of MDPI and/or the editor(s). MDPI and/or the editor(s) disclaim responsibility for any injury to people or property resulting from any ideas, methods, instructions or products referred to in the content.

Carbohydrate Polymers 230 (2020) 115708

Contents lists available at ScienceDirect

Carbohydrate Polymers

journal homepage: www.elsevier.com/locate/carbpol

Chitosan-glucan complex hollow fibers reinforced collagen wound dressing embedded with aloe vera. Part I: Preparation and characterization

A.M. Abdel-Mohsen[a,b,c,*], R.M. Abdel-Rahman[a], I. Kubena[d], L. Kobera[e], Z. Spotz[a], M. Zboncak[a], R. Prikryl[f], J. Brus[e], J. Jancar[a,b,f]

[a] CEITEC-Central European Institute of Technology, Brno University of Technology, Purkyňova 656/123, Brno 612 00, Czechia
[b] SCITEG, a.s., Brno, Czechia
[c] Department of Pretreatment and Finishing of Cellulosic based Textiles, Textile Industries Research Division, National Research Centre, 33 EL Buhouth St., Dokki, Giza 12622, Egypt
[d] Institute of Physics of Materials, Academy of Sciences of the Czechia, Žižkova 22, CZ 61662, Brno, Czechia
[e] Institute of Macromolecular Chemistry of the Czech Academy of Sciences, HeyRovskeho Nam. 2, 162 06, Prague 6, Czechia
[f] Institute of Materials Chemistry, Faculty of Chemistry, Brno University of Technology, Purkyňova 464/118, Brno, 612 00, Czechia

ARTICLE INFO

Keywords:
Chitosan-glucan
Hollow fiber
Collagen
Aloe vera
Degradation
Release properties
Wound dressing

ABSTRACT

Collagen (CO)/chitosan-glucan complex (CSGC) hollow fibers encapsulated aloe vera (AV) dressing scaffold (CO/CSGC@AV) were fabricated for the first time by the freeze-dried process. Extraction process, morphology, mechanical properties, pore size, porosity, swelling ability, and degradation behavior of composites scaffold were investigated. CSGC hollow fibers were extracted from *mycelium* of *Schizophyllum commune* CSGC hollow fiber exhibited inner diameter of (600 ± 250 nm) and outer fiber diameter of (2.5 ± 0.5 μm). The results of swelling and hydrolytic degradation studies demonstrated that the physicochemical of CO/CSGC@AV was significantly enhanced by CSGC in a concentration-dependent manner. The mechanical property of the CO/CSGC@AV was improved after encapsulated AV into CSGC hollow fibers compared with native CO. The pore size and porosity of the CO/CSGC@AV were slightly decreased in the presence of AV. All these results suggested that the new dressing scaffold has a potential for clinical skin regeneration, particularly for infected chronic wounds and ulcers.

1. Introduction

Polysaccharide-protein complex, existing in different cell walls of fungi as a part of the extracellular matrix, have been investigated because of their biologically attractive functions such as antibacterial, antitumor, anti-nociceptive, anti-inflammatory, anti-oxidative, immune-stimulatory activities and healing properties (Abdel-Mohsen et al., 2016; Burkatovskaya et al., 2006). Chitin and glucan are the main components of fungi cell wall occurring in two forms, free chitin and chitin covalently bonded to β-glucan (Abdel-Mohsen et al., 2016). Intensive research efforts are concentrating on modifying the natural polymers, such as cellulose (Kontturi et al., 2018), chitin and chitosan (Abdel-Mohsen et al., 2016), (Nakashima et al., 2018; Zhao et al., 2018) and polyesters from a different type of bacteria, fungi, etc. (Irimia-Vladu, 2014). Non-animal sources reveal a huge advantage over the animal ones, due to their inherent non-allergenicity and biodegradability in the human organs (François, 2007; Kang et al., 2018). *Mycelium* from *Schizophyllum commune* (non-animal source), the vegetative lower part of fungi. Mycelium has been recognized as the major living organism on nature (HUMFELD, 1948; van der Linde et al., 2018). Mycelium has a porous structure composed of tubular filaments called hypha. To date, chitin microfibrils are connected next to the plasma membrane following the biosynthesis of different chains and the fibril formation process through physical hydrogen bonding (Kang et al., 2018; Ruiz-Herrera & Bartnicki-Garcia, 1974).

These micro-fibrils are covalently linked to β-1,3-glucans that extend through the cell wall and tether mannoproteins and lipids on the cell wall surface through branched networks with β-1,6-linked glucans (Duran et al., 1979; François, 2007). Chitin-glucan complex (ChGC) has been extracted from different sources of mycelium (Geißel et al., 2018) by chemical or enzymatic processes. The resultant chitosan–glucan complexes from ChGC were used as flocculants for cultivation of mammalian cells. Unfortunately, the extracted ChGC or CSGC complex is only in powder form (Skorik et al., 2010). Fibers derived from natural

* Corresponding author at: Central European Institute of Technology (CEITEC), Brno University of Technology, Purkyňova 656/123, Brno 612 00, Czechia.
E-mail address: abdel-mohsen@ceitec.vutbr.cz (A.M. Abdel-Mohsen).

https://doi.org/10.1016/j.carbpol.2019.115708
Received 6 August 2019; Received in revised form 27 November 2019; Accepted 5 December 2019
Available online 05 December 2019
0144-8617/ © 2019 Elsevier Ltd. All rights reserved.

polymer sources is an indispensable class of materials that has versatility for a wide range of structural and functional applications in the medical and environmental protection area (Kim et al., 2017).

Hollow fibers have revealed an interesting advantages due to their large surface-to-volume ratios and the ability to trap, isolate or release materials engaged in it (Yoon et al.). Coaxial and tri-axial electrospinning are an interesting methods to fabricate high-aspect-ratio hollow micro/ nanofibers with a controlled inner and outer diameter(Yin et al., 2017) (Yoon et al.). The principle is to use solvent dissolving only the core material while preserving the shell structure (Dzenis, 2004). The challenges of preparing hollow fibers include the choice of the solvent for core and shell (Halaui et al., 2017). In addition, the poor mechanical properties of the existing hollow fibers remain a great challenge (Bedford et al., 2012; Jiang et al., 2014). In our study, a novel source and a simple process were used to fabricate hollow fibers without applying any hazard solvent for extraction chitosan-glucan complex hollow fibers. The second advantage of our new hollow chitosan-glucan fiber was stability and high compatibility with human cells compared with synthetic materials such as polyacrylonitrile, polycaprolactone, acetylacetonate, and polyaniline (Bedford et al., 2012; Han et al., 2017).

Collagen is known to be one of the most promising materials and has been found in diverse applications in tissue engineering for their excellent biocompatibility (Marinucci et al., 2003), biodegradability, and non-toxicity (Marone et al., 2010). However, the fast biodegradation rate and the low mechanical strength of the native collagen scaffolds are the crucial problems that limit its broader application. Cross-linking of the collagen is an effective method to modify the biodegradation rate and to optimize its mechanical properties (Khor, 1997; Marelli et al., 2015; Merrett et al., 2009; Yao et al., 2008). Currently, there are two different kinds of crosslinking methods used in improving the chemical, physical and mechanical properties of the collagen-based scaffolds, i.e., covalent cross-links (Jorge-Herrero et al., 1999) and physical cross-links (Yunoki et al., 2003), (Saito & Marumo, 2010). The reagents used in the covalent cross-linking treatment involved traditional glutaraldehyde (GA), 1-ethyl-3-(3-dimethylaminopropyl)-carbodiimide (EDC), polyglycidyl ether, genipin and polyepoxidic resins, etc (Osborne et al., 1999; Sung et al., 1996), (Kumar et al., 2004).

Aloe vera (AV) has been used in traditional medicine for a long time and It is one of the most familiar herbs in the world. The compositions of AV include many interesting nutrients, such as amino acids, vitamins, sugars, minerals, and enzymes, that support general healthiness. In addition, it has been widely used for the treatment of burns in the last century (Paichit et al., 2012). Many studies shows various biological properties of AV including biological activity, antidiabetic, and anti-inflammatory properties (Ashraf et al., 2016). Furthermore, it has been described that aloe vera can accelerate wound healing in streptozotocin-induced diabetic rats due to their ability to stimulate fibroblasts and enhance the healing process such as collagen synthesis and maturation and wound contraction (Mijatović et al., 2018).

Different wound dressings based on collagen in combination with different polysaccharides like cellulose (Wu et al., 2017), chitosan (Kirichenko et al., 2013; Rezaii et al., 2019), hyaluronan (Rezaii et al., 2019), alginate and chitosan incorporated nanoparticles (Rezaii et al., 2019; You et al., 2017) are prepared by different techniques and applied as new wound healing have shown many disadvantages like (i) need external crosslinker agents to improve the dressing stability (Doillon & Silver, 1986; Doillon et al., 1987; Gentleman et al., 2003), (ii) many of these crosslinkers are toxic or can inhibit the cell viability, (iii) mechanical and degradation properties of the collagen-based dressing are not significant enough for long-term of applications (Ghodbane & Dunn, 2016), (iv) lack of drug control release due to deficiency of mechanical stability and fast biodegradation (Fujioka et al., 1995).

To our knowledge, hollow fibers with controlled fibers dimension extracted from *Schizophyllum commune* for the first time *and* 2/3D structures were fabricated from it. In our study, we hypothesis that (1) CSGC hollow fibers could be trapped and encapsulate the AV, drug or any other bioactive substances inside it and controlled the release of these materials, (2) The CSGC can work as crosslinker agent, without external hazard crosslinker agent for collagen dressing scaffold, (3) New CSGC hollow fibers could improve the hydrolytic stability of collagen sponge, that could be supposed to use it in different areas of application especially in bone, cartilage or skin regeneration.

In this work, a novel dressing from collagen (CO)/chitosan-glucan complex (CSGC) hollow fiber/aloe vera (AV) composite was prepared and characterized by different techniques. They demonstrated significant enhancement swelling, suitable mechanical property, hydrolytic degradation, and controlled release.

2. Experimental part

2.1. Materials

Bovine collagen type I was supplied as an 8 wt. % of bulk material (VUP, Brno, Czechia) and then, freeze-dried (−70 °C, 48 h) obtained dry collagen (CO). Mycelium was produced from an extracellular product by *Schizophyllum commune* cultured under standard cultivation conditions. All the other chemicals were used without further purifications from commercial sources in the Czechia and were of analytical grade.

2.2. Methods

2.2.1. Cultivation of mycelium

Schizophyllum commune strain (*F-795*) Czech collection of microorganisms strain and cultivated on agar slants with potato dextrose agar (PDA) at 4 °C as described in the literature with a small modification (Mohammadi et al., 2018; Sung et al., 2018). The strain was transferred into a petri dish that was cultivated for 7 days at 30 °C. 100 ml of medium (Inoculum I) in Erlenmeyer flask was inoculated with 0.5 × 0.5 cm from native mycelium from the petri dishes and incubated in rotary shakers at 30 °C, for 5 days without any disruption of the cell wall bead of mycelium using homogenizer. 50 ml were used for inoculation of 1000 ml Erlenmeyer flasks with 500 ml medium. 1000 ml Erlenmeyer flasks were cultivated in rotary shakers at 30 °C, for 7 days. Medium for the seed cultures and production cultivations contained 35 g/l sucrose, 3 g/l yeast extract, 2.5 g/l disodium hydrogen phosphate, 0.5 g/l magnesium sulfate, initial pH 5.5. Mycelium (insoluble part) and *schizophyllan* yields were measured as follows: 500 ml of cultural broth were centrifuged (10 000 rpm, 25 °C, 20 min), and schizophyllan was obtained from the supernatant after. Insoluble (mycelium) was re-suspended in 250 ml of Milli-Q water, centrifuged again and discarded the supernatant. The insoluble mycelium was placed into a petri dish, freeze-dried (−70 °C, 15 Pa, 48 h) obtained dry mycelium beads.

2.2.2. Extraction of hollow fibers and AV powder preparation

Extraction of chitin-glucan (ChGC) and chitosan-glucan (CSGC) hollow fibers from mycelium beads were done by the chemical way under mild conditions. Firstly, the dry mycelium bead was treated with 5 % of sodium hydroxide (solid to liquid ratio 1/100) at 50 °C for 2 h with 200 rpm. This step was repeated many times until obtained transparent supernatant. The hollow fiber ChGC was washed with Milli-Q water until naturalized at pH 7. Finally, the hollow ChGC fibers were freeze-dried. For extraction of chitosan-glucan hollow fiber (CSGC); chitin-glucan complex (ChGC) was treated with sodium hydroxide 20 % wt.% at 40 °C for 24 h under low speed (200 rpm). The CSGC was washed with Milli-Q water until naturalized at pH 7. Finally, the hollow CSGC fibers with different degree of deacetylation (DDA) was freeze-dried for 48 h.

Aloe vera powder was prepared from fresh aloe vera leaves and the

leaves were washed well with Millli-Q water and the green part was carefully removed from the inner gel. The parenchyma part was homogenized using homogenizer then centrifuged at 15000 rpm for 30 min at 4 °C. The isolated gel was freeze-dried for 2 days, and the powder was kept in dissector to prevent the humidity.

2.3. Fabrication of dressing scaffolds

Wound dressing from collagen (CO)/chitosan-glucan complex (CSGC) hollow fibers and in the presence or absence of different concentrations of AV were fabricated by freeze-drying technique. 0.5 (wt. %) of dry CO was swelled in 10 mM of acetic acid at 4 °C for two days then, homogenized in ice bath (0 °C) for 5 min at 12000 rpm using Ultra-Turrax VD125 homogenizer (VWR International Ltd., UK). Dispersed collagen was centrifuged at 4500 rpm for 10 min (Hermle Z300, Labortechnik, Germany) removed air bubbles, cast into stainless steel molds, kept overnight at −35 °C and lyophilized at −50 °C for 48 h.

Collagen/chitosan-glucan complex hollow fiber (CO/CSGC) dressing sheet was fabricated using different ratios of CSGC to CO. CO (0.5 %) was mixed with CSGC (0.25; 0.5, 1 wt. %) in 10 mM of acetic acid and swelled at 4 °C for two days then homogenized in ice bath (0 °C) for 15 min at 12000 rpm using Ultra-Turrax VD125 homogenizer. The processing of preparation of CO-CSGC dressing scaffolds was the same as used in CO scaffold preparation. The samples coded as CO/CSGC (1/0.5); CO/CSGC (1/1); CO/CSGC (1/2) for 0.25, 0.5 and 1 wt. % of CSGC hollow fibers.

Different ratios between collagen and aloe vera (1/1, 1/2 w/w), AV was dissolved in Milli-Q (certain volume) then, blended with CO dispersed in 10 mM of acetic acid and swelled at 4 °C for two days then homogenized in ice bath (0 °C) for 15 min at 12000 rpm using homogenizer. Processing of preparation of CO/AV dressing scaffolds was the same as used in CO scaffold preparation and samples coded as CO/AV (1/1); CO/AV(1/2); for 0.5 and 1 wt. % of AV powder.

For CO/CSGC@AV dressing scaffolds were fabricated using different concentrations of AV (0.5, 1 %) the latter was dissolved in Milli-Q (certain volume) then blended with different concentrations ratios of CSGC hollow fibers (0.25, 05, 1 wt. %) then a gaited for 2 days at 4 °C, the pH of the medium was 3-4. The mixed solution was homogenized on ice bath (0 °C) for 30 min at 12000 rpm. Different ratios between CSGC@AV (0.25/0.5; 0.5/0.5; 1/0.5; 0.25/1; 0.5/1, 1/1) were mixed with net CO (0.5 wt.%) in 10 mM of acetic acid and all suspension solution (CO/CSGC@AV) were swelled at 4 °C for two days, homogenized in ice bath (0 °C) for 15 min at 12000 rpm. The air bubbles were removed from the suspension by centrifuged at 4500 rpm for 10 min. The obtained CO/CSGC@AV suspensions were poured into stainless steel molds and for a 3D scaffold the solution was poured in 48 well plates and kept overnight at −35 °C, then freeze-drier (−50 °C, 15 Pa, 48 h; CHRIST ALPHA 1-4 LSC). All the samples after freeze-dried were neutralized using phosphate buffer solution (pH 7.5) for 5 times each 30 min, kept overnight at −35 °C and lyophilized -50 °C for 48 h). The samples coded as (Table S1) CO/CSGC@AV (1/0.5/1); CO/CSGC@AV (1/1/1); CO/CSGC (1/2/1); CO/CSGC@AV (1/0.5/2); CO/CSGC@AV (1/1/2); CO/CSGC 1/2/2 for 0.25, 0.5, 1 wt. % of CSGC and 0.5, 1 wt. % of AV with constant CO concentration.

3. Scaffold characterization

Attenuated total reflectance Fourier-transformed infrared spectroscopy (ATR-FTIR): were recorded to study the chemical composition of the obtained dressing mats using Bruker Vertex80 V spectrometer equipped with the diamond crystal over the wavenumbers ranging from 4000 to 650 cm^{-1}. Each spectrum consists of 128 scans and the obtained spectra were analyzed utilizing OPUS software (version 6.5).

Transmission electron microscope (TEM) investigations were performed employing the JEOL JEM-2010 (HT) electron microscope (JEOL, Japan), with an accelerating voltage of 120 kV. The samples were dispersed in Milli-Q water with a concentration of 0.5 mg/ml, and a drop was placed on Cu grids pre-coated with carbon films and dried in air.

X-ray diffraction *(XRD)* was measured at 3 kW diffractometer Smart lab from Rigaku using Cu Kx radiation (λ. = 1.54 Å) and detector Dtex-Ultra with Bragg-Brentano geometry. Diffraction angle 2-Theta was measured in a range from 5° to 70° with step size 0.02° at speed 4°/min. A generator was operated at the current 30 mA and voltage 40 kV.

Scanning electron microscopy (SEM, JEOL JSM-6340 F) was used to examine the morphology of the fibers and scaffold dressing. The average fiber diameter and pore size of the dressing scaffolds was determined by collecting data from 100 different locations within SEM images, and Image J software was used for subsequent measurements and analysis. The surface elemental analysis was determined by Energy Dispersive X-ray spectroscopy (EDX) (Oxford Instruments, England) and evaluated by Aztec 2.1a software. Hollow fiber diameters were measured using Image J software. Samples were then air-dried at room temperature prior to sputter coating with 20 nm of Au/Pd layer and imaged at 10 kV in SEM (Tescan, Brno, Czechia).

Thermal gravimetric analysis (TGA) in this case was used for the study of thermal stability and moisture content of the different composition of wound dressing sheets. Measurements were carried out in the inert nitrogen with a temperature rate of 10 °C/min up to 800 °C.

Mechanical properties of prepared dressing scaffolds were evaluated by Zwick/Roell-Z010 test instrument (Zwick/Roell, Germany) with a 10 N load cell at a crosshead speed of 5 mm. min^{-1} at room temperature (20 °C). All samples were cut into rectangles with dimensions of 30 mm × 5 mm. At least ten samples were tested for each type of dressing scaffold and data were averaged to get the standard deviation. The thickness of samples was measured with a micrometer (Prominent s.r.o., Czechia).

Solid-state NMR spectroscopy: ^{13}C CP/MAS NMR spectra were recorded on a Bruker AVANCE III HD spectrometer (Larmor frequencies $\nu^{13}C$ = 125.783 MHz) using a 3.2 mm MAS probe. The spinning speed of the rotor sample was 20 kHz. The number of scans for the accumulation of ^{13}C CP/MAS NMR spectra was 2048, repetition delay of 5 s, and spinlock of 1 ms. During detection, the high-power dipolar decoupling (SPINAL 64) was used to eliminate strong hetero-nuclear dipolar couplings. The isotropic chemical shift of the ^{13}C NMR scale was calibrated with glycine as an external standard (176.03 ppm to carbonyl signal). In all cases, the dried samples were placed into the ZrO_2 rotors and all NMR experiments were performed at 303 K. Temperature calibration was performed on $Pb(NO_3)_2$ using a procedure described in the literature (Brus, 2000). The mol (%) of chitin units were calculated from equation referred to in the literature (Spěváček & Brus, 2008) accord icing to Eq. (1):

$$mol\%(N-acetylglucosamine) = \frac{\boldsymbol{I}_{C_3}}{(\boldsymbol{I}_{C1} + \boldsymbol{I}_{C2} + \boldsymbol{I}_{C3} + \boldsymbol{I}_{C4} + \boldsymbol{I}_{C5} + \boldsymbol{I}_{C6})/6} \times 100 \quad (1)$$

Calcium ion measurement: The kinetics of calcium release was studied from the prepared dressing scaffold. Collagen/aloe vera (CO/AV; 1/2), collagen complex/ aloe vera (CO/CSGC@AV) with different concentration of CSGC (0.25, 0, 5, 1 wt.). The dressing scaffolds were cut into pieces in a diameter of 10 mm. These samples were then immersed in 10 ml saline buffered solution (SB, pH = 7.0) at 37 °C. 1 ml solution was taken at regular time intervals (1, 12, 24, 48, 72, 96, and 144 h) and analyzed for the amount of calcium released using Inductively Coupled Plasma Mass Spectrometry (ICP-MS), and then the same volume of fresh saline solution was added.

Degradation measurement: the wound dressing mats were cut into 1 × 1 cm strips and weight then immersed into phosphate buffer solution (PBS) solution and placed in an incubator at 37 °C to test their

hydrolytically stability at body conditions. After removing the swollen samples from the solutions at regular intervals, samples were freeze-dried until constant weight. Hydrolytic degradation was examined gravimetrically by recording weight decrements as a function of time (0, 1, 3, 5, 10, 14, and 21 days). Weight loss was calculated according to the Eq. (2).

$$Weight\ loss\ (\%) = \frac{Wi - Wf}{Wi} \times 100 \quad (2)$$

Where W_i was the weight of dried sample and W_f. was the weight of the sample in the regular time. The resulting value is an average of five measurements.

Swelling percentage: 0.5 × 0.5 cm dressing specimens were gravimetrically evaluated in PBS solution (pH = 7.5) at 37 °C. In regular time intervals (0.5, 1, 3, 6, 12, 24, 48, 72, 96, 120, and 168 h) swollen pieces were removed, the excess surface water was quickly swiped out by blotting paper and reweighed. The water uptake of CO; CO/CSGC; CO/CSGC@AV dressing mats were defined according to the Eq. (3).

$$Swelling\ percentage\ (\%) = \frac{Ws - Wd}{Wd} \times 100 \quad (3)$$

Where W_s was the weight of the swollen samples at the given time and W_d is the weight of the dry sample. The resulting value is an average of 5 measurements (n = 5).

Porosity measurements: the porosity of the prepared dressing scaffold was determined by using the reported method(Liang et al., 2016). The scaffold was immersed in absolute ethyl alcohol until it was saturated. The weight of the scaffold was measured before and after the immersion. The porosity (*P*) was calculated from the following Eq. (4).

$$Porosity\ (\%) = \frac{M2 - M1}{\rho v} \times 100 \quad (4)$$

Where, M_1 and M_2 weight of dressing before and after immersion, V was the volume of dressing before immersion, which was calculated from the formula of length × width × height. ρ the density of the alcohol. All the samples were triplicate (n = 3).

4. Results and discussion

4.1. Extraction of hollow fibers

Mycelium yield after twelve days of *Schizophyllum commune (S. commune)* cultivation varied between 12.3 ± 0.3 g/l. To prevent the deformation of the shape of the mycelium bead structure, only gentle mechanical processes had to be employed. Scheme 1 shows the sequence of extraction steps from mycelium bead. In native mycelium, the main component was the *β*-(1→3, 1→6)-D-glucan with different ratio between *β*-(1→3) and branched *β*-(1→6) (Scheme 1a, g) covalently bonded to proteins and lipids (Kang et al., 2018). The chitin chains were covalently connected with glucan matrix (Scheme 1a; g). After deprotenization step (DP), large amounts of lipids and proteins were removed from the mycelium matrix (Scheme 1b). By repeating the DP step 10 times, partially deacetylated chitin was obtained (DDA = 50 %). The 5 wt. % of NaOH could not remove all proteins (residual protein measured by solid-state NMR was 7 %) but it was quite enough to remove all lipids (0 %) from the mycelium matrix (DP step) (Scheme 1g). In the de-acetylation step (DA), a high concentration of sodium hydroxide (20 wt. %) was used for 24 h with changing the supernatant solution each 2 h by adding a fresh solution of NaOH. The reaction temperature was 40 °C under low mechanical stirring at 200 rpm. The chitosan-glucan complex was generated with 90 and 100 % acetylation with 0 % proteins (solid-state NMR) with the DDA depending on the reaction time (Scheme 1g). The CSGC with 90 % DDA was used to preserve a low amount of acetamide groups needed can improve the mechanical properties of the dressing scaffolds (Hsu et al., 2004; Liu et al., 2012; Wenling et al., 2005).

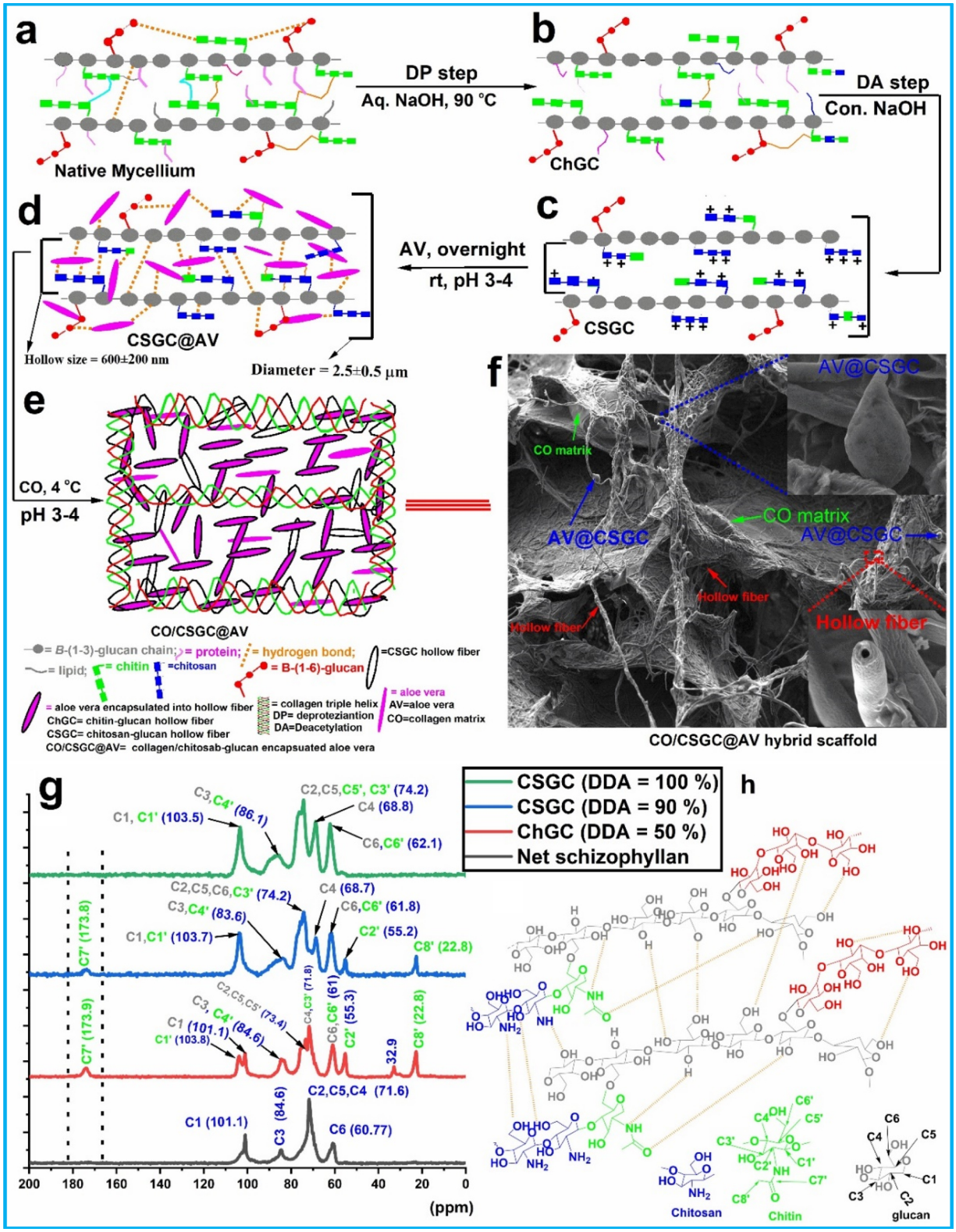
The chemical structure of chitin-glucan and chitosan-glucan hollow fiber complex wasn't confirmed in literature and there weren't more details about the chemical bonds between chitin or chitosan and glucan (linear and branched chains). ^{13}C CP/MAS NMR experiments were used to confirm the chemical structure of both ChGC and CSGC and pure schizophyllan. The experimental ^{13}C CP/MAS NMR spectrum of plain glucan was confirmed the structure of *β*-(1→3, 1→6)-D-glucan as depicted in Scheme 1g. The peak position at 101.1 ppm corresponds with C1 atoms in the *β*-glycosidic bond. The peak at 84.6 ppm can be assigned to the (1→3) linked C3 carbon. The shows overlapped signal sat 71.6 ppm reflects the C5, C2 and C4 atoms of glucan units while the C6 atoms have the resonance at 60.6 ppm. From the recorded spectra C6 and C1 carbons were characterized by two signals, which could be attributed to the (1→3) and (1→6) linkage of the glycosidic bond. The ratio of linear and branched glucosidic bonds (1-3) and (1-6) was 1:1, respectively (Y.-T. Kim et al., 2000).

For the sample chitin/chitosan-glucan hollow fibers, the chitin/chitosan-glucan complex was confirmed by splitting of signal at 103.8 and 101.1 ppm, which could be assigned to C1` and C1 carbons from chitosan and glucan, respectively. The splitting of these signals (C1/C1`) indicated that the complicated bonding in the analyzed complex could be expected. It has been revealed three superimposed resonances by deconvolution (fitting) of C1/C1` signals (Scheme 1h). The resonances at 101.1 ppm and 102.7 ppm were corresponding to (1→3) and (1→6) glycosidic bonds of β-glucan, respectively. The resonance at 103.8 ppm, which was attributed to chitin/chitosan units, from the intensities of resonances at 101.7 ppm and 102.7 ppm has been revealed a dominant fraction of (1→3) glycosidic bonds (approximately 90 %). The degree of deacetylation of chitosan was 50 %, for the sample chitin-glucan hollow fiber (ChGC; DDA = 50 %). Additionally, the signal at 32.9 ppm was clearly visible in ^{13}C CP/MAS NMR spectrum of sample ChGC (Scheme 1g), which corresponds to the residual proteins and/or lipids (Roca et al., 2012; Spěváček & Brus, 2008).

The ratio of chitin/chitosan and anomeric glucan was (1:1), and the *β*-(1-6) glucosidic bonds approximately 10 mol % of anomeric glucan. The degree of deacetylation was 50 mol % ratio between chitin and chitosan. The spectrum of the chitosan-glucan complex (CSGC; DDA = 90 %; Scheme 1g) shows the typical pattern that was for chitosan-glucan complex polysaccharide. The characteristic peaks at 174.2, 55.3 and 22.8 ppm correspond with carbonyl (C7`), methine atoms near the nitrogen (C2`) and methylene carbons (C8`), respectively, from chitin units (Roca et al., 2012; Spěváček & Brus, 2008; Tishchenko et al., 2011). On the other hand, the absence of a peak at 33 ppm, eventually other signals, in ^{13}C CP/MAS NMR spectrum of sample CSGC (DDA = 90 %) implies the absence of impurities in chitosan-glucan complex hollow fiber (CSGC). The calculated % deacetylation degree of the hollow fiber complex was 90 %. The complex contains 15 % of chitin/chitosan units (this data was obtained from fitting of C1 signal, as in previous cases) and the degree of deacetylation of chitin/chitosan was 90 % from the chitin/chitosan weight ratio.

^{13}C-CP/MAS NMR spectrum of chitin/chitosan-glucan complex with completely deacetylated the amino groups (ChGC; DDA = 100 %) is depicted in Scheme 1g confirms the structure of β-(1→3, 1→6)-D-glucan and reflects characteristic peaks of a complex polysaccharide. The peaks appeared at 103.5, 86.1, 74.4, 68.8 and 62.1 correspond to C1-C6 carbons of anomeric β-glucan, respectively (Roca et al., 2012). However, the presence of a peak at 57.0 ppm was indicated that the polysaccharide complex also contains a certain amount of chitosan units. The mentioned resonance was typical to C2` (Scheme 1h) atoms of the chitosan structure.

Consequently, we conclude that the analyzed hollow fiber chitosan-glucan complex was β-(1→3, 1→6)-D-glucan/chitosan complex. The degree of deacetylation of chitin/chitosan was 100 % (CSGC; DDA = 100 %; Scheme 1g) and the ratio of chitosan to glucan was (95:5), respectively. Furthermore, from the considerable similarity of



Scheme 1. Schematic illustration extracting sequence process of hollow fibers, hollow fibers encapsulated aloe vera and engineered dressing scaffolds.
Notes: (a) native mycelium beads after fermentation chemical bonded with proteins and lipids; (b) mycelium beads after deprotenization step (DP) with low proteins and lipids contents (chitin-glucan hollow fiber complex (ChGC); (c) chitosan-glucan hollow fiber after deacetylation step (CSGC) with zero proteins; (d) hollow fiber encapsulated aloe vera (CSGC@AV); (e) collagen/chitosan-glucan hollow fiber encapsulated aloe vera (CO/CSGC@AV; (f) representative SEM of CO/CSGC@AV dressing scaffold; (g) ^{13}C CP/MAS NMR spectra of native *Schizophyllum commune,* ChGC (DDA = 50 %), CSGC with different degree of deacetylation (DDA = 90, 100 %), respectively for the carbon resonance assignments and signal numbering; (h) proposed chemical structure of chitosan-glucan hollow fiber complex (DDA = 90 %).

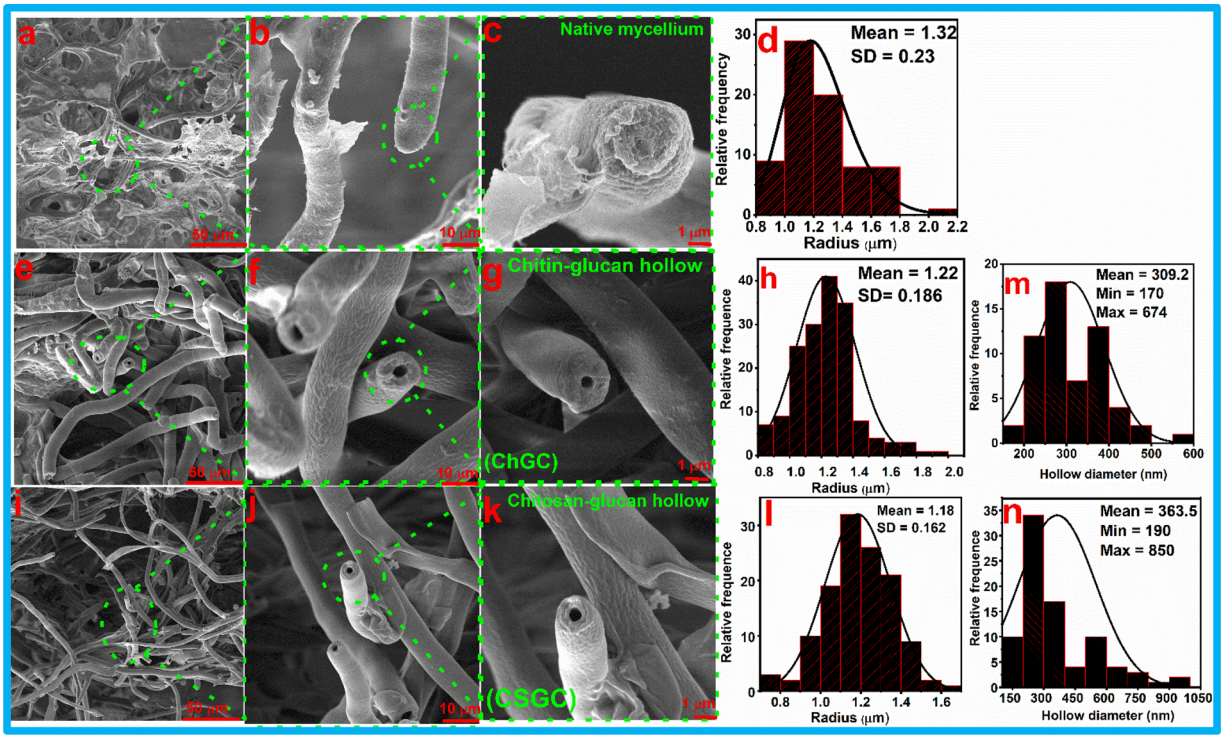


Fig. 1. Morphological visualization of native mycelium, extracted chitin-glucan (ChGC) and chitosan-glucan (CSGC) complex hollow fibers.
Notes: (a, b, c) SEM of native mycelium beads at different magnifications (scale bars were 50, 10 and 1 μm); (e, f, g) SEM of the extracted ChGC from mycelium with hollow fibers with 50 % DDA (scale bars were 50, 10 and 1 μm); (I, j, k) SEM of CSGC with 90 % DDA (scale bars were 50, 10 and 1 μm); (d, h, l) fiber radius histograms of mycelium, ChGC and CSGC, respectively; (m, n) histograms of hollow diameters of ChGC and CSGC, respectively. The histograms of fiber radius were plotted from 200 points and for hollow size was plotted from 100 points.

^{13}C CP/MAS NMR spectra of samples CSGC (DDA = 90 and 100 %; Scheme 1g) could be expected similar structure (anomeric β-glucan bonded with chitin or chitosan units) with different degree of deacetylation. The chemical structure of Ch/CSGC hollow fiber complex was not well known and need to be precisely studied and confirmed. The chemical composition depended on the source and the extraction process. From ^{13}C solid-state NMR spectroscopy (Scheme 1g) the most formed of *β*-(1, 3)-glucans with short branched *β*-(1, 6)-glucans and chitin/chitosan β-(1, 4)-*N*-acetyl glucosamine/ glucosamine connected covalently by glycosidic bonds (Scheme 1h).

Fig. 1a–c depict surface morphology and cross-section of native mycelium. The fiber diameter was 1.32 μm (Fig. 1d). The extraction of ChGC hollow fibers was done under a mild condition with low rotation speed of mechanical stirrer to prevent the destruction of the hollow fiber shape. Fig. 1e–g show the ChGC fibers after the treatment of mycelium beads with low concentrated sodium hydroxide. Fibers were well disturbed without bundled together and the surface morphology of the ChGC was more smooth, homogeneous and clear compared with native mycelium fiber (Fig. 1a). Fig. 1f explored visualization of hollow structure of ChGC appeared after mycelium beads treated with sodium hydroxide for certain time (10 h) and 50 ℃ with changed the alkaline aqueous medium every 2 h prevented back interactions between ChGC functional groups and proteins molecules and also to obtain pure ChGC hollow without residual of proteins or lipids that was confirmed by solid NMR and obtained clear/transparent supernatant solution.

The hollow structure was appeared, due to the extraction of proteins and pigments from the internal structure of ChGC fibers. Fig. 1g shows the cross-section of ChGC fiber with hollow shape displayed smooth surface without noticeable roughness indicated that CSGC hollow fiber has a clean surface with circular cross-section. The ChGC fiber show a radius of 1.22 0.186 ± μm (Fig. 1h) and the average inner diameter (Fig. 1m) was 674–170 nm.

Fig. 1i–k represents the CSGC after the ChGC treatment with sodium hydroxide de-acetylated the acetamide groups on the surface and inside the hollow fibers and the extraction process was investigated and optimized at 40 ℃ under low mechanical stirring (200 rpm). Using high temperature (90 ℃) and high speed (1000 rpm) to de-acetylate the chitin part damaged completely the fiber structure obtained (Fig. S1a,b; supporting information) and the optical morphology of the complex before and after treatment was visualized by digital camera (Fig. S1c,d). The fibers were more separated without any bundling (Fig. 1i, k) with a smooth surface and a radius of 1.18 ± 0.162 μm (Fig. 1l). The inner diameter of hollow CSGC fibers (Fig. 1n) was about 363 − 850 nm. After purifications, proteins and other impurities like pigments in native mycelium were removed successfully. Thus, the purified chitosan-glucan hollow fiber was suitable for the fabrication of biomaterials. From SEM of ChGC (Fig. 1f) and CSGC (Fig. 1j) the hollow size was increased from (400–600 nm) by increasing the degree of deacetylation from 50 % to 90 % for ChGC (Fig. 1f) and CSGC (Fig. 1j), respectively. This increase in hollow size could confirm that the majority of the chitin chains in complex macromolecule was connected inside the fiber not only on the surface of complex matrix without significant changes in surface morphology of ChGC and CSGC fibers (Fig. 1g, k). Chitosan-glucan hollow fiber (CSGC) with fiber diameters (2.5 ± 0.5 μm) and hollow size (800 nm ± 200) was prepared and used to encapsulate the AV molecule (Scheme 1d, Fig. 1n).

In the presence of CO matrix, the interactions between CSGC and AV were improved, due to the presence of different groups of CO that could be connected physically/ionically with CSGC@AV or CSGC, AV separated. In Scheme 1 shows the cross-section of collagen/hollow fibers encapsulated aloe vera (CO/CSGC@AV) and CSGC@AV well adhere and distributed onto the surface of CO matrix.

4.2. Morphological characteristics

The microstructure was investigated employing scanning electron

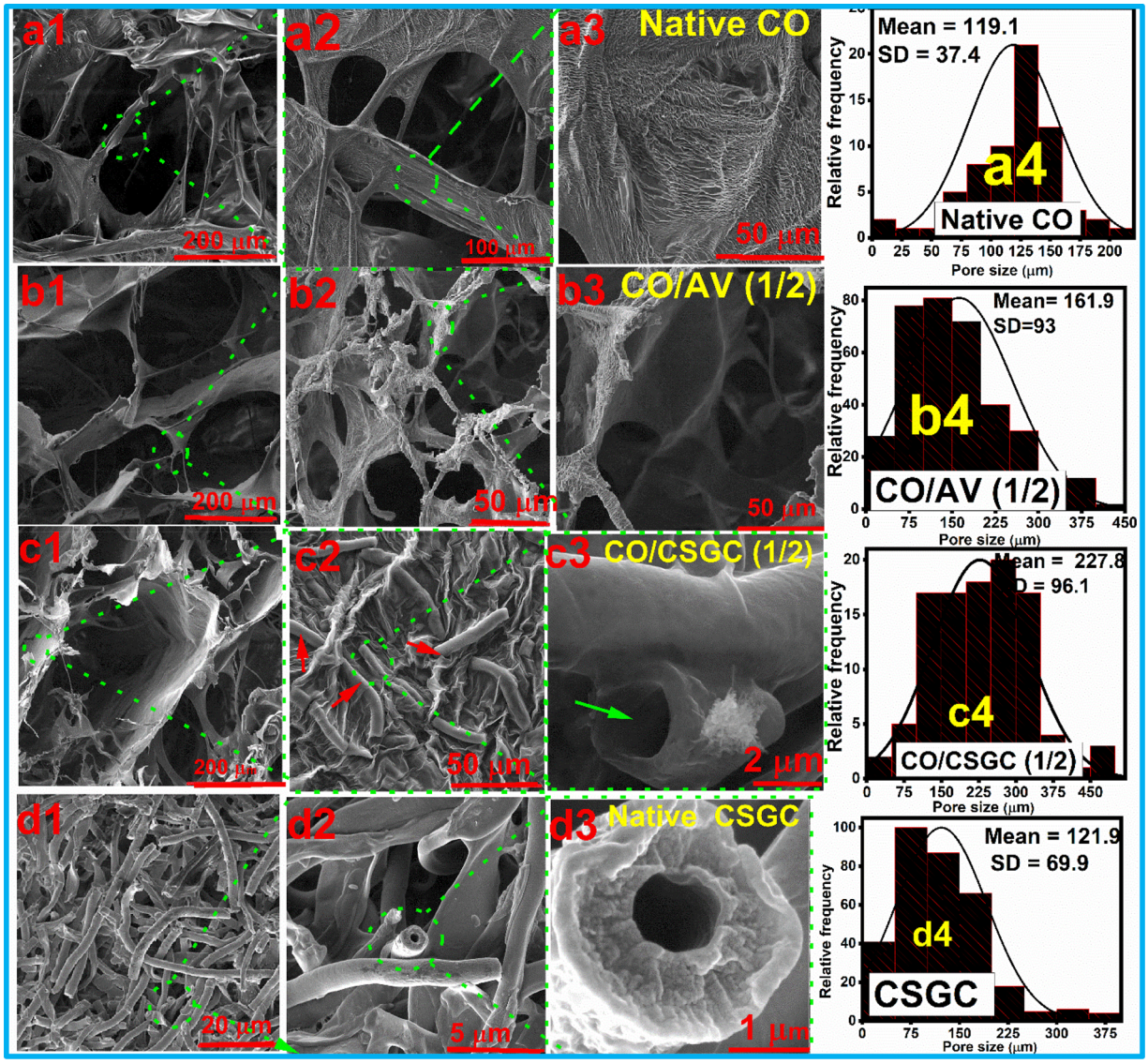
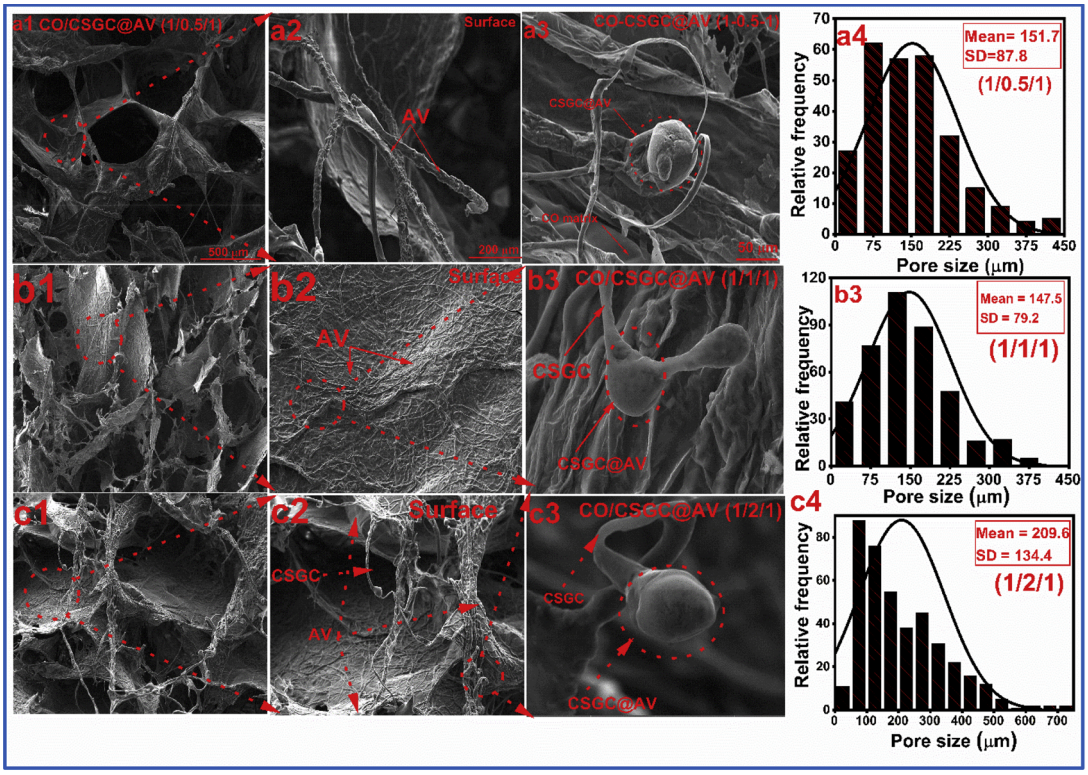


Fig. 2. Representative SEM and pore size histograms of dressing scaffold.
Notes: (a1-a4) SEM and pore size histogram of native CO; (b1-b4) SEM photographs and pore size histogram of CO/AV (1/2); (c1-c4) SEM and pore size histogram of CO/CSGC (1/2); (d1-d4) SEM and pore size histogram of native CSGC (1/2). Scale bars of (a1, a2, a3) were 200, 100 and 50 µm, respectively for (b1, b2, b3) were 200, 100 and 50 µm, respectively for (c1, c2, c3) were 200, 50 and 2 µm, respectively. For d1(20 µm), d2 (5 µm) and d3 (200 nm). The pore size histograms were plotted from 200 points.

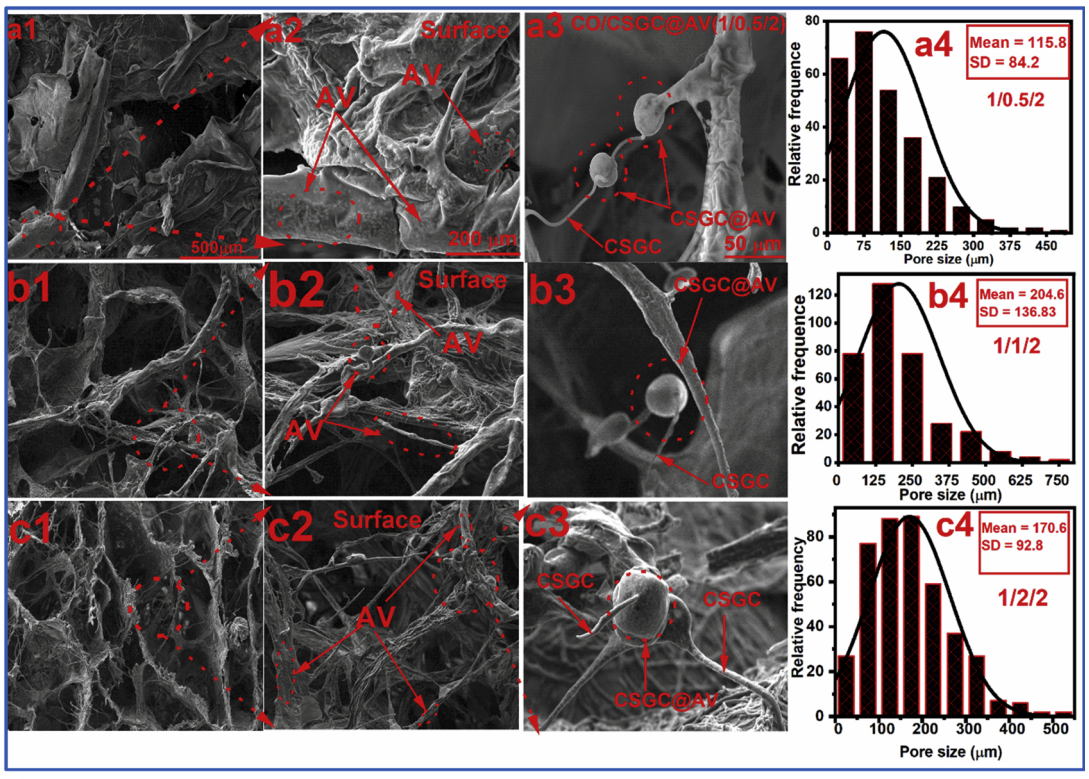
microscopy (SEM) as shown in Figs. 2, 3. Fig. 2a_{1-3} depicts micrographs of the scaffold architecture and pore size histogram of native CO (0.5 wt. %). The CO scaffold has a heterogeneous lamellar pore structure surrounded by flake-like collagen sheets with a mean pore size of 119 ± 37 µm (Fig. 2a_4). At the same mass ratio between CO and AV (1:1), the pore size was increased to the average pore size of 207 ± 109 µm (Fig. S2a_{1-3}; Fig. S2a_4; supporting information). At 1:2 ratio between collagen/aloe vera presented in Fig. 2b_{1-3}, the pore size was decreased slightly from 207 ± 109–162 ± 93 µm, respectively (Fig. 2b_4). This might be due to AV acted as crosslinked agent between CO functional groups and excess of AV worked as bridge lines between CO matrix. The improvement of pore size of CO/AV, might be due to the AV molecules decreased the attraction forces between the functional groups of CO (carboxylic, hydroxyl and amino groups) and increased the pore size, as well as AV, have been reported (Rahman et al., 2017) to contain several biologically active and nutritionally compounds such as glycoproteins, saccharides, vitamins and antioxidants could interact with CO functional groups and increased the pore size.

The appearance of the collagen/chitosan-glucan (CO/CSGC) porous scaffold is shown in Fig. 2c_{1-3}. SEM observation clearly showed the different pore structures of the CO/CSGC (1/2) scaffolds that were prepared in the absence of AV compared to the neat CO scaffold. The CO/CSGC (1/2) porous scaffold with large spherical pores (277 ± 96 µm; Fig. 2c_4) were formed in the CO/CSGC scaffold in an absence of AV (Fig. 2c_{1-3}). The large spherical pores evenly distributed throughout the volume and well stacked. The hollow fibers adhered to the surface of collagen matrix with physical bonds as shown in Fig. 2c_2, (red rows) as well as keeping open the hollow as depicted in Fig. 2c_3, (green row). Fig. 2d_{1-4} shows the native CSGC hollow fibers scaffold with very smooth and homogenous fiber surface and pore size was (122 ± 70 µm).

Fig. 3A and B exhibits the SEM micrographs and histograms of pore size of scaffolds fabricated using different contractions of CSGC (0.25, 0.5, 1 wt.%) and AV (0.5, 1 wt. %). The surface morphology of the dressing scaffold (CO/CSGC@AV) differed from the native mycelium. The pores were interconnected, and the size was significantly increased with the increase of the CSGC concentrations (0.25–1 wt. %). Using different concentrations of CSGC as shown in Fig. 3A (a_{1-3}; b_{1-3}; c_{1-3})



A



B

Fig. 3. (A) Representative SEM of dressing scaffolds using AV (0.5 wt.).
Notes: (a1-a4) SEM and pore size histograms of CO/CSGC@AV (1/0.5/1); (b1-b4) SEM and pore size histogram of CO/CSGC@AV (1/1/1); (c1-c4) SEM and pore size histogram of CO/CSGC@AV (1/2/1); (500 μm scale bars of (a1, b1, c1); 200 μm of (a2, b2, c2); 50 μm of (a3, b3, c3). The histograms of pore size measurements were plotted from 200 points. (B) Representative SEM of dressing scaffolds using AV (1 wt.).
Notes: (a1-a4) SEM and pore size histograms of CO/CSGC@AV (1/0.5/2); (b1-b4) SEM and pore size histogram of CO/CSGC@AV (1/1/2); (c1-c4) SEM and pore size histogram of CO/CSGC@AV (1/2/2); (500 μm scale bars of (a1, b1, c1); 200 μm of (a2, b2, c2); 50 μm of (a3, b3, c3). The histograms of pore size measurements were plotted from 200 points.

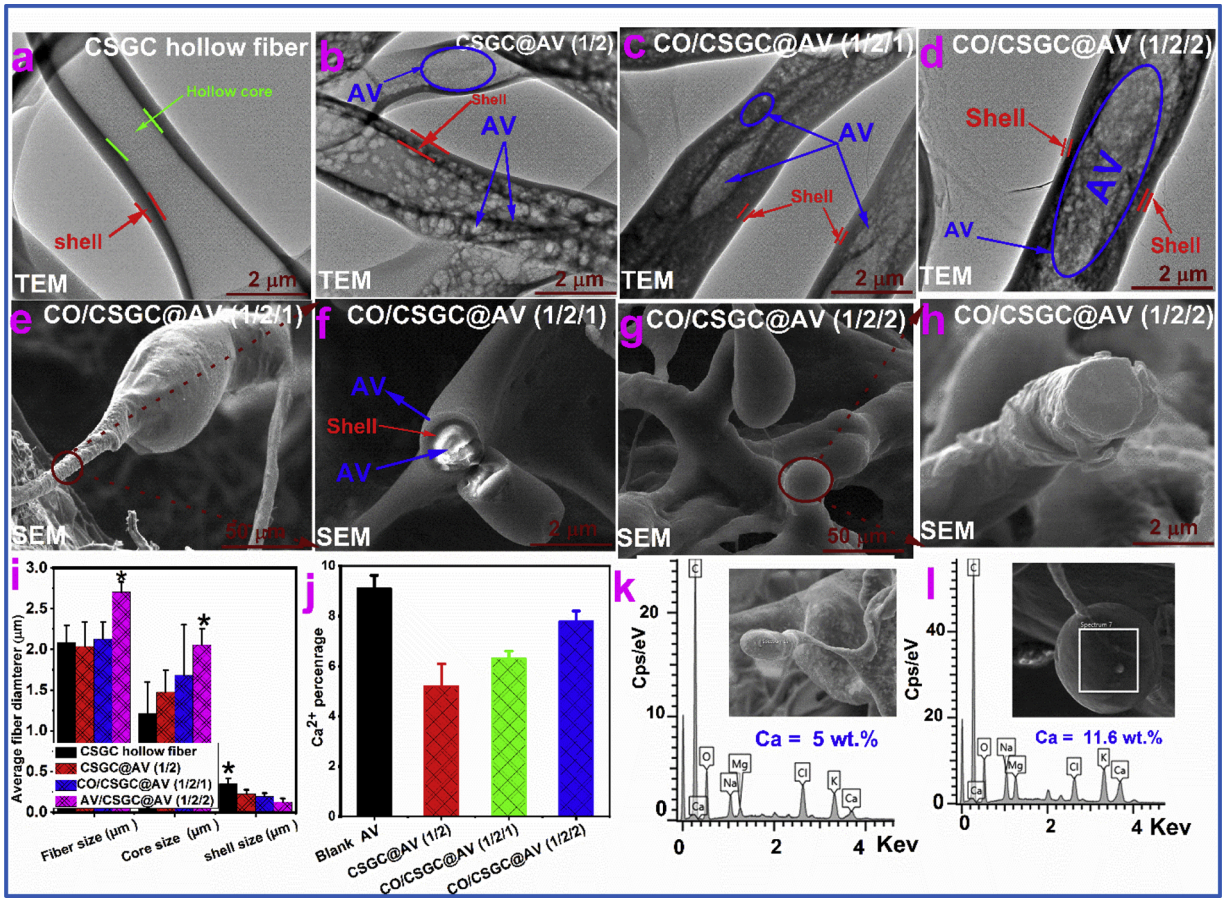


Fig. 4. TEM, SEM-EDX and cross-sectional of CO/CSGC@AV wound dressing scaffold.
Notes: (a) TEM images of native CSGC; (b) CSGC@AV (1/2); (c) CO/CSGC@AV (1/2/1); (d) CO/CSGC@AV (1/2/2). (e) SEM images of CO/CSGC@AV (1/2/1); (f) cross-section of CO/CSGC@AV (1/2/1); (g) SEM images of CO/CSGC@AV (1/2/2); (h) cross-section of CO/CSGC@AV (1/2/2); (i) Effect of AV on average size diameters of hollow fiber, core, and shell before and after encapsulation of AV; (j) Effect of hollow fibers on calcium ions percentage trapped into dressing scaffold; (k) EDX of CO/CSGC@AV (1/2/1); (l) EDX of CO/CSGC@AV (1/2/2). ($p^* > 0.01$).

the AV (0.5 wt. %) molecules were well dispersed inside (Fig. 3Aa$_3$,b$_3$,c$_3$) the CSGC hollow fibers (Fig. 4c) as well as on the surface of scaffold matrix (Fig. 3Aa$_2$,b$_2$,c$_2$). The pore size of CO/CSGC@AV (1/0.5/1; 1/1/1; 1/2/1) dressing scaffolds was 151 ± 87, 147 ± 97, 209 ± 104 μm as shown in Fig. 3Aa$_4$, b$_4$, c$_4$, respectively.

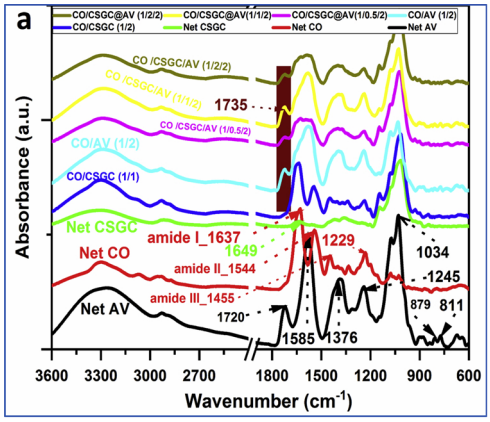
Fig. 3B shows the effect of 1 wt. % of AV on the surface morphology of dressing scaffold using different concentrations of CSGC hollow fibers (0.25, 0.5, 1 wt.%). Interestingly, high loaded of AV was observed (loading efficiency = 85 %; 1/2/2) into the CSGC hollow fibers. AV was encapsulated into the hollow fibers and hollow fiber size was increased slightly from 1.2 to 1.5 μm (Fig. 4i) by increased the AV concentration from 0.5 to 1 wt. %. Due to the AV was dissolved in slightly acid medium pH (4.5–5) could enhance the loading capacity of AV into CSGC and activated the amino groups in chitosan chains to absorb more AV. In addition, enhanced the adhesion properties between CO and CSGC (Fig. 3Ba$_1$-c$_2$), could create strong physical bonds between these functional groups (−COO$^-$,−NH$_2$) and CSGC (−NH$_2$,−NHCOCH$_3$,−OH groups). From the histograms (Fig. 3Ba$_4$,b$_4$,c$_4$), the pore size of dressing scaffold was slightly decreased compared with 0.5 wt. % AV, but still much higher than CO dressing alone.

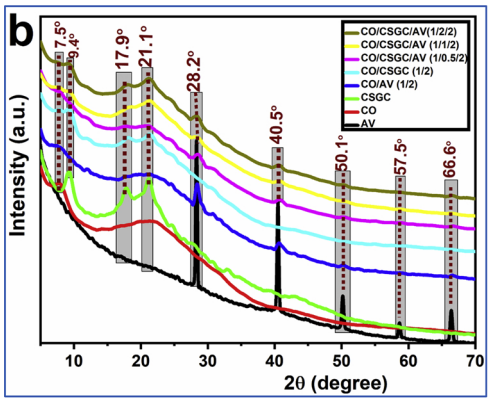
The hollow fiber composition was observed using transmission electron microscopy (TEM) for native chitosan-glucan complex CSGC, complex encapsulated aloe vera (CSGC@AV;1/2) and collagen/hollow encapsulated aloe vera (CO/CSGC@AV) with two different ratios of AV (1/2/1, 1/2/2). Fig. 4a depicts the plain CSGC hollow fiber with the hollow size (363 − 850 nm) and fiber radius (1.18 ± 0.162 μm). Fig. 4b shows the TEM of CSGC@ AV (1/2) without CO matrix with sharp interface boundary after encapsulated the aloe vera into CSGC fibers. CSGC/AV (1/2) exhibited homogeneous and well distribution of AV molecules inside the hollow structure of complex with slightly decreased in shell diameter 0.22 ± 0.051 μm (Fig. 4i) compared with native CSGC (Fig. 4a,i).

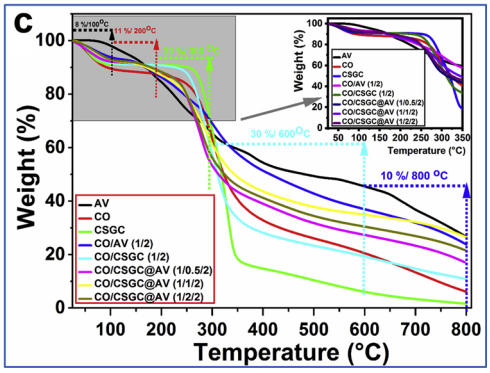
Collagen did not induce any significant changes in the morphology and diameter of the CSGC fibers. Fig. 4c,d shows dressing scaffold with different concentrations of AV (1/2/1, 1/2/2). Comparing between the dressing scaffold engineered from a different concentration of AV, the CSGC exhibited more AV trapped inside the hollow fiber (Fig. 4d), due to the ionic and physical interactions between functional groups of CSGC and the AV. We can conclude that the chitosan-glucan complex hollow fibers were very interesting candidates for trapping and releasing bioactive moieties. The surface morphology and cross-section of CSGC hollow fibers were slightly changed after encapsulated the AV (Fig. 4e,g). from the cross-section, AV generated thick layer inside the CSGC fiber (Fig. 4f, h). At a higher concentration of AV, the fibers trapped more AV inside and on the surface of CSGC (Fig. 4j) with loading efficiency about 85 % compared with native AV (from Ca ions measurement). Fig. 4h suggests that the AV filled completely the hole in the CSGC fibers (1/2/2). The EDX spectra (Fig. 4k, l) captured at different locations on CO/CSGC/AV revealed 5 and 11.5 wt. % of calcium from the AV for 1/2/1 and 1/2/2 dressing scaffold, respectively.

The trapping or encapsulation mechanism of AV into CSGC hollow fibers unclear and will need more studies. Here, we proposed different mechanisms of immobilized the AV inside the CSGC fibers. (i) Under acidic conditions, amino groups of CSGC were protonated and formed

quaternary salt that could interact with components of AV generated amphiphilic property between cationic chitosan part in CSGC and anionic part of AV (acetylated mannan, anthracene derivatives), (ii) The presence of minerals like Ca and Zn ions in AC composition could form complex bridge with cationic amino groups of chitosan and attract inside the AV, (iii) The AV solution connected to the CSGC hollow fibers, a capillary force imposed on the solution, and the AV solution flowed in the hollow tube under the impact of capillary force and velocity of the fluidic depends on the concentration of AV (Fig. 2C,c,d) as well as of intermolecular forces between the AV solution and surrounding CSGC surfaces, and (iv) The size of the CSGC hollow quite sufficient bigger than the size of AV, might be surface tension of AV (caused by cohesion within the gel of AV) solution and adhesive property (Scheme 1f) between the AV solution and hollow fiber wall act to propel the solution of AV inside the hollow of CSGC. From the above hypothesis, the complex hollow fiber encapsulated the AV molecules formed ionic interactions with the protonated amino groups inside the hollow fiber.







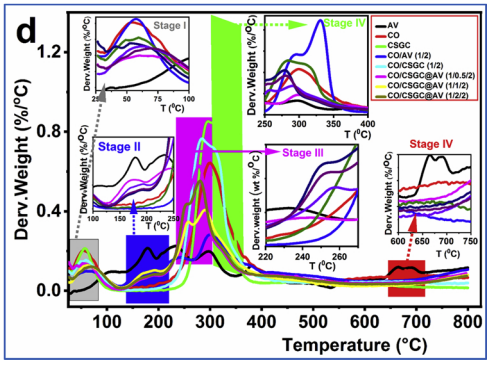


Fig. 5. FTIR of natives and hybrid scaffolds.
Notes: (a) ATR-FTIR of powder aloe vera (AV); native collagen (CO); native chitosan-glucan hollow fibers (CSGC); collagen/chitosan-glucan hollow (CO/CSGC;1/2); collagen/aloe vera (CO/AV; 1/2); collagen/chitosan-glucan hollow encapsulated Aloe Vera using different ratio of CSGC (1/0.5/2, 1/1/2, 1/2/2). (B) XRD of CO/CSGC@AV hybrid scaffolds.
Notes: (b) XR-diffraction of AV; CO; CSGC; CO/AV (1/2); CO/CSGC (1/2); CO/CSGC@AV (1/0.5/2); CO/CSGC@AV (1/1/2); CO/CSGC@AV (1/2/2). (C) TG of CO/CSGC@AV hybrid scaffolds.
Notes: (c) TG of native AV, CO; CSGC and hybrid scaffold CO/AV (1/2); CO/CSGC (1/2); CO/CSGC@AV (1/0.5/2); CO/CSGC@AV (1/1/2); CO/CSGC@AV (1/2/2), respectively. The measurement was conducted under a nitrogen atmosphere at a heating rate of 10 °C/min. (D) DTG of CO/CSGC@AV hybrid scaffolds.
Notes: (d) DTG of native AV, CO; CSGC and hybrid scaffold CO/AV (1/2); CO/CSGC (1/2); CO/CSGC@AV (1/0.5/2); CO/CSGC@AV (1/1/2); CO/CSGC@AV (1/2/2), respectively. The measurement was conducted under a nitrogen atmosphere at a heating rate of 10 °C/min.

4.3. Characterization of dressing sheets

For the dressing scaffold system composed of three different components of biomaterials, ATR-FTIR could be used as an effective technique to define the existence of each component. Fig. 5 depict ATR-FTIR, XRD, and TGA-DTG of the composite scaffold. Fig. 5a shows the ATR-FTIR of different dressing scaffold compositions compared with net CO, CSGC, and AV. Native CO scaffold displayed the characteristic absorption bands in region of 3427 cm^{-1} for υ_s stretching vibration of hydroxyl groups, 3279 cm^{-1} amide A, υ_s (NH) stretching vibration of amine group of protein, 3052 cm^{-1} amide B, overtone amide II, 2962 υ_{as} (CH_3), asymmetric stretching vibration of methyl group and 2924 υ_{as} (CH_2) asymmetric stretching vibration of methylene group in collagen chains (Fig. 5a).

The triple helix structure of collagen I show four absorption peaks at 1637,1544, 1449,1263 cm^{-1} for amide I, II, CH_3, and amide III, respectively. The magnitude of absorbance ratios between A_{1235} and A_{1450} peak intensity was 1.13 ± 0.05. from our data we conclude that after acid treatment of collagen there wasn't any denaturized and fully triple-helical confirmation of CO. Our results completely fit with reported results in literature (Gordon et al., 1974; Sylvester et al., 1989; Yannas et al., 1980).

FTIR of AV shows different peaks for amide 1 υ_s (C═O) stretching vibration bands of peptide bond were appeared at 1733 and 1248 cm^{-1} a correspond to carbonyl groups of the organic components of AV and o-acetyl esters and asymmetric and symmetric (C–H) stretching vibration band of methylene groups, respectively. These acetyl groups were necessary for the biological activity of AV, they mask hydrophilic hydroxyl groups thus make the molecule more as the main component of AV (Paichit et al., 2012). Another peak was appeared at 1585 cm^{-1} (C═C groups or from aromatic rings) in main component of AV (Logaranjan et al., 2016). A further peak at 1032 cm^{-1} could owing the

glucan units as well as glucosidic bonds (Silva et al., 2013). The pyranoside ring absorption band at 879 cm^{-1} (C—H ring vibration) and mannose absorption peak at 811 cm^{-1} were also detected for AV.

Chitosan-glucan hollow fiber complex (CSGC) shows different specific peaks at 3320 cm^{-1} correspond to hydroxyl groups on CSGC compositions, beaks at 2930 cm^{-1} related to asymmetrical stretch of methylene groups of the complex, 1649 cm^{-1} was a characteristic vibration for carbonyl groups residual in chitosan chain, 1550 cm^{-1} correspond to primary free amino groups of chitosan chains in the CSGC complex. 1070, and 1040 cm^{-1} were characteristic peaks for ether linkage (—C—O—C—) of chitosan and glucan backbone (Abdel-Mohsen et al., 2016). β-anomeric configuration was signalized by absorption at 890 and 1371 cm^{-1} **(**Fig. 5a**)**. Chitosan-glucan was extracted from α-chitin form not β-form was confirmed from chitin-glucan and observed that amide I band clearly divided into two peaks at 1653 and 1638 cm^{-1} confirmed chitin-glucan complex was in α-form.

A spectrum of CO/CSGC was depicted in Fig. 5a showed characteristic absorption band in region 3310 cm^{-1} for O—H stretch (low intensity) compared with net CO, peak at 1645 cm^{-1} for CO/CSGC, with low beak intensity compared with 1645 cm^{-1} for native CO, which might be due to the physical interaction between CO and CSGC. The peak of (—C—O—C—) ether linkage at 1040 cm^{-1} was shifted to 1020 cm^{-1} with high intensity compared with net CO, due to the generation of hydrogen bonds between hydroxyl groups of CSGC and CO. The interactions between CO and CSGC might be occurred by the formation of H-bonds. The —OH groups, COO^- and $-NH_2$ groups in CO were capable of forming hydrogen bonds with —OH, $-NHCOCH_3$ and $-NH_2$ groups in chitosan-glucan hollow fiber (Tamate et al., 2018). Additionally, ionic bonds might be formed between CO and CSGC. These molecules were capable of forming a complex with oppositely charged ionic polymers, and these interactions might be formed polycationic/polyanionic complexation, obviously, owing to their same main functional groups with thermal stability **(**Fig. 5c, d).

Spectra of collagen/chitosan-glucan/ aloe vera (CO/CSGC@AV) with different ratios of CSGC (1/0.5/2, 1/1/2, 1/2/2) were shown in Fig. 5a. CO/CSGC@AV depicted a shifting peak from 3314 cm^{-1} to 3281 cm^{-1} due to the hydrogen bonds that were generated between the functional groups of AV and (—OH, —COOH and $-NH_2$) groups in CO and/or CSGC hollow fiber. A new peak was appeared at 1735 cm^{-1} and the intensity of this peak was increased by increasing the ratio of CSGC component, could be due to the formation of amide reaction (Belbachir et al., 2009; Lee et al., 2017).

From the above results, native collagen scaffold still exhibits all the characteristic peaks of the triple helical structure of neat collagen. The spectra of CSGC Fig. 3a proved that the chitosan-glucan was extracted from α-chitin by observing that the amide I band clearly divided into two peaks at 1653 and 1638 cm^{-1}, confirming the α-form. Analysis of the ATR-FTIR spectra suggested that fabricating the 3D scaffolds did not create any significant change in the molecular structure of any of the components.

Fig. 5b shows the X-ray diffraction (XRD) patterns of dressing scaffold. The diffraction curves of all materials CO, CSGC and fabricated scaffold with different ratios of CSGC devolved exhibited mainly amorphous patterns with small crystalline fraction except native AV. Powder AV demonstrated the peaks observed for native AV at 28.2°, 40.5°, 50.1°, 57.5° and 66.6° corresponded to Ca^{2+} as well as the organic polysaccharides (glucomannan, a mannose-rich polysaccharide, and gibberellin) as the main components of AV. CO scaffold shows mainly amorphous patterned with small peak intensity at 2θ = 7.5° and other broad peak appeared at 2θ = 18–22° indicated a tendency to the structural organization of collagen triple helix structure. We further investigated the semi-crystalline structure of our new hollow fibers scaffold using X-ray diffraction (XRD). In nature, chitin occurs as supramolecular semi-crystalline and exists in two major distinct polymorphs: α-chitin (orthorhombic) and β-chitin (monoclinic). These chitin crystals have different molecular conformations (i.e., antiparallel for α-chitin vs parallel for β-chitin) with dissimilar hydrogen-bond densities, which could be intuitively distinguished through ATR-FTIR and XRD analyses; each material presents different characteristic peaks. As revealed in the FTIR spectra (Fig. 3a), β-chitin has a single broad absorption peak at around 1630 cm^{-1} because of the intramolecular C═O···HO hydrogen bonds. Meanwhile, α-chitin was characterized by split peaks at 1653 and 1638 cm^{-1} (ATR-FTIR; Fig. 5a) which raised from the antiparallel molecular arrangement whereby the intramolecular C═O···HO hydrogen bonds were simultaneously engaged with the inter-sheet C═O···HN hydrogen bonds (Jin et al., 2016; Kim et al., 2017).

For plain CSGC scaffold exhibited mainly semi-crystalline pattern with three different phases at 2θ = 9.4, 17.9 and 21.1°, these three peaks corresponded to three components of the complex (chitin, chitosan and branched glucan). Due to the degree of deacetylation of chitosan was only 50 % (DDA = 50 %), and chitin was 50 %. These results obviously indicate that the residual chitin in the chitosan-glucan complex was in α-form structure. In collagen/aloe vera scaffold with ratio (1/2) showed only one broad beak for collagen at 2θ around 20–25° as well as two beaks related to AV in the same position compared with native AV at 2θ = 28.2, 40.3° indicated that there wasn't signification interaction between CO and AV, was only physically hydrogen bond generated between functional groups of CO and AV as well as in interaction was on the surface of collagen scaffold (Fig. 5b).

The XRD of dressing scaffold with different ratios of hollow fiber complex represented in Fig. 5b. CO/CSGC@AV (1/0.5/2; 1/1/2; 1/2/2) shows different pattern peaks related to the composition of the scaffolds. Collagen peak at 2θ = 7.5° with lower peak intensity, might be due to strong physical interaction with CSGC and/ or AV functional groups. Peak related to complex at 2θ = 9.4° (chitin part) was observed with very low intensity compared with native complex, but the intensity of this peak was raised using high ratio of the complex to CO. Amorphous two peaks of chitosan/glucan components in complex appeared 2θ = 17.9° and 21.1° were visualized in scaffold also with lower intensity. Interestingly, peaks correspond to AV were appeared in the same position in dressing scaffold with low intensity as compared with native AV.

From x-ray diffraction patterns (Fig. 5b), dressing scaffold was synthesized without significant changes in the chemical structure of the scaffold components and the interactions between collagen, chitin/chitosan-glucan hollow fibers complex and aloe vera were only on the surface and between the functional groups like (carboxylic, amino, hydroxyl) in CO, (amino, acetamide, hydroxyl) in CSGC, and (acetyl, hydroxyl, carbonyl) as well as residual metals in AV.

The thermal stability of the dressing sheets was measured using Thermogravimetric analysis (TGA) for the experimental samples CO, AV, CSGC, CO/CSGC (1/2), CO/AV (1/2), CO/CSGC@AV (1/0.5/2; 1/1/2; and ½/2) as represented in Fig. 5c, d and correspond thermal degradation values were displayed in table S2 (supporting information). From TG curves, we determined the mass loss during the heating process from 25 to 800 °C. The temperature of maximum speed process (T_{max}) was determined from the maximum on DTG curve (Table S2; supporting information). For CO scaffold a weight loss from room temperature to 100 °C is 4.5 % (stage I), probably resulting from the evaporation of non-bounded water absorbed into the surface of triple helix collagen structure. The second stage of collagen scaffold appeared at maximum decomposition temperature at 298 °C (stage II, Fig. 5c, d), which might be due to water bounded and small molecules liberated after degradation of helix structure of collagen to small monomer molecules (Udhayakumar et al., 2017).

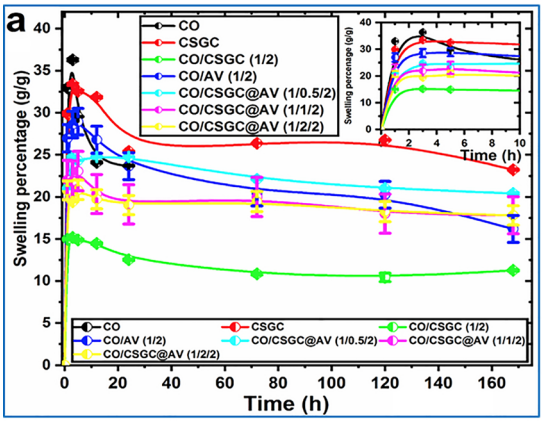
The TG/DTG of chitosan-glucan hollow fiber (CSGC) was shown in Fig. 5c, d with three different decomposition stages. The first stage was appeared at 58 °C, due to the evaporation of water physically connected with a complex chain. In stage II, the complex mass loss about 29 % at 294 °C, might be due to cleaving the chain bonds *β-(1-4, 1-3, 1-6)* between the different components of the hollow fiber complex (chitin,

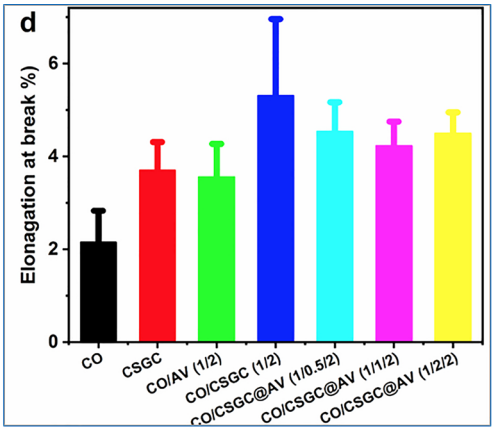
chitosan, glucan). The third stage beak was appeared at a maximum decomposing temperature about 331 °C with mass loss 66.4 %, due to the decomposition of linear and branched glucose chains, acetyl glucosamine and *N*- acetyl glucosamine (Abdel-Mohsen et al., 2016). Pure aloe vera (AV) shows five different decomposition peaks at 110, 178, 299, and 382 °C for 3.2, 11.5, 34.1, and 43.8 % mass loss, respectively.

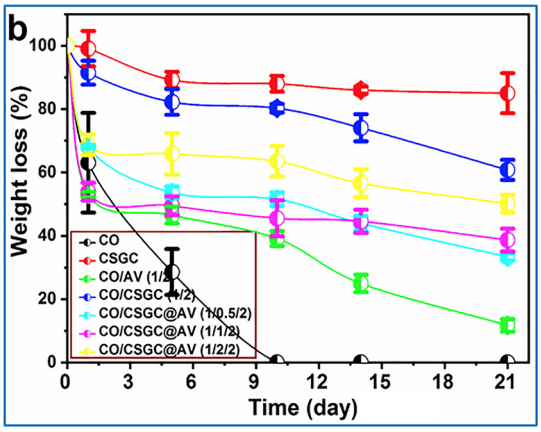
Different decomposition stages of AV, related to the multi-components of aloe vera structure such as vitamins, enzymes, minerals, sugars, anthraquinone, fatty acid, and hormones (Silva et al., 2013; Surjushe et al., 2008). The dressing scaffold CO/CSGC@AV with different mass ratio of CSGC (0.5, 1, 2) and a constant ratio of AV (2) was shown in Fig. 5c, d and Table S2 (supporting information). Interestingly, the combination of CO, CSGC, and AV enhanced the thermal stability of scaffold compared with net CO scaffold showed weight loss only 23 % up to 250 °C that was lower compared to other scaffolds. From the thermogravimetric data, we can conclude that different compositions of the CSGC did not show significant changes in the thermal stability of the scaffold. The addition of the AV improved the thermal stability slightly, due to the strong interaction between collagen and hollow fibers in the presence of aloe vera.

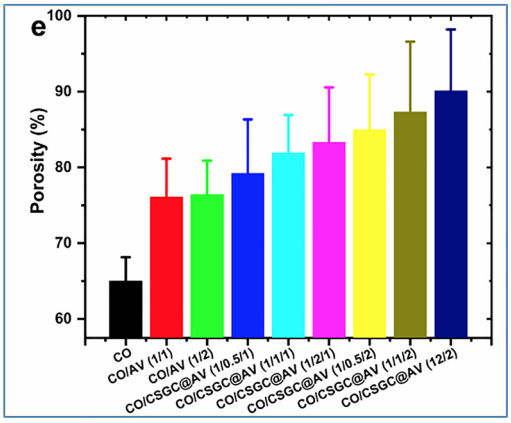
4.4. Swellability, degradability and mechanical properties of dressing sheets

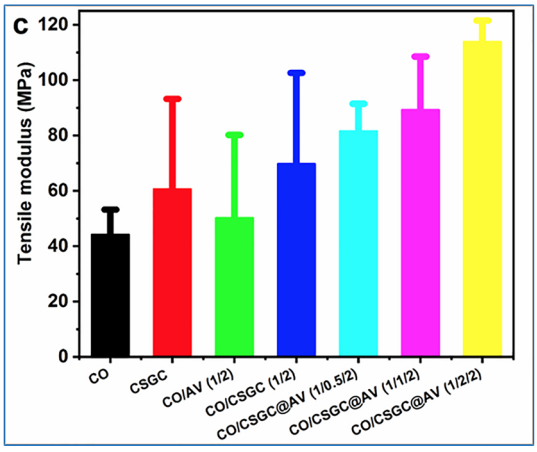
Swelling rate (%) of different dressing scaffold engendered with/without aloe vera at different intervals of phosphate buffer solution (PBS) contact time was depicted in Fig. 6a. the swelling percentage (g/g) of collagen (CO) scaffold was rapidly increased up to (25 g/g) of CO in the initial 2.5 h, due to the hydrophilic character of collagen chains, then decreased up to (15 g/g) after 120 h. After 5 days of immersing of collagen in PBS buffer at 37 °C, the scaffold started to hydrolysis to

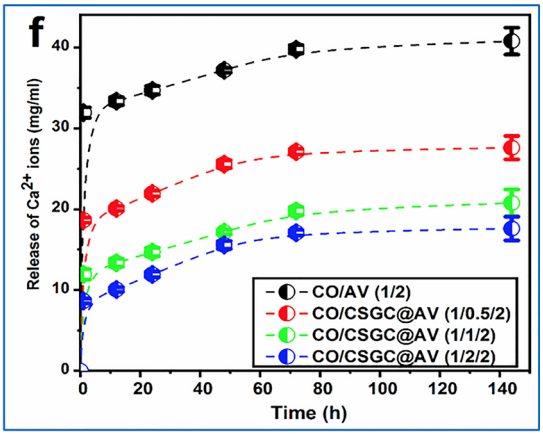












(caption on next page)

Fig. 6. (a) Swelling percentage (g/g) of dressing scaffold.
Notes: Water uptake of native collagen (CO); native chitosan-glucan hollow fibers (CSGC); collagen/aloe vera (CO/AV; 1/2); collagen/chitosan-glucan hollow (CO/CSGC; 1/2); collagen/chitosan-glucan hollow/Aloe Vera (CO/**CSGC**@AV; 1/0.5/2); collagen/chitosan-glucan hollow/aloe vera (CO/CSGC@AV; 1/1/2); collagen/chitosan-glucan hollow/Aloe Vera (CO/CSGC@AV; 1/2/2); The samples were measured three times (n = 3), using PBS at 37 ^{0}C at different time (0.5, 3, 5, 12, 24, 48, 72, 120, and after 168 h). (B) Representative hydrolytic degradation of dressing scaffold.
Notes: Weight loss percentage as a function of time for pure native CO; CSGC; CO/AV (1/2); CO/CSGC (1/2); CO/CSGC@AV; (1/0.5/2); CO/CSGC@AV (1/1/2); CO/CSGC@AV (1/2/2), the samples were measured three times (n = 3), using PBS at 37 ^{0}C at different time (1, 3, 7, 14, and 21d). (c) Tensile strength of native hybrid scaffold.
Notes: Tensile modulus of native CO; native CSGC; CO/AV (1/2); CO/CSGC (1/2); CO/CSGC@AV (1/0.5/2); CO/CSGC@AV (1/1/2); CO/CSGC@AV (1/2/2). (D) Elongation at break of native and hybrid scaffold.
Notes: Elongation at break of native (CO); native CSGC; CO/AV (1/2); CO/CSGC (1/2); CO/CSGC@AV (1/0.5/2); CO/CSGC@AV (1/1/2); CO/CSGC@AV (1/2/2), The samples were measured three times (n = 5) for (±) SD. (E) Porosity of natives and dressing scaffold.
Notes: Porosity measurements of hybrid scaffold using different concentrations of CSGC and AV. Natives collagen (CO), chitosan-glucan complex hollow fibers (CSGC), collagen/aloe vera (CO/AV; 1/1), collagen/aloe vera (CO/AV; 1/2), collagen/chitosan-glucan complex/ aloe vera (CO/CSGC@AV; 1/0.5/1), collagen/chitosan-glucan complex/ aloe vera (CO/CSGC@AV; 1/1/1), collagen/chitosan-glucan complex/ aloe vera (CO/CSGC@AV; 1/2/1), collagen/chitosan-glucan complex/ aloe vera (CO/CSGC@AV; 1/0.5/2), collagen/chitosan-glucan complex/ aloe vera (CO/CSGC@AV; 1/1/2), and collagen/chitosan-glucan complex/ aloe vera (CO/CSGC@AV; 1/2/2). (F) Representative release of calcium ions from dressing scaffold.
Notes: (f) Release measurement of calcium ions in saline solution (n = 5 for the test of $Ca2^{+}$ contains). collagen/aloe vera (CO/AV; 1/2), collagen/chitosan-glucan complex/ aloe vera (CO/CSGC@AV; 1/0.5/2), collagen/chitosan-glucan complex/ aloe vera (CO/CSGC@AV; 1/1/2), and collagen/chitosan-glucan complex/ aloe vera (CO/CSGC@AV; 1/2/2).

small pieces inside the solution but not completely hydrolysis. Chitosan-glucan hollow fiber scaffold show the highest water absorption scaffold and the swelling percent (SP) was rapidly increased to (30 g/g) in the initial 4 h interval and reached a saturation of (35 g/g), then was constant absorption after 25 h. after 1 day of swelling, CSGC scaffold, the SP (%) was slightly decreased but still highly water absorption capacity compared with the other scaffold. The higher swelling capacity of CSGC related to the hydrophilic properties of the complex (a lot of hydroxyl in chitin, chitosan, glucan units, and amino groups) as well as the hollow structure shape of the fiber that could trap water inside the hollow structure. Scaffold CO/CSGC (1/2) ratio was the lowest water absorption capacity compared with CO, CSGC and another scaffold, and the SP (%) increase in the first 25 h with constant swelling percent (15 g/g), after was slightly decreased up to 6 days of immersing in PBS.

The lower water absorption of CO/CSGC, related to the strong physical interactions on the surface of CO or between the matrix layers (physically interact between the different groups, −COO, NH_2, −OH, and $-NHCOCH_3$) prevented CO to absorb the water molecules (Fig. 6a). The swelling percentage (%) of collagen/aloe vera scaffold (1/2) was higher than the native collagen scaffold in the first 3 h (27 g/g), due to the hydrophilic properties of AV (presence of polysaccharide in the chemical composition of aloe vera). The effect of concentration of CSGC on the swelling percentage of a hybrid scaffold in the presence of AV (1 %) was depicted in Fig. 6a. increase the mass ratio of CSGC in scaffold was increased the swelling percent with a constant value up to 160 h. Due to the hydrophilic characters of CSGC, AV, and CO. At equilibrium of swelling, the composite hybrid scaffold contains (1/2/2) ratio between CO, CSGC, AV has the highest swelling percentage. Based on the above observation, the optimum concentration of CSGC to be used in the hybrid scaffold was fixed as 1 %. High water/ fluid holding capacity of such a scaffold was very important for cell adhesion, proliferation, and growths. The wide range of swelling ratios obtained for CO/CSGC@AV hybrid scaffold is advantageous for tissue engineering applications since they could finely be tuned based on their final application. In addition, the increased swelling of the scaffold at a higher ratio of CSGC can enhance their cell adherence and viability of cells *in-vivo*. For wound closure, this could greatly accelerate healing by providing high oxygen and exudate permeable and flexible wound seal (Annabi et al., 2017; Peppas et al., 2006). Results revealed that the *in-vitro* degradation rate of native and hybrid scaffolds depends on the ratio of complex to collagen

Another technical advantage of scaffold used for wound closure applications was their control degradation in wet environments. Therefore, we aimed to investigate the *in-vitro* degradation of a hybrid scaffold under physiological body application. Results revealed that the in-vitro degradation rate of native and hybrid scaffold depends on the ratio of complex to collagen and final scaffold concentrations. Fig. 6b shows the weight loss percent (%) of different hybrid scaffolds was measured under physiological conditions (PBS pH = 7.5; 37 °C) after 1, 3, 5, 10, 14, and 21 days of immersed in PBS. Collagen scaffold was significant decrease the mass after 6 days (mass loss = 40 %), and in day ten was completely degraded in PBS (mass loss = 100 %), due to CO triple helix would be gain access to the cleavage site by binding to the metal attachment domains along the chains followed by unwinding of the triple helix and then destroyed the collagen chains (Foglia et al., 2013; Rajan et al., 2007).

Native chitosan-glucan hollow fiber scaffold was more stable with less degree of degradation compared with other scaffolds. After 1 day of immersed the mass loss was only 0.9 %, after 10 days the mass loss (%) was 12 % after incubation at 37 °C. After 21 days of seeding in PBS, the mass loss was only 15 %. This might be a strong physical and chemical interaction between the different components chain in the complex (chitin, chitosan, glucan). Scaffold engineered from CO/CSGC@AV incubated in PBS using a different ratio of CSGC exhibited lower degradability compared with native CO scaffold. In addition, the rate of degradability decreased with increased of CSGC concentration. The incorporation of AV resulted in no significant changes in the degradability rate of the composite hybrid scaffold (Fig. 6b, Table S3). In contrast, previous studies have shown that the encapsulated/ incorporations of antimicrobial agents in proteins-based biomaterials, could significantly alter the degradability percentage of the obtained biomaterials (Annabi et al., 2017; Kumar et al., 2012).

Mechanical properties of CO/CSGC@AV dressing scaffold were characterized through tensile tests. The tensile tests on the hybrid scaffold revealed that the tensile modulus (Fig. 6c) and elongation at break (Fig. 6d) of the fabricated scaffolds could be modulated by varying the collagen/ chitosan-glucan hollow fiber ratio in presence/ absence of aloe vera and the total polymer concentration. The tensile modulus of the hybrid scaffold increased consistently from 44.2 ± 8.9 kPa (native CO) to 69.7 ± 12.8 kPa (CO/CSGC; 1/2) and 50. ± 19.9 (CO/AV; 1/2) to 81.5 ± 9.8, 89.3 ± 19.2, 113.8 ± 7.6 kPa for CO/CSGC@AV (1/0.5/2; 1/1/2; 1/2/2), respectively. Elastic modulus of the scaffold was significantly increased in presence of CSGC and AV compared with native CO, due to the hydrogen/ionic interactions (presence of Ca^{2+} and Zn^{2+} in composition of AV) between their functional groups *via* hydroxyl, amino, and acetamide carboxyl of CO, CSGC and AV as well as between carboxylic groups/amino groups of CO/CSGC and metal ions (Ca^{2+} and Zn^{2+}) components of AV. These ionic interactions served as ionic cross-linker for hybrid scaffolds. In Fig. 6d, the elongation at break of hybrid scaffold (%) increased with increased concentration of CSGC (0.25, 0.5, and1 %) in presence of AV suggested that the CSGC and AV enhanced

the elasticity of the scaffold and resulted in more stretchable scaffold.

The porosity of the engineered scaffold was shown in Fig. 6e. The porosity (%) of plain CO scaffold, CO/AV (1/2), CO/CSGC (1/2) CO/CSGC@AV (1/0.5/1;1/1/1;1/2/2; 1/0.5/2; 1/1/2; and 1/2/2) was 65 ± 3.14, 76.1 ± 5.05, 76.4 ± 4.49, 79.2 ± 7.12, 81.9 ± 5.02, 83.3 ± 7.26, 85 ± 7.26, 87.3 ± 9.3, and 90.1 ± 8.1 (%), respectively. The porosity was slightly increased with increasing the concentrations of CSGC from 65 to 90 %, with small changes in pore size and pore architecture. Enhancement in porosity could improve the water absorption of a hybrid scaffold and could easily absorb culture medium to facility the cell migration, adhesive and proliferation into and on the surface of the hybrid scaffolds.

Since one of the aims of this study to demonstrate the possibility of different agents loaded into the hollow fiber and control release of each agent for biomedical application. Regarding our target, aloe vera was used as as a drug model and investigated the release of calcium ions (one of AV component) by using ICP-MS. CO/AV (1/2) scaffold showed high release percentage at the same time compared with scaffold contain hollow fiber (Fig. 6f). The concentration of calcium ions released in the presence of different contractions of CSGC hollow fibers was smaller without CSGC. The release of calcium ion was decreased by increasing the concentration of complex (form 0.25–1 wt. %) into the dressing scaffold. This owing to the interactions (ionic, physical, electrostatic) between calcium ions and functional groups of CSGC (amino, amide, hydroxyl) (Arias & Fernández, 2008; Li et al., 2012; Qi et al., 2018) which could reduce the release percentage of calcium from the dressing scaffold (Fig. 6f). The loading capacity of AV was increased with increasing the concentrations of CSGC (increase the encapsulated Ca^{2+}) into the hollow structure (Fig. 4 k, l). This means that the complex strongly interacts with AV components and reduced the release percentage of calcium ions. From Fig. 6 we can conclude that the presence of CSGC (different concentrations) had a significant influence on hydrogel physical properties (swelling hydrolytic degradation and porosity) mechanical properties as well as a promising material to control release different types of drugs.

5. Conclusions

A novel dressing scaffold from collagen/chitosan-glucan complex hollow fibers in presence or absence aloe vera (CO/CSGC@AV) was fabricated by freeze-dried technique for the first time with enhanced the physical, chemical and mechanical properties of collagen scaffold. CSGC hollow fibers were extracted from *Schizophyllum commune* with controlled the degree of deacetylation (DDA 50–100 %), fiber diameter (2.5 ± 0.5 μm) and hollow size (800 ± 200 nm) by green chemical treatment of native mycelium. The degree of deacetylation and surface morphology of CSGC hollow fiber was confirmed and visualized by solid-NMR and SEM spectroscopy. CO/CSGC@AV fabricated with different concentrations of CSGC (0.25, 0.5 1 wt. %) show significantly enhanced swelling percentage and stability of scaffold in the presence of AV for up to three weeks compared with native CO. The pore size and porosity of CO/CSGC@AV exhibited enhanced in the presence of high ratio f CSGC and concentration independent of AV. CSGC complex hollow fibers could control the released of calcium ions from the scaffold matrix compared with dressing scaffold in absence of CSGC. We believe that the new CO/CSGC@AV hybrid dressing scaffold opens a new approach of application in biomedical areas that could be employed for soft tissue engineering especially for skin wound healing and drug delivery application.

Authors contribution sections

Author Contributions: Conceptualization, Methodology A.M.A; R.M.A; I.K; L.K; Z.S; M.Z; R.P; J.B; J.J. Writing original manuscript, A.M.A; R.M.A; I.K; L.K; Z.S; M.Z; R.P; J.B; J.J

Writing-Review, and editing manuscript A.M.A; R.M.A; I.K; L.K; Z.S; M.Z; R.P; J.B; J.J. Funding acquisition.

Acknowledgments

This research was carried out under the project CEITEC 2020 (LQ1601) with financial support from the Ministry of Education, Youth and Sports of the Czechia under the National Sustainability Programme II.

Appendix A. Supplementary data

Supplementary material related to this article can be found, in the online version, at doi:https://doi.org/10.1016/j.carbpol.2019.115708.

References

Abdel-Mohsen, A. M., Jancar, J., Massoud, D., Fohlerova, Z., Elhadidy, H., Spotz, Z., & Hebeish, A. (2016). Novel chitin/chitosan-glucan wound dressing: Isolation, characterization, antibacterial activity and wound healing properties. *International Journal of Pharmaceutics, 510*(1), 86–99.

Annabi, N., Rana, D., Shirzaei Sani, E., Portillo-Lara, R., Gifford, J. L., Fares, M. M., & Weiss, A. S. (2017). Engineering a sprayable and elastic hydrogel adhesive with antimicrobial properties for wound healing. *Biomaterials, 139*, 229–243.

Arias, J. L., & Fernández, M. S. (2008). Polysaccharides and proteoglycans in calcium carbonate-based biomineralization. *Chemical Reviews, 108*(11), 4475–4482.

Ashraf, J. M., Ansari, M. A., Khan, H. M., Alzohairy, M. A., & Choi, I. (2016). Green synthesis of silver nanoparticles and characterization of their inhibitory effects on AGEs formation using biophysical techniques. *Scientific Reports, 6*, 20414.

Bedford, N. M., Dickerson, M. B., Drummy, L. F., Koerner, H., Singh, K. M., Vasudev, M. C., & Steckl, A. J. (2012). Nanofiber-based bulk-heterojunction organic solar cells using coaxial electrospinning. *Advanced Energy Materials, 2*(9), 1136–1144.

Belbachir, K., Noreen, R., Gouspillou, G., & Petibois, C. (2009). Collagen types analysis and differentiation by FTIR spectroscopy. *Analytical and Bioanalytical Chemistry, 395*(3), 829–837.

Brus, J. (2000). Heating of samples induced by fast magic-angle spinning. *Solid State Nuclear Magnetic Resonance, 16*(3), 151–160.

Burkatovskaya, M., Tegos, G. P., Swietlik, E., Demidova, T. N., P Castano, A., & Hamblin, M. R. (2006). Use of chitosan bandage to prevent fatal infections developing from highly contaminated wounds in mice. *Biomaterials, 27*(22), 4157–4164.

Doillon, C. J., & Silver, F. H. (1986). Collagen-based wound dressing: Effects of hyaluronic acid and firponectin on wound healing. *Biomaterials, 7*(1), 3–8.

Doillon, C. J., Silver, F. H., & Berg, R. A. (1987). Fibroblast growth on a porous collagen sponge containing hyaluronic acid and fibronectin. *Biomaterials, 8*(3), 195–200.

Duran, A., Cabib, E., & Bowers, B. (1979). Chitin synthetase distribution on the yeast plasma membrane. *Science, 203*(4378), 363–365.

Dzenis, Y. (2004). Spinning continuous fibers for nanotechnology. *Science, 304*(5679), 1917–1919.

Foglia, M. L., Camporotondi, D. E., Alvarez, G. S., Heinemann, S., Hanke, T., Perez, C. J., & Desimone, M. F. (2013). A new method for the preparation of biocompatible silica coated-collagen hydrogels. *Journal of Materials Chemistry B, 1*(45), 6283–6290.

François, J. M. (2007). A simple method for quantitative determination of polysaccharides in fungal cell walls. *Nature Protocols, 1*, 2995.

Fujioka, K., Takada, Y., Sato, S., & Miyata, T. (1995). Novel delivery system for proteins using collagen as a carrier material: The minipellet. *Journal of Controlled Release, 33*(2), 307–315.

Geißel, B., Loiko, V., Klugherz, I., Zhu, Z., Wagener, N., Kurzai, O., & Wagener, J. (2018). Azole-induced cell wall carbohydrate patches kill Aspergillus fumigatus. *Nature Communications, 9*(1), 3098.

Gentleman, E., Lay, A. N., Dickerson, D. A., Nauman, E. A., Livesay, G. A., & Dee, K. C. (2003). Mechanical characterization of collagen fibers and scaffolds for tissue engineering. *Biomaterials, 24*(21), 3805–3813.

Ghodbane, S. A., & Dunn, M. G. (2016). Physical and mechanical properties of cross-linked type I collagen scaffolds derived from bovine, porcine, and ovine tendons. *Journal of Biomedical Materials Research Part A, 104*(11), 2685–2692.

Gordon, P. L., Huang, C., Lord, R. C., & Yannas, I. V. (1974). The far-infrared Spectrum of collagen. *Macromolecules, 7*(6), 954–956.

Halaui, R., Zussman, E., Khalfin, R., Semiat, R., & Cohen, Y. (2017). Polymeric microtubes for water filtration by co-axial electrospinning technique. *Polymers for Advanced Technologies, 28*(5), 570–582.

Han, D., Sherman, S., Filocamo, S., & Steckl, A. J. (2017). Long-term antimicrobial effect of nisin released from electrospun triaxial fiber membranes. *Acta Biomaterialia, 53*, 242–249.

Hsu, S.-h., Whu, S. W., Tsai, C.-L., Wu, Y.-H., Chen, H.-W., & Hsieh, K.-H. (2004). Chitosan as scaffold materials: Effects of molecular weight and degree of deacetylation. *Journal of Polymer Research, 11*(2), 141–147.

HUMFELD, H. (1948). The production of mushroom mycelium in submerged culture. *Science, 107*(2780), 373.

Irimia-Vladu, M. (2014). "Green" electronics: biodegradable and biocompatible materials and devices for sustainable future. *Chemical Society Reviews, 43*(2), 588–610.

Jiang, H., Wang, L., & Zhu, K. (2014). Coaxial electrospinning for encapsulation and controlled release of fragile water-soluble bioactive agents. *Journal of Controlled*

Release, 193, 296–303.
Jin, J., Lee, D., Im, H.-G., Han, Y. C., Jeong, E. G., Rolandi, M., & Bae, B.-S. (2016). Chitin nanofiber transparent paper for flexible green electronics. *Advanced Materials, 28*(26), 5169–5175.
Jorge-Herrero, E., Fernández, P., Turnay, J., Olmo, N., Calero, P., García, R., & Castillo-Olivares, J. L. (1999). Influence of different chemical cross-linking treatments on the properties of bovine pericardium and collagen. *Biomaterials, 20*(6), 539–545.
Kang, X., Kirui, A., Muszyński, A., Widanage, M. C. D., Chen, A., Azadi, P., & Wang, T. (2018). Molecular architecture of fungal cell walls revealed by solid-state NMR. *Nature Communications, 9*(1), 2747.
Khor, E. (1997). Methods for the treatment of collagenous tissues for bioprostheses. *Biomaterials, 18*(2), 95–105.
Kim, J.-K., Kim, D. H., Joo, S. H., Choi, B., Cha, A., Kim, K. M., & Jin, J. (2017). Hierarchical chitin fibers with aligned nanofibrillar architectures: A nonwoven-mat separator for Lithium metal batteries. *ACS Nano, 11*(6), 6114–6121.
Kim, Y.-T., Kim, E.-H., Cheong, C., Williams, D. L., Kim, C.-W., & Lim, S.-T. (2000). Structural characterization of β-d-(1→3, 1→6)-linked glucans using NMR spectroscopy. *Carbohydrate Research, 328*(3), 331–341.
Kirichenko, A. K., Bolshakov, I. N., Ali-Rizal, A. E., & Vlasov, A. A. (2013). Morphological study of burn wound healing with the use of collagen-chitosan wound dressing. *Bulletin of Experimental Biology and Medicine, 154*(5), 692–696.
Kontturi, E., Laaksonen, P., Linder, M. B., Nonappa, Gröschel, A. H., Rojas, O. J., & Ikkala, O. (2018). Advanced Materials through Assembly of Nanocelluloses. *Advanced Materials, 30*(24), 1703779.
Kumar, M. N. V. R., Muzzarelli, R. A. A., Muzzarelli, C., Sashiwa, H., & Domb, A. J. (2004). Chitosan chemistry and pharmaceutical perspectives. *Chemical Reviews, 104*(12), 6017–6084.
Kumar, P. T. S., Lakshmanan, V.-K., Biswas, R., Nair, S. V., & Jayakumar, R. (2012). Synthesis and biological evaluation of chitin Hydrogel/Nano ZnO composite bandage as antibacterial wound dressing. *Journal of Biomedical Nanotechnology, 8*(6), 891–900.
Lee, Y.-C., Chiang, C.-C., Huang, P.-Y., Chung, C.-Y., Huang, T. D., Wang, C.-C., & Reisz, R. R. (2017). Evidence of preserved collagen in an Early Jurassic sauropodomorph dinosaur revealed by synchrotron FTIR microspectroscopy. *Nature Communications, 8*, 14220.
Li, Y., Rodrigues, J., & Tomás, H. (2012). Injectable and biodegradable hydrogels: Gelation, biodegradation and biomedical applications. *Chemical Society Reviews, 41*(6), 2193–2221.
Liang, D., Lu, Z., Yang, H., Gao, J., & Chen, R. (2016). Novel asymmetric wettable AgNPs/Chitosan wound dressing: In vitro and in vivo evaluation. *ACS Applied Materials & Interfaces, 8*(6), 3958–3968.
Liu, Z., Ge, X., Lu, Y., Dong, S., Zhao, Y., & Zeng, M. (2012). Effects of chitosan molecular weight and degree of deacetylation on the properties of gelatine-based films. *Food Hydrocolloids, 26*(1), 311–317.
Logaranjan, K., Raiza, A. J., Gopinath, S. C. B., Chen, Y., & Pandian, K. (2016). Shape- and size-controlled synthesis of silver nanoparticles using Aloe vera plant extract and their antimicrobial activity. *Nanoscale Research Letters, 11*(1), 520.
Marelli, B., Le Nihouannen, D., Hacking, S. A., Tran, S., Li, J., Murshed, M., & Barralet, J. E. (2015). Newly identified interfibrillar collagen crosslinking suppresses cell proliferation and remodelling. *Biomaterials, 54*(0), 126–135.
Marinucci, L., Lilli, C., Guerra, M., Belcastro, S., Becchetti, E., Stabellini, G., & Locci, P. (2003). Biocompatibility of collagen membranes crosslinked with glutaraldehyde or diphenylphosphoryl azide: An in vitro study. *Journal of Biomedical Materials Research Part A, 67A*(2), 504–509.
Marone, P. A., Lau, F. C., Gupta, R. C., Bagchi, M., & Bagchi, D. (2010). Safety and toxicological evaluation of undenatured type II collagen. *Toxicology Mechanisms and Methods, 20*(4), 175–189.
Merrett, K., Liu, W., Mitra, D., Camm, K. D., McLaughlin, C. R., Liu, Y., & Fogg, D. E. (2009). Synthetic neoglycopolymer-recombinant human collagen hybrids as biomimetic crosslinking agents in corneal tissue engineering. *Biomaterials, 30*(29), 5403–5408.
Mijatović, S., Bramanti, A., Nicoletti, F., Fagone, P., Kaluđerović, G. N., & Maksimović-Ivanić, D. (2018). Naturally occurring compounds in differentiation based therapy of cancer. *Biotechnology Advances, 36*(6), 1622–1632.
Mohammadi, A., Shojaosadati, S. A., Tehrani, H. J., Mousavi, S. M., Saleh, T., & Khorasani, A. C. (2018). Schizophyllan production by newly isolated fungus Schizophyllum commune IBRC-M 30213: Optimization of culture medium using response surface methodology. *Annals of Microbiology, 68*(1), 47–62.
Nakashima, K., Kimura, S., Ogawa, Y., Watanabe, S., Soma, S., Kaneko, T., & Satoh, N. (2018). Chitin-based barrier immunity and its loss predated mucus-colonization by indigenous gut microbiota. *Nature Communications, 9*(1), 3402.
Osborne, C. S., Reid, W. H., & Grant, M. H. (1999). Investigation into the biological stability of collagen/chondroitin-6-sulphate gels and their contraction by fibroblasts and keratinocytes: The effect of crosslinking agents and diamines. *Biomaterials, 20*(3), 283–290.
Paichit, I., Atchariya, F., Anan, O., Anuphan, S., & Jarupa, V. (2012). Effects of the blended fibroin/aloe gel film on wound healing in streptozotocin-induced diabetic rats. *Biomedical Materials, 7*(3), 035008.
Peppas, N. A., Hilt, J. Z., Khademhosseini, A., & Langer, R. (2006). Hydrogels in biology and medicine: From molecular principles to bionanotechnology. *Advanced Materials, 18*(11), 1345–1360.
Qi, C., Lin, J., Fu, L.-H., & Huang, P. (2018). Calcium-based biomaterials for diagnosis, treatment, and theranostics. *Chemical Society Reviews, 47*(2), 357–403.
Rahman, S., Carter, P., & Bhattarai, N. (2017). Aloe Vera for tissue engineering applications. *Journal of Functional Biomaterials, 8*(1), 6.
Rajan, N., Habermehl, J., Coté, M.-F., Doillon, C. J., & Mantovani, D. (2007). Preparation of ready-to-use, storable and reconstituted type I collagen from rat tail tendon for tissue engineering applications. *Nature Protocols, 1*, 2753.
Rezaii, M., Oryan, S., & Javeri, A. (2019). Curcumin nanoparticles incorporated collagen-chitosan scaffold promotes cutaneous wound healing through regulation of TGF-β1/Smad7 gene expression. *Materials Science and Engineering C, 98*, 347–357.
Roca, C., Chagas, B., Farinha, I., Freitas, F., Mafra, L., Aguiar, F., & Reis, M. A. M. (2012). Production of yeast chitin–glucan complex from biodiesel industry byproduct. *Process Biochemistry, 47*(11), 1670–1675.
Ruiz-Herrera, J., & Bartnicki-Garcia, S. (1974). Synthesis of Cell Wall Microfibrils in vitro by a "Soluble" Chitin Synthetase from Mucor rouxii. *Science, 186*(4161), 357–359.
Saito, M., & Marumo, K. (2010). Collagen cross-links as a determinant of bone quality: A possible explanation for bone fragility in aging, osteoporosis, and diabetes mellitus. *Osteoporosis International, 21*(2), 195–214.
Silva, S. S., Popa, E. G., Gomes, M. E., Cerqueira, M., Marques, A. P., Caridade, S. G., & Reis, R. L. (2013). An investigation of the potential application of chitosan/aloe-based membranes for regenerative medicine. *Acta Biomaterialia, 9*(6), 6790–6797.
Skorik, Y. A., Pestov, A. V., & Yatluk, Y. G. (2010). Evaluation of various chitin-glucan derivatives from Aspergillus niger as transition metal adsorbents. *Bioresource Technology, 101*(6), 1769–1775.
Spěváček, J., & Brus, J. (2008). Solid-state NMR studies of polysaccharide systems. *Macromolecular Symposia, 265*(1), 69–76.
Sung, H.-W., Hsu, H.-L., Shih, C.-C., & Lin, D.-S. (1996). Cross-linking characteristics of biological tissues fixed with monofunctional or multifunctional epoxy compounds. *Biomaterials, 17*(14), 1405–1410.
Sung, K. H., Josewski, J., Dübel, S., Blankenfeldt, W., & Rau, U. (2018). Structural insights into antigen recognition of an anti-β-(1,6)-β-(1,3)-D-glucan antibody. *Scientific Reports, 8*(1), 13652.
Surjushe, A., Vasani, R., & Saple, D. G. (2008). Aloe Vera: A Short Review. *Indian Journal of Dermatology, 53*(4), 163–166.
Sylvester, M. F., Yannas, I. V., Salzman, E. W., & Forbes, M. J. (1989). Collagen banded fibril structure and the collagen-platelet reaction. *Thrombosis Research, 55*(1), 135–148.
Tamate, R., Hashimoto, K., Horii, T., Hirasawa, M., Li, X., Shibayama, M., & Watanabe, M. (2018). Self-healing micellar ion gels based on multiple hydrogen bonding. *Advanced Materials, 30*(36), 1802792.
Tishchenko, G., Šimůnek, J., Brus, J., Netopilík, M., Pekárek, M., Walterová, Z., & Lenfeld, J. (2011). Low-molecular-weight chitosans: Preparation and characterization. *Carbohydrate Polymers, 86*(2), 1077–1081.
Udhayakumar, S., Shankar, K. G., Sowndarya, S., Venkatesh, S., Muralidharan, C., & Rose, C. (2017). l-Arginine intercedes bio-crosslinking of a collagen–Chitosan 3D-hybrid scaffold for tissue engineering and regeneration: In silico, in vitro, and in vivo studies. *RSC Advances, 7*(40), 25070–25088.
van der Linde, S., Suz, L. M., Orme, C. D. L., Cox, F., Andreae, H., Asi, E., & Bidartondo, M. I. (2018). Environment and host as large-scale controls of ectomycorrhizal fungi. *Nature, 558*(7709), 243–248.
Wenling, C., Duohui, J., Jiamou, L., Gong, Y., Nanming, Z., & Zhang, X. (2005). Effects of the degree of deacetylation on the physicochemical properties and schwann cell affinity of chitosan films. *Journal of Biomaterials Applications, 20*, 157–177.
Wu, S., Applewhite, A. J., Niezgoda, J., Snyder, R., Shah, J., Cullen, B., & Treadwell, T. (2017). Oxidized regenerated Cellulose/Collagen dressings: Review of evidence and recommendations. *Advances in Skin & Wound Care, 30*(11S Suppl. 1), S1–S18.
Yannas, I. V., Burke, J. F., Gordon, P. L., Huang, C., & Rubenstein, R. H. (1980). Design of an artificial skin. II. Control of chemical composition. *Journal of Biomedical Materials Research, 14*(2), 107–132.
Yao, C., Markowicz, M., Pallua, N., Magnus Noah, E., & Steffens, G. (2008). The effect of cross-linking of collagen matrices on their angiogenic capability. *Biomaterials, 29*(1), 66–74.
Yin, L., Wang, K., Lv, X., Sun, R., Yang, S., Yang, Y., & Yu, Z. (2017). The fabrication of an ICA-SF/PLCL nanofibrous membrane by coaxial electrospinning and its effect on bone regeneration in vitro and in vivo. *Scientific Reports, 7*(1), 8616.
Yoon, J., Yang, H.-S., Lee, B.-S., & Yu, W.-R. (2019). Recent Progress in Coaxial Electrospinning: New Parameters, Various Structures, and Wide Applications. *Advanced Materials, 0*(0), 1704765.
You, C., Li, Q., Wang, X., Wu, P., Ho, J. K., Jin, R., & Han, C. (2017). Silver nanoparticle loaded collagen/chitosan scaffolds promote wound healing via regulating fibroblast migration and macrophage activation. *Scientific Reports, 7*(1), 10489.
Yunoki, S., Suzuki, T., & Takai, M. (2003). Stabilization of low denaturation temperature collagen from fish by physical cross-linking methods. *Journal of Bioscience and Bioengineering, 96*(6), 575–577.
Zhao, X., Guo, B., Wu, H., Liang, Y., & Ma, P. X. (2018). Injectable antibacterial conductive nanocomposite cryogels with rapid shape recovery for noncompressible hemorrhage and wound healing. *Nature Communications, 9*(1), 2784.

Science of the Total Environment 745 (2020) 140975

Contents lists available at ScienceDirect

Science of the Total Environment

journal homepage: www.elsevier.com/locate/scitotenv

Review

A critical review of the overlooked challenge of determining micro-bioplastics in soil

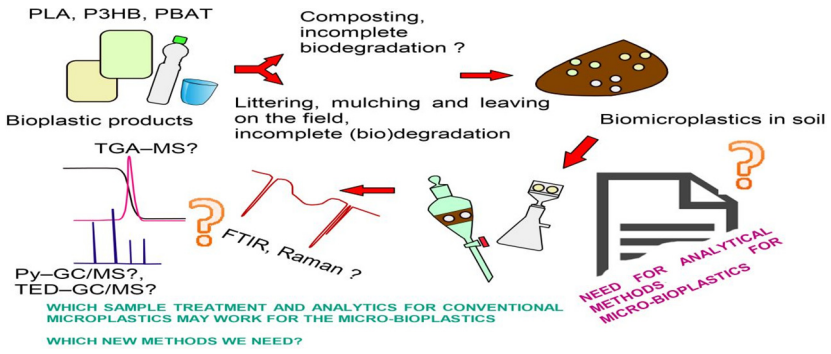
Jakub Fojt [a], Jan David [b], Radek Přikryl [c], Veronika Řezáčová [a], Jiří Kučerík [a,*]

[a] Institute of Chemistry and Technology of Environmental Protection, Faculty of Chemistry, Brno University of Technology, Purkyňova 118, 612 00 Brno, Czech Republic
[b] iES Landau, Institute for Environmental Sciences, Group of Environmental and Soil Chemistry, University of Koblenz–Landau, Fortstraße 7, 76829 Landau, Germany
[c] Institute of Material Science, Faculty of Chemistry, Brno University of Technology, Purkyňova 118, 612 00 Brno, Czech Republic

HIGHLIGHTS

- Biodegradable plastics may turn into micro-bioplastics with unknown life-time.
- There are no extraction and analytical techniques for micro-bioplastics in soil.
- Methods of micro-bioplastics analysis are inspired by conventional microplastics.
- Pyrolysis is among the most promising approaches for micro-bioplastics analysis.

GRAPHICAL ABSTRACT



ARTICLE INFO

Article history:
Received 14 April 2020
Received in revised form 12 July 2020
Accepted 12 July 2020
Available online 18 July 2020

Editor: Thomas Kevin V

Keywords:
Micro-bioplastics
PLA
PHB
PBAT
Biodegradation
Analysis

ABSTRACT

Currently, non-biodegradable oil-based plastics are gradually being replaced by bio-based biodegradable plastics to prevent the formation of microplastics. For biodegradable materials to decompose completely, however, they require specific conditions that are rarely met in ecosystems. Paradoxically, this may lead to the fast production of microplastics from biodegradable materials, i.e. micro-bioplastics. Until recently, the scientific focus has been solely on the estimation of conventional microplastics. As a result, there is a lack of analytical methods for determining the amount of micro-bioplastics in soil. In this review, we address this problem by summarising sample pre-treatments and analytical techniques suitable for the determination of conventional microplastics, which serve as inspiration for the determination of micro-bioplastics from polyhydroxybutyrates, polylactic acid and polybutylene adipate terephthalate in soil. The analytical techniques include both pyrolysis-based techniques, i.e. thermoanalytical and non-thermoanalytical approaches including sample pre-separation and respective detection limits. We conclude that due to the incomplete knowledge of the production rate of micro-bioplastics, fate, sorption properties and toxicity, it is necessary to develop and validate a rapid and suitable method for their determination. Indeed, the use of thermoanalytical approaches seems to be the most promising strategy. Furthermore, we suggest how the development and analysis of micro-bioplastics should be addressed in future research.

© 2020 Elsevier B.V. All rights reserved.

* Corresponding author.
E-mail address: kucerik@fch.vut.cz (J. Kučerík).

https://doi.org/10.1016/j.scitotenv.2020.140975
0048-9697/© 2020 Elsevier B.V. All rights reserved.

Contents

1. Introduction . . . 2
   1.1. Biodegradation and biodegradation tests . . . 3
   1.2. Biodegradable polymers used in agriculture . . . 4
2. Methods . . . 5
3. Determination of conventional microplastics . . . 5
   3.1. Extraction and purification . . . 5
   3.2. Qualitative and semi-quantitative determination of conventional microplastics . . . 5
   3.3. Quantitative determination of conventional microplastics . . . 6
4. Determination of P3HB, PLA and PBAT in various matrices . . . 6
   4.1. P3HB . . . 6
   4.2. PLA . . . 7
   4.3. PBAT . . . 8
5. Directions for future studies . . . 8
6. Conclusions . . . 9

Declaration of competing interest . . . 9
Acknowledgement . . . 9
References . . . 9

1. Introduction

In 2016, 335 million tons of plastic materials were produced worldwide (PlasticsEurope, 2017). This was mainly due to their resistance to corrosive chemicals, hydrolysis, microorganisms, heat and light; their low density; and their useful mechanical properties (Bagheri et al., 2017). Some of these advantages can turn into disadvantages in terms of processing waste and environmental pollution, however. For example, only 9% of all plastics produced in the last 65 years was recycled, while 12% was incinerated in waste incinerators and the remaining 79% was landfilled, i.e. stored in the environment (Geyer et al., 2017). Current studies estimate that five trillion pieces of plastics with a total mass of 250 million tons are floating in oceans across the world and that an additional eight million tons are added each year (Andrady, 2011; Guo and Wang, 2019).

Concentrations of microplastics in soil are more difficult to estimate because of complications caused by a multitude of soil biotic and abiotic processes, the interaction of particles with various components of soil, strong matrix effects and challenging extraction methods. A limited number of studies have focused on the determination of soil microplastic concentrations (Rillig, 2012), however, some estimates suggest that microplastic concentrations in terrestrial ecosystems could be 4–23 times higher than in aquatic ecosystems (de Souza Machado et al., 2018). Several authors have estimated that the microplastic content in soils can reach from $5.5 \cdot 10^{-3}$ wt% in protected Swiss floodplain soils (Scheurer and Bigalke, 2018) to 6.7 wt% in Australian urban/industrial area soils (Fuller and Gautam, 2016).

Conventional (oil-based) plastics are supposed to degrade very slowly in environmental conditions (Ward et al., 2019), and their gradual decomposition leads to the formation of mesoplastics (longest dimension 1 to 10 mm), microplastics (1 to 1000 μm) and nanoplastics (1 to 1000 nm) (Hartmann et al., 2018). In general, microplastics are categorised as either primary or secondary (Wong et al., 2020). Primary microplastics are made intentionally and used in cosmetics, cleaning products and abrasive mixtures, whereas secondary microplastics are formed by abrasion or disintegration of larger plastic objects or particles (Laskar and Kumar, 2019).

Once microplastics enter the soil, they become part of complex soil organic matter and mineral substituents, which further increases its persistence (Bläsing and Amelung, 2018). As a result, the particles accumulate in all ecosystems, raising concerns about their negative side effects (Thompson, 2004). The particles are dangerous because of their ability to adsorb and concentrate hazardous chemicals from water, such as pharmaceuticals or pesticides, and thereby serve as carriers of these compounds to organisms (Guo et al., 2019). When reaching certain concentrations, microplastics in aquatic ecosystems can cause chronic reproductive toxicity in microorganisms, higher mortality, food intake problems, endocrine disruption and oxidative stress; immune and nervous system disorders have also been observed (Jaikumar et al., 2019; Bosker et al., 2019; Lu et al., 2016). In general, as the radius of the particles decreases, their active surface increases, which can be assumed to cause greater biological activity and adsorption capacity of nanoplastics. Plastic nanoparticles can also penetrate the cell wall, thereby transporting the adsorbed substances directly to the cells (Ferreira et al., 2019). Information regarding the difference between conventional and biodegradable microplastics is very limited, however, some studies have shown that biodegradable microplastics are better sorbents (Gong et al., 2019; Zuo et al., 2019) and affect natural environments (Green et al., 2016; Chen et al., 2020).

In January 2018, the European Commission responded to the problems of recycling and disposing of plastics by confirming its continued promotion of recycling and identifying the possible benefits and risks of using biodegradable plastics (Haider et al., 2018). Bioplastics are defined according to the source of their material or how long they take

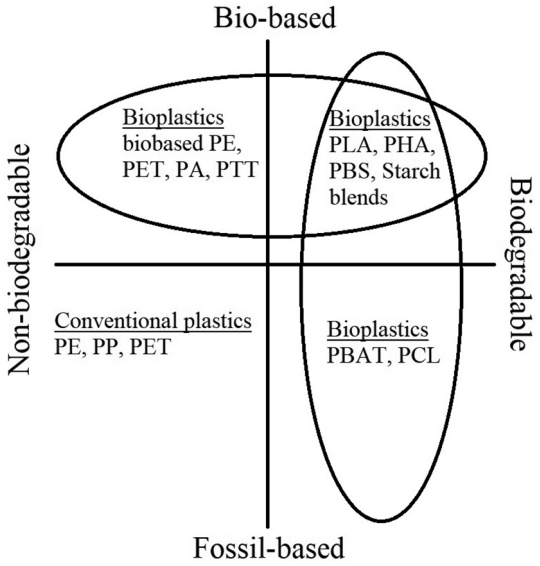


Fig. 1. Types of bioplastics and some examples (Ashter, 2016).

to biodegrade, for example, bioplastics made from plants or animals are called biobased bioplastics. However, not all biobased bioplastics are biodegradable and not all biodegradable plastics are biobased (Ashter, 2016) (see Fig. 1). The biodegradable bioplastics are supposed to undergo significant microbial biodegradation in a short period of time (according to biodegradation standards this should be 180 days) under favourable conditions (temperature, pH, humidity, etc.). The decomposition of these plastics is accompanied by the formation of water, methane and/or CO_2 and biomass. In this review, we focus on problems with the determination of biodegradable bioplastics.

One of the first disciplines to use bioplastics was medicine, which has used biodegradable plastics since the late 1980s as a specific active substance carrier, a replacement for human tissues and as surgical implants (Van de Velde and Kiekens, 2002). More recently, bioplastics have also gained great popularity in 3D printing (Ferreira et al., 2017). As materials, biodegradable plastics are promising alternatives to conventional, mostly non-biodegradable, plastics (Haider et al., 2018). This has led to them being used for food packaging, mulch films, geotextiles, waste bags, cosmetics and clothing (Van de Velde and Kiekens, 2002). In 2017, 2.05 million tons of biobased plastics were produced worldwide, of which 43.2% were biodegradable namely bioplastics (polybutylene adipate terephthalate (PBAT), polybutylene succinate (PBS), polylactic acid (PLA), polyhydroxybutyrates (PHA), starch-, pectin-, chitosan-based blends/composites (Bertolino et al., 2020; Cavallaro et al., 2019) and other biodegradable bioplastics) (Fig. 2). By 2022, this is expected to increase to 2.44 million tons (Agnihotri et al., 2019).

The complete biodegradation of bioplastics occurs only under very specific conditions, the most important being suitable temperature and pH, optimum humidity, a rich environment for microorganisms and sufficient nutrients (Bastioli, 2005). The most suitable environments for biodegradation are therefore compost (temperature, fungi, bacteria) > soil (fungi, bacteria) > freshwater (bacteria) > marine water (dilute bacteria). In fact, only industrial compost meets the optimal and controllable conditions for biodegradation, and in natural ecosystems, biodegradation conditions are often not feasible, leading to a significant slowdown in biodegradation. One of the first and most important steps of degradation is biofragmentation, which is dependent on the type and number of enzymes. Enzymes are produced intracellularly, and relatively specific conditions are required for their excretion.

Paradoxically, if the conditions are not met, microplastics are produced much faster in the case of biodegradable plastics than in conventional oil-based plastics (Sintim et al., 2019). Multiple biodegradation studies have been conducted and only a few achieved complete biodegradation (Emadian et al., 2017). Therefore, it is very likely that most of the unbiodegraded material is fragmented into microplastics or nanoplastics. As there are no analytical techniques for their determination, the presence of PHB biomicroplastics can only be proven by microscopy (Shruti and Kutralam-Muniasamy, 2019), and unlike conventional plastics (Rillig, 2012), the fate of these microplastics (Bläsing and Amelung, 2018) is not studied or discussed in any way.

With growing production and use of bioplastics, this topic clearly needs to be studied further. The first step in deciding the presence and impact of microplastics in the environment is their unambiguous identification and quantification. Although there are currently no analytical methods for the determination of biodegradable microplastics in water, soil or compost (Crawford and Quinn, 2017), it is possible to be inspired, at least methodically, by the research dealing with the analysis of conventional microplastics.

In this review, we focus on three types of biodegradable bioplastics: PBAT, PLA and PHB. PLA and PBAT were selected due their wide use and the controversy regarding their biodegradability and compostability (Tsuji and Suzuyoshi, 2002; Karamanlioglu et al., 2017; Tabasi and Ajji, 2015), while PHB was chosen due its promising potential as food-waste material (Obruca et al., 2010). The number of papers related to selected bioplastics is steadily increasing (Fig. 3). This review does not deal with bioplastics from starch and modified starches (even though they represent about 20% of all bioplastics) because PHB, PBAT and PLA represent bioplastics with a higher potential for microplastics formation according to their life-cycle assessment results as they can be made from waste and their production does not compete with food.

1.1. Biodegradation and biodegradation tests

The International Union for Pure and Applied Chemistry defines biodegradable polymers as polymers 'that are susceptible to degradation by biological activity, with the degradation accompanied by a lowering of its mass' (Vert et al., 2012). As this definition can refer to both water-soluble and biodegradable polymers, however, some other organisations also require the complete mineralisation of the plastics to carbon dioxide, water and biomass when defining biodegradable plastics (CEN/TR 15351:2006) (Haider et al., 2018; Horie et al., 2004). This extra definition has also been adopted by various national and international organisations, such as the International Organisation for Standardisation, to standardise biodegradability tests in fresh water, seawater, soil and compost, such as EN ISO 14851:1999, EN ISO 17556, ASTM D 5338 or ASTM D 6400.

Biodegradation has four stages. The first stage is biodeterioration, where the surface of the material is covered with a biofilm that causes fragmentation into smaller particles. During the second stage, the debris

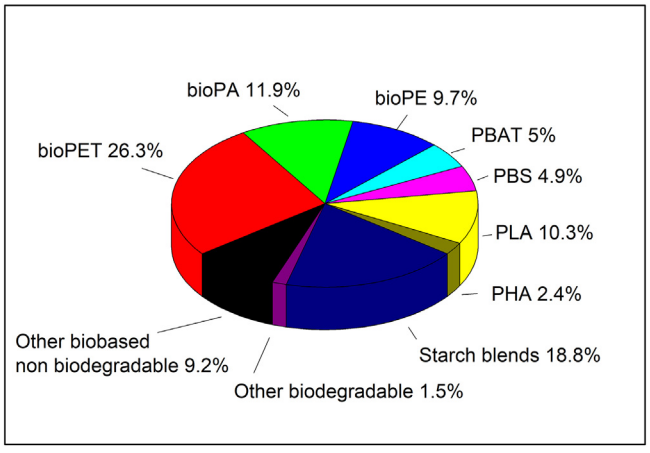


Fig. 2. Worldwide production of biobased plastics in 2017. Modified from Agnihotri et al. (2019).

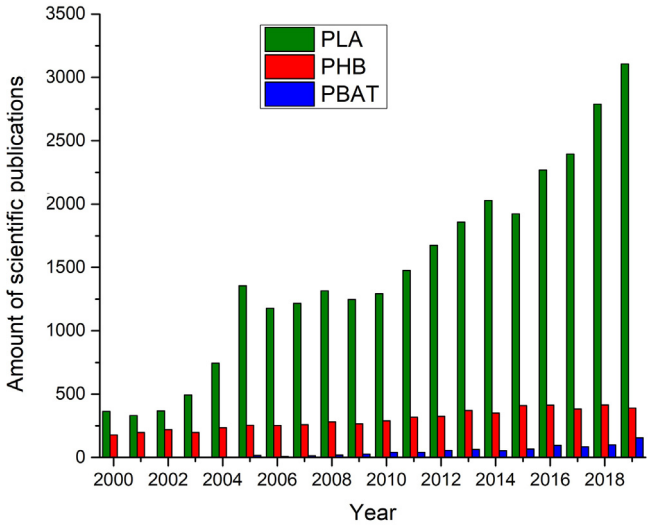


Fig. 3. The number of works related to P3BH, PLA and PBAT from 2000 to 2019.

is depolymerised by extracellular enzymes from microorganisms in the biofilm. In the third stage, the resulting small molecules are transported into the cells of the microorganism, which is called bio-assimilation. Then, in the final stage, mineralisation occurs, producing water, nitrogen and carbon dioxide for aerobic biodegradation and methane for anaerobic biodegradation (Bagheri et al., 2017; Haider et al., 2018).

The simplest way to measure biodegradation is by observing the sample mass loss during the biodegradation test (Chinaglia et al., 2018). This experiment is only suitable for larger pieces of plastics or foils, which means that as these pieces break down into smaller particles, inaccurate results are obtained (Emadian et al., 2017). For this reason, more advanced methods have been developed. For example, tests for aerobic biodegradation are based on the measurement of microbial oxygen consumption (biological oxygen demand), released carbon dioxide or total organic carbon (Emadian et al., 2017; Harrison et al., 2018). In contrast, tests for anaerobic degradation are based on the measurement of methane production (Ryan et al., 2017; Bátori et al., 2018). As a rule, these experiments are conducted under controlled conditions in artificial or well-defined natural test media.

The biodegradability of polymer products should be guaranteed, when a polymer obtains a certificate, e.g. "Vincotte OK biodegradable". The certification is based on a series of tests of biodegradation, disintegration and ecotoxicological safety (Harrison et al., 2018). Nonetheless, these tests do not include seasonal variations or extent of polymer degradation. In addition, the testing environments tend to be defined for a specific purpose. For this reason, aerobic and anaerobic biodegradation in wastewater, freshwater ecosystems and marine ecosystems are tested separately. Distortion of results may also occur due to different approaches to inoculum, insufficient reproducibility of results and a lack of ways to test in uncontrolled environments (Harrison et al., 2018). As a result, the rate of biodegradation is highly dependent on various parameters and also certified materials may not be biodegradable an open environment (Harrison et al., 2018). Indeed, under unfavourable conditions, the biodegradation of bioplastics can take several decades to produce microplastics similar to conventional plastics (Bagheri et al., 2017; Harrison et al., 2018).

1.2. Biodegradable polymers used in agriculture

Plastic mulching has become a global agricultural practice, therefore, the risk of plastic residue remaining in the soil and likely breaking down into microplastics is enhanced in agricultural soils (Steinmetz et al., 2016). 'Plasticulture', as it is known, includes films, foils, nonwoven fabrics for mulching, rods and tubes for tunnel structures, anti-hail and shading nets, seedling pots, stings and clips for tying plants and biodegradable seed covers and discs. About 60% of crops would not thrive without the use of plasticulture and because of this, 1 ha of agricultural soil may leave 80–200 kg of plastics after one season (Siwek et al., 2019). The benefits of mulch use include soil humidity reduction and water retention, which reduces the potential development of fungal diseases as well as lowering the potential of hypoxia in plant roots (Siwek et al., 2019).

Concerns about plastic waste in agriculture have broadened the focus of plasticulture to include biodegradable plastic mulching, which is now gaining popularity. As a result, the current trend is to replace conventional plastics with biodegradable plastics in agriculture (Shruti and Kutralam-Muniasamy, 2019). The latter's biodegradability is rarely 100%, however (Kasirajan and Ngouajio, 2012) (or such biodegradability success is simply uncertain, often due to seasonal changes in temperature and humidity), and they are suspected of contributing to the microplastic issue, especially as they can exhibit the same or similar issues as conventional microplastics (ecotoxicological effects, sorption of persistent contaminants, etc.). Therefore, the possibility of biodegradable plastics forming microplastics in agricultural fields and the environment is presumed (Sintim et al., 2019).

PLA, PHB and PBAT are among the biodegradable materials used in plasticulture. PHB consists of biodegradable and biocompatible polymers that are synthesised by bacteria as energy storage polymers (Obruca et al., 2014; Obruca et al., 2010). PHB can be completely biodegraded in all ecosystems, however, through industrial composting may be biodegraded only up to 78% (Hermann et al., 2011). The most common representative of PHB is poly-3-hydroxybutyrate (P3HB), which is produced by gram-negative and gram-positive bacteria (*Pseudomonas sp.*, *Bacillus sp.*, *Methylobacterium sp.*) under nutrient-deficient stress conditions (Ansari et al., 2016). P3HB is a hydrophobic material that exhibits increased crystallinity, a high melting point and high fragility, which complicates its processing and limits its potential use on an industrial scale (Obruca et al., 2014).

The mechanical properties of P3HB can be improved by adding other polymers (e.g. polylactic acid) to form copolymers (with 3-hydroxyvaleric acid) or by adding plasticisers (Ansari et al., 2016; Obruca et al., 2014). As these additives can significantly slow down the biodegradation of the final product (Bagheri et al., 2017), biodegradation enhancers such as starch are added to these blends. Another factor that makes it difficult to use PHB is its economic demands on production, but cost reduction can be achieved by producing P3HB from waste materials. A very good source of carbon for P3HB synthesising bacteria is rapeseed oil, which also has a high yield. Therefore, in theory, more than 1 g of PHA can be obtained per gram of oil (Obruca et al., 2010). Other promising waste materials include products from the sugar industry and hydrolysate coffee grounds (Obruca et al., 2014).

The second biodegradable polymer of interest is PBAT. PBAT is susceptible to biodegradation via aerobic bacteria and fungi and is suitable for industrial and home composting. According to various studies, the extent of its biodegradation can reach values between 65 and 90 wt% of C degradation depending on the industrial composting conditions. Its largest producer is the Germany-based company BASF (about 75 kt *p.a.*), which trades under the names Ecoflex® and Ecovio® and produces it as a blend with polylactic acid (PLA). PBAT is a synthetic polyester copolymer produced by melting polycondensation from 1,4-butanediol and adipic acid, employing tetrabutoxytitanium as the transesterification catalyst (Zhao et al., 2010; Koltzenburg et al., 2014).

PBAT is claimed to be non-toxic and non-ecotoxic and is industrially compostable in several weeks (n.d.) according to EN 13432 or ASTM 6400 (Siegenthaler et al., 2012). It can also be blended with starches (Shi et al., 2011) and PHAs (Hutníková and Fričová, 2016). It is used for the production of shopping bags, mulching foils for tillage into the soil and various horticulture products such as seed/fertilizer tapes, plant pots and erosion control nets (Siegenthaler et al., 2012) Therefore, there is potential for PBAT particles to be present in soil. Foils can also be blended with PBAT and nitrile rubber for increased toughness (Fernandes et al., 2017), which may put micro rubber particles into the soil. In terms of the medical field, the use of PBAT is very rare and is not predicted to increase.

Another widely used biodegradable polymer is polylactic acid (PLA), which is a biobased aliphatic polyester. It can be biodegraded under aerobic as well as anaerobic conditions by both bacteria and fungi (C degradation between 55 and 95%), but not generally through home composting. In contrast to biodegradation in organisms, non-enzymatic degradation of this biopolymer occurs in the environment (Shimao, 2001). As PLA can be absorbed by human and animal bodies, its use in medical implants is significantly increasing, and it is also very popular in 3D printing (Ferreira et al., 2017; Ezeh and Susmel, 2018). Due to the ease of processing it and its general yield strength and low gas permeability compared to other polymers (biodegradable as well as oil-based), much attention has been paid to this material in the past 20 years (Hamad et al., 2018).

Despite the advantages of PLA, however, it is almost always possible to find better and cheaper oil-based plastics. The price for PLA

pellets currently starts at $500 per tonne (Fahim et al., 2019), but costs can be reduced by adding cheaper biomass-based additives or other agricultural products, such as sawdust or starches. This not only reduces production costs but also speeds up the biodegradation of this plastic material, which otherwise biodegrades very slowly (Wan et al., 2019). Adding some of these materials to PLA is not always in line with sustainable development goals, however, as there may be competition for land as a systemic resource for agricultural food production (Karan et al., 2019).

2. Methods

We performed a literature search on Clarivate Analytics, Web of Science and Google Scholar that focused on the three biodegradable polymers most likely to be used for agriculture (P3HB, PLA, PBAT and their blends), as well as their utilisation, biodegradability and the possible analytical methods leading to their determination in various substrates, possibly in a soil matrix. We did not filter by publication date, and both the abbreviations and complete names of the polymers were searched together with the terms 'microplastics', 'analysis', 'determination', 'assay' and 'characterization'. To obtain an overview of any existing analytical techniques for these polymers, we also included some characterisation methods that are connected to the biopolymers' technology, production and material analysis. The material characterisation and biotechnological analysis were highly specified, however. For comparison, we reviewed analytical methods that have been used in the determination of microplastics from conventional polymers.

3. Determination of conventional microplastics

Man-made microplastics have been introduced into all parts of the environment, including animals (He et al., 2018; Rainieri and Barranco, 2019; Sun et al., 2019; Prata et al., 2019), and due to their harmful effects on living organisms (Jaikumar et al., 2019), quantitative and qualitative methods for their determination are being developed (Guo et al., 2019; Bosker et al., 2019; Elert et al., 2017). This makes it possible to assess the degree of primary and secondary microplastic contamination in different sites and the ability of sewage treatment plants to retain microplastics (Sun et al., 2019).

3.1. Extraction and purification

The matrix containing microplastics often consists of organic and inorganic mixtures (He et al., 2018). The easiest and cheapest way to remove larger particles from the sample is by sieving (He et al., 2018; Sun et al., 2019; Bläsing and Amelung, 2018). If the sample contains excess water, it can be removed by drying, filtration or evaporation. It is also possible to utilise different densities from the rest of the matrix and use density fractionation to separate the microplastics from the sample. Salt solutions are used for this purpose (NaCl, $CaCl_2$, $ZnCl_2$, NaI) (He et al., 2018; Sun et al., 2019; Silva et al., 2018). For the extraction of low-density plastics such as polyethylene (PE) and polypropylene (PP), only distilled water may be used in combination with sonication (Zhang et al., 2018).

Liu et al. (2018) used a saturated solution of NaCl with a density of 1.19 $g \cdot cm^{-3}$ to extract higher density plastics (such as polyethersulfone [PES]), whereas for the extraction of polyvinyl chloride (PVC) and polyethylene terephthalate (PET), Scheurer and Bigalke (2018) used a saturated solution of $CaCl_2$. Due to its higher density, this latter method also has greater efficiency. The disadvantage of this method is the interaction of calcium ions with the organic soil component, resulting in aggregates that complicate further analysis. Imhof et al. (2012) and Liebezeit and Dubaish (2012) developed a separation method for extraction using a zinc chloride solution with a density of 1.6 to 1.7 $g \cdot cm^{-3}$, while Dekiff et al. (2014) and Van Cauwenberghe et al. (2013) used a solution of NaI with a density of up to 1.8 $g \cdot cm^{-3}$ for extraction. The use of NaI and $ZnCl_2$ solutions are very effective due to their high densities, but they are more expensive, generate waste and are more dangerous than using NaCl or $CaCl_2$.

Organic compounds in the sample that could adversely affect the assay can be removed by decomposition (He et al., 2018). As conventional plastics are mostly resistant to an aggressive chemical environment, strong oxidising agents, bases and acids can be used to decompose the organic component of the sample. Indeed, decomposition by catalytic wet oxidation is very common (He et al., 2018; Sun et al., 2019; Silva et al., 2018). Hydrogen peroxide, sodium hypochlorite and Fenton's reagent or solutions of alkaline hydroxides and strong acids are mostly used for this method (Sun et al., 2019; Hurley et al., 2018). This type of degradation is not suitable for a bulk sample, however, as the entire process would take too long. The use of concentrated nitric acid is also not suitable for pH-sensitive plastics such as polystyrene (PS) or nylon (Erni-Cassola et al., 2017).

Hydrogen peroxide decomposition uses a 30% solution of peroxide, but the method is very slow and takes up to seven days to complete. By using Fenton's reagent instead of hydrogen peroxide, the degradation time can be shortened significantly (to 10 min or less) without destroying the microplastics in the sample (Tagg et al., 2017). A mixture of technical enzymes, such as lipases, amylases, proteinases, chitinases and cellulases, can also be used for decomposition (Sun et al., 2019; Silva et al., 2018). Cole et al. (2015) used the enzyme Proteinase-K for this purpose, achieving decomposition higher than 97% (for comparison, 72.1 ± 9.2% decomposition was achieved with the 2 M HCl and 91.3 ± 0.4% was achieved with 10 M NaOH at 60 °C). Meanwhile, Löder et al. (2017) developed a multistep decomposition method combining multiple enzymes (protease, chitinase, cellulase), a surfactant (sodium dodecyl sulfate) and hydrogen peroxide with an efficiency of 98.3 ± 0.1%.

3.2. Qualitative and semi-quantitative determination of conventional microplastics

Qualitative methods for the determination of microplastics can distinguish them from the matrix and other particles (e.g. cellulose, sand and glass) and identify the type of polymer, whereas semi-quantitative methods can determine, for example, the number of microplastics particles per volume or matrix weight or the proportion of microplastic areas occupied by a microscopic substrate. The most commonly used method is visual identification by microscope, which is a quick and simple process that makes it possible to determine the shape, texture and surface type of a particle. Particles smaller than 100 μm cannot be identified in this way, however (Song et al., 2015; Shim et al., 2017). Furthermore, this method may result in the false-positive identification of microplastics or vice versa as they may not be distinguishable from other matrix components (He et al., 2018; Silva et al., 2018).

It is also possible to make a mistake in particle counting when using a Petri dish divided into sectors (Carr et al., 2016). To confirm the composition of the microplastics and its differentiation from other particles, this method must be combined with Fourier transform infrared (FTIR) or Raman spectroscopy. For example, using FTIR Browne et al. (2011) identified polyamides, PES, PE, PP and PVC microplastics in effluent from sewage treatment plants, marine sediments and water from washing machines. Lares et al. (2018) used FTIR and Raman microscopy and identified PES, PE, PA and PP microplastic particles and fibres in sewage sludge and lake water. Further refinement of matrix analyses can be achieved using an electron microscope.

FTIR should be used for the qualitative determination of microplastics larger than 10 μm and Raman spectroscopy can be used to characterise particles larger than 1 μm. Polymers sensitive to photodegradation, such as PVC, are harder to determine using this method, however. Instead, PVC particles can be identified by means of attenuated total reflectance (ATR)–FTIR (Käppler et al., 2018). FTIR

and Raman spectroscopy are complementary and should be selected according to the structure of the microplastics expected in the sample. The FTIR method is used to determine microplastics with a structure where the vibrations of atoms in a molecule change its dipole moment, while Raman spectroscopy can determine microplastics with a structure of molecules where the vibrations of atoms change their polarizability (He et al., 2018).

For quicker determination of microplastics in German sediments, Primpke et al. (2017) used automatised focal-plane-array FTIR microscopy, where each array element works as an independent IR sensor. This allows the measurement of wide fields together with in-house automated data processing and a spectral database comparison. Renner et al. (2017) used ATR–FTIR automated peak detection software to analyse microplastic standards in reference samples, while Serranti et al. (2018) characterised marine microplastics using hyperspectral imaging that consists of a short-wavelength infrared spectrograph and lens with automated data evaluation from various software, a database comparison and principal component analysis statistical evaluation. Piehl et al. (2018) tested agricultural soil for plastic debris using sampling, sieving, filtration and ATR–FTIR and found 0.3 ± 0.4 particles·ha^{-1}. They had to omit all particles smaller than 1 mm, however, due to challenges with the sample pre-treatment.

Destructive methods are increasingly being used for the qualitative analysis of microplastics in various environments, including pyrolysis gas chromatography with mass spectrometry detection (Py–GC/MS), desorption-GC/MS and liquid chromatography (LC). For example, Dümichen et al. (2015 and 2017) used GC/MS for the thermodesorption of PP, PE and PS in fermentation residues taken from a biogas plant and PE, PS and PET in river water. This method is advantageous due to the speed of analysis and low sample consumption (20 mg) but involves high demands on sample homogenisation (Dümichen et al., 2017). To make vibrational-spectrometric microscopy methods quicker and more robust, Hufnagl et al. (2019) used a chemometric approach with a combination of spectral descriptors, such as random decision forest (RDF) classifiers, together with FTIR microscopy with a focal plane array (FPA) detector. In this preliminary study, the authors were able to identify PE, PP, PMMA (polymethyl methacrylate), PS and PAN (polyacrylonitrile) particles in the artificially microplastic-fortified samples of freshwater plankton (Hufnagl et al., 2019).

3.3. Quantitative determination of conventional microplastics

Quantitative determination of microplastics (especially in soil and other complex solid or colloidal matrices) is currently a major analytical challenge. The complexity of the samples makes analysis difficult because of possible interferences with the analyte creating a false-positive or negative signal (David et al., 2019). A quantitative determination is one that can distinguish between plastics and matrices or other materials, gives information about the type of plastics (at least approximately) and indicates the concentration of the microplastics in the chemical sense (i.e. by weight or volume).

A promising quantitative method for the determination of microplastics is Py–GC/MS, where the sample is pyrolyzed in an inert atmosphere and the resulting gaseous products are captured in a solvent or passed (most commonly by capillary) directly to the GC–MS. The advantage is that multiple plastics can be determined in a mixture and the sample can be analysed without any pre-treatment. The disadvantage is that it does not provide information on the number, size and shape of the microplastics (He et al., 2018). Fries et al. (2013) used a Py–GC/MS method to identify sediment from the island of Norderney, where due to strong tidal phenomena, a high accumulation of PE, PS and PVC sediments occur. They also identified additives contained therein (Fries et al., 2013). Nuelle et al. (2014) also used this method to determine PP, PET and PVC in sea sediments. The known methods of quantitative determination of microplastics in solid matrices are summarised in Table 1.

4. Determination of P3HB, PLA and PBAT in various matrices

Introducing biodegradable plastics products into the market could be connected with the formation of microplastics in a short time due to their imperfect or slow biodegradation (Sintim et al., 2019). Although the environmental persistence of biodegradable microplastics should be shorter than that of conventional plastics, they may have similar negative properties (Haider et al., 2018). Methods for the qualitative and quantitative determination of such microplastic particles are not available, which is in stark contrast to the number of methods available for bulk bioplastic materials. These tests would be useful for assessing environmental contamination and for verifying biodegradability tests as it is currently not possible to satisfactorily analyse the test medium for any residues of these materials once the test is over.

Only some of the methods used in conventional microplastics can be used to extract bioplastics from soil or other solid matrices. These are mainly physical processes such as filtration, sieving or sedimentation fractionation (Sun et al., 2019). Aggressive chemicals cannot be used to decompose the organic constituents of the matrix due to the poor resistance of microplastics. One of the alternatives seems to be the dissolution of bioplastics in chloroform (Krishnan et al., 2017). As other organic substances can be co-extracted (mainly humic fractions), however, the extract must be thoroughly purified.

Extraction using ionic liquids, which are more specific for dissolution, could be a promising alternative. Two different strategies can be used. The first is the dissolution of the biomass and the release of microplastics into a solution where they can be easily filtered out (Kobayashi et al., 2015; Lee and Yang, 2016; Dubey et al., 2017), with Kobayashi et al. (2015) indicating recovery of up to 98%. Only samples with a specific matrix can be analysed, e.g. matrices formed by bodies of microorganisms, and it is not yet clear if these methods will work for soil-type matrices. Additionally, the large consumption of ionic liquid has relatively low yields and little solvent recycling. The second strategy involves dissolving a suitable PHA bioplastics in ionic liquid and precipitating it again after filtering out the remaining biomass, as described in the US007763715B2 patent (Hecht et al., 2010).

4.1. P3HB

To determine P3HB (density 1.18–1.26 g·cm^{-3}) using the separation method, it must be depolymerised and determined as a monomer, i.e. hydroxybutyric acid. One possibility is the use of hydrosulfuric methanolysis. This method is not quantitative, however, as by-products such as crotonic acid and propene derivatives may be formed. The yields of this method are between 30 and 40% (Grubelnik et al., 2008; Comeau et al., 1988). Another possibility is cleavage with tetraethoxytitanate and trifluoroacetic acid ethyl ester (TFA). This method is suitable for further GC analysis, whereby the TFA chain may be lost and derivatisation is required (Grubelnik et al., 2008). The most suitable method for P3HB depolymerisation is to use reduction lithium aluminium hydride depolymerisation. The resulting monomer can then be determined using high-performance liquid chromatography with mass spectrometric detection and electrospray ionisation (HPLC–ESI/MS; detection limits range from 4.2 wt% in 10 μL aliquot from 2 mg of polymer) (Grubelnik et al., 2008).

Methods for determining intercellular P3HB in activated sludge cells can also be used to determine P3HB microplastics. These methods are based on the propanolytic or hydrolytic depolymerisation of plastics and the determination of the resulting products by ion chromatography (semi-quantitative, detection limits not stated) (Hesselmann et al., 1999). The determination of extraneous P3HB microplastics in activated sludge complicates the occurrence of natural P3HB that is a part of the cells of the microorganisms in the sludge. In fact, P3HB can form up to 10 times the percentage of the cell weight of microorganisms (Li et al., 2019).

Table 1
Summarised quantitative methods for detection of microplastics in solid matrices.

Microplastic type	Matrix	Pre-separation	Method	Detection results	Reference
Thermoanalytical methods					
PE	Sandy topsoil	None	TED–GC/MS	10,000 ppm (evaluable) 2500 ppm (detectable)	(Dümichen et al., 2015)
PS, PP, tire wear as SBR	Highway street runoff sludge	None	TED–GC/MS	0.2; 0.44 and 0.23 μg LOD respectively	(Dümichen et al., 2017)
PET	Model loamy sand	None	TGA–MS	600–2500 ppm LOD 17,200–184,000 ppm LOQ	(David et al., 2018)
PE, PP, PET, PS, PA6, PVC, PC, PMMA	Fish tissue	Enzymatic & chemical digestion + density separation	CP Py–GC/MS	0.4 to 290 μg (found evaluable)	(Fischer and Scholz-Böttcher, 2017)
PS	Tidal sediment	Chemical digestion + density separation	MF Py–GC/MS	LOD = 3 ng; LOQ = 16 ng	(Fischer and Scholz-Böttcher, 2019)
PE, PP, PS	Model loamy sand	Dissolution in TCB	Filament Py–GC/MS	1–86 ppm method LODs	(Steinmetz et al., 2020)
PET, PS, PVC	Model loamy sand	None	TGA + modeling	*Preliminary modeled*: PET: 3300 ppm LOD, 11500 ppm LOQ; PS: 9100 ppm LOD, 30800 ppm LOD; PVC: 22200 ppm LOD.	(David et al., 2019)
Non-thermoanalytical methods					
PE, PP	Cosmetic products	Extraction, dissolution	HTGPC (high-temperature gel-permeation chromatography)	For conc. 700–3700 ppm RSD 2.3–13.4% and recovery 92–96%	(Hintersteiner et al., 2015)
PC, PET	Landfill sludge	Alkali hydrolysis heating depolymerization	LC/MS/MS of depolymerization products	LOD 0.00832 ppm PC LOD 0.053 ppm PET	(Wang et al., 2017)
PS, PET	Model loamy sand	Extraction by solvents	RP–LC	Recovery >99% PS, >80% PET	(Elert et al., 2017)
PS, PVC	Sea sediments	Not mentioned	TGA–FTIR	LOQ 0.050 mg (PVC), 0.025 mg (PS)	Yu et al., 2019
Several types	Floodplain soil	Density separation, oxidative digestion	FTIR	As low as 5 ppm conc., LOD not specified	Scheurer and Bigalke, 2018

P3HB in bacterial biomass can be quantified using FTIR spectrometry and subsequent statistical data processing using partial least squares regression and further modeling (Kansiz et al., 2000). Arcos-Hernandez et al. (2010) developed an FTIR method to determine PHB in mixed cell cultures in concentrations from 0.011 *w*/w, and the R^2 was between 0.911 and 0.985 (see Isak et al., 2016 for further information), while Samek et al. (2016) employed Raman spectrometry to quantify the P3HB content in *Cupriavidus necator* H16 media with the lowest calibration point being 1.395 μmol·L^{-1}. It should be noted that the latter method only worked for amorphous P3HB. These two publications did not state any limits of detection in their methods, however, the methods were optimised for the determination of P3HB in cells and it is not clear if they would work for the determination of P3HB in soil.

Extracted P3HB can also be dissolved in chloroform when sulfuric acid is added. Crotonic acid is formed, the solution turns brown and the P3HB content can be determined spectrophotometrically (Krishnan et al., 2017). Detection limits were not stated, but the amount of P3HB in the sample should have been between 5 and 50 μg (Law and Slepecky, 1961). For the determination of P3HB in *Synechocystis sp.*, it is possible to use a commercial set that uses enzymatic depolymerisation, with the resulting solution analysed spectrophotometrically (Zilliges and Damrow, 2017). Very efficient extraction is needed to analyse micro-bioplastics in soil as the organic matter can form turbidity or substances with a similar absorption spectrum in the solution.

Karr et al. (1983) used HPLC/UV–VIS to determine P3HB in a *Rhizobium japonicum* culture after complicated digestion with sodium hypochlorite and digestion and depolymerisation to crotonic acid following extraction. The lowest concentration observed was 140 nmol·L^{-1}, and further detection limits were not stated. In contrast, Elhottová et al. (2000) employed GC/MS–MS to determine derivatised products of methanolysis of glycolipid extracts/isolates to determine the P3HB content in sandy loam soil, wastewater treatment sludge and *Bacillus megaterium* CC M 1464 culture. The lowest observed concentration was 1.16 nmol·L^{-1}, and further detection parameters were not published. Monteil-Rivera et al. (2007) used both methanolysis and acid hydrolysis of P3HB to obtain depolymerisation products and hydroxyalkeonic acids and then analysed them via SPME–GC/FID, with LODs from 1.6 to 53 mg·L^{-1}, LOQs of 5.5–175 mg·L^{-1}, recovery of 98–100% and RSDs of 2–8 (Monteil-Rivera et al., 2007). Similarly, Werker et al. (2008) used GC/FID after acid alcoholysis and hexane extraction to determine the P3HB content in activated sludge from various laboratory-scale bioreactors treating wastewater, with the lowest detectable concentration of 14 μmol of 3-hydroxybutyric acid/butyl ester corresponding to 1.2 mg of P3HB.

Torri et al. (2014) utilised offline Py–GC/FID to determine 2-alkenoic acids in bacterial biomass with a LOD of 100 μg (1 wt% of P3HB in biomass) and RSD ≤ 15%, stating that such a method was comparable to methods using methanolysis. Abbondanzi et al. (2017) further developed and reworked this method to enable even quicker and easier in-vial-thermolysis suitable for P3HB amounts of 0.5–2.5 mg (10–50% of P3HB in mixed microbial culture samples) detected by GC/MS. Similarly, Velasco Alvarez et al. (2017) performed a gas chromatography isotope dilution mass spectrometry (GC/IDMS) analysis of P3HB in *Escherichia coli* microbial biomass (after propanolysis and derivatisation) with ^{13}C–P3HB internal standard, with a LOD of 0.01 μg·g^{-1} (or 0.11 nmol·L^{-1}).

Another possibility is the method based on sample thermal decomposition followed by an analysis of gaseous products, which allows direct determination of P3HB in the matrix, similar to conventional microplastics (Nuelle et al., 2014; Yu et al., 2019; David et al., 2018). In the case of P3HB, which has low resistance to thermal degradation, chain cleavage occurs leading to a decrease in molecular weight (Fig. 4). The product of thermal degradation is crotonic acid with a molecular weight of 86.09 g/mol and its oligomers.

4.2. PLA

The mechanism of PLA (density 1.24 g·cm^{-3}) thermal degradation is more complicated and is attributed to random cleavage of the backbone

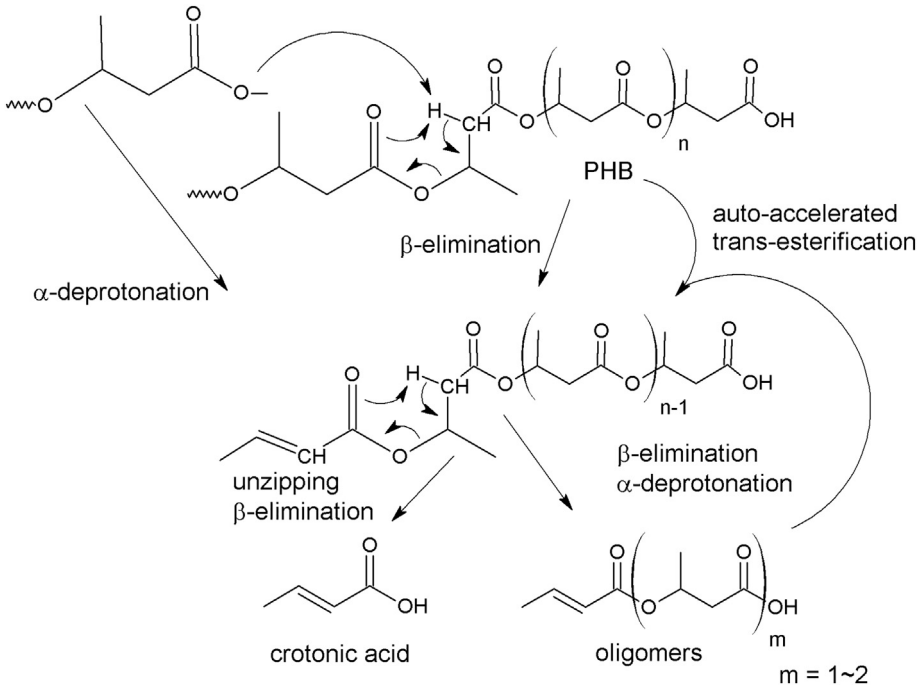


Fig. 4. Mechanism of P3HB thermal degradation (Bugnicourt et al., 2015).

(Hyon et al., 1998), depolymerisation (Gupta and Deshmukh, 1982) and transesterification reactions (Signori et al., 2009). Primary pyrolysis products are carbon monoxide, carbon dioxide, methyl ketene, acetaldehyde, water and cyclic oligomers. The secondary products are methane and butanedione, which are probably products of acetaldehyde degradation. Degradation is also affected by reactive end groups, catalyst residues, unreacted monomers and other impurities. In this case, the use of pyrolysis is more problematic. Pyrolysis can be used only if degradation products are not the same as matrix degradation products. The sample would then have to be pre-treated, which could lead to further problems.

For the determination of PLA as a film without a matrix, Arrieta et al. (2013) developed a sequential pyrolysis method (using Py–GC/MS) with detection limits starting at 0.1 μg according to an analyte, an R^2 from 0.841 to 0.985 and an RSD from 4.68 to 2.65. Moreover, by using the sophisticated hyphenated techniques used in food nanoanalysis, such as ultraperformance liquid chromatography-quadrupole/time-of-flight mass spectrometry (UPLC–QTOF–MS) or ultraperformance liquid chromatography-ion mobility spectroscopy-quadrupole time-of-flight mass spectrometry (UPLC–IMS–QTOF–MS), they were able to analyse various cyclic and linear oligomers of PLA (masses from 257 to 1175) in food simulants (solutions of ethanol and acetic acid) in concentrations around thousands ng/g (Ubeda et al., 2019). Moreover, atmospheric solid analysis probe-ion mobility mass spectrometry (ASAP–IM–MS) enables qualitative differentiation between PLA, PBS and PE in PLA–PBS and PLA–PE blends after the melting of the sample and thermal desorption of the analyte (Barrère et al., 2014).

4.3. PBAT

There have been many material characterisation works published regarding PBAT, but no analytical ones (e.g. how to quantify PBAT within a matrix). Some authors have tried to distinguish PBAT (density 1.25 $g{\cdot}cm^{-3}$) in blends from other polymers (mainly PLA) qualitatively, which can be achieved by differential scanning calorimetry (DSC), thermogravimetry (TG), Fourier transform infrared spectroscopy (FTIR) and elemental analysis (EA) (Zhao et al., 2010; Weng et al., 2013). Similar results obtained by Sikorska et al. (2017) confirmed these results. PBAT can be distinguished from P3HB in blends by utilising ^{1}H MAS NMR and ^{13}C CP/MAS NMR (Hutníková and Fričová, 2016) and Rizzarelli et al. (2016) were able to identify PE qualitatively from PBAT and PLA in PE/PBAT/PLA blends utilising TGA and Py–GC/MS (as well as quantifying PE in terms of 1–10 wt% in the blends). Chen et al. (2016) determined PBAT in blends with PLA and polypropylene carbonate (PPC) qualitatively via MIR (mid-infrared) and Raman spectrometry. They also quantitatively employed NIR (near-infrared) and Raman spectrometry following chemometrical data evaluation in tenths of wt%. R^2 was determined to be between 0.399 and 0.999 and the root mean square error of prediction (RMSEP) values were between 2.54% and 3.58% (Chen et al., 2016).

Recently, Duemichen et al. (2014) performed pyrolysis of polybutylene terephthalate (PBT) via TGA–FTIR, TGA–MS and TED–GC/MS. The question is whether the pyrolysis products characteristic for PBT, i.e. benzoic acid (m/z = 105/122), but-3-enyl benzoate (m/z = 105/77), biphenyl (m/z = 154/76), propyl 4-methyl benzoate (m/z = 119/136) and terephthalic acid di(but-3-enyl)ester (m/z = 203/149) are useful also for determination of PBTA.

5. Directions for future studies

The following research questions regarding the formation of microplastics from biodegradable plastics need to be investigated. This can be achieved by looking at the possibility of applying the existing analytical methods for conventional microplastics to microplastics from biodegradable plastics and developing tailored analytical methods to track the concentrations of microplastics from biodegradable plastics in soil. Then, it can be decided if biodegradable plastics that are left to biodegrade via industrial or household composting and those used in agriculture or littered present a future environmental issue.

Research question 1: Is it possible that rapidly formed microbioplastics also decompose more rapidly than conventional microplastics?

Research question 2: Is the use of mulch foils and composting bioplastic products and packaging another source of microplastics in the environment, especially in soil?

Research question 3: Is the impact of micro-bioplastics on the environment comparable to the known effect of conventional microplastics?

Research question 4: In what ways is it possible to identify micro-bioplastics in the soil and to differentiate them from conventional microplastics or even from each other? Are the analytical methods for determining the content of bioplastics or conventional plastics suitable for this?

6. Conclusions

Products made from biodegradable bioplastics are beginning to replace products made from conventional plastics due to pressure from legislation, organisations and customers. Consumers may also mistakenly believe that these materials are not a threat to the environment, which can lead to increased littering. For example, studies have shown that many people do not know how to handle bioplastic waste and can unintentionally harm the environment with it (Taufik et al., 2020). According to Jevons' paradox (a phenomenon where precautionary savings will generate more consumption), biobased plastics may also be consumed more and thus the production of (bio)plastic waste will rise (Alcott, 2005). This is a material for which there is currently no recycling infrastructure.

Composting is a very common method of bioplastic disposal, but the compost formed may contain many micro-bioplastic particles resulting from incomplete biodegradation, through which the soil may be contaminated. This has led to some composting plants separating bioplastics from biowaste, meaning they end up in incinerators or landfills together with conventional plastics (Barrett, 2019). It is not entirely clear if this waste will be responsible for a massive microparticle formation with high sorption capacity or chronic toxicity to living organisms. Therefore, a reliable and rapid method for the determination of these particles in all environmental situations, especially in soil, must be developed.

As is evident from this review, methods for determining micro-bioplastics could be inspired by the approaches already developed for conventional plastics, however, bioplastics have specificities that need to be considered when choosing the appropriate method. This is mainly due to their chemical instability, which makes it impossible to use aggressive chemicals when decomposing the matrix. This significantly complicates the analysis and requires methods that do not involve any pre-treatment of the sample. Also, the natural occurrence of the analysed polymer or its monomers may interfere with the analytical signal that the micro-bioplastic contamination gives.

Until now, it has been unknown which extraction methods and analytical methods should be developed or re-adopted for the determination of bio-microplastics in solid environmental matrices, particularly in soil.

Based on the reviewed techniques, it can be concluded that the best methods for the analysis of conventional microplastics are the methods based on pyrolysis and thermal analysis (TGA–MS, TGA and chemometrics, Py–GC/MS and TED–GC/MS). For extraction, only mild techniques can be used so as not to deteriorate and exclude the analyte. As for a Py–GC/MS with the injection of a liquid sample to the pyrolyzer, suitable solvents have to be found to dissolve the maximal amount of the biopolymer but a minimal amount of the matrix.

From the known characterisation methods for the biopolymers, for P3HB, the selective depolymerisation and determination using HPLC–ESI/MS according to Grubelnik et al. (2008) is promising. Another option is methanolysis and acid hydrolysis of P3HB to hydroxyalkeonic acids and subsequent analysis via SPME–GC/FID (Monteil-Rivera et al., 2007). For PLA, so far, only UPLC–IMS–QTOF–MS seems to be convenient (Ubeda et al., 2019), but this is not accessible to most labs.

As for analysis of PBAT, no analytical techniques are yet known, except for the material-characterisation ones. Here, the results of analysis of identification of PBAT and PLA in PE/PBAT/PLA blends utilising TGA and Py–GC/MS as published by Rizzarelli et al. (2016) might be a good starting point. Also, applicable seem to be use of pyrolysis products of polybutylene terephthalate (PBT) published by Duemichen et al. (2014).

Declaration of competing interest

The authors declare that they have no known competing financial interests or personal relationships that could have appeared to influence the work reported in this paper.

Acknowledgement

The financial support of projects FCH-S-20-6446 of Ministry of Education, Youth and Sports and FV40094 of Ministry of Industry and Trade of the Czech Republic are acknowledged.

References

Abbondanzi, F., Biscaro, G., Carvalho, G., Favaro, L., Lemos, P., Paglione, M., Samorì, C., Torri, C., 2017. Fast method for the determination of short-chain-length polyhydroxyalkanoates (scl-PHAs) in bacterial samples by In Vial-Thermolysis (IVT). New Biotechnol. 39, 29–35. https://doi.org/10.1016/j.nbt.2017.05.012.

Agnihotri, S., Shukla, S., Pilla, S., 2019. Sustainability Issues in Bioplastics. Reference Module in Materials Science and Materials Engineering. https://doi.org/10.1016/B978-0-12-803581-8.10610-1.

Alcott, B., 2005. Jevons' paradox. Ecol. Econ. 54, 9–21. https://doi.org/10.1016/j.ecolecon.2005.03.020.

Andrady, A., 2011. Microplastics in the marine environment. Mar. Pollut. Bull. 62, 1596–1605. https://doi.org/10.1016/j.marpolbul.2011.05.030.

Ansari, S., Fatma, T., Appanna, V., 2016. Cyanobacterial polyhydroxybutyrate (PHB): screening, optimization and characterization. PLoS ONE 11. https://doi.org/10.1371/journal.pone.0158168.

Arcos-Hernandez, M., Gurieff, N., Pratt, S., Magnusson, P., Werker, A., Vargas, A., Lant, P., 2010. Rapid quantification of intracellular PHA using infrared spectroscopy: an application in mixed cultures. J. Biotechnol. 150, 372–379. https://doi.org/10.1016/j.jbiotec.2010.09.939.

Arrieta, M., Parres, F., López, J., Jiménez, A., 2013. Development of a novel pyrolysis-gas chromatography/mass spectrometry method for the analysis of poly(lactic acid) thermal degradation products. J. Anal. Appl. Pyrolysis 101, 150–155. https://doi.org/10.1016/j.jaap.2013.01.017.

Ashter, S., 2016. Introduction to Bioplastics Engineering. 1st. William Andrew, USA.

Bagheri, A., Laforsch, C., Greiner, A., Agarwal, S., 2017. Fate of so-called biodegradable polymers in seawater and freshwater. Global Chall. 1, 1–5. https://doi.org/10.1002/gch2.201700048.

Barrère, C., Selmi, W., Hubert-Roux, M., Coupin, T., Assumani, B., Afonso, C., Giusti, P., 2014. Rapid analysis of polyester and polyethylene blends by ion mobility-mass spectrometry. Polym. Chem. 5, 3576–3582. https://doi.org/10.1039/C4PY00164H.

Barrett, A., 2019. The battle between Oregon composters and the biodegradable products institute. Bioplastics NEWS.

Bastioli, C., 2005. Handbook of Biodegradable Polymers. Rapra Technology, Shrewsbury.

Bátori, V., Åkesson, D., Zamani, A., Taherzadeh, M., Sárvári Horváth, I., 2018. Anaerobic degradation of bioplastics: a review. Waste Manag. 80, 406–413. https://doi.org/10.1016/j.wasman.2018.09.040.

Bertolino, V., Cavallaro, G., Milioto, S., Lazzara, G., Kryuchkova, M., Khaertdinov, N., Fakhrullin, R., 2020. Polysaccharides/halloysite nanotubes for smart bionanocomposite materials. Carbohydr. Polym. 245, 40553–40564. https://doi.org/10.1016/j.carbpol.2020.116502.

Bläsing, M., Amelung, W., 2018. Plastics in soil: analytical methods and possible sources. Sci. Total Environ. 612, 422–435. https://doi.org/10.1016/j.scitotenv.2017.08.086.

Bosker, T., Olthof, G., Vijver, M., Baas, J., Barmentlo, S., 2019. Significant decline of Daphnia magna population biomass due to microplastic exposure. Environ. Pollut. 250, 669–675. https://doi.org/10.1016/j.envpol.2019.04.067.

Browne, M., Crump, P., Niven, S., Teuten, E., Tonkin, A., Galloway, T., Thompson, R., 2011. Accumulation of microplastic on shorelines woldwide: sources and sinks. Environ. Sci. Technol. 45, 9175–9179. https://doi.org/10.1021/es201811s.

Bugnicourt, E., Cinelli, P., Lazzeri, A., Alvarez, V., 2015. The main characteristics, properties, improvements, and market data of polyhydroxyalkanoates. Handbook of Sustainable Polymers, pp. 899–928 https://doi.org/10.1201/b19600-25.

Carr, S., Liu, J., Tesoro, A., 2016. Transport and fate of microplastic particles in wastewater treatment plants. Water Res. 91, 174–182. https://doi.org/10.1016/j.watres.2016.01.002.

Cavallaro, G., Lazzara, G., Rozhina, E., Konnova, S., Kryuchkova, M., Khaertdinov, N., Fakhrullin, R., 2019. Organic-nanoclay composite materials as removal agents for environmental decontamination. RSC Adv. 9, 40553–40564. https://doi.org/10.1039/C9RA08230A.

Chen, R., Huang, X., Wang, M., Jin, G., 2016. Evaluation and comparison of mid-infrared, Raman and near-infrared spectroscopies for characterization and determination of the compositions in fully biodegradable poly(lactic acid)/poly(propylene

carbonate)/poly(butylene adipate-co-terephthalate) blends combined with chemometrics. J. Macromol. Sci. A 53, 354–361. https://doi.org/10.1080/10601325.2016.1166001.
Chen, H., Wang, Y., Sun, X., Peng, Y., Xiao, L., 2020. Mixing effect of polylactic acid microplastic and straw residue on soil property and ecological function. Chemosphere 243. https://doi.org/10.1016/j.chemosphere.2019.125271.
Chinaglia, S., Tosin, M., Degli-Innocenti, F., 2018. Biodegradation rate of biodegradable plastics at molecular level. Polym. Degrad. Stab. 147, 237–244. https://doi.org/10.1016/j.polymdegradstab. 2017.12.011.
Cole, M., Webb, H., Lindeque, P., Fileman, E., Halsband, C., Galloway, T., 2015. Isolation of microplastics in biota-rich seawater samples and marine organisms. Sci. Rep. 4. https://doi.org/10.1038/srep04528.
Comeau, Y., Hall, K., Oldham, W., 1988. Determination of poly-β-hydroxybutyrate and poly-β-hydroxyvalerate in activated sludge by gas-liquid chromatography. Appl. Environ. Microbiol. 54.
Crawford, C., Quinn, B., 2017. Microplastic Pollutants, 2017. Elsevier, Amsterdam.
David, J., Steinmetz, Z., Kučerík, J., Schaumann, G., 2018. Quantitative analysis of poly(ethylene terephthalate) microplastics in soil via thermogravimetry–mass spectrometry. Anal. Chem. 90, 8793–8799. https://doi.org/10.1021/acs.analchem.8b00355.
David, J., Weissmannová, H., Steinmetz, Z., Kabelíková, L., Demyan, M., Šimečková, J., Tokarski, D., Siewert, C., Schaumann, G., Kučerík, J., 2019. Introducing a soil universal model method (SUMM) and its application for qualitative and quantitative determination of poly(ethylene), poly(styrene), poly(vinyl chloride) and poly(ethylene terephthalate) microplastics in a model soil. Chemosphere 225, 810–819. https://doi.org/10.1016/j.chemosphere.2019.03.078.
de Souza Machado, A., Kloas, W., Zarfl, C., Hempel, S., Rillig, M., 2018. Microplastics as an emerging threat to terrestrial ecosystems. Glob. Chang. Biol. 24, 1405–1416. https://doi.org/10.1111/gcb.14020.
Dekiff, J., Remy, D., Klasmeier, J., Fries, E., 2014. Occurrence and spatial distribution of microplastics in sediments from Norderney. Environ. Pollut. 186, 248–256. https://doi.org/10.1016/j.envpol.2013.11.019.
Dubey, S., Bharmoria, P., Gehlot, P., Agrawal, V., Kumar, A., Mishra, S., 2017. 1-Ethyl-3-methylimidazolium diethylphosphate based extraction of bioplastic "polyhydroxyalkanoates" from bacteria: green and sustainable approach. 6, 766–773. https://doi.org/10.1021/acssuschemeng.7b03096.
Duemichen, E., Braun, U., Senz, R., Fabian, G., Sturm, H., 2014. Assessment of a new method for the analysis of decomposition gases of polymers by a combining thermogravimetric solid-phase extraction and thermal desorption gas chromatography mass spectrometry. J. Chromatogr. A 1354, 117–128. https://doi.org/10.1016/j.chroma.2014.05.057.
Dümichen, E., Barthel, A., Braun, U., Bannick, C., Brand, K., Jekel, M., Senz, R., 2015. Analysis of polyethylene microplastics in environmental samples, using a thermal decomposition method. Water Res. 85, 451–457. https://doi.org/10.1016/j.watres.2015.09.002.
Dümichen, E., Eisentraut, P., Bannick, C., Barthel, A., Senz, R., Braun, U., 2017. Fast identification of microplastics in complex environmental samples by a thermal degradation method. Chemosphere 174, 572–584. https://doi.org/10.1016/j.chemosphere.2017.02.010.
Elert, A., Becker, R., Duemichen, E., Eisentraut, P., Falkenhagen, J., Sturm, H., Braun, U., 2017. Comparison of different methods for MP detection: what can we learn from them, and why asking the right question before measurements matters? Environ. Pollut. 231, 1256–1264. https://doi.org/10.1016/j.envpol.2017.08.074.
Elhottová, D., Tříska, J., Petersen, S., 2000. Analysis of poly-β-hydroxybutyrate in environmental samples by GC-MS/MS. Fresenius J. Anal. Chem. 367, 157–164. https://doi.org/10.1007/s002160051617.
Emadian, S., Onay, T., Demirel, B., 2017. Biodegradation of bioplastics in natural environments. Waste Manag. 59, 526–536. https://doi.org/10.1016/j.wasman.2016.10.006.
Erni-Cassola, G., Gibson, M., Thompson, R., Christie-Oleza, J., 2017. Lost, but found with Nile Red: a novel method for detecting and quantifying small microplastics (1 mm to 20 μm) in environmental samples. Environ. Sci. Technol. 51, 13641–13648. https://doi.org/10.1021/acs.est.7b04512.
Ezeh, O., Susmel, L., 2018. Fatigue behaviour of additively manufactured polylactide (PLA). Procedia Structural Integrity 13, 728–734. https://doi.org/10.1016/j.prostr.2018.12.121.
Fahim, I., Chbib, H., Mahmoud, H., 2019. The synthesis, production & economic feasibility of manufacturing PLA from agricultural waste. Sustain. Chem. Pharm. 12. https://doi.org/10.1016/j.scp.2019.100142.
Fernandes, T., Leite, M., de Sousa, A., Furtado, C., Escócio, V., da Silva, A., 2017. Improvement in toughness of polylactide/poly(butylene adipate-co-terephthalate) blend by adding nitrile rubber. Polym. Bull. 74, 1713–1726. https://doi.org/10.1007/s00289-016-1798-9.
Ferreira, R., Amatte, I., Dutra, T., Bürger, D., 2017. Experimental characterization and micrography of 3D printed PLA and PLA reinforced with short carbon fibers. Compos. Part B 124, 88–100. https://doi.org/10.1016/j.compositesb.2017.05.013.
Ferreira, I., Venâncio, C., Lopes, I., Oliveira, M., 2019. Nanoplastics and marine organisms: what has been studied? Environ. Toxicol. Pharmacol. 67, 1–7. https://doi.org/10.1016/j.etap.2019.01.006.
Fischer, M., Scholz-Böttcher, B., 2017. Simultaneous trace identification and quantification of common types of microplastics in environmental samples by pyrolysis-gas chromatography–mass spectrometry. Environmental Science & Technology Letters 51, 5052–5060. https://doi.org/10.1021/acs.est.6b06362.
Fischer, M., Scholz-Böttcher, B., 2019. Microplastics analysis in environmental samples – recent pyrolysis-gas chromatography-mass spectrometry method improvements to increase the reliability of mass-related data. Anal. Methods 11, 2489–2497. https://doi.org/10.1039/C9AY00600A.
Fries, E., Dekiff, J., Willmeyer, J., Nuelle, M., Ebert, M., Remy, D., 2013. Identification of polymer types and additives in marine microplastic particles using pyrolysis-GC/MS and scanning electron microscopy. Environ Sci Process Impacts 15, 1949–1956. https://doi.org/10.1039/c3em00214d.
Fuller, S., Gautam, A., 2016. A procedure for measuring microplastics using pressurized fluid extraction. Environ. Sci. Technol. 50, 5774–5780. https://doi.org/10.1021/acs.est.6b00816.
Geyer, R., Jambeck, J., Law, K., 2017. Production, use, and fate of all plastics ever made. Sci. Adv. 3. https://doi.org/10.1126/sciadv.1700782.
Gong, W., Jiang, M., Han, P., Liang, G., Zhang, T., Liu, G., 2019. Comparative analysis on the sorption kinetics and isotherms of fipronil on nondegradable and biodegradable microplastics. Environ. Pollut. 254. https://doi.org/10.1016/j.envpol.2019.07.095.
Green, D., Boots, B., Sigwart, J., Jiang, S., Rocha, C., 2016. Effects of conventional and biodegradable microplastics on a marine ecosystem engineer (Arenicola marina) and sediment nutrient cycling. Environ. Pollut. 208, 426–434. https://doi.org/10.1016/j.envpol.2015.10.010.
Grubelnik, A., Wiesli, L., Furrer, P., Rentsch, D., Hany, R., Meyer, V., 2008. A simple HPLC-MS method for the quantitative determination of the composition of bacterial medium chain-length polyhydroxyalkanoates. J. Sep. Sci. 31, 1739–1744. https://doi.org/10.1002/jssc.200800033.
Guo, X., Wang, J., 2019. The chemical behaviors of microplastics in marine environment: a review. Mar. Pollut. Bull. 142, 1–14. https://doi.org/10.1016/j.marpolbul.2019.03.019.
Guo, X., Chen, C., Wang, J., 2019. Sorption of sulfamethoxazole onto six types of microplastics. Chemosphere 228, 300–308. https://doi.org/10.1016/j.chemosphere.2019.04.155.
Gupta, M., Deshmukh, V., 1982. Thermal oxidative degradation of poly-lactic acid. Colloid Polym. Sci. 260, 308–311.
Haider, T., Völker, C., Kramm, J., Landfester, K., Wurm, F., 2018. Plastics of the future? The impact of biodegradable polymers on the environment and on society. Angew. Chem. Int. Ed. 3, 1–5. https://doi.org/10.1002/anie.201805766.
Hamad, K., Kaseem, M., Ayyoob, M., Joo, J., Deri, F., 2018. Polylactic acid blends: the future of green, light and tough. Prog. Polym. Sci. 85, 83–127. https://doi.org/10.1016/j.progpolymsci.2018.07.001.
Harrison, J., Boardman, C., O'Callaghan, K., Delort, A., Song, J., 2018. Biodegradability standards for carrier bags and plastic films in aquatic environments: a critical review. R. Soc. Open Sci. 5. https://doi.org/10.1098/rsos.171792.
Hartmann, N., Hüffer, T., Thompson, R., Hassellöv, M., Verschoor, A., Daugaard, A., Rist, S., Karlsson, T., Brennholt, N., Cole, M., Herrling, M., Hess, M., Ivleva, N., Lusher, A., Wagner, M., 2018. Are we speaking the same language? Recommendations for a definition and categorization framework for plastic debris. Environ. Sci. Technol. 53, 1039–1047. https://doi.org/10.1021/acs.est.8b05297.
He, D., Luo, Y., Lu, S., Liu, M., Song, Y., Lei, L., 2018. Microplastics in soils: analytical methods, pollution characteristics and ecological risks. TrAC Trends Anal. Chem. 109, 163–172. https://doi.org/10.1016/j.trac.2018.10.006.
Hecht, S., Niehoff, R., Narasimhan, K., Neal, C., Forshey, P., Phan, D., Deepali, A., Brooker, M., Combs, K., 2010. Extracting Biopolymers From Biomass Using Ionic Liquids.
Hermann, B., Debeer, L., De Wilde, B., Blok, K., Patel, M., 2011. To compost or not to compost: carbon and energy footprints of biodegradable materials' waste treatment. Polym. Degrad. Stab. 96, 1159–1171. https://doi.org/10.1016/j.polymdegradstab.2010.12.026.
Hesselmann, R., Fleischmann, T., Hany, R., Zehnder, A., 1999. Determination of polyhydroxyalkanoates in activated sludge by ion chromatographic and enzymatic methods. J. Microbiol. Methods 35, 111–119. https://doi.org/10.1016/S0167-7012(98)00107-9.
Hintersteiner, I., Himmelsbach, M., Buchberger, W., 2015. Characterization and quantitation of polyolefin microplastics in personal-care products using high-temperature gel-permeation chromatography. Anal. Bioanal. Chem. 407, 1253–1259. https://doi.org/10.1007/s00216-014-8318-2.
Horie, K., Barón, M., Fox, R., He, J., Hess, M., Kahovec, J., Kitayama, T., Kubisa, P., Maréchal, E., Mormann, W., Stepto, R., Tabak, D., Vohlídal, J., Wilks, E., Work, W., 2004. Definitions of terms relating to reactions of polymers and to functional polymeric materials (IUPAC recommendations 2003). Pure Appl. Chem. 76, 889–906. https://doi.org/10.1351/pac200476040889.
Hufnagl, B., Steiner, D., Renner, E., Löder, M., Laforsch, C., Lohninger, H., 2019. A methodology for the fast identification and monitoring of microplastics in environmental samples using random decision forest classifiers. Anal. Methods 11, 2277–2285. https://doi.org/10.1039/C9AY00252A.
Hurley, R., Lusher, A., Olsen, M., Nizzetto, L., 2018. Validation of a method for extracting microplastics from complex, organic-rich, environmental matrices. Environ. Sci. Technol. 52, 7409–7417. https://doi.org/10.1021/acs.est.8b01517.
Hutníková, M., Fričová, O., 2016. Solid-state NMR study of poly(3-hydroxybutyrate) and Ecoflex reser blends. Acta Phys. Pol. A 129, 388–393. https://doi.org/10.12693/APhysPolA.129.388.
Hyon, S., Jamshidi, K., Ikada, Y., 1998. Effects of residual monomer on the degradation of DL-lactide polymer. Polym. Int. 46, 196–202.
Imhof, H., Schmid, J., Niessner, R., Ivleva, N., Laforsch, C., 2012. A novel, highly efficient method for the separation and quantification of plastic particles in sediments of aquatic environments. Limnol. Oceanogr. Methods 10, 524–537. https://doi.org/10.4319/lom.2012.10.524.
Isak, I., Patel, M., Riddell, M., West, M., Bowers, T., Wijeyekoon, S., Lloyd, J., 2016. Quantification of polyhydroxyalkanoates in mixed and pure cultures biomass by Fourier transform infrared spectroscopy: comparison of different approaches. Lett. Appl. Microbiol. 63, 139–146. https://doi.org/10.1111/lam.12605.
Jaikumar, G., Brun, N., Vijver, M., Bosker, T., 2019. Reproductive toxicity of primary and secondary microplastics to three cladocerans during chronic exposure. Environ. Pollut. 249, 638–646. https://doi.org/10.1016/j.envpol.2019.03.085.
Kansiz, M., Billman-Jacobe, H., McNaughton, D., 2000. Quantitative determination of the biodegradable polymer poly(β-hydroxybutyrate) in a recombinant Escherichia

coli strain by use of mid-infrared spectroscopy and multivariative statistics. Appl. Environ. Microbiol. 66.
Käppler, A., Fischer, M., Scholz-Böttcher, B., Oberbeckmann, S., Labrenz, M., Fischer, D., Eichhorn, K., Voit, B., 2018. Comparison of μ-ATR-FTIR spectroscopy and py-GCMS as identification tools for microplastic particles and fibers isolated from river sediments. Anal. Bioanal. Chem. 410, 5313–5327. https://doi.org/10.1007/s00216-018-1185-5.
Karamanlioglu, M., Preziosi, R., Robson, G.D., 2017. Abiotic and biotic environmental degradation of the bioplastic polymer poly(lactic acid): a review. Polym. Degrad. Stab. 137, 122–130. https://doi.org/10.1016/j.polymdegradstab. 2017.01.009.
Karan, H., Funk, C., Grabert, M., Oey, M., Hankamer, B., 2019. Green bioplastics as part of a circular bioeconomy. Trends Plant Sci. 24, 237–249. https://doi.org/10.1016/j.tplants.2018.11.010.
Karr, D., Waters, J., Emerich, D., 1983. Analysis of poly-β-hydroxybutyrate in Rhizobium japonicum bacteroids by ion-exclusion high-pressure liquid chromatography and UV detection. Appl. Environ. Microbiol. 46, 1339–1344.
Kasirajan, S., Ngouajio, M., 2012. Polyethylene and biodegradable mulches for agricultural applications: a review. Agron. Sustain. Dev. 32, 501–529. https://doi.org/10.1007/s13593-011-0068-3.
Kobayashi, D., Fujita, K., Nakamura, N., Ohno, H., 2015. A simple recovery process for biodegradable plastics accumulated in cyanobacteria treated with ionic liquids. Appl. Microbiol. Biotechnol. 99, 1647–1653. https://doi.org/10.1007/s00253-014-6234-1.
Koltzenburg, S., Maskos, M., Nuyken, O., 2014. Polymere: Synthese, Eigenschaften und Anwendungen. Springer-Verlag, Berlin Heidelberg https://doi.org/10.1007/978-3-642-34773-3.
Krishnan, S., Chinnadurai, G., Perumal, P., 2017. Polyhydroxybutyrate by Streptomyces sp: production and characterization. Int. J. Biol. Macromol. 104, 1165–1171. https://doi.org/10.1016/j.ijbiomac.2017.07.028.
Lares, M., Ncibi, M., Sillanpää, M., Sillanpää, M., 2018. Occurrence, identification and removal of microplastic particles and fibers in conventional activated sludge process and advanced MBR technology. Water Res. 133, 236–246. https://doi.org/10.1016/j.watres.2018.01.049.
Laskar, N., Kumar, U., 2019. Plastics and microplastics: a threat to environment. Environ. Technol. Innov. 14. https://doi.org/10.1016/j.eti.2019.100352.
Law, J., Slepecky, R., 1961. Assay of poly-β-hydroxybutyric acid. Bacteriol 82, 33–36.
Lee, L., Yang, C., 2016. Investigations on green blends comprising biodegradable polymer and ionic liquid. Polymers 8. https://doi.org/10.3390/polym8120444.
Li, H., Zhang, J., Shen, L., Chen, Z., Zhang, Y., Zhang, C., Li, Q., Wang, Y., 2019. Production of polyhydroxyalkanoates by activated sludge: correlation with extracellular polymeric substances and characteristics of activated sludge. Chem. Eng. J. 361, 219–226. https://doi.org/10.1016/j.cej.2018.12.066.
Liebezeit, G., Dubaish, F., 2012. Microplastics in beaches of the East Frisian islands Spiekeroog and Kachelotplate. Bull. Environ. Contam. Toxicol. 89, 213–217. https://doi.org/10.1007/s00128-012-0642-7.
Liu, M., Lu, S., Song, Y., Lei, L., Hu, J., Lv, W., Zhou, W., Cao, C., Shi, H., Yang, X., He, D., 2018. Microplastic and mesoplastic pollution in farmland soils in suburbs of Shanghai, China. Environ. Pollut. 242, 855–862. https://doi.org/10.1016/j.envpol.2018.07.051.
Löder, M., Imhof, H., Ladehoff, M., Löschel, L., Lorenz, C., Mintenig, S., Piehl, S., Primpke, S., Schrank, I., Laforsch, C., Gerdts, G., 2017. Enzymatic purification of microplastics in environmental samples. Environ. Sci. Technol. 51, 14283–14292. https://doi.org/10.1021/acs.est.7b03055.
Lu, Y., Zhang, Y., Deng, Y., Jiang, W., Zhao, Y., Geng, J., Ding, L., Ren, H., 2016. Uptake and accumulation of polystyrene microplastics in zebrafish (Danio rerio) and toxic effects in liver. 50, 4054–4060. https://doi.org/10.1021/acs.est.6b00183.
Monteil-Rivera, F., Betancourt, A., Van Tra, H., Yezza, A., Hawari, J., 2007. Use of headspace solid-phase microextraction for the quantification of poly(3-hydroxybutyrate) in microbial cells. J. Chromatogr. A 1154, 34–41. https://doi.org/10.1016/j.chroma.2007.03.121.
Nuelle, M., Dekiff, J., Remy, D., Fries, E., 2014. A new analytical approach for monitoring microplastics in marine sediments. Environ. Pollut. 184, 161–169. https://doi.org/10.1016/j.envpol.2013.07.027.
Obruca, S., Marova, I., Snajdar, O., Mravcova, L., Svoboda, Z., 2010. Production of poly(3-hydroxybutyrate-co-3-hydroxyvalerate) by Cupriavidus necator from waste rapeseed oil using propanol as a precursor of 3-hydroxyvalerate. Biotechnol. Lett. 32, 1925–1932. https://doi.org/10.1007/s10529-010-0376-8.
Obruca, S., Benesova, P., Petrik, S., Oborna, J., Prikryl, R., Marova, I., 2014. Production of polyhydroxyalkanoates using hydrolysate of spent coffee grounds. Process Biochem. 49, 1409–1414. https://doi.org/10.1016/j.procbio.2014.05.013.
Piehl, S., Leibner, A., Löder, M., Dris, R., Bogner, C., Laforsch, C., 2018. Identification and quantification of macro- and microplastics on an agricultural farmland. Sci. Rep. 8. https://doi.org/10.1038/s41598-018-36172-y.
PlasticsEurope, 2017. Plastics – The Facts 2017: An Analysis of European Plastics Production, Demand and Waste Data. Plastics europe.
Prata, J., da Costa, J., Duarte, A., Rocha-Santos, T., 2019. Methods for sampling and detection of microplastics in water and sediment: a critical review. TrAC Trends Anal. Chem. 110, 150–159. https://doi.org/10.1016/j.trac.2018.10.029.
Primpke, S., Lorenz, C., Rascher-Friesenhausen, R., Gerdts, G., 2017. An automated approach for microplastics analysis using focal plane array (FPA) FTIR microscopy and image analysis. Anal. Methods 9, 1499–1511. https://doi.org/10.1039/C6AY02476A.
Rainieri, S., Barranco, A., 2019. Microplastics, a food safety issue? Trends Food Sci. Technol. 84, 55–57. https://doi.org/10.1016/j.tifs.2018.12.009.
Renner, G., Schmidt, T., Schram, J., 2017. A new chemometric approach for automatic identification of microplastics from environmental compartments based on FT-IR spectroscopy. Anal. Chem. 89, 12045–12053. https://doi.org/10.1021/acs.analchem.7b02472.
Rillig, M., 2012. Microplastic in terrestrial ecosystems and the soil? Environ. Sci. Technol. 46, 6453–6454. https://doi.org/10.1021/es302011r.
Rizzarelli, P., Rapisarda, M., Perna, S., Mirabella, E., La Carta, S., Puglisi, C., Valenti, G., 2016. Determination of polyethylene in biodegradable polymer blends and in compostable carrier bags by Py-GC/MS and TGA. J. Anal. Appl. Pyrolysis 117, 72–81. https://doi.org/10.1016/j.jaap.2015.12.014.
Ryan, C., Billington, S., Criddle, C., 2017. Assessment of models for anaerobic biodegradation of a model bioplastic: poly(hydroxybutyrate-co-hydroxyvalerate). Bioresour. Technol. 227, 205–213. https://doi.org/10.1016/j.biortech.2016.11.119.
Samek, O., Obruča, S., Šiler, M., Sedláček, P., Benešová, P., Kučera, D., Márova, I., Ježek, J., Bernatová, S., Zemánek, P., 2016. Quantitative Raman spectroscopy analysis of polyhydroxyalkanoates produced by Cupriavidus necator H16. Sensors 16. https://doi.org/10.3390/s16111808.
Scheurer, M., Bigalke, M., 2018. Microplastics in Swiss floodplain soils. Environ. Sci. Technol. 52, 3591–3598. https://doi.org/10.1021/acs.est.7b06003.
Serranti, S., Palmieri, R., Bonifazi, G., Cózar, A., 2018. Characterization of microplastic litter from oceans by an innovative approach based on hyperspectral imaging. Waste Manag. 76, 117–125. https://doi.org/10.1016/j.wasman.2018.03.003.
Shi, B., Shlepr, M., Palfery, D., 2011. Effect of blend composition and structure on biodegradation of starch/ecoflex-filled polyethylene films. J. Appl. Polym. Sci. 120, 1808–1816. https://doi.org/10.1002/app.33309.
Shim, W., Hong, S., Eo, S., 2017. Identification methods in microplastic analysis: a review. Anal. Methods 9, 1384–1391. https://doi.org/10.1039/C6AY02558G.
Shimao, M., 2001. Biodegradation of plastics. Curr. Opin. Biotechnol. 12, 242–247. https://doi.org/10.1016/S0958-1669(00)00206-8.
Shruti, V., Kutralam-Muniasamy, G., 2019. Bioplastics: missing link in the era of microplastics. Sci. Total Environ. 697. https://doi.org/10.1016/j.scitotenv.2019.134139.
Siegenthaler, K., Künkel, A., Skupin, G., Yamamoto, M., 2012. Ecoflex® and Ecovio®: biodegradable, performance-enabling plastics. Synthetic biodegradable polymers. Adv. Polym. Sci. 245, 91–136. https://doi.org/10.1007/12_2010_106.
Signori, F., Coltelli, M., Bronco, S., 2009. Thermal degradation of poly(lactic acid) (PLA) and poly(butylene adipate-co-terephthalate) (PBAT) and their blends upon melt processing. Polym. Degrad. Stab. 94, 74–82. https://doi.org/10.1016/j.polymdegradstab.2008.10.004.
Sikorska, W., Rydz, J., Wolna-Stypka, K., Musioł, M., Adamus, G., Kwiecień, I., Janeczek, H., Duale, K., Kowalczuk, M., 2017. Forensic engineering of advanced polymeric materials—part V: prediction studies of aliphatic–aromatic copolyester and polylactide commercial blends in view of potential applications as compostable cosmetic packages. Polymers 9. https://doi.org/10.3390/polym9070257.
Silva, A., Bastos, A., Justino, C., da Costa, J., Duarte, A., Rocha-Santos, T., 2018. Microplastics in the environment: challenges in analytical chemistry - a review. Anal. Chim. Acta 1017, 1–19. https://doi.org/10.1016/j.aca.2018.02.043.
Sintim, H., Bary, A., Hayes, D., English, M., Schaeffer, S., Miles, C., Zelenyuk, A., Suski, K., Flury, M., 2019. Release of micro- and nanoparticles from biodegradable plastic during in situ composting. Sci. Total Environ. 675, 686–693. https://doi.org/10.1016/j.scitotenv.2019.04.179.
Siwek, P., Domagala-Swiatkiewicz, I., Bucki, P., Puchalski, M., 2019. Biodegradable agroplastics in 21st century horticulture. Polimery 64, 480–486. https://doi.org/10.14314/polimery.2019.7.2.
Song, Y., Hong, S., Jang, M., Han, G., Rani, M., Lee, J., Shim, W., 2015. A comparison of microscopic and spectroscopic identification methods for analysis of microplastics in environmental samples. Mar. Pollut. Bull. 93, 202–209. https://doi.org/10.1016/j.marpolbul.2015.01.015.
Steinmetz, Z., Wollmann, C., Schaefer, M., Buchmann, C., David, J., Tröger, J., Muñoz, K., Frör, O., Schaumann, G., 2016. Plastic mulching in agriculture. Trading short-term agronomic benefits for long-term soil degradation? Sci. Total Environ. 550, 690–705. https://doi.org/10.1016/j.scitotenv.2016.01.153.
Steinmetz, Z., Kintzi, A., Muñoz, K., Schaumann, G., 2020. A simple method for the selective quantification of polyethylene, polypropylene, and polystyrene plastic debris in soil by pyrolysis-gas chromatography/mass spectrometry. J. Anal. Appl. Pyrolysis 147. https://doi.org/10.1016/j.jaap.2020.104803.
Sun, J., Dai, X., Wang, Q., van Loosdrecht, M., Ni, B., 2019. Microplastics in wastewater treatment plants: detection, occurrence and removal. Water Res. 152, 21–37. https://doi.org/10.1016/j.watres.2018.12.050.
Tabasi, R.Y., Ajji, A., 2015. Selective degradation of biodegradable blends in simulated laboratory composting. Polym. Degrad. Stab. 120, 435–442. https://doi.org/10.1016/j.polymdegradstab. 2015.07.020.
Tagg, A., Harrison, J., Ju-Nam, Y., Sapp, M., Bradley, E., Sinclair, C., Ojeda, J., 2017. Fenton's reagent for the rapid and efficient isolation of microplastics from wastewater. Chem. Commun. 53, 372–375. https://doi.org/10.1039/C6CC08798A.
Taufik, D., Reinders, M., Molenveld, K., Onwezen, M., 2020. The paradox between the environmental appeal of bio-based plastic packaging for consumers and their disposal behaviour. Sci. Total Environ. 705. https://doi.org/10.1016/j.scitotenv.2019.135820.
Thompson, R., 2004. Lost at sea: where is all the plastic? Science 304, 838. https://doi.org/10.1126/science.1094559.
Torri, C., Cordiani, H., Samorì, C., Favaro, L., Fabbri, D., 2014. Fast procedure for the analysis of poly(hydroxyalkanoates) in bacterial cells by off-line pyrolysis/gas-chromatography with flame ionization detector. J. Chromatogr. A 1359, 230–236. https://doi.org/10.1016/j.chroma.2014.07.008.
Tsuji, H., Suzuyoshi, K., 2002. Environmental degradation of biodegradable polyesters 1. Poly(ε-caprolactone), poly[(R)-3-hydroxybutyrate], and poly(L-lactide) films in controlled static seawater. Polym. Degrad. Stab. 75, 347–355. https://doi.org/10.1016/S0141-3910(01)00240-3.
Ubeda, S., Aznar, M., Alfaro, P., Nerín, C., 2019. Migration of oligomers from a food contact biopolymer based on polylactic acid (PLA) and polyester. Anal. Bioanal. Chem. 411, 3521–3532. https://doi.org/10.1007/s00216-019-01831-0.

Van Cauwenberghe, L., Claessens, M., Vandegehuchte, M., Mees, J., Janssen, C., 2013. Assessment of marine debris on the Belgian Continental Shelf. Mar. Pollut. Bull. 73, 161–169. https://doi.org/10.1016/j.marpolbul.2013.05.026.

Van de Velde, K., Kiekens, P., 2002. Biopolymers: overview of several properties and consequences on their applications. Polym. Test. 21, 433–442. https://doi.org/10.1016/S0142-9418(01)00107-6.

Velasco Alvarez, M., ten Pierick, A., van Dam, P., Maleki Seifar, R., van Loosdrecht, M., Wahl, S., 2017. Microscale quantitative analysis of polyhydroxybutyrate in prokaryotes using IDMS. Metabolites 7. https://doi.org/10.3390/metabo7020019.

Vert, M., Doi, Y., Hellwich, K., Hess, M., Hodge, P., Kubisa, P., Rinaudo, M., Schué, F., 2012. Terminology for biorelated polymers and applications (IUPAC recommendations 2012). Pure Appl. Chem. 84, 377–410. https://doi.org/10.1351/PAC-REC-10-12-04.

Wan, L., Zhou, S., Zhang, Y., 2019. Parallel advances in improving mechanical properties and accelerating degradation to polylactic acid. Int. J. Biol. Macromol. 125, 1093–1102. https://doi.org/10.1016/j.ijbiomac.2018.12.148.

Wang, L., Zhang, J., Hou, S., Sun, H., 2017. A simple method for quantifying polycarbonate and polyethylene terephthalate microplastics in environmental samples by liquid chromatography–tandem mass spectrometry. Environmental Science & Technology Letters 4, 530–534. https://doi.org/10.1021/acs.estlett.7b00454.

Ward, C., Armstrong, C., Walsh, A., Jackson, J., Reddy, C., 2019. Sunlight converts polystyrene to carbon dioxide and dissolved organic carbon. Environmental Science & Technology Letters 6, 669–674. https://doi.org/10.1021/acs.estlett.9b00532.

Weng, Y., Jin, Y., Meng, Q., Wang, L., Zhang, M., Wang, Y., 2013. Biodegradation behavior of poly(butylene adipate-co-terephthalate) (PBAT), poly(lactic acid) (PLA), and their blend under soil conditions. Polym. Test. 32, 918–926. https://doi.org/10.1016/j.polymertesting.2013.05.001.

Werker, A., Lind, P., Bengtsson, S., Nordström, F., 2008. Chlorinated-solvent-free gas chromatographic analysis of biomass containing polyhydroxyalkanoates. Water Res. 42, 2517–2526. https://doi.org/10.1016/j.watres.2008.02.011.

Wong, J.K.H., Lee, K.K., Tang, K.H.D., Yap, P.S., 2020. Microplastics in the freshwater and terrestrial environments: prevalence, fates, impacts and sustainable solutions. Sci. Total Environ. 719, 137512. https://doi.org/10.1016/j.scitotenv.2020.137512.

Yu, J., Wang, P., Ni, F., Cizdziel, J., Wu, D., Zhao, Q., Zhou, Y., 2019. Characterization of microplastics in environment by thermal gravimetric analysis coupled with Fourier transform infrared spectroscopy. Mar. Pollut. Bull. 145, 153–160. https://doi.org/10.1016/j.marpolbul.2019.05.037.

Zhang, S., Yang, X., Gertsen, H., Peters, P., Salánki, T., Geissen, V., 2018. A simple method for the extraction and identification of light density microplastics from soil. Sci. Total Environ. 616-617, 1056–1065. https://doi.org/10.1016/j.scitotenv.2017.10.213.

Zhao, P., Liu, W., Wu, Q., Ren, J., 2010. Preparation, mechanical, and thermal properties of biodegradable polyesters/poly(lactic acid) blends. J. Nanomater. 2010, 1–8. https://doi.org/10.1155/2010/287082.

Zilliges, Y., Damrow, R., 2017. Quantitative determination of poly-β-hydroxybutyrate in Synechocystis sp. PCC 6803. BIO-PROTOCOL 7. https://doi.org/10.21769/BioProtoc.2402.

Zuo, L., Li, H., Lin, L., Sun, Y., Diao, Z., Liu, S., Zhang, Z., Xu, X., 2019. Sorption and desorption of phenanthrene on biodegradable poly(butylene adipate co-terephtalate) microplastics. Chemosphere 215, 25–32. https://doi.org/10.1016/j.chemosphere.2018.09.173.

polymers

MDPI

Article

Slow-Release Nitrogen Fertilizers with Biodegradable Poly(3-hydroxybutyrate) Coating: Their Effect on the Growth of Maize and the Dynamics of N Release in Soil

Soňa Kontárová [1,*], Radek Přikryl [1], Petr Škarpa [2], Tomáš Kriška [2], Jiří Antošovský [2], Zuzana Gregušková [1], Silvestr Figalla [1], Vojtěch Jašek [1], Marek Sedlmajer [1], Přemysl Menčík [1] and Mária Mikolajová [3]

[1] Institute of Materials Chemistry, Faculty of Chemistry, Brno University of Technology, 61200 Brno, Czech Republic
[2] Department of Agrochemistry, Soil Science, Microbiology and Plant Nutrition, Mendel University in Brno, 61200 Brno, Czech Republic
[3] Institute of Natural and Synthetic Polymers, Faculty of Chemical and Food Technology, Slovak University of Technology in Bratislava, Radlinského 9, 812 37 Bratislava, Slovakia
* Correspondence: kontarova@fch.vut.cz

Abstract: Fertilizers play an essential role in agriculture due to the rising food demand. However, high input fertilizer concentration and the non-controlled leaching of nutrients cause an unwanted increase in reactive, unassimilated nitrogen and induce environmental pollution. This paper investigates the preparation and properties of slow-release fertilizer with fully biodegradable poly(3-hydroxybutyrate) coating that releases nitrogen gradually and is not a pollutant for soil. Nitrogen fertilizer (calcium ammonium nitrate) was pelletized with selected filler materials (poly(3-hydroxybutyrate), struvite, dried biomass). Pellets were coated with a solution of poly(3-hydroxybutyrate) in dioxolane that formed a high-quality and thin polymer coating. Coated pellets were tested in aqueous and soil environments. Some coated pellets showed excellent resistance even after 76 days in water, where only 20% of the ammonium nitrate was released. Pot experiments in Mitscherlich vegetation vessels monitored the effect of the application of coated fertilizers on the development and growth of maize and the dynamics of N release in the soil. We found that the use of our coated fertilizers in maize nutrition is a suitable way to supply nutrients to plants concerning their needs and that the poly(3-hydroxybutyrate) that was used for the coating does not adversely affect the growth of maize plants.

Keywords: slow-release; nitrogen fertilizers; coating; poly(3-hydroxybutyrate); ammonium nitrate; biodegradable; dioxolane; biomass; control-release; maize

check for updates

Citation: Kontárová, S.; Přikryl, R.; Škarpa, P.; Kriška, T.; Antošovský, J.; Gregušková, Z.; Figalla, S.; Jašek, V.; Sedlmajer, M.; Menčík, P.; et al. Slow-Release Nitrogen Fertilizers with Biodegradable Poly(3-hydroxybutyrate) Coating: Their Effect on the Growth of Maize and the Dynamics of N Release in Soil. *Polymers* **2022**, *14*, 4323. https://doi.org/10.3390/polym14204323

Academic Editors: Gabriella Santagata, Arash Moeini and Pierfrancesco Cerruti

Received: 22 September 2022
Accepted: 12 October 2022
Published: 14 October 2022

Publisher's Note: MDPI stays neutral with regard to jurisdictional claims in published maps and institutional affiliations.

Copyright: © 2022 by the authors. Licensee MDPI, Basel, Switzerland. This article is an open access article distributed under the terms and conditions of the Creative Commons Attribution (CC BY) license (https://creativecommons.org/licenses/by/4.0/).

1. Introduction

The importance of fertilizers for the human population is indisputable. Without the Haber–Bosch synthesis of ammonia (commercialized in 1913), and the subsequent synthetic nitrogen compounds and their applications, we would not be able to produce more than half of today's world food [1]. Due to the rapid growth of the population by 2–3 million people in the next 80 years, more crop production will be needed, which will also increase the need for fertilizers [2,3]. Fertilizers provide plants with fundamental macronutrients (nitrogen/phosphorus/potassium), where nitrogen is essential to plant growth [4]. However, crops' poor absorption of nutrients from fertilizers and the related losses of nitrogen in the soil, water, and air caused a cascade of environmental problems [5]. Despite the fact that the use of nitrogen fertilizers plays an essential role in meeting the demand for crop production, nitrogen use efficiency is relatively low due to their excessive use (in general between 25 and 50%), which often leads to losses of redundant nitrogen from agroecosystems [6]. Environmental problems include eutrophication and the expansion of

dead zones in coastal ocean waters resulting from the leaching of nitrates into rivers, lakes, ponds, and ground waters. The atmospheric deposition of ammonia and nitrates affects natural ecosystems; nitrous oxide (N_2O) is now the third most crucial greenhouse gas, following CO_2 and CH_4 [1,4]. The excessive use of fertilizers can cause soil acidification, depletion of soil cations, reduction of carbon uptake, and contamination with heavy metals. All this negatively influences animal and human health, the environment, biodiversity, and the climate [7,8]. Even more significant losses of nitrogen in the environment (that will occur with a growing population) could be reduced by more moderate meat consumption, low-protein animal feeding, better agronomic management, and a portfolio that includes split applications and balanced use of fertilizers, precision farming, optimized crop rotations, and the use of expensive slow-release compounds [1].

Controlled- and slow-release fertilizers (CRFs and SRFs) provide a more efficient, economical, and safe way to deliver nutrients to plants. They are able to retain nutrients in the soil for a longer period, as they are available for the plants at the desired rate or concentration level. Thus, nutrient utilization efficiency (NUE) improves due to less frequent dosing and reduced nutrient removal from the soil by rain or irrigation, which also reduces environmental hazards [4,9–12]. Slow- or controlled-release fertilizers are a good alternative to conventional mineral fertilizers, and their use allows for a reduction of the fertilizer rate by 20% or 30% of the recommended value to achieve the same yield [13]. Slow-release fertilizers are described as "low solubility compounds with a complex/high molecular weight chemical structure that releases nutrients through either microbial or chemically decomposable compound" [4,14]. Controlled-release fertilizers (CRFs) can be described as "products containing sources of water-soluble nutrients, the release of which in the soil is controlled by a coating applied to the fertilizer" [4,15]. SRFs are usually classified into "condensation products of urea-aldehydes, fertilizers with a physical barrier (coated or incorporated into the matrix), and super granules. CRF is a subset of SRF, which falls under the category of fertilizer with a physical barrier" [4].

Current commercial CRFs with polymer coatings are often made of a thermoplastic resin such as polyolefin, polyvinylidene chloride, and copolymers, which cannot degrade easily in soil and accumulate over time. Generally, these CRFs containing synthetic, non-biodegradable polymers accumulate up to 50 kg/ha per year in the soil after releasing their nutrients, remaining and causing white pollution [4,16]. With the agreement of the European Green Deal, EU Fertilizing Products Regulation (FPR), and Circular Economy Action Plan, manufacturers are faced with significant challenges; they will have to adapt their current practices to the new FPR requirements, including biodegradability criteria for polymer coatings of controlled-release fertilizers [4,17].

The present study aimed to prepare CRFs with a coating of a biodegradable nature. The pelletization of powder fertilizer ammonium nitrate with dolomite (CAN) with selected additive materials (poly(3-hydroxybutyrate) P3HB, struvite, dried biomass containing P3HB) has become the most technologically feasible. Using struvite and biomass from P3HB extraction meets the requirements of the circular economy. P3HB can be made from waste cooking oil and a variety of byproducts [18–21]. However, pellets alone without a non-defective coating would not meet the requirements of slow release. A 6% solution of fully biodegradable P3HB with green solvent dioxolane [22] was applied to the pellets by 6-fold immersion [23] and produced a good quality coating.

The kinetics of fertilizer release from coated pellets in an aqueous environment was monitored by the conductometry method. The results showed the high quality of the prepared water-barrier polymer coating. The dynamics of mineral nitrogen release of these CRFs were studied under laboratory conditions, followed by an evaluation of the effectiveness of the newly developed coated fertilizers on maize growth and an assessment of their effects on soil mineral nitrogen content. We assumed that the coated CAN-based fertilizers would reduce the environmental load in the soil without simultaneously limiting plant growth.

2. Materials and Methods

2.1. Preparation of Coated and Encapsulated Fertilizers

2.1.1. The Fertilizer

The fertilizer used in pellets was calcium ammonium nitrate (CAN) supplied by Lovochemie, a.s. (Lovosice, Czech Republic) [24]. CAN is a nitrogen fertilizer containing 27% of nitrogen (up to 13.5% N-NH_4^+ and 13.5% N-NO_3^-) and 21% of dolomite (CAS 16389-88-1). It is a mixture of ammonium nitrate with finely ground dolomite in the form of whitish to light brown granules. Most particles (up to 90%) of CAN had a size in the range of 2–5 mm. Before pelletization, it was necessary to grind CAN into a powder on a grain mill (Sana Products Ltd., České Budějovice, Czech Republic) and sieve (Sana mesh sieve, pore size 0.5 × 0.5 (mm × mm)). Thus, the CAN was finally below 0.5 mm.

2.1.2. Filling Material in Pellets

The primary filler material (together with the fertilizer) in the pellets prepared manually using a hydraulic press was poly-3-hydroxybutyrate (P3HB, ρ = 1.23 g·cm^{-3}, M_w = 450,000 g·mol^{-1}, purity 98–99%) supplied by TianAn Biopolymer (Ningbo, People's republic of China) [25] and commercially purified in acetone as a white powder (Nafigate Corporation, Prague, Czech Republic) [26].

Another filler material used in some fertilizer mixtures was a struvite ($NH_4MgPO_4 \cdot 6H_2O$). A homogenized mixture of struvite from Nafigate and Aldrich (Merck KGaA, St. Louis, Missouri, USA) [27], in the form of a white powder, free of lumps by sieving, was used.

Dried biomass was also used in some mixtures with fertilizer as a filler material. The biomass was supplied by Nafigate Corporation and was produced from waste cooking oil by fermentation with a bacterial culture of *Cupriavidus necator* H16. The specific procedure for biomass production is described in [18]. After cultivation, the biomass was concentrated by centrifugation to 50% dry matter and stored frozen at −20 °C. It was dried at 105 °C to constant weight before use. Before pelletization, the lumps were removed by sieving. The dried biomass contained about 60% P3HB.

2.1.3. Preparation of Fertilizer Pellets

Pelletization was performed by compressing powdered materials of fertilizer CAN and other filler materials (P3HB, struvite, dried biomass containing P3HB) into pellets using a manual hydraulic press SPECAC (Orpington, Great Britain) [28] with a compressive force equivalent to 2 tons. Each resulting pellet had weight = 0.5 g, height = 4 mm, and diameter = 10 mm (approx.). Before the powder mixture preparation and homogenization, the fertilizer powder and P3HB powder were dried in an oven at 60 °C overnight and freed of lumps with a sieve (other filler materials: struvite and biomass were also sieved, and the sieve pore size was 0.5 × 0.5 (mm × mm)). Several series of cold-pressed pellets were prepared and composed of: 50% fertilizer CAN + 50% P3HB, 50% CAN + 50% biomass, 50% CAN + 25% P3HB + 25% struvite and 100% CAN serving as reference.

2.1.4. The Material for the Coating Solution

Coatings were prepared with a 6% solution of P3HB dissolved in chloroform with amylene (($CHCl_3$, M_r = 119.38; 99.93%, stabilized with amylene max. 55 ppm, supplied by Lach-Ner Ltd. (Neratovice, Czech Republic) [29]), then a 7% solution of P3HB in chloroform with ethanol ((99.8%, stabilized with approx. 1% ethanol p.a., supplied by PENTA Ltd. (Chrudim, Czech Republic) [30]) and 6% solution of P3HB in 1,3-dioxolane (($C_3H_6O_2$, M_w = 74.08 g·mol^{-1}, density 1.07 kg/L, stabilized with 0.03% BHT (2,6-Di-Tert-Butyl-4-Methylphenol), supplied by VWR International Ltd. (Stříbrná Skalice, Czech Republic) [31]). The solutions were prepared for preliminary tests of coating solutions and for dip coating of pelletized fertilizers purposes.

2.1.5. Coating of Fertilizer Pellets and Encapsulation

Finally, after preliminary tests of coating solutions, dioxolane was chosen as the best solvent for preparing the coating solution. The prepared pellets were coated manually by dipping them six times in a beaker with a 6% coating solution of P3HB in dioxolane.

The preparation of 6% P3HB in dioxolane for manual coating was first carried out by dissolving in an oven at a temperature of 90–95 °C approx. 1.5–2 h. However, new and faster ways of preparing larger volumes of solutions (at least 2000 mL) for later coating in a coating drum were sought (will be part of another article).

The resulting coating solution had suitable viscosity, and the final coating weight was only 12–17% of the original pellet weight (depending on the composition of the pellet to which the coating was applied).

The prepared pellets of 50% CAN + 50% P3HB were also encapsulated in an experimental biodegradable film based on P3HB, thermoplastic starch TPS, and PLA instead of coating. The biodegradable film was prepared by Panara Nitra (Slovakia, [32]) with Slovak University of Technology in Bratislava (Bratislava, Slovakia, [33]). The intention was to use biodegradable films based on P3HB and auxiliary polymers that were developed for complete decomposition in environmental components. These foils were prepared to use fully degradable agricultural foils, both in compost and in soils. An annular welding head was tailor-made for encapsulation that was electrically heated to a suitable temperature close to the melting point of the film (approx. 160 °C). By applying the appropriate pressure and time, a defect-free connection around the entire pellet was achieved. These encapsulated pellets were also tested in aqueous and soil environments.

2.2. Testing Nitrogen Release from Coated Fertilizer

The conductometric method monitored the release of ammonium and nitrate nitrogen in the aqueous medium from our six times hand-coated and encapsulated pellets prepared on a hydraulic press.

Ammonium nitrate is an inorganic, highly soluble fertilizer that dissociates into individual ions in aqueous environments: ammonium (NH_4^+) and nitrate (NO_3^-). The solubility of ammonium nitrate is 213 g/100 g H_2O [34], and conductometry can be used to determine the solvated fraction. Conductometry is a method based on measuring the conductivity of the second type of conductor: a solution whose conductivity is ensured by the ions present. The specific conductivity of the solution (κ) is related to the conductance (G), which can be determined by measuring the electric current flowing between the two electrodes of the conductometric probe through free charge carriers (ions). The conductance (G) is a quantity depending on the geometry of the measuring probe, and therefore it is used only to obtain a specific conductance (κ). Since, in the case of fertilizer analysis, there is a fundamental relationship between ion concentration (c_{Ion}) and specific conductance (κ), we describe the dependence of conductivity on ion concentration by the molar conductivity quantity (Λ_m):

$$G = \kappa \cdot \frac{A}{l} \quad (1)$$

G ... conductance (S)
κ ... specific conductivity ($S \cdot cm^{-1}$)
A ... probe electrode area (cm^2)
l ... probe electrode distance (cm)

$$\kappa = \Lambda_m \cdot c_{Ion} \quad (2)$$

Λ_m ... molar conductivity ($S \cdot cm^2 \cdot mol^{-1}$)
c_{Ion} ... ion concentration ($mol \cdot cm^{-3}$) [35]

The measurements of nutrient loss from the prepared pellets were performed in closable plastic test tubes with a volume of 50 mL. For all tests, one pellet (approx. 0.5 g) of fertilizer compressed into the form of a carrier with additives was placed in test tubes with

a volume of distilled water of 40 mL. Ten pellets were measured for each experimental formulation, and the results were averaged. The measurements were performed at laboratory conditions (temperature 22 °C). The current signal was electronically converted to a frequency. The dependence of the change in the frequency of the alternating current on time was measured using a METEX® M-3850D multimeter (Metex Corporation, Toronto, Canada) [36]. Values were recorded initially after 24 h, and then the frequency of monitoring was reduced as necessary, and the time interval between measurements was usually 48 h. The method of calibration dependence between the frequency of alternating current and electrolyte concentration was used to monitor the mass transport of the nutrients from controlled release fertilizer. The calibration dependences were fitted using the Origin program (OriginLab, Northampton, MA, USA) [37] with two exponential fits to obtain the calibration dependence equation. Finally, the weight loss of the fertilizer was determined from this calibration dependence equation. We counted 21% dolomite content in the CAN fertilizer in the calculations of ammonium and nitrate loss from the pellets.

2.3. The Greenhouse Pot Experiment

The pot greenhouse experiment aimed to verify the effect of the application of coated fertilizers on the development and growth of maize and the dynamics of N release in the soil. A pot experiment was established in the vegetation hall of Mendel University in Brno (Brno, Czech Republic), evaluating the effect of fertilizing of coated fertilizers applied during the sowing period of maize.

2.3.1. Experimental Design

The experiment was performed in Mitscherlich vegetation pots (on 6.5 kg of soil). Five kg of soil was weighed into each pot. Maize (6 seeds per pot) was sown on the soil surface followed by uniform coverage with soil (750 g). Fertilizers were manually spread on the surface of this layer and evenly covered with another 750 g of soil (Figure 1). The basic agrochemical properties of the soil used in the pot experiment are presented in Table 1. SY Orpheus maize variety from Syngenta (Oseva, a.s., Bzenec, Czech Republic) [38] was used in the experiment. The pot experiment was performed under semi-natural conditions (rain shelter) in the vegetation hall. An identical controlled watering regime was used for all pots during the experiment. Plants were watered to 70% of maximum water holding capacity throughout the growing season. The pots were hand-watered with demineralized water on the soil surface.

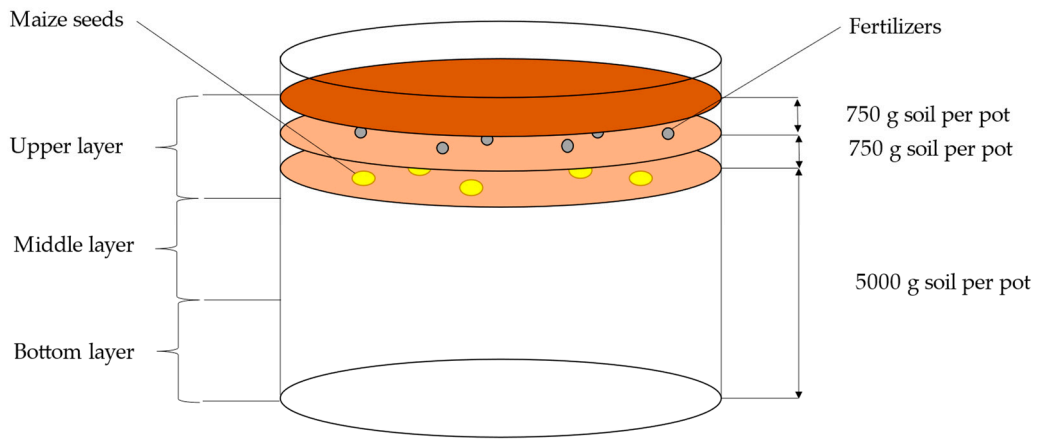


Figure 1. Scheme of Mitscherlich vegetation pot.

Table 1. Agrochemical properties of used soil in the pot experiment.

Soil Parameters	Value	Ref.
Clay	20%	
Dust	27%	[39]
Sand	53%	
Oxidizable C content (Cox)	0.80%	[40]
pH ($CaCl_2$)	6.09	
Cation exchange capacity	164 mmol/kg	
Noverall	0.19%	
NH_4^+ (K_2SO_4)	1.48 mg/kg	
NO_3^- (K_2SO_4)	17.2 mg/kg	[41]
P (Mehlich 3)	36.4 mg/kg	
K (Mehlich 3)	400 mg/kg	
Ca (Mehlich 3)	2720 mg/kg	
Mg (Mehlich 3)	214 mg/kg	

The fertilization treatments used in the experiment are presented in Table 2.

Table 2. Scheme of the pot experiment with maize.

Treatment	Composition of Pellets Used in Vegetation Tests	Number of Pellets (pcs/Pot)	N Dose (g/Pot)
CAN-c	100% CAN with P3HB coating	4	0.54
CAN/P-c	50% CAN + 50% P3HB with P3HB coating	8	0.54
CAN/P/S-c	50% CAN + 25% P3HB + 25% struvite with P3HB coating	8	0.54
CAN/P/B-c	50% CAN + 50% biomass with P3HB coating	8	0.54
CAN/P-bf	50% CAN + 50% P3HB encapsulated in biodegradable film	8	0.54
CAN	100% CAN (positive reference)	4	0.54
CON-c	without fertilizer (negative reference)	0	0

Each of these treatments was based on 12 replicates (pots) distributed in the vegetation hall at random. Maize was sown on 18 March 2021. The influence was monitored of the applied fertilizers on plant growth and nitrogen content in the soil profile after the establishment of the experiment (sowing) in regular 3-week intervals (t_1 = 8 April; t_2 = 29 April; and t_3 = 20 May 2021). After emergence (29 March 2021), the maize plants were adjusted to a final number of three plants per pot. Soil and plant analyses were performed during the vegetation.

2.3.2. Soil and Plant Sampling and Analyses

Soil sampling was carried out at the observed intervals (t_1–t_3) for each variant (each variant from four pots in each term). Soil samples were collected from each pot from three soil profile depths (upper, middle, and bottom layer, Figure 1). The contents of mineral nitrogen (Nmin)—ammonium (NH_4^+) and nitrate (NO_3^-) were determined in the soil samples [42].

The effects of the coated fertilizers on the growth of maize plants were monitored during the experiment at identical intervals (terms t_1–t_3). Chlorophyll content (N tester value), vegetative index (NDVI), basic photosynthetic parameters based on the action and measurement of light signal in PS II, dry weight of maize aboveground biomass (AGB), nitrogen content in AGB and capacitance of the root system were evaluated in plants (Table 3).

Table 3. Observed plant growth parameters.

Plant Parameter	Device Used	Terms	Ref.
Chlorophyll content (N-tester value)	Yara N-Tester chlorophyll meter (Yara International ASA, Oslo, Norway)	t1–t3	[43]
Vegetation index (NDVI)	PlanPen NDVI310 device (Photon Systems Instruments, Drásov, Czech Republic)	t1–t3	
Quantum yield of the PSII (Φ_{PSII})	PAR-Fluorpen FP110-LM/D device (Photon Systems Instruments, Drásov, Czech Republic)	t1–t3	[44]
Dry weight of AGB	Laboratory-scale PCB Kern (KERN & Sohn GmbH, Balingen, Germany)	t1–t3	
N content in AGB	Kjeltec 2300 device (Foss Analytical, Hillerød, Denmark)	t1–t3	[45]
Root electrical capacitance (C_R)	VOLTCRAFT LCR 4080 (Conrad Electronic GmbH, Wels, Austria)	t3	[44]

2.3.3. Statistical Data Analysis

The soils and plants were analyzed in STATISTICA 12 software [46] using Tukey's analysis of variance followed by testing at the 95% level of significance ($p \leq 0.05$). Normality and homogeneity of variances were checked using the Shapiro–Wilk test and Levene's test. In the case of the greenhouse pot experiment, the results are expressed as arithmetic mean ± standard error (SE).

3. Results

Several mixtures (formulations) of fertilizer and filler materials were successfully prepared by compressing powdered fertilizer (CAN) with filler materials (P3HB, struvite, dried biomass containing P3HB) into pellets using a manual hydraulic press. The coating was performed manually by dipping them six times in a beaker with a 6% coating solution of P3HB in dioxolane.

3.1. Preliminary Tests of Coating Solutions

Dioxolane was finally chosen as a solvent for P3HB in the coating solution based on preliminary tests that compared coating solutions of 6% P3HB in dioxolane, 7% P3HB in chloroform with ethanol, and 6% P3HB in chloroform with amylene. A solution of 6% P3HB in dioxolane was prepared for this test in an oven at 90–95 °C for 2 h (however, now, we are able to reduce the time required to prepare the solution to only 25 min using stirred autoclave with a heating jacket). Coating solutions of P3HB with chloroform were prepared under reverse reflux at 65 °C for 1 h. Pellets prepared on a manual press composed of 50% CAN + 50% P3HB were selected for preliminary coating solution tests. After preparing the individual P3HB coating solutions, the pre-weighed pellets were soaked in beakers with these individual solutions, pulled out after 2–5 s, and dried on glass material for at least 30 min (under laboratory conditions). After each soaking and drying (coating layer formation), the pellets were weighed again. Six layers of the coating were applied in this way. The pellets were weighed again the next day to determine the final weight of the pellets after applying six coats of coating to ensure all solvents were evaporated. For clarity, we present the final evaluation of coating weights of the pellets after applying six layers of coating (see Table 4) and the overall evaluation of individual coating solutions.

Table 4. Average coating weights (in%) and standard deviation of the weight of the original pellets (n = 10) after applying six layers of coating.

Coating Solution	Coating Weights of the Pellets (%)
7% P3HB in chloroform with ethanol	82.4 ± 4.6
6% P3HB in dioxolane	19.9 ± 1.5
6% P3HB in chloroform with amylene	Failed to form an acceptable coating

A solution of 7% P3HB in chloroform with ethanol seemed to be more gel-like. It was harder to apply and evaporated more slowly but created a quality coating that did not crack. Still, the resulting coating is too heavy. Boyandin et al. [23] acquired after the application of 6 layers approx. 60% extra pellet weight. A solution of 6% P3HB in dioxolane was applied well and quickly (lower viscosity), evaporated faster than chloroform, created a quality coating that does not crack, and the significant advantage was that the resulting 6-times coating was only (19.9 ± 1.5)% of the weight of the original pellet. A solution of 6% P3HB in chloroform with amylene was unusable; the solution was applied well at first, but the coating cracked at the second layer and was highly defective (see Figure S1). Although six-layer pellets were finally weighed, the resulting weight was irrelevant.

Although these individual solutions were not tested on a large number of pellets, the differences were so significant that in terms of quality and weight of the formed 6-times coating, a solution of 6% P3HB in dioxolane was a clear choice. A solution of 7% P3HB in chloroform with ethanol also produced a quality coating. However, due to the enormous weight of the applied coating (due to the high viscosity of the solution), this solution is disadvantageous and not so well used for manual coating on a laboratory scale, even when coating in a coating drum. Using a solution of P3HB in dioxolane, which has a suitable viscosity, we achieved a high-quality multiple coating: only 20% of the extra coating weight on the pellet is a significant improvement. Therefore, the solution of P3HB in dioxolane was best for application; dioxolane evaporated the fastest, and the resulting 6-times coating had excellent quality and the lowest weight. Legislative changes (Green Deal) have also contributed to the choice of dioxolane as a coating solvent. The advantage is also lower health risks when working with dioxolane. The disadvantages are its flammability and high price compared with chloroform.

3.2. Slow-Release Fertilizers

Pellets of various formulations were successfully prepared on a hydraulic press for further testing in aqueous and soil environments. These pellets contained CAN fertilizer, P3HB, struvite, and biomass in different composition. Approximately 120 pellets for each formulation were prepared. The pellets were coated manually with six layers using a solution of P3HB in dioxolane. Schematic representation of coated pellets can be seen in Figure 2 and coated pellets of different experimental formulations in Figure S2. Details of the pellet preparation and coating process were already described in the experimental part.

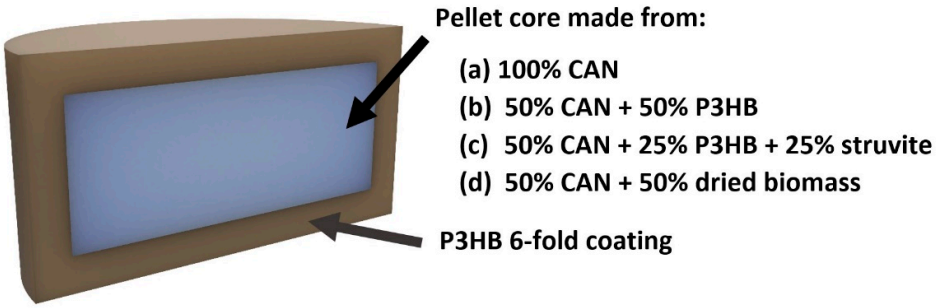


Figure 2. Schematic representation of coated pellets.

From each formulation, ten pellets were weighed before manual coating, and after pellets were coated with six layers of P3HB coating in dioxolane. The weighing of the coated pellets did not take place until the second day after manual coating so that the solvent could evaporate. Table 5 presents the calculated arithmetic mean ± standard deviation of the weight of the 6-fold coating applied to the pellets of different formulations (% of the original weight of the pellets). The resulting 6-fold coating of P3HB in dioxolane had finally even less weight than expected. In the case of pellets 50% P3HB with 50% CAN, the coating was approx. 17% by weight of the original pellet. For pellets that contained 50% CAN + 25% P3HB + 25% struvite or 50% CAN + 50% biomass, the resulting coating

had approx. 14% by weight of the original pellet. Finally, for pellets containing 100% CAN fertilizer, the coating had only approximately 12% by weight of the original pellet.

Table 5. Calculated average weight (%, n = 10) and standard deviation of manually applied 6-fold coating for all pellet formulations prepared on a hydraulic press.

Formulation	6-Fold Additional Coating Applied (% of Original Pellet Weight, Average and Standard Deviation)
100% CAN	11.9 ± 1.6
50% CAN + 50% P3HB	16.9 ± 2.5
50% CAN + 25% P3HB + 25% struvite	13.8 ± 2.8
50% CAN + 50% biomass	14.4 ± 2.4

3.3. Pellets Encapsulated in Foils

A special foil was used for the manual encapsulation of 0.5 g pellets with a composition of 50% CAN + 50% P3HB instead of coating (details described in Section 2). Pellets were created on a hydraulic press in the laboratory, and an experimental biodegradable film marked NR/75/267 (Manufacturer Panara Nitra, Slovakia, P3HB content 13%, thermoplastic starch TPS 22%) was used for encapsulation. The film achieves 50% decomposition in the soil, measured on the basis of exhaled CO_2 after 420 days. The biodegradability test leading to the complete decomposition of the film has not yet been completed.

The first versions of the pellets with the starch-containing films were too permeable in the weld. Foil welds were first solved by folding the foil and closing with a weld on three sides. As it turned out, it was not possible to prepare a weld without a defect in the corners. Therefore, the encapsulation geometry was changed to a circular shape. Thus, an annular welding head was made to measure, which was electrically heated to a suitable temperature close to the melting point of the film (approx. 160 °C). Both welded foils were placed in the mating piece between the Teflon foils to prevent the molten foil from adhering to the welding head and the mating piece. A defect-free connection around the entire pellet was achieved by applying the appropriate pressure and time. Thus, 120 pellets with a composition of 50% fertilizer CAN + 50% P3HB were encapsulated in the film for further testing in aqueous and soil environments (see Figures S3 and S4).

3.4. The Nitrogen Release from Coated Fertilizer in the Aquatic Environment

Measuring the loss of fertilizer from the prepared defined carriers in the aquatic environment (distilled water, laboratory conditions, conductometry method described in the experimental part) provided us only an indicative prediction for the subsequent use of fertilizers in the soil in terms of their "slow-release" quality. Nevertheless, it could early on be deduced from these tests whether the pellets and their subsequent coating were designed correctly in terms of their chemical composition and whether they were well prepared and coated so that there would be a gradual release of nitrogen in the soil.

The compositions of the individual manually coated fertilizer formulations prepared on a hydraulic press that were tested in the aqueous medium can be seen in Table 6. The release of ammonium nitrate (AN) in the aqueous medium from our six-fold manually-coated pellets (containing CAN fertilizer) was investigated by the conductometric method. Figure 3 shows the results of the measurement completed on day 76.

Table 6. The composition of six-fold manually coated fertilizer formulations prepared on a hydraulic press and tested in the aqueous medium.

Composition of 6-Fold Manually Coated Fertilizer Pellets	
CAN/P/B-$_C$	50% CAN + 50% biomass + coating P3HB in dioxolane
CAN/P-$_C$	50% CAN + 50% P3HB + coating P3HB in dioxolane
CAN/P/S-$_C$	50% CAN + 25% P3HB + 25% struvite + coating P3HB in dioxolane
CAN-c	100% CAN + coating P3HB in dioxolane
CAN	100% CAN (positive reference)
CAN/P-$_{bf}$	50% CAN + 50% P3HB + biodegradable polymeric film (encapsulation)

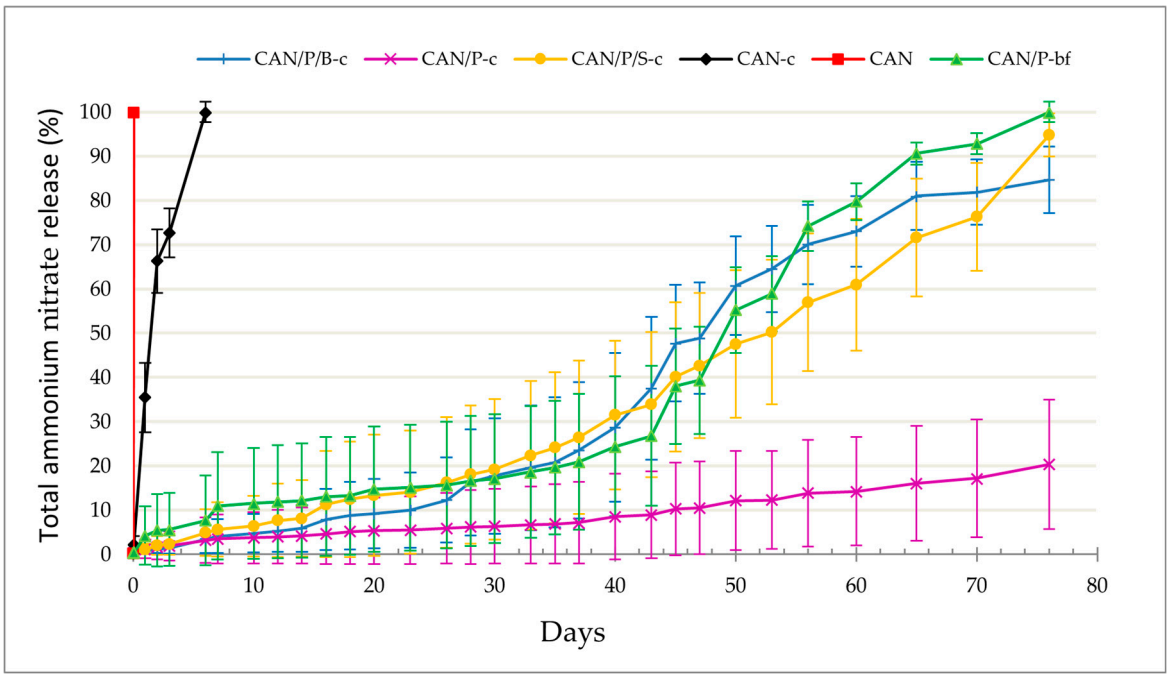


Figure 3. Release of ammonium nitrate (AN) from pellets of different compositions in the aquatic environment as a function of time. Total ammonium nitrate release in% is expressed as mean (n = 10), and the error bars represent the standard deviation. CAN-c: 100% CAN with P3HB coating; CAN/P-c: 50% CAN + 50% P3HB with P3HB coating; CAN/P/S-c: 50% CAN + 25% P3HB + 25% struvite with P3HB coating; CAN/P/B-c: 50% CAN + 50% biomass with P3HB coating; CAN/P-bf: 50% CAN + 50% P3HB encapsulated in biodegradable film; CAN: 100% CAN (positive reference).

As can be seen, all ammonium nitrate fertilizer was released immediately (in 1 h in the aquatic environment) from the reference (100% CAN without coating). The rapid release of fertilizer was also observed in coated pellets containing 100% CAN. Half of the AN was released from these pellets after approximately 1.5 days and all in 6 days. The adhesion of the 6-fold coating prepared on these pellets containing 100% CAN fertilizer was probably not as great as for pellets containing P3HB in addition to the fertilizer.

The release of AN from the coated pellets containing struvite, biomass, and pellets with foil instead of coating showed a similar course of fertilizer release. Half of the AN was released from pellets containing struvite on day 53, from pellets containing biomass approximately day 48, and from pellets with foil approximately day 49. However, at the end of the measurement (day 76), all ammonium nitrate was released from the foil pellets, while 95% of AN was released from the struvite-containing pellets and 85% of the AN from the pellets containing biomass. Significantly, the least AN was released from coated pellets containing 50% CAN and 50% P3HB. After 76 days, only 20% of the ammonium nitrate

was released. The nitrogen ammonium release curve of the fertilizer has an almost linear course in this interval (lag phase and linear phase [4]), which indicates a perfectly flawless coating. This flawless coating could have been formed due to the high adhesion of the P3HB coating (dissolved in dioxolane) to the pellets of this composition. This indicates that P3HB inside the pellet is essential as an adhesion promotor. In this case, a well-made coating acts as a polymer layer almost impermeable to water.

The results of water tests show that these pellets have the potential for the gradual release of nitrogen even in the soil environment. It is also clear that for a quality coating that adhered well to our pellets, it was necessary to add P3HB as an additive. On the 100% CAN pellets without P3HB, no coating was formed that would withstand the action of water for a long time. In comparison, the coating on the pellets containing 50% P3HB showed high resistance even after 76 days in water.

3.5. Efect of Coated Fertilizers in Greenhouse Experiment

Based on the identified potential of the coated and encapsulated fertilizers under aqueous test conditions, the pot vegetation experiment aimed to verify the effect of our different fertilizer formulations on the development and growth of maize and the dynamics of N release in the soil. The experiment took place in Mitscherlich's vegetation pots in the vegetation hall at the Mendel University Brno (Figure S5).

3.5.1. The Nitrogen Release from the Fertilizers in the Soil

During plant growth, soil sampling was performed at regular 3-week intervals to determine the mineral nitrogen content (described in the experimental part). Based on the content of mineral N (NH_4^+ and NO_3^-) determined in individual soil layers of the pot (upper, middle, and bottom layer) over time, the effect of coating on the dynamics of nitrogen release from our tested fertilizers was assessed.

In the first term (t_1) of soil collection (3 weeks after sowing/fertilization), it is evident that from uncoated fertilizer (CAN), nitrogen is released very quickly and leaches in the lower layer of soil profile due to watering. The NH_4^+ nitrogen supply in this treatment is relatively low, which is a consequence of the rapid release of this form N from fertilizer and its rapid nitrification (Figure S6a,b).

Coated fertilizers (CAN-c, CAN/P-c, CAN/P/S-c, and CAN/P/B-c) showed the ability to gradually release N. This was evidenced by the significantly high contents of ammonium N in the upper layer of the soil. In contrast with uncoated fertilizer (CAN), NH_4^+ was later released from modified coated fertilizers. The gradual release of N from these fertilizers was also evidenced by the low content of nitrates in the lower soil layer (Figure S6b). Its lowest values were reached in treatment with encapsulated fertilizer CAN/P-bf. The hydrolysis of encapsulated fertilizer was slowed down, and thus, the nitrification of the released NH_4^+ did not occur so intensively). Thus, the CAN/P-bf fertilizer (encapsulated pellets) showed the slowest N release. This is evidenced by the content of ammonium N in the soil (all layers), which was statistically the lowest in this treatment option.

The gradual nutrient release from coated fertilizers is evident in the soil analysis results performed 6 weeks after sowing of maize (t_2). The significantly highest NH_4^+ content in the upper and middle soil layer was recorded for all treatments with coated (CAN-c, CAN/P-c, CAN/P/S-c, and CAN/P/B-c) and encapsulated fertilizer CAN/P-bf (Figure S7a). There was a quite change in the content of soil N, especially at CAN-c (100% CAN with P3HB coating). The determined NH_4^+ content was the lowest of the coated fertilizers. This indicates its nitrification and horizontal shift (between t_1 and t_2). In the treatment fertilized with uncoated fertilizer (CAN), the nitrogen released from the fertilizer has long been uptake by plants or nitrified and leached into the lower layers, as evidenced by the ammonium ion supply in the soil, which was at the level of the non-fertilized treatment (CON-nf).

The highest nitrate nitrogen content in the soil was also recorded in the upper and middle part of the soil profile in treatments fertilized with coated fertilizers, especially in treatments CAN/P/S-c, and CAN/P/B-c (Figure S7b). Its increased amount in the soil is due to the gradual release of nitrates from coated CAN and gradual nitrification of ammonium N. The content of nitrates in the lower soil layer was compared between the treatments. If we compare this amount of NO_3^- with the values found in the term t_1 for treatment CAN (79.6 mg/kg), the use of coated fertilizers significantly reduced the risk of its leaching.

In soil analyses performed 9 weeks after sowing (t_3), it is evident that the plants depleted mineral nitrogen from the soil. This is evidenced by the very low contents of the ammonium and nitrate forms of N in all soil layers (Figure S8a,b). However, for both forms of acceptable nitrogen, there are apparent differences between the fertilizers used at this time. The significantly highest supply of NH_4^+ and NO_3^- was found on treatments fertilized with coated fertilizers (especially CAN/P/S-c, CAN/P/B-c) and encapsulated fertilizer CAN/P-bf.

The dynamics of the release of the monitored forms of mineral nitrogen from fertilizers are presented in Figure 4a,b. It is clear that coated fertilizers tend to retain nitrogen in the soil (soil profile), delay its conversion into leachable N (nitrate), contribute to eliminating its loss by leaching, and thus increase the efficiency of fertilization using nitrogen by plants.

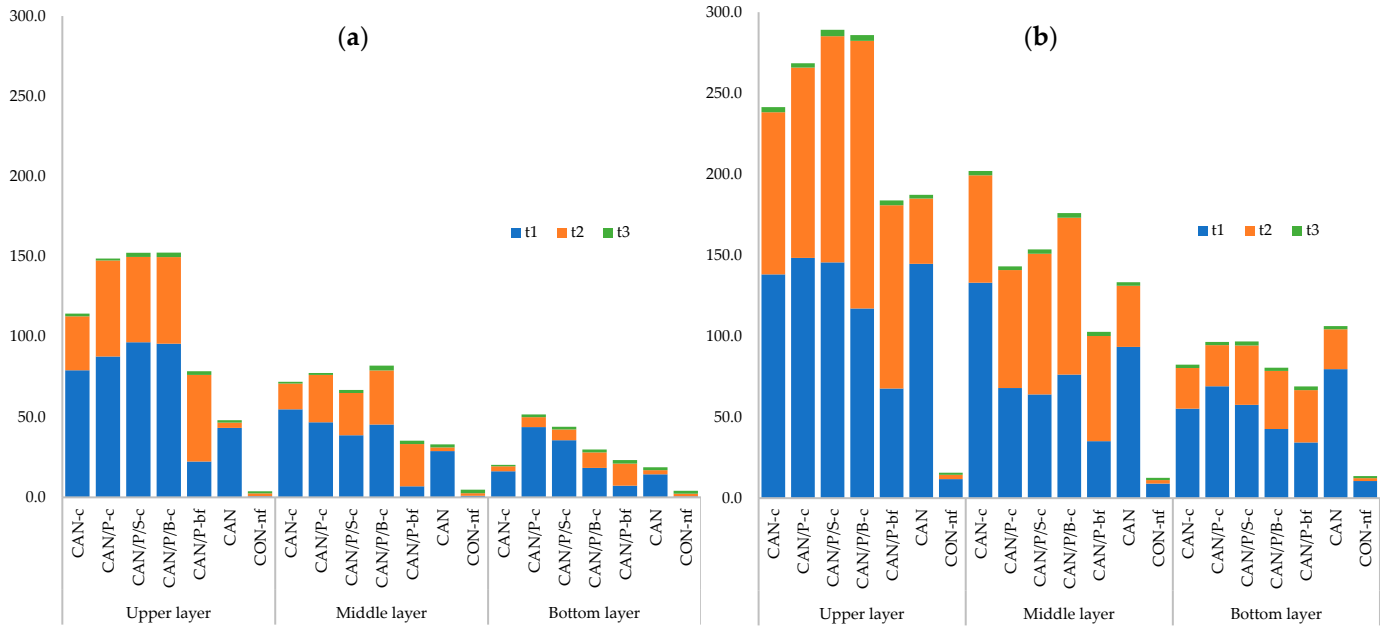


Figure 4. Development of ammonium (**a**) and nitrate (**b**) soil nitrogen content (mg/kg of soil) over time. CAN-c: 100% CAN with P3HB coating; CAN/P-c: 50% CAN + 50% P3HB with P3HB coating; CAN/P/S-c: 50% CAN + 25% P3HB + 25% struvite with P3HB coating; CAN/P/B-c: 50% CAN + 50% biomass with P3HB coating; CAN/P-bf: 50% CAN + 50% P3HB encapsulated in biodegradable film; CAN: 100% CAN (positive reference); CON-nf: without fertilizer (negative reference).

3.5.2. Effect of Coated and Encapsulated Fertilizers on Plant Biomass of Maize

In addition to the nitrogen content in the soil, the effect of the tested fertilizers on the production of plant matter and its quality was evaluated in a pot experiment. Plant biomass production was evaluated based on the assessment of the dry weight of maize plants in terms of t_1–t_3 and root system size (t_3). Biomass quality was determined by measuring chlorophyll content (N tester), development of vegetation index (NDVI), and selected photosynthetic parameters during vegetation (t_1–t_3).

Above-Ground Biomass Production and Root Size

The development of dry weight of maize aboveground biomass (AGB) production is presented in Figure 5. The dry weight of AGB was not significantly affected by fertilization in the initial stage (t_1). No significant differences between the fertilized treatments were found in other plant collection dates (t_2 and t_3) either. In this growth phase, the expected reduction in dry matter of AGB on the nitrogen unfertilized treatment (CON-nf) was confirmed. While the relatively highest dry matter yield of AGB was found on the CAN at t_2, at the end of the experiment (t_3) the highest dry matter production was obtained on the CAN/P/B-c coated fertilizer treatment.

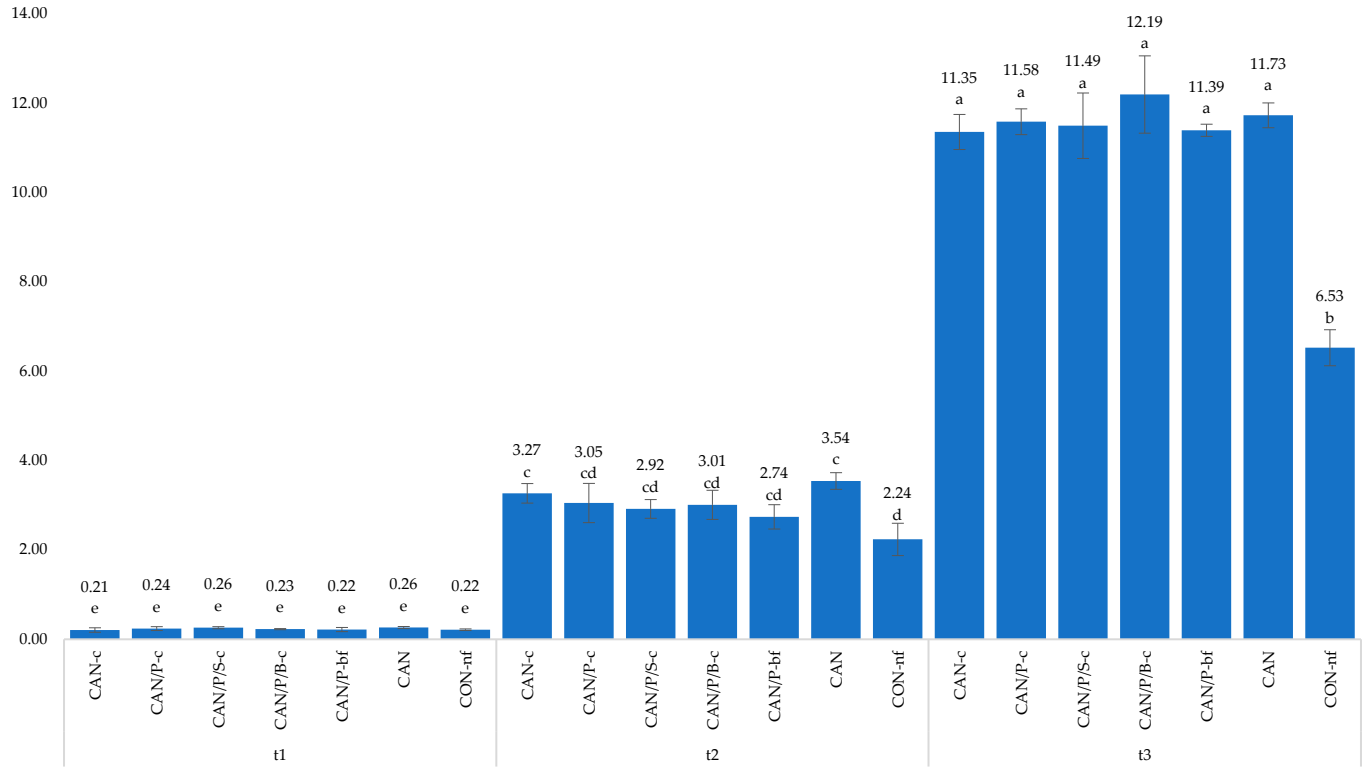


Figure 5. Dry matter weight of maize AGB (g/1 plant). The weights of AGB are expressed as mean (n = 4); the error bars represent the standard deviation. Different letters above error bars denote statistically significant differences among treatments using Tukey's post hoc tests. CAN-c: 100% CAN with P3HB coating; CAN/P-c: 50% CAN + 50% P3HB with P3HB coating; CAN/P/S-c: 50% CAN + 25% P3HB + 25% struvite with P3HB coating; CAN/P/B-c: 50% CAN + 50% biomass with P3HB coating; CAN/P-bf: 50% CAN + 50% P3HB encapsulated in biodegradable film; CAN: 100% CAN (positive reference); CON-nf: without fertilizer (negative reference).

The size (capacity) of the root system of maize plants was determined only at term t_3 using the so-called electric root capacity (C_R). The C_R values are presented in Figure 6. The size of plant roots strongly correlates with the weight of AGB dry matter in a given phase ($r = 0.851$; $p < 0.001$). The significantly highest value was reached in treatment with relatively highest AGB production (CAN/P/B-c). On this variant, C_R was 16.5% higher compared to maize grown on the variant fertilized with CAN.

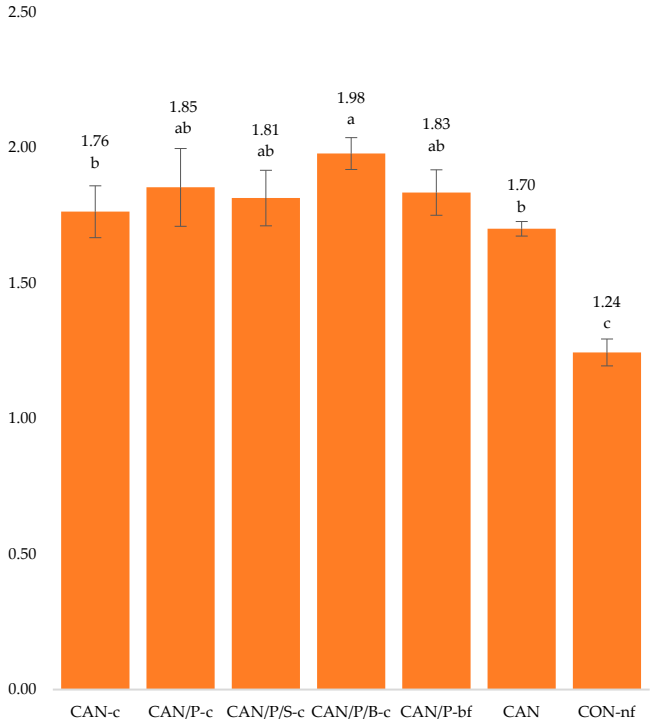


Figure 6. The maize root system size (nF) determined by root electrical capacitance (C_R). The values of C_R are expressed as mean (n = 4); the error bars represent the standard deviation. Different letters above error bars denote statistically significant differences among treatments using Tukey's post hoc tests. CAN-c: 100% CAN with P3HB coating; CAN/P-c: 50% CAN + 50% P3HB with P3HB coating; CAN/P/S-c: 50% CAN + 25% P3HB + 25% struvite with P3HB coating; CAN/P/B-c: 50% CAN + 50% biomass with P3HB coating; CAN/P-bf: 50% CAN + 50% P3HB encapsulated in biodegradable film; CAN: 100% CAN (positive reference); CON-nf: without fertilizer (negative reference).

Nitrogen Content in Plant, Chlorophyll Content, NDVI, and Quant Yield of PSII

The nitrogen content determined in AGB of maize plants decreased logically over time (t_1 to t_3). The effect of fertilizer application on its amount in tissues was observed mainly in treatment CAN-c (see Table 7). The nitrogen content in plants was the significantly highest in t_1 and t_2 after fertilization with this treatment. The nitrogen contents in the AGB of maize plants were equal in the fertilized variants at the end of the experiment (t_3). These contents of N in plant correlate with the state of mineral N amount in the soil, especially the NO_3^- form (t_1: r = 0.729, $p < 0.001$; t_2: r = 0.753, $p < 0.001$; t_3: r = 0.845, $p < 0.001$).

In addition to the N content in the AGB of maize plants, the normalized difference vegetation index (NDVI) and chlorophyll content, expressed as N-tester value, were determined (Table 7). The amount of chlorophyll in the plants was also determined using a Yara N-tester. N tester values significantly correlated with nitrogen contents in AGB (r = 0.740, $p < 0.001$). Since the chlorophyll content in the plant is directly dependent on the amount of nitrogen in the tissues, this fact can be explained by the gradual release of nutrients from coated fertilizers in time and its relative deficiency in the later stages of growth (t_3) in plants fertilized with conventional, non-coated fertilizers. While in the terms t_1 and t_2, the plants fertilized with uncoated CAN showed the significant highest N tester value, in the term t_3 the significant highest content of chlorophyll was found in treatments CAN/P-c, CAN/P/S-c and CAN/P-bf.

Table 7. Nitrogen content in the above-ground mass of maize plants (% DM), N tester value, NDVI, and quantum yield of photosystem II (Φ_{PSII}) in maize. The values represent the mean (n = 4) ± standard deviation. Different letters denote statistically significant differences among treatments using Tukey's post hoc tests. CAN-c: 100% CAN with P3HB coating; CAN/P-c: 50% CAN + 50% P3HB with P3HB coating; CAN/P/S-c: 50% CAN + 25% P3HB + 25% struvite with P3HB coating; CAN/P/B-c: 50% CAN + 50% biomass with P3HB coating; CAN/P-bf: 50% CAN + 50% P3HB encapsulated in biodegradable film; CAN: 100% CAN (positive reference); CON-nf: without fertilizer (negative reference).

Term of Measured	Treatments	N Content in AGB (% of DM ± SD)	N-Tester Value	NDVI	Φ_{PSII}
t1	CAN-c	5.99 a ± 0.25	519 def ± 8	0.75 cdefgh ± 0.01	0.835 abc ± 0.006
	CAN/P-c	5.81 ab ± 0.04	529 def ± 12	0.77 abcde ± 0.01	0.835 abc ± 0.006
	CAN/P/S-c	5.70 ab ± 0.20	518 def ± 8	0.75 defgh ± 0.02	0.838 abc ± 0.005
	CAN/P/B-c	5.58 bc ± 0.08	506 ef ± 7	0.76 abcdefg ± 0.02	0.825 abcd ± 0.006
	CAN/P-bf	5.57 bc ± 0.07	506 ef ± 13	0.76 abcdefg ± 0.02	0.825 abcd ± 0.006
	CAN	5.64 ab ± 0.06	565 abc ± 7	0.76 abcdefg ± 0.02	0.825 abcd ± 0.006
	CON-nf	5.25 c ± 0.08	498 f ± 10	0.77 abcdef ± 0.01	0.833 abc ± 0.005
t2	CAN-c	3.54 d ± 0.25	574 ab ± 20	0.79 abcd ± 0.01	0.833 abc ± 0.005
	CAN/P-c	3.32 de ± 0.13	538 cd ± 9	0.80 abc ± 0.01	0.840 ab ± 0.000
	CAN/P/S-c	3.47 de ± 0.11	530 de ± 12	0.80 a ± 0.00	0.840 ab ± 0.008
	CAN/P/B-c	3.30 de ± 0.16	543 bcd ± 16	0.80 ab ± 0.01	0.835 abc ± 0.013
	CAN/P-bf	3.14 e ± 0.23	541 cd ± 9	0.79 abcd ± 0.01	0.843 a ± 0.005
	CAN	3.29 de ± 0.12	579 a ± 3	0.78 abcd ± 0.02	0.825 abcd ± 0.010
	CON-nf	1.48 f ± 0.20	397 g ± 13	0.75 bcdefg ± 0.02	0.830 abc ± 0.008
t3	CAN-c	1.57 f ± 0.04	366 hi ± 19	0.71 gh ± 0.02	0.823 abcd ± 0.010
	CAN/P-c	1.50 f ± 0.04	405 g ± 7	0.71 gh ± 0.01	0.823 abcd ± 0.010
	CAN/P/S-c	1.58 f ± 0.06	399 g ± 3	0.70 h ± 0.01	0.820 bcd ± 0.000
	CAN/P/B-c	1.55 f ± 0.06	358 hi ± 23	0.73 efgh ± 0.02	0.818 cd ± 0.010
	CAN/P-bf	1.62 f ± 0.06	388 gh ± 8	0.72 gh ± 0.01	0.823 abcd ± 0.013
	CAN	1.52 f ± 0.06	350 i ± 7	0.72 fgh ± 0.00	0.808 de ± 0.010
	CON-nf	0.80 g ± 0.04	249 j ± 8	0.62 i ± 0.05	0.790 e ± 0.008

A significant dependence was found between the measured values of N tester and NDVI (r = 0.822, $p < 0.001$). However, fertilization did not have a significant effect on the values of the vegetation index, as shown in Table 7.

Quantum yield of photosystem II (Φ_{PSII}) is a measure of photosystem II (PSII) efficiency and corresponds to the F_V/F_M ratio, where F_V is the maximum variable chlorophyll fluorescence yield in the light-adapted state and F_M is the maximum chlorophyll fluorescence yield in the light-adapted state. The quantum yield thus provides an accurate estimate of photosynthetic activity. The value of Φ_{PSII} was not significantly affected by coated fertilizer fertilization (Table 7). The actual capacity of the PSII for photochemical processes by availability of reaction centers of the photosystem II significantly corelated with NDVI values (r = 0.713, $p < 0.001$). Nevertheless, its values at the end of the vegetation (*t3*) were relatively highest in plants fertilized with coated and encapsulated fertilizers (0.821), compared to the Φ_{PSI} value on the CAN (0.808) and unfertilized treatment (0.790).

4. Discussion

Several controlled-release fertilizer formulations have been successfully prepared: coated pellets containing CAN fertilizer and fillers that align with the circular economy's intentions (fully biodegradable P3HB, struvite, and biomass). The behavior and release dynamics of the fertilizer in aqueous environments and vegetation pot experiments were tested.

Boyandin et al. [23] investigated the release of ammonium nitrate in an aqueous medium in pellets with a 6-fold coating of P3HB in chloroform. Its pellets contained only 25% of ammonium nitrate, and the rest was made up of P3HB or other additives (wood

flour). Testing in water in research lasted seven days. (18.3 ± 7.9)% of fertilizer was released after seven days from its coated pellets containing ammonium nitrate and P3HB, and (13.4 ± 7.9)% of fertilizer was released from its coated pellets also containing wood flour. Our coated pellets containing fertilizer with 50% P3HB, or struvite, or biomass had only 3.5–5.7% released ammonium nitrate after seven days. Pellets in foils released 11.5% of ammonium nitrate. The differences in a more extended experiment would be even more pronounced. In addition, we also achieved a small coating thickness on the pellets (approx. 12–17% of the weight of the original pellet for various formulations) due to using "green" dioxolane as a P3HB solvent [22].

The release of fertilizer into water is also described, e.g., by Rashidzadeh and Olad [47]. Their slow-released NPK fertilizer, encapsulated by superabsorbent nanocomposite and prepared via the in situ free radical polymerization of sodium alginate, acrylic acid, acrylamide, and montmorillonite in the presence of fertilizer compounds, also possessed excellent slow-release property. The release of fertilizer was 14.66% on the first day, 28.54% after one week, and 57.66% after one month.

Our coated pellets containing 50% fertilizer with 50% P3HB showed excellent resistance even after 76 days in water. After 76 days, only 20% of the ammonium nitrate was released. According to a review of controlled-release fertilizers by Lawrencia et al. [4], such fertilizer release in the water environment corresponds more to fertilizer with a synthetic polymer-based coating than fertilizer with a natural polymer-based coating. We proved the feasibility of P3HB as a filler and coating material. By adjusting filler content and coating thickness, we could design the period of the agrochemical release from the formulation. Effective P3HB coating could also be used for seed protection [48].

The pot experiment results proved coated CAN fertilizers as a possible option to improve nutrient use efficiency, reduce nitrogen losses, and minimize environmental pollution while providing nitrogen to plants more gradually during vegetation, which is also described by several authors [9,49–52]. The release of nitrogen from coated CAN fertilizers affected dynamic changes in the soil mineral N content during the vegetation of maize. Contents of N_{min} and its ionic forms (NO_3^-, NH_4^+) were determined in the soil in three terms (t_1–t_3). Although enough of the available nitrogen can be essential for direct plant consumption, the excessive content may inevitably increase its loss in soil [53]. One of the important aspects of coated fertilizers is the longevity of nutrient release at optimal levels for plant uptake. The application of coated CAN fertilizers showed a positive effect on the N_{min} (NO_3^-, NH_4^+) release pattern, as seen in Figures S6–S8. The statistically lowest values of nitrogen content in the soil in the t_1 term were observed after CAN/Pbf treatment, possibly because of the encapsulation, which slowed down the hydrolysis of this fertilizer and resulted in more gradual nitrogen release. This fact possibly resulted in slower nitrification and thereby reduced loss from leaching. Positive effects were found of fertilizers coated with different types of polymers such as polyolefin [54,55], multiorganic polymer, diamide of oxalic acid [55,56], and sulfur [57] on nitrate leaching. The results obtained from t_2 and t_3 clearly demonstrate the effects of coated fertilizers: each treatment provided a higher amount of nitrogen (both ammonia and nitrate) in comparison with common uncoated CAN. Nitrogen after this treatment was taken up by the plants and leached in the middle and lower layers of the soil, while the coated treatments continued to provide both forms of nitrogen more gradually. One of the highest supplies of nitrogen in both later terms was provided by coated treatments CAN/P/B-c and CAN/P/S-c; a similar result was also provided by encapsulated treatment CAN/Pbf. Zheng et al. [58] similarly describe the enhanced content of soil mineral nitrogen in later vegetation stages after applying sulfur-coated fertilizers. Figure 4 describes the development of nitrogen in the soil layers over time; a similar result with gradually increasing content of N in the top layer while maintaining the high amount of nitrogen in the middle layer is also presented by Xiao et al. [59]. Their controlled-release N fertilizer coated with paper-plastic composite material (composed of paper and polyethylene) reduced nitrogen leaching and ammonia evaporation from soil.

The aboveground biomass of maize after fertilization with coated CAN treatments was, as expected, higher in comparison with unfertilized treatment and comparable with the treatment without coating (CAN). These results proved that coated fertilizers present a potential alternative to common fertilizers, as their application has no negative effect on yield while minimizing the environmental losses of nitrogen. The same conclusions are presented by Škarpa et al. [60]. Trenkel [13] even describes the possibility of lowering the application doses of coated fertilizers while achieving similar yields. Some authors also describe increases in crop yields after coated fertilizer application [61–65]. After the use of CRF fertilizers based on polyhydroxyalkanoate, a significant increase in total fresh plant biomass was found compared with the quick-release NPK fertilizer [66]. In our experiment, the increase in aboveground biomass was observed only in t_3 after the treatment CAN/P/B-c in comparison with uncoated CAN. A strong correlation between aboveground biomass and root size was observed in our experiment. The highest value of root size was measured on the treatment CAN/P/B-c with the highest biomass production. The correlation between the nitrogen content (especially nitrate form) in the soil and N content in the aboveground biomass of plants was observed, the same as the correlation between nitrogen content in AGB and N-tester values. Similar findings were presented by Koning et al. [67]. The content of chlorophyll plants is dependent on the amount of nitrogen in the tissues [68]; these results can be explained by the gradual release of nitrogen from coated treatment in time and its relative deficiency in the later stages of growth (t_3) in plants fertilized with conventional, non-coated fertilizers. Although the effect of fertilization was not significant in terms of N-tester values and NDVI index, the coated treatment CAN/P/B-c and encapsulated treatment CAN/Pbf provided one of the highest values, especially in later terms of vegetation. A single pre-planting application of these controlled-release fertilizers can fill a crop's nutritional requirements throughout its growing season.

Our research on controlled-release fertilizers with biodegradable coating involved coated formulations with urea and P3HB filler. We were able to prepare these pellets on a quarter-operational pelletizing device and coat them in larger quantities in a coating drum. This technology could be transferable to the industry. A careful study of the biodegradation of these fertilizer formulations in soil and research into the long-term effect on soil composition under field conditions will also be needed.

Supplementary Materials: The following supporting information can be downloaded at: https://www.mdpi.com/article/10.3390/polym14204323/s1. Figure S1: Six coating layers applied manually to pellets composed of 50% P3HB with 50% CAN: coated with a solution of (a) 7% P3HB in chloroform with ethanol, (b) 6% P3HB in dioxolane, (c) 6% P3HB in amylene; Figure S2: Manually-coated pellets of different experimental formulations (prepared on a hydraulic press); Figure S3: Encapsulation of pellets containing 50% CAN and 50% P3HB into a biodegradable film; Figure S4: The final appearance of the encapsulated pellets; Figure S5: Grown maize in Mitscherlich vegetation pots in the rain shelter; Figure S6: The ammonium (a) and nitrate (b) soil nitrogen content (mg/kg of soil) in the first term (t1) of soil collection (3 weeks after sowing/fertilization). The nitrogen contents of the different soil layers (up—upper, mi—middle, bo—bottom) are expressed as mean (n = 4); the error bars represent the standard deviation. The mean values marked with an asterisk are significantly different ($p \leq 0.05$) from the treatment without coated (CAN) by the Tukey test (each of the soil layers was statistically evaluated separately). CAN-c: 100% CAN with P3HB coating; CAN/P-c: 50% CAN + 50% P3HB with P3HB coating; CAN/P/S-c: 50% CAN + 25% P3HB + 25% struvite with P3HB coating; CAN/P/B-c: 50% CAN + 50% biomass with P3HB coating; CAN/P-bf: 50% CAN + 50% P3HB encapsulated in biodegradable film; CAN: 100% CAN (positive reference); CON-nf: without fertilizer (negative reference); Figure S7: The ammonium a) and nitrate b) soil nitrogen content (mg/kg of soil) in the second term (t_2) of soil collection (6 weeks after sowing/fertilization). The nitrogen contents of the different soil layers (up—upper, mi—middle, bo—bottom) are expressed as mean (n = 4); the error bars represent the standard deviation. The mean values marked with an asterisk are significantly different ($p \leq 0.05$) from the treatment without coated (CAN) by the Tukey test (each of the soil layers was statistically evaluated separately). CAN-c: 100% CAN with P3HB coating; CAN/P-c: 50% CAN + 50% P3HB with P3HB coating; CAN/P/S-c: 50% CAN + 25% P3HB + 25% struvite with

P3HB coating; CAN/P/B-c: 50% CAN + 50% biomass with P3HB coating; CAN/P-bf: 50% CAN + 50% P3HB encapsulated in biodegradable film; CAN: 100% CAN (positive reference); CON-nf: without fertilizer (negative reference); Figure S8: The ammonium (a) and nitrate (b) soil nitrogen content (mg/kg of soil) in the third term (t_3) of soil collection (9 weeks after sowing/fertilization). The nitrogen contents of the different soil layers (up—upper, mi—middle, bo—bottom) are expressed as mean (n = 4), the error bars represent the standard deviation. The mean values marked with an asterisk are significantly different ($p \leq 0.05$) from the treatment without coated (CAN) by the Tukey test (each of the soil layers was statistically evaluated separately). CAN-c: 100% CAN with P3HB coating; CAN/P-c: 50% CAN + 50% P3HB with P3HB coating; CAN/P/S-c: 50% CAN + 25% P3HB + 25% struvite with P3HB coating; CAN/P/B-c: 50% CAN + 50% biomass with P3HB coating; CAN/P-bf: 50% CAN + 50% P3HB encapsulated in biodegradable film; CAN: 100% CAN (positive reference); CON-nf: without fertilizer (negative reference).

Author Contributions: Conceptualization, R.P. and S.K.; methodology, R.P., S.K., S.F., P.Š. and V.J.; validation, P.M. and M.M.; formal analysis, S.K., R.P., Z.G., S.F., M.S., V.J., P.M., P.Š., T.K., J.A. and M.M.; investigation, S.K., M.S., Z.G., V.J., S.F., R.P. and P.M.; resources, R.P.; data curation, S.K., V.J., S.F., P.Š. and M.M.; writing—original draft preparation, S.K.; writing—review and editing, S.K., R.P., P.Š., T.K. and J.A.; supervision, R.P., S.K. and P.Š.; project administration, R.P., Z.G. and P.Š.; funding acquisition, R.P. All authors have read and agreed to the published version of the manuscript.

Funding: This research was funded by Ministry of Industry and Trade of the Czech Republic, grant number FV40095 and by the grant Internal Grant Agency AF-IGA2020-TP007: Use of superabsorbent polymers with controlled nutrient release in field-crop cultivation systems in arid areas.

Institutional Review Board Statement: Not applicable.

Informed Consent Statement: Not applicable.

Data Availability Statement: Not applicable.

Acknowledgments: We would like to thank Nafigate Corporation for the support in the form of supplies of P3HB material, struvite and biomass.

Conflicts of Interest: The authors declare no conflict of interest.

References

1. Smil, V. Nitrogen Cycle and World Food Production. *World Agric.* **2011**, *2*, 9–13.
2. United Nations, Department of Economic and Social Affairs, Population Division. World Population Prospects 2019: Highlights (ST/ESA/SER.A/423). 2019. Available online: https://population.un.org/wpp/publications/files/wpp2019_highlights.pdf (accessed on 1 July 2022).
3. Adam, D. How Far Will Global Population Rise. *Nature* **2021**, *597*, 462–465. [CrossRef]
4. Lawrencia, D.; Wong, S.K.; Low, D.Y.S.; Goh, B.H.; Goh, J.K.; Ruktanonchai, U.R.; Soottitantawat, A.; Lee, L.H.; Tang, S.Y. Controlled Release Fertilizers: A Review on Coating Materials and Mechanism of Release. *Plants* **2021**, *10*, 238. [CrossRef] [PubMed]
5. Galloway, J.N.; Townsend, A.R.; Erisman, J.W.; Bekunda, M.; Cai, Z.; Freney, J.R.; Martinelli, L.A.; Seitzinger, S.P.; Sutton, M.A. Transformation of the nitrogen cycle: Recent trends, questions, and potential solutions. *Science* **2008**, *320*, 889–892. [CrossRef]
6. Zhang, X.; Davidson, E.; Mauzerall, D.; Searchinger, T.D.; Dumas, P.; Shen, Y. Managing nitrogen for sustainable development. *Nature* **2015**, *528*, 51–59. [CrossRef] [PubMed]
7. Bisht, N.; Chauhan, P.S. Excessive and Disproportionate Use of Chemicals Cause Soil Contamination and Nutritional Stress. In *Soil Contamination—Threats and Sustainable Solutions*; Larramendy, M.L., Soloneski, S., Eds.; IntechOpen: London, UK, 2020. [CrossRef]
8. Fan, L.-T.; Singh, S.K. Introduction. In *Controlled Release: A Quantitative Treatment*, 1st ed.; Fan, L.-T., Singh, S.K., Eds.; Springer Science & Business Media: Berlin/Heidelberg, Germany, 2012; Volume 13, pp. 1–8.
9. Gil-Ortiz, R.; Naranjo, M.Á.; Ruiz-Navarro, A.; Atares, S.; García, C.; Zotarelli, L.; San Bautista, A.; Vicente, O. Enhanced Agronomic Efficiency Using a New Controlled-Released, Polymeric-Coated Nitrogen Fertilizer in Rice. *Plants* **2020**, *9*, 1183. [CrossRef] [PubMed]
10. Wang, Y.; Liu, M.; Ni, B.; Xie, L. κ-Carrageenan–sodium alginate beads and superabsorbent coated nitrogen fertilizer with slow-release, water-retention, and anticompaction properties. *Ind. Chem. Eng. Res.* **2012**, *51*, 1413–1422. [CrossRef]
11. Cole, J.C.; Smith, M.W.; Penn, C.J.; Cheary, B.S.; Conaghan, K.J. Nitrogen, phosphorus, calcium, and magnesium applied individually or as a slow release or controlled release fertilizer increase growth and yield and affect macronutrient and micronutrient concentration and content of field-grown tomato plants. *Sci. Hortic.* **2016**, *211*, 420–430. [CrossRef]

12. Cong, Z.; Yazhen, S.; Changwen, D.; Jianmin, Z.; Huoyan, W.; Xiaoqin, C. Evaluation of waterborne coating for controlled-release fertilizer using Wurster fluidized bed. *Ind. Eng. Chem. Res.* **2010**, *49*, 9644–9647. [CrossRef]
13. Trenkel, M.E. *Slow- and Controlled-Release and Stabilized Fertilizers: An Option for Enhancing Nutrient Efficiency in Agriculture*, 2nd ed.; IFA: Paris, France, 2010; p. 160.
14. Shaviv, A. Controlled release fertilizers. In Proceedings of the IFA International Workshop on Enhanced-Efficiency Fertilizers, Frankfurt, Germany, 28–30 June 2005.
15. AAPFCO. *Official Publication No. 48*; Association of American Plant Food Control Officials, Inc.: West Lafayette, IA, USA, 1995.
16. Lubkowski, K.; Smorowska, A.; Grzmil, B.; Kozłowska, A. Controlled-release fertilizer prepared using a biodegradable aliphatic copolyester of poly (butylene succinate) and dimerized fatty acid. *J. Agric. Food. Chem.* **2015**, *63*, 2597–2605. [CrossRef] [PubMed]
17. Fertilizers Europe. 2019/2020 Overview. Available online: https://www.fertilizerseurope.com/wp-content/uploads/2020/07/AR-2019_20_32-pager-screen.pdf (accessed on 16 July 2022).
18. Obruca, S.; Benesova, P.; Oborna, J.; Marova, I. Application of protease-hydrolyzed whey as a complex nitrogen source to increase poly(3-hydroxybutyrate) production from oils by *Cupriavidus necator*. *Biotechnol. Lett.* **2014**, *36*, 775–781. [CrossRef]
19. Silva, L.F.; Taciro, M.K.; Raicher, G.; Piccoli, R.A.M.; Mendonça, T.T.; Lopes, M.S.G.; Gomez, J.G.C. Perspectives on the production of polyhydroxyalkanoates in biorefineries associated with the production of sugar and ethanol. *Int. J. Biol. Macromol.* **2014**, *71*, 2–7. [CrossRef] [PubMed]
20. Dietrich, K.; Dumont, M.-J.; Rio, L.F.D.; Orsat, V. Producing PHAs in the bioeconomy—Towards a sustainable bioplastic. *Sustain. Prod. Consum.* **2017**, *9*, 58–70. [CrossRef]
21. Surendran, A.; Lakshmanan, M.; Chee, J.Y.; Sulaiman, A.M.; Thuoc, D.V.; Sudesh, K. Can Polyhydroxyalkanoates Be Produced Efficiently From Waste Plant and Animal Oils? *Front. Bioeng. Biotechnol.* **2020**, *8*, 169. [CrossRef]
22. Nuttipon, Y.; Suchada, C.N. Toward non-toxical and simple recovery process of poly(3-hydroxybutyrate) using the green solvent 1,3-dioxolane. *Process Biochem.* **2018**, *69*, 197–207. [CrossRef]
23. Boyandin, A.N.; Kazantseva, E.A.; Varygina, D.E.; Volova, T.G. Constructing Slow-Release Formulations of Ammonium Nitrate Fertilizer Based on Degradable Poly(3-hydroxybutyrate). *J. Agric. Food Chem.* **2017**, *65*, 6745–6752. [CrossRef] [PubMed]
24. Lovochemie, a.s. Available online: https://www.lovochemie.cz/en (accessed on 26 July 2022).
25. TianAn Biopolymer. Available online: www.tianan-enmat.com (accessed on 26 July 2022).
26. Nafigate Corporation. Available online: https://www.nafigate.com/ (accessed on 26 July 2022).
27. Merck. Available online: https://www.sigmaaldrich.com/CZ/en (accessed on 26 July 2022).
28. SPECAC. Available online: https://specac.com/ (accessed on 26 July 2022).
29. Lach:ner. Available online: https://www.lach-ner.cz/en (accessed on 26 July 2022).
30. PENTA Chemicals Unlimited. Available online: https://www.pentachemicals.eu/en/ (accessed on 26 July 2022).
31. AvantorTM Delivered by VWRTM. Available online: https://www.vwr.com/ (accessed on 26 July 2022).
32. Panara. Available online: https://panaraplast.com/ (accessed on 26 July 2022).
33. STU. Available online: https://www.stuba.sk/english.html?page_id=132 (accessed on 26 July 2022).
34. PubChem: Ammonium Nitrate. Available online: https://pubchem.ncbi.nlm.nih.gov/compound/Ammonium-nitrate (accessed on 26 July 2022).
35. Miller, R.L.; Bradford, W.L.; Peters, N.E. *Specific Conductance: Theoretical Considerations and Application to Analytical Quality Control*; US Government Printing Office: Washington, DC, USA, 1988.
36. Metex Corporation Limited. Available online: https://www.metexcorporation.com/hand-held-instruments.html (accessed on 26 July 2022).
37. OriginLab. Available online: https://www.originlab.com/ (accessed on 26 July 2022).
38. Oseva. Available online: https://oseva.com/about-oseva/ (accessed on 26 July 2022).
39. Gee, G.W.; Bauder, J.W. Particle-size analysis. In *Methods of Soil Analysis Part 1—Physical and Mineralogical Methods*; Klute, A., Ed.; ASA and SSSA: Madison, WI, USA, 1986; pp. 383–411.
40. Schumacher, B.A. *Methods for the Determination of Total Organic Carbon (TOC) in Soils and Sediments*; United States Environmental Protection Agency, Environmental Sciences Division National, Exposure Research Laboratory: Las Vegas, NV, USA, 2002.
41. Zbíral, J.; Malý, S.; Váňa, M. (Eds.) *Soil Analysis III*, 3rd ed.; Central Institute for Supervising and Testing in Agriculture: Brno, Czech Republic, 2011; pp. 18–52. (In Czech)
42. Zbíral, J. *Analysis of Soils I. Unified Techniques*, 2nd ed.; Central Institute for Supervising and Testing in Agriculture: Brno, Czech Republic, 2002; p. 197. (In Czech)
43. Netto, A.L.; Campostrini, E.; Goncalves de Oliverira, J.; Bressan-Smith, R.E. Photosynthetic pigments, nitrogen, chlorophyll a fluorescence and SPAD-502 readings in coffee leaves. *Sci. Hortic.* **2005**, *104*, 199–209. [CrossRef]
44. Škarpa, P.; Klofáč, D.; Krčma, F.; Šimečková, J.; Kozáková, Z. Effect of Plasma Activated Water Foliar Application on Selected Growth Parameters of Maize (*Zea mays* L.). *Water* **2020**, *12*, 3545. [CrossRef]
45. Zbíral, J. *Plant Analysis: Integrated Work Procedures*; Central Institute for Supervising and Testing in Agriculture: Brno, Czech Republic, 2005; p. 192. (In Czech)
46. StatSoft, Inc. STATISTICA (Data Analysis Software System), Version 12. 2013. Available online: http://www.statsoft.com/ (accessed on 13 May 2021).

47. Rashidzadeh, A.; Olad, A. Slow-released NPK fertilizer encapsulated by NaAlg-g-poly(AA-co-AAm)/MMT superabsorbent nanocomposite. *Carbohydr. Polym.* **2014**, *114*, 269–278. [CrossRef]
48. Grubbs, J.B., III; Locklin, J.J. PLA/PHA Biodegradable Coatings for Seeds and Fertilizers. U.S. Patent Application Number 16/880083, 26 November 2020.
49. Liu, C.; Chen, F.; Li, Z.; Cocq, K.L.; Liu, Y.; Wu, L. Impact of nitrogen practices on yield, grain quality, and nitrogen-use efficiencyof crops and soil fertility in three paddy-upland cropping systems. *J. Sci. Food Agric.* **2021**, *101*, 2218–2226. [CrossRef]
50. Zhu, S.; Liu, L.; Yang, Y.; Shi, R. Application of controlled release urea improved grain yield and nitrogen use efficiency: Ameta-analysis. *PLoS ONE* **2020**, *15*, e0241481. [CrossRef] [PubMed]
51. Zhang, K.; Wang, Z.; Yu, Q.; Liu, B.; Duan, M.; Wang, L. Effect of controlled-release urea fertilizers for oilseed rape (*Brassica napus* L.) on soil carbon storage and CO_2 emission. *Environ. Sci. Pollut. Res.* **2020**, *27*, 31983–31994. [CrossRef]
52. Liao, J.; Liu, X.; Song, H.; Chen, X.; Zhang, Z. Effects of biochar-based controlled release nitrogen fertilizer on nitrogen-use efficiency of oilseed rape (*Brassica napus* L.). *Sci. Rep.* **2020**, *10*, 11063. [CrossRef] [PubMed]
53. Zhu, Z.L. Loss of fertilizer N from plants-soil system and the strategies and techniques for its reduction. *Soil Environ. Sci.* **2000**, *9*, 1–6.
54. Zvomuya, F.; Rosen, C.J.; Russelle, M.P.; Gupta, S.C. Nitrate leaching and nitrogen recovery following application of polyolefin-coated urea to potato. *J. Environ. Qual.* **2003**, *32*, 480–489. [CrossRef]
55. Mikkelsen, R.L.; Williams, H.M.; Behel, A.D., Jr. Nitrogen leaching and plant uptake from controlled-release fertilizers. *Fertil. Res.* **1994**, *37*, 43–50. [CrossRef]
56. Cabrera, R.I. Comparative evaluation of nitrogen release patterns from controlled-release fertilizers by nitrogen leaching analysis. *Hort. Sci.* **1997**, *32*, 669–673. [CrossRef]
57. Zheng, W.; Wan, Y.; Li, Y.; Liu, Z.; Chen, J.; Zhou, H.; Gao, Y.; Chen, B.; Zhang, M. Developing water and nitrogen budgets of a wheat-maize rotation system using auto-weighing lysimeter: Effects of blended application of controlled-release an un-coated urea. *Environ. Pollut.* **2020**, *263*, 114383. [CrossRef] [PubMed]
58. Zheng, W.; Zhang, M.; Liu, Z.; Zhou, H.; Lu, H.; Zhang, W.; Yang, Y.; Li, C.; Chen, B. Combining controlled-release urea and normal urea to improve the nitrogen use efficiency and yield under wheat-maize double cropping system. *Field Crops Res.* **2016**, *197*, 52–62. [CrossRef]
59. Xiao, Y.; Peng, F.; Zhang, Y.; Wang, J.; Zhuge, Y.; Zhang, S.; Gao, H. Effect of bag-controlled release fertilizer on nitrogen loss, greenhouse gas emissions, and nitrogen applied amount in peach production. *J. Clean. Prod.* **2019**, *234*, 258–274. [CrossRef]
60. Škarpa, P.; Mikušová, D.; Antošovský, J.; Kučera, M.; Ryant, P. Oil-Based Polymer Coatings on CAN Fertilizer in Oilseed Rape (*Brassica napus* L.) Nutrition. *Plants* **2021**, *10*, 1605. [CrossRef] [PubMed]
61. Tian, C.; Zhou, X.; Liu, O.; Peng, J.; Wang, W.; Zhang, Z.; Yang, Y.; Song, H.; Guan, C. Effects of a controlled-release fertilizer on yield, nutrient uptake, and fertilizer usage efficiency in early ripening rapeseed (*Brassica napus* L.). *J. Zhejiang Univ. Sci.* **2016**, *17*, 775–786. [CrossRef]
62. Wei, H.; Chen, Z.; Xing, Z.; Zhou, L.; Liu, Q.; Zhang, Z.; Jiang, Y.; Hu, Y.; Zhu, J.; Cui, P.; et al. Effects of slow or controlled release fertilizer types and fertilization modes on yield and quality of rice. *J. Integr. Agric.* **2018**, *17*, 2222–2234. [CrossRef]
63. Ma, Q.; Wang, M.; Zheng, G.; Yao, Y.; Tao, R.; Zhu, M.; Ding, J.; Li, C.; Guo, W.; Zhu, X. Twice-split application of controlled-release nitrogen fertilizer met the nitrogen demand of winter wheat. *Field Crops Res.* **2021**, *267*, 108163. [CrossRef]
64. Ye, Y.; Liang, X.; Chen, Y.; Liu, J.; Gu, J.; Guo, R.; Li, L. Alternate wetting and drying irrigation and controlled-release nitrogen fertilizer in late-season rice. Effects on dry matter accumulation, yield, water and nitrogen use. *Field Crops Res.* **2013**, *144*, 212–224. [CrossRef]
65. Lu, Y.; Sun, Y.; Liao, Y.; Nie, J.; Yie, J.; Yang, Z.; Zhoiu, X. Effects of the application of controlled release nitrogen fertilizer on rapeseed yield, agronomic characters and soil fertility. *Agric. Sci. Technol.* **2015**, *16*, 1226.
66. Murugan, P.; Ong, S.Y.; Hashim, R.; Kosugi, A.; Arai, T.; Sudesh, K. Development and evaluation of controlled release fertilizer using P(3HB-co-3HHx) on oil palm plants (nursery stage) and soil microbes. *Biocatal. Agric. Biotechnol.* **2020**, *28*, 101710. [CrossRef]
67. Koning, L.A.; Veste, M.; Freese, D.; Lebzien, S. Effects of nitrogen and phosphate fertilization on leaf nutrient content, photosynthesis, and growth of the novel bioenergy crop *Fallopia sachalinensis* cv. 'Igniscum Candy'. *J. Appl. Bot. Food Qual.* **2015**, *88*, 22–28.
68. Gianquinto, G.; Goffart, J.P.; Olivier, M.; Guarda, G.; Colauzzi, M.; Dalla Costa, L.; Delle Vedove, G.; Vos, J.; Mackerron, D.K.L. The Use of Hand-held Chlorophyll Meters As a Tool to Assess the Nitrogen Status and to Guide Nitrogen Fertilization of Potato Crop. *Potato Res.* **2004**, *47*, 35–80. [CrossRef]

polymers

MDPI

Article

High-Pressure Depolymerization of Poly(lactic acid) (PLA) and Poly(3-hydroxybutyrate) (PHB) Using Bio-Based Solvents: A Way to Produce Alkyl Esters Which Can Be Modified to Polymerizable Monomers

Vojtěch Jašek [1,*], Jan Fučík [2], Lucia Ivanová [2], Dominik Veselý [2], Silvestr Figalla [1], Ludmila Mravcova [2], Petr Sedlacek [3], Jozef Krajčovič [2] and Radek Přikryl [1]

[1] Institute of Materials Chemistry, Faculty of Chemistry, Brno University of Technology, 61200 Brno, Czech Republic
[2] Institute of Environmental Chemistry, Faculty of Chemistry, Brno University of Technology, 61200 Brno, Czech Republic
[3] Institute of Physical and Applied Chemistry, Faculty of Chemistry, Brno University of Technology, 61200 Brno, Czech Republic
* Correspondence: xcjasekv@vutbr.cz

check for updates

Citation: Jašek, V.; Fučík, J.; Ivanová, L.; Veselý, D.; Figalla, S.; Mravcova, L.; Sedlacek, P.; Krajčovič, J.; Přikryl, R. High-Pressure Depolymerization of Poly(lactic acid) (PLA) and Poly(3-hydroxybutyrate) (PHB) Using Bio-Based Solvents: A Way to Produce Alkyl Esters Which Can Be Modified to Polymerizable Monomers. *Polymers* **2022**, *14*, 5236. https://doi.org/10.3390/polym14235236

Academic Editors: Antonio M. Borrero-López, Concepción Valencia-Barragán, Esperanza Cortés Triviño, Adrián Tenorio-Alfonso and Clara Delgado-Sánchez

Received: 8 November 2022
Accepted: 29 November 2022
Published: 1 December 2022

Publisher's Note: MDPI stays neutral with regard to jurisdictional claims in published maps and institutional affiliations.

Copyright: © 2022 by the authors. Licensee MDPI, Basel, Switzerland. This article is an open access article distributed under the terms and conditions of the Creative Commons Attribution (CC BY) license (https://creativecommons.org/licenses/by/4.0/).

Abstract: The polyesters poly(lactic acid) (PLA) and poly(3-hydroxybutyrate) (PHB) used in various applications such as food packaging or 3D printing were depolymerized by biobased aliphatic alcohols—methanol and ethanol with the presence of *para*-toluenesulphonic acid (*p*-TSA) as a catalyst at a temperature of 151 °C. It was found that the fastest depolymerization is reached using methanol as anucleophile for the reaction with PLA, resulting in the value of reaction rate constant (k) of 0.0425 min^{-1} and the yield of methyl lactate of 93.8% after 120 min. On the other hand, the value of constant k for the depolymerization of PHB in the presence of ethanol reached 0.0064 min^{-1} and the yield of ethyl 3-hydroxybutyrate was of 76.0% after 240 min. A kinetics study of depolymerization was performed via LC–MS analysis of alkyl esters of lactic acid and 3-hydroxybutanoic acid. The structure confirmation of the products was performed via FT-IR, MS, ^{1}H NMR, and ^{13}C NMR. Synthesized alkyl lactates and 3-hydroxybutyrates were modified into polymerizable molecules using methacrylic anhydride as a reactant and potassium 2-ethylhexanoate as a catalyst at a temperature of 80 °C. All alkyl esters were methacrylated for 24 h, guaranteeing the quantitative yield (which in all cases reached values equal to or of more than 98%). The methacrylation rate constants (k') were calculated to compare the reaction kinetics of each alkyl ester. It was found that lactates reach afaster rate of reaction than 3-hydroxybutyrates. The value of k' for themethacrylated methyl lactate reached 0.0885 $dm^3/(mol \cdot min)$. Opposite to this result, methacrylated ethyl 3-hydroxybutyrate's constant k' was 0.0075 $dm^3/(mol \cdot min)$. The reaction rate study was conducted by the GC-FID method and the structures were confirmed via FT-IR, MS, ^{1}H NMR, and ^{13}C NMR.

Keywords: poly(lactic acid); poly(3-hydroxybutyrate); depolymerization; alcoholysis; methacrylation; polymerizable monomers; kinetics

1. Introduction

In recent years, processes producing plastic materials mostly use fossil-based polymers due to the fact that these molecules are cheap to obtain and their properties can be determined efficiently. However, this type of manufacturing is dependent on non-renewable resources which might lead to potential supply risks [1–4]. Therefore, various biopolymers based on bio-source inputs such as PLA or PHB attract a significant amount of attention [5,6]. Poly(lactic acid) (PLA) is a particular biopolymer used for numerous applications such as food packaging or 3D filament printing [2,7,8]. The increasing usage of this polymer leads to considerable problems—the rate of degradation of PLA in

moderate environmental conditions is very slow; therefore, the accumulation of waste can occur [1,9,10]. There are ways to handle PLA waste, such as composting, incinerating, or mechanical recycling [7,11,12]. The first two processes do not generate any usable material and the mechanical recycling of PLA results in the production of a polymer with considerably worse properties than the original one. The reason for this outcome is that the thermal and photochemical degradation takes place during the mechanical processing of the PLA polymer, which leads to the decrease in molecular weight of the material [2,7,13,14]. Poly(3-hydroxybutyrate) (PHB) is a biopolymer that is produced by various microorganisms and can be degraded by living systems as well. The biodegradability of PHB is aconsiderable benefit of this polyester [2,15,16]. Nevertheless, PHB suffers rapid thermal degradation during the potential mechanical recycling, similarly to PLA, particularly at temperatures starting at 170–180 °C [2,17]. These two biopolymers are miscible, which is beneficial for a potential 3D printing usage, for example [18,19]. However, the fact that mixtures of numerous polymers and plasticizers are used complicates their potential recycling [20].

The chemical recycling of polyesters such as PLA or PHB is another way of handling leftover polymers or those with bad quality or properties such as low values of MW. This type of process results in forming monomers out of the polyester polymer chain. The produced monomers can either be carboxylic acids or esters depending on the chosen nucleophile. When water is used as a nucleophile, hydrolysis takes the place of the depolymerization process. Alcoholysis, on the other hand, requires alcohol to undergo the reaction, resulting in the formation of an ester via the transesterification mechanism [21–27]. These processes involve either specific reaction conditions (high pressure, high temperature) or the presence of a particular catalyst and appropriate organic solvents. Extreme conditions such as high temperature (above 120 °C) and high pressure (depending on the chosen nucleophile) can be complicated in terms of up-scaling or energy consumption [28–31]. On the other hand, specific catalysts can be expensive, and particularly organic solvents may be inappropriate for regeneration in the production process and lower temperatures could result in a decrease in the reaction rate [30,32]. The hydrolysis of PLA was experimentally verified using a temperature of 250 °C and high pressure. The molar ratio of 1:20 (PLA:H_2O) and a reaction time of 10–20 min resulted in a 90% conversion to L-lactic acid [33–35]. Adding microwave irradiation to the process of hydrolysis with aratio of 1:3 (PLA:H_2O) provided a 45% conversion to l-lactic acid after 120 min [34,35]. PHB alcoholysis was observed using ionic liquids as catalysts and methanol as a nucleophile. The highest yield of methyl 3-hydroxybutyrate (83.75%) was reached with the mixture of the molar ratio 5:1 (MeOH:PHB) and of the mass ratio 1:0.03 (PHB:cat.) with the conditions of a temperature of 140 °C and a reaction time of 3 h [36–38].

The main aim of this work is to describe a depolymerization process of the polyesters PLA and PHB in high-pressure and high-temperature conditions. The nucleophiles chosen for the reactions are methanol and ethanol and the reaction takes place in ahigh-pressure reactor. *Para*-toluensulphonic acid serves as an acidic catalyst for all alcoholyses. The monoester product structures are verified via numerous analyses (MS, FT-IR, ^{1}H NMR, ^{13}C NMR) and their reaction kinetics are studied. All synthesized monoesters (lactates and 3-hydroxybutyrates) undergo a methacrylation process to produce methacrylated esters which can be polymerized. The methacrylation reaction uses methacrylic anhydride as areagent and the chosen catalyst for this reaction is potassium 2-ethylhexanoate. The polymerizable products' structures are verified by numerous methods (MS, FT-IR, ^{1}H NMR, ^{13}C NMR) as well.

2. Materials and Methods

2.1. Materials

PLA granulate was supplied from Fillamentum Manufacturing Czech s.r.o., Hulín, Czech Republic. Measured polymer parameters were as follows: number-average molecular weight (M_n), 123,500 g/mol; weight-average molecular weight (MW), 235,300 g/mol; dispersity, 1.90. PHB powder was acquired from NAFIGATE Corporation a.s., Prague,

Czech Republic. Measured polymer parameters were as follows: number-average molecular weight (M_n), 85,040 g/mol; weight-average molecular weight (MW), 211,400 g/mol; dispersity, 2.49. All measurements of polymer properties were measured via GPC (Agilent 1100, Santa Clara, CA, USA) in chloroform ($CHCl_3$) and the analysis parameters were as follows: mobile phase flow 1 mL/min; column temperature 30 °C, used column: PLgel 5 µm MIXED-C (300 × 7.5 mm). Aliphatic alcohols for depolymerization (methanol 99%, ethanol 99%) were supplied by Honeywell Research Chemicals, Charlotte, NC, USA (used alcohols were not claimed either synthetic or bio-source by the supplier). The catalyst for alcoholyses (*p*-toluensulphonic acid monohydrate), methacrylic anhydride (94%), potassium hydroxide (p.a.), d-chloroform ($CDCl_3$; 99.8%), and 2-ethylhexanoic acid (for synthesis) were all acquired from Sigma-Aldrich, Prague, Czech Republic.

2.2. Methods for the Characterization of Products

2.2.1. Fourier-Transform Infrared Spectrometry (FT-IR)

Infrared spectrometry was used as one of the structure verification methods, but itwas mainly supposed to serve as a confirmation of –OH hydroxyl functional groups in alkyl esters of either lactic acid or 3-hydroxybutanoic acid. Analyses were performed on the infrared spectrometer Bruker Tensor 27 (Billerica, MA, USA) by the attenuated total reflectance (ATR) method using diamond as a dispersion component. The irradiation source in this type of spectrometer is a diode laser. Due to the fact that instrumentation uses Fourier transformation, the Michelson interferometer was used for the quantification of the signal. Spectra were composed out of 32 total scans with a measurement resolution of 2 cm^{-1}.

2.2.2. Mass Spectrometry (MS)

MS conditions were as follows: ESI in positive mode; spray voltage: 3500 V; cone temperature 350 °C; cone gas flow: 35 a.u.; heated probe temperature: 650 °C; probe gas flow: 40 a.u., nebulizer gas flow: 55 a.u., and exhaust gas: ON. For quantification, MRM mode was used with the following MRM transitions for MeLa (RT 1.24 min; 105.1 > 84.6 with CE 0.25 eV;105.1 > 93.9 with CE 0.25 eV and 105.1 > 45.0 with CE 2 eV), for EtLa (RT 2.35 min; 119.1 > 47.3 with CE 2.0 eV and 119.1 > 91.1 with CE 2.0 eV) for M3HB (RT 1.91 min; 119.1 > 59.0 with CE 10 eV; 119.1 > 87.2 with CE 2.5 eV; and 119.1 > 101.2 with CE 1.0 eV), and for E3HB (RT 3.58 min; 133.1 > 73.3 CE with 5 eV and 133.1 > 87.2 with CE 5 eV). The collision gas Argon was used ata pressure of 1.5 mTorr.

Additionally, by the same MS method, newly synthesized monomers methacrylated methyl lactate (MeLaMMA), methacrylated ethyl lactate (EtLaMMA), methacrylated methyl 3-hydroxybutyrate (M3HBMMA), and methacrylated ethyl 3-hydroxybutyrate (E3HBMMA) were qualitatively characterized by product scan; therefore, themass spectra of these compounds were obtained. The precursor of MeLAaMMA (*m/z* 173.1) was fragmented (CE 10 eV) and the following product ions were obtained: 57.3 and 74.2. The precursor of EtLaMMA (*m/z* 187.0) was fragmented (CE 2.5 eV) and the following product ions were obtained: 69.2; 113.1 and 141.1. The precursor of M3HBMMA (*m/z* 187.1) was fragmented (CE 2.5 eV) and the following product ions were obtained: 59.3; 69.2; 101.1 and 155.1. The precursor of E3HBMMA (*m/z* 201.0) was fragmented (CE 2.5 eV) and the following product ions were obtained: 69.0; 73.3; 115.1; and 155.0.

2.2.3. Nuclear Magnetic Resonance (NMR)

Nuclear magnetic resonance was used to obtain ^1H and ^{13}C spectra to confirm the structure of synthesized molecules. The measurements were conducted by instrument Bruker Avance III 500 MHz (Bruker, Billerica, MA, USA) with the measuring frequency of 500 MHz for ^1H NMR and 126 MHz for ^{13}C NMR at the temperature of 30 °C using d-chloroform ($CDCl_3$) as a solvent with tetramethylsilane (TMS) as an internal standard. The chemical shifts (δ) are expressed in part per million (ppm) units which are referenced

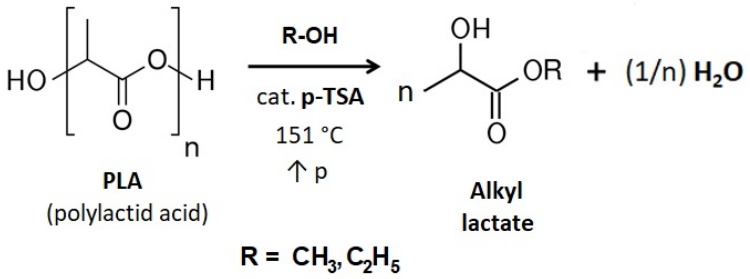
by a solvent. Coupling constant *J* has (Hz) unit with coupling expressed as s—singlet, d—doublet, t—triplet, q—quartet, p—quintet, m—multiplet.

2.3. Alcoholyses of Polyesters

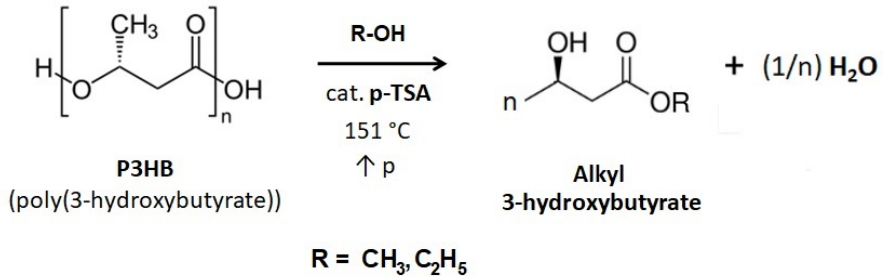
All depolymerization reactions took place in the high-pressure reactor of a volume reservoir of 1.8 L. Mixtures consisting of the polyester (PLA or PHB) and the alcohol (methanol or ethanol) in amolar ratio 1:4 (PLA/PHB:MeOH/EtOH) with the presence of dissolved catalyst p-toluensulphonic acid in a molar ratio 1:0.01 (PLA/PHB:*p*-TSA) were transferred into the reactor (see Scheme 1 for PLA and Scheme 2 for PHB). The reactor was heated up to 151 °C and the pressure increased regarding the particular type of suspense according to the vapor-pressure characteristics of the alcohol and forming ester product (ranging from 7 to 15 bar). The samples for kinetics analysis were taken directly from the reactor and cooled down immediately. The kinetics of forming monoesters was monitored via LC–MS analysis. The conversion of the particular polyester was calculated from the leftover polymer acquired by mixing the reaction solution sample with water. The unreacted polymer was precipitated and weighed. After the alcoholyses were stopped (depending on the particular combination of reagents) the leftover alcohol and the formed monoester were distilled from the solution. Products of the depolymerization were analyzed via MS, FT-IR, ^{1}H NMR, and^{13}C NMR for structure verification. Yields of monoester (Yield) and polymer conversions (*X*) were calculated as follows:

$$X = \frac{\text{Starting polymer weight} - \text{leftover polymer weight}}{\text{Starting polymer weight}} \times 100\% \quad (1)$$

$$\text{Yield} = \frac{\text{Measured quantity of ester}}{\text{Theoretical quantity of ester}} \times 100\% \quad (2)$$



Scheme 1. Alcoholysis of polylactic acid (PLA) catalyzed by *p*-TSA (↑ p means pressure's increase).



Scheme 2. Alcoholysis of poly(3-hydroxybutyrate) (PHB) catalyzed by p-TSA (↑ p means pressure's increase).

Methyl lactate (MeLa): ^{1}H NMR (Figure S1) ($CDCl_3$, 500 MHz): δ(ppm) 4.30–4.26 (q; *J* = 6.9 Hz; 1H), 3.78 (s; 3H), 2.80 (s; 1H), 1.42–1.41 (d; *J* = 6.9 Hz; 3H). ^{13}C NMR (Figure S5) ($CDCl_3$, 126 MHz): *δ*(ppm) 176.26; 66.90; 52.65; 20.50.

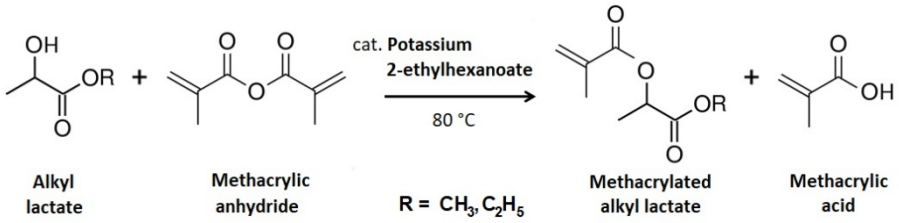
Ethyl lactate (EtLa): ^{1}H NMR (Figure S2) ($CDCl_3$, 500 MHz): δ (ppm) 4.27–4.21 (m; 3H), 2.84 (s; 1H), 1.41–1.40 (d; *J* = 6.9 Hz; 3H), 1.31–1.28 (t; *J* = 7.16; 7.16 Hz; 3H). ^{13}C NMR (Figure S6) ($CDCl_3$, 126 MHz): δ (ppm) 175.72; 66.76; 61.64; 20.38; 14.15.

Methyl 3-hydroxybutyrate (M3HB): ^{1}H NMR (Figure S3) ($CDCl_3$, 500 MHz): δ (ppm) 4.22–4.16 (qd; *J* = 8.54; 6.30; 6.27; 6.27 Hz; 1H), 3.70 (s; 3H), 2.93 (s; 1H), 2.51–2.40 (m; 2H), 1.23–1.22 (d; *J* = 6.30 Hz 3H). ^{13}C NMR (Figure S7) ($CDCl_3$, 126 MHz): δ (ppm) 173.29; 64.28; 51.71; 42.63; 22.49.

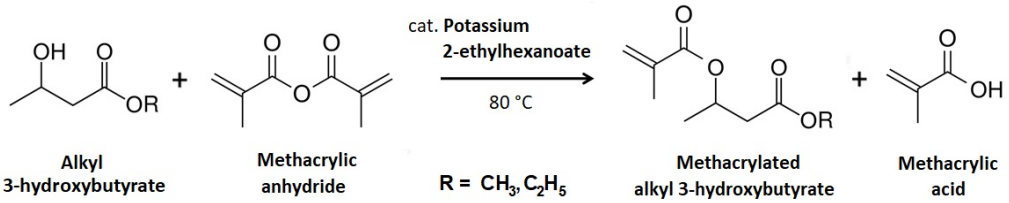
Ethyl 3-hydroxybutyrate (E3HB): ^{1}H NMR (Figure S4) ($CDCl_3$, 500 MHz): δ 4.22–4.15 (q; *J* = 7.16; 7.12; 7.12 Hz; 3H), 2.98 (s; 1H), 2.50–2.46 (dd; *J* = 16.38; 3.48 Hz; 1H), 2.43–2.38 (dd; *J* = 16.40; 8.68 Hz; 1H), 1.28–1.25 (t; *J* = 6.52; 6.52 Hz; 3H), 1.23–1.22 (d; *J* = 6.93 Hz; 3H). ^{13}CNMR (Figure S8) ($CDCl_3$, 126 MHz): δ (ppm) 172.93; 64.30; 60.67; 42.83; 22.45, 14.19.

2.4. Methacrylation of Alkyl Esters

Synthesized alkyl esters of either lactic acid or 3-hydroxybutanoic acid did undergo a reaction with methacrylic anhydride (MAA) in order to form a polymerizable monomer. The reaction mixtures were prepared in a molar ratio 1:1 (ester:MAA) (see Scheme 3 for lactates and Scheme 4 for 3-hydroxybutyrates). The reaction mixture was poured into a three-necked round bottom flask and placed in an oil bath tempered at 80 °C and stirred via a magnetic stirrer. The reactions were catalyzed by a 50% solution of potassium 2-ethylhexanoate in 2-ethylhexynoic acid (2-EHA) that was prepared via a neutralization reaction of 2-ethylhexanoic acid with potassium hydroxide in a mass ratio 1:2 (KOH:acid) while the reaction water was evaporated. The catalyst was added to the mixture in a molar ratio 1:0.02 (ester:catalyst). The reaction started the moment the catalyst was added and all reactions took 24 h of reaction time. The conversions of reactants and the yields of forming products were monitored via GC-FID analysis. The formed methacrylic acid was neutralized by potassium hydroxide aqueous solution and separated from the metracrylated product. Methacrylated alkyl ester structures were verified via MS, FT-IR, ^{1}H NMR, and^{13}C NMR methods.



Scheme 3. Methacrylation of alkyl lactate esters by methacrylic anhydride (MAA).



Scheme 4. Methacrylation of alkyl 3-hydroxybutyrate esters by methacrylic anhydride (MAA).

Methacrylated methyl lactate (MeLaMMA): ^{1}H NMR (Figure S9) ($CDCl_3$, 500 MHz): δ(ppm) 6.20–6.19 (dd; *J* = 1.54; 0.94 Hz; 1H), 5.63–5.62 (p; *J* = 1.53; 1.53; 1.52; 1.52 Hz; 1H), 5.17–5.13 (q; *J* = 7.08; 7.07; 7.07 Hz; 1H), 3.75 (s; 3H), 1.97–1.96 (dd; *J* = 1.6; 1.00 Hz; 3H), 1.53(d; *J* = 7.00 Hz; 3H). ^{13}C NMR (Figure S13) ($CDCl_3$, 126 MHz): δ (ppm)171.30; 166.68; 135.63; 126.44; 68.77; 52.27; 18.13; 16.96.

Methacrylated ethyl lactate (EtLaMMA): ^{1}H NMR (Figure S10) ($CDCl_3$, 500 MHz): δ(ppm) 6.20–6.19 (p; *J* = 1.07; 1.07; 1.07; 1.07 Hz; 1H), 5.63–5.61 (p; *J* = 1.57; 1.57; 1.57; 1.57Hz; 1H), 5.14–5.10 (q; *J* = 7.07; 7.07; 7.03 Hz; 1H), 4.23–4.18 (q; *J* = 7.16; 7.16; 7.15 Hz; 2H), 1.97–1.96 (dd; *J* = 1.58; 1.01 Hz; 3H), 1.53–1.52 (d; *J* = 7.05 Hz; 3H), 1.28–1.26 (t; *J* = 7.15; 7.15 Hz; 3H); 1.53–1.52 (d; *J* = 7.05 Hz; 3H), 1.28–1.26 (t; *J* = 7.15; 7.15 Hz; 3H). ^{13}C NMR (Figure S14) ($CDCl_3$, 126 MHz): δ (ppm) 170.86; 166.76; 135.74; 126.35; 68.93; 61.31; 18.18; 16.97; 14.11.

Methacrylated methyl 3-hydroxybutyrate (M3HBMMA): ^{1}H NMR (Figure S11) ($CDCl_3$, 500 MHz): δ (ppm) 6.07–6.06 (dq; *J* = 1.96; 1.02; 0.98; 0.98 Hz; 1H), 5.56–5.53 (p; *J* = 1.60; 1.60; 1.58; 1.58 Hz; 1H), 5.35–5.29 (dp; *J* = 7.32; 6.26; 6.26; 6.25; 6.25 Hz; 1H), 3.68 (s; 3H), 2.72–2.67 (dd; *J* = 15.34; 7.29 Hz; 1H), 2.57–2.53 (dd; *J* = 15.35; 5.79 Hz; 1H), 1.92 (dd; *J* = 1.63; 1.01 Hz; 3H), 1.35–1.34 (d; *J* = 6.36 Hz; 3H). ^{13}C NMR (Figure S15) ($CDCl_3$, 126MHz): δ (ppm) 170.70; 166.59; 136.47; 125.41; 67.68; 51.73; 40.74; 19.89; 18.23.

Methacrylated ethyl 3-hydroxybutyrate (E3HBMMA): ^{1}HNMR (Figure S12) ($CDCl_3$, 500 MHz): δ (ppm) 6.07–6.06 (dd; *J* = 1.75; 0.97 Hz; 1H), 5.54–5.53 (q; *J* = 1.63; 1.63; 1.63 Hz; 1H), 5.35–5.29 (dp; *J* = 7.50; 6.24; 6.24; 6.24; 6.24 Hz; 1H), 4.16–4.10 (qd; *J* = 7.11; 7.06; 7.06; 0.96Hz; 2H), 2.69–2.65 (dd; *J* = 15.28; 7.42 Hz; 1H), 2.55–2.51 (dd; *J* = 15.29; 5.75 Hz; 1H), 1.94–1.91 (m; 3H), 1.34–1.33 (d; *J* = 6.28 Hz; 3H), 1.25–1.22 (t; *J* = 7.13; 7.13 Hz; 3H). ^{13}C NMR (Figure S16) ($CDCl_3$, 126 MHz): δ (ppm) 170.21; 166.54; 136.46; 125.33; 67.71; 60.57; 41.01; 19.85; 18.19; 14.14.

2.5. Methods for the Reaction Kinetics Study

2.5.1. LC–MS Method for Depolymerization Kinetics

Samples were obtained from the reactor during organic synthesis, followed by quantification of products methyl lactate (MeLa), ethyl lactate(EtLa), methyl 3-hydroxybutyrate(M3HB), and ethyl 3-hydroxybutyrate(E3HB) by ultra-performance liquid chromatography (UHPLC Agilent 1290 Infinity LC) in tandem with triple quadruple (Bruker EVOQ LC-TQ) (Billerica, MA, USA) with atmospheric pressure electrospray ionization (ESI). An external generator of gases was used as the source of nitrogen and air (Peak Scientific—Genius 3045) (Inchinnan, UK). As a stationary phase column, Luna® Omega Polar C18 Phenomenex (100 × 2.1 mm, 1.6 μm) was used. The optimum column temperature was adjusted to 40 °C and the flow rate was set to 0.5 mL/min. The mobile phases were as follows: (A) 0.1% HCOOH in H_2O and (B) ACN were used with the following gradient program of An eluent (%): t (0 min) = 90, t (0.5 min) = 85, t (3.5 min) = 5, t (4.5 min) = 95. Stop time was set to 6.0 min and re-equilibration time was set to 2.0 min. The injection volume applied in all analyses was 7 μL.

MS conditions were as follows: ESI in positive mode; spray voltage: 3500 V; cone temperature 350 °C; cone gas flow: 35 a.u.; heated probe temperature: 650 °C; probe gas flow: 40 a.u., nebulizer gas flow: 55a.u. and exhaust gas: ON. For quantification, MRM mode was used with the following MRM transitions for MeLa (RT 1.24 min; 105.1 > 84.6 with CE 0.25 eV; 105.1 > 93.9 with CE 0.25 eV and 105.1 > 45.0 with CE 2 eV), for EtLa (RT 2.35 min; 119.1 > 47.3 with CE 2.0 eV and 119.1 > 91.1 with CE 2.0 eV), for M3HB (RT 1.91 min; 119.1 > 59.0 with CE 10eV; 119.1 > 87.2 with CE 2.5 eV and 119.1 > 101.2 with CE 1.0 eV), and for E3HB (RT 3.58 min; 133.1 > 73.3 CE with 5eV and 133.1 > 87.2 with CE 5 eV). The collision gas Argon was used ata pressure of 1.5 mTorr.

2.5.2. GC-FID Method for Methacrylation Kinetics

Samples were obtained from the reactor during organic synthesis, followed by quantification of reactants (alkyl esters, methacrylic anhydride) by gas chromatography (Hewlett Packard 5890 Series II) (Palo Alto, CA, USA) with a flame ionization detector (FID). Gas bottles of nitrogen (as auxiliary gas for FID), air (as an oxidizer for FID), and hydrogen (as carrier gas and fuel for FID) were used. Capillary GC column ZB-624 (60 m × 0.32 mm, 1.8 μm) served as a stationary phase. The temperature of the inlet was set to 200 °C and the temperature of the detector to 260 °C. Substances were separated with atemperature gradient, with an initial temperature of 60 °C (held for 1 min) followed by atemperature rate of 20 °C/min with a final temperature of 250 °C (held for 15 min). The column flow rate set for the analyses was 3 mL/min and the split ratio was 1:40. The injection volume applied in all analyses was 1 μL. The retention time of peaks: MeLa (RT6.15 min); EtLa (RT 7.05 min); M3HB (RT 7.76 min); E3HB (RT 8.53 min); MAA (RT 9.88 min); MeLaMMA (RT 9.80); EtLaMMA (RT10.45 min); M3HBMMA (RT 10.85); E3HBMMA (RT 14.48 min).

3. Results

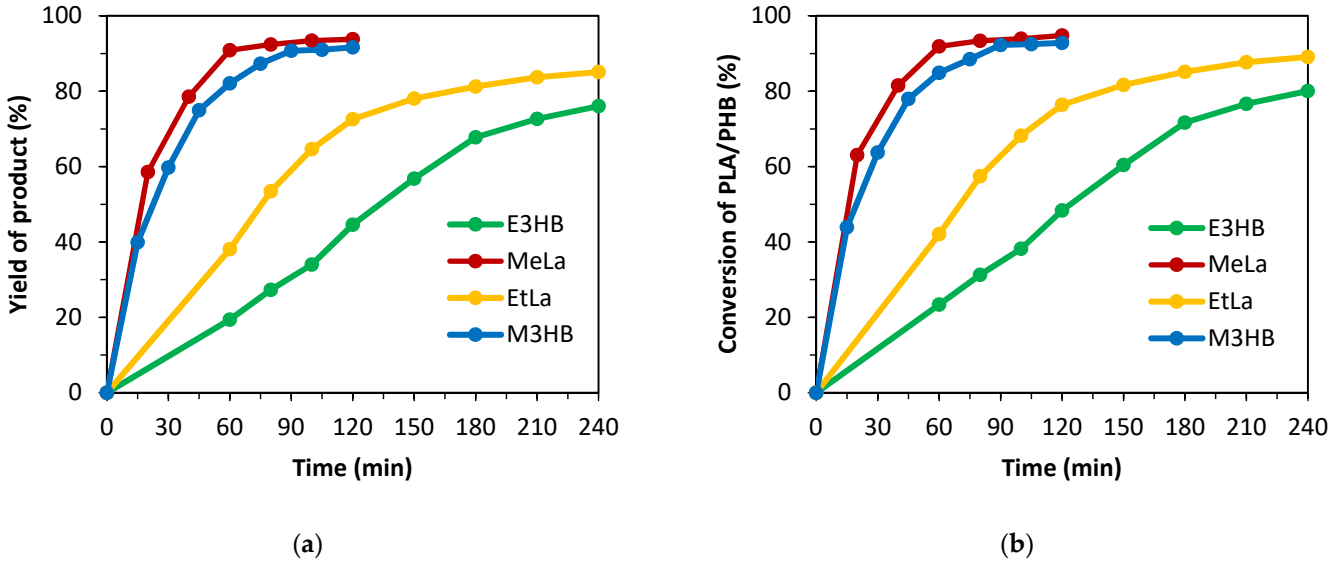
3.1. Depolymerization of PLA and PHB via Alcoholysis

The reaction mixtures for the depolymerization were prepared according to the mass proportion shown in Table 1. The mass of a particular polymer in every mixture was constant and the amount of reacting nucleophile (alcohol) changed depending on the molar ratio of the treactants. The amounts of catalyst (*p*-TSA) for each reaction solution are written in the table as well. Table 1 also contains information on the boiling points of each alkyl ester that was synthesized.

Table 1. Depolymerization mixture components and boiling point values of synthesized monoesters.

		Methyl Lactate	Ethyl Lactate	Methyl 3-Hydroxybutyrate	Ethyl 3-Hydroxybutyrate
Reaction mixture	Polymer	200 g PLA	200 g PLA	200 g PHB	200 g PHB
	Alcohol	356 g MeOH	511 g EtOH	298 g MeOH	428 g EtOH
	Catalyst	5.28 g *p*-TSA	5.28 g *p*-TSA	4.42 g *p*-TSA	4.42 g *p*-TSA
Boiling point		145 °C [39]	154 °C [40]	159 °C [41]	185 °C [42]

The results of the LC–MS analysis in Figure 1a show that methyl esters of each lactic or 3-hydroxybutanoic acid reach their reaction equilibria after about 90 min of depolymerization (MeLawas slightly faster than M3HB), resulting in yields of 93.8% for MeLa and 91.6% for M3HB. On the other hand, the ethyl esters of both carboxylic acids did not reach their total yield value after 4 h of reaction. The reaction rate of ethyl 3-hydroxybutyrate seems to be the slowest, reaching a yield of 76.0% after 240 min. The ethyl lactate's yield after the same reaction time reached 85.1%. The differences between the product yields could be caused by the steric effects of the particular molecules involved in the reaction.



(**a**) (**b**)

Figure 1. (**a**) The increase in particular yields of monoesters during the depolymerization reaction of PLA or PHB; (**b**) the increase in particular conversions of polymers during the depolymerization reaction of PLA or PHB.

The conversion signs of progress of either PLA or PHB during the depolymerization reactions are displayed in Figure 1b. They have been acquired by weighing the residual polymer from the taken sample. The precipitated content of the unreacted polymer was measured and the percentage of conversion was calculated. The results have very similar data curves as the values of the products' yields due to the fact that these values are connected. The conversion of PLA is 94.8% for methanolysis (after 120 min) and the

conversion of PLA is 89.1% for ethanolysis (after 240 min). PHB reached conversions values of 92.8% (MeOH, 120 min) and 80.0% (EtOH, 240 min).

The pressure of the reacting mixture was monitored during every alcoholysis. The results shown in Figure 2 confirm the progressing depolymerization for each mixture. Due to the incorporation of alcohol into the structure of the alkyl ester, the pressure in the system should decrease as a result of decreasing the presence of evaporating alcohol. These expectations are fulfilled except for the methyl lactate. The pressure of the system for the methanolysis of PLA increases after 45 min of reaction. This elevation is caused by the forming MeLa since the reaction temperature was 151 °C and the boiling point value of MeLa is below this temperature (shown in Table 1). Therefore, the occurring monoester participates in the pressure increase.

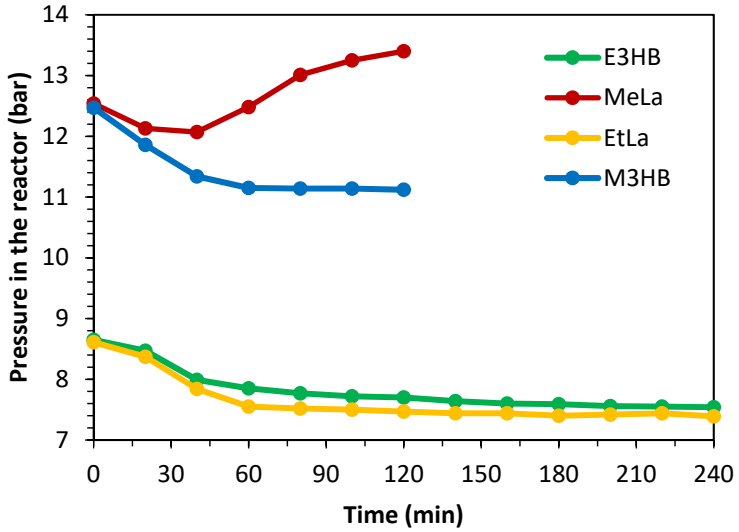


Figure 2. Pressure values dependence on time during depolymerization.

3.2. Kinetics of the Depolymerization of PLA and PHB via Alcoholysis

The first-order reaction order is mostly used to describe the alcoholysis depolymerization due to the fact that if the excess of alcohol is added to the mixture, the concentration of polymer molecules affects the reaction kinetics directly due to its lesser molar amount of mixture [43,44]. If the first-order reaction is used for the calculation, the equations are the following:

$$r = \frac{dc_{polymer}}{dt} = -kc_{polymer}, \quad (3)$$

where r is the reaction rate (mol/(dm^3·min)), k represents the reaction constant (min^{-1}), and $c_{polymer}$ stands for the molar concentration of the polymer (mol/dm^3) at time t (min). The molar concentration of the polymer as a reagent can be substituted by the following conversion values:

$$c_{polymer} = (1 - X), \quad (4)$$

where the molar concentration ($c_{polymer}$) is expressed by conversion (X). This equation is applied for the values of conversion from the number interval of <0,1>. If the molar concentration is replaced with the conversion, the first-order equation has to be rewritten:

$$\frac{dX}{dt} = k(1 - X) \quad (5)$$

If Equation (5) is calculated generally, the steps are as follows:

$$\frac{dX}{(1 - X)} = kdt \quad (6)$$

$$\int_0^X \frac{dX}{(1-X)} = k\int_0^t dt \tag{7}$$

$$-[\ln(1-X) - \ln(1)] = kt \tag{8}$$

$$\ln\frac{1-X}{1} = -kt \tag{9}$$

$$\ln\frac{1}{1-X} = kt \tag{10}$$

Equation (10) was applied to the kinetics values measured by LC–MS analysis. The conversion was transferred into a modified form using the logarithm of a fraction and the dependence on time, as shown in Figure 3. There is evidence that the highest reaction rate constant comprises the depolymerization of PLA in methanol (producing MeLa) with the value of approximately 0.0425 min^{-1}. On the other hand, the depolymerization of PHB in ethanol provided the lowest value of reaction rate constant, reaching approx. 0.0064 min^{-1}. The rest of the reaction rate constants (k) are shown in Table 2.

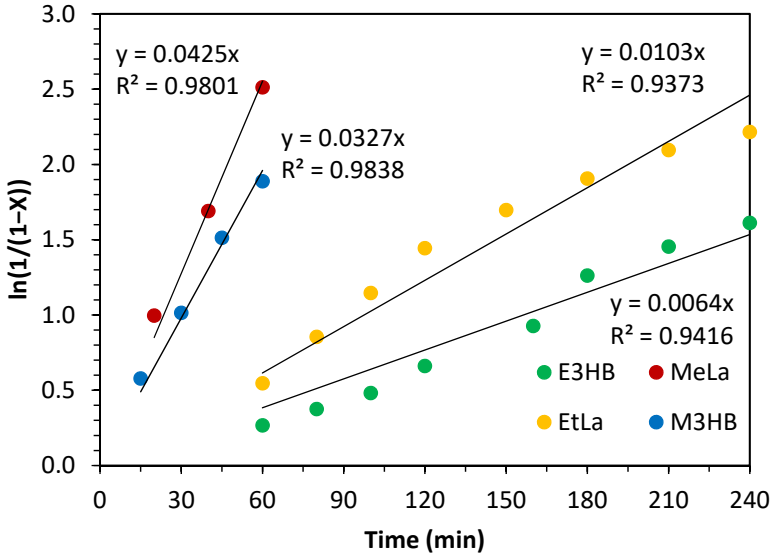


Figure 3. Kinetics of depolymerization of PLA and PHB polymers providing reaction rate constants (k).

Table 2. The values of reaction rate constants (k) for depolymerization of PLA and PHB via alcoholysis.

	Methyl Lactate	Ethyl Lactate	Methyl 3-Hydroxybutyrate	Ethyl 3-Hydroxybutyrate
Reaction rate constant k (min^{-1})	0.0425	0.0327	0.0103	0.0064

3.3. Structural Characterization of Synthesized Alkyl Esters

3.3.1. FT-IR Analyses of Alkyl Esters

Infrared spectrometry using Fourier transformation was used as the first method to confirm the distilled synthesized product. The main peaks shown in Figure 4 lay in the intervals of wave numbers of either 3700–3200 cm^{-1} (–OH stretching) or the values of 1210–1163 cm^{-1} (C=O stretching) and 1750–1735 cm^{-1} (C–O stretching). In particular, the ester bond stretching signals are important since the initial suspension mixture would contain aliphatic alcohol, which provides the signal for the hydroxyl functional groups as well.

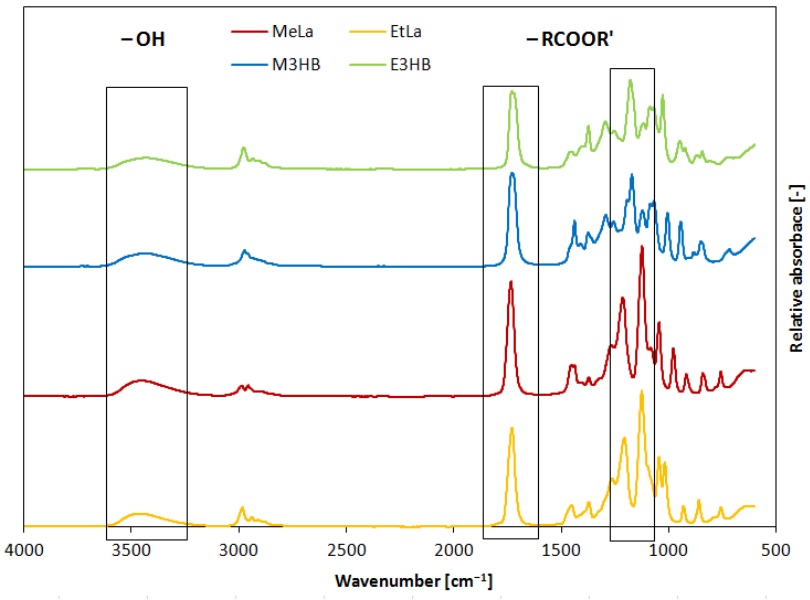


Figure 4. FT-IR spectra of the synthesized alkyl esters as products of the depolymerization reaction of PLA and PHB.

3.3.2. MS Analyses of Alkyl Esters

The analytic procedure to obtain all MS spectra of synthesized alkyl esters of lactic and 3-hydroxybutyric acid is described above (see Section 2.2.2). All molecular precursor ions have been measured as products of the ESI ionization process. Other signals are particular product ions occurring due to the fragmentation of the molecules apart during the MS/MS analysis. All spectra are shown in Figure 5.

3.4. Methacrylation of the Alkyl Esters of Lactic and 3-Hydroxybutanoic Acid

The reaction mixtures for the syntheses of methacrylated alkyl esters of carboxylic acids were prepared according to the mass proportion shown in Table 3. The mass of a particular alkyl ester in every mixture was constant and the amount of reacting methacrylic anhydride changed depending on the molar ratio of the reactants. The amount of catalyst (50% solution of potassium 2-ethylhexanoate in 2-ethylhexanoic acid) was calculated according to the particular reacting alkyl ester.

Table 3. Methacrylation mixture components for the synthesis of methacrylated alkyl monoesters.

		Methacrylated Methyl Lactate	**Methacrylated Ethyl Lactate**	**Methacrylated Methyl 3-Hydroxybutyrate**	**Methacrylated Ethyl 3-Hydroxybutyrate**
Reaction mixture	Ester	30 g MeLa	30 g EtLa	30 g M3HB	30 g E3HB
	Anhydride	44.4 g MAA	39.2 g MAA	39.2 g MAA	35.0 g MAA
	Catalyst	2.1 g solution	1.85 g solution	1.85 g solution	1.66 g solution
Mixture volume		70.42 cm^3	66.92 cm^3	66.26 cm^3	63.31 cm^3

The results of the methacrylation reaction that forms methacryled alkyl esters of lactic or 3-hydroxybutanoic acid are shown in Figure 6. Both reactants which were monitored (alkyl ester and methacrylic anhydride) via GC-FID analysis have similar time progressions of their conversion values due to the fact that their molar ratio in the reacting mixtures was 1:1 mol in all cases. The conversion values of methacrylic anhydride are slightly higher, likely due to the fact that the anhydride participated in secondary reactions in the reaction mixture (water hydrolysis, etc.). It is evident that the esters of lactic acid (MeLa and EtLa), formed into the products MeLaMMA and EtLaMMA, respectively, progressed faster in time

than the alkyl esters of 3-hydroxybutanoic acid. These results may have been determined by the steric effects of each ester and due to their varying polarity which could have affected the effectiveness of the catalyst.

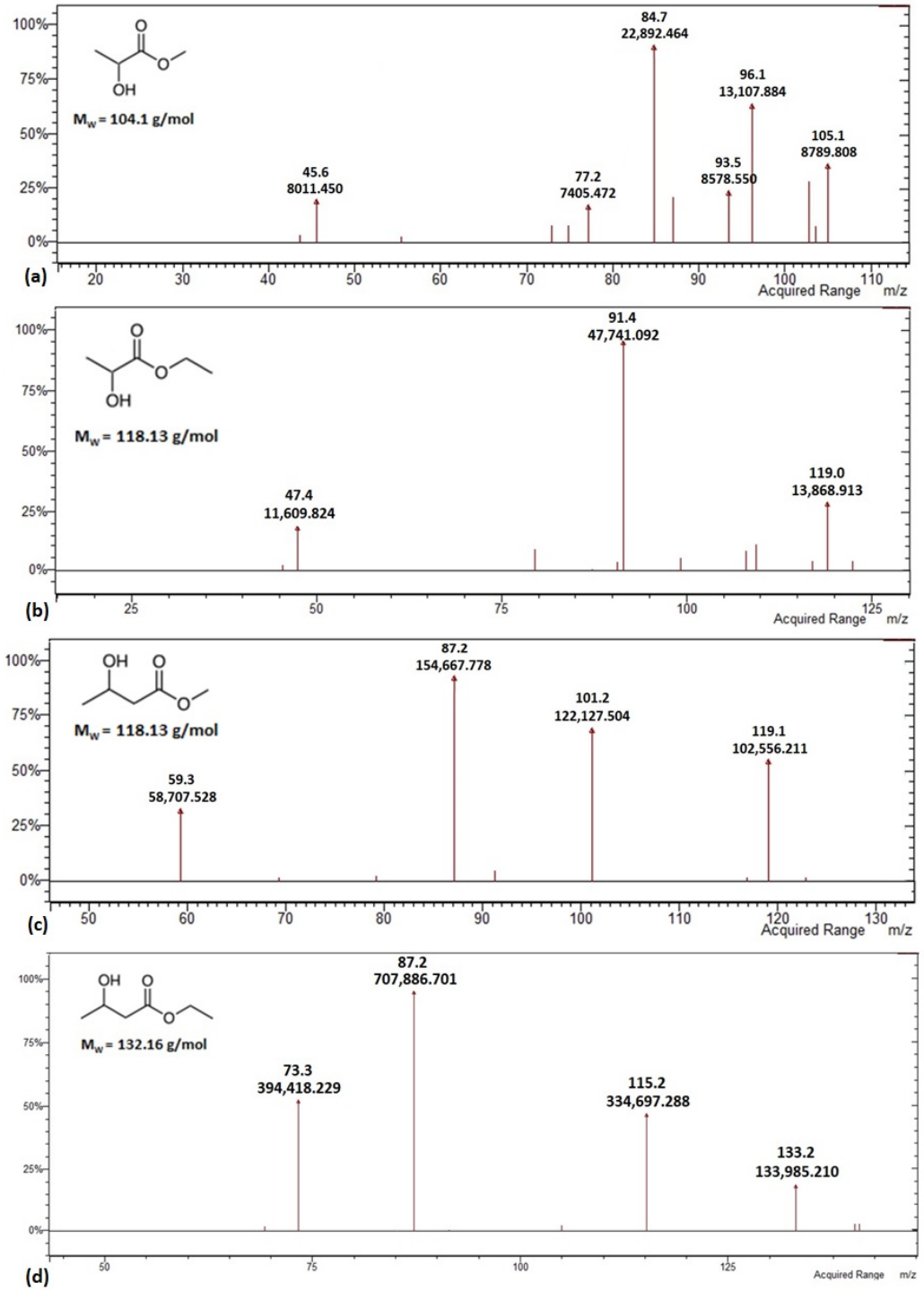
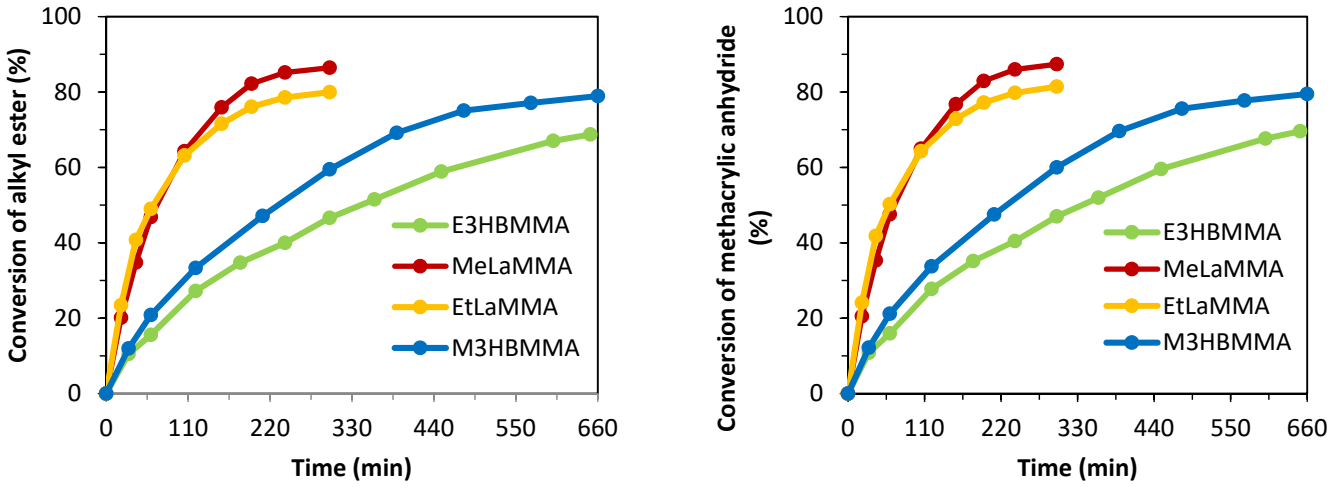


Figure 5. MS spectra of the synthesized alkyl monoesters based on PLA and PHB. (**a**) Methyl lactate (MeLa); (**b**) Ethyl lactate (EtLa); (**c**) Methyl 3-hydroxybutyrate (M3HB); (**d**) Ethyl 3-hydroxybutyrate (E3HB).



(**a**) (**b**)

Figure 6. (**a**) The increase in particular conversions of alkyl esters of lactic and 3-hydroxybutanoic acid in time during the methacrylation reactions; (**b**) The increase in conversion of methacrylic anhydride in time during the methacrylation reactions.

The methacrylation reactions were performed for 24 h to obtain the highest yields of the methacrylated product. The graphs below are presented in order to compare the rates of each particular reaction which served for the calculation of reaction rate constants. The yields of methacrylated alkyl esters products increasing in time are shown in Table 4. The yield quantified after 5 h of reaction is shown for comparison.

Table 4. Methacrylated alkyl ester yields compared after 5 h and 24 h of methacrylation reaction.

		Methacrylated Methyl Lactate	Methacrylated Ethyl Lactate	Methacrylated Methyl 3-Hydroxybutyrate	Methacrylated Ethyl 3-Hydroxybutyrate
Yield of product	5 h	86.2%	80.2%	59.5%	45.6%
	24 h	99.5%	99.4%	98.3%	98.0%

3.5. Kinetics of the Methacrylation Reactions

It is assumed that when equimolar amounts of both reactants (alkyl ester and methacrylic anhydride) are used, the rate of methacrylation is dependent on the concentration of both reactants. The acylation of hydroxyl functional groups using homogeneous catalysis was considered as potential reaction kinetics (methacrylation reaction is a type of the acylation) [45]. The Equations defining the dependence of the concentration of both reactants (alkyl ester and methacrylic anhydride) on time leading to acquiring the reaction rate constant are as follows:

$$r' = \frac{dc_{ester}}{dt} = \frac{dc_{MAA}}{dt} = -k' c_{ester} c_{MAA}, \quad (11)$$

Equation (11) defines the conventional second-order rate where r' is the reaction rate (mol/(dm^3·min)), k' represents the reaction constant (dm^3/(mol·min)), c_{ester} stands for the molar concentration of a particular alkyl ester (mol/dm^3), and c_{MAA} stands for the molar concentration of methacrylic anhydride (mol/dm^3) at time t (min). To solve the second-order rate of reaction, several mathematical adjustments need to be made:

$$c^0{}_{ester} = a \quad (12)$$

$$c^0{}_{MAA} = b \quad (13)$$

$$c_{ester} = a - x \tag{14}$$

$$c_{MAA} = b - x, \tag{15}$$

where x stands for the concentration of each reactant in particular time t (min), $c^0{}_{ester}$ (mol/dm^3) is the initial concentration of alkyl ester, and $c^0{}_{MAA}$ (mol/dm^3) is the initial concentration of methacrylic anhydride. Considering these additional defined quantities, Equation (11) can be rearranged and solved:

$$-\frac{dx}{dt} = -k'\left(c^0{}_{ester} - x\right)\left(c^0{}_{MAA} - x\right) \tag{16}$$

$$\int_0^x \frac{dx}{(c^0{}_{ester} - x)(c^0{}_{MAA} - x)} = k' \int_0^t dt \tag{17}$$

$$\frac{1}{b-a}\left(\ln\frac{1}{a-x} - \ln\frac{1}{b-x}\right) = k't \tag{18}$$

$$\frac{1}{c^0{}_{MAA} - c^0{}_{ester}}\left(\ln\frac{c^0{}_{ester}}{c^0{}_{ester} - x} - \ln\frac{c^0{}_{MAA}}{c^0{}_{MAA} - x}\right) = k't, \tag{19}$$

The left side of Equation (19) can be simplified by applying the rule of logarithm, and when the simplified equation has been rearranged, the dependence of the actual concentration during the reaction on time can be formed:

$$\frac{1}{c^0{}_{MAA} - c^0{}_{ester}} \ln\frac{c^0{}_{ester}c_{MAA}}{c^0{}_{MAA}c_{ester}} = k't \tag{20}$$

$$\ln\frac{c^0{}_{ester}c_{MAA}}{c^0{}_{MAA}c_{ester}} = k'\left(c^0{}_{MAA} - c^0{}_{ester}\right)t \tag{21}$$

Equation (21) can be used to obtain the reaction rate constant k'. If the graphic solution is applied, the slope of the linear curve acquired from the graph contains the constant k'. All data gathered during the reaction progress in time recalculated for mathematical purposes are shown in Figure 7. All reaction rate constants are written in Table 5. It is evident from the results that, in general, the methacrylation reactions of alkyl esters of lactic acid have higher reaction rate constants than the alkyl esters of 3-hydroxybutanoic acid. It is assumed that the availability of the hydroxyl functional group of lactates is better than for 3-hydroxybutyrates.

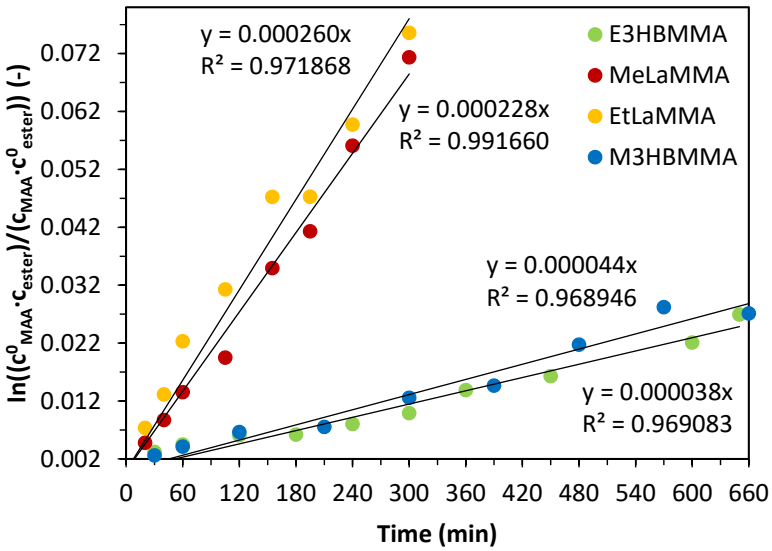


Figure 7. The graphic solution of second-order reaction rate of methacrylation reaction of alkyl esters.

Table 5. The calculated values of reaction rate constants (k') for methacrylation of alkyl esters of lactic and 3-hydroxybutyric acid from the slope of the graphic solutions.

	Methacrylated Methyl Lactate	Methacrylated Ethyl Lactate	Methacrylated Methyl 3-Hydroxybutyrate	Methacrylated Ethyl 3-Hydroxybutyrate
Reaction rate constant k' ($dm^3/(mol \cdot min)$)	0.0885	0.0554	0.0092	0.0079

3.6. Structural Characterization of Synthesized Methycrylated Alkyl Esters

3.6.1. FT-IR Analyses of Methacrylated Alkyl Esters

Infrared spectrometry using Fourier transformation's results for the confirmation of the structures of the synthesized methacrylated alkyl esters are displayed in Figure 8. Peaks showing the presence of signals, which belong to ester bonds, lay in the intervals of wave numbers of either 1210–1163 cm^{-1} (C=O stretching) or the values of 1750–1735 cm^{-1} (C–O stretching). The signals referring to C–O stretching are split in every spectrum. The reason for the splitting of the peak is the presence of two different types of ester bonding in molecules. One bond belongs to the ester of lactic or 3-hydroxybutanoic acid and aliphatic alcohol. The other signal refers to the ester bond between the formed alkyl ester of carboxylic acid and the methacrylic acid. The second type of signal that can be found in FT-IR spectra reaches the values of wave numbers of either 1670–1600 cm^{-1} (C=C stretching) or 1000–650 cm^{-1} (C=C bending). These peaks uncover the presence of unsaturated double bonds within the structures of synthesized products that belong to methacrylates. Another confirmation of the successful methacrylation is the absence of signal in the area of 3700–3200 cm^{-1} (–OH stretching). These functional groups were supposed to react with methacrylic anhydride. Therefore, their peaks are missing in comparison with FT-IR spectra in Figure 4.

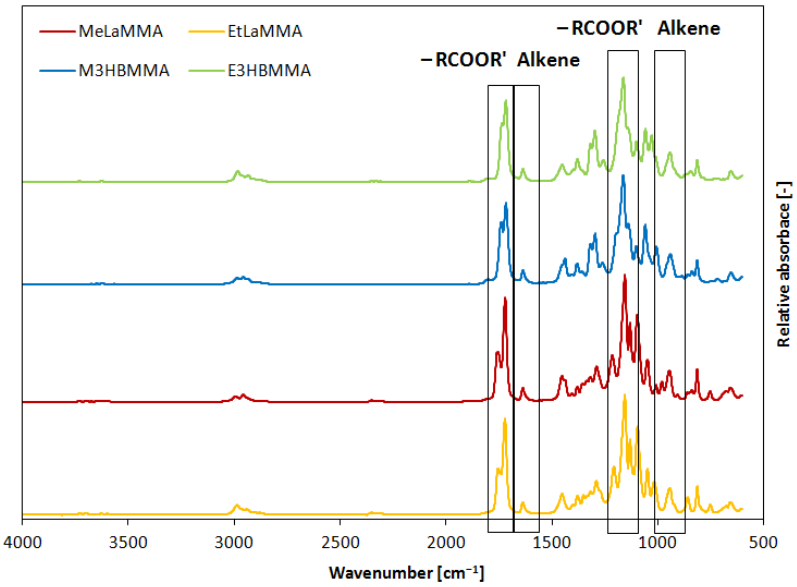


Figure 8. FT-IR spectra of the synthesized methacryled alkyl esters as products of the methacrylation reaction of alkyl esters of lactic acid or 3-hydroxybutanoic acid and methacrylic anhydride.

3.6.2. MS Analyses of Methacrylated Alkyl Esters

The analytic procedure to obtain all MS spectra of synthesized methacrylated alkyl esters is described above (see Section 2.2.2). All molecular precursor ions have been measured as products of the ESI ionization process. Other signals are particular product ions occurring due to the fragmentation of the molecules during the MS/MS analysis. All spectra are shown in Figure 9.

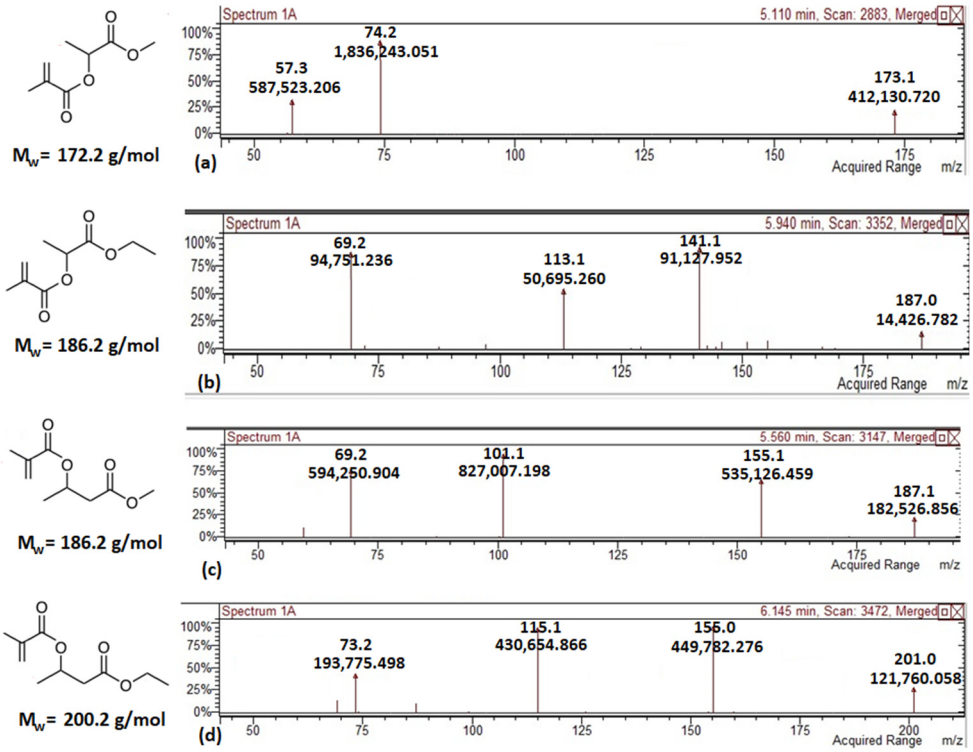


Figure 9. MS spectra of the synthesized methacrylated alkyl esters of lactic acid or 3-hydroxybutanoic acid. (**a**) Methacrylated methyl lactate (MeLaMMA); (**b**) methacrylated ethyl lactate (EtLaMMA); (**c**) methacrylated methyl 3-hydroxybutyrate (M3HB); (**d**) methacrylated ethyl 3-hydroxybutyrate (E3HB).

4. Discussion

This work was focused on the experimental confirmation of the depolymerization of poly(lactic acid) (PLA) and poly(3-hydroxybutyrate) (PHB) via alcoholysis. All reactions were performed in identical conditions, which were a temperature of 151 °C, the presence of the constant amount of molar alcohol access (4:1) and the catalyst *para*-toluenesulphonic acid, particularly 1% mol. of the particular polyester. The pressure of the reaction solution differed regarding the used alcohol and the particular reaction combination. In all cases, the pressure in the reactor decreased over time except for the mixture containing methanol and poly(lactic acid). This mixture's pressure elevated from 12.54 bar to 13.40 due to the boiling point value of methyl lactate being 145 °C, which means this ester evaporated in the reactor as well. Generally, lower pressure values were measured for theethanolyses of both PLA and PHB, which decreased from an approximate value of 8.63 bar to 7.54 (E3HB) and 7.39 (M3HB). The decrease is the consequence of lowering the volatility of the reacting solution due to the forming of alkyl esters. It was also found that the rates of methanolyses are faster than the rates of ethanolyses. Depolymerization reaction rate constants (k) were calculated for all experimental reactions, resulting in the highest one of 0.0425 (min^{-1}) for the methanolysis of PLA and the lowest constant related to ethanolysis of PHB, reaching a value of 0.0064 (min^{-1}). These differences are probably caused by the steric effects of particular reactants. The yields of each product were: 93.79% MeLa (120 min); 91.64% M3HB (120 min); 85.08% EtLa (240 min); and 76.03% E3HB (240 min).

The synthesized alkyl esters from the depolymerization of PLA and PHB were modified by the methacrylation reaction with methacrylic anhydride (MAA) to methacrylated alkyl esters, which are polymerizable. The reaction mixtures were composed of equal mass amounts of alkyl esters and different amounts of methacrylic anhydride in equimolar ratio to the esters. The catalyst used for the methacrylation was potassium 2-ethylheaxoate (50% mass solution) in 2-ethylhexanoic acid. The amount of catalyst was 2% mol. The rates of the methacrylation at 80 °C of each alkyl ester define the calculated reaction rate constants (k').

It has been observed that in general, the methacrylation of alkyl lactates was faster than in the case of alkyl 3-hydroxybutyrates. The highest value of methacrylation rate constant comprises the mixture containing methyl lactate (k' = 0.0885 $dm^3/(mol \cdot min)$).On the other hand, the lowest one belongs to ethyl 3-hydroxybutyrate (k' = 0.0079 $dm^3/(mol \cdot min)$). These constants have been calculated according to the reactions' progress in time to evaluate a comparison for all reactants, but the methacrylation reactions of all alkyl esters were performed for 24 h to ensure the biggest possible yield. All yields reached values equal to or higher than 98%.

5. Conclusions

Several conclusions from the performed experiments can be summarized. The type of aliphatic alcohol plays a major role in the rate of depolymerization of the polyesters PLA and PHB. Methanol ensures a faster depolymerization process than ethanol. However, using methanol can be problematic regarding the used equipment due to the fact that these mixtures produce a higher overpressure. The methacrylation of all alkyl esters of lactic or 3-hydroxybutanoic acid reaches high yields after 24 h, close to 100%. Nevertheless, the lactic esters undergo methacrylation reaction at a faster rate than the 3-hydroxybutyrates. The distillation of the forming methacrylic acid could be performed instead of neutralizing and washing the acid; however, the appropriate stabilization against spontaneous polymerization has to be ensured.

Supplementary Materials: The following supporting information can be downloaded at: https://www.mdpi.com/article/10.3390/polym14235236/s1, Figure S1: ^{1}H NMR spectrum of methyl lactate (MeLa). ^{1}H NMR ($CDCl_3$, 500 MHz): δ (ppm) 4.30–4.26 (q; *J* = 6.9 Hz; 1H), 3.78 (s; 3H), 2.80 (s; 1H), 1.42–1.41 (d; *J* = 6.9 Hz; 3H). Figure S2: ^{1}H NMR spectrum of ethyl lactate (EtLa). ^{1}H NMR ($CDCl_3$, 500 MHz): δ (ppm) 4.27–4.21 (m; 3H), 2.84 (s; 1H), 1.41–1.40 (d; *J* = 6.9 Hz; 3H), 1.31–1.28 (t; *J* = 7.16; 7.16 Hz; 3H). Figure S3: ^{1}H NMR spectrum of methyl 3-hydroxybutyrate (M3HB). ^{1}H NMR ($CDCl_3$, 500 MHz): δ (ppm) 4.22–4.16 (qd; *J* = 8.54; 6.30; 6.27; 6.27 Hz; 1H), 3.70 (s; 3H), 2.93 (s; 1H), 2.51–2.40 (m; 2H), 1.23–1.22 (d; *J* = 6.30 Hz 3H). Figure S4: ^{1}H NMR spectrum of ethyl 3-hydroxybutyrate (E3HB). ^{1}H NMR ($CDCl_3$, 500 MHz): δ 4.22–4.15 (q; *J* = 7.16; 7.12; 7.12 Hz; 3H), 2.98 (s; 1H), 2.50–2.46 (dd; *J* = 16.38; 3.48 Hz; 1H), 2.43–2.38 (dd; *J* = 16.40; 8.68 Hz; 1H), 1.28–1.25 (t; *J* = 6.52; 6.52 Hz; 3H), 1.23–1.22 (d; *J* = 6.93 Hz; 3H). Figure S5: ^{13}C NMR spectrum of methyl lactate (MeLa). ^{13}C NMR ($CDCl_3$, 126 MHz): δ (ppm) 176.26; 66.90; 52.65; 20.50. Figure S6: ^{13}C NMR spectrum of ethyl lactate (EtLa). ^{13}C NMR ($CDCl_3$, 126 MHz): δ (ppm) 175.72; 66.76; 61.64; 20.38; 14.15. Figure S7: ^{13}C NMR spectrum of methyl 3-hydroxybutyrate (M3HB). ^{13}C NMR ($CDCl_3$, 126 MHz): δ (ppm) 173.29; 64.28; 51.71; 42.63; 22.49. Figure S8: ^{13}C NMR spectrum of ethyl 3-hydroxybutyrate (E3HB). ^{13}C NMR ($CDCl_3$, 126 MHz): δ (ppm) 172.93; 64.30; 60.67; 42.83; 22.45, 14.19. Figure S9: ^{1}H NMR spectrum of methacrylated methyl lactate (MeLaMMA). ^{1}H NMR ($CDCl_3$, 500 MHz): δ (ppm) 6.20–6.19 (dd; *J* = 1.54; 0.94 Hz; 1H), 5.63–5.62 (p; *J* = 1.53; 1.53; 1.52; 1.52 Hz; 1H), 5.17-5.13 (q; *J* = 7.08; 7.07; 7.07 Hz; 1H), 3.75 (s; 3H), 1.97–1.96 (dd; *J* = 1.6; 1.00 Hz; 3H), 1.53 (d; *J* = 7.00 Hz; 3H). Figure S10: ^{1}H NMR spectrum of methacrylated ethyl lactate (EtLaMMA). ^{1}H NMR ($CDCl_3$, 500 MHz): δ (ppm) 6.20–6.19 (p; *J* = 1.07; 1.07; 1.07; 1.07 Hz; 1H), 5.63–5.61 (p; *J* = 1.57; 1.57; 1.57; 1.57 Hz; 1H), 5.14–5.10 (q; *J* = 7.07; 7.07; 7.03 Hz; 1H), 4.23–4.18 (q; *J* = 7.16; 7.16; 7.15 Hz; 2H), 1.97–1.96 (dd; *J* = 1.58; 1.01 Hz; 3H), 1.53–1.52 (d; *J* = 7.05 Hz; 3H), 1.28–1.26 (t; *J* = 7.15; 7.15 Hz; 3H). Figure S11: ^{1}H NMR spectrum of methacrylated methyl 3-hydroxybutyrate (M3HBMMA). ^{1}H NMR ($CDCl_3$, 500 MHz): δ (ppm) 6.07–6.06 (dq; *J* = 1.96; 1.02; 0.98; 0.98 Hz; 1H), 5.56–5.53 (p; *J* = 1.60; 1.60; 1.58; 1.58 Hz; 1H), 5.35–5.29 (dp; *J* = 7.32; 6.26; 6.26; 6.25; 6.25 Hz; 1H), 3.68 (s; 3H), 2.72–2.67 (dd; *J* = 15.34; 7.29 Hz; 1H), 2.57–2.53 (dd; *J* = 15.35; 5.79 Hz; 1H), 1.92 (dd; *J* = 1.63; 1.01 Hz; 3H), 1.35-1.34 (d; *J* = 6.36 Hz; 3H). Figure S12: ^{1}H NMR spectrum of methacrylated ethyl 3-hydroxybutyrate (E3HBMMA). ^{1}H NMR ($CDCl_3$, 500 MHz): δ (ppm) 6.07–6.06 (dd; *J* = 1.75; 0.97 Hz; 1H), 5.54–5.53 (q; *J* = 1.63; 1.63; 1.63 Hz; 1H), 5.35–5.29 (dp; *J* = 7.50; 6.24; 6.24; 6.24; 6.24 Hz; 1H), 4.16–4.10 (qd; *J* = 7.11; 7.06; 7.06; 0.96 Hz; 2H), 2.69–2.65 (dd; *J* = 15.28; 7.42 Hz; 1H), 2.55–2.51 (dd; *J* = 15.29; 5.75 Hz; 1H), 1.94–1.91 (m; 3H), 1.34–1.33 (d; *J* = 6.28 Hz; 3H), 1.25–1.22 (t; *J* = 7.13; 7.13 Hz; 3H). Figure S13: ^{13}C NMR spectrum of methacrylated methyl lactate (MeLaMMA). ^{13}C NMR ($CDCl_3$, 126 MHz): δ (ppm) 171.30; 166.68; 135.63; 126.44; 68.77; 52.27; 18.13; 16.96. Figure S14: ^{13}C NMR spectrum of methacrylated ethyl lactate (EtLaMMA). ^{13}C NMR ($CDCl_3$, 126 MHz): δ (ppm) 170.86; 166.76; 135.74; 126.35; 68.93; 61.31; 18.18; 16.97; 14.11.

Figure S15: ^{13}C NMR spectrum of methacrylated methyl 3-hydroxybutyrate (M3HBMMA). ^{13}C NMR ($CDCl_3$, 126 MHz): δ (ppm) 170.70; 166.59; 136.47; 125.41; 67.68; 51.73; 40.74; 19.89; 18.23. Figure S16: ^{13}C NMR spectrum of methacrylatedethyl 3-hydroxybutyrate (E3HBMMA). ^{13}C NMR ($CDCl_3$, 126 MHz): δ (ppm) 170.21; 166.54; 136.46; 125.33; 67.71; 60.57; 41.01; 19.85; 18.19; 14.14.

Author Contributions: V.J.: conceptualization, experimental work, mathematical calculation, gas chromatography analysis, and infrared analysis; J.F.: liquid chromatography analysis, mass spectrometry analysis, and conceptualization; L.I.: nuclear magnetic resonance analysis; D.V.: nuclear magnetic resonance analysis; L.M.: gas chromatography supervision; S.F., R.P., P.S. and J.K.: supervision; J.K. and P.S.: investigation. All authors have read and agreed to the published version of the manuscript.

Funding: This work was supported by the Materials Research Centre. L.I.: Appreciation to Brno City Municipality (Brno Ph.D. Talent Scholarship) for the financial support. V.J., J.F., L.I. and D.V.: Appreciation to the Ministry of Education, Youth and Sport of the Czech Republic (project No. FCH-S-22-8012) and (project No. FCH-S-22-8001).

Institutional Review Board Statement: Not applicable.

Informed Consent Statement: Not applicable.

Data Availability Statement: Not applicable.

Acknowledgments: We would like to thank Nafigate Corporation a.s. for the support in the form of supplies of PHB material.

Conflicts of Interest: The authors declare no conflict of interest.

References

1. Beltrán, F.R.; Barrio, I.; Lorenzo, V.; Del Río, B.; Martínez Urreaga, J.; de La Orden, M.U. Valorization of poly(lactic acid) wastes via mechanical recycling: Improvement of the properties of the recycled polymer. *Waste Manag. Res. J. A Sustain. Circ. Econ.* **2019**, *37*, 135–141. [CrossRef]
2. Arrieta, M.P.; Samper, M.D.; Aldas, M.; López, J. On the Use of PLA-PHB Blends for Sustainable Food Packaging Applications. *Materials* **2017**, *10*, 1008. [CrossRef] [PubMed]
3. Ray, S.S.; Bousmina, M. Biodegradable polymers and their layered silicate nanocomposites: In greening the 21st century materials world. *Prog. Mater. Sci.* **2005**, *50*, 962–1079.
4. Hottel, T.; Bilec, M.; Landis, A. Sustainability assessments of bio-based polymers. *Polym. Degrad. Stab.* **2013**, *98*, 1898–1907. [CrossRef]
5. Reddy, M.M.; Vivekanandhan, S.; Misra, M.; Bhatia, S.K.; Mohanty, A.K. Biobased plastics and bionanocomposites: Current status and future opportunities. *Prog. Polym. Sci.* **2013**, *38*, 1653–1689. [CrossRef]
6. Gough, C.R.; Callaway, K.; Spencer, E.; Leisy, K.; Jiang, G.; Yang, S.; Hu, X. Biopolymer-Based Filtration Materials. *ACS Omega* **2021**, *6*, 11804–11812. [CrossRef]
7. Beltrán, F.; Arrieta, M.; Moreno, E.; Gaspar, G.; Muneta, L.; Carrasco-Gallego, R.; Yáñez, S.; Hidalgo-Carvajal, D.; de la Orden, M.; Urreaga, J.M. Evaluation of the Technical Viability of Distributed Mechanical Recycling of PLA 3D Printing Wastes. *Polymers* **2021**, *13*, 1247. [CrossRef] [PubMed]
8. Moreno, E.; Beltrán, F.R.; Arrieta, M.P.; Gaspar, G.; Muneta, L.M.; Carrasco-Gallego, R.; Yáñez, S.; Hidalgo-Carvajal, D.; de la Orden, M.U.; Martínez Urreaga, J. Technical Evaluation of Mechanical Recycling of PLA 3D Printing Wastes. In Proceedings of the First International Conference on "Green" Polymer Materials, Basel, Switzerland, 4 November 2020; MDPI: Basel, Switzerland, 2021; p. 19.
9. Leejarkpai, T.; Mungcharoen, T.; Suwanmanee, U. Comparative assessment of global warming impact and eco-efficiency of PS (polystyrene), PET (polyethylene terephthalate) and PLA (polylactic acid) boxes. *J. Clean. Prod.* **2016**, *125*, 95–107. [CrossRef]
10. Piemonte, V.; Gironi, F. Kinetics of Hydrolytic Degradation of PLA. *J. Polym. Environ.* **2013**, *21*, 313–318. [CrossRef]
11. Castro-Aguirre, E.; Iniguez-Franco, F.; Samsudin, H.; Fang, X.; Auras, R. Poly(lactic acid)—Mass production, processing, industrial applications, and end of life. *Adv. Drug Deliv. Rev.* **2016**, *107*, 333–366. [CrossRef] [PubMed]
12. Papong, S.; Malakul, P.; Trungkavashirakun, R.; Wenunun, P.; Chom-in, T.; Nithitanakul, M.; Sarobol, E. Comparative assessment of the environmental profile of PLA and PET drinking water bottles from a life cycle perspective. *J. Clean. Prod.* **2014**, *65*, 539–550. [CrossRef]
13. Chen, H.; Chen, F.; Chen, H.; Liu, H.; Chen, L.; Yu, L. Thermal degradation and combustion properties of most popular synthetic biodegradable polymers. *Waste Manag. Res. J. A Sustain. Circ. Econ.* **2022**, 0734242X221129054. [CrossRef] [PubMed]
14. Zhou, Q.; Xanthos, M. Nanosize and microsize clay effects on the kinetics of the thermal degradation of polylactides. *Polym. Degrad. Stab.* **2009**, *94*, 327–338. [CrossRef]
15. Uğur, A.; Şahin, N.; Beyatli, Y. Accumulation of Poly-\beta-Hydroxybutyrate in Streptomyces Species During Growth with Different Nitrogen Sources. *Turk. J. Biol.* **2002**, *26*, 171–174.

16. Lenz, R.W.; Marchessault, R.H. Bacterial Polyesters: Biosynthesis, Biodegradable Plastics and Biotechnology. *Biomacromolecules* **2005**, *6*, 1–8. [CrossRef]
17. Arrieta, M.P.; Fortunati, E.; Dominici, F.; Rayón, E.; López, J.; Kenny, J.M. Multifunctional PLA–PHB/cellulose nanocrystal films: Processing, structural and thermal properties. *Carbohydr. Polym.* **2014**, *107*, 16–24. [CrossRef]
18. Kervran, M.; Vagner, C.; Cochez, M.; Ponçot, M.; Saeb, M.R.; Vahabi, H. Thermal degradation of polylactic acid (PLA)/polyhydroxybutyrate (PHB) blends: A systematic review. *Polym. Degrad. Stab.* **2022**, *201*, 109995. [CrossRef]
19. Kontárová, S.; Přikryl, R.; Melčová, V.; Menčík, P.; Horálek, M.; Figalla, S.; Plavec, R.; Feranc, J.; Sadílek, J.; Pospíšilová, A. Printability, Mechanical and Thermal Properties of Poly(3-Hydroxybutyrate)-Poly(lactic acid)-Plasticizer Blends for Three-Dimensional (3D) Printing. *Materials* **2020**, *13*, 4736. [CrossRef]
20. Plavec, R.; Hlaváčiková, S.; Omaníková, L.; Feranc, J.; Vanovčanová, Z.; Tomanová, K.; Alexy, P. Recycling possibilities of bioplastics based on PLA/PHB blends. *Polym. Test.* **2020**, *92*, 106880. [CrossRef]
21. Elsawy, M.A.; Kim, K.H.; Park, J.W.; Deep, A. Hydrolytic degradation of polylactic acid (PLA) and its composites. *Renew. Sustain. Energy Rev.* **2017**, *79*, 1346–1352. [CrossRef]
22. Piemonte, V.; Sabatini, S.; Gironi, F. Chemical Recycling of PLA: A Great Opportunity Towards the Sustainable Development? *J. Polym. Environ.* **2013**, *21*, 640–647. [CrossRef]
23. Coszach, P.; Bogaert, J.C.; Willocq, J. Chemical Recycling of PLA by Hydrolysis. U.S. Patent No 8,431,683, 2013.
24. Cosate de Andrade, M.F.; Souza, P.; Cavalett, O.; Morales, A.R. Life Cycle Assessment of Poly(lactic acid) (PLA): Comparison Between Chemical Recycling, Mechanical Recycling and Composting. *J. Polym. Environ.* **2016**, *24*, 372–384. [CrossRef]
25. McKeown, P.; Jones, M.D. The Chemical Recycling of PLA: A Review. *Sustain. Chem.* **2020**, *1*, 1–22. [CrossRef]
26. Cristina, A.M.; Rosaria, A.; Sara, F.; Fausto, G. PLA Recycling by Hydrolysis at High Temperature. In *AIP Conference Proceedings*; AIP Publishing LLC: Melville, NY, USA, 2016; p. 020011.
27. Tsuji, H.; Daimon, H.; Fujie, K. A New Strategy for Recycling and Preparation of Poly(l-lactic acid): Hydrolysis in the Melt. *Biomacromolecules* **2003**, *4*, 835–840. [CrossRef] [PubMed]
28. Li, S.M.; Rashkov, I.; Espartero, J.L.; Manolova, N.; Vert, M. Synthesis, characterization, and hydrolytic degradation of PLA/PEO/PLA triblock copolymers with long poly (l-lactic acid) blocks. *Macromolecules* **1996**, *29*, 57–62. [CrossRef]
29. Piemonte, V.; Gironi, F. Lactic Acid Production by Hydrolysis of Poly(Lactic Acid) in Aqueous Solutions: An Experimental and Kinetic Study. *J. Polym. Environ.* **2013**, *21*, 275–279. [CrossRef]
30. Majgaonkar, P.; Hanich, R.; Malz, F.; Brüll, R. Chemical Recycling of Post-Consumer PLA Waste for Sustainable Production of Ethyl Lactate. *Chem. Eng. J.* **2021**, *423*, 129952. [CrossRef]
31. Grewell, D.; Srinivasan, G.; Cochran, E. Depolymerization of Post-Consumer Polylactic Acid Products. *J. Renew. Mater.* **2014**, *2*, 157–165. [CrossRef]
32. Lee, S.H.; Song, W.S. Enzymatic Hydrolysis of Polylactic Acid Fiber. *Appl. Biochem. Biotechnol.* **2011**, *164*, 89–102. [CrossRef]
33. Payne, J.; McKeown, P.; Jones, M.D. A circular economy approach to plastic waste. *Polym. Degrad. Stab.* **2019**, *165*, 170–181. [CrossRef]
34. Hirao, K.; Ohara, H. Synthesis and Recycle of Poly(L-lactic acid) using Microwave Irradiation. *Polym. Rev.* **2011**, *51*, 1–22. [CrossRef]
35. Hirao, K.; Nakatsuchi, Y.; Ohara, H. Alcoholysis of Poly(l-lactic acid) under microwave irradiation. *Polym. Degrad. Stab.* **2010**, *95*, 925–928. [CrossRef]
36. Song, X.; Liu, F.; Wang, H.; Wang, C.; Yu, S.; Liu, S. Methanolysis of microbial polyester poly(3-hydroxybutyrate) catalyzed by Brønsted-Lewis acidic ionic liquids as a new method towards sustainable development. *Polym. Degrad. Stab.* **2018**, *147*, 215–221. [CrossRef]
37. Song, X.; Wang, H.; Liu, F.; Yu, S. Kinetics and mechanism of monomeric product from methanolysis of poly (3-hydroxybutyrate) catalyzed by acidic functionalized ionic liquids. *Polym. Degrad. Stab.* **2016**, *130*, 22–29. [CrossRef]
38. Siddiqui, M.N.; Redhwi, H.H.; Al-Arfaj, A.A.; Achilias, D.S. Chemical Recycling of PET in the Presence of the Bio-Based Polymers, PLA, PHB and PEF: A Review. *Sustainability* **2021**, *13*, 10528. [CrossRef]
39. National Center for Biotechnology Information. Methyl Lactate. PubChem Compound Database. Available online: https://pubchem.ncbi.nlm.nih.gov/compound/Methyl-lactate (accessed on 30 October 2022).
40. National Center for Biotechnology Information. Ethyl Lactate. PubChem Compound Database. Available online: https://pubchem.ncbi.nlm.nih.gov/compound/Ethyl-lactate (accessed on 30 October 2022).
41. National Center for Biotechnology Information. Methyl 3-Hydroxybutyrate. PubChem Compound Database. Available online: https://pubchem.ncbi.nlm.nih.gov/compound/Methyl-3-hydroxybutyrate (accessed on 30 October 2022).
42. National Center for Biotechnology Information. Ethyl 3-Hydroxybutyrate. PubChem Compound Database. Available online: https://pubchem.ncbi.nlm.nih.gov/compound/Ethyl-3-hydroxybutyrate (accessed on 30 October 2022).
43. Amarasekara, A.S.; Owereh, O.S. Synthesis of a sulfonic acid functionalized acidic ionic liquid modified silica catalyst and applications in the hydrolysis of cellulose. *Catal. Commun.* **2010**, *11*, 1072–1075. [CrossRef]
44. Codari, F.; Lazzari, S.; Soos, M.; Storti, G.; Morbidelli, M.; Moscatelli, D. Kinetics of the hydrolytic degradation of poly(lactic acid). *Polym. Degrad. Stab.* **2012**, *97*, 2460–2466. [CrossRef]
45. Hill, C.A.S.; Jones, D.; Strickland, G.; Cetin, N.S. Kinetic and Mechanistic Aspects of the Acetylation of Wood with Acetic Anhydride. *Holzforschung* **1998**, *52*, 623–629. [CrossRef]